

**NUMERICAL
COMPUTATION
of
INTERNAL
and
EXTERNAL FLOWS**

Volume 2

*Computational Methods
for Inviscid and
Viscous Flows*

C. HIRSCH

Numerical Computation

of

**INTERNAL AND EXTERNAL
FLOWS**

**Volume 2: Computational Methods for Inviscid and
Viscous Flows**

**WILEY SERIES IN
NUMERICAL METHODS IN ENGINEERING**

Consulting Editors

R. H. Gallagher, *Worcester Polytechnic Institute,
Worcester, Massachusetts, USA*

and

O. C. Zienkiewicz, *Department of Civil Engineering,
University College of Swansea*

Rock Mechanics in Engineering Practice

Edited by K. G. Stagg and O. C. Zienkiewicz

Optimum Structural Design: Theory and Applications

Edited by R. H. Gallagher and O. C. Zienkiewicz

Finite Elements in Fluids

Vol. 1 Viscous Flow and Hydrodynamics

Vol. 2 Mathematical Foundations, Aerodynamics and Lubrication

Edited by R. H. Gallagher, J. T. Oden, C. Taylor, and O. C. Zienkiewicz

Finite Elements in Geomechanics

Edited by G. Gudehus

Numerical Methods in Offshore Engineering

Edited by O. C. Zienkiewicz, R. W. Lewis, and K. G. Stagg

Finite Elements in Fluids

Vol. 3

*Edited by R. H. Gallagher, O. C. Zienkiewicz, J. T. Oden, M. Morandi Cecchi,
and C. Taylor*

Energy Methods in Finite Element Analysis

Edited by R. Glowinski, E. Rodin, and O. C. Zienkiewicz

Finite Elements in Electrical and Magnetic Field Problems

Edited by M. V. K. Chari and P. Silvester

Numerical Methods in Heat Transfer

Vol. I

Edited by R. W. Lewis, K. Morgan, and O. C. Zienkiewicz

Finite Elements in Biomechanics

Edited by R. H. Gallagher, B. R. Simon, P. C. Johnson, and J. F. Gross

Soil Mechanics—Transient and Cyclic Loads

Edited by G. N. Pande and O. C. Zienkiewicz

Finite Elements in Fluids

Vol. 4

Edited by R. H. Gallagher, D. Norrie, J. T. Oden, and O. C. Zienkiewicz

Foundations of Structural Optimization: A Unified Approach

Edited by A. J. Morris

Numerical Methods in Heat Transfer

Vol. II

Edited by R. W. Lewis, K. Morgan, and B. A. Schrefler

Numerical Methods in Coupled Systems

Edited by R. W. Lewis, E. Hinton, and P. Bettess

New Directions in Optimum Structural Design

Edited by E. Atrek, R. H. Gallagher, K. M. Ragsdell, and O. C. Zienkiewicz

Mechanics of Engineering Materials

Edited by C. S. Desai and R. H. Gallagher

Numerical Analysis of Forming Processes

Edited by J. F. T. Pittman, O. C. Zienkiewicz, R. D. Wood, and J. M. Alexander

Finite Elements in Fluids

Vol. 5

Edited by R. H. Gallagher, J. T. Oden, O. C. Zienkiewicz,

T. Kawai, and M. Kawahara

Mechanics of Geomaterials: Rocks, Concretes, Soils

Edited by Z. P. Bažant

Finite Elements in Fluids

Vol. 6

Edited by R. H. Gallagher, G. F. Carey, J. T. Oden, and O. C. Zienkiewicz

Numerical Methods in Heat Transfer

Vol. III

Edited by R. W. Lewis and K. Morgan

Accuracy Estimates and Adaptive Refinements in Finite Element Computations

Edited by I. Babuška, J. Gago, E. R. de Arantes e Oliveira, and O. C. Zienkiewicz

**The Finite Element Method in the Deformation and Consolidation
of Porous Media**

R. W. Lewis and B. A. Schrefler

Numerical Methods for Transient and Coupled Problems

Edited by R. W. Lewis, E. Hinton, P. Bettess, and B. A. Schrefler

Microcomputers in Engineering Applications

Edited by B. A. Schrefler and R. W. Lewis

Numerical Computation of Internal and External Flows

Vol. 1: Fundamentals of Numerical Discretization

C. Hirsch

Finite Elements in Fluids

Vol. 7

Edited by R. H. Gallagher, R. Glowinski, P. M. Gresho,

J. T. Oden, and O. C. Zienkiewicz

Mathematical Modeling of Creep and Shrinkage of Concrete

Edited by Z. P. Bažant

Numerical Computation of Internal and External Flows

Vol. 2: Computational Methods for Inviscid and Viscous Flows

C. Hirsch

Numerical Computation
of
INTERNAL AND EXTERNAL
FLOWS

**Volume 2: Computational Methods for
Inviscid and Viscous Flows**

Charles Hirsch

*Department of Fluid Mechanics,
Vrije Universiteit Brussel,
Brussels, Belgium*

A Wiley-Interscience Publication

JOHN WILEY & SONS

Chichester · New York · Brisbane · Toronto · Singapore

Copyright © 1990 by John Wiley & Sons Ltd.
Baffins Lane, Chichester, West Sussex PO19 1UD, England
Reprinted November 1991
Reprinted August 1992
Reprinted August 1994

All rights reserved.

No part of this book may be reproduced by any means,
or transmitted, or translated into a machine language
without the written permission of the publisher.

Other Wiley Editorial Offices

John Wiley & Sons, Inc., 605 Third Avenue,
New York, NY 10158-0012, USA

Jacaranda Wiley Ltd, G.P.O. Box 859, Brisbane,
Queensland 4001, Australia

John Wiley & Sons (Canada) Ltd, 22 Worcester Road,
Rexdale, Ontario M9W 1L1, Canada

John Wiley & Sons (SEA) Pte Ltd, 37 Jalan Pemimpin #05-04,
Block B, Union Industrial Building, Singapore 2057

Library of Congress Cataloging-in-Publication Data:

Hirsch, Ch.

Numerical computation of internal and external flows.

(Wiley series in numerical methods in engineering)
"A Wiley-Interscience publication."

Contents: v. 1. Fundamentals of numerical discretiza-
tion—v. 2. Computational methods for inviscid and
viscous flows.

I. Fluid dynamics—Mathematical models. I. Title.

II. Title: Numerical computation of internal and external
flows. III. Series.

TA357.H574 1988 620.1'064 87-23116

ISBN 0471 91762 1 (v. 1)

ISBN 0471 92351 6 (v. 2)

ISBN 0471 92452 0 (pbk.:v. 2)

British Library Cataloguing in Publication Data:

Hirsch, Ch. (Charles)

Numerical computation of internal and external flows.

Vol. 2. Computational methods for inviscid and viscous flows

I. Fluids. Flow. Simulations. Numerical methods

I. Title

532'.051'0724

ISBN 0471 92351 6 (Pbk: 0471 92452 0)

Typeset by Thomson Press (India) Ltd
Printed and bound in Great Britain by
Redwood Books, Trowbridge, Wiltshire

TA
357
H/578
1988
V. 2

To A. F.

CONTENTS

PREFACE	xv
NOMENCLATURE	xix
PART V: THE NUMERICAL COMPUTATION OF POTENTIAL FLOWS	1
Chapter 13 The Mathematical Formulations of the Potential Flow Model	4
13.1 Conservative Form of the Potential Equation	4
13.2 The Non-conservative Form of the Isentropic Potential Flow Model	6
13.2.1 Small-perturbation potential equation	7
13.3 The Mathematical Properties of the Potential Equation	9
13.3.1 Unsteady potential flow	9
13.3.2 Steady potential flow	9
13.4 Boundary Conditions	14
13.4.1 Solid wall boundary condition	14
13.4.2 Far field conditions	15
13.4.3 Cascade and channel flows	17
13.4.4 Circulation and Kutta condition	18
13.5 Integral or Weak Formulation of the Potential Model	18
13.5.1 Bateman variational principle	19
13.5.2 Analysis of some properties of the variational integral	20
Chapter 14 The Discretization of the Subsonic Potential Equation	26
14.1 Finite Difference Formulation	27
14.1.1 Numerical estimation of the density	29
14.1.2 Curvilinear mesh	31
14.1.3 Consistency of the discretization of metric coefficients	34
14.1.4 Boundary conditions—curved solid wall	36
14.2 Finite Volume Formulation	38
14.2.1 Jameson and Caughey's finite volume method	39
14.3 Finite Element Formulation	42
14.3.1 The finite element–Galerkin method	43
14.3.2 Least squares or optimal control approach	47
14.4 Iteration Scheme for the Density	47

Chapter 15	The Computation of Stationary Transonic Potential Flows	57
15.1	The Treatment of the Supersonic Region: Artificial Viscosity—Density and Flux Upwinding	61
15.1.1	Artificial viscosity—non-conservative potential equation	62
15.1.2	Artificial viscosity—conservative potential equation	66
15.1.3	Artificial compressibility	67
15.1.4	Artificial flux or flux upwinding	70
15.2	Iteration Schemes for Potential Flow Computations	77
15.2.1	Line relaxation schemes	77
15.2.2	Guidelines for resolution of the discretized potential equation	81
15.2.3	The alternating direction implicit method—approximate factorization schemes	88
15.2.4	Other techniques—multigrid methods	98
15.3	Non-uniqueness and Non-isentropic Potential Models	104
15.3.1	Isentropic shocks	105
15.3.2	Non-uniqueness and breakdown of the transonic potential flow model	105
15.3.3	Non-isentropic potential models	112
15.4	Conclusions	117
PART VI: THE NUMERICAL SOLUTION OF THE SYSTEM OF EULER EQUATIONS		125
Chapter 16	The Mathematical Formulation of the System of Euler Equations	132
16.1	The Conservative Formulation of the Euler Equations	132
16.1.1	Integral conservative formulation of the Euler equations	133
16.1.2	Differential conservative formulation	134
16.1.3	Cartesian system of coordinates	134
16.1.4	Discontinuities and Rankine–Hugoniot relations—entropy condition	135
16.2	The Quasi-linear Formulation of the Euler Equations	138
16.2.1	The Jacobian matrices for conservative variables	138
16.2.2	The Jacobian matrices for primitive variables	145
16.2.3	Transformation matrices between conservative and non-conservative variables	147
16.3	The Characteristic Formulation of the Euler Equations—Eigenvalues and Compatibility Relations	150
16.3.1	General properties of characteristics	151
16.3.2	Diagonalization of the Jacobian matrices	153
16.3.3	Compatibility equations	154
16.4	Characteristic Variables and Eigenvalues for One-dimensional Flows	157
16.4.1	Eigenvalues and eigenvectors of Jacobian matrix	158
16.4.2	Characteristic variables	162
16.4.3	Characteristics in the xt -plane—shocks and contact discontinuities	168
16.4.4	Physical boundary conditions	171
16.4.5	Characteristics and simple wave solutions	173
16.5	Eigenvalues and Compatibility Relations in Multidimensional Flows	176

16.5.1	Jacobian eigenvalues and eigenvectors in primitive variables	177
16.5.2	Diagonalization of the conservative Jacobians	180
16.5.3	Mach cone and compatibility relations	184
16.5.4	Boundary conditions	191
16.6	Some Simple Exact Reference Solutions for One-dimensional Inviscid Flows	196
16.6.1	The linear wave equation	196
16.6.2	The inviscid Burgers equation	196
16.6.3	The shock tube problem or Riemann problem	204
16.6.4	The quasi-one-dimensional nozzle flow	211
Chapter 17 The Lax–Wendroff Family of Space-centred Schemes		224
17.1	The Space-centred Explicit Schemes of First Order	226
17.1.1	The one-dimensional Lax–Friedrichs scheme	226
17.1.2	The two-dimensional Lax–Friedrichs scheme	229
17.1.3	Corrected viscosity scheme	233
17.2	The Space-centred Explicit Schemes of Second Order	234
17.2.1	The basic one-dimensional Lax–Wendroff scheme	234
17.2.2	The two-step Lax–Wendroff schemes in one dimension	238
17.2.3	Lerat and Peyret's S_x^β family of non-linear two-step Lax–Wendroff schemes	246
17.2.4	One-step Lax–Wendroff schemes in two dimensions	251
17.2.5	Two-step Lax–Wendroff schemes in two dimensions	258
17.3	The Concept of Artificial Dissipation or Artificial Viscosity	272
17.3.1	General form of artificial dissipation terms	273
17.3.2	Von Neumann–Richtmyer artificial viscosity	274
17.3.3	Higher-order artificial viscosities	279
17.4	Lerat's Implicit Schemes of Lax–Wendroff Type	283
17.4.1	Analysis for linear systems in one dimension	285
17.4.2	Construction of the family of schemes	288
17.4.3	Extension to non-linear systems in conservation form	292
17.4.4	Extension to multi-dimensional flows	296
17.5	Summary	296
Chapter 18 The Central Schemes with Independent Time Integration		307
18.1	The Central Second-order Implicit Schemes of Beam and Warming in One Dimension	309
18.1.1	The basic Beam and Warming schemes	310
18.1.2	Addition of artificial viscosity	315
18.2	The Multidimensional Implicit Beam and Warming Schemes	326
18.2.1	The diagonal variant of Pulliam and Chaussee	328
18.3	Jameson's Multistage Method	334
18.3.1	Time integration	334
18.3.2	Convergence acceleration to steady state	335
Chapter 19 The Treatment of Boundary Conditions		344
19.1	One-dimensional Boundary Treatment for Euler Equations	345
19.1.1	Characteristic boundary conditions	346
19.1.2	Compatibility relations	347

19.1.3	Characteristic boundary conditions as a function of conservative and primitive variables	349
19.1.4	Extrapolation methods	353
19.1.5	Practical implementation methods for numerical boundary conditions	357
19.1.6	Nonreflecting boundary conditions	369
19.2	Multidimensional Boundary Treatment	372
19.2.1	Physical and numerical boundary conditions	372
19.2.2	Multidimensional compatibility relations	376
19.2.3	Farfield treatment for steadystate flows	377
19.2.4	Solid wall boundary	379
19.2.5	Nonreflective boundary conditions	384
19.3	The Far-field Boundary Corrections	385
19.4	The Kutta Condition	395
19.5	Summary	401
Chapter 20 Upwind Schemes for the Euler Equations		408
20.1	The Basic Principles of Upwind Schemes	409
20.2	One-dimensional Flux Vector Splitting	415
20.2.1	Steger and Warming flux vector splitting	415
20.2.2	Properties of split flux vectors	417
20.2.3	Van Leer's flux splitting	420
20.2.4	Non-reflective boundary conditions and split fluxes	425
20.3	One-dimensional Upwind Discretizations Based on Flux Vector Splitting	426
20.3.1	First-order explicit upwind schemes	426
20.3.2	Stability conditions for first-order flux vector splitting schemes	428
20.3.3	Non-conservative firstorder upwind schemes	438
20.4	Multi-dimensional Flux Vector Splitting	438
20.4.1	Steger and Warming flux splitting	440
20.4.2	Van Leer flux splitting	440
20.4.3	Arbitrary meshes	441
20.5	The Godunov-type Schemes	443
20.5.1	The basic Godunov scheme	444
20.5.2	Osher's approximate Riemann solver	453
20.5.3	Roe's approximate Riemann solver	460
20.5.4	Other Godunov-type methods	469
20.5.5	Summary	472
20.6	First-order Implicit Upwind Schemes	473
20.7	Multi-dimensional First-order Upwind Schemes	475
Chapter 21 Second-order Upwind and High-resolution Schemes		493
21.1	General Formulation of Higher-order Upwind Schemes	494
21.1.1	Higher-order projection stages—variable extrapolation or MUSCL approach	495
21.1.2	Numerical flux for higher-order upwind schemes	498
21.1.3	Second-order space- and time-accurate upwind schemes based on variable extrapolation	499
21.1.4	Linearized analysis of second-order upwind schemes	502

21.1.5	Numerical flux for higher-order upwind schemes—flux extrapolation	504
21.1.6	Implicit second-order upwind schemes	512
21.1.7	Implicit second-order upwind schemes in two dimensions	514
21.1.8	Summary	516
21.2	The Definition of High-resolution Schemes	517
21.2.1	The generalized entropy condition for inviscid equations	519
21.2.2	Monotonicity condition	525
21.2.3	Total variation diminishing (TVD) schemes	528
21.3	Second-order TVD Semi-discretized Schemes with Limiters	536
21.3.1	Definition of limiters for the linear convection equation	537
21.3.2	General definition of flux limiters	550
21.3.3	Limiters for variable extrapolation—MUSCL—method	552
21.4	Timeintegration Methods for TVD Schemes	556
21.4.1	Explicit TVD schemes of first-order accuracy in time	557
21.4.2	Implicit TVD schemes	558
21.4.3	Explicit second-order TVD schemes	560
21.4.4	TVD schemes and artificial dissipation	564
21.4.5	TVD limiters and the entropy condition	568
21.5	Extension to Non-linear Systems and to Multi-dimensions	570
21.6	Conclusions to Part VI	583
PART VII: THE NUMERICAL SOLUTION OF THE NAVIER–STOKES EQUATIONS		595
Chapter 22 The Properties of the System of Navier–Stokes Equations		597
22.1	Mathematical Formulation of the Navier–Stokes Equations	597
22.1.1	Conservative form of the Navier–Stokes equations	597
22.1.2	Integral form of the Navier–Stokes equations	599
22.1.3	Shock waves and contact layers	600
22.1.4	Mathematical properties and boundary conditions	601
22.2	Reynolds-averaged Navier–Stokes Equations	603
22.2.1	Turbulent-averaged energy equation	604
22.3	Turbulence Models	606
22.3.1	Algebraic models	608
22.3.2	One- and two-equation models— k - ϵ models	613
22.3.3	Algebraic Reynolds stress models	615
22.4	Some Exact One-dimensional Solutions	618
22.4.1	Solutions to the linear convection–diffusion equation	618
22.4.2	Solutions to Burgers equation	620
22.4.3	Other simple test cases	621
Chapter 23 Discretization Methods for the Navier–Stokes Equations		624
23.1	Discretization of Viscous and Heat Conduction Terms	625
23.2	Time-dependent Methods for Compressible Navier–Stokes Equations	627
23.2.1	First-order explicit central schemes	628
23.2.2	One-step Lax–Wendroff schemes	629
23.2.3	Two-step Lax–Wendroff schemes	630

23.2.4	Central schemes with separate space and time discretization	636
23.2.5	Upwind schemes	648
23.3	Discretization of the Incompressible Navier–Stokes Equations	654
23.3.1	Incompressible Navier–Stokes equations	654
23.3.2	Pseudo-compressibility method	656
23.3.3	Pressure correction methods	661
23.3.4	Selection of the space discretization	666
23.4	Conclusions to Part VII	674
INDEX		685

Preface

This volume, divided into Parts V to VII, is a continuation of the first one which was devoted to fundamentals of numerical discretizations. It contains a presentation of computational methods for inviscid and viscous flow models as they have evolved over the last decade.

Over the last twenty to thirty years considerable progress has been achieved and the field of Computational Fluid Dynamics (CFD) is reaching a mature stage, where most of the basic methodology is, and will remain, well established. Basically, the 1970s can be considered as the development period for the foundations of the discretization methods for transonic potential models and for the foundations of the central discretization methods for the Euler and Navier–Stokes equations, following on the landmark introduction of the Lax–Wendroff scheme.

Although prepared by earlier fundamental developments in the line of Godunov’s method for physically based discretizations of the Euler equations, the upwind, high resolution methods have reached their maturity and been established on solid theoretical grounds in the 1980s. They are by now as firmly established as the central methods. Hence a large variety of techniques are available and a considerable experience has already been accumulated with various discretizations of the Euler equations.

The concomitant tremendous development of computer performance over the same period has resulted in the present capacity of solving two-dimensional Euler equations in seconds of computer time, and simple three-dimensional problems in minutes of CPU times, with the best available codes on the powerful supercomputers. Hence more attention can be given to the validation, accuracy and reliability of numerical flow simulations and to their extensions to complex industrial design and analysis applications.

Another consequence is the current possibility of obtaining Navier–Stokes solutions, within the Reynolds-averaged approximation, in rather short computer times (at least for two-dimensional problems and simple three-dimensional configurations). Although the accumulated experience with Navier–Stokes solutions is not yet as large as with the inviscid models, it is rapidly building up. Due to the strong connection between Euler and Navier–Stokes equations at high Reynolds numbers, most of the inviscid methods are of application to the viscous flows. The major topic of uncertainty remains

essentially connected to the fundamental problems of turbulence and its modelization within the Reynolds-averaged approximation.

The content of this volume reflects in a certain way the situation just described.

Part V deals with the simplest inviscid approximation which is, in certain flow regimes, equivalent to the full system of Euler equations, namely the full potential model. It contains three chapters, 13 to 15, covering the mathematical formulations (Chapter 13), the discretization of subsonic potential flows (Chapter 14) and the treatment of transonic situations (Chapter 15).

Part VI is devoted to a detailed presentation of the Euler equations and of the basic numerical techniques developed in order to discretize the complex system of inviscid, compressible conservation laws. It covers Chapters 16 to 21, dealing with the algebra of the Euler equations (Chapter 16), the central schemes (Chapter 17 and 18), the treatment of boundary conditions (Chapter 19) and the upwind methods (Chapters 20 and 21).

Part VII finally introduces the discretization methods for the Navier–Stokes equations and contains two chapters, 22 and 23. Chapter 22 covers the basic mathematical formulation of Reynolds-averaged Navier–Stokes equations with an introduction to turbulence models and the last chapter summarizes the approaches for compressible and incompressible viscous conservation laws.

The present text is directed at students at the graduate level as well as at scientists and engineers already engaged, or starting to be engaged, in Computational Fluid Dynamics. Although Computational Fluid Dynamics requires a good theoretical base, it remains for the large part an experimental science since many properties depend on the non-linear character of the flow equations and cannot be fully analysed. Therefore, a fraction of the problems added to each chapter request the writing of a program, mainly for the one-dimensional flow equations.

Since the development of a code covers many aspects: selection of a scheme, implementation of boundary conditions, selection of a time integration method, definition of control mechanisms of non-linear instabilities, . . . , it is recommended to experiment intensively with as many variants as possible, either individually or by sharing the number of selected options and different test cases within a group or a class of students. A single modular code with many options is a remarkably effective and instructive ‘numerical laboratory’.

Initial versions of some chapters have been written while holding the NAVAIR Research Chair at the Naval Postgraduate School in Monterey. I am particularly grateful to Ray Shreeve for this opportunity and for his friendship.

Some sections on Euler equations have been written during a summer stay at ICASE, NASA Langley, and I would like to acknowledge particularly Dr Milton Rose, former Director of ICASE, for his hospitality and the stimulating atmosphere.

I have also had the privilege to benefit from results of computations performed, at my request, on different test cases by several groups and I would like to thank D. Caughey at Cornell University, T. Holst at NASA Ames, A. Jameson

at Princeton University, M. Salas at NASA Langley, and J. South and C. Gumbert also at NASA Langley, for their willingness and effort.

During the redaction of this book, I have had some stimulating discussions on the subject of the Kutta condition with T. Pulliam and A. Rizzi for which I am grateful.

I have also the pleasure to thank my coworkers C. Lacor and G. Van Dijk for their comments and support, as well as my secretary J. D'haes for her considerable help with figures and text.

Ch. HIRSCH
BRUSSELS, JULY 1988

Nomenclature

a	convection velocity or wave speed
\bar{A}	Jacobian of flux vector with respect to conservative variables, with components A, B, C
c	speed of sound
c_p	specific heat at constant pressure
c_v	specific heat at constant volume
D	artificial dissipation function
e	internal energy per unit mass
E	total energy per unit mass
f	scalar flux function
f^*	numerical flux function
\bar{f}_e	external force vector
\bar{F}	flux vector with components f, g, h
$g^{\alpha\beta}, g_{\alpha\beta}$	contravariant and covariant metric tensor
G	amplification factor/matrix; convergence operator of iterative schemes
h	enthalpy per unit mass
H	stagnation enthalpy per unit mass
I	rothalpy
J	Jacobian of coordinate transformation
k	coefficient of thermal conductivity
k	wave number
K	stiffness matrix
$K = \bar{A} \cdot \bar{\kappa}$	projection of Jacobian matrix on propagation direction $\bar{\kappa}$
K_T	Jacobian matrix of differential operator L
$l^{(i)}$	left eigenvector of Jacobian matrix
L	differential operator
M	Mach number
n	normal distance
\bar{n}	normal vector
N_I	finite element interpolation function for node I
p	pressure
P	convergence or conditioning operator
Pr	Prandtl number
q	modulus of velocity; source term
Q	source term column-vector
r	gas constant per unit mass
$r^{(i)}$	right eigenvector of Jacobian matrix
R	residual of iterative scheme

Re	Reynolds number
s	entropy per unit mass
S	characteristic surface, area of nozzle cross-section
\vec{S}	surface vector
t	time
T	temperature
u	scalar dependent variable
U	column-vector of conservative variables
\vec{v}	velocity vector cartesian components u, v, w
V	column-vector of primitive variables
w	characteristic variable
W	column-vector of characteristic variables
\vec{x}	position vector
x, y, z	cartesian coordinates
α	diffusivity coefficient
γ	specific heat ratio
Γ	circulation; boundary of domain Ω
δ	central-difference operator: $\delta u_i = u_{i+1/2} - u_{i-1/2}$
$\bar{\delta}$	central-difference operator: $\bar{\delta} u_i = (u_{i+1} - u_{i-1})/2$
δ^+	forward difference operator $\delta^+ u_i = u_{i+1} - u_i$
δ^-	backward difference operator $\delta^- u_i = u_i - u_{i-1}$
Δ	Laplace operator
Δt	time step
$\Delta x, \Delta y$	spatial mesh size in x and y directions
ε	turbulence dissipation rate
ε_D	dissipation or diffusion error
ε_ϕ	dispersion error
$\vec{\zeta}$	vorticity vector
$\vec{\kappa}$	wave-number vector; wave propagation direction
$\lambda(A)$	eigenvalue of matrix A
μ	coefficient of dynamic viscosity
μ	averaging difference operator: $\mu u_i = (u_{i+1/2} + u_{i-1/2})/2$
μ	switching function for transonic potential flow
ξ, η, ζ	curvilinear coordinates
ρ	density
$\rho(A)$	spectral radius of matrix A
σ	Courant number
$\bar{\sigma}$	internal stress tensor
τ	ratio $\Delta t/\Delta x$
$\bar{\tau}$	viscous shear stress tensor
ν	kinematic viscosity
ϕ	velocity potential function
ϕ	phase angle in Von Neumann analysis
Φ	phase angle of amplification factor
ω	time frequency of plane wave
ω	overrelaxation parameter
Ω	volume
$\bar{I}_x, \bar{I}_y, \bar{I}_z$	unit vectors along the x, y, z directions

Subscripts

e	external variable
i, j	mesh point locations in x, y directions
I, J	nodal point index
J	eigenvalue number
L, R	left and right states
min	minimum
max	maximum
n	normal or normal component
o	stagnation values
v	viscous term
x, y, z	components in x, y, z directions
x, y, z	partial differentiation with respect to x, y, z
∞	freestream value
ξ, η, ζ	components in ξ, η, ζ directions

Superscripts

AV	artificial viscosity
n	iteration level
n	time level
-	exact solution of discretized equation
-	exact solution of differential equation

Symbols

\times	vector product of two vectors
\otimes	tensor product of two vectors
$\bar{\nabla}$	gradient or divergence operator

PART V: THE NUMERICAL COMPUTATION OF POTENTIAL FLOWS

The potential flow model is the simplest inviscid description that takes full account of compressibility effects. The lower levels of approximation, such as the small disturbance equation and the linearized potential flows, will not be discussed here since they do not contain all the geometrical or compressibility properties of the full potential equation. Moreover, the computational speed of modern computers allows the computation of full non-linear potential flows at only a marginal increase in computer cost, compared to the cost of applications of small disturbance equations or Panel methods (Kutler, 1983). Therefore there does not seem to be a strong justification to develop operational codes based on approximation levels lower than the full potential model.

The development of numerical methods for the solution of the full potential equation, in particular for transonic and supersonic flow configurations with the presence of shock and sonic surfaces, has been an essential topic of research in the 1970s. Presently, this problem can be considered as solved, and three-dimensional potential codes are operational tools in industry and applied systematically in preliminary design stages. Due to the advancement in computer technology and in algorithms, computational times have evolved from several hours to a few seconds for a three-dimensional computation—typically of the order of five seconds on a CRAY-X-MP supercomputer for 50 000 mesh points. (Holst and Thomas, 1983; Shankar, 1985.) The reader will find in this last reference a synthesis of the level of achievement reached in the numerical solution of potential flows, while the review of Holst *et al.* (1982) gives an overview of the state of the art typical of the end of the 1970s.

Chapter 13 will describe the various mathematical formulations of the potential model as they can be used for space discretizations.

A first distinction is to be made between stationary and unsteady flow situations. Many, if not all, of the computational methods for unsteady potential flows do rely on, or are close to, the approaches developed for steady flows. Therefore steady-state computational methods form the basis of nearly all the potential flow applications and we will restrict our presentation of potential flow discretizations to steady flows.

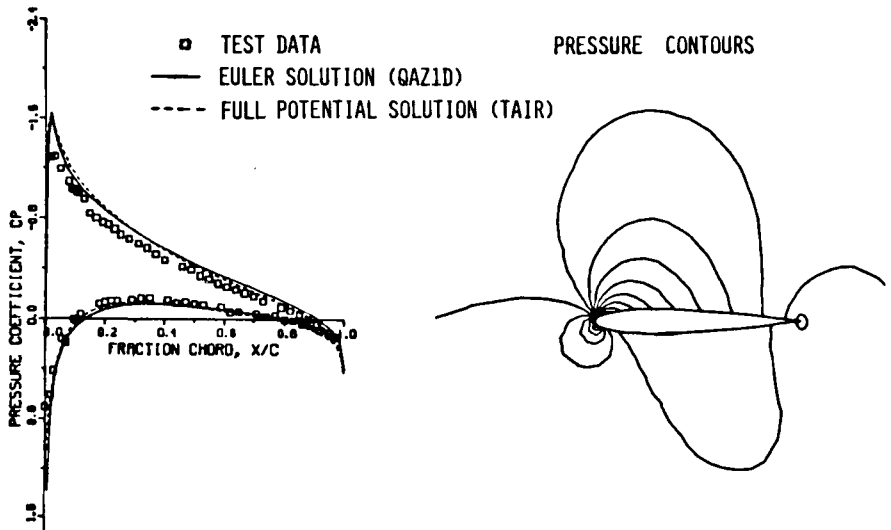


Figure V.1 Comparison of Euler and potential flow computations for a NACA 0012 profile under incidence at subsonic flow conditions. (Courtesy A. Verhoff, McDonnell Aircraft Co., USA)

Another basic distinction is to be made between subcritical and supercritical flows. As discussed in Section 2.9.2 in Volume 1, the subsonic potential flow model is fully equivalent to the full system of Euler equations if the initial flow is irrotational. In this case, the potential model is an exact description of the inviscid flow. An example is shown in Figure V.1 for a two-dimensional NACA 0012 airfoil under 3.5 degrees of incidence. The Euler and potential flow computations are nearly identical and the discrepancy with experimental data on the suction surface is most probably tied to viscous effects generated at the leading edge.

Chapter 14 will deal with the rather simple and by now classical computation of subsonic potential flows. The steady-state potential equation is of the elliptic type and a very large variety of techniques can be used to discretize and solve the non-linear algebraic system of equations. Most of the methods described in Chapter 12 to Volume 1 can be, or have been, applied together with various approaches to treat the non-linearity due to compressibility.

We would like to mention at this point that the methods presented in Chapter 14 can be applied to other elliptic or parabolic problems having the same mathematical structure, such as the heat conduction equation defining the temperature distribution in a stationary medium, electrostatic potentials, etc.

The much more complex problem of transonic potential flows will be treated in Chapter 15.

The hyperbolic character of the potential equation in supersonic flow regions, as well as the possible occurrence of shocks, require a particular treatment,

since the straightforward extrapolation of the subsonic algorithms into the supersonic zones leads to unstable codes.

It will be seen that the final outcome of the analysis of the transonic behaviour will lead to the possibility of maintaining the subsonic discretization methods in all flow regions, but with the addition of some form of upwind estimation of the density or mass flux, or alternatively by the addition of artificial viscosity terms.

Since the transonic, isentropic potential model is at a lower level of approximation of inviscid flows, compared to the Euler equations, as seen in Chapter 2 in Volume 1, large differences in shock position and strength, compared to Euler solutions, can be observed.

Section 15.3 will discuss the consequences of this fact, in particular the observed non-uniqueness of transonic isentropic potential flows, resulting from a progressive breakdown of this model with increasing shock strength. Some of the techniques which could be applied in order to overcome these isentropic limitations connected to a potential shock will then be presented. This requires the introduction of non-isentropic corrections.

As an illustration of the achievement of different methods, several results of computations performed with high accuracy or (and) on very fine meshes for two- and three-dimensional flow configurations will be presented. Many of them could be considered as reference potential solutions and we would like to thank particularly at this point D. Caughey, C. Gumbert, A. Jameson, M. Salas and J. South for their willingness to perform these computations.

References

- Holst, T., and Thomas S. (1933). 'Numerical solution of transonic wing flowfields.' *AIAA Journal*, **21**, 863-70.
- Holst, T. L., Slooff, J. W., Yoshihara, H., and Ballhaus, W. F. (1982). 'Applied computational transonic aerodynamics.' *AGARD AG-266*.
- Kutler, P. (1983). 'A perspective of theoretical and applied computational fluid dynamics,' *AIAA Paper 83-0037*, AIAA 21st Aerospace Sciences Meeting.
- Shankar, V. (1985). 'A unified full potential scheme for subsonic, transonic and supersonic flows.' *AIAA Paper 85-1643*, AIAA 18th Fluid Dynamics, Plasmadynamics and Lasers Conference.

Chapter 13

The Mathematical Formulations of the Potential Flow Model

The potential flow model can be expressed in several ways, through differential as well as integral, weak, formulations. The differential form is certainly the most common and, if the conservative form is the only one appropriate for numerical discretizations, the quasi-linear form is best adapted to the analysis of the characteristic properties of the potential flow model. Finite difference methods will be based on the conservative differential equation, while the finite volume method will take as starting point the integral form. This will also be the case for the finite element applications, which require a weak, integral formulation.

These various formulations will be defined in the following sections.

13.1 CONSERVATIVE FORM OF THE POTENTIAL EQUATION

The basic assumption for the existence of a potential, inviscid flow is the condition of irrotationality, that is the condition of vanishing vorticity vector. If the initial flow field is irrotational it will remain so according to Kelvin's theorem and the flow will be isentropic.

For inviscid irrotational flows, one can define a potential function ϕ by

$$\vec{v} = \vec{\nabla}\phi \quad (13.1.1)$$

The conservative form of the potential model is obtained from the continuity equation (1.2.2):

$$\frac{\partial \rho}{\partial t} + \vec{\nabla} \cdot (\rho \vec{\nabla}\phi) = 0 \quad (13.1.2)$$

Remember that the term under the gradient is the mass flux $\vec{F} = \rho \vec{v}$ with Cartesian components $f = \rho u$, $g = \rho v$, $h = \rho w$.

The momentum and energy equation reduce to the following relation for the stagnation enthalpy:

$$\frac{\partial \phi}{\partial t} + H = H_0 \quad (13.1.3)$$

where H_0 is constant over the whole flow field. The density is a unique function

of $\bar{\nabla}\phi$ and $\partial_t\phi$ and can be written for a perfect gas, with stagnation density ρ_0 and stagnation enthalpy H_0 , following equation (2.9.6):

$$\frac{\rho}{\rho_0} = \left[1 - \frac{(\bar{\nabla}\phi)^2}{2H_0} - \frac{\partial_t\phi}{H_0} \right]^{1/(\gamma-1)} \quad (13.1.4)$$

since the potential flow is considered as isentropic.

The steady-state form of the potential equation reduces to

$$\bar{\nabla} \cdot (\rho \bar{\nabla}\phi) = 0 \quad (13.1.5)$$

with the isentropic density law

$$\frac{\rho}{\rho_0} = \left[1 - \frac{(\bar{\nabla}\phi)^2}{2H_0} \right]^{1/(\gamma-1)} \quad (13.1.6)$$

and the energy equation

$$H \equiv h + \frac{\bar{v}^2}{2} = H_0 \quad (13.1.7)$$

In the following, the partial derivatives of ϕ and other scalar quantities with respect to an independent variable will be indicated by a subscript when no ambiguity can arise; that is we will write ϕ_t for $\partial_t\phi$, ρ_t for $\partial_t\rho$, and so on. Subscripts on vector quantities such as velocities will represent the corresponding projections.

In many practical computations, the explicit form of equation (13.1.2) is required in general curvilinear coordinate systems.

Example 13.1.1 Two-dimensional potential equation in arbitrary coordinates

If the coordinate transformation is defined by

$$\begin{aligned} \xi &= \xi(x, y) \\ \eta &= \eta(x, y) \end{aligned} \quad (E13.1.1)$$

the potential equation is written as

$$\frac{\partial}{\partial t} \left(\frac{\rho}{J} \right) + \frac{\partial}{\partial \xi} \left(\rho \frac{U}{J} \right) + \frac{\partial}{\partial \eta} \left(\rho \frac{V}{J} \right) = 0 \quad (E13.1.2)$$

The contravariant velocity components U, V can be defined in function of the Cartesian components as

$$U = \frac{\partial \xi}{\partial x} \phi_x + \frac{\partial \xi}{\partial y} \phi_y = \xi_{x,u} + \xi_{y,v} \quad (E13.1.3a)$$

$$V = \frac{\partial \eta}{\partial x} \phi_x + \frac{\partial \eta}{\partial y} \phi_y = \eta_{x,u} + \eta_{y,v} \quad (E13.1.3b)$$

where u, v are the Cartesian velocity components.

The stationary potential equation is also to be obtained as

$$\bar{\nabla} \cdot (\rho \bar{v}) = \frac{\partial}{\partial \xi} \left[(g^{11} \phi_\xi + g^{12} \phi_\eta) \frac{\rho}{J} \right] + \frac{\partial}{\partial \eta} \left[g^{21} \phi_\xi + g^{22} \phi_\eta \right] \frac{\rho}{J} = 0 \quad (\text{E13.1.4})$$

since one has also

$$\begin{aligned} U &= g^{11} \phi_\xi + g^{12} \phi_\eta \\ V &= g^{21} \phi_\xi + g^{22} \phi_\eta \end{aligned} \quad (\text{E13.1.5})$$

The matrix tensor \bar{g} has the following components:

$$\begin{aligned} g^{11} &= \xi_x^2 + \xi_y^2 \\ g^{12} &= g^{21} = \xi_x \eta_x + \xi_y \eta_y \\ g^{22} &= \eta_x^2 + \eta_y^2 \end{aligned} \quad (\text{E13.1.6})$$

In practical computations, one will often have to determine the metric coefficients through the inverse relations

$$\begin{aligned} x &= x(\xi, \eta) \\ y &= y(\xi, \eta) \end{aligned} \quad (\text{E13.1.7})$$

This is obtained by the relations

$$\begin{aligned} \xi_x &= J y_\eta & \xi_y &= -J x_\eta \\ \eta_x &= -J y_\xi & \eta_y &= J x_\xi \end{aligned} \quad (\text{E13.1.8})$$

with the Jacobian J :

$$J = \frac{1}{x_\xi y_\eta - x_\eta y_\xi} \quad (\text{E13.1.9})$$

Example 13.1.2 Potential equation in cylindrical coordinates

In cylindrical coordinates (r, θ, z) , one has an orthogonal coordinate system, with metric coefficients $h_1 = 1$, $h_2 = r$, $h_3 = 1$ and $J = 1/r$. The components g^{ab} are diagonal with $g^{11} = 1$, $g^{22} = 1/r^2$, $g^{33} = 1$.

The potential equation becomes, in steady-state conditions,

$$\frac{\partial}{\partial r} \left(\rho r \frac{\partial \phi}{\partial r} \right) + \frac{\partial}{\partial z} \left(\rho r \frac{\partial \phi}{\partial z} \right) + \frac{\partial}{\partial \theta} \left(\frac{\rho}{r} \frac{\partial \phi}{\partial \theta} \right) = 0 \quad (\text{E13.1.10})$$

13.2 THE NON-CONSERVATIVE FORM OF THE ISENTROPIC POTENTIAL FLOW MODEL

The isentropic potential model can be written in non-conservative form by working out the derivatives of the density (see Problem 13.1):

$$\begin{aligned} \frac{1}{c^2} [\phi_{tt} + \partial_t (\bar{\nabla} \phi)^2] &= (1 - M_x^2) \phi_{xx} + (1 - M_y^2) \phi_{yy} + (1 - M_z^2) \phi_{zz} - 2M_x M_y \phi_{xy} \\ &\quad - 2M_x M_z \phi_{xz} - 2M_y M_z \phi_{zy} \end{aligned} \quad (\text{13.2.1})$$

As mentioned above, the subscript on ϕ indicates a partial derivative with respect to the corresponding coordinate, but the same subscript on the Mach number M indicates the corresponding velocity component.

The second term in the left-hand side of this equation can be explicitly calculated by

$$\partial_t(\bar{\nabla}\phi)^2 = 2(\phi_x\phi_{xt} + \phi_y\phi_{yt} + \phi_z\phi_{zt}) \quad (13.2.2)$$

and the Mach numbers are defined in the coordinate direction x, y, z by

$$\begin{aligned} M_x &= \frac{\phi_x}{c} & M_y &= \frac{\phi_y}{c} & M_z &= \frac{\phi_z}{c} \\ M^2 &= \frac{\bar{v}^2}{c^2} \end{aligned} \quad (13.2.3)$$

The speed of sound c is given by

$$\begin{aligned} c^2 &= \left(\frac{\partial p}{\partial \rho} \right)_s = \frac{\gamma p}{\rho} \\ &= (\gamma - 1)h = (\gamma - 1) \left[H_0 - \frac{(\bar{\nabla}\phi)^2}{2} - \phi_t \right] \end{aligned} \quad (13.2.4)$$

for perfect gases.

For steady flows, the left-hand side of equation (13.2.1) vanishes, and one obtains the non-conservative equivalent to equation (13.1.5) in Cartesian coordinates. It can be written in condensed notation, with a summation convention on $i, j = x, y, z$:

$$(\delta_{ij} - M_i M_j) \phi_{ij} = 0 \quad (13.2.5)$$

13.2.1 Small-perturbation potential equation

The small-perturbation potential equation has been for a long time the basis for potential flow theories, particularly for transonic flows where it is known as the transonic small-perturbation (TSP) equation, as it is a simplified form valid for flow fields along slender bodies aligned with the x axis (Figure 13.2.1).

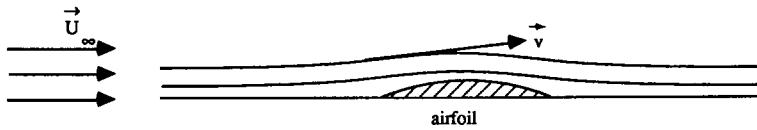
It can be written in various ways from a small-perturbation expansion of the full potential equations (13.1.5) or (13.2.5). Defining the perturbation potential Φ by

$$\phi = U_\infty(x + \Phi) \quad (13.2.6)$$

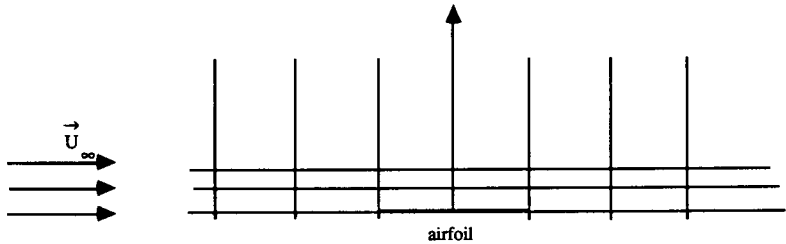
the velocity components are defined by

$$\begin{aligned} u &= U_\infty(1 + \Phi_x) \\ v &= U_\infty\Phi_y \end{aligned} \quad (13.2.7)$$

where U_∞ is the free-stream velocity. With the assumption of a dominating



(a) Physical plane



(b) Computational plane

Figure 13.2.1 Small-perturbation potential flow along slender body

x component of the velocity field, that is $v \ll u$, the two-dimensional form of equation (13.2.5) reduces to

$$(1 - M_\infty^2)\Phi_{xx} + \Phi_{yy} = 0 \quad (13.2.8)$$

neglecting second-order terms in Φ_y and assuming $M_\infty^2 \ll 1$.

The factor of the first term can be worked out by introducing the free-stream Mach number M_∞ and the relation

$$c^2 \left(1 + \frac{\gamma - 1}{2} M_\infty^2 \right) = c_\infty^2 \left(1 + \frac{\gamma - 1}{2} M_\infty^2 \right) \quad (13.2.9)$$

derived from the energy equation (13.1.7) for a perfect gas.

This leads to the following form of the small-perturbation potential equation see Problem 13.10):

$$[1 - M_\infty^2 - (\gamma + 1)M_\infty^2 \Phi_x] \Phi_{xx} + [1 - (\gamma - 1)M_\infty^2 \Phi_x] \Phi_{yy} = 0 \quad (13.2.10)$$

neglecting terms proportional to Φ_x^2 and Φ_y^2 .

This equation is generally further simplified to the more classical form

$$[1 - M_\infty^2 - (\gamma + 1)M_\infty^2 \Phi_x] \Phi_{xx} + \Phi_{yy} = 0 \quad (13.2.11)$$

The sonic condition corresponds to $u = \Phi_x = (1 - M_\infty^2)/[(\gamma + 1)M_\infty^2]$. The first-order TSP equation is the Prandtl–Glauert equation

$$(1 - M_\infty^2)\Phi_{xx} + \Phi_{yy} = 0 \quad (13.2.12)$$

If $y = f(x)$ is the equation of the thin airfoil surface, it is customary with the

small-disturbance hypothesis to set the surface boundary condition on the x axis, that is at $y = 0$. Hence, the flow is calculated in the half-plane where the airfoil occupies a portion of the x axis. The presence of the airfoil will appear in the computation only through the boundary condition (Figure 13.2.1)

$$v = (U_{\infty} + u)f'(x) \approx U_{\infty}f'(x) \quad (13.2.13)$$

where $f'(x)$ is the derivative of f .

Other formulations of the small-perturbation equations as well as references to earlier work can be found in J. Slooff (1982).

13.3 THE MATHEMATICAL PROPERTIES OF THE POTENTIAL EQUATION

The mathematical properties of the potential flow equation can best be obtained from an analysis of the non-conservative form (13.2.1).

13.3.1 Unsteady potential flow

The time-dependent potential equation is a quasi-linear, second-order partial differential equation and it is of importance to determine its type: hyperbolic, parabolic or elliptic (see Chapter 3 in Volume 1).

Since this equation contains a second derivative with respect to time, and since a coordinate system can always be chosen such that one of the velocity components is locally zero, at least one of the second-order space derivatives will have a positive coefficient, indicating that the equation is hyperbolic with respect to time, independently of Mach number.

In many unsteady potential flow computations, the additional approximation of low-frequency unsteady motion is introduced, allowing the second-order time derivative in the potential equation to be neglected. However, this does not change the type of the equation.

13.3.2 Steady potential flow

For steady potential flows, the situation with respect to the type of the equation is more complex.

In two dimensions, x, y , it was shown in Chapter 3 that the potential equation is hyperbolic in (x, y) for supersonic velocities, parabolic along sonic lines, $M = 1$ and elliptic in the subsonic flow regime.

In three-dimensional flows, the situation is somewhat more complicated, since at each point one has an infinity of possible characteristic directions and the properties of the system in supersonic flows also depend on the coordinate selected to act as a time-like direction.

Following the guidelines of Chapter 3, the stationary form of the three-dimensional potential equation (13.2.5) is first cast into a system of

first-order equations by addition of the irrotationality condition

$$\bar{\nabla} \times \bar{v} = 0 \quad (13.3.1)$$

Defining the column vector U as

$$U = \begin{vmatrix} u \\ v \\ w \end{vmatrix} = \begin{vmatrix} \phi_x \\ \phi_y \\ \phi_z \end{vmatrix} \quad (13.3.2)$$

representing the velocity field and adding the y and z projections of the irrotationality equation (13.3.1), under the form

$$\begin{aligned} \frac{\partial v}{\partial x} - \frac{\partial u}{\partial y} &= 0 \\ \frac{\partial w}{\partial x} - \frac{\partial u}{\partial z} &= 0 \end{aligned} \quad (13.3.3)$$

to the potential equation (13.2.1) written as

$$\begin{aligned} (1 - M_x^2)u_x + (1 - M_y^2)v_y + (1 - M_z^2)w_z - M_x M_y (u_y + v_x) - M_y M_z (w_y + v_z) \\ - M_x M_z (u_z + w_x) = 0 \end{aligned} \quad (13.3.4)$$

one obtains the following equivalent first-order system:

$$(A_1 \partial_x + A_2 \partial_y + A_3 \partial_z)U = 0 \quad (13.3.5)$$

The three matrices A_i are defined by

$$A_1 = \begin{vmatrix} 1 - M_x^2 & -M_x M_y & -M_x M_z \\ 0 & 1 & 0 \\ 0 & 0 & 1 \end{vmatrix} \quad (13.3.6a)$$

$$A_2 = \begin{vmatrix} -M_x M_y & 1 - M_y^2 & -M_y M_z \\ -1 & 0 & 0 \\ 0 & 0 & 0 \end{vmatrix} \quad (13.3.6b)$$

$$A_3 = \begin{vmatrix} -M_x M_z & -M_y M_z & 1 - M_z^2 \\ 0 & 0 & 0 \\ -1 & 0 & 0 \end{vmatrix} \quad (13.3.6c)$$

The system (13.3.5) will be hyperbolic, if normals $\bar{n}(n_x, n_y, n_z)$ can be found, satisfying the condition (3.2.22) for the vanishing of the determinant

$$\det |A_1 n_x + A_2 n_y + A_3 n_z| = 0 \quad (13.3.7)$$

Since \bar{n} is defined up to an arbitrary scale factor, each solution of (13.3.7) represents a one-parameter family of characteristic surfaces, defined by a relation of the form $n_x/n_z = f(n_y/n_z)$.

A straightforward calculation, which is left to the reader as an exercise (see

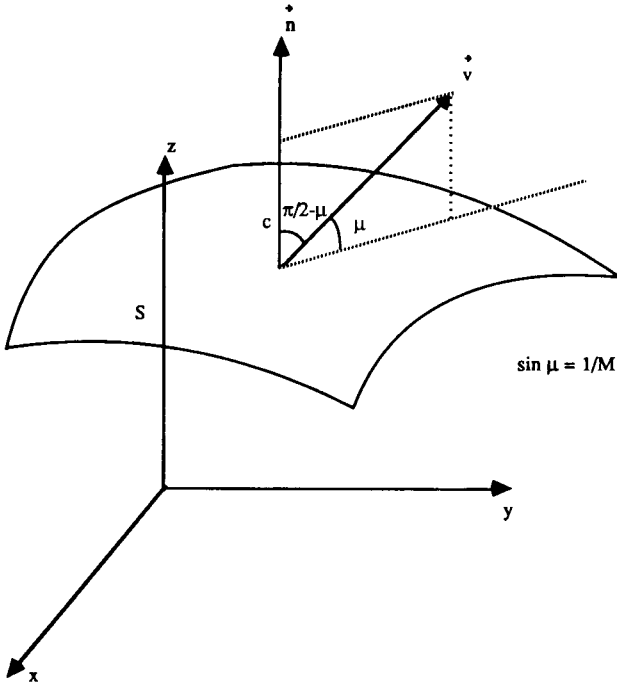


Figure 13.3.1 Condition for \bar{n} to be the normal to a characteristic surface S

Problem 13.3), leads to the characteristic condition

$$\bar{n}^2 - \frac{(\bar{v} \cdot \bar{n})(\bar{v} \cdot \bar{n})}{c^2} = 0 \quad (13.3.8)$$

or

$$(\bar{v} \cdot \bar{1}_n)^2 = c^2 \quad (13.3.9)$$

after removal of a trivial solution $n_x = 0$, with $\bar{1}_n$ representing the unit vector along the normal \bar{n} .

Hence, the normals to the characteristic surfaces are the directions along which the projection of the velocity is sonic (see Figure 13.3.1). If the velocity \bar{v} is subsonic, there is no solution to (13.3.9) and the potential equation (13.1.4) or (13.3.4) is elliptic. When the velocity is supersonic directions \bar{n} satisfying equation (13.3.9) can be defined and the potential equation is hyperbolic. The directions \bar{n} generate a cone around the velocity vector \bar{v} of opening angle 2β such that (see Figure 13.3.2)

$$\cos \beta = \frac{1}{M} \quad (13.3.10)$$

or

$$\beta = \frac{\pi}{2} - \mu \quad (13.3.11)$$

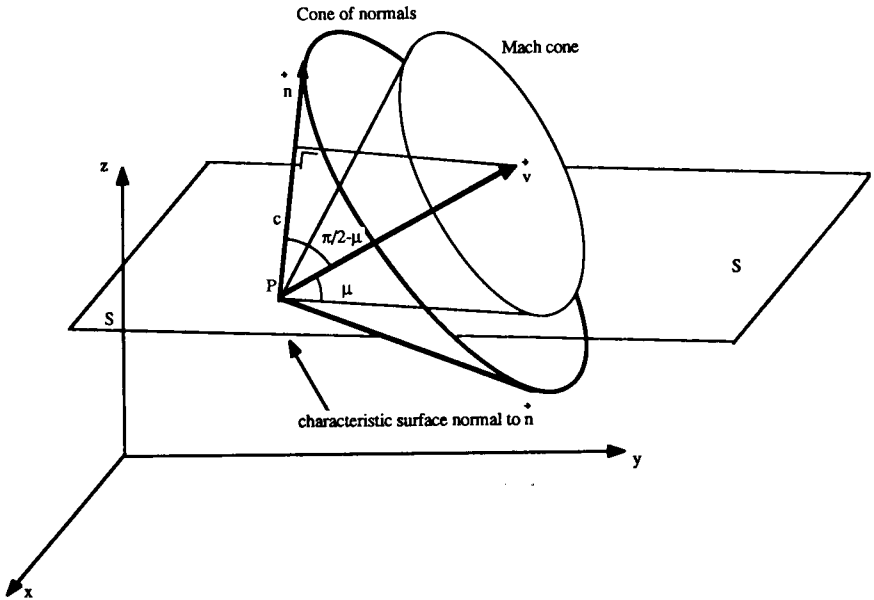


Figure 13.3.2 Mach cone and cone of the normals \vec{n} to the characteristic surfaces S

where μ is the Mach angle defined by

$$\sin \mu = \frac{1}{M} \tag{13.3.12}$$

Each normal \vec{n} lying on the cone of opening angle $(\pi - 2\mu)$ centered on the velocity defines a characteristic surface. The envelope of the characteristic surfaces when \vec{n} sweeps its cone forms a second cone, of opening angle 2μ centered on the velocity, the *Mach cone*. The Mach cone limits the *zone of influence* of point P and the downstream prolongation of the cone defines the *domain of dependence* of P.

However, if for supersonic absolute velocities the potential equation is hyperbolic, it is yet not clear which coordinate direction can be taken as a *time-like* variable. This is of importance since, following the developments of Chapter 3, Section 3.4, a time-like direction z implies that an arbitrary perturbation in the direction $\vec{\kappa}(n_x, n_y)$ of the x, y plane will propagate in the z direction with a ‘frequency’ ω equal to $-n_z$. The component n_z is the solution of equation (13.3.8), written as follows after multiplication by c^2 and development of the scalar products:

$$n_z^2(c^2 - w^2) - 2wn_z(\vec{v} \cdot \vec{\kappa}) + c^2\vec{\kappa}^2 - (\vec{v} \cdot \vec{\kappa})^2 = 0 \tag{13.3.13}$$

where

$$\vec{v} \cdot \vec{\kappa} = un_x + vn_y \tag{13.3.14}$$

A real solution n_z to the quadratic equation (13.3.13) will exist for all $\vec{\kappa}$, if the

discriminant is positive, that is if

$$w^2(\vec{v} \cdot \vec{\kappa})^2 - (c^2 - w^2)[c^2 \vec{\kappa}^2 - (\vec{v} \cdot \vec{\kappa})^2] > 0$$

or

$$w^2 \vec{\kappa}^2 + (\vec{v} \cdot \vec{\kappa})^2 > c^2 \vec{\kappa}^2 \quad (13.3.15)$$

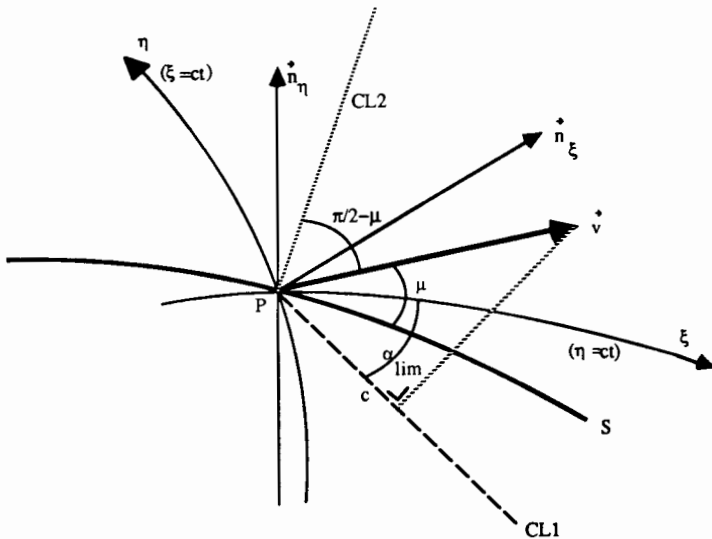
Since one can always choose $\vec{\kappa}^2 = 1$, this equation will be satisfied for all $\vec{\kappa}$ if

$$w^2 > c^2 \quad (13.3.16)$$

that is if the velocity projection in the considered direction is supersonic. For subsonic flows, equation (13.3.13) has no real solutions.

Referring to Figure 13.3.2, the condition (13.3.16) implies that all time-like directions are located inside the cone of normals. In a curvilinear system of coordinates, a particular coordinate direction, say $\xi^1 = \xi$, will be time-like if the associated covariant component of the normal direction, n_1 , is real for all values of n_2, n_3 . Applying the above procedure, one obtains the condition on the *contravariant* velocity component U :

$$\frac{U}{\sqrt{g^{11}}} > c \quad (13.3.17)$$



S : characteristic line

CL1, CL2 : limit directions for which $\vec{v} \cdot \vec{n} = c$

intersections with cone of normals

\vec{n}_ξ : normal to $\xi = ct$ line

\vec{n}_η : normal to $\eta = ct$ line

Figure 13.3.3 Conditions for the directions ξ to be a time-like coordinate

that is the 'physical' value of the velocity projection in the direction normal to the ξ^1 -constant lines has to be supersonic (Figure 13.3.3); see also Problem 13.5.

A direction outside the cone of normals will correspond to an elliptic behaviour and will be called a *space-like* direction.

In Figure 13.3.3 the line S is the intersection of the surface $\xi^3 \equiv \zeta$ with the characteristic surface and the lines CL1 and CL2 are the intersections with the cone of normals. Hence, CL2 is perpendicular to S and makes an angle $(\pi/2 - \mu)$ with the direction of the local velocity. All the normals between the limit lines CL1 and CL2 correspond to time-like directions since the projection of the velocity on this direction is larger than the sonic velocity. This is the case for the normal \bar{n}_ξ to the η -coordinate line (a line $\xi = ct$). Note that the projection of the velocity along this direction is equal to the left-hand side of equation (13.3.17). On the other hand, the normal \bar{n}_η to the ξ -coordinate line (a line $\eta = ct$) is outside the lines CL1 and CL2 and therefore the associated η -coordinate line is space-like.

The application of these considerations to the computation of three-dimensional supersonic potential flows with embedded subsonic regions has been developed by Shankar and Osher (1983) and Shankar *et al.* (1983).

In practical computations, the separation surface between subsonic and supersonic regions is not known and is part of the solution. Next to the occurrence of shock discontinuities, this makes up for the difficulties of transonic potential flows.

13.4 BOUNDARY CONDITIONS

A computational domain has to be selected, limited by a boundary Γ and the boundary conditions for the potential flow computations have to be defined.

13.4.1 Solid wall boundary condition

At solid boundaries, the normal velocity is

$$\rho \frac{\partial \phi}{\partial n} \equiv \rho \phi_n = q \quad (13.4.1)$$

where

$$q = 0 \quad (13.4.2a)$$

if the solid wall is at rest, while

$$q = \rho \bar{v}_w \cdot \bar{I}_n \quad (13.4.2b)$$

if the solid wall has a velocity \bar{v}_w , where \bar{I}_n is the unit vector along the normal to the boundary. If a local mass flux \dot{m}_w per area unit is injected through the wall surface (Figure 13.4.1), then

$$q = \dot{m}_w \quad (13.4.2c)$$

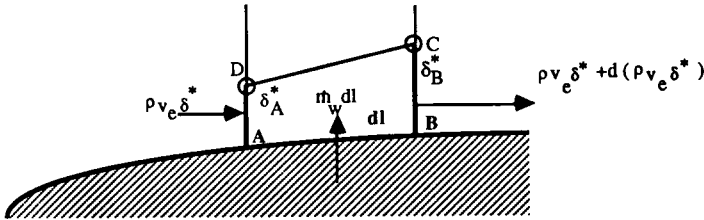


Figure 13.4.1 Boundary conditions along a wall with real or simulated mass flow injection

For instance, in viscid–inviscid interaction computations where the potential flow is corrected for the boundary layer thickness, the displaced boundary of the inviscid region is the edge of the boundary layer. For small boundary layer thicknesses the displaced boundary of the computational region can be modelled by the introduction of the displacement thickness δ^* . In this case a mass balance over the domain ABCD gives

$$\dot{m}_w = \frac{d}{dl}(\rho v_e \delta^*) \quad (13.4.3)$$

where v_e is the velocity at the edge of the boundary layer and dl the elementary distance along the wall.

13.4.2 Far field conditions

At the external boundaries of the computational domain, the flow field is assumed to be known. In external flow problems, such as the flow around a body under uniform inflow \vec{V}_∞ , the potential flow is known by

$$\phi = \vec{V}_\infty \cdot \vec{x} + \phi_0 \quad (13.4.4)$$

where ϕ_0 is an arbitrary constant and \vec{x} the distance to a point on the boundary with respect to a chosen reference.

Single airfoil

For lifting bodies with circulation Γ_B the contribution of the circulation to the potential flow at large distance has to be taken into account (Figure 13.4.2). This is best represented, for a two-dimensional airfoil, by a vortex singularity, corrected for compressibility effects (Ludford, 1951):

$$\phi_{\text{far field}} = \vec{V}_\infty \cdot \vec{x} + \frac{\Gamma_B}{2\pi} \tan^{-1}[\sqrt{1 - M_\infty^2} \tan(\theta - \alpha_\infty)] + \phi_0 \quad (13.4.5)$$

where θ is the angular position of a far field point, Γ_B the circulation and M_∞ the Mach number corresponding to the free-stream velocity \vec{V}_∞ under an incidence angle of α_∞ .

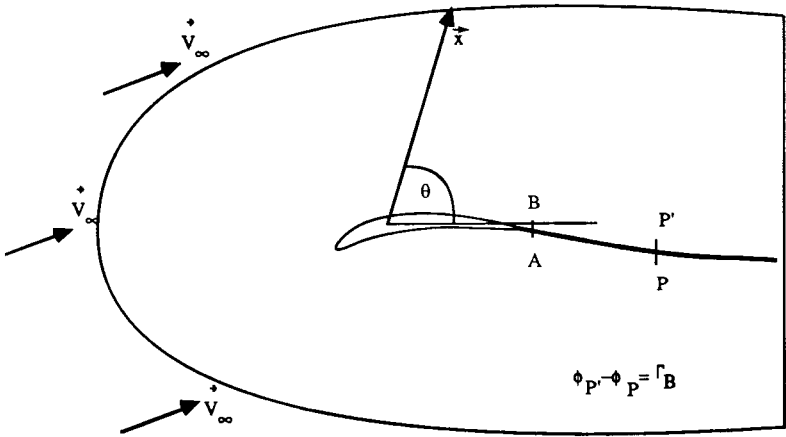


Figure 13.4.2 Computational domain and boundary conditions for isolated airfoils

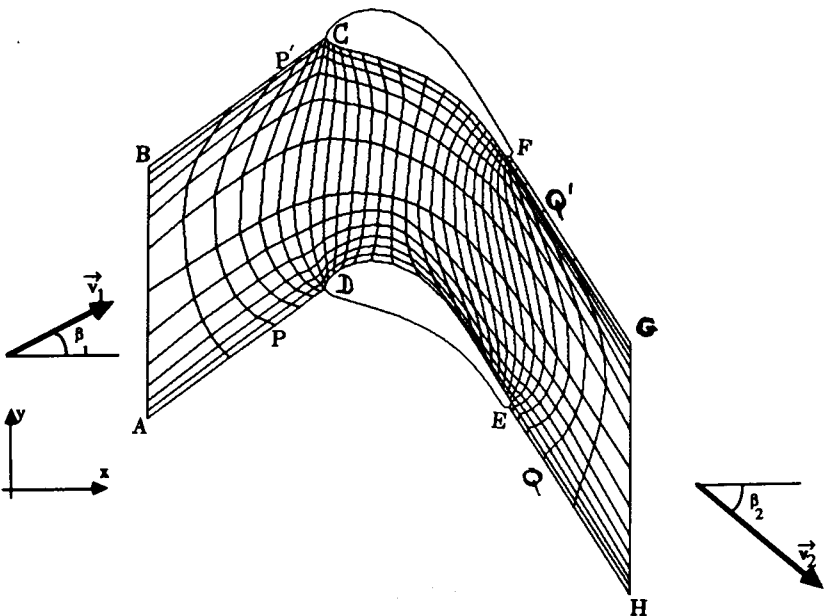


Figure 13.4.3 Computational domain for cascade configurations

13.4.3 Cascade and channel flows

(Figure 13.4.3) The upstream velocity field is assumed to be known and the potential field along AB can be determined. Hence, a Dirichlet condition $\phi = \phi_{AB}(y)$ can be applied along the inlet section AB. At the outlet, the flow is generally not completely known and the potential at point H is unknown.

Therefore the most appropriate boundary condition is a Neumann condition expressing conservation of mass flow through the cascade channel, assuming uniform flow conditions along the outlet section of the computational domain GH:

$$(\rho\phi_n)_{GH} = (\rho_1 v_{1n}) \frac{A_1}{A_2} \quad (13.4.6)$$

where ρ_1 is the inlet specific mass, \bar{v} the inlet velocity with normal component v_{1n} and A_1, A_2 the inlet and outlet areas.

For *transonic* cascade and channel flows, additional problems arise when shock waves are present under choked conditions due to the non-uniqueness of the potential solutions for given physical inlet and outlet conditions (see Section 2.9 in volume 1). In addition, for choking conditions occurring when the flow is accelerated through sonic conditions at a minimum area section of the channel, the mass flow is fixed by the critical, sonic conditions and is therefore unknown. Consequently, a Neumann boundary condition cannot be applied and the condition (13.4.6) has to be replaced by a more appropriate condition. A detailed analysis has been given by Deconinck and Hirsch (1983) and the following boundary treatment can be applied.

Choked flow with subsonic inlet and outlet flow conditions

This will occur, for instance, in a convergent-divergent channel when the pressure difference between inlet and exit is sufficiently large. The flow is accelerated through sonic velocity in the throat and further accelerated to supersonic velocities. The supersonic region is terminated by a strong shock which brings the flow back to subsonic conditions. As discussed in Section 2.9.2, the shock position cannot be defined by the physical variables, since the outlet isentropic variables such as velocity, pressure and density are uniquely determined by the subsonic isentropic flow conditions. In addition the mass flow is unknown and only Dirichlet conditions can be applied. The following approach will lead to a unique isentropic potential flow with shocks:

Dirichlet condition at inlet: $\phi = \phi_1$

Dirichlet condition at outlet: $\phi = \phi_2$ based on a uniformity assumption

The potential difference $(\phi_2 - \phi_1)$ fixes the shock position and the mass flow results from the computation. The same situation occurs for a divergent channel with sonic inlet and subsonic outlet.

Divergent channel with shock

If the inlet is supersonic with a subsonic outlet the flow is not necessarily choked but a shock is present. Therefore one has to impose:

- (1) A Neumann condition at inlet (or outlet) to fix the mass flow;
- (2) A potential difference by imposing the value of the potential at one point on the Neumann boundary.

13.4.4 Circulation and Kutta condition*Single airfoil*

As discussed in Section 2.9, lifting airfoils require a circulation whose intensity is defined by the Kutta condition. In practical computations a branch cut is to be defined along which the potential will have a discontinuity given by equation (2.9.11). (Figure 13.4.2):

$$\phi_{P'} - \phi_P = \Gamma_B = \phi_B - \phi_A \quad (13.4.7)$$

The value of the circulation is updated during the iterative process by imposing equal velocities or pressures at both sides of the trailing edge.

Cascades

For cascades, along the boundaries BC and AD all physical flow variables are identical. The circulation around the closed contour of Figure 13.4.3, ABGHA, is equal to

$$\Gamma_B = s(v_{2y} - v_{1y}) \quad (13.4.8)$$

where s is the spacing between consecutive blades. Therefore, the periodicity condition can be satisfied by imposing

$$\phi_B - \phi_A = \phi_{P'} - \phi_P = sv_{1y} \quad (13.4.9a)$$

$$\phi_G - \phi_H = \phi_{Q'} - \phi_Q = sv_{2y} \quad (13.4.9b)$$

The value of $v_{2y} = v_{2x} \cos \beta_2$ is obtained either by imposing β_2 as an outlet variable or by applying a Kutta condition at the trailing edge, under the form of requiring equal velocities at E and F.

13.5 INTEGRAL OR WEAK FORMULATION OF THE POTENTIAL MODEL

The weak formulation forms the common basis for finite element and finite volume discretizations. For any smooth function W , the weak form of the potential equation in conservation form (13.1.2) is obtained after multiplica-

tion by W and integration over the computational domain Ω . A partial integration is performed, leading to

$$\int_{\Omega} \rho_1 W \, d\Omega - \int_{\Omega} \rho \bar{\nabla} \phi \cdot \bar{\nabla} W \, d\Omega + \oint_{\Gamma} \rho \phi_n W \, d\Gamma = 0 \quad (13.5.1)$$

In general, W is chosen to be zero on the part S_0 of the boundary where the function ϕ is known and the boundary integral reduces to a contribution on the part of the boundary where a Neumann boundary condition is imposed.

If a discontinuity surface Σ propagating with speed \bar{C} exists in the flow domain Ω , the application of the approach followed in Section 2.7 leads to the jump condition valid locally along Σ and expressing mass conservation over the discontinuity),

$$[\rho \phi_n] - \bar{C} \cdot \bar{1}_n [\rho] = 0 \quad (13.5.2)$$

where $\bar{1}_n$ is the unit vector normal to the discontinuity surface Σ and the square brackets indicate the discontinuous variation over the surface, $[\rho] = \rho_2 - \rho_1$.

Comparing with the Rankine–Hugoniot relations derived in Section 2.7, it is seen that the potential discontinuities do not satisfy the jump relations for the momentum components. Instead they satisfy the isentropic condition $[s] = 0$, which is not valid for the Rankine–Hugoniot discontinuities. Since the latter represent the correct, inviscid conservation laws over discontinuities, the potential shocks will represent an isentropic approximation to the Euler shocks. These shocks are connected to an entropy increase proportional to $(M^2 - 1)^3$ and hence the potential shocks might be valid for Mach numbers close enough to 1, say $M < 1.25$; see Section 2.9.2 for a more detailed discussion and comparison.

The finite volume discretization for a given mesh point will be obtained with $W = 1$ in the control volume associated to the mesh point and zero outside.

For finite element formulations, with a Galerkin method, W is equal to the element interpolation functions.

13.5.1 Bateman variational principle

The weak formulation (13.5.1) can also be obtained from Bateman's variational principal (Bateman, 1929), stating that the pressure integral

$$I = \int_{\Omega} p \, d\Omega \, dt \quad (13.5.3)$$

is extremum, where $d\Omega \, dt$ is a space–time domain element and where the initial and boundary conditions are supposed to be satisfied for all variations $\delta\phi$.

If not, their contribution has to be added to the functional (13.5.3). For instance, the boundary condition $\rho \phi_n = g$ on Γ_1 will give a contribution $\int_{\Gamma_1} g \phi \, d\Gamma \, dt$.

The pressure p is considered as a unique function of the potential derivatives defined by the isentropic relations for a perfect gas:

$$\frac{p}{p_0} = \left(\frac{h}{h_0}\right)^{\gamma/(\gamma-1)} = \left(\frac{\rho}{\rho_0}\right)^\gamma = \left(1 - \frac{\bar{v}^2}{2H_0} - \frac{\phi_t}{H_0}\right)^{\gamma/(\gamma-1)} \quad (13.5.4)$$

The first variation δI is obtained by

$$\delta I = \int_{\Omega} \delta p \, d\Omega \, dt = \int_{\Omega} \left(\frac{\partial p}{\partial \phi_x} \delta \phi_x + \frac{\partial p}{\partial \phi_y} \delta \phi_y + \frac{\partial p}{\partial \phi_z} \delta \phi_z + \frac{\partial p}{\partial \phi_t} \delta \phi_t \right) d\Omega \, dt \quad (13.5.5)$$

From equation (13.5.4) one has, with a straightforward calculation (see Problem 13.7),

$$\delta p = -\rho [\bar{v} \cdot \delta \bar{v} + \delta \phi_t] = \left(\frac{\partial p}{\partial \rho} \right) \cdot \delta \rho = c^2 \cdot \delta \rho \quad (13.5.6)$$

and

$$\delta \rho = -\rho \frac{\bar{v} \cdot \delta \bar{v}}{c^2} - \rho \frac{\delta \phi_t}{c^2} \quad (13.5.7)$$

Hence, with the potential definition $\bar{v} = \bar{\nabla} \phi$, one obtains

$$\delta I = - \int_{\Omega} (\rho \bar{\nabla} \phi \cdot \delta \bar{\nabla} \phi + \rho \delta \phi_t) \, d\Omega \, dt = - \int_{\Omega} (\rho \bar{\nabla} \phi \cdot \bar{\nabla} \delta \phi + \rho \partial_t \delta \phi) \, d\Omega \, dt \quad (13.5.8)$$

which gives, after integration by part, with $\delta \phi = 0$ on the boundaries,

$$\delta I = \int_{\Omega} [\bar{\nabla} \cdot (\rho \bar{\nabla} \phi) + \partial_t \rho] \delta \phi \, d\Omega \, dt = 0 \quad (13.5.9)$$

Hence, the vanishing of the first variation is equivalent to the mass conservation equation (13.1.2), written for the potential function. Note also that equation (13.5.8) put to zero is equivalent to the weak formulation (13.5.1) with $W = \delta \phi$ and a partial integration of the time derivative term.

13.5.2 Analysis of some properties of the variational integral

It is interesting to estimate the second variation of the pressure functional, since its sign will indicate if the functional extremum is a maximum or a minimum. Since this is of particular importance for steady-state potential flows, we will develop this analysis for the stationary formulation (13.1.5), (13.1.6).

The variational Bateman integral can be written without the time variable, and the first variation δI becomes

$$\delta I = - \int_{\Omega} \rho \bar{v} \cdot \delta \bar{v} \, d\Omega \quad (13.5.10)$$

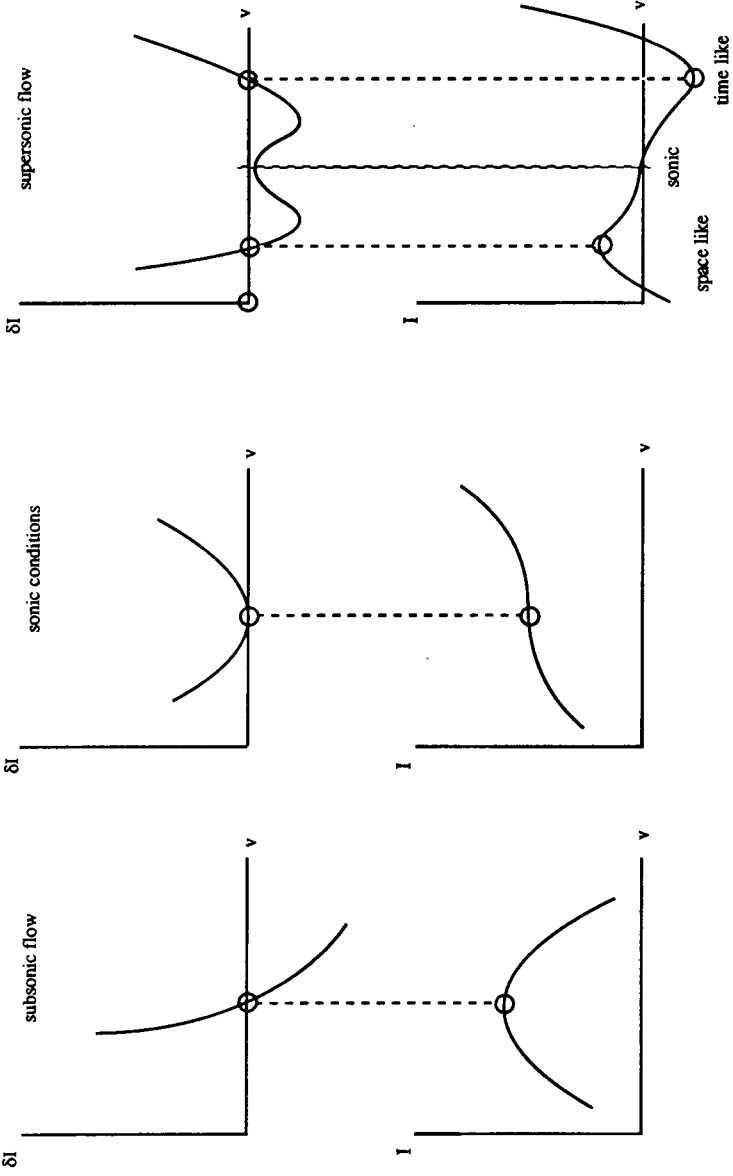


Figure 13.5.1 Representation of the dependence of the variational pressure integral with Mach number

The second variation is obtained by the following steps:

$$\begin{aligned}\delta^2 I &= -\delta \int_{\Omega} \rho \bar{v} \cdot \delta \bar{v} \, d\Omega \\ &= -\int_{\Omega} \delta \rho (\bar{v} \cdot \delta \bar{v}) \, d\Omega - \int_{\Omega} \rho (\delta \bar{v} \cdot \delta \bar{v}) \, d\Omega - \int_{\Omega} \rho (\bar{v} \cdot \delta^2 \bar{v}) \, d\Omega \quad (13.5.11)\end{aligned}$$

In the last term $\delta^2 \bar{v}$ is taken to be zero, since $\delta \bar{v}$ is the independent variable.

With $\delta \rho$ defined by equation (13.5.7), one obtains for the second variation

$$\delta^2 I = -\int_{\Omega} \rho \left[(\delta \bar{v})^2 - \frac{(\bar{v} \cdot \delta \bar{v})^2}{c^2} \right] d\Omega \quad (13.5.12)$$

The two terms under the integral can be written out explicitly, in Cartesian coordinates,

$$\begin{aligned}(\delta \bar{v})^2 - \frac{(\bar{v} \cdot \delta \bar{v})^2}{c^2} &= \left(1 - \frac{u^2}{c^2}\right) \delta u^2 + \left(1 - \frac{v^2}{c^2}\right) \delta v^2 + \left(1 - \frac{w^2}{c^2}\right) \delta w^2 - \frac{2uv}{c^2} \delta u \cdot \delta v \\ &\quad - \frac{2uw}{c^2} \delta u \cdot \delta w - \frac{2vw}{c^2} \delta v \cdot \delta w \quad (13.5.13)\end{aligned}$$

This expression parallels completely the right-hand side of the potential equation (13.2.5). This is of course not by accident, since the same type of information is contained in both equations. The sign of the second variation $\delta^2 I$ can best be analysed by comparing the expression under the integral in equation (13.5.12) with the characteristic relation (13.3.8).

Both expressions are identical, if $\delta \bar{v}$ is replaced by \bar{n} . Therefore, one has immediately the following results:

- (1) The quantity $[(\delta \bar{v})^2 - ((\bar{v} \cdot \delta \bar{v})^2/c^2)]$ is always positive for arbitrary variations $\delta \bar{v}$ if the flow is subsonic. In this case, $\delta^2 I < 0$ and the extremum of the variational pressure integral is a maximum.
- (2) Along sonic surfaces, $\delta^2 I = 0$ for certain variations and the curve representing the relation between I and the velocity variation goes through an inflection point.
- (3) If the flow is supersonic, one has to distinguish, following the relations (13.3.13) to (13.3.15), between space-like and time-like variations $\delta \bar{v}$. If $\delta \bar{v}$ is a space-like variation, that is if $\delta \bar{v}$ lies outside the cone of normals of Figure 13.3.2, the second variation $\delta^2 I$ remains negative. When $\delta \bar{v}$ is time-like, within the cone of normals, $\delta^2 I$ is positive and I has a minimum.

This is summarized in Figure 13.5.1 by a one-dimensional representation of the functional I in the function of v .

An essential guideline in the supersonic case will be to avoid velocity variations during the computations which cause a change of sign of the second variation

$\delta^2 I$. This would have in consequence a loss in unicity of the computed solutions associated with a loss of positive definiteness of the iteration matrix, which could become singular.

This will become clearer in the next chapter, where it will be seen that the Jacobian iteration matrix applied on $\delta\phi$ for a Newton iteration on the density is identical to the quadratic form defining the second variation $\delta^2 I$. This should not be surprising to the reader, since the first variation δI is precisely the potential flow equation applied to $\delta\phi$.

References

- Bateman, H. (1929). 'Notes on a differential equation which occurs in the two-dimensional motion of a compressible fluid and the associated variational problem.' *Proc. Roy. Soc., Series A*, **125**, 598–618.
- Deconinck, H., and Hirsch, Ch. (1983). 'Boundary conditions for the potential equation in transonic internal flow calculations.' *ASME Paper 83-GT-135*, 26th International ASME Gas Turbine Conference.
- Ludford, G. S. (1951). 'The behavior at infinity of the potential function of a two-dimensional compressible flow.' *Journal of Mathematical Physics*, **30**, 117–30.
- Shankar, V., and Osher, S. (1983). 'An efficient, full potential implicit method based on characteristics for supersonic flows.' *AIAA Journal*, **21**, 1262–70.
- Shankar, V., Szema, K. Y., and Osher, S. (1983). 'A conservative type dependent full potential method for the treatment of supersonic flows with embedded subsonic regions.' *Proc. AIAA 6th Computational Fluid Dynamics Conf., AIAA Paper 83-1887*, pp. 36–47.
- Slooff, J. (1982). 'General theory.' In *Applied Computational Transonic Aerodynamics*, Chap. 2, AGARDograph AGARD-AG-206.

PROBLEMS

Problem 13.1

Derive the quasi-linear potential equation (13.2.1) by applying the relation (13.5.7) to the conservative form (13.1.2).

Hint: Work out the spatial gradients and replace the derivative of the density by derivatives of the potential function based on equation (13.5.7).

Problem 13.2

Obtain the matrices (13.3.6).

Problem 13.3

Obtain, by working out the determinant (13.3.7), the relation (13.3.8) for the characteristic normals.

Hint: Introduce the scalar product

$$\frac{1}{c}(\vec{v} \cdot \vec{n}) = M_x n_x + M_y n_y + M_z n_z$$

Problem 13.4

Derive the relations for the characteristic lines for a two-dimensional potential flow. Show by an explicit calculation that they form an angle $\mu = \sin^{-1} 1/M$ with the velocity vector.

Hint: Solve for the directions (n_x, n_y) of the normals. The characteristic lines are orthogonal to \vec{n} .

- (1) Define $\lambda = n_y/n_x$ and obtain the characteristic normal directions as

$$\lambda_{\pm} = \frac{M_x M_y \pm (M^2 - 1)^{1/2}}{1 - M_y^2}$$

- (2) Obtain the characteristic directions as s_{\pm} :

$$s_{\pm} = \frac{M_x M_y \mp (M^2 - 1)^{1/2}}{1 - M_x^2}$$

and consider a local coordinate system with the x axis aligned with the velocity vector.

Problem 13.5

Obtain the condition (13.3.17) for the coordinate line $\xi^1 = \xi$ to be time-like, taking into account that the scaled contravariant component $U/\sqrt{g^{11}}$ is the projection of the velocity in the direction normal to the line $\xi = \text{constant}$.

Hint: Take $\vec{\kappa} = n_2 \vec{e}^2 + n_3 \vec{e}^3$ and develop $\vec{v} \cdot \vec{n} = \vec{v} \cdot \vec{\kappa} + v^1 n_1$, and $\vec{n}^2 = \vec{\kappa}^2 + (n_1)^2 g^{11} + 2\kappa^1 n_1$. Follow the reasoning which led to equation (13.3.15) and choose $\kappa^1 = 0$.

Apply also to the two-dimensional case of Figure 13.3.3.

Problem 13.6

Obtain equation (13.5.2).

Problem 13.7

Obtain the relation (13.5.6) for the pressure variations from the isentropic relation (13.5.4).

Hint: Apply the density relation (13.1.4) and the perfect gas law for the stagnation quantities.

Problem 13.8

Define the critical speed of sound c_* by the condition $|\vec{v}_*| = c_*$ and obtain the steady-density relation as a function of a non-dimensional velocity ratio:

$$M_*^2 = \frac{\vec{v}^2}{c_*^2}$$

Define the critical density and show that one can distinguish the supersonic from the subsonic points by comparing the expression

$$\left(1 - M_*^2 \frac{\gamma - 1}{\gamma + 1}\right) \quad \text{with} \quad \frac{2}{\gamma + 1} \quad \text{or} \quad \rho \quad \text{with} \quad \rho^*$$

Hint: Apply the constancy of energy to relate c_* and H_0 . Obtain

$$\frac{\rho}{\rho_0} = \left(1 - M_*^2 \frac{\gamma - 1}{\gamma + 1} \right)^{1/(\gamma - 1)}$$

The last observation is often used in programs where the density is evaluated in order to detect supersonic points.

Problem 13.9

Repeat the calculations of Example 13.1.1 for the three-dimensional potential equation, with the coordinate transformations $\xi = \xi(x, y, z)$, $\eta = \eta(x, y, z)$, $\zeta = \zeta(x, y, z)$.

Note that the gradients of ξ define the transformation between the Cartesian and contravariant components of velocity; for instance $U = \vec{v} \cdot \vec{\nabla} \xi$. The metric tensor $g^{\alpha\beta}$ defines the transformation between the gradients of the potential in the curvilinear system and the contravariant velocity components; for instance $U^\alpha = g^{\alpha\beta} \phi_\beta$, where $\phi_\beta = \partial\phi/\partial\xi^\beta$ with $\xi^1 = \xi$, $\xi^2 = \eta$, $\xi^3 = \zeta$.

Problem 13.10

Obtain the small perturbation potential equations (13.2.10) and (13.2.11). Derive first equation (13.2.9) using equation (13.2.4).

Hint: Write M_x^2 as follows:

$$M_x^2 = M_\infty^2 (1 + \Phi_x)^2 \frac{c_\infty^2}{c^2}$$

and work out using equation (13.2.9), neglecting quadratic terms in Φ_x^2 .

Problem 13.11

Write the small perturbation potential equation in conservation form and derive the corresponding shock relations. Compare with the Rankine–Hugoniot relations derived from the Euler equations.

Hint: Obtain

$$\left[(1 - M_\infty^2) \phi_x - \frac{\gamma + 1}{2} \Phi_x^2 \right]_x + \phi_{yy} = 0$$

and the jump relations

$$\left[(1 - M_\infty^2) \phi_x - \frac{\gamma + 1}{2} \phi_x^2 \right] \frac{dy}{dx} + [\phi_y] = 0$$

where the square brackets now represent the jump over the discontinuity: $[A] = A_2 - A_1$ and dy/dx is the slope of the discontinuity in the xy plane.

Chapter 14

The Discretization of the Subsonic Potential Equation

Since the stationary subsonic potential flows are governed by an elliptic equation they can be computed in a straightforward way, the numerical resolution of smooth elliptic problems being nowadays an easy task.

The main steps to be defined are the following:

- (1) The selection of a discretization scheme. One has the choice between finite difference, finite volume and finite element representations. All of them have been applied and are in use at different places with equal success. The choice is therefore more a matter of personal taste than of efficiency.
- (2) The iteration method to deal with the non-linearity introduced by the density.
- (3) The algorithm for the resolution of the obtained algebraic system.

In addition the interaction between the last two steps and the implementation of the boundary conditions will completely define the numerical scheme.

With subsonic flows, which have a smooth behaviour, we will be able to operate with rather coarse meshes, with the exception of certain localized regions such as corners, leading or trailing edges of airfoils, and other regions where strong flow gradients can be expected. Hence, the total number of mesh points will be restricted and nearly any of the methods described in Chapter 12 in volume 1 for the resolution of algebraic systems, will be sufficiently effective.

Therefore, readers only interested in subsonic potential flows will be able to limit themselves to this chapter. It could be mentioned at this point that the algorithms for subsonic potential flows are equally applicable to all problems governed by a similar equation, such as heat conduction in solid bodies, electrical potential distributions, groundwater flows, etc.

The particular problems attached to transonic flows will be dealt with in the following chapter. They concern essentially steps 2 and 3 since the density variations contain all the non-linearities, in particular the transition from subsonic to supersonic regions and the eventual presence of shock discontinuity surfaces.

We will deal essentially with the conservative form (13.1.5) of the potential equation. As discussed in Chapter 6, a non-conservative formulation of a

conservation law, in the present case mass conservation, generates internal sources, although for smooth flows these contributions will be of the same order as the truncation errors. However, in regions with strong gradients or with discontinuities, unacceptable errors are introduced in this way and the conservative form has to be used.

Also, for the sake of simplicity, we will present the various discretizations for two-dimensional flow problems. In most cases the generalization to a higher dimension will be straightforward and we refer readers to the appropriate literature for more details concerning three-dimensional applications.

14.1 FINITE DIFFERENCE FORMULATION

In Cartesian coordinates, the most straightforward discretization, of second-order accuracy, is the central symmetrical form following equation (4.4.7) in volume 1.

○ potential evaluation

X density evaluation

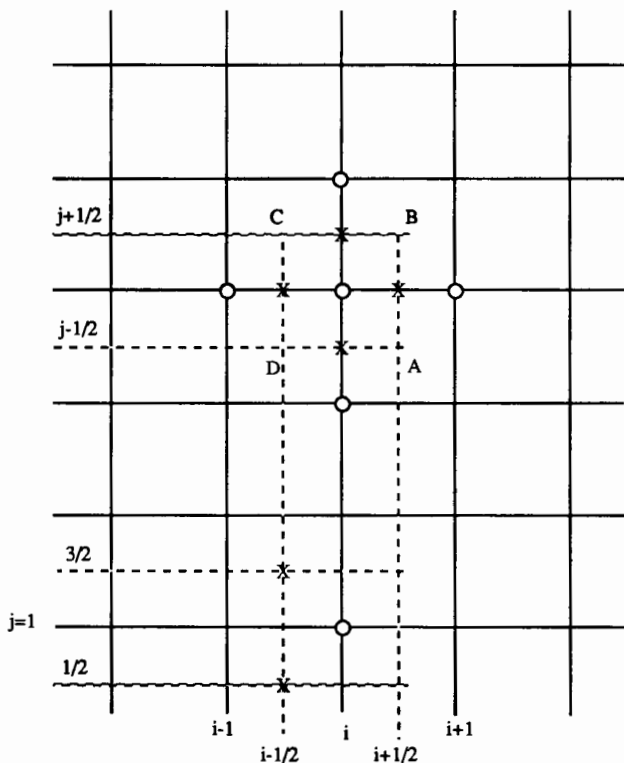


Figure 14.1.1 Cartesian two-dimensional finite difference computational mesh

Referring to Figure 14.1.1, the following two-dimensional scheme can be defined:

$$\left(\frac{1}{\Delta x^2} \delta_x^+ \rho_{i-1/2,j} \delta_x^- + \frac{1}{\Delta y^2} \delta_y^+ \rho_{i,j-1/2} \delta_y^- \right) \phi_{ij} = 0 \quad (14.1.1)$$

where δ^+ and δ^- are defined in Chapter 4 as the forward and backward difference operators, acting on all the terms to their right. The subscripts indicate the variable on which the difference operators act. For memory, we recall the definitions

$$\begin{aligned} \delta^+ \phi_i &= \phi_{i+1} - \phi_i & \delta^- \phi_i &= \phi_i - \phi_{i-1} & \delta \phi_i &= \phi_{i+1/2} - \phi_{i-1/2} \\ \mu \phi_i &= \frac{\phi_{i+1/2} + \phi_{i-1/2}}{2} & \bar{\delta} \phi_i &= \frac{\phi_{i+1} - \phi_{i-1}}{2} = \mu \delta \phi_i \end{aligned} \quad (14.1.2)$$

Worked out explicitly, equation (14.1.1) becomes, for $\Delta x = \Delta y$,

$$\begin{aligned} \rho_{i+1/2,j}(\phi_{i+1,j} - \phi_{ij}) - \rho_{i-1/2,j}(\phi_{ij} - \phi_{i-1,j}) + \rho_{i,j+1/2}(\phi_{i,j+1} - \phi_{ij}) \\ - \rho_{i,j-1/2}(\phi_{ij} - \phi_{i,j-1}) = 0 \end{aligned} \quad (14.1.3)$$

As seen from Figure 14.1.1, the discretized equation will involve the five points marked on this figure. Note that the densities have to be evaluated at the mid-point locations, while the potential values are evaluated at the corners of the mesh. This standard five-point molecule is shown in Figure 14.1.2 and reduces to the five-point Laplace operator for incompressible flows.

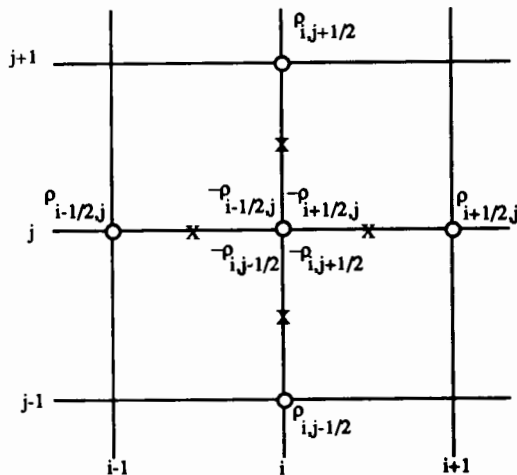


Figure 14.1.2 Computational molecule for the finite difference scheme (14.1.3)

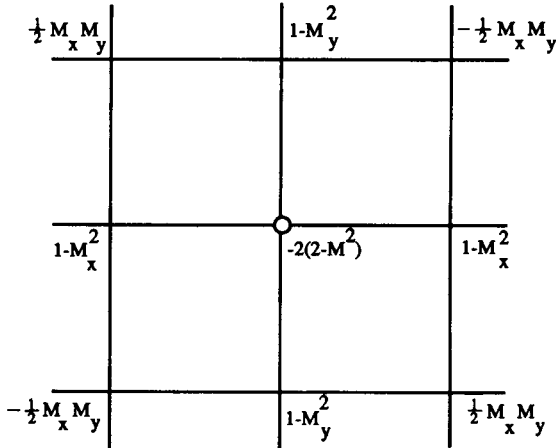


Figure E14.1.1 Computational molecule for the non-conservative potential equation and second-order central differences

Example 14.1.1 Non-conservative potential equation in two dimensions

In a Cartesian mesh, the following equation has to be discretized:

$$(1 - M_x^2)\phi_{xx} + (1 - M_y^2)\phi_{yy} - 2M_x M_y \phi_{xy} = 0 \quad (\text{E14.1.1})$$

With central differences, one obtains in point (i, j) for $\Delta x = \Delta y$, with second-order accuracy,

$$(1 - M_x^2)_{ij}(\phi_{i+1,j} - 2\phi_{i,j} + \phi_{i-1,j}) + (1 - M_y^2)_{i,j}(\phi_{i,j+1} - 2\phi_{i,j} + \phi_{i,j-1}) - \frac{1}{2}(M_x M_y)_{ij}(\phi_{i+1,j+1} - \phi_{i+1,j-1} - \phi_{i-1,j+1} + \phi_{i-1,j-1}) = 0 \quad (\text{E14.1.2})$$

The computational molecule can be visualized as in Figure E14.1.1.

Observe that the matrix of the system (E14.1.2) is diagonal dominant for subsonic flows. In supersonic flows, for instance for a flow in the x direction, the matrix does not remain diagonal dominant. This is easily seen and left as an exercise for the reader.

14.1.1 Numerical estimation of the density

The numerical estimation of ρ^n at the mid-point locations is obtained from the velocity field, since ρ is a unique function of the velocity squared.

In order to obtain the mid-point velocities, for instance at point $(i + 1/2, j)$, one can apply the following operations:

$$u_{i+1/2,j} = \frac{1}{\Delta x} \delta_x^+ \phi_{ij} = \frac{1}{\Delta x} (\phi_{i+1,j} - \phi_{ij}) \quad (14.1.4)$$

$$\begin{aligned}
 v_{i+1/2,j} &= \frac{1}{\Delta y} \mu_x \delta_y^+ \phi_{i+1/2,j} = \frac{1}{\Delta y} \mu_x (\phi_{i+1/2,j+1} - \phi_{i+1/2,j}) \\
 &= \frac{1}{2\Delta y} (\phi_{i+1,j+1} + \phi_{i,j+1} - \phi_{i+1,j} - \phi_{ij}) \quad (14.1.5)
 \end{aligned}$$

Another alternative for the estimation of $v_{i+1/2,j}$ is to consider the central derivative with respect to j since equation (14.1.5) is only a first-order estimate of $v_{i+1/2,j}$ (it is actually a second-order estimation of $v_{i+1/2,j+1/2}$). To second order, one has

$$v_{i+1/2,j} = \frac{1}{\Delta y} \mu_x \delta_y \phi_{i+1/2,j} = \frac{1}{4\Delta y} (\phi_{i+1,j+1} + \phi_{i,j+1} - \phi_{i+1,j-1} - \phi_{i,j-1}) \quad (14.1.6)$$

Various alternatives can be applied to evaluate the densities needed in equation (14.1.3):

- (1) Evaluate the densities at the mid-points of Figure 14.1.1 by

$$\rho_{i+1/2,j} = \rho(\bar{v}_{i+1/2,j}^2) \quad (14.1.7)$$

Each mesh point requires the evaluation of two densities, $\rho_{i+1/2,j}$ and $\rho_{i,j+1/2}$, and, if needed, the density at a mesh point can be obtained by averaging the four surrounding mid-cell values. For instance,

$$\rho_{ij} = \frac{1}{4} (\rho_{i+1/2,j} + \rho_{i-1/2,j} + \rho_{i,j+1/2} + \rho_{i,j-1/2}) \quad (14.1.8)$$

- (2) Estimate the density at the centres ABCD of the finite difference mesh of Figure 14.1.1. For instance,

$$\rho_{i+1/2,j+1/2} = \rho(\bar{v}_{i+1/2,j+1/2}^2) \quad (14.1.9)$$

where the corresponding velocity component could be evaluated by

$$u_{i+1/2,j+1/2} = \frac{1}{2} (u_{i+1/2,j+1} + u_{i+1/2,j}) \quad (14.1.10)$$

$$v_{i+1/2,j+1/2} = \frac{1}{2} (v_{i+1,j+1/2} + v_{i,j+1/2})$$

and

$$\bar{v}_{i+1/2,j+1/2}^2 = (u^2 + v^2)_{i+1/2,j+1/2} \quad (14.1.11)$$

The velocity components at mid-point are evaluated with the help of equations (14.1.4) and (14.1.6) to second-order accuracy (see also Problem 14.1).

Another variant could be to use equations (14.1.10) and (14.1.11) directly for the squares of the velocity components.

The densities at the mid-points in Figure 14.1.1, needed for equation (14.1.3), can then be obtained by averaging the corresponding centre-point values. For instance,

$$\rho_{i+1/2,j} = \frac{1}{2} (\rho_{i+1/2,j+1/2} + \rho_{i+1/2,j-1/2}) \quad (14.1.12)$$

This variant is more economical since the number of density evaluations

per mesh point is one instead of two (or three in a three-dimensional problem). This is a welcome gain, since the fractional power in the expression of the density is a costly numerical operation.

- (3) Evaluate the density at the mesh points, via

$$\begin{aligned}\rho_{i+1/2,j} &= \frac{1}{2}(\rho_{ij} + \rho_{i+1,j}) \\ \rho_{i,j+1/2} &= \frac{1}{2}(\rho_{ij} + \rho_{i,j+1})\end{aligned}\quad (14.1.13)$$

with

$$\rho_{ij} = \rho(\bar{v}_{ij}^2) \quad (14.1.14)$$

and

$$\begin{aligned}u_{ij} &= \frac{1}{2}(u_{i+1/2,j} + u_{i-1/2,j}) \\ v_{ij} &= \frac{1}{2}(v_{i,j+1/2} + v_{i,j-1/2})\end{aligned}\quad (14.1.15)$$

Clearly many other variants can be defined and the precise method adopted has been found to have little influence on the results (Jameson, 1976) if the order of accuracy is maintained.

14.1.2 Curvilinear mesh

In practice, one seldom has Cartesian meshes, but instead one attempts to adapt the mesh to the geometry of the flow configuration via various mesh generation techniques.

Figure 13.4.3 is an example of a numerically generated mesh for a cascade and Figure 14.1.3 provides some typical topologies for isolated airfoil geometries.

In order to apply a finite difference discretization on a general mesh, the lines are considered as forming a set of curvilinear coordinates $\zeta^\alpha(\xi, \eta)$. The coordinate transformation laws $\xi = \xi(x, y)$, $\eta = \eta(x, y)$ generate a mapping of the physical space (x, y) to a computational domain (ξ, η) where a Cartesian mesh is set up (Figure 14.1.4).

By writing the potential equation in the curvilinear coordinate system (ξ, η) , equation (E13.1.2), it can be discretized directly in the Cartesian computational space (ξ, η) .

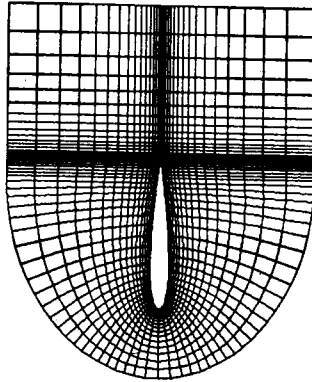
The following two-dimensional scheme is a direct generalization of the Cartesian finite difference scheme (14.1.1), with $\Delta\xi = \Delta\eta = 1$:

$$\delta_\xi^- \left(\rho \frac{U}{J} \right)_{i+1/2,j} + \delta_\eta^- \left(\rho \frac{V}{J} \right)_{i,j+1/2} = 0 \quad (14.1.16)$$

The contravariant velocities are defined by the relations of Example 13.1.1 and can be discretized as follows.

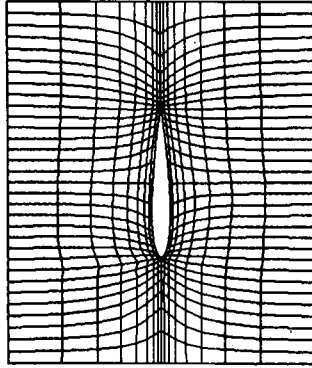
$$\begin{aligned}U_{i+1/2,j} &= g_{i+1/2,j}^{11} \delta_\xi^+ \phi_{ij} + g_{i+1/2,j}^{12} \mu_\xi \delta_\eta^- \phi_{i+1/2,j} \\ &= g_{i+1/2,j}^{11} (\phi_{i+1,j} - \phi_{i,j}) \\ &\quad + \frac{1}{4} g_{i+1/2,j}^{12} (\phi_{i+1,j+1} + \phi_{i,j+1} - \phi_{i+1,j-1} - \phi_{i,j-1})\end{aligned}\quad (14.1.17)$$

MESH SIZE : 97* 17



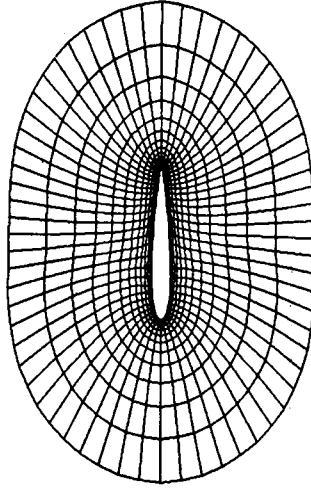
(a) C - mesh

MESH SIZE : 33* 9



(b) H - mesh

MESH SIZE : 65* 13



(c) O - mesh

Figure 14.1.3 Some typical mesh configurations

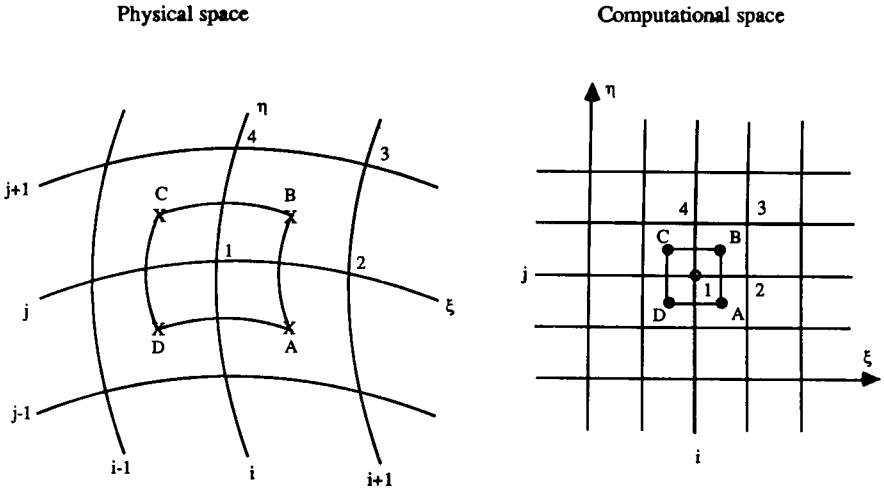


Figure 14.1.4 Mapping from the physical space (x, y) to a computational domain (ξ, η)

and

$$V_{i,j+1/2} = g_{i,j+1/2}^{21} \mu_\eta \delta_\xi^- \phi_{i,j+1/2} + g_{i,j+1/2}^{22} \delta_\eta^+ \phi_{ij} \quad (14.1.18)$$

Similar formulas are easily derived for the other components (see Problem 14.2).

Example 14.1.2 Discretization of metric coefficients

An interesting way of discretizing the metric coefficients is based on a representation of the mapping $x(\xi, \eta)$, $y(\xi, \eta)$ on a cell-by-cell basis and considering locally a bilinear isoparametric transformation compatible with second-order accuracy. This particular transformation is used to compute the coordinate derivatives appearing in the metric coefficients.

In Scheme (14.1.16) the metric is required at the mid-points $(i \pm 1/2, j)$ and $(i, j \pm 1/2)$. If A, B, C, D are the centres of the four cells surrounding mesh point (i, j) (Figure 14.1.4), the metric coefficient at $(i + 1/2, j)$ can be defined by averaging the values computed first at points A and B.

Considering point B within the quadrilateral 1234, the isoparametric transformation with bilinear shape functions $N_I(\xi, \eta)$ is written as

$$\bar{x} = \sum_{I=1}^4 \bar{x}_I N_I(\xi, \eta) \quad (E14.1.3)$$

with

$$N_I(\bar{\xi}) = \frac{1}{4}(1 + \xi \xi_I)(1 + \eta \eta_I) \quad (E14.1.4)$$

where $I = 1, 2, 3, 4$ and ξ, η range from -1 to $+1$ following the standard finite element representation of Table 5.1 in Chapter 5, Volume 1, with $\xi_I = \pm 1$,

$\eta_I = \pm 1$. This representation corresponds to a local ξ, η coordinate system centred in point B with an overall variation $\Delta\xi = \Delta\eta = 2$.

Derivatives such as x_ξ, x_η are computed from

$$x_\xi = \sum_I x_I \frac{\partial N_I}{\partial \xi} = \frac{1}{4} \sum_I x_I (1 + \eta \eta_I) \xi_I \quad (\text{E14.1.5})$$

$$x_\eta = \sum_I x_I \frac{\partial N_I}{\partial \eta} = \frac{1}{4} \sum_I x_I (1 + \xi \xi_I) \eta_I \quad (\text{E14.1.6})$$

where the sum ranges from 1 to 4 over the four nodes of the considered element. At the centre B ($\xi = 0, \eta = 0$) of element 1234 the following discretization formulas are obtained:

$$x_\xi|_B = \frac{x_2 + x_3 - x_4 - x_1}{2} \quad (\text{E14.1.7a})$$

$$x_\eta|_B = \frac{x_3 + x_4 - x_2 - x_1}{2} \quad (\text{E14.1.7b})$$

which can be written as a finite difference formula for point B

$$x_\xi|_B = \mu_\eta \sigma_\xi x_{i+1/2, j+1/2} \quad (\text{E14.1.8a})$$

$$x_\eta|_B = \mu_\xi \delta_\eta x_{i+1/2, j+1/2} \quad (\text{E14.1.8b})$$

Similar relations are derived for the other derivatives. With the relations of Example 13.1.1, one has

$$g^{11} = J(x_\eta^2 + y_\eta^2) = \frac{x_\eta^2 + y_\eta^2}{x_\xi y_\eta - x_\eta y_\xi} \quad (\text{E14.1.9a})$$

$$g^{12} = -J(x_\xi x_\eta + y_\xi y_\eta) = \frac{x_\xi x_\eta + y_\xi y_\eta}{x_\eta y_\xi - x_\xi y_\eta} \quad (\text{E14.1.9b})$$

and

$$g_{i+1/2, j}^{11} = \frac{g_A^{11} + g_B^{11}}{2} \quad (\text{E14.1.10a})$$

$$g_{i+1/2, j}^{12} = \frac{g_A^{12} + g_B^{12}}{2} \quad (\text{E14.1.10b})$$

14.1.3 Consistency of the discretization of metric coefficients

Generally, the metric coefficients will be evaluated in the computational plane (ξ, η) through the relations of Example 13.1.1, and particular care has to be exercised in the discretization of these relations in order to avoid the introduction of systematic errors, which would appear as numerical mass sources. In particular, the consistency of free-stream or uniform flow conditions must be

ensured numerically, that is equation (14.1.16) with (14.1.17) and (14.1.18) must be satisfied identically by the numerical discretization for a uniform flow field \bar{v}_∞ .

Written out explicitly, this implies, in two dimensions with U_∞, V_∞ being the contravariant components of \bar{v}_∞ ,

$$\frac{\partial}{\partial \xi} \left(\frac{\rho_\infty U_\infty}{J} \right) + \frac{\partial}{\partial \eta} \left(\frac{\rho_\infty V_\infty}{J} \right) = 0 \quad (14.1.19a)$$

or

$$\frac{\partial}{\partial \xi} \left(\frac{\xi_x u_\infty + \xi_y v_\infty}{J} \rho_\infty \right) + \frac{\partial}{\partial \eta} \left(\frac{\eta_x u_\infty + \eta_y v_\infty}{J} \rho_\infty \right) = 0 \quad (14.1.19b)$$

where u_∞ and v_∞ are the Cartesian components of \bar{v}_∞ .

If Δ_ξ and Δ_η represent the selected finite difference discretization operator of the mass flux derivatives, this equation is discretized in the scheme as

$$\Delta_\xi \left(\frac{\xi_x u_\infty + \xi_y v_\infty}{J} \rho_\infty \right) + \Delta_\eta \left(\frac{\eta_x u_\infty + \eta_y v_\infty}{J} \rho_\infty \right) = 0 \quad (14.1.20)$$

Since u_∞ and v_∞ are to be considered as independent constants, the following equations, which are algebraic identities, have to be satisfied by the discretization. With ξ_x and η_x computed via relations (E13.1.8), one has

$$\Delta_\xi(y_\eta) - \Delta_\eta(y_\xi) = 0 \quad \text{or analytically} \quad y_{\xi\eta} = y_{\eta\xi} \quad (14.1.21)$$

and

$$\Delta_\xi(-x_\eta) + \Delta_\eta(x_\xi) = 0 \quad \text{or analytically} \quad x_{\xi\eta} = x_{\eta\xi} \quad (14.1.22)$$

The metric coefficients are not necessarily estimated via the same difference operators as applied to the flux components. If one denotes by Δ_ξ^m and Δ_η^m the difference operators applied for the metric coefficients, the above conditions imply that the two sets of difference operators have to commute. More precisely, one should select $\Delta_\xi, \Delta_\eta, \Delta_\xi^m, \Delta_\eta^m$ such that

$$\Delta_\xi \Delta_\eta^m y_{ij} - \Delta_\eta \Delta_\xi^m y_{ij} = 0 \quad (14.1.23)$$

and similarly on x .

If both operators are obtained from second-order central differences, this condition is satisfied since

$$\Delta_\eta^m y_{ij} = \frac{1}{2}(y_{i,j+1} - y_{i,j-1})$$

and

$$\begin{aligned} \Delta_\xi \Delta_\eta^m y_{ij} &= \bar{\delta}_\xi \bar{\delta}_\eta y_{ij} \\ &= \frac{1}{4}(y_{i+1,j+1} - y_{i-1,j+1} - y_{i+1,j-1} + y_{i-1,j-1}) \\ &= \Delta_\eta \Delta_\xi^m y_{ij} \end{aligned} \quad (14.1.24)$$

However, this is not true in general. For instance, if one-sided, backward formulas are applied for the fluxes and central differences for the metric, one

obtains

$$\begin{aligned} (\Delta_{\xi}\Delta_{\eta}^m - \Delta_{\eta}\Delta_{\xi}^m)y_{ij} &= (\delta_{\xi}^{-}\bar{\delta}_{\eta} - \delta_{\eta}^{-}\bar{\delta}_{\xi})y_{ij} \\ &= \frac{1}{2}(y_{i,j+1} - y_{i,j-1} - y_{i-1,j+1} + y_{i-1,j-1}) \\ &\quad - \frac{1}{2}(y_{i+1,j} - y_{i+1,j-1} - y_{i-1,j} + y_{i-1,j-1}) \end{aligned} \quad (14.1.25)$$

which is clearly different from zero (see Problems 14.3 and 14.4).

The situation is still more complex in three dimensions, where one would have, instead of (14.1.21) and (14.1.22), with coordinates ξ, η, ζ (refer to Problem 13.9),

$$\Delta_{\xi}(y_{\eta}z_{\zeta} - y_{\zeta}z_{\eta}) - \Delta_{\eta}(y_{\xi}z_{\zeta} - y_{\zeta}z_{\xi}) + \Delta_{\zeta}(y_{\xi}z_{\eta} - y_{\eta}z_{\xi}) = 0 \quad (14.1.26)$$

with two other similar relations.

Contrary to the two-dimensional case (14.1.24), this relation is not satisfied for central differences (see also Problem 14.5).

In general, the error introduced by the non-consistency of the metric discretization is small for smoothly varying meshes, remaining of the order of the truncation error of the difference operators used. However, when the mesh cells are highly distorted or in regions with large mesh spacings, this error can have a significant effect on the accuracy of the computation.

A detailed investigation and analysis of the consistency of metric discretizations with regard to potential flows, including additional requirements with regard to the consistent estimation of free-stream density and velocities, is to be found in Flores *et al.* (1983).

A simple and effective way to cancel any remaining consistency errors due to metric discretizations consists in subtracting the free-stream equation (14.1.19) from the basic equation, when both are of course discretized in the same way (Pulliam and Steger, 1980). Hence one discretizes instead the equation

$$\frac{\partial}{\partial \xi} \left(\rho \frac{U}{J} \right) + \frac{\partial}{\partial \eta} \left(\rho \frac{V}{J} \right) = \frac{\partial}{\partial \xi} \left(\frac{\rho_{\infty} U_{\infty}}{J} \right) + \frac{\partial}{\partial \eta} \left(\frac{\rho_{\infty} V_{\infty}}{J} \right) \quad (14.1.27)$$

This procedure is recommended for all finite difference codes operating on non-Cartesian grids.

14.1.4 Boundary conditions—curved solid wall

The implementation of the boundary conditions is straightforward for the Dirichlet conditions as well as for the Kutta condition. The Neuman boundary condition $\rho(\partial\phi/\partial n) = 0$ is most generally implemented by a one-sided difference along the corresponding boundary. Various forms can be given to this implementation and one of the most accurate methods, with second-order schemes such as equation (14.1.3), is obtained by the *reflecting boundary condition*. Along the boundary corresponding to the plane coordinate surface $j = 1$ (Figure 14.1.1), this condition is expressed by

$$(\rho v)_{i,1/2} = -(\rho v)_{i,3/2} \quad (14.1.28)$$

This leads to a contribution to equation (14.1.3) along $j = 1$ of

$$\frac{2}{\Delta y^2} \rho_{i,3/2} (\phi_{i,2} - \phi_{i,1}) \quad (14.1.29)$$

instead of the complete expression for the second y derivative applied in equation (14.1.3).

If the solid wall is curved, the condition of vanishing normal velocity is expressed by the corresponding contravariant velocity component being zero.

Referring to Figure 14.1.4, for a boundary defined as a $\eta = \text{constant}$ line, the contravariant velocity V is normal to the solid wall and hence is set to zero:

$$V = 0 \quad \text{along the solid wall boundary} \quad (14.1.30)$$

A more precise formulation is to express the corresponding mass flux as zero, that is

$$\frac{\rho V}{J} = 0 \quad (14.1.31)$$

which can be discretized by a reflecting boundary condition leading to

$$\left(\frac{\rho V}{J} \right)_{i,1/2} = - \left(\frac{\rho V}{J} \right)_{i,3/2} \quad (14.1.32)$$

The velocity has to be estimated in order to obtain the density and one might use the wall velocity for the density at point $(i, 1/2)$. A more accurate boundary condition formulation can be obtained from the condition of vanishing vorticity,

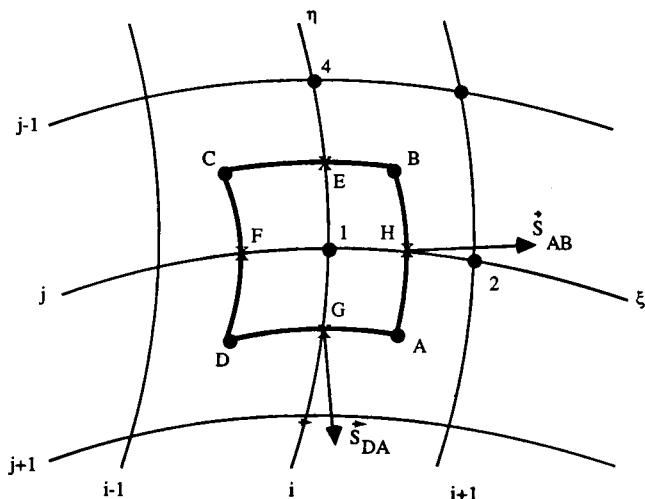


Figure 14.2.1 Finite volume discretization in physical space

which relates the normal velocity gradient to the wall curvature R_w .

$$\frac{\partial v_1}{\partial n} = -\frac{v_1}{R_w} \quad (14.1.33)$$

where v_1 is the local velocity component tangent to the wall boundary and $\partial/\partial n$ denotes the derivative in the direction normal to the wall.

For a boundary formed by a j -line on Figure 14.1.4, for instance the line ($j = 1$), the direction of positive values of n is towards the inside of the flow domain, and the radius of curvature is defined as positive.

This relation can be used to estimate a velocity magnitude at $(i, 1/2)$ by an appropriate extrapolation of $(v_1)_{i,1}$ to $(v_1)_{i,1/2}$.

14.2 FINITE VOLUME FORMULATION

Finite volume methods have the advantage of allowing a direct discretization in the physical space, for arbitrary mesh configurations, without the necessity of an explicit computation of metric coefficients.

Since one discretizes directly the integral conservation laws over a control volume cell, errors connected to the free-stream consistency requirements discussed in the previous section should also be strongly reduced if not eliminated.

Referring to Figure 14.2.1, we consider the element ABCD as attached to the mesh point (i, j) . The mass conservation law is integrated as follows:

$$\oint_{\text{ABCD}} \vec{F} \cdot d\vec{S} = 0 \quad \text{with } \vec{F} = \rho \vec{v} = \rho \vec{\nabla} \phi \quad (14.2.1)$$

or

$$(\vec{F} \cdot \vec{S})_{\text{AB}} + (\vec{F} \cdot \vec{S})_{\text{BC}} + (\vec{F} \cdot \vec{S})_{\text{CD}} + (\vec{F} \cdot \vec{S})_{\text{DA}} = 0 \quad (14.2.2)$$

where the surface vectors all point outwards.

The four fluxes can be evaluated directly in physical space, referring to Chapter 6 in Volume 1,

$$(\vec{F} \cdot \vec{S})_{\text{AB}} = (\rho \vec{v} \cdot \vec{S})_{\text{AB}} = [\rho(u\Delta y - v\Delta x)]_{\text{AB}} \quad (14.2.3)$$

If the control volume ABCD is referred to a local ξ, η coordinate system, then the equivalence of the discretizations (14.2.3) with (14.1.16) can easily be seen from the direct application of the relations of Example 13.1.1.

Considering transformation laws $\xi = \xi(x, y)$, $\eta = \eta(x, y)$ with the side AB of unit length in the η direction, that is $\Delta\eta_{\text{AB}} = 1$, one has

$$\begin{aligned} U_{\text{AB}} &= (\xi_x u + \xi_y v)_{\text{AB}} = [J(y_\eta u - x_\eta v)]_{\text{AB}} \\ &= [J(u\Delta y - v\Delta x)] \end{aligned} \quad (14.2.4)$$

Hence, comparing with (14.2.3),

$$(\vec{F} \cdot \vec{S})_{\text{AB}} = (\rho \vec{v} \cdot \vec{S})_{\text{AB}} = \left(\rho \frac{U}{J} \right)_{\text{AB}} \quad (14.2.5)$$

Actually $1/J$ is a measure of the area of the element ABCD, when AB is considered of unit length along the η axis.

This shows that the integral conservation law (14.2.2) can be written as

$$f_{AB} - f_{CD} + g_{CB} - g_{DA} = 0 \quad (14.2.6)$$

where f and g are the ξ, η components of the flux vector \vec{F} , that is

$$f = \rho \frac{U}{J} \quad g = \rho \frac{V}{J} \quad (14.2.7)$$

It appears, therefore, that the finite volume method can be considered as a finite difference method applied directly in the computational space if the flux components are evaluated in a similar way. It is easily seen that the finite difference discretization (14.1.16) is identical to the finite volume approach if $f_{AB} = (\vec{F} \cdot \vec{S})_{AB}$ is defined as the mid-point value $f_{i+1/2,j}$ (see Problem 14.6).

A large number of possible finite volume methods can be generated, according to the choice of the control volume ABCD and, for a given control cell ABCD, according to the way the flux components are evaluated on the cell faces; see Chapter 6 for a presentation of various options.

It is recommended to the reader to investigate a large number of formulations in order to become familiar with the definition of finite volume discretizations (see Problems 14.7 to 14.14).

14.2.1 Jameson and Caughey's finite volume method

In the approach developed by Jameson and Caughey (1977) for two- and three-dimensional flows, and applied to various configurations by Caughey and

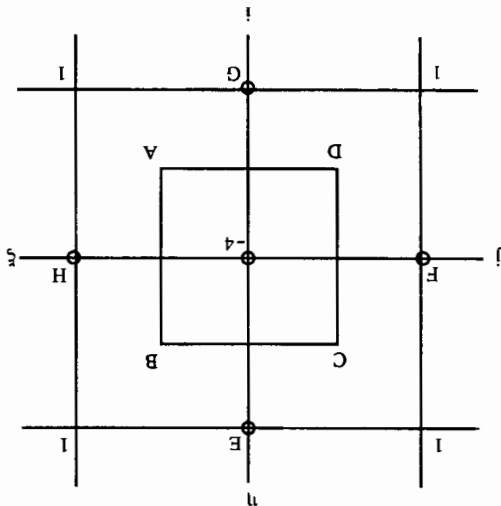
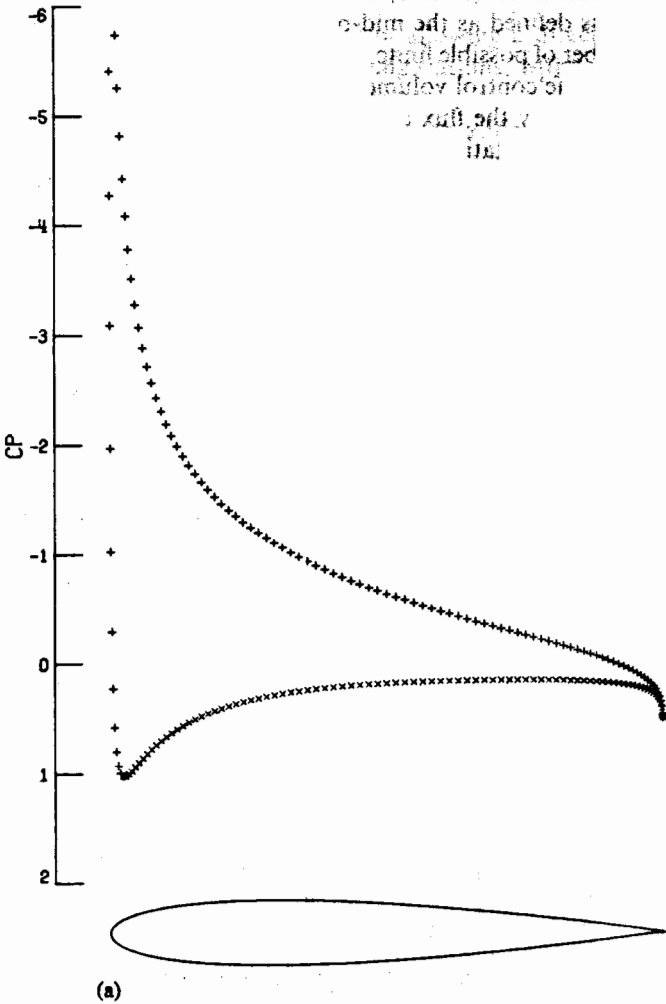


Figure 14.2.2 Computational molecule for the scheme (14.2.11)

Jameson (1979, 1980), the flux at the faces is obtained from the average of the corner values. For face AB,

$$f_{AB} = \frac{f_A + f_B}{2} \tag{14.2.8}$$

and similarly for the other faces.



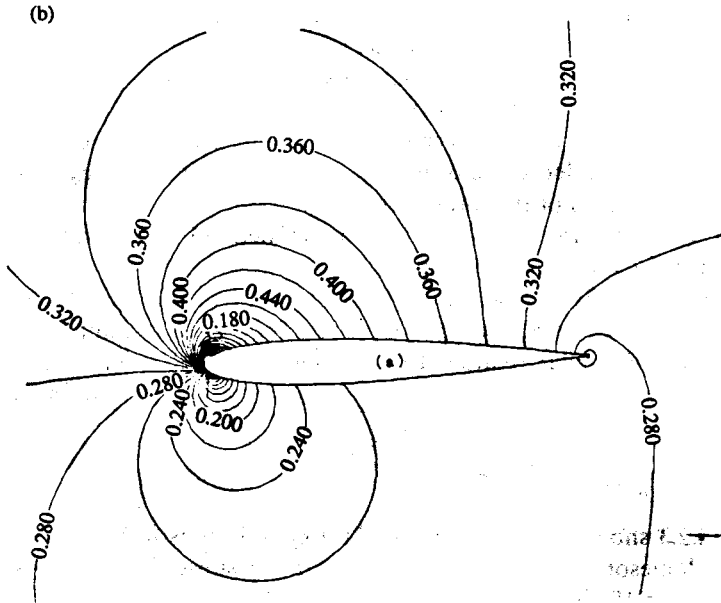


Figure 14.2.3 (a) Pressure distribution and (b) iso-Mach lines for the potential flow on an NACA 0012 airfoil at 10° incidence and upstream Mach number of 0.3. (From Salas *et al.*, 1983)

When applied to the form (14.2.6), the sum of the f components ($f_{AB} - f_{CD}$) becomes

$$\begin{aligned} f_{AB} - f_{CD} &= \frac{f_A + f_B}{2} - \frac{f_C + f_D}{2} \\ &= \frac{1}{2}(f_{i+1/2,j+1/2} + f_{i+1/2,j-1/2} - f_{i-1/2,j+1/2} - f_{i-1/2,j-1/2}) \\ &= \mu_\eta \delta_\xi f_{ij} \end{aligned} \quad (14.2.9)$$

This leads to the scheme, written in the two-dimensional computational space, for $\Delta\xi = \Delta\eta = 1$:

$$(\mu_\eta \delta_\xi f + \mu_\xi \delta_\eta g)_{i,j} = 0 \quad (14.2.10)$$

or

$$\mu_\eta \delta_\xi^- f_{i+1/2,j} + \mu_\xi \delta_\eta^- g_{i,j+1/2} = 0 \quad (14.2.11)$$

showing the difference with the finite difference formula (14.1.16).

The velocities, densities and metric coefficients at the points A, B, C, D are computed by equations (14.1.9) to (14.1.11).

This scheme is more compact than (14.1.16) and requires only one density evaluation per computational cell (point B for cell 1234 of Figure 14.2.1). However, a consequence of this compactness is that the even and odd numbered points are decoupled from each other and a tendency towards oscillatory behaviour of the solutions has been noticed; refer to the discussion in Section 4.4

in Volume 1. This can be seen from the application of scheme (14.2.11) to the incompressible form of the potential equation, which would lead to the molecule shown in Figure 14.2.2 for the Laplace operator. The set of points E, F, G, H is not connected to corner points and two different error levels could subsist (see Problem 14.7). This can be corrected by the explicit addition of recoupling terms and we refer the reader to the original references and to Caughey and Jameson (1982) for the details of this procedure.

Other finite volume schemes can be defined following various options described in Chapter 6 in Volume 1.

An interesting finite volume approach, worth mentioning because of its simplicity, has been developed by Wedan and South (1983), defining a Cartesian mesh, with a particular treatment of the boundary cells which are cut by the solid walls.

Practical example

Figure 14.2.3 shows the pressure distribution and the iso-Mach lines obtained with the Jameson and Caughey method for the subsonic flow on an NACA 0012 airfoil at 10° incidence and $M_\infty = 0.3$ (Salas *et al.*, 1983).

14.3 FINITE ELEMENT FORMULATION

The first application of finite element methods to potential flows were developed by Argyris *et al.* (1969) and De Vries and Norrie (1971) for incompressible flows and Thompson (1974), Periaux (1975) and Shen and Habashi (1976) for compressible, subsonic flows. These authors apply various elements, linear or quadratic triangles, bilinear and biquadratic quadrilaterals with either the potential function or stream function formulations for two-dimensional problems. Other earlier applications have been developed by Hirsch and Warzee (1977) and Prince (1978) for subsonic cascade flows in two dimensions and by Laskaris (1978) for three-dimensional potential flows in the subsonic range. For transonic flow computations, finite elements were used initially by Glowinski *et al.* (1976), Ecer and Akay (1976), Eberle (1977), Deconinck and Hirsch (1979a, 1979b) and Habashi and Hafez (1982). An account of the evolution of transonic finite element computation methods can be found in Hirsch and Deconinck (1982).

As discussed in Chapter 5 in Volume 1, the application of the finite element method requires the definition of an integral formulation to initiate the discretization. For subsonic applications, and for many transonic methods, the weak Galerkin formulation, equivalent to Bateman's variational principle, is the best appropriate choice. However, in order to treat the problems of the supersonic regions, other variational formulations can be defined. One alternative, which has been strongly developed, is the least squares or optimal control approach (Glowinski *et al.*, 1976; Glowinski and Periaux, 1983). Various

other variational formulations have been attempted and the interested reader will find a review of these attempts in Hafez *et al.* (1978).

The simplest method is still the weighted residual or weak formulation coupled to a Galerkin method, and we will follow this approach in this section.

14.3.1 The finite element—Galerkin method

With interpolation functions $N_J(\bar{x})$ attached to a mesh point J , the weak formulation (13.5.1) becomes, with $W = N_J(\bar{x})$,

$$-\int_{\Omega} \rho \bar{\nabla} \phi \cdot \bar{\nabla} N_J \, d\Omega + \int_{\Gamma} q N_J \, d\Gamma = 0 \quad (14.3.1)$$

where Γ is the part of the boundary where the Neumann condition

$$\rho \phi_n = q \quad (14.3.2)$$

is imposed.

With the finite element representation

$$\phi = \sum_I \phi_I N_I(\bar{x}) \quad (14.3.3)$$

one obtains

$$-\sum_I \phi_I \int_{\Omega} \rho \bar{\nabla} N_I \cdot \bar{\nabla} N_J \, d\Omega + \int_{\Gamma} q N_J \, d\Gamma = 0 \quad (14.3.4)$$

The stiffness matrix

$$K_{IJ} = \int_{\Omega} \rho \bar{\nabla} N_I \cdot \bar{\nabla} N_J \, d\Omega \quad (14.3.5)$$

is non-linear and the system

$$K_{IJ} \phi_I = q_J \quad (14.3.6)$$

where q_J

$$q_J = \int_{\Gamma} q N_J(\bar{x}) \, d\Gamma \quad (14.3.7)$$

has to be solved iteratively.

Note that the subscripts I, J correspond to mesh point or node numbers in a general triangulation of the space domain Ω . If a mesh is generated by families of lines as in finite difference discretizations, where each mesh point lies on one line of each family, then each node number I corresponds to a set (i, j) in a finite difference notation.

One of the most commonly used elements next to the linear triangles (or tetrahedra) is the bilinear (or trilinear) element with four node quadrilaterals (or eight node bricks) because of its good compromise between simplicity and

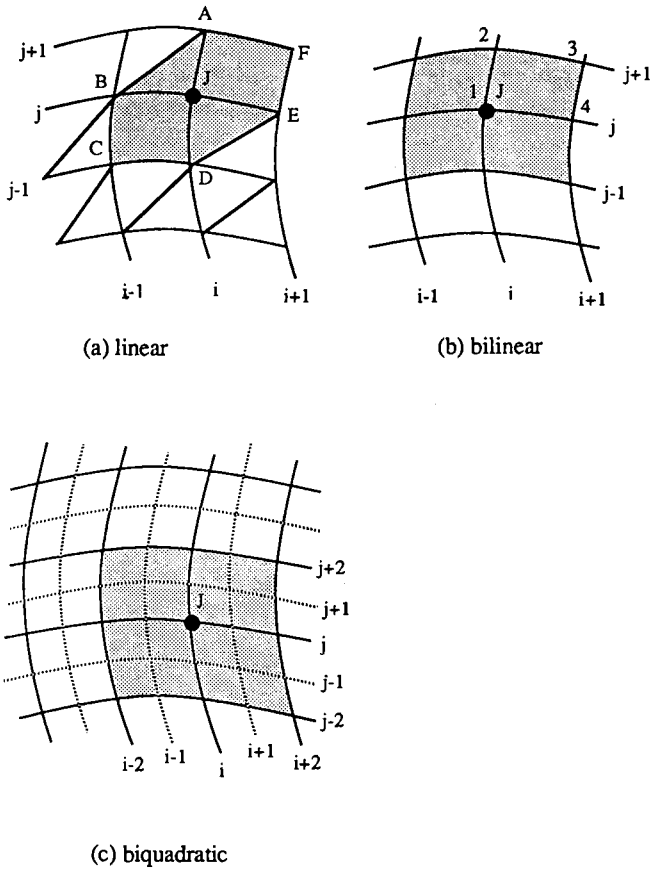


Figure 14.3.1 Elements contributing to the equation for node $J(i, j)$ are in shaded area

accuracy. This element gives a second-order accuracy for the potential function and is therefore equivalent to the use of second-order difference formulas. However, second-order elements, such as quadratic triangles or quadrilaterals, are also applied, when third-order accuracy is required (Deconinck and Hirsch, 1980; Chen, 1982). In this last reference, third-order isoparametric elements are actually used to improve a finite difference discretization.

The integration domain Ω_J , attached to node J is defined by the region around J in which the interpolation functions N_J are different from zero. Since these functions have local support only, this implies that only the elements which contain the node J will contribute to the integral over Ω_J . An example is shown in figure 14.3.1, where the shaded areas represent the domain Ω_J . For bilinear elements, eight surrounding points will contribute to the discretized equation at node J , while 25 nodes will contribute for biquadratic elements and six for linear triangles.

The integrations in equation (14.3.4) are performed numerically by Gauss point integrations (see Chapter 5 in Volume 1). Note that with the exception of the density, the other factors of the stiffness matrix are only dependent on the geometry and the chosen elements. Therefore an important simplification and reduction in the computational work is obtained if the density is assumed constant over an element, equal for instance to its value at the centre of the element. This leads to

$$K_{ij} = \sum_{(e)} \rho^{(e)} \int_{(\Omega_e^j)} \bar{\nabla} N_I \cdot \bar{\nabla} N_J \, d\Omega \equiv \sum_e \rho^{(e)} K_{IJ}^{(e)} \quad (14.3.8)$$

where the summation extends to all the elements Ω_e^j contained in Ω_j . Hence, for each element (e), the elemental stiffness matrix $K^{(e)}$ has to be computed only once and can be stored for its use during the iterative process. For linear triangles, this procedure is an exact one since the velocity is constant over each triangular element and so is the density. In general, the density at the centre of the element will be evaluated through the central value of the velocity. For instance, for quadrilateral elements,

$$\bar{v}_c^2 = |\bar{\nabla} \phi|_c^2 = \left| \sum_I \phi_I \bar{\nabla} N_I(0,0) \right|^2 \quad (14.3.9)$$

since the origin of the local coordinate system is the centre of the quadrilateral and where the summation extends over all the nodes of the element. For instance, in element 1234 of Figure 14.3.1(b), the summation extends over the four nodes 1, 2, 3 and 4.

It is instructive to compare the computational molecules obtained on an orthogonal mesh with these assumptions, using finite elements with linear triangles and bilinear quadrilaterals, and the corresponding molecules obtained with second-order finite difference discretizations. Figure 14.3.2 illustrates the configurations obtained where the notation ρ_i indicates the constant value of ρ in element i . It is seen that with bilinear elements the residual at the central node depends on all the surrounding nodes, including the corner nodes. This is not the case for the finite difference formulation, which is closer to a discretization as obtained from linear triangles and actually identical to it for the Laplace equation corresponding to incompressible flow (see Problems 14.12 to 14.14).

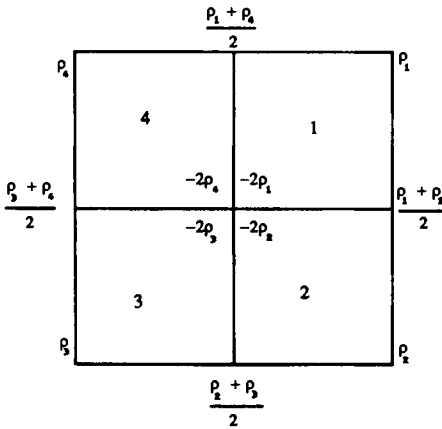
The computational molecules in Figure 14.3.2 are obtained from equation (14.3.8) either by an exact integration or by a Gauss quadrature formula, with two or more points. If an approximate, one-point Gauss formula is applied with bilinear elements, an explicit calculation would lead to

$$K_{IJ} = \sum_{(e)} \rho^{(e)} (\xi_I \xi_J + \eta_I \eta_J)^{(e)} \quad (14.3.10)$$

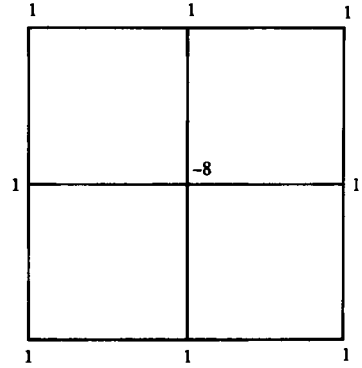
with $\xi_I, \xi_J, \eta_I, \eta_J$ being equal to ± 1 . For the potential equation, this leads to the scheme given by Figure 14.3.3, with the corresponding scheme for the

Bilinear elements

Potential equation

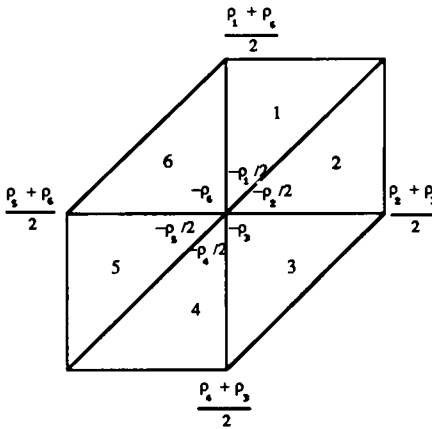


Laplace equation



Linear triangles

Potential equation



Laplace equation

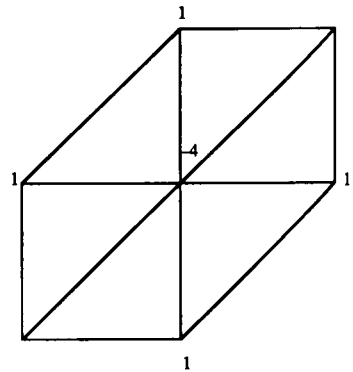


Figure 14.3.2 Comparison of computational molecules from bilinear and triangular elements, for compressible and incompressible potential flows

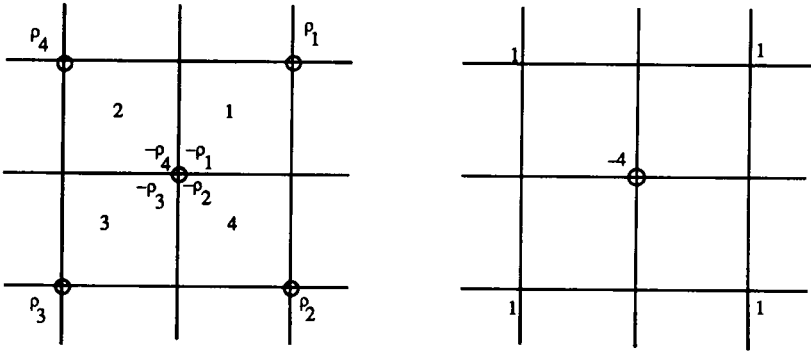


Figure 14.3.3 Computational molecule obtained with equation (14.3.10)

Laplace equation. This scheme is actually identical to the finite volume scheme of Jameson and Caughey introduced in Section 14.2.

Practical example

An example of a finite element subsonic computation performed for a turbine cascade is shown in Figure 14.3.4. A finite element Galerkin method was used, with biquadratic interpolation functions as developed by Hirsch and Warzee (1977). The mesh is shown in Figure 14.3.4(a) and Mach number distributions are displayed in Figure 14.3.4(b).

14.3.2 Least squares or optimal control approach

This approach has been developed by Glowinski *et al.* (1976) for transonic flow computations and is extensively applied in the French aeronautical industry (Bristeau *et al.*, 1980; Glowinski and Periaux, 1983) as an alternative to the Galerkin formulation. We refer the reader to these references for more details.

14.4 ITERATION SCHEME FOR THE DENSITY

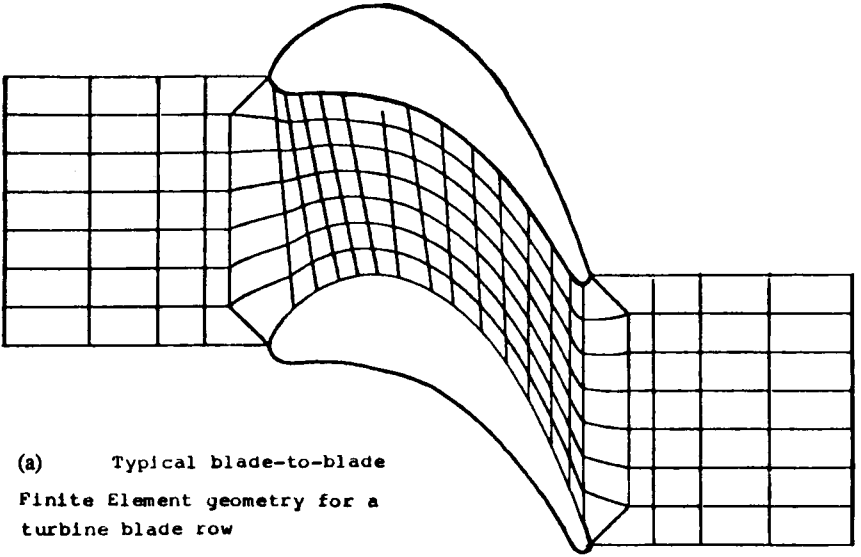
The evaluation of the density is an essential aspect in potential flow computations since it contains the full non-linearity effects of the flow. The simplest approach is a linearization method whereby the density is calculated from the known values of the velocities obtained at the previous iteration. Symbolically this would lead, if n indicates the iteration number in an iterative procedure, to the formulation

$$\bar{\nabla} \cdot (\rho^n \bar{\nabla} \phi^{n+1}) = 0 \quad (14.4.1)$$

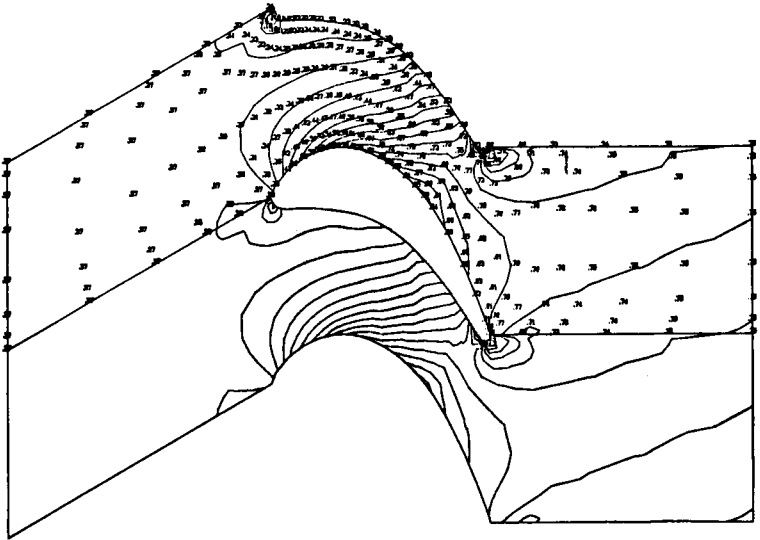
where

$$\rho^n = \rho(|\bar{\nabla} \phi^n|^2) \quad (14.4.2)$$

Some authors call this method Taylor linearization (Shen, 1978; Caspar, 1980)



(a) Typical blade-to-blade
Finite Element geometry for a
turbine blade row



TURBINE BLADE VKI-LS59-BL.2 -15
INLET ANGLE = 30.00 DEG OUTLET ANGLE = -65.95 DEG
INLET MACH NUMBER = .2675 OUTLET MACH NUMBER = .7500

(b) Iso - Mach lines

Figure 14.3.4 Subsonic potential flow through a turbine cascade

and in the finite element literature it is called the secant stiffness method (Section 12.4 in Volume 1). This approach is the most widely used, in subsonic as well as supersonic flow situations.

A Newton method to handle the non-linearity can also be considered, following equation (12.4.3). The Jacobian matrix can be computed analytically in this case, and one obtains the following iteration scheme with $\delta\phi = \phi^{n+1} - \phi^n$. Writing formally

$$K_T \delta\phi = -\bar{\nabla} \cdot (\rho^n \bar{\nabla} \phi^n) \equiv -R^n \quad (14.4.3)$$

the Jacobian operator K_T is computed as follows. Newton's method is written as

$$\begin{aligned} \bar{\nabla} \cdot (\rho^{n+1} \bar{\nabla} \phi^{n+1}) &= \bar{\nabla} \cdot [(\rho^n + \delta\rho) \bar{\nabla} (\phi^n + \delta\phi)] \\ &= \bar{\nabla} \cdot (\rho^n \bar{\nabla} \phi^n) + \bar{\nabla} \cdot (\delta\rho \bar{\nabla} \phi^n) + \bar{\nabla} \cdot (\rho^n \bar{\nabla} \delta\phi) = 0 \end{aligned} \quad (14.4.4)$$

where the higher-order term containing products of $\delta\rho$ and $\delta\phi$ has been neglected.

Introducing equation (13.5.7), with $\phi_i = 0$ for a steady formulation, the $\delta\rho$ term becomes, with $\bar{v} = \bar{\nabla} \phi$,

$$\bar{\nabla} \cdot (\delta\rho \bar{\nabla} \phi) = \bar{\nabla} \cdot (\bar{v} \delta\rho) = -\bar{\nabla} \cdot \left[\rho \bar{v} \left(\frac{\bar{v} \cdot \delta\bar{v}}{c^2} \right) \right] = -\bar{\nabla} \cdot \left[\rho \frac{\bar{v} (\bar{v} \cdot \bar{\nabla}) \delta\phi}{c^2} \right] \quad (14.4.5)$$

and

$$\begin{aligned} K_T \delta\phi &= \bar{\nabla} \cdot (\rho^n \bar{\nabla} \delta\phi) + \bar{\nabla} \cdot (\delta\rho \bar{\nabla} \phi^n) \\ &= \bar{\nabla} \cdot \rho^n \left[\bar{\nabla} - \frac{\bar{v} (\bar{v} \cdot \bar{\nabla})}{c^2} \right] \delta\phi \end{aligned} \quad (14.4.6)$$

The Newton operator can be written in Cartesian coordinates:

$$K_T = \partial_i [\rho (\delta_{ij} - M_i M_j) \partial_j] \quad (14.4.7)$$

which, written out explicitly in two dimensions, becomes

$$K_T = \partial_x \left[\rho \left(1 - \frac{u^2}{c^2} \right) \partial_x \right] - \partial_x \left[\rho \frac{uv}{c^2} \partial_y \right] - \partial_y \left[\rho \frac{uv}{c^2} \partial_x \right] + \partial_y \left[\rho \left(1 - \frac{v^2}{c^2} \right) \partial_y \right] \quad (14.4.8)$$

This method is rarely used, however, due to the increased computational cost involved in the evaluation of the Jacobian matrix K_T . It has been applied by Prince (1978) and Laskaris (1978) to two- and three-dimensional subsonic potential flows. It has exceptionally been applied to transonic potential flow computations, but an analysis of the properties of equations (14.4.3) and (14.4.6) is most instructive. It reveals the source and the nature of the problems connected to the transition from subsonic to supersonic flow regimes. Indeed, one can consider that for sufficiently small variations $\delta\phi$, any iterative method, even a linearization (14.4.1), will actually be an approximation to equation (14.4.3), which contains all the effects of the density variations.

Therefore, the properties of equation (14.4.3) are representative of the properties of the non-linear potential equation. The structure of the Jacobian operator is closely related to the structure of the non-conservative form of the potential equations (13.2.5), as can be seen from a direct comparison with equation (14.4.7). However, it is also related to the expression appearing in the second variation of the pressure functional, equation (13.5.12), and both provide indeed the same information.

In order to analyse the Jacobian operator, let us consider its eigenvalues for a wave-like solution of the form of a Fourier mode

$$\delta\phi = \delta\phi_0 e^{i\vec{\kappa}\cdot\vec{x}} \quad (14.4.9)$$

where $\vec{\kappa}$ is a wave-number vector in space of components $(\kappa_x, \kappa_y, \kappa_z)$ and $\delta\phi_0$ a constant dependent on the boundary values.

Introducing (14.4.9) into equation (14.4.6), one obtains, for the left-hand side operator, at fixed ρ^n , the eigenvalue equation

$$K_T \delta\phi = -\rho^n \left[\vec{\kappa}^2 - \frac{(\vec{v}\cdot\vec{\kappa})^2}{c^2} \right] \delta\phi \quad (14.4.10)$$

Hence, the eigenvalues $\lambda_{\vec{\kappa}}$ of the Jacobian operator of the potential equation are given by

$$\lambda_{\vec{\kappa}} = -\rho^n \left[\vec{\kappa}^2 - \frac{(\vec{v}\cdot\vec{\kappa})^2}{c^2} \right] \quad (14.4.11)$$

For incompressible flows, $c^2 \rightarrow \infty$ and one recognizes the eigenvalue $-\vec{\kappa}^2$ of the Laplace operator for Fourier eigenmodes.

The expression between brackets in (14.4.11) is identical to the left-hand side of the characteristic condition (13.3.8), and also to the expression defining the second variation of the pressure functional (13.5.12). All three approaches do express the same information with regard to the influence of compressibility.

One has therefore the following properties:

- (1) For subsonic flows, $\lambda_{\vec{\kappa}}$ is always negative and the operator $(-K_T)$ is positive definite.
- (2) Zero eigenvalues will appear for supersonic flows, making the operator K_T singular, for directions $\vec{\kappa}$ lying on the cone of normals defined by equation (13.3.8).
- (3) For supersonic flows, the eigenvalues $\lambda_{\vec{\kappa}}$ change sign and become positive for directions $\vec{\kappa}$ inside the cone of normals, that is for time-like vectors $\vec{\kappa}$.

It is seen that the second term dominates the first in this case as a consequence of the dominating contribution from the density variations (14.4.5). This is another expression of the fact that in supersonic flows the variations of density have a stronger influence on the flow properties than the velocity variations.

- (4) When the $\vec{\kappa}$ directions are outside the cone of normal, that is for space-like directions, the eigenvalues remain negative and $(-K_T)$ will remain positive

definite. In this case, since $\bar{\kappa}$ is normal to the wave-front surface $\delta\phi$, the potential variations remain inside the domain of dependence (see Figures 13.3.2 and 13.3.3).

These properties reveal that the Jacobian $(-K_T)$, which is positive definite in the subsonic flow regions, can become singular and non-positive definite in the supersonic domains. This makes equation (14.4.3) ill-defined, and unless a resolution algorithm can be devised to handle non-positive definite operators, one has to define a numerical formulation based on positive definite operators able to handle the above properties.

The alternatives are indicated by equation (14.4.10):

- (1) Attempt to avoid the singularities of K_T , that is discretize the potential equation in a way that prevents the eigenvalues of K_T from becoming zero or changing sign.
- (2) Define an iterative scheme P such that $P^{-1}K_T$ does not generate negative eigenvalues when λ_κ is positive. Remember that P should have negative eigenvalues in order to be considered as conditioning operator (see Section 12.4 in Volume 1).

The replacement of equation (14.4.3) by a preconditioned system $P\delta\phi = -R^n$, where P is an elliptic operator, is currently applied for subsonic problems (see also equation (14.4.1)). With ρ^n fixed, P is equal or very close to a Laplace operator, and this is a very effective method for subsonic problems. However, the same method will tend to diverge in the presence of supersonic regions, since the eigenvalues of K_T can become positive. As a consequence, the corresponding eigenvalues of the amplification matrix

$$G = 1 - P^{-1}K_T \quad (14.4.12)$$

will become larger than one.

References

- Argyris, J. H., Mareczek, G., Sharpf, D. W. (1969). 'Two and three dimensional flow using finite elements.' *Aeronautical Journal of the Royal Aero. Society*, **73**, 961–964.
- Bristeau, M. O., Glowinski, R., Periaux, J., Perrier, P., Pironneau, P., Poirier, G. (1980). 'Transonic flow simulation by finite element and least squares,' *Finite Elements in Fluids*, Vol. 4, Chichester, J. Wiley & Sons.
- Caspar, J. R. (1980). 'A model problem study of transonic potential flow procedures.' AIAA 18th Aerospace Sciences Meeting—*AIAA Paper 80-0337*.
- Caughey, D. A., Jameson, A. (1979). 'Numerical calculation of transonic potential flow about wing-body combinations.' *AIAA Journal*, **17**, 175–181.
- Caughey, D. A., and Jameson, A. (1980). 'Progress in finite volume calculations for wing-fuselage combinations.' *AIAA Journal*, **18**, 1281–1288.
- Caughey, D. A., Jameson, A. (1982). 'Basic Advances in the finite volume method for transonic potential flow calculations.' In Cebeci, T. (eds.), *Numerical and Physical Aspects of Aerodynamic Flows*, Berlin: Springer Verlag.

- Chen, L. T. (1982). 'Improved finite difference scheme for transonic airfoil flowfield calculations.' *AIAA Journal*, **20**, 218–226.
- Deconinck, H., Hirsch, Ch. (1979a). 'A finite element method solving the full potential equation with boundary layer interaction in transonic cascade flow.' AIAA 17th Aerospace Sciences Meeting—*AIAA Paper 79-0132*.
- Deconinck, H., Hirsch, Ch. (1979b). 'Transonic flow calculations with finite elements.' In Rizzi, A. & Viviand, H. (eds.), *Notes on Numerical Fluid Dynamics*, Vol. 3, *Proc. GAMM Workshop on Numerical Methods for the Computation of Inviscid Transonic Flows with Shock Waves*, Vieweg.
- Deconinck, H., Hirsch, Ch. (1980). 'Transonic flow calculations with higher order finite elements.' *Proc. Seventh Int. Conf. on Numerical Methods in Fluid Dynamics*, Reynolds, W. C. (Ed.) *Lecture Notes in Physics*, Vol. 141, Berlin: Springer Verlag.
- De Vries, G., Norrie, D. H. (1971). 'The application of the finite element technique to potential flow problems.' *Trans. ASME—Journal of Applied Mechanics*, 798–802.
- Doria, M. L., South, J. C. (1982). 'Transonic potential flow and coordinate generation for bodies in a wind tunnel.' *AIAA Paper 82-0223*—AIAA 20th Aerospace Sciences Meeting.
- Eberle, A. (1977). 'Eine Methode Finiter Elemente zur Berechnung der Transsonischen Potential-Stromung um Profile.' *MBB Rapport MBB-UFE 1352*. (English Translation—NASA TM-75324).
- Ecer, A., Akay, H. U. (1976). 'Application of finite element method for the solution of transonic flow.' *Finite Elements in Fluids*, Vol. 3, pp. 191–201, Chichester, J. Wiley & Sons.
- Flores, J., Holst, T. L., Kwak, D., Batiste, D. (1983). 'A new consistent spatial differencing scheme for the transonic full potential equation.' AIAA 21st Aerospace Sciences Meeting, Reno—*AIAA Paper 83-0373*.
- Glowinski, R., Periaux, J., Pironneau, O. (1976). 'Transonic flow simulation by the finite element method via optimal control.' *Finite Elements in Fluids*. Vol. 3, pp. 249–259, Chichester, J. Wiley & Sons.
- Glowinski, R., Periaux, J. (1983). 'Least squares and domain decomposition methods applied to the numerical solution of non-linear problems in fluid dynamics.' *Von Karman Institute Lecture Series*, 1983-04, Belgium, Rhode St. Genese.
- Habashi, W. G., Hafez, M. M. (1982). 'Finite element solutions of transonic flow problems.' *AIAA Journal*, **20**, 1368–1376.
- Hafez, M. M., Wellford, L. C., Murman, E. M. (1978). 'Finite elements and finite differences for transonic flow calculations.' *Finite Elements in Fluids*, Vol. 3, Chichester, J. Wiley & Sons.
- Hirsch, Ch., Warzee, G. (1977). 'Finite element computation of subsonic cascade flows'. *Proc. 6th Canadian Congress on Applied Mechanics*, Vancouver.
- Hirsch, Ch., Warzee, G. (1980). 'Quasi 3D finite element computation of flows in centrifugal compressors.' In *Performance Prediction of Centrifugal Pumps and Compressors*, pp. 69–75, ASME Publications.
- Hirsch, Ch., Deconinck, H. (1982). 'A survey of finite element methods for transonic flows.' In Roe, P. J. (ed.), *Numerical Methods in Aeronautical Fluid Mechanics*, London: Academic Press.
- Jameson, A. (1976). 'Transonic flow calculations.' *Von Karman Institute Lecture Series on Computational Fluid Dynamics LS-87*, Belgium: Rhode-St-Genese.
- Jameson, A., Caughey, D. E. (1977). 'A finite volume method for transonic potential flow calculations.' *Proc. AIAA Third Computational Fluid Dynamics Conference*, Albuquerque, pp. 35–54.
- Laskaris, T. E. (1978). 'Finite element analysis of three-dimensional potential flow in turbomachines.' *AIAA Journal*, **16**.
- Periaux, J. (1979). 'Resolution de quelques problemes non-lineaires en Aerodynamique par des methodes d'elements finis et de moindres carres fonctionnels.' *Ph.D. Thesis, Universite Paris VI, France*.

- Prince, T. C. (1978). 'Prediction of steady inviscid compressible flow on a blade-to-blade surface by finite element method.' AIAA 16th Aerospace Sciences Meeting—*AIAA Paper 78-244*.
- Pulliam, T. H., Steger, J. L. (1980). 'Implicit finite difference simulations of three dimensional compressible flows.' *AIAA Journal*, **18**, 159–167.
- Salas, M. D., Jameson, A., Melnik, R. E. (1983). 'A comparative study of the non-uniqueness problem of the potential equation.' Proc. AIAA 6th Computational Fluid Dynamics Conference—*AIAA Paper 83-1888*, pp. 48–60.
- Shen, S. F., Habashi, W. (1976). 'Local linearization of the finite element method and its applications to compressible flows.' *Int. Journal for Num. Meth. in Engineering*, **10**, 565–577.
- Shen, S. F. (1978). 'Transonic aerodynamic computation with finite element method.' *Finite Elements in Fluids*, Vol. 3, Chichester, J. Wiley & Sons.
- Schulz, H. D., Neuhoﬀ, F., Hirsch, Ch., Shreeve, R. P. (1984). 'Application of finite element code Q3DFLO-81 to turbomachinery flow fields.' *Naval Postgraduate School Report*, NPS67-84-005-PR, NPS, Dept. Aeronautics, Monterey, U.S.A.
- Thompson, D. S. (1974). 'Flow through a cascade of airfoils.' In Oden, J. T. (Ed.), *Finite Elements in Flow Problems*, URH Press.
- Wedan, B., South, J. (1983). 'A method for solving the transonic full potential equation for general configurations.' Proc. AIAA 6th Computational Fluid Dynamics Conference—*AIAA Paper 83-1889*, pp. 515–526.

PROBLEMS

Problem 14.1

Express the velocity components at the corners ABCD of the computational cell of Figure 14.1.1 as a function of the potential values at the mesh points, following equations (14.1.10), by applying (14.1.4) and (14.1.5). Draw the corresponding computational molecules for the two velocity components. Repeat the calculation by applying (14.1.4) with (14.1.6).

Problem 14.2

Write the equations (14.1.17) and (14.1.18) for the velocity components at the points $(i - 1/2, j)$ and $(i, j - 1/2)$ and write out explicitly the scheme (14.1.16) for ϕ_{ij} . Determine the coefficients of the computational molecule.

Problem 14.3

Show that a central differencing of the Jacobian matrix coefficients at the mesh points, followed by an averaging to obtain the values at mid-side points $(i \pm 1/2, j)$ and $(i, j \pm 1/2)$, does not satisfy the consistency relations (14.1.23) when the flux difference operators are defined by equations (14.1.16) to (14.1.18).

Hint: Coefficients such as x_ξ , x_η are discretized by

$$(x_\xi)_{ij} = \bar{\delta}_\xi x_{ij} = \frac{x_{i+1,j} - x_{i-1,j}}{2}$$

$$(y_\eta)_{ij} = \bar{\delta}_\eta y_{ij} = \frac{y_{i,j+1} - y_{i,j-1}}{2}$$

and

$$(x_\xi)_{i+1/2,j} = \mu_\xi (x_\xi)_{i+1/2,j} = \frac{1}{2} [(x_\xi)_{i+1,j} + (x_\xi)_{ij}]$$

Problem 14.4

Show that the metric discretization defined in a way similar to the difference expressions of (14.1.18), namely a different discretization dependent on the mid-cell point location, for instance:

$$\begin{aligned}\Delta_{\xi}^m x_{i+1/2,J} &= \delta_{\xi}^+ x_{ij} \\ \Delta_{\eta}^m x_{i+1/2,J} &= \mu_{\xi} \bar{\delta}_{\eta} x_{i+1/2,J} \\ \Delta_{\xi}^m y_{i,J+1/2} &= \mu_{\eta} \bar{\delta}_{\xi} y_{i,J+1/2} \\ \Delta_{\eta}^m y_{i,J+1/2} &= \delta_{\eta}^+ y_{ij}\end{aligned}$$

satisfies the consistency condition for the scheme (14.1.16) to (14.1.18).

Problem 14.5

Verify by an explicit calculation that the three-dimensional consistency condition (14.1.26) is not verified for central difference operators on the flux components and on the metric coefficients evaluated at mesh point ijk . Show also that if the central operators on the metric are replaced by central differences averaged in the associated direction the condition will be satisfied.

Hint: For instance, for the first term in equation (14.1.26), associated with ξ_x , one replaces the central difference

$$\bar{\delta}_{\eta} y_{ijk} \bar{\delta}_{\xi} z_{ijk} - \bar{\delta}_{\xi} y_{ijk} \bar{\delta}_{\eta} z_{ijk}$$

by the averaged form, with $\bar{\mu} u_i = \frac{1}{2} (u_{i+1} + u_{i-1}) = \frac{1}{2} (\delta^+ + \delta^-) u_i$,

$$\bar{\mu}_{\xi} \bar{\delta}_{\eta} y_{ijk} \cdot \bar{\mu}_{\eta} \bar{\delta}_{\xi} z_{ijk} - \bar{\mu}_{\eta} \bar{\delta}_{\xi} y_{ijk} \cdot \bar{\mu}_{\xi} \bar{\delta}_{\eta} z_{ijk}$$

The other terms are obtained by cyclic permutation.

Problem 14.6

Show that the finite volume formulation (14.2.2) is identical to the finite difference discretization (14.1.16) with the choice

$$f_{AB} = (\bar{F} \cdot \bar{S})_{AB} = f_{i+1/2,J}$$

Problem 14.7

Obtain the computational molecule for the scheme (14.2.11) and prove Figure 14.2.2 for an incompressible flow on a Cartesian mesh.

Problem 14.8

Apply the scheme (14.1.16) to the flow around a cylinder in polar coordinates (r, θ) and solve for an incompressible flow as well as for an incident Mach number of $M_{\infty} = 0.2$.

Hint: Define a mesh formed by circles and radial lines, taking $\xi = r$, $\eta = \theta$. Solve the algebraic system with a relaxation method or a direct method. Compare with the exact incompressible solution $\phi(r, \theta) = U_{\infty} (r + a^2/r) \cos \theta$ for a cylinder of radius a .

Problem 14.9

Repeat Problem 14.8 for the scheme (14.2.11).

Problem 14.10

Apply a finite volume formulation to the cell 1234 of Figure 14.2.1 and develop the scheme for a Cartesian mesh.

Define u, v, ρ at the corners of the cell, that is at $(i, j), (i + 1, j)$, etc., but define the potential function at the cell centres, that is at $(i + 1/2, j + 1/2)$ for cell 1234 (Doria and South, 1982).

Hint: Define the fluxes at the cell face centres, that is at $(i, j + 1/2)$ and $(i + 1, j + 1/2)$ for the f component and at $(i + 1/2, j)$ and $(i + 1/2, j + 1)$ for the g component. Define also the velocities by second-order central differences, such as

$$u_{i,j+1/2} = \frac{\phi_{i+1/2,j+1/2} - \phi_{i-1/2,j+1/2}}{\Delta x}$$

Show that, in the incompressible case, one obtains the five-point Laplace operator centred at point B, and compare with the finite difference scheme (14.1.1).

Problem 14.11

Apply the scheme of the preceding problem to the flow around a cylinder, with various formulas for the evaluation of the density. Solve, by direct methods, for an incident flow at Mach number $M_\infty = 0.2$ and for an incompressible flow.

Problem 14.12

Compute the stiffness matrix elements on a rectangular mesh for bilinear elements for the potential equation. Do the explicit exact integrations for each element and obtain the molecule of Figure 14.3.2(a).

Hint: Take

$$N_I = \frac{1}{4}(1 + \xi\xi_I)(1 + \eta\eta_I)$$

and apply

$$K_{IJ} = \sum_e \rho^{(*)} \int \left[\left(\frac{\partial N_I}{\partial \xi} \right) \left(\frac{\partial N_J}{\partial \xi} \right) + \left(\frac{\partial N_I}{\partial \eta} \right) \left(\frac{\partial N_J}{\partial \eta} \right) \right] \frac{d\xi d\eta}{\Delta x \Delta y / 4}$$

Problem 14.13

Perform the same calculations for linear triangles on a rectangular mesh. Prove the molecule of Figure 14.3.2(b).

Problem 14.14

Apply the finite element–Galerkin formulation to the flux form of the potential equation on linear triangles, and show that one obtains a finite volume formulation for the control volume ABCDEF of Figure 14.3.1.

Define the formulas to be applied to the potential derivatives in order to obtain the molecule of Figure 14.3.2(b).

Hint: Calculate, with $f = \rho u = \rho \phi_x$, $g = \rho v = \rho \phi_y$, as components of the flux vector \vec{F} ,

$$\begin{aligned} \int_{\Omega} (\vec{\nabla} \cdot \vec{F}) N_I d\Omega &= - \int_{\Omega} (\vec{F} \cdot \vec{\nabla}) N_I d\Omega + \oint_{\Gamma} F_n \cdot N_I d\Gamma \\ &= - \int_{\Omega} \left(f \frac{\partial N_I}{\partial x} + g \frac{\partial N_I}{\partial y} \right) d\Omega + \oint_{\Gamma} F_n N_I d\Gamma \end{aligned}$$

and show that one obtains the expression

$$\sum_{\text{sides}} (f \Delta y - g \Delta x) = 0$$

using the relations to be found in Chapter 5 in Volume 1.

Problem 14.15

Derive the complete expressions, as a function of the mesh point coordinates, of all the metric coefficients in Example 14.1.2.

Show that these metric derivatives based on a local isoparametric finite element representation with bilinear interpolation functions do not satisfy the metric compatibility conditions (14.1.23) when applied with scheme (14.1.16).

Show that they do satisfy the metric compatibility conditions (14.1.23) when applied to scheme (14.2.11).

Problem 14.16

Solve the small disturbance potential equation (13.2.11) for a 4% circular arc airfoil and a cartesian mesh for incident Mach numbers of 0.2 and 0.4.

Chapter 15

The Computation of Stationary Transonic Potential Flows

As pointed out in the previous chapter, the standard solution methods for subsonic potential flows break down when the flow becomes supersonic. This results from the transition of the potential equation from elliptic to hyperbolic type, indicating that the flow changes from a diffusive character to a propagation-dominated behaviour. Consequently the typical elliptic numerical operators will not be able to simulate correctly the propagation properties of the supersonic flow regions. This shows up in the properties of the Jacobian matrix K_T for a Newton iteration on the density, which ceases to be positive definite, or in the fact that the matrix of the coefficients of the algebraic system of the central difference potential equation ceases to be diagonally dominant for supersonic flows. These are various illustrations of the same difficulties and the supersonic region will require an appropriate treatment. Moreover, the specific field of transonic flows, with mixed supersonic and subsonic regions, has the additional complication that the sonic transition line between the two regions is unknown and is part of the solution and that the transition from supersonic to subsonic flow can occur through a shock discontinuity which has also to be computed. Figures 15.1.1 and 15.1.2 show typical transonic flow configurations for an isolated airfoil and a more complex channel flow with supersonic inlet and subsonic outlet flow.

Therefore, the following steps have to be considered for transonic potential flow computations:

- (1) Define an appropriate discretization in the supersonic regions which takes into account the existence of domains of dependence of the flow properties limited by the characteristics of the hyperbolic equation.
- (2) Define an appropriate iteration scheme for the non-linear system of algebraic equations which ensures that during the evolution towards the converged steady state the computed solution remains within the proper regions of dependence.
- (3) Avoid the appearance of non-physical expansion shocks, which are also solution of the isentropic potential equation.

Actually the introduction of the first step automatically ensures condition 3

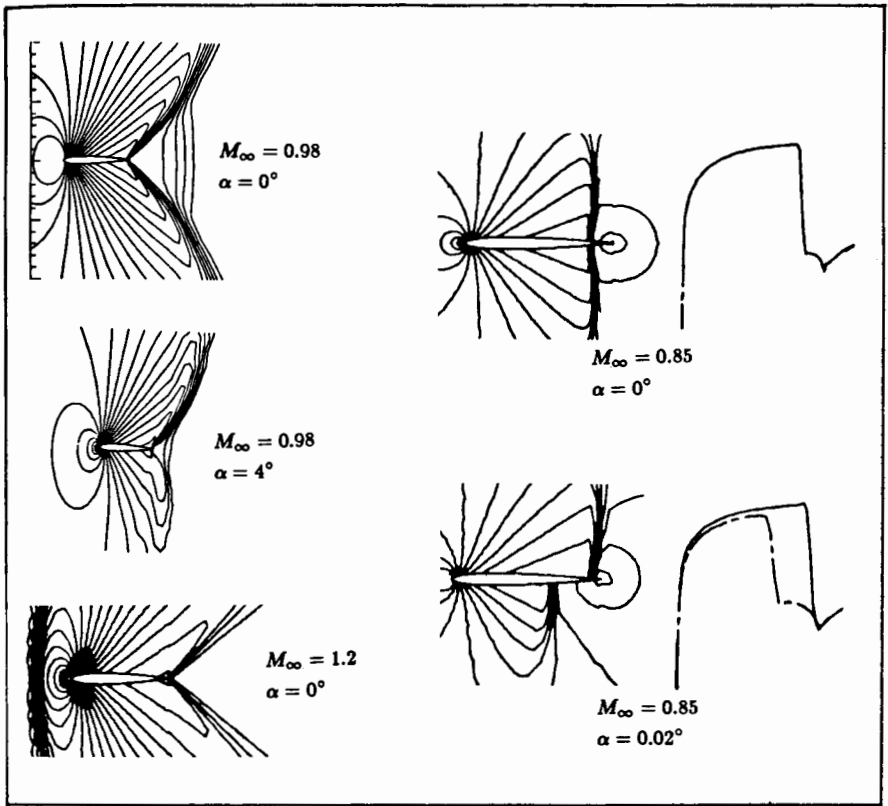


Figure 15.1.1 Typical transonic flow configurations for an isolated airfoil. (From Shankar *et al.*, 1985)

so there are no particular measures to take for this step, once step 1 is ensured. The reason behind this situation is that the introduction of typical supersonic distretization methods leads to schemes which, when compared to the elliptic central-type discretizations, appear as equivalent to *the addition of an artificial viscosity* term added to the subsonic elliptic schemes. This explains also why the resolution of step 1 is often referred to in the literature as the introduction of artificial viscosity.

The first successful computation of a steady transonic potential flow was obtained by Murman and Cole (1971) for the small disturbance equation in two dimensions. This basic work marked a breakthrough that initiated considerable activity in this field, giving rise to an extremely rapid development which led, in about ten years time, to the situation where the computation of transonic potential flows can be considered as a practically solved problem. A large number of operational codes exist by now, which compute three-dimensional transonic potential flows in a few seconds of CPU time on the most advanced computers (Thomas and Holst, 1983).

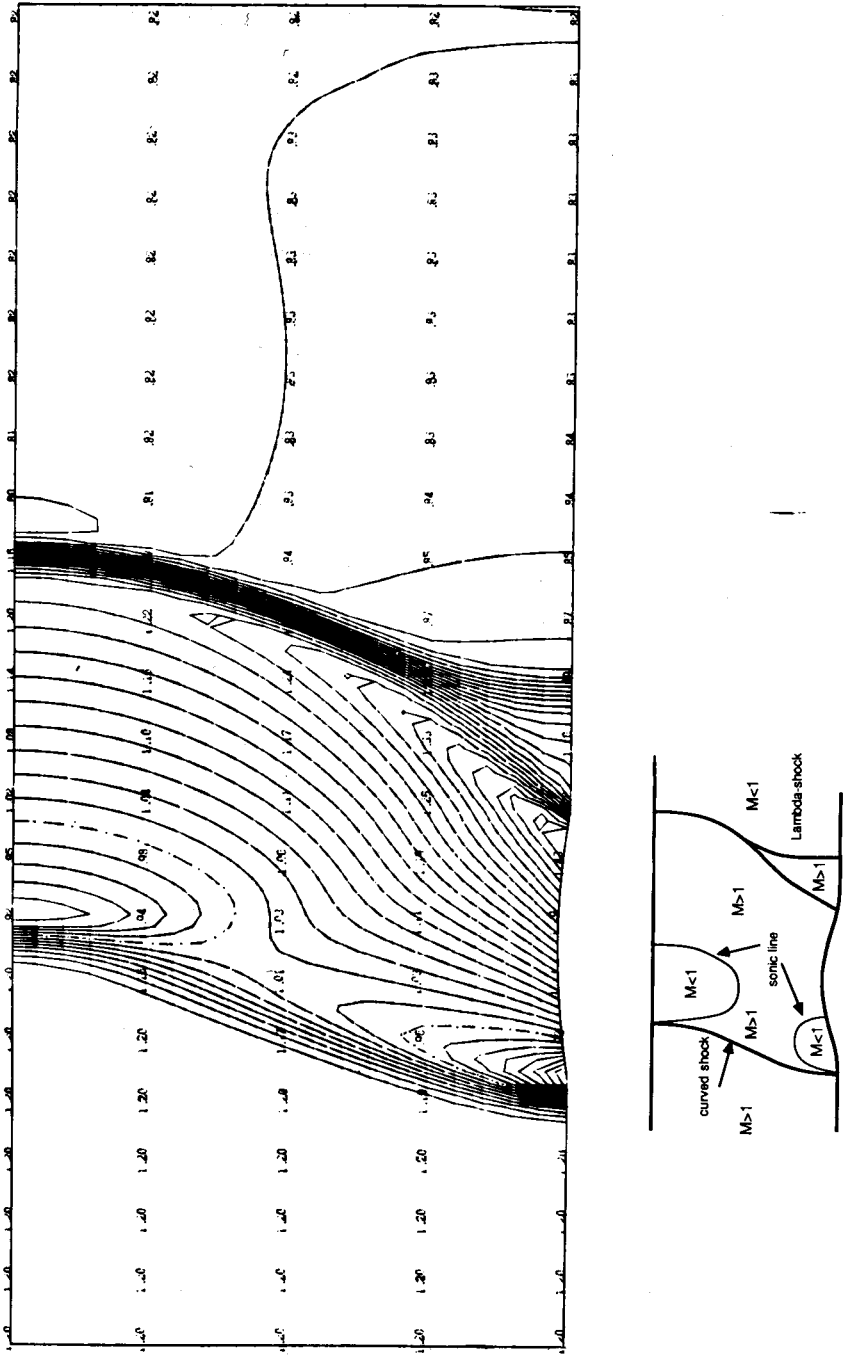


Figure 15.1.2 Typical transonic channel flow with multiple shock configuration; isentropic potential computation. (From Deconinck, 1983)

The original idea of Murman and Cole consisted of using different finite difference formulas in the supersonic, sonic and subsonic regions. As with many ideas which appear simple afterwards, the original development required deep understanding of the underlying problems both numerical and physical. It is fascinating and instructive to read the historical account of the genesis of these ideas, as reported by Hall (1981), and which we cannot resist quoting here for our and, we hope, for the reader's pleasure.

Earl Murman had been working for a year or so at Boeing on finite difference methods for integrating the compressible Navier–Stokes equations when, in 1968, Julian Cole arrived on a one-year visit. Cole writes: ‘it was Goldberg who suggested that transonic flow was a timely subject. I decided on a joint analytical and numerical approach and he said that Earl and I could work together (since my programming was feeble). Our approach was founded on several bits of previous experience.

- i) The fact that Lax–Wendroff could give the correct shock jumps (had) made a deep impression and I (had) learned about artificial viscosity, diffusion and dispersion of difference schemes. Yosh (Yoshihara) was convinced that steady flows could not be calculated directly but I decided while at Boeing to try using a conservative scheme (*à la* Lax) in order to catch shocks.
- ii) I was aware of Howard Emmon's very early ‘successful’ relaxation calculations of mixed flows in nozzles and decided to try a relaxation method.
- iii) I had studied the fundamentals of small disturbance theory... rather extensively earlier. I knew it had all the essential difficulties and could even be a good approximation. It was clear that it would make the numerical work easier.

Murman writes that Cole

...spent several months systematically deriving a small disturbance theory from the complete Euler equations.

It laid the theoretical groundwork for our later developments.

In January 1969 we started some computations solving Laplace equations and then the TSP using centered finite differences. By April we found that we could not get the calculations to converge for supercritical flow. It was in the following several months that we hit upon the idea of switching and type dependent schemes. I believe that the idea grew out of an afternoon brainstorming session when we were discussing finite difference methods for elliptic and hyperbolic problems and how the two were basically different. Julian, I believe, threw out a comment that maybe we could combine them somehow.

I have often reflected back on that event to realise how important it is in research to be open-minded, imaginative, and receptive to unconventional suggestions.

Cole adds:

I knew enough numerical analysis to know that hyperbolic schemes were unstable if the domain of dependence was incorrect. Even though the time-like direction was unclear I thought that perhaps we should have only downstream influence. So we decided to switch schemes: explicit hyperbolic was ruled out by the CFL condition near the sonic line.

Murman continues:

My experience the previous year on the Navier–Stokes computations allowed us to make rapid progress. It was clear that we should maintain conservation form to calculate shock waves. Unfortunately we missed the essential point of the shock point operator. For stability reasons, the hyperbolic operator had to be implicit. This naturally led to a line relaxation algorithm so that the method would work in the limits of both purely supersonic and purely subsonic flow. In July we programmed up the first code and it worked almost immediately.

After this initial work, Murman and Cole's procedure was extended to three-dimensions by Ballhaus and Bailey (1972), to the non-conservative full potential equation for two-dimensions by Steger and Lomax (1972) and Garabedian and Korn (1972), and for three-dimensions by Jameson (1974). The conservative full potential equation was solved initially by Jameson (1975) for two-dimensional flows and extended to three-dimensional configurations by Jameson and Caughey (1977). Subsequently, improvements were introduced with regard to the treatment of the artificial viscosity terms, leading to the concept of artificial compressibility (Eberle, 1977; Holst and Ballhaus, 1979; Hafez *et al.*, 1978). Also an important effort was made towards the improvement of the convergence rate of the iterative techniques.

The above-mentioned initial developments were based on line relaxation iterative methods but Ballhaus and Steger (1975) and Ballhaus *et al.* (1978) introduced variants of the implicit alternative direction ADI techniques, called approximate factorization (AF) methods. These have been extended to the full potential equation by Holst and Ballhaus (1979) and Holst (1979) and by Holst (1980) for three-dimensional computations. Multi-grid acceleration techniques were introduced by Jameson (1979) for finite difference methods and by Deconinck and Hirsch (1981) for finite element potential flow discretizations.

15.1 THE TREATMENT OF THE SUPERSONIC REGION: ARTIFICIAL VISCOSITY—DENSITY AND FLUX UPWINDING

The original scheme of Murman and Cole was based on the observation that in the supersonic region, with the flow oriented in the x -direction, the central difference operator does not respect the proper region of dependence. Indeed, a central difference operator for the second-order derivative ϕ_{xx} at point P (Figure 15.1.3)

$$\phi_{xx}^{(C)}|_{i,j} = \frac{\phi_{i+1,j} - 2\phi_{i,j} + \phi_{i-1,j}}{\Delta x^2} = \frac{1}{\Delta x^2} \delta_x^2 \phi_{i,j} \quad (15.1.1)$$

would suggest that the solution in P(i, j) is dependent on a downstream point ($i + 1, j$). This is in opposition to the physical properties of supersonic flows since only the points located within the region of dependence of P can have an effect on the flow properties at this point. Therefore, if a backward or upwind difference

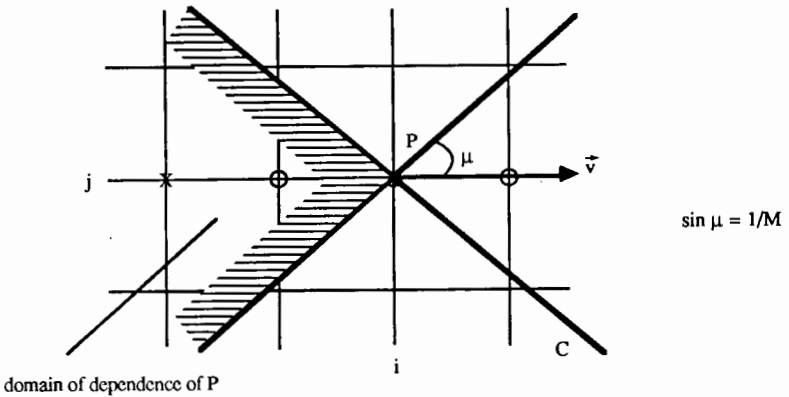


Figure 15.1.3 Region of dependence of P in supersonic flow

operator is used instead, at supersonic points, such as

$$\phi_{xx}^{(B)}|_{ij} = \frac{\phi_{i-2,j} - 2\phi_{i-1,j} + \phi_{ij}}{\Delta x^2} = \frac{1}{\Delta x^2} E_x^{-1} \delta_x^2 \phi_{ij} \quad (15.1.2)$$

this would be in agreement with the physical reality of supersonic flow.

Hence, a *type-dependent* differencing is introduced whereby the *derivatives in the flow direction are upwind differenced*. It is to be noted that the difference formula (15.1.2) is a first-order approximation to the second derivative at point (i, j) and hence, while the subsonic regions have second-order accuracy, the supersonic regions have only first-order accuracy. This will be the case for most of the transonic potential flow methods, although attempts to work with second-order accurate upwind differencing have been developed.

15.1.1 Artificial viscosity—non-conservative potential equation

When the two formulas (15.1.2) and (15.1.1) are compared one obtains

$$\begin{aligned} \phi_{xx}^{(B)} &= \phi_{xx}^{(C)} - \frac{\phi_{i+1,j} - 3\phi_{i,j} + 3\phi_{i-1,j} - \phi_{i-2,j}}{\Delta x^2} \\ &= \phi_{xx}^{(C)} - \Delta x \phi_{xxx} \end{aligned} \quad (15.1.3)$$

where the difference expression is seen to be a formula for the third-order derivative ϕ_{xxx} .

Hence, the upwind differencing of Murman and Cole can be interpreted as the addition of an artificial viscosity term proportional to $\Delta x \phi_{xxx} = \Delta x u_{xx}$ to the centrally differenced second-order derivative. Two equivalent points of view can therefore be taken: either the streamwise derivatives are upwind differenced in the supersonic regions or all derivatives are *centrally differenced everywhere* but an artificial viscosity term is added to the equations.

The form of the artificial viscosity terms are obviously not arbitrary, but, as shown by Lax (1954) (see Section 21.2), any form of non-vanishing dissipation will be sufficient to implement the entropy condition and exclude expansion shocks. Therefore, the upwind differencing automatically adds an entropy condition under the form of artificial dissipation terms proportional to the mesh size. However, some care is required in order to prevent these terms vanishing over a shock transition, where the flow changes from supersonic to subsonic regime, or over a sonic point, where the inverse transition takes place.

When applied to the small disturbance equation, under the two-dimensional form

$$(1 - M^2)\phi_{xx} + \phi_{yy} = 0 \quad (15.1.4)$$

an artificial viscosity term $(1 - M^2)\Delta x \phi_{xxx}$ for $M > 1$ is obtained and either we write the scheme

$$(1 - M^2)\phi_{xx}^{(B)} + \phi_{yy}^{(C)} = 0 \quad (15.1.5)$$

or we introduce first the artificial viscosity term and discretize subsequently the left-hand side centrally:

$$\begin{aligned} (1 - M^2)\phi_{xx}^{(C)} + \phi_{yy}^{(C)} &= -\Delta x(M^2 - 1)\phi_{xxx} & \text{for } M > 1 \\ &= 0 & \text{for } M < 1 \end{aligned} \quad (15.1.6)$$

In order to apply these concepts to the full potential equation, we have to take into account the local flow direction and define an upwind differencing with respect to the local velocity direction. Such a procedure has been introduced

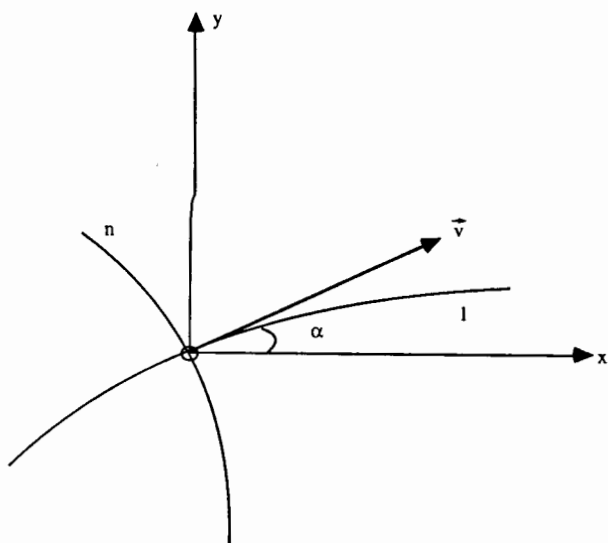


Figure 15.1.4 Transformation between local streamline and Cartesian coordinate systems (l, n) , (x, y)

by Jameson (1974) for the non-conservative form of the potential equations and was termed the 'rotated difference scheme'.

The potential equation can be written locally in streamline coordinates (l, n) under the form

$$(1 - M^2)\phi_{ll} + \phi_{nn} = 0 \quad (15.1.7)$$

where the local streamline coordinate system (l, n) is related to the Cartesian coordinates by a rotation of angle α , with $\cos \alpha = u/q$, where q is the modulus of the velocity vector $\vec{v} = q\vec{1}_l = u\vec{1}_x + v\vec{1}_y$ (see Figure 15.1.4).

Hence, one has

$$\begin{aligned} x &= l \cos \alpha - n \sin \alpha = \frac{ul - vn}{q} \\ y &= l \sin \alpha + n \cos \alpha = \frac{vl + un}{q} \end{aligned} \quad (15.1.8)$$

and applying standard transformation rules

$$\begin{aligned} \phi_{ll} &= \frac{u^2 \phi_{xx} + 2uv \phi_{xy} + v^2 \phi_{yy}}{q^2} \\ \phi_{nn} &= \frac{v^2 \phi_{xx} - 2uv \phi_{xy} + u^2 \phi_{yy}}{q^2} \end{aligned} \quad (15.1.9)$$

The rotated difference scheme consists in differencing all the derivatives contributing to ϕ_{nn} centrally while the derivatives contributing to ϕ_{ll} are upwind differenced at supersonic points. For instance, equation (15.1.1) is applied for ϕ_{xx} when used for the estimation of ϕ_{nn} while equation (15.1.2) will be applied in the computation of ϕ_{ll} for the same second derivative ϕ_{xx} . Similarly, the other derivatives such as ϕ_{xy} are discretized centrally in ϕ_{nn} as

$$\begin{aligned} \phi_{xy}^{(C)} &= \frac{1}{4\Delta x \Delta y} (\delta_x^+ + \delta_x^-) (\delta_y^+ + \delta_y^-) \phi_{ij} = \frac{1}{\Delta x \Delta y} \bar{\delta}_x \bar{\delta}_y \phi_{ij} \\ &= \frac{1}{4\Delta x \Delta y} (\phi_{i+1, j+1} - \phi_{i+1, j-1} - \phi_{i-1, j+1} + \phi_{i-1, j-1}) \end{aligned} \quad (15.1.10)$$

and in the upwind manner in ϕ_{ll} as

$$\begin{aligned} \phi_{xy}^{(B)} &= \frac{1}{\Delta x \Delta y} \delta_y^- \delta_x^- \phi_{ij} = \frac{1}{\Delta x \Delta y} (\phi_{ij} - \phi_{i-1, j} - \phi_{i, j-1} + \phi_{i-1, j-1}) \\ &= \phi_{xy}^{(C)} - \frac{\Delta x}{2} \phi_{xxy} - \frac{\Delta y}{2} \phi_{xyy} \end{aligned} \quad (15.1.11)$$

These expressions are written for $u > 0$ and $v > 0$. If the sign of these components is negative the upwinding direction has to be reversed. The corresponding artificial viscosity terms can be obtained by comparing the upwinded expressions

with the central differenced ones, and one obtains, with equations (15.1.3) and (15.1.11), for $u > 0, v > 0$,

$$\phi_{ii}^{(B)} = \phi_{ii}^{(C)} - \frac{u^2}{q} \Delta x \phi_{xxx} - \frac{v^2}{q} \Delta y \phi_{yyy} - \frac{uv}{q} (\Delta x \phi_{xxy} + \Delta y \phi_{xyy}) \quad (15.1.12)$$

When all the terms are grouped, an artificial viscosity term (AVT) appears of the form

$$\text{AVT} = \frac{1}{q^2} (M^2 - 1) [\Delta x (u^2 \phi_{xxx} + uv \phi_{xxy}) + \Delta y (v^2 \phi_{yyy} + uv \phi_{xyy})] \quad (15.1.13)$$

and the centrally differenced equation becomes

$$(1 - M^2) \phi_{ii}^{(C)} + \phi_{nn}^{(C)} = \text{AVT} \quad (15.1.14)$$

It is to be noted from equation (15.1.3) that the artificial viscosity terms must be discretized in an appropriate way corresponding to their original derivation. For instance, ϕ_{xxx} in equation (15.1.3) has to be upwind differenced as $\delta_x^- \delta_x^2 \phi_{ij}$ and not otherwise. Similar conclusions appear when equation (15.1.11) is worked out in detail. It is a general rule that the artificial viscosity terms have to be differenced with formulas containing upwind contributions (see Problem 15.2).

Example 15.1.1 Murman and Cole method on the small disturbance equation

Consider the small disturbance equation for the perturbation potential Φ , in the form (13.2.11):

$$[1 - M_\infty^2 - (\gamma + 1)M_\infty^2 \Phi_x] \Phi_{xx} + \Phi_{yy} = 0 \quad (E15.1.1)$$

The discretization is performed on a Cartesian mesh for thin airfoils. Designating by A the coefficient of the Φ_{xx} term, A_{ij} is obtained from a second-order central difference of Φ_x :

$$\Phi_{x,ij} = \frac{\Phi_{i+1,j} - \Phi_{i-1,j}}{2\Delta x} \quad (E15.1.2)$$

where the central discretization in the subsonic region would be, with $\Delta x = \Delta y$,

$$A_{ij}(\Phi_{i+1,j} - 2\Phi_{ij} + \Phi_{i-1,j}) + (\Phi_{i,j+1} - 2\Phi_{ij} + \Phi_{i,j-1}) = 0 \quad (E15.1.3)$$

In the supersonic region, the first term is backward differenced:

$$A_{i-1,j}(\Phi_{ij} - 2\Phi_{i-1,j} + \Phi_{i-2,j}) + (\Phi_{i,j+1} - 2\Phi_{ij} + \Phi_{i,j-1}) = 0 \quad (E15.1.4)$$

The two equations can be combined with the introduction of a switch factor μ , such that $\mu = 0$ for subsonic flows or $A > 0$ and $\mu = 1$ in the supersonic regions where $A < 0$:

$$\begin{aligned} \mu_{ij} A_{i-1,j} (\Phi_{ij} - 2\Phi_{i-1,j} + \Phi_{i-2,j}) + (\Phi_{i,j+1} - 2\Phi_{ij} + \Phi_{i,j-1}) \\ + (1 - \mu_{ij}) A_{ij} (\Phi_{i+1,j} - 2\Phi_{ij} + \Phi_{i-1,j}) = 0 \end{aligned} \quad (E15.1.5)$$

This scheme is not in conservative form, since the switch coefficient is taken at point (i, j) for the subsonic as well as the supersonic term. A conservative form is obtained when μ is taken at $(i-1, j)$ with the first term. In this case the scheme can be written as, see Problem 15.9,

$$A_{ij} \delta_x^2 \Phi_{ij} + \delta_y^2 \Phi_{ij} = \mu_{ij} A_{ij} \delta_x^2 \Phi_{ij} - \mu_{i-1,j} A_{i-1,j} \delta_x^2 \Phi_{i-1,j} \quad (\text{E15.1.6})$$

The boundary condition (13.2.13) is introduced in the discretization via the second y derivative of Φ at points $i, j = 1$ of the airfoil surface on the x axis (see Figure 13.2.1). Considering Figure 14.1.1 and a fictive point $j = 0$, symmetric of $j = 1$,

$$\delta_y^2 \Phi_{i,1} = \Phi_{i,2} - 2\Phi_{i,1} + \Phi_{i,0} \quad (\text{E15.1.7})$$

The value at $j = 0$ is obtained by expressing the boundary condition as a central difference

$$v_{i,1} = \frac{\Phi_{i,2} - \Phi_{i,0}}{2\Delta y} = f'_i \quad (\text{E15.1.8})$$

and the second y derivative becomes

$$\delta_y^2 \Phi_{i,1} = 2(\Phi_{i,2} - \Phi_{i,1} - \Delta y f'_i) \quad (\text{E15.1.9})$$

15.1.2 Artificial viscosity—conservative potential equation

The expression (15.1.13) is not in conservative form and cannot be used for the conservative potential equation, which requires that all the terms appear in divergence form. Hence, one should be able to write the artificial viscosity terms under the form of the divergence of a vector quantity,

$$\text{AVT} = \vec{\nabla} \cdot \vec{A} = A_x + B_y \quad (\text{15.1.15})$$

in such a way that the potential equation becomes

$$\vec{\nabla} \cdot (\rho \vec{\nabla} \phi + \vec{A}) = 0 \quad (\text{15.1.16})$$

This equation would subsequently be centrally discretized everywhere in the flow field, with \vec{A} going to zero as the mesh size is reduced.

The method followed by Jameson (1975) was to adopt a form for \vec{A} that contained, to the highest-order derivatives of ϕ , the corresponding terms of equation (15.1.13), multiplied by the density ρ .

If one considers the first term of equation (15.1.13), the x -component of equation (15.1.15) should contain the expression

$$\Delta x \frac{\rho}{q^2} (M^2 - 1) (u^2 \phi_{xxx} + uv \phi_{xxy})$$

and an obvious generalization is

$$A_x = \left[\frac{\rho}{q^2} (M^2 - 1) (u^2 \phi_{xx} + uv \phi_{xy}) \right] \Delta x \quad (\text{15.1.17})$$

The artificial viscosity terms are switched off for subsonic flows by the switching function

$$\mu = \max \left[0, \left(1 - \frac{1}{M^2} \right) \right] \quad (15.1.18)$$

and the artificial viscosity terms of Jameson can be written, for $u > 0, v > 0$, as

$$A = \frac{\rho}{c^2} \mu (u^2 u_x + uvv_x) \Delta x \quad (15.1.19)$$

$$B = \frac{\rho}{c^2} \mu (uvu_y + v^2 v_y) \Delta y \quad (15.1.20)$$

Applying equation (13.5.7) with $\phi_t = 0$, these expressions can be written in a very convenient way as derivatives of the density ρ , since

$$\rho_x = -\frac{\rho}{c^2} \vec{v} \cdot \frac{\partial \vec{v}}{\partial x} = -\frac{\rho}{c^2} (uu_x + vv_x) \quad (15.1.21)$$

$$\rho_y = -\frac{\rho}{c^2} \vec{v} \cdot \frac{\partial \vec{v}}{\partial y} = -\frac{\rho}{c^2} (uu_y + vv_y) \quad (15.1.22)$$

and the artificial viscosity terms become

$$\vec{A} = -\mu (u \rho_x \Delta x \vec{1}_x + v \rho_y \Delta y \vec{1}_y) \quad (15.1.23)$$

where the derivatives of the density are *upwind differenced*.

These terms are of first order and reduce the overall second-order accuracy of the subsonic regions to first-order accuracy in the supersonic zones. Second-order variants of the conservative artificial viscosity can be found in Jameson (1976a) and Caughey and Jameson (1982).

15.1.3 Artificial compressibility

The form of equation (15.1.23) leads to the concept of *artificial compressibility*. Indeed, with equation (15.1.23) the potential equation (15.1.16) can be written as follows:

$$\frac{\partial}{\partial x} (\bar{\rho} \phi_x) + \frac{\partial}{\partial y} (\bar{\rho} \phi_y) = 0 \quad (15.1.24)$$

with

$$\begin{aligned} \bar{\rho} &= \rho - \mu \rho_x \Delta x \\ \bar{\bar{\rho}} &= \rho - \mu \rho_y \Delta y \end{aligned} \quad (15.1.25)$$

This form was introduced by Holst and Ballhaus (1979).

In curvilinear coordinates, one would have, instead of equation (15.1.24),

$$\frac{\partial}{\partial \xi} \left(\bar{\rho} \frac{U}{J} \right) + \frac{\partial}{\partial \eta} \left(\bar{\bar{\rho}} \frac{V}{J} \right) = 0 \quad (15.1.26a)$$

with

$$\begin{aligned}\bar{\rho} &= \rho - \mu \rho_{\xi} \Delta \xi \\ \bar{\rho} &= \rho - \mu \rho_{\eta} \Delta \eta\end{aligned}\quad (15.1.26b)$$

The implications of equations (15.1.24) and (15.1.26a) are extremely important. These equations show indeed that the correct discretization of the supersonic regions, which has to be consistent with the physical upstream regions of dependence, can be fully described and obtained by an upwind estimation of the density, according to equations (15.1.25) and (15.1.26b). This upwinding is introduced prior to discretization and the resulting equation is then treated centrally as in the subsonic case.

Example 15.1.2 Discretization on a Cartesian mesh

With a finite difference scheme on a Cartesian mesh and a discretization of the form (14.1.1), the artificial densities are needed at the mid-points $(i \pm 1/2, j)$ and $(i, j \pm 1/2)$. Hence, if $u_{i+1/2, j} > 0$,

$$\bar{\rho}_{i+1/2, j} = \rho_{i+1/2, j} - \mu_{ij}(\rho_{i+1/2, j} - \rho_{i-1/2, j}) \quad (E15.1.10)$$

and if $u_{i+1/2, j} < 0$,

$$\bar{\rho}_{i+1/2, j} = \rho_{i+1/2, j} + \mu_{i+1, j}(\rho_{i+1/2, j} - \rho_{i+3/2, j}) \quad (E15.1.11)$$

and similar relations for $\bar{\rho}$. If $v_{i, j+1/2} > 0$,

$$\bar{\rho}_{i, j+1/2} = \rho_{i, j+1/2} - \mu_{ij}(\rho_{i, j+1/2} - \rho_{i, j-1/2}) \quad (E15.1.12)$$

and if $v_{i, j+1/2} < 0$,

$$\bar{\rho}_{i, j+1/2} = \rho_{i, j+1/2} + \mu_{i, j+1}(\rho_{i, j+1/2} - \rho_{i, j+3/2}) \quad (E15.1.13)$$

Another form of the artificial density was introduced independently by Eberle (1977). If the supersonic influence is taken into account by an upwind effect on the mass flux, one can estimate these fluxes in a point H situated in the streamwise direction at a distance Δl upstream of the discretization point P (Figure 15.1.4).

Hence,

$$(\rho u)_H = (\rho u)_P - \Delta l \frac{\partial(\rho u)}{\partial l} \quad (15.1.27)$$

The second term can be approximated by

$$\frac{\partial}{\partial l}(\rho u) = \frac{\partial}{\partial l} \left(\rho q \frac{u}{q} \right) \simeq \frac{u}{q} \frac{\partial(\rho q)}{\partial l} \quad (15.1.28)$$

neglecting the local effect of the streamline curvature. With equation (13.5.7), one obtains

$$\frac{\partial \rho}{\partial l} = - \frac{\rho q}{c^2} \frac{\partial q}{\partial l} \quad (15.1.29)$$

and

$$\Delta l \frac{\partial}{\partial l}(\rho u) = \Delta l u \left(1 - \frac{1}{M^2} \right) \frac{\partial \rho}{\partial l} \quad (15.1.30)$$

Similar expressions are obtained for the other mass flux components and hence the potential equation can be discretized as

$$\bar{\nabla} \cdot (\bar{\rho} \bar{\nabla} \phi) = 0 \quad (15.1.31)$$

where $\bar{\rho}$ is the artificial density defined by

$$\bar{\rho} = \rho - \mu \frac{\partial \rho}{\partial l} \Delta l = \rho - \mu \delta l \left(\frac{u}{q} \rho_x + \frac{v}{q} \rho_y \right) \quad (15.1.32)$$

Hafez *et al.* (1978) obtained a very similar expression where, instead of equation (15.1.32), one computes $\bar{\rho}$ by the relations

$$\bar{\rho} = \rho - \mu \left(\frac{u}{q} \rho_x \Delta x + \frac{v}{q} \rho_y \Delta y \right) \quad (15.1.33)$$

Note that the derivations in the artificial density are upwind differenced, according to the sign of u, v or of (U, V) . Equation (15.1.31) with either (15.1.32) or (15.1.33) is an extremely convenient form, particularly with finite element formulations, since third-order derivatives are explicitly avoided, and is widely used in many transonic potential flow computations. This concept of artificial, upwinded density has actually some analogy to an upwinding method introduced by Hughes and Brooks (1982) for the treatment of advective-diffusive transport equations and further generalized to the Euler equations by Hughes and Mallet (1986).

In practical computations, it appeared that some empirical corrections had to be introduced on the switching function μ , in order to ensure better stability in shock regions as a consequence of the ambiguity of μ at the sonic transition. Various expressions have been attempted, such as

$$\mu = \max \left[0, \left(1 - \frac{M_c^2}{M^2} \right) \right] C \cdot M^2$$

where M_c^2 is a cut-off Mach number of the order of $M \approx 0.95$ and C a coefficient between one and two. The cut-off Mach number M_c activates the switching function in the small subsonic region $M_c \leq M \leq 1$, close to the sonic lines. This appears to improve the stability in some cases. The constant C and the additional factor M^2 increase the amount of artificial viscosity and have also a stabilizing effect.

Other variants can be found in the literature; see, for instance, Habashi and Hafez (1981). Figure 15.1.5 compares various options for the switching function as applied to the transonic flow over a NACA 0012 profile at zero angle of incidence and free-stream Mach number of 0.85. The calculations are performed with a finite element discretization and artificial compressibility. The

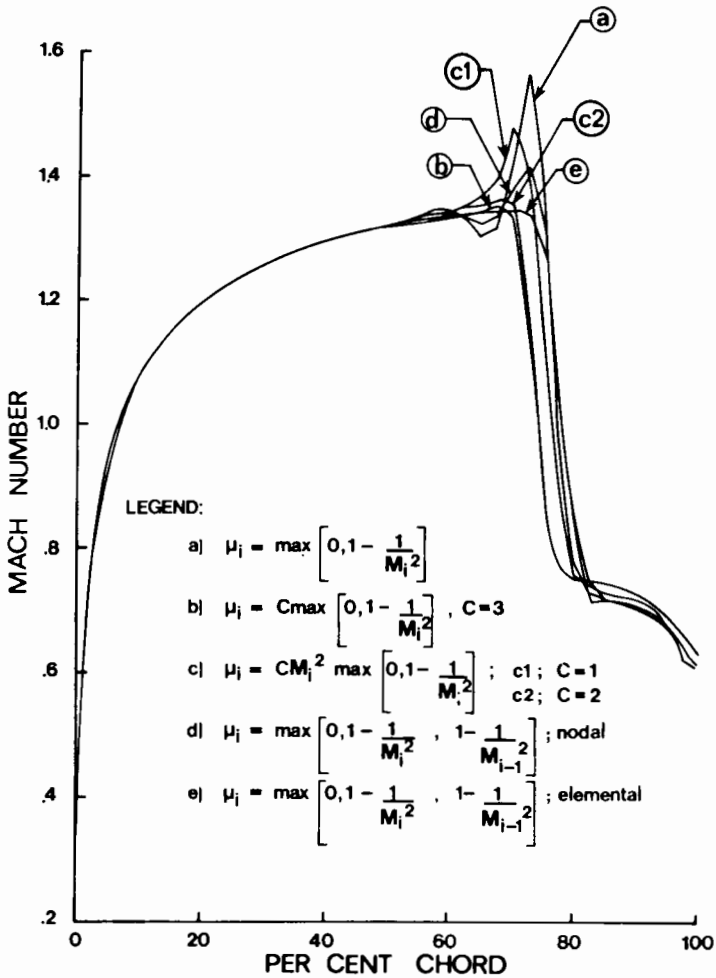


Figure 15.15 Comparison of various options for the switching function as applied to a finite element computation with artificial compressibility by Habashi and Hafez (1981). (Courtesy M. Hafez, University of California, Davis, USA)

considerable influence of a proper choice of the switching function on the shock position and the shock resolution can clearly be seen.

The concept of artificial density is, however, superseded by the flux upwinding approach, which completely removes the sonic transition uncertainty of the switching function.

15.1.4 Artificial flux or flux upwinding

The upwinding techniques leading to artificial viscosity or artificial compressibility concepts have been widely used, but a more precise formulation can be

defined, inspired by the developments of controlled, monotone schemes for Euler equations (see Chapter 20).

These developments attempt to control the generation of non-linear pre- or postshock oscillations (over- or undershoots) in the vicinity of strong discontinuities such as shocks or contact discontinuities. Conditions are imposed in order to prevent the appearance of unwanted peaks in the numerical solution instead of having them occur and damped afterwards by the addition of artificial dissipation terms.

These concepts have some application in transonic potential flow problems as a consequence of the unsatisfactory treatment of the sonic transition region by the artificial viscosity or density methods. Indeed, the switching function defined by equation (15.1.18) goes through zero at sonic points and hence the dissipation vanishes around the sonic transition region. This can lead to the appearance of expansion shocks or to instabilities when the sonic point is passed with steep gradients, for instance in leading edge regions of certain profiles. It is known that the one-dimensional time-dependent small-disturbance equation with the Murman–Cole switching will not damp an initial expansion shock (Jameson, 1976b; Goorjian and Van Buskirk, 1981).

In order to avoid these effects the switching at sonic points should be better controlled in such a way as to avoid the possibilities of unwanted expansion peaks.

These concepts have been introduced initially by Engquist and Osher (1980), and applied by Goorjian and Van Buskirk (1981) for the small disturbance equations and by Boerstael (1981) and Osher (1982) for the full potential equation. Further applications are discussed in Hafez (1983), Boerstael and Kassies (1983), Goorjian *et al.* (1983), Hafez *et al.* (1984), Osher *et al.* (1985) and Shankar *et al.* (1985).

A first observation can be made with regard to the concept of flux upwinding. The artificial density form of equation (15.1.32) can be written as an artificial flux, since one has, using equation (15.1.29),

$$\begin{aligned} \frac{\partial(\rho q)}{\partial l} &\equiv (\rho q)_l = -\frac{\rho}{a^2} q^2 \frac{\partial q}{\partial l} + \rho \frac{\partial q}{\partial l} = \rho(1 - M^2) \frac{\partial q}{\partial l} \\ &= q \left(1 - \frac{1}{M^2}\right) \frac{\partial \rho}{\partial l} \end{aligned} \quad (15.1.34)$$

where l is the streamwise direction and the subscript l indicates derivatives with respect to the streamwise direction l . Hence, the corrected upwinded flux $\tilde{\rho}q$ can be written in supersonic regions as

$$\tilde{\rho}q = \rho q - q \left(1 - \frac{1}{M^2}\right) \frac{\partial \rho}{\partial l} \Delta l \quad (15.1.35a)$$

or

$$\tilde{\rho}q = \rho q - \frac{\partial(\rho q)}{\partial l} \Delta l \quad (15.1.35b)$$

In order to obtain a better treatment of the sonic region and to avoid expansion shocks, the upwinded flux correction is referred to the sonic mass flux value ρ^*q^* . The artificial mass flux is defined by

$$\overline{\rho q} = \rho q - \frac{\partial}{\partial l} [v(\rho q - \rho^*q^*)] \Delta l \quad (15.1.36)$$

where

$v = 0$ for subsonic flow and at the sonic line, that is for $M \leq 1$ or $q \leq q^*$ or $\rho \geq \rho^*$
 $v = 1$ for supersonic flows, that is $M > 1$ or $q > q^*$ or $\rho < \rho^*$

This allows a clear distinction between subsonic, supersonic, sonic and shock points while the artificial density methods allow only a distinction between subsonic and supersonic points (see Figure 15.1.6).

The discretized form of equation (15.1.36) will be written as follows, for instance at a face centre of a two-dimensional cell:

$$\begin{aligned} (\overline{\rho q})_{i+1/2,j} = & (\rho q)_{i+1/2,j} - v_{i+1/2,j}(\rho q - \rho^*q^*)_{i+1/2,j} \\ & + v_{i-1/2,j}(\rho q - \rho^*q^*)_{i-1/2,j} \end{aligned} \quad (15.1.37)$$

and similar expressions at other points.

At subsonic points the artificial or upwinded mass flux (15.1.36) gives the same result as the artificial density, since ρ^*q^* is constant for steady flows, depending only on the flow conditions at infinity (see Problem 15.5).

At a subsonic point, $M < 1$ both at $(i-1/2, j)$ and $(i+1/2, j)$ and

$$(\overline{\rho q})_{i+1/2,j} = (\rho q)_{i+1/2,j} \quad \text{for a subsonic point} \quad (15.1.38)$$

At a supersonic point, $M > 1$ both at $(i-1/2, j)$ and $(i+1/2, j)$ and

$$(\overline{\rho q})_{i+1/2,j} = (\rho q)_{i-1/2,j} \quad \text{for a supersonic point} \quad (15.1.39)$$

At a sonic point transition, from subsonic to supersonic velocities, $q > q^*$ ($M > 1$) at $(i+1/2, j)$ but $q < q^*$ or $M < 1$ at $(i-1/2, j)$ (Figure 15.1.6), equation (15.1.37) reduces to

$$(\overline{\rho q})_{i+1/2,j} = (\rho^*q^*) \quad \text{at a sonic point transition} \quad (15.1.40)$$

Note that this guarantees that expansion shocks will not occur, since in this case one would have $(\rho q)_{i+1/2,j} < \rho^*q^*$.

At a shock transition, $q < q^*$ ($M < 1$) at $(i+1/2, j)$ and $q > q^*$ ($M > 1$) at $(i-1/2, j)$, equation (15.1.37) becomes (see also Problem 15.6)

$$(\overline{\rho q})_{i+1/2,j} = (\rho q)_{i+1/2,j} + (\rho q - \rho^*q^*)_{i-1/2,j} \quad (15.1.41)$$

At shock points, the switching ensures that there is only one mesh point in the shock region since the corresponding cell is treated either as fully supersonic or fully subsonic as soon as the shock cell is left. This generates very sharp shocks, as demonstrated by Figure 15.1.7, from Hafez *et al.* (1984), for the flow

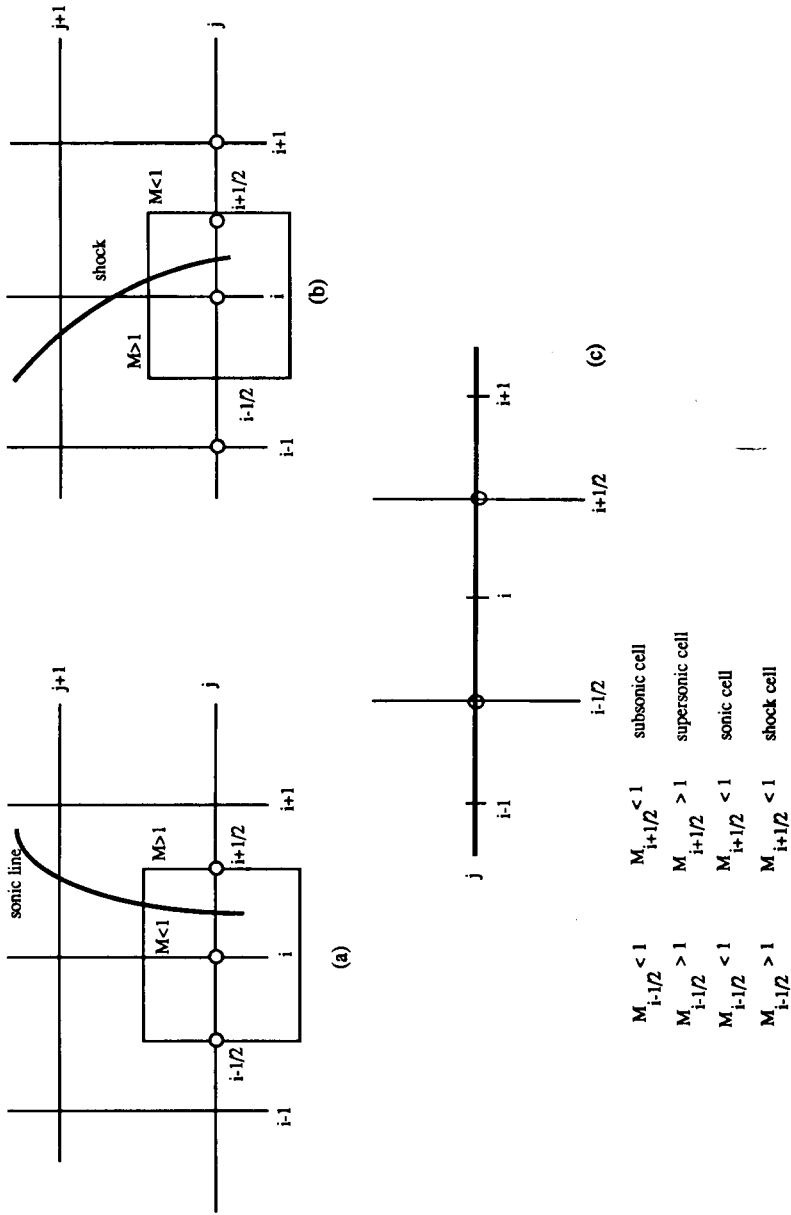


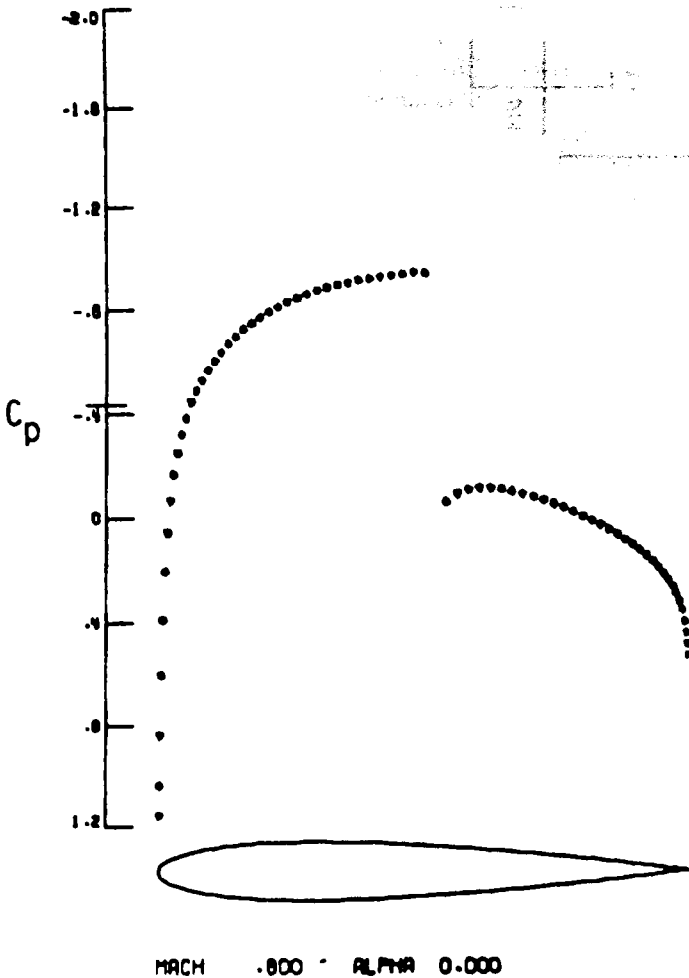
Figure 15.1.6 Flux upwinding at sonic and shock point transitions. (a) Sonic cell. (b) Shock cell. (c) Computational cell attached to point i

over a NACA 0012 airfoil at incident Mach number of 0.8 and zero angle of incidence, to be compared with Figure 15.1.5, and at $M_\infty = 0.75$ and 2° incidence.

When the potential equation is written in curvilinear coordinates, the flux terms are written as

$$\rho \frac{v^\alpha}{J} = (\rho q) \frac{v^\alpha}{qJ} \quad (15.1.42)$$

and the first mass flux factor (ρq) is unwinded as described above in the coordinate direction corresponding to the index α of the considered flux component. Hence, the conservative potential equation will be discretized in



(a)

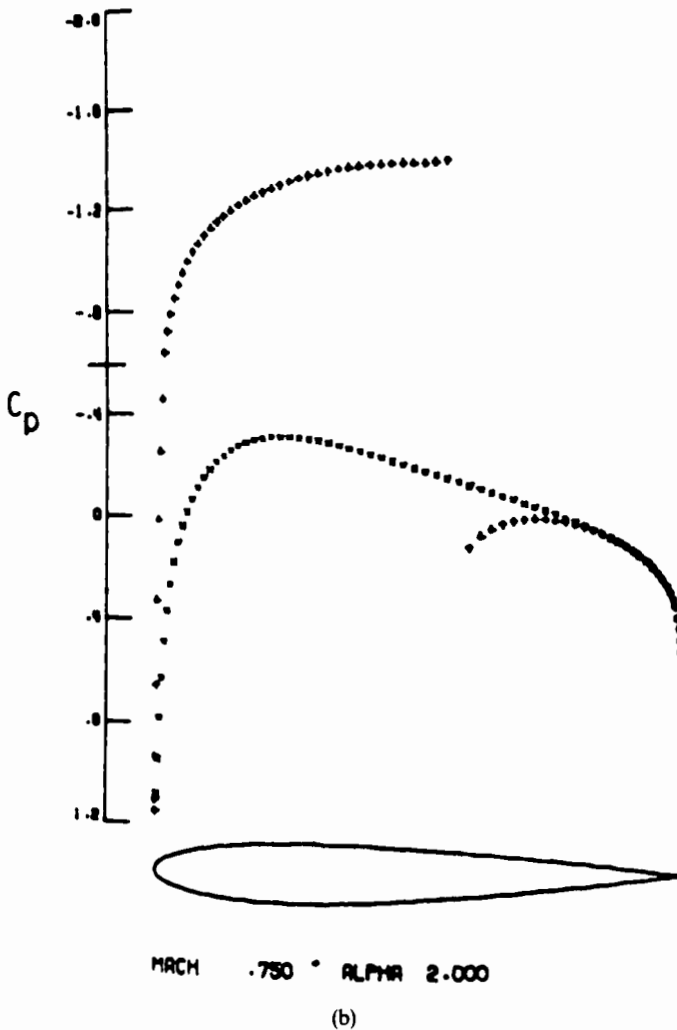


Figure 15.17 Pressure distribution on a NACA 0012 airfoil at (a) $M = 0.8$ and zero angle of attack, (b) $M = 0.75, 2^\circ$ incidence, calculated with flux upwinding. (From Hafez *et al.*, 1984)

finite difference form, with the artificial mass flux approach, as

$$\delta_{\xi}^{-} \left[(\bar{\rho q})_{i+1/2,j} \left(\frac{U}{Jq} \right)_{i+1/2,j} \right] + \delta_{\eta}^{-} \left[(\bar{\rho q})_{i,j+1/2} \left(\frac{V}{Jq} \right)_{i,j+1/2} \right] = 0 \quad (15.1.43)$$

In supersonic flows, the upwinding directions have to correspond to time-like directions, as defined in Chapter 13. Hence the ξ term, for instance, of equation (15.1.41) will be upwinded only if the associated contravariant velocity

component is supersonic, that is if

$$\frac{U}{\sqrt{g^{11}}} > c \quad (15.1.44)$$

When this condition is not satisfied, the ξ derivative is centrally discretized without upwinding. The reason behind this rule can be understood from an explicit calculation of the Murman and Cole procedure applied to the ξ -derivative term of the potential equation written in curvilinear coordinates (see Problem 15.8).

All the transonic potential calculations performed with the upwinded mass flux instead of the upwinded density indicate improved shock and sonic point treatment, improved stability with strong gradients and better convergence properties. In particular, Goorjian *et al.*, (1983) present some interesting comparisons between the two approaches (see also Volpe, 1986). In addition, the flux upwinding does not require any user—specified constants. Therefore this approach to the transonic treatment of the potential equation is to be recommended.

In conclusion, it is seen that the original type of differencing method of Murman and Cole has evolved into the artificial density and flux upwinding concepts, which, when introduced before discretization, allow a full subsonic type of discretization to be performed on the potential equation while correctly taking into account the supersonic properties of the flow.

In addition, the entropy condition is thereby automatically fulfilled ensuring that no expansion shocks will occur and that the shocks captured by the computation will be physical compression shocks.

It has to be remembered, however (see Section 2.9.2 in Volume 1), that the shock produced by the isentropic potential model is an isentropic shock, in contrast with the exact Rankine–Hugoniot shocks which are connected to discontinuous positive entropy variations. As a consequence, the shock intensity will differ from the intensity obtained from solution of the Euler equations, but also the position of the shock might be different from the one obtained from an Euler solution. We will come back to this in a later section, 15.3, where some approximate methods will be discussed that allow the potential flow solutions to be corrected for non-isentropic effects.

Similar differences with respect to the captured shocks are obtained between the non-conservative and conservative computations. It is a general observation that non-conservative computations produce shocks that are closer to the experimental data than the conservative ones. This comes about because the mass deficit due to non-conservation of mass flux at the shock, in the non-conservative calculations, simulates in some sense the effects of shock–boundary layer interactions occurring in practice. However, the correct way is to respect the conservation laws during computations and add the physical interactions, such as a boundary layer viscid–inviscid interaction, in order to have good control of the various effects contributing to a given flow configuration.

15.2 ITERATION SCHEMES FOR POTENTIAL FLOW COMPUTATIONS

Once a proper discretization and a linearization procedure for the density have been set up, the algebraic system of mesh point values has to be solved by an appropriate method.

For subsonic problems, direct methods would leave only iterations on the density non-linearity and are most appropriate when the number of mesh points is not too high.

For very fine meshes and for three-dimensional flow problems with a large number of unknowns, direct methods will generally lead to prohibitive computational times and computer storage requirements. In these cases, iterative methods for the solution of the algebraic system of equations will be more appropriate. In addition, preconditioning, multi-grid and conjugate gradient methods have led to the development of very efficient iterative schemes.

As described in the introduction, this step in the solution of potential flow equations is an essential part of the whole computation. It has to ensure that the iterative process towards the final solution is convergent and, secondly, that this convergent process is as fast as possible.

An additional problem arises in the computation of transonic and supersonic flows. In order to ensure the convergence of the iterative method, the problems referred to earlier, and connected to the fact that the passage to supersonic regions makes the Jacobian matrix K_T non-positive definite, have to be solved. The iterative technique will have to be chosen in such a way as to maintain the sign of the quadratic form in equation (14.4.10) which is equivalent to the requirement that the successive computed values of the potential all satisfy the conditions imposed by the supersonic region of dependence.

15.2.1 Line relaxation schemes

The initial success of Murman and Cole's approach for transonic flows was not only due to the introduction of the type differencing but essentially to the result of the application of a line relaxation method to solve the system of algebraic equations by a series of tridiagonal systems along the vertical lines perpendicular to the flow directions, sweeping with the flow. Furthermore, it can be shown by a Von Neumann analysis of the iterative scheme, following Section 12.1.5 in Volume 1, that an explicit method is unstable (see Problem 15.12).

A standard line overrelaxation (SLOR) iteration method, following equation (12.2.43) in Volume 1, can be applied to equation (15.1.5) on a Cartesian mesh, with $\Delta x = \Delta y$. In the supersonic region the scheme becomes

$$(1 - M^2)_{ij}(\phi_{i-2,j}^{n+1} - 2\phi_{i-1,j}^{n+1} + \phi_{ij}^{\overline{n+1}}) + (\phi_{i,j+1}^{\overline{n+1}} - 2\phi_{ij}^{\overline{n+1}} + \phi_{i,j-1}^{\overline{n+1}}) = 0 \quad (15.2.1a)$$

$$\phi^{n+1} = \phi^n + \omega(\phi^{\overline{n+1}} - \phi^n) \quad (15.2.1b)$$

This equation can be written in correction form $P\Delta\phi = -R^n$ (see Chapter 12),

where $\Delta\phi = \phi^{n+1} - \phi^n$ and R^n is the residual equal to the left-hand side of equation (15.2.1) taken at the level n :

$$(M^2 - 1)_{ij}(\omega \Delta\phi_{i-2,j} - 2\omega \Delta\phi_{i-1,j} + \Delta\phi_{ij}) - (\Delta\phi_{i,j+1} - 2\Delta\phi_{ij} + \Delta\phi_{i,j-1}) = \omega R_{ij}^n \quad (15.2.2)$$

This relaxation scheme can be analysed by representing the conditioning operator P as a differential operator, following the presentation of Section 12.5. This leads to the representation (see Problem 15.13)

$$(M^2 - 1)[\omega E_x^{-1} \delta_x^2 + (1 - \omega)]\Delta\phi_{ij} - \delta_y^2 \Delta\phi_{ij} = \omega R_{ij}^n \quad (15.2.3)$$

where the standard finite difference operators are used (equation (14.1.2)); E is the shift operator $E_x \phi_{ij} = \phi_{i+1,j}$ and δ^2 is the central second difference operator. The equivalent artificial time-dependent formulation is

$$(M^2 - 1)[\omega \phi_{xxt} + (1 - \omega)\phi_t] - \phi_{yyt} = \frac{\omega}{\tau} R \quad (15.2.4)$$

where $\Delta\phi$ has been represented by the pseudo-time derivative $\phi_t \simeq \Delta\phi/\tau$, with τ being a fictive time step, and where ϕ_{xxt} is backward differenced. R in the right-hand side has now to be interpreted as the differential potential equation.

This iterative scheme has to be evaluated in function of the compatibility of the iterative process with the condition that $\Delta\phi$ should not leave the proper region of dependence (see Section 14.4).

The ϕ_{yy} term is represented in equation (15.2.3) by $\delta_y^2 \phi^{n+1} + (\omega - 1)\delta_y^2 \phi^n$, but the appropriate procedure in the supersonic region is to march in the flow direction, such that ϕ_{ij}^{n+1} can be determined only in function of the new values $\phi_{i-2,j}^{n+1}$ and $\phi_{i-1,j}^{n+1}$ determined on the previous columns. This implies that ϕ_{yy} should be represented by $\delta_y^2 \phi^{n+1}$ in the supersonic region. Note that the scheme (15.2.1) satisfies this requirement for $\omega = 1$. For a general relaxation procedure, this condition can be satisfied by taking the y -derivative terms at the new level $n + 1$, instead of the intermediate level, introducing hereby a factor ω in front of the y second difference operator of equation (15.2.3).

An additional modification to the standard SLOR method has been introduced by Jameson (1974) for the treatment of the x -derivative terms. In the first term of equation (15.2.1), the second ϕ derivative is replaced by the expression

$$(\phi_{i-2,j}^n - 2\phi_{i-1,j}^{n+1} + 2\phi_{ij}^{n+1} - \phi_{ij}^n)$$

and the iterative scheme (15.2.1) is now replaced by

$$(1 - M^2)_{ij}(\phi_{i-2,j}^n - 2\phi_{i-1,j}^{n+1} + 2\phi_{ij}^{n+1} - \phi_{ij}^n) + (\phi_{i,j+1}^{n+1} - 2\phi_{ij}^{n+1} + \phi_{i,j-1}^{n+1}) = 0 \quad (15.2.5)$$

The conditioning operator becomes

$$2(M^2 - 1)\delta_x^- \Delta\phi_{ij} - \delta_y^2 \Delta\phi_{ij} = R_{ij}^n \quad (15.2.6)$$

and the equivalent artificial time-dependent equation is

$$\left[\frac{2(M^2 - 1)}{\Delta x} \phi_{xt} - \phi_{yyt} \right] = \frac{1}{\tau} R \quad (15.2.7)$$

This treatment leads to the appearance of a ϕ_{xt} term in the convergence operator P , where t is the artificial time, reflecting the convergence history.

The reason behind the introduction of this term comes from a more general analysis, performed by Jameson (1974), investigating the requirements on the operator P in order to maintain, during the iterative process, the appropriate regions of dependence in the supersonic zones.

A general iterative relaxation procedure applied to equation (15.1.4), or more generally to equation (15.1.7) in the local streamline coordinates, will lead to a time-dependent equation of the following form, as seen in Section 12.5 in Volume 1:

$$2\alpha\phi_{it} + 2\beta\phi_{nt} + \gamma\phi_t = (1 - M^2)\phi_{ii} + \phi_{nn} \quad (15.2.8)$$

where ϕ_t represents $\Delta\phi/\tau$ and where the residual in the right-hand side is taken at iteration level n .

For instance, applying a decomposition of the form (15.2.5) to the derivatives in the rotated difference scheme (15.1.14) leads to

$$\begin{aligned} \alpha &= (M^2 - 1) \left[\frac{\tau u}{\Delta x q} + \frac{\tau v}{\Delta y q} \right] \\ \beta &= \frac{1}{2} \frac{\tau v}{\Delta x q} \\ \gamma &= 0 \end{aligned} \quad (15.2.9)$$

where ϕ_{it} is differenced upwind in space, with respect to the local velocity direction, in order to provide the correct sign for increasing the magnitude of the matrix diagonal. The left-hand side of equation (15.2.8) can be diagonalized by the following transformation:

$$T = t - \frac{\alpha l}{M^2 - 1} + \beta n \quad (15.2.10)$$

leading to the equation

$$(1 - M^2)\phi_{ii} + \phi_{nn} + \left(\frac{\alpha^2}{M^2 - 1} - \beta^2 \right) \phi_{TT} - \gamma\phi_T = 0 \quad (15.2.11)$$

which is of the form

$$K\phi_{TT} + \gamma\phi_T = (1 - M^2)\phi_{ii} + \phi_{nn} \quad (15.2.12)$$

For subsonic flows, $K = \alpha^2/(1 - M^2) + \beta^2$ is always positive and equation (15.2.12) is hyperbolic in T ; hence a stationary solution $\phi_T = 0$ will be obtained

if the coefficient γ provides a positive damping. This requires

$$\gamma > 0 \quad \text{for subsonic flows } M < 1$$

On the other hand, for supersonic flows, the coefficients of ϕ_{ii} and ϕ_{nn} have opposite signs and the steady-state equation is hyperbolic in l , where l is a time-like direction. The iterative evolution has to respect this property and therefore equation (15.2.12) must remain hyperbolic in l . This requires that $K\phi_{TT}$ should have the opposite sign to ϕ_{nn} and hence $K < 0$, or

$$\alpha > \beta\sqrt{(M^2 - 1)} \quad \text{for } M > 1 \quad (15.2.13)$$

In addition, in order to maintain the hyperbolic character, no damping term is allowed and, therefore, γ should be zero. This is also confirmed by a Von Neumann analysis (Jameson, 1974). Hence

$$\gamma = 0 \quad \text{for } M > 1$$

These are necessary conditions to ensure the compatibility between the convergence process and the physical properties of the supersonic flow, but it does not guarantee the unconditional convergence to the steady-state solution. It shows, nevertheless, that the presence of a ϕ_{ii} term, with positive coefficient, increasing with Mach number, is necessary in the equivalent artificial time-dependent equations (15.2.8).

The modification in equation (15.2.5) introduces such a ϕ_{ii} term when marching with the flow direction, but this may not be the case with other iterative schemes. Even with relaxation schemes the intensity of the naturally introduced ϕ_{ii} term might not be sufficient to satisfy equation (15.2.13)—for instance in the vicinity of the sonic line where α as given by equation (15.2.9) approaches zero. In both cases, additional ϕ_{ii} terms can be introduced explicitly, for instance under the form

$$\alpha\phi_{ii} = \varepsilon \left(\frac{\tau}{\Delta x} \frac{u}{q} \phi_{xi} + \frac{\tau}{\Delta y} \frac{v}{q} \phi_{yi} \right) \quad (15.2.14)$$

where ϕ_{xi} and ϕ_{yi} are upwind differenced.

The parameter ε is a user-specified constant which should be proportional to Mach number in order to maintain stability of the scheme. However, a too large value of ε could slow down the convergence rate.

The SLOR technique is a simple and effective method for transonic flows although its convergence rate is not always very efficient. Nevertheless, it is one of the most widely used methods and can be very effectively coupled with multi-grid acceleration techniques.

A simple way of improving the convergence properties of line relaxation methods is to use a sequence of grids ranging from coarse to fine. The solution is computed initially on the coarser mesh and after a certain number of relaxation sweeps transferred to the next finer mesh. Since the line relaxation method is very effective in reducing the high-frequency components of the error, the

solution transferred to the next mesh will be closer to the exact solution than the first guess. If this is performed on a series of grids, the starting solution on the fine grid will already be a good guess and allow a substantial gain compared to a calculation with the initial solution used from the start on the fine mesh. This procedure is also of benefit because the line relaxation computation on the coarser meshes is relatively inexpensive compared to a relaxation sweep on the fine mesh.

For most of the schemes described in the previous sections, the line relaxation method will involve the solution of tridiagonal systems along each line. This can be done in a very effective way by applying the Thomas algorithm. Since relaxation along the n lines perpendicular to the streamlines gives the highest coefficients for the ϕ_{ii} terms, the 'natural' relaxation sweeping direction is in the streamwise direction solving along n lines.

15.2.2 Guidelines for resolution of the discretized potential equation

Once the proper region of dependence of supersonic flows has been introduced in the discretization, through one or the other form of artificial viscosity, density of flux upwinding, one could ask if direct methods can be applied, or any other method for the resolution of algebraic systems, next to relaxation techniques.

To gain more insight into the convergence process of transonic potential flow computations, Caspar (1980) studied a simple model problem, which allows a very enlightening analysis of the convergence properties and conditions of transonic numerical procedures. This analysis, which we will summarize in the following, explains the role of the artificial viscosity or upwinding in removing multiple solutions, as well as the effect of ϕ_{ii} terms in ensuring better convergence behaviour. Also, this simple model leads to certain guidelines for ensuring unconditional stability of the iterative process and explains, for instance, why subsonic potential codes can still converge in the presence of small, shock-free, supersonic pockets.

A uniform flow U_∞ in a rectangular domain is considered with an inflow section at $x = 0$ and an outlet section at $x = a$ (Figure 15.2.1). The boundary conditions are taken to be periodic in the x direction and Dirichlet conditions are imposed:

$$\phi(x, 0) = \phi(x, b) = U_\infty x \quad (15.2.15)$$

$$\phi(x + a, y) = \phi(x, y) + U_\infty a \quad (15.2.16)$$

The solution is given by the uniform flow

$$\phi(x, y) = U_\infty x \quad (15.2.17)$$

and the density

$$r = \frac{\rho}{\rho_\infty} = \left\{ 1 - \frac{\gamma - 1}{2} M_\infty^2 \frac{|\bar{\nabla} \phi|^2}{1 + [(\gamma - 1)/2] M_\infty^2} \right\}^{1/(\gamma - 1)} \equiv (1 - K |\bar{\nabla} \phi|^2)^{1/(\gamma - 1)} \quad (15.2.18)$$

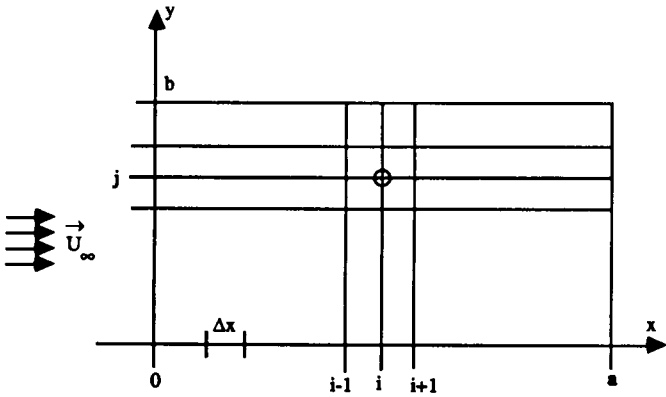


Figure 15.2.1 Model problem analysis with uniform flow

has the solution

$$r^* = (1 - K)^{1/(\gamma - 1)} = \left\{ \frac{1}{1 + [(\gamma - 1)/2]M_\infty^2} \right\}^{1/(\gamma - 1)} \tag{15.2.19}$$

since $|\bar{\nabla}\phi|^2 = U_\infty^2$. An orthogonal Cartesian finite difference mesh is defined with $(N + 1)$ points in the x direction and $(L + 2)$ points in the y direction (Figure 15.2.1), and the potential equation is differenced centrally, following equation (14.1.1):

$$L(\phi)_{ij} \equiv \bar{\nabla} \cdot (r \bar{\nabla} \phi)_{ij} = \frac{1}{\Delta x^2} (\delta_x^+ r_{i+1/2,j} \delta_x^- \phi_{ij}) + \frac{1}{\Delta y^2} (\delta_y^+ r_{i,j+1/2} \delta_y^- \phi_{ij}) = 0 \tag{15.2.20}$$

with

$$\begin{aligned} r_{i+1/2,j} &= \mu_x r_{i,j} \\ r_{i,j+1/2} &= \mu_y r_{i,j} \\ r_{i,j} &= r(|\bar{\nabla}\phi|_{i,j}^2) \\ |\bar{\nabla}\phi|_{i,j}^2 &= \left(\frac{\bar{\delta}_x \phi_{i,j}}{\Delta x} \right)^2 + \left(\frac{\bar{\delta}_y \phi_{i,j}}{\Delta y} \right)^2 \end{aligned} \tag{15.2.21}$$

Since the exact solution is known, the various iterative procedures can be analysed. Following the general framework developed in Chapter 12, Section 12.4, the iterative solution of equation (15.2.20), $P\Delta\phi = -R^n$, $\Delta\phi = \phi^{n+1} - \phi^n$, will converge for the non-singular conditioning operator P , if the convergence operator

$$G = 1 - P^{-1}K_T \tag{15.2.22}$$

where K_T is the Jacobian matrix $\partial L/\partial \phi$, has all its eigenvalues lower than one; that is the spectral radius of the matrix G should be lower than one. Note that when some eigenvalues reach the value of one, K_T is singular and hence multiple solutions of $R(\phi) = 0$ are possible (Ortega and Rheinboldt, 1970).

The eigenvalues of $K_T = \partial L/\partial \phi$ can easily be obtained for the present model problem, applying equation (14.4.8) at the point corresponding to the exact solution:

$$K_T = \left[\frac{r^*}{\Delta x^2} (1 - M_\infty^2) \delta_x^2 + \frac{r^*}{\Delta y^2} \delta_y^2 \right] \quad (15.2.23)$$

The operator P , on the other hand, is dependent on the selected iterative process.

The standard, subsonic, linearized iteration technique is defined by equation (14.4.1), with central difference operators, and the convergence operator P being the Laplace operator. This is actually a good approximation to the Jacobian matrix K_T and should therefore lead to rapid convergence. On the small-disturbance equation, equation (15.1.4), this choice corresponds to the iterative scheme

$$\phi_{xx}^{n+1} + \phi_{yy}^{n+1} = M^2 \phi_{xx}^n \quad (15.2.24)$$

On the full potential equation, one obtains the following scheme (also called the constant stiffness scheme in the finite element literature):

$$\rho^* (\Delta \phi_{xx} + \Delta \phi_{yy}) = -(\bar{\nabla} \rho \bar{\nabla} \phi)^n \quad (15.2.25)$$

where ρ^* is the density taken at a previous iteration.

These methods are very effective in subsonic flows, but are not valid in supersonic flows without appropriate modification, as discussed next. The convergence operator, obtained for the present model problem, is given by $P_{D/C}$, with $\sigma = \Delta x/\Delta y$:

$$P_{D/C} = \frac{r^*}{\Delta x^2} (\delta_x^2 + \sigma^2 \delta_y^2) \quad (15.2.26)$$

and hence the amplification matrix G becomes

$$G_{D/C} = M_\infty^2 \frac{\delta_x^2}{\delta_x^2 + \sigma^2 \delta_y^2} \quad (15.2.27)$$

The eigenvalues of this amplification operator can best be analysed by a Fourier representation for periodic boundary conditions in x . Denoting by λ the eigenvalues of the operator G , one obtains

$$\lambda_{D/C} = M_\infty^2 \frac{\sin^2 \Phi_x/2}{\sin^2 \Phi_x/2 + \sigma^2 \sin^2 \Phi_y/2} \quad (15.2.28)$$

where

$$\Phi_x = \frac{2\pi}{N}m = \frac{2\pi \Delta x}{a}m, \quad m = 1, \dots, N$$

$$\Phi_y = \frac{\pi l}{L+1} = \frac{\pi \Delta y}{b}l, \quad l = 1, \dots, L+1 \quad (15.2.29)$$

These eigenvalues are always lower than one for subsonic Mach numbers, which explains the rapid convergence of the method for subsonic flows (Gelder, 1971; Hirsch and Warzee, 1977; Shen, 1978).

For supersonic flows, there is a maximum value of Mach number, say M_s , above which the method will diverge since $\max \lambda_{D/C} \geq 1$. The maximum value of $\lambda_{D/C}$ at a given Mach number is obtained for the high frequencies $\Phi_x = \pi$ and for the low frequency in y , $\Phi_y = \pi/(L+1)$, and hence one has approximately

$$\max \lambda_{D/C} \approx M_\infty^2 \frac{1}{1 + \frac{\pi^2 \Delta x^2}{(4b^2)}} \quad (15.2.30)$$

The limiting Mach number M_s is given by

$$M_s^2 \approx 1 + \left(\frac{\pi \Delta x}{2b} \right)^2 > 1 \quad (15.2.31)$$

and the stability condition for supersonic flows is $M_\infty < M_s$.

Thus, the scheme can remain stable for slightly supersonic flows, but the limit decreases with the mesh size. This explains the observation of various authors that the subsonic codes still converge in the presence of shock-free, small, supersonic regions (Prince, 1978; Caspar *et al.*, 1979; Shen, 1978; Deconinck and Hirsch, 1980a).

When eigenvalues of G pass through one, eigenvalues of the Jacobian matrix K_T become zero, independently of the iterative operator P . This leads to multiple solutions of equation (15.2.20) as an explicit calculation shows (Caspar, 1980).

Artificial compressibility

If artificial compressibility is introduced (equation (15.1.25)) to account for the supersonic flow regions,

$$\tilde{r} = r - \mu \delta_x^- r \quad (15.2.32)$$

the Jacobian matrix becomes, replacing (15.2.23),

$$K_T|_{AC} = \frac{r^*}{\Delta x^2} [\delta_x^2 + \sigma^2 \delta_y^2 - M_\infty^2 (1 - \mu \delta_x^-) \delta_x^2] \quad (15.2.33)$$

The eigenvalues of $K_T|_{AC}$ are, with $I = \sqrt{-1}$,

$$\lambda(K_T|_{AC}) = \frac{-r^*}{\Delta x^2} 4 \{ \sin^2 \Phi_x / 2 + \sigma^2 \sin^2 \Phi_y / 2 - M_\infty^2 [1 - \mu(1 - e^{-I\Phi_x})] \sin^2 \Phi_x / 2 \} \quad (15.2.34)$$

Due to the complex factor $(1 - e^{-I\Phi_x})$, these eigenvalues can never be zero and hence the matrix $K_T|_{AC}$ is never singular (and positive definite). An explicit calculation confirms that multiple solutions do not appear (Caspar, 1980).

With the same Laplace iterative operator the amplification matrix $G_{D/AC}$ becomes

$$G_{D/AC} = G_{D/C}(1 - \mu\delta_x^-) \quad (15.2.35)$$

and the eigenvalues of $G_{D/AC}$ are given by

$$\begin{aligned} \lambda_{D/AC} &= \lambda_{D/C} [1 - \mu(1 - e^{-I\Phi_x})] \\ &= \lambda_{D/C} [1 + (M_\infty^2 - 1)e^{-I\Phi_x}] \frac{1}{M_\infty^2} \quad \text{when } M_\infty > 1 \end{aligned} \quad (15.2.36)$$

Hence, with artificial viscosity the linear Laplace direct method will be only *conditionally stable* with a limit proportional to Mach number. The limit is, however, larger than the limit value M_s obtained from equation (15.2.31), but still proportional to the mesh size. Therefore the stability limit is reduced when the mesh is refined. For instance, at the highest frequencies in x , $\Phi_x = \pi$, the modulus of the eigenvalue becomes, for $M_\infty > 1$,

$$|\lambda|_{D/AC} = |M_\infty^2 - 2| \frac{1}{1 + \sigma^2 \sin^2 \Phi_y / 2} \quad (15.2.37)$$

which is to be compared to equation (15.2.30) when $\Phi_y = \pi/(L+1)$; that is one should have $M_\infty^2 < (2 + M_s^2)$.

Jameson (1976a) has used the rapid convergence properties of the direct Laplace operator, applying fast Poisson solvers, to accelerate the overall iterative transonic convergence process by combining it with another method which would remove the high-frequency errors introduced in the supersonic regions by the non-convergent Laplace operator. Since the line relaxation method is effective for this purpose, one could apply several relaxation sweeps after each Poisson solver solution. This combined scheme converges for transonic flows with shocks at a much faster rate than relaxation alone (Jameson, 1976a), when five to eight relaxation sweeps are performed after each direct solution. The direct, Poisson solution leads to rapid convergence in the subsonic zones while the relaxation sweeps dominate the convergence behaviour in the supersonic regions.

Another approach has been followed by Ecer and Akay (1981) using a direct method for the solution of the algebraic system and a finite element discretization. Their analysis of the error propagation and amplification confirms the

results of the present model problem. These authors also deduce a sequence of increased artificial viscosity coefficients α in $\bar{\rho} = \rho - \alpha\mu(\partial\rho/\partial l)\Delta l$ in order to maintain convergence.

However, increasing the artificial viscosity to stabilize a conditionally convergent scheme can lead to inaccuracy in the shock position and intensity since the effect of the viscosity persists in the converged solution on a finite mesh. Therefore the artificial viscosity should be kept at a minimum value, while convergence should be enhanced by appropriate iteration techniques and additional terms, such as the ϕ_{xt} terms mentioned above.

The addition of ϕ_{xt} terms to the iteration scheme can be performed in various ways, when coupled to direct methods for the algebraic system.

Introduction of ϕ_{xt} terms

This leads to an operator $P_{D/LT}$ (see equation (15.2.14)):

$$P_{D/LT}\Delta\phi = -\varepsilon\mu M_\infty^2 \frac{\tau}{\Delta x} r\phi_{xt} + \tau\bar{\mathbf{V}} \cdot (\bar{\rho}\bar{\mathbf{V}}\phi_t) = -R^n \quad (15.2.38)$$

where the ϕ_{xt} term can be handled in two ways:

- (1) Explicitly by $\phi_{xt} = \Delta\phi^n/\tau$, leading to an operator $P_{D/LTE}$
- (2) Implicitly by $\phi_{xt} = \Delta\phi^{n+1}/\tau$, leading to an operator $P_{D/LTI}$

In this last case a linearization procedure is necessary.

When added implicitly, the convergence operator $P_{D/LTI}$ has an additional term proportional to εM_∞^2 , while the explicitly added ϕ_{xt} term will give an additional εM_∞^2 term in the expression of K_T . Therefore, the M_∞^2 dependence of the maximum eigenvalue will remain in this latter case, but with the implicit operator $P_{D/LTI}$ the limiting value will be independent of Mach number since the amplification matrix $G = 1 - P^{-1} \cdot K_T$ will have a Mach number dependence in the denominator which will compensate the corresponding factor in the numerator of equations (15.2.28) and (15.2.36). Therefore, the presence of the ϕ_{xt} term will enhance the stability when added explicitly, but will not allow unconditional stability with a direct method when the mesh size is reduced or the Mach number increased. However, an implicitly added ϕ_{xt} term, with a coefficient proportional to M_∞^2 , will allow unconditional stability for reduced mesh sizes or increased Mach number. Note that the M_∞^2 dependence of the ϕ_{xt} term is essential to obtain unconditional stability in this case.

Introduction of ϕ_{xt} terms in the density

Hafez *et al.* (1978) suggested another alternative for the introduction of artificial

time-dependent terms, namely the addition of a ϕ_t term in the expression of the density, following the time-dependent exact expression (equation (13.1.4)):

$$\frac{\rho}{\rho_0} = \left(1 - \frac{|\bar{\nabla}\phi|^2}{2H_0} - \varepsilon\mu\phi_t \right)^{1/\gamma-1}. \quad (15.2.39)$$

In this case, too, the added ϕ_t term can be treated explicitly or implicitly. Similar conclusions as above are obtained for a direct method resolution, namely the implicit artificial time term in the density will lead to unconditional stability, while the explicit treatment will improve the convergence properties but will not lead to unconditional stability. Figure 15.2.2, taken from Caspar (1980), illustrates these properties for the model problem of Figure 15.2.1. The figure displays the evolution of the spectral radius of the amplification operator with increasing Mach number for the different options discussed. The 'Taylor' denomination stands for a linearized direct method. The improvement brought by the artificial time-dependent terms—either ϕ_t in the density or ϕ_{xt} —is clearly seen, but remains conditional while the implicit treatment of these terms allows an unconditional stability.

Similar results are obtained when the spectral radius is computed for decreasing mesh size. Only the implicit artificial time dependence will lead to unconditional stability.

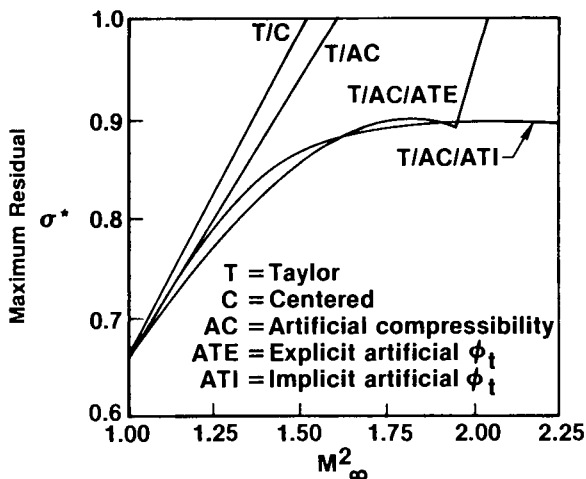


Figure 15.2.2 Spectral radius of amplification operators for the model problem. (Courtesy J. Caspar, United Technology Research Center, USA)

Linearized line relaxation method

If the same linearization procedure is coupled to a line relaxation iteration and artificial compressibility, one obtains from the vertical SLOR on equation (15.2.20) the convergence operator

$$P_{\text{SLOR}} = \frac{r^*}{\Delta x^2} \left[\left(\frac{2}{\omega} - 1 \right) - \frac{\sigma^2}{\omega} \delta_y^2 + \delta_x^- \right] \quad (15.2.40)$$

and the amplification operator G_{SLOR} is given by

$$G_{\text{SLOR}} = 1 - P_{\text{SLOR}}^{-1} K_T \quad (15.2.41)$$

where K_T is given by equation (15.2.33).

Here, again, the M_∞^2 term in K_T will limit the stability region of the scheme and hence only conditional stability will be achieved. The method will not converge if the space discretization is continuously refined or the Mach number is increased.

This can be improved, and unconditional stability achieved, if an additional ϕ_{xt} term proportional to M_∞^2 is added to the SLOR operator, that is in an implicit way. Note that introducing the density terms as part of the SLOR iteration will produce these implicit ϕ_{xt} terms.

Linearized approximate factorization method

The approximate factorization techniques, derived from ADI methods, will be discussed in the next section and are widely used in transonic potential flow computations.

The model problem analysis shows that standard ADI is stabilized unconditionally by the addition of implicit ϕ_t in the density or ϕ_{xt} terms in close analogy with SLOR behaviour, but are only conditionally stable otherwise.

15.2.3 The alternating direction implicit method—approximate factorization schemes

The alternating direction implicit scheme—ADI—has already been discussed in Chapter 12, Section 12.3.2. It provides a locally one-dimensional space splitting, together with an implicit treatment in each direction, generally leading to tridiagonal systems for three-point discretization formulas as developed in the previous sections. Hence convergence rates higher than obtainable by line relaxation methods can be achieved, since the influence of one mesh point on the others is transmitted in a faster way.

It was therefore tempting to consider the application of these schemes to the transonic full potential equation. This was introduced by Ballhaus and Steger (1975) for the unsteady transonic small disturbance equation and for steady flows by Ballhaus *et al.* (1978). It was then extended to the full potential equation by Holst and Ballhaus (1979). The original ADI formulation is adapted to

elliptic problems and, as mentioned above, is not expected to provide unconditional stability for higher Mach numbers or finer meshes in the transonic regime. Some adaptations will therefore be necessary, introducing ϕ_{xi} terms in the convergence operator, leading to the so-called AF2 schemes.

The basic ADI scheme—AF1 scheme

In a general curvilinear coordinate system, the ADI scheme will take the following form, referring to a discretization of equations (14.1.16) to (14.1.18):

$$C_{ADI} \Delta \phi_{ij} = (1 - \sigma \delta_{\xi}^{+} A_i \delta_{\xi}^{-}) \cdot (1 - \sigma \delta_{\eta}^{+} A_j \delta_{\eta}^{-}) \Delta \phi = \sigma \omega R_{ij}^n \quad (15.2.42)$$

In the above formulation the right-hand side is the residual, as would be obtained by any of the discretization methods discussed in the previous sections. The coordinates ξ, η represent curvilinear coordinates and the coefficients A are defined as follows:

$$A_i = \left(\frac{g^{11} \rho}{J \Delta \xi^2} \right)_{i-1/2, j} \quad (15.2.43a)$$

$$A_j = \left| \frac{g^{22} \rho}{J \Delta \eta^2} \right|_{i, j-1/2} \quad (15.2.43b)$$

Note that only the diagonal elements of the metric tensor g appear in the above coefficients. In the case of a discretization in a Cartesian mesh, the variables ξ, η become identical to the x, y coordinates and the coefficients A reduce to the density divided by the mesh spacing squared, in the corresponding direction. In practical calculations the density will be replaced by some form of artificial density in the supersonic regions.

As usual the ADI method is solved by a local one-dimensional splitting in the following steps:

$$(1 - \sigma \delta_{\xi}^{+} A_i \delta_{\xi}^{-}) f_{ij} = \sigma \omega R_{ij}^n \quad (15.2.44a)$$

$$(1 - \sigma \delta_{\eta}^{+} A_j \delta_{\eta}^{-}) \Delta \phi_{ij} = f_{ij} \quad (15.2.44b)$$

An alternative form, requiring less computational effort, but which might be less efficient in iteration counts, consists in setting the A coefficients outside the difference operator.

In the formulation of equations (15.2.43) corresponding to second-order discretizations, each of these equations represents a set of tridiagonal matrix equations along the corresponding lines. Hence, the whole mesh is swept through twice for each iteration step, once along the different coordinate directions. The parameters σ and ω have to be optimized and can be selected according to the guidelines mentioned in Section 12.3.2 in Volume 1. This scheme gives excellent convergence rates in subsonic flows.

Since this iteration scheme, unlike the line relaxation method, does not generate the equivalent of the ϕ_{ii} terms, it is not expected to have good

convergence properties for transonic flow regimes, unless some form of ϕ_{it} upwind term is artificially added. In order to generate these upwind terms within the iteration scheme, the variant called AF2 has been introduced by Holst and Ballhaus (1979) and Holst (1980).

The AF2 scheme for transonic potential flows

In order to provide a natural build-in ϕ_{it} term in the convergence operator, the derivative in the mainstream direction, taken here as the ξ direction, is split over two factors as follows, written for a two-dimensional flow:

$$(1 - \sigma \delta_{\xi}^{+} A_i)(\delta_{\xi}^{-} - \sigma \delta_{\eta}^{+} A_j \delta_{\eta}^{-}) \Delta \phi_{ij} = \sigma \omega R_{ij}^n \quad (15.2.45)$$

This is implemented in a two-step procedure:

$$(1 - \sigma \delta_{\xi}^{+} A_i) f_{ij} = \sigma \omega R_{ij}^n \quad (15.2.46a)$$

$$(\delta_{\xi}^{-} - \sigma \delta_{\eta}^{+} A_j \delta_{\eta}^{-}) \Delta \phi_{ij} = f_{ij} \quad (15.2.46b)$$

The first step, along the ξ lines, is a bidiagonal matrix system which is solved by sweeping in the negative ξ direction. The second step solves a tridiagonal system in the η direction for each constant ξ line, sweeping in the positive ξ direction.

As for the ADI-AF1 scheme, the parameters σ and ω have to be optimized. The latter is generally taken close to the theoretical optimum of two. Large values of σ are effective in reducing the low-frequency errors, while small values will be effective at the high-frequency end of the error frequency bandwidth. Therefore it is suggested, following Ballhaus *et al.* (1978), that a sequence of values of σ be used, ranging from low to high in order to cover the largest possible range of error frequencies (see also Section 12.3.2 in Volume 1).

One of the problems of ADI factorization methods is the definition of boundary conditions for the intermediate solution f in equations (15.2.44) and (15.2.46). In many cases a Dirichlet condition on f is imposed, setting the function value to zero at the boundary, or a Von Neumann condition can be chosen. Restrictions on the stability conditions can follow from the boundary conditions, and limitations on σ and ω might have to be imposed. This is discussed in South and Hafez (1983). In particular, the α coefficients in the AF2 scheme have to be restricted at the boundaries in order to ensure convergence.

As mentioned earlier, the density is to be replaced by an upwinded form in the residual and in the convergence operator on the left-hand side of the factored equation. However, tests performed by Holst (1980) with the AF2 scheme show that introducing the upwinded density in the residual only and not in the factored convergence operators does not reduce the convergence rate. Moreover, replacing the density by a constant in the left-hand side also produced stable results, but with a convergence rate slowed down by a factor of two to three.

Figure 15.2.3, from Holst and Ballhaus (1979), shows a comparison of convergence rates between the AF1, AF2 and SLOR schemes as applied to a

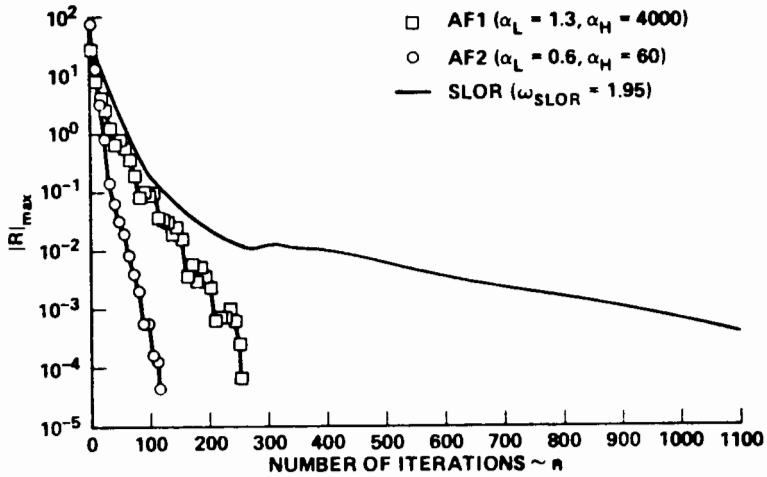


Figure 15.2.3 Maximum residual convergence history for SLOR, AF1 and AF2 iterative schemes applied to the transonic potential flow over a circular arc airfoil of 10 per cent thickness, at a free-stream Mach number of 0.84. (From Holst and Ballhaus, 1979)

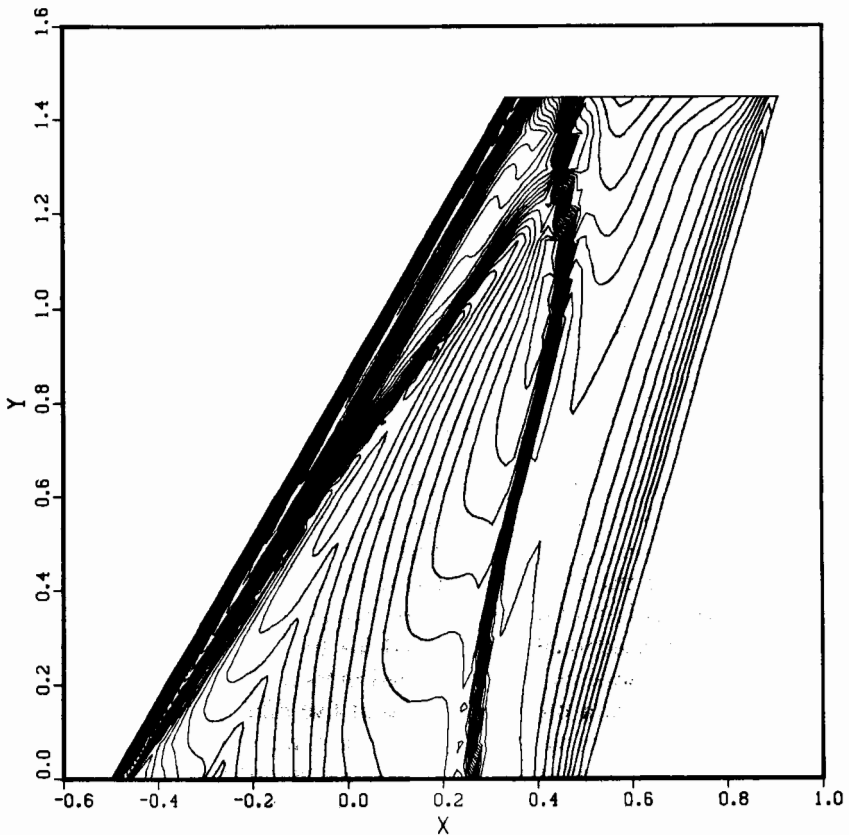


Figure 15.2.4 Mach number distribution on the upper surface of the ONERA M6 wing at a free-stream Mach number of 0.84 and 3.0° incidence, with a $225 \times 30 \times 30$ mesh. (Courtesy T. Holst, NASA Ames Research Center, USA)

10 per cent thick, circular arc airfoil at a free-stream Mach number of 0.84. The convergence rate is expressed by the maximum residual. The marked improvement in convergence rate over SLOR is clearly seen as well as the superiority of the AF2 formulation compared with the standard AF1-ADI method. However, the AF1 scheme behaves better with subsonic flows. The excellent behaviour of these schemes is tied to an optimization procedure of the σ parameter as described in Section 12.3.2, and some trial and error is required to find the optimal range.

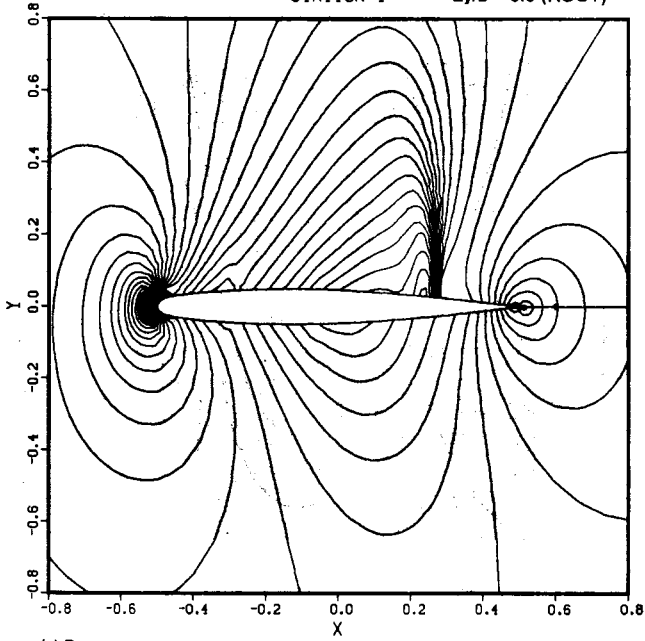
Most of the stability and convergence properties of ADI schemes and their approximate factorization versions are based on uniform grid assumptions and do not take into account the effects of strongly stretched or distorted grids. Computations show, however, a significant decrease in convergence rates in these cases, when compared to the same flow problem calculated on a uniform grid. A detailed investigation of the influence of the grid distortion on the convergence properties of approximate factorization schemes has been presented by Catherall (1982), following the introduction of a very successful variant called AF3 by Baker (1981). The AF3 variant is similar to the AF2 or backward difference operator, but the coefficients A are also factorized and distributed between the various factors. In particular, the metric coefficients can be explicitly factorized in order to take into account the effects of grid stretching, and an analysis of the optimal choices for the factorization of the A coefficients can be found in Catherall (1982).

The ADI approximation factorization techniques can be applied to finite element discretizations if the mesh is generated by intersections of families of lines, as obtained from curvilinear coordinate systems. Applications to (transonic) potential flow computations on arbitrary, body-fitted meshes were developed by Deconinck and Hirsch (1979, 1980a, 1980b) for various bilinear and biquadratic elements.

The ADI approximate factorization method has been extended by Holst and Thomas (1983) to the computation of three-dimensional potential flows over swept wings. The following figures show the results of a computation on the ONERA M6 wing at a free-stream Mach number of 0.84 and 3.0° incidence, for which experimental data are available (AGARD Report AR-138, 1979), performed by T. Holts (private communication) with a very fine mesh of $225 \times 30 \times 30$ points using the TAIR code, Dougherty *et al.* (1981). Figure 15.2.4 shows the Mach number distribution on the upper surface, while Figure 15.2.5 presents the Mach number cross-sectional plots at five stations and a typical cross-sectional O-grid used for the computation with a nearly constant chordwise spacing. The computed pressure coefficients are compared to the experimental data on Figure 15.2.6 at five different stations. Note that the spanwise locations of the experimental data and the computed results are not identical. As expected, the potential shock is downstream of the experimentally observed position, but the high resolution gives an excellent prediction. In particular, at 80 per cent span the double-shock structure is still well captured.

MACH CONTOURS
STATION 1

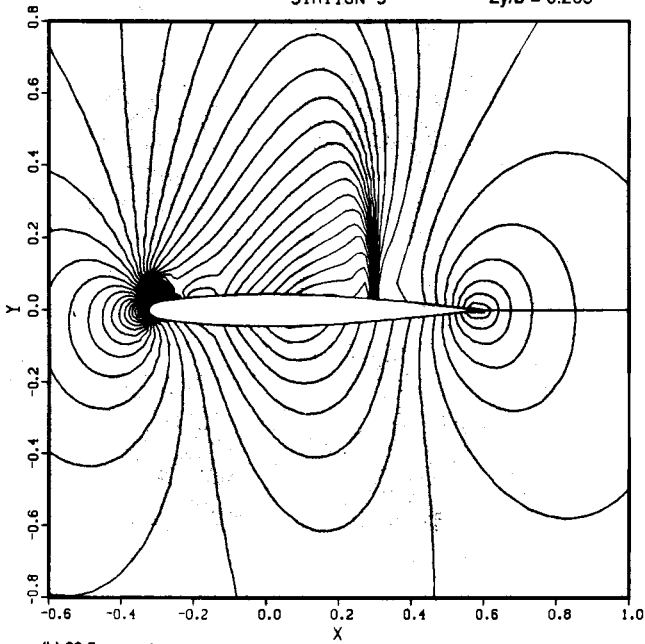
ONERA M6
 $2y/b = 0.0$ (ROOT)



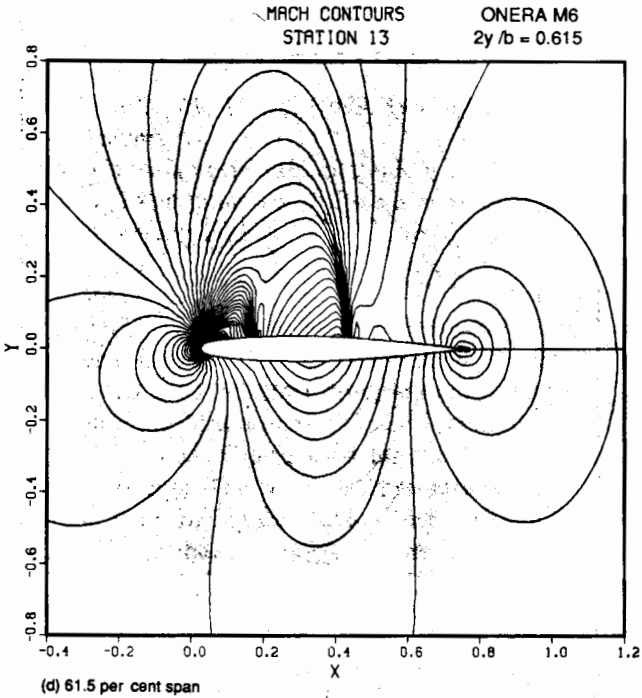
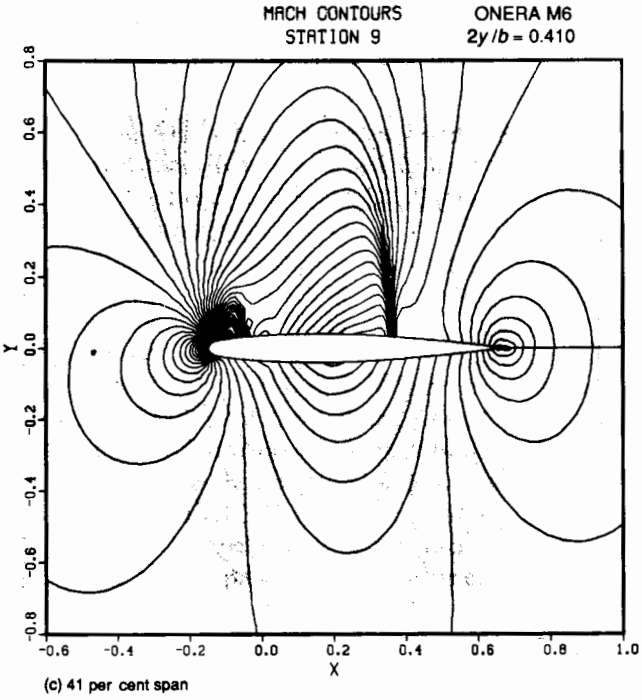
(a) Root section

MACH CONTOURS
STATION 5

ONERA M6
 $2y/b = 0.205$



(b) 20.5 percent span



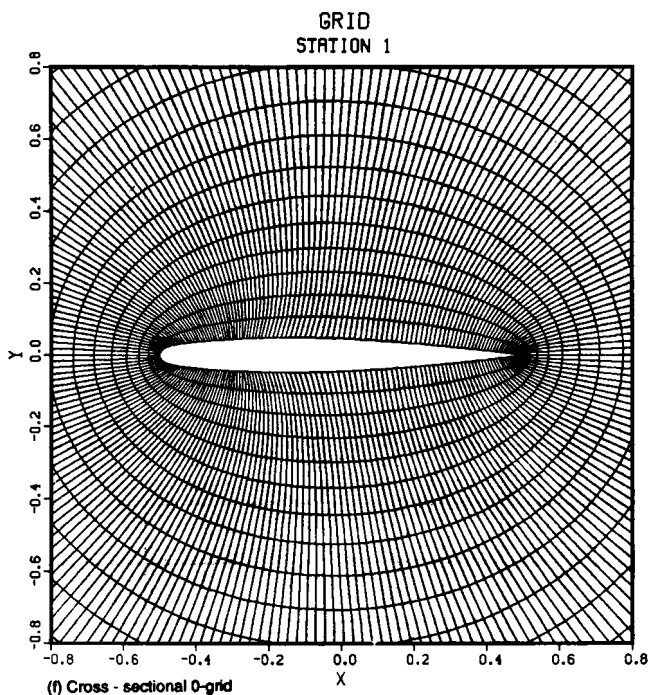
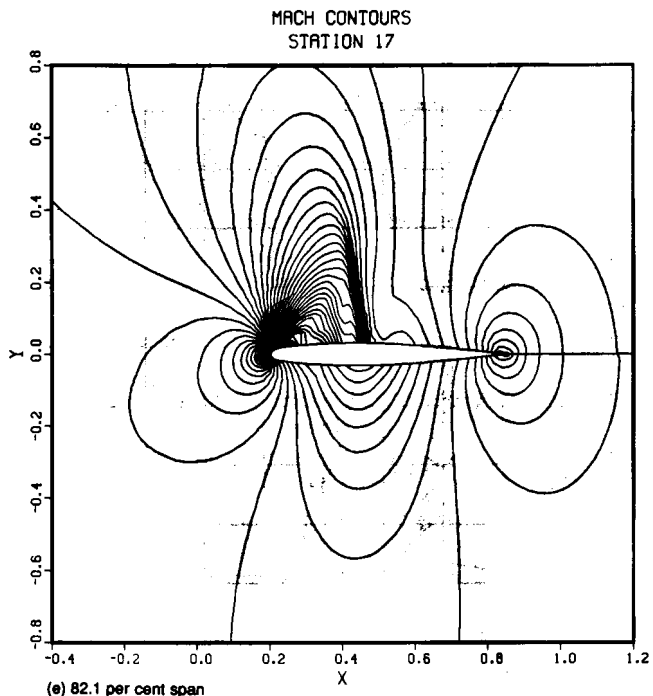
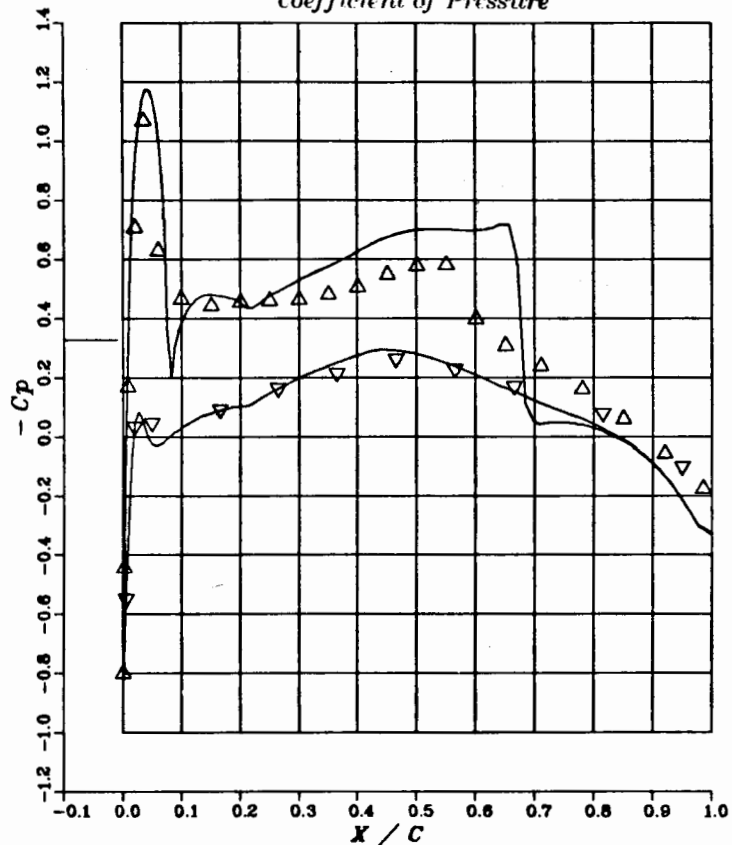


Figure 15.2.5 Mach number cross-sectional plots at five spanwise stations of the ONERA M6 wing at a free-stream Mach number of 0.84 and 3.0° incidence with a $225 \times 30 \times 30$ grid. (Courtesy T. Holst, NASA Ames Research Center, USA)

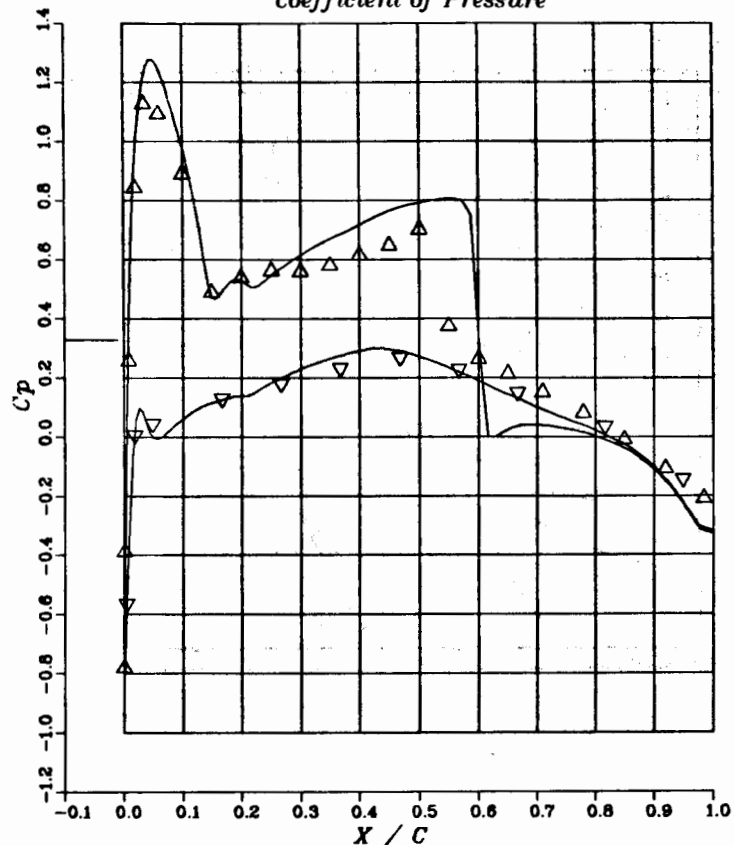
	M_∞	α_w	$2y/b$	
$\Delta \nabla$	0.8395	3.0600	0.2000	EXP
—	0.8400	3.0000	0.2051	TWING

Coefficient of Pressure



	M_∞	α_w	$2y/b$	
$\Delta \nabla$	0.8395	3.0600	0.4400	EXP
	0.8400	3.0000	0.4615	TWING

Coefficient of Pressure



\triangle	∇	0.8395	3.0600	0.6500	EXP
—	—	0.8400	3.0000	0.6154	TWING

\triangle	∇	0.8395	3.0600	0.8000	EXP
—	—	0.8400	3.0000	0.7692	TWING

Coefficient of Pressure

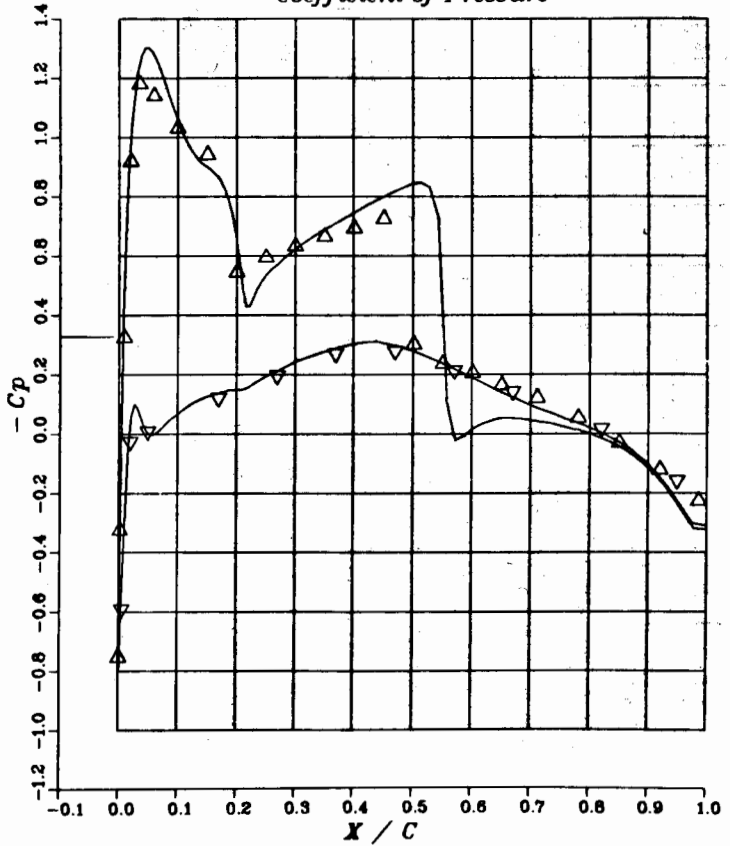


Figure 15.2.6 (c) 61.5 per cent span - exp. 65 per cent span

Coefficient of Pressure

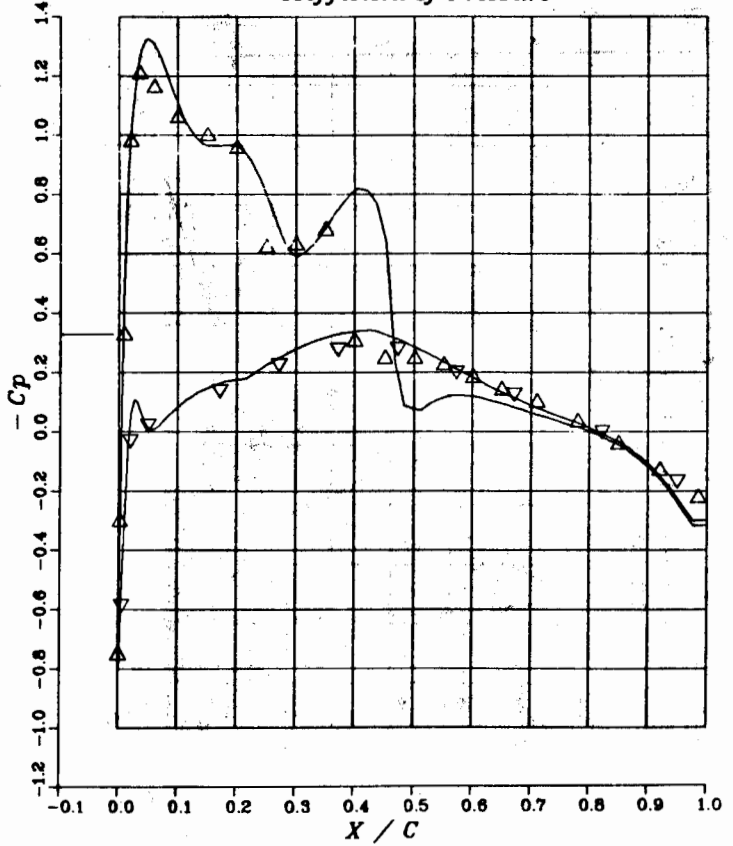
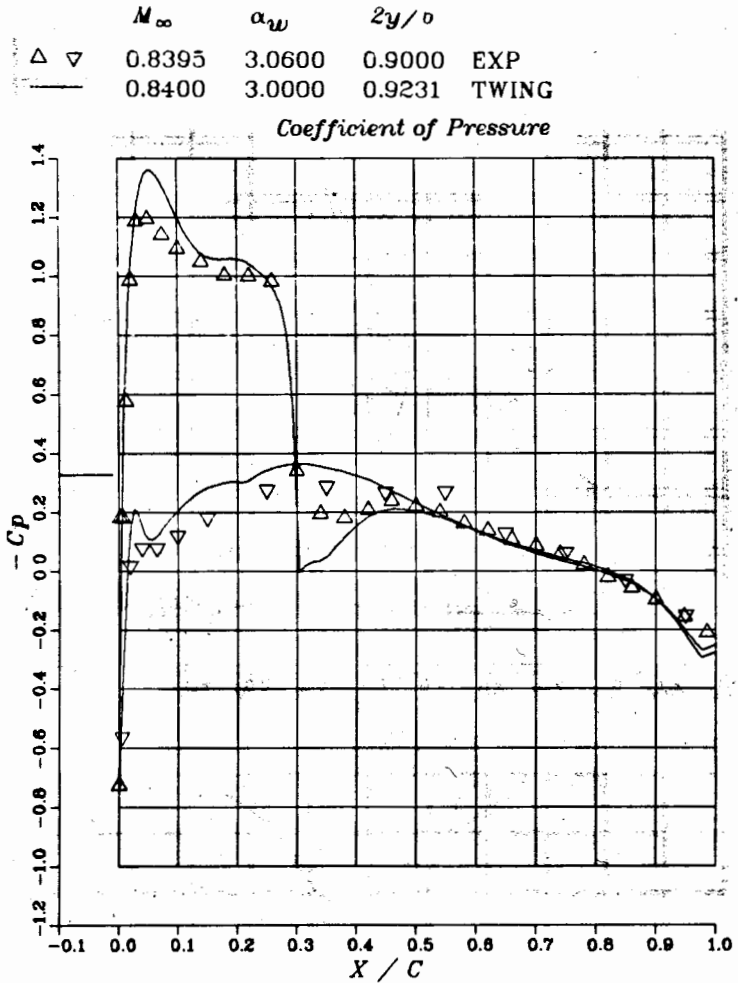


Figure 15.2.6 (d) 76.9 per cent span - exp. 80 per cent span



(e) 92.3 per cent span – exp. 90 per cent span

Figure 15.2.6 Computed pressure coefficients at five spanwise stations of the ONERA M6 wing at a free-stream Mach number of 0.84 and 3.0° incidence compared to experimental data. (Courtesy T. Holst, NASA Ames Research Center, USA)

15.2.4 Other techniques—multi-grid methods

Although line relaxation and approximate factorization methods are most widely used in potential flow computations and are applied in many of the available potential codes, many other methods have been investigated which have shown prospects for equal or better convergence properties than SLOR or approximate factorization.

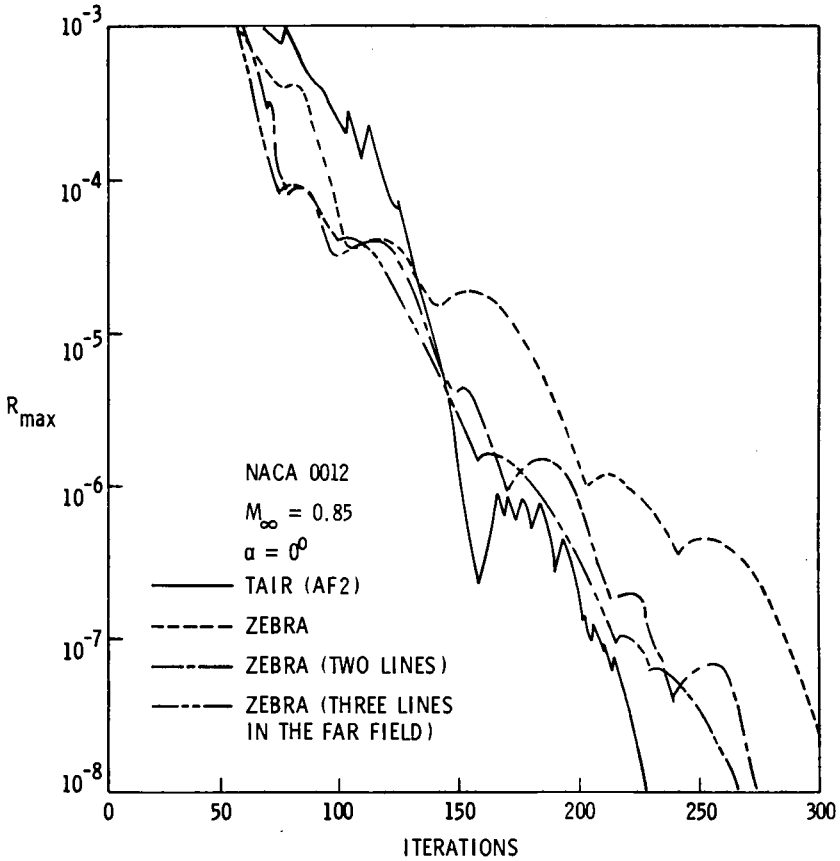


Figure 15.2.7 Comparison of convergence rates of the AF2 scheme and Zebra line relaxation—three variants—for the flow on a NACA 0012 airfoil at a free-stream Mach number of 0.85 and 0° incidence. (From Hafez and Lovell, 1983a)

Among successful variants, Zebra line relaxation, easily vectorizable, can be mentioned (Hafez and South, 1981; Hafez and Lovell, 1983a), as well as several conjugate gradient preconditioning techniques (Habashi and Hafez, 1982; Wong and Hafez, 1982; Wong, 1983; Hafez, 1983). Figure 15.2.7, from Hafez and Lovell (1983a), compares the convergence rates of the AF2 scheme with several variants of Zebra relaxation for an NACA 0012 calculation at 0.85 Mach number.

For practical computations on coarse meshes, simple SLOR, eventually under Zebra form, or approximate factorization can be recommended as a good compromise between simplicity and performance.

For more advanced codes, and if minimization of computer time is of concern, then the multi-grid method should be strongly recommended. It has been applied initially by Jameson (1979) to the conservative full potential equation with considerable success, producing converged results in a few multi-grid cycles.

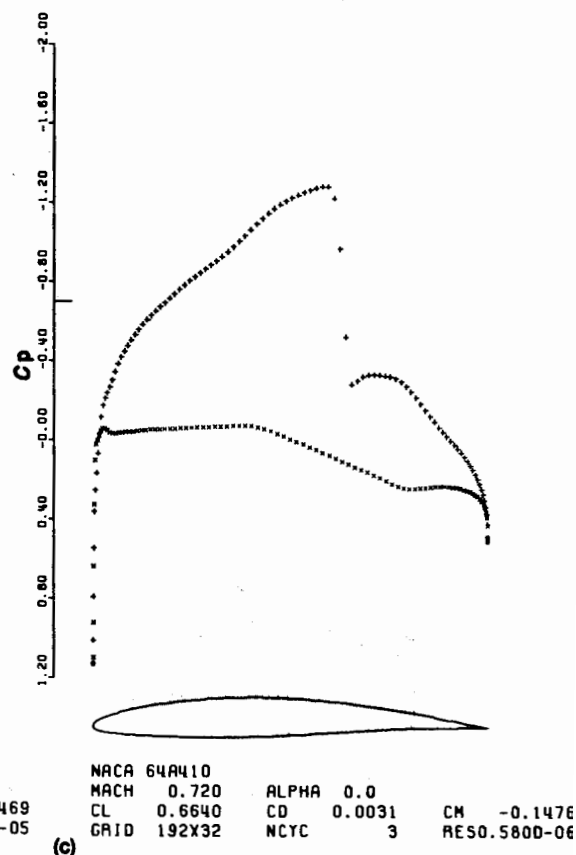
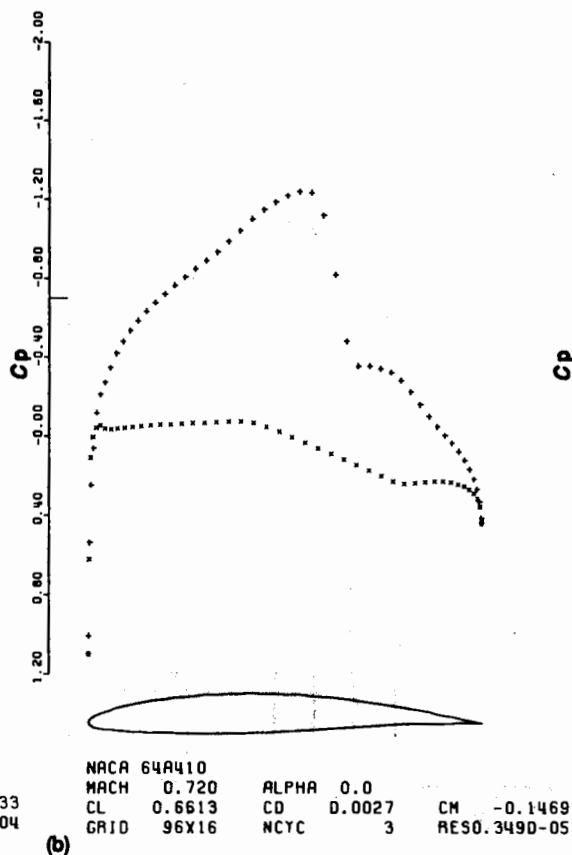
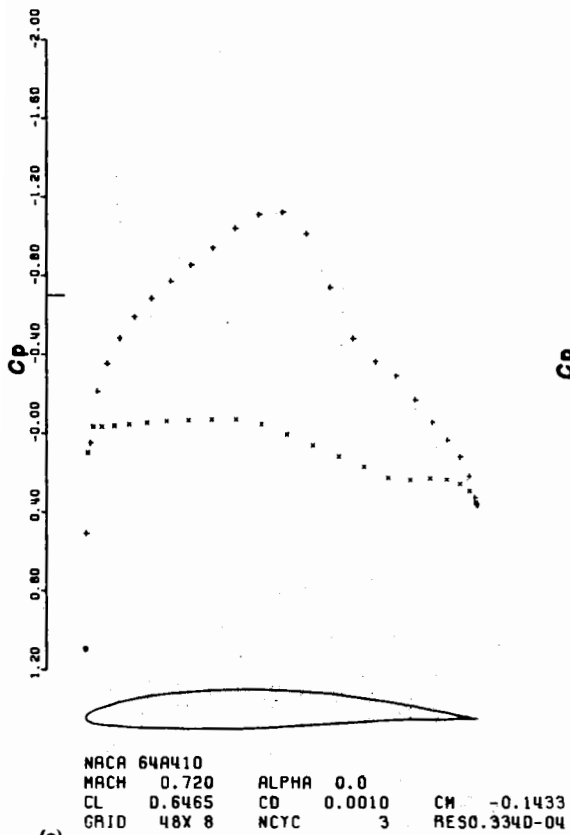
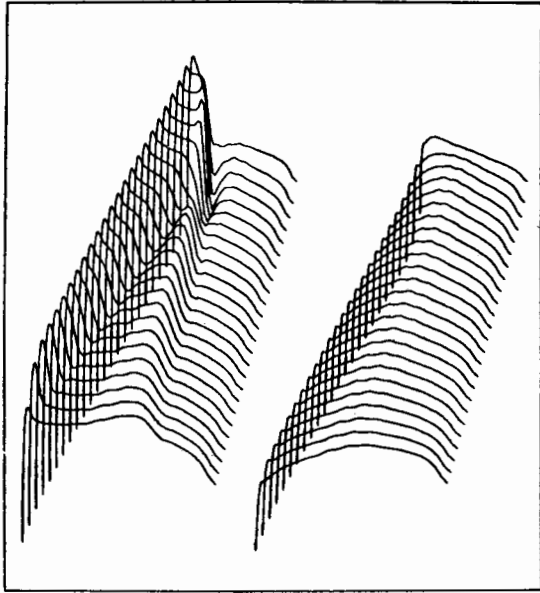
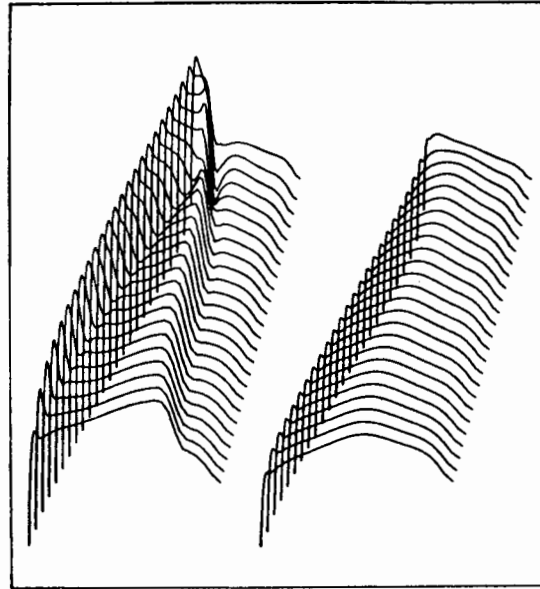


Figure 15.2.8 Pressure coefficients on three successive meshes of 48×8 , 96×16 and 192×32 , obtained with the multi-grid method, for an NACA 64A410 airfoil at a free-stream Mach number of 0.72 and 0° incidence. (Courtesy A. Jameson, University of Princeton, USA)



UPPER SURFACE PRESSURE LOWER SURFACE PRESSURE

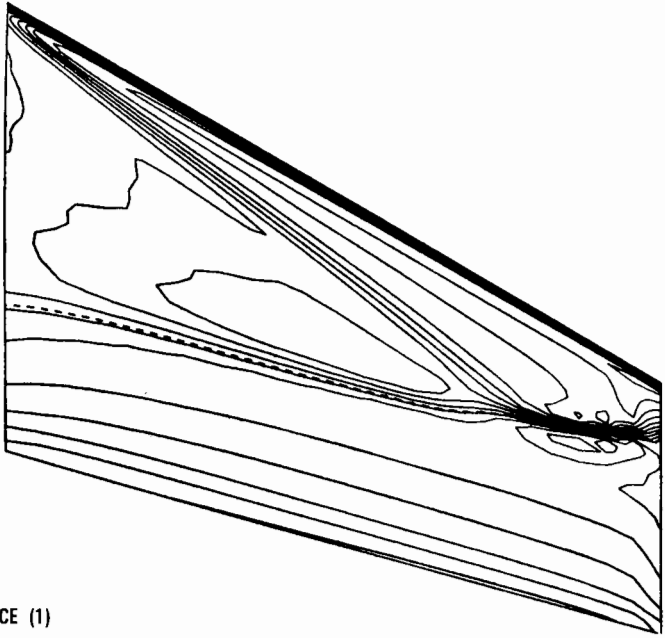
ONERA WING ON CYLINDRICAL FUSELAGE
 MACH 0.840 ALPHA 3.000
 CL 0.3960 CD 0.0131 CM -0.2032
 GRID 160X24 NCYC 14 RESO.2740-06



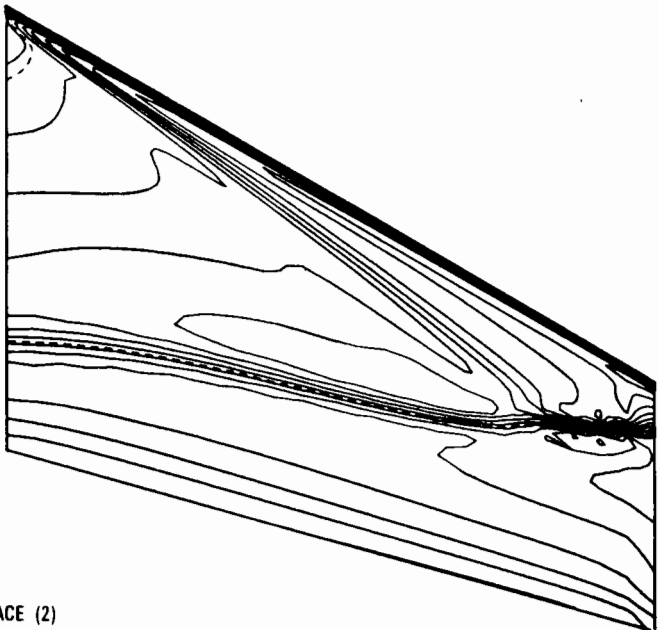
UPPER SURFACE PRESSURE LOWER SURFACE PRESSURE

ONERA WING ON WALL
 MACH 0.840 ALPHA 3.000
 CL 0.2853 CD 0.0104 CM -0.2157
 GRID 160X24 NCYC 14 RESO.5880-07

(a) Pressure coefficients for cylindrical fuselage (1) and plane wall (2)

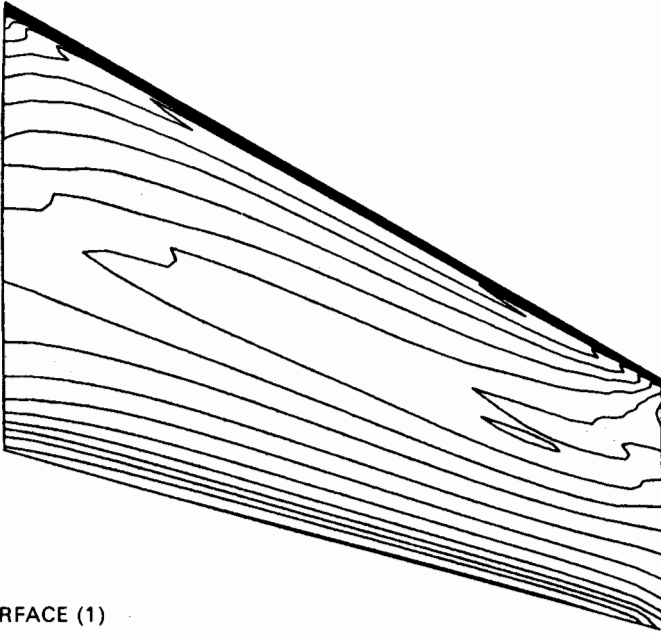


UPPER SURFACE (1)

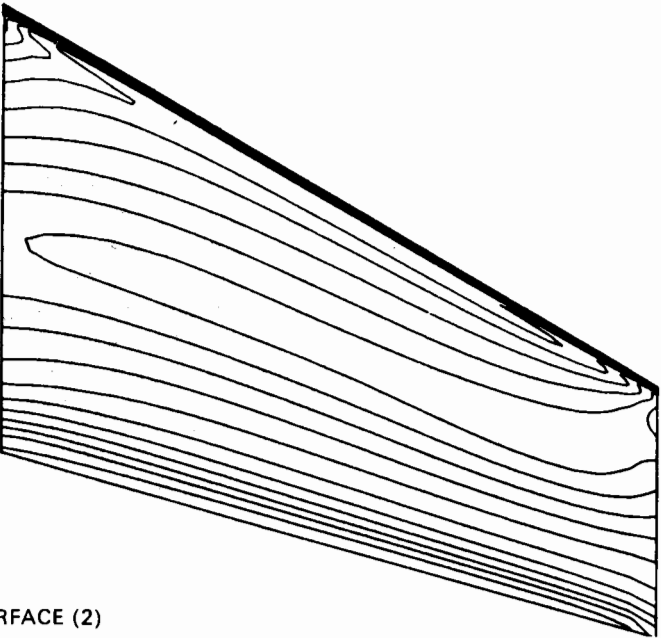


UPPER SURFACE (2)

(b) Upper surface isobars for cylindrical fuselage (1) and plane wall (2)



LOWER SURFACE (1)



LOWER SURFACE (2)

(c) Lower surface isobars for cylindrical fuselage (1) and plane wall (2)

Figure 15.2.9 Comparison of the influence of two wing-body combinations on the ONERA M6 wing at a free-stream Mach number of 0.84 and 3° incidence. (Courtesy D. Caughey, Cornell University, USA)

An enhanced approximate factorization approach with increased sensitivity to the high-frequency errors is used as a smoothing operator. Compared to the ADI scheme (15.2.42), Jameson applies the scheme

$$(S - \sigma\delta_z^+ A_i\delta_z^-)(S - \sigma\delta_\eta^+ A_i\delta_\eta^-)\Delta\phi_{ij} = \sigma\omega SR_{ij} \quad (15.2.47)$$

where

$$S = 1 + \alpha\delta_z^- + \beta\delta_\eta^- \quad (15.2.48)$$

The coefficients α and β depend on the flow type and are user input and a single ADI iteration sweep is performed on each mesh before passing to the other mesh.

Figure 15.2.8 shows results of a transonic flow on an NACA 64A410 airfoil at $M_\infty = 0.72$ and 0° incidence obtained with this multi-grid technique. Pressure coefficients on three successive meshes of 48×8 , 96×16 and 192×32 are shown after only three multi-grid cycles (A. Jameson, private communication). The residual reduction rate has a remarkably low value of 0.4637 on the fine mesh and after ten cycles the residual has dropped to 10^{-8} with no change in the lift coefficient of 0.6640 obtained after three cycles.

Other variants have been developed with finite element discretizations by Deconinck and Hirsch (1981) and subsequently improved by Bredif (1983). A detailed investigation of multi-grid strategies and smoothing operators applied to the potential equation is to be found in Van der Wees *et al.* (1983).

Three-dimensional applications of the multi-grid method have also been developed by McCarthy and Reyhner (1982), Caughey (1983) and others. Although convergence rates are generally not as impressive as in two-dimensions, excellent results can be achieved.

Figure 15.2.9 compares the influence of two different wing-body combinations on the ONERA M6 wing at a free-stream Mach number of 0.84 and 3.0° incidence, namely a cylindrical fuselage and a plane wall. The importance of the three-dimensional interference effects can be seen on the upper as well as lower surface pressure and distributions. In particular, the shock intensity in the root area is markedly reduced by a circular fuselage, while the leading edge expansion is enhanced. These calculations were obtained after fourteen multi-grid cycles, with SLOR relaxation, on a $160 \times 24 \times 25$ grid by D. Caughey (private communication).

15.3 NON-UNIQUENESS AND NON-ISENTROPIC POTENTIAL MODELS

As discussed in Section 2.9.2 in Volume 1, the isentropic assumption leads to a restricted validity range of the potential flow model for transonic flows with shocks, as compared to the exact inviscid flow description provided by the system of Euler equations. As soon as shocks appear in the flow, consequences of the isentropicity are twofold.

15.3.1 Isentropic shocks

The shock intensity as resulting from the constancy of entropy cannot be equal to the correct non-isentropic shock jumps as defined by the Rankine–Hugoniot relations. The Rankine–Hugoniot shock relations are obtained through the satisfaction of all the conservation laws, mass, momentum, energy, and lead to an entropy increase through the shock discontinuity, while the potential model imposes constancy of entropy and can only satisfy mass and energy conservation.

Compared to the correct shock intensity and position, the potential shocks are stronger and located further downstream on airfoils and in channel flows. The difference between potential and Euler shocks increases with increasing Mach number levels but remains relatively limited for non-lifting airfoils. For lifting airfoils, however, these differences can become very strong and lead to very different flow configurations at the same incident conditions.

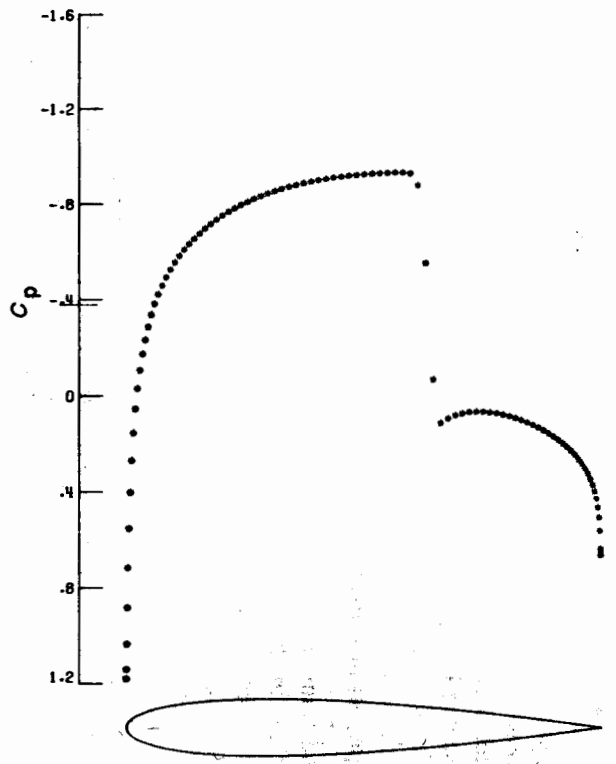
Figure 15.3.1 to 15.3.3 show comparisons between potential and Euler solutions. The potential solution is obtained with Jameson's finite volume code (Jameson and Caughey, 1977), using artificial viscosity and the multi-grid acceleration scheme (Jameson, 1979). This code allows the residual to converge up to machine accuracy due to the effective multi-grid scheme. The second solution is obtained by solving the Euler equations with a modified version of a code developed by Jameson and described in Chapter 18. Figure 15.3.1 compares the two solutions for a non-lifting NACA 0012 airfoil at 0° incidence and an incident Mach number of 0.82.

Figure 15.3.2 and 15.3.3 show a similar comparison of pressure coefficients and iso-Mach lines at a free-stream Mach number of 0.75 and an incidence angle of 2° . The potential calculation has been performed on a very fine O-mesh of 384×64 points, while the Euler calculation was obtained on a more standard mesh of 192×33 shown in Figure 15.3.3(c). The consistently stronger potential shock is clearly seen; the potential model predicts a lift coefficient of 0.615 while the Euler model leads to a value of 0.439. Additional examples at higher Mach numbers are presented in Figures 2.9.5 to 2.9.7 in Volume 1.

15.3.2 Non-uniqueness and breakdown of the transonic potential flow model

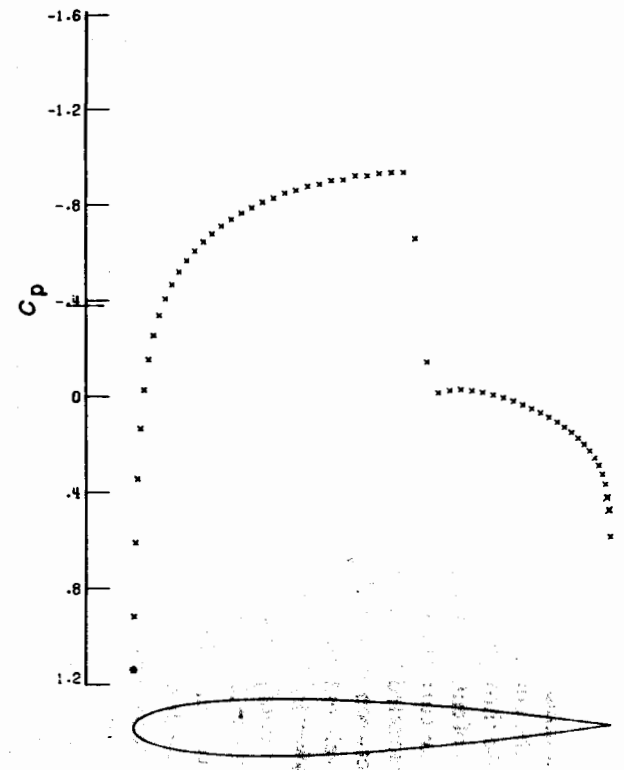
It has been found numerically that the isentropic potential flow model has non-unique solutions in the transonic range. This is well known for internal flows but has also been found in external flows, as discussed in Section 2.9.3 (Steinhoff and Jameson, 1982; Salas *et al.*, 1983); see Figures 2.9.15 and 2.9.16 in Volume 1. Non-physical solutions are found with negative lift coefficients at positive angles of incidence or non-symmetrical solutions at zero incidence.

The extremely careful investigation of Salas *et al.* (1983) and Salas and Gumbert (1985) shows, without any doubt, that this is a feature of the mathematical model of the conservative differential equation for the isentropic potential function. These non-unique, non-physical solutions do not seem to appear with the Euler equations and nor are they found when the same flow



NACA 0012
 MACH .820 ALPHA 0.000
 CL -.0000 CD .0186 CM .0000
 GRID 192X32 NCYC 71 RES .660E-12

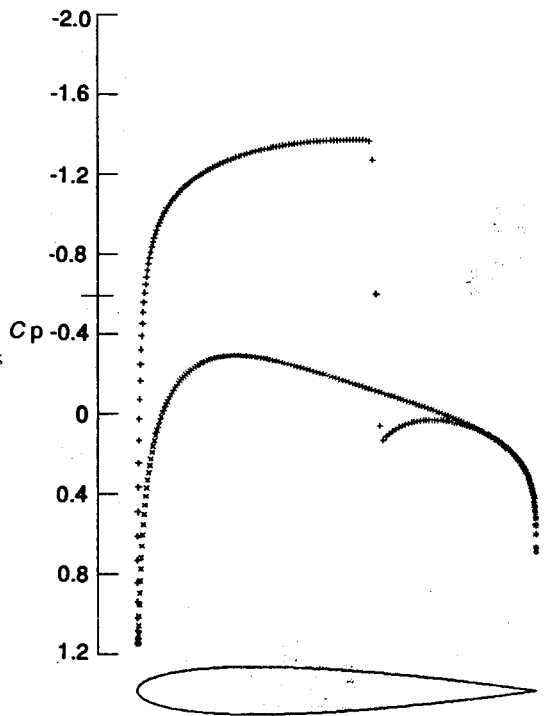
(a) Potential flow model



NACA 0012
 MACH .820 ALPHA 0.000
 CL .0000 CD .0190 CM -.0000
 GRID 120X34 NCYC 2000 RES .165E-06

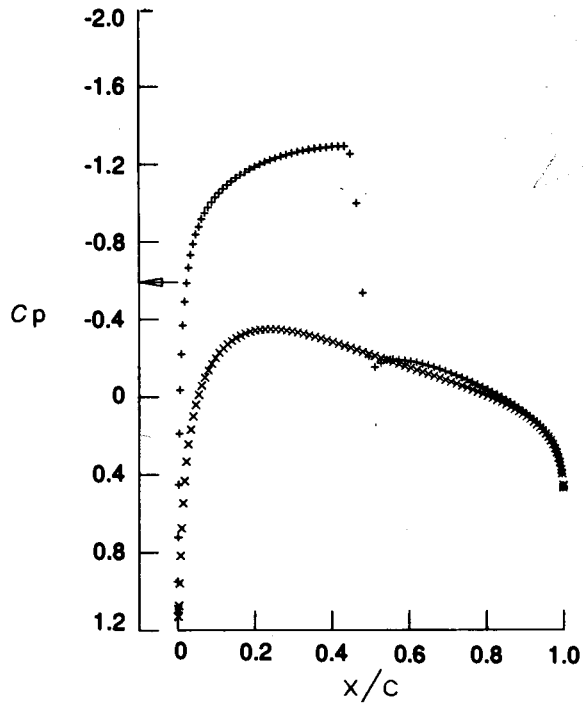
(b) Euler model

Figure 15.3.1 Comparison of pressure coefficients on a NACA 0012 airfoil at $M = 0.82$ and 0° incidence. (Courtesy M. Salas, NASA Langley Research Center, USA)



NACA 0012
 MACH .750 ALPHA 2.000
 CL .6151 CD .0219 CM -.0333
 GRID 384X64 NCYC 150 RES .404E-11

(a)

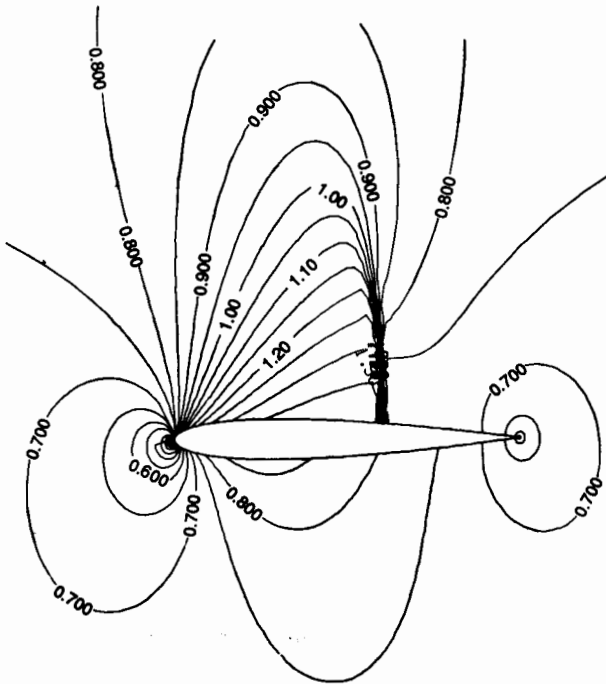


NACA 0012
 M = .750 ALPHA = 2.000 CD, CL = .01282 .4386
 192 X 33 GRID

(b)

Figure 15.3.2 Comparison of pressure coefficients on a NACA 0012 airfoil at $M=0.75$ and 2° incidence, computed with: (a) Potential flow model. (Courtesy C. R. Gumbert and J. South, NASA Langley Research Center, USA). (b) Euler model. (Courtesy M. Salas, NASA Langley Research Center, USA)

LOCAL MACH NUMBER

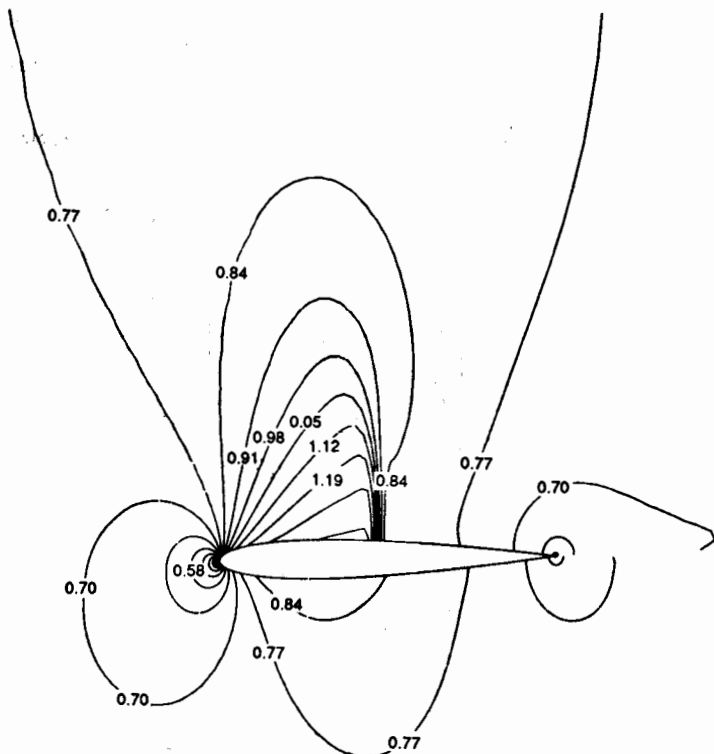


NACA 0012
 ORID=384X64, AM= .750, ALPHA= 2.0000
 MIN= 0., MAX= 1.35E+00, INC= 5.00E-02
 (a)

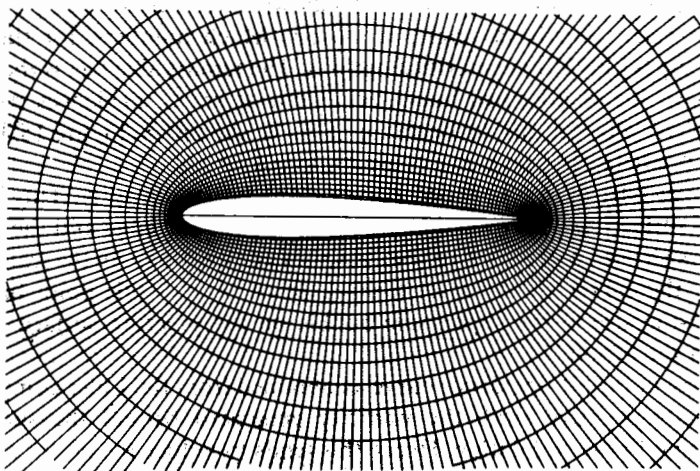
Figure 15.3.3 Comparison of iso-Mach lines on a NACA 0012 airfoil at $M = 0.75$ and 2° incidence, computed with: (a) Potential flow model. (Courtesy C. R. Gumbert and J. South, NASA Langley Research Center, USA.) (b) Euler model. (Courtesy M. Salas, NASA Langley Research Center, USA.) (c) O-Mesh of 192×33 points around an NACA 0012 airfoil

is computed with a non-conservative potential code, which leads to shock jumps of lower strength than the isentropic conservative ones. Figure 15.3.4 shows a comparison for the NACA 0012 airfoil between the lift-incidence angle curves as computed by these three flow models. The potential results show a lift-incidence relation which is unphysical, since the slope at the origin has to be positive. For certain incidence angles there can be three different solutions, none of them having physical significance.

It seems, therefore, that the non-uniqueness is strongly connected with the isentropic condition of the conservative potential model which is not satisfied, at the shock, by the other two computations. Actually a more detailed investigation, by Salas and Gumbert (1985), of the transonic potential flow over



MACH CONTOURS MIN VALUE= .0387 MAX= 1.3498
 NACA 0012
 192 X 33 GRID M = .750 ALPHA = 2.000 CD, CL = .01282 .4386
 (b)



(c) OUTPUT GRID
 NACA 0012
 193 X 33 GRID

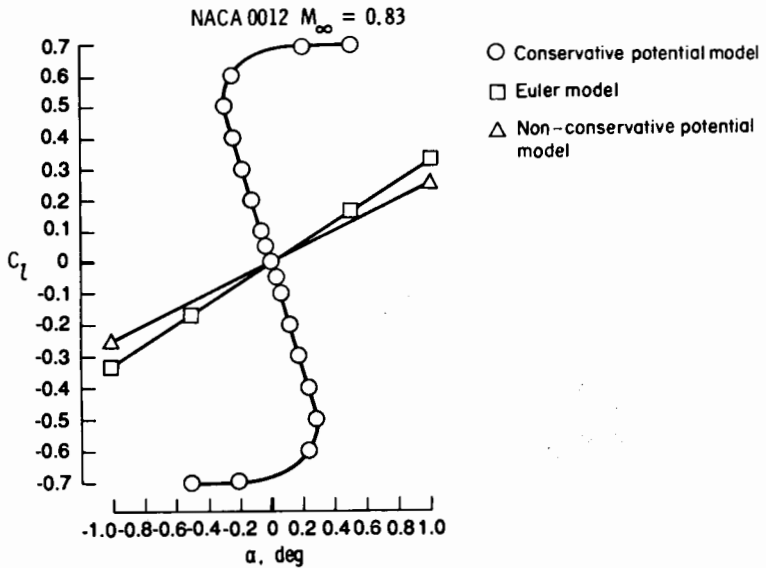
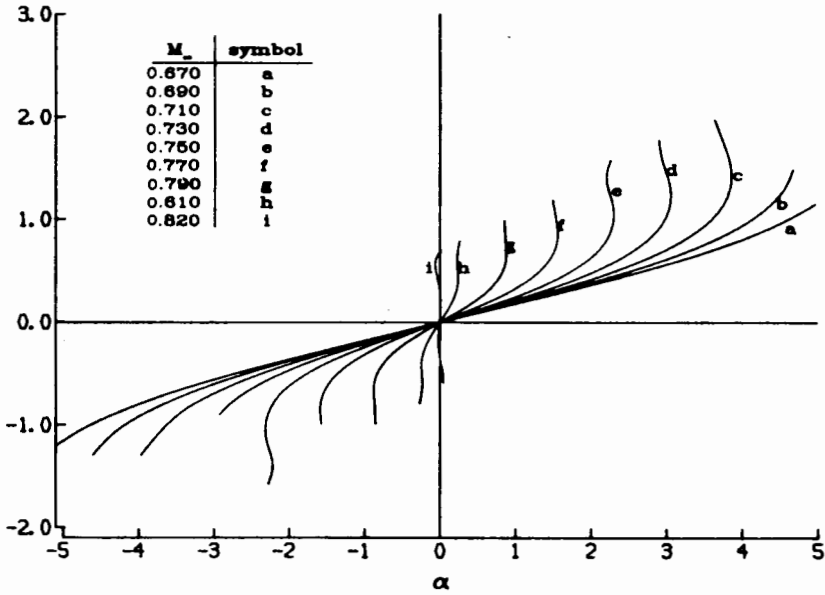


Figure 15.3.4 Calculated variation of lift coefficient with incidence angle for a NACA 0012 airfoil at an incident Mach number of 0.83 obtained with Euler, conservative and non-conservative potential model. (Courtesy M. Salas, NASA Langley Research Center, USA)

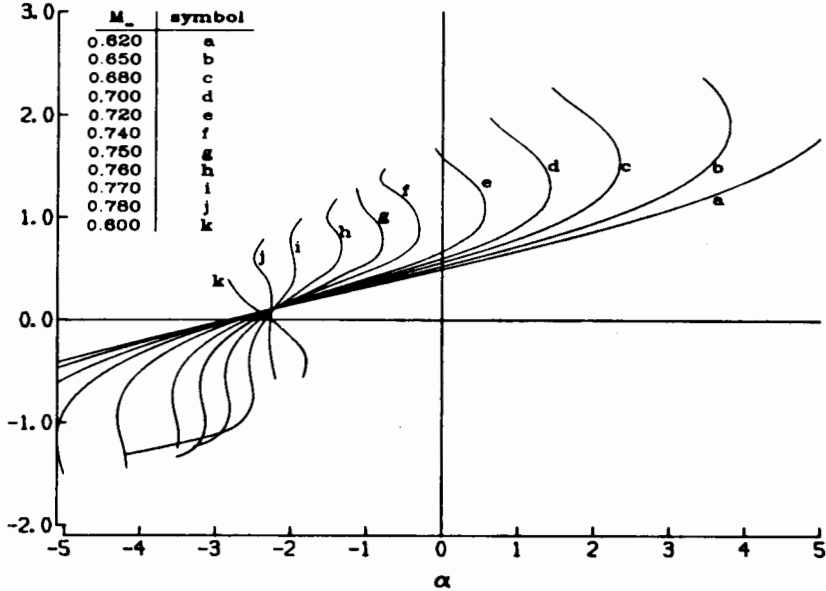
several airfoil sections, covering a wide range of Mach numbers, has shown that the observed non-uniqueness of the potential equation is the continuation of a progressive breakdown of the isentropic potential model. This breakdown is illustrated by the increasing deviation between the potential model behaviour and the physically correct behaviour, in the inviscid approximation, predicted by the Euler equations. Figure 15.3.5 shows a computed diagram of lift coefficient versus incidence angle, at various Mach numbers, for the NACA 0012 and the NLR 7301 supercritical airfoils. The remarkable fact is the increase in lift above the well-known linear behaviour at small incidences where one expects physically the lift to decrease. This is shown in Figure 15.3.6 to be correctly predicted by the Euler computations.

The upper part of the S-shaped curves stops rather abruptly. This is due to the upper surface shock wave reaching the airfoil trailing edge and the difficulty of the O-mesh used in the code to resolve shocks downstream of the trailing edge. Normally the curves should start turning down beyond this point because of the increasing size of the supersonic bubble on the pressure surface, reducing the lift on the airfoil.

The slope of the lift-incidence curve as obtained from the Euler computations is essentially negative since the vorticity generated behind the shock is of opposite sign to the circulation. Hence this tends to reduce the lift for increasing angles of attack. Since the potential model is irrotational, the vorticity created downstream of a shock is not taken into account and the lift will increase with

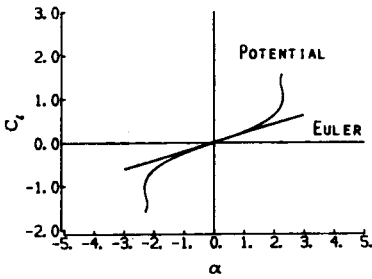


(a) NACA 0012 airfoil

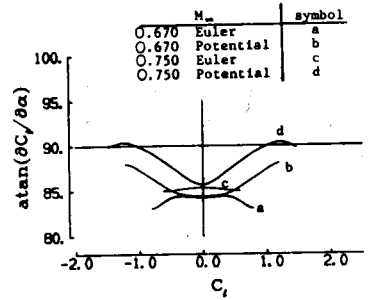


(b) NLR 7301 supercritical airfoil

Figure 15.35 Calculated variations of lift coefficient with incidence angle at different Mach numbers, obtained with the conservative potential model. (From Salas and Gumbert, 1985)



(a) Lift coefficient versus incidence angle at incident Mach number of 0.75



(b) Slope of lift – incidence curve in function of lift coefficient at two incident Mach numbers

Figure 15.3.6 Comparative variation of lift–incidence curves for a NACA 0012 airfoil, as obtained from potential and Euler models. (From Salas and Gumbert, 1985)

shock strength. Figure 15.3.6(b) shows the behaviour of the slope lift–incidence at two values of incident Mach number, demonstrating these effects. The same behaviour of the potential model is found for all airfoils tested (Salas and Gumbert, 1985). From these curves a diagram can be generated, displaying the Mach number–incidence range above which the potential model breaks down, as indicated by the values where the slope of the curve lift–incidence deviates from the linear behaviour. This is shown in Figure 15.3.7 for five airfoil sections. The regions above the curves can be considered as the region of non-validity of the potential flow model. Note the design points of the two shock-free supercritical airfoils (b) and (c), which are isolated shockless solutions appearing as singular points surrounded by solutions with shocks.

These severe limitations of the standard potential flow models could be reduced if the isentropic assumptions at the shocks are removed and replaced by some approximations of the correct Rankine–Hugoniot jump relations. This would maintain the advantage of potential flow models with regard to their economy and reduced computer cost, and extend their applicability range.

15.3.3 Non-isentropic potential models

An illuminating analysis has been presented by Klopfer and Nixon (1983) of the various assumptions at the basis of potential theories. Klopfer and Nixon investigated the different options available within the isentropic assumptions with regard to the conservation laws over a shock discontinuity. The standard potential model conserves mass and energy but not momentum. Other alternatives consist in conserving mass and momentum or energy and momentum. A one-dimensional analysis shows that conserving mass and momentum leads to shock intensities which are the closest to the Rankine–Hugoniot relations, followed by the standard potential model assumptions. The last option, which does not conserve mass, leads to large deviations and is not

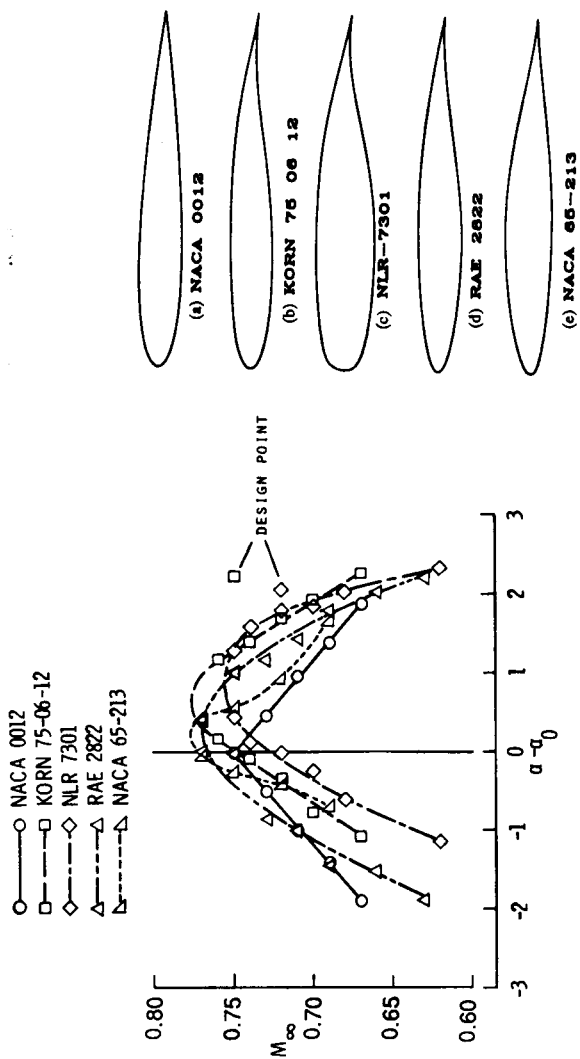


Figure 15.3.7 Mach number-incidence range above which the potential model breaks down for five different airfoils. Design points of the two shock-free supercritical airfoils are indicated. (From Salas and Gumbert, 1985)

to be recommended. Discussions of these various options can be found also in Viviand (1980) and Hafez and Lovell (1983b).

If, instead of satisfying all the conservation equations, errors are introduced by the model assumptions, for instance by the non-conservation of momentum in the isentropic potential model, one has the following steady-state equations:

$$\bar{\nabla} \cdot [\rho \bar{v} (1 + \varepsilon_\rho)] = 0 \quad (15.3.1)$$

$$\bar{\nabla} \cdot [\rho \bar{v} \otimes \bar{v} + p(1 + \varepsilon_m)] = 0 \quad (15.3.2)$$

$$\bar{\nabla} \cdot [\rho \bar{v} H(1 + \varepsilon_e)] = 0 \quad (15.3.3)$$

where ε_ρ , ε_m , ε_e are the errors in the conservation of mass, momentum and energy respectively. For the standard potential model $\varepsilon_\rho = \varepsilon_e = 0$, $\varepsilon_m \neq 0$ at shock discontinuities. Introducing Crocco's form of the momentum equation, equation (2.7.4) of Volume 1, leads to

$$-\bar{v} \times \bar{\zeta} = T \bar{\nabla} s - \bar{\nabla} H \left(\frac{1 + \varepsilon_e}{1 + \varepsilon_\rho} \right) - \frac{1}{\rho} [\bar{\nabla} (p \varepsilon_m) - \bar{v} \cdot \bar{\nabla} (\rho \bar{v} \varepsilon_\rho)] \quad (15.3.4)$$

This shows that the conservation errors appear as vorticity sources unless their gradient is zero, which is highly unlikely in a general flow configuration. For the isentropic potential model, equation (15.3.4) reduces to

$$-\bar{v} \times \bar{\zeta} = -\frac{1}{\rho} \bar{\nabla} (p \varepsilon_m) \quad (15.3.5)$$

showing that the non-conservation of momentum through a shock produces vorticity and hence the potential function does not exist any more downstream of a shock. This is a basic inconsistency of the potential model for flows with shocks. Actually, a non-uniform shock will generate an entropy gradient downstream of the shock and hence the correct inviscid flow with $\varepsilon_\rho = \varepsilon_m = \varepsilon_e = 0$ satisfies

$$-\bar{v} \times \bar{\zeta} = (T \bar{\nabla} s)_{\text{shock}} \quad (15.3.6a)$$

or

$$q \cdot \bar{\zeta} = T \frac{ds}{dn} \quad (15.3.6b)$$

and is also not irrotational. However, a small-perturbation analysis shows (Klopfer and Nixon, 1983) that the vorticity produced at an isentropic potential shock, with Mach number M_1 upstream of the shock, due to non-conservation of momentum is of the order of $(M_1^2 - 1)$, while it is of the order of $(M_1^2 - 1)^3$ for the non-isentropic shock satisfying all the conservation equations, that is for the Rankine-Hugoniot shocks. Hence, a non-isentropic correction to the potential shocks can be expected to have better accuracy than the isentropic potential shock.

The approach followed by Klopfer and Nixon consists in modifying the relation between density and velocity in such a way as to introduce the entropy

variation over the shock, writing instead of equation (13.1.6)

$$\frac{\rho}{\rho_0} = \left[K \left(1 - \frac{\bar{v}^2}{2H_0} \right) \right]^{1/(\gamma-1)} \quad (15.3.7)$$

where (see equation (2.1.27) in Volume 1)

$$K = e^{-\Delta s/c_v} \quad (15.3.8)$$

and Δs is the entropy increase over the shock. Actually, this is equivalent to a modification of the stagnation density ρ_0 , since one has ahead of the shock $\rho_0 = \rho_{01} = p_{01}/rT_0$ and downstream of the shock $\rho_{02} = p_{02}/rT_0 \neq \rho_{01}$ where p_{02}/p_{01} is the total pressure loss over the shock given by equation (2.9.21) in Volume 1. Hence equation (15.3.7) can be rewritten as

$$\rho = \rho_{02} \left(1 - \frac{\bar{v}^2}{2H_0} \right)^{1/(\gamma-1)} \quad (15.3.9)$$

where ρ_{02} is given by

$$\rho_{02} = \rho_{01} \left(\frac{p_{02}}{p_{01}} \right) \quad (15.3.10)$$

This approach has been considered independently by Deconinck and Hirsch (1983) in order to resolve the non-uniqueness of the potential flow with shocks in internal flows and to be able to establish a relation between the physical downstream pressure and the potential difference boundary condition necessary to locate the shock position according to the procedure developed in Section 13.4. The same approach has been applied to transonic nozzles and transonic cascades by Habashi *et al.* (1983).

Of course this requires that the computational procedure be adapted in order to find the shock position and subsequently to assume that the one-dimensional shock relations for a normal shock are valid. This is justified for simple shock structures but is undoubtedly more difficult to apply for complex shock configurations such as the ones illustrated in Figure 15.1.2.

Figure 15.3.8, from Whitlow (1988), shows a comparison between a potential flow and a Euler solution for an NLR 7301 airfoil at $M_\infty = 0.70$ and 2° incidence. As can be seen from this figure, the isentropic potential model gives a strong shock close to the trailing edge and no shock on the pressure surface, while the Euler solution has a weaker shock close to the 60 per cent chord. With the isentropic corrections closer agreement with the Euler solution is obtained.

For external flow problems an additional adaptation has to be introduced with regard to the Kutta condition, since a relation exists between the shock position, which fixes the circulation, and the jump in potential at the trailing edge cut. A detailed investigation of the relation between the shock position and trailing edge flow, in particular the flow angle of the stagnation streamline for lifting airfoils, has been applied by Lucchi (1983) in order to introduce non-isentropic shock corrections to a potential flow computation.

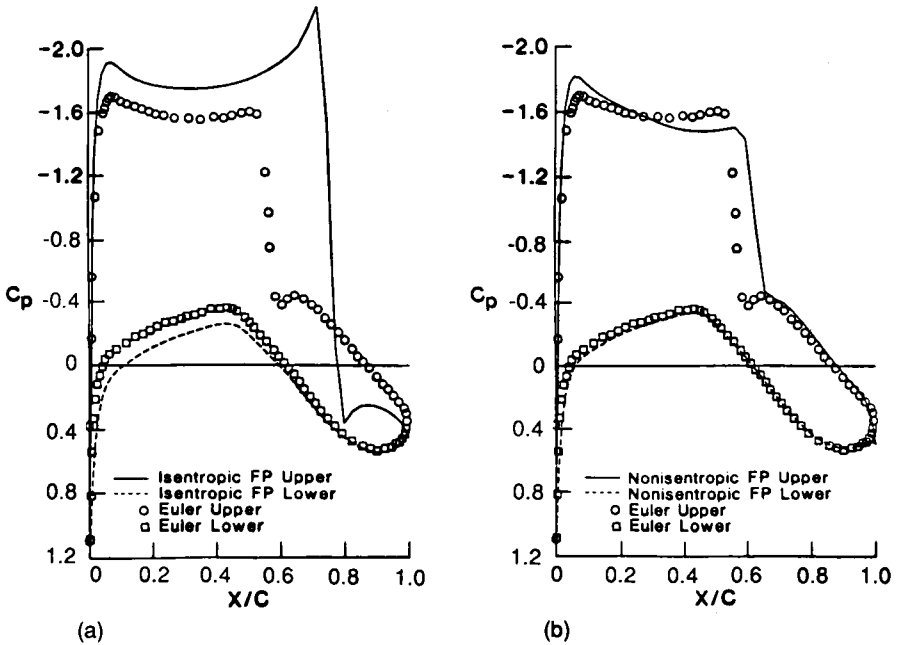


Figure 15.38 Pressure distribution on an NLR 7301 airfoil at $M_\infty = 0.7$ and 2° incidence, obtained from the potential model, Euler model and non-isentropic corrections to the potential model. (a) Isentropic potential and Euler solutions. (b) Non-isentropic potential and Euler solutions. (From Whitlow, 1988)

The Kutta condition satisfied by the potential calculation corresponds to equal static pressures on both sides of the trailing edge, since the stagnation pressures are equal in the isentropic assumption. Hence, the dividing streamline leaves the trailing edge along the bisector direction. However, with a non-isentropic shock the stagnation pressures are different on pressure and suction surfaces and the bisector direction is not a force-free streamline. The stagnation streamline will in this case leave the trailing edge under an angle α_{le} with the bisector directed towards the suction surface. This angle is a measure of the stagnation pressure difference between both sides of the airfoil, and therefore allows the position of the isentropic shocks to be fixed. Although the shock positions are extremely sensitive to small variations in the angle of the stagnation streamline (Lucchi, 1983), good results are obtained by correcting the potential pressure distribution by a constant shift defined by the Rankine–Hugoniot relation and iterating over the streamline angle at the trailing edge in order to satisfy the condition of equal static pressures.

All the methods based on corrections to a potential function do require some form of shock detection and some simplifying assumption with regard to the normal shock relations. This is also the case for the non-isentropic calculation of Ecer and Akay (1983). In this approach the Clebsch representation (equations (2.8.12) and (2.8.14) in Volume 1) is used and the rotational function

ψ is obtained through equation (2.8.14) and the generated entropy over the shock.

Clearly the introduction of non-isentropic corrections into conservative potential is to be recommended as a simple way to increase the validity range of potential flow models. Examples of applications can be found in Siclari and Rubel (1984) and Chen *et al.* (1985).

15.4 CONCLUSIONS

The potential model is actually a correct inviscid representation for subsonic flows as well as for shock-free supersonic flows and can be used in this range with excellent results as long as no strong shocks are present. A large number of applications exist currently in industry.

The problems connected with the hyperbolic properties of the potential equation in the supersonic regions can be treated by the introduction of artificial viscosity, density upwinding or flux upwinding, while maintaining the subsonic, central differencing of the potential equation. This has to be coupled to an appropriate iterative scheme of the algebraic system of equations.

For weak normal shocks, the inconsistencies with regard to the full Euler model can be circumvented in various ways, through non-isentropic corrections, as long as the maximum Mach number remains below values of the order of $M \simeq 1.3$. Also, within this range, the interactive computation with the boundary layer development provides a valid approximation to the viscous effects, as illustrated by the examples of Figure 2.5.3 in Volume 1.

The computational methods for potential flows have reached a strongly developed stage and three-dimensional flows can be computed today in a few seconds of computer time on the present available computers. Although the isentropic potential flow model has a limited range of validity and problems of non-uniqueness for the conservative formulation, its usefulness in the subsonic, low transonic and fully supersonic flow regimes is well established.

Outside this range, the full system of Euler equations should be advocated for the computation of inviscid flows.

REFERENCES

- Baker, J. T. (1981). 'Potential flow calculations by the approximate factorization method.' *Journal Computational Physics*, **42**, 1-19.
- Ballhaus, W. F., and Bailey, F. R. (1972). 'Numerical calculation of transonic flow about swept wings.' *AIAA Paper 72-677*.
- Ballhaus, W. F., and Steger, J. L. (1975). 'Implicit approximate factorization schemes for the low-frequency transonic equations.' *NASA TM X-73082*.
- Ballhaus, W. F., Jameson, A., Albert, J. (1978). 'Implicit approximate factorization schemes for steady transonic flow problems.' *AIAA Journal*, **16**, 573-9.
- Boerstoel, J. W. (1981). 'A multi-grid algorithm for steady transonic potential flows around airfoils using Newton iteration.' *NASA CP 2022*, pp. 151-72; also *Journal Computational Physics*, **48**, 314-43 (1982).

- Boerstol, J. W., and Kassies, A. (1983). 'Integrating multigrid relaxation into a robust fast-solver for transonic potential flows around lifting airfoils.' *AIAA Paper 83-1885*, AIAA 6th Computational Fluid Dynamics Conference, Danvers.
- Bredif, M. (1983). 'A fast finite element method for transonic flow calculations.' *AIAA Paper 83-0507*, AIAA 21st Aerospace Sciences Meeting, Reno.
- Caspar, J. R. (1980). 'A model problem study of transonic potential flow procedures.' *AIAA Paper 80-0337*, AIAA 18th Aerospace Sciences Meeting.
- Caspar, J. R., Hobbs, D. E., Davis, R. L. (1979). 'The calculation of potential flow in cascades using finite area techniques.' *AIAA Paper 79-0077*, AIAA 17th Aerospace Sciences Meeting. See also *AIAA Journal*, **18**, 103–109, 1980.
- Catherall, D. (1982). 'Optimum approximate factorization schemes for two-dimensional steady potential flows.' *AIAA Journal*, **20**, 1057–63.
- Caughey, D. A. (1983). 'Multigrid calculation of three dimensional transonic potential flows.' *AIAA Paper 83-0374*, AIAA 21st Aerospace Sciences Meeting.
- Caughey, D. A., and Jameson, A. (1982). 'Basic advances in the finite volume method for transonic potential flow calculations.' In T. Cebeci (ed.), *Numerical and Physical Aspects of Aerodynamic Flows*, Berlin: Springer Verlag.
- Chen, L. T., Clark, R. W., and Vassberg, J. C. (1985). 'Improvements in transonic airfoil potential flow calculations.' *AIAA Paper 85-1642*, AIAA 18th Fluid Dynamics and Plasmadynamics and Lasers Conference.
- Deconinck, H. (1983). 'The numerical computation of transonic potential flows.' Ph.D. Thesis, Department of Fluid Mechanics, Vrije universiteit Brussel, Brussels, Belgium.
- Deconinck, H., and Hirsch, Ch. (1979). 'Transonic flow calculations with finite elements.' In A. Rizzi, and H. Viviand (eds), *Notes on Numerical Fluid Dynamics*, Vol. 3, *Proc. GAMM Workshop on Numerical Methods for the Computation of Inviscid Transonic Flows with Shock Waves*, Braunschweig: Vieweg.
- Deconinck, H., Hirsch, Ch. (1980a). 'Subsonic and transonic computations of cascade flows.' In Glöwinski, R. and Lions, J. (eds), *Computing Methods in Applied Sciences and Engineering*, North Holland.
- Deconinck, H., and Hirsch, Ch. (1980b). 'Transonic flow calculations with higher order finite elements.' In W. C. Reynolds, (ed.), *Proc. Seventh International Conference on Numerical Method in Fluid Dynamics, Lecture Notes in Physics*, Vol. 141, Springer Verlag.
- Deconinck, H., and Hirsch, Ch. (1981). 'A multigrid method for the transonic full potential equation discretized with finite elements on an arbitrary body fitted mesh.' *NASA CP 2022*, pp. 61–81; also *Journal Computational Physics*, **48**, 344–65 (1982).
- Deconinck, H., Hirsch, Ch. (1983). 'Boundary conditions for the potential equation in transonic internal flow calculations.' *26th International ASME Gas Turbine Conference—ASME Paper 83-GT-135*.
- Dougherty, F. C., Holst, T. L., Gundy, K. L., and Thomas, S. D. (1981). 'TAIR—a transonic airfoil analysis computer code.' *NASA TM-81296*.
- Eberle, A. (1977). 'Eine methode finiter Elemente zur Berechnung der Transsonischen Potential-Stromung um Profile.' *MBB Rapport MBB-UFE 1352*; English Translation, *NASA TM-75324*.
- Ecer, A., and Akay, H. U. (1981). 'Investigation of transonic flow in a cascade using finite element method.' *AIAA Journal*, **19**, 1174–82.
- Ecer, A., and Akay, H. U. (1983). 'A finite element formulation for steady transonic Euler equations.' *AIAA Journal*, **21**, 343–50.
- Engquist, B., and Osher, S. (1980). 'Stable and entropy satisfying approximations for transonic flow calculations.' *Mathematics of Computation*, **34**, 45–75.
- Garabedian, P. R., and Korn, D. (1972). 'Analysis of transonic airfoils.' *Comm. Pure and Applied Mathematics*, **24**, 841–51.
- Gelder, D. (1971). 'Solution of the compressible flow equations.' *Int. Journal for Numerical Methods in Engineering*, **3**, 35–43.

- Goorjian, P. M., Van Buskirk, R. (1981). 'Implicit calculation of transonic flows using monotone methods.' *AIAA Paper 81-0331*, AIAA 19th Aerospace Sciences Meeting, St. Louis.
- Goorjian, P. M., Meagher, M. E., Van Buskirk, R. (1983). 'Monotone implicit algorithms for the small disturbance and full potential equations applied to transonic flows.' *AIAA Paper 83-0371*, AIAA 21st Aerospace Sciences Meeting, Reno.
- Habashi, W. G., and Hafez, M. M. (1981). 'Finite element method for transonic cascade flows.' *AIAA Paper 81-1472*, AIAA/SAE/ASME 17th Joint Propulsion Conference, Colorado Springs.
- Habashi, W. G., and Hafez, M. M. (1982). 'Finite element solutions of transonic flow problems.' *AIAA Journal*, **20**, 1368-76.
- Habashi, W. G., Hafez, M., and Kotiuga, P. I. (1983). 'Finite element methods for internal flow calculations.' *AIAA Paper 83-1404*, AIAA/SAE/ASME 19th Joint Propulsion Conference.
- Hafez, M. M. (1983). 'Progress in finite element techniques for transonic flows.' *AIAA Paper 83-1919*, Proc. AIAA 6th Computational Fluid Dynamics Conference, Danvers, pp. 243-50.
- Hafez, M. M., and Lovell, D. R. (1983a). 'Improved relaxation schemes for transonic potential calculations.' *AIAA Paper 83-0372*, AIAA 21st Aerospace Sciences Meeting, Reno.
- Hafez, M. M., and Lovell, D. (1983b). 'Entropy and vorticity corrections for transonic flows.' *AIAA Paper 83-1926*, Proc. AIAA 6th Computational Fluid Dynamics Conference, pp. 630-44.
- Hafez, M. M., and South, J. C. (1981). 'Vectorization of relaxation methods for solving transonic full potential equation.' In A. Rizzi, and H. Viviand (eds), *GAMM Workshop on Numerical Methods for the Computation of Inviscid Transonic Flows with Shock Waves*, Vieweg Verlag (1981).
- Hafez, M. M., South, J. C., and Murman, E. M. (1978). 'Artificial compressibility methods for the numerical solution of the full potential equation.' *AIAA Paper 78-1148*; see also *AIAA Journal*, **17**, 838-44.
- Hafez, M. M., Osher, S., and Whitlow, W. (1984). 'Improved finite difference schemes for transonic potential calculations.' *AIAA Paper 84-0092*, AIAA 22nd Aerospace Sciences Meeting.
- Hall, M. G. (1981). 'Computational fluid dynamics—a revolutionary force in aerodynamics.' *AIAA Paper 81-1014*, Proc. Fifth AIAA Computational Fluid Dynamics Conference, pp. 176-88.
- Hirsch, Ch., and Warzee, G. (1977). 'Finite element computation of subsonic cascade flows.' *Proc. 6th Canadian Congress on Applied Mechanics, Vancouver*.
- Holst, T. L. (1979). 'An implicit algorithm for the conservative transonic full potential equation using an arbitrary mesh.' *AIAA Journal*, **17**, 1038-45.
- Holst, T. L. (1980). 'A fast, conservative algorithm for solving the transonic full potential equation.' *AIAA Journal*, **18**, 1431-9.
- Holst, T. L., and Ballhaus, W. F. (1979). 'Fast, conservative schemes for the full potential equation applied to transonic flows.' *AIAA Journal*, **17**, 145-52.
- Holst, T., and Thomas, S. (1983). 'Numerical solution of transonic wing flowfields.' *AIAA Journal*, **21**, 863-70.
- Hughes, T. J. R., and Brooks, A. N. (1982). 'A theoretical framework for Petrov-Galerkin methods with discontinuous weighting functions: application to the streamline upwind procedure.' In R. H. Gallagher *et al.* (eds), *Finite Elements in Fluids*, London: John Wiley and Sons.
- Hughes, T. J. R., and Mallet, M. (1986). 'A new finite element formulation for computational fluid dynamics: III. The generalized streamline operator for multi-dimensional advective-diffusive systems.' *Computer Methods for Applied Mechanical Engineering*, **58**, 305-28.

- Jameson, A. (1974). 'Iterative solutions of transonic flows over airfoils and wings, including flows at Mach 1.' *Comm. Pure and Applied Mathematics*, **27**, 283–309.
- Jameson, A. (1975). 'Transonic potential flow calculations using conservative form.' *Proc. AIAA Second Computational Fluid Dynamics Conference, Hartford*, pp. 148–61.
- Jameson, A. (1976a). 'Numerical computation of transonic flows with shock waves.' In *Symposium Transonicum*, Vol. II, Springer Verlag.
- Jameson, A. (1976b). 'Numerical solutions of nonlinear partial differential equations of mixed type.' In *Numerical Solutions of Partial Differential Equations*, Vol. III, Academic Press, New York, pp. 275–320.
- Jameson, A. (1979). 'Acceleration of transonic potential flow calculations on arbitrary meshes by the multi-grid method.' *AIAA Paper 79-1458*, AIAA 4th Computational Fluid Dynamics Conference.
- Jameson, A., and Caughey, D. E. (1977). 'A finite volume method for transonic potential flow calculations.' *Proc. AIAA 3rd Computational Fluid Dynamics Conference, Albuquerque*, pp. 35–54.
- Klopper, G. H., and Nixon, D. (1983). 'Non isentropic potential formulation for transonic flows.' *AIAA Paper 83-0375*, AIAA 21st Aerospace Sciences Meeting, Reno.
- Lax, P. D. (1954). 'Weak solutions of non linear hyperbolic equations and their numerical computation.' *Comm. Pure and Applied Mathematics*, **7**, 159–93.
- Lucchi, C. W. (1983). 'Shock connection and trailing edge pressure jump in two dimensional transonic potential flows at subsonic uniform mach numbers.' *Pro. AIAA 6th Computational Fluid Dynamics Conf. AIAA Paper 83-1884*, pp. 23–29.
- Murman, E. M., and Cole, J. D. (1971). 'Calculation of plane steady transonic flows.' *AIAA Journal*, **9**, 114–21.
- McCarthy, D. R., and Reyhner, T. A. (1982). 'Multigrid code for three dimensional transonic potential flow about inlets.' *AIAA Journal*, **20**, 45–50.
- Ortega, J. M., and Rheinboldt, W. C. (1970). *Iterative Solutions of Non-Linear Equations in Several Variables*, London: John Wiley and Sons.
- Prince, T. C. (1978). 'Prediction of steady inviscid compressible flow on a blade-to blade surface by finite element method.' *AIAA 16th Aerospace Sciences Meeting—AIAA Paper 78-244*.
- Osher, S. (1982). 'Shock modelling in aeronautics.' In K. W. Morton and M. J. Baines (eds), *Numerical Methods for Fluid Dynamics*, pp. 179–218, London: Academic Press.
- Osher, S., Hafez, M., and Whitlow, W. Jr. (1985). 'Entropy condition satisfying approximations for the full potential equation of transonic flow.' *Mathematics of Computation*, **44**, 1–29.
- Salas, M. D., Gumbert, C. R. (1985). 'Breakdown of the conservative potential equation.' *AIAA Paper 85-0367*, AIAA 23rd Aerospace Sciences Meeting.
- Salas, M. D., Jameson, A., and Melnik, R. E. (1983). 'A comparative study of the non uniqueness problem of the potential equation.' *AIAA Paper 83-1888, Proc. AIAA 6th Computational Fluid Dynamics Conference*, pp. 48–60.
- Shankar, V., Hiroshi, I., Gorski, J., and Osher, S. (1985). 'A fast, time accurate unsteady full potential scheme.' *AIAA Paper 85-1512, Proc. AIAA 7th Computational Fluid Dynamics Conference*, pp. 214–27.
- Shen, S. F. (1978). 'Transonic aerodynamic computation with finite element method.' In *Finite Elements in Fluids*, Vol. 3, London: John Wiley and Sons.
- Siclari, M. J., and Rubel, A. (1984). 'Entropy corrections to supersonic conical nonlinear potential flows.' *AIAA-Paper 84-1683*, AIAA 17th Fluid Dynamics, Plasma Dynamics and Lasers Conference.
- South, J. C., and Hafez, M. M. (1983). 'Stability analysis of intermediate boundary conditions in approximate factorization schemes.' *AIAA Paper 83-1896, Proc. AIAA 6th Computational Fluid Dynamics Conference, Danvers*, pp. 527–34.
- Steger, J. L., and Lomax, H. (1972). 'Transonic flow about two-dimensional airfoils by relaxation procedures.' *AIAA Journal*, **10**, 49–54.

- Steinhoff, J., and Jameson, A. (1982). 'Multiple solutions of the transonic potential flow equation.' *AIAA Journal*, **20**, 1521–5.
- Thomas, S. D., and Holst, T. L. (1983). 'Numerical computation of transonic flows about wing-fuselage configurations on a vector computer.' *AIAA Paper 83-0499, AIAA 26th Aerospace Sciences Meeting*.
- Van der Wees, A. J., Van der Vooren, J., and Meelker, J. H. (1983). 'Robust calculation of 3D transonic potential flow based on the non-linear FAS multi-grid method and incomplete LU decomposition.' *AIAA Paper 83-1950, Proc. AIAA 6th Computational Fluid Dynamics Conference*, pp. 584–601.
- Viviand, H. (1980). 'Pseudo-unsteady methods for transonic flow computations.' *Proc. 7th Int. Conference on Numerical Methods in Fluid Dynamics*, Springer Verlag (1981).
- Volpe, G. (1986). 'Transonic potential flow calculations by two artificial density methods.' *AIAA Paper 86-1084, AIAA/ASME 4th Fluid Mechanics, Plasma Dynamics and Lasers Conference*.
- Whitlow, W. Jr (1988). 'Application of a nonisentropic full potential method to AGARD standard airfoils.' *AIAA Paper 88-0710, AIAA 26th Aerospace Sciences Meeting*.
- Wong, Y. S. (1983). 'Calculation of Transonic Potential Flows by a Parameter Free Procedure.' *AIAA Paper 83-1886, Proc. AIAA 6th Computational Fluid Dynamics Conference*, pp. 30–5.
- Wong, Y. S., and Hafez, M. M. (1982). 'Conjugate gradient methods applied to transonic finite difference and finite element calculations.' *AIAA Journal*, **20**, 1526–33.

PROBLEMS

Problem 15.1

Obtain the relations (15.1.9) analytically.

Problem 15.2

Work out explicitly the difference form of equation (15.1.9) applying equations (15.1.10) and (15.1.11) and derive the rotated difference scheme in the Cartesian system of coordinates.

Show the validity of equation (15.1.12).

Problem 15.3

Apply the artificial density formulation to the finite difference discretization of Problem 14.8 for the flow along a cylinder. Try various expressions and coefficients of the artificial density.

Problem 15.4

Repeat Problem 15.3 with a finite volume scheme (Problem 14.10) and artificial viscosity (15.1.19). Compare with the formulations of Problem 15.3.

Problem 15.5

Show that the sonic conditions are related to the reference conditions of the flow at

infinity, by the following relations:

$$q_*^2 = c_*^2 = \left\{ \frac{1 + [(\gamma - 1)/2]M_\infty^2}{[(\gamma + 1)/2]M_\infty^2} \right\} U_\infty^2$$

$$\frac{\rho_*}{\rho_\infty} = \left(\frac{2}{\gamma + 1} \right)^{1/(\gamma - 1)} \quad \text{or} \quad \frac{\rho_*}{\rho_\infty} = \left(\frac{q_*}{U_\infty} M_\infty \right)^{2/(\gamma - 1)}$$

Hint: Apply the perfect gas relations and the conservation of energy $H_0 = h + \bar{V}^2/2$ to obtain the relations for the critical, sonic conditions $q_* = c_*$. The velocity at infinity is U_∞ .

Problem 15.6

Compare the upwinded fluxes (15.1.37) at sonic and shock points with the fluxes obtained from the corresponding upwinded densities, according to the following equations:

$$\bar{\rho}_{i+1/2,j} = [(1 - \mu)\rho]_{i+1/2,j} + \mu_{i+1/2,j}\rho_{i+1/2+l,j}$$

$$\mu_{i+1/2,j} = \begin{cases} \max \left[0, \left(1 - \frac{M_c^2}{M_{ij}^2} \right) \right] CM_{ij}^2 & \text{if } U_{i+1/2,j} > 0 \\ \max \left[0, \left(1 - \frac{M_c^2}{M_{i+1,j}^2} \right) \right] CM_{i+1,j}^2 & \text{if } U_{i+1/2,j} < 0 \end{cases}$$

The subscript l is equal to minus the sign of $U_{i+1/2,j}$.

Analyse the differences and observe the effects of the constant M_c^2 on the spreading of the shock.

Problem 15.7

Apply the artificial flux formulation, equation (15.1.37) to Problem 15.3. Compare both cases.

Problem 15.8

Consider the conservative potential equation in two dimensions, in curvilinear coordinates, Example 13.1.1, and apply the Murman–Cole upwinding in the ξ direction, following equation (15.1.3). Develop the difference equations by applying the formulas (14.1.17) and (14.1.18).

Show that the additional term from the upwinding is proportional to

$$\frac{\rho g^{11}}{J} \left(\frac{U^2}{g^{11}c^2} - 1 \right) \phi_{\xi\xi\xi} \Delta \xi$$

Observe that for subsonic contravariant ξ velocities this artificial viscosity coefficient has the wrong sign and hence the scheme will not converge.

Hint: Apply equation (15.1.21) in curvilinear coordinates, as

$$\frac{\partial \rho}{\partial \xi} = -\frac{\rho}{c^2} \bar{v} \cdot \frac{\partial \bar{v}}{\partial \xi} = -\frac{\rho}{c^2} \bar{v} \cdot \bar{\nabla} \frac{\partial \phi}{\partial \xi}$$

and

$$\rho_\xi = -\frac{\rho}{c^2} \left(U \frac{\partial}{\partial \xi} + V \frac{\partial}{\partial \eta} \right) \phi_\xi$$

Introduce in $(\partial/\partial\xi)(\rho(U/J))$ and show that this leads to a term

$$\frac{\rho}{J} \left(g^{11} - \frac{U^2}{c^2} \right) \phi_{\xi\xi} + \frac{\rho}{J} \left(g^{12} - \frac{UV}{c^2} \right) \phi_{\xi\eta}$$

Problem 15.9

Show that the Murman–Cole equation (15.1.6) can be written as follows, with the introduction of a switch coefficient μ , such that $\mu = 0$ for $M < 1$ and $\mu = 1$ for $M > 1$:

$$(1 - M^2)_{ij} \delta_x^2 \phi_{ij} + \delta_y^2 \phi_{ij} = \mu_{ij} (1 - M^2)_{ij} (\delta_x^2 \phi_{ij} - \delta_x^2 \phi_{i-1,j})$$

Write out the discretized equation at a shock point, namely for $M > 1$ at $(i-1, j)$ and $M < 1$ at (i, j) .

Compare the shock point treatment with a conservative formulation

$$(1 - M^2)_{ij} \delta_x^2 \phi_{ij} + \delta_y^2 \phi_{ij} = \mu_{ij} (1 - M^2)_{ij} \delta_x^2 \phi_{ij} - \mu_{i-1,j} (1 - M^2)_{i-1,j} \delta_x^2 \phi_{i-1,j}$$

Hint: Observe that equation (15.1.2) can be written as

$$\phi_{xx}^{(B)}|_{ij} = \phi_{xx}^{(C)}|_{i-1,j}$$

Problem 15.10

Apply the flux upwinding technique to the small-disturbance potential equation (13.2.12) and compare with the Murman–Cole approach of the previous problem.

Problem 15.11

Apply the flux upwinding method to the steady Burgers equation $(\phi_x^2)_x = 0$ and compare with the original Murman–Cole switch.

Problem 15.12

Show that an explicit scheme applied to the Murman–Cole differencing (15.1.5) is unstable by a Von Neumann analysis.

Apply also a Von Neumann analysis to the scheme (15.2.1) and show that it is unconditionally stable.

Hint: Consider the scheme, valid for $M > 1$,

$$(1 - M^2)(\phi_{i-1,j}^n - 2\phi_{i-1,j}^{n+1} + \phi_{ij}^{n+1}) + (\phi_{i,j+1}^n - 2\phi_{ij}^{n+1} + \phi_{i,j-1}^n) = 0$$

and analyse the extreme cases $\phi_y = \pm \pi$ with $\phi_x = 0, \pi$.

Problem 15.13

Derive equations (15.2.2) to (15.2.4), (15.2.6) and (15.2.7).

Problem 15.14

Verify the SLOR equation (15.2.5), and write explicitly the tridiagonal system of equations to solve along the y lines.

Problem 15.15

Apply the SLOR technique to solve the flow around a cylinder following Problem 15.3. Solve for free-stream Mach numbers of 0.2, 0.4 and for the supercritical values of 0.51. Consider only half a circle on a symmetry plane.

Problem 15.16

Repeat Problem 15.15 for the scheme of Problem 15.4.

Problem 15.17

Write the discretized equations for the AF2 scheme in full, following equations (15.2.46).

Problem 15.18

Repeat Problem 15.15 with the ADI and AF2 methods and compare with the SLOR iterations. Investigate the influence of the parameters σ, ω .

Problem 15.19

Apply the line relaxation to the matrix system obtained by the finite element discretization with bilinear quadrilateral elements on a rectangular mesh. Notice the similarity and differences with the equations obtained in Problem 15.14.

Hint: In the limiting case of an incompressible flow, the finite element tridiagonal matrix structure is $(1 \ -8 \ 1)$ instead of $(1 \ -4 \ 1)$ for the finite difference schemes.

Problem 15.20

Applying the results of Problem 15.2, obtain equation (15.1.14).

Problem 15.21

Obtain the eigenvalues (15.2.34) from a Von Neumann analysis of the operator (15.2.33).

Problem 15.22

Apply the SLOR technique to solve the flow over a thin circular arc airfoil of 4 per cent thickness applying the small-disturbance approximation.

Consider a uniform Cartesian mesh with the airfoil replaced by a segment $0 < x < 1$. The airfoil is introduced via the boundary condition $u/v = df/dx$, where $y = f(x)$ is the airfoil's surface. Solve for a free-stream Mach number of 0.6 and 0.85 with the artificial viscosity concept.

Problem 15.23

Solve the same problem (15.22) and apply an artificial density method for the transonic cases.

Solve the algebraic system of equations by line relaxations along the radii.

Problem 15.24

Introduce the non-isentropic corrections (15.3.10) into Problem 15.22 for the incident Mach number of 0.85 and comment on the observed differences with regard to shock position and intensity.

PART VI: THE NUMERICAL SOLUTION OF THE SYSTEM OF EULER EQUATIONS

The system of Euler equations constitutes the most complete description of inviscid, non-heat-conducting flows and hence, is the highest level of approximation for non-viscous fluids (see Section 2.7 in Volume 1). In this sense, it should simulate physical flows in the limit of vanishing viscosities.

Although the inviscid flow models are obviously not of universal validity, the importance of their accurate numerical simulation resides in the dominating convective character of the Navier–Stokes equations at high Reynolds numbers.

Therefore most, if not all, of the methods developed for the Euler equations are also valid for the Navier–Stokes equations, with the addition of centrally discretized shear stress terms. Actually, many of them were originally developed for the Navier–Stokes equations. It is only at very low Reynolds numbers, when the flow is diffusion dominated, that specific methods for the Navier–Stokes equations have to be defined. However, since the overwhelming majority of flow situations encountered in industry and nature have high Reynolds numbers, they are essentially dominated by convective effects and hence close to the Euler equations, to which they reduce outside the viscous regions.

A large number of methods and approaches have been developed in order to handle the complex, non-linear system of convection-dominated conservation laws.

The history of numerical techniques for the resolution of the inviscid Euler equations goes back to the early 1950s, with the first-order methods of Courant *et al.* (1952) and Lax and Friedrichs (Lax, 1954). Since these early days, a very large number of schemes have been developed, some of them having already been introduced in Volume 1 as applied to the one-dimensional linear convection equation.

The milestone for the modern development of numerical schemes for time-dependent Euler (and also compressible Navier–Stokes) equations is undoubtedly to be found in the pioneering work of Lax and Wendroff (Lax, 1957; Lax and Wendroff, 1960, 1964). An account of the earlier work in the field of numerical developments for Euler equations can be found in Richtmyer and Morton (1967).

The second-order accurate Lax–Wendroff method has led to a whole family of variants when applied to non-linear systems, characterized by their common property of being space centred, reducing to three-point central schemes in one-dimension, explicit in time and derived from a combined space and time discretization. The most popular of these variants is due to MacCormack (1969) and a more general family, with two parameters, has been developed by Lerat and Peyret (1974).

When time accuracy is not required, as for steady-state calculations or when the time-step restriction imposed by the conditional stability of explicit schemes is much smaller than the typical time constant of unsteady phenomena, implicit methods can be considered. Implicit generalizations of the Lax–Wendroff schemes have been developed by Lerat (1979, 1983).

Many other variants can be developed in this framework and the bidiagonal, compact schemes presented by MacCormack (1981), Casier *et al.* (1983) have some attractive properties.

Another approach to space-centred schemes is based on a separate space and time discretization, unlike the Lax–Wendroff family which is basically derived from a combined space and time discretization. As a consequence, the steady-state limit of the numerical solution depends on the time-step used in the computation. Although the error attached to the time-step terms is of the same order as the truncation error, because of the CFL condition, it nevertheless represents a conceptual drawback, since it introduces a numerical parameter in the predicted steady-state flow.

This drawback is avoided when the time integration is separated from the space discretization. By performing first the space discretization, a system of ordinary differential equations in time is obtained and the steady-state solution is reached when the sum of the space terms vanishes.

Space-centred schemes (three-point schemes in one dimension) of second-order accuracy in space belonging to this approach were initially introduced with implicit, linear multi-step time-integration methods by Briley and McDonald (1975), Beam and Warming (1976) and Warming and Beam (1978).

An explicit scheme, applying a fourth-order Runge–Kutta time-integration method has been introduced by Jameson *et al.* (1981), based on essentially similar second-order space discretization methods.

The basic concept behind space-centred schemes is the application of Taylor expansions and analytic continuation to equations that are essentially of a convective nature and hence directionally biased.

Alternative discretization methods can be developed which relate to the physical propagation properties of the solutions of the Euler equations. These ‘non-space-centred’ schemes are classified as *upwind* schemes in a global sense, since many variants can be defined. Their common point is the relation established between the characteristic propagation properties and the differencing such as to apply directional space discretizations in accordance with the physical behaviour of the inviscid flows.

The first explicit upwind scheme was introduced by Courant *et al.* (1952), and several extensions to second-order accuracy and implicit time integrations have been developed. The flux vector splitting methods of Steger and Warming (1981) and Van Leer (1982) can be considered as members of the same subgroup, based on a directional discretization of the flux derivatives. A second subgroup of schemes is in the line of Godunov's (1959) method which solves, over each mesh interval, the locally one-dimensional Euler equations for discontinuous neighbouring states (the Riemann problem). This most original approach, which introduces in the numerical discretization information from the exact, local, non-linear solutions of the Euler equations, has generated a series of schemes that introduce different approximate Riemann solvers (Engquist and Osher, 1980; Osher, 1982; Roe, 1981a, 1981b). They are also known as flux difference splitting methods.

The extension of this approach has generated some remarkable mathematical analysis, leading to a deep understanding of basic properties of the discretization of non-linear systems of hyperbolic equations and to the introduction of non-linear components in the discretizations. Essential contributions in these directions are due to Van Leer (1974, 1979), Harten (1983, 1984), Osher (1984), Osher and Chakravarthy (1984) and others.

The outcome of these investigations is the ability to generate numerical algorithms which allow a high resolution of discontinuities, such as shock waves and contact discontinuities, without oscillations. This last aspect is of considerable importance since the appearance of shocks, and other discontinuities, is a frequent and essential phenomenon of high-speed inviscid flows.

Practically all the schemes for Euler equations behave in a satisfactory way for stationary, smooth flows without strong gradients, but they can have very different behaviours in the presence of shock waves, for instance. Therefore, particular attention will be given to the numerical simulation of discontinuities and to the behaviour of different schemes in dealing with these situations. Most of the originally developed schemes, such as the Lax–Wendroff type of central schemes, generate oscillations around shock discontinuities. Various methods have been attempted to control or limit these oscillations through the introduction of artificial viscosity, which is required, on the other hand, by the entropy condition to exclude non-physical shocks.

Another approach aims at preventing the generation of numerical oscillations, instead of damping them after they have been allowed. This approach is based on the concepts of non-linear *limiters* introduced initially by Boris and Book (1973) and Van Leer (1974) and later generalized via the important concept of *total variation diminishing* (TVD) schemes, introduced by Harten (1983), whereby the variation of the numerical solution is controlled in a non-linear way, such as to forbid the appearance of any new extremum. This concept, when applied to central schemes, leads to particular forms of artificial viscosity without empirical constants.

A simplified classification of some of the most important and widely applied schemes is given in Table VI.1. This classification is by far not exhaustive and

Table VI.1. Schemes for Euler and Navier–Stokes equations

	Combined space–time discretization	Separate space discretization and time integration
Space-centred schemes	<i>Explicit schemes</i>	<i>Implicit schemes of</i>
	Lax–Friedrichs scheme (1954)—first order	Briley and McDonald (1975)
	Lax–Wendroff schemes (1960)—second order	Beam and Warming (1976)
	<i>Two-step schemes</i>	<i>Multi-stage Runge–Kutta explicit schemes of</i>
	Richtmyer and Morton (1967)	Jameson, Schmidt and Turkel (1981)
	MacCormack (1969)	
	Lerat and Peyret (1974)	
	<i>Implicit schemes</i>	
	MacCormack (1981); Casier, Deconinck and Hirsch (1983)	
	Lerat (1979, 1983)	
Upwind schemes		Flux vector splitting
		Courant, Isaacson and Reeves (1952)—First-order upwind
		Moretti (1979)—non-conservative schemes plus shock fitting
		Steger and Warming (1981)
		Van Leer (1982)
		Godunov-type methods—Riemann solvers
		<i>Exact Riemann problem solution</i>
		Godunov (1959)—first order
		Van Leer (1979)—second order
		Woodward and Colella (1984); Ben-Artzi and Falcovitz (1984)
	<i>Approximate Riemann solvers</i>	
	Roe (1981a, 1981b)	
	Engquist and Osher (1980); Osher (1982)	
	Harten, Lax and Van Leer (1983)	
High-resolution TVD schemes (non-linear schemes)		Explicit TVD upwind schemes
		Boris and Book (1973); Van Leer (1974, 1979)
		Harten (1983, 1984)
		Osher (1984); Osher and Chakravarthy (1984)
		Implicit TVD upwind schemes
	Yee and Harten (1985)	
	Central TVD schemes (implicit or explicit)	
	Davis (1984); Roe (1985); Yee (1985, 1987)	

it is hardly possible to list all the existing schemes. A more complete list, of essentially space-centred schemes, can be found in Yanenko *et al.* (1983, 1984) and in Shokin (1983). This classification is to be viewed as a presentation of general boxes where most existing schemes can be placed, with the aim of providing some guideline to the reader.

Like all classifications, loopholes can be found. For instance, one can extract concepts from the techniques applied to generate high-resolution upwind schemes, following the total variation controlled (TVD) approach, and introduce them in the space-centred schemes, generating in this way improved shock resolutions in the Lax–Wendroff schemes (Davis, 1984; Roe, 1985; Yee, 1985, 1987).

It is our goal, in this part composed of Chapters 16 to 21, to present an overview of some of the most important methods and their properties.

Chapter 16 will deal essentially with the algebra of the coupled non-linear system formed by the Euler equations. Due to the strong coupling between the five equations (in three dimensions) a large variety of options are open for the selection of the set of basic variables. Each choice results in a different formulation, with different Jacobian matrices of the fluxes with respect to the basic dependent variables. Transformations from one set of variables to another have to be defined, since one often has to deal with two or more sets simultaneously, particularly when treating the boundary conditions.

Chapter 17 will introduce the second-order Lax–Wendroff family of schemes, characterized by the combined space–time discretization. The original explicit versions and the two-step variants of MacCormack, Lerat and Peyret, as well as the implicit variants of Lerat, will be discussed.

Chapter 18 is devoted to the explicit as well as implicit space-centred methods based on separate space (second-order) and time discretizations. This covers essentially the schemes of Beam and Warming and of Jameson. An essential element with this approach is the introduction of artificial dissipation terms required to maintain stability.

Chapter 19 discusses the important problem of boundary conditions for the Euler equations.

Chapter 20 is devoted to a presentation of the first-order upwind schemes. This covers the flux vector splitting methods and the Godunov-type schemes, also known as flux difference splitting methods, based on either exact or approximate solutions to the Riemann problem.

Chapter 21 introduces the reader to the techniques for the generation of second-order upwind schemes. Since these schemes still generate numerical oscillations in the vicinity of discontinuities a deeper analysis of the properties of numerical discretizations is required. Some recent developments are presented, leading to the introduction of non-linear components in second- or higher-order schemes, in order to satisfy general requirements such as monotonicity, total variation diminishing schemes, entropy conditions, which guarantee unique, oscillation-free solutions of scalar conservation laws.

References

- Beam, R. M., and Warming, R. F. (1976). 'An implicit finite-difference algorithm for hyperbolic system in conservation law form.' *Journal Computational Physics*, **22**, 87–109.
- Ben-Artzi, M., and Falcovitz, J. (1984). 'A second order Godunov-type scheme for compressible fluid dynamics.' *Journal Computational Physics*, **55**, 1–32.
- Boris, J. P., Book, D. L. (1973). 'Flux corrected transport I. SHASTA, a fluid transport algorithm that works.' *Journal Computational Physics*, **11**, pp. 38–69.
- Briley, W. R., McDonald, H. (1975). 'Solution of the three-dimensional Navier–Stokes equations by an implicit technique.' *Proc. Fourth International Conference on Numerical Methods in Fluid Dynamics, Lecture Notes in Physics*, Vol. 35, Berlin: Springer.
- Casier, F., Deconinck, H., and Hirsch, Ch. (1983). 'A class of central bidiagonal schemes with implicit boundary conditions for the solution of Euler's equations.' *AIAA Paper 83-0126*, AIAA 21st Aerospace Sciences Meeting; see also *AIAA Journal*, **22**, 1556–1563.
- Courant, R., Isaacson, E., and Reeves, M. (1952). 'On the solution of nonlinear hyperbolic differential equations by finite differences.' *Comm. Pure and Applied Mathematics*, **5**, 243–55.
- Davis, S. F. (1984). 'TVD finite difference schemes and artificial viscosity.' *ICASE Report 84-20*, NASA CR-172373, NASA Langley Research Center.
- Engquist, B., and Osher, S. (1980). 'Stable and entropy satisfying approximations for transonic flow calculations.' *Mathematics of Computation*, **34**, 45–75.
- Godunov, S. K. (1959). 'A difference scheme for numerical computation of discontinuous solution of hydrodynamic equations.' *Math. Sbornik*, **47**, 271–306 (in Russian). Translated US Joint Publ. Res. Service, *JPRS 7226* (1969).
- Harten, A. (1983). 'High resolution schemes for hyperbolic conservation laws.' *Journal Computational Physics*, **49**, 357–93.
- Harten, A., Lax, P. D., and Van Leer B. (1983). 'On upstream differencing and Godunov-type schemes for hyperbolic conservation laws,' *SIAM Review*, **25**, 35–61.
- Harten, A. (1984). 'On a class of high resolution total variation stable finite difference schemes.' *SIAM Journal of Numerical Analysis*, **21**, 1–23.
- Jameson, A., Schmidt, W., and Turkel, E. (1981). 'Numerical simulation of the Euler equations by finite volume methods using Runge–Kutta time stepping schemes.' *AIAA Paper 81-1259*, AIAA 5th Computational Fluid Dynamics Conference.
- Lax, P. D. (1954). 'Weak solutions of non linear hyperbolic equations and their numerical computation.' *Comm Pure and Applied Mathematics*, **7**, 159–93.
- Lax, P. D. (1957). 'Hyperbolic systems of conservation laws II.' *Comm. Pure and Applied Mathematics*, **10**, 537–66.
- Lax, P. D., and Wendroff, B. (1960). 'Systems of conservation laws.' *Comm. Pure and Applied Mathematics*, **13**, 217–37.
- Lax, P. D., and Wendroff, B. (1964). 'Difference schemes for hyperbolic equations with high order of accuracy.' *Comm. Pure and Applied Mathematics*, **17**, 381–98.
- Lerat, A. (1979). *Une Classe de Schemas aux Differences Implicites pour les Systemes Hyperboliques de Lois de Conservation*, Vol. A288, pp. 1033–6, Paris: Comptes Rendus Academie des Sciences.
- Lerat, A. (1983). 'Implicit methods of second order accuracy for the Euler equations.' *AIAA Paper 83-1925*, AIAA 6th Computational Fluid Dynamics Conference; also *AIAA Journal*, **23**, 33–40.
- Lerat, A., and Peyret, R. (1974). 'Non centered schemes and shock propagation problems.' *Computers and Fluids*, **2**, 35–52.
- MacCormack, R. W. (1969). 'The effect of viscosity in hypervelocity impact cratering.' *AIAA Paper 69-354*.
- MacCormack, R. W. (1981). 'A numerical method for solving the equations of

- compressible viscous flow.' *AIAA Paper 81-0110*, AIAA 19th Aerospace Sciences Meeting.
- Moretti, G. (1979). 'The λ -scheme.' *Computers and Fluids*, **7**, 191–205.
- Osher, S. (1982). 'Shock modelling in aeronautics.' In K. W. Morton and M. J. Baines (eds), *Numerical Methods for Fluid Dynamics*, pp. 179–218, London: Academic Press.
- Osher, S. (1984). 'Riemann solvers, the entropy condition and difference approximations.' *SIAM Journal Numerical Analysis*, **21**, 217–35.
- Osher, S., and Chakravarthy, S. R. (1984). 'High resolution schemes and the entropy condition.' *SIAM Journal Numerical Analysis*, **21**, 955–84.
- Richtmyer, R. D., and Morton, K. W. (1967). *Difference Methods for Initial Value Problems*, 2nd edn, New York: John Wiley and Sons.
- Roe, P. L. (1981a). 'The use of the Riemann problem in finite difference schemes.' *Lecture Notes in Physics*, Vol. 141, 354–9, Berlin: Springer Verlag.
- Roe, P. L. (1981b). 'Approximate Riemann solvers, parameter vectors and difference schemes.' *Journal Computational Physics*, **43**, 357–72.
- Roe, P. L. (1985). 'Some contributions to the modelling of discontinuous flows.' *Proc. 1983 AMS-SIAM Summer Seminar on Large Scale Computing in Fluid Mechanics, Lecture in Applied Mathematics*, **22**, 163–93.
- Shokin, Yu. I. (1983). *The Method of Differential Approximation*, New York, Springer Verlag.
- Steger, J. L., and Warming, R. F. (1981). 'Flux vector splitting of the inviscid gas-dynamic equations with application to finite difference methods.' *Journal Computational Physics*, **40**, 263–93.
- Van Leer, B. (1974). 'Towards the ultimate conservative difference scheme. II. Monotonicity and conservation combined in a second order scheme.' *Journal Computational Physics*, **14**, 361–70.
- Van Leer, B. (1979). 'Towards the ultimate conservative difference scheme. V. A second order sequel to Godunov's method.' *Journal Computational Physics*, **32**, 101–36.
- Van Leer, B. (1982). 'Flux vector splitting for the Euler equations.' In *Proc. 8th International Conference on Numerical Methods in Fluid Dynamics*, Springer Verlag.
- Warming, R. F., and Beam, R. M. (1978). 'On the construction and application of implicit factored schemes for computational fluid dynamics.' *SIAM-AMS Proc.*, **11**, 85–129.
- Woodward, P. R., and Colella, P. (1984). 'The piecewise parabolic method (PPM) for gas dynamical calculations.' *Journal Computational Physics*, **54**, 174–201.
- Yanenko, N. N., Fedotova, Z. I., Tusheva, L. A., Shokin, Yu. I. (1983). 'Classification of difference schemes of gas dynamics by the method of differential approximation—one dimensional case.' *Computers and Fluids*, **11**, 187–99.
- Yanenko, N. N., Fedotova, Z. I., Kompaniets, L. A., Shokin, Yu. I. (1984). 'Classification of difference schemes of gas dynamics by the method of differential approximation—two-dimensional case.' *Computers and Fluids*, **12**, 93–119.
- Yee, H. C. (1985). 'On symmetric and upwind TVD schemes.' *Proc. 6th GAMM Conference on Numerical Methods in Fluid Mechanics*, pp. 399–407, Braunschweig: Vieweg.
- Yee, H. C. (1987). 'Construction of explicit and implicit symmetric TVD schemes and their applications.' *Journal Computational Physics*, **68**, 151–79.
- Yee, H. C., and Harten, A. (1985). 'Implicit TVD schemes for hyperbolic conservation laws in curvilinear coordinates.' *AIAA Paper 85-1513, Proc. AIMM 7th Computational Fluid Dynamics Conference*, 228–41.

Chapter 16

The Mathematical Formulation of the System of Euler Equations

The system of inviscid conservation laws, called the Euler equations, forms a first-order system of non-linear coupled equations, which can be written in various equivalent forms.

Since the physical basis of the Euler equations is the expression of the conservation laws for mass, momentum and energy, the basic formulation will be derived from the integral form of these conservation laws. As shown earlier in Chapter 6 in Volume 1, the conservation form of the equations is essential in order to compute correctly the propagation speed and the intensity of discontinuities, such as contact discontinuities or shocks that can occur in inviscid flows. However, when discontinuities are not expected, non-conservative formulations can be used.

Various algebraical formulations can be defined depending on the choice of the dependent flow variables. The vectors of variables formed by density, momentum and total energy, obeying the conservation form of the equations, and called the *conservative variables*. The more 'direct' variables, however, are those that can be directly controlled experimentally and are defined as density, velocity and pressure. These variables will generally be imposed by the physical boundary conditions and are called the *primitive variables*. In addition, as the system of Euler equations is hyperbolic in time, quantities that propagate along characteristics can be defined and the system of equations can be transformed to the *characteristic form*.

From the mathematical point of view, one can write equivalently the equations in either form and transformation matrices between the three sets can be defined.

16.1 THE CONSERVATIVE FORMULATION OF THE EULER EQUATIONS

The natural form of the flow equations is connected to the quantities satisfying conservation laws, as discussed in Chapter 1 in Volume 1. These quantities are mass, momentum and total energy per unit volume, and the expression of the Euler equations in terms of these basic variables constitutes the framework of the conservative form of the inviscid flow equations.

16.1.1 Integral conservative formulation of the Euler equations

This formulation has been derived in Chapter 1 (see Table 1.1 for a summary) and was discussed in Section 2.7 in Volume 1.

For a three-dimensional flow through a volume Ω , enclosed by the surface S , the conservation laws are expressed by

$$\frac{\partial}{\partial t} \int_{\Omega} \rho \, d\Omega + \oint_S \rho \bar{v} \cdot d\bar{S} = 0 \quad (16.1.1)$$

$$\frac{\partial}{\partial t} \int_{\Omega} \rho \bar{v} \, d\Omega + \oint_S (\rho \bar{v} \otimes \bar{v} + p) d\bar{S} = \int_{\Omega} \rho \bar{f}_e \, d\Omega \quad (16.1.2)$$

$$\frac{\partial}{\partial t} \int_{\Omega} \rho E \, d\Omega + \oint_S \rho H \bar{v} \cdot d\bar{S} = \int_{\Omega} \rho \bar{f}_e \cdot \bar{v} \, d\Omega \quad (16.1.3)$$

where \bar{f}_e are the external forces.

These equations can be written in a rotating frame of reference, when a steady rotation $\bar{\omega}$ is imposed on the reference system, with an entrainment velocity equal to $\bar{\omega} \times \bar{r}$, \bar{r} being the local position vector. In this case the velocity \bar{v} has to be replaced everywhere by the relative velocity $\bar{w} = \bar{v} - \bar{\omega} \times \bar{r}$, and the Coriolis and centrifugal forces $[-2\rho\bar{\omega} \times \bar{w} - \rho\bar{\omega} \times (\bar{\omega} \times \bar{r})]$ have to be added to $\rho\bar{f}_e$ in the right-hand side of equation (16.1.2). In the energy equation (16.1.3), the total energy E is to be replaced by

$$E^* = e + \frac{\bar{w}^2}{2} - \frac{(\bar{\omega} \times \bar{r})^2}{2} = E - (\bar{\omega} \times \bar{r}) \cdot \bar{v} \quad (16.1.4)$$

and the stagnation enthalpy H is to be replaced by the rothalpy I , h denoting the static enthalpy:

$$I = H - (\bar{\omega} \times \bar{r}) \cdot \bar{v} = h + \frac{\bar{w}^2}{2} - \frac{(\bar{\omega} \times \bar{r})^2}{2} \quad (16.1.5)$$

while \bar{f}_e remains unchanged in the right-hand side.

The system of equations (16.1.1) to (16.1.3) can be written in a compact form, introducing the column hypervectors and tensors U and \bar{F} , and \bar{I} representing the 3×3 unit matrix:

$$U = \begin{vmatrix} \rho \\ \rho \bar{v} \\ \rho E \end{vmatrix} \equiv \begin{vmatrix} \rho \\ \rho u \\ \rho v \\ \rho w \\ \rho E \end{vmatrix} \quad (16.1.6)$$

$$\bar{F} = \begin{vmatrix} \rho \bar{v} \\ \rho \bar{v} \otimes \bar{v} + p \bar{I} \\ \rho \bar{v} H \end{vmatrix} = \bar{v} U + \begin{vmatrix} 0 \\ \bar{I} \\ \bar{v} \end{vmatrix} p \quad (16.1.7)$$

as well as the source column Q :

$$Q = \begin{vmatrix} 0 \\ \rho \vec{f}_e \\ \rho \vec{f}_e \cdot \vec{v} \end{vmatrix} \quad (16.1.8)$$

The integral compact form of the Euler equations becomes

$$\frac{\partial}{\partial t} \int_{\Omega} U \, d\Omega + \oint_S \vec{F} \cdot d\vec{S} = \int_{\Omega} Q \, d\Omega \quad (16.1.9)$$

The column vector U contains the *conservative variables*, while \vec{F} contains the conserved fluxes.

The system of equations (16.1.9) has to be completed by an equation of state defining the thermodynamical properties of the considered fluid. In general, an equation of the form $p = p(\rho, T)$ with the definitions of the internal energy, for instance $e = e(p, T)$ or $e = e(p, S)$, are required. For a perfect gas, one has $p/\rho = rT$ and $e = c_v T$.

Various equivalent thermodynamic relations, valid for perfect gases, are given in Section 2.1.1 in Volume 1.

16.1.2 Differential conservative formulation

In the vector form, the system of five Euler equations has been derived previously, and can be summarized as follows, following Section 2.1:

$$\frac{\partial \rho}{\partial t} + \vec{\nabla} \cdot (\rho \vec{v}) = 0 \quad (16.1.10)$$

$$\frac{\partial(\rho \vec{v})}{\partial t} + \vec{\nabla} \cdot (\rho \vec{v} \otimes \vec{v} + p \vec{I}) = \rho \vec{f}_e \quad (16.1.11)$$

$$\frac{\partial(\rho E)}{\partial t} + \vec{\nabla} \cdot (\rho \vec{v} H) = \rho \vec{f}_e \cdot \vec{v} \quad (16.1.12)$$

or in condensed notation:

$$\frac{\partial U}{\partial t} + \vec{\nabla} \cdot \vec{F} = Q \quad (16.1.13)$$

The Cartesian formulation of the above equations has been given in Section 2.7, equations (2.7.1) to (2.7.2), and is repeated here for convenience.

16.1.3 Cartesian system of coordinates

We write equation (16.1.13) in Cartesian coordinates x, y, z , with the velocity vector \vec{v} having components u, v, w and magnitude

$$q = (\vec{v} \cdot \vec{v})^{1/2} = (u^2 + v^2 + w^2)^{1/2} \quad (16.1.14)$$

as

$$\frac{\partial U}{\partial t} + \frac{\partial f}{\partial x} + \frac{\partial g}{\partial y} + \frac{\partial h}{\partial z} = Q \quad (16.1.15)$$

The components f, g, h of the flux vector-tensor \bar{F} are defined by equations (2.7.2)

$$f = \begin{vmatrix} \rho u \\ \rho u^2 + p \\ \rho uv \\ \rho uw \\ \rho uH \end{vmatrix} \quad g = \begin{vmatrix} \rho v \\ \rho uv \\ \rho v^2 + p \\ \rho vw \\ \rho vH \end{vmatrix} \quad h = \begin{vmatrix} \rho w \\ \rho uw \\ \rho vw \\ \rho w^2 + p \\ \rho wH \end{vmatrix} \quad (16.1.16)$$

The Cartesian components of U are

$$U = \begin{vmatrix} \rho \\ \rho u \\ \rho v \\ \rho w \\ \rho E \end{vmatrix} \quad (16.1.17)$$

and the equation (16.1.15) becomes explicitly

$$\frac{\partial}{\partial t} \begin{vmatrix} \rho \\ \rho u \\ \rho v \\ \rho w \\ \rho E \end{vmatrix} + \frac{\partial}{\partial x} \begin{vmatrix} \rho u \\ \rho u^2 + p \\ \rho uv \\ \rho uw \\ \rho uH \end{vmatrix} + \frac{\partial}{\partial y} \begin{vmatrix} \rho v \\ \rho vu \\ \rho v^2 + p \\ \rho vw \\ \rho vH \end{vmatrix} + \frac{\partial}{\partial z} \begin{vmatrix} \rho w \\ \rho wu \\ \rho wv \\ \rho w^2 + p \\ \rho wH \end{vmatrix} = \begin{vmatrix} 0 \\ f_{ex} \\ f_{ey} \\ f_{ez} \\ W_f \end{vmatrix} \quad (16.1.18)$$

In many applications, the Euler equations are discretized on arbitrary curvilinear meshes and the conservative formulation in general coordinates is therefore required.

16.1.4 Discontinuities and Rankine–Hugoniot relations—entropy condition

Inviscid flows can undergo a discontinuous behaviour, namely shocks or contact discontinuities can appear in the flow. These situations are described by solutions of the integral conservation equations or by weak generalized solutions, in the sense of distribution theories, of the Euler equations. The relations between flow variables on both sides of a discontinuity surface moving with a velocity \bar{C} have been derived in Section 2.7.1. They are known as the *Rankine–Hugoniot* relations and are given by equation (2.7.11) if it is assumed that the external forces \bar{f}_e are continuous:

$$[\bar{F}] \cdot \bar{1}_n - \bar{C} [U] \cdot \bar{1}_n = 0 \quad (16.1.19)$$

In this equation, $\bar{1}_n$ is the unit vector normal to the discontinuity surface and

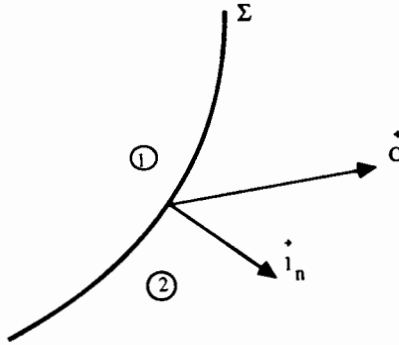


Figure 16.1.1 Discontinuity surface

$[A]$ represents the jump in the quantity A over the discontinuity surface when following a streamline; that is

$$[A] = A_2 - A_1 \quad (16.1.20)$$

where the subscripts 1 and 2 designate respectively upstream and downstream states with respect to the discontinuity surface (Figure 16.1.1).

If the discontinuity surface is defined by an equation of the form

$$\Sigma(\vec{x}, t) = 0 \quad (16.1.21)$$

the unit vector along the normal is

$$\vec{i}_n = \frac{\vec{\nabla}\Sigma}{|\vec{\nabla}\Sigma|} \quad (16.1.22)$$

By definition of the discontinuity propagation speed \vec{C} , the following relation must hold, expressing that the surface $\Sigma = \text{constant}$ moves with velocity \vec{C} :

$$\frac{\partial \Sigma}{\partial t} + \vec{C} \cdot \vec{\nabla}\Sigma = 0 \quad (16.1.23)$$

and equation (16.1.19) can be written as

$$[\vec{F}] \cdot \vec{\nabla}\Sigma + \frac{\partial \Sigma}{\partial t} [U] = 0 \quad (16.1.24)$$

Worked out explicitly, the Rankine–Hugoniot relations become

$$[\rho \vec{v} \cdot \vec{i}_n] - \vec{C} \cdot \vec{i}_n [\rho] = 0 \quad (16.1.25)$$

$$[(\rho \vec{v} \cdot \vec{i}_n) \vec{v} + p \cdot \vec{i}_n] - \vec{C} \cdot \vec{i}_n [\rho \vec{v}] = 0 \quad (16.1.26)$$

$$[H \cdot \rho \vec{v} \cdot \vec{i}_n] - \vec{C} \cdot \vec{i}_n [\rho E] = 0 \quad (16.1.27)$$

For a stationary discontinuity surface, these equations simplify to

$$[\rho \vec{v} \cdot \vec{i}_n] = 0 \quad (16.1.28)$$

$$[\vec{v}] \rho \vec{v} \cdot \vec{1}_n + [p] \vec{1}_n = 0 \quad (16.1.29)$$

$$[H] = 0 \quad (16.1.30)$$

Various forms of discontinuities are physically possible: *shocks*, where all flow variables undergo a discontinuous variation, *contact discontinuities* and *vortex sheets*, also called slip lines, across which no mass transfer takes place but where density, as well as the tangential velocity, may be discontinuous, although pressure and normal velocity remain continuous.

Seen from a reference system moving with the discontinuity, the following properties result from the Rankine–Hugoniot relations.

Contact discontinuities/slip lines

They are defined by the condition of no mass flow through the discontinuity

$$v_{n1} = v_{n2} = 0 \quad (16.1.31)$$

and of continuous pressure

$$[p] = 0 \quad (16.1.32)$$

allowing non-zero values for the jump in specific mass and tangential velocity:

$$\begin{aligned} [\rho] &\neq 0 \\ [v_t] &\neq 0 \end{aligned} \quad (16.1.33)$$

Shock surfaces

Shocks are solutions of the Rankine–Hugoniot relations with non-zero mass flow through the discontinuity. Consequently, pressure and normal velocity undergo discontinuous variations, while the tangential velocity remains continuous. Hence shocks satisfy the following properties:

$$\begin{aligned} [\rho] &\neq 0 \\ [p] &\neq 0 \\ [v_n] &\neq 0 \\ [v_t] &= 0 \end{aligned} \quad (16.1.34)$$

Note that since the stagnation pressure p_0 is not constant across the shock, the inviscid shock relations nevertheless imply a discontinuous entropy variation through the shock. This variation has to be positive, corresponding to compression shocks and excluding thereby expansion shocks, for physical reasons connected to the second principle of thermodynamics.

It has to be added that expansion shocks, whereby the entropy jump is negative, are valid solutions of the inviscid equations since, in the absence of heat transfer, they describe reversible flow variations. Hence, there is no mechanism that allows a distinction to be made between discontinuities with entropy increase (positive entropy jump) or entropy decrease (negative entropy variation).

A condition has to be imposed on the entropy in order to ensure that the obtained solutions of the inviscid equations are indeed limits, for vanishing viscosity, of the real fluid behaviour.

This condition is expressed as

$$\frac{\partial}{\partial t}(\rho s) + \bar{\mathbf{V}} \cdot (\rho \bar{\mathbf{v}} s) \geq 0 \quad (16.1.35)$$

This form of the entropy condition, in the absence of heat conduction effects, ensures that unphysical solutions, such as expansion shocks, will not appear.

One has also

$$\left(\frac{\partial s}{\partial t} + (\bar{\mathbf{v}} \cdot \bar{\mathbf{V}}) s \right) \geq 0 \quad (16.1.36)$$

The introduction of this property into numerical schemes will be presented in Chapter 21.

16.2 THE QUASI-LINEAR FORMULATION OF THE EULER EQUATIONS

In order to investigate the mathematical properties of the system of Euler equations, it is necessary, following Chapter 3 in Volume 1, to write these equations in a quasi-linear form. The Euler system of equations contains only first-order derivatives and if the external forces $\bar{\mathbf{f}}_e$ are independent of the flow gradients, the system of Euler equations is of first order in the variables U .

16.2.1 The Jacobian matrices for conservative variables

The quasi-linear form of equations (16.1.13) or (16.1.15) is written as

$$\frac{\partial U}{\partial t} + \left(\frac{\partial \bar{\mathbf{F}}}{\partial U} \right) \cdot \bar{\mathbf{V}} U = Q \quad (16.2.1a)$$

or

$$\frac{\partial U}{\partial t} + \bar{\mathbf{A}} \cdot \nabla U = Q \quad (16.2.1b)$$

or explicitly

$$\frac{\partial U}{\partial t} + A \frac{\partial U}{\partial x} + B \frac{\partial U}{\partial y} + C \frac{\partial U}{\partial z} = Q \quad (16.2.2)$$

where A, B, C are the three Jacobian matrices of the flux vector $\bar{\mathbf{F}}$. They can be condensed into a vector form $\bar{\mathbf{A}}$ (A, B, C):

$$\bar{\mathbf{A}} \equiv \frac{\partial \bar{\mathbf{F}}}{\partial U} \quad (16.2.3)$$

having the components A, B, C defined by

$$A = \frac{\partial f}{\partial U} \quad B = \frac{\partial g}{\partial U} \quad C = \frac{\partial h}{\partial U} \quad (16.2.4)$$

The flux components f, g, h have the very remarkable property of being homogeneous functions of degree 1 of the conservative variable vector U in the case of a perfect gas or, more generally, for fluids satisfying the relation

$$p = \rho f(e) \quad (16.2.5)$$

where e is the internal energy (Beam and Warming, 1976; Steger and Warming, 1981). This implies that

$$\bar{F}(\lambda U) = \lambda \bar{F}(U) \quad \text{for any } \lambda \quad (16.2.6)$$

and by differencing with respect to λ and setting $\lambda = 1$, one obtains the relation

$$\bar{F}(U) = \frac{\partial \bar{F}}{\partial U} U = \bar{A} U \quad (16.2.7)$$

or in component form

$$f = AU \quad g = BU \quad h = CU \quad (16.2.8)$$

Inserting these relations in the conservative form of equations (16.1.13) or (16.1.15) shows that one can write the Euler equations in the form

$$\frac{\partial U}{\partial t} + \frac{\partial(AU)}{\partial x} + \frac{\partial(BU)}{\partial y} + \frac{\partial(CU)}{\partial z} = Q \quad (16.2.9)$$

Compared with equation (16.2.2), it appears that it makes no difference whether the Jacobian matrices A, B, C are inside or outside the derivatives as long as the functions are continuous. However, from the numerical point of view, the two formulations do not lead to identical discretizations. One must have the following identities, using condensed notation:

$$(AU)_x = AU_x \quad (16.2.10)$$

Then

$$A_x U = 0 \quad (16.2.11)$$

and similarly for B and C , namely

$$B_y U = C_z U = 0 \quad (16.2.12)$$

The homogeneous property is demonstrated by writing the vector U and the fluxes \bar{F} as a function of the conservative variables $\rho, \bar{m} = \rho \bar{v}, \varepsilon = \rho E$. Hence, with

$$U = \begin{vmatrix} \rho \\ \bar{m} \\ \varepsilon \end{vmatrix} \quad \bar{m} = \begin{vmatrix} m \\ n \\ l \end{vmatrix} \quad (16.2.13)$$

the flux vector components can be written as

$$f = \begin{pmatrix} m \\ \frac{m^2}{\rho} + p \\ \frac{mn}{\rho} \\ \frac{ml}{\rho} \\ \frac{m}{\rho}(\varepsilon + p) \end{pmatrix} \quad (16.2.14a)$$

and similar relations for g and h :

$$g = \begin{pmatrix} n \\ \frac{mn}{\rho} \\ \frac{n^2}{\rho} + p \\ \frac{nl}{\rho} \\ \frac{n}{\rho}(\varepsilon + p) \end{pmatrix} \quad (16.2.14b)$$

$$h = \begin{pmatrix} l \\ \frac{ml}{\rho} \\ \frac{nl}{\rho} \\ \frac{l^2}{\rho} + p \\ \frac{l}{\rho}(\varepsilon + p) \end{pmatrix} \quad (16.2.14c)$$

Since

$$\varepsilon = \rho e + \frac{\bar{m}^2}{2\rho} \quad (16.2.15)$$

the internal energy e is a function of degree zero in U and therefore the above fluxes will be homogeneous of degree one in the variables $\rho, \bar{m}, \varepsilon$ if the pressure p is of degree one. This implies that p can be expressed as the density times a function of degree zero. This is expressed by the relation (16.2.5).

Some methods do explicitly use this homogeneity property in the discretization scheme (Steger and Warming, 1981), and it should be kept in mind that the relation (16.2.5) might not be true for real fluids, such as air at very high temperatures, combustion gases or steam, for instance.

The Jacobian matrices can be determined explicitly if the fluid constitutive relations are specified. For a perfect gas assumption, one has (see Section 2.1.1)

$$p = (\gamma - 1)\rho e = (\gamma - 1)\left(\varepsilon - \frac{\bar{m}^2}{2\rho}\right) \quad (16.2.16)$$

The rather abstract compact notation $\partial\bar{F}/\partial U$ is to be interpreted as representing the three Jacobian matrices A, B, C formed by assembling the column vectors obtained by differencing the corresponding flux components with respect to the dependent conservative variables $\rho, \bar{m}, \varepsilon$. For instance,

$$A = \frac{\partial f}{\partial U} = \left| \frac{\partial f}{\partial \rho}, \frac{\partial f}{\partial m}, \frac{\partial f}{\partial n}, \frac{\partial f}{\partial l}, \frac{\partial f}{\partial \varepsilon} \right| \equiv \left| \frac{\partial f}{\partial \rho}, \frac{\partial f}{\partial \bar{m}}, \frac{\partial f}{\partial \varepsilon} \right| \quad (16.2.17)$$

where each derivative is a 5×1 column. The compact notation $\partial f/\partial \bar{m}$ represents a 5×3 matrix, which is introduced in order to obtain a formulation valid for any number of space variables, from one to three.

A detailed computation gives, for f ,

$$\frac{\partial f}{\partial \rho} = \begin{vmatrix} 0 \\ -\frac{m^2}{\rho^2} + \frac{\partial p}{\partial \rho} \\ -\frac{nm}{\rho^2} \\ -\frac{lm}{\rho^2} \\ -\frac{m}{\rho^2}(\varepsilon + p) + \frac{m}{\rho} \frac{\partial p}{\partial \rho} \end{vmatrix} \quad (16.2.18)$$

The derivatives of p with respect to the conservative variables are obtained from the above relation (16.2.16). Hence,

$$\frac{\partial p}{\partial \rho} = (\gamma - 1) \frac{\bar{m}^2}{2\rho^2} = \frac{\gamma - 1}{2} \bar{v}^2 \quad (16.2.19)$$

$$\frac{\partial p}{\partial \bar{m}} = -(\gamma - 1) \frac{\bar{m}^T}{\rho} = -(\gamma - 1) \bar{v}^T \quad (16.2.20)$$

$$\frac{\partial p}{\partial \varepsilon} = \gamma - 1 \quad (16.2.21)$$

The notation $\partial p / \partial \bar{m}$ represents a 1×3 line vector and since the vectors are considered as columns, \bar{m}^T or \bar{v}^T are line vectors, T indicating the transpose.

The first column of the Jacobian A becomes

$$\frac{\partial f}{\partial \rho} = \begin{vmatrix} 0 \\ -\frac{m^2}{\rho^2} + \frac{\gamma - 1}{2} \frac{\bar{m}^2}{\rho^2} \\ -\frac{mn}{\rho^2} \\ -\frac{ml}{\rho^2} \\ -\frac{m}{\rho^2} \left[\gamma \varepsilon - (\gamma - 1) \frac{\bar{m}^2}{\rho} \right] \end{vmatrix} \quad (16.2.22)$$

One obtains for the 5×3 matrix $\partial f / \partial \bar{m}$ the following form:

$$\frac{\partial f}{\partial \bar{m}} = \begin{vmatrix} 1 & 0 & 0 \\ 2\frac{m}{\rho} - (\gamma - 1)\frac{m}{\rho} & -(\gamma - 1)\frac{n}{\rho} & -(\gamma - 1)\frac{1}{\rho} \\ \frac{n}{\rho} & \frac{m}{\rho} & 0 \\ \frac{1}{\rho} & 0 & \frac{m}{\rho} \\ \frac{\gamma \varepsilon}{\rho} - \frac{\gamma - 1}{2\rho^2}(\bar{m}^2 + 2m^2) & -(\gamma - 1)\frac{mn}{\rho^2} & -(\gamma - 1)\frac{lm}{\rho^2} \end{vmatrix} \quad (16.2.23)$$

which can be written out explicitly as

$$\frac{\partial f}{\partial \bar{m}} = \begin{vmatrix} 1 & 0 & 0 \\ (3 - \gamma)u & -(\gamma - 1)v & -(\gamma - 1)w \\ v & u & 0 \\ w & 0 & u \\ \gamma E - \frac{\gamma - 1}{2}(\bar{v}^2 + 2u^2) & -(\gamma - 1)uv & -(\gamma - 1)uw \end{vmatrix} \quad (16.2.24)$$

Finally,

$$\frac{\partial f}{\partial \varepsilon} = \begin{vmatrix} 0 \\ \gamma - 1 \\ 0 \\ 0 \\ \gamma u \end{vmatrix} \quad (16.2.25)$$

and the Jacobian matrix A can be written in the general form

$$A = \begin{vmatrix} 0 & 1 & 0 & 0 & 0 \\ -u^2 + \frac{\gamma-1}{2}\bar{v}^2 & (\gamma-1)u & -(\gamma-1)v & -(\gamma-1)w & \gamma-1 \\ -uv & v & u & 0 & 0 \\ -uw & w & 0 & u & 0 \\ -u[\gamma E - (\gamma-1)\bar{v}^2] & \gamma E - \frac{\gamma-1}{2}(\bar{v}^2 + 2u^2) & -(\gamma-1)uv & -(\gamma-1)uw & \gamma u \end{vmatrix} \quad (16.2.26)$$

The other Jacobians B and C are obtained by cyclic permutation of u, v, w :

$$B = \begin{vmatrix} 0 & 0 & 1 & 0 & 0 \\ -uv & v & u & 0 & 0 \\ -v^2 + \frac{\gamma-1}{2}\bar{v}^2 & -(\gamma-1)u & (\gamma-1)v & -(\gamma-1)w & \gamma-1 \\ -vw & 0 & w & v & 0 \\ -v[\gamma E - (\gamma-1)\bar{v}^2] & -(\gamma-1)uv & \gamma E - \frac{\gamma-1}{2}(\bar{v}^2 + 2v^2) & -(\gamma-1)vw & \gamma v \end{vmatrix} \quad (16.2.27)$$

$$C = \begin{vmatrix} 0 & 0 & 0 & 1 & 0 \\ -uw & w & 0 & u & 0 \\ -vw & 0 & w & v & 0 \\ -w^2 + \frac{\gamma-1}{2}\bar{v}^2 & -(\gamma-1)u & -(\gamma-1)v & (\gamma-1)w & \gamma-1 \\ -w[\gamma E - (\gamma-1)\bar{v}^2] & -(\gamma-1)uw & -(\gamma-1)vw & \gamma E - \frac{\gamma-1}{2}(\bar{v}^2 + 2w^2) & \gamma w \end{vmatrix} \quad (16.2.28)$$

Note that E can also be expressed as $E = c^2/\gamma(\gamma-1) + \bar{v}^2/2$.

The structure of the conservative Jacobian matrices A, B, C is quite complicated, so much so that in order to assert the hyperbolicity of the Euler equations it is necessary to find the eigenvalues of linear combinations of A, B, C . Indeed, referring to Chapter 3 in Volume 1, the Euler equations will be

hyperbolic with respect to time if the matrix K defined by

$$K = \bar{A} \cdot \bar{\kappa} = A \cdot \kappa_x + B \cdot \kappa_y + C \cdot \kappa_z \quad (16.2.29)$$

has real eigenvalues for any set of values of $\bar{\kappa}$.

Example 16.2.1 One-dimensional Jacobians in conservative variables

For the one-dimensional Euler equations, the system contains three equations for the vector

$$U = \begin{vmatrix} \rho \\ \rho u \\ \rho E \end{vmatrix} = \begin{vmatrix} \rho \\ m \\ \varepsilon \end{vmatrix} \quad (16.2.1)$$

and the flux vector \bar{F} reduces to its x component f :

$$f = \begin{vmatrix} \rho u \\ \rho u^2 + p \\ \rho u H \end{vmatrix} = \begin{vmatrix} m \\ m^2/\rho + p \\ m(\varepsilon + p) \end{vmatrix} \quad (16.2.2)$$

The Jacobian matrix $A = \partial f / \partial U$ is obtained from equation (16.2.26) by removing the third and fourth lines and the third and fourth columns (associated with $\partial f / \partial n$ and $\partial f / \partial l$). Hence, one has

$$A = \begin{vmatrix} 0 & 1 & 0 \\ -(3-\gamma)\frac{u^2}{2} & (3-\gamma)u & \gamma-1 \\ (\gamma-1)u^3 - \gamma u E & \gamma E - 3\frac{\gamma-1}{2}u^2 & \gamma u \end{vmatrix} \quad (16.2.3)$$

Example 16.2.2 Two-dimensional Jacobians in conservative variables

In the two-dimensional case, the conservative variables ^{form} from the vector

$$U = \begin{vmatrix} \rho \\ \rho u \\ \rho v \\ \rho E \end{vmatrix} = \begin{vmatrix} \rho \\ m \\ n \\ \varepsilon \end{vmatrix} \quad (16.2.4)$$

The Jacobians A and B are obtained from equations (16.2.26) and (16.2.27) by removing the fourth column and line in both matrices. This leads to

$$A = \begin{vmatrix} 0 & 1 & 0 & 0 \\ \frac{\gamma-3}{2}u^2 + \frac{\gamma-1}{2}v^2 & (3-\gamma)u & -(\gamma-1)v & \gamma-1 \\ -uv & v & u & 0 \\ -\gamma u E + (\gamma-1)u\bar{v}^2 & \gamma E - \frac{\gamma-1}{2}(v^2 + 3u^2) & -(\gamma-1)uv & \gamma u \end{vmatrix} \quad (16.2.5)$$

$$B = \begin{vmatrix} 0 & 0 & 1 & 0 \\ -uv & v & u & 0 \\ \frac{\gamma-3}{2}v^2 + \frac{\gamma-1}{2}u^2 & -(\gamma-1)u & (3-\gamma)v & \gamma-1 \\ -\gamma vE + (\gamma-1)v\bar{v}^2 & -(\gamma-1)uv & \gamma E - \frac{\gamma-1}{2}(u^2 + 3v^2) & \gamma v \end{vmatrix} \quad (\text{E16.2.6})$$

16.2.2 The Jacobian matrices for primitive variables

It is easier to obtain the eigenvalues of the system of Euler equations when these are written in non-conservative form as a function of the primitive variables ρ, \bar{v}, p . Referring to Table 1.1, Chapter 1, one can write the inviscid flow equations in the absence of heat conduction and heat sources as

$$\begin{aligned} \frac{\partial \rho}{\partial t} + (\bar{v} \cdot \bar{\nabla})\rho + \rho \bar{\nabla} \cdot \bar{v} &= 0 \\ \frac{\partial \bar{v}}{\partial t} + (\bar{v} \cdot \bar{\nabla})\bar{v} + \frac{\bar{\nabla} p}{\rho} &= \bar{f}_e \\ \frac{\partial E}{\partial t} + (\bar{v} \cdot \bar{\nabla})E + \frac{1}{\rho} \bar{\nabla} \cdot (\bar{v} p) &= \bar{f}_e \cdot \bar{v} \end{aligned} \quad (16.2.30)$$

The last equation has to be transformed to an equation for the pressure p . In order to obtain this equation, the isentropic assumption will be introduced, through the relations

$$e = e(p, s) \quad (16.2.31)$$

and

$$\left. \frac{\partial p}{\partial \rho} \right|_s = c^2 \quad (16.2.32)$$

defining the speed of sound c . If the flow is isentropic, one can write for any variation δe :

$$\delta e = \left. \frac{\partial e}{\partial p} \right|_s \cdot \delta p \quad (16.2.33)$$

and the isentropic derivative $\partial e / \partial p|_s$ can be deduced from the thermodynamic relations

$$T ds = dh - \frac{dp}{\rho} = de + p d\left(\frac{1}{\rho}\right) \quad (16.2.34)$$

Introducing the isentropic condition, the isentropic derivatives satisfy

$$dh - \frac{dp}{\rho} = de + p d\left(\frac{1}{\rho}\right) = 0 \quad \text{at constant } s \quad (16.2.35)$$

Hence

$$\left. \frac{\partial h}{\partial p} \right|_s = \frac{1}{\rho} \quad (16.2.36)$$

and

$$\left. \frac{\partial e}{\partial p} \right|_s = \left. \frac{\partial h}{\partial p} \right|_s - \frac{1}{\rho} + \frac{p}{\rho^2} \left(\frac{\partial \rho}{\partial p} \right)_s = \frac{p}{\rho^2 c^2} \quad (16.2.37)$$

The energy equation becomes, after subtracting the momentum equation scalarly multiplied by \vec{v} and introducing the definition of $E = e + \vec{v}^2/2$,

$$\frac{\partial p}{\partial t} + (\vec{v} \cdot \vec{\nabla})p + \rho c^2 (\vec{\nabla} \cdot \vec{v}) = 0 \quad (16.2.38)$$

Actually this equation, compared to the continuity equation, is an alternative form of the isentropic law, namely

$$dp = c^2 d\rho \quad (16.2.39)$$

where the differentials in dp and $d\rho$ designate the total convective derivatives $(\partial/\partial t + \vec{v} \cdot \vec{\nabla})$. The system (16.2.30) becomes

$$\begin{aligned} \frac{\partial \rho}{\partial t} + (\vec{v} \cdot \vec{\nabla})\rho + \rho(\vec{\nabla} \cdot \vec{v}) &= 0 \\ \frac{\partial \vec{v}}{\partial t} + (\vec{v} \cdot \vec{\nabla})\vec{v} + \frac{1}{\rho} \vec{\nabla} p &= \vec{f}_e \\ \frac{\partial p}{\partial t} + (\vec{v} \cdot \vec{\nabla})p + \rho c^2 (\vec{\nabla} \cdot \vec{v}) &= 0 \end{aligned} \quad (16.2.40)$$

With the primitive variables vector V ,

$$V = \begin{vmatrix} \rho \\ \vec{v} \\ p \end{vmatrix} = \begin{vmatrix} \rho \\ \vec{m} \\ \rho \\ (\gamma - 1) \left(\varepsilon - \frac{\vec{m}^2}{2\rho} \right) \end{vmatrix} \quad (16.2.41)$$

one obtains the system of Euler equations in the form

$$\frac{\partial V}{\partial t} + (\vec{A} \cdot \vec{\nabla})V = \vec{Q} \quad (16.2.42)$$

or

$$\frac{\partial V}{\partial t} + \vec{A} \frac{\partial V}{\partial x} + \vec{B} \frac{\partial V}{\partial y} + \vec{C} \frac{\partial V}{\partial z} = \vec{Q} \quad (16.2.43)$$

where $\vec{A}, \vec{B}, \vec{C}$ are the components of the Jacobian vector matrix \vec{A} . Compare

with the expression for the Jacobian \bar{A} , it is obvious that $\bar{\bar{A}}$ has a much simpler structure. Explicitly, one obtains for the components ($\bar{\bar{A}}, \bar{\bar{B}}, \bar{\bar{C}}$),

$$\bar{\bar{A}} = \begin{vmatrix} u & \rho & \cdot & \cdot & \cdot \\ \cdot & u & \cdot & \cdot & 1/\rho \\ \cdot & \cdot & u & \cdot & \cdot \\ \cdot & \cdot & \cdot & u & \cdot \\ \cdot & \rho c^2 & \cdot & \cdot & u \end{vmatrix} \quad (16.2.44)$$

and similar relations for $\bar{\bar{B}}$ and $\bar{\bar{C}}$:

$$\bar{\bar{B}} = \begin{vmatrix} v & \cdot & \rho & \cdot & \cdot \\ \cdot & v & \cdot & \cdot & \cdot \\ \cdot & \cdot & v & \cdot & 1/\rho \\ \cdot & \cdot & \cdot & v & \cdot \\ \cdot & \cdot & \rho c^2 & \cdot & v \end{vmatrix} \quad (16.2.45)$$

$$\bar{\bar{C}} = \begin{vmatrix} w & \cdot & \cdot & \rho & \cdot \\ \cdot & w & \cdot & \cdot & \cdot \\ \cdot & \cdot & w & \cdot & \cdot \\ \cdot & \cdot & \cdot & w & 1/\rho \\ \cdot & \cdot & \cdot & \rho c^2 & w \end{vmatrix} \quad (16.2.46)$$

16.2.3 Transformation matrices between conservative and non-conservative variables

The Jacobian matrix of the transformation from the conservative to the non-conservative variables is defined by

$$M = \frac{\partial U}{\partial V} \quad (16.2.47)$$

and its evaluation requires the explicit formulation of the fluid constitutive relations. It is important to notice that the definition of the non-conservative Jacobians *does not require* an explicit definition of the fluid constitutive relations, and therefore has a larger validity range; that is they are not necessarily connected to a perfect gas assumption as is the case with the conservative Jacobians \bar{A} . For a perfect gas, using relation (16.2.16), one obtains the condensed form (see Problem 16.7):

$$M = \left| \frac{\partial U}{\partial \rho} \quad \frac{\partial U}{\partial \bar{v}} \quad \frac{\partial U}{\partial p} \right| = \begin{vmatrix} 1 & 0 & 0 \\ \bar{v} & \rho \bar{I} & 0 \\ \frac{\bar{v}^2}{2} & \rho \bar{v}^T & \frac{1}{\gamma - 1} \end{vmatrix} \quad (16.2.48)$$

and its inverse

$$M^{-1} = \begin{vmatrix} \frac{\partial V}{\partial \rho} & \frac{\partial V}{\partial \bar{m}} & \frac{\partial V}{\partial \varepsilon} \end{vmatrix} = \begin{vmatrix} 1 & 0 & 0 \\ -\frac{\bar{v}}{\rho} & \frac{1}{\rho} \bar{I} & 0 \\ (\gamma-1)\frac{\bar{v}^2}{2} & -(\gamma-1)\bar{v}^T & \gamma-1 \end{vmatrix} \quad (16.2.49)$$

The determinant of M^{-1} is $(\gamma-1)/\rho$; hence

$$\det M = \frac{\rho}{\gamma-1} \quad (16.2.50)$$

The relations between the conservative and the non-conservative jacobians \bar{A} and $\bar{\bar{A}}$ can be expressed through a similarity transformation with matrix M . Indeed, introducing the Jacobian matrix M in equation (16.2.1) leads to

$$M \frac{\partial V}{\partial t} + \bar{A} M \cdot \bar{\nabla} V = Q$$

or, after multiplication by M^{-1} ,

$$\frac{\partial V}{\partial t} + (M^{-1} \bar{A} M) \cdot \bar{\nabla} V = M^{-1} Q \quad (16.2.51)$$

Identifying with the non-conservative form, equation (16.2.42), gives the relation

$$\bar{\bar{A}} = M^{-1} \bar{A} M \quad \text{or} \quad \bar{A} = M \bar{\bar{A}} M^{-1} \quad (16.2.52)$$

and for the source terms

$$\bar{\bar{Q}} = M^{-1} Q \quad (16.2.53)$$

With regard to the analysis of the eigenvalues of the Euler system of equations, it is easier to work with the non-conservative Jacobians $\bar{\bar{A}}$, which are of a simple structure. From the above transformations, the matrix $K = \bar{A} \cdot \bar{\kappa}$ and the matrix $\bar{\bar{K}} = \bar{\bar{A}} \cdot \bar{\kappa}$ have the same eigenvalues, since they are connected by the similarity transformation

$$\bar{\bar{K}} = M^{-1} K M \quad (16.2.54)$$

Therefore, the characteristic properties of the system of Euler equations will be analysed on the non-conservative, primitive variable formulation.

Example 16.2.3 Non-conservative Jacobians in one and two dimensions

For one-dimensional flows, the transformation matrix M reduces to

$$M = \begin{vmatrix} 1 & \cdot & \cdot \\ u & \rho & \cdot \\ \frac{u^2}{2} & \rho u & \frac{1}{\gamma-1} \end{vmatrix} \quad (\text{E16.2.7})$$

and its inverse M^{-1} is obtained from equation (16.2.49):

$$M^{-1} = \begin{vmatrix} 1 & \cdot & \cdot \\ -\frac{u}{\rho} & \frac{1}{\rho} & \cdot \\ \frac{\gamma-1}{2}u^2 & -(\gamma-1)u & \gamma-1 \end{vmatrix} \quad (\text{E16.2.8})$$

The Jacobian \tilde{A} becomes

$$\tilde{A} = \begin{vmatrix} u & \rho & 0 \\ 0 & u & \frac{1}{\rho} \\ 0 & \rho c^2 & u \end{vmatrix} \quad (\text{E16.2.9})$$

In two dimensions, one has

$$M = \begin{vmatrix} 1 & \cdot & \cdot & \cdot \\ u & \rho & \cdot & \cdot \\ v & \cdot & \rho & \cdot \\ \frac{\bar{v}^2}{2} & \rho u & \rho v & \frac{1}{\gamma-1} \end{vmatrix} \quad (\text{E16.2.10})$$

$$M^{-1} = \begin{vmatrix} 1 & \cdot & \cdot & \cdot \\ -\frac{u}{\rho} & \frac{1}{\rho} & \cdot & \cdot \\ -\frac{v}{\rho} & \cdot & \frac{1}{\rho} & \cdot \\ \frac{\gamma-1}{2}(u^2 + v^2) & -(\gamma-1)u & -(\gamma-1)v & \gamma-1 \end{vmatrix} \quad (\text{E16.2.11})$$

and for the two Jacobians \tilde{A} and \tilde{B} :

$$\tilde{A} = \begin{vmatrix} u & \rho & \cdot & \cdot \\ \cdot & u & \cdot & \frac{1}{\rho} \\ \cdot & \cdot & u & \cdot \\ \cdot & \rho c^2 & \cdot & u \end{vmatrix} \quad (\text{E16.2.12})$$

$$\tilde{B} = \begin{vmatrix} v & \cdot & \rho & \cdot \\ \cdot & v & \cdot & \cdot \\ \cdot & \cdot & v & \frac{1}{\rho} \\ \cdot & \cdot & \rho c^2 & v \end{vmatrix} \quad (\text{E16.2.13})$$

16.3 THE CHARACTERISTIC FORMULATION OF THE EULER EQUATIONS—EIGENVALUES AND COMPATIBILITY RELATIONS

The eigenvalues of the matrix $\tilde{K} = \vec{A} \cdot \vec{\kappa}$, associated to an arbitrary direction of propagation $\vec{\kappa}$, define for a large part the behaviour of the solutions to the Euler equations. It is therefore essential to have a clear understanding of the characteristic properties, since they represent essential aspects of inviscid flows, namely the propagation of disturbances. We refer the reader to Chapter 3 of Volume 1 for a general introduction to hyperbolic properties and characteristics.

For the first-order system of equation, written in non-conservative form with the primitive variable V , equations (16.2.42) and (16.2.43),

$$\frac{\partial V}{\partial t} + (\vec{A} \cdot \vec{\nabla})V = \tilde{Q} \quad (16.3.1)$$

or

$$\frac{\partial V}{\partial t} + \tilde{A} \frac{\partial V}{\partial x} + \tilde{B} \frac{\partial V}{\partial y} + \tilde{C} \frac{\partial V}{\partial z} = \tilde{Q} \quad (16.3.2)$$

the condition for hyperbolicity is expressed by the existence of simple wave-like solutions of the form

$$V = \hat{V} e^{I S(\vec{x}, t)} = \hat{V} e^{I(\vec{\kappa} \cdot \vec{x} - \omega t)} \quad I = \sqrt{-1} \quad (16.3.3)$$

The function

$$S(\vec{x}, t) = \vec{\kappa} \cdot \vec{x} - \omega t \quad (16.3.4)$$

represents the phase of the wave propagating in the direction $\vec{\kappa}$, with a pulsation ω (for an observer moving with the group velocity of the wave packet).

Wave-like solutions will exist if the eigenvalues of the matrix $\tilde{K} = \vec{A} \cdot \vec{\kappa}$, for arbitrary $\vec{\kappa}$, are real with linear independence of the corresponding left eigenvectors \vec{l} .

If $\lambda_{(j)}$ denotes an eigenvalue of the matrix \tilde{K} , obtained from

$$\det |\lambda \vec{l} - \vec{A} \cdot \vec{\kappa}| = 0 \quad (16.3.5)$$

the left eigenvectors $l^{(j)}$, defined as *line vectors* in the five-dimensional space of the vectors V , are solutions of

$$\vec{l}^{(j)} \tilde{K} = \lambda_{(j)} \vec{l}^{(j)} \quad \text{no summation on } j \quad (16.3.6a)$$

or explicitly

$$\vec{l}_i^{(j)} (\vec{A} \cdot \vec{\kappa})_{ik} = \lambda_{(j)} \vec{l}_k^{(j)} \quad i, j, k = 1, \dots, 5 \quad (16.3.6b)$$

with summation only on i .

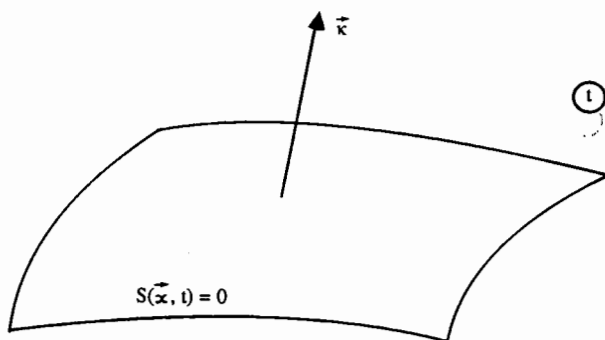


Figure 16.3.1 Characteristic surface in space at a given time t

16.3.1 General properties of characteristics

To each eigenvalue $\lambda_{(j)}(\vec{\kappa})$ and vector $\vec{\kappa}$ one can associate a *characteristic surface* $S(\vec{x}, t) = \text{constant}$ (Figure 16.3.1), *normal to the vector* $\vec{\kappa}$ at instant t and defined by the relations

$$\partial_t S = -\lambda_{(j)}(\vec{\kappa}) \quad (16.3.7)$$

$$\vec{\nabla} S = \vec{\kappa} \quad (16.3.8)$$

To each eigenvalue $\lambda_{(j)}$ one can associate an infinity of characteristic surfaces by varying the vector $\vec{\kappa}$ up to a normalization constant.

From the definition of the eigenvalue $\lambda_{(j)}$ one has

$$\omega = +\lambda_{(j)} \quad (16.3.9)$$

Hence the eigenvalues of \vec{K} represent the frequency, up to a factor 2π , of the propagating wave. This wave propagates with a *phase velocity* \vec{a} , defined by the usual wave relations

$$\vec{a} = \frac{\omega}{\kappa} \quad (16.3.10)$$

$$\vec{a} = a \vec{l}_{\kappa} = +\lambda_{(j)} \frac{\vec{\kappa}}{\kappa^2} \quad (16.3.11)$$

in the direction of $\vec{\kappa}$, that is normal to the constant wave phase surface $S(\vec{x}, t) = \text{constant}$.

Characteristic speed of propagation

If one defines a direction, locally tangent to the phase velocity,

$$\frac{d\vec{x}}{dt} = \vec{a} = \lambda_{(j)} \frac{\vec{\kappa}}{\kappa^2} \quad (16.3.12)$$

the characteristic surface will follow this direction, since

$$\frac{dS}{dt} = 0 \quad \text{along} \quad \frac{d\vec{x}}{dt} = \vec{a} \quad (16.3.13)$$

Indeed, along this curve,

$$\frac{dS}{dt} = \partial_t S + \vec{a} \cdot \vec{\nabla} S = -\lambda_{(j)} + \vec{a} \cdot \vec{\kappa} = 0 \quad (16.3.14)$$

by definition of \vec{a} . This expresses also that the four-dimensional space-time vector $(\vec{a}, 1)$ lies in the surface $S(\vec{x}, t) = \text{constant}$ since $-\lambda_{(j)} = S_t$ is the time component of the normal n to $S(\vec{x}, t)$ with components $(\vec{n}, n_t) = (\vec{\nabla} S, S_t) = (\vec{\kappa}, -\lambda_{(j)})$. Hence, the characteristic surface attached to a normal κ propagates in this direction with a velocity a , the *characteristic velocity*.

The relation (16.3.12) above can be considered as defining the characteristic surfaces.

For each eigenvalue (j) , one has an infinity of characteristic surfaces, propagating in the arbitrary direction $\vec{\kappa}$. The envelope of all these wave surfaces obtained by varying $\vec{\kappa}$ constitutes the *Mach conoid* and the curves of tangency between a wave surface and the Mach conoid are called the *bicharacteristics*. The Mach conoid, the bicharacteristics and the wave surface $S(\vec{x}, t)$ are all to be considered in the four-dimensional space-time (\vec{x}, t) .

Since the bicharacteristics lie in the wave surface $S(\vec{x}, t) = \text{constant}$, they must obey the following condition:

$$-\frac{\partial b}{\partial t} \lambda_{(j)} + \vec{b} \cdot \vec{\kappa} = 0 \quad (16.3.15)$$

where \vec{b} and b , are the space-time components of the bicharacteristic. Since one can always choose $\partial_t b = 1$, one has the condition

$$\vec{b} \cdot \vec{\kappa} = \lambda_{(j)} \quad (16.3.16)$$

One solution is $\vec{b} = \vec{a}$, which was just shown to be on the wave surface, but this is not the bicharacteristic since \vec{a} is the direction of $\vec{\kappa}$. If the eigenvalue can be written as

$$\lambda_{(j)} = \vec{e} \cdot \vec{\kappa} \quad (16.3.17)$$

with \vec{e} not in the direction of $\vec{\kappa}$, then the intersection of the characteristic surface and its envelope (the Mach conoid) is given by the particular value

$$\vec{b} = \vec{e} \quad (16.3.18)$$

The bicharacteristic direction is therefore defined by

$$b: (\vec{e}, 1) \quad (16.3.19)$$

On the other hand, the characteristic surface is also defined by the property that an appropriate linear combination of the equations will result in a form

that contains only derivatives in directions lying in this surface. As shown in Chapter 3 in Volume 1, when this is the case, the coefficients of the linear combination are the left eigenvectors $\tilde{l}^{(j)}$. The transformed equation, given by equation (3.3.6), becomes here, for the eigenvalue $\lambda_{(j)}$,

$$\tilde{l}^{(j)} \frac{\partial V}{\partial t} + \tilde{l}^{(j)} (\tilde{A} \cdot \tilde{\nabla}) V = \tilde{l}^{(j)} \tilde{Q} \quad (16.3.20)$$

and is the *compatibility equation* for the eigenvalue $\lambda_{(j)}$. Since the eigenvalue $\lambda_{(j)}$ is a function of the normal vector $\tilde{\kappa}$, there is an *infinity* of compatibility relations that can be associated with a given eigenvalue. As will be discussed later, certain compatibility relations can be more significant than others. In particular, for points lying on a given surface, for instance an inlet or an outlet boundary of a computational domain or a solid wall boundary embedded in a flow, the direction of propagation normal to these surfaces is of particular significance.

16.3.2 Diagonalization of the Jacobian matrices

It is seen from equation (16.3.6) that a matrix L^{-1} can be defined that will diagonalize the matrix \tilde{K} . Indeed, constructing a matrix L^{-1} with the left eigenvectors $\tilde{l}^{(j)}$, that is the j th line of L^{-1} is the left eigenvector $\tilde{l}^{(j)}$, equation (16.3.6) for all the eigenvalues grouped together can be written as

$$L^{-1} \tilde{K} = \Lambda L^{-1} \quad (16.3.21)$$

where Λ is the diagonal matrix of all the eigenvalues; that is

$$\Lambda = \begin{vmatrix} \lambda_1 & & & & \\ & \lambda_2 & & & \\ & & \cdot & & \\ & & & \cdot & \\ & & & & \lambda_n \end{vmatrix} \quad (16.3.22)$$

where all $\lambda_{(j)}$ are functions of $\tilde{\kappa}$. Hence with $\Lambda = \Lambda(\tilde{\kappa})$ one has

$$\tilde{K} = \Lambda L^{-1} \quad (16.3.23)$$

or

$$\Lambda = L^{-1} (\tilde{A} \cdot \tilde{\kappa}) L \quad (16.3.24)$$

It is of particular importance to notice here that one can diagonalize any linear combination $\tilde{A} \cdot \kappa_x + \tilde{B} \cdot \kappa_y + \tilde{C} \cdot \kappa_z \equiv \tilde{A} \cdot \tilde{\kappa}$ by the appropriate matrix $L(\tilde{\kappa})$, but it is *not possible* to diagonalize simultaneously the three jacobians \tilde{A} , \tilde{B} , \tilde{C} . By selecting $\kappa_x = 1$, $\kappa_y = \kappa_z = 0$, a matrix L_1 will be defined which will diagonalize \tilde{A} , and similarly a matrix L_2 defined by $\kappa_x = 0$, $\kappa_y = 1$, $\kappa_z = 0$ will diagonalize \tilde{B} , but it will be shown in the following that $L_1 \neq L_2$ and hence \tilde{A} and \tilde{B} cannot be diagonalized by the same matrix. This follows from the fact that the Jacobian matrices \tilde{A} , \tilde{B} , \tilde{C} actually do not commute and have, therefore, not the same set of eigenvalues.

Right eigenvectors

Since the matrix $\tilde{K} = \vec{A} \cdot \vec{\kappa}$ is not symmetric, there exists a set of right eigenvectors $\vec{r}^{(j)}$ associated with the same eigenvalues $\lambda_{(j)}$. These column vectors $r^{(j)}$ are defined by

$$\tilde{K}\vec{r}^{(j)} = \lambda_{(j)}\vec{r}^{(j)} \quad \text{no summation on } j \quad (16.3.25a)$$

or explicitly

$$\tilde{K}_{ik}\vec{r}_k^{(j)} = \lambda_{(j)}\vec{r}_i^{(j)} \quad i, j, k = 1, \dots, 5 \quad (16.3.25b)$$

with a summation only on k .

Comparing with the equations for the left eigenvectors $\vec{l}^{(j)}$, it is seen that, grouping all the vectors $\vec{r}^{(j)}$ in a matrix R , where the j th column is the vector $\vec{r}^{(j)}$, the above equations can be written as

$$\tilde{K} \cdot R = R\Lambda \quad (16.3.26a)$$

or

$$\tilde{K} = R\Lambda R^{-1} \quad (16.3.26b)$$

Hence, the matrix of the right eigenvectors is the inverse of the matrix L^{-1} of the left eigenvectors; that is

$$R = L \quad (16.3.27)$$

From equations (16.3.25) one has the orthogonality property between the left and right eigenvectors

$$\vec{l}^{(j)} \cdot \vec{r}^{(k)} = \delta_{jk} \quad (16.3.28)$$

which is another expression for the identity $LL^{-1} = 1$.

The right eigenvectors have the important property to be proportional to the intensity of the propagating disturbance, as seen from equation (3.3.13).

16.3.3 Compatibility equations

With the introduction of the matrices L and L^{-1} , one can write the compatibility equations in a compact form, since equations (16.3.20) can be grouped as

$$(L^{-1}\partial_t + L^{-1}\vec{A} \cdot \vec{\nabla})V = L^{-1}\vec{Q} \quad (16.3.29)$$

It is easy to see that the compatibility relations can be expressed as a function of the conservative variables by application of the matrix $L^{-1}M^{-1}$. Indeed, the above equation can be written as

$$L^{-1}M^{-1}(\partial_t + \vec{A} \cdot \vec{\nabla})U = L^{-1}M^{-1}\vec{Q} \quad (16.3.30)$$

The matrix P defined by

$$P^{-1} = L^{-1}M^{-1} \quad \text{and} \quad P = ML \quad (16.3.31)$$

plays the same role, with respect to the conservative variables, as the matrix L with the primitive variables.

In particular, the matrix P will diagonalize the matrix $K = \vec{A} \cdot \vec{\kappa}$ in the same way as L diagonalizes the matrix $\vec{K} = \vec{A} \cdot \vec{\kappa}$. Indeed, from equation (16.3.24) and the relation between \vec{A} and \vec{A} ,

$$\vec{A} = M^{-1} \vec{A} M \quad (16.3.32)$$

one has

$$\Lambda = L^{-1} M^{-1} (\vec{A} \cdot \vec{\kappa}) M L = P^{-1} K P \quad (16.3.33)$$

The lines of P^{-1} are therefore the left eigenvectors of K , while the columns of P are the right eigenvectors of the same matrix, associated with the conservative variables.

The compatibility relations (16.3.29) lead to the introduction of a new set of *characteristic variables*.

They are defined as a 5×1 column vector by the relation valid for arbitrary variations δ (either ∂_t or $\vec{\nabla}$):

$$\delta W = L^{-1} \delta V \quad (16.3.34a)$$

or explicitly

$$\delta w_k = \sum_i l_i^{(k)} \delta v_i \quad (16.3.34b)$$

Hence, the component δw_k of δW is obtained from the linear combination of the primitive variables with coefficients equal to the components of the k th left eigenvector. Inversely, one has

$$\delta V = L \delta W \quad (16.3.35)$$

the compatibility relations can be written as follows:

$$L^{-1} \frac{\partial V}{\partial t} + (L^{-1} \vec{A} L) L^{-1} \vec{\nabla} V = L^{-1} \vec{Q} \quad (16.3.36)$$

or

$$\frac{\partial W}{\partial t} + (L^{-1} \vec{A} L) \cdot \vec{\nabla} W = L^{-1} \cdot \vec{Q} \quad (16.3.37)$$

Note that the characteristic variables are now associated with a given direction of propagation $\vec{\kappa}$, and therefore these variables are a function of $\vec{\kappa}$.

The definition (16.3.35) expresses the increments δW as a linear combination of the increments of the primitive variables, δV , with coefficients equal to the components of the left eigenvectors. Since the left eigenvectors are generally functions of the flow variables, the coefficients are not constant. Therefore, the variables W will exist if the Pfaff conditions of integrability of a differential form are satisfied; see, for instance, Narasimhan (1973). This is the case when the coefficients of the L matrix are constant, that is for linear equations, whereby W is defined by

$$W = L^{-1} V \quad \text{if } L^{-1} \text{ constant} \quad (16.3.38)$$

The characteristic variable W can also be defined for non-constant coefficients if no more than two differentials appear in the linear combination (16.3.34). This is the case for the one-dimensional time-dependent Euler equations, or for supersonic stationary two-dimensional flows. For more general flows, the integrability conditions cannot be satisfied and the variables W cannot be defined. However, δW always exists and we will maintain the above characteristic formulation (16.3.37) as a shorthand notation for the compatibility equations, keeping in mind that in general only the variations δW are meaningful.

The characteristic variables can also be related to the conservative variables U by

$$\delta W = P^{-1} \delta U \quad (16.3.39a)$$

or

$$\delta U = P \delta W \quad (16.3.39b)$$

Hence, the relation between the three sets of variables can be summarized as shown in Figure 16.3.2.

One can also observe the particular situation of one-dimensional flows, where the matrix $L^{-1} \bar{A} L$ is diagonal, so that the characteristic equations (16.3.37) become decoupled and appear as a set of *scalar* equations. This is a unique feature of one-dimensional flows.

Equations (16.3.39) can also be read differently, if one remembers that the columns of L (or P) are the right eigenvectors of \bar{K} (or \bar{K}). Hence, equation (16.3.39) reads

$$\delta U = \sum_{k=1}^5 \delta w_k r^{(k)} \quad (16.3.40)$$

where δw_k are the components of the column vector δW . This expresses the decomposition of δU in simple waves described by the right eigenvectors of the matrix K , with amplitudes equal to the characteristic δw_k component. The above

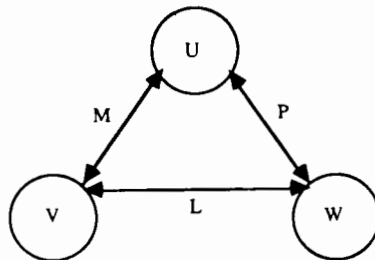


Figure 16.3.2 Relation between the conservative variables U , the primitive variables V and the characteristic variables W

relation is at the basis of a most original method developed by Roe (1981), to be discussed in Chapter 20.

The numerical schemes and their properties, as well as the mathematical formulation of the equations, are dominated by the hyperbolic character (in time) of the system of Euler equations. Since the basic phenomena are of propagation or convective nature, the characteristics of the system and their properties will play an essential role in the mathematical description and in many numerical discretization techniques.

The situation is actually more complex with respect to the space variables, where the stationary form of the Euler equations is of mixed or hybrid type, depending on Mach number and the considered spatial direction. This explains why nearly all the schemes developed for the numerical solution of the Euler equations take as a starting point the time-dependent formulation, even when only the steady state is of interest. In this case, the time evolution of the system is of no importance and the goal of an efficient numerical scheme will be to reach the steady-state conditions in a minimum of time steps.

16.4 CHARACTERISTIC VARIABLES AND EIGENVALUES FOR ONE-DIMENSIONAL FLOWS

One-dimensional flows play an important role in the computation and analysis of solutions to the Euler equations. They are altogether simple enough to warrant a detailed analysis of the non-linear propagation effects and representative of higher-dimensional flows, allowing in many cases local applications of one-dimensional properties. In particular, the application of local one-dimensional concepts for the definition of boundary conditions is an extremely important outcome of the properties of one-dimensional characteristics.

The most general case is described by the quasi one-dimensional flow in a channel of varying cross-section S (Figure 16.4.1). The conservative form of the

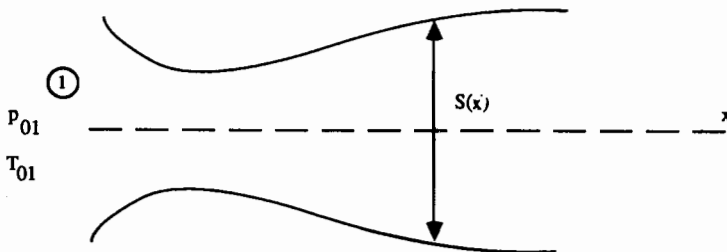


Figure 16.4.1 Quasi one-dimensional flow in channel of varying cross-section $S(x)$

Euler equations can be written as follows (see, for instance, Shapiro, 1953):

$$\begin{aligned}\frac{\partial(\rho S)}{\partial t} + \frac{\partial(\rho u S)}{\partial x} &= 0 \\ \frac{\partial(\rho u S)}{\partial t} + \frac{\partial(\rho u^2 + p)S}{\partial x} &= p \frac{dS}{dx} \\ \frac{\partial(\rho E S)}{\partial t} + \frac{\partial(\rho u H S)}{\partial x} &= 0\end{aligned}\quad (16.4.1)$$

This system can be transformed into primitive variables ρ, u, p , leading to the system (see Problem 16.8)

$$\begin{aligned}\frac{\partial \rho}{\partial t} + u \frac{\partial \rho}{\partial x} + \rho \frac{\partial u}{\partial x} &= -\frac{\rho u}{S} \frac{dS}{dx} \\ \frac{\partial u}{\partial t} + u \frac{\partial u}{\partial x} + \frac{1}{\rho} \frac{\partial p}{\partial x} &= 0 \\ \frac{\partial p}{\partial t} + u \frac{\partial p}{\partial x} + \rho c^2 \frac{\partial u}{\partial x} &= -\frac{\rho u c^2}{S} \frac{dS}{dx}\end{aligned}\quad (16.4.2)$$

Defining the source vector \tilde{Q} ,

$$\tilde{Q} = \begin{vmatrix} -\rho u \\ 0 \\ -\rho c^2 u \end{vmatrix} \frac{1}{S} \frac{dS}{dx}\quad (16.4.3)$$

the equations can be written for the primitive variable vector $V = (\rho, u, p)^T$:

$$\frac{\partial V}{\partial t} + \tilde{A} \frac{\partial V}{\partial x} = \tilde{Q}\quad (16.4.4)$$

where the Jacobian matrix \tilde{A} is given by equation (E16.2.9).

16.4.1 Eigenvalues and eigenvectors of Jacobian matrix

The vector $\bar{\kappa}$ is one dimensional, $\bar{\kappa} = \kappa \bar{1}_x$, and since its magnitude is arbitrary, one can take $\kappa = 1$. The eigenvalue equation (16.3.5) becomes

$$\det|\lambda I - \tilde{A}| = 0\quad (16.4.5)$$

or

$$\begin{vmatrix} u - \lambda & \rho & 0 \\ 0 & u - \lambda & \frac{1}{\rho} \\ 0 & \rho c^2 & u - \lambda \end{vmatrix} = 0\quad (16.4.6)$$

A direct calculation gives the eigenvalues

$$\begin{aligned}\lambda_1 &= u \\ \lambda_2 &= u + c \\ \lambda_3 &= u - c\end{aligned}\tag{16.4.7}$$

and the three left eigenvectors of \tilde{A} , defined up to an arbitrary normalizations, are

$$\begin{aligned}\tilde{l}^{(1)} &= \begin{pmatrix} \alpha & 0 & -\frac{\alpha}{c^2} \end{pmatrix} \\ \tilde{l}^{(2)} &= \begin{pmatrix} 0 & \beta & \frac{\beta}{\rho c} \end{pmatrix} \\ \tilde{l}^{(3)} &= \begin{pmatrix} 0 & \delta & -\frac{\delta}{\rho c} \end{pmatrix}\end{aligned}\tag{16.4.8}$$

where α, β, δ are three normalization coefficients.

Example 16.4.1 Determination of the left eigenvector of Jacobian matrix \tilde{A}

The left eigenvectors $\tilde{l}^{(j)}$ are defined by

$$\tilde{l}^{(j)} \tilde{A} = \lambda_{(j)} \tilde{l}^{(j)}\tag{E16.4.1}$$

Writing this equation explicitly for a given eigenvalue λ , the components l_1, l_2, l_3 of the left eigenvector l are solutions of

$$(l_1, l_2, l_3) \begin{vmatrix} u & \rho & 0 \\ 0 & u & \frac{1}{\rho} \\ 0 & \rho c^2 & u \end{vmatrix} = \lambda(l_1, l_2, l_3)\tag{E16.4.2}$$

For the first eigenvalue $\lambda = u$, we obtain

$$\begin{aligned}ul_1 &= ul_1 \\ \rho l_1 + ul_2 + \rho c^2 l_3 &= ul_2 \\ \frac{1}{\rho} l_2 + ul_3 &= ul_3\end{aligned}\tag{E16.4.3}$$

The last equation gives $l_2 = 0$ and the first one is satisfied for arbitrary values of l_1 . Taking $l_1 = \alpha$ as an arbitrary normalization factor, the second equation gives $l_3 = -\alpha/c^2$.

For the second and third eigenvalues $\lambda = u \pm c$, we obtain the system

$$\begin{aligned} ul_1 &= (u \pm c)l_1 \\ \rho l_1 + ul_2 + \rho c^2 l_3 &= (u \pm c)l_2 \\ \frac{1}{\rho} l_2 + ul_3 &= (u \pm c)l_3 \end{aligned} \quad (\text{E16.4.4})$$

The first equation shows that $l_1 = 0$, and the two others are satisfied for $l_2 = \pm \rho c l_3$. This leads to equations (16.4.8).

Taking $\alpha = \beta = \delta = 1$, the following diagonalization matrix is obtained:

$$L^{-1} = \begin{vmatrix} 1 & 0 & -\frac{1}{c^2} \\ 0 & 1 & \frac{1}{\rho c} \\ 0 & 1 & -\frac{1}{\rho c} \end{vmatrix} \quad (\text{16.4.9})$$

and

$$L = \begin{vmatrix} 1 & \frac{\rho}{2c} & -\frac{\rho}{2c} \\ 0 & \frac{1}{2} & \frac{1}{2} \\ 0 & \frac{\rho c}{2} & -\frac{\rho c}{2} \end{vmatrix} \quad (\text{16.4.10})$$

Note that the columns of L are the right eigenvectors of \tilde{A} , corresponding to the normalization of L^{-1} .

The conservative Jacobian matrix A can also be diagonalized by application of the transformation matrix P , following equation (16.3.33). With the above normalization one obtains, with M^{-1} defined by equation (E.16.2.8),

$$P^{-1} = L^{-1}M^{-1} = \begin{vmatrix} 1 - \frac{\gamma-1}{2} \frac{u^2}{c^2} & (\gamma-1) \frac{u}{c^2} & -\frac{\gamma-1}{c^2} \\ \left(\frac{\gamma-1}{2} u^2 - uc\right) \frac{1}{\rho c} & \frac{1}{\rho c} [c - (\gamma-1)u] & \frac{\gamma-1}{\rho c} \\ -\left(\frac{\gamma-1}{2} u^2 + uc\right) \frac{1}{\rho c} & \frac{1}{\rho c} [c + (\gamma-1)u] & -\frac{\gamma-1}{\rho c} \end{vmatrix} \quad (\text{16.4.11})$$

The matrices L^{-1} and P^{-1} corresponding to other normalizations are obtained by multiplying the first row by α , the second by β and the third by δ .

Similarly, one obtains the inverse of the above matrix by direct multiplication of M and L , with M defined by equation (E16.2.7):

$$P = ML = \begin{vmatrix} 1 & \frac{\rho}{2c} & -\frac{\rho}{2c} \\ u & \frac{\rho}{2c}(u+c) & -\frac{\rho}{2c}(u-c) \\ \frac{u^2}{2} & \frac{\rho}{2c}\left(\frac{u^2}{2} + uc + \frac{c^2}{\gamma-1}\right) & -\frac{\rho}{2c}\left(\frac{u^2}{2} - uc + \frac{c^2}{\gamma-1}\right) \end{vmatrix} \quad (16.4.12)$$

The matrices L and P for other normalizations are obtained by dividing the first column by α , the second by β and the third by δ . A normalization that is often found in the literature is $\alpha = 1$, $\beta = -\delta = 1/\sqrt{2}$ (Warming *et al.*, 1975). Note also that the terms $u^2/2 + c^2/(\gamma-1) = H$, the stagnation enthalpy.

The lines of P^{-1} are the left eigenvectors of the Jacobian A in the conservative variables, while the columns of P are the right eigenvectors of the same matrix, associated with the same eigenvalues.

The compatibility relations are obtained after multiplication from the left by the matrix L^{-1} , following equation (16.3.29). With

$$L^{-1}\tilde{A} = \begin{vmatrix} u & 0 & -\frac{u}{c^2} \\ 0 & u+c & \frac{1}{\rho c}(u+c) \\ 0 & u-c & -\frac{1}{\rho c}(u-c) \end{vmatrix} \quad (16.4.13)$$

we obtain the compatibility relations from equations (16.3.36):

$$L^{-1}\frac{\partial V}{\partial t} + (L^{-1}\tilde{A}L)L^{-1}\frac{\partial V}{\partial x} = L^{-1}\tilde{Q} \quad (16.4.14)$$

or

$$L^{-1}\frac{\partial V}{\partial t} + \Lambda L^{-1}\frac{\partial V}{\partial x} = L^{-1}\tilde{Q} \quad (16.4.15)$$

introducing the diagonal matrix of the eigenvalues Λ

$$\Lambda = \begin{vmatrix} u & & \\ & u+c & \\ & & u-c \end{vmatrix} \quad (16.4.16)$$

Explicitly, these equations are written as

$$\begin{aligned} \frac{\partial \rho}{\partial t} - \frac{1}{c^2} \frac{\partial p}{\partial t} + u \frac{\partial \rho}{\partial x} - \frac{u}{c^2} \frac{\partial p}{\partial x} &= 0 \\ \frac{\partial u}{\partial t} + \frac{1}{\rho c} \frac{\partial p}{\partial t} + (u+c) \left(\frac{\partial u}{\partial x} + \frac{1}{\rho c} \frac{\partial p}{\partial x} \right) &= -\frac{uc}{S} \frac{dS}{dx} \\ \frac{\partial u}{\partial t} - \frac{1}{\rho c} \frac{\partial p}{\partial t} + (u-c) \left(\frac{\partial u}{\partial x} - \frac{1}{\rho c} \frac{\partial p}{\partial x} \right) &= \frac{uc}{S} \frac{dS}{dx} \end{aligned} \quad (16.4.17)$$

16.4.2 Characteristic variables

Applying the definition (16.3.34), the following definitions of the characteristic variables $\delta W = (\delta w_1, \delta w_2, \delta w_3)^T$, with δW representing an arbitrary variation, either ∂_t or ∂_x , are obtained from $\delta W = L^{-1} \delta V$: from (6.4.9),

in 1-dim.

$$V = \begin{pmatrix} \rho \\ u \\ p \end{pmatrix} \quad \delta V = \begin{pmatrix} \delta \rho \\ \delta u \\ \delta p \end{pmatrix}$$

$$\begin{aligned} \delta w_1 &= \delta \rho - \frac{1}{c^2} \delta p \\ \delta w_2 &= \delta u + \frac{1}{\rho c} \delta p \\ \delta w_3 &= \delta u - \frac{1}{\rho c} \delta p \end{aligned} \quad (16.4.18)$$

The characteristic form of the one-dimensional Euler equations can be decoupled in the W variables and written as

$$\frac{\partial W}{\partial t} + \Lambda \frac{\partial W}{\partial x} = L^{-1} \tilde{Q} \quad (16.4.19a)$$

or

$$\frac{\partial}{\partial t} \begin{vmatrix} w_1 \\ w_2 \\ w_3 \end{vmatrix} + \begin{vmatrix} u & \cdot & \cdot \\ \cdot & u+c & \cdot \\ \cdot & \cdot & u-c \end{vmatrix} \frac{\partial}{\partial x} \begin{vmatrix} w_1 \\ w_2 \\ w_3 \end{vmatrix} = \begin{vmatrix} 0 \\ -uc \\ uc \end{vmatrix} \frac{1}{S} \frac{dS}{dx} \quad (16.4.19b)$$

Riemann variables

The decoupling of the equations shows that the quantities w_j propagate along the corresponding characteristics with the speed $\lambda_{(j)}$. Hence,

$$\delta w_1 = \delta \rho - \frac{1}{c^2} \delta p$$

propagates with velocity u along the characteristic C_0 defined by $dx/dt = u$.

This characteristic is the path line of the fluid. On the other hand,

$$\begin{aligned}\delta w_2 &= \delta u + \frac{1}{\rho c} \delta p \\ &= \delta u + \frac{c \delta \rho}{\rho}\end{aligned}$$

propagates with velocity $u + c$ along the characteristic C_+ defined by $dx/dt = u + c$ and

$$\begin{aligned}\delta w_3 &= \delta u - \frac{1}{\rho c} \delta p \\ &= \delta u - c \frac{\delta \rho}{\rho}\end{aligned}$$

propagates with velocity $u - c$ along the characteristic C_- defined by $dx/dt = u - c$. The C_+ and C_- characteristics are also called *Mach lines* (Figure 16.4.2).

When the right-hand side of the equations is zero, the corresponding characteristic variables are strictly conserved during their propagation along the characteristic; that is the quantity w , satisfying

$$\frac{\partial w}{\partial t} + \lambda \frac{\partial w}{\partial x} = 0 \quad (16.4.20)$$

remains constant along the characteristic C , defined by

$$\frac{dx}{dt} = \lambda \quad (16.4.21)$$

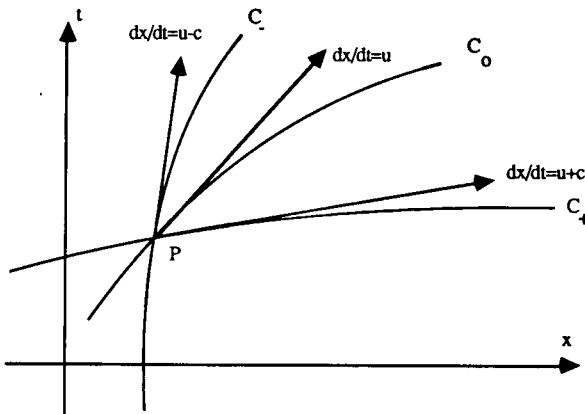


Figure 16.4.2 Characteristic lines for a one-dimensional flow

since along C,

$$\frac{dw}{dt} = \frac{\partial w}{\partial t} + \frac{dx}{dt} \frac{\partial w}{\partial x} = 0 \quad (16.4.22)$$

The variables w are also called *Riemann variables* and *Riemann invariants* when they remain constant. The system of equations in characteristic form can also be written as follows:

$$\begin{aligned} d^{(0)}\rho - \frac{1}{c^2} d^{(0)}p &= 0 & d^{(0)} &= \partial_t + u\partial_x \\ d^{(+)}u + \frac{1}{\rho c} d^{(+)}p &= -\frac{uc}{S} \frac{dS}{dx} & d^{(+)} &= \partial_t + (u+c)\partial_x \\ d^{(-)}u - \frac{1}{\rho c} d^{(-)}p &= +\frac{uc}{S} \frac{dS}{dx} & d^{(-)} &= \partial_t + (u-c)\partial_x \end{aligned} \quad (16.4.23)$$

with the definitions of the three characteristics

$$\begin{aligned} \text{on } C_0: \quad \frac{dx}{dt} &= u \\ \text{on } C_+: \quad \frac{dx}{dt} &= u + c \\ \text{on } C_-: \quad \frac{dx}{dt} &= u - c \end{aligned} \quad (16.4.24)$$

It is of interest also to notice that the first characteristic equation expresses the constant transport of entropy along the path line $dx/dt = u$. From equation (2.1.17) in Volume 1, one has, for the variations of entropy s ,

$$ds = -\frac{\gamma c_v}{\rho} \left(d\rho - \frac{dp}{c^2} \right) \quad (16.4.25)$$

and the first equation is equivalent to the condition

$$d^{(0)}s = 0 \quad \text{along} \quad \frac{dx}{dt} = u \quad (16.4.26)$$

or

$$\frac{\partial s}{\partial t} + u \frac{\partial s}{\partial x} = 0 \quad (16.4.27)$$

Hence, the entropy propagates along the path line and is conserved along this characteristic, as long as discontinuities do not appear.

For isentropic flows, the Riemann or characteristic variables can be integrated

as follows, for either C_+ or C_- . For instance, on C_+ ,

$$w_2 = u + \int \frac{dp}{\rho c} = u + \int c(\rho) \frac{d\rho}{\rho} \quad (16.4.28)$$

where the isentropic relations

$$p = k\rho^\gamma \quad \text{and} \quad c^2 = k\gamma\rho^{\gamma-1} \quad (16.4.29)$$

can be introduced, k being a constant. This gives

$$w_2 = u + \frac{2}{\gamma-1}c \quad (16.4.30)$$

and similarly

$$w_3 = u - \frac{2}{\gamma-1}c \quad (16.4.31)$$

for the two Riemann variables on the characteristics C_+ and C_- . The system of one-dimensional Euler equations is then equivalent to the following characteristic form:

$$\begin{aligned} \frac{\partial s}{\partial t} + u \frac{\partial s}{\partial x} &= 0 \\ \frac{\partial}{\partial t} \left(u + \frac{2c}{\gamma-1} \right) + (u+c) \frac{\partial}{\partial x} \left(u + \frac{2c}{\gamma-1} \right) &= -cu \frac{1}{S} \frac{dS}{dx} \\ \frac{\partial}{\partial t} \left(u - \frac{2c}{\gamma-1} \right) + (u-c) \frac{\partial}{\partial x} \left(u - \frac{2c}{\gamma-1} \right) &= +cu \frac{1}{S} \frac{dS}{dx} \end{aligned} \quad (16.4.32)$$

This formulation expresses the propagation or the convection of entropy along the streamlines and the propagation of pressure waves as described by the Riemann variables w_2 and w_3 along the characteristics C_+ and C_- .

Other formulations in characteristic variables can be found in Liepmann and Roshko (1957).

Example 16.4.2 Steady two-dimensional supersonic flow

We consider a stationary, two-dimensional supersonic isentropic flow written in non-conservative form with the variables u, v, p as basic dependent variables.

By transforming the continuity equation, via the isentropic relation, into an equation for the pressure, as done in Section 16.2.2, equation (16.2.40), the system of stationary Euler equations becomes

$$\begin{aligned} u \frac{\partial u}{\partial x} + v \frac{\partial u}{\partial y} + \frac{1}{\rho} \frac{\partial p}{\partial x} &= 0 \\ u \frac{\partial v}{\partial x} + v \frac{\partial v}{\partial y} + \frac{1}{\rho} \frac{\partial p}{\partial y} &= 0 \\ u \frac{\partial p}{\partial x} + v \frac{\partial p}{\partial y} + \rho c^2 \frac{\partial u}{\partial x} + \rho c^2 \frac{\partial v}{\partial y} &= 0 \end{aligned} \quad (\text{E16.4.5})$$

This can be written as a system for the variable

$$V = \begin{vmatrix} u \\ v \\ p \end{vmatrix} \quad (\text{E16.4.6})$$

under the form

$$A_1 \frac{\partial V}{\partial x} + A_2 \frac{\partial V}{\partial y} = 0 \quad (\text{E16.4.7})$$

Taking the x direction as time like, the system can be transformed to

$$\frac{\partial V}{\partial x} + A \frac{\partial V}{\partial y} = 0 \quad (\text{E16.4.8})$$

where the Jacobian matrix A is obtained from $A = A_1^{-1} \cdot A_2$:

$$A = \begin{vmatrix} uv & -c^2 & -\frac{v}{\rho} \\ 0 & \frac{v}{u}(u^2 - c^2) & \frac{u^2 - c^2}{\rho u} \\ -\rho v c^2 & \rho u c^2 & uv \end{vmatrix} \frac{1}{u^2 - c^2} \quad (\text{E16.4.9})$$

It is seen that $(u^2 - c^2)$ may not vanish for the matrix A to exist, that is the flow should be supersonic in the x direction. This is the condition for the selection of x as a time-like direction, as seen in Chapter 13, Section 13.3.

The properties of the stationary system are defined by the eigenvalue structure, solutions of $\det|A - \lambda I| = 0$.

A straightforward calculation gives the three eigenvalues

$$\begin{aligned} \lambda_1 &= \frac{v}{u} \\ \lambda_2 &= \frac{uv + c^2 \alpha}{u^2 - c^2} \equiv \frac{u + v\alpha}{u\alpha - v} \\ \lambda_3 &= \frac{uv - c^2 \alpha}{u^2 - c^2} \equiv \frac{v\alpha - u}{u\alpha + v} \end{aligned} \quad (\text{E16.4.10})$$

where

$$\alpha = \sqrt{M^2 - 1} \quad \text{and} \quad M^2 = \frac{u^2 + v^2}{c^2} \equiv \frac{q^2}{c^2} \quad (\text{E16.4.11})$$

They are real and the system is hyperbolic in x if $\alpha > 0$, that is for supersonic flows. Otherwise there is one real and two complex eigenvalues and the system is hybrid.

The first eigenvalue defines the characteristic C_0 , identical to the streamline, while the two other eigenvalues define the characteristics C_+ and C_- and are the Mach lines (see also Chapter 13 and Problem 13.4).

The diagonalization matrix L^{-1} , such that $L^{-1}AL = \Lambda$, where Λ is the diagonal matrix of the eigenvalues, is obtained from the left eigenvectors of the matrix A . Applying the method of Example 16.4.1, with the third component l_3 normalized to 1, one obtains

$$L^{-1} = \begin{pmatrix} \rho u & \rho v & 1 \\ -\frac{\rho v}{\alpha} & \frac{\rho u}{\alpha} & 1 \\ \frac{\rho v}{\alpha} & -\frac{\rho u}{\alpha} & 1 \end{pmatrix} \quad (\text{E16.4.12})$$

The inverse matrix, containing the right eigenvectors as columns, is

$$L = \begin{pmatrix} \frac{u}{\rho q^2} & -\frac{u+v\alpha}{2\rho q^2} & \frac{v\alpha-u}{2\rho q^2} \\ \frac{v}{\rho q^2} & \frac{u\alpha-v}{2\rho q^2} & -\frac{v+u\alpha}{2\rho q^2} \\ 0 & \frac{1}{2} & \frac{1}{2} \end{pmatrix} \quad (\text{E16.4.13})$$

The characteristic variables are defined by $\delta W = L^{-1}\delta V$, or

$$\begin{aligned} \delta w_1 &= \rho u \delta u + \rho v \delta v + \delta p \\ \delta w_2 &= \delta p - \frac{\rho u^2}{\alpha} \delta\left(\frac{v}{u}\right) = \delta p - \frac{\rho v}{\alpha} \delta u + \frac{\rho u}{\alpha} \delta v \\ \delta w_3 &= \delta p + \frac{\rho u^2}{\alpha} \delta\left(\frac{v}{u}\right) = \delta p + \frac{\rho v}{\alpha} \delta u - \frac{\rho u}{\alpha} \delta v \end{aligned} \quad (\text{E16.4.14})$$

The compatibility relations can be written as follows by defining the directional derivatives $d^{(k)}$ along the characteristic k :

$$\begin{aligned} d^{(k)} &= \frac{\partial}{\partial x} + \lambda_{(k)} \frac{\partial}{\partial y} \\ \rho u d^{(1)}u + \rho v d^{(1)}v + d^{(1)}p &= 0 \\ \frac{\rho v}{\alpha} d^{(2)}u - \frac{\rho u}{\alpha} d^{(2)}v - d^{(2)}p &= 0 \\ \frac{\rho v}{\alpha} d^{(3)}u - \frac{\rho u}{\alpha} d^{(3)}v + d^{(3)}p &= 0 \end{aligned} \quad (\text{E16.4.15})$$

These relations can also be written in characteristic form for the variables W :

$$\begin{aligned} \frac{\partial w_1}{\partial t} + \frac{v}{u} \frac{\partial w_1}{\partial x} &= 0 \\ \frac{\partial w_2}{\partial t} + \frac{uv + c^2 \alpha}{u^2 - c^2} \frac{\partial w_2}{\partial x} &= 0 \\ \frac{\partial w_3}{\partial t} + \frac{uv - c^2 \alpha}{u^2 - c^2} \frac{\partial w_3}{\partial x} &= 0 \end{aligned} \tag{E16.4.16}$$

where w_1 is constant along the streamline, the quantity w_2 is constant along the Mach line C_+ and w_3 is constant along C_- .

16.4.3 Characteristics in the xt plane—shocks and contact discontinuities

One can interpret the physical state at a given point in a one-dimensional isentropic inviscid flow as resulting from the quantities transported along the characteristics.

At a given point $P(x, t)$ (Figure 16.4.3), the physical flow condition will be determined by the entropy transported along C_0 at speed u , that is along the streamline. The velocity u and the pressure or the density are determined from the quantities $[u \pm 2c/(\gamma - 1)]$ transported at velocity $(u \pm c)$ along C_{\pm} . Hence,

$$\left(u + \frac{2c}{\gamma - 1} \right)_P = \left(u + \frac{2c}{\gamma - 1} \right)_{P_+} \tag{16.4.33a}$$

$$\left(u - \frac{2c}{\gamma - 1} \right)_P = \left(u - \frac{2c}{\gamma - 1} \right)_{P_-} \tag{16.4.33b}$$

$$s_P = s_{P_0} \tag{16.4.33c}$$

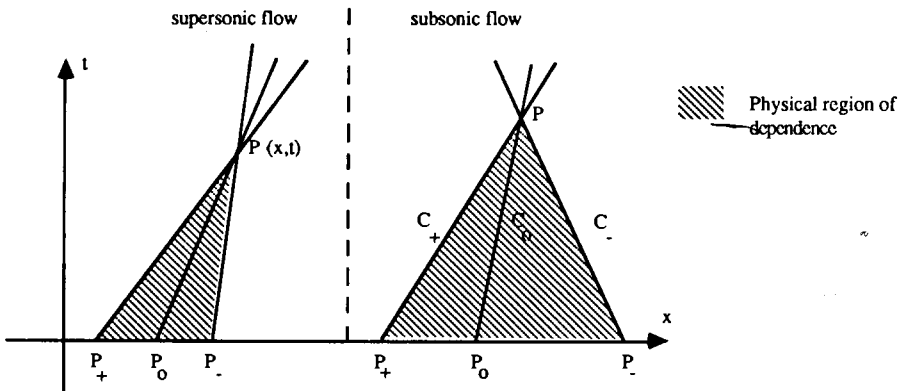


Figure 16.4.3 Propagation of flow quantities in a one-dimensional inviscid flow

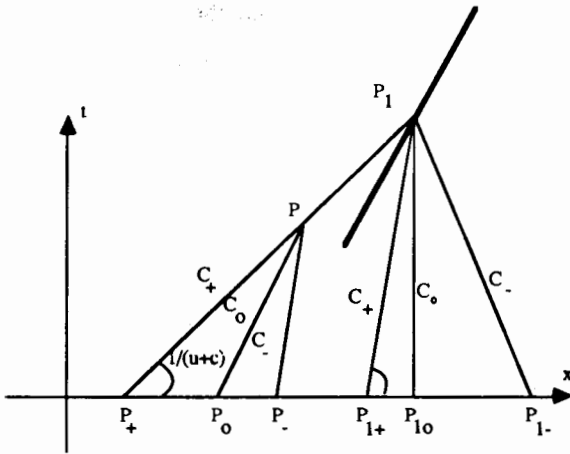


Figure 16.4.4 Intersecting characteristics for $\partial_x(u+c) < 0$

The left side of Figure 16.4.3 is drawn for the case of a supersonic flow, while for a subsonic flow, the C_- characteristic has a negative slope and one has the situation shown on the right side of the figure.

Each point P in the (x, t) plane is reached by one characteristic of each type and therefore the flow situation at a given position x , at the time t , is solely dependent on the domain between P_+ and P_- . This is the *domain of dependence* of P . Inversely, referring to Figure 16.4.2, the region included between the characteristics issuing from P forms the *domain of influence* of P .

Due to the non-linearity of the flow equations, the streamline slopes may decrease, in particular if $\partial_x(u+c) < 0$, that is when $(u+c)$ decreases with increasing x , and one can have the situation illustrated in Figure 16.4.4, where the C_+ characteristic emanating from P_{1+} intersects the C_+ characteristic from P_+ , and hence multi-valued quantities would occur in P_1 ; that is one would have

$$\left(u + \frac{2c}{\gamma - 1}\right)_{P_1} = \left(u + \frac{2c}{\gamma - 1}\right)_{P_+} \quad (16.4.34a)$$

and

$$\left(u + \frac{2c}{\gamma - 1}\right)_{P_1} = \left(u + \frac{2c}{\gamma - 1}\right)_{P_{1+}} \quad (16.4.34b)$$

where

$$\left(u + \frac{2c}{\gamma - 1}\right)_{P_+} \neq \left(u + \frac{2c}{\gamma - 1}\right)_{P_{1+}} \quad (16.4.34c)$$

This impossible situation leads to a *discontinuous* flow behaviour called a shock wave.

It is shown (see, for instance, Shapiro, 1953 and Whitham, 1974 for a more

detailed discussion of shock properties) that the shock velocity C satisfies

$$(u + c)_{P_{1+}} < C < (u + c)_{P_+} \quad (16.4.35)$$

This implies also that all the variables satisfy the relation

$$(\rho, u, p)_{P_+} > (\rho, u, p)_{P_{1+}} \quad (16.4.36)$$

and also

$$(c)_{P_+} > (c)_{P_{1+}} \quad (16.4.37)$$

in order for a shock to occur.

The fact that $(\partial_x p)$ should be negative implies that a fixed observer sees a wave of increasing pressure, that is a *compression wave*, in order to generate a shock. On the other hand, an expansion wave will not give rise to discontinuities in physical situations, but will lead to an *expansion fan*.

Hence, with respect to a fixed observer, a shock situation will be characterized by the following properties shown in Figure 16.4.5(a), while for a stationary shock, one has the situation of Figure 16.4.5(b), with the conditions that the velocity towards the shock is supersonic and subsonic when going away from the shock.

Another discontinuity that can arise is the *contact discontinuity* representing an interface between two fluid regions of different densities but equal pressure. However, since the contact interface moves with the fluid particles, the velocity has to be continuous over a contact discontinuity.

These various aspects of one-dimensional inviscid flows will be illustrated by the solution of the so-called shock-tube problem described in Section 16.6. This problem forms a non-trivial solution of unsteady Euler flows.

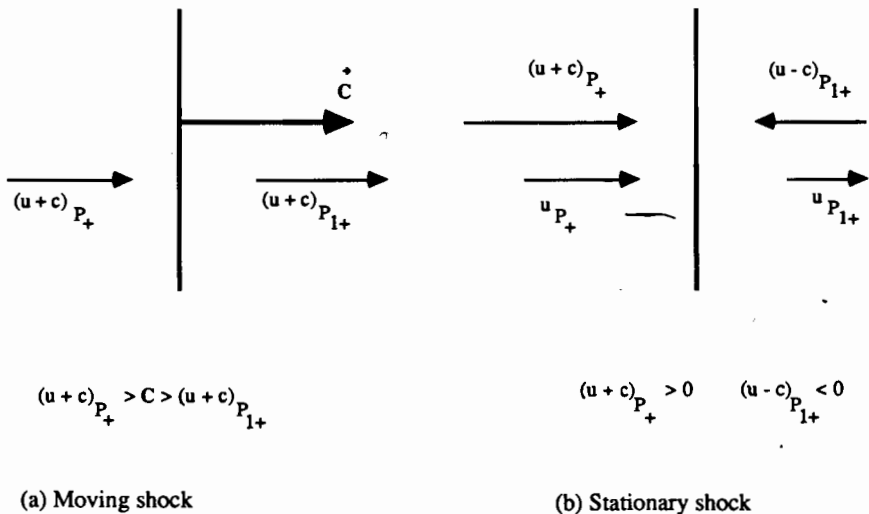


Figure 16.4.5 Shock condition for fixed observer and for an observer moving with the shock

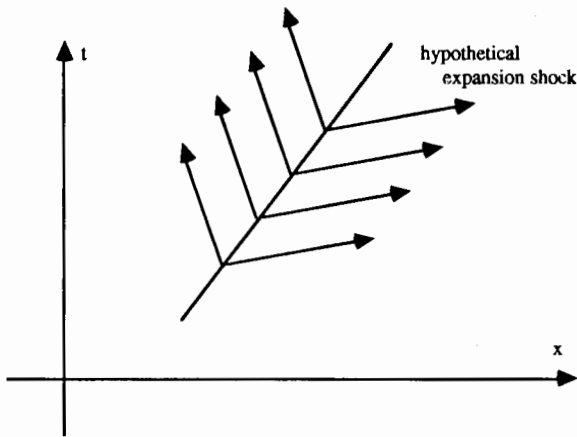


Figure 16.4.6 Situation with an hypothetical expansion shock

Note that the condition for the occurrence of a compression shock can be expressed by the fact that the characteristics on both sides intersect the shock. This means that the information carried by the characteristics is propagated towards the discontinuity. A hypothetical expansion shock would lead to a situation where $(u + c)_{P_+} < C < (u + c)_{P_1+}$, instead of equation (16.4.35) and to characteristics carrying information away from the discontinuity. This is illustrated in Figure 16.4.6. The conceptualization of these conditions to the definition of an entropy condition, which would exclude the above expansion shock, is discussed in Chapter 21.

16.4.4 Physical boundary conditions

The above considerations have a direct bearing on the number of boundary conditions to be imposed in a one-dimensional inviscid flow problem. Consider an inlet plane $x = x_0$, an outlet plane $x = x_1$ and points P_0 and P_1 at a given time on these boundaries. The number of boundary conditions to be imposed will depend on the way the information transported along the characteristics interacts with the boundaries (Figure 16.4.7).

At an inlet point P_0 , the characteristics C_+ and C_0 have ^{speeds $u+c$ and u} slopes u and $c + u$, which are always positive, for a flow in the positive x direction. Therefore, they will always carry information from the boundaries towards the inside of the domain. This requires the values of the transported quantities to be known at P_0 .

The third characteristic C_- has a slope whose sign depends on the inlet Mach number. For supersonic inlet flow conditions, C_- will have a positive slope, but a negative slope at subsonic inlet conditions.

In the first case, the information from the inlet surface enters the domain and a corresponding boundary condition has to be imposed. On the other hand, at

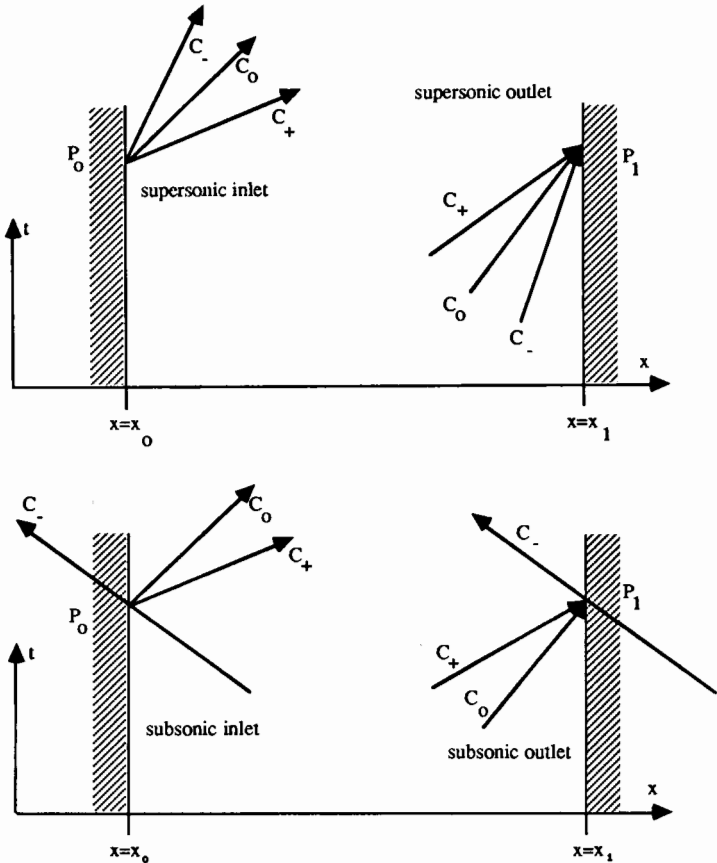


Figure 16.4.7 Boundary conditions for one-dimensional inviscid flows

subsonic inlet conditions, information from inside the domain reaches the boundary along C_- and no boundary condition associated with C_- is allowed to be fixed arbitrarily.

Similar considerations can be made at the outlet. Two characteristics, C_0 and C_+ , always reach the outlet from inside the domain and therefore they determine two of the three independent characteristic variables in the outlet plane from the behaviour of the interior flow.

The third condition is dependent on the outlet flow Mach number. For supersonic outlet velocities no boundary condition is to be imposed, while at subsonic outlet velocities one boundary condition is to be fixed at the outlet section.

This is summarized in Table 16.1. Table 16.1 shows the number and the nature of the boundary conditions required by the physical properties of the flow. However, this raises several problems with regard to the numerical formulations.

Table 16.1. Physical boundary conditions for one-dimensional inviscid flows

	Subsonic	Supersonic
Inlet	Two conditions w_1 and w_2 given	Three conditions w_1, w_2, w_3 given
Outlet	One condition w_3 given	Zero conditions

- (1) The physical conditions to be imposed are the entropy and the values of the characteristic or Riemann variables. This is not a very practical requirement, since these variables are generally not known. Instead, the conditions that are fixed in practical situations in experimental set-ups are velocities and pressures, and therefore the characteristic information might have to be defined in an iterative or approximate way, particularly at subsonic boundaries.
- (2) On the other hand, the numerical schemes generally require the values of all the variables at the boundaries. Hence, additional conditions of numerical origin will have to be added to the physical conditions in order to define completely the numerical problem. These conditions, called the *numerical boundary conditions*, correspond to the boundary variables defined by the inner flow. They should reflect in some way this information, which is dependent on the yet-unknown internal flow conditions. Therefore, these numerical conditions should be compatible with the physical flow behaviour and should not influence the physical boundary conditions.

The importance of the numerical boundary conditions is considerable and can not be emphasized enough. In addition, it can be shown from the theoretical point of view, as well as through numerical experiments, that the choice of the numerical boundary conditions can have a dominating effect on the accuracy, stability and convergence rate of many schemes. For instance, many implicit schemes which are linearly, unconditionally stable, appear to be only conditionally stable in practice if an unadapted boundary treatment is introduced.

A large number of methods have been and still are being investigated in order to find the most appropriate boundary formulation for a given discretization scheme, and this will be discussed in more detail in Chapter 19.

16.4.5 Characteristics and simple wave solutions

The characteristic attached to an eigenvalue $\lambda_{(j)}$ is a curve in the space-time domain (x, t) , defined by equation (16.4.20), which expresses that its direction is equal to $\lambda_{(j)}$. Under certain circumstances, such as one-dimensional isentropic flows, the characteristic variables are constant along the associated

characteristics in the (x, t) space. However, as mentioned at the end of Section 16.3, the W variables cannot always be integrated.

Following Lax (1957), more general solutions to systems of hyperbolic equations can be defined by considering characteristics or *simple wave* solutions in phase space, that is in the space of the variables U .

We consider a scalar variable v , constant along the characteristic (j) , that satisfies

$$\frac{\partial v}{\partial t} + \lambda^{(j)} \frac{\partial v}{\partial x} = 0 \tag{16.4.38}$$

and we look for solutions defined by $U^{(j)} = U^{(j)}(v)$, everywhere tangent to the right eigenvector $r^{(j)}(v)$ associated to the eigenvalue $\lambda_{(j)}(v)$. This solution defines a wave path in phase space, as illustrated in Figure 16.4.8, and is such that

$$\frac{dU^{(j)}}{dv} = r^{(j)} \tag{16.4.39}$$

Hence $U^{(j)}$ satisfies the conservation equation $\partial U/\partial t + A\partial U/\partial x = 0$, because of

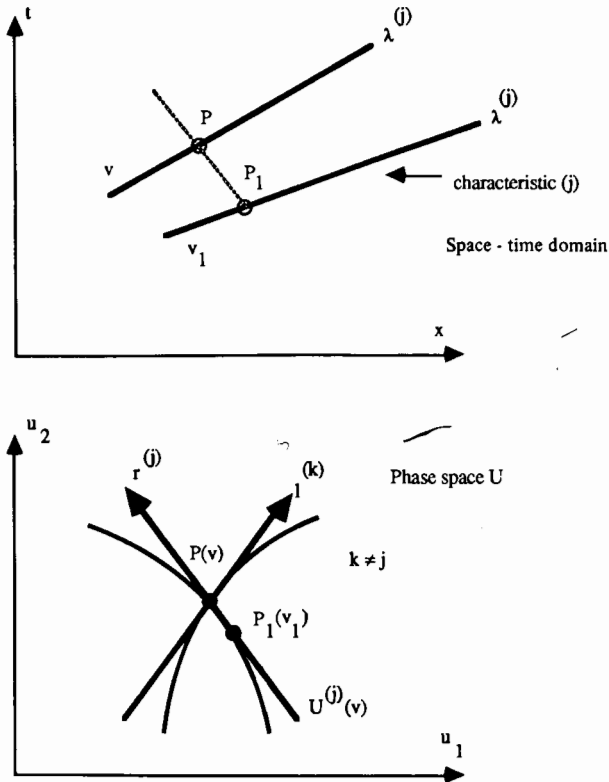


Figure 16.4.8 Characteristics and simple wave solutions in space-time and phase space domains

equation (16.4.38), since

$$\begin{aligned}\frac{\partial U^{(j)}}{\partial t} &= \frac{dU^{(j)}}{dv} \frac{\partial v}{\partial t} = r^{(j)} \frac{\partial v}{\partial t} \\ A \frac{\partial U^{(j)}}{\partial x} &= A \frac{dU^{(j)}}{dv} \frac{\partial v}{\partial x} = \lambda_{(j)} r^{(j)} \frac{\partial v}{\partial x}\end{aligned}\quad (16.4.40)$$

Along this wave path quantities can be defined that remain invariant.

The functional $R^{(j)}(v)$ is *invariant along the wave path* $U^{(j)}$ if

$$\frac{dR^{(j)}}{dv} = 0 \quad (16.4.41a)$$

or

$$\frac{dR^{(j)}}{dv} = \frac{\partial R^{(j)}}{\partial U} \cdot \frac{dU^{(j)}}{dv} = \frac{\partial R^{(j)}}{\partial U} \cdot r^{(j)} = 0 \quad (16.4.41b)$$

This equation indicates that the gradient of $R^{(j)}$ with respect to the U variables is orthogonal to the corresponding j -right eigenvector. Since the $(n-1)$ left eigenvectors $l^{(k)}$, $k \neq j$, are also orthogonal to $r^{(j)}$, there are $(n-1)$ independent $R^{(j)}$ invariants whose U gradients can be expressed as linear combinations of these $(n-1)$ left eigenvectors.

Note that $\partial R/\partial U$ is a line vector with the following elements in conservative variables $\partial R/\partial U \equiv (\partial R/\partial p, \partial R/\partial m, \partial R/\partial \varepsilon)$.

For each eigenvalue (j), one can write

$$\frac{dR^{(j)}}{dU} = \sum_{k \neq j} \alpha_k l^{(k)} \quad (16.4.42)$$

with $(n-1)$ arbitrary constants α_k . Hence $(n-1)$ independent invariants $R_m^{(j)}$, $m = 1, \dots, n-1$, can be defined for each j eigenvalue.

It is easily shown (see Lax, 1957) that the boundaries of a region of constant state U in the xt space are characteristics that are necessarily straight lines.

The compatibility relation (16.4.15) can be written separately for each eigenvalue, considered for the conservative variables:

$$l^{(k)} \left(\frac{\partial U}{\partial t} + \lambda^{(k)} \frac{\partial U}{\partial x} \right) = 0 \quad (16.4.43)$$

For $j \neq k$, the k th left eigenvector can be expressed as a linear combination of the $(n-1)$ invariants $R_m^{(j)}$ by inverting the relations (16.4.42):

$$l^{(k)} = \sum_{m=1}^{n-1} \beta_m^{(k)} \frac{dR_m^{(j)}}{dU} \quad k \neq j \quad (16.4.44)$$

Inserting this relation in equation (16.4.43), we obtain

$$\sum_m \beta_m^{(k)} \left(\frac{\partial R_m^{(j)}}{\partial t} + \lambda^{(k)} \frac{\partial R_m^{(j)}}{\partial x} \right) = 0 \quad k \neq j \quad (16.4.45)$$

and if the j characteristic is the boundary of a constant-state region, each term should vanish separately; hence, for all $k \neq j$,

$$\frac{\partial R_m^{(j)}}{\partial t} + \lambda^{(k)} \frac{\partial R_m^{(j)}}{\partial x} = 0 \quad k \neq j \quad (16.4.46)$$

indicating that the j invariants are constant along the $(n - 1)$ other characteristics in the $x-t$ space.

Consequently, a solution in a region of the $x-t$ space for which all j invariants are constant is called a j simple wave. Simple wave solutions separate regions of constant state.

Referring to Figure 16.4.8 for the purpose of a simple illustration, the invariants $R_m^{(j)}$ are constant along the wave path $r^{(j)}$ in phase space. However, since this wave path is generated by varying the parameter v , that is by crossing the associated characteristic in the physical space-time domain, it is also seen from equation (16.4.46) that the j invariants are constant across the j characteristic in the $x-t$ space.

Multiplying equation (16.4.39), which defines the j invariants, by the k th left eigenvector for $k \neq j$ and introducing the characteristic variables defined by equation (16.3.35) leads to the following relation:

$$l^{(k)} \frac{dU^{(j)}}{dv} = \frac{dw_k}{dv} = 0 \quad k \neq j \quad (16.4.47)$$

Hence, the $(n - 1)$ characteristic variables w_k , for $k \neq j$, defined for the simple wave solution, satisfy equation (16.4.41) and are therefore j invariants. They are called *Riemann invariants*, following the definition given in Section 16.4.2. When a j characteristic is followed in *physical space-time*, the variable w_j remains constant, but when the simple wave path defined by the j th right eigenvector is followed in *phase space*, then the $(n - 1)$ other characteristic variables w_k , $k \neq j$, are constant. Both points of view are actually consistent since in following the wave path in phase space one crosses the j characteristics in $x-t$ space and thereby follows the various other k characteristics in the $x-t$ domain.

For the one-dimensional Euler equation, three characteristics exist. For the wave of speed $u - c$, the quantity $[u - 2c/(\gamma - 1)]$ is constant along the associated characteristic in the $x-t$ space, while the two other variables s and $[u + 2c/(\gamma - 1)]$ are constant when this simple wave is crossed. Similarly, $[u - 2c/(\gamma - 1)]$ and s are constant when the $u + c$ characteristic is crossed. For the third wave of speed u , it is seen from equation (16.4.18) that w_2 and w_3 can be combined for the simple wave solutions to u and p as invariants.

Finally we mention here a general property shown by Lax (1957); namely when crossing a shock of intensity ε , the j invariants all undergo a change of third order in ε .

16.5 EIGENVALUES AND COMPATIBILITY RELATIONS IN MULTI-DIMENSIONAL FLOWS

The eigenvalues of the system of multi-dimensional Euler equations are surprisingly simple, in view of the complexity of the Jacobian matrices. The associated eigenvectors are easily derived for the Jacobians in primitive variables.

16.5.1 Jacobian eigenvalues and eigenvectors in primitive variables

The eigenvalues are obtained as solutions of equation (16.3.5):

$$\det |\lambda \vec{I} - \vec{A} \cdot \vec{\kappa}| = 0 \quad (16.5.1)$$

or explicitly with \vec{A} defined by equations (16.2.44) to (16.2.46):

$$\det \begin{vmatrix} (\vec{v} \cdot \vec{\kappa} - \lambda) & \rho \kappa_x & \rho \kappa_y & \rho \kappa_z & 0 \\ 0 & (\vec{v} \cdot \vec{\kappa} - \lambda) & 0 & 0 & \kappa_x / \rho \\ 0 & 0 & (\vec{v} \cdot \vec{\kappa} - \lambda) & 0 & \kappa_y / \rho \\ 0 & 0 & 0 & (\vec{v} \cdot \vec{\kappa} - \lambda) & \kappa_z / \rho \\ 0 & \rho c^2 \kappa_x & \rho c^2 \kappa_y & \rho c^2 \kappa_z & (\vec{v} \cdot \vec{\kappa} - \lambda) \end{vmatrix} = 0 \quad (16.5.2)$$

The above eigenvalue equation becomes

$$(\vec{v} \cdot \vec{\kappa} - \lambda)^3 [(\vec{v} \cdot \vec{\kappa} - \lambda)^2 - c^2 \kappa^2] = 0 \quad (16.5.3)$$

leading to the following eigenvalues:

$$\begin{aligned} \lambda_1 = \lambda_2 = \lambda_3 &= \vec{v} \cdot \vec{\kappa} \\ \lambda_4 &= \vec{v} \cdot \vec{\kappa} + c\kappa \\ \lambda_5 &= \vec{v} \cdot \vec{\kappa} - c\kappa \end{aligned} \quad (16.5.4)$$

where κ is the modulus of the vector $\vec{\kappa}$.

The first eigenvalue has a multiplicity corresponding to the space dimension, that is three for a general three-dimensional flow or two in a two-dimensional flow system. The other two eigenvalues are the obvious generalizations of the one-dimensional case with a very similar physical interpretation. The corresponding speeds of propagation of the waves are respectively

$$\begin{aligned} \vec{a}_1 = \vec{a}_2 = \vec{a}_3 &= (\vec{v} \cdot \vec{I}_\kappa) \cdot \vec{I}_\kappa \\ \vec{a}_4 &= [(\vec{v} \cdot \vec{I}_\kappa) + c] \vec{I}_\kappa \\ \vec{a}_5 &= [(\vec{v} \cdot \vec{I}_\kappa) - c] \vec{I}_\kappa \end{aligned} \quad (16.5.5)$$

The first three propagation velocities are the projection of \vec{v} along the direction of the wave vector $\vec{\kappa}$, while the two remaining velocities are identical to the one-dimensional propagation velocities when viewed along the direction of $\vec{\kappa}$. According to equation (16.3.19), the bicharacteristic directions are given by $(\vec{v}, 1)$, and $(\vec{v} \pm c \cdot \vec{I}_\kappa, 1)$.

The left eigenvectors $\vec{l}^{(j)}$ can readily be found by solving the homogeneous problem (16.3.6). For the triple eigenvalue $\lambda = \vec{v} \cdot \vec{\kappa}$, one obtains the following equations for the components of $\vec{l}^{(j)}$:

$$\begin{aligned} l_1 &\text{ arbitrary} \\ l_1 + c^2 l_5 &= 0 \\ l_1 + c^2 l_3 &= 0 \\ l_1 + c^2 l_5 &= 0 \\ \kappa_x l_2 + \kappa_y l_3 + \kappa_z l_4 &= 0 \end{aligned} \quad (16.5.6)$$

where $\kappa_x, \kappa_y, \kappa_z$ are the Cartesian projections of $\vec{\kappa}$.

This system, which occurs three times, has nevertheless three linearly independent solutions, which are defined, up to two arbitrary normalization factors, by

$$\begin{aligned}\tilde{l}_1^{(1)} &= (\mu_1^{(1)}, 0, \kappa_z \mu_2^{(1)}, -\kappa_y \mu_2^{(1)}, -\mu_1^{(1)}/c^2) \\ \tilde{l}_2^{(2)} &= (\mu_1^{(2)}, -\kappa_z \mu_2^{(2)}, 0, \kappa_x \mu_2^{(2)}, -\mu_1^{(2)}/c^2) \\ \tilde{l}_3^{(3)} &= (\mu_1^{(3)}, +\kappa_y \mu_2^{(3)}, -\kappa_x \mu_2^{(3)}, 0, -\mu_1^{(3)}/c^2)\end{aligned}\quad (16.5.7)$$

For the two remaining eigenvalues, one obtains

$$\begin{aligned}l_1 &= 0 \\ l_2 &= \pm c \hat{\kappa}_x \rho l_5 \\ l_3 &= \pm c \hat{\kappa}_y \rho l_5 \\ l_4 &= \pm c \hat{\kappa}_z \rho l_5 \\ l_5 &\text{ arbitrary}\end{aligned}\quad (16.5.8)$$

and

$$\begin{aligned}\tilde{l}^{(4)} &= (0, \hat{\kappa}_x \mu^{(4)}, \hat{\kappa}_y \mu^{(4)}, \hat{\kappa}_z \mu^{(4)}, \mu^{(4)}/\rho c) \\ \tilde{l}^{(5)} &= (0, -\hat{\kappa}_x \mu^{(5)}, -\hat{\kappa}_y \mu^{(5)}, -\hat{\kappa}_z \mu^{(5)}, \mu^{(5)}/\rho c)\end{aligned}\quad (16.5.9)$$

where $\hat{\kappa}_x, \hat{\kappa}_y, \hat{\kappa}_z$ are the Cartesian components of the unit vector $\bar{1}_\kappa$ along the direction of $\bar{\kappa}$.

The μ coefficients are arbitrary normalization coefficients which can be freely chosen.

Since the norm of $\bar{\kappa}$ is of no physical significance, it is customary to select the coefficients μ of the three first eigenvectors to be proportional to $1/\kappa$. For instance, one can take

$$\begin{aligned}\mu_2^{(1)} = \mu_2^{(2)} = \mu_2^{(3)} &= \frac{1}{\kappa} \\ \mu^{(4)} = \mu^{(5)} &= 1\end{aligned}\quad (16.5.10)$$

and

$$\mu_1^{(1)} = \hat{\kappa}_x \quad \mu_1^{(2)} = \hat{\kappa}_y \quad \mu_1^{(3)} = \hat{\kappa}_z \quad (16.5.11)$$

This leads to a diagonalization matrix L^{-1} , of $\tilde{K} = \bar{A} \bar{\kappa}$, formed by lines equal to the left eigenvectors $\tilde{l}^{(j)}$ of the following form:

$$L^{-1} = \begin{vmatrix} \hat{\kappa}_x & 0 & \hat{\kappa}_z & -\hat{\kappa}_y & \frac{-\hat{\kappa}_x}{c^2} \\ \hat{\kappa}_y & -\hat{\kappa}_z & 0 & \hat{\kappa}_x & \frac{-\hat{\kappa}_y}{c^2} \\ \hat{\kappa}_z & \hat{\kappa}_y & -\hat{\kappa}_x & 0 & \frac{-\hat{\kappa}_z}{c^2} \\ 0 & \hat{\kappa}_x & \hat{\kappa}_y & \hat{\kappa}_z & \frac{1}{\rho c} \\ 0 & -\hat{\kappa}_x & -\hat{\kappa}_y & -\hat{\kappa}_z & \frac{1}{\rho c} \end{vmatrix} \quad (16.5.12)$$

The inverse of L^{-1} is composed of columns equal to the right eigenvectors of $\tilde{K} = \tilde{A} \cdot \tilde{\kappa}$ and is equal to (see Problem 16.10)

$$L = \begin{pmatrix} \hat{\kappa}_x & \hat{\kappa}_y & \hat{\kappa}_z & \frac{\rho}{2c} & \frac{\rho}{2c} \\ 0 & -\hat{\kappa}_z & \hat{\kappa}_y & \frac{\hat{\kappa}_x}{2} & \frac{-\hat{\kappa}_x}{2} \\ \hat{\kappa}_z & 0 & -\hat{\kappa}_x & \frac{\hat{\kappa}_y}{2} & \frac{-\hat{\kappa}_y}{2} \\ -\hat{\kappa}_y & \hat{\kappa}_x & 0 & \frac{\hat{\kappa}_z}{2} & \frac{-\hat{\kappa}_z}{2} \\ 0 & 0 & 0 & \frac{\rho c}{2} & \frac{\rho c}{2} \end{pmatrix} \quad (16.5.13)$$

Note that the two-dimensional matrices, for flows in the xy plane, are obtained by removing the fourth column and the second line of L^{-1} and setting $\kappa_z = 0$ in the remaining elements. Similarly, the second column and fourth line have to be removed for the two-dimensional form of L (see Problem 16.11). It is interesting to observe that the determinant of L is equal to

$$\det(L) = \frac{\rho c}{2} = \frac{1}{\det(L^{-1})} \quad (16.5.14)$$

Many other choices can be made for the normalization coefficients μ . For instance, a current choice is $\mu^{(4)} = \mu^{(5)} = 1/\sqrt{2}$ (Warming *et al.*, 1975); see also Problem 16.12.

As noted earlier, the matrix L diagonalizes the linear combination $(\tilde{A}\tilde{\kappa}_x + \tilde{B}\tilde{\kappa}_y + \tilde{C}\tilde{\kappa}_z)$ but *does not diagonalize the individual matrices* $\tilde{A}, \tilde{B}, \tilde{C}$. Of course, the matrix L_1 corresponding to $\hat{\kappa}_x = 1, \hat{\kappa}_y = \hat{\kappa}_z = 0$ will diagonalize the Jacobian \tilde{A} , but not \tilde{B} and \tilde{C} . Since these three Jacobians do not commute they cannot be diagonalized simultaneously. For instance, if L is written as a function of $\hat{\kappa}_x, \hat{\kappa}_y, \hat{\kappa}_z$ as $L(\hat{\kappa}_x, \hat{\kappa}_y, \hat{\kappa}_z)$ then the matrix L_1 is equal to $L(1, 0, 0)$, while the matrix $L_2 = L(0, 1, 0)$ will diagonalize \tilde{B} and the matrix $L_3 = L(0, 0, 1)$ will diagonalize \tilde{C} .

Explicitly, we have

$$L_1^{-1} = \begin{pmatrix} 1 & 0 & 0 & 0 & \frac{-1}{c^2} \\ 0 & 0 & 0 & 1 & 0 \\ 0 & 0 & -1 & 0 & 0 \\ 0 & 1 & 0 & 0 & \frac{1}{\rho c} \\ 0 & -1 & 0 & 0 & \frac{1}{\rho c} \end{pmatrix} \quad (16.5.15a)$$

$$L_1 = \begin{pmatrix} 1 & 0 & 0 & \frac{\rho}{2c} & \frac{\rho}{2c} \\ 0 & 0 & 0 & \frac{1}{2} & \frac{-1}{2} \\ 0 & 0 & -1 & 0 & 0 \\ 0 & 1 & 0 & 0 & 0 \\ 0 & 0 & 0 & \frac{\rho c}{2} & \frac{\rho c}{2} \end{pmatrix} \tag{16.5.15b}$$

and the eigenvalues of \tilde{A} are obtained from $\lambda_{(j)}(\tilde{\kappa})$ for the values $\kappa_x = 1, \kappa_y = \kappa_z = 0$ if $\tilde{\kappa}$ is normalized to a unit length. Hence,

$$L_1^{-1} \tilde{A} L_1 = \begin{pmatrix} u & \cdot & \cdot & \cdot & \cdot \\ \cdot & u & \cdot & \cdot & \cdot \\ \cdot & \cdot & u & \cdot & \cdot \\ \cdot & \cdot & \cdot & u+c & \cdot \\ \cdot & \cdot & \cdot & \cdot & u-c \end{pmatrix} \tag{16.5.16}$$

and similarly

$$L_2^{-1} \tilde{B} L_2 = \begin{pmatrix} v & \cdot & \cdot & \cdot & \cdot \\ \cdot & v & \cdot & \cdot & \cdot \\ \cdot & \cdot & v & \cdot & \cdot \\ \cdot & \cdot & \cdot & v+c & \cdot \\ \cdot & \cdot & \cdot & \cdot & v-c \end{pmatrix} \tag{16.5.17}$$

$$L_3^{-1} \tilde{C} L_3 = \begin{pmatrix} w & \cdot & \cdot & \cdot & \cdot \\ \cdot & w & \cdot & \cdot & \cdot \\ \cdot & \cdot & w & \cdot & \cdot \\ \cdot & \cdot & \cdot & w+c & \cdot \\ \cdot & \cdot & \cdot & \cdot & w-c \end{pmatrix} \tag{16.5.18}$$

Note that L_1^{-1} contains the left eigenvectors of \tilde{A} and similarly L_2^{-1} and L_3^{-1} contain the left eigenvectors of \tilde{B} and \tilde{C} respectively.

16.5.2 Diagonalization of the conservative Jacobians

The conservative Jacobians will be diagonalized by applying the transformation matrix M :

$$\Lambda = L^{-1}(\tilde{A} \cdot \tilde{\kappa})L = L^{-1}M^{-1}(\tilde{A} \cdot \tilde{\kappa})ML \tag{16.5.19}$$

and the matrix $P = ML$ will diagonalize the conservative Jacobians in the form

$$P^{-1}(\tilde{A} \cdot \tilde{\kappa})P = \Lambda \tag{16.5.20}$$

where Λ is the diagonal matrix of the eigenvalues $\lambda_{(j)}$:

$$\Lambda = \begin{pmatrix} \bar{v} \cdot \bar{\kappa} & \cdot & \cdot & \cdot & \cdot \\ \cdot & \bar{v} \cdot \bar{\kappa} & \cdot & \cdot & \cdot \\ \cdot & \cdot & \bar{v} \cdot \bar{\kappa} & \cdot & \cdot \\ \cdot & \cdot & \cdot & \bar{v} \cdot \bar{\kappa} + c\kappa & \cdot \\ \cdot & \cdot & \cdot & \cdot & \bar{v} \cdot \bar{\kappa} - c\kappa \end{pmatrix} \tag{16.5.21}$$

From a direct multiplication of M and L , which is left as an exercise to the reader (Problem 16.13), one obtains the following form for P , with the variables

$$\bar{b} = \left(\frac{\bar{v}^2}{2}\right) \cdot \bar{1}_x + \rho(\bar{v} \times \bar{1}_x)$$

$$H = \frac{\bar{v}^2}{2} + \frac{c^2}{\gamma - 1} = h + \frac{\bar{v}^2}{2} \quad (16.5.22)$$

$$P = \begin{vmatrix} \hat{\kappa}_x & \hat{\kappa}_y & \hat{\kappa}_z & \frac{\rho}{2c} & \frac{\rho}{2c} \\ u\hat{\kappa}_x & u\hat{\kappa}_y - \rho\hat{\kappa}_z & u\hat{\kappa}_z + \rho\hat{\kappa}_y & \frac{\rho}{2c}(u + \hat{\kappa}_x c) & \frac{\rho}{2c}(u - \hat{\kappa}_x c) \\ v\hat{\kappa}_x + \rho\hat{\kappa}_z & v\hat{\kappa}_y & v\hat{\kappa}_z - \rho\hat{\kappa}_x & \frac{\rho}{2c}(v + \hat{\kappa}_y c) & \frac{\rho}{2c}(v - \hat{\kappa}_y c) \\ w\hat{\kappa}_x - \rho\hat{\kappa}_y & w\hat{\kappa}_y + \rho\hat{\kappa}_x & w\hat{\kappa}_z & \frac{\rho}{2c}(w + \hat{\kappa}_z c) & \frac{\rho}{2c}(w - \hat{\kappa}_z c) \\ \bar{b} \cdot \bar{1}_x & \bar{b} \cdot \bar{1}_y & \bar{b} \cdot \bar{1}_z & \frac{\rho}{2c}(H + c\bar{v} \cdot \bar{1}_x) & \frac{\rho}{2c}(H - c\bar{v} \cdot \bar{1}_x) \end{vmatrix} \quad (16.5.23)$$

For other choices of the normalization coefficients $\mu^{(4)}$ and $\mu^{(5)}$, the fourth column has to be divided by $\mu^{(4)}$ and the fifth by $\mu^{(5)}$. As with the corresponding matrix L , the two-dimensional version of P is obtained by removing the second column and fourth line and by setting $\hat{\kappa}_z = w = 0$ in the remaining terms.

Similarly, from L^{-1} and M^{-1} one obtains for P^{-1} , with the auxiliary variables

$$\bar{B}_0 = \left(1 - \frac{\gamma - 1}{2} M^2\right) \bar{1}_x - \frac{1}{\rho}(\bar{v} \times \bar{1}_x) \quad (16.5.24)$$

$$\bar{C}_\pm = \pm \frac{\bar{1}_x}{\rho} - \frac{\gamma - 1}{\rho c} \bar{v} \quad (16.5.25)$$

$$P^{-1} = \begin{vmatrix} \bar{B}_0 \cdot \bar{1}_x & (\gamma - 1) \frac{u}{c^2} \hat{\kappa}_x & (\gamma - 1) \frac{v}{c^2} \hat{\kappa}_x + \frac{\hat{\kappa}_z}{\rho} & (\gamma - 1) \frac{w}{c^2} \hat{\kappa}_x - \frac{\hat{\kappa}_y}{\rho} & -\frac{\gamma - 1}{\rho^2} \hat{\kappa}_x \\ \bar{B}_0 \cdot \bar{1}_y & (\gamma - 1) \frac{u}{c^2} \hat{\kappa}_y - \frac{\hat{\kappa}_z}{\rho} & (\gamma - 1) \frac{v}{c^2} \hat{\kappa}_y & (\gamma - 1) \frac{w}{c^2} \hat{\kappa}_y + \frac{\hat{\kappa}_x}{\rho} & -\frac{\gamma - 1}{\rho^2} \hat{\kappa}_y \\ \bar{B}_0 \cdot \bar{1}_z & (\gamma - 1) \frac{u}{c^2} \hat{\kappa}_z + \frac{\hat{\kappa}_y}{\rho} & (\gamma - 1) \frac{v}{c^2} \hat{\kappa}_z - \frac{\hat{\kappa}_x}{\rho} & (\gamma - 1) \frac{w}{c^2} \hat{\kappa}_z & -\frac{\gamma - 1}{\rho^2} \hat{\kappa}_z \\ \frac{c}{\rho} \left(\frac{\gamma - 1}{2} M^2 - \frac{\bar{v} \cdot \bar{1}_x}{c}\right) & \bar{C}_+ \cdot \bar{1}_x & \bar{C}_+ \cdot \bar{1}_y & \bar{C}_+ \cdot \bar{1}_z & \frac{\gamma - 1}{\rho c} \\ \frac{c}{\rho} \left(\frac{\gamma - 1}{2} M^2 + \frac{\bar{v} \cdot \bar{1}_x}{c}\right) & \bar{C}_- \cdot \bar{1}_x & \bar{C}_- \cdot \bar{1}_y & \bar{C}_- \cdot \bar{1}_z & \frac{\gamma - 1}{\rho c} \end{vmatrix} \quad (16.5.26)$$

The two-dimensional form for P^{-1} is obtained by removing the fourth column and second line. Note also that the columns of P are the right eigenvectors of the matrix $K = \vec{A} \cdot \vec{\kappa}$. Similarly, the left eigenvectors of $\vec{A} \cdot \vec{\kappa}$ are obtained from the lines of $P^{-1} = L^{-1}M^{-1}$.

The matrix $P_1 = ML_1$ will diagonalize the Jacobian A and can be constructed from M and L_1 . One obtains by direct multiplication or by taking $\hat{\kappa}_x = 1$, $\hat{\kappa}_y = \hat{\kappa}_z = 0$ in the general expression (16.5.23) of P :

$$P_1 = \begin{vmatrix} 1 & 0 & 0 & \frac{\rho}{2c} & \frac{\rho}{2c} \\ u & 0 & 0 & \frac{\rho(u+c)}{2c} & \frac{\rho(u-c)}{2c} \\ v & 0 & -\rho & \frac{\rho v}{2c} & \frac{\rho v}{2c} \\ w & \rho & 0 & \frac{\rho w}{2c} & \frac{\rho w}{2c} \\ \frac{\vec{v}^2}{2} & \rho w & -\rho v & \frac{\rho}{2c}(H+uc) & \frac{\rho}{2c}(H-uc) \end{vmatrix} \quad (16.5.27)$$

and one has

$$P_1^{-1} \cdot A \cdot P_1 = \begin{vmatrix} u & & & & \\ \cdot & u & & & \\ \cdot & \cdot & u & & \\ \cdot & \cdot & \cdot & u+c & \\ \cdot & \cdot & \cdot & \cdot & u-c \end{vmatrix} \quad (16.5.28)$$

Similar properties are obtained for the other two components B and C .

Example 16.5.1 Two-dimensional matrices of eigenvectors

For a two-dimensional flow, one obtains, with the orthogonality condition $L^{-1}L = 1$, the following forms:

$$L^{-1} = \begin{vmatrix} 1 & 0 & 0 & \frac{-1}{c^2} \\ 0 & \hat{\kappa}_y & -\hat{\kappa}_x & 0 \\ 0 & \hat{\kappa}_x & \hat{\kappa}_y & \frac{1}{\rho c} \\ 0 & -\hat{\kappa}_x & -\hat{\kappa}_y & \frac{1}{\rho c} \end{vmatrix} \quad (\text{E16.5.1})$$

and

$$L = \begin{vmatrix} 1 & 0 & \frac{\rho}{2c} & \frac{\rho}{2c} \\ 0 & \hat{\kappa}_y & \frac{\hat{\kappa}_x}{2} & -\frac{\hat{\kappa}_x}{2} \\ 0 & -\hat{\kappa}_x & \frac{\hat{\kappa}_y}{2} & -\frac{\hat{\kappa}_y}{2} \\ 0 & 0 & \frac{\rho c}{2} & \frac{\rho c}{2} \end{vmatrix} \quad (\text{E16.5.2})$$

The associated P matrices are obtained from equations (16.5.23) by removing the second column and fourth line, with $\kappa_z = w = 0$ in the remaining terms:

$$P = \begin{vmatrix} 1 & 0 & \frac{\rho}{2c} & \frac{\rho}{2c} \\ u & \rho \hat{\kappa}_y & \frac{\rho}{2c}(u + c \hat{\kappa}_x) & \frac{\rho}{2c}(u - c \hat{\kappa}_x) \\ v & -\rho \hat{\kappa}_x & \frac{\rho}{2c}(v + c \hat{\kappa}_y) & \frac{\rho}{2c}(v - c \hat{\kappa}_y) \\ \frac{\bar{v}^2}{2} & \rho(u \hat{\kappa}_y - v \hat{\kappa}_x) & \frac{\rho}{2c}(H + c \bar{v} \cdot \bar{\Gamma}_\kappa) & \frac{\rho}{2c}(H - c \bar{v} \cdot \bar{\Gamma}_\kappa) \end{vmatrix} \quad (\text{E16.5.3})$$

and the two-dimensional form for P^{-1} is obtained by removing the fourth column and second line from the three-dimensional form, with $\kappa_z = w = 0$,

$$P^{-1} = \begin{vmatrix} 1 - \frac{\gamma-1}{2} M^2 & (\gamma-1) \frac{u}{c^2} & (\gamma-1) \frac{v}{c^2} & -\frac{\gamma-1}{c^2} \\ \frac{1}{\rho}(v \hat{\kappa}_x - u \hat{\kappa}_y) & \frac{\hat{\kappa}_y}{\rho} & -\frac{\hat{\kappa}_x}{\rho} & 0 \\ \frac{c}{\rho} \left(\frac{\gamma-1}{2} M^2 - \frac{\bar{v} \cdot \bar{\Gamma}_\kappa}{c} \right) & \frac{1}{\rho} \left[\hat{\kappa}_x - (\gamma-1) \frac{u}{c} \right] & \frac{1}{\rho} \left[\hat{\kappa}_y - (\gamma-1) \frac{v}{c} \right] & \frac{\gamma-1}{\rho c} \\ \frac{c}{\rho} \left(\frac{\gamma-1}{2} M^2 + \frac{\bar{v} \cdot \bar{\Gamma}_\kappa}{c} \right) & -\frac{1}{\rho} \left[\hat{\kappa}_x + (\gamma-1) \frac{u}{c} \right] & -\frac{1}{\rho} \left[\hat{\kappa}_y + (\gamma-1) \frac{v}{c} \right] & \frac{\gamma-1}{\rho c} \end{vmatrix} \quad (\text{E16.5.4})$$

An alternative expression for the L^{-1} matrix

Other choices for the left eigenvector normalization coefficients lead to different

combinations for the compatibility relations. For instance, the choice

$$\begin{aligned} \mu_1^{(1)} &= \mu^{(4)} = \mu^{(5)} = 1 \\ \mu_2^{(1)} &= \mu_1^{(2)} = \mu_1^{(3)} = 0 \\ \mu_2^{(2)} &= \mu_2^{(3)} = \frac{1}{\kappa} \end{aligned} \tag{16.5.29}$$

leads to the following form:

$$\bar{L}^{-1} = \begin{pmatrix} 1 & 0 & 0 & 0 & -\frac{1}{c^2} \\ 0 & -\hat{\kappa}_z & 0 & \hat{\kappa}_x & 0 \\ 0 & \hat{\kappa}_y & -\hat{\kappa}_x & 0 & 0 \\ 0 & \hat{\kappa}_x & \hat{\kappa}_y & \hat{\kappa}_z & \frac{1}{\rho c} \\ 0 & -\hat{\kappa}_x & -\hat{\kappa}_y & -\hat{\kappa}_z & \frac{1}{\rho c} \end{pmatrix} \tag{16.5.30}$$

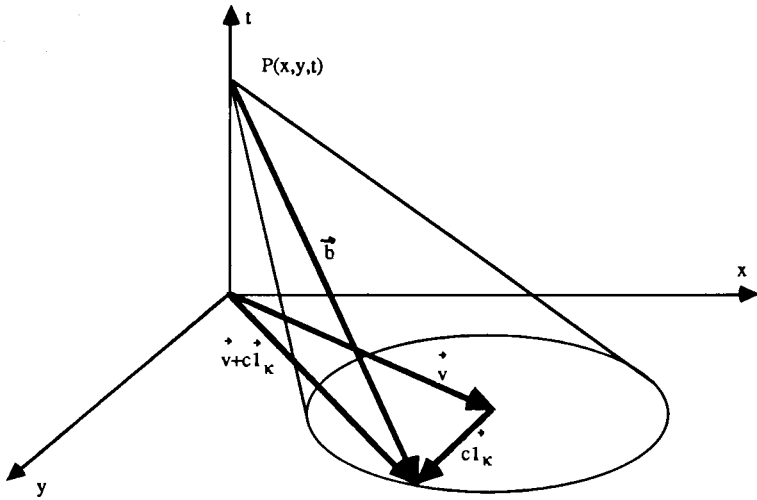
with the following matrix of the right eigenvectors:

$$\bar{L} = \begin{pmatrix} 1 & 0 & 0 & \frac{\rho}{2c} & \frac{\rho}{2c} \\ 0 & -\hat{\kappa}_z & \hat{\kappa}_y & \frac{\hat{\kappa}_x}{2} & -\frac{\hat{\kappa}_x}{2} \\ 0 & \frac{-\hat{\kappa}_y \hat{\kappa}_z}{\hat{\kappa}_x} & \frac{-(\hat{\kappa}_z^2 + \hat{\kappa}_x^2)}{\hat{\kappa}_x} & \frac{\hat{\kappa}_y}{2} & \frac{\hat{\kappa}_y}{2} \\ 0 & \frac{\hat{\kappa}_y^2 + \hat{\kappa}_x^2}{\hat{\kappa}_x} & \frac{\hat{\kappa}_y \hat{\kappa}_z}{\hat{\kappa}_x} & \frac{\hat{\kappa}_z}{2} & -\frac{\hat{\kappa}_z}{2} \\ 0 & 0 & 0 & \frac{\rho c}{2} & \frac{\rho c}{2} \end{pmatrix} \tag{16.5.31}$$

The other matrices \bar{P}^{-1} and \bar{P} can be derived by direct calculations (see Problem 16.13).

16.5.3 Mach cone and compatibility relations

The characteristic surfaces in a three-dimensional flow are easily obtained from the knowledge of the eigenvalues of the Jacobian matrices. For the multiple eigenvalue $\lambda = \bar{v} \cdot \bar{\kappa}$, all characteristic surfaces contain not only the vector $((\bar{v} \cdot \bar{1}_\kappa) \bar{1}_\kappa, 1)$ in the space-time domain but also the vector $(\bar{v}, 1)$, as shown in Section 16.3.1. The characteristic surfaces are therefore the stream surfaces and this vector is called the *pseudo-path line*. This projection on the space-like



(a) Supersonic flows

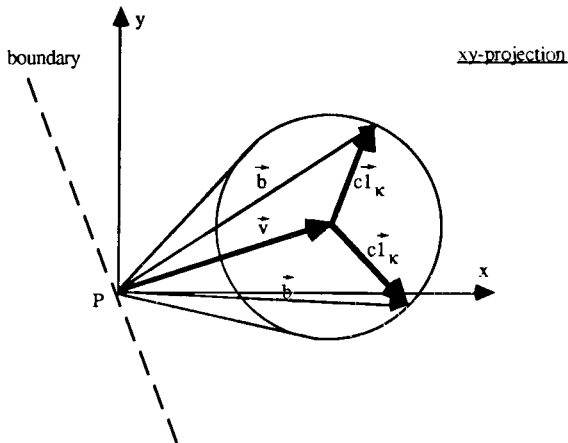
(b) The xy projection of bicharacteristics

Figure 16.5.1 Characteristic surface and Mach conoid for a supersonic flow configuration

domain $t = \text{constant}$ is the velocity vector. Hence, the envelope of all the corresponding characteristic surfaces are the pseudo-path line $(\vec{v}, 1)$, since this vector is independent of the normal $\vec{\kappa}$ and the Mach conoid attached to this multiple eigenvalue reduces to the pseudo-path line.

The two remaining eigenvalues generate the same Mach conoid, whose

intersection with a $t = \text{constant}$ surface is the sphere, or the circle in a two-dimensional flow, obtained by the rotation of the vector $(c\bar{1}_\kappa)$ around the extremity of the vector \bar{v} . Indeed, since the characteristic surface contains the bicharacteristics, defined by equations (16.3.18) and (16.3.19), $b = (\bar{v} \pm c\bar{1}_\kappa, 1)$ and the vector $(\bar{a}, 1) = ((\bar{v} \cdot \bar{1}_\kappa \pm c)\bar{1}_\kappa, 1)$, the projection of the envelope of the wave phase surfaces may be obtained by varying $\bar{1}_\kappa$ on all the space components of the bicharacteristics b . For a two-dimensional flow, Figures 16.5.1 and 16.5.2 represent the two possible situations for supersonic and subsonic flows respectively.

It is seen that the axis of the Mach conoid is the pseudo-path line $(\bar{v}, 1)$ and that the point P lies within the circle of radius c around \bar{v} in the $t = \text{constant}$ projection for a subsonic flow, while it lies outside this circle for supersonic flows.

The compatibility relations in multi-dimensional flow

The compatibility equations can be obtained by multiplying the system of non-conservative equations in primitive variables by each of the left eigenvectors following equation (16.3.20).

A practical way to proceed is to calculate first a vector $\bar{Z}^{(j)}$ defined as three-line vectors by

$$\bar{Z}^{(j)} = l^{(j)} \bar{A} \quad \bar{Z}^{(j)} \equiv (Z_x, Z_y, Z_z)^{(j)} \quad (16.5.32a)$$

$$Z_x^{(j)} \equiv (Z_{x1}, Z_{x2}, Z_{x3}, Z_{x4}, Z_{x5})^{(j)} \quad (16.5.32b)$$

such that equation (16.3.20) becomes

$$l^{(j)} \frac{\partial V}{\partial t} + (\bar{Z}^{(j)} \cdot \bar{\nabla}) V = l^{(j)} \bar{Q} \quad (16.5.33)$$

If one defines the following directional derivatives as a 1×5 line vector of operators

$$\bar{d}^{(j)} = (\bar{l}^{(j)} \partial_t + \bar{Z}^{(j)} \cdot \bar{\nabla}) \quad (16.5.34)$$

the compatibility equation (16.3.20) can be written as

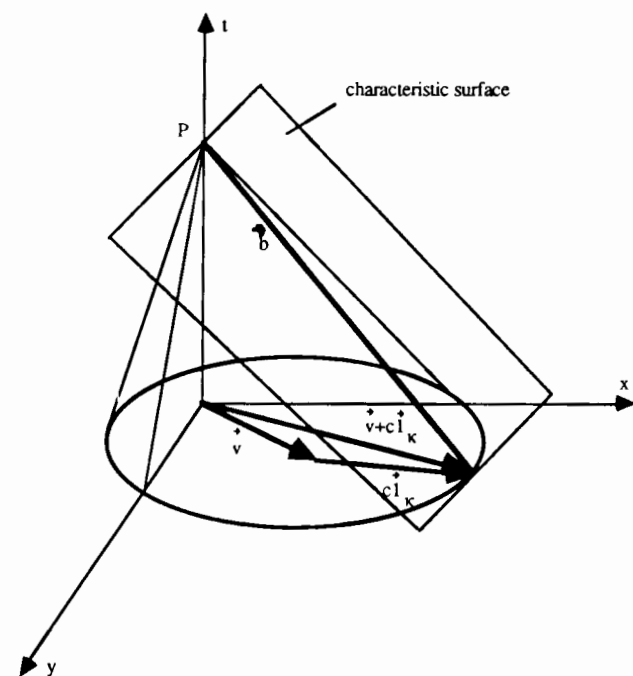
$$\bar{d}^{(j)} V = (\bar{l}^{(j)} \bar{Q}) \quad \text{for a given eigenvalue } \lambda_{(j)} \quad (16.5.35a)$$

Denoting by a subscript k the k th component of $\bar{d}^{(j)}$ associated with a vector $\bar{Z}^{(j)}$, it can be observed that the k th directional derivative acts only on the corresponding component of V ; that is the derivative in the direction of \bar{Z}_1 will act on the density ρ , the derivative \bar{d}_2 associated with \bar{Z}_2 will act on the velocity component u , and so on. Hence, this equation reads

$$\bar{d}_1^{(j)} \rho + \bar{d}_2^{(j)} u + \bar{d}_3^{(j)} v + \bar{d}_4^{(j)} w + \bar{d}_5^{(j)} p = \bar{l}^{(j)} \cdot \bar{Q} \quad (16.5.35b)$$

for a given eigenvalue $\lambda_{(j)}$.

Since the eigenvalues are a function of the normal $\bar{\kappa}$, one can define an infinity of sets of vectors $\bar{Z}^{(j)}$ associated to the *same eigenvalue* by orienting the



(a) Subsonic flows

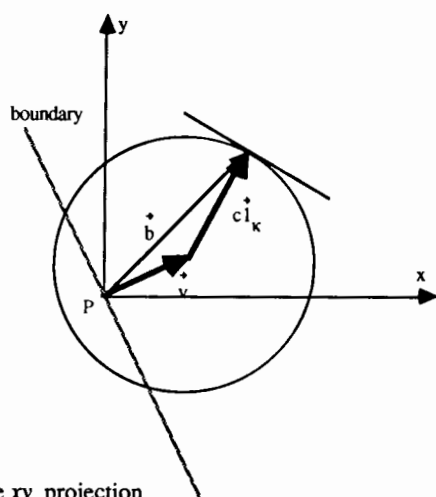
(b) The xy projection

Figure 16.5.2 Characteristic surface and Mach conoid for a subsonic flow configuration

wave-number vector $\vec{\kappa}$ in various directions. Note that the magnitude of κ plays no physical role since it can always be set to one by an appropriate normalization.

Since the set of Euler equations can be replaced by an equivalent set of compatibility equations for each of the eigenvalues (five in a three-dimensional flow), it is seen that there is an infinite manifold of equivalent formulations of the form $\vec{d}_k v_k = \vec{l} \vec{Q}$, which can replace the original form of the Euler equations.

It must be ensured, of course, that the selected characteristic compatibility equations form an independent set. One guideline is to define one compatibility equation for each eigenvalue number (j). Since the five space-time vectors ($\vec{l}^{(j)}, Z^{(j)}$) all lie in the four-dimensional characteristic surface $S(\vec{x}, t) = \text{constant}$ (see Chapter 3 in Volume 1), they are not independent from each other. Hence, one can always recombine the compatibility equation $\sum_k \vec{d}_k v_k = \vec{l} \vec{Q}$ into derivatives along four independent directions. For instance, one can always select the bicharacteristic direction in order to define a directional derivative and three orthogonal directions within the characteristic surface. Another alternative is to select different values of $\vec{\kappa}$ and then combine the equations. In particular, selecting $\vec{\kappa}$ along the coordinate directions will allow the connection with one-dimensional propagation properties to be expressed; see, for instance, Zannetti and Colasurdo (1981) for an application of these properties.

Example 16.5.2 Determination of Z direction

Consider the form (16.5.12) for the matrix of the left eigenvectors. The components of $\vec{Z}^{(1)}(Z_x, Z_y, Z_z)^{(1)}$ are obtained from the products $l^{(1)} \vec{A}, l^{(1)} \vec{B}, l^{(1)} \vec{C}$. With

$$l^{(1)} = \left| \hat{\kappa}_x, 0, \hat{\kappa}_z, -\hat{\kappa}_y, \frac{-\hat{\kappa}_x}{c^2} \right| \quad (\text{E16.5.5})$$

one obtains, by direct multiplication of \vec{A} from the left by $l^{(1)}$,

$$Z_x^{(1)} = \left| u\hat{\kappa}_x, 0, u\hat{\kappa}_z, -u\hat{\kappa}_y, \frac{-u\hat{\kappa}_x}{c^2} \right| \quad (\text{E16.5.6})$$

The y -component of $\vec{Z}^{(1)}$ is obtained by a similar operation on the jacobian \vec{B} :

$$Z_y^{(1)} = \left| v\hat{\kappa}_x, 0, v\hat{\kappa}_z, -v\hat{\kappa}_y, -\left[\frac{u\hat{\kappa}_x \rho + c^2 \hat{\kappa}_z}{\bar{\rho} c^2} \right] \right| \quad (\text{E16.5.7})$$

and with $Z_z^{(1)} = l^{(1)} \vec{C}$,

$$Z_z^{(1)} = \left| w\hat{\kappa}_x, 0, w\hat{\kappa}_z, -w\hat{\kappa}_y, -\left[\frac{w\hat{\kappa}_x \rho + c^2 \hat{\kappa}_z}{\rho c^2} \right] \right| \quad (\text{E16.5.8})$$

Similar forms are derived for the second and third eigenvectors, by permutation of the x, y, z components of $\vec{\kappa}$.

The fourth eigenvector

$$l^{(4)} = \left| 0, \hat{\kappa}_x, \hat{\kappa}_y, \hat{\kappa}_z, \frac{1}{\rho c} \right| \quad (\text{E16.5.9})$$

generates the following components of $\vec{Z}^{(4)} = l^{(4)} \vec{A}$:

$$Z_x^{(4)} = \left| 0, u\hat{\kappa}_x + c, u\hat{\kappa}_y, u\hat{\kappa}_z, \frac{\hat{\kappa}_x c + u}{\rho c} \right| \quad (\text{E16.5.10})$$

$$Z_y^{(4)} = \left| 0, v\hat{\kappa}_x, v\hat{\kappa}_y + c, v\hat{\kappa}_z, \frac{\hat{\kappa}_y c + v}{\rho c} \right| \quad (\text{E16.5.11})$$

$$Z_z^{(4)} = \left| 0, w\hat{\kappa}_x, w\hat{\kappa}_y, w\hat{\kappa}_z + c, \frac{\hat{\kappa}_z c + w}{\rho c} \right| \quad (\text{E16.5.12})$$

These components now allow a straightforward determination of the compatibility relations.

For any of the three first eigenvectors, for instance $\vec{l}^{(1)}$, the following compatibility relation is obtained, applying directly equation (16.5.33) in the absence of source terms:

$$\begin{aligned} & \hat{\kappa}_x \left[(\partial_t + \vec{v} \cdot \vec{\nabla}) \rho - \frac{1}{c^2} (\partial_t + \vec{v} \cdot \vec{\nabla}) p \right] + \hat{\kappa}_z \left[(\partial_t + \vec{v} \cdot \vec{\nabla}) v + \frac{1}{\rho} \partial_y p \right] \\ & - \hat{\kappa}_y \left[(\partial_t + \vec{v} \cdot \vec{\nabla}) v + \frac{1}{\rho} \partial_z p \right] = 0 \end{aligned} \quad (\text{16.5.36})$$

The last two terms are the projections of the momentum equation along the y and z directions and the compatibility equation reduces to

$$d_v \rho - \frac{1}{c^2} d_v p = 0 \quad d_v = \partial_t + \vec{v} \cdot \vec{\nabla} \quad (\text{16.5.37})$$

where the derivative d_v indicates the convective derivative along the pseudo-path line. As shown for the one-dimensional case, this is equivalent to the conservation of entropy along the path line for continuous flow variations.

The eigenvectors $\vec{l}^{(4)}$ and $\vec{l}^{(5)}$ corresponding to the eigenvalues $(\vec{v} \cdot \vec{\kappa} \pm c\kappa)$ lead to the following compatibility equations:

$$\begin{aligned} & \hat{\kappa}_x (\partial_t + \vec{v} \cdot \vec{\nabla}) u + \hat{\kappa}_y (\partial_t + \vec{v} \cdot \vec{\nabla}) v + \hat{\kappa}_z (\partial_t + \vec{v} \cdot \vec{\nabla}) w \pm c \cdot \vec{\nabla} \cdot \vec{v} \\ & \pm \frac{1}{\rho c} [\partial_t + (\vec{v} \pm c \vec{\kappa}) \cdot \vec{\nabla}] p = 0 \end{aligned} \quad (\text{16.5.38})$$

The pressure term represents a contribution from the derivatives along the bicharacteristic $(\vec{v} \pm c \vec{\kappa})$ and will be written as d_b^\pm :

$$d_b^\pm = \partial_t + (\vec{v} \pm c \vec{\kappa}) \cdot \vec{\nabla} \quad (\text{16.5.39})$$

The first terms can also be transformed into variations along the bicharacteristic, leading to the following expression:

$$\bar{1}_\kappa \cdot d_b^\pm \bar{v} \pm \frac{1}{\rho c} d_b^\pm p \pm c[\bar{\nabla} \cdot \bar{v} - \bar{1}_\kappa \cdot (\bar{1}_\kappa \cdot \bar{\nabla}) \bar{v}] = 0 \quad (16.5.40)$$

This compatibility equation has a close resemblance to the one-dimensional form, at least for the first two terms. These two terms correspond exactly to the one-dimensional Riemann variables, but written for the velocity component in the direction of $\bar{\kappa}$. Hence, for isentropic flows, one can define one-dimensional Riemann variables associated with an arbitrary direction $\bar{\kappa}$, but these will not be invariants because of the two last terms, with the exception of one-dimensional flows. Defining

$$R_{(\kappa)}^\pm = \bar{v} \cdot \bar{1}_\kappa \pm \frac{2c}{\gamma - 1} \quad (16.5.41)$$

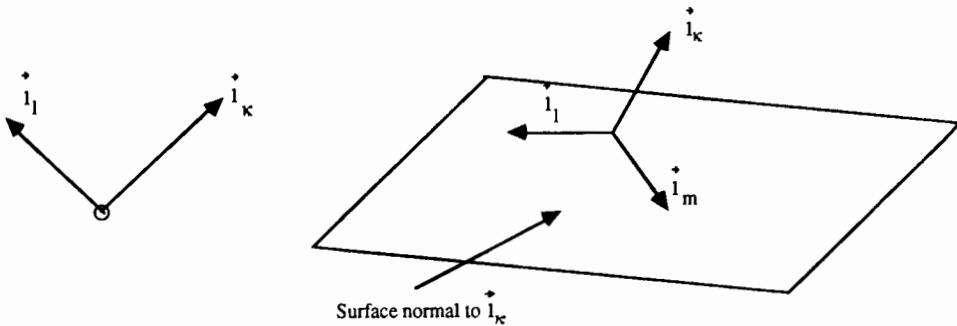
the above compatibility equation can be written as

$$d_b^\pm R_{(\kappa)}^\pm = \pm c[\bar{1}_\kappa (\bar{1}_\kappa \cdot \bar{\nabla}) \bar{v} - \bar{\nabla} \cdot \bar{v}] + \bar{v} \cdot d_b^\pm \bar{1}_\kappa \quad (16.5.42)$$

The last term on the right-hand side vanishes when the selected propagation direction $\bar{\kappa}$ is constant along the bicharacteristic. The term between brackets on the right-hand side represents the components of the divergence of \bar{v} in the subspace normal to $\bar{1}_\kappa$. Denoting this subspace by \bar{n}_κ we have, referring to Figure 16.5.3,

$$\bar{\nabla} \cdot \bar{v} = \bar{1}_\kappa \cdot (\bar{1}_\kappa \cdot \bar{\nabla}) \bar{v} + \bar{n}_\kappa \cdot (\bar{n}_\kappa \cdot \bar{\nabla}) \bar{v} \quad (16.5.43)$$

In a two-dimensional space, \bar{n}_κ represents the unit vector $\bar{1}_l$ in the direction normal to $\bar{1}_\kappa$, while in a three-dimensional space, \bar{n}_κ represents the unit vectors



Two-dimensional space

Three-dimensional space

Figure 16.5.3 Subspaces normal to the κ direction

$\bar{\Gamma}_l$ and $\bar{\Gamma}_m$ normal to $\bar{\Gamma}_\kappa$. Hence

$$\bar{n}_\kappa \cdot (\bar{n}_\kappa \cdot \bar{\nabla}) \bar{v} = \bar{\Gamma}_l \cdot (\bar{\Gamma}_l \cdot \bar{\nabla}) \bar{v} \quad \text{in a two-dimensional space} \quad (16.5.44)$$

with $\bar{\Gamma}_l \cdot \bar{\Gamma}_\kappa = 0$ and

$$\bar{n}_\kappa \cdot (\bar{n}_\kappa \cdot \bar{\nabla}) \bar{v} = \bar{\Gamma}_l \cdot (\bar{\Gamma}_l \cdot \bar{\nabla}) \bar{v} + \bar{\Gamma}_m \cdot (\bar{\Gamma}_m \cdot \bar{\nabla}) \bar{v} \quad \text{in a three-dimensional space} \quad (16.5.45)$$

with $\bar{\Gamma}_l$, $\bar{\Gamma}_m$, $\bar{\Gamma}_\kappa$ forming an orthogonal set. Equation (16.5.45) represents the contribution of the divergence originating from the surface normal to $\bar{\kappa}$, that is from the characteristic surface.

The compatibility condition (16.5.42) can then be written, in the absence of source terms and for constant $\bar{\kappa}$, as follows:

$$d_b^\pm R_{(\kappa)}^\pm = \mp c \bar{n}_\kappa \cdot (\bar{n}_\kappa \cdot \bar{\nabla}) \bar{v} \quad (16.5.46)$$

This has been used by different authors (Moretti, 1979, 1983; Zanetti and Colasurdo, 1981; Pandolfi, 1983, 1984) to develop numerical schemes with the aim of following the physical propagation phenomena as closely as possible. The compatibility equation is applied in various directions, for instance the coordinate directions, and combined in order to obtain a set of equations for the time derivatives \bar{v}_t and p_t (ρ_t being connected to p_t by the other compatibility conditions).

Another important and widespread application of the compatibility relations is their use as additional, 'numerical' conditions at the boundaries of the computational domain in order to provide the necessary information for the variables that are not imposed by the physical boundary conditions. In this case the direction $\bar{\kappa}$ is mostly chosen along the normal to the boundaries. However, it can also be used, in a modified form, in order to express the physical boundary conditions such as to avoid parasitic wave reflections at the boundaries. This is known as 'non-reflecting boundary conditions' and will be discussed in Chapter 19.

Relations (16.5.40) or (16.5.42) are often used in the far field in external aerodynamics or at inlet and outlet surfaces with internal flows in a local one-dimensional form by setting the right-hand side to zero. Some caution is in order here, since this will be valid only if the velocity is uniform in the boundary surfaces.

16.5.4 Boundary conditions

The number of boundary conditions to be imposed at a given boundary is connected to the amount of information, that is the number of bicharacteristics, entering or leaving the domain.

Considering the Mach conoid on the boundary surface, say the surface $x = \text{constant}$, one can decompose the bicharacteristic propagation into the

direction parallel to the boundary and a component normal to the boundary. The former will describe information that remains within this boundary surface and neither enters nor leaves the domain. The latter, on the other hand, will represent information that effectively enters or leaves the domain. *Hence, the number of conditions to be imposed at a boundary will correspond to the number of bicharacteristics associated with $\vec{k} = \vec{n}$, the normal to the boundary surfaces, that enter the computational domain.*

For a supersonic flow entering the domain, there will be four (or five) for two- (or three-) dimensional flow conditions, all of which have to be imposed. If the inlet is subsonic, certain bicharacteristics will leave the domain, those associated with $(\vec{v} \cdot \vec{n} - c) < 0$, and only three (or four) conditions have to be imposed. Similarly, at the outlet no conditions are to be given if the velocity is supersonic and one condition is to be imposed for a subsonic outlet speed.

The remaining variables will have to be determined by appropriate numerical procedures, which have to be compatible with the physical flow conditions and the numerical scheme. As discussed in the previous section for one-dimensional configurations, this is an important and difficult problem to which careful attention has to be given in the development of a computational method.

This is best illustrated by Figures 16.5.1 and 16.5.2, considering the dashed line through P as an inlet or an outlet boundary of the computational domain. In the supersonic flow case (Figure 16.5.1), the projection of all bicharacteristics will be on one side of the boundary. On the other hand, the same boundary for a subsonic inlet velocity will always have bicharacteristics on both sides of the projected boundary (Figure 16.5.2).

Example 16.5.3 Two-dimensional compatibility relations

We apply the same procedure as described above to the two-dimensional case, with the matrix of the left eigenvectors defined by equation (E16.5.1)

a. *First compatibility relation* With

$$l^{(1)} = \left| 1, 0, 0, \frac{-1}{c^2} \right| \quad (\text{E16.5.13})$$

one obtains

$$\begin{aligned} Z_x^{(1)} &= \left| u, 0, 0, \frac{-u}{c^2} \right| \\ Z_y^{(1)} &= \left| v, 0, 0, \frac{-v}{c^2} \right| \end{aligned} \quad (\text{E16.5.14})$$

and the compatibility equation for the first eigenvalue is identical to the

three-dimensional form (16.5.37):

$$d_v \rho - \frac{1}{c^2} d_v p = 0 \quad d_v = \partial_t + \bar{v} \cdot \bar{\nabla} \quad (\text{E16.5.15})$$

b. Second compatibility relation With the second left eigenvector equal to

$$l^{(2)} = |0, \hat{\kappa}_y, -\hat{\kappa}_x, 0| \quad (\text{E16.5.16})$$

one has

$$\begin{aligned} Z_x^{(2)} &= \left| 0, u\hat{\kappa}_y, -u\hat{\kappa}_x, \frac{\hat{\kappa}_y}{\rho} \right| \\ Z_y^{(2)} &= \left| 0, v\hat{\kappa}_y, -v\hat{\kappa}_x, \frac{-\hat{\kappa}_x}{\rho} \right| \end{aligned} \quad (\text{E16.5.17})$$

and the compatibility relation becomes

$$\partial_t(u\hat{\kappa}_y - v\hat{\kappa}_x) + (\bar{v} \cdot \bar{\nabla})(u\hat{\kappa}_y - v\hat{\kappa}_x) + \frac{1}{\rho}(\hat{\kappa}_y \partial_x - \hat{\kappa}_x \partial_y)p = 0 \quad (\text{E16.5.18})$$

c. Third and fourth compatibility relations They can both be treated simultaneously, since they correspond to opposite propagation directions, as seen from the structure of the eigenvectors. Hence, with

$$l^{(3)} = \left| 0, \hat{\kappa}_x, \hat{\kappa}_y, \frac{1}{\rho c} \right| \quad (\text{E16.5.19})$$

one has, in full similarity with the three-dimensional case,

$$\begin{aligned} Z_x^{(3)} &= \left| 0, u\hat{\kappa}_x + c, u\hat{\kappa}_y, \frac{\kappa_x c + u}{\rho c} \right| \\ Z_y^{(3)} &= \left| 0, v\hat{\kappa}_x, v\hat{\kappa}_y + c, \frac{\kappa_y c + v}{\rho c} \right| \end{aligned} \quad (\text{E16.5.20})$$

and the compatibility relations become

$$\hat{\kappa}_x(\partial_t + \bar{v} \cdot \bar{\nabla})u + \hat{\kappa}_y(\partial_t + \bar{v} \cdot \bar{\nabla})v \pm c\bar{\nabla} \cdot \bar{v} \pm \frac{1}{\rho c}[\partial_t + (\bar{v} \pm c\bar{1}_x) \cdot \bar{\nabla}]p = 0 \quad (\text{E16.5.21})$$

Characteristic variables

In treating boundary conditions through the compatibility relations it is most appropriate to work with characteristic variables defined in the same way as in the one-dimensional case. They are defined by multiplication of the primitive variable vector V by the left eigenvectors; that is the j th component of δW is obtained by

$$\delta w_j = l^{(j)} \delta V \quad (\text{16.5.47})$$

In the three-dimensional case, it is simpler to operate with the alternate form (16.5.30) for the matrix of the left eigenvectors. Hence one obtains

$$\begin{aligned}
 \delta w_1 &= \delta \rho - \frac{1}{c^2} \delta p \\
 \delta w_2 &= \hat{\kappa}_x \delta w - \hat{\kappa}_z \delta u = (\bar{\mathbf{I}}_x \times \bar{\mathbf{I}}_y) \cdot \delta \bar{\mathbf{v}} = -(\bar{\mathbf{I}}_x \times \delta \bar{\mathbf{v}}) \cdot \bar{\mathbf{I}}_y \\
 \delta w_3 &= \hat{\kappa}_y \delta u - \hat{\kappa}_x \delta v = (\bar{\mathbf{I}}_z \times \bar{\mathbf{I}}_x) \cdot \delta \bar{\mathbf{v}} = (\bar{\mathbf{I}}_x \times \delta \bar{\mathbf{v}}) \cdot \bar{\mathbf{I}}_z \\
 \delta w_4 &= \bar{\mathbf{I}}_x \cdot \delta \bar{\mathbf{v}} + \frac{1}{\rho c} \delta p \\
 \delta w_5 &= -\bar{\mathbf{I}}_x \cdot \delta \bar{\mathbf{v}} + \frac{1}{\rho c} \delta p
 \end{aligned} \tag{16.5.48}$$

The first characteristic variables describe entropy perturbations, as analysed in the one-dimensional case. The second and the third characteristic variables correspond to shear layer or vorticity waves in the characteristic surface normal to the direction of propagation $\bar{\kappa}$. The last two variables are associated with acoustic pressure waves. Note the change of sign of w_4 and w_5 with respect to their one-dimensional counterpart.

As noticed in Section 16.3.3, the characteristic variables W cannot be integrated in the general case, although the variations δW can always be defined. However, the variables W can always be defined locally if a linearization around a constant state is performed, such that equation (16.3.38) is valid locally. In all cases the characteristic equations can always be considered as a convenient representation of the compatibility relations for the variations δW .

The characteristic equations can be obtained by writing the space gradient terms of equation (16.3.37) as $\bar{\mathbf{Z}} \cdot L \bar{\mathbf{V}} W$, leading to the system

$$\begin{aligned}
 \left(\frac{\partial}{\partial t} + \bar{v} \cdot \bar{\nabla} \right) w_1 &= 0 \\
 \left(\frac{\partial}{\partial t} + \bar{v} \cdot \bar{\nabla} \right) w_2 - \frac{c}{2} (\bar{\mathbf{I}}_y \times \bar{\mathbf{I}}_x) \cdot \bar{\nabla} (w_4 + w_5) &= 0 \\
 \left(\frac{\partial}{\partial t} + \bar{v} \cdot \bar{\nabla} \right) w_3 + \frac{c}{2} (\bar{\mathbf{I}}_z \times \bar{\mathbf{I}}_x) \cdot \bar{\nabla} (w_4 + w_5) &= 0 \\
 \left[\frac{\partial}{\partial t} + (\bar{v} + c \bar{\mathbf{I}}_x) \cdot \bar{\nabla} \right] w_4 + c \bar{n}_x \cdot (\bar{n}_x \cdot \bar{\nabla}) \bar{v} &= 0 \\
 \left[\frac{\partial}{\partial t} + (\bar{v} - c \bar{\mathbf{I}}_x) \cdot \bar{\nabla} \right] w_5 + c \bar{n}_x \cdot (\bar{n}_x \cdot \bar{\nabla}) \bar{v} &= 0
 \end{aligned} \tag{16.5.49}$$

Observe that the first term of each equation is purely convective and that the characteristic equations would be totally decoupled, as in the one-dimensional case, if the other terms would vanish. This is, however, not the case, unless directions $\bar{\kappa}$ could be chosen to make the other, non-diagonal, terms vanish.

These properties have been used by Deconinck *et al.* (1986) and Hirsch *et al.* (1987) in order to define multi-dimensional upwind algorithms independently of the mesh orientation.

The non-diagonal terms in the second and third equations are equal to the y and z projections of the term

$$\frac{c}{2}(\bar{\mathbf{I}}_{\kappa} \times \bar{\mathbf{V}})(w_4 + w_5) = \left(\bar{\mathbf{I}}_{\kappa} \times \frac{\bar{\nabla} p}{\rho} \right) \quad (16.5.50)$$

and depend only on the pressure gradient. The non-diagonal terms in the fourth and fifth equations, on the other hand, do not contain the pressure term, since this term is identical to the right-hand side of the compatibility relation (16.5.46).

This system of equations is fully equivalent to the Euler equations in primitive variables. It indicates that the variations of w_1, w_2, w_3 along the pseudo-path line is due to the variations of the pressure gradient in the direction normal to the wave-number vector $\bar{\kappa}$. The variations of the characteristic variables w_4 and w_5 along the bicharacteristic, which represents the transport of pressure waves, are due, for their part, to the variations of the velocity field in the wave-front surface perpendicular to $\bar{\kappa}$.

These relations can be used to solve the Euler equations or can be applied to generate numerical boundary conditions.

Two-dimensional characteristic relations

In the two-dimensional case, the characteristic variables reduce to

$$\delta W = \begin{pmatrix} \delta w_1 \\ \delta w_2 \\ \delta w_3 \\ \delta w_4 \end{pmatrix} = \begin{pmatrix} \delta \rho - \frac{\delta p}{c^2} \\ \hat{\kappa}_y \delta u - \hat{\kappa}_z \delta v \\ \bar{\mathbf{I}}_{\kappa} \cdot \delta \bar{\mathbf{v}} + \frac{\delta p}{\rho c} \\ -\bar{\mathbf{I}}_{\kappa} \cdot \delta \bar{\mathbf{v}} + \frac{\delta p}{\rho c} \end{pmatrix} \quad (16.5.51)$$

The characteristic system becomes

$$\begin{aligned} \left(\frac{\partial}{\partial t} + \bar{\mathbf{v}} \cdot \bar{\nabla} \right) w_1 &= 0 \\ \left(\frac{\partial}{\partial t} + \bar{\mathbf{v}} \cdot \bar{\nabla} \right) w_2 - \frac{c}{2} (\hat{\kappa}_x \partial_y - \hat{\kappa}_y \partial_x) (w_3 + w_4) &= 0 \\ \left[\frac{\partial}{\partial t} + (\bar{\mathbf{v}} + c \bar{\mathbf{I}}_{\kappa}) \cdot \bar{\nabla} \right] w_3 - c (\hat{\kappa}_x \partial_y - \hat{\kappa}_y \partial_x) w_2 &= 0 \\ \left[\frac{\partial}{\partial t} + (\bar{\mathbf{v}} - c \bar{\mathbf{I}}_{\kappa}) \cdot \bar{\nabla} \right] w_3 - c (\hat{\kappa}_x \partial_y - \hat{\kappa}_y \partial_x) w_2 &= 0 \end{aligned} \quad (16.5.52)$$

This is easily obtained from the relations of Example 16.5.3 (see Problem 16.15).

16.6 SOME SIMPLE EXACT REFERENCE SOLUTIONS FOR ONE-DIMENSIONAL INVISCID FLOWS

We will present in this section some exact solutions, which can be used as test cases for the validation of one-dimensional schemes.

16.6.1 The linear wave equation

This equation represents a wave propagating at a velocity a in the positive x direction or the convective transport of a scalar quantity u in a flow of velocity equal to a . This equation has been used extensively in Volume 1 and we mention it here again for completeness:

$$\frac{\partial u}{\partial t} + a \frac{\partial u}{\partial x} = 0 \quad (16.6.1)$$

Its general solution is

$$u = f(x - at) \quad (16.6.2)$$

and allows a variety of test cases, from smooth solutions, like a sinusoidal wave, to discontinuities. For instance, an initial distribution

$$u(x, 0) = \sin kx \quad t = 0 \quad (16.6.3)$$

will lead to the solution

$$u(x, t) = \sin k(x - at) \quad t > 0 \quad (16.6.4)$$

This test case allows us to test the diffusion and dispersion properties of schemes and to define the accuracy of the scheme on smooth functions as a function of the wave-number k . On the other hand, the following discontinuous variation

$$\begin{aligned} u(x, 0) &= 1 & x < 0 \\ u(x, 0) &= +b & x > 0 \end{aligned} \quad \text{with } b < 1 \quad (16.6.5)$$

leads to a discontinuity of amplitude $(1 - b)$, moving with the velocity a in the positive x direction.

This extremely simple test case is by far not trivial, as shown in Volume 1, indicating that its numerical treatment can be very instructive with regard to the properties of the scheme at handling propagating discontinuities.

When $b > 1$, the discontinuity is typical of an expansion shock and the scheme should not propagate this discontinuity (although it is an exact solution of the wave equation (16.6.1)) but instead damp this expansion through an introduced entropy condition or any form of dissipative mechanism.

16.6.2 The inviscid Burgers equation

This equation has a non-linear flux term, proportional to the square of the basic variable u , identical to the convection term of the Euler equations. It is

therefore representative for the non-linearities occurring in the flow equations. It is written in standard form as

$$\frac{\partial u}{\partial t} + \frac{\partial u^2}{\partial x} = 0 \quad (16.6.6)$$

or in quasi-linear form as

$$\frac{\partial u}{\partial t} + u \frac{\partial u}{\partial x} = 0 \quad (16.6.7)$$

The Jacobian is equal to u and the characteristics are defined by

$$\frac{dx}{dt} = u \quad (16.6.8)$$

The general solution is given by

$$du = 0 \quad \text{along} \quad \frac{dx}{dt} = u \quad (16.6.9)$$

expressing that u remains constant on the characteristic (16.6.8).

For an initial distribution

$$u(x, 0) = g(x) \quad -\infty < x < \infty, \quad t = 0 \quad (16.6.10)$$

the characteristics in the xt plane are straight lines given by the parametric equations as a function of the initial position x_0 :

$$x = x_0 + g(x_0) \cdot t \quad (16.6.11)$$

and the general solution is

$$u(x, t) = u(x_0, 0) = g(x_0) = g(x - g(x_0)t) \quad (16.6.12)$$

Note that the gradients of u are given by

$$\frac{\partial u}{\partial x} = \frac{g'(x_0)}{1 + g'(x_0) \cdot t} \quad (16.6.13)$$

and

$$\frac{\partial u}{\partial t} = -g(x_0) \cdot \frac{\partial u}{\partial x} = -\frac{g(x_0) \cdot g'(x_0)}{1 + g'(x_0) \cdot t} \quad (16.6.14)$$

where g' denotes the derivative of g with respect to its argument.

The characteristics have a slope proportional to $1/g(x_0)$ in the xt plane (Figure 16.6.1), and if $g'(x_0)$ is positive, which is typical for an expansion profile, they will never intersect. However, for a decreasing initial distribution of u , that is $g'(x_0) < 0$, typical for a compression profile, the characteristics will intersect.

The time evolution of the 'compression' branch of the initial distribution $u = g(x)$ is shown in Figure 16.6.1(c). Since point A propagates with a speed $u_A = g(x_{03})$ greater than the speed of point B, $u_B = g(x_{04})$, point A will

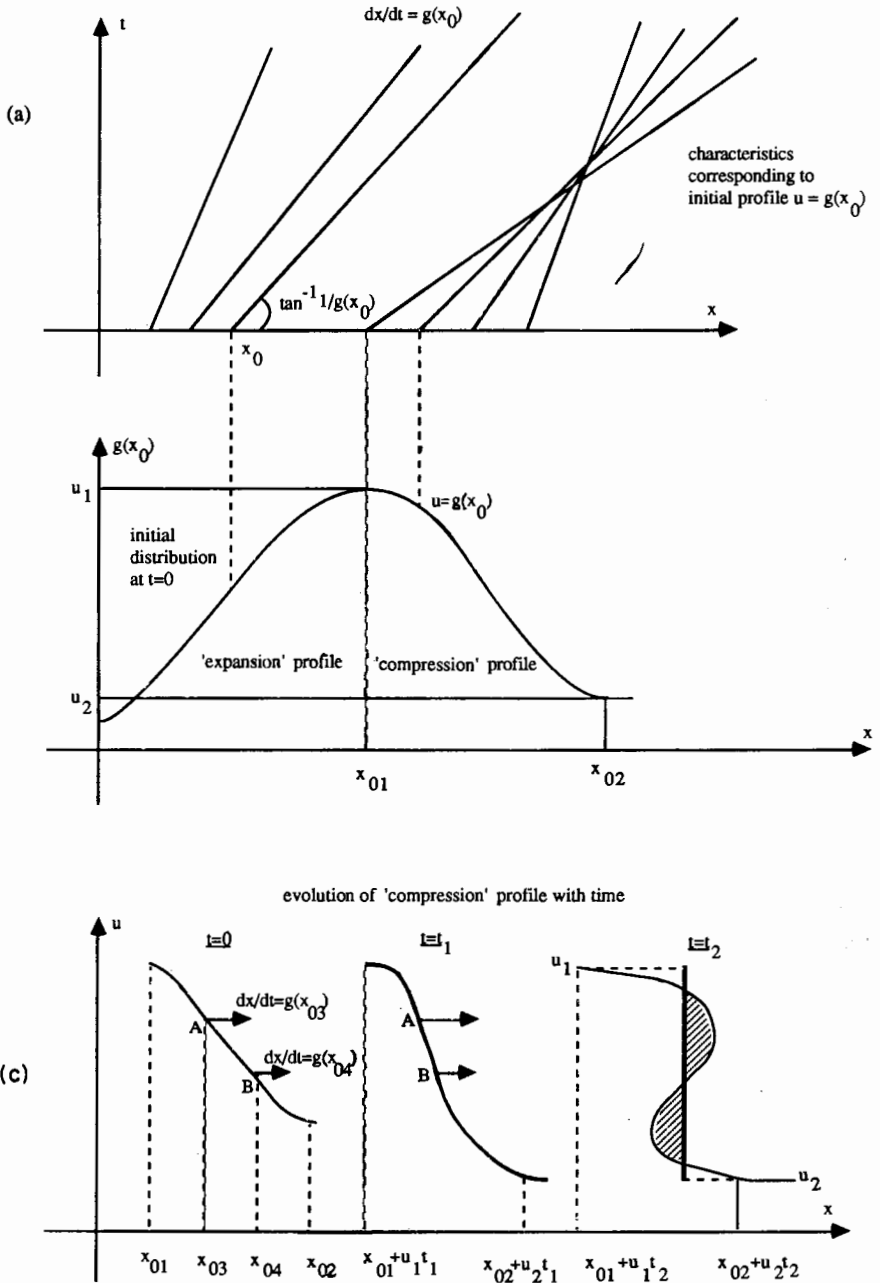


Figure 16.6.1 Behaviour of solutions to Burgers equation. (a) Characteristics corresponding to initial profile shown in (b) and (c) time evolution of compression profile with shock formation

progressively take over point B, resulting in a multi-valued profile as shown at time $t = t_2$. The solution at time $t = t_2$ has clearly no physical significance, since the function u cannot take on different values at the same time t_2 and in the same location x . Therefore an initial profile with decreasing intensities will lead to a breakdown of the continuous solution and to the appearance of a *shock discontinuity*.

The shock will appear only when $g'(x_0) < 0$ or $u_x < 0$ and at the time t_s given by the condition that the tangent to the $u(x)$ profiles becomes vertical. This happens at first for

$$t_s = \frac{-1}{\max |g'(x_0)|} \quad (16.6.15)$$

The shock will move at a velocity C satisfying the Rankine–Hugoniot relation, which becomes here

$$\left[\frac{u^2}{2} \right] - C[u] = 0 \quad (16.6.16)$$

leading to the shock speed

$$C = \frac{1}{2}(u_2 + u_1) \quad (16.6.17)$$

where u_1 and u_2 are the values upstream and downstream of the shock, with $u_2 < u_1$. Note that

$$u_2 < C < u_1 \quad (16.6.18)$$

that is the upstream waves propagate faster than the shock, feeding waves into the shock, while the downstream waves propagate at a slower velocity.

If the initial profile covers values between u_2 and u_1 , these limits will define the shock intensity. Let x_{02} and x_{01} denote the respective initial positions corresponding to these values (Figure 16.6.1). It is easily shown (Whitham, 1974) that the conservation property of the area under the curve $u = g(x)$ implies that the shaded areas in Figure 16.6.1(c) are equal and that

$$\int_{x_{01}}^{x_{02}} g(x) dx = \frac{1}{2}[g(x_{01}) + g(x_{02})](x_{02} - x_{01}) \quad (16.6.19)$$

The conditions for the shock position $x_s = x_s(t)$ can be expressed as

$$\begin{aligned} x_s(t) &= x_{01} + g(x_{01})t \\ x_s(t) &= x_{02} + g(x_{02})t \end{aligned} \quad (16.6.20)$$

These three conditions define the quantities x_{01} , x_{02} and x_s , and also allow the development of the shock in time to be followed. A more detailed discussion can be found in Whitham (1974).

Sinusoidal wave profile

An interesting test case for unsteady flows with shock formation and propagation is provided by the time evolution of a *single sinusoidal wave profile*:

$$g(x) = \begin{cases} u(x, 0) = A \sin \frac{\pi x}{L} + u_0 & 0 \leq x \leq L \\ u_0 & x < 0 \text{ and } x > L \end{cases} \quad (16.6.21)$$

The relations (16.6.19) and (16.6.20) allow the time evolution and the shock formation to be followed, but a simple asymptotic situation results, which is given by the following relations.

For $t \gg t_s$, the shock moves at a speed

$$C = u_0 t + \sqrt{Bt} \quad (16.6.22)$$

and has an intensity

$$[u] = \sqrt{\frac{B}{t}} \quad (16.6.23)$$

where $B/2$ is the area under the sinusoidal curve, which remains constant following (16.6.19); that is

$$B = 2 \int_0^L [g(x) - u_0] dx = \frac{4AL}{\pi} \quad (16.6.24)$$

The expansion part takes on a linear shape asymptotically:

$$u \approx \frac{x}{t} \quad u_0 t < x < u_0 t + \sqrt{Bt} \quad (16.6.25)$$

Note that the amplitude decreases as $t \rightarrow \infty$, while the shock velocity increases, both at a rate $\propto \sqrt{t}$ if $u_0 = 0$. This solution is illustrated in Figure 16.6.2.

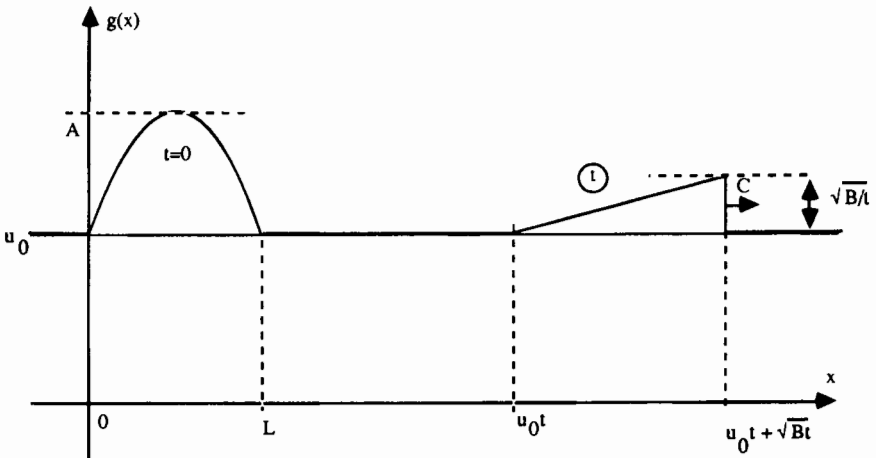


Figure 16.6.2 Solution of Burgers equation for an initial sinusoidal distribution

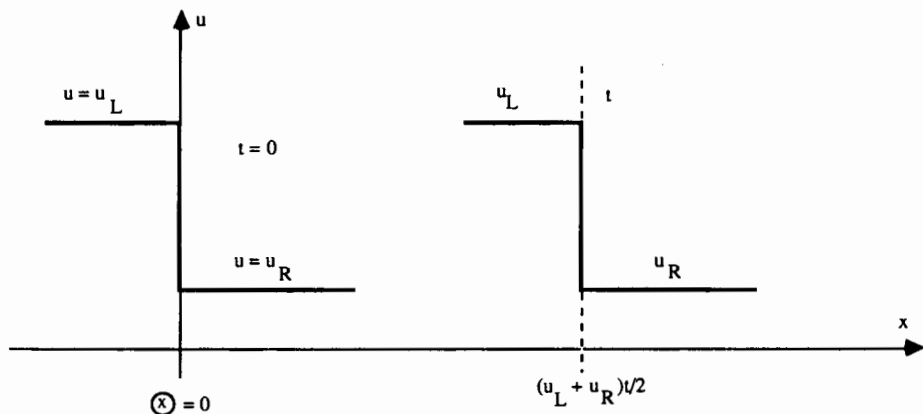


Figure 16.6.3 Burgers solution for a propagating discontinuity

Initial shock discontinuity

A rather simple test case, which can be used both for steady and unsteady computations, is provided by an initial discontinuous distribution (Figure 16.6.3):

$$u(x, 0) = g(x) = \begin{cases} u_L & x < 0, \quad t = 0 \\ u_R & x > 0, \quad t = 0 \end{cases} \quad (16.6.26)$$

The solution is given by (16.6.17), namely a shock propagating at speed $C = (u_L + u_R)/2$ with unmodified intensity $[u] = u_L - u_R$. If $u_R = -u_L$, the shock is stationary and this forms a simple, although non-linear, test case for steady-state methods.

Initial linear distribution

Actually, any initial distribution with $g'(x) < 0$ between u_1 and u_2 will lead to the same shock structure. For instance, a linear distribution (Figure 16.6.4)

$$u(x, 0) = g(x) = \begin{cases} u_1 & x < 0, \quad t = 0 \\ u_1 \left(1 - \frac{x}{L}\right) + u_2 \frac{x}{L} & 0 \leq x \leq L, \quad t = 0 \\ u_2 & x > L, \quad t = 0 \end{cases} \quad (16.6.27)$$

will lead to the solution shown in Figure 16.6.4, where the characteristics are also indicated. The shock is formed at a time given by equation (16.6.15), which becomes here

$$t_s = \frac{L}{u_1 - u_2} \quad (16.6.28)$$

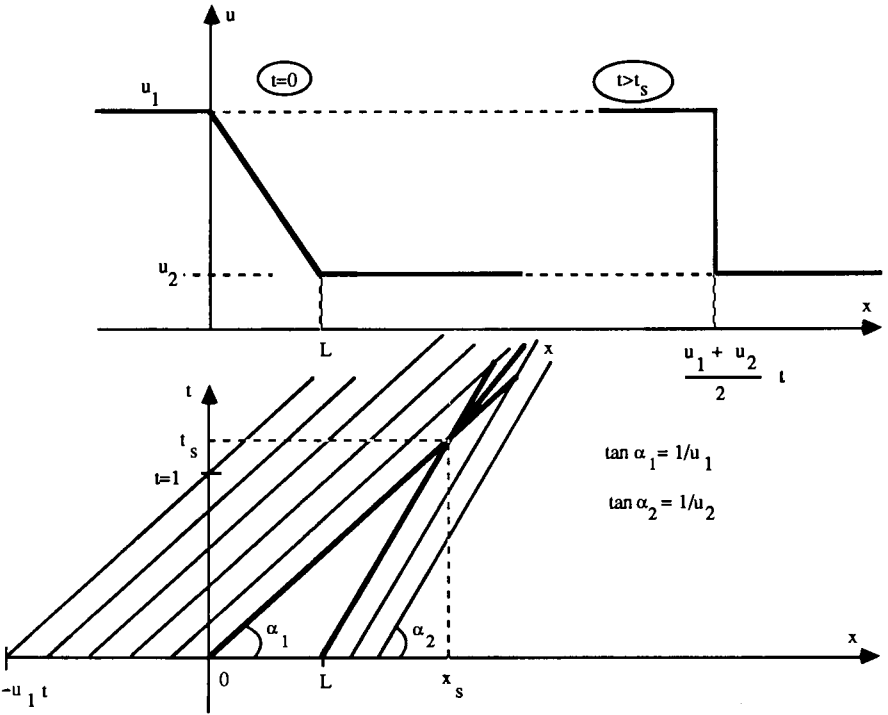


Figure 16.6.4 Shock formation for an initial linear distribution

and at the position

$$x_s = t_s \cdot u_1 = L + t_s \cdot u_2 \tag{16.6.29}$$

The solution is therefore, for $t > t_s$,

$$u(x, t) = \begin{cases} u_1 & \text{for } x < \frac{u_1 + u_2}{2} t \\ u_2 & \text{for } x > \frac{u_1 + u_2}{2} t \end{cases} \tag{16.6.30}$$

Expansion fan

If the initial distribution corresponds to $g'(x) > 0$, there will be no shock formation as described above. For an initial discontinuity

$$u(x, 0) = g(x) = \begin{cases} u_1 & x < 0, \quad t = 0 \\ u_2 & x > 0, \quad t = 0 \end{cases} \tag{16.6.31}$$

with $u_1 < u_2$, the characteristics behave as shown in Figure 16.6.5. Between the points $u_1 t < x < u_2 t$, there is no information available and the solution is not

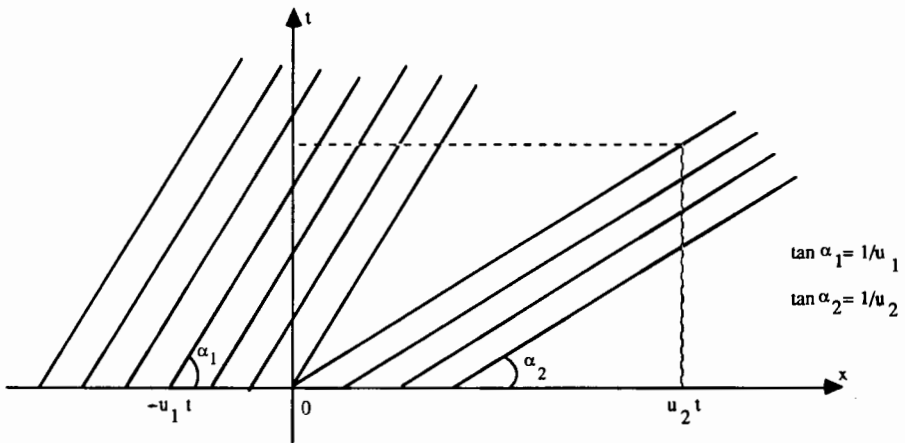
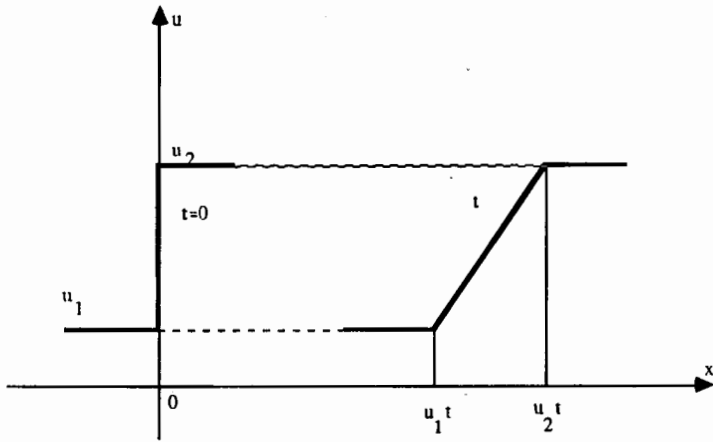


Figure 16.6.5 Initial expansion discontinuity for Burger's equations

Burgers'

determined by the intersection of characteristics. Hence a continuous solution is possible and is given by

$$u(x, t) = \begin{cases} u_1 & x/t < u_1 \\ x/t & u_1 < x/t < u_2 \\ u_2 & x/t > u_2 \end{cases} \quad (16.6.32)$$

This continuous solution, which corresponds to a series of characteristics emanating from the origin with continuous slopes between u_1 and u_2 , is called an *expansion fan*.

However, a discontinuous solution can also be defined for the same initial

conditions. The solution

$$u(x, t) = \begin{cases} u_2 & x/t < \frac{u_1 + u_2}{2} \\ u_1 & x/t > \frac{u_1 + u_2}{2} \end{cases} \quad (16.6.33)$$

satisfies the jump conditions and is clearly a solution to Burgers equation.

This solution, which corresponds to an *expansion shock*, has to be rejected on physical grounds since it would violate the entropy condition. It can be shown, by the analysis of the complete Burgers equation $u_t + uu_x = \nu u_{xx}$, that the continuous solution, equation (16.6.32), is the limit for $\nu \rightarrow 0$ of solutions of the dissipative Burgers equation, while this is not the case for the discontinuous solutions (see Whitham, 1974). Therefore an additional entropy condition is necessary to restore the unicity of the inviscid solutions. Any scheme that would maintain, or create, an expansion discontinuity on the test case of the type defined by equation (16.6.31) would have to be modified by the addition of some dissipative mechanism.

16.6.3 The shock tube problem or Riemann problem

The shock tube problem constitutes a particularly interesting and difficult test case, since it presents an exact solution to the full system of one-dimensional Euler equations containing simultaneously a shock wave, a contact discontinuity and an expansion fan.

This particular problem, also called the *Riemann problem*, is altogether of practical and theoretical interest. It can be realized experimentally by the sudden breakdown of a diaphragm in a long one-dimensional tube separating two initial gas states at different pressures and densities. The initial conditions are the following:

$$\begin{array}{lllll} u = u_L, & p = p_L & \rho = \rho_L & x < x_0 & t = 0 \\ u = u_R, & p = p_R & \rho = \rho_R & x > x_0 & t = 0 \end{array} \quad (16.6.34)$$

with $p_R < p_L$ and the diaphragm is located at $x = x_0$. We will assume that the two regions contain the same gas.

If viscous effects can be neglected along the tube walls and if an infinitely long tube is considered, avoiding reflections at the tube ends, the exact solution to the Euler equations can easily be obtained on the basis of simple waves separating regions of uniform conditions.

At the bursting of the diaphragm, at time $t = 0$, the pressure discontinuity propagates to the right in the low-pressure gas and simultaneously an expansion fan propagates to the left in the high-pressure gas. In addition, a contact discontinuity separating the two gas regions propagates to the right in the tube. This is illustrated in Figures 16.6.6 and 16.6.7, which show also the characteristics and the discontinuities.

Since the shock and the contact discontinuity move in regions of uniform conditions, they will have a constant velocity and the expansion is centred at the diaphragm position x_0 , $t = 0$.

We will distinguish the following regions: region R contains the undisturbed gas at the low pressure p_R . It is separated by a shock wave from region 2 which represents the disturbed low-pressure gas. The contact discontinuity separates region 2 from the disturbed high-pressure gas region 3, which in turn has been influenced by the expansion fan propagating to the left into the undisturbed high-pressure region L. The expansion fan region, through which the flow quantities vary continuously, is defined as region 5.

Shock wave

The shock is generated between region R and 2, and for values of fluid velocities u_2 and pressure p_2 , the normal shock relations, equation (16.1.28) to (16.1.30), hold. As a function of Mach numbers or pressure ratio, the normal shock relations are applied in Section 2.9 in Volume 1. One has, as a function of the pressure ratio $p_2/p_R \equiv P$,

$$\frac{\rho_2}{\rho_R} = \frac{1 + \alpha P}{\alpha + P} \quad \text{with } \alpha = \frac{\gamma + 1}{\gamma - 1} \quad (16.6.35)$$

$$\frac{u_2 - u_R}{c_R} = \frac{P - 1}{(1 + \alpha P)^{1/2}} \cdot \frac{1}{\sqrt{\gamma(\gamma - 1)/2}} \quad (16.6.36)$$

$$M = \frac{C - u_R}{c_R} = \frac{(P - 1)c_R}{\gamma(u_2 - u_R)} \quad (16.6.37)$$

$$\left| \frac{c_2}{c_R} \right|^2 = P \frac{\alpha + P}{1 + \alpha P} \quad (16.6.38)$$

The quantity C is the propagation speed of the shock in the undisturbed region R.

Contact surface

The contact surface sustains a discontinuity in density but the pressures and velocities normal to the surfaces are continuous. Therefore the contact discontinuity propagates at a velocity V equal to u_2 .

Along this surface, the following conditions have to be satisfied:

$$p_3 = p_2 \quad (16.6.39)$$

$$u_3 = u_2 \equiv V \quad (16.6.40)$$

Expansion fan

The expansion fan is formed by the left running characteristics of slopes $(u - c)$, and the information between regions L and 3 is transmitted along the C_0 and

C_+ characteristics. Hence, along the C_0 characteristics, the path line, the entropy is constant:

$$s_3 = s_L \quad (16.6.41a)$$

or

$$\frac{p_3}{\rho_3^\gamma} = \frac{p_L}{\rho_L^\gamma} \quad (16.6.41b)$$

and along the C_+ characteristic, the Riemann variable is constant:

$$\frac{\gamma - 1}{2} u_L + c_L = \frac{\gamma - 1}{2} u_3 + c_3 \quad (16.6.42)$$

or, when $u_L = 0$ and $u_3 = V$,

$$c_L = c_3 + \frac{\gamma - 1}{2} V \quad (16.6.43)$$

From (16.6.41) and (16.6.42) one obtains the relation between V and p_3 :

$$V - u_L = \frac{2}{\gamma - 1} c_L \left[1 - \left(\frac{p_3}{p_L} \right)^{(\gamma - 1)/2\gamma} \right] \quad (16.6.44)$$

The above relations allow the determination of all the constant states in the regions 2, 3 and L. In particular, expressing equation (16.6.40) in equation (16.6.36) leads to a relation between $u_2 = V$ and the pressure ratio P , while another relation between V and P is obtained by introducing the condition of pressure continuity across the contact surface, equation (16.6.39), in equation (16.6.44). Eliminating V between these two relations leads to an implicit equation for P .

One obtains

$$\sqrt{\frac{2}{\gamma(\gamma - 1)} \frac{P - 1}{(1 + \alpha P)^{1/2}}} = \frac{2}{\gamma - 1} \frac{c_L}{c_R} \left[\left(\frac{p_L}{p_R} \right)^{(\gamma - 1)/2\gamma} - P^{(\gamma - 1)/2\gamma} \right] + \frac{u_L - u_R}{c_R} \quad (16.6.45)$$

which can be solved for known pressure ratios p_L/p_R by an iterative method, for instance a Newton iteration. With the knowledge of P , all other variables are determined, using the above relations.

Variations through expansion fan—region 5

Finally, the continuous evolution of the flow variables through region 5 separating the regions 3 and L has to be determined. The gas state in region 5 is determined by conditions (16.6.41) and (16.6.42), which express the constancy of the information carried by the characteristics C_0 and C_+ . Hence

$$\frac{p_5}{\rho_5^\gamma} = \frac{p_L}{\rho_L^\gamma} \quad (16.6.46)$$

and

$$\frac{\gamma - 1}{2} u_5 + c_5 = \frac{\gamma - 1}{2} u_L + c_L \quad (16.6.47)$$

In addition, the expansion fan is formed by the C_- characteristics along which

$$\frac{\gamma - 1}{2} u_5 - c_5 = \text{constant} \quad \text{along} \quad \frac{dx}{dt} = u_5 - c_5 \quad (16.6.48)$$

Each characteristic of the expansion fan is defined by

$$\frac{dx}{dt} = \frac{\gamma + 1}{2} u_5 - c_L - \frac{\gamma - 1}{2} u_L \quad (16.6.49)$$

using equation (16.6.47). The combination of equations (16.6.48) and (16.6.47) also shows that u_5 and c_5 are separately constant along this characteristic, implying that they can be defined by $x/t = u_5 - c_5$.

Hence, since u_5 varies between zero and V , one has, within the expansion fan, considering the diaphragm to be initially located at $x = 0$ (otherwise x is to be replaced by $(x - x_0)$ for an initial position x_0),

$$\begin{aligned} u_5 &= \frac{2}{\gamma + 1} \left(\frac{x}{t} + c_L + \frac{\gamma - 1}{2} u_L \right) \\ \text{for} \quad - \left(\frac{\gamma - 1}{2} u_L + c_L \right) &< \frac{x}{t} < \left(\frac{\gamma + 1}{2} V - c_L - \frac{\gamma - 1}{2} u_L \right) \\ c_5 &= c_L - \frac{\gamma - 1}{2} (u_5 - u_L) = u_5 - \frac{x}{t} \\ p_5 &= p_L \left(\frac{u_5}{c_L} \right)^{2\gamma/(\gamma - 1)} \end{aligned} \quad (16.6.50)$$

This completes the solution of the shock tube problem.

An important observation is that the complete solution of the shock tube problem is only a function of the ratio x/t and the initial conditions $(\rho, u, p)_L$, $(\rho, u, p)_R$. Also, it can be seen from the second of the above equations that the flow acceleration through the expansion fan will reach sonic conditions, $u_5 = c_5$, at the original diaphragm position $x = 0$.

Typical solutions are shown in Figures 16.6.8 and 16.6.9 for the following data, in SI units for a perfect gas with $\gamma = 1.4$ (see Problem 16.25):

Figure 16.6.8: $p_L = 10^5$; $\rho_L = 1$; $p_R = 10^4$; $\rho_R = 0.125$; $u_L = u_R = 0$
corresponding to an initial pressure ratio of 10.

Figure 16.6.9: $p_L = 10^5$; $\rho_L = 1$; $p_R = 10^3$; $\rho_R = 0.010$; $u_L = u_R = 0$
corresponding to an initial pressure ratio of 100

These test data correspond to those applied by Sod (1978).

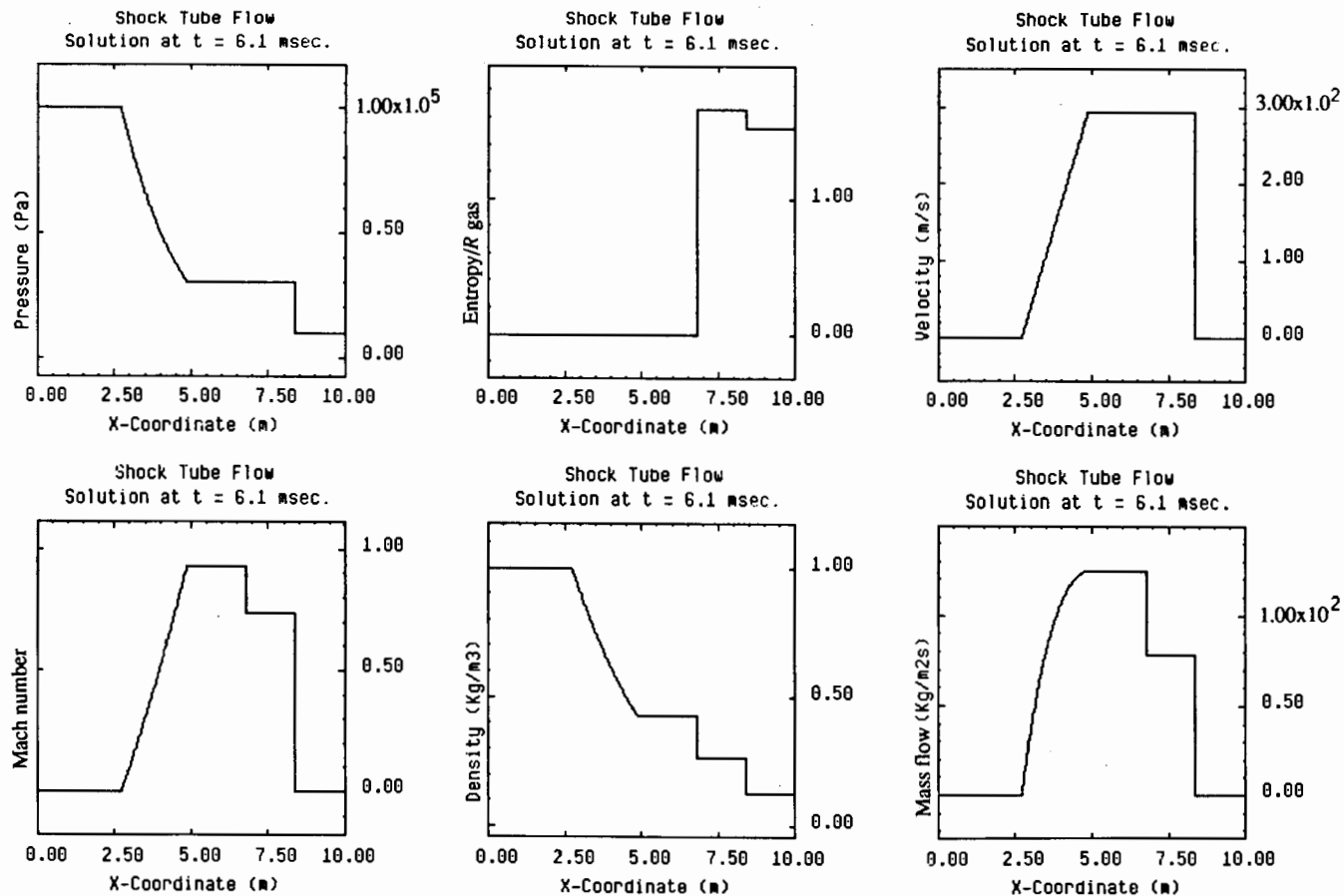


Figure 16.6.8 Variation of flow quantities in the shock tube—Riemann—problem for $p_L = 10^5$; $\rho_L = 1$; $p_R = 10^4$; $\rho_R = 0.125$; $u_L = u_R = 0$

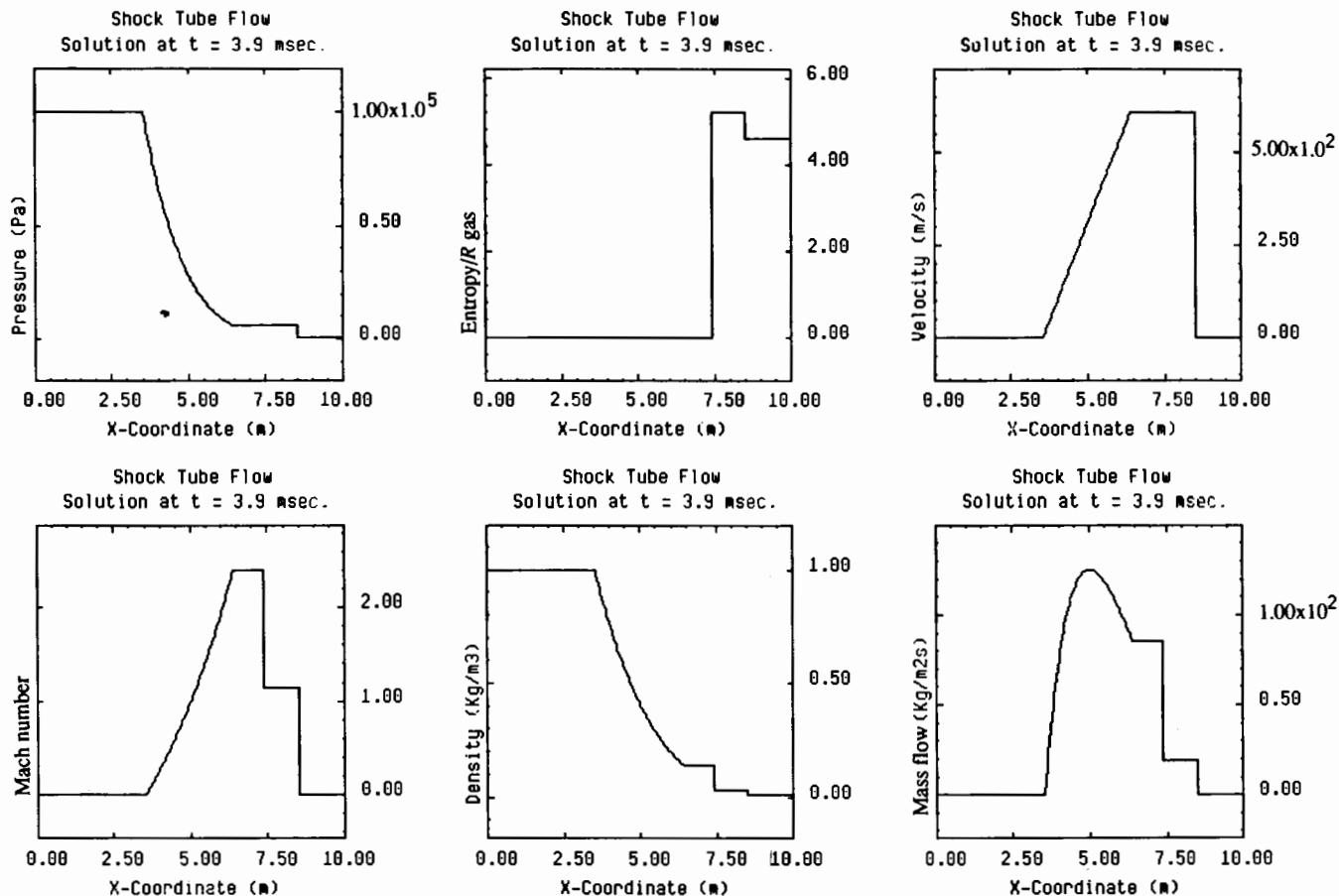


Figure 16.6.9 Variation of flow quantities in the shock tube—Riemann—problem for $p_L = 10^5$; $\rho_L = 1$; $p_R = 10^3$; $\rho_R = 0.010$; $u_L = u_R = 0$

In the first case the shock pressure ratio is moderate, $P = 3.031$, while the second case in Figure 16.6.9 corresponds to a strong shock with a pressure ratio $P = 7.155$ and supersonic Mach numbers after the expansion. The variations of pressure, density, Mach number, entropy, velocity and mass flux ρu are shown as a function of distance.

Looking at the Mach number evolution from right to left, the first discontinuity is due to the shock wave propagating downstream, followed by the contact discontinuity. By analysing the other curves it is seen that the shock wave corresponds to discontinuous variations of all the variables including entropy, while velocity and pressure are continuous over the contact discontinuity. Upstream of the contact discontinuity, the smooth variation represents the expansion waves. Observe the linear variation of the velocity in the expansion region and its isentropic nature.

16.6.4 The quasi-one-dimensional nozzle flow

This flow forms an excellent family of test cases for steady-state computations, allowing a variety of conditions to be tested: in particular, subsonic flows, supersonic flows without shocks, subsonic-supersonic transition without shocks, subsonic-supersonic-subsonic flow with shocks. Also the impact of boundary conditions on convergence and accuracy can be investigated.

The exact one-dimensional flow in a nozzle of varying cross-section $S(x)$ is solved in many textbooks (see, for instance, Shapiro, 1953, or Zucrow and Hoffman, 1976).

For isentropic continuous flow one has, with subscript 1 indicating inlet conditions and referring to Figure 16.4.1, p. 157

$$\begin{aligned} p_0 &= p_{01} \\ T_0 &= T_{01} \end{aligned} \quad (16.6.51)$$

$$\frac{T_0}{T} = 1 + \frac{\gamma - 1}{2} M^2 = \left(\frac{p_0}{p}\right)^{(\gamma-1)/\gamma} = \left(\frac{\rho_0}{\rho}\right)^{\gamma-1} = \frac{c_0^2}{c^2} \quad (16.6.52)$$

The critical conditions are defined by

$$\rho^* c^* = \rho_0 c_0 \left(\frac{2}{\gamma + 1}\right)^{(\gamma+1)/(2(\gamma-1))} \quad (16.6.53)$$

and the critical mass flow rate by

$$\dot{m}^* = \rho^* c^* S^* \quad (16.6.54)$$

The critical section S^* is the minimal area where sonic conditions are reached when the mass flow is at the critical value \dot{m}^* .

The relations defining the mass flow rate at a section S can be written as

$$\dot{m} = \rho_0 c_0 M S \left(1 + \frac{\gamma - 1}{2} M^2 \right)^{-(\gamma + 1)/[2(\gamma - 1)]}$$

$$\frac{\dot{m} \sqrt{\gamma r T_0}}{p_0 S} = \gamma M \left(1 + \frac{\gamma - 1}{2} M^2 \right)^{-(\gamma + 1)/[2(\gamma - 1)]} \quad (16.6.55)$$

Expressing constancy of mass flow, one obtains the ratio of the current section area to the critical area S^* :

$$\frac{S}{S^*} = \frac{1}{M} \left(\frac{2}{\gamma + 1} \cdot \frac{T_0}{T} \right)^{(\gamma + 1)/[2(\gamma - 1)]} = \frac{1}{M} \left[\frac{2}{\gamma + 1} \left(1 + \frac{\gamma - 1}{2} M^2 \right) \right]^{(\gamma + 1)/[2(\gamma - 1)]} \quad (16.6.56a)$$

$$M = \frac{u}{c} = \frac{u}{\sqrt{\gamma p / \rho}} \quad (16.6.56b)$$

Choked flow conditions, that is $\dot{m} = \rho^* S^* c^* = \dot{m}^*$, are obtained if the throat area S_t equals the critical area S^* . For instance, in a Laval nozzle with throat area $S_t = S^*$, the mass flow rate will be equal to the maximum value allowed and the throat Mach number will be equal to 1.

If, on the other hand, S^* is selected such that $S^* < S_t$, the flow is unchoked and M_t , the throat Mach number, will never reach the sonic value of 1. Its value will depend on whether the inlet flow is subsonic or supersonic. In the subsonic case ($M_1 < 1$) M_t will also be subsonic and in the supersonic case ($M_1 > 1$) M_t will also remain supersonic. Hence, by selecting the stagnation conditions at the inlet, p_{01} , T_{01} , as well as the critical area S^* , a variety of shock-free test cases can be defined.

Since, for a given mass flow $\dot{m} > \dot{m}^*$, two solutions are always possible, a subsonic and a supersonic one, the inlet value of the Mach number has also to be selected; refer to Figure 2.9.6 in Volume 1.

If shocks are to be considered, the Rankine–Hugoniot relations have to be satisfied, that is over the shock

$$T_0 = T_{01}$$

$$M_R^2 = \frac{2 + (\gamma - 1)M_L^2}{2\gamma M_L^2 - (\gamma - 1)}$$

$$\frac{p_R}{p_L} = \frac{2\gamma M_L^2 - (\gamma - 1)}{\gamma + 1} \quad (16.6.57)$$

$$\frac{p_{0R}}{p_{0L}} = \frac{([\gamma + 1]/2)M_L^2 / \{1 + [(\gamma - 1)/2]M_L^2\}}{\{[2\gamma/(\gamma + 1)]M_L^2 - (\gamma - 1)/(\gamma + 1)\}^{1/(\gamma - 1)}}$$

where the subscripts R and L denote respectively the conditions at the right (downstream) and the left (upstream) sides of the shock.

The definition of a test case is then as follows:

- (1) Define $S(x)$, S^* , p_{01} , T_{01} , M_1 , x_{shock} . The Mach number variation $M(x)$ is obtained from the iterative solution of above equations, where the initial value M_1 will allow selection of the subsonic or supersonic branch.
- (2) When a sonic point is reached, at the throat of a converging-diverging nozzle for instance, a choice has to be made again between the subsonic or supersonic evolution.
- (3) If a shock point is reached, the shock relations (16.6.57) are applied to find the conditions downstream of the shock, fixing the shock intensity and the stagnation pressure downstream of the shock.
- (4) Downstream of the shock, the isentropic relations (16.6.51) to (16.6.56) are applied again with the new value of the stagnation pressure.

References

- Deconinck, H., Hirsch, Ch., and Peuteman, J. (1986) 'Characteristic decomposition methods for the multidimensional Euler equations.' *Proc. Tenth International Conference on Numerical Methods in Fluid Dynamics, Lecture Notes in Physics*, Vol. 264, 216–21.
- Hirsch, Ch., Lacor, C., and Deconinck, H. (1987). 'Convection algorithms based on a diagonalization procedure for the multidimensional Euler equations.' *AIAA Paper 87-1163, Proc. AIAA 8th Computational Fluid Dynamics Conference*, 667–76.
- Liepmann, H. W., and Roshko, A. (1957). *Elements of Gas Dynamics*, New York, John Wiley and Sons.
- Moretti, G. (1983). 'A fast Euler solver for steady flows.' *AIAA Paper 83-1940, Proc. AIAA 6th Computational Fluid Dynamics Conference*, 357–362.
- Pandolfi, M. (1983). 'A contribution to the numerical prediction of unsteady flows.' *AIAA Paper 83-0121, AIAA 21st Aerospace Sciences Meeting*.
- Pandolfi, M. (1984). 'On the flux difference splitting method in multidimensional unsteady flows.' *AIAA Paper 84-0166, AIAA 22nd Aerospace Sciences Meeting*.
- Shapiro, A. H. (1953). *The Dynamics and Thermodynamics of Compressible Fluid Flow*, New York: Ronald Press.
- Sod, G. A. (1978). 'A survey of several finite difference methods for systems of nonlinear hyperbolic conservation laws.' *Journal Computational Physics*, **27**, 1–31.
- Warming, R. F., Beam, R. M., and Hyett, B. J. (1975). 'Diagonalization and simultaneous symmetrization of gas-dynamic matrices.' *Mathematics of Computation*, **29**, 1037.
- Whitham, G. B. (1974). *Linear and Nonlinear Waves*, New York: John Wiley and Sons.
- Zanetti, L., and Colasurdo, G. (1981). 'Unsteady compressible flow: a computational method consistent with the physical phenomena.' *AIAA Journal*, **19**, 852–56.
- Zucrow, M. J., and Hoffman, J. D. (1976). *Gas Dynamics*, Vols I and II, New York: John Wiley and Sons.

?
Narasimh
(1973)

PROBLEMS

Problem 16.1

Show that a vortex sheet discontinuity is always associated with a discontinuous density variation, implying a discontinuous entropy, if constancy of total enthalpy is assumed. Investigate the case $[s] = 0$ with $[H] \neq 0$.

Hint: Consider the possibility $[\rho] = 0$ and show that this implies $[s] = 0$ and $[\rho v_i^2] = 0$ from the relation between entropy and stagnation pressure and the definition of stagnation pressure as a function of Mach number.

Problem 16.2

Show that the flux hypervector \bar{F} can be written in a condensed form as

$$\bar{F} = \begin{vmatrix} \bar{m} \\ \bar{m} \otimes \frac{\bar{m}}{\rho} + pI \\ \bar{m} \cdot \left(\frac{\varepsilon}{\rho} + \frac{p}{\rho} \right) \end{vmatrix}$$

where

$$I = \begin{vmatrix} 1 & 0 & 0 \\ 0 & 1 & 0 \\ 0 & 0 & 1 \end{vmatrix} \equiv (I_x, I_y, I_z)$$

defines the three column vectors I_x, I_y, I_z as the matrix representation of the unit vectors $\bar{1}_x, \bar{1}_y, \bar{1}_z$:

$$I_x = \begin{vmatrix} 1 \\ 0 \\ 0 \end{vmatrix} \quad I_y = \begin{vmatrix} 0 \\ 1 \\ 0 \end{vmatrix} \quad I_z = \begin{vmatrix} 0 \\ 0 \\ 1 \end{vmatrix}$$

Obtain also the condensed form of the flux vector components

$$f = \begin{vmatrix} m \\ \bar{m} \cdot \frac{m}{\rho} + p \cdot I_x \\ \frac{m}{\rho} (\varepsilon + p) \end{vmatrix}$$

and similar relations for g and h :

$$g = \begin{vmatrix} n \\ \bar{m} \cdot \frac{n}{\rho} + p \cdot I_y \\ \frac{n}{\rho} (\varepsilon + p) \end{vmatrix}$$

$$h = \begin{vmatrix} l \\ \bar{m} \cdot \frac{l}{\rho} + p \cdot I_z \\ \frac{l}{\rho} (\varepsilon + p) \end{vmatrix}$$

Problem 16.3

Derive equations (16.2.22) to (16.2.25) for the components of the flux Jacobians in conservative variables.

Problem 16.4

Derive by a direct calculation the Jacobians B and C of the flux components g and h given in equations (16.2.27) and (16.2.28).

Problem 16.5

Derive the pressure equation in primitive ^{live} variables (16.2.38).

Problem 16.6

Show that the set of three Jacobian matrices in primitive variables (16.2.44) to (16.2.46) can be written as

$$\vec{A} = \begin{vmatrix} \bar{v} & \rho \bar{I}^T & 0 \\ 0 & \bar{v} \bar{I} & \frac{1}{\rho} \bar{I} \\ 0 & \rho c^2 \cdot \bar{I}^T & \bar{v}^T \end{vmatrix}$$

where the unit matrices are defined by

$$\bar{I}^T = |I_x^T, I_y^T, I_z^T|$$

with

$$I_x^T = (1, 0, 0) \quad I_y^T = (0, 1, 0) \quad I_z^T = (0, 0, 1)$$

Problem 16.7

Derive the explicit form of the transformation matrix between conservative and primitive variables (16.2.48) and its inverse (16.2.49).
p. 147

Problem 16.8

Derive the quasi-one-dimensional Euler equations for the flow in a nozzle of varying cross-section $S(x)$ for the conservative variable U , taking as the starting point the conservative form (16.4.1).
p. 158

Hint: Obtain the form

$$\begin{aligned} \frac{\partial \rho}{\partial t} + \frac{\partial(\rho u)}{\partial x} &= -\frac{1}{S} \frac{dS}{dx} \rho u \\ \frac{\partial(\rho u)}{\partial t} + \frac{\partial(\rho u^2 + p)}{\partial x} &= -\frac{1}{S} \frac{dS}{dx} \rho u^2 \\ \frac{\partial(\rho E)}{\partial t} + \frac{\partial(\rho u H)}{\partial x} &= -\frac{1}{S} \frac{dS}{dx} \rho u H \end{aligned}$$

Problem 16.9

Obtain the diagonalization matrix P^{-1} and its inverse P for the one-dimensional Euler equation, given by equations (16.4.11) and (16.4.12) by a direct calculation of the left eigenvectors of the Jacobian matrix A in conservative variables.

Problem 16.10

Obtain the matrix (16.5.13) of the right eigenvectors L in primitive variables by a direct determination of the right eigenvectors of the matrix \tilde{K} , following the procedure applied to obtain the left eigenvectors. Determine the normalization coefficients by the condition $LL^{-1} = 1$, using the form (16.3.29).

Problem 16.11

Obtain the matrices L^{-1} and L of the left and right eigenvectors of the matrix \tilde{K} in two dimensions by a direct determination of the eigenvectors. Fix the normalization constants such as to obtain equation (E16.4.5) and (E16.4.6).

Problem 16.12

Obtain the matrices L^{-1} and L of the left and right eigenvectors of the matrix \tilde{K} in two and three dimensions for the normalization $\mu^{(4)} = \mu^{(5)} = 1/\sqrt{2}$.

Problem 16.13

Calculate the matrix P of the right eigenvectors of the conservative Jacobians K , equation (16.5.23), by direct multiplication $P = ML$.

Obtain the same matrix by a direct computation of the eigenvectors of K .

Problem 16.14

Derive the matrices \bar{L} , \bar{P}^{-1} and \bar{P} associated with the choice defined by equations (16.5.29) and (16.5.30) for \bar{L}^{-1} by finding the right eigenvectors corresponding to the normalization (16.5.29).

Problem 16.15

Obtain the characteristic variables (16.5.48) and the characteristic form (16.5.49). Show that it reduces to equations (16.5.51) and (16.5.52) in the two-dimensional case.

Problem 16.16

Consider the quasi-one-dimensional system in the variables

$$U = \begin{pmatrix} \rho S \\ \rho u S \\ \rho E S \end{pmatrix}$$

and calculate the Jacobian of the source term with respect to U .

Hint: The Jacobian of the source term is given by

$$(\gamma - 1) \frac{1}{S} \frac{\partial S}{\partial x} \begin{vmatrix} 0 & 0 & 0 \\ \frac{u^2}{2} & -u & 1 \\ 0 & 0 & 0 \end{vmatrix}$$

Problem 16.17

Consider the quasi-one-dimensional system in the variables

$$X = \begin{vmatrix} \rho S \\ u S \\ p S \end{vmatrix}$$

and derive the Jacobian of the flux and of the source term.

Problem 16.18

Consider the stationary, two-dimensional supersonic isentropic flow analysed in Example 16.4.2. Work out all the equations and in particular the matrices of left and right eigenvectors.

Repeat the analysis when the continuity equation is added, leading to a system of four equations for the variables (ρ, u, v, p) . Show that the same eigenvalues are obtained with the first one appearing twice and derive the associated eigenvectors.

Show also that the additional characteristic equation expresses the constancy of entropy along the streamline.

Problem 16.19

Define the Jacobians, their eigenvalues and left and right eigenvectors for the quasi-one-dimensional Euler equations, written in the variables

$$X = \begin{vmatrix} s \\ c \\ u \end{vmatrix}$$

where c is the speed of sound and the entropy s has been non-dimensionalized by the specific heat coefficient c_v .

Obtain the compatibility relations and the source term as well as the characteristic variables and equations.

Derive the transformation matrix $Y = \partial U / \partial X$ between the X variables and the conservative variable U of Problem 16.16.

Hint: The entropy is defined as a function of p and ρ by the relation $ds/c_v = dp/p - \gamma d\rho/\rho$ and in non-dimensional form by $ds = dp/p - \gamma d\rho/\rho$.

The Jacobian matrix is

$$\begin{vmatrix} u & 0 & 0 \\ 0 & u & \frac{\gamma-1}{2}c \\ \frac{-c^2}{\gamma(\gamma-1)} & \frac{2c}{\gamma-1} & u \end{vmatrix}$$

The characteristic variables are

$$\delta w_1 = \delta s$$

$$\delta w_2 = \frac{2}{\gamma-1} \delta c + \delta u - \frac{c}{\gamma(\gamma-1)} \delta s$$

$$\delta w_3 = \frac{-2}{\gamma-1} \delta c + \delta u + \frac{c}{\gamma(\gamma-1)} \delta s$$

Problem 16.20

Define the Jacobians, their eigenvalues and left and right eigenvectors for the quasi-one-dimensional Euler equations, written in the variables

$$X = \begin{vmatrix} \rho \\ u \\ s \end{vmatrix}$$

where c is the speed of sound and the entropy s has been non-dimensionalized by the specific heat coefficient c_v .

Obtain the compatibility relations and source term as well as the characteristic variables and equations.

Derive the transformation matrix $Y = \partial U / \partial X$ between the X variables and the conservative variable U of Problem 16.16.

Hint: The Jacobian matrix is

$$\begin{vmatrix} u & \rho & 0 \\ \frac{c^2}{\rho} & u & \frac{c^2}{\gamma} \\ 0 & 0 & u \end{vmatrix}$$

and the matrix of the left eigenvectors

$$L^{-1} = \begin{vmatrix} 0 & 0 & 1 \\ c & \rho & \frac{c\rho}{\gamma} \\ -c & \rho & -\frac{c\rho}{\gamma} \end{vmatrix}$$

Problem 16.21

Define the Jacobians, their eigenvalues and left and right eigenvectors for the quasi-one-dimensional Euler equations, written in the variables

$$X = \begin{pmatrix} \rho \\ \rho u \\ p \end{pmatrix}$$

Obtain the compatibility relations and the source term as well as the characteristic variables and equations.

Derive the transformation matrix $Y = \partial U / \partial X$ between the X variables and the conservative variable U of Problem 16.16.

Hint: Obtain

$$A = \begin{pmatrix} 0 & 1 & 0 \\ -u^2 & 2u & 1 \\ -uc^2 & c^2 & u \end{pmatrix} \quad \Lambda = \begin{pmatrix} u & & \\ & u-c & \\ & & u+c \end{pmatrix}$$

$$L^{-1}AL = \Lambda \quad L^{-1} = \begin{pmatrix} 1 & 0 & -1/c^2 \\ \frac{u}{2c} & -\frac{1}{2c} & \frac{1}{2c^2} \\ \frac{u}{2c} & \frac{1}{2c} & \frac{1}{2c^2} \end{pmatrix}$$

$$L = \begin{pmatrix} 1 & 1 & 1 \\ u & u-c & u+c \\ 0 & c^2 & c^2 \end{pmatrix}$$

Problem 16.22

Define the Jacobians, their eigenvalues and left and right eigenvectors for the quasi-one-dimensional Euler equations, written in the variables

$$X = \begin{pmatrix} P \\ c \\ u \end{pmatrix}$$

where c is the speed of sound and P the logarithm of the pressure $P = \ln p$.

Obtain the compatibility relations and the source term as well as the characteristic variables and equations.

Derive the transformation matrix $Y = \partial U / \partial X$ between the X variables and the conservative variable U of Problem 16.16.

Problem 16.23

Consider the one-dimensional Euler equation for isenthalpic flows $H = H_0$.

By extracting the pressure from $H = H_0$, write the system of equations for the

variables

$$\begin{vmatrix} \rho \\ \rho u \end{vmatrix}$$

Calculate the eigenvalues and eigenvectors of the Jacobian matrix. Obtain the compatibility relations as well as the characteristic variables and equations.

Hint: The Jacobian matrix is

$$\begin{vmatrix} 0 & 1 \\ \frac{\gamma-1}{\gamma} H - \frac{\gamma+1}{2\gamma} u^2 & \frac{\gamma+1}{\gamma} u \end{vmatrix}$$

and has the eigenvalues

$$\lambda_{1,2} = \frac{\gamma+1}{2\gamma} u \pm b(u) \quad b^2(u) = \frac{\gamma-1}{\gamma} \left(H - \frac{\gamma+1}{4\gamma} u^2 \right)$$

The matrix of the left eigenvectors is

$$L^{-1} = \begin{vmatrix} -\lambda_2 & 1 \\ -\lambda_1 & 1 \end{vmatrix}$$

and the inverse matrix L , containing the right eigenvectors as columns, is

$$L = \begin{vmatrix} 1 & -1 \\ \lambda_1 & -\lambda_2 \end{vmatrix} \frac{1}{2b^2}$$

Problem 16.24

Define a transformation matrix P with columns, equal to the right eigenvectors of A , such that one can write

$$U = \sum_{j=1}^3 r^{(j)}$$

Hint: Choose the normalization coefficients α, β, δ in order to satisfy this property. Obtain $1/\alpha = \rho(\gamma-1)/\gamma$; $\beta = -\delta = \gamma/c$.

Problem 16.25

Write a program to solve the Riemann problem (shock tube problem) for the following initial data (all data in SI units) for air taken as a perfect gas with $\gamma = 1.4$:

$$\text{Case 1: } p_L = 10^5; \quad \rho_L = 1; \quad p_R = 10^4; \quad \rho_R = 0.125; \quad u_L = u_R = 0$$

$$\text{Case 2: } p_L = 10^5; \quad \rho_L = 1; \quad p_R = 5 \times 10^3; \quad \rho_R = 0.050; \quad u_L = u_R = 0$$

$$\text{Case 3: } p_L = 10^5; \quad \rho_L = 1; \quad p_R = 10^3; \quad \rho_R = 0.010; \quad u_L = u_R = 0$$

Generate plots of the x variation of pressure, density, entropy, Mach number, velocity and mass flux at fixed times. Take the initial position of the diaphragm at $x = 5$.

Hint: Solve the equation (16.6.45) for P with a Newton-Raphson method. Obtain the

following values:

$$\text{Case 1: } P = 3.031; \quad p_2 = 30313; \quad u_2 = 293; \quad C = 544$$

$$\text{Case 2: } P = 3.729; \quad p_2 = 18643; \quad u_2 = 399; \quad C = 684$$

$$\text{Case 3: } P = 7.155; \quad p_2 = 7155; \quad u_2 = 587; \quad C = 838$$

Problem 16.26

Write a program to calculate the exact solutions of the stationary flow in a diverging nozzle of cross-section

$$S(x) = 1.398 + 0.347 \tanh [0.8(x - 4)] \quad 0 \leq x \leq 10$$

Consider the following cases, with $T_0 = 300$ K and $p_{01} = 1$ bar and air considered as a perfect gas $\gamma = 1.4$:

Subsonic flow: $S^* = 0.8$ with a subsonic inlet Mach number

Supersonic flow: $S^* = 0.8$ with a supersonic inlet Mach number

Transonic flow with a shock at $x = 4$ and $S^* = 0.8$ and supersonic inlet Mach number

Hint: Solve equation (16.6.56) by a Newton–Raphson method and select an initial guess to be subsonic or supersonic according to the chosen solution. Note that all these cases are unchoked.

Problem 16.27

Write a program to calculate the exact solutions of the stationary flow in a converging–diverging nozzle of cross-section

$$S(x) = \begin{cases} 1 + 1.5 \left(1 - \frac{x}{5}\right)^2 & 0 \leq x \leq 5 \\ 1 + 0.5 \left(1 - \frac{x}{5}\right)^2 & 5 \leq x \leq 10 \end{cases}$$

Consider the following cases, with $T_0 = 300$ K and $p_{01} = 1$ bar and air considered as a perfect gas $\gamma = 1.4$:

Subsonic flow in the whole domain: $S^* = 0.8$

Subsonic flow in the whole nozzle with sonic velocity at the throat: $S^* = 1$ (select the subsonic branches at all points)

Subsonic–supersonic flow without shock: $S^* = 1$ (select the subsonic solution upstream of the throat and the supersonic solution downstream of the throat)

Supersonic flow in the whole domain: $S^* = 0.8$

Transonic flow with a shock at $x = 7$ with a subsonic inlet Mach number and $S^* = 1$

Transonic flow with a shock at $x = 7$ with a supersonic inlet Mach number and $S^* = 0.8$

Hint: Solve equation (16.6.56) by a Newton–Raphson method and select an initial guess to be subsonic or supersonic according to the chosen solution.

The cases with $S^* = 0.8$ are unchoked since the throat area corresponds to $S = 1$.

Problem 16.28

Define the Jacobians, their eigenvalues and left and right eigenvectors for the quasi-one-

dimensional Euler equations, written in the variables

$$X = \begin{vmatrix} p \\ u \\ s \end{vmatrix}$$

where c is the speed of sound and the entropy s has been non-dimensionalized by the specific heat coefficient c_v .

Obtain the compatibility relations and the source term as well as the characteristic variables and equations.

Derive the transformation matrix $Y = \partial U / \partial X$ between the X variables and the conservative variable U of Problem 16.16.

Hint: The Jacobian matrix is

$$Y = \begin{vmatrix} u & \rho c^2 & 0 \\ \frac{1}{\rho} & u & 0 \\ 0 & 0 & u \end{vmatrix}$$

and the matrix of the left eigenvectors is

$$L^{-1} = \begin{vmatrix} 0 & 0 & 1 \\ \frac{c}{2\gamma p} & \frac{1}{2} & 0 \\ \frac{c}{2\gamma p} & -\frac{1}{2} & 0 \end{vmatrix}$$

and the inverse matrix L is defined as

$$L = \begin{vmatrix} 0 & \frac{\gamma p}{c} & \frac{\gamma p}{c} \\ 0 & 1 & -1 \\ 1 & 0 & 0 \end{vmatrix}$$

Problem 16.29

Define the Jacobians, their eigenvalues and left and right eigenvectors for the quasi-one-dimensional Euler equations, written in the variables

$$X = \begin{vmatrix} \rho \\ c \\ M \end{vmatrix}$$

where c is the speed of sound and M is the Mach number.

Obtain the compatibility relations and the source term as well as the characteristic variables and equations.

Derive the transformation matrix $Y = \partial U / \partial X$ between the X variables and the conservative variable U of Problem 16.16.

Hint: The transformation matrix Y is defined by

$$Y = \begin{vmatrix} 1 & 0 & 0 \\ cM & \rho M & \rho c \\ E & \frac{2\rho E}{c} & \rho c^2 M \end{vmatrix}$$

where the total energy is written as $E = c^2[1/\gamma(\gamma - 1) + M^2/2]$.

Problem 16.30

Write the Rankine–Hugoniot relations in one dimension. Show that the Rankine–Hugoniot relations for a moving shock of velocity C are identical to the stationary shock relations (16.1.28) to (16.1.30) for the velocities $u_1 - C$ and $u_2 - C$.

Show that the pressure increase over the stationary shock is given by

$$[p] = \rho_1 \frac{\gamma + 1}{4} [u]^2 + \rho_1 [u] \left\{ \left(\frac{\gamma + 1}{4} \right)^2 [u]^2 + c_1^2 \right\}^{1/2}$$

where the subscripts 1 and 2 correspond to the regions upstream and downstream of the shock.

Problem 16.31

Derive the exact solution of Burgers equation for a block wave defined as

$$\begin{aligned} u &= u_0 & \text{for } x \leq 0 \\ u &= u_1 & \text{for } 0 \leq x \leq x_1 \\ u &= u_0 & \text{for } x \geq x_1 \end{aligned}$$

with $u_0 < u_1$.

Show that the exact solution is composed of an expansion (linear variation) followed by a shock. Show also that the initial square wave takes a triangular shape for all times after the expansion wave reaches the shock.

Hint: The top of the expansion moves at a speed u_1 and the shock at speed $(u_0 + u_1)/2$, while the foot of the expansion has a speed equal to u_0 .

Chapter 17

The Lax–Wendroff Family of Space-Centred Schemes

The space-centred algorithms for the Euler equations were historically the first to be derived and still form the basis and the reference for all the other schemes derived since then.

The second-order accurate scheme of Lax and Wendroff is the most important of them, due to its uniqueness for linear equations (it is the unique second-order central explicit scheme for the linear convection equation on a three-point support) and its essential role as the guideline for all schemes attempting to improve certain of its deficiencies. Since all centred second-order accurate schemes refer to the Lax–Wendroff algorithm, its weaknesses, such as the generation of oscillations at discontinuities, play an essential role in the understanding of the behaviour of centrally discretized schemes.

The essential property of the Lax–Wendroff schemes lies in the combination of time and space-centred discretizations. This is required in order to achieve second-order accuracy with an explicit time integration on a three-point support, and the Lax–Wendroff schemes are therefore the simplest explicit schemes of second-order accuracy.

Although this scheme is unique for the one-dimensional linear convection equation, many variants can be defined for non-linear fluxes, even in one dimension. They all reduce to the same linear form and are generally structured as predictor–corrector algorithms with an explicit time integration. However, implicit extensions have been developed and will be presented in Section 17.4.

We will consider in the following all centred explicit or implicit schemes of second-order accuracy with combined space–time discretization as belonging to the Lax–Wendroff family.

We will generally present the various schemes in their one-dimensional form and after a one-dimensional analysis we will introduce their multi-dimensional formulations and illustrate some properties by examples of applications.

The one-dimensional scalar, non-linear conservative form will be considered as

$$\frac{\partial u}{\partial t} + \frac{\partial f}{\partial x} = q$$

or in quasi-linear form as

$$\frac{\partial u}{\partial t} + a(u) \frac{\partial u}{\partial x} = q \quad \text{with } a(u) = \frac{\partial f}{\partial u}$$

When written as a system we will use U as the basic set of variables and $A(U)$ as the Jacobian matrix. Similar conventions apply to the multi-dimensional case.

The field of one-dimensional flows offers a wide test space for methods and algorithms for the numerical computation of inviscid, steady or unsteady flows. This is due to a combination of complexity of the one dimensional Euler equations, making them representative of the full non-linearity of real flows and of sufficient simplicity, allowing the existence of exact solutions for both stationary and time-dependent situations.

In addition, the idealized one-dimensional Burgers equation, $u_t + uu_x = 0$, and the even simpler case of the linearized, first-order wave equation, $u_t + au_x = 0$, offer non-trivial test cases for accuracy and convergence properties of numerical schemes for hyperbolic equations, particularly with regard to the extremely difficult problem of representing accurately propagating discontinuities such as shock waves or contact discontinuities; several examples were presented in Volume 1.

Nearly all existing schemes have initially been analysed and developed on a one-dimensional basis and a considerable literature on the properties of one-dimensional algorithms, including topics such as stability and dissipation properties, influence of boundary conditions on convergence and accuracy, treatment of discontinuities, etc., is available.

An existing scheme that behaves satisfactory on a one-dimensional basis might lead to difficulties in its extension to two- or three-dimensional flows. However, there is no example of a scheme that failed in the one-dimensional version and still worked well in its multi-dimensional extensions. It is therefore safe to say and to recommend that any scheme should first be tested on a one-dimensional basis before extending it to multi-dimensional problems.

An essential property of discretized schemes, already discussed in Section 6.1 in Volume 1, is the *conservative* property. Essentially, this property requires that the time derivative of the integral of U over a given space domain only depends on the boundary fluxes and not on the fluxes within this domain. This ensures that the discretization technique actually represents a discrete approximation to the integral form of the conservation laws.

The conservative property of a discretization leads to a unified formulation of a scheme by the introduction of a *numerical flux* \bar{F}^* , where \bar{F}^* is a function of mesh point values U_j with components f^* , g^* see Lax (1957). All conservative explicit schemes have to be expressed in the following form, written here in two dimensions:

$$U_{ij}^{n+1} - U_{ij}^n = \frac{-\Delta t}{\Delta x} (f_{i+1/2,j}^* - f_{i-1/2,j}^*) - \frac{\Delta t}{\Delta y} (g_{i,j+1/2}^* - g_{i,j-1/2}^*)$$

with the consistency condition

$$\begin{aligned} f^*(U_j, \dots, U_{j+k}) &= f(U) & \text{when all } U_j &= U \\ g^*(U_j, \dots, U_{j+k}) &= g(U) & \text{when all } U_j &= U \end{aligned}$$

In Section 17.1, we will introduce the first-order Lax–Friedrichs scheme which, although not belonging to the Lax–Wendroff family, has in common the combined space–time and space-centred discretization. Historically, it is the unsatisfactory behaviour of this scheme that has led Lax and Wendroff to search for a second-order discretization.

The other sections will be devoted to the analysis of the basic explicit Lax–Wendroff scheme in one and two dimensions, including the non-linear variant of MacCormack and their generalization by Lerat and Peyret.

Several properties of these schemes have already been introduced in Chapters 8 and 9 of Volume 1 for the linear scalar case and eventually for the Burgers equation, and we refer the reader to the appropriate sections for an introduction and stability analysis.

Section 17.3 will introduce the important concept of artificial viscosity or dissipation which plays an essential role in space-centred discretizations, particularly in the vicinity of strong gradients and discontinuities.

Section 17.4 will present the very interesting family of implicit variants of the Lax–Wendroff schemes developed by Lerat.

17.1 THE SPACE-CENTRED EXPLICIT SCHEMES OF FIRST ORDER

The family of schemes considered in this section are perhaps the first representatives of the modern developments in the field of numerical discretizations of the Euler equations. They are known as the schemes of Lax or Lax–Friedrichs (Lax, 1954).

They are not applied in their original form any longer, due to their poor first-order accuracy, but several variants with improved accuracy are still in use (see Section 17.1.3). They form, however, an interesting base for comparisons with other schemes, and can be used as intermediate step in higher-order schemes, as in the Richtmyer two-step variant of the second-order Lax–Wendroff method, to be discussed in Section 17.2.

17.1.1 The one-dimensional Lax–Friedrichs scheme

The basic idea behind this scheme is to stabilize the explicit, unstable central scheme obtained from a central differencing of the first derivative of the flux term.

When applied to the linearized convection equation $u_t + au_x = 0$, it has been shown in Chapter 7 in Volume 1 that the explicit scheme

$$u_i^{n+1} - u_i^n = -\frac{\sigma}{2}(u_{i+1}^n - u_{i-1}^n) \quad (17.1.1)$$

is unstable. The variable σ is the *Courant number*, also called the *CFL number*:

$$\sigma = \frac{a \Delta t}{\Delta x} \quad (17.1.2)$$

The stabilizing procedure consists of replacing u_i^n by $(u_{i+1}^n + u_{i-1}^n)/2$, leading to the scheme

$$u_i^{n+1} = \frac{1}{2}(u_{i+1}^n + u_{i-1}^n) - \frac{\sigma}{2}(u_{i+1}^n - u_{i-1}^n) \quad (17.1.3)$$

When applied to the conservative form $U_t + f_x = 0$, the Lax–Friedrichs scheme is

$$U_i^{n+1} = \frac{U_{i+1}^n + U_{i-1}^n}{2} - \frac{\tau}{2}(f_{i+1}^n - f_{i-1}^n) \quad (17.1.4)$$

where

$$\tau = \frac{\Delta t}{\Delta x} \quad (17.1.5)$$

Comparing equation (17.1.3) with equation (17.1.1) it is seen that the stabilization procedure of Lax corresponds to the addition of a *dissipative* term proportional to the second derivative of u . Equation (17.1.4) can also be written as

$$U_i^{n+1} = U_i^n - \frac{\tau}{2}(f_{i+1}^n - f_{i-1}^n) + \frac{1}{2}(U_{i+1}^n - 2U_i^n + U_{i-1}^n) \quad (17.1.6)$$

Since the last term between parentheses can be considered as the discretization of $(\Delta x^2/2\Delta t \cdot U_{xx})$, the Lax–Friedrichs scheme can be viewed as being obtained from an explicit Euler time integration of an equation of the form

$$\frac{\partial U}{\partial t} + \frac{\partial f}{\partial x} = \alpha \frac{\partial^2 U}{\partial x^2} \quad (17.1.7)$$

which is a *dissipative equation* with the numerical viscosity α .

This scheme has been analysed in Chapter 8 in Volume 1 for the linear convection equation and from the truncation error analysis, in the linearized case $f = aU$, with constant a :

$$\alpha = \frac{a}{2\sigma} \Delta x (1 - \sigma^2) = \frac{\Delta x^2}{2\Delta t} (1 - \sigma^2) \quad (17.1.8)$$

For a non-linear equation, one can deduce, from equations (9.4.21) and (9.4.24),

$$\alpha = \frac{\Delta x^2}{2\Delta t} (1 - \tau^2 a^2) + \frac{\Delta x^2}{2} (3\tau^2 a^2 - 1) a_U \cdot U_x \quad (17.1.9)$$

This shows that the system is first-order accurate at constant σ , that is for a fixed ratio $\Delta t/\Delta x$. For independent variations of Δx and Δt , one could consider the scheme to be second-order accurate in space and first-order accurate in time. In practice, however, one operates at a fixed Courant number, so that the Lax–Friedrichs scheme is to be considered as a first-order scheme in space and time. Equation (17.1.9) contains a non-linear contribution to the numerical

dissipation, under the form of a term proportional to $a_x = a_v \cdot U_x$ (the subscripts indicate partial derivatives).

Linearized stability analysis

It has been shown in Chapter 8 that the linearized, one-dimensional Lax–Friedrichs scheme is conditionally stable by a Von Neumann analysis, satisfying the Courant–Friedrichs–Lewy condition, in brief the *CFL condition*.

Applying the analysis to the linearized system $U_t + AU_x = 0$, for a finite Fourier mode k , with $\phi = k \Delta x$ with $I = \sqrt{-1}$, one obtains

$$G = \cos \phi - I \tau A \sin \phi \quad (17.1.10)$$

The eigenvalues $\lambda(G)$ of G are determined from

$$\lambda(G) = \cos \phi - I \frac{\Delta t}{\Delta x} \lambda(A) \sin \phi = |\lambda(G)| e^{I\Phi} \quad (17.1.11)$$

We define

$$\bar{\sigma} = \frac{\Delta t}{\Delta x} \lambda(A) \quad (17.1.12)$$

where $\lambda(A)$ is an eigenvalue of the Jacobian matrix A and the Courant number of the system is

$$\sigma = \frac{\Delta t}{\Delta x} \lambda(A)_{\max} \equiv \tau \rho(A) \quad (17.1.13)$$

The stability condition $\rho(G) \leq 1$ is satisfied for the CFL condition, since A has real eigenvalues:

$$\sigma = \frac{\Delta t}{\Delta x} \rho(A) = \frac{\Delta t}{\Delta x} |u + c| \leq 1 \quad (17.1.14)$$

where $\rho(A)$ is the spectral radius of the matrix A equal to $|u + c|$ for the system of one-dimensional Euler equations. This is a necessary and sufficient stability condition.

The dispersion and diffusion errors are obtained from the amplification matrix by separating the phase and the amplitude.

The error analysis can be performed on G , through the eigenvectors $\lambda(G)$, as shown in Chapter 8, where σ is defined by equation (17.1.13).

The phase Φ of G is given by

$$\tan \Phi = + \sigma \tan \phi \quad (17.1.15)$$

and the error in phase is obtained by the ratio of Φ and of the phase of the exact solution $\sigma \phi$. The relative phase error is

$$\varepsilon_\Phi = \frac{\tan^{-1}(\sigma \tan \phi)}{\sigma \phi} \quad (17.1.16)$$

Since ε_Φ is mostly greater than 1, in particular for $\phi = \pi/2$, $\varepsilon_\Phi = 1/\sigma$, the phase error is a leading error, namely the numerical computed waves propagate at a higher velocity than the physical waves, since the numerical phase speed $a_{\text{num}} = \Phi/(\kappa \Delta t) = a\Phi/\sigma\phi$ and the ratio of propagation speeds is equal to $a_{\text{num}}/a = \varepsilon_\Phi$.

The dissipation error is defined by

$$\varepsilon_D = |G| = (\cos^2 \phi + \sigma^2 \sin^2 \phi)^{1/2} \quad (17.1.17)$$

The highest damping occurs for $\phi = \pi/2$, that is in the mid-range frequencies with $|G|_{\text{min}} = \sigma$, and any discontinuity will be strongly smoothed out for low CFL numbers σ and therefore this scheme is not very accurate.

Observe that $\sigma = 1$ reproduces the exact solution $U_i^{n+1} = U_{i-1}^n$, since it corresponds to $G = 1$. Note also that, since $G(\pi) = 1$, the scheme is not dissipative in the sense of Kreiss.

Non-linear formulations

The general form of a conservative discretization is based on the introduction of numerical fluxes f^* , such that the scheme can be written under the form

$$U_i^{n+1} = U_i^n - \tau(f_{i+1/2}^{*n} - f_{i-1/2}^{*n}) \quad (17.1.18)$$

When compared to the formulation (17.1.4), one obtains

$$\begin{aligned} f_{i+1/2}^* &= \frac{1}{2}(f_i + f_{i+1}) - \frac{1}{2\tau}(U_{i+1} - U_i) \\ &= f_{i+1/2} - \frac{1}{2\tau}(U_{i+1} - U_i) \end{aligned} \quad (17.1.19)$$

as the numerical flux defining the Lax–Friedrichs scheme. Here $f_{i+1/2}$ is defined as $f_{i+1/2} = (f_i + f_{i+1})/2$, which is distinct from $f[(U_i + U_{i+1})/2]$ in the non-linear case.

In the steady-state limit, the numerical scheme solves for the balance of the numerical fluxes $f_{i+1/2}^* = f_{i-1/2}^*$ as an approximation to the balance of the physical fluxes $f_{i+1/2} = f_{i-1/2}$. The resulting stationary solution satisfies $f_{i+1/2} - f_{i-1/2} = (U_{i+1} - 2U_i + U_{i-1})/2\tau$ instead, and is dependent on the ratio $\tau = \Delta t/\Delta x$.

17.1.2 The two-dimensional Lax–Friedrichs scheme

Applied to the two-dimensional system of Euler equations, written as

$$\frac{\partial U}{\partial t} + \frac{\partial f}{\partial x} + \frac{\partial g}{\partial y} = 0 \quad (17.1.20)$$

the generalization of the one-dimensional scheme (17.1.4) is

$$U_{ij}^{n+1} = \frac{1}{4}(U_{i+1,j}^n + U_{i-1,j}^n + U_{i,j+1}^n + U_{i,j-1}^n) - \frac{\tau_x}{2}(f_{i+1,j}^n - f_{i-1,j}^n) - \frac{\tau_y}{2}(g_{i,j+1}^n - g_{i,j-1}^n) \quad (17.1.21)$$

where

$$\tau_x = \frac{\Delta t}{\Delta x} \quad \tau_y = \frac{\Delta t}{\Delta y} \quad (17.1.22)$$

This scheme can be represented by the stencil in Figure 17.1.1.

The linearized stability condition is obtained from the constant coefficient quasi-linear form

$$\frac{\partial U}{\partial t} + A \frac{\partial U}{\partial x} + B \frac{\partial U}{\partial y} = 0 \quad (17.1.23)$$

Applying a standard Von Neumann analysis, with $\phi_x = \kappa_x \Delta x$ and $\phi_y = \kappa_y \Delta y$, one obtains the amplification matrix

$$G = \frac{1}{2}(\cos \phi_x + \cos \phi_y) - IA\tau_x \sin \phi_x - IB\tau_y \sin \phi_y \quad (17.1.24)$$

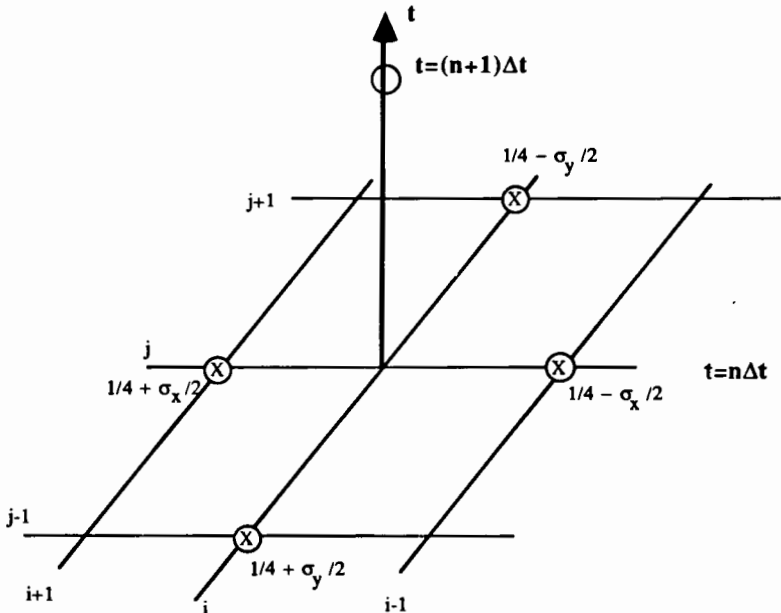


Figure 17.1.1 Computational stencil for the standard two-dimensional Lax-Friedrichs scheme applied to the linearized Euler equations

If the matrices A and B would commute (which is *not* the case for the Euler equations), they would have the same eigenvectors and one would obtain $\lambda(G)$ for the eigenvalues of G :

$$\lambda(G) = \frac{1}{2}(\cos \phi_x + \cos \phi_y) - I \frac{\Delta t}{\Delta x} \lambda(A) \sin \phi_x - I \frac{\Delta t}{\Delta y} \lambda(B) \sin \phi_y \quad (17.1.25)$$

Defining

$$\sigma_x = \frac{\Delta t}{\Delta x} \lambda(A)_{\max} \equiv \tau \rho(A) \quad \sigma_y = \frac{\Delta t}{\Delta y} \lambda(B)_{\max} \equiv \tau \rho(B) \quad (17.1.26)$$

$\lambda(A)_{\max}$ and $\lambda(B)_{\max}$ being the maximum eigenvalues of the Jacobians A and B , the necessary and sufficient stability condition, obtained in Chapter 8, Section 8.6.2, is

$$\sigma_x^2 + \sigma_y^2 \leq \frac{1}{2}$$

or

$$\frac{\Delta t^2}{\Delta x^2} (u+c)^2 + \frac{\Delta t^2}{\Delta y^2} (v+c)^2 \leq \frac{1}{2} \quad (17.1.27)$$

This is illustrated in Figure 17.1.2 in a diagram of σ_x and σ_y , where the stability region is inside a circle of radius $\sqrt{2}/2$.

When the matrices A and B do not commute, there are no general conditions known that are necessary and sufficient for the Von Neumann stability. However, some sufficient conditions can be obtained for A, B being *real symmetric* matrices. As seen in the previous chapter for the full system of Euler equations, the Jacobians A and B are not symmetric but a similarity trans-

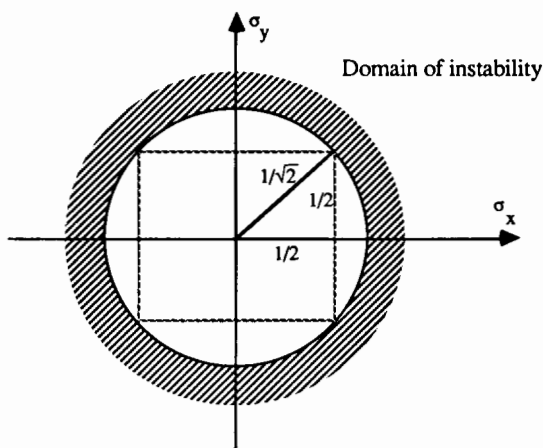


Figure 17.1.2 Two-dimensional Lax–Friedrichs scheme. Necessary and sufficient Von Neumann stability condition for commuting Jacobian matrices

formation S can be found, which simultaneously symmetrizes A and B (Turkel, 1973; Harten, 1983a); that is there exist non-singular matrices S such that

$$SAS^{-1} = A_0 \quad \text{and} \quad SBS^{-1} = B_0 \quad (17.1.28)$$

where A_0 and B_0 are symmetric matrices. In this case, the following conjecture has been made by Turkel (1977), which provides a guideline for obtaining sufficient conditions for stability in the non-commuting case:

Turkel's conjecture: If the amplification matrix G of a symmetric hyperbolic difference scheme is power bounded (that is the scheme is stable) for commuting matrices A, B, \dots , when their real eigenvalues are restricted to some subset R_s , then G is also power bounded for all real symmetric matrices having their eigenvalues restricted to the same subset R_s .

The scheme is said to be symmetric hyperbolic if G is symmetric, that is its real and imaginary parts are both real symmetric matrices. Within this conjecture, the above condition (17.1.27) can be considered as sufficient for stability of the Lax–Friedrichs scheme (17.1.21). Other sufficient conditions are summarized for a variety of explicit central schemes in Yanenko *et al.* (1984). For instance,

$$\sigma_x \leq \frac{1}{2} \quad \text{and} \quad \sigma_y \leq \frac{1}{2} \quad (17.1.29)$$

which is represented by the region inside the square of Figure 17.1.1.

A variant of the scheme (17.1.21) can be defined where the corner points of the mesh cell are used for the averaging term as in Figure 17.1.3 (Yanenko *et al.*, 1984):

$$\begin{aligned} U_{ij}^{n+1} = & \frac{1}{4}(U_{i+1,j+1}^n + U_{i+1,j-1}^n + U_{i-1,j+1}^n + U_{i-1,j-1}^n) \\ & - \frac{\tau_x}{4}(f_{i+1,j+1}^n + f_{i+1,j-1}^n - f_{i-1,j+1}^n - f_{i-1,j-1}^n) \\ & - \frac{\tau_y}{4}(g_{i+1,j+1}^n + g_{i-1,j+1}^n - g_{i+1,j-1}^n - g_{i-1,j-1}^n) \end{aligned} \quad (17.1.30)$$

or introducing the difference operators

$$\begin{aligned} \bar{\mu}_x U_{ij} &= \frac{1}{2}(U_{i+1,j} + U_{i-1,j}) & \bar{\mu}_y U_{ij} &= \frac{1}{2}(U_{i,j+1} + U_{i,j-1}) \\ \bar{\delta}_x U_{ij} &= \frac{1}{2}(U_{i+1,j} - U_{i-1,j}) & \bar{\delta}_y U_{ij} &= \frac{1}{2}(U_{i,j+1} - U_{i,j-1}) \end{aligned} \quad (17.1.31)$$

$$U_{ij}^{n+1} = \bar{\mu}_x \bar{\mu}_y u_{ij} - \bar{\tau}_x \bar{\mu}_y \delta_x^n f_{ij} - \bar{\tau}_y \bar{\mu}_x \delta_y^n g_{ij} \quad (17.1.32)$$

From Figure 17.1.3, it is seen that the modified scheme decouples the even- and odd-numbered mesh points. This could generate some oscillations; see Chapter 4 in Volume 1 for a discussion on this problem.

The linearized amplification matrix is (see Problem 17.2)

$$G = \cos \phi_x \cos \phi_y - I \sigma_x \sin \phi_x \cos \phi_y - I \sigma_y \cos \phi_x \sin \phi_y \quad (17.1.33)$$

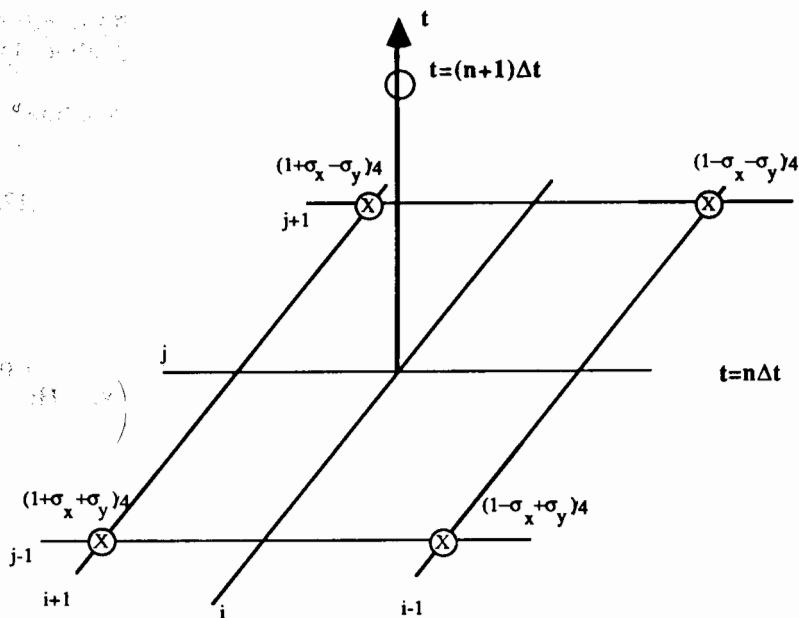


Figure 17.13 Computational stencil for the two-dimensional Lax–Friedrichs scheme (17.1.30)

and sufficient stability conditions are given by

$$\sigma_x \leq 1 \quad \text{and} \quad \sigma_y \leq 1 \quad (17.1.34)$$

increasing the stability range with respect to the original scheme (17.1.21).

17.1.3 Corrected viscosity scheme

An attempt to improve the accuracy of the Lax–Friedrichs scheme by achieving asymptotically second-order accuracy for steady-state problems has been introduced by McDonald (1971) and further analysed by Couston *et al.* (1975).

In the one-dimensional case, the quantity $(\beta \Delta x^2 / \Delta t) u_{xx}$ is subtracted from the right-hand side of equation (17.1.7), leading to a scheme

$$u_i^{n+1} = u_i^n - \frac{\tau}{2}(f_{i+1}^n - f_{i-1}^n) + \frac{1}{2}(u_{i+1}^n - 2u_i^n + u_{i-1}^n) - \frac{\beta}{2}(u_{i+1}^l - 2u_i^l + u_{i-1}^l) \quad (17.1.35)$$

where the last term is updated every N iterations; that is l is kept constant between two updatings and set equal to $l = N \cdot \text{mod}(n, N)$, where $\text{mod}(n, N)$ is the integer part of n/N .

When this term is not updated, the scheme has the properties of the original Lax scheme, but the solution is regularly corrected every N iterations for the accumulated truncation error.

The solution of the difference equation converges to the solution of the corrected equation

$$u_t + f_x = (1 - \beta - \sigma^2) \frac{\Delta x^2}{2\Delta t} u_{xx} \quad (17.1.36)$$

and if the coefficient β is chosen as $\beta = 1 - \sigma^2 - O(\Delta x)$, the final accuracy will approach second order. An improvement in accuracy is obtained, however calibrations of N and β are required. In particular, the corrected scheme is linearly stable only if N is larger than the maximum number of mesh points on the x axis. The interested reader will find more details in Van Hove and Arts (1979). Note that the Lax–Friedrichs version of McDonald (1971) is probably the first application of a finite volume method to the Euler equations (see Problem 17.3).

Another scheme based on a first-order discretization with corrected viscosity in order to approach second-order accuracy has been developed by Denton (1975, 1982) and is widely used in the field of internal turbomachinery flows.

17.2 THE SPACE-CENTRED EXPLICIT SCHEMES OF SECOND ORDER

The second-order space-centred explicit schemes are all derived from the basic Lax–Wendroff scheme (1960). It has already been shown in Chapter 9 in Volume 1 that this scheme is the unique second-order space-centred discretization on the three-point support $(i-1, i, i+1)$ for the linear one-dimensional convection equation. Therefore, the numerous variants of the Lax–Wendroff scheme differ in the treatment of the non-linearities and in their multi-dimensional aspects, but reduce to the same linearized, one-dimensional form.

The popularity of these schemes, and in particular the two-step version of MacCormack (1969), is due to their second-order accuracy and simplicity, although their behaviour around discontinuities is not fully satisfactory.

We will review first the one-dimensional, linear and non-linear versions of the Lax–Wendroff schemes (Sections 17.2.1, 17.2.2 and 17.2.3) and then discuss in Sections 17.2.4 and 17.2.5 the two-dimensional extensions.

17.2.1 The basic one-dimensional Lax–Wendroff scheme

The idea behind the Lax–Wendroff scheme is to stabilize the unstable central scheme (17.1.1), while obtaining second-order accuracy in space and time. A close look at the origin of the instability of this scheme shows that it is due to the combination of a first-order time difference with a second-order space discretization of the flux term.

Indeed, developing equation (17.1.1) in a Taylor series, gives a truncation error of the form

$$u_t + au_x = -\frac{\Delta t}{2} u_{tt} + O(\Delta x^2, \Delta t^2) \quad (17.2.1)$$

leading to a negative numerical viscosity.

Hence, if the term $\Delta t u_{tt}/2$ is added to the left-hand side, the truncation error would be of second order in Δx and Δt .

The basic approach is therefore as follows: in the time series development

$$U^{n+1} = U^n + \Delta t U_t + \frac{\Delta t^2}{2} U_{tt} + \frac{\Delta t^3}{6} U_{ttt} \quad (17.2.2)$$

the Δt^2 term is maintained and replaced by the space derivative term

$$\frac{\partial^2 U}{\partial t^2} = -\frac{\partial^2 f}{\partial x \partial t} = -\frac{\partial}{\partial x} \left(A \frac{\partial U}{\partial t} \right) = \frac{\partial}{\partial x} \left(A \frac{\partial f}{\partial x} \right) \quad (17.2.3)$$

where the Jacobian $A = \partial f / \partial U \equiv f_U$ is introduced.

Equation (17.2.2) becomes

$$U^{n+1} = U^n - \Delta t \frac{\partial f}{\partial x} + \frac{\Delta t^2}{2} \frac{\partial}{\partial x} \left(A \frac{\partial f}{\partial x} \right) + O(\Delta t^3) \quad (17.2.4)$$

and is discretized at point i with second-order central differences, leading to the *one-step* non-linear version of the Lax-Wendroff scheme:

$$U_i^{n+1} = U_i^n - \frac{1}{2} \tau (f_{i+1}^n - f_{i-1}^n) + \frac{1}{2} \tau^2 [A_{i+1/2}^n (f_{i+1}^n - f_i^n) - A_{i-1/2}^n (f_i^n - f_{i-1}^n)] \quad (17.2.5a)$$

with

$$A_{i+1/2} = A(U_{i+1/2}) \quad (17.2.5b)$$

or

$$A_{i+1/2} = \frac{1}{2} (A_i + A_{i+1}) \quad (17.2.5c)$$

The linearized form can be written as

$$u_i^{n+1} = u_i^n - \frac{1}{2} \sigma (u_{i+1}^n - u_{i-1}^n) + \frac{1}{2} \sigma^2 (u_{i+1}^n - 2u_i^n + u_{i-1}^n) \quad (17.2.6)$$

Equation (17.2.5a) can also be written in conservative form as the difference in numerical fluxes f^* :

$$U_i^{n+1} - U_i^n = -\tau (f_{i+1/2}^* - f_{i-1/2}^*) \quad (17.2.7)$$

with

$$f_{i+1/2}^* = f_{i+1/2} - \frac{\tau}{2} A_{i+1/2} (f_{i+1} - f_i) \quad (17.2.8)$$

$$f_{i+1/2} = \frac{f_i + f_{i+1}}{2}$$

Introducing the compact difference notations defined in Chapter 4,

$$\begin{aligned}\delta U_i &= U_{i+1/2} - U_{i-1/2} \\ \mu U_i &= \frac{U_{i+1/2} + U_{i-1/2}}{2} \\ \delta^+ U_i &= U_{i+1} - U_i \\ \delta^- U_i &= U_i - U_{i-1}\end{aligned}\tag{17.2.9}$$

the Lax–Wendroff scheme can be rewritten as follows:

$$U_i^{n+1} - U_i^n = -\tau \bar{\delta} f_i^n + \frac{1}{2} \tau^2 \delta^+ (A_{i-1/2} \delta^- f_i^n)\tag{17.2.10}$$

or

$$U_i^{n+1} - U_i^n = -\tau \bar{\delta} f_i^n + \frac{1}{2} \tau^2 \delta (A_i \delta f_i^n)\tag{17.2.11}$$

The stability conditions for the Lax–Wendroff scheme are obtained from a linearized Von Neumann analysis, leading to the amplification matrix

$$G = 1 - I\tau A \sin \phi - \tau^2 A^2 (1 - \cos \phi)\tag{17.2.12}$$

The stability condition on the spectral radius of G requires the computation of its eigenvalues $\lambda(G)$:

$$\rho(G) = \lambda(G)_{\max} = 1 - I\sigma \sin \phi - \sigma^2 (1 - \cos \phi)\tag{17.2.13}$$

defining σ by

$$\sigma = \frac{\Delta t}{\Delta x} \lambda(A)_{\max}\tag{17.2.14}$$

In the complex $\lambda(G)$ plane, this represents an ellipse centred on the real axis at the abscissa $(1 - \sigma^2)$ with a semi-axis of σ^2 along the real axis and σ along the vertical axis, leading to the CFL condition (see Chapter 8). We recall here that for the Euler equations, the CFL condition is to be applied to the highest eigenvalue ($u + c$). The modulus of the amplification factor is given by

$$|\rho(G)|^2 = 1 - 4\sigma^2(1 - \sigma^2) \sin^2 \frac{\phi}{2}\tag{17.2.15}$$

and the phase Φ is defined by

$$\tan \Phi = \frac{\sigma \sin \phi}{1 - 2\sigma^2 \sin^2 \phi/2}\tag{17.2.16}$$

The relative phase error

$$\varepsilon_\phi = \frac{\Phi}{\sigma \phi}\tag{17.2.17}$$

is mostly lower than one, indicating a dominating lagging phase error. The highest frequencies, corresponding to $\phi = \pi$, are damped by a factor $|G|_\pi = 1 - 2\sigma^2$, while the phase angle ϕ goes to zero if $\sigma^2 < \frac{1}{2}$ and tends to π if $\sigma^2 > \frac{1}{2}$.

At low CFL values, for $\sigma^2 < \frac{1}{2}$, the phase error is the largest at the high frequencies, since $\varepsilon_\phi = 0$ for $\phi = \pi$. Hence, this will tend to accumulate the high-frequency errors generated at a discontinuity and oscillations will appear, for instance for a propagating discontinuity, since the phase error indicates a lagging computed phase.

The truncation error of the Lax–Wendroff scheme is, in the linear case,

$$\begin{aligned} \varepsilon_T &= -\frac{\sigma^2}{6} u_{iii} - \frac{\Delta x^3}{6} \frac{\sigma}{\Delta t} u_{xxx} = \frac{\Delta x^3}{6} (1 - \sigma^2) u_{xxt} \\ &= \frac{-\Delta x^2 a}{6} (1 - \sigma^2) u_{xxx} \end{aligned} \quad (17.2.18)$$

The equivalent equation has now a dispersive term in the right-hand side. The dissipation of the scheme is of fourth order, since for small $\phi = k \Delta x$, one has, from equation (17.2.15),

$$|\rho(G)|^2 \simeq 1 - \frac{\sigma^2}{4} (1 - \sigma^2) \phi^4 \quad (17.2.19)$$

showing that the Lax–Wendroff scheme is dissipative to the fourth order, in the sense of Kreiss, for $0 < \sigma < 1$.

Non-linear variant

The non-linear formulation of the Lax–Wendroff scheme requires the evaluation of the Jacobian $A_{i+1/2}$, defined by equation (17.2.5b) or (17.2.5c). However, other definitions are possible, leading to alternative, non-linear variants of the basic scheme (17.2.5a). Instead of evaluating analytically the Jacobian A and calculating its values at $U_{i+1/2} = (U_i + U_{i+1})/2$, one can perform a direct numerical evaluation of $A_{i+1/2}$ by the following formula (Roe, 1981; Harten, 1983b):

$$A_{i+1/2} = \begin{cases} \frac{f_{i+1} - f_i}{U_{i+1} - U_i} & \text{if } U_{i+1} - U_i \neq 0 \\ A(U_i) & \text{if } U_{i+1} = U_i \end{cases} \quad \begin{array}{l} \text{for vector equations} \\ \text{this must be rewritten} \\ A_{i+1/2}(U_{i+1}, U_i) = f_{i+1} - f_i \\ (17.2.20) \end{array}$$

With this definition, the Lax–Wendroff scheme takes the form

$$U_i^{n+1} = U_i^n - \frac{\tau}{2} (f_{i+1}^n - f_{i-1}^n) + \frac{1}{2} \tau^2 [A_{i+1/2}^2 (U_{i+1}^n - U_i^n) - A_{i-1/2}^2 (U_i^n - U_{i-1}^n)] \quad (17.2.21)$$

and the associated numerical flux becomes, instead of (17.2.8),

$$f_{i+1/2}^* = f_{i+1/2} - \frac{\tau}{2} A_{i+1/2}^2 (U_{i+1} - U_i) \quad (17.2.22)$$

In order to generalize the above definition of $A_{i+1/2}$ to non-linear systems of equations, one can apply a decomposition in simple waves of the form (16.3.40):

$$\delta U_{i+1/2} = U_{i+1} - U_i = \sum_k \delta w_{i+1/2}^k r_{i+1/2}^k \quad (17.2.23)$$

where r^k are the right eigenvectors of the Jacobian matrix A and δw^k are the characteristic variables.

The operator $A_{i+1/2}^2(U_{i+1} - U_i)$ is decomposed as

$$A_{i+1/2}^2(U_{i+1} - U_i) = \sum_k (a_{i+1/2}^k)^2 \delta w_{i+1/2}^k r_{i+1/2}^k \quad (17.2.24)$$

This can be realized in a most natural way by the linearization introduced by Roe (1981) (see Section 20.5.3), where a Jacobian matrix $A_{i+1/2}$ is defined which satisfies *exactly* the numerical relation

$$f_{i+1} - f_i = A_{i+1/2}(U_{i+1} - U_i) \quad (17.2.25)$$

with

$$A_{i+1/2} = A_{i+1/2}(U_i, U_{i+1})$$

such that

$$A_{i+1/2}(U_i, U_i) = A(U_i) \quad (17.2.26)$$

17.2.2 The two-step Lax–Wendroff schemes in one dimension

The scheme represented by equation (17.2.5a) requires the evaluation of the Jacobian matrices A , which can be a costly operation in practical computations. Hence a two-step procedure has been introduced by Richtmyer and Morton (1967) that avoids the estimation of the Jacobians. This scheme, known as the *Richtmyer scheme*, is at the basis of many modern two-step predictor–corrector methods which are able to handle non-linearities in a straightforward way.

An intermediate state is introduced which can be considered as the solution at a time $t = (n + \frac{1}{2})\Delta t$, followed by a second step which brings the solution to the final time step $t = (n + 1)\Delta t$. Richtmyer's scheme is then defined as

$$\begin{aligned} U_{i+1/2}^{n+1/2} &= \frac{1}{2}(U_i^n + U_{i+1}^n) - \frac{\tau}{2}(f_{i+1}^n - f_i^n) \\ U_i^{n+1} &= U_i^n - \tau(f_{i+1/2}^{n+1/2} - f_{i-1/2}^{n+1/2}) \end{aligned} \quad (17.2.27)$$

The first step is identical to the Lax–Friedrichs scheme (LF) applied to the mid-point ($i + \frac{1}{2}$) between times n and $(n + \frac{1}{2})$, while the second step is a leapfrog scheme, applied at $(n + \frac{1}{2})$ (see Figure 17.2.1).

This second step is of second-order accuracy at the points $(i, n + \frac{1}{2})$, while the first step has first-order accuracy at the points $(i + \frac{1}{2}, n + \frac{1}{2})$ at fixed Courant number. Globally, the two-step scheme is second order in space and time at $(i, n + 1)$. It is easily seen that in the linear case $f = a \cdot u$, the two-step scheme becomes identical to the single-step Lax–Wendroff scheme equation (17.2.6).

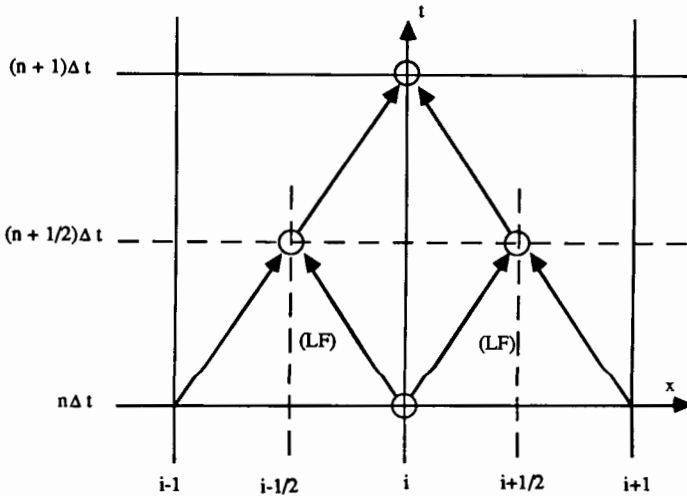


Figure 17.2.1 Computational stencil for the two-step Richtmyer variant of the Lax-Wendroff scheme

MacCormack's scheme

The two-step predictor-corrector scheme of MacCormack (1969) is another version of the Lax-Wendroff discretization to which it becomes identical in the linear case. This scheme is probably the most widely applied version of the Lax-Wendroff schemes. Predictor values are defined at $(n+1)$ and point i , followed by a corrector step, where $\bar{f}_i = f(\bar{U}_i)$:

$$\begin{aligned}\bar{U}_i &= U_i^n - \tau(f_{i+1}^n - f_i^n) \\ U_i^{n+1} &= \frac{1}{2}(U_i^n + \bar{U}_i) - \frac{\tau}{2}(\bar{f}_i - \bar{f}_{i-1})\end{aligned}\quad (17.2.28)$$

This scheme has been introduced in a linearized version in Chapter 11 in Volume 1.

The first step is a first-order forward discretization in space, which is actually unstable for positive eigenvalues of A , that is for supersonic velocities.

The second, corrector, step is a backward first-order scheme, which will be unstable for negative characteristic speeds of propagation, that is for subsonic flows. However, the overall combined scheme is stable and of second order due to the cancellations of the truncation errors of each step.

MacCormack's scheme can be written more explicitly in a predictor-corrector sequence where the symmetry between the two steps is more apparent:

$$\bar{U}_i = U_i^n - \tau(f_{i+1}^n - f_i^n) \quad (17.2.29a)$$

$$\bar{\bar{U}}_i = U_i^n - \tau(\bar{f}_i - \bar{f}_{i-1}) \quad (17.2.29b)$$

Updating gives

$$U_i^{n+1} = \frac{1}{2}(\bar{U}_i + \bar{\bar{U}}_i) \quad (17.2.29c)$$

An alternative is to reverse the order of the predictor and the corrector:

$$\text{Predictor:} \quad \bar{U}_i = U_i^n - \tau(f_i^n - f_{i-1}^n) \quad (17.2.30a)$$

$$\text{Corrector:} \quad \bar{\bar{U}}_i = U_i^n - \tau(\bar{f}_{i+1} - \bar{f}_i) \quad (17.2.30b)$$

$$\text{Updating:} \quad U_i^{n+1} = \frac{1}{2}(\bar{U}_i + \bar{\bar{U}}_i) \quad (17.2.30c)$$

Note that, for non-linear problems, the three versions (17.2.27), (17.2.29) and (17.2.30) will lead to different results, although they are identical on linear problems.

Since the predictor of the version (17.2.30) only transmits downwind influences, an error generated at a shock discontinuity, for instance, will tend to propagate downstream. Hence, this version will be better adapted for discontinuities moving from right to left, while the version (17.2.29) might be more suitable in the opposite situation. This is confirmed by Lerat and Peyret (1975), where it is shown that this choice gives the best non-linear dissipation properties. However, this can be strongly dependent on the way the boundary conditions are treated and on the presence of artificial viscosity.

When the boundary conditions are applied at the downstream end of the x domain the predictor of (17.2.30) will treat the last point in the same way as all the others, while a numerical boundary condition will be imposed in this point at the corrector sequence. Similar situations occur at the other end of the interval with the predictor and corrector roles inverted.

The MacCormack schemes can also be written for the variations ΔU , as follows for the version (17.2.29):

$$\overline{\Delta U}_i = -\tau \cdot \delta^+ f_i^n \quad (17.2.31a)$$

$$\overline{\overline{\Delta U}}_i = -\tau \cdot \delta^- \bar{f}_i \quad (17.2.31b)$$

$$\Delta U_i \equiv U_i^{n+1} - U_i^n = \frac{1}{2}(\overline{\Delta U}_i + \overline{\overline{\Delta U}}_i) = -\frac{\tau}{2}[f_{i+1}^n - f_i^n + \bar{f}_i - \bar{f}_{i-1}] \quad (17.2.31c)$$

where $\overline{\Delta U}$ is the predictor variation ($\bar{U} - U^n$), $\overline{\overline{\Delta U}}$ is the corrector variation ($\bar{\bar{U}} - U^n$) and ΔU the global variation of the solution over one full step.

A similar form is obtained for scheme (17.2.30) by interchanging the forward and backward differences. Equation (17.2.31c) shows that the MacCormack schemes are in the conservation form with the numerical fluxes $f_{i+1/2}^*$ equal to

$$\begin{aligned} f_{i+1/2}^* &= \frac{1}{2}(\bar{f}_i + f_{i+1}^n) \\ &= \frac{1}{2}[f(U_{i+1}^n) + f^n[U_i - \tau(f_{i+1}^n - f_i^n)]] \\ &= f_{i+1/2} - \frac{\tau}{2}A_{i+1/2}(f_{i+1} - f_i) + O(\Delta t^2) \end{aligned} \quad (17.2.32)$$

It is of importance to notice here that the steady-state solution satisfies the balance of the numerical flux f^* :

$$f_{i+1/2}^* = f_{i-1/2}^*$$

or from (17.2.32), for scheme (17.2.29),

$$f_{i+1} + f[U_i - \tau(f_{i+1} - f_i)] = f_i + f[U_{i-1} - \tau(f_i - f_{i-1})]$$

The steady-state solution will therefore depend on the time step Δt , $\tau = \Delta t/\Delta x$. This is considered as a drawback, since it introduces a dependence on a non-physical parameter unless the predictor and the corrector converge separately to the steady state. This is, however, not the case generally.

Indeed, if the predictor step would converge to zero residual, that is to $\bar{U}_i = U_i^n$, implying $f_i = f_{i+1}$, the residual of the corrector step would be proportional to $(f_{i+1} - f_{i-1})$ and of the order of the truncation error. Hence, the final residual after the two steps is

$$\Delta U_i = U_i^{n+1} - U_i = -\Delta t \cdot R_i^n \equiv -\tau(f_{i+1/2}^* - f_{i-1/2}^*)$$

where R^n is the difference of the numerical fluxes and will not necessarily converge to machine zero but may remain at the level of the truncation error of the discretization.

Predictor-corrector sequences using the same operator for each step will not be subject to this problem and the residual will be able to converge to machine zero. This in turn will lead to the same steady-state solution, independent of the time step size Δt .

Example 17.2.1 MacCormack scheme for the Euler equations with source term

The quasi-one-dimensional Euler equations for the flow in a nozzle of varying cross-section $S(x)$ are given by equation (16.4.1). The adaptation of the scheme (17.2.29) to a system with a source term can be done in a straightforward way. Denoting by Q the source term vector for the system

$$\frac{\partial U}{\partial t} + \frac{\partial f}{\partial x} = Q \quad (\text{E17.2.1})$$

the scheme (17.2.29) is extended as follows:

$$\bar{U}_i = U_i^n - \tau(f_{i+1}^n - f_i^n) + \Delta t Q_i^n \quad (\text{E17.2.2a})$$

$$\bar{\bar{U}}_i = U_i^n - \tau(\bar{f}_i - \bar{f}_{i-1}) + \Delta t \bar{Q}_i \quad (\text{E17.2.2b})$$

Updating gives

$$U_i^{n+1} = \frac{1}{2}(\bar{U}_i + \bar{\bar{U}}_i) \quad (\text{E17.2.2c})$$

In the corrector step the source term is evaluated as $\bar{Q} = Q(\bar{U})$. With the numerical flux (17.2.32) the scheme can be written as

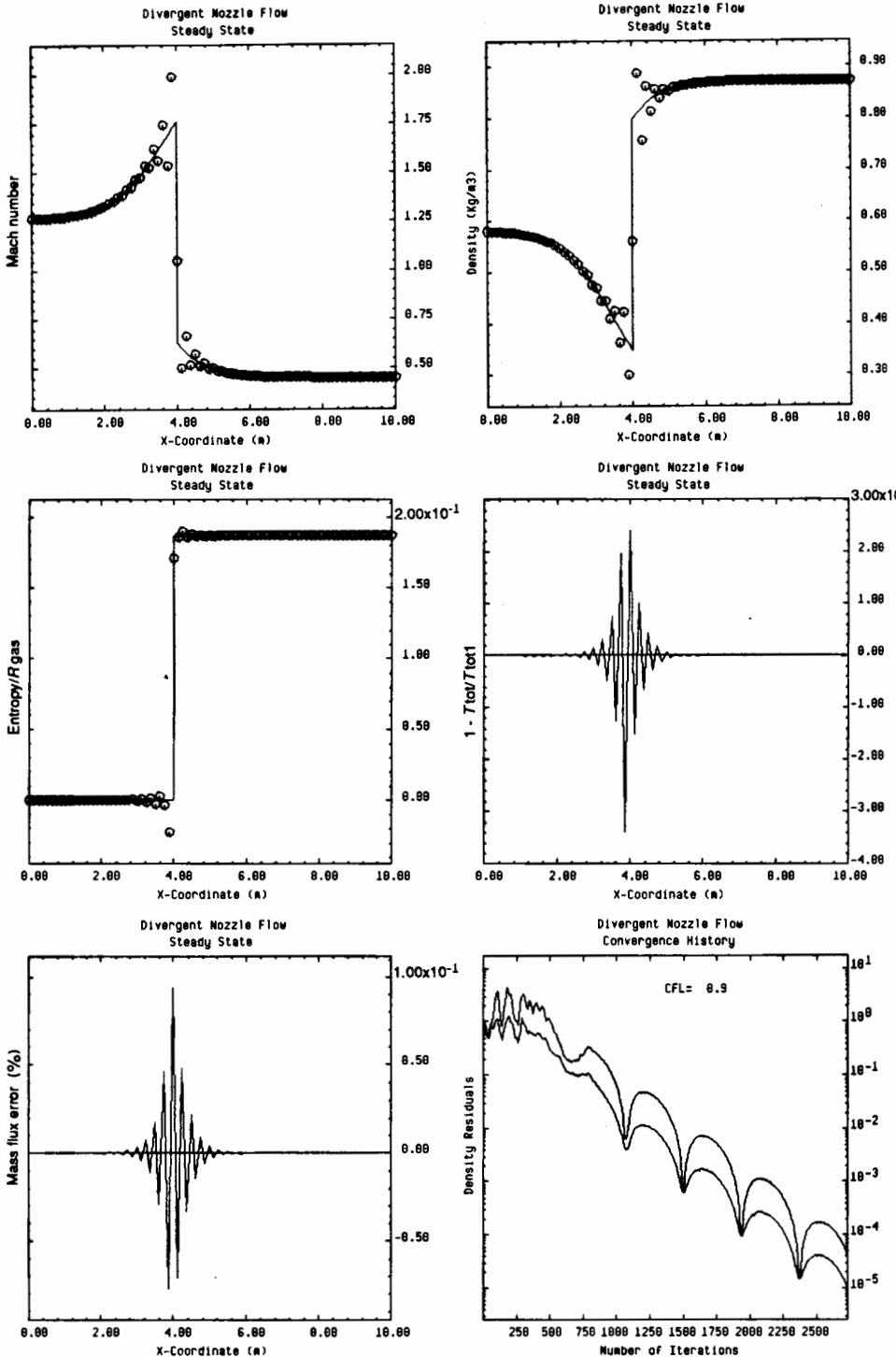


Figure 17.2.2 Results of MacCormack's scheme applied to the stationary flow in a diverging nozzle with 81 mesh points at CFL = 0.9. Calculated results ooo Exact solution —

$$\Delta U_i = U_i^{n+1} - U_i^n = -\tau(f_{i+1/2}^* - f_{i-1/2}^*) + \frac{\Delta t}{2}(Q_i^n + \bar{Q}_i) \quad (\text{E17.2.3})$$

See also Problem 17.11 for a formulation of the one-step Lax–Wendroff scheme in the presence of source terms.

Figure 17.2.2 shows a computation of the stationary transonic flow in the diverging nozzle of Problem 16.26 with MacCormack's scheme (17.2.29) at a Courant number of 0.9 with 81 mesh points. Results for Mach number, density, entropy and stagnation temperature variations are plotted as a function of distance, next to the exact solution shown by a continuous line. Figure 17.2.2 also displays the streamwise evolution of the error in mass flux, expressed as a percentage of the exact value $(\rho u)_{\text{ex}}$. The plotted quantity is $[(\rho u)/(\rho u)_{\text{ex}} - 1]$ as a percentage. The convergence history is also shown via the L_2 and max norms of the density residuals.

As can be observed, excellent accuracy is obtained in the smooth regions, but strong oscillations appear around the shock. The plots of entropy and stagnation temperature are very instructive with regard to the hidden deficiencies or qualities of a scheme, since both are derived quantities. Entropy should remain constant everywhere with the exception of the discontinuity, while stagnation temperature has to remain constant for stationary flows, even over discontinuities. The errors occurring in the shock region are an indication of the way the scheme treats discontinuous variations, and in the present case the behaviour of the mass flux error is an additional indication of the generated high-frequency oscillations.

This is typical of all the central second-order algorithms and requires the introduction of some mechanism to damp the high-frequency errors generated at discontinuities.

Figure 17.2.3 presents a computation of the unsteady shock tube flow with the same version of MacCormack's scheme (17.2.29) at CFL = 0.95 after 35 time steps.

This test case corresponds to the data of Figure 16.6.8 and shows an expansion shock at the original position ($x = 5$) of the diaphragm, where sonic conditions would occur if the expansion fan would reach this location. The acceleration phase through the expansion fan comes close enough to sonic velocities, as can be seen from the Mach number distribution, to generate the expansion shock. This is due to the lack of dissipation of the scheme at the points where the Courant number goes to zero (see equation (17.2.13)). This equation shows indeed that the eigenvalues of the amplification matrix are equal to one when the eigenvalues of the Jacobian matrix vanish, that is for sonic conditions. Hence there is no mechanism to ensure the increase in entropy required by the second law of thermodynamics. This is confirmed by the entropy diagram in Figure 17.2.3, showing no entropy variation over the expansion shock at $x = 5$.

Similar results are obtained in Figure 17.2.4 which displays the computations for the test case of Figure 16.6.9, corresponding to an expansion fan acceleration

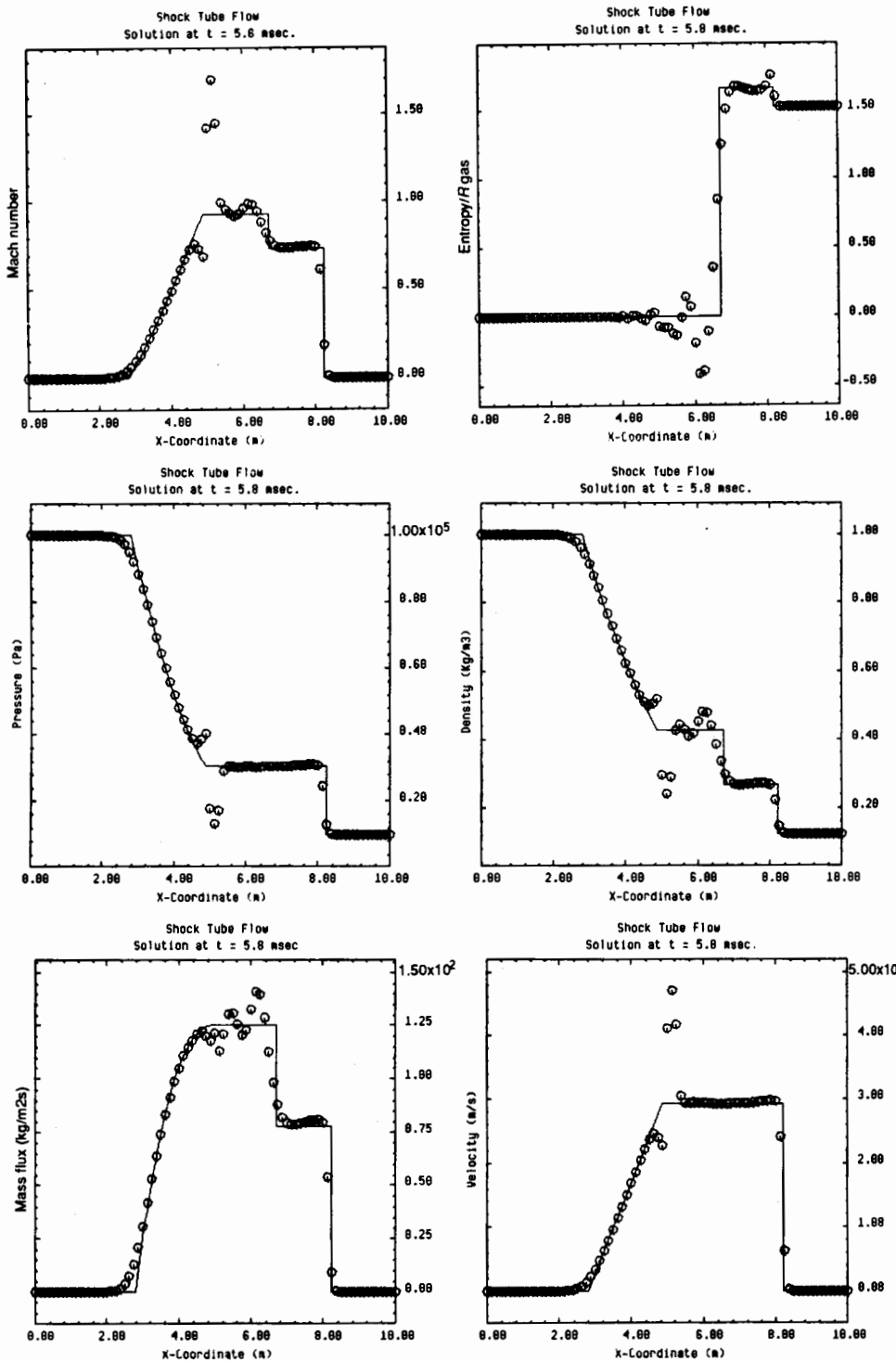


Figure 17.2.3 Results of MacCormack's scheme applied to the shock tube problem of Figure 16.6.8, with 81 mesh points at $CFL = 0.95$ after 35 time steps. Calculated results ○○ Exact solution —

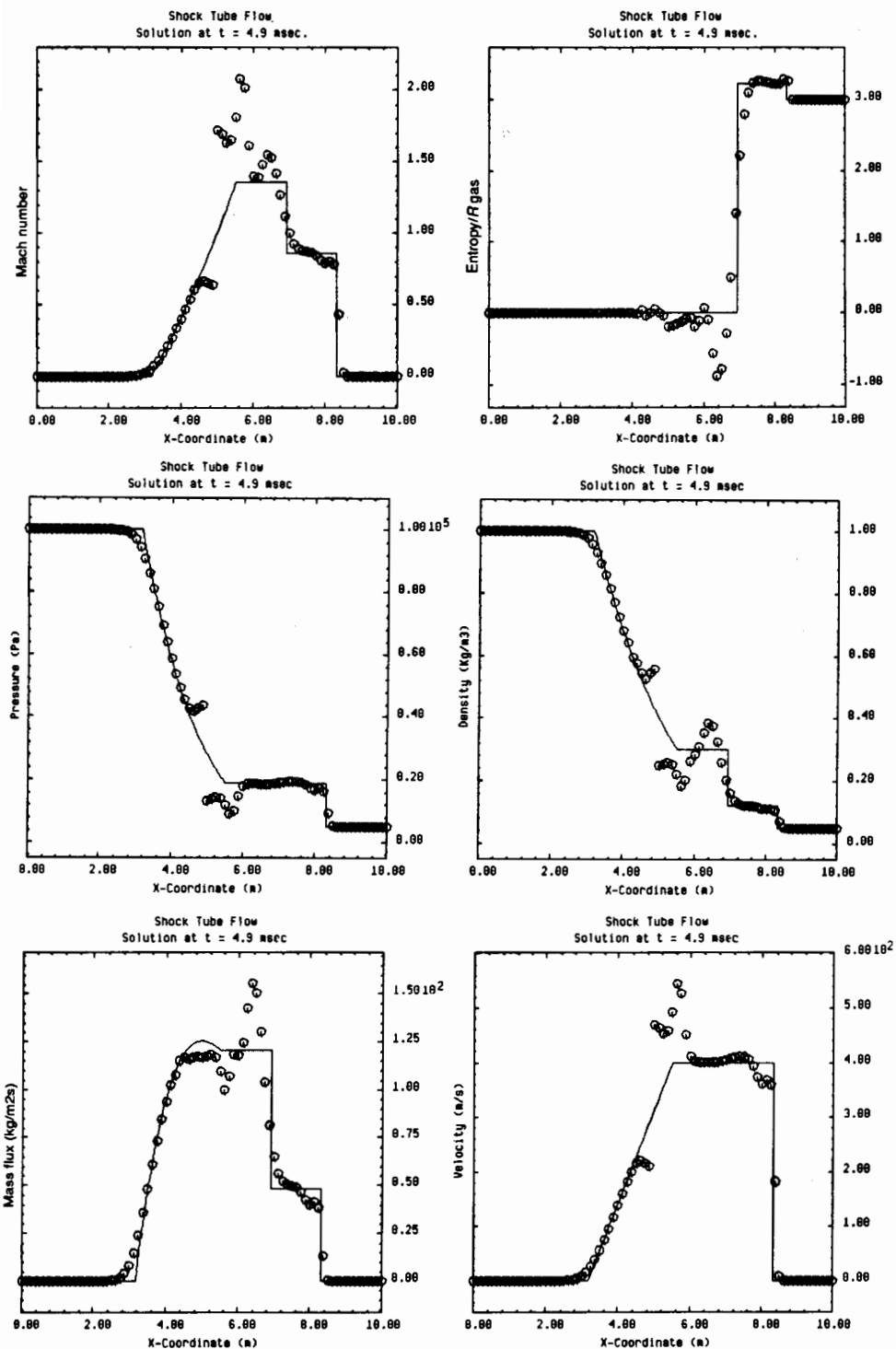


Figure 17.2.4 Results of MacCormack's scheme applied to the shock tube problem of Figure 16.6.9, with 81 mesh points at CFL = 0.95 after 35 time steps. Calculated results ○○○ Exact solution —

to supersonic velocities. The expansion shock at $x = 5$ is clearly seen. On the other hand, the shock is sharply resolved but the contact discontinuity is smeared. This is a feature common to many schemes.

The cure to the stationary shock oscillations as well as to the expansion shock lies in the introduction of additional dissipative terms proportional to the mesh size and of the same order or higher than the truncation error. This will be discussed in Section 17.3.

The semi-explicit variant of Casier, Deconinck and Hirsch (1983)

From a bidiagonal implicit family of schemes developed by Casier *et al.* (1983), a subclass can be extracted that can be considered as a generalization of MacCormack's schemes. The following represents a quasi-explicit extension of the explicit scheme (17.2.31):

$$(\xi + \frac{1}{2})\overline{\Delta U}_i = -\tau \cdot \delta^+ f_i^n + (\xi - \frac{1}{2})\overline{\Delta U}_{i-1} \quad (17.2.33a)$$

$$(\xi + \frac{1}{2})\overline{\Delta U}_i = -\tau \cdot \delta^- \bar{f}_i + (\xi - \frac{1}{2})\overline{\Delta U}_{i+1} \quad (17.2.33b)$$

$$\Delta U_i^n = \frac{1}{2}(\overline{\Delta U}_i + \overline{\Delta U}_i) \quad (17.2.33c)$$

This scheme is conditionally stable for the CFL condition

$$|\sigma| \leq 2\xi \quad (17.2.34)$$

and reduces to (17.2.31) for $\xi = \frac{1}{2}$.

Each step involves only two mesh points and is a bidiagonal system, which is solved by a single sweep through the mesh. Details concerning the properties of the sweeps and the related boundary conditions are given in the original reference.

For steady calculations in particular, computations at high Courant numbers can be performed by appropriate choices of ξ . Hence the number of iterations to reach steady state can be considerably reduced, as shown in Figure 17.2.5 at similar computational cost per iteration. In addition the parameter ξ introduces a dissipation at each step level. Figure 17.2.5 shows the results obtained with scheme (17.2.33) at $\xi = 20$, CFL = 39 for a supersonic flow in a converging-diverging nozzle. Observe the excellent shock resolution, typical of compact box-type schemes, to be compared with Figure 17.2.2. The comparison of the convergence histories with MacCormack's scheme shows the considerable improvement obtained with the above scheme.

17.2.3 Lerat and Peyret's S_2^b family of non-linear, two-step Lax-Wendroff schemes

Lerat and Peyret (1974, 1975) made a systematic investigation of all the explicit second-order accurate schemes in space and time, which are centrally differenced

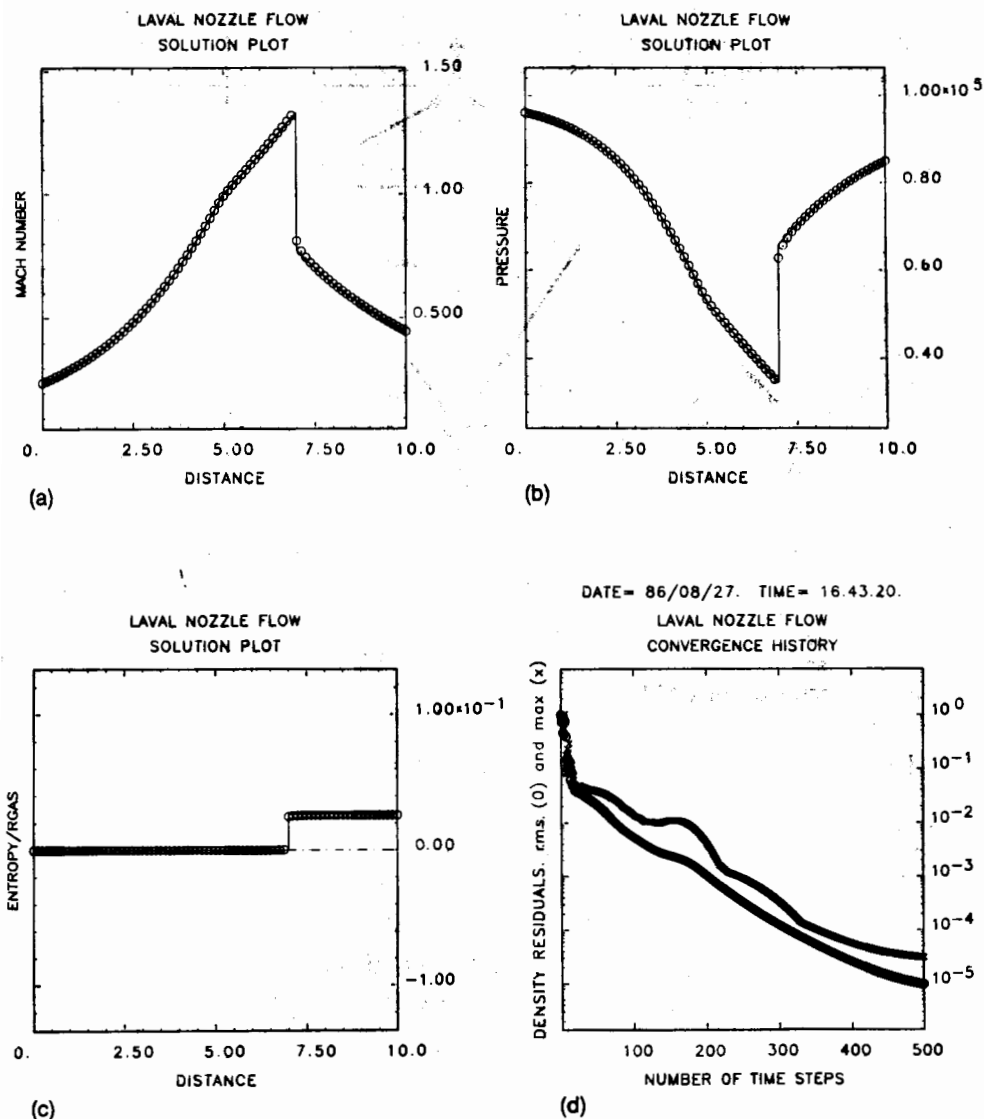


Figure 17.2.5 Results of scheme (17.2.33) with $CFL = 39$ and $\xi = 20$ applied to a stationary, transonic nozzle flow

with respect to $(i - 1)$, i , $(i + 1)$ and have a predictor–corrector two-step structure between the time levels n and $n + 1$.

These schemes correspond to an explicit discretization of the predictor variables in $(i + \beta)$ at time level $(n + \alpha)$ (Figure 17.2.6). The predictor step leads to the following equations, for a forward differencing choice, by performing a

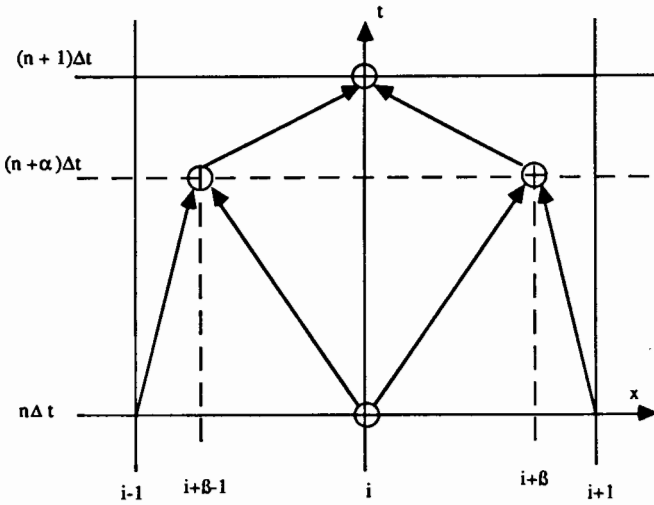


Figure 17.2.6 Computational molecule in Lerat and Peyret's S_{α}^{β} schemes

Taylor expansion of $U_{i+\beta}^{n+\alpha}$:

$$\begin{aligned}
 U_{i+\beta}^{n+\alpha} &= U_{i+\beta}^n + \alpha \Delta t (U_t)_{i+\beta} + \frac{\alpha^2 \Delta t^2}{2} (U_{tt})_{i+\beta} + \dots \\
 &= U_i^n + \beta \Delta x (U_x)_i^n + \alpha \Delta t (U_t)_i^n + \alpha \beta \Delta t \Delta x U_{tx} + \frac{\beta^2 \Delta x^2}{2} U_{xx} + \frac{\alpha^2 \Delta t^2}{2} U_{tt}
 \end{aligned}
 \tag{17.2.35}$$

The last three terms are the truncation error of the predictor step at (n, i) . Applying forward difference formulas for the space derivatives after replacing U_i by $-f_x$ leads to

$$U_{i+\beta}^{n+\alpha} \equiv \bar{U}_i = U_i^n + \beta(U_{i+1}^n - U_i^n) - \alpha\tau(f_{i+1}^n - f_i^n)
 \tag{17.2.36}$$

The corrector step is defined as to obtain overall second-order accuracy and can be written as

$$U_i^{n+1} = U_i^n - \frac{\tau}{2\alpha}(\bar{f}_i - \bar{f}_{i-1}) - \frac{\tau}{2\alpha}[(\alpha - \beta)f_{i+1}^n + (2\beta - 1)f_i^n + (1 - \alpha - \beta)f_{i-1}^n]
 \tag{17.2.37}$$

This family of schemes for arbitrary (α, β) are designated as the S_{α}^{β} schemes by Lerat and Peyret. They can be written in the alternative way by introducing the predictor and corrector variations $\overline{\Delta U}, \underline{\Delta U}$ with the same definitions as for

MacCormack's scheme (17.2.29), namely

$$\overline{\Delta U}_i = -\tau(f_{i+1}^n - f_i^n) \quad (17.2.38a)$$

$$\overline{\overline{\Delta U}}_i = -\tau(\bar{f}_i - \bar{f}_{i-1}) \quad (17.2.38b)$$

where

$$\bar{f}_i = f(\bar{U}_i) \equiv f(U_{i+\alpha}^{n+\alpha}) \quad (17.2.38c)$$

The S_α^β schemes take the following form:

$$\bar{U}_i = U_i^n + \beta(U_{i+1}^n - U_i^n) + \alpha \overline{\Delta U}_i \quad (17.2.39a)$$

$$\Delta U_i \equiv U_i^{n+1} - U_i^n = \frac{1}{2\alpha} [(\alpha - \beta)\overline{\Delta U}_i + (\alpha + \beta - 1)\overline{\Delta U}_{i-1} + \overline{\overline{\Delta U}}_i] \quad (17.2.39b)$$

The interpretation of the predictor variation ($\bar{U}_i - U_i^n$) is clear from the Taylor expansion (17.2.35). It represents the flux contribution to the solution at the predictor level at point $(i + \beta)$, $(n + \alpha)$. The corrector variation $\overline{\Delta U}$ is also to be considered as a flux contribution at level $(n + \alpha)$ to the final correction $\Delta U = U^{n+1} - U^n$, which can be written as

$$\Delta U_i = \frac{1}{2}(\overline{\Delta U}_i + \overline{\Delta U}_{i-1}) - \frac{1}{2\alpha} [\beta \overline{\Delta U}_i + (1 - \beta)\overline{\Delta U}_{i-1} + \overline{\overline{\Delta U}}_i] \quad (17.2.40)$$

With regard to the conservative form of the equations, the numerical flux of the S_α^β scheme is

$$\begin{aligned} f_{i+1/2}^* &= \frac{1}{2\alpha} [(\alpha - \beta)f_{i+1} + (\alpha + \beta - 1)f_i + \bar{f}_i] \\ &= \frac{1}{2}(f_{i+1} + f_i) - \frac{1}{2\alpha} [\beta f_{i+1} + (1 - \beta)f_i] + \frac{1}{2\alpha} \bar{f}_i \end{aligned} \quad (17.2.41)$$

For $\alpha = \beta = \frac{1}{2}$ one obtains exactly the Richtmyer two-step version of the Lax-Wendroff scheme, while $\alpha = 1$, $\beta = 0$ gives MacCormack's scheme (17.2.29) and $\alpha = 1$, $\beta = 1$ gives the variant (17.2.30). The family of schemes $\alpha, \beta = \frac{1}{2}$, $S_\alpha^{1/2}$, has been considered by McGuire and Morris (1973), while the particular case $\alpha = 1$, $\beta = \frac{1}{2}$ has been proposed by Rubin and Burstein (1967). Another family $\alpha, \beta = 0$, S_α^0 , or $\beta = 1$, S_α^1 , has also been investigated independently by Warming *et al.* (1973).

All the S_α^β schemes reduce to the Lax-Wendroff scheme in the linear case $f = a \cdot u$ and have therefore identical linear properties. Hence, they represent a family of non-linear splittings of the Lax-Wendroff scheme into two steps. Lerat and Peyret (1975) made an investigation of the optimal properties for non-linear problems, in particular for Burgers equation, which allows a detailed analysis of the truncation errors, with the aim of reducing the oscillations around shock waves generated by the insufficient dissipation of three-point, explicit, central, second-order schemes.

Computing the truncation error of the S_α^β schemes in the general non-linear case up to the highest order (see Section 9.4, equations (9.4.21) to (9.4.24) in Volume 1) leads to the equivalent differential equation of the scheme

$$U_t + f_x = \varepsilon_T \quad (17.2.42)$$

where ε_T is the truncation error.

From the definition of the numerical flux $f_{i+1/2}^*$, the contribution to the truncation error arising from the non-linearity contains a term proportional to the mixed derivative of f^* with respect to U_i and U_{i+1} . This is the term g_{12} in equations (9.4.21) to (9.4.25), where

$$g_{12} = \frac{\partial^2 f_{i+1/2}^*}{\partial U_i \partial U_{i+1}} = \frac{1}{2\alpha} A_U (1 - \beta + \alpha\tau A)_i (\beta - \alpha\tau A)_i \quad (17.2.43)$$

Hence, the truncation error becomes, with $\sigma = \tau A$,

$$\varepsilon_T = \frac{\Delta x^2}{6} \frac{\partial}{\partial x} \left[(\sigma^2 - 1) f_{xx} + \frac{3}{2\alpha} A_U (\beta - \alpha\sigma) (1 - \beta + \alpha\sigma) U_x^2 + 2\sigma^2 A_U U_x^2 \right] \quad (17.2.44)$$

By applying the relation $AU_x = f_x$, an alternative expression for the truncation error is

$$\varepsilon_T = \frac{\Delta x^2}{6} \frac{\partial}{\partial x} \left\{ (\tau^2 A^2 - 1) f_{xx} + \frac{3}{2\alpha} A_U (\beta U - \alpha\tau f)_x [(1 - \beta)U + \alpha\tau f]_x + 2\tau^2 A_U f_x^2 \right\} \quad (17.2.45)$$

where the subscripts indicate derivatives, in particular A_U is the derivative of the Jacobian with respect to U , $A_U = f_{UU}$.

The first term is the only one in the linear case $A_U = 0$, and is of a dispersive nature as discussed earlier. The second term is proportional to the second derivative f_{uu} and, hence, if the coefficient is appropriately chosen, could allow a non-linear dissipation to be introduced in order to damp the oscillations created at shock or contact discontinuities. However, since the coefficient of this term is proportional to f_x , the scheme can be made dissipative for compression shocks but would then be antidissipative for expansion waves. A detailed analysis, based on Burgers equation, shows that the choice

$$\begin{aligned} \alpha &= 1 + \sqrt{\frac{5}{2}} \\ \beta &= \frac{1}{2} \end{aligned} \quad (17.2.46)$$

gives a maximum dissipation with compression shocks and keeps the antidissipation to a minimum with rarefaction waves (Lerat and Peyret, 1975).

It is to be noted that the effect of the antidissipative term is partly counter-balanced by a higher-order term proportional to $\Delta x^4 (\partial^4 f / \partial x^4)$ with a negative coefficient. The optimum values above are confirmed by numerical experiments on Euler equations, to minimize the non-linear oscillations at discontinuities.

17.2.4 One-step Lax–Wendroff schemes in two dimensions

The one-step Lax–Wendroff scheme for the multi-dimensional Euler equations is obtained from equation (17.2.2), following the same procedure as in one dimension. In two dimensions, the equation $U_t + f_x + g_y = 0$ leads to the following estimation of U_{ii} :

$$\begin{aligned}
 U_{ii} &= \frac{\partial}{\partial t}(-f_x - g_y) \\
 &= -\frac{\partial}{\partial x}\left(A\frac{\partial U}{\partial t}\right) - \frac{\partial}{\partial y}\left(B\frac{\partial U}{\partial t}\right) \\
 &= \frac{\partial}{\partial x}[A(f_x + g_y)] + \frac{\partial}{\partial y}[B(f_x + g_y)] \\
 &= \frac{\partial}{\partial x}\left(A\frac{\partial f}{\partial x}\right) + \frac{\partial}{\partial y}\left(B\frac{\partial g}{\partial y}\right) + \frac{\partial}{\partial x}\left(A\frac{\partial g}{\partial y}\right) + \frac{\partial}{\partial y}\left(B\frac{\partial f}{\partial x}\right) \quad (17.2.47)
 \end{aligned}$$

The mixed derivatives that appear in the last two terms are somewhat cumbersome, so much so that A and B do not commute.

The direct generalization of equation (17.2.11), with central symmetric difference formulas for the mixed derivatives, leads to the following scheme, written in difference operators notation:

$$\begin{aligned}
 U_{ij}^{n+1} &= U_{ij}^n - \tau_x \bar{\delta}_x f_{ij}^n - \tau_y \bar{\delta}_y g_{ij}^n + \frac{\tau_x^2}{2} \delta_x (A_{ij} \delta_x f_{ij}) + \frac{\tau_y^2}{2} \delta_y (B_{ij} \delta_y g_{ij}) \\
 &\quad + \frac{\tau_x \tau_y}{2} [\bar{\delta}_x (A_{ij} \bar{\delta}_y g_{ij}) + \bar{\delta}_y (B_{ij} \bar{\delta}_x f_{ij})] \quad (17.2.48)
 \end{aligned}$$

where

$$\tau_x = \frac{\Delta t}{\Delta x} \quad \tau_y = \frac{\Delta t}{\Delta y} \quad (17.2.49)$$

and the central difference operators $\bar{\delta}_x$ and $\bar{\delta}_y$ are defined by equation (17.1.31), while δ_x, δ_y are the operators in the x and y directions defined as in equation (17.2.9).

This scheme uses all of the nine points surrounding (ij) , and various other variants can be defined by treating the mixed derivative terms differently (see Problem 17.4).

The stability of the two-dimensional Lax–Wendroff scheme (17.2.48) is analysed by the Von Neumann method. The following amplification matrix is obtained for constant Jacobians A, B and linearized fluxes $f = Au, g = Bu$:

$$\begin{aligned}
 G &= 1 - I(\tau_x A \sin \phi_x + \tau_y B \sin \phi_y) - \tau_x^2 A^2 (1 - \cos \phi_x) - \tau_y^2 B^2 (1 - \cos \phi_y) \\
 &\quad - \frac{\tau_x \tau_y}{2} (AB + BA) \sin \phi_x \sin \phi_y \quad (17.2.50)
 \end{aligned}$$

For real, symmetric and commuting matrices A, B , Turkel (1977) has shown that the following condition is necessary and sufficient for the Von Neumann stability:

$$|\tau_x \rho(A)|^{2/3} + |\tau_y \rho(B)|^{2/3} \leq 1 \tag{17.2.51}$$

Since the matrices A and B do not commute, this condition is only sufficient (Turkel, 1977). Weaker conditions had been given originally by Lax and Wendroff (1964) as

$$\tau_x \rho(A) \leq \frac{1}{\sqrt{8}} \quad \text{and} \quad \tau_y \rho(B) \leq \frac{1}{\sqrt{8}} \tag{17.2.52}$$

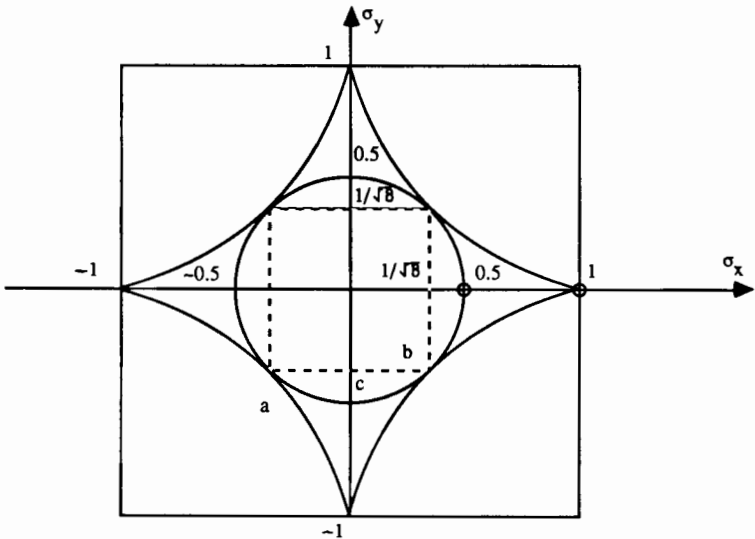
and an improvement found by Tadmor is reported by Turkel (1977) as

$$[\tau_x \rho(A)]^2 + [\tau_y \rho(B)]^2 \leq \frac{1}{4} \tag{17.2.53}$$

All of the above sufficient relations are valid for real, symmetric matrices A and B are compared in Figure 17.2.7, in a diagram (σ_x, σ_y)

$$\sigma_x = \tau_x \rho(A) \quad \sigma_y = \tau_y \rho(B) \tag{17.2.54}$$

It is worth mentioning that for a scalar equation with $\Delta x = \Delta y$, a numerical study of the amplification factor (17.2.50) performed by Burstein (1967) has led



- a - condition (17.2.51)
- b - condition (17.2.52)
- c - condition (17.2.53)

Figure 17.2.7 Comparison of different sufficient stability conditions for the one-step Lax–Wendroff scheme in two dimensions

to the stability condition

$$\tau(|\bar{v}| + c) < 0.5406$$

which is close to the condition (17.2.53).

Although interesting conceptually, the one-step Lax–Wendroff schemes are rarely applied since they require many Jacobian matrices evaluations; therefore one favours, in practice, extensions of the two-step methods.

Reinterpretation of the one-step Lax–Wendroff scheme

The one-step Lax–Wendroff schemes have recently gained a renewed interest for practical computations in the framework of multi-grid schemes (Ni, 1982; Hall, 1985; see also Koeck, 1985). Ni (1982) reformulated the Taylor expansion in time (17.2.2) as a ‘distribution’ formula for the finite variation $\Delta U = U^{n+1} - U^n$ at a mesh point.

The guiding idea is obtained from rewriting the Lax–Wendroff algorithm in the form (17.2.7), (17.2.8) as a two-step procedure:

$$\overline{\Delta U}_{i+1/2} = -\tau(f_{i+1}^n - f_i^n) \tag{17.2.55}$$

$$f_{i+1/2}^* = f_{i+1/2} + \frac{1}{2}A_{i+1/2}^n \overline{\Delta U}_{i+1/2} \tag{17.2.56}$$

$$\Delta U^n = -\tau(f_{i+1/2}^* - f_{i-1/2}^*) \tag{17.2.57}$$

The variation $\Delta U_i^n = U_i^{n+1} - U_i^n$ from time n to time level $n + 1$ is considered to result from contributions of the flux imbalance over the cells $(i + 1, i)$ and $(i, i - 1)$ (Figure 17.2.8). The flux imbalance over cell $(i + 1/2)$ is $(f_{i+1} - f_i)$ and contributes to the overall variation ΔU_i^n by an amount

$$\overline{\Delta U}_{i+1/2} \equiv -\tau(f_{i+1}^n - f_i^n) = -\tau\delta f_{i+1/2}^n \tag{17.2.58}$$

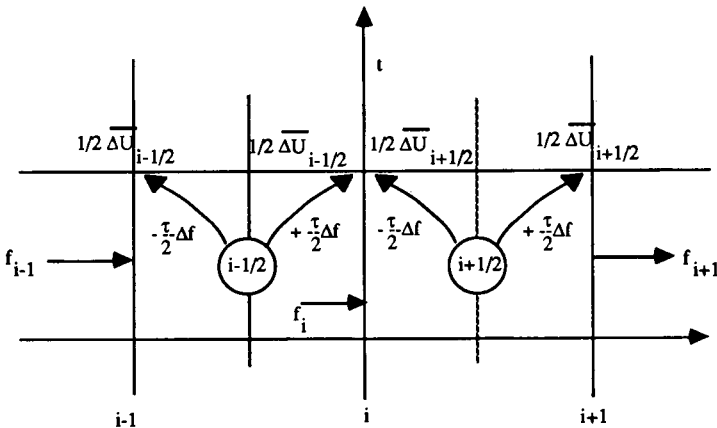


Figure 17.2.8 Distribution of flux imbalances in the distribution interpretation of the one-step Lax–Wendroff scheme

Similarly, the cell $(i - 1/2)$ contributes with

$$\overline{\Delta U}_{i-1/2} \equiv -\tau(f_i^n - f_{i-1}^n) = -\tau \delta f_{i-1/2}^n \quad (17.2.59)$$

If no other contributions to ΔU_i are taken into account, the formula

$$\Delta U_i^n = \frac{1}{2}(\overline{\Delta U}_{i+1/2} + \overline{\Delta U}_{i-1/2}) = -\frac{\tau}{2}(f_{i+1}^n - f_{i-1}^n) \quad (17.2.60)$$

is the unstable central difference scheme.

The contributions from the second time derivative U_{tt} stabilizes the central scheme while maintaining second-order accuracy. As seen from equation (17.2.5), the stabilizing terms can be viewed as arising from a contribution

$$\overline{\Delta f}_{i-1/2} \equiv A_{i-1/2} \cdot \overline{\Delta U}_{i-1/2} = \left(\frac{\partial f}{\partial U} \right)_{i-1/2} \cdot \overline{\Delta U}_{i-1/2} \quad (17.2.61)$$

from cell $(i - 1/2)$ and

$$\Delta f_{i+1/2} \equiv A_{i+1/2} \cdot \overline{\Delta U}_{i+1/2} = \left(\frac{\partial f}{\partial U} \right)_{i+1/2} \cdot \overline{\Delta U}_{i+1/2} \quad (17.2.62)$$

from cell $(i + 1/2)$.

The total contribution from cell $(i - 1/2)$ to U_i^{n+1} is defined in the Lax-Wendroff scheme as

$$\Delta U_{i-1/2}^+ \equiv \frac{1}{2}(\overline{\Delta U}_{i-1/2} + \tau \overline{\Delta f}_{i-1/2}) \quad (17.2.63)$$

and the contribution from the downstream cell $(i + 1/2)$ is

$$\Delta U_{i+1/2}^- \equiv \frac{1}{2}(\overline{\Delta U}_{i+1/2} - \tau \overline{\Delta f}_{i+1/2}) \quad (17.2.64)$$

The Lax-Wendroff scheme can then be written as

$$\Delta U_i \equiv U_i^{n+1} - U_i^n = (\Delta U_{i+1/2}^- + \Delta U_{i-1/2}^+) \quad (17.2.65)$$

Within each cell, for instance cell $(i + 1/2)$, the first variation $\overline{\Delta U}_{i+1/2}$ is equally distributed to the points i and $i + 1$, while the second contribution $\overline{\Delta f}_{i+1/2}$ is added to the downstream point and subtracted from the upstream point; that is one has

$$\Delta U_{i+1/2}^+ = \frac{1}{2}(\overline{\Delta U}_{i+1/2} + \tau \overline{\Delta f}_{i+1/2}) \quad (17.2.66)$$

such that

$$\Delta U_{i+1/2}^- + \Delta U_{i+1/2}^+ = \overline{\Delta U}_{i+1/2} \quad (17.2.67)$$

Although the resultant scheme is central, each separate contribution has an upwind character. This can best be seen for a scalar (characteristic) equation where A or its eigenvalue a is taken as positive.

In this case, with $\sigma = \tau a > 0$,

$$\Delta U_{i-1/2}^+ = \frac{1}{2}(1 + \sigma) \overline{\Delta U}_{i-1/2} \quad (17.2.68)$$

and

$$\Delta U_{i+1/2}^- = \frac{1}{2}(1 - \sigma)\overline{\Delta U}_{i+1/2} \quad (17.2.69)$$

showing that the upstream cell provides a larger correction to ΔU_i than the downstream cell. This is in agreement with the physical properties of wave propagations. The central properties of the Lax–Wendroff scheme result from the equal distribution of Δf contained in equation (17.2.65).

The interpretation of Lax–Wendroff scheme as distribution formulas of corrections is used by Ni (1982) and Hall (1985) in order to define multi-grid strategies, whereby the above formulas are applied on a succession of coarser meshes.

It is interesting to observe at this point that MacCormack's scheme (17.2.29) can be interpreted as a distribution scheme whereby

$$\Delta U_{i+1/2}^+ = \frac{1}{2}\overline{\Delta U}_{i+1/2} \quad (17.2.70)$$

and

$$\Delta U_{i-1/2}^- = \frac{1}{2}\tilde{\Delta U}_{i-1/2} \quad (17.2.71)$$

where the tilde indicates that the variation in the upstream cell ($i - 1/2$) is considered to have been already affected by the downstream cell variation; that is

$$\Delta U_{i-1/2}^- = \frac{1}{2}\overline{\Delta U}_{i-1/2}(U_i^n + \Delta U_{i+1/2}^+, U_{i-1}^n + \Delta U_{i-1/2}^+) \equiv \frac{1}{2}\tilde{\Delta U}_{i-1/2} \quad (17.2.72)$$

with

$$\Delta U_{i-1/2}^+ = \frac{1}{2}\overline{\Delta U}_{i-1/2}(U_i^n, U_{i-1}^n) \quad (17.2.73)$$

The alternative version (17.2.30) is obtained by considering the downstream cell variations to be affected by the prior, upstream corrections.

Various ways can be defined for the computation of the flux corrections $\Delta f_{i\pm 1/2}$. A straightforward way, avoiding the calculation of the Jacobian matrices, consists in the following equations:

$$\Delta f = \Delta \begin{vmatrix} \rho u \\ \rho u^2 + p \\ \rho u + 1 \end{vmatrix} = \begin{vmatrix} \Delta(\rho u) \\ u \Delta(\rho u) + \rho u \Delta u + \Delta p \\ H \Delta(\rho u) + \rho u \Delta H \end{vmatrix} \quad (17.2.74)$$

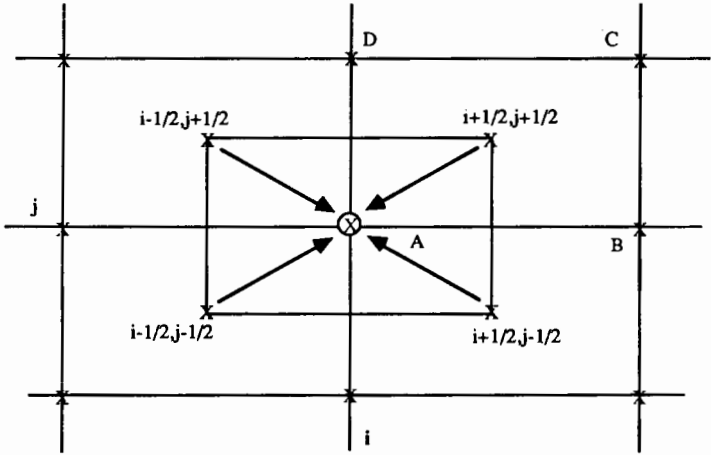
where Δ represents the appropriate finite difference and

$$\Delta U = \begin{vmatrix} \Delta \rho \\ \Delta(\rho u) \\ \Delta(\rho E) \end{vmatrix} \quad (17.2.75)$$

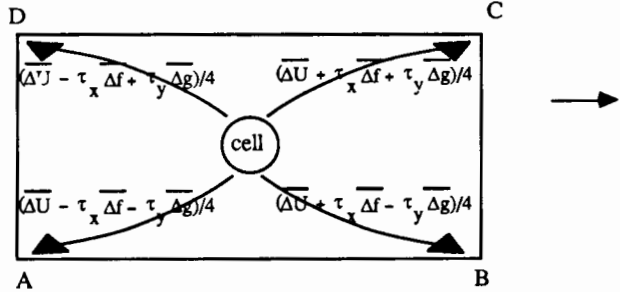
is used to derive the values of Δp , Δu and ΔH from their relations to the conservative variables seen in Chapter 16.

Two-dimensional distribution formulas

The extension of the above interpretation to two dimensions has the additional advantage that the mixed derivative terms of equation (17.2.48) do not appear



CONTRIBUTIONS TO POINT A FROM SURROUNDING CELLS



DISTRIBUTION WITHIN A CELL

Figure 17.2.9 Two-dimensional distribution interpretation of the Lax-Wendroff one-step schemes

explicitly in the calculation. Indeed, referring to Figure 17.2.9, four cells will contribute to the variation $\Delta U_{ij}^n = U_{ij}^{n+1} - U_{ij}^n$.

Considering cell $(i + 1/2, j + 1/2)$, the variations associated to the first derivative terms of equation (17.2.48) lead to a contribution

$$\overline{\Delta U}_{i+1/2, j+1/2} = -\tau_x (f_{i+1, j+1/2} - f_{i, j+1/2}) - \tau_y (g_{i+1/2, j+1} - g_{i+1/2, j}) \quad (17.2.76)$$

where

$$f_{i, j+1/2} = \frac{1}{2}(f_{i, j} + f_{i, j+1}) \quad (17.2.77)$$

and similar formulas for the other flux components at mid-side points.

For an arbitrary mesh, the contribution $\Delta U_{i+1/2, j+1/2}$ will be defined by a finite volume discretization with a control volume ABCD having the mesh

points at its corners:

$$\overline{\Delta U}_{i+1/2,j+1/2} = -\frac{\Delta t}{S_{i+1/2,j+1/2}} \sum_{ABCD} (f \Delta y - g \Delta x) \quad (17.2.78)$$

where $S_{i+1/2,j+1/2}$ is the area of ABCD and the summation extends to the four sides of the cell.

This variation is distributed equally to the four corners of the cell with a weight coefficient of $\frac{1}{4}$ and when these contributions from the four cells common to point (i, j) are added to form ΔU_{ij}^n , one obtains again the central unstable scheme.

The stabilizing terms arising from the U_{ii} contributions are evaluated from the second line of equation (17.2.47). With

$$\overline{\Delta f}_{i+1/2,j+1/2} = A_{i+1/2,j+1/2} \overline{\Delta U}_{i+1/2,j+1/2} \quad (17.2.79)$$

$$\overline{\Delta g}_{i+1/2,j+1/2} = B_{i+1/2,j+1/2} \overline{\Delta U}_{i+1/2,j+1/2}$$

the following distributions occur within the cell $(i+1/2, j+1/2)$ towards the four corners:

$$\Delta U_{i+1/2,j+1/2}^{\pm\pm} = \frac{1}{4} (\overline{\Delta U} \pm \tau_x \overline{\Delta f} \pm \tau_y \overline{\Delta g})_{i+1/2,j+1/2} \quad (17.2.80)$$

with obvious definitions of the four combinations of signs. For instance

$$\Delta U_{i+1/2,j+1/2}^{(C)} = \Delta U_{i+1/2,j+1/2}^{++} \quad (17.2.81)$$

$$\Delta U_{i+1/2,j+1/2}^{(B)} = \Delta U_{i+1/2,j+1/2}^{+-}$$

Finally, the distribution form of the Lax-Wendroff scheme can be written as

$$\begin{aligned} \Delta U_{ij} = U_{ij}^{n+1} - U_{ij}^n = & \Delta U_{i+1/2,j+1/2}^{--} + \Delta U_{i+1/2,j-1/2}^{+-} \\ & + \Delta U_{i-1/2,j-1/2}^{++} + \Delta U_{i-1/2,j+1/2}^{+-} \end{aligned} \quad (17.2.82)$$

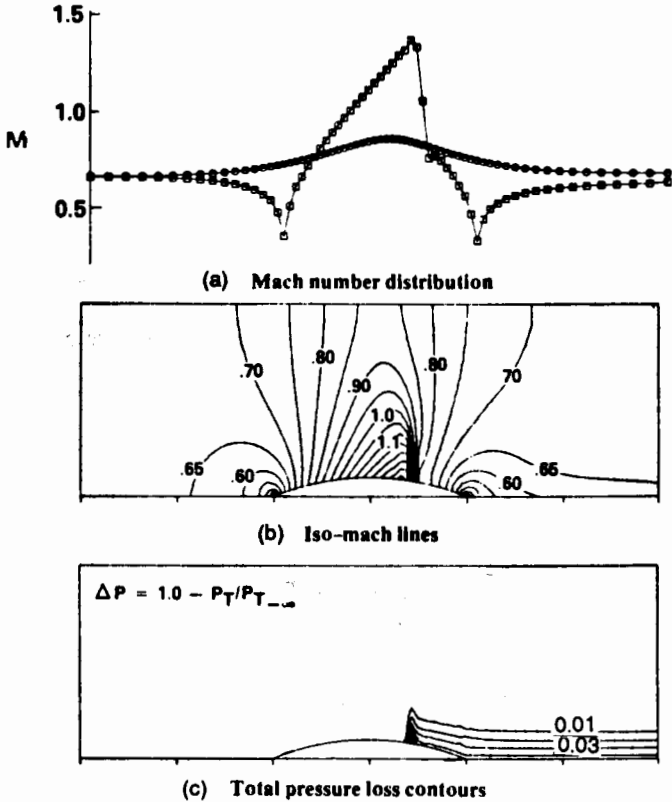
For unequal mesh sizes, the above formula can be replaced by volume-weighted averages.

For more details on the multi-grid application we refer the reader to the above-mentioned references for two-dimensional applications and to the extension to three dimensions developed by Koeck (1985).

Figure 17.2.10, from Ni (1982), is an example of a transonic flow in a channel with a circular arc obstacle on the lower wall. The height of the channel is equal to the chord of the circular arc, and its thickness to chord ratio is 10 per cent.

For an incident Mach number of $M_\infty = 0.675$, a supersonic region terminated by a normal shock is obtained. Behind the non-uniform shock, the flow is known to become rotational, and this can be seen from the way the iso-mach lines intersect the flat surfaces. Upstream of the circular arc, the flow is irrotational and the iso-mach lines are perpendicular to the surface, which is not the case any-longer in the downstream part (see Problem 17.12).

The stagnation pressure contours (Figure 17.2.10(c)) show the generated



Transonic solution for flow in the channel at $M_\infty = 0.675$.

Figure 17.2.10 Transonic flow in a channel with a circular arc obstacle on the lower wall. (From Ni, 1982)

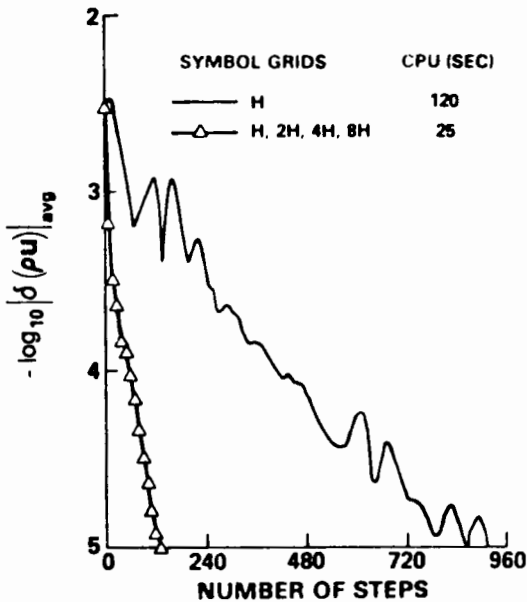
entropy at the shock being convected further downstream. The convergence history in Figure 17.2.11 shows the improvement achieved by the multi-grid strategy using four successive grids.

17.2.5 Two-step Lax–Wendroff schemes in two dimensions

As with one-dimensional problems, the one-step Lax–Wendroff schemes also suffer from the difficulty of requiring calculations of Jacobian matrices. This can be avoided by the two-step versions, such as the Richtmyer and MacCormack schemes, which are generalized by the two-dimensional versions of the S_α^β schemes of Lerat and Peyret.

The two-step Richtmyer scheme

Equation (17.2.27) can be generalized to two (or three) dimensions in a straightforward way by applying a first-step Lax–Friedrichs scheme (17.1.21), followed



Convergence history for transonic flow in the channel.

Figure 17.2.11 Convergence history for the transonic channel flow of Figure 17.2.10. (From Ni, 1982)

by a leapfrog step. One obtains, in two dimensions,

$$U_{ij}^{n+1/2} = \frac{1}{4}(U_{i+1,j}^n + U_{i-1,j}^n + U_{i,j+1}^n + U_{i,j-1}^n) - \frac{\tau_x}{2}(f_{i+1,j}^n - f_{i-1,j}^n) - \frac{\tau_y}{2}(g_{i,j+1}^n - g_{i,j-1}^n) \quad (17.2.83)$$

$$U_{ij}^{n+1} = U_{ij}^n - \tau_x(f_{i+1/2,j}^{n+1/2} - f_{i-1/2,j}^{n+1/2}) - \tau_y(g_{i,j+1/2}^{n+1/2} - g_{i,j-1/2}^{n+1/2})$$

This scheme involves the points $(i \pm 1, j)$ and $(i, j \pm 1)$ at two different time levels, since the first step is written at integer mesh points.

The more direct generalization of equation (17.2.27) has also been considered as follows (Zwas, 1973):

$$U_{i+1/2,j+1/2}^{n+1/2} = \frac{1}{4}(U_{i+1,j+1}^n + U_{i+1,j}^n + U_{i,j+1}^n + U_{i,j}^n) - \frac{\tau_x}{2}(f_{i+1,j+1/2}^n - f_{i,j+1/2}^n) - \frac{\tau_y}{2}(g_{i+1/2,j+1}^n - g_{i+1/2,j}^n) \quad (17.2.84)$$

$$U_{ij}^{n+1} = U_{ij}^n - \tau_x(f_{i+1/2,j}^{n+1/2} - f_{i-1/2,j}^{n+1/2}) - \tau_y(g_{i,j+1/2}^{n+1/2} - g_{i,j-1/2}^{n+1/2})$$

These two versions are equivalent but not identical. In the version (17.2.84), the half-integer mesh point values can be estimated as

$$\begin{aligned}
 f_{i+1,j+1/2}^n &= f\left(\frac{U_{i+1,j+1}^n + U_{i+1,j}^n}{2}\right) \\
 f_{i+1/2,j}^{n+1/2} &= f\left(\frac{U_{i+1/2,j+1/2}^{n+1/2} + U_{i+1/2,j-1/2}^{n+1/2}}{2}\right)
 \end{aligned}
 \tag{17.2.85}$$

The alternative option

$$\begin{aligned}
 f_{i+1/2,j}^{n+1/2} - f_{i-1/2,j}^{n+1/2} &= \frac{1}{2}(f_{i+1/2,j+1/2}^{n+1/2} + f_{i+1/2,j-1/2}^{n+1/2}) \\
 &\quad - \frac{1}{2}(f_{i-1/2,j+1/2}^{n+1/2} + f_{i-1/2,j-1/2}^{n+1/2})
 \end{aligned}
 \tag{17.2.86}$$

is a third-order estimation.

The stability conditions of these two versions are also different. Applying a Von Neumann analysis, scheme (17.2.83) gives, in the linearized case,

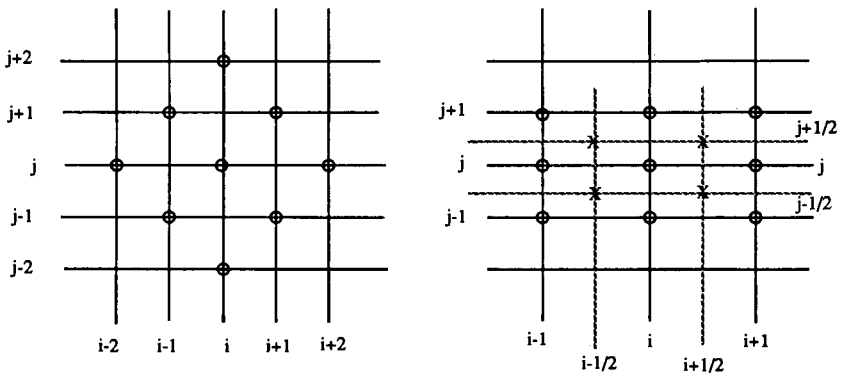
$$G = 1 - I(\tau_x A \sin \phi_x + \tau_y B \sin \phi_y)(\cos \phi_x + \cos \phi_y) - 2(\tau_x A \sin \phi_x + \tau_y B \sin \phi_y)^2
 \tag{17.2.87}$$

When the scheme (17.2.83) is reduced to a single equation, it involves points $(i \pm 2, j)$ and $(i, j \pm 2)$ shown in Figure 17.2.12.

The necessary and sufficient stability property can be found in this case (Richtmyer and Morton, 1967), and for $\Delta x = \Delta y$ can be written as

$$\frac{\Delta t}{\Delta x} (|\bar{v}| + c) \leq \frac{1}{\sqrt{2}}
 \tag{17.2.88}$$

which is a CFL condition with the limit $1/\sqrt{2}$.



(a) Computational stencil for scheme (17.2.83)

(b) Computational stencil for scheme (17.2.84)

Figure 17.2.12 Computational molecules for schemes (17.2.83) and (17.2.84)

The variant (17.2.84) is more compact and involves the nine points indicated in Figure 17.2.12(b), leading to the amplification matrix

$$G = 1 - \frac{I}{2} [\tau_x A \sin \phi_x (1 + \cos \phi_y) + \tau_y B \sin \phi_y (1 + \cos \phi_x)] - \left(\tau_x A \sin \frac{\phi_x}{2} \cos \frac{\phi_y}{2} + \tau_y B \cos \frac{\phi_x}{2} \sin \frac{\phi_y}{2} \right)^2 \quad (17.2.89)$$

Here, also, a necessary and sufficient condition for stability can be found (Zwas, 1973; Turkel, 1977), for $\Delta x = \Delta y$:

$$\frac{\Delta t}{\Delta x} (|\bar{v}| + c) \leq 1 \quad (17.2.90)$$

which is a CFL condition limited by one. Hence this version of the Richtmyer scheme allows a maximum time step larger by a factor $\sqrt{2}$ compared to the scheme (17.2.83).

The two-step MacCormack scheme

This scheme is the most popular two-step variant of the explicit Lax-Wendroff family as it involves only seven points instead of nine.

Since MacCormack's scheme combines forward and backward differences in separate predictor and corrector steps, four different schemes can be defined in two dimensions, through various combinations of the one-sided differences on the flux components f and g . For instance, in the line of scheme (17.2.29), one would write the following version of MacCormack's scheme:

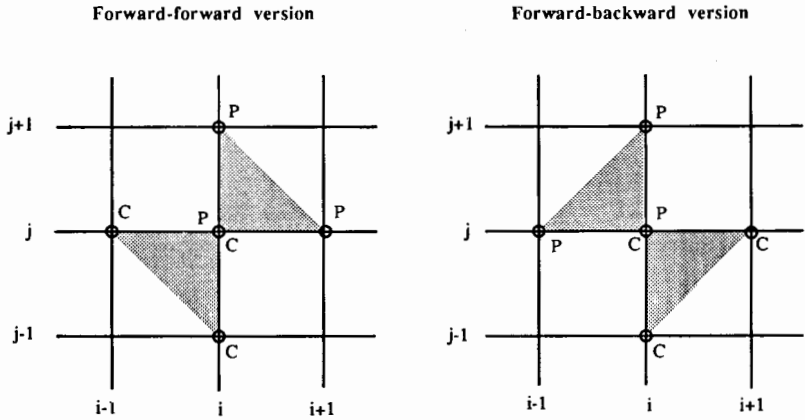
$$\begin{aligned} \bar{U}_{ij} &= U_{ij}^n - \tau_x (f_{i+1,j}^n - f_{ij}^n) - \tau_y (g_{i,j+1}^n - g_{ij}^n) \\ \bar{\bar{U}}_{ij} &= U_{ij}^n - \tau_x (\bar{f}_{ij} - \bar{f}_{i-1,j}) - \tau_y (\bar{g}_{ij} - \bar{g}_{i,j-1}) \\ U_{ij}^{n+1} &= \frac{1}{2} (\bar{U}_{ij} + \bar{\bar{U}}_{ij}) \end{aligned} \quad (17.2.91)$$

Figure 17.2.13 shows the computational molecule associated to scheme (17.2.91) where the points marked P indicate the values used at the predictor level.

The amplification matrix of the two-dimensional MacCormack scheme can be derived for the version (17.2.91) by defining \bar{G} as $\bar{U} = \bar{G}U^n$, $\bar{\bar{G}}$ as $\bar{\bar{U}} = \bar{\bar{G}}U^n$ and $G = (\bar{G} + \bar{\bar{G}})/2$, leading to

$$\begin{aligned} \bar{G} &= 1 - \tau_x A (e^{I\phi_x} - 1) \tau_y B (e^{I\phi_y} - 1) \\ \bar{\bar{G}} &= 1 - \bar{G} [\tau_x A (1 - e^{-I\phi_x}) + \tau_y B (1 - e^{-I\phi_y})] \\ G &= 1 - I (\tau_x A \sin \phi_x + \tau_y B \sin \phi_y) \\ &\quad - \left[(\tau_x^2 A^2 (1 - \cos \phi_x) + \tau_y^2 B^2 (1 - \cos \phi_y)) \right. \\ &\quad \left. + 4 \tau_x \tau_y AB \sin \frac{\phi_x}{2} \sin \frac{\phi_y}{2} \cos \frac{\phi_x - \phi_y}{2} \right] \end{aligned} \quad (17.2.92)$$

written for commuting matrices A, B .



P : Predictor points
C : Corrector points

Figure 17.2.13 Computational molecule for MacCormack's scheme

This expression is quite complicated and no analytically derived stability condition is known. An experimentally derived necessary condition for stability is obtained by MacCormack and Paullay (1972) as a CFL condition, indicating that the physical domain of dependence should be contained in the numerical one:

$$(\tau_x |\lambda(A)|_{\max} + \tau_y |\lambda(B)|_{\max}) \leq 1 \tag{17.2.93}$$

or

$$\Delta t \leq \left[\frac{|\lambda(A)|_{\max}}{\Delta x} + \frac{|\lambda(B)|_{\max}}{\Delta y} \right]^{-1}$$

This condition is obtained from the stability condition $\rho(G) \leq 1$ for $\phi_x = \phi_y = \pi$. See also Tong (1987) for an independent confirmation through a numerical evaluation of the amplification factor G . In Cartesian coordinates, $|\lambda(A)|_{\max} = |u| + c$ and $|\lambda(B)|_{\max} = |v| + c$, where u and v are the x and y components of the velocity vector \vec{v} . Hence, one obtains for the Euler equations

$$\Delta t \leq \frac{1}{(|u| + c)/\Delta x + (|v| + c)/\Delta y} < \frac{\Delta x \Delta y}{|u|\Delta y + |v|\Delta x + c\sqrt{\Delta x^2 + \Delta y^2}} \tag{17.2.94}$$

where the right-hand side is the current form, as generally found in the literature.

A backward-backward predictor version is described by the scheme

$$\begin{aligned} \bar{U}_{ij} &= U_{ij}^n - \tau_x (f_{ij}^n - f_{i-1,j}^n) - \tau_y (g_{ij}^n - g_{i,j-1}^n) \\ \bar{\bar{U}}_{ij} &= U_{ij}^n - \tau_x (\bar{f}_{i+1,j} - \bar{f}_{ij}) - \tau_y (\bar{g}_{i,j+1} - \bar{g}_{ij}) \\ U_{ij}^{n+1} &= \frac{1}{2} (\bar{U}_{ij} + \bar{\bar{U}}_{ij}) \end{aligned} \tag{17.2.95}$$

A comparative study of the four variants has led Lerat and Sides (1977) to the conclusion that the best results are obtained in steady flows when the corrector step is upwind with regard to the flow direction, in concordance with the one-dimensional observations. A dynamic switch between the four variants as a function of the flow direction is applied by Lerat and Sides (1977), but most of the applications use a fixed version. In this case, it is recommended to cycle between the four possibilities during a computation, in order to avoid a bias provided by an eventual accumulation of errors.

Finite volume formulation of MacCormack's scheme

Due to its importance, we present here a finite volume formulation of MacCormack's scheme on an arbitrary mesh, which was actually one of the first applications of the finite volume method (see Chapter 6 in Volume 1).

The current approach consists of a discretization of both predictor and corrector steps on the same control volume ABCD with mesh points (i, j) at its centre (Figure 17.2.14). The two steps are distinguished by the way the fluxes are estimated. In the predictor forward-forward version, for instance, the flux along the downstream side BC is defined as being equal to the flux value at point Q $(i + 1, j)$ and along the side CD to the value at point R $(i, j + S)$. In the corrector step, the upstream flux values are selected.

Designating the cell side normals by $\vec{S}_{i\pm 1/2}$ and $\vec{S}_{j\pm 1/2}$, the predictor step is defined by

$$\bar{U}_{ij} = U_{ij}^n - \frac{\Delta t}{\Omega_{ij}} (\bar{F}_{i+1,j} \cdot \vec{S}_{i+1/2} + \bar{F}_{i,j+1} \cdot \vec{S}_{j+1/2} + \bar{F}_{ij} \cdot \vec{S}_{i-1/2} + \bar{F}_{ij} \cdot \vec{S}_{j-1/2}) \quad (17.2.96)$$

where Ω_{ij} is the area of the cell.

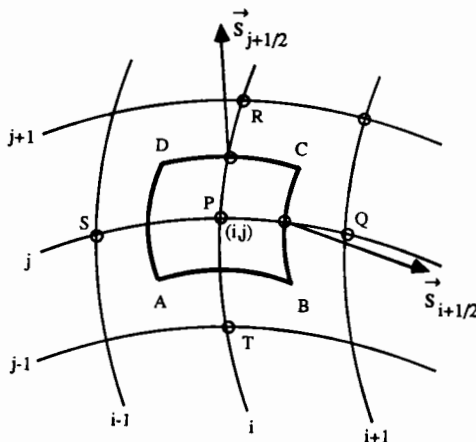


Figure 17.2.14 Control volume ABCD for finite volume discretization of MacCormack's scheme

The corrector step is

$$\bar{U}_{ij} = U_{ij}^n - \frac{\Delta t}{\Omega_{ij}} (\bar{F}_{ij} \cdot \bar{S}_{i+1/2} + \bar{F}_{ij} \cdot \bar{S}_{j+1/2} + \bar{F}_{i-1} \cdot \bar{S}_{i-1/2} + \bar{F}_{j-1} \cdot \bar{S}_{j-1/2}) \quad (17.2.97)$$

and

$$U_{ij}^{n+1} = \frac{1}{2} (\bar{U}_{ij} + \bar{U}_{ij}) \quad (17.2.98)$$

The flux contributions are evaluated, for instance, as follows:

$$\begin{aligned} \bar{S}_{i+1/2} &= (y_{i+1/2,j+1/2} - y_{i+1/2,j-1/2}) \bar{I}_x \\ &\quad - (x_{i+1/2,j+1/2} - x_{i+1/2,j-1/2}) \bar{I}_y \quad (17.2.99) \\ &\equiv \Delta y_{i+1/2} \bar{I}_x - \Delta x_{i+1/2} \bar{I}_y \\ \bar{F}_{i+1,j} \bar{S}_{i+1/2} &= f_{i+1,j} \Delta y_{i+1/2} - g_{i+1,j} \Delta x_{i+1/2} \end{aligned}$$

Computational note With the definitions of the flux components f and g in conservative variables, the above contributions can be calculated as follows, where U is the vector of the conservative variables:

$$\bar{F} \cdot \bar{S} = \begin{vmatrix} \rho(u \Delta y - v \Delta x) \\ \rho u(u \Delta y - v \Delta x) + p \Delta y \\ \rho v(u \Delta y - v \Delta x) - p \Delta x \\ \rho H(u \Delta y - v \Delta x) \end{vmatrix} = U(u \Delta y - v \Delta x) + p \begin{vmatrix} 0 \\ \Delta x \\ -\Delta x \\ 0 \end{vmatrix} \quad (17.2.100)$$

The scalar quantity

$$q \equiv u \Delta y - v \Delta x = \bar{v} \cdot \bar{S} \quad (17.2.101)$$

is the volume flow rate through the cell side \bar{S} . Hence, it is computationally advantageous and recommended to follow this approach, defining

$$\bar{F}_{i+1,j} \bar{S}_{i+1/2} = U_{i+1,j} q_{i+1,j} + p_{i+1,j} \begin{vmatrix} 0 \\ \Delta y \\ -\Delta x \\ 0 \end{vmatrix} \quad (17.2.102)$$

Other variants can be defined by selecting different control volumes for predictor and corrector steps and defining the points at which the fluxes are estimated in an appropriate way; see, for instance, Thompkins *et al.* (1983) and Problem 17.24.

A three-dimensional finite volume formulation can be found in Rizzi and Inouye (1973).

A necessary CFL condition for stability is expressed by the condition that the numerical domain of dependence should contain all of the physical one.

This can be expressed by the general form

$$\Delta t \leq \min_{(ij)} \left(\frac{\Omega_{ij}}{|\bar{v}_{ij} S_{i-1/2}| + |\bar{v}_{ij} \bar{S}_{j-1/2}| + c_{ij} \sqrt{|\bar{S}_{i+1/2}|^2 + |\bar{S}_{i+1/2}|^2}} \right) \quad (17.2.103)$$

The operator splitting approach to multi-dimensional explicit schemes

An alternative to the multi-dimensional schemes of the previous section consists in splitting the discretized space operators into products of one-dimensional operators. This is also known as the fractional step method, advocated by Yanenko (1971).

A similar, but not identical, concept has been introduced for the resolution of multi-dimensional implicit schemes in Chapter 11 in Volume 1, known as ADI factorization. In the present context, the operator splitting has to be handled with more care than the ADI factorization, since the splitting acts directly on the order of accuracy of the scheme.

As a result it is expected that the split formulation will lead to improved stability properties or to reduced computational work. For instance, the two-dimensional Lax-Wendroff scheme could be replaced by a product of one-dimensional schemes as follows. Defining the Lax-Wendroff discretization operator for a one-dimensional equation, following equation (17.2.10),

$$\begin{aligned} U_{ij}^{n+1} &= L_x^{(LW)} U_{ij}^n = U_{ij}^n - \tau_x \bar{\delta}_x f_{ij} + \frac{\tau_x^2}{2} \delta_x^+ (A_{i-1/2, j} \delta_x^- f_{ij}^n) \\ &= \left[1 - \tau_x A_{ij} \bar{\delta}_x + \frac{\tau_x^2}{2} \delta_x (A_{ij}^2 \delta_x) \right] U_{ij}^n \end{aligned} \quad (17.2.104)$$

one can define a two-dimensional Lax-Wendroff scheme as

$$U_{ij}^{n+1} = L_x^{(LW)} L_y^{(LW)} U_{ij}^n \quad (17.2.105)$$

The Von Neumann stability analysis for linear equations is readily obtained as the product of the one-dimensional amplification matrices (17.2.12):

$$G = G_x G_y \quad (17.2.106)$$

where G_x and G_y are the expressions (17.2.12) for the x and y variables respectively. Hence, the stability conditions will be

$$|\sigma_x| \leq 1 \quad \text{and} \quad |\sigma_y| \leq 1 \quad (17.2.107)$$

These conditions are more favourable than those represented in Figure 17.2.7.

Working out the product $L_x^{(LW)} L_y^{(LW)}$, it is seen that third- and fourth-order terms in τ^3 and τ^4 appear in the development that are not present in the original two-dimensional form (17.2.48) (see Problem 17.15). If the matrices A, B do not commute, all the terms of (17.2.48) cannot be obtained by the product $L_x L_y$, and the second-order accuracy might be lost. Therefore, the symmetric splitting

$$U_{ij}^{n+1} = \frac{1}{2} (L_x L_y + L_y L_x) U_{ij}^n \quad (17.2.108)$$

will reproduce all the $\tau_x \tau_y$ terms, plus additional terms, but the resulting scheme will remain second order in Δt and Δx .

Split MacCormack scheme

The two-dimensional MacCormack scheme can be formulated in split form by products of one-dimensional operators. The operator $L_x^{(M)}(\Delta t/2)$ is defined by the scheme (17.2.29) as

$$U_{ij}^{n+1/2} \equiv L_x^{(M)}\left(\frac{\Delta t}{2}\right)U_{ij}^n \quad (17.2.109)$$

where $L_x^{(M)}$ results from the predictor corrector sequence

$$\bar{U}_{ij} = U_{ij}^n - \tau_x(f_{i+1,j}^n - f_{ij}^n) \quad (17.2.110)$$

$$U_{ij}^{n+1/2} = \frac{1}{2}(U_{ij}^n + \bar{U}_{ij}) - \frac{\tau_x}{2}(\bar{f}_i - \bar{f}_{i-1}) \quad (17.2.111)$$

The operator $L_y^{(M)}(\Delta t)$ is defined in a similar way by interchanging the roles of i and j as well as f and g . Hence, the scheme

$$U_{ij}^{n+1} = L_x^{(M)}\left(\frac{\Delta t}{2}\right)L_y^{(M)}\left(\frac{\Delta t}{2}\right)U_{ij}^n \quad (17.2.112)$$

is an alternative to MacCormack's scheme (17.2.91). The linear stability analysis is identical to the one just described, since each factor L_x^M, L_y^M has the amplification matrix of the corresponding one-dimensional Lax-Wendroff scheme. Hence, one also obtains the conditions (17.2.107).

Here, again, it is seen by developing the operator product $L_x^M \cdot L_y^M$ that an order of accuracy is lost when the Jacobian matrices A, B do not commute.

In order to maintain the second order of accuracy, it is necessary to define symmetric sequences of split operators (see Strang, 1976). The following alternatives are valid:

- (1) Alternate the sequences $L_x^{(M)}L_y^{(M)}$ and $L_y^{(M)}L_x^{(M)}$; a $2\Delta t$ cycle is defined whereby

$$\begin{aligned} U_{ij}^{n+1} &= L_x^{(M)}\left(\frac{\Delta t}{2}\right)L_y^{(M)}\left(\frac{\Delta t}{2}\right)U_{ij}^n \\ U_{ij}^{n+2} &= L_y^{(M)}\left(\frac{\Delta t}{2}\right)L_x^{(M)}\left(\frac{\Delta t}{2}\right)U_{ij}^{n+1} \\ &= L_y^{(M)}\left(\frac{\Delta t}{2}\right)L_x^{(M)}\left(\frac{\Delta t}{2}\right)L_x^{(M)}\left(\frac{\Delta t}{2}\right)L_y^{(M)}\left(\frac{\Delta t}{2}\right)U_{ij}^n \end{aligned} \quad (17.2.113)$$

- (2) Distribute the time interval in fractions through the scheme

$$U_{ij}^{n+2} = L_y^{(M)}\left(\frac{\Delta t}{2}\right)L_x^{(M)}(\Delta t)L_y^{(M)}\left(\frac{\Delta t}{2}\right)U_{ij}^n \quad (17.2.114)$$

or

$$U_{ij}^{n+2} = L_x^{(M)} \left(\frac{\Delta t}{2} \right) L_y^{(M)} (\Delta t) L_x^{(M)} \left(\frac{\Delta t}{2} \right) U_{ij}^n \quad (17.2.115)$$

advancing the solution by two time steps $2\Delta t$.

(3) A still more general splitting sequence is

$$U_{ij}^{n+2} = \left[L_y^{(M)} \left(\frac{\Delta t}{2N} \right) \right]^N L_x^{(M)} \left[L_y^{(M)} \left(\frac{\Delta t}{2N} \right) \right]^N U_{ij}^n \quad (17.2.116)$$

In these sequences the one-dimensional operators have different time steps. For unequal mesh sizes $\Delta x \neq \Delta y$, larger time steps can be chosen for the direction with the larger mesh size. If $\Delta y > \Delta x$, one can allow $L_y(\Delta t_y)$ with the CFL limitation $\Delta t_y \leq \Delta y/\rho(B)$ and combine in a symmetric set with $L_x(\Delta t_x)$ operators, such that the sum of all Δt equals the interval ΔT over which the solution is advanced in time.

The two-dimensional version of the S_α^p schemes

The extension of the S_α^p schemes to two-dimensional problems has been investigated by Lerat (1981) in a systematic analysis of predictor–corrector schemes, which reduce in the linear case to the two-dimensional Lax–Wendroff schemes (see also Lerat and Sides, 1982).

A first extension with one predictor in unsplit form did not appear to be satisfactory. Consequently, Lerat considered schemes with two predictors and a single corrector, in an approach which resembles the operator splitting concept. However, the predictors are not pure one-dimensional operators.

Requiring the schemes to be restricted to nine points around (i, j) to be second-order accurate in space and time leads to a family with four parameters $\alpha_1, \alpha_2, \beta_1, \beta_2$, which can be extracted from the original 67 parameters and defined as follows:

$$\begin{aligned} \bar{U}_{ij} = & U_{ij}^n + \beta_1 (U_{i+1,j}^n - U_{ij}^n) - \alpha_1 \tau_x (f_{i+1,j}^n - f_{ij}^n) \\ & - \alpha_1 \frac{\tau_y}{4} (g_{i+1,j+1}^n + g_{i,j+1}^n - g_{i+1,j-1}^n - g_{i,j-1}^n) \end{aligned} \quad (17.2.117)$$

$$\begin{aligned} \bar{\bar{U}}_{ij} = & U_{ij}^n + \beta_2 (U_{i,j+1}^n - U_{ij}^n) - \alpha_2 \tau_y (g_{i,j+1}^n - g_{ij}^n) \\ & - \alpha_2 \frac{\tau_x}{4} (f_{i+1,j+1}^n + f_{i+1,j}^n - f_{i-1,j+1}^n - f_{i-1,j}^n) \end{aligned} \quad (17.2.118)$$

$$U_{ij}^{n+1} = U_{ij}^n - \tau_x (f_{i+1/2}^* - f_{i-1/2}^*) - \tau_y (g_{i,j+1/2}^* - g_{i,j-1/2}^*) \quad (17.2.119)$$

$$\begin{aligned} f_{i+1/2}^* = & \frac{1}{2\alpha_1} [(\alpha_1 - \beta_1) f_{i+1,j}^n + (\alpha_1 + \beta_1 - 1) f_{ij}^n + \bar{f}_{ij}] \\ g_{i,j+1/2}^* = & \frac{1}{2\alpha_2} [(\alpha_2 - \beta_2) g_{i,j+1}^n + (\alpha_2 + \beta_2 - 1) g_{ij}^n + \bar{\bar{g}}_{ij}] \end{aligned} \quad (17.2.120)$$

The numerical flux $f_{i+1/2,j}^*$ is defined as in equation (17.2.41) with $\alpha = \alpha_1$ and $\beta = \beta_1$ while $g_{i,j+1/2}^*$ is obtained from a similar expression with j taking the role of i , with $\alpha = \alpha_2$, $\beta = \beta_2$ and f replaced by g . In addition, \bar{f}_{ij} is defined by $f(\bar{U}_{ij})$ in $f_{i+1/2,j}^*$ and by $\bar{g}_{ij} = g(\bar{U}_{ij})$ in $g_{i,j+1/2}^*$.

It can be observed that the predictor steps are close to the one-dimensional predictors (17.2.38), except for the last terms, which represent a two-dimensional contribution. Hence these schemes are a straightforward extension of the one-dimensional S_α^β schemes.

This family of predictor-corrector schemes contains several known schemes as a particular case. For $\alpha_1 = \alpha_2 = \beta_1 = \beta_2 = \frac{1}{2}$ one obtains a scheme proposed earlier by Thommen (1966) for the Navier-Stokes equations and applied by Singleton (1968) and Magnus and Yoshihara (1975) to the Euler equations.

The choice $\alpha_1 = \alpha_2 = 1$, $\beta_1 = \beta_2 = \frac{1}{2}$ corresponds to a scheme proposed by Palumbo and Rubin (1972).

It is to be noticed, however, that the two-dimensional MacCormack schemes are not included in the above four-parameter family, in contrast to the one-dimensional case where the choice $\alpha = 1$, $\beta = 0$ or $\alpha = 1$, $\beta = 1$ reduce to

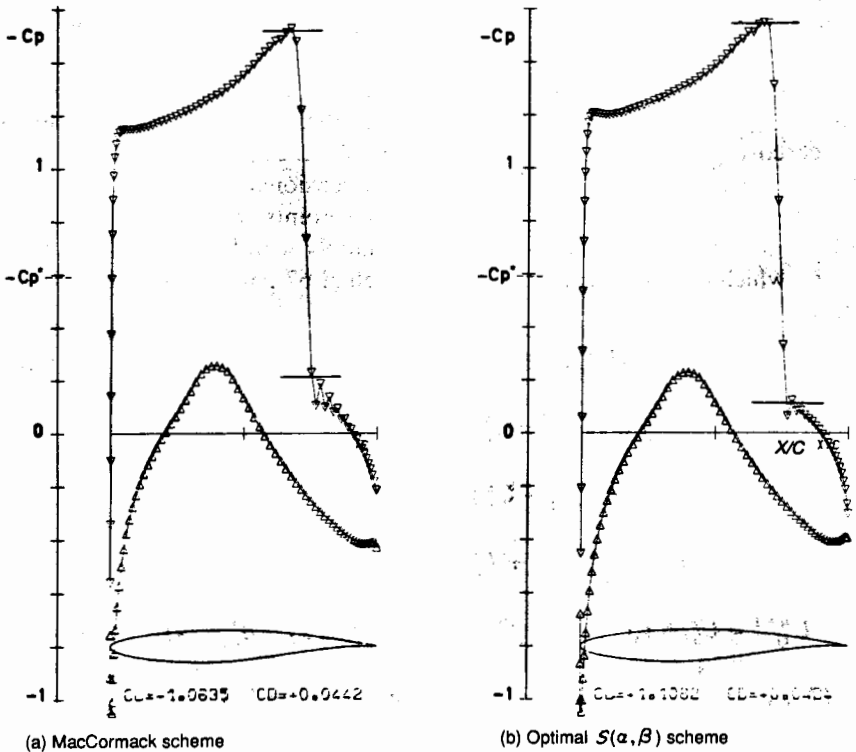


Figure 17.2.15 Pressure distribution on an RAE 2822 airfoil at $M_\infty = 0.75$ and 3° incidence. (From Lerat and Sides, 1982)

the MacCormack schemes. Observe also that for $\beta_1 = \beta_2 = \frac{1}{2}$, the schemes are symmetric around $i + \frac{1}{2}$ and $j + \frac{1}{2}$.

All the schemes reduce to the Lax–Wendroff form (17.2.48) for constant matrices A and B , independently of the $\alpha_1, \alpha_2, \beta_1, \beta_2$ coefficients. They represent therefore a family of non-linear multi-step variants of the Lax–Wendroff scheme.

In calculating the equivalent differential equations, the coefficients of Δx^2 and Δy^2 are identical to the corresponding one-dimensional terms (17.2.45) and hence an optimal scheme selection can be made, which would, as in the one-dimensional S_2^p schemes, have an optimal dissipation for the compression waves due to the non-linear contributions in the truncation error, while keeping to a minimum the antidissipation of the expansion waves. This can then be obtained for the same set of values; that is

$$\alpha_1 = \alpha_2 = 1 + \sqrt{\frac{5}{2}} \quad \beta_1 = \beta_2 = \frac{1}{2}$$

Figure 17.2.15 shows a comparison between MacCormack's scheme and the above optimal scheme for a transonic airfoil computation, from Lerat and Sides (1982). Both calculations have been performed on the same mesh of 224×29

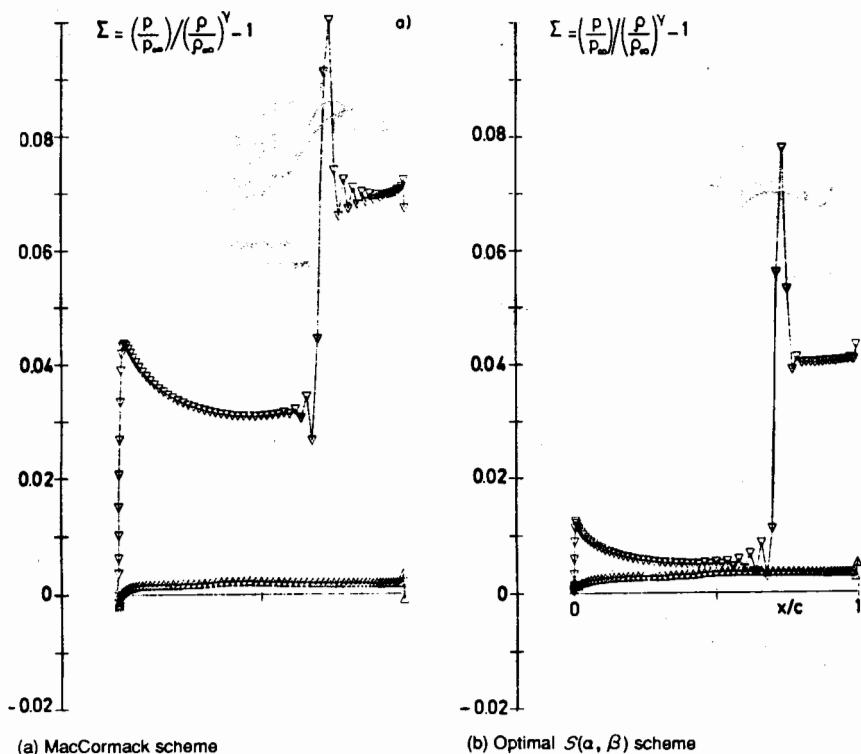


Figure 17.2.16 Entropy distribution on an RAE 2822 airfoil at $M_\infty = 0.75$ and 3° incidence. (From Lerat and Sides, 1982)

cells, with the same boundary conditions and additional artificial viscosity (see Section 17.3 for more details on this last aspect).

The calculations performed on an RAE 2822 airfoil at $M_\infty = 0.75$ and 3° incidence show the postshock oscillations with MacCormack's method on the pressure distributions (Figure 17.2.15(a)), compared to the results of the optimal scheme (Figure 17.2.15(b)). The horizontal bars indicate the Rankine–Hugoniot jump, which appears somewhat inaccurate with the MacCormack computation. The plot of the surface entropy distribution on Figure 17.2.16 gives a better view of the difference in behaviour of the two schemes.

It can be seen that the strong expansion at the leading edge produces a large entropy rise with the MacCormack scheme—about four times as large as with the optimal scheme.

The plotted quantity $\Sigma = (\rho/\rho^y)(p_0/\rho_0^y) - 1$ is a measure of the entropy errors, since the entropy should remain zero in this isentropic flow, except at the shock,

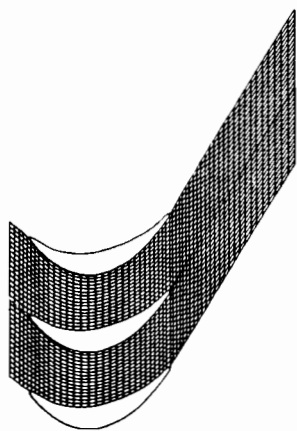
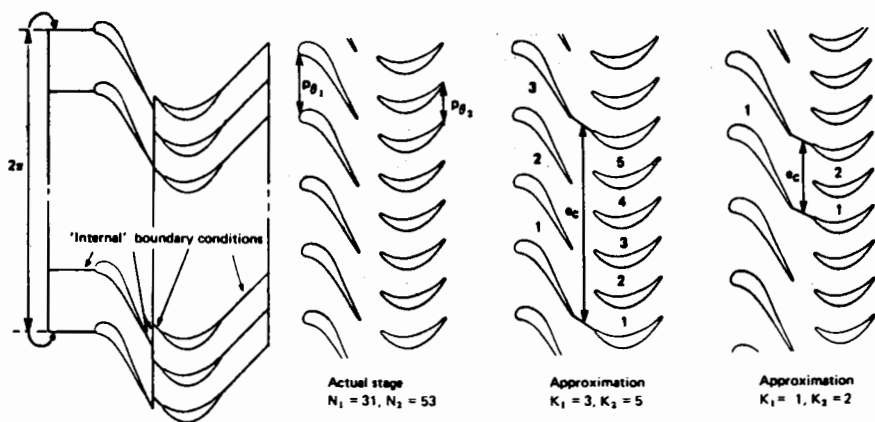


Figure 17.2.17 Geometry and mesh for the stator–rotor interaction in the two-dimensional section of a turbine stage. (From Fourmaux and Le Meur, 1987)

where the Rankine–Hugoniot conservation laws impose an entropy discontinuity. Hence any deviation from this behaviour indicates a generation of numerical (unwanted) viscosity.

Observe also that the entropy has a maximum inside the numerical shock structure. A similar property is actually obtained when physical shock structures are analysed on the basis of the Navier–Stokes equations; see, for example, Zeldovich and Rainer (1967).

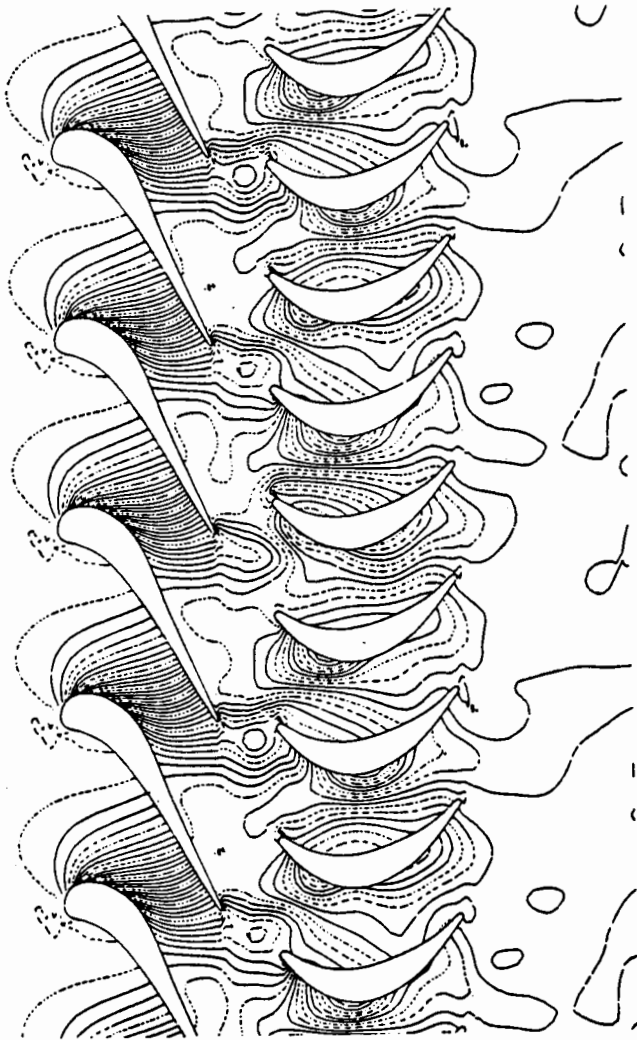


Figure 17.2.18 Instantaneous pressure field for the stator–rotor interaction in the two-dimensional section of a turbine stage. (From Fourmaux and Le Meur, 1987)

Example 17.2.2 Unsteady flow in a two-dimensional section of a turbine stage

The interaction between the rotor and stator in turbomachines creates an unsteady flow component which can have a non-negligible effect on performance. Calculations of this interaction on a domain composed of three stator and five rotor blades have been performed at ONERA with MacCormack's scheme (Fourmaux and Le Meur, 1987). Figure 17.2.17 displays the mesh between two consecutive blades and several of the full-stage arrangements considered. The total mesh contains 40 000 points and characteristic relations are applied as boundary conditions. A typical instantaneous pressure field is shown in Figure 17.2.18 for steady inflow conditions in front of the stator demonstrating the unsteady flow pattern.

17.3 THE CONCEPT OF ARTIFICIAL DISSIPATION OR ARTIFICIAL VISCOSITY

All the second-order, three-point central schemes of the Lax–Wendroff family generate oscillations around sharp discontinuities, as shown in Figures 17.2.2 to 17.2.4. Similar effects were also observed with the linear convection equation in Chapters 8 and 9 in Volume 1.

First-order schemes, on the other hand, have truncation errors proportional to a second derivative which acts as an added numerical viscosity (see equation (17.1.7)). Therefore, these schemes will damp the high-frequency components and smooth out strong gradients.

An alternative explanation for the oscillatory behaviour of the shock transition with Lax–Wendroff schemes is given by Lax and Wendroff (1960) in their original paper. This remarkable paper contains many basic ideas and considerations which are still highly up to date and we strongly recommend a careful reading of this work.

A stationary solution, in particular a stationary discontinuity, will satisfy the asymptotic part of the scheme (17.2.6), that is the steady state \bar{u}_i will satisfy in the linearized case

$$-\frac{\sigma}{2}(\bar{u}_{i+1} - \bar{u}_{i-1}) + \frac{1}{2}\sigma^2(\bar{u}_{i+1} - 2\bar{u}_i + \bar{u}_{i-1}) = 0 \quad (17.3.1)$$

When this solution is approached, for $u_i^{n+1} = u_i^n$, the spatial error $\varepsilon_i = u_i^n - \bar{u}_i$ satisfies the same equation

$$-\frac{\sigma}{2}(\varepsilon_{i+1} - \varepsilon_{i-1}) + \frac{1}{2}\sigma^2(\varepsilon_{i+1} - 2\varepsilon_i + \varepsilon_{i-1}) = 0 \quad (17.3.2)$$

Following the normal mode analysis of Section 10.5 in Volume 1, an exact solution of the form $\varepsilon_i = \kappa^i$ can be found, leading to

$$\kappa = \frac{1 + \sigma}{\sigma - 1} \quad (17.3.3)$$

Since the stability limit is $|\sigma| < 1$, κ will always be negative. Hence at consecutive points $i, i + 1$, the error $\varepsilon_i = \kappa^i$ will change sign, leading to an oscillatory behaviour of the numerical solution. This behaviour represents an 'odd-even' point error of wavelength $2\Delta x$, that is of high frequency. Since $G(\pi) = 1 - 2\sigma^2$, these oscillations will not be damped when $\sigma \simeq 0$, that is when a sonic point is encountered.

For the Lax–Friedrichs first-order scheme, κ is always positive, since $\kappa = (1 + \sigma)/(1 - \sigma)$ in this case.

In order to remove the unavoidable high-frequency oscillations around discontinuities in second-order central schemes, Von Neumann and Richtmyer (1950) introduced the concept of *artificial viscosity* or *artificial dissipation*. These additional terms should simulate the effects of the physical viscosity, *on the scale of the mesh*, locally around the discontinuities and be negligible, that is of an order equal or higher than the truncation error, in smooth regions. Additional dissipation is also required to avoid the appearance of expansion shocks, as seen in Figures 17.2.3 and 17.2.4, by providing enough dissipation when the intrinsic dissipation of the scheme vanishes at sonic transitions.

17.3.1 General form of artificial dissipation terms

Lax and Wendroff (1960) made a general analysis on the conditions to be fulfilled by an additional dissipative term added to a difference scheme of second-order accuracy.

The numerical fluxes $f_{i+1/2}^*$ given by equations (17.2.8), (17.2.32) or (17.2.41) for the different versions of the non-linear Lax–Wendroff schemes do all have the same structure and are members of a general family, which can be written according to Lax and Wendroff (1960) as

$$f_{i+1/2}^* = \frac{f_{i+1} + f_i}{2} - \frac{1}{2}\tau A_{i+1/2}(f_{i+1} - f_i) - D(U_i, U_{i+1}) \cdot (U_{i+1} - U_i) \quad (17.3.4)$$

where D is any positive function of $(U_{i+1} - U_i)$ which goes to zero at least linearly with $(U_{i+1} - U_i)$.

All the numerical fluxes of the form (17.3.4) satisfy the requirement derived in Section 9.4 for second-order accuracy (equation (9.4.22)), written here as

$$\left(\frac{\partial f^*}{\partial U_{i+1}} - \frac{\partial f^*}{\partial U_i} \right)_{v_i} = -\tau A_i^2 \quad (17.3.5)$$

The freedom in the choice of the function D can be used to generate additional dissipation in the scheme in order to control the high-frequency oscillations generated around discontinuities.

The function D must have the dimensions of A , that is the dimension of a velocity, and therefore $D \Delta x$ has the dimensions of a viscosity if u represents a velocity component; Lax and Wendroff call D the *artificial viscosity*. Introducing (17.3.4) into the general form of the conservative scheme (17.2.7) leads to the

Lax–Wendroff scheme (17.2.5) with an additional contribution from D :

$$U_i^{n+1} - U_i^n = -\tau(f_{i+1/2}^* - f_{i-1/2}^*)_{LW} + \tau[D_{i+1/2}(U_{i+1} - U_i) - D_{i-1/2}(U_i - U_{i-1})] \quad (17.3.6)$$

where the artificial viscosity term can be considered as a discretization of $\Delta x(\partial/\partial x)((D(\partial U/\partial x))$. Hence, the addition of an artificial viscosity (AV) term can be considered as a modification of the numerical flux f^* which is replaced by

$$f^{(AV)*} = f^* - \Delta x D \frac{\partial U}{\partial x} \quad (17.3.7a)$$

and in discretized form

$$f_{i+1/2}^{(AV)*} = f_{i+1/2}^{(LW)*} - D_{i+1/2}(U_{i+1} - U_i) \quad (17.3.7b)$$

where D is at least proportional to Δx in order to maintain the second-order accuracy. Note the similarity of equation (17.3.7a) with the viscous flux terms of the Navier–Stokes equations, where $D \Delta x$ plays the role of the viscosity.

The additional terms will have a non-negligible influence at points where the solution undergoes strong variations, but will be negligible in smooth regions where they are at least of the order of the truncation error.

In order for $D_{i+1/2}$ to have a stabilizing influence, it has to be positive.

However, one can also define D as a polynomial function of $(U_{i+1} - U_i)$, which is often done in practical implementations of artificial viscosity terms.

17.3.2 Von Neumann–Richtmyer artificial viscosity

The original method applied by Von Neumann and Richtmyer (1950) can be written for a one-dimensional flow in the above form, when the conservative variable U is replaced by the velocity u for the momentum and energy equations and is not considered with the continuity equation. The origin of the method is based on the consideration of an additional pressure term, which is added only to the momentum and energy equations, under the following form, for a one-dimensional case:

$$D \frac{\partial u}{\partial x} = \alpha \Delta x \rho \begin{vmatrix} 0 \\ 1 \\ u \end{vmatrix} \left| \frac{\partial u}{\partial x} \right| \frac{\partial u}{\partial x} \quad (17.3.8)$$

The discretized form of the associated dissipation terms is

$$D_{i+1/2}(u_{i+1} - u_i) = \alpha \rho_{i+1/2} \begin{vmatrix} 0 \\ 1 \\ u \end{vmatrix}_{i+1/2} |u_{i+1} - u_i| (u_{i+1} - u_i) \quad (17.3.9a)$$

or as alternative

$$D_{i+1/2}(u_{i+1} - u_i) = \alpha \rho_i \begin{vmatrix} 0 \\ 1 \\ u \end{vmatrix}_i |u_{i+1} - u_i| (u_{i+1} - u_i) \quad (17.3.9b)$$

The coefficient α is of the order of unity and has to be adjusted empirically.

In multi-dimensional problems, similar terms are added to each flux component separately.

The Von Neumann and Richtmyer artificial viscosity can be generalized to the following form:

$$f^{(AV)*} = f^* - \varepsilon \cdot \Delta x^2 \psi \left| \frac{\partial U}{\partial x} \right| \frac{\partial U}{\partial x} \quad (17.3.10)$$

where ψ are positive coefficients, which could depend on the mesh point i , such that $\psi \cdot U$ has the dimension of a velocity. Equation (17.3.10) is not to be interpreted as matrix products, but is to be read componentwise.

The artificial dissipation of Von Neumann and Richtmyer is non-linear and proportional to Δx^2 . Lower-order expressions have been attempted, for instance of the form

$$D = \alpha \Delta x (|u| + c) \quad (17.3.11)$$

but this gives generally too much dissipation in smooth flow regions and is not sufficiently selective in regions of sharp discontinuities.

Example 17.3.1 MacCormack scheme with artificial dissipation

In MacCormack's scheme the dissipation terms are generally added both at the predictor and corrector levels. In this case the scheme can be written as follows:

$$\overline{\Delta U}_i = -\tau(f_{i+1} - f_i)^n + \Delta t Q_i^n + \tau D_{i+1/2}^n (U_{i+1} - U_i)^n - \tau D_{i-1/2}^n (U_i - U_{i-1})^n \quad (E17.3.1)$$

$$\overline{\overline{\Delta U}}_i = -\tau(\bar{f}_i - \bar{f}_{i-1}) + \Delta t \bar{Q}_i + \tau \bar{D}_{i+1/2} (\bar{U}_{i+1} - \bar{U}_i) - \tau \bar{D}_{i-1/2} (\bar{U}_i - \bar{U}_{i-1}) \quad (E17.3.2)$$

The modified numerical flux of the explicit MacCormack scheme with the addition of artificial viscosity becomes

$$f_{i+1/2}^{(AV)*} = \frac{1}{2}(f_{i+1} + \bar{f}_i) - \frac{1}{2}[D_{i+1/2}(U_{i+1} - U_i) + \bar{D}_{i+1/2}(\bar{U}_{i+1} - \bar{U}_i)] \quad (E17.3.3)$$

Figure 17.3.1 shows the result of the application of MacCormack's scheme to the stationary nozzle flow of Figure 17.2.2 under the same conditions but with the addition of the Von Neumann-Richtmyer artificial viscosity. As can be seen, the oscillations at the shock have been damped and the mass flux error is reduced in amplitude from a maximum of 10 per cent to 0.4 per cent, but remains still spread over a large part of the flow region.

Figures 17.3.2 and 17.3.3 show the effects of the same dissipation terms on the shock tube flows of Figures 17.2.3 and 17.2.4. The artificial dissipation has prevented the appearance of the expansion shocks at the sonic transition. Observe also the smearing of the contact discontinuity and the good resolution of the shock. However, the results are not totally satisfactory, since some oscillations can still be observed.

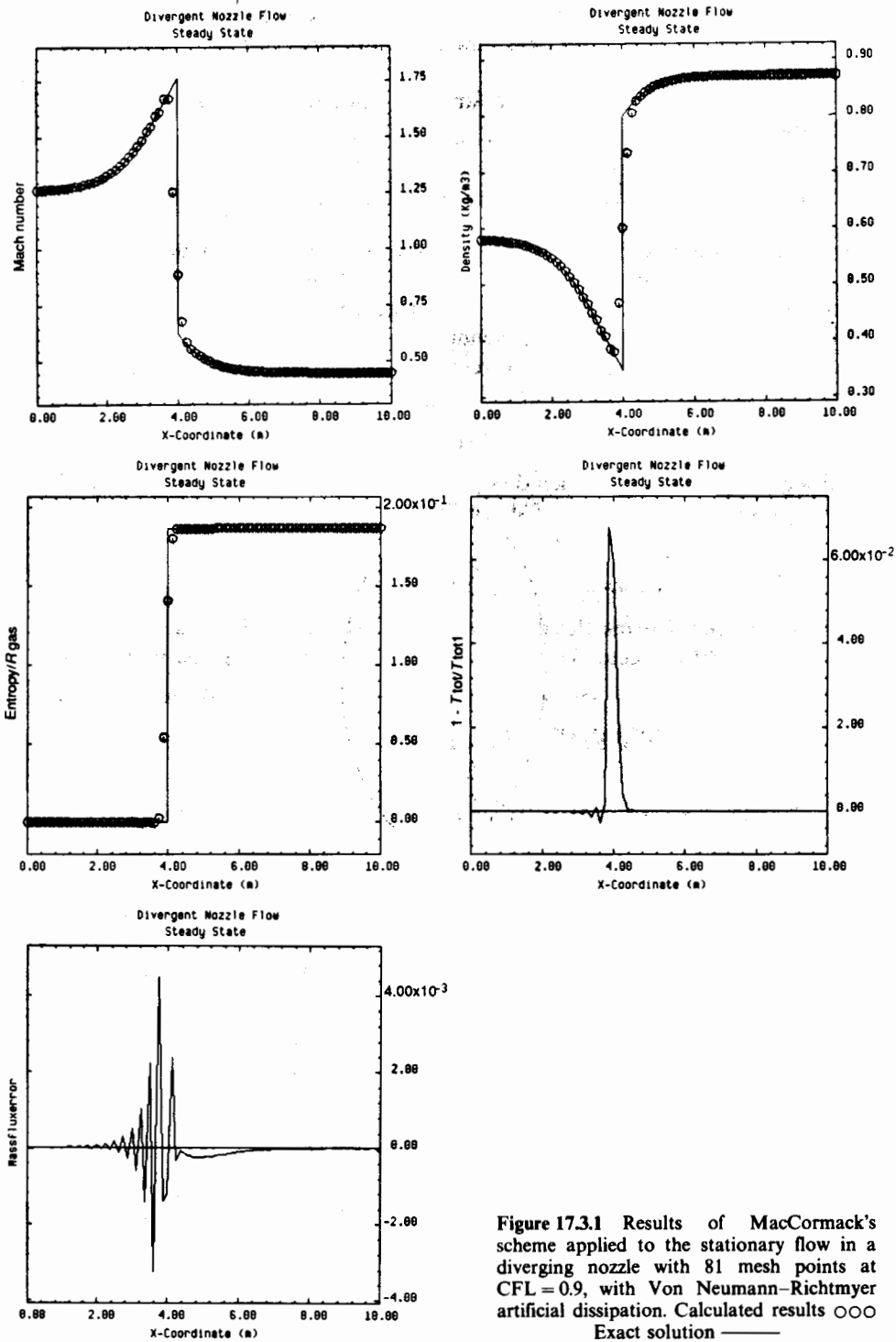


Figure 17.3.1 Results of MacCormack's scheme applied to the stationary flow in a diverging nozzle with 81 mesh points at CFL = 0.9, with Von Neumann-Richtmyer artificial dissipation. Calculated results ○○ Exact solution —

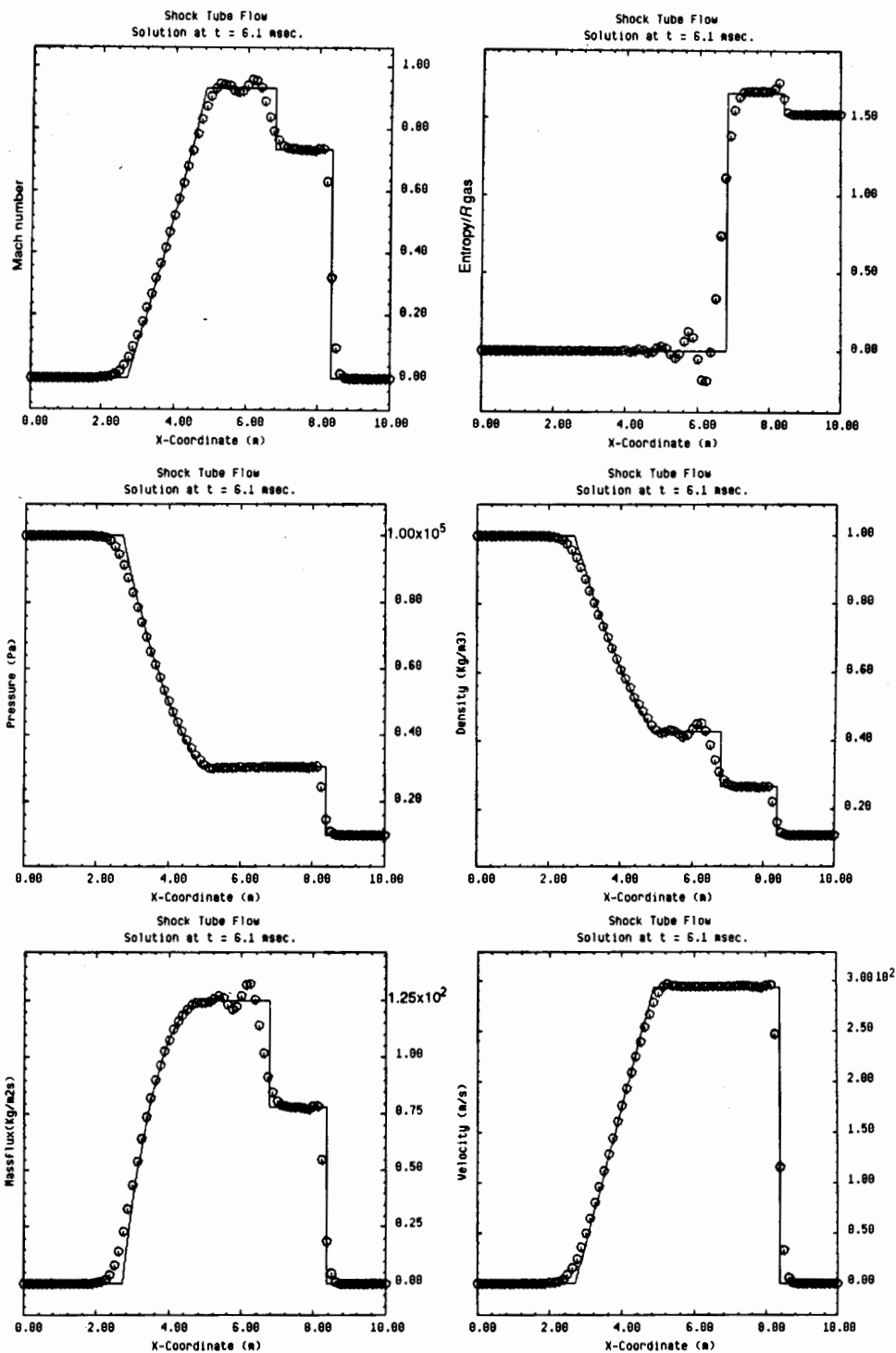


Figure 17.3.2 Results of MacCormack's scheme applied to the shock tube problem of Figure 16.6.8, with 81 mesh points at CFL = 0.95, after 35 time steps, with Von Neumann-Richtmyer artificial dissipation. Calculated results $\circ\circ$ Exact solution —

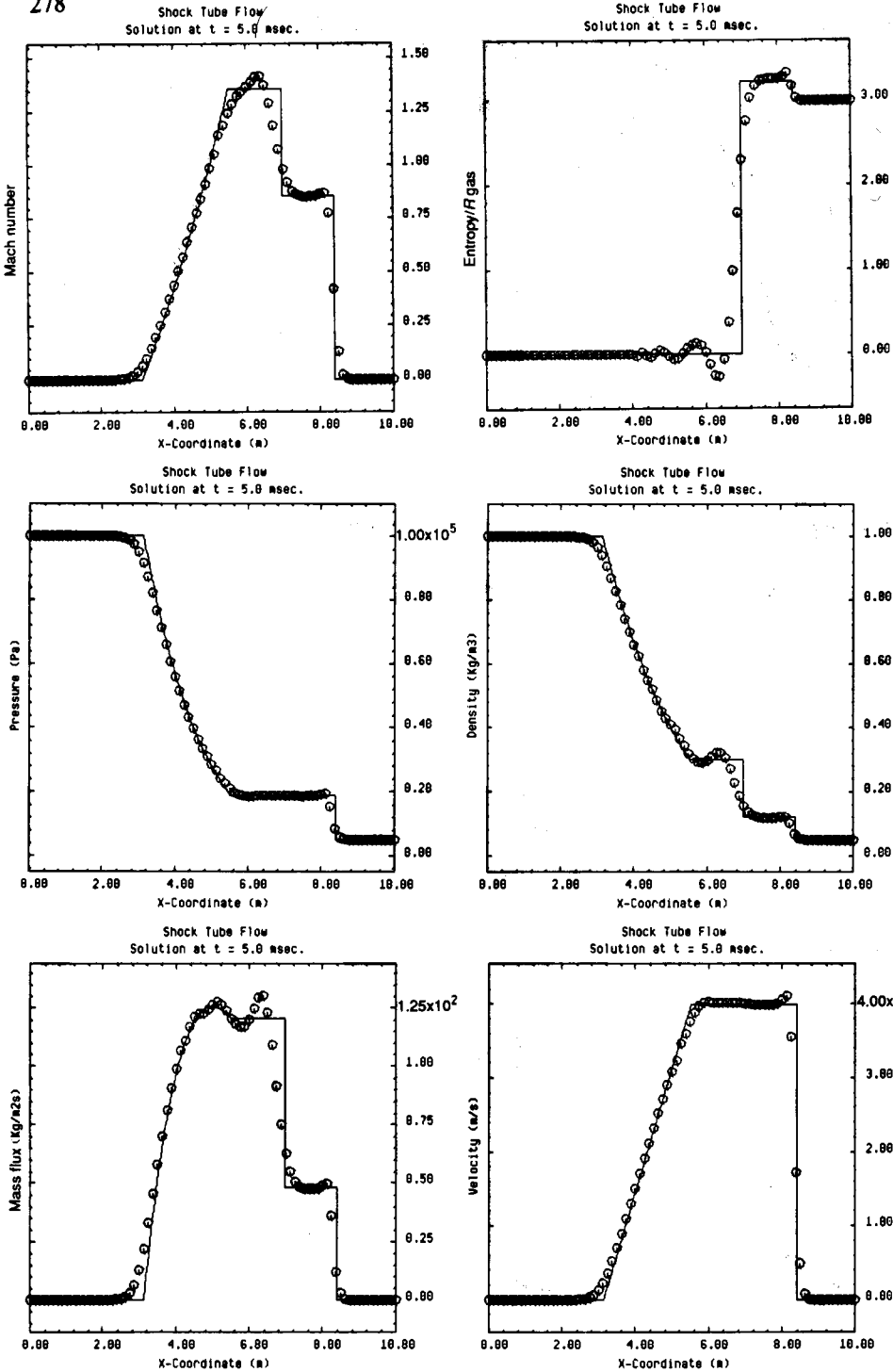


Figure 17.3.3 Results of MacCormack's scheme applied to the shock tube problem of Figure 16.6.9, with 81 mesh points at CFL = 0.95, after 35 time steps, with Von Neumann-Richtmyer artificial dissipation. Calculated results ○○ Exact solution —

17.3.3 Higher-order artificial viscosities

A third-order artificial viscosity has been applied by MacCormack and Baldwin (1975), whereby D is made proportional to a second derivative of the pressure field in order to enhance the effect of the dissipation in the presence of strong pressure gradients and to reduce it in the smooth flow regions.

The D factor is defined as follows:

$$D = \varepsilon \Delta x^2 \frac{|u| + c}{p} \left| \frac{\partial^2 p}{\partial x^2} \right| \quad (17.3.12)$$

and the modified numerical flux becomes

$$f^{(AV)*} = f^* - \varepsilon \Delta x^3 \frac{|u| + c}{p} \left| \frac{\partial^2 p}{\partial x^2} \right| \frac{\partial U}{\partial x} \quad (17.3.13)$$

It is generally computed as follows:

$$f_{i+1/2}^{(AV)*} = f_{i+1/2}^{(LW)*} - \varepsilon (|u| + c)_{i+1/2} \frac{|p_{i+1} - 2p_i + p_{i-1}|}{p_{i+1} + 2p_i + p_{i-1}} (U_{i+1} - U_i) \quad (17.3.14)$$

Another form of artificial viscosity is based on the addition of higher-order derivatives. It cannot be written as (17.3.7) but takes the form, with $a = |u| + c$ as the scaling velocity,

$$f^{(AV)*} = f^* + \varepsilon \Delta x^3 (|u| + c) \frac{\partial^3 U}{\partial x^3} \quad (17.3.15)$$

and represents a dissipation proportional to a fourth difference, linear in U .

This last expression has been introduced by Steger (1978) in the Beam and Warming schemes to be discussed in the following chapter.

Jameson's artificial dissipation

Jameson and others (Jameson *et al.*, 1981; Jameson, 1982) apply a blend of the expressions (17.3.14) and (17.3.15) with excellent shock-capturing properties. In this approach the third derivative term is switched off when the quantity (17.3.12) dominates. The same formulation has also been applied by Pulliam (1984) and Pulliam and Steger (1985) into the Beam and Warming codes with excellent results.

The corrected numerical flux is defined by

$$f_{i+1/2}^{(AV)*} = f_{i+1/2}^* - d_{i+1/2} \quad (17.3.16)$$

where d combines the MacCormack–Baldwin artificial dissipation with the linear fourth-order dissipation (17.3.15) in the following way:

$$d_{i+1/2} = \varepsilon_{i+1/2}^{(2)} (U_{i+1} - U_i) - \varepsilon_{i+1/2}^{(4)} (U_{i+2} - 3U_{i+1} + 3U_i - U_{i-1}) \quad (17.3.17)$$

where $\varepsilon^{(2)}$ is defined according to equation (17.3.14) and $\varepsilon^{(4)}$ according to equation (17.3.15).

The non-linear coefficient $\varepsilon^{(2)}$ is evaluated by

$$\varepsilon_{i+1/2}^{(2)} = \frac{1}{2}(\varepsilon_i^{(2)} + \varepsilon_{i+1}^{(2)}) \quad (17.3.18)$$

or

$$\varepsilon_{i+1/2}^{(2)} = \max(\varepsilon_i^{(2)}, \varepsilon_{i+1}^{(2)}) \quad (17.3.19)$$

where

$$\varepsilon_i^{(2)} = \alpha^{(2)}(|u| + c)_i \frac{|p_{i+1} - 2p_i + p_{i-1}|}{p_{i+1} + 2p_i + p_{i-1}} \quad (17.3.20)$$

The pressure term in $\varepsilon^{(2)}$ is generally of second order, except in regions of strong pressure gradients, where it reduces to first order or becomes of the order of one. Hence, around shocks, the $\varepsilon^{(2)}$ term is dominating.

This did not appear to be sufficient to avoid completely some small oscillations, of the order of 1 per cent in density variation, preventing the complete convergence to the steady state. They are noticeable mostly near regions with sharp gradients, such as airfoil trailing edges.

These oscillations were removed by the introduction of the third derivative term (17.3.15), providing some background dissipation through the domain, but led to the reappearance of overshoots around the shockwaves. Hence, the background dissipation is turned off when $\varepsilon^{(2)}$ is large and one defines

$$\varepsilon_{i+1/2}^{(4)} = \max[0, (\alpha^{(4)} - \varepsilon_{i+1/2}^{(2)}) / (u + c)] \quad (17.3.21)$$

where $\alpha^{(4)}$ is an adjustable constant.

Typical values of $\alpha^{(2)}$ and $\alpha^{(4)}$ are

$$\alpha^{(2)} \approx \frac{1}{4} \quad \alpha^{(4)} \approx \frac{1}{256} \quad (17.3.22)$$

The dissipation terms are added to the four equations, but in the energy equation the fourth component of U , namely ρE , is replaced by ρH in equation (17.3.17). This ensures that the steady state satisfies $H = H_\infty = \text{constant}$. Details of implementation and considerations of boundary treatment of these dissipation terms can be found in Pulliam (1985) and Swanson and Turkel (1987).

Many other forms of artificial viscosity can be found in the literature, and although the introduction of artificial viscosity may appear somewhat arbitrary it is by far not as 'artificial' as a first impression might lead us to think.

It will be shown indeed in Chapter 20 that any upwind scheme can be written as a central scheme plus dissipation terms. This fact has already been introduced in Chapter 15 when dealing with the calculation of transonic potential flows.

It shows that the dissipation terms introduce an upwind correction to the central schemes, such as to remove non-physical effects arising from the central discretization of wave propagation phenomena. These effects arise mainly around discontinuities, where a sudden change in the propagation direction of certain waves occurs. Due to its nature, the central discretization is not able to

handle this discontinuous change and generates oscillations. On the other hand, the upwind schemes are on the contrary defined as a function of the signs of the propagation velocities. Some form of equivalence is obtained in this way between upwind schemes, on one hand, and central schemes with artificial viscosity, on the other hand. It will even be shown in Chapter 21 that the introduction of upwind, second-order non-linear algorithms, controlling and preventing the appearance of unwanted oscillations, called TVD (total variation diminishing) schemes, allow the definition of artificial viscosity terms for Lax–Wendroff schemes, rendering them equivalent to upwind TVD schemes. This approach leads to artificial viscosity forms, without adjustable and empirical constants.

In the following we will refer to various forms of artificial viscosity and we encourage the reader to experiment with various forms on simple test cases.

Figure 17.3.4 shows the same test case as Figure 17.3.1 with the MacCormack–Baldwin dissipation (17.3.12) and $\varepsilon = 0.625$. Comparing to Figure 17.3.1 one notices the sharper shock, which is resolved over two mesh cells. The mass flux error is also extremely narrow and concentrated over the shock only. This indicates that the filter provided by the pressure derivatives in the dissipation terms is indeed very effective. Note, however, that the maximum mass flux error remains here at the level reached without artificial dissipation.

When applied to the shock tube problems of Figures 17.3.2 and 17.3.3, similar observations can be made with regard to the shock definition, namely that the shock is sharper with the MacCormack–Baldwin dissipation.

Remark

Some ambiguity is found in the literature with regard to the definition of numerical and artificial viscosities.

Lax and Wendroff call the function D in equation (17.3.4) the *artificial viscosity* defined as the contribution in the numerical flux *above* the Lax–Wendroff term $\frac{1}{2}\tau A_{i+1/2}(f_{i+1} - f_i)$ or, according to (17.2.22), $(\tau/2)A_{i+1/2}^2(U_{i+1} - U_i)$.

More recent trends write the numerical flux as

$$f_{i+1/2}^* = \frac{f_{i+1} + f_i}{2} - \frac{1}{2}\bar{D}_{i+1/2}(U_{i+1} - U_i) \quad (17.3.23)$$

and call the function $\bar{D}_{i+1/2} = \bar{D}(A_{i+1/2})$ the coefficient of numerical viscosity.

The significance of these denominations should be related to the numerical dissipation as obtained from the truncation errors. A first observation should be kept in mind, namely that the truncation error will have the structure of an effective viscosity or dissipation only if the scheme is first order. In this case, the truncation error has a term proportional to U_{xx} .

For instance, in the Lax–Friedrichs scheme, equation (17.1.19) shows that $\bar{D}(A_{i+1/2}) = 1/\tau$, but from the truncation error one has an expression of the form of equation (17.1.7), where $\alpha = (\Delta x^2/2\Delta t)(1 - \tau^2 A^2)$ plays the role of an effective numerical dissipation coefficient.

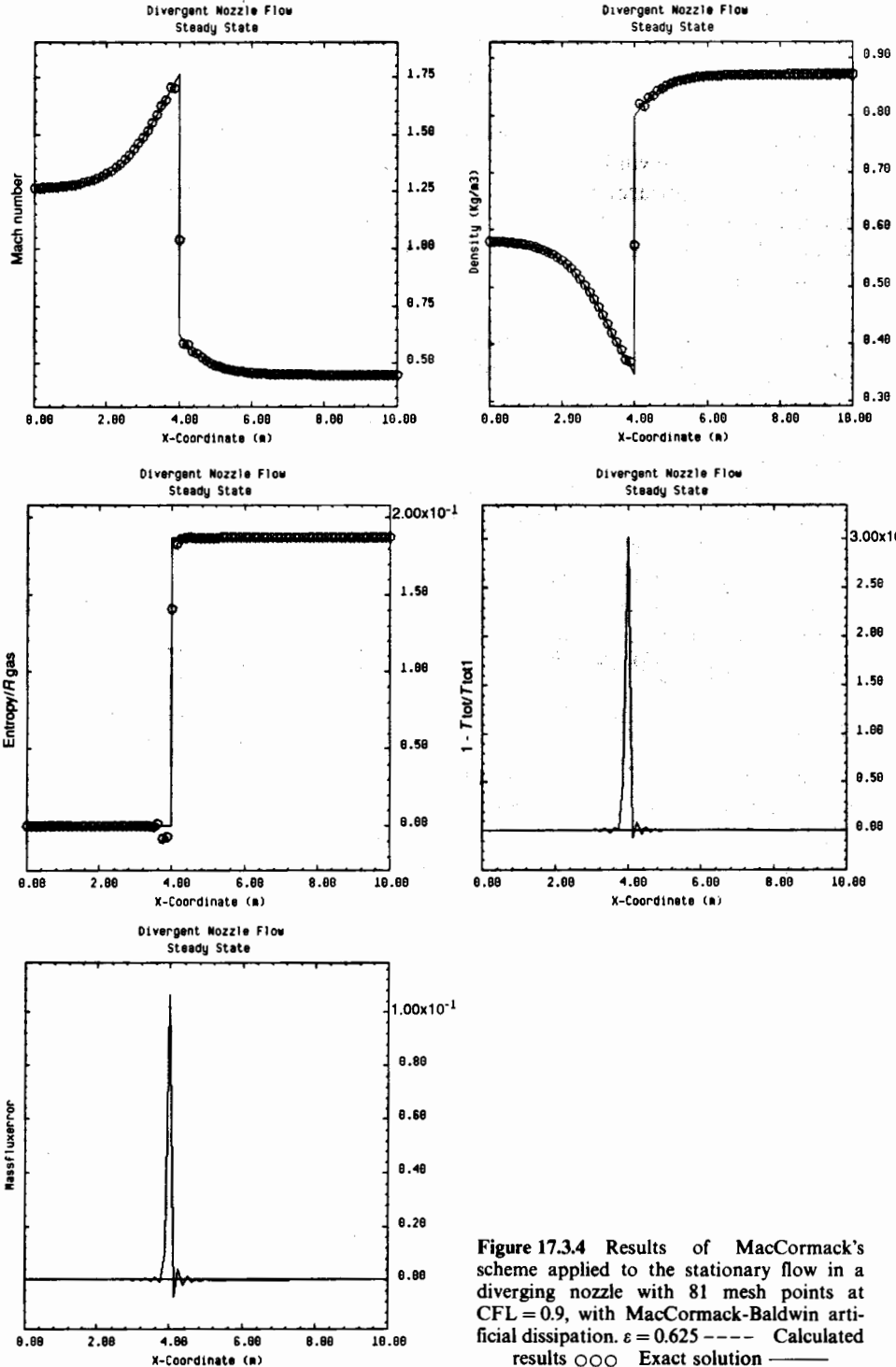


Figure 17.3.4 Results of MacCormack's scheme applied to the stationary flow in a diverging nozzle with 81 mesh points at CFL = 0.9, with MacCormack-Baldwin artificial dissipation. $\epsilon = 0.625$ --- Calculated results ○○ Exact solution —

More generally, the first-order truncation term of a scheme in conservative form with a numerical flux f^* is given by equation (9.4.21), Chapter 9 in Volume 1. Applied to the above equation (17.3.16), the coefficient of the U_{xx} term can be written as

$$\frac{\partial f^*}{\partial U_{i+1}} - \frac{\partial f^*}{\partial U_i} + \tau A^2 = -\bar{D} + \tau A^2 \quad (17.3.24)$$

and the effective numerical dissipation coefficient, to be compared to the physical viscosity, is

$$\alpha = \frac{\Delta x}{2} (\bar{D} - \tau A^2) \quad (17.3.25)$$

The Lax–Wendroff scheme corresponds to $\bar{D} = \tau A^2$ and equation (17.3.4) corresponds to $\bar{D} = \tau A^2 + 2D$, where D goes to zero with $(U_{i+1} - U_i)$. Hence D is proportional to Δx and does not contribute to the U_{xx} truncation error.

For second-order schemes, the lowest-order truncation error is a dispersive error of the form $\beta \Delta x^2 U_{xxx}$. Hence, the dominating effect is not of a dissipative nature and care has to be exercised in the interpretation of terms like \bar{D} and D as ‘viscosity’ coefficients in a strict sense.

17.4 LERAT’S IMPLICIT SCHEMES OF LAX–WENDROFF TYPE

The schemes of the Lax–Wendroff family presented in the previous sections are explicit as an outcome of the initial derivation by a Taylor expansion in time, followed by a central space discretization. When compared to the straightforward central space discretization of the flux terms, $f_x = (f_{i+1} - f_{i-1})/2\Delta x$, which is unstable with an explicit forward difference in time, the Lax–Wendroff approach can be considered as a means to introduce some dissipation in the scheme through the time derivative terms. This dissipation is proportional to the time step and is sufficient to stabilize the central flux difference, although additional dissipation has to be introduced in order to resolve the shock oscillations.

A similar line of development can be adopted to generate implicit schemes, in the line of the Lax–Wendroff ‘methodology’, by combining time and space discretizations in order to achieve certain desirable properties. This approach has been applied by Lerat (1979, 1985) to generate a family of implicit, central, second-order schemes depending on three parameters that are unconditionally stable and have dissipative properties, resulting in an implicit extension of the Lax–Wendroff schemes.

The reason behind the development of implicit schemes is to be found in the severe limitation on the permissible time step of explicit schemes as a consequence of the CFL-condition. If a_{\max} is the maximum speed of propagation of a one-dimensional problem $a_{\max} = (|u| + c)_{\max}$, the time step Δt is limited by

$$\Delta t < \text{CFL} \frac{\Delta x_{\min}}{a_{\max}} = \frac{\Delta x_{\min}}{(|u| + c)_{\max}} \text{CFL}$$

where CFL is the maximum Courant number. The maximum allowable time step Δt can become very small, particularly with fine meshes.

With steady-state problems, where the stationary solution is sought and convergence is reached when the variations $\Delta U = U^{n+1} - U^n$ come below an imposed limit, explicit schemes will require a large number of time steps, of the order of several thousands. Although this concern becomes less severe with the development of new generations of vector and parallel processors and with the introduction of multi-grid techniques, it is still important to be able to reach the computed steady-state flow in a minimum of time steps.

When time accuracy is not required for stationary flows solved with a time-dependent method, one can apply a simple convergence acceleration technique by using *local time steps* which differ from one point to the other as a function of the local propagation speeds and corresponding local CFL condition. Hence, one will allow the solution to progress in time towards the steady-state conditions, at a different pace in each point.

The local time step at point i will be defined by

$$\text{CFL} \frac{\Delta x_{\min}}{(|u| + c)_{\max}} < \Delta t_i < \frac{\Delta x_{\min}}{(|u| + c)_i} \text{CFL}$$

The time evolution of the solution loses its physical significance since the time-dependent problem which is solved in this way corresponds to the pseudo time-dependent equation $U_{r^*} + f_x = 0$, where $t^* = t \cdot (|u| + c)_{\max} / (|u| + c)$. An alternative for strongly varying mesh sizes is to select

$$t^* = t \frac{(|u| + c)_{\max}}{(|u| + c)} \cdot \frac{\Delta x}{\Delta x_{\min}}$$

leading to a local permissible time step

$$\Delta t_i = \text{CFL} \frac{\Delta x_i}{(|u| + c)_i} \quad (17.4.1)$$

This leads to significant improvements of convergence rates but remains limited since the overall convergence rate will still depend on the slowest progressing zones.

Implicit schemes can also be important for time-dependent problems when the time scale of the unsteady phenomena is much larger than the time step allowed by the CFL condition. Although time-accurate solutions are required in this case, the possibility of allowing larger time steps than the CFL limit leads to a welcome gain in computational efficiency.

Therefore an alternative to the explicit schemes lies in the development of implicit methods that allow, as a consequence of their unconditional stability, higher time steps, limited only by accuracy requirements and eventual non-linear stability problems or boundary condition treatment.

We will present the developments of Lerat in some detail in this section, not only because of the interest and importance of the resulting schemes but also

because of the considerable didactic value of the rigorous and systematic analysis at the basis of these developments. As we will see from the following, all the properties of numerical schemes will be called upon in order to specify conditions on the parameters of the scheme. The truncation error analysis will lead to conditions on the order of accuracy and the development of the equivalent differential equation will provide guidelines for optimization of the dispersion and diffusion errors. The Von Neumann analysis will lead to conditions for the stability of the scheme and also to conditions for the solvability of the implicit operators (non-vanishing of the implicit operator). Furthermore, the error analysis will allow conditions to be set for maximal dissipation of high-frequency errors; in particular it can be requested that the Kreiss dissipative condition be satisfied for the parameters of the schemes. The available degrees of freedom also allow the imposition of an additional condition on the implicit operator, namely strict diagonal dominance.

Finally, the resulting three-parameter family of schemes can be tuned to optimize certain desirable properties: for instance, maximize convergence rates for stationary problems, or minimize dissipation and dispersion errors for unsteady flows, or fix the order of accuracy of the first, explicit, step, opening a wide range of Lax–Wendroff variants for this step.

17.4.1 Analysis for linear systems in one dimension

The starting point is the following, most general, implicit scheme with two time levels and three-point support for the linear system $U_t + AU_x = 0$, which generalizes the explicit form (9.2.10) in Volume 1:

$$c_{-1}U_{i-1}^{n+1} + c_0U_i^{n+1} + c_1U_{i+1}^{n+1} = b_{-1}U_{i-1}^n + b_0U_i^n + b_1U_{i+1}^n \quad (17.4.2)$$

The coefficients b_j and c_j are general functions of $\tau = \Delta t/\Delta x$ and A . The following considerations are an extension of the procedures developed in Section 9.2 in Volume 1, to which the reader is referred for the details of the calculations concerning the truncation errors and the consistency conditions.

A first consistency condition, expressing that a constant U should be a possible solution, is

$$\sum_{j=-1}^{+1} b_j = \sum_{j=-1}^{+1} c_j = 1 \quad (17.4.3)$$

Performing a Taylor expansion in the same way as in Section 9.2.1, the $(p+1)$ conditions for the scheme (17.4.2) to be accurate of order p in space and time for fixed ratios $\tau = \Delta t/\Delta x$ are obtained as

$$\sum_j j^m b_j = \sum_j c_j (j - \sigma)^m \quad \text{for } m = 0, 1, 2, \dots, p \quad (17.4.4)$$

where σ is defined by

$$\sigma = \tau A \quad (17.4.5)$$

For a scalar equation, $A = a$ and σ is the Courant number. For a system of equations, σ is a matrix whose maximum eigenvalue will represent the Courant number of the scheme, following equation (17.2.14).

It can be seen that equation (17.4.4) is a direct generalization of equation (9.2.23) and that the coefficients b_j and c_j are only dependent on σ .

Eliminating b_0 and c_0 via equation (17.4.3), four coefficients are left, and defining

$$\begin{aligned} b_+ &= b_1 + b_{-1} & b_- &= b_1 - b_{-1} \\ c_+ &= c_1 + c_{-1} & c_- &= c_1 - c_{-1} \end{aligned} \quad (17.4.6)$$

the schemes (17.4.2) can be written as follows (see problem 17.31):

$$U_i^{n+1} + c_- \bar{\delta} U_i^{n+1} + \frac{1}{2} c_+ \delta^2 U_i^{n+1} = U_i^n + b_- \bar{\delta} U_i^n + \frac{1}{2} b_+ \delta^2 U_i^n \quad (17.4.7)$$

The difference operators have been defined earlier (equation (14.1.2)) and δ^2 is the central second difference $\delta^2 U_i = U_{i+1} - 2U_i + U_{i-1}$. In Δ form, equation (17.4.7) can be written as

$$[1 + c_- \bar{\delta} + \frac{1}{2} c_+ \delta^2] \Delta U_i^n = (b_- - c_-) \bar{\delta} U_i^n + \frac{1}{2} (b_+ - c_+) \delta^2 U_i^n \quad (17.4.8)$$

Note that it is assumed for the moment that A is a constant matrix and therefore the coefficients b and c are also independent of the mesh point index i .

Obviously we require that the schemes be at least first-order accurate and the first consistency condition (17.4.4) for $m = 1$,

$$b_- - c_- = -\sigma \quad (17.4.9)$$

imposes the condition that the coefficient of the first difference in the right-hand side of equation (17.4.8) be equal to $-\sigma$. This merely shows that this term should be an approximation to the space derivative $A \partial U / \partial x$.

Equation (17.4.8) becomes

$$[1 + c_- \bar{\delta} + \frac{1}{2} c_+ \delta^2] \Delta U_i^n = -\sigma \bar{\delta} U_i^n + \frac{1}{2} (b_+ - c_+) \delta^2 U_i^n \quad (17.4.10)$$

The choice $b_+ = c_+ = 0$ and $c_- = \theta \sigma$ reproduces the Beam and Warming schemes (18.1.10) with $\xi = 0$ to be introduced in the following chapter (see also Problem 17.30).

In addition, if the coefficient of the second difference term in the right-hand side is set equal to γ , the explicit scheme obtained by $c_{\pm} = 0$ reproduces the family of first-order schemes (9.3.3).

If we look for, at least, *second-order schemes in space and time*, the relations (17.4.4) for $m = 2$, expressed as a function of the b_{\pm} and c_{\pm} coefficients, become

$$b_+ - c_+ = -2\sigma c_- + \sigma^2 \quad (17.4.11)$$

and equation (17.4.10) can be expressed as a function of the parameters c_{\pm} defining the *implicit part* of the algorithm as

$$[1 + c_- \bar{\delta} + \frac{1}{2} c_+ \delta^2] \Delta U_i = -\sigma \bar{\delta} U_i^n + \frac{1}{2} (\sigma - 2c_-) \sigma \delta^2 U_i^n \quad (17.4.12)$$

The explicit scheme, obtained by setting the c_{\pm} coefficients to zero, is the unique second-order space-centred scheme on the three-point support, namely the Lax–Wendroff scheme (17.2.6). For *any* other choice of the c_{\pm} coefficients, an implicit scheme is obtained, which maintains the second-order accuracy on the same three-point support.

The Beam and Warming schemes to be discussed in the following chapter are defined by the central discretization of the flux terms in the right-hand side of the Δ formulation. This implies the absence of any second difference term in the right-hand side residuals, hence, $c_- = \sigma/2$, leading to the trapezoidal scheme $\theta = \frac{1}{2}$, when $c_+ = 0$.

For third-order accuracy, the additional condition

$$c_+ = \sigma c_- + \frac{1 - \sigma^2}{3} \quad (17.4.13)$$

has to be satisfied, while the unique fourth-order accurate scheme will satisfy, in addition, the condition

$$c_- = \frac{\sigma}{2} \quad (17.4.14)$$

Von Neumann analysis: stability and solvability

A classical Von Neumann stability analysis is applied to the general scheme (17.4.7), leading to the amplification matrix G defined by

$$[1 + Ic_- \sin \phi - c_+(1 - \cos \phi)]G = 1 + Ib_- \sin \phi - b_+(1 - \cos \phi) \quad (17.4.15)$$

A first condition to be imposed on the implicit operator is that the factor multiplying G (which is equal to one for an explicit scheme) should not vanish in the range $\phi[-\pi, \pi]$. This ensures that the scheme will always be *solvable*.

Hence this will be the case if

$$c_+ < \frac{1}{2} \quad (17.4.16)$$

The stability of the scheme can be analysed following Section 8.6.1 in Volume 1, where the conditions (8.6.7) can be directly applied. The following necessary and sufficient conditions are obtained in this linear case:

$$b_-^2 - c_-^2 \leq b_+ - c_+ \quad (17.4.17a)$$

$$b_+^2 - c_+^2 \leq b_+ - c_+ \quad (17.4.17b)$$

For an explicit scheme, where $c_+ = c_- = 0$, the stability conditions reduce to

$$b_-^2 \leq b_+ \leq 1 \quad (17.4.18)$$

For the Lax–Wendroff scheme, with $b_- = \sigma$ and $b_+ = \sigma^2$, one obtains the CFL condition $|\sigma| \leq 1$.

Dissipative properties

The schemes (17.4.7) will be dissipative in the sense of Kreiss (see

equation (8.5.13)) if the spectral radius of G satisfies the condition

$$\rho(G) \leq 1 - K\phi^{2r} \quad \text{for } K > 0 \quad \text{and} \quad \phi[-\pi, \pi] \quad (17.4.19)$$

From an analysis of the amplification matrix in the limit as $\phi \rightarrow 0$ and in the region $\phi = \pi$, it can be shown (Lerat, 1981) that the schemes considered are dissipative in the sense of Kreiss if the stability conditions (17.4.17) are satisfied with a strict inequality in (17.4.17b). This implies, next to stability, that

$$b_+ \neq c_+ \quad \text{and} \quad b_+ \neq 1 - c_+ \quad (17.4.20)$$

for all eigenvalues of A .

For an explicit scheme, these conditions reduce to

$$b_+ \neq 0 \quad \text{and} \quad b_+ \neq 1 \quad (17.4.21)$$

When the schemes are dissipative, the order of dissipation is four, with the exception of the first-order schemes which are dissipative of order two only.

For the Lax-Wendroff schemes, $b_+ = \sigma^2$ and the scheme is dissipative when the Jacobian matrix A does not have zero eigenvalues.

Diagonal dominance

A property on the implicit operator that guarantees the convenient resolution of the algebraic system of the unknowns U^{n+1} either by direct or by iterative methods, is the condition of strict diagonal dominance. For the system (17.4.2) applied to a scalar equation, this is expressed by

$$|c_0| > |c_1| + |c_{-1}| \quad (17.4.22)$$

or in function of the c_{\pm} coefficients as

$$|1 - c_+| > |c_+ + c_-| + |c_+ - c_-| \quad (17.4.23)$$

By simple inspection it is seen that the condition of strict diagonal dominance is satisfied if

$$c_+ < \frac{1}{2} \quad \text{and} \quad c_+ + |c_-| < 1 \quad (17.4.24)$$

Observe that the conditions (17.4.24) are more severe than the solvability condition (17.4.16).

17.4.2 Construction of the family of schemes

The above-derived properties have to be satisfied by the coefficients b_{\pm} and c_{\pm} , considered as arbitrary functions of $\sigma = A \Delta t / \Delta x$.

Realistic algorithms will be obtained if the schemes are restricted to coefficients that are polynomials of σ . Although one could define more complex schemes, they do not appear to be of general interest.

In addition, at least second-order accuracy in space and time is requested and the schemes with the lowest number of free parameters are obtained for

polynomials with degree lower or equal to two, as can be seen from equations (17.4.9) and (17.4.11).

Equation (17.4.11) shows that c_- may not be of degree higher than one and the most general form is then

$$\begin{aligned}c_- &= \alpha\sigma + \mu \\c_+ &= \beta\sigma^2 + \nu\sigma + \gamma\end{aligned}\tag{17.4.25}$$

where $\alpha, \beta, \gamma, \mu, \nu$ are real numbers.

If the condition (17.4.13) for third-order accuracy is introduced the coefficients have to be restricted to $\beta = \alpha - \frac{1}{3}$, $\gamma = \frac{1}{3}$, $\mu = \nu$, with $\alpha \neq \frac{1}{2}$. For $\alpha < \frac{1}{2}$, the third-order schemes are solvable and stable for $\sigma \leq 1$, and if the CFL number σ is restricted to $\sigma < 1$, the scheme is also dissipative and strictly diagonal dominant. A simple choice is $\alpha = 0$, $\beta = \frac{1}{3}$ and $\gamma = \frac{1}{3}$. The unique fourth-order scheme, $\alpha = \frac{1}{2}$, $\beta = \frac{1}{6}$, $\gamma = \frac{1}{3}$, $\mu = \nu = 0$ is solvable only if $\sigma^2 < 1$ but in this case the scheme is not dissipative. It has been analysed in some detail by Harten and Tal-Ezer (1981).

Family of schemes are now constructed which are implicit and space centred, second-order accurate in space and time, unconditionally stable, dissipative, solvable and satisfying the scalar condition for strict diagonal dominance.

The requirement of space-centred schemes implies that the scheme remains invariant when $(i - 1)$ is changed into $(i + 1)$ while A changes into $-A$. Hence, from the formulation (17.4.7), it is seen that one should have

$$\begin{aligned}c_-(-\sigma) &= -c_-(\sigma) & \text{and} & & c_+(-\sigma) &= c_+(\sigma) \\b_-(-\sigma) &= -b_-(\sigma) & \text{and} & & b_+(-\sigma) &= b_+(\sigma)\end{aligned}\tag{17.4.26}$$

With the choice (17.4.25) these conditions will be satisfied when $\mu = \nu = 0$ and one obtains

$$\begin{aligned}c_- &= \alpha\sigma & b_- &= (\alpha - 1)\sigma \\c_+ &= \beta\sigma^2 + \gamma & b_+ &= (1 - 2\alpha + \beta)\sigma^2 + \gamma\end{aligned}\tag{17.4.27}$$

The schemes (17.4.12) then take the following form:

$$[1 + \alpha\sigma\bar{\delta} + \frac{1}{2}(\beta\sigma^2 + \gamma)\delta^2]\Delta U_i^n = -\sigma\bar{\delta}U_i^n + \frac{1}{2}(1 - 2\alpha)\sigma^2\delta^2U_i^n\tag{17.4.28}$$

Some of the schemes to be discussed in the next chapter belong to the family (17.4.28). The choice $\alpha = \frac{1}{2}$, $\beta = \gamma = 0$ is the trapezoidal Beam and Warming scheme corresponding to $\theta = \frac{1}{2}$, $\xi = 0$. The choice $\alpha = \frac{1}{2}$, $\beta = 0$, $\gamma = \frac{1}{3}$ reproduces the scheme (18.1.14) for $\theta = \frac{1}{2}$, $\xi = 0$, which has fourth-order spatial accuracy but is only second order in time.

More insight is obtained when the algorithm (17.4.28) is written as a two-step scheme, whereby the explicit part is separated from the implicit operations.

Defining an intermediate variation $\overline{\Delta U}$ by

$$\overline{\Delta U}_i = -\sigma\bar{\delta}\cdot U_i^n + (\frac{1}{2} - \alpha)\sigma^2\delta^2U_i^n\tag{17.4.29a}$$

$$[1 + \alpha\sigma\bar{\delta} + \frac{1}{2}(\beta\sigma^2 + \gamma)\delta^2]\Delta U_i^n = \overline{\Delta U}_i\tag{17.4.29b}$$

The first step, (17.4.29a), is an explicit operation that defines $\overline{\Delta U}_i$ by a Lax–Wendroff-type scheme. For $\alpha = 0$, this step is identical to the Lax–Wendroff scheme and has the same CFL limitations on the maximum time step for stability. However, the second step introduces an implicit correction on $\overline{\Delta U}_i$, which extends the admissible maximum Courant number and provides additional dissipation through the parameters α, β and γ .

When $\alpha = \beta = \gamma = 0$, the scheme is identical to the explicit Lax–Wendroff scheme. However, for $\alpha \neq 0$, the explicit step is only first-order accurate and the implicit step provides a correction on the truncation error of the first step, such that the overall solution $U^{n+1} = U^n + \Delta U^n$ is second-order accurate.

The above general requirements can now be translated into conditions on the coefficients α, β, γ . The solvability condition (17.4.16) has to be valid for all values of σ , and from

$$\beta\sigma^2 + \gamma < \frac{1}{2} \quad (17.4.30)$$

we deduce

$$\beta \leq 0 \quad \text{and} \quad \gamma < \frac{1}{2} \quad (17.4.31)$$

Adding the conditions for unconditional linear stability requires

$$\beta \leq \alpha - \frac{1}{2}, \quad \gamma < \frac{1}{2}, \quad \alpha \leq \frac{1}{2} \quad (17.4.32)$$

In order to ensure a dissipative scheme, the conditions (17.4.20) have to be satisfied, that is

$$(1 - 2\alpha)\sigma^2 \neq 0 \quad (17.4.33)$$

When the eigenvalues of A are different from zero, the parameter α may not take the value $\frac{1}{2}$. Hence the last condition in (17.4.32) is to be replaced by

$$\alpha < \frac{1}{2} \quad (17.4.34)$$

It is to be observed at this point that the schemes will not be dissipative when the eigenvalues of the Jacobian matrix go through zero, that is at sonic and stagnation points. Therefore, these schemes might still need some artificial dissipation to damp oscillations that would occur at shock discontinuities (Sides, 1985). However, further extensions by Lerat and Sides (1986) indicate that with an appropriate treatment of the explicit step and the addition of implicit boundary conditions, excellent shock-capturing properties are obtained without any artificial viscosity.

Finally, the conditions (17.4.24) for diagonal dominance are satisfied for all values of σ if

$$\beta < -\frac{\alpha^2}{4(1-\gamma)} \quad \text{or} \quad \alpha = \beta = 0 \quad (17.4.35)$$

and

$$\gamma < \frac{1}{2}$$

Hence all the properties will be satisfied for all values of the CFL number σ if

$$\beta \leq \alpha - \frac{1}{2}, \quad \gamma < \frac{1}{2}, \quad \alpha < \frac{1}{2} \quad \text{and} \quad \beta < -\frac{\alpha^2}{4(1-\gamma)} \quad (17.4.36)$$

This still leaves a large number of possible schemes, and additional conditions can be imposed in order to satisfy certain properties, such as the maximum convergence rate or minimal error generation.

Selection of parameters

The parameter γ does not seem to play an important role in the definition of the properties of the second-order schemes (17.4.29). This can be seen, for instance, on the expression of the amplification matrix G (equation (17.4.15)), which takes on the following form when the definitions (17.4.27) are introduced:

$$G - 1 = \frac{-I\sigma \sin \phi - (1 - 2\alpha)\sigma^2(1 - \cos \phi)}{1 + I\alpha\sigma \sin \phi - (\beta\sigma^2 + \gamma)(1 - \cos \phi)} \quad (17.4.37)$$

As in the implicit step (17.4.29b), the parameter γ appears always in the combination $(\beta\sigma^2 + \gamma)$ and its influence can be overtaken by the parameter β . Hence, setting $\gamma = 0$ will not affect the generality of the schemes, nor limit the influence of the remaining parameters α and β .

Analysing further the amplification matrix, it is seen that for $\alpha = \frac{1}{2}$, the scheme does not damp the high-frequency errors, since in this case $G = 1$ for $\phi = \pi$. Hence the scheme is not dissipative in the sense of Kreiss when $\alpha = \frac{1}{2}$. For other values of α , the parameter $(1 - 2\alpha)$ controls the dissipation of the high-frequency errors, since

$$G(\phi = \pi) = 1 - \frac{2\sigma^2(1 - 2\alpha)}{1 - 2(\beta\sigma^2 + \gamma)} \quad (17.4.38)$$

On the other hand, the parameter β controls the behaviour of the scheme at high Courant numbers, that is for very large time steps. This is particularly interesting for steady-state computations, where it is expected to reach the stationary conditions as fast as possible.

Steady-state computations

For increasing σ , the amplification matrix tends to the limits

$$G \underset{\sigma \rightarrow \infty}{\approx} 1 + \frac{1 - 2\alpha}{\beta} \quad (17.4.39)$$

and the maximum convergence rate is achieved for

$$\beta = 2\alpha - 1 \quad (17.4.40)$$

since $G \rightarrow 0$ in this case.

The behaviour at the low-frequency end of the error spectrum is obtained

from an expansion of the amplification matrix in powers of ϕ or, alternatively, from the first terms of the truncation error.

Applying the Taylor expansion technique to the scheme (17.4.29), following the approach outlined in Section 9.2 in Volume 1 leads to the following equivalent differential equation of scheme (17.4.29) (see Problem 17.33):

$$U_t + AU_x = -\frac{\Delta x^2}{6} A[(1-3\gamma) + \sigma^2(3\alpha - 3\beta - 1)]U_{xxx} - \frac{\Delta x^3}{8} \sigma A(1-2\alpha)[(1-2\gamma) + \sigma^2(2\alpha - 2\beta - 1)]U_{xxxx} \quad (17.4.41)$$

From the conditions (17.4.36) it is seen that the coefficient of the U_{xxx} term describing the dispersion error never vanishes, which is to be expected from a second-order scheme. Observe that the conditions $\gamma = \frac{1}{3}$, $\beta = \alpha - \frac{1}{3}$, which make the dispersion error vanish, are precisely the conditions for third-order accuracy of the scheme.

Unsteady flow computations

Many unsteady flows have time scales much larger than the time scale of the propagation of the acoustic waves. In this case, the Courant number limitation of an explicit Lax–Wendroff-type method will lead to allowable time steps that are much smaller than the time steps requested by an accurate simulation of the physical phenomena. In these circumstances, occurring for instance for the flow along an oscillating airfoil, there is much to be gained by the use of implicit methods, where one can adapt the time steps to the desired accuracy without being limited by CFL conditions of explicit methods.

One would like, in such a situation, to minimize the dispersion and diffusion errors during computation. This can be achieved by looking at the dominant contributions to these errors from the right-hand side of equation (17.4.41) for large values of the Courant number σ , namely the coefficients of the σ^2 terms.

From the conditions (17.4.36), it is seen that the coefficient of σ^2 in the dispersion error never vanishes and reaches its lowest value for the choice

$$\beta = \alpha - \frac{1}{2} \quad (17.4.42)$$

which is also the value for which the σ^2 term vanishes in the dissipation error term. Observe also that the coefficient of the U_{xxxx} term is always negative, as it should be for stability, as seen in Section 9.2 in Volume 1.

17.4.3 Extension to non-linear systems in conservation form

The derived family of implicit schemes (17.4.29) can be extended in a straightforward way to the non-linear system in conservation form

$$\frac{\partial U}{\partial t} + \frac{\partial f}{\partial x} = 0 \quad (17.4.43)$$

as follows:

$$\overline{\Delta U}_i = -\tau \bar{\delta} f_i^n + \left(\frac{1}{2} - \alpha\right) \tau^2 \delta(A_i^n \delta f_i^n) \quad (17.4.44a)$$

$$\left[1 + \alpha \tau \bar{\delta} A_i^n + \frac{\beta}{2} \tau^2 \delta(A_i^2 \delta) + \frac{\gamma}{2} \delta^2 \right] \Delta U_i = \overline{\Delta U}_i \quad (17.4.44b)$$

The scheme (17.4.44) can be considered as constituted of an explicit step of the Lax–Wendroff type, to which it reduces exactly for $\alpha = 0$ (see equation (17.2.5)), followed by an implicit operator defined by equation (17.4.44b).

Introducing the numerical flux of the scheme

$$f_{i+1/2}^* = \frac{f_i + f_{i+1}}{2} - (1 - 2\alpha) \frac{\tau}{2} A_{i+1/2} (f_{i+1} - f_i) \quad (17.4.45)$$

equation (17.4.44) becomes

$$\left[1 + \alpha \tau \bar{\delta} A_i + \frac{\beta}{2} \tau^2 \delta(A_i^2 \delta) + \frac{\gamma}{2} \delta^2 \right]^n \Delta U_i = -\tau \delta f_i^* \quad (17.4.46)$$

The choice $\alpha = 0$ is of particular interest since the explicit step becomes of second-order accuracy and is then identical to the Lax–Wendroff scheme. In addition the β term in the implicit operator,

$$\beta \tau^2 \delta(A^2 \delta \Delta U) \sim \beta \Delta t^3 A^2 U_{,xxx} \sim \beta \Delta t^3 U_{,iii} \quad (17.4.47)$$

is of the same order as the truncation error of the Lax–Wendroff scheme.

The implicit step can therefore be considered as an implementation of a correction to the explicit truncation error without affecting the overall accuracy of the scheme.

Note that in the non-linear case, the maximum order of accuracy cannot exceed two, since the non-linear fluxes introduce truncation terms proportional to Δx^2 , as seen in Section 9.4 in Volume 1.

A similar idea of increasing the accuracy of a scheme by solving a modified equation, obtained after subtracting a fraction of the leading non-linear truncation error, has also been analysed and exploited by Klopfer and McRae (1983).

With the choice $\gamma = 0$, the simplified schemes with $\alpha = 0$ become

$$\overline{\Delta U}_i = -\tau \bar{\delta} f_i^n + \frac{1}{2} \tau^2 \delta(A_i^n \delta f_i^n) \quad (17.4.48a)$$

$$\left[1 + \frac{\beta}{2} \tau^2 \delta(A_i^2 \delta) \right] \Delta U_i = \overline{\Delta U}_i \quad (17.4.48b)$$

The choice $\alpha = 0$ allows the substitution of the explicit step by any other scheme which is linearly equivalent to the Lax–Wendroff schemes. Therefore, any of the methods discussed in Section 17.2 can be used. Lerat (1981) and Lerat *et al.*, (1982, 1985) have applied various versions of the S_a^β scheme, in particular the optimal choice $(1 + \sqrt{5/2}, 0)$ for the explicit step.

For steady-state calculations, optimal convergence rates will be obtained with

the choice (17.4.40), that is $\beta = -1$, while unsteady calculations will be optimized by selecting $\beta = -\frac{1}{2}$, following (17.4.42).

Since the first, explicit, step has the full second-order accuracy of the scheme, the intermediate value $\overline{\Delta U}$ can be considered as equal to $\Delta t \cdot R^n$, where R^n is the residual of the space balance of the fluxes.

The implicit step can therefore be viewed as a way of redistributing the residuals, producing a new value ΔU from the explicit initial approximation $\overline{\Delta U}$. In particular, considering A^2 as a constant in the implicit step is identical to the residual smoothing step applied by Jameson, as will be seen in next chapter, equation (18.3.10).

For steady-state computations, the *physical* solution corresponds to $\overline{\Delta U} = 0$, that is to the right-hand side of the first, explicit, step equal to zero. The second, implicit, step improves the convergence rate by allowing large time steps through the unconditional stability and provides additional dissipation to damp undesirable high-frequency errors. However, it has no effect on the final converged solution which is completely defined by the first, explicit, step. Hence, the second step can be viewed, for steady-state problems, as a *mathematical* or *numerical* step.

Simplification of the schemes

The block tridiagonal system in (17.4.48b) can be replaced by scalar tridiagonal inversions if A_i is approximated by its maximum eigenvalue $a_{\max} = |u| + c_{\max}$. The system (17.4.48b) becomes, with $\rho(A)$ representing the spectral radius of the matrix A ,

$$\left[1 + \frac{\beta}{2} \tau^2 \delta (\rho^2(A_i) \delta) \right] \Delta U_i = \overline{\Delta U}_i \quad (17.4.49)$$

The implicit operator is simplified to scalar tridiagonal operations instead of the block tridiagonal. This reduces the computational cost of the scheme but slows down the convergence rate, as can be seen from the amplification matrix, which becomes, instead of (17.4.37),

$$G - 1 = \frac{-\sigma I \sin \phi + \sigma^2 (\cos \phi - 1)}{1 + \beta \sigma_{\max}^2 (\cos \phi - 1)} \quad (17.4.50)$$

In the large time step limit

$$G \approx 1 - \frac{\sigma^2}{\beta \sigma_{\max}^2} \quad (17.4.51)$$

Hence, the asymptotic value $G \rightarrow_{\Delta t \rightarrow \infty} 0$ cannot be reached and slower convergence rates are to be expected. This is confirmed by computations in a diverging nozzle by Lerat *et al.* (1985), as shown in Figure 17.4.1. The results shown in Figure 17.4.1 have been obtained with the simplified schemes (17.4.48) and (17.4.49).

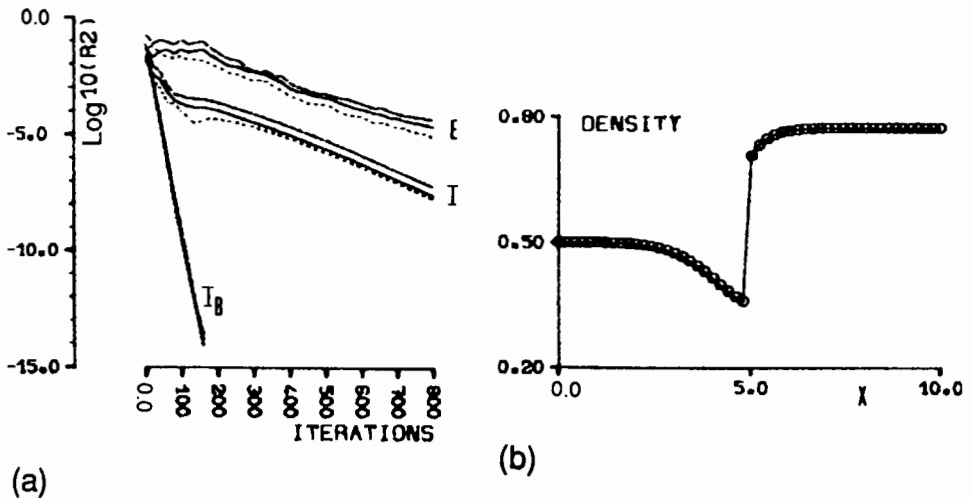


Figure 17.4.1 (a) Convergence history for a one-dimensional nozzle flow with Lerat's implicit (Lax-Wendroff) schemes.

E Explicit Lax-Wendroff scheme, (CFL = 1)

I Implicit diagonalized version (17.4.49), $\beta = -1$, CFL = 20

I_B Implicit block tridiagonal version (17.4.48), $\beta = -1$, CFL = 20

(b) Computed density variation with run I_B . (From Lerat *et al.*, 1985)

Figure 17.4.1(a) shows a comparison at a CFL number of 20 of the convergence rates for the implicit steps with block tridiagonal inversions (17.4.48b) and with the scalar inversion (17.4.49).

The rate of convergence of the Lax-Wendroff explicit step (E) is also shown at CFL = 1. The converged density distribution is shown in Figure 17.4.1(b), illustrating the good shock-capturing properties of the scheme. The simplification introduction by equation (17.4.49) will therefore only be interesting at low CFL numbers.

Boundary conditions

A detailed analysis of the impact of the boundary conditions on stability of the implicit schemes (17.4.48) and (17.4.49) has been performed by Daru (1983) and Daru and Lerat (1985) for the one-dimensional nozzle flows. The results of the analysis can be summarized as follows, referring to Chapter 19 for more details on the various options and to the original references for the detailed derivations:

- (1) At supersonic inlet $\Delta U = 0$ may be taken at the boundaries.
- (2) At a supersonic outlet section, the unknowns can be obtained by zero-order extrapolation in a stable way.
- (3) At a subsonic outlet, zero-order extrapolation is always stable. Linear extrapolation is also always stable with the exception of the case $\beta = -1$ for the scheme (17.4.48) for which the stability is conditional and restricted to CFL < 5. Quadratic extrapolation is always unstable.

17.4.4 Extension to multi-dimensional flows

The family of schemes with $\alpha = \gamma = 0$ has an explicit step which is identical to the Lax–Wendroff scheme and therefore the extension to two-dimensional flows can be obtained by taking any of the two-dimensional versions of Section 17.2 as the first, explicit, step.

If $\overline{\Delta U}_{ij}$ is the explicit variation at mesh point (i, j) , the generalization of the implicit step can be defined as

$$\left[1 + \frac{\beta}{2} \tau_x^2 \delta_x (A_{ij}^2 \delta_x) + \frac{\beta}{2} \tau_y^2 \delta_y (B_{ij}^2 \delta_y) \right] \Delta U_{ij} = \overline{\Delta U}_{ij} \quad (17.4.52)$$

In order to avoid block pentadiagonal systems, an ADI factorization is applied, reducing the implicit part of the algorithm to a two-step procedure

$$\begin{aligned} \left[1 + \frac{\beta}{2} \tau_x^2 \delta_x (A_{ij}^2 \delta_x) \right] \Delta U_{ij}^* &= \overline{\Delta U}_{ij} \\ \left[1 + \frac{\beta}{2} \tau_y^2 \delta_y (B_{ij}^2 \delta_y) \right] \Delta U_{ij} &= \Delta U_{ij}^* \end{aligned} \quad (17.4.53)$$

For steady-state problems, the value $\beta = -1$ is recommended.

A further simplification can be considered, losing, however, the optimal convergence rates for high CFL numbers, by replacing the Jacobians A and B by their spectral radius. This leads to implicit systems that are scalar tridiagonal, as in equation (17.4.49), and the implicit steps (17.4.53) reduce to

$$\begin{aligned} \left[1 + \frac{\beta}{2} \tau_x^2 \delta_x (\rho^2(A_{ij}) \delta_x) \right] \Delta U_{ij}^* &= \overline{\Delta U}_{ij} \\ \left[1 + \frac{\beta}{2} \tau_y^2 \delta_y (\rho^2(B_{ij}) \delta_y) \right] \Delta U_{ij} &= \Delta U_{ij}^* \end{aligned} \quad (17.4.54)$$

Applications of this approach to steady and unsteady two-dimensional inviscid flows can be found in Sides (1985), Lerat *et al.* (1982, 1985) and Lerat and Sides (1986), where the explicit step is based on the two-dimensional version of the S_x^β schemes presented in Section 17.2.

17.5 SUMMARY

The Lax–Wendroff family of schemes has been presented at some length in this chapter, since they play a major role in the development of discretization methods for compressible Euler and Navier–Stokes equations. They are still widely used, in particular under the form of the MacCormack predictor–corrector formulation.

An important feature is the requirement of the addition of artificial dissipation terms in order to remove the oscillations around discontinuities. This requires

good judgement and empiricism and several possible forms have been described, although many others can be defined. A rational method for the determination of artificial dissipation terms will also be presented in Chapter 21, in connection with TVD upwind schemes, leading to a bridge between the central and the upwind methods.

If the one-dimensional form of the Lax–Wendroff schemes is straightforward to apply, a larger variety exists in multidimensions. In this connection, the two-step formulation of Ni can be recommended as an interesting alternative, in particular when coupled to a multigrid approach. This can actually be generalized to any two-step formulation: the explicit Lax–Wendroff schemes should best be applied with multigrid schemes for stationary problems in order to compensate for the unfavourable CFL limitations on the allowable time step.

Another interesting approach for steady state problems is the implicit version of Lerat, which can be tuned to optimal convergence for high CFL and shows also excellent shock resolution without artificial dissipation, Lerat and Sides (1986, 1988).

References

- Burstein, S. Z. (1967). 'High order accurate difference methods in hydrodynamics.' In F. Ames (ed.), *Nonlinear Partial Difference Equations*, pp. 279–90, New York: Academic Press.
- Casier, F., Deconinck, H., and Hirsch Ch. (1983). 'A class of central bidiagonal schemes with implicit boundary conditions for the solution of Euler's equations.' *AIAA Paper 83-0126*, AIAA 21st Aerospace Sciences Meeting. See also *AIAA Journal*, Vol. 22, 1556–1563.
- Couston, M. McDonald, P. W., and Smolderen, J. (1975). 'The Damping surface technique for time dependent solutions to fluid dynamics problems.' *Von Karman Institute Report VKI-TN 109*, Brussels, Belgium.
- Daru, V. (1983). 'Contribution a l'etude d'une methode numerique implicite pour resoudre les equations d'Euler.' These de 3eme cycle, Universite de Paris VI.
- Daru, V., and Lerat, A. (1985). 'Analysis of an implicit Euler solver.' In Angrand *et al.* (eds), *Numerical Methods for the Euler Equations of Fluid Dynamics*. Philadelphia: SIAM Publications.
- Denton, J. (1975). 'A time marching method for two and three dimensional blade to blade flows.' *R & M 3795*, Aeronautical Research Council.
- Denton, J. (1982). 'An improved time marching method for turbomachinery flow calculations.' In P. L. Roe (ed.), *Numerical Methods in Aeronautical Fluid Dynamics*, London: Academic Press.
- Fourmaux, A., and Le Meur, A. (1987). 'Computation of unsteady phenomena in transonic turbines and compression.' *Onera Report TP 131*, Onera, France.
- Hall, M. G. (1985). 'Cell-vertex multigrid schemes for solutions of the Euler equations.' In *Proc. IMA Conference on Numerical Methods in Fluids*, Oxford: Oxford University Press.
- Harten, A. (1983a). 'On the symmetric form of systems of conservation laws with entropy.' *Journal Computational Physics*, **49**, 151–64.
- Harten, A. (1983b). 'High resolution schemes for hyperbolic conservation laws.' *Journal Computational Physics*, **49**, 357–93.
- Harten, A., and Tal-Ezer, H. (1981). 'On a fourth order accurate implicit scheme for hyperbolic conservation laws.' *Mathematics of Computation*, **36**, 353.

- Jameson, A. (1982). 'Transonic aerofoil calculations using the Euler equations.' In P. L. Roe (ed.), *Numerical Methods in Aeronautical Fluid Dynamics*, New York: Academic Press.
- Jameson, A., Schmidt, W., and Turkel, E. (1981). 'Numerical simulation of the Euler equations by finite volume methods using Runge-Kutta time stepping schemes.' *AIAA Paper 81-1259*, AIAA 5th Computational Fluid Dynamics Conference.
- Klopper, G. H., and McRae, D. S. (1983). 'Nonlinear truncation error analysis of finite difference schemes for the Euler equations.' *AIAA Journal*, **21**, 487-94.
- Koeck, C. (1985). 'Computation of three-dimensional flow using the Euler equations and a multiple-grid scheme.' *Int. Journal for Numerical Methods in Fluids*, **5**, 483-500.
- Lax, P. D. (1954). 'Weak solutions of non linear hyperbolic equations and their numerical computation.' *Comm. Pure and Applied Mathematics*, **7**, 159-93.
- Lax, P. D. (1957). 'Hyperbolic systems of conservation laws II.' *Comm. Pure and Applied Mathematics*, **10**, 537-66.
- Lax, P. D., and Wendroff, B. (1960). 'Systems of conservation laws.' *Comm. Pure and Applied Mathematics*, **13**, 217-37.
- Lax, P. D., and Wendroff, B. (1964). 'Difference schemes for hyperbolic equations with high order of accuracy.' *Comm. Pure and Applied Mathematics*, **17**, 381-98.
- Lerat, A. (1979). *Une Classe de Schémas aux Differences Implicites pour les Systemes Hyperboliques de Lois de Conservation*, Vol. 288A, pp. 1033-6, Paris: Comptes Rendus Academie des Sciences.
- Lerat, A. (1981). 'Sur le calcul des solutions faibles des systemes hyperboliques de lois de conservations a l'aide de schemas aux differences.' *Publication ONERA 1981-1*.
- Lerat, A. (1985). 'Implicit methods of second order accuracy for the Euler equations.' *AIAA Journal*, **23**, 33-40.
- Lerat, A., and Peyret, R. (1974). 'Non centered schemes and shock propagation problems.' *Computers and Fluids*, **2**, 35-52.
- Lerat, A., and Peyret, R. (1975). 'The problem of spurious oscillations in the numerical solution of the equations of gas dynamics.' *Lecture Notes in Physics*, Vol. 35, pp. 251-256, New York: Springer Verlag.
- Lerat, A., and Sides, J. (1977). 'Calcul numerique d'ecoulements transsoniques instationnaires.' *AGARD Conference Proc. CP-226*, pp. 15.1-15.10.
- Lerat, A., and Sides, J. (1982). 'A new finite volume method for the Euler equations with applications to transonic flows.' In P. L. Roe (ed.), *Numerical Methods in Aeronautical Fluid Dynamics*, New York: Academic Press.
- Lerat, A., and Sides, J. (1986). 'Implicit transonic calculations without artificial viscosity or upwinding.' *GAMM Workshop on Numerical Simulation of Compressible Euler Flows*, Vieweg and Sols, Branschei. Also, ONERA TP, 87-195.
- Lerat, A., Sides, J., and Daru, V. (1982). 'An implicit finite volume method for solving the Euler equations.' *Lecture Notes In Physics*, Vol. 170, pp. 343-9.
- Lerat, A., Sides, J., and Daru, V. (1985). 'Efficient computation of steady and unsteady transonic flows by an implicit solver.' In W. G. Habashi (ed.), *Advances in Computational Transonics*, London: Pineridge Press.
- Lerat, A., and Sides, J. (1988). 'Efficient solution of the steady Euler equations with a centered implicit method.' In Morton and Baines (eds), *Numerical Methods for Fluid Dynamics III*, 65-86, Clarendon Press, Oxford.
- MacCormack, R. W. (1969). 'The effect of viscosity in hypervelocity impact cratering.' *AIAA Paper 69-354*.
- MacCormack, R. W., and Baldwin, B. S. (1975). 'A numerical method for solving the Navier-Stokes equations with application to shock-boundary layer interaction.' *AIAA Paper 75-1*.
- MacCormack, R. W., and Paullay, A. J. (1972). 'Computational efficiency achieved by time splitting of finite difference operators.' *AIAA Paper 72-154*.
- MaDonald, P. W. (1971). 'The computation of transonic flow through two-dimensional gas turbine cascades.' *ASME Paper 71-GT-89*.

- Magnus, R., and Yoshihara, H. (1975). 'Unsteady transonic flows over an airfoil.' *AIAA Journal*, **13**, 1622–8.
- McGuire, G. R., Morris, J. L. (1973). 'A class of second order accurate methods for the solution of systems of conservation laws: *Journal Computational Physics*, **11**, pp. 531–549.
- Ni, R. N. (1982). 'A multiple grid scheme for solving the Euler equations.' *AIAA Journal*, **20**, 1565–71.
- Palumbo, D. J., and Rubin, D. L. (1972). 'Solution of the two-dimensional unsteady compressible Navier–Stokes equations using a second order accurate numerical scheme.' *Journal Computational Physics*, **9**, 466–95.
- Pulliam, T. H. (1984). 'Euler and thin layer Navier–Stokes codes: ARC2D, ARC3D.' *Proc. Computational Fluid Dynamics User's Workshop*, The University of Tennessee Space Institute, Tullahoma, Tennessee.
- Pulliam, T. H. (1985). 'Artificial dissipation models for the Euler equations.' *AIAA Paper 85-0438*, AIAA 23th Aerospace Sciences Meeting.
- Pulliam, T. H., and Steger, J. L. (1985). 'Recent improvements in efficiency, accuracy and convergence for implicit approximate factorization algorithms.' *AIAA Paper 85-0360*, AIAA 23rd Aerospace Sciences Meeting.
- Richtmyer, R. D., and Morton, K. W. (1967). *Difference Methods for Initial Value Problems*, 2nd eds, New York: John Wiley and Sons.
- Rizzi, A. W., and Inouye, M. (1973). 'Time split finite volume method for three-dimensional blunt-body flows.' *AIAA Journal*, **11**, 1478–85.
- Roe, P. L. (1981). 'The use of the Riemann Problem in finite difference schemes.' *Lecture Notes in Physics*, Vol. 141, pp. 354–9, Berlin: Springer Verlag.
- Rubin, E. L., Burstein, S. Z. (1967). 'Difference methods for the inviscid and viscous equations of a compressible gas' *Journal Computational Physics*, **2**, pp. 178–196.
- Sides, J. (1985). 'Computation of unsteady transonic flows with an implicit numerical method for solving the Euler equations.' *La Recherche Aerospaciale*, **1985-2**, 17–39.
- Singleton, R. E. (1968). 'Lax–Wendroff difference scheme applied to the transonic airfoil problem.' *AGARD Conference Proc.*, **CP-35**, 2.1–2.9.
- Steger, J. L. (1978). 'Implicit finite difference simulation of flow about two-dimensional geometries.' *AIAA Journal*, **16**, 679–86.
- Strang, G. (1976). *Linear Algebra and Its Applications*, New York: Academic Press.
- Swanson, R. C., and Turkel, E. (1987). 'Artificial dissipation and central difference schemes for the Euler and Navier–Stokes equations.' *AIAA Paper 87-1107*, *Proc. AIAA 8th Computational Fluid Dynamics Conference*, pp. 55–69.
- Tadmor, E. (1984). 'The large time behaviour of the scalar, genuinely nonlinear Lax–Friedrichs Scheme.' *Mathematics of Computation*, **43**, pp. 353–368.
- Thompkins, W. T., Tong, S. S., Bush, R. H., Usab, W. J., and Norton, R. J. G. (1983). 'Solution procedures for accurate numerical simulations of flow in turbomachinery cascades.' *AIAA Paper 83-0257*, AIAA 21st Aerospace Sciences Meeting.
- Thommen, H. U. (1966). 'Numerical integration of the Navier–Stokes equations.' *ZAMP*, **17**, 369–84.
- Tong, S. S. (1987). 'The impact of smoothing formulations on the stability and accuracy of various time marching schemes.' *AIAA Paper 87-1106*, *Proc. AIAA 8th Computational Fluid Dynamics Conference*, pp. 47–54.
- Turkel, E. (1973). 'Symmetrization of the fluid dynamic matrices with applications.' *Mathematics of Computation*, **27**, 729–36.
- Turkel, E. (1977). 'Symmetric hyperbolic difference schemes and matrix problems.' *Linear Algebra and Applications*, **16**, 109–29.
- Van Hove, W., and Arts, A. (1979). 'Comparison of several finite difference schemes for time marching methods as applied to one dimensional nozzle flow.' *Von Karman Institute Report VKI-TN132*, Brussels, Belgium.
- Von Neumann, J., and Richtmyer, R. D. (1950). 'A method for the numerical calculations of hydrodynamical shocks.' *Journal Mathematical Physics*, **21**.

- Warming, R. F., Kutler, P., Lomax, H. (1973). 'Second and third order non centered difference schemes for non linear hyperbolic equations.' *AIAA Journal*, **11**, pp. 189–195.
- Yanenko, N. N. (1971). *The Method of Fractional Steps*, New York: Springer Verlag.
- Yanenko, N. N., Fedotova, Z. I., Kompaniets, L. A., and Shokin, Yu. I. (1984). 'Classification of difference schemes of gas dynamics by the method of differential approximation—two dimensional case.' *Computers and Fluids*, **12**, 93–119.
- Zeldovich, Y. B., Ranzer, Y. P. (1967). *Physics of Shock Waves and High Temperature Hydrodynamic Phenomena*. Academic Press, New York.
- Zwas, G. (1973). 'On two step Lax–Wendroff methods in several dimensions.' *Numerische Mathematik*, **20**, 350–5.

PROBLEMS

Problem 17.1

Consider a modified one-dimensional Lax–Friedrichs scheme, applied to the scalar hyperbolic equation $u_t + f_x = 0$, instead of (17.1.4) (Tadmor, 1984):

$$u_i^{n+1} = \frac{1}{4}(u_{i+1} + 2u_i + u_{i-1}) - \frac{\tau}{2}(f_{i+1} - f_{i-1})$$

Analyse the stability, error spectrum and truncation error for this scheme. Show that the stability condition is now restricted to $|\sigma| \leq 1/\sqrt{2}$.

Derive the expression of the numerical flux f^* and observe that the above scheme corresponds to the addition of half of the stabilizing dissipation by comparing with equation (17.1.6).

Problem 17.2

Derive the amplification matrix for the modified Lax–Friedrichs scheme (17.1.30) and show that the conditions (17.1.34) are sufficient for stability in the linear case.

Problem 17.3

Apply the Lax–Friedrichs scheme in finite volume form to the hexagonal control volume ABCDEF of Figure 6.2.4 in Volume 1 on a Cartesian mesh, and a Lax–Friedrichs averaging over the six nodes. Derive the Von Neumann amplification matrix.

Hint: Write

$$\frac{\partial}{\partial t}(U\Omega) + \oint_{\text{ABCDEF}} (f dy - g dx) = 0$$

and take average values for the fluxes. For instance, $f_{\text{AB}} = (f_{i+1,j} + f_{i,j-1})/2$.

Obtain the following scheme, with $\Omega = 3\Delta x \Delta y$:

$$\begin{aligned} U_{ij}^{n+1} = & \frac{1}{6}(U_{i+1,j} + U_{i+1,j+1} + U_{i,j+1} + U_{i-1,j} + U_{i-1,j-1} + U_{i,j-1}) \\ & - \frac{1}{6\Delta y}(g_{i+1,j+1} + f_{i,j-1} + 2f_{i+1,j} - 2f_{i-1,j} - f_{i-1,j-1} - f_{i,j+1}) \\ & - \frac{1}{6\Delta y}(g_{i+1,j+1} + 2g_{i,j+1} + g_{i-1,j} - g_{i-1,j-1} - 2g_{i,j-1} - g_{i+1,j}) \end{aligned}$$

Problem 17.4

Solve Burger's equation $u_t + uu_x = 0$ for a stationary discontinuity with the Lax-Friedrichs scheme.

Hint: Take $u_L = 1$ and $u_R = -1$ where u_L and u_R are the value of the solution left and right of the discontinuity. The shock velocity is equal to $(u_L + u_R)/2$; therefore this choice gives a stationary shock.

Consider two cases:

- (1) Shock placed in a mesh point;
- (2) Shock located between two mesh points.

Start with an initial solution, linear over 20 mesh points, and take different CFL numbers, such as 0.2, 0.5, 0.8, 1. Plot and compare the results of these two cases every five time steps.

Problem 17.5

Repeat Problem 17.4 for a moving discontinuity by taking $u_L = 1$, $u_R = -0.8$. Compare with the case $u_L = 1$, $u_R = 0.8$.

Problem 17.6

Apply the Lax-Friedrichs scheme to the shock tube problem of Figure 16.5.8. Take $\text{CFL} = 0.95$ and generate plots of the flow variables as a function of x after 15, 25 and 35 time steps. Compare with the exact solution.

Problem 17.7

Apply the Lax-Friedrichs scheme to the diverging nozzle with a shock at $x = 4$, shown in Figure 17.2.2. Take the same data and refer to Chapter 19 for the treatment of the boundary conditions. Apply a simple zero-order extrapolation technique for the numerical boundary conditions.

For the physical condition of downstream pressure, take the value of the exact solution.

Generate plots of the flow variables as a function of x and compare with the exact solution.

Problem 17.8

Find the amplification matrix for the two-step Richtmyer schemes (17.2.83) and (17.2.84). Reduce the scheme to a one-step form for the linearized case and compare with the Lax-Wendroff scheme.

Hint: Define an intermediate amplification matrix \bar{G} for the intermediate step by

$$U^{n+1/2} = \bar{G}U^n$$

and

$$U^{n+1} = GU^n$$

Calculate \bar{G} from the first step and the relation between G and \bar{G} from the second step.

Problem 17.9

Show that the form (17.2.21) can be obtained also from an analytical derivation of equation (17.2.4) where the flux derivative in the last term is replaced by AU_x , leading to a term $(A^2U_x)_x$.

Calculate directly the matrix A^2 for the conservative variables and compare the discretized form of $A^2 U_x$ with the expression (17.2.24) taking the right eigenvectors as defined in Chapter 16 and δw as $w_{i+1} - w_i$.

Hint: Obtain

$$A^2 = \begin{pmatrix} \frac{(\gamma-3)u^2}{2} & (3-\gamma)u & \gamma-1 \\ \left[\frac{(3\gamma-7)u^2}{2} - c^2 \right] u & 3(2-\gamma)u^2 + c^2 & 3(\gamma-1)u \\ (5\gamma-9)\frac{u^4}{4} - \frac{3+\gamma}{2(\gamma-1)}c^2u^2 & \frac{7-5\gamma}{2}u^3 + \frac{2uc^2}{\gamma-1} & \frac{5\gamma-3}{2}u^2 + c^2 \end{pmatrix}$$

Problem 17.10

Obtain the amplification matrices (17.2.50) and (17.2.92) for the one-step, two-dimensional Lax-Wendroff scheme and the two-step MacCormack version.

Compare the two expressions, in particular the high-frequency behaviour, and observe that MacCormack's scheme has a stronger damping of the high frequency for the same values of Courant numbers, and obtain the condition (17.2.93).

Write a programme to plot the lines of constant amplification in a diagram (ϕ_x, ϕ_y) for a range of values of the x and y Courant numbers.

Problem 17.11

Extend the Lax-Wendroff derivation to the quasi-one-dimensional Euler equations for a nozzle flow (equation (16.4.1)).

Refer to Example 17.2.1 and obtain the following scheme generalizing equation (17.2.10):

$$U_i^{n+1} - U_i^n = -\tau \bar{\delta} f_i^n + \frac{1}{2} \tau^2 \delta^+ (A_{i-1/2} \delta^- f_i^n) + \Delta t \left[Q_i - \frac{\tau}{2} \bar{\delta} (A_i Q_i) + X_i (\Delta t Q_i - \tau \bar{\delta} f_i) \right]$$

where $X = \partial Q / \partial U$ is the Jacobian matrix of the source term (see Problem 16.16).

Work out completely the matrix products of the terms containing the source vector and write out the three components of the additional corrections to $\Delta t Q$ arising from the Taylor expansion in time.

Compare with the MacCormack formulation of Example 17.2.1 and derive the above result from the two-step version.

Problem 17.12

Show that constant velocity lines should intersect a flat s. f. face at right angles for an irrotational flow.

Hint: Calculate the direction of the constant velocity line $q = \text{const.}$ as

$$\tan \alpha = \frac{dy}{dx} = -\frac{\partial q / \partial y}{\partial q / \partial x}$$

with the x direction along the surface.

Introduce the irrotational condition at the wall with $v = 0$ to show that $\alpha = 90^\circ$.

Problem 17.13

Write the forward–backward and backward–forward versions of the MacCormack scheme on a Cartesian mesh.

Calculate the amplification factors.

Problem 17.14

Write the forward–backward and backward–forward versions of the MacCormack scheme in a finite volume form on an arbitrary mesh, on the control volume ABCD of Figure 17.2.14.

Write out all the terms explicitly and recover the versions of problem 17.13 on a regular mesh.

Problem 17.15

Develop the products $L_x^{(LW)}L_y^{(LW)}$ in the split operator version (17.2.105) of the Lax–Wendroff scheme, assuming that the matrices A and B do not commute. Show that one does not recover all the terms of the unsplit version (17.2.48). Show by a Taylor expansion that the split scheme is no longer of second-order accuracy.

Problem 17.16

Show, by an explicit calculation, that Lerat's two-dimensional family of schemes reduces to the single-step Lax–Wendroff scheme (17.2.48) for constant matrices A, B and for all values of $\alpha_1, \alpha_2, \beta_1, \beta_2$ coefficients.

Problem 17.17

Write out in full the Thommen scheme by introducing $\alpha_1 = \alpha_2 = \beta_1 = \beta_2 = \frac{1}{2}$ in the general family of Lerat's predictor–corrector schemes. Calculate the amplification matrix and show that it is identical to the Lax–Wendroff amplification matrix (17.2.50).

Problem 17.18

Solve Burger's equation for the stationary discontinuity of Problem 17.4 with the distributive formulation of Lax and Wendroff. Compare the results with those obtained from the original Lax–Wendroff scheme and with MacCormack's scheme. Test with different Courant numbers.

Problem 17.19

Repeat the previous problem for the moving discontinuities of Problem 17.5.

Problem 17.20

Obtain the results of Figure 17.2.2 with MacCormack's scheme

Take the same data and refer to Chapter 19 for the treatment of the boundary conditions. Apply a simple zero-order extrapolation technique for the numerical boundary conditions.

For the physical condition of downstream pressure, take the value of the exact solution.

Generate plots of the flow variables as a function of x and compare with the exact solution. Plot in particular entropy, stagnation temperature and mass flux error in addition to the other variables.

Problem 17.21

Solve Problem 17.20 with the S_a^β scheme of Lerat and Peyret. Compare different values of (α, β) and observe that the choice $\alpha = 1 + \sqrt{5/2}, \beta = \frac{1}{2}$ is indeed optimal.

Problem 17.22

Obtain the results of Figure 17.2.3 with MacCormack's scheme.

Take the same data and generate plots of the flow variables as a function of x and compare with the exact solution after 15, 25 and 35 time steps.

Experiment with other CFL numbers.

Test the alternative scheme (17.2.30).

Note that the expansion shock appears only when the end of the expansion fan is close enough to the sonic value.

Problem 17.23

Repeat Problem 17.22 with the S_x^β scheme and compare the results for different values of the parameters α, β .

Problem 17.24

Derive a finite volume formulation for the forward-forward version of MacCormack's scheme by considering the triangle PQR for the predictor step and PST for the corrector step, referring to Figure 17.2.14.

Apply the integration formulas (6.2.26) and (6.2.27) in Volume 1 to define average values of the flux derivatives over the triangles.

Show that one recovers the scheme (17.2.91) on a Cartesian mesh.

Obtain the other three versions of the two-dimensional MacCormack scheme by permutation of the triangles. For instance, the forward-backward version is obtained by selecting the triangle PRS for the predictor and PTQ for the corrector.

Hint: The integral of $\partial f / \partial x$ over the triangle PQR leads to a discretization of the average value of this derivative as

$$\frac{\bar{\partial f}}{\partial x} = \frac{1}{\Omega_{\text{PQR}}} [f_{i+1,j}(y_{ij} - y_{i,j-1}) - f_{ij}(y_{i+1,j} - y_{i,j-1}) + f_{i,j-1}(y_{i+1,j} - y_{ij})]$$

and similar relations for the other derivatives.

Problem 17.25

Show the result (17.3.3) for the normal mode analysis of the stationary part of the Lax-Wendroff scheme.

Repeat the same normal mode analysis for the Lax-Friedrichs scheme.

Problem 17.26

Add the artificial viscosity of fourth order (17.3.15) to the Lax-Wendroff scheme applied to Burger's equation for the stationary discontinuity case of Problems 17.4 and 17.18. Compare with the results obtained without artificial dissipation.

Problem 17.27

Compare the effects of the artificial viscosity of fourth order with (a) Von Neumann-Richtmyer artificial viscosity and (b) MacCormack-Baldwin artificial viscosity applied to the test case of Problem 17.26.

Problem 17.28

Repeat Problem 17.20 by applying (a) Von Neumann–Richtmyer artificial viscosity and (b) MacCormack–Baldwin artificial viscosity, and obtain Figures 17.2.1 and 17.2.4. Experiment with different values of the adjustable coefficient and observe the influence of increasing this parameter.

Problem 17.29

Repeat Problem 17.22 by applying (a) Von Neumann–Richtmyer artificial viscosity and (b) MacCormack–Baldwin artificial viscosity, and obtain Figures 17.2.2 and 17.2.3. Compare with the outcome of the MacCormack–Baldwin artificial viscosity.

Experiment with different values of the adjustable coefficient and observe the influence of increasing this parameter.

Problem 17.30

Derive the conditions (17.4.4) by following the developments of Section 9.2.1 in Volume 1. Write out explicitly the conditions for the schemes (17.4.2) to be first-, second- and third-order accurate. Compare with the Beam and Warming schemes (18.1.10) and show that one can reproduce only the schemes $\theta, \xi = 0$. Explain the reason for this fact.

Problem 17.31

Obtain equations (17.4.7) and (17.4.8) and write the schemes explicitly by working out the difference operators.

Problem 17.32

Derive the stability conditions (17.4.17) by applying the method presented in Section 8.6.1 in Volume 1.

Obtain also the conditions for dissipation in the sense of Kreiss, by deriving the limit of the amplification matrix G for $\phi \rightarrow 0$ and for $\phi = \pi$.

Problem 17.33

Obtain the equivalent differential equation (17.4.41) of Lerat's implicit schemes, by a Taylor series development of the scheme (17.4.29) following the method described in Chapter 9 in Volume 1.

Problem 17.34

Write the scheme (17.4.48) with $\beta = -1$ as a one-step algorithm for U^{n+1} .

Observe that in this case the second difference disappears from the right-hand side explicit operator.

Compare and comment on the differences with the Beam and Warming scheme (18.1.10) for $\xi = 0$ and $\theta = 1$.

Hint: The Scheme (17.4.48) with $\beta = -1$ reads

$$U_i^{n+1} - \frac{1}{2}\tau^2\delta(A_i^{2n}\delta U_i^{n+1}) = U_i^n - \tau\bar{\delta}f_i^n$$

or explicitly

$$U_i^{n+1} - \frac{\tau^2}{2}[A_{i+1/2}^{2n}(U_{i+1}^{n+1} - U_i^{n+1}) - A_{i-1/2}^{2n}(U_i^{n+1} - U_{i-1}^{n+1})] = U_i^n - \frac{\tau}{2}(f_{i+1}^n - f_{i-1}^n)$$

while the Beam and Warming scheme reduces to

$$U_i^{n+1} + \tau \bar{\delta}(A_i^n U_i^{n+1}) = U_i^n - \tau \bar{\delta} f_i^n + \tau \bar{\delta}(A_i^n U_i^n)$$

Problem 17.35

Solve the inviscid Burger equation for a stationary shock with the implicit Lerat scheme (17.4.48) with $\beta = -1$ at increasing CFL number σ .

Consider a linear initial distribution and solve for the cases where the shock is on a mesh point and between mesh points.

Observe the shock resolution and the convergence rate with increasing values of Courant number σ .

Problem 17.36

Repeat Problem 17.35 by replacing the explicit step by the MacCormack two-step scheme.

Problem 17.37

To the programme developed in Problem 17.28 add an implicit step (17.4.48) using the block tridiagonal solver.

Compare the convergence rate at different CFL values, with $\beta = -1$. Observe the effects of increasing the CFL number towards very high values.

Compare with the diagonalized version of equation (17.4.49).

Test different values of β and its influence on the convergence rate.

Chapter 18

The Central Schemes with Independent Time Integration

The schemes presented in this chapter share the common property of being based on a central, second-order discretization of the flux gradients and a *separate* time-integration method. If the first property can also be found in the Lax–Wendroff family the second is not, as seen in the previous chapter.

Schemes with these properties have been applied by Briley and McDonald (1975), and extensively developed by Beam and Warming (1976, 1978) in conjunction with implicit linear multi-step time-integration methods and by Jameson *et al.* (1981) with explicit fourth-order multistage Runge–Kutta time-integration schemes.

Both Beam and Warming's as well as Jameson's schemes have essentially the *same* central space discretization of the flux terms, although they can differ in their practical application, mainly for historical reasons: the former having been developed in a finite difference formulation of the flow equations (Euler or Navier–Stokes) in curvilinear coordinates, the latter having been formulated with a finite volume approach.

When applied on a Cartesian uniform mesh the space discretization of these schemes is the simplest one can consider with second-order accuracy, namely

$$\frac{\partial f}{\partial x} + \frac{\partial g}{\partial y} \Rightarrow \frac{f_{i+1,j}^n - f_{i-1,j}^n}{2\Delta x} + \frac{g_{i,j+1}^n - g_{i,j-1}^n}{2\Delta y}$$

The time-dependent Euler equations are transformed, after the space discretization, into a system of ordinary differential equations (ODE) in time, of the form

$$\frac{dU_{ij}}{dt} = -\frac{1}{2} \left[\frac{f_{i+1,j} - f_{i-1,j}}{\Delta x} + \frac{g_{i,j+1} - g_{i,j-1}}{\Delta y} \right] \quad (18.1.1)$$

Referring to Chapter 11 in Volume 1, various integration methods can be adopted for this system of ODEs under the condition that the stability region of the time-integration operators contains the spectrum of the matrix representing the space discretization. The analysis is performed on the linearized equations and as shown in Chapter 10 the spectrum of the central difference operator lies on the imaginary axis. Hence the time-integration methods to be considered must contain at least part of the imaginary axis in their stability domain. This

is the case for the multistage Runge–Kutta methods, while the linear multi-step methods have the whole left-hand side of the complex $\Omega\Delta t$ plane as the stability region, implying unconditional stability.

It has also been seen that the straightforward Euler explicit method (forward difference in time) is unstable, while the central difference in time, the leapfrog method, is marginally stable. However, even with a stable time integration the central schemes suffer from certain tendencies to instability. It has to be observed that the central difference generates odd–even point decoupling of the type already described in Chapter 4 and also in Section 17.3. Reducing equation (18.1.1) to the one-dimensional scalar case leads to

$$\frac{du_i}{dt} = -\frac{a}{2\Delta x}(u_{i+1} - u_{i-1}) \quad (18.1.2)$$

and a steady solution where u takes the value b at even points and c at the odd-numbered points satisfies the steady-state limit of equation (18.1.2). This decoupling corresponds to a wavelength of $2\Delta x$ and is therefore a high-frequency error.

Although this can be removed in linear problems by an appropriate treatment of the boundary conditions, in non-linear problems the convection terms produce a non-linear interaction of modes, the aliasing effect mentioned in Section 8.5.3 of Volume 1. Thereby the high-frequency modes generate low-frequency errors that can affect the smoothly varying solution. It is therefore essential to damp the high-frequency error modes, and the addition of dissipation terms forms an undissociable part of the central schemes.

In addition, dissipation terms are required to damp the oscillations around shock discontinuities and to prevent the appearance of expansion shocks.

The origin of the application of the linear multi-step methods considered by Beam and Warming is to be found in the search for implicit time-integration methods.

An important requirement for implicit methods, particularly when they are to be used with large time steps, is that the achieved steady state should be independent of the values of the time steps applied to reach the stationary solution. This property is not satisfied by the explicit methods of the Lax–Wendroff type, as already discussed in Section 17.2. This problem is not too severe with explicit methods since the CFL stability condition guarantees that the associated error remains of the order of the truncation error. However, with the larger time steps allowed by the implicit methods, the time-step dependence of the steady-state solution can lead to large errors and should be avoided.

Earlier attempts to introduce implicit schemes were based on local iterative techniques which made them too costly per time step compared to equivalent explicit methods. With the introduction of an adapted linearization of the implicit operators. (Briley and McDonald, 1975; Beam and Warming, 1976, 1978), the implicit operators are reduced to tridiagonal or block tridiagonal inversions which can be performed in an efficient way through the Thomas algorithm.

These developments for the Euler equations were systematically investigated by Beam and Warming and a recent account of their approach and related concepts is to be found in Beam and Warming (1982). These methods have been largely developed to two- and three-dimensional flows, including Navier–Stokes solutions, and a large body of research has been devoted to the analysis and the treatment of associated implicit boundary conditions and to the control of non-linear high-frequency oscillations.

18.1 THE CENTRAL SECOND-ORDER IMPLICIT SCHEMES OF BEAM AND WARMING IN ONE DIMENSION

The time discretization and linearization are defined by applying linear multi-step integration schemes to the space-discretized Euler equations, considered as a system of ordinary differential equations in time, following the developments of Chapter 11 in Volume 1.

The general, two-level time-integration formula (11.1.23) applied to the one-dimensional equation $U_t + f_x = 0$ leads to the semi-discretized scheme

$$(1 + \xi)\Delta U^n - \xi\Delta U^{n-1} = -\Delta t \left[\theta \frac{\partial f^{n+1}}{\partial x} + (1 - \theta) \frac{\partial f^n}{\partial x} \right] + \left(\theta - \frac{1}{2} - \xi \right) O(\Delta t^2) + O(\Delta t^3) \quad (18.1.3)$$

An essential aspect of the implicit schemes is connected to the linearization process of the flux derivative terms $\partial f^{n+1}/\partial x$.

The following linearization technique was introduced by Briley and McDonald (1975) and Beam and Warming (1976). The fluxes at time level $(n + 1)$ are obtained by

$$\begin{aligned} f^{n+1} &= f^n + \Delta t \left(\frac{\partial f}{\partial t} \right)^n + O(\Delta t^2) \\ &= f^n + \Delta t \left(A \cdot \frac{\partial U}{\partial t} \right)^n + O(\Delta t^2) \\ &= f^n + A^n (U^{n+1} - U^n) + O(\Delta t^2) \end{aligned} \quad (18.1.4)$$

Equation (18.1.3) becomes, applying the procedure of (18.1.4) to the flux derivative f_x ,

$$\left[(1 + \xi) + \Delta t \theta \frac{\partial}{\partial x} A^n \right] \Delta U^n = -\Delta t \frac{\partial f^n}{\partial x} + \xi \Delta U^{n-1} + \left(\theta - \frac{1}{2} - \xi \right) O(\Delta t^2) \quad (18.1.5)$$

Obviously, this scheme can be of second order in time only for $\theta = \xi + \frac{1}{2}$ and is a three-level scheme, containing U^{n-1} , U^n and U^{n+1} for $\xi \neq 0$. This general scheme has been introduced by Beam and Warming (1978) and is part of the family of linear multi-step methods of order two. For particular values of θ and ξ one obtains some well-known schemes, summarized in Table 18.1.

Table 18.1. Currently applied linear multi-step methods

θ	ξ	Name	Scheme	Accuracy in time
0	0	Euler explicit scheme	$\Delta U^n = -\Delta t \frac{\partial f^n}{\partial x}$	$O(\Delta t)$
0	$-\frac{1}{2}$	Explicit leapfrog scheme	$U^{n+1} - U^{n-1} = -2\Delta t \frac{\partial f^n}{\partial x}$	$O(\Delta t^2)$
$\frac{1}{2}$	0	Implicit trapezoidal scheme	$\left(1 + \frac{\Delta t}{2} \frac{\partial}{\partial x} A\right) \Delta U^n = -\Delta t \frac{\partial f^n}{\partial x}$	$O(\Delta t^2)$
1	0	Euler implicit scheme	$\left(1 + \Delta t \frac{\partial}{\partial x} A\right) \Delta U^n = -\Delta t \frac{\partial f^n}{\partial x}$	$O(\Delta t)$
1	$\frac{1}{2}$	Three-point backward implicit scheme	$\left(\frac{3}{2} + \Delta t \frac{\partial}{\partial x} A\right) \Delta U^n = -\Delta t \frac{\partial f^n}{\partial x} + \frac{1}{2} \Delta U^{n-1}$	$O(\Delta t^2)$

Linear stability properties

The linear stability properties of the above scheme have been investigated within the framework of the theory of ordinary differential equations as a function of the eigenvalue range of the space-discretized matrix of f_x^n .

It can be shown, (see Beam Warming, 1982, for a detailed discussion and original references and also see Chapter 11, Section 11.1 in Volume 1) that the scheme (18.1.5) is A stable for the following range of parameters (θ, ξ):

$$\begin{aligned} \xi &\geq -\frac{1}{2} \\ 2\theta &\geq \xi + 1 \end{aligned} \quad (18.1.6)$$

From Table 18.1, it is seen that next to the first-order explicit Euler method only the leapfrog method is not A stable or unconditionally stable for the Euler equations. There is also an interesting theorem by Dahlquist (1963) showing that an A -stable method cannot have an order of accuracy higher than two and must be implicit.

Note that the trapezoidal scheme lies on the boundary of the A -stability region and hence will be only marginally stable for hyperbolic problems, since some errors could not be sufficiently damped. The stability region of equation (18.1.5) is not necessarily identical to the A -stability region of equation (18.1.3) because of the way the implicit terms are treated, in particular in multi-dimensional problems where a separate analysis is necessary. Warming and Beam (1978) and Beam and Warming (1980) have analysed these schemes for linear parabolic and hyperbolic model equations in several dimensions.

18.1.1 The basic Beam and Warming schemes

The schemes discussed in this chapter refer to central discretized flux terms,

that is

$$f_{xi} = \frac{f_{i+1} - f_{i-1}}{2\Delta x} + O(\Delta x^2) \quad (18.1.7)$$

$$(A\Delta U)_{xi} = \frac{A_{i+1} \Delta U_{i+1} - A_{i-1} \Delta U_{i-1}}{2\Delta x} + O(\Delta x^2) \quad (18.1.8)$$

A large number of other space discretizations could be selected for the scheme (18.1.5). In particular, various upwind formulas can be applied to the flux terms as well as to the implicit terms on the left-hand side, and examples of implicit schemes of this type will be presented in Chapter 20.

When second-order central differences are applied on the implicit operators, the implicit matrix transforms into block tridiagonal systems which can be solved in an economical way with a minimum of arithmetic operations. Applying the central discretizations, the following schemes of second-order spatial accuracy are obtained, known as the *Beam and Warming schemes*:

$$[(1 + \xi) + \tau\theta\bar{\delta}A_i^n]\Delta U_i^n = -\tau\bar{\delta}f_i^n + \xi\Delta U_i^{n-1} \quad (18.1.9a)$$

or explicitly

$$(1 + \xi)\Delta U_i^n + \frac{\tau}{2}\theta(A_{i+1}\Delta U_{i+1}^n - A_{i-1}\Delta U_{i-1}^n) = -\frac{\tau}{2}(f_{i+1}^n - f_{i-1}^n) + \xi\Delta U_i^{n-1} \quad (18.1.9b)$$

In the linearized case $A = a$, the tridiagonal system has the following form:

$$(1 + \xi)\Delta U_i^n + \frac{1}{2}\theta\sigma\Delta U_{i+1}^n - \frac{1}{2}\theta\sigma\Delta U_{i-1}^n = -\frac{\sigma}{2}(U_{i+1}^n - U_i^n) + \xi\Delta U_i^{n-1} \quad (18.1.10)$$

The Beam and Warming schemes can also be written under the standard form (17.2.7) with a numerical flux f^* :

$$\Delta U_i^n + \xi(\Delta U_i^n - \Delta U_i^{n-1}) = -\tau(f_{i+1/2}^* - f_{i-1/2}^*) \quad (18.1.11)$$

where the numerical flux f^* is defined by

$$f_{i+1/2}^* = \frac{f_{i+1} + f_i}{2} + \frac{\theta}{2}(A_{i+1}^n\Delta U_{i+1}^n + A_i^n\Delta U_i^n) \quad (18.1.12)$$

which reduces to $(f_{i+1} + f_i)/2$ in the steady-state limit. Note also that the steady-state limit, attained when all $\Delta U_i = 0$, is $f_{i+1} = f_{i-1}$ and is independent of the time step Δt .

Higher-order spatial accuracy can be obtained by taking advantage of the implicit character of the equations while maintaining the tridiagonal structure of the matrix. This is achieved through implicit difference formulas, as presented in Section 4.3 in Volume 1, which define implicitly the first derivative up to

fourth-order accuracy:

$$\left(\frac{\partial U}{\partial x}\right)_i = \frac{1}{\Delta x} \frac{\bar{\delta}}{1 + \delta^2/6} U_i + O(\Delta x^4) \quad (18.1.13)$$

If this approximation is introduced into equation (18.1.9), the following variant of the Beam and Warming schemes, with fourth-order spatial accuracy, is obtained after formal multiplication by $(1 + \delta^2/6)$:

$$\left[(1 + \xi) + \tau \cdot \theta \bar{\delta} A_i^n + \frac{1}{6}(1 + \xi)\delta^2 \right] \Delta U_i^n = -\tau \bar{\delta} f_i + \xi \left(1 + \frac{\delta^2}{6} \right) \Delta U_i^{n-1} \quad (18.1.14a)$$

Written out in full:

$$\begin{aligned} & \frac{2}{3}(1 + \xi)\Delta U_i^n + \left(\frac{\tau}{2}\theta A_{i+1} + \frac{1 + \xi}{6} \right) \Delta U_{i+1}^n - \left(\frac{\tau}{2}\theta A_{i-1} - \frac{1 + \xi}{6} \right) \Delta U_{i-1}^n \\ & = -\frac{\tau}{2}(f_{i+1}^n - f_{i-1}^n) + \frac{\xi}{6}(\Delta U_{i-1}^{n-1} + 4\Delta U_i^{n-1} + \Delta U_{i+1}^{n-1}) \end{aligned} \quad (18.1.14b)$$

This scheme is basically no more expensive to run than the second-order version (18.1.9); see Harten and Tal-Ezer (1981) for an analysis of similar implicit fourth-order schemes.

Von Neumann analysis and overall accuracy

The stability and accuracy of the above schemes can be investigated through a Von Neumann analysis of the linearized forms of the schemes.

For schemes (18.1.10), the amplification factor G is obtained from

$$(1 + \xi + I\sigma\theta \cdot \sin \phi)(G - 1) = -I\sigma \sin \phi + \frac{\xi}{G}(G - 1) \quad (18.1.15)$$

For $\xi \neq 0$, G is defined by a quadratic expression which can be analysed by the method of Section 8.6.3. This analysis confirms the conditions (18.1.6); see also Problem 18.1.

For the particular case $\xi = 0$, which is mostly used in practice, the amplification factor is

$$G = 1 - \frac{I\sigma \sin \phi}{1 + I\sigma\theta \sin \phi} = |G|e^{-i\Phi} \quad (18.1.16)$$

The amplitude $|G|$ and the relative phase error $\varepsilon_\phi = \Phi/\sigma\phi$ are given by

$$|G|^2 = \frac{1 + \sigma^2(\theta - 1)^2 \sin^2 \phi}{1 + \sigma^2\theta^2 \cdot \sin^2 \phi} \quad (18.1.17)$$

and

$$\varepsilon_\phi = \frac{1}{\sigma\phi} \tan^{-1} \left[\frac{\sigma \sin \phi}{1 + \sigma^2\theta(\theta - 1)\sin^2 \phi} \right] \quad (18.1.18)$$

From equation (18.1.17) it is seen that the stability condition $|G| \leq 1$ for any value of ϕ is satisfied for $\theta \geq \frac{1}{2}$.

The polar plots of $|G|$ and ε_ϕ as a function of the parameter ϕ , from 0 to the highest frequency $\phi = \pi$ for the schemes $(\theta = \frac{1}{2}, \xi = 0)$, $(\theta = 1, \xi = 0)$ and $(\theta = 1, \xi = \frac{1}{2})$, have already been shown in Figure 11.1.3 in Chapter 11 in Volume 1. It is seen, from equation (18.1.17) that the trapezoidal scheme $(\xi = 0, \theta = \frac{1}{2})$ is only marginally stable since $|G| = 1$.

The phase errors become increasingly large with increasing frequency for all three schemes indicated in Figure 11.1.3 and correspond to a lagging error since $\varepsilon_\phi \leq 1$. Indeed, the high-frequency waves tend to a zero phase speed, compared to $\pi\sigma$ for the exact phase speed of a linear wave. Hence, since $G = 1$ for $\phi = \pi$, these high-frequency waves are, in addition, undamped and the schemes are not dissipative in the sense of Kreiss. As a consequence large oscillations can be expected in the vicinity of rapid variations of the solution.

Note also that for increasing Courant numbers σ , the amplification factor $|G|$ tends to $(\theta - 1)/\theta$, and the tangent of the phase Φ tends to zero, like $1/\sigma\theta(\theta - 1)$ when $\theta \neq 1$, and to infinity, like σ for the Euler implicit scheme $(\theta = 1, \xi = 0)$. For low frequencies, $\phi = k\Delta x \rightarrow 0$, the schemes have a second-order dissipation since

$$|G|^2 \simeq 1 - \sigma^2(2\theta - 1)\phi^2 \quad (18.1.19)$$

with the exception of the trapezoidal scheme, corresponding to $\theta = \frac{1}{2}$.

Performing a Taylor series expansion on the linearized equation (18.1.10) leads to the following truncation error terms in the equivalent equation (see also Problems 18.2 and 18.3):

$$u_t + au_x = a\Delta t \left(\theta - \xi - \frac{1}{2} \right) u_{tt} - \frac{a}{6} \Delta x^2 u_{xxx} \\ - \Delta x^2 \sigma^2 a \left[\frac{1}{3} + (2\xi - \theta)(1 + \xi - \theta) \right] u_{xxx} + O(\Delta x^3) \quad (18.1.20)$$

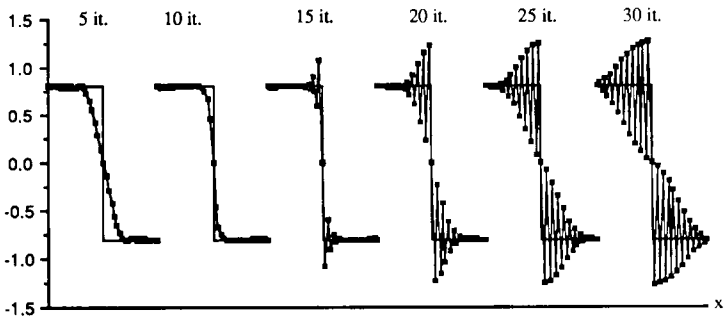
The first-order schemes in time, $\theta \neq \xi + \frac{1}{2}$, lead to a viscosity-like contribution from the time discretization which, however, disappears as the steady state is approached. The remaining terms have a dominant dispersive error proportional to u_{xxx} , and this contributes to the lack of build-in dissipation.

Some of these properties are illustrated in Figure 18.1.1 showing results of a computation of solutions to the inviscid Burgers equation with the Euler implicit scheme.

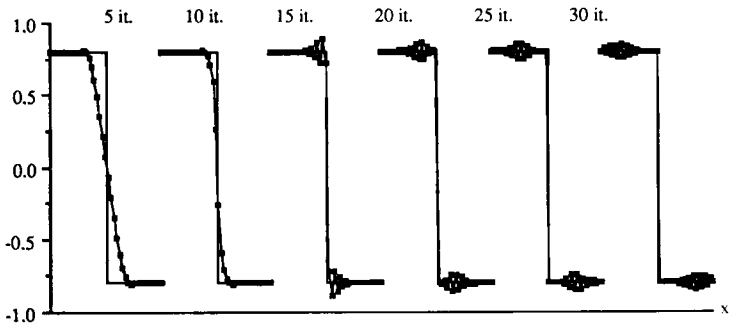
Three cases are shown corresponding to a stationary shock located in a mesh point (case 1), to the shock located between two mesh points (case 2) and a third case with slowly moving shock with a velocity = 0.05. The shock discontinuity is from $u_L = 0.8$ to $u_R = -0.8$ for cases 1 and 2, and between 0.8 and -0.7 for the propagating shock.

Figure 18.1.1 shows a series of diagrams containing the exact solution and the computed profiles after respectively 5, 10, 15, 20, 25 and 30 time steps. All cases are computed at a Courant number of 0.8.

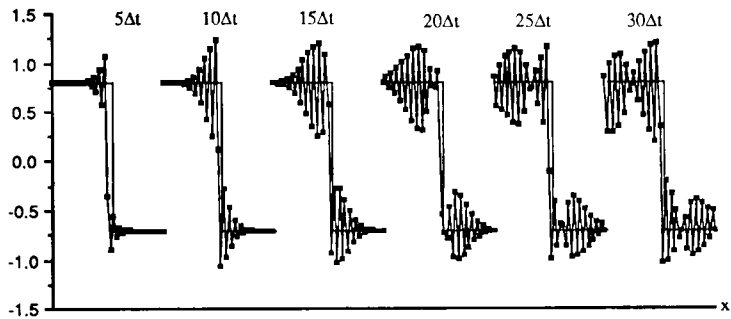
Beam and Warming scheme



Test case 1 : steady - state problem with shock placed in a point



Test case 2 : steady - state problem with shock between two points



Test case 3 : non stationary problem with moving shock

Figure 18.1.1 Application of the schemes (18.1.9) to Burgers equation. Results are given for CFL = 0.8, after respectively 5, 10, 15, 20, 25 and 30 iterations

The differences between case 1 and case 2 illustrate in a spectacular way the generation of high-frequency oscillations when the amplification factor is equal to 1. This occurs for all wavelengths when the eigenvalues of the Jacobian A go through zero, leading to a zero value of the Courant number σ . These errors are then undamped since $G = 1$ for $\sigma = 0$. When the shock is located at a mesh point, the propagation velocity is sonic at this point and the oscillations are undamped, while this is not the case when the shock is located between mesh points. In this latter case there is no mesh point where the sonic velocity is attained. In test cases 2 and 3, one can observe the relative displacement of the high-frequency error waves, which form a wave-packet that should be travelling at the numerical group velocity, as seen in Section 8.3.5 in Volume 1. The numerical group velocity can readily be calculated by writing the amplification factor (18.1.16) under the form $G = \exp(-I\omega \Delta t)$ and taking the derivative of both sides. This leads to the expression, valid for linearized equations with phase speed a :

$$v_G = \text{Re} \left(\frac{d\omega}{dk} \right) = a \frac{\cos \phi [1 - \sigma^2 \theta (\theta - 1) \sin^2 \phi]}{(1 + \sigma^2 \theta^2 \sin^2 \phi) [1 + \sigma^2 (\theta - 1)^2 \sin^2 \phi]} \quad (18.1.21)$$

At the highest frequencies $\phi \simeq \pi$, the group velocity equals $-a$, indicating that the numerical waves travel in the opposite direction to the convection of the flow properties. Hence, in front of the shock, where $u_L > 0$, v_G will be negative and the wave-packet will travel to the left. The opposite situation occurs downstream of the shock, where the convection velocity is negative. Hence the error waves will travel to the right. This is the case in Figure 18.1.1, and considering test case 2, for instance, with $u_L = -u_R = 0.8$, at a CFL number of 0.8 the ratio $\Delta x / \Delta t = 1$ and after five time steps the wave has covered a distance equal to $0.8 \times 5\Delta t = 4\Delta x$. This is confirmed by the figures, where it can be seen that the error waves have moved by four mesh points from one plot to the other.

Case 1 in Figure 18.1.1 shows the generation of the oscillations at the discontinuity and their propagation throughout the flow field, destroying the accuracy of the complete solution. A similar behaviour is to be observed for the non-stationary shock. Clearly these results indicate the need for additional damping or dissipation in the implicit schemes.

18.1.2 Addition of artificial viscosity

As seen from the previous examples, artificial viscosity is required to damp the high-frequency waves and a fourth-order dissipation term of the form (17.3.15) has been added (Beam and Warming, 1976; Steger, 1978).

This leads to an additional term in the right-hand side of scheme (18.1.9), equal to

$$-\varepsilon \frac{\tau}{2} \Delta x^3 a_i \left[\left(\frac{\partial^3 U}{\partial x^3} \right)_{i+1} - \left(\frac{\partial^3 U}{\partial x^3} \right)_{i-1} \right] \quad \text{where } a = |u| + c \quad (18.1.22)$$

Since τ has the dimensions of the inverse of a velocity, the product $\varepsilon\tau a$ can be absorbed into a constant ε_E , producing a linear dissipation term

$$-\varepsilon_E \Delta x^4 \frac{\partial^4 U}{\partial x^4} \equiv -\varepsilon_E^* \text{CFL} \Delta x^4 \frac{\partial^4 U}{\partial x^4} \quad (18.1.23)$$

where ε_E and ε_E^* are artificial viscosity coefficients. Observe that this linear dissipation is obtained also if $a_i = (|u| + c)_i$ and a local time step such as (17.4.1) is selected.

At steady-state conditions, all ΔU tend to zero and the stationary solution corresponds to

$$f_{i+1} = f_{i-1} - \frac{2\Delta x}{\Delta t} \varepsilon_E \delta^4 U_i + O(\Delta x^3)$$

If ε_E is fixed the steady state would depend on the time step, which is not desirable. Hence this coefficient has to remain proportional to the time step, and since ε_E is a non-dimensional coefficient, one can take ε_E proportional to a Courant number, for instance the reference Courant number of the computation. This is applied in equation (18.1.23) where the dissipation coefficient is taken as $\varepsilon_E = \varepsilon_E^* \text{CFL}$.

The corrected scheme can be written as

$$[(1 + \xi) + \tau\theta \cdot \bar{\delta} A_i^n] \Delta U_i^n = -\tau \bar{\delta} f_i^n + \xi \Delta U_i^{n-1} - \varepsilon_E \delta^4 U_i^n \quad (18.1.24)$$

where δ^4 is a central approximation for the fourth-order derivative:

$$\delta^4 U_i = U_{i+2} - 4U_{i+1} + 6U_i - 4U_{i-1} + U_{i-2} \quad (18.1.25)$$

Of course, this fourth-order term does not modify the overall accuracy of the scheme.

For $\xi = 0$, the Von Neumann analysis applied to the linearized equation leads to the following amplification factor (see Problem 18.4):

$$G - 1 = -\frac{I\sigma \sin \phi + 4\varepsilon_E(1 - \cos \phi)^2}{1 + I\sigma\theta \sin \phi} \quad (18.1.26)$$

For the highest frequencies, we now have a dissipative contribution, since

$$G = 1 - 16\varepsilon_E \quad \text{for } \phi = \pi \quad (18.1.27)$$

with a stability limit determined by $|G| \leq 1$, that is

$$0 \leq \varepsilon_E \leq \frac{1}{8} \quad (18.1.28)$$

The value $\varepsilon_E = \frac{1}{16}$ is linearly the optimal choice since $G = 0$ for $\phi = \pi$ and the high frequencies are completely damped.

When $\xi \neq 0$, the stability limit for the artificial viscosity coefficients is extended to (see Problem 18.5)

$$0 \leq \varepsilon_E \leq \frac{1 + 2\xi}{8} \quad (18.1.29)$$

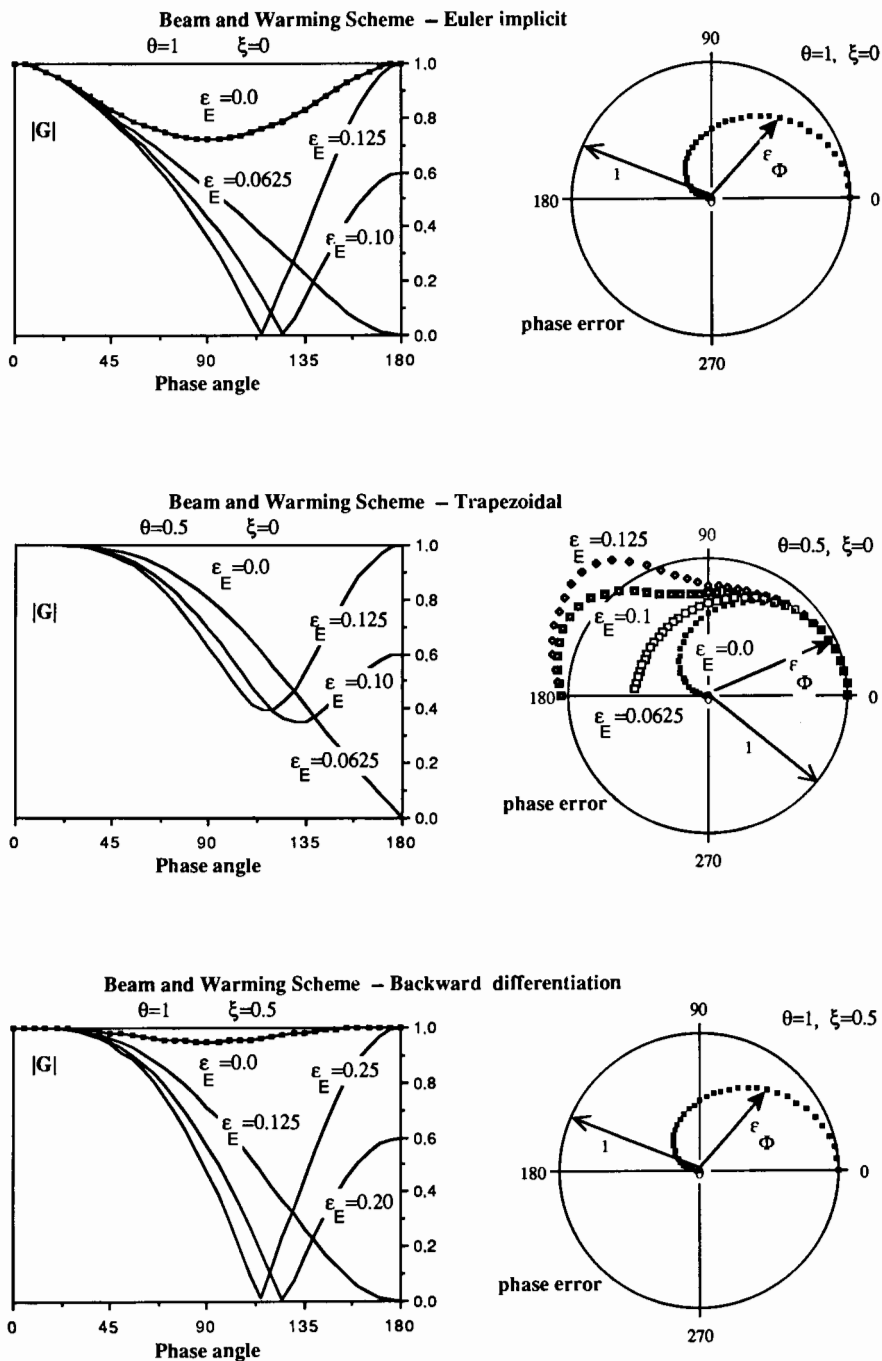


Figure 18.1.2 Amplification modulus and phase error for scheme (18.1.24) with explicit, linear fourth-order dissipation

Figure 18.1.2 shows the influence of ϵ_E on the amplitude (diffusion error) and the phase ratio ϕ/ϕ_e (dispersion error) for the schemes (18.1.24) for different values of the dissipation coefficient at a Courant number of 0.95. Three different schemes are represented, the Euler implicit ($\theta = 1, \xi = 0$), the trapezoidal ($\theta = \frac{1}{2}, \xi = 0$) and the backward differenced ($\theta = 1, \xi = 0.5$) schemes. Compared to the situation without dissipation terms, represented by the curves labelled $\epsilon_E = 0.00$, the reduction in the modulus of the amplification factor is representative of the increased dissipation of the scheme.

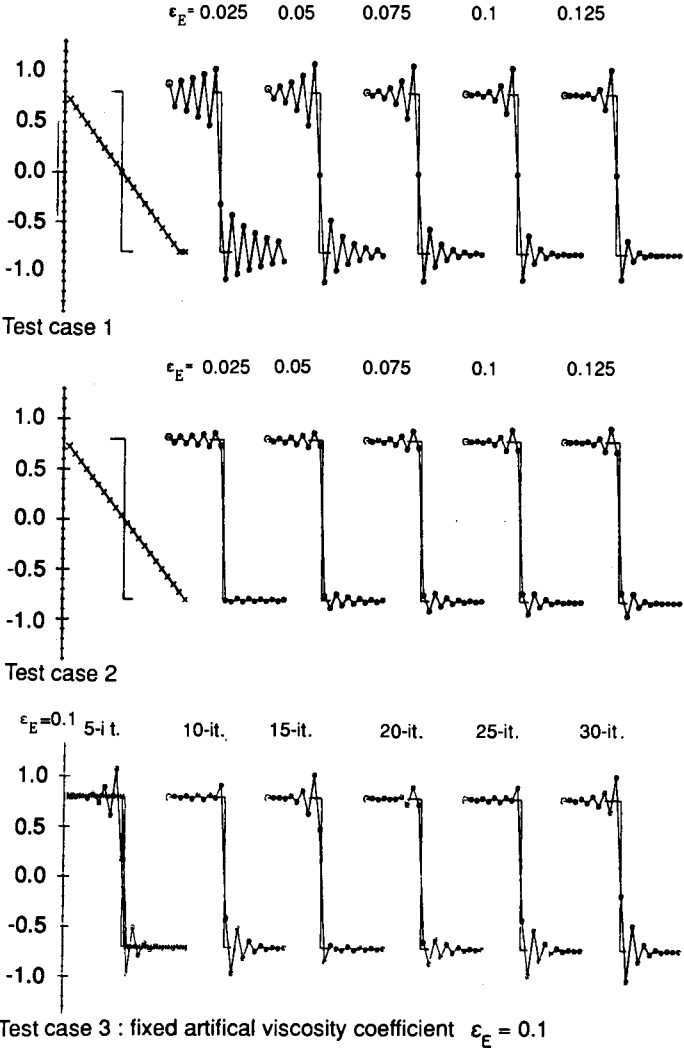


Figure 18.1.3 Application of explicit artificial viscosity (18.1.22). Comparison of converged shock structures as a function of ϵ_E for Burgers equation and the test cases of Figure 18.1.1 at CFL = 3.2

Figure 18.1.3 presents the effect of increasing the artificial viscosity coefficient ε_E on the same test case of Burgers equation as shown in Figure 18.1.1, at higher values of the Courant number, namely $\sigma = 3.2$. At these high CFL numbers, the steady-state solution is obtained in a few iterations.

The values of ε_E cover the whole range from $\varepsilon_E = \frac{1}{40}$ to the stability limit $\varepsilon_E = \frac{1}{8}$. The results of test cases 1 and 2 correspond to the converged profiles with different values of the dissipation parameter, while test case 3 shows the evolution of the non-stationary shock at $\varepsilon_E = \frac{1}{10}$, where the different profiles are obtained after 5, 10, 15, 20, 25 and 30 time steps. This last calculation is unstable at the same CFL number of 3.2 in the absence of the dissipation term.

Clearly this higher-order dissipation term is insufficient to damp completely the oscillations at larger CFL values, although it allows computations at values of the Courant number that otherwise would be unstable in the absence of this term.

Implicit dissipation terms

When performing computations at higher Courant numbers, which is the goal of implicit methods, it appears that increasing values of the dissipation coefficient ε_E are required in order to obtain sufficient dissipation. However, the stability limit (18.1.29) precludes the increase of ε_E . In order to extend the stability range of the dissipation terms an implicit dissipation D_1 of second order has been introduced by Pulliam and Steger (1978), in addition to the explicit term. This term, which operates on the left-hand side in the implicit operator of equation (18.1.24), has the form

$$D_1 = -\varepsilon_1 \Delta x^2 \frac{\partial^2 \Delta U}{\partial x^2} \quad (18.1.30)$$

Discretized centrally, the corrected equation (18.1.24) becomes

$$[(1 + \zeta) + \tau \theta \bar{\delta} A_i^n - \varepsilon_1 \delta^2] \Delta U_i^n = -\tau \bar{\delta} f_i^n + \zeta \Delta U_i^{n-1} - \varepsilon_E \delta^4 U_i^n \quad (18.1.31)$$

A Von Neumann analysis on the linearized equation gives the amplification function G , for $\zeta = 0$, as

$$G - 1 = -\frac{I \sigma \sin \phi + 4 \varepsilon_E (1 - \cos \phi)^2}{1 + I \sigma \theta \sin \phi + 2 \varepsilon_1 (1 - \cos \phi)} \quad (18.1.32)$$

In the high-frequency limit, $\phi = \pi$, the amplification factor becomes equal to

$$G = \frac{1 + 4 \varepsilon_1 - 16 \varepsilon_E}{1 + 4 \varepsilon_1} \quad (18.1.33)$$

and the stability limit requires

$$0 \leq 8 \varepsilon_E \leq 1 + 4 \varepsilon_1 \quad (18.1.34)$$

instead of equation (18.1.28).

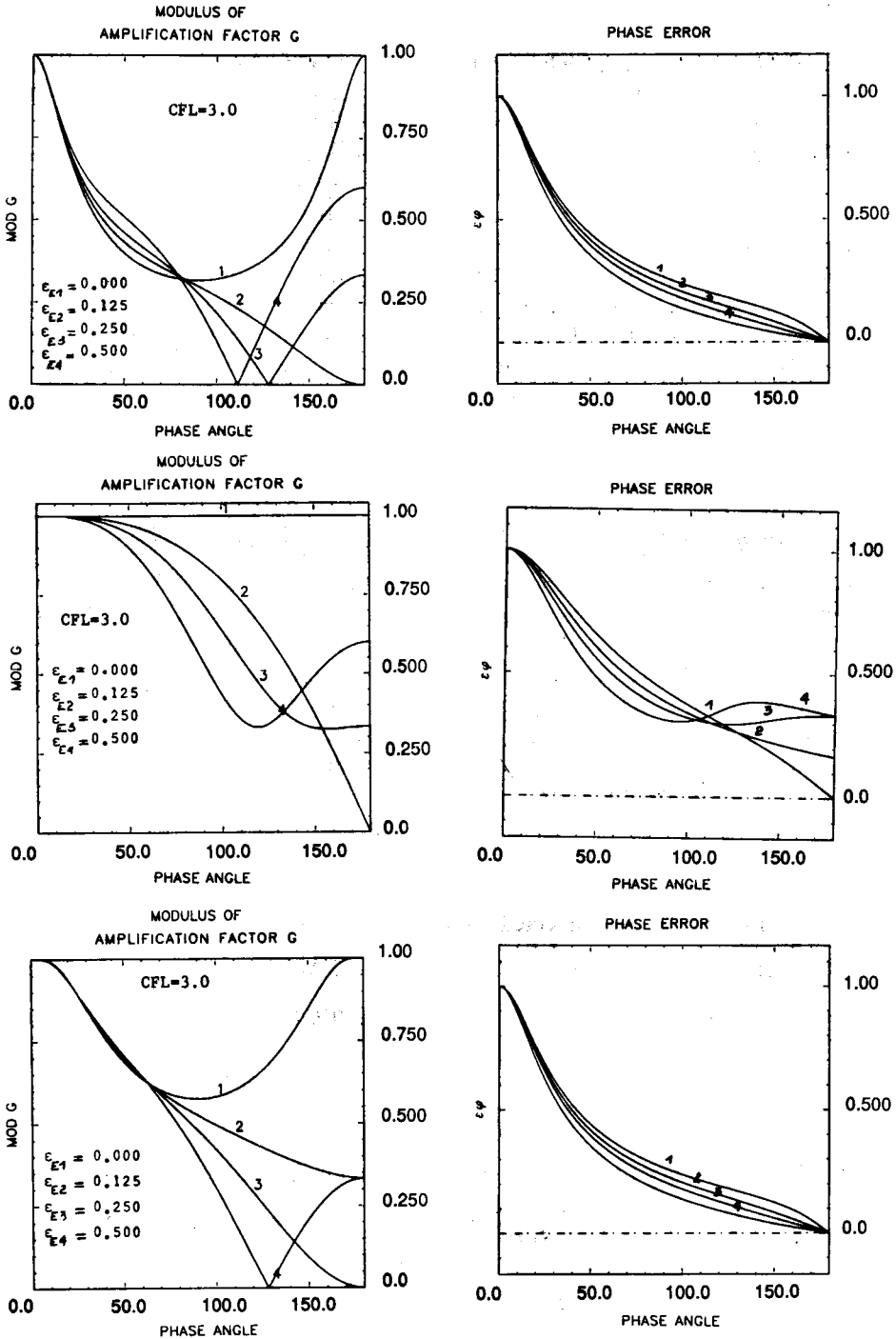


Figure 18.1.4 Amplification amplitude and phase error for scheme (18.1.31) with explicit, linear, fourth-order dissipation and second-order implicit dissipation

With $\zeta \neq 0$, the stability limit is easily seen to be (see Problem 18.6)

$$0 \leq 8\varepsilon_E \leq (1 + 2\zeta + 4\varepsilon_I) \quad (18.1.35)$$

Hence, a choice of the form (Pulliam and Steger, 1978)

$$\varepsilon_I = 2\varepsilon_E \quad (18.1.36)$$

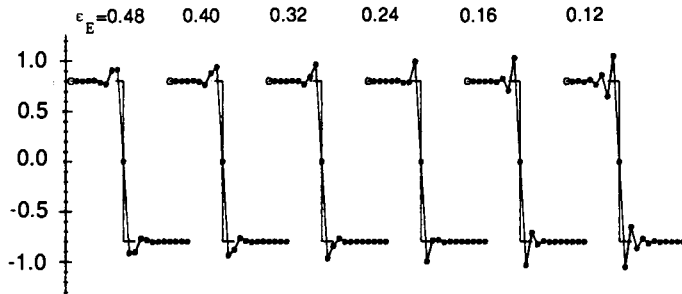
guarantees linear stability for all values of ε_E .

Figure 18.1.4 presents the effects of the implicit dissipation terms on the amplification factor and on the dispersion error for different values of ε_E , while ε_I is selected according to equation (18.1.36), at a CFL = 3. This is to be compared with Figure 18.1.2.

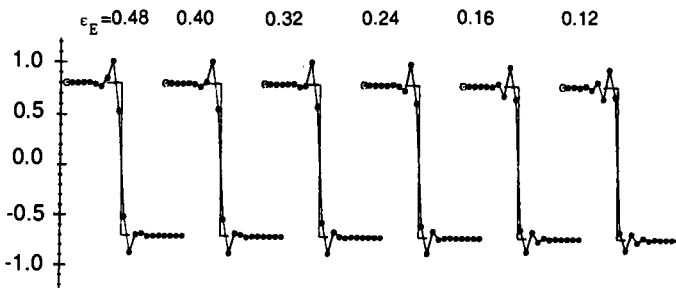
Figure 18.1.5 shows, the effect of the implicit dissipation term on the solutions of Burgers equation of Figure 18.1.3 for different values of ε_E and for $\varepsilon_I = 2\varepsilon_E$. Due to the presence of the implicit term, higher values of ε_E could be used, leading to an improved accuracy.

These examples show that the shock structure is essentially dependent on the explicit coefficient ε_E , while ε_I only allows the range of ε_E to be extended.

The following figures show results obtained for a quasi-one-dimensional nozzle flow, solving the full system of one-dimensional Euler equations, with



Test case 1 : CFL = 5.2



Test case 2 : CFL = 3.2

Figure 18.1.5 Application of the scheme (18.1.31) to Burgers equation, with explicit and implicit viscosity ($\varepsilon_I = 2\varepsilon_E$) for CFL = 3.2 and several values of ε_E to the test cases 1 and 2 of Figure 18.1.3

the three-point backward scheme ($\theta = 1, \xi = \frac{1}{2}$) and the implicit, first order in time Euler scheme ($\theta = 1, \xi = 0$).

The basic scheme (18.1.31) is adapted as follows for the quasi-one-dimensional nozzle, where a non-zero source term Q appears in the right-hand side (see equations (16.4.1)):

$$\left[(1 + \xi) + \theta \Delta t \frac{\partial}{\partial x} A^n - \theta \Delta t B^n \right] \Delta U^n = - \Delta t \frac{\partial}{\partial x} f^n + \Delta t Q^n + \xi \Delta U^{n-1} \quad (18.1.37)$$

Adding the central space discretization leads to, instead of equation (18.1.9),

$$[(1 + \xi) + \theta \tau \bar{\delta} A_i^n - \theta \Delta t B_i^n] \Delta U_i^n = - \tau \bar{\delta} f_i^n + \Delta t Q_i^n + \xi \Delta U_i^{n-1} \quad (18.1.38)$$

where A_i is the standard Jacobian matrix $A = \partial f / \partial U$ at point i and B is the Jacobian of the source terms, $B = \partial Q / \partial U$. B is given for a perfect gas by

$$B = \frac{1}{S} \left(\frac{dS}{dx} \right) \begin{vmatrix} 0 & 0 & 0 \\ (\gamma - 1)u^2 & -(\gamma - 1)u & \gamma - 1 \\ 0 & 0 & 0 \end{vmatrix} \quad (18.1.39)$$

Note that the source term can also be treated explicitly, leading to a slightly simpler scheme, with, however, a penalty on the convergence rate for stationary problems. This alternative is obtained from scheme (18.1.38) by setting $B = 0$:

$$[(1 + \xi) + \theta \tau \bar{\delta} \bar{A}_i^n] \Delta U_i^n = - \tau \bar{\delta} \bar{f}_i^n + \Delta t Q_i^n + \xi \Delta U_i^{n-1} \quad (18.1.40)$$

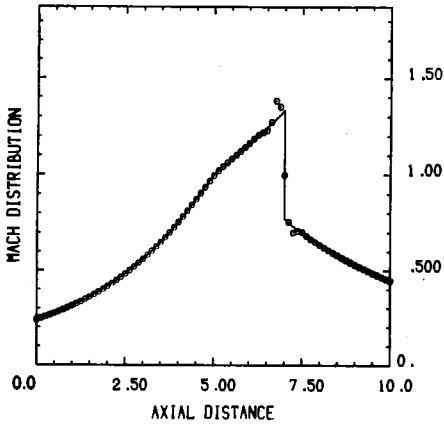
The considered test case is obtained for the converging-diverging nozzle of Problem 16.27 with inlet stagnation conditions of $p_0 = 1$ bar and $T_0 = 300$ K and the shock positioned at $x = 7$.

The figures display the convergence history, the density and Mach number distributions and also two diagrams showing the spatial variation of the errors generated by the scheme, namely the absolute value (on a logarithmic scale) of the mass flux error as defined earlier in relation to Figure 17.2.2, and the entropy distribution. All cases correspond to $\varepsilon_E^* = 5$ and $\varepsilon_1 = 2\varepsilon_E$.

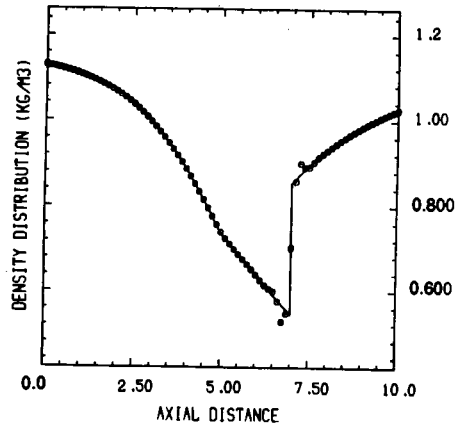
The three-point backward scheme (Figure 18.1.6) converges to machine accuracy in approximately 100 iterations for a CFL number of 40 using local time stepping. This is roughly 30 per cent faster than the Euler implicit scheme (Figure 18.1.7) under the same conditions, although the former scheme requires an additional storage level. Both schemes give identical converged results, which is to be expected since the steady state is independent on the implicit iterative algorithm.

An example of a non-stationary computation run at CFL = 0.95 with the Euler implicit scheme is shown in Figure 18.1.8 for the shock tube problem and artificial dissipation coefficients of $\varepsilon_1 = 2\varepsilon_E$ with $\varepsilon_E^* = 0.500$. As seen in Figure 18.1.8, the accuracy in the discontinuity regions is not very good, since the contact discontinuity is completely smeared out and the shock is distributed

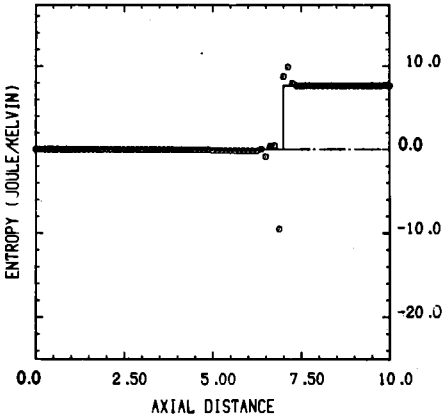
MACH NUMBER VERSUS AXIAL DISTANCE



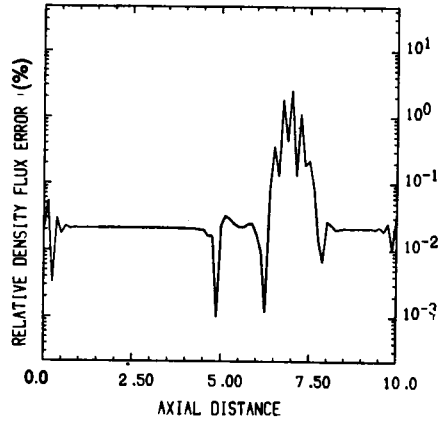
DENSITY VERSUS AXIAL DISTANCE



ENTROPY VERSUS AXIAL DISTANCE



DENSITY FLUX ERROR VERSUS AXIAL DISTANCE



CONVERGENCE HISTORY

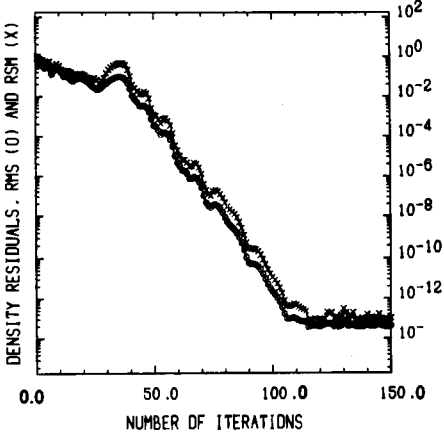


Figure 18.16 One-dimensional Euler flow in a nozzle, computed with the Beam and Warming scheme (18.1.38), with implicit and explicit linear dissipation terms. Three-point backward scheme $\theta = 1$, $\xi = \frac{1}{2}$

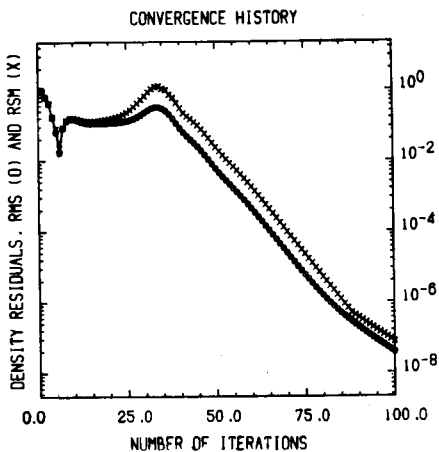
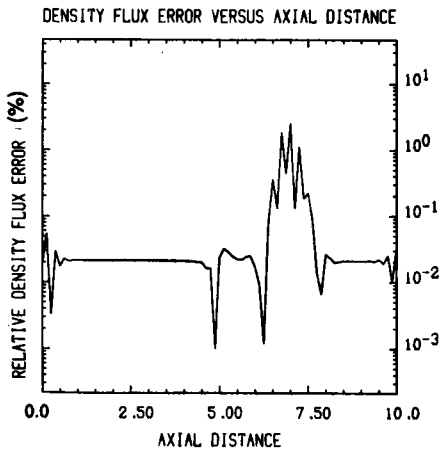
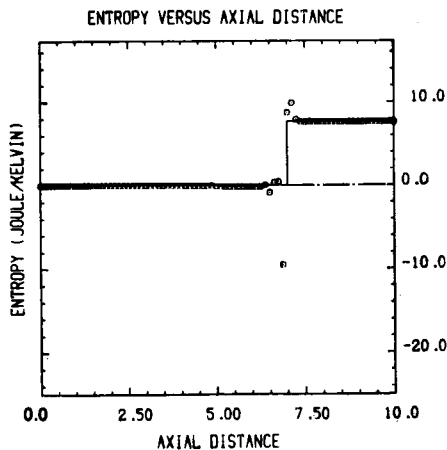
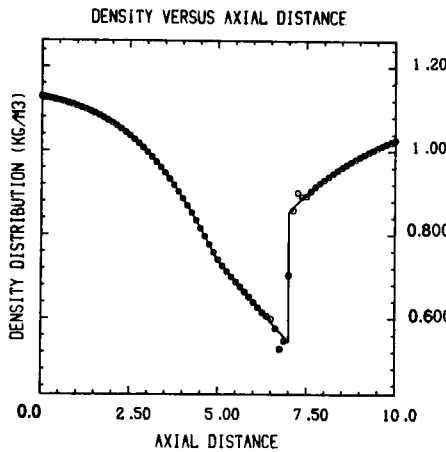
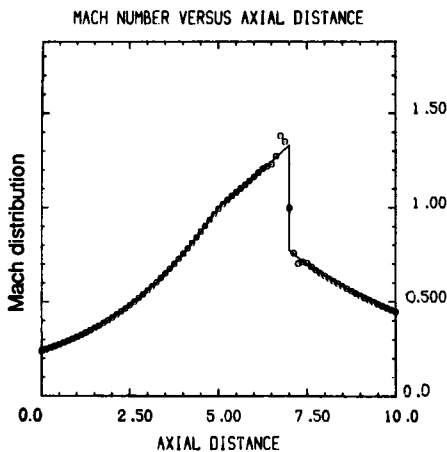
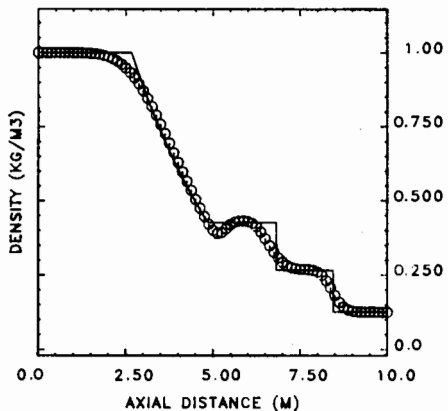
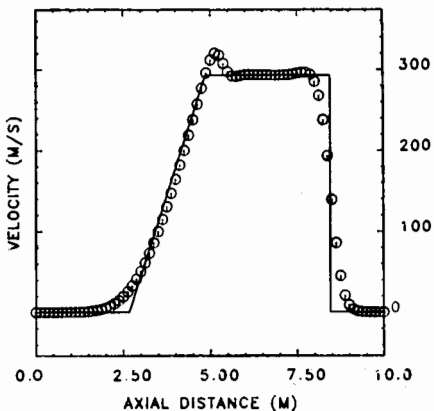


Figure 18.17 One-dimensional Euler flow in a nozzle, computed with the Beam and Warming scheme (18.1.38), with implicit and explicit linear dissipation terms. Euler implicit scheme $\theta = 1$, $\xi = 0$

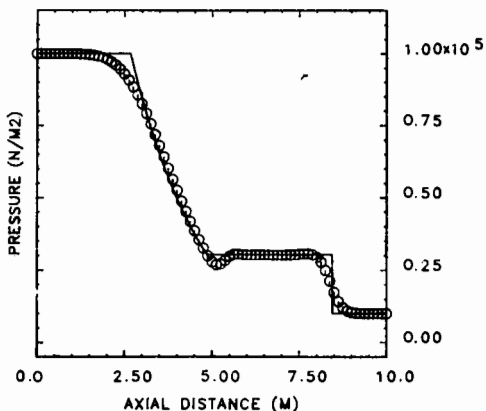
SHOCK TUBE FLOW T-STEP =35 CFL =0.95
WARMING AND BEAM SCHEME



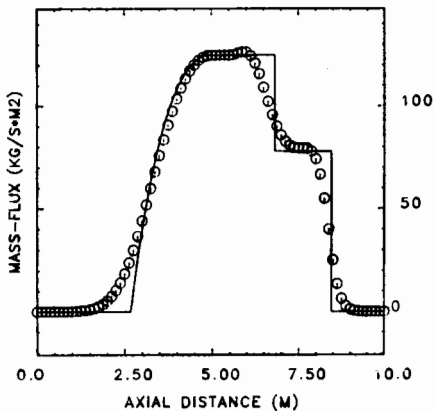
SHOCK TUBE FLOW T-STEP =35 CFL =0.95
WARMING AND BEAM SCHEME



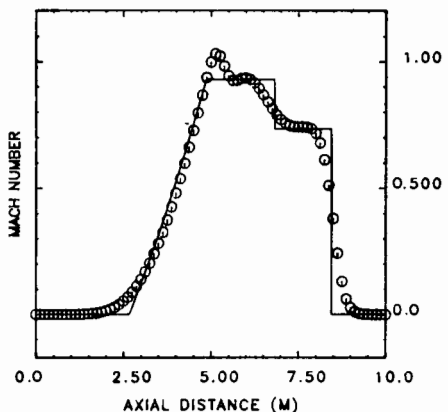
SHOCK TUBE FLOW T-STEP =35 CFL =0.95
WARMING AND BEAM SCHEME



SHOCK TUBE FLOW T-STEP =35 CFL =0.95
WARMING AND BEAM SCHEME



SHOCK TUBE FLOW T-STEP =35 CFL =0.95
WARMING AND BEAM SCHEME



SHOCK TUBE FLOW T-STEP =35 CFL =0.95
WARMING AND BEAM SCHEME

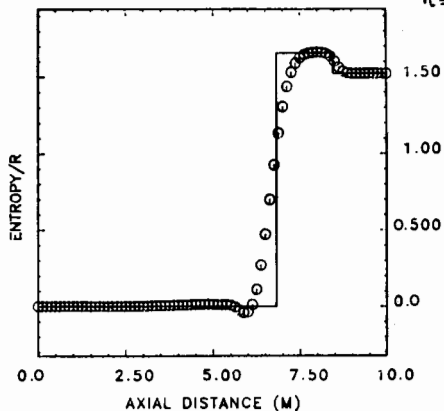


Figure 18.1.8 Shock tube problem (pressure ratio 10) computed with the Beam and Warming scheme (18.1.38), with implicit and explicit linear dissipation terms. Euler implicit scheme $\theta = 1, \xi = 0$

over roughly ten points. Reducing the dissipation coefficients does not alter this situation but increases the oscillations at the limits of the expansion fan.

Compared to the results obtained with McCormack's scheme on similar test cases, it can be seen that McCormack's scheme captures the discontinuities in a sharper way, the shock being distributed over three mesh points. This is one of the properties that made McCormack's scheme very popular for aeronautical applications, as a consequence of its excellent shock-capturing properties. However, the two computations have not been performed with the same artificial viscosity.

The linear artificial dissipation as described above appears generally sufficiently effective, although other forms of artificial dissipation can be introduced such as the MacCormack-Baldwin form or the Jameson combination presented in Section 17.3. The latter has been introduced in the Beam and Warming schemes by Pulliam (1986), with improved results, as shown in next section.

18.2 THE MULTI-DIMENSIONAL IMPLICIT BEAM AND WARMING SCHEMES

Since the time integration is distinct from the space discretization the multi-step method (11.1.23) applied to the one-dimensional form in (18.1.3) is readily generalized to two and three dimensions.

Let us consider the two-dimensional system of Euler equations:

$$\frac{\partial U}{\partial t} + \frac{\partial f}{\partial x} + \frac{\partial g}{\partial y} = 0 \quad (18.2.1)$$

Applying the two level time-integration formulas (11.1.23) leads to

$$(1 + \xi)\Delta U^n + \Delta t \theta \left(\frac{\partial f}{\partial x} + \frac{\partial g}{\partial y} \right)^{n+1} = -\Delta t \left(\frac{\partial f}{\partial x} + \frac{\partial g}{\partial y} \right)^n + \xi \Delta U^{n-1} \quad (18.2.2)$$

The linearization (18.1.4) is applied to f and g separately and the above equation becomes

$$\left[(1 + \xi) + \Delta t \theta \left(\frac{\partial}{\partial x} A + \frac{\partial}{\partial y} B \right)^n \right] \Delta U^n = -\Delta t \left(\frac{\partial f}{\partial x} + \frac{\partial g}{\partial y} \right)^n + \xi \Delta U^{n-1} \quad (18.2.3)$$

Applying a central space discretization in Cartesian coordinates leads to the following two-dimensional form of the Beam and Warming schemes:

$$(1 + \xi)\Delta U_{ij}^n + \theta(\tau_x \bar{\delta}_x A + \tau_y \bar{\delta}_y B)^n \Delta U_{ij}^n = -(\tau_x \bar{\delta}_x f_{ij}^n + \tau_y \bar{\delta}_y g_{ij}^n) + \xi \Delta U_{ij}^{n-1} \quad (18.2.4)$$

or explicitly

$$\begin{aligned}
 (1 + \xi)\Delta U_{ij}^n + \theta \frac{\Delta t}{2\Delta x} (A_{i+1,j}\Delta U_{i+1,j} - A_{i-1,j}\Delta U_{i-1,j})^n \\
 + \theta \frac{\Delta t}{2\Delta y} (B_{i,j+1}\Delta U_{i,j+1} - B_{i,j-1}\Delta U_{i,j-1})^n \\
 = -\Delta t \left(\frac{f_{i+1,j}^n - f_{i-1,j}^n}{2\Delta x} + \frac{g_{i,j+1}^n - g_{i,j-1}^n}{2\Delta y} \right) + \xi \Delta U_{ij}^{n-1} \quad (18.2.5)
 \end{aligned}$$

The implicit operator on the left-hand side is a block pentadiagonal matrix and is quite costly to invert. Therefore an ADI factorization is applied, following the methodology described in Section 11.4 in Volume 1.

For $\xi = 0$, the ADI factorization results in

$$(1 + \theta\tau_x \bar{\delta}_x A)(1 + \theta\tau_y \bar{\delta}_y B^n)\Delta U_{ij}^n = -(\tau_x \bar{\delta}_x f_{ij}^n + \tau_y \bar{\delta}_y g_{ij}^n) \quad (18.2.6)$$

and is solved by the two-step procedure

$$(1 + \theta\tau_x \bar{\delta}_x A^n)\bar{\Delta U}_{ij} = -(\tau_x \bar{\delta}_x f_{ij}^n + \tau_y \bar{\delta}_y g_{ij}^n) \quad (18.2.7a)$$

$$(1 + \theta\tau_y \bar{\delta}_y B^n)\Delta U_{ij}^n = \bar{\Delta U}_{ij} \quad (18.2.7b)$$

Each step is a tridiagonal system along the x lines for $\bar{\Delta U}$ and along the y lines for ΔU .

On arbitrary curvilinear meshes the above schemes have generally been applied after transforming equation (18.2.1) to curvilinear coordinates. However, one could as well start from an equivalent finite volume discretization as described in Section 6.2 in Volume 1; see Jameson and Yoon (1986) for example.

When discretized with finite differences in curvilinear coordinates, care should be taken to satisfy numerically the geometrical consistency relations. This has already been discussed in Chapter 14, Section 14.1, dealing with the numerical solutions of potential flows. A useful guideline is to discretize the metric coefficients similarly to the formulas derived from finite volume methods. Another way, valid for external flow problems, is to subtract the equation written for the far field from the general equation; that is one discretizes the following equation:

$$\frac{\partial}{\partial t} \left(\frac{U - U_\infty}{J} \right) + \frac{\partial}{\partial \xi^\alpha} \left(\frac{F^\alpha - F_\infty^\alpha}{J} \right) = 0 \quad (18.2.8)$$

This guarantees that the conservation equations are numerically identically satisfied for uniform flow conditions; see also Hindman (1981) and Pulliam and Steger (1978, 1980) for a detailed discussion.

The linear dissipation terms are added for each coordinate direction separately, as described above. However, an improved damping of the oscillations has been obtained with Jameson's combination of artificial viscosity, as described in

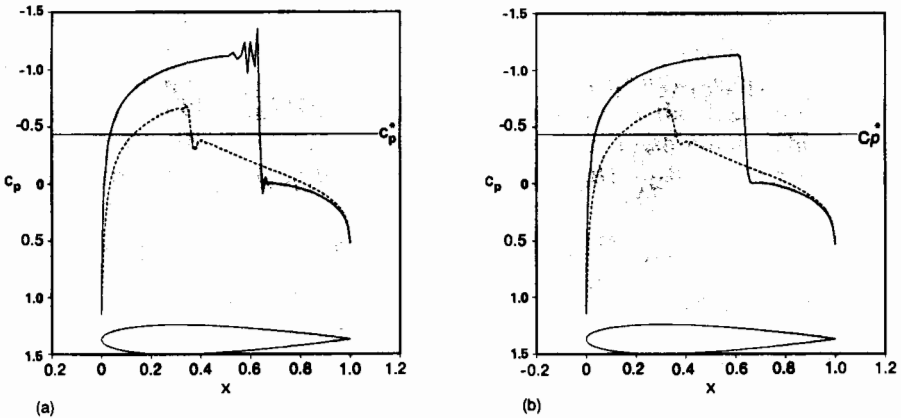


Figure 18.2.1 Comparison of shock resolution for the flow over an NACA 0012 between (a) the linear fourth difference and (b) Jameson's dissipation terms. (From Pulliam, 1986)

Section 17.3 (Pulliam, 1986). Figure 18.2.1 from this last reference shows the improvement in the shock resolution obtained by replacing the above linear terms by the combined dissipation terms of Jameson.

The extension to three dimensions is obvious from the equations (18.2.6), where a third factor is to be introduced. However, it has been shown in Section 11.4 in Volume 1 that the three-dimensional factorization is linearly unconditionally *unstable* for the centrally discretized convection equations. This instability is nevertheless weak and can be removed by the presence of dissipation terms, so that in practice instability problems do not seem to occur (Pulliam, 1986).

18.2.1 The diagonal variant of Pulliam and Chaussee

The tridiagonal system in the left-hand side of equations (18.1.9) defining the standard Beam and Warming scheme is in fact a block tridiagonal system where each element is a 3×3 matrix for the one-dimensional Euler equations and a 5×5 matrix when considered as a factor of a three-dimensional computation.

The solution of this system is the most costly operation at each time step because of the necessity to invert the Jacobian matrices. Hence, a worthwhile gain in computational work could be obtained if the implicit operations were to contain only scalar tridiagonal inversions. This has been suggested by Pulliam and Chaussee (1981).

We will discuss this approach in one dimension, since it applies without transformation to the factorized multi-dimensional case when each factor is treated separately. The method is based on the introduction of the transformation matrix P which diagonalizes A (see Section 16.3):

$$A = PAP^{-1} \quad (18.2.9)$$

where Λ is the diagonal matrix of the eigenvalues.

With this relation the Beam and Warming implicit scheme (18.1.9) becomes

$$[(1 + \xi) + \theta\tau\bar{\delta}(P\Lambda P^{-1})]_i \Delta U_i = -\tau\bar{\delta}f_i + \xi \Delta U_i^{n-1} \quad (18.2.10)$$

Scalar tridiagonal systems are obtained by displacing the matrix P outside of the differencing operator, leading to

$$P[(1 + \xi) + \theta\tau\bar{\delta}\cdot\Lambda]_i P^{-1} \cdot \Delta U_i^n = -\tau\bar{\delta}f_i^n + \xi \Delta U_i^{n-1} \quad (18.2.11)$$

Since the Jacobian Λ is a diagonal matrix, the block tridiagonal system reduces to three independent tridiagonal scalar equations.

An error is introduced by the above manipulation since the matrix P is not a constant matrix. Comparing the two equations (18.2.10) and (18.2.11), the additional error introduced in equation (18.2.11) is

$$\theta\tau(\Lambda P^{-1}) \cdot \bar{\delta}(P \cdot \Delta U_i) \quad (18.2.12)$$

which is proportional to Δt^2 since ΔU is first order in time.

Hence the error is of the same order as the $(\theta - \frac{1}{2} - \xi)$ truncation error in equation (18.1.5). This procedure reduces the accuracy to first order in time and would destroy the highest-order time accuracy for the family of schemes satisfying $\theta = \xi + \frac{1}{2}$. However, the spatial accuracy remains unchanged by this modification to the basic scheme. Note that the variables $P^{-1}\Delta U_i$ are the characteristic variables $\Delta W_i = P^{-1}\Delta U_i$.

Actually, a further simplification can be introduced for steady-state computations, considering that the convergence operator on the left-hand side is a numerical procedure for driving the solution to the converged conditions.

If the diagonal matrix Λ of the eigenvalues is replaced by its spectral radius, that is by its maximum eigenvalue $(|u| + c)_{\max} \equiv a_{\max}$, equation (18.2.10) becomes

$$[(1 + \xi) + \theta\bar{\delta}\sigma]_i \Delta U_i^n = -\tau\bar{\delta}f_i^n + \xi \Delta U_i^{n-1} \quad (18.2.13)$$

where $\sigma = \tau a_{\max}$.

This simplification of the Beam and Warming scheme has been also applied by Lerat (1985), as seen in Section 17.4. It has the advantage, over the full tridiagonal system, of ensuring diagonal dominance of the left-hand side operator since σ is never zero or negative, while not affecting the accuracy of the scheme. Of course, it reduces the time accuracy to first order as does equation (18.2.11).

Since the left-hand side operator is not exactly equal to the Jacobian of the right-hand side flux terms, it is to be expected that the convergence rate to steady state will be reduced, compared to the full system (18.1.7). This is indeed confirmed by Pulliam and Chaussee (1981), as well as by the calculations of Lerat *et al.* (1984). Therefore, the reduced computational cost of the simplified schemes (18.2.11) or (18.2.13) has to be balanced against the loss in convergence rate.

The schemes presented in this section have been developed into an effective operational code for two- and three-dimensional Euler (and also Navier–Stokes) equations at NASA Ames Research Center (USA) under the code name ARC2D

and ARC3D. A description of the components of these codes can be found in Pulliam and Steger (1985).

Practical example Three-dimensional inviscid flow in a 90° elbow passage

The considered internal flow in a 90° elbow duct has been investigated experimentally by Stanitz *et al.* (1953) with different shear flow profiles at inlet, generated by spoilers placed upstream of the duct. The original experiments have been repeated recently by Kreatsoulas *et al.* (1988) on a half-scale replica

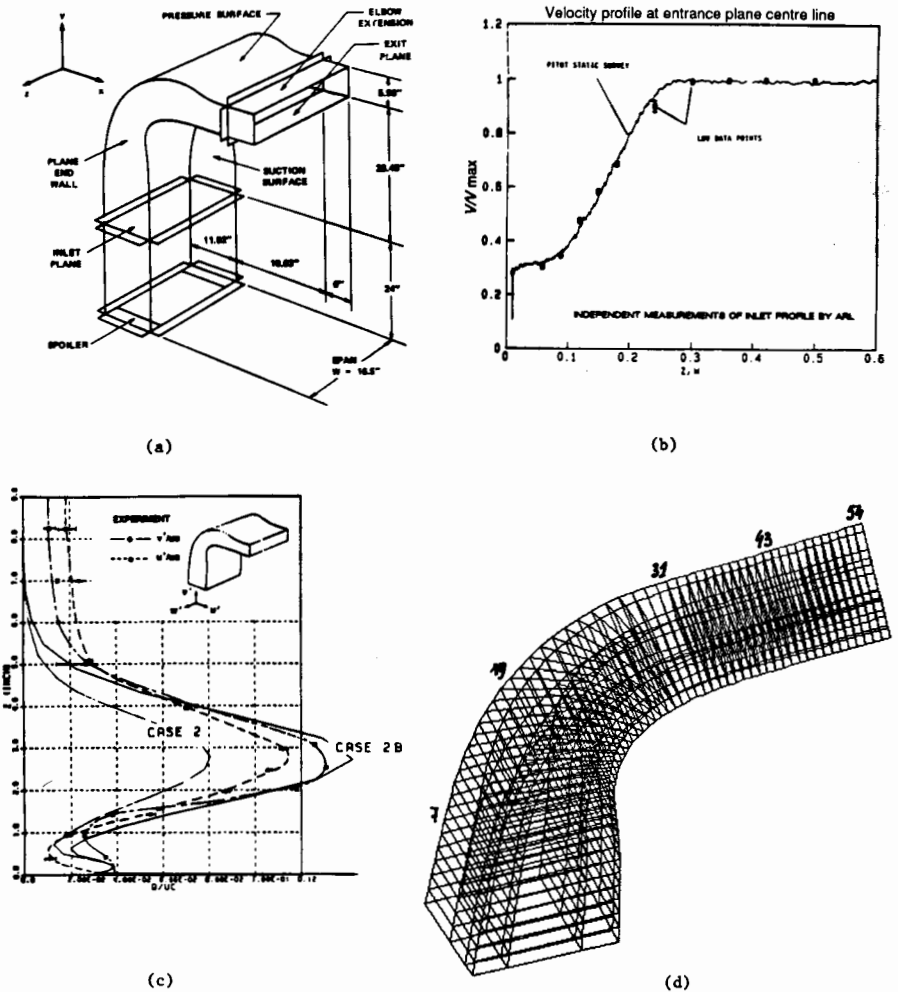


Figure 18.2.2 Original geometry, inlet profile and partial mesh for Stanitz duct. (a) Original geometry. (b) Inlet velocity profiles. (From Kreatsoulas *et al.*, 1988.) (c) Inlet turbulence profiles. (From Kreatsoulas *et al.*, 1988.) (d) Partial mesh. (Courtesy C. Lacor, Vrije Universiteit Brussel)

of Stanitz's duct, adding, however, detailed turbulence profiles at the inlet in order to allow more reliable validations of turbulence models.

The present results correspond to a spoiler size of 2.5 inch and a nominal outlet Mach number of 0.4. The inlet axial velocity distribution produced by the spoiler and taken as the inlet boundary condition is shown in Figure 18.2.2 together with the duct geometry, the inlet turbulence profiles and the discretized duct domain. The grid has 55 cross-sectional planes and 25×25 mesh points per cross-section, and only part of the mesh is shown for reasons of clarity.

Since the flow is symmetric about the mid-span section, only half of the duct is discretized. The calculations have been performed with the ARC3D code in the diagonalized version by C. Lacor with the support of W. Chan and T. Pulliam at NASA Ames.

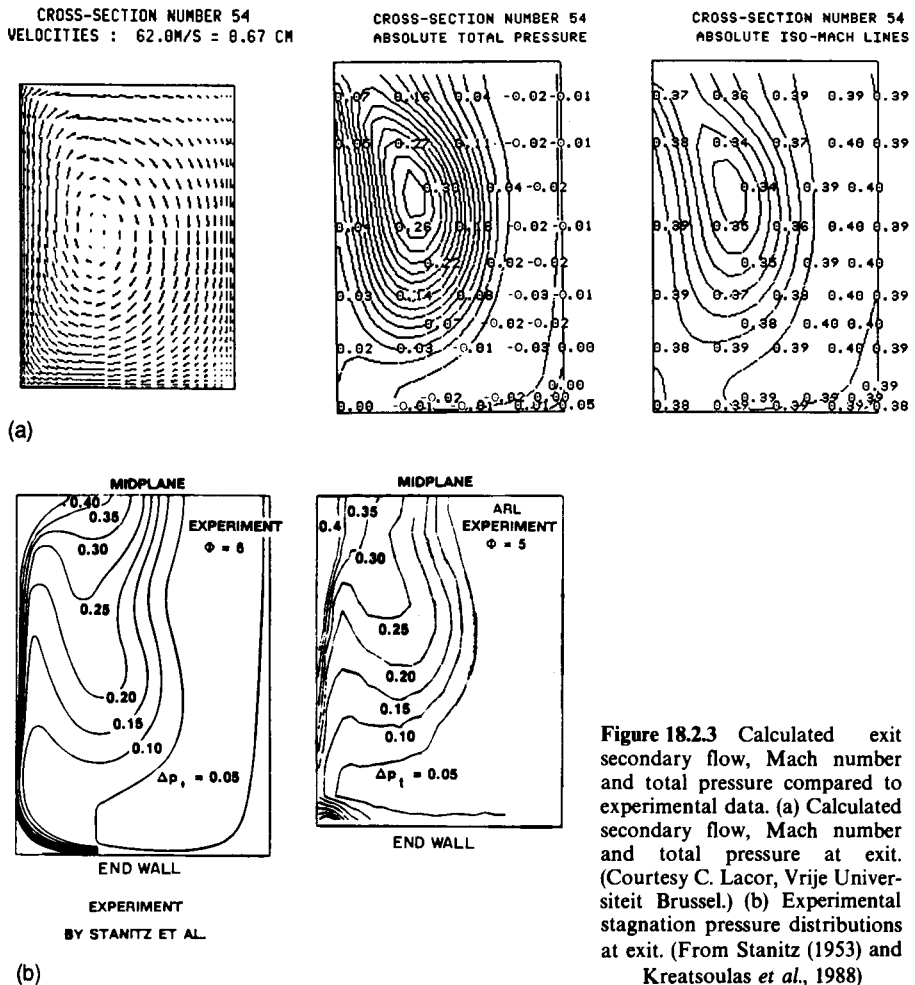


Figure 18.2.3 Calculated exit secondary flow, Mach number and total pressure compared to experimental data. (a) Calculated secondary flow, Mach number and total pressure at exit. (Courtesy C. Lacor, Vrije Universiteit Brussel.) (b) Experimental stagnation pressure distributions at exit. (From Stanitz (1953) and Kretsoulas *et al.*, 1988)

Due to the combination of the non-uniform inlet velocity with the turning of the streamlines, streamwise vorticity is generated, creating a rotating flow pattern in the cross-sectional planes, designated as secondary flow.

This is seen in Figure 18.2.3 where the calculated secondary flow in the exit section of the duct is displayed, together with the calculated total pressure distributions and the experimental data from Stanitz *et al.* (1953) and Kreatsoulas *et al.* (1988). The development of the secondary flow can be observed

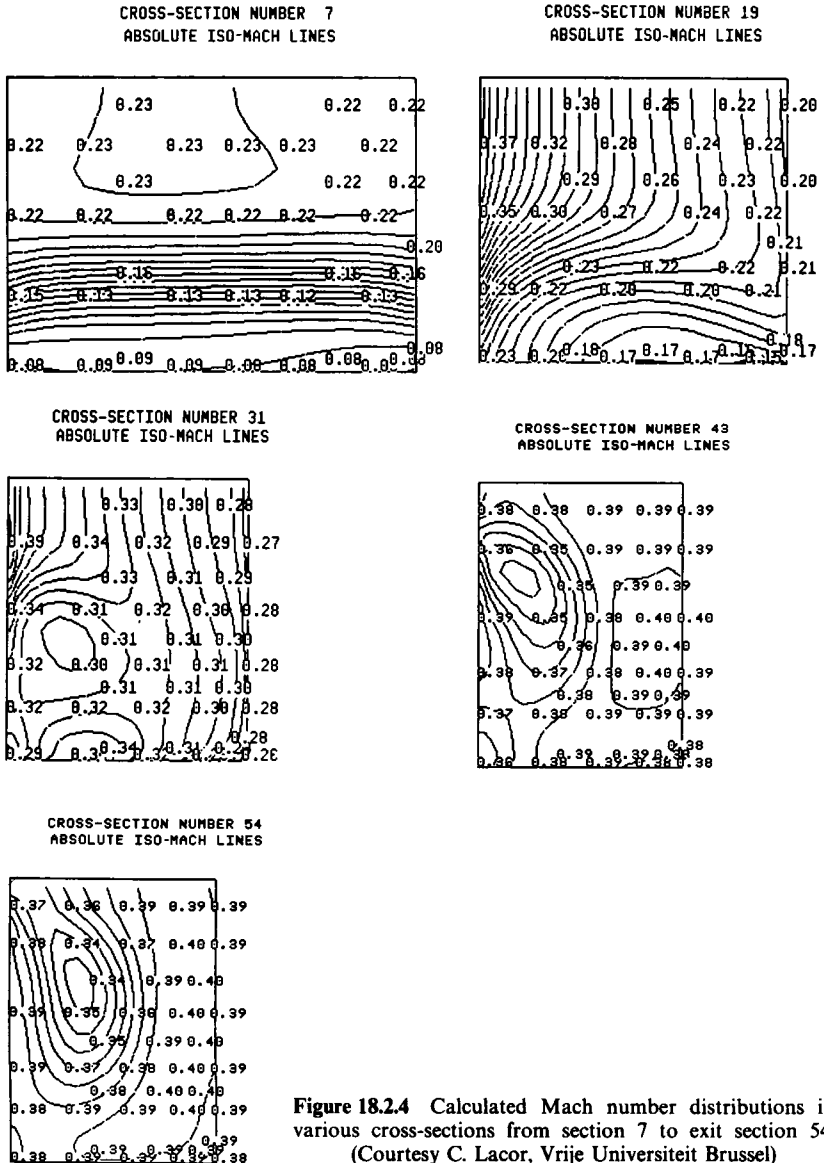


Figure 18.2.4 Calculated Mach number distributions in various cross-sections from section 7 to exit section 54. (Courtesy C. Lacor, Vrije Universiteit Brussel)

in more detail by following the iso-Mach and isostagnation pressure lines in the sections numbered 7, 19, 31, 43 and 54 (exit section) (Figures 18.2.4 and 18.2.5). The progressive rolling up of the stagnation pressure lines is a measure of the secondary flow, since in this subsonic inviscid flow the stagnation pressure remains constant along streamlines.

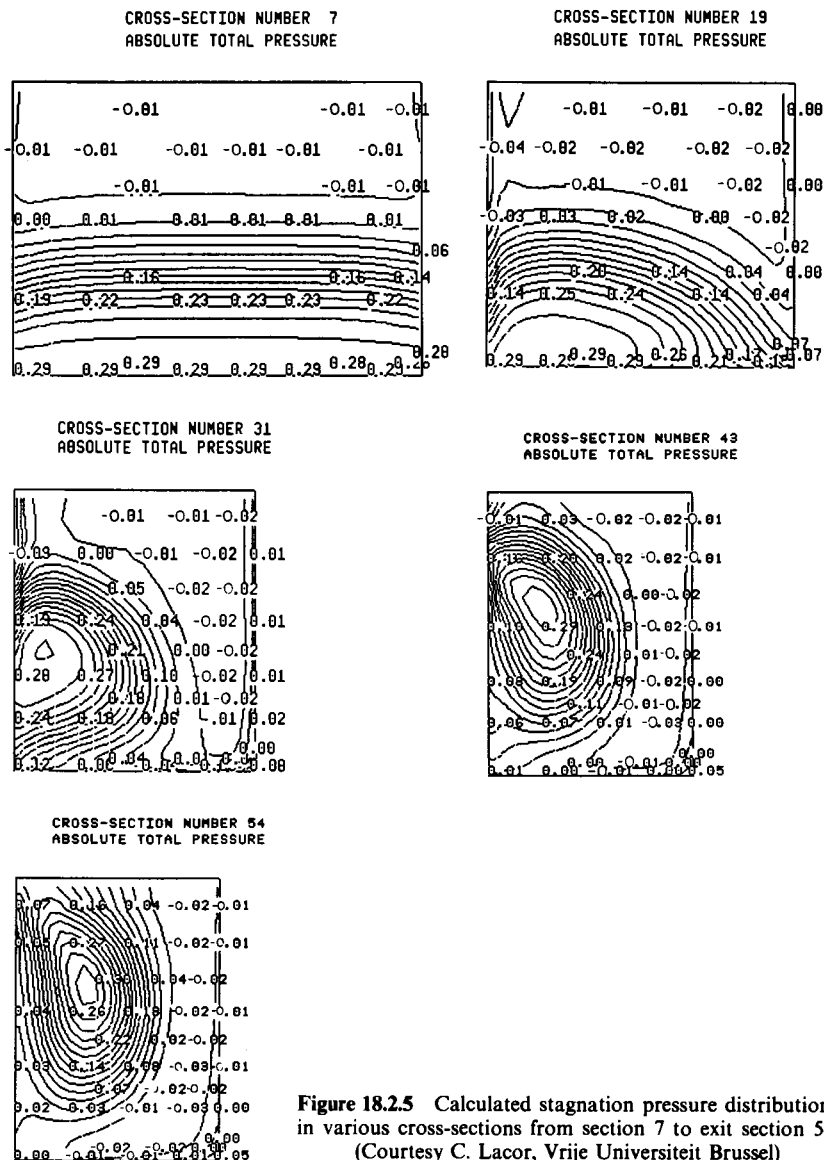


Figure 18.2.5 Calculated stagnation pressure distributions in various cross-sections from section 7 to exit section 54. (Courtesy C. Lacor, Vrije Universiteit Brussel)

Compared to the experimental total pressure distribution at the exit, it is seen that an excellent agreement is obtained from the inviscid calculation, confirming that the main contributions to the secondary flow in this geometry are of inviscid origin.

18.3 JAMESON'S MULTI-STAGE METHOD

The method developed by Jameson *et al.* (1981), Jameson (1982, 1987) and listed references applies a Runge–Kutta multi-stage time integration to the central discretization of the flux balance. This time-integration scheme contains part of the imaginary axis in its stability domain, as seen in Chapter 11, Section 11.5. It is therefore well adapted to centrally discretized hyperbolic convection operators that have pure imaginary eigenvalues. Additional dissipation terms are, however, still required to control the high-frequency waves, which are not damped by the scheme.

The method developed by Jameson and coworkers is a remarkable combination of components such as efficient dissipation terms, convergence acceleration ingredients and multi-grid techniques, leading to most efficient and accurate prediction codes. In addition, the properties of the Runge–Kutta multi-stage method are fully exploited to provide optimized smoothing properties as required by the multi-grid method.

The space discretization is identical to equation (18.1.1), namely a central differencing of the fluxes, although in practice a finite volume method is applied as outlined in Chapter 6 of Volume 1.

The dissipation terms are defined by equations (17.3.16) to (17.3.21) and added to the numerical flux 2.

18.3.1 Time integration

A four-step Runge–Kutta integration is applied, following Section 11.5 in Volume 1. For instance, in version (11.5.1), writing $-R^{(AV)}$ for the right-hand-side residual of equation (18.1.1) when $f^{(AV)}$ and $g^{(AV)}$ are introduced instead of f and g ,

$$\begin{aligned}
 U_{ij}^{(0)} &= U_{ij}^n \\
 U_{ij}^{(1)} &= U_{ij}^n - \alpha_1 \Delta t R^{(AV)}(U_{ij}^{(0)}) \\
 U_{ij}^{(2)} &= U_{ij}^n - \alpha_2 \Delta t R^{(AV)}(U_{ij}^{(1)}) \\
 U_{ij}^{(3)} &= U_{ij}^n - \alpha_3 \Delta t R^{(AV)}(U_{ij}^{(2)}) \\
 U_{ij}^{n+1} &= U_{ij}^n - \Delta t R^{(AV)}(U_{ij}^{(3)})
 \end{aligned} \tag{18.3.1}$$

A fourth-order accurate scheme (in time) can be obtained for

$$\alpha_2 = \frac{1}{4} \quad \alpha_3 = \frac{1}{3} \quad \alpha_4 = \frac{1}{2} \tag{18.3.2}$$

This integration scheme is explicit with a CFL condition of

$$\text{CFL} \leq 2\sqrt{2} \quad (18.3.3)$$

To reduce the computational cost of the evaluation of the dissipation term at each stage of the Runge–Kutta time integration, the $d_{i+1/2,j}$ terms are frozen at the time level n . Hence, if one writes

$$R_{ij}^{(\text{AV})} = R_{ij} + D_{ij} \quad (18.3.4)$$

where D contains all the dissipation terms and R_{ij} is the right-hand side of equation (18.1.1), at each stage $R^{(\text{AV})}$ is calculated as

$$R^{(\text{AV})}(U_{ij}^{(k)}) = R(U_{ij}^{(k)}) + D(U_{ij}^{(1)}) \quad (18.3.5)$$

The implications of this decomposition on stability properties are analysed in Jameson and Baker (1984).

18.3.2 Convergence acceleration to steady state

Several ingredients have been introduced by Jameson in order to accelerate the convergence towards the steady-state solution.

Local time step

Within each cell the solution is allowed to advance in time at the maximum rate compatible with a fixed Courant number and the size of the cell following equation (17.4.1).

Enthalpy damping

It has been seen in the treatment of the transonic potential equation that a $\partial\phi/\partial t$ term has a damping effect when the problem is hyperbolic in the variable t (see Chapter 15, Section 15.2).

Since the general form of the energy equation (13.1.3) is

$$\phi_t + H = H_\infty = \text{constant} \quad (18.3.6)$$

adding a term of the form $(H - H_\infty)$ could have a similar effect.

Since the discretization described in this section guarantees that $H = H_\infty$ will be satisfied by the discrete equations at convergence, one is ensured that $(H - H_\infty)$ will tend to zero.

It is interesting to observe at this point that McCormack's scheme, with different flux balance estimations for the predictor and the corrector, will not converge exactly to a constant stagnation enthalpy at steady state. Hence, the

following terms are added to the residuals:

$$R^{(AV)} \Rightarrow \bar{R} \equiv R^{(AV)} + \alpha U(H - H_\infty) \quad (18.3.7)$$

For reasons of homogeneity the fourth variable of the last term should be ρE or ρH . However, as pointed out by Jameson *et al.* (1981), this would give a quadratic term in the energy equation for H , making it close to a Riccati equation, which could have destabilizing effects. The replacement of ρH by 1 in the damping term for the energy equation appeared to be effective (see also Volpe *et al.*, 1987).

Residual smoothing

This step has been introduced to give an additional implicit character and increase thereby the maximum allowable Courant number. In addition this has the effect of smoothing the high-frequency variations of the residual and is essential to multi-grid convergence accelerations.

After \bar{R} has been calculated, an additional explicit step can be added in order to average the residual variations, for instance defining an averaged residual $R^{(T)}$:

$$\begin{aligned} R_{ij}^{(T)} &= \bar{R}_{ij} + \varepsilon(\delta_x^2 + \delta_y^2)\bar{R}_{ij} \\ &= \varepsilon(\bar{R}_{i-1,j} + \bar{R}_{i+1,j} + \bar{R}_{i,j-1} + \bar{R}_{i,j+1}) + (1 - 4\varepsilon)\bar{R}_{ij} \end{aligned} \quad (18.3.8)$$

which also increases the support of the scheme.

However, performing a Fourier analysis on this averaging operator when \bar{R}_{ij} is developed in a finite Fourier series leads to

$$R_{ij}^{(T)} = [2\varepsilon(\cos \phi_x + \cos \phi_y) + (1 - 4\varepsilon)]\bar{R}_{ij} \quad (18.3.9)$$

for an individual mode defined by ϕ_x, ϕ_y .

It is seen that for values of ε such that $\varepsilon > \frac{1}{8}$, the amplification factor of the averaging operator could have zero eigenvalues, since the factor between brackets could vanish in the range $-2 \leq \cos \phi_x + \cos \phi_y \leq 2$. This would have as a consequence that $R_{ij}^{(T)}$ could be zero when \bar{R}_{ij} is not, which is an undesirable property.

Therefore, the step (18.3.8) is replaced by an implicit averaging of the form

$$[1 - \varepsilon(\delta_x^2 + \delta_y^2)]R_{ij}^{(T)} = \bar{R}_{ij} \quad (18.3.10)$$

This leads to a pentadiagonal system and a more efficient formulation is obtained from an ADI factorization:

$$(1 - \varepsilon\delta_x^2)(1 - \varepsilon\delta_y^2)R_{ij}^{(T)} = \bar{R}_{ij} \quad (18.3.11)$$

Observe that each tridiagonal step has an explicit solution on an infinite support. For instance the solution of

$$(1 - \varepsilon\delta_x^2)R_{ij}^{(T)} = R_{ij}^* \quad (18.3.12)$$

or

$$-\varepsilon R_{i+1,j}^{(T)} + (1 - 2\varepsilon)R_{ij}^{(T)} - \varepsilon R_{i-1,j}^{(T)} = R_{ij}^* \quad (18.3.13)$$

is

$$R_{ij}^{(T)} = \frac{1 - \kappa}{1 + \kappa} [R_{ij}^* + \kappa(R_{i+1,j}^* + R_{i-1,j}^*) + \kappa^2(R_{i+2,j}^* + R_{i-2,j}^*) + \dots] \quad (18.3.14)$$

where κ is a solution of

$$\varepsilon \kappa^2 + (1 - 2\varepsilon)\kappa - \varepsilon = 0 \quad (18.3.15)$$

or

$$\varepsilon = \frac{\kappa}{(1 - \kappa)^2} \quad (18.3.16)$$

This indicates that after the residual smoothing, \bar{R}^T is made dependent on all the R_{ij} , with terms proportional to κ^k for $R_{i+k,j}$.

Hence, ε should be chosen such as to allow a solution of (18.3.15) such that $\kappa < 1$. This is always possible for $\varepsilon > 0$, since the product of the two solutions to (18.3.15) is equal to one.

Applying a Fourier analysis, one obtains, instead of equation (18.3.9),

$$R_{ij}^{(T)} = \frac{\bar{R}_{ij}}{(1 + 2\varepsilon - 2\varepsilon \cos \phi_x)(1 + 2\varepsilon - 2\varepsilon \cos \phi_y)} \quad (18.3.17)$$

The denominator attains a maximum for the high frequencies $\cos \phi_x \simeq \pi$, $\cos \phi_y \simeq \pi$, showing that the implicit operator provides maximum residual smoothing at these frequencies.

With regard to amplification factors, it is to be noticed from equation (18.3.1) that the Fourier transform of the residual is $(\bar{G} - 1)$, where \bar{G} is the amplification factor of the explicit scheme. Hence, equation (18.3.11) leads to the amplification factor

$$G^{(T)} - 1 = \frac{\bar{G} - 1}{(1 + 2\varepsilon - 2\varepsilon \cos \phi_x)(1 + 2\varepsilon - 2\varepsilon \cos \phi_y)} \quad (18.3.18)$$

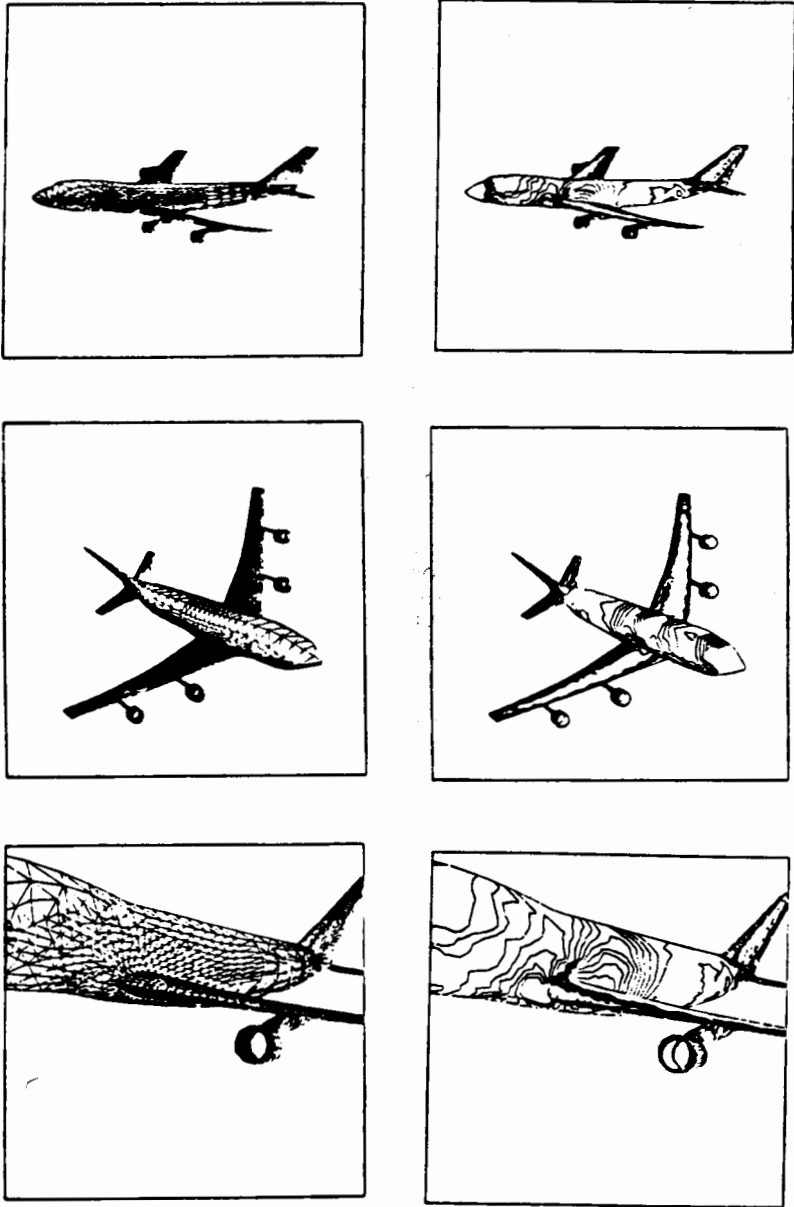
and any Courant number can now be selected provided ε is made large enough.

It is sufficient to apply the smoothing at alternate stages, provided the smoothing parameter ε is sufficiently increased, for instance at the second and fourth stage in the four-stage Runge-Kutta time integration.

This additional step of residual smoothing is similar to the implicit step in the general family of implicit schemes developed by Lerat and analysis in Section 17.4.

Multi-grid acceleration

By transferring to coarser meshes, the convergence to steady state is accelerated since larger time steps can be used on the coarser mesh. The corrections are then interpolated back to the fine grid, where a smoothing operator removes the high-frequency errors.



(a) Views of the mesh

(b) Surface pressure contours

Figure 18.3.1 Transonic flow over a complete Boeing 747-200 aircraft at incident Mach number of 0.84 and 2.73° incidence. (From Jameson, 1987)

The details of the multi-grid technique can be found in the mentioned references, in particular in Jameson (1983a, 1987).

This method has been developed into very efficient two- and three-dimensional codes (Jameson, 1987) and Figure 18.3.1 is an example of the flow over a complete Boeing 747-200 aircraft calculated with a version of the method applied with a non-structured mesh. The mesh contained 35 370 points and 181 952 tetrahedra. Although this mesh is rather coarse, the significant flow features are predicted, such as the supersonic region on the wings and the interference effects between the components.

It is to be observed that the treatment of the dissipation terms, in particular at the solid boundaries, can have strong effects on accuracy and the convergence rate of the inviscid flow computations. Detailed discussions of the influence of these damping terms can be found in Rizzi (1984), Pulliam (1986), Swanson and Turkel (1987) and Caughey and Turkel (1988). One of the important conclusions is the necessity to reduce the second-order dissipation terms at the solid boundaries.

References

- Beam, R. M., and Warming, R. F. (1976). 'An implicit finite-difference algorithm for hyperbolic systems in conservation law form.' *Journal Computational Physics*, **22**, 87-109.
- Beam, R. M., and Warming, R. F. (1978). 'An implicit factored scheme for the compressible Navier-Stokes equations.' *AIAA Journal*, **16**, 393-402.
- Beam, R. M., and Warming, R. F. (1980). 'Alternating direction implicit methods for parabolic equations with a mixed derivative.' *SIAM Journal of Sci. Stat. Comp.*, **1**, 131-59.
- Beam, R. M., and Warming, R. F. (1982). 'Implicit numerical methods for the compressible Navier-Stokes and Euler equations.' Von Karman Institute Lecture Series 1982-04, Rhode Saint Genese, Belgium.
- Briley, W. R., and McDonald, H. (1975). 'Solution of the three-dimensional Navier-Stokes equations by an implicit technique.' *Proc. Fourth International Conference on Numerical Methods in Fluid Dynamics, Lecture Notes in Physics*, Vol. 35, Berlin: Springer.
- Caughey, D. A., and Turkel, E. (1988). 'Effects of numerical dissipation of finite volume solutions of compressible flow problems.' *AIAA Paper 88-0621*, AIAA 26th Aerospace Sciences Meeting.
- Dahlquist, G. (1963). 'A special stability problem for linear multistep methods.' *BIT*, **3**, 27-43.
- Harten, A., and Tal-Ezer, H. (1981). 'On a fourth order accurate implicit scheme for hyperbolic conservation laws.' *Mathematics of Computation*, **36**, 353.
- Hindman, R. G. (1981). 'Geometrically induced errors and their relationship to the form of the governing equations and the treatment of generalized mappings.' *AIAA Paper 81-1008, Proc. Fifth AIAA Computational Fluid Dynamics Conference*, pp. 113-25.
- Jameson, A. (1982). 'Transonic aerofoil calculations using the Euler equations. In P. L. Roe (ed.), *Numerical Methods in Aeronautical Fluid Dynamics*, New York: Academic Press.
- Jameson, A. (1983a). 'Solution of the Euler equations for two dimensional transonic flow by a multigrid method.' *Applied Math. and Computation*, **13**, 327-55.
- Jameson, A. (1983b). 'The evolution of computational methods in aerodynamics.' *Journal of Applied Mechanics*, **50**, 1052-70.

- Jameson, A. (1987). 'Successes and challenges in computational aerodynamics.' *AIAA Paper 87-1184, Proc. AIAA 8th Computational Fluid Dynamics Conference.*
- Jameson, A., and Baker, T. J. (1984). 'Multigrid solution of the Euler equations for aircraft configurations.' *AIAA Paper 84-0093, AIAA 22nd Aerospace Sciences Meeting.*
- Jameson, A., and Yoon S. (1986). 'Multigrid solution of the Euler equations using implicit schemes.' *AIAA Journal*, **24**, 1734–43.
- Jameson, A., Schmidt, W., and Turkel, E. (1981). 'Numerical simulation of the Euler equations by finite volume methods using Runge–Kutta time stepping schemes.' *AIAA Paper 81-1259, AIAA 5th Computational Fluid Dynamics Conference.*
- Kreatsoulas, J. C., Lee, D., Ballantyne, A., and Knight, C. J. (1988). 'Experimental/computational study of viscous flow in an accelerating, 90 degree rectangular duct.' *AIAA Paper 88-0186, AIAA 26th Aerospace Sciences Meeting.*
- Lerat, A. (1983). 'Implicit methods of second order accuracy for the Euler equations.' *AIAA Paper 83-1925, AIAA 6th Computational Fluid Dynamics Conference.*
- Lerat, A. (1985). 'Implicit methods of second order accuracy for the Euler equations.' *AIAA Journal*, **23**, 33–40.
- Lerat, A., Sides, J., and Daru, V. (1984). 'Efficient computation of steady and unsteady transonic flows by an implicit solver.' In W. G. Habashi (ed.), *Advances in Computational Transonics*, Pineridge Press.
- Pulliam, T. H. (1984). 'Euler and thin layer Navier–Stokes codes: ARC2D, ARC3D.' *Proc. Computational Fluid Dynamics User's Workshop*, The University of Tennessee Space Institute, Tullahoma, Tennessee.
- Pulliam, T. H. (1986). 'Artificial dissipation models for the Euler equations.' *AIAA Journal*, **24**, 1931–40.
- Pulliam, T. H., and Chaussee, D. S. (1981). 'A diagonal form of an implicit approximate factorization algorithm.' *Journal Computational Physics*, **39**, 347–63.
- Pulliam, T. H., and Steger, J. L. (1978). 'On implicit finite difference simulations of three dimensional flows.' *AIAA Paper 78-10, AIAA 16th Aerospace Sciences Meeting.*
- Pulliam, T. H., and Steger, J. L. (1980). 'Implicit finite difference simulations of three dimensional compressible flows.' *AIAA Journal*, **18**, 159–67.
- Pulliam, T. H., and Steger, J. L. (1985). 'Recent improvements in efficiency, accuracy and convergence for implicit approximate factorization algorithms.' *AIAA Paper 85-0360, AIAA 23rd Aerospace Sciences Meeting.*
- Rizzi, A. (1984). 'Spurious entropy production and very accurate solutions to the Euler equations.' *AIAA Paper 84-1644, AIAA 17th Fluid Dynamics, Plasma Dynamics and Lasers Conference.*
- Stanitz, J. D., Osborn, W. M., and Misizin, J. (1953). 'An experimental investigation of secondary flow in an accelerating rectangular elbow with 90° of turning.' *NACA TN-3015 Report.*
- Steger, J. L. (1978). 'Implicit finite difference simulation of flow about two-dimensional geometries.' *AIAA Journal*, **16**, 697–86.
- Swanson, R. C., and Turkel, E. (1987). 'Artificial dissipation and central difference schemes for the Euler and Navier–Stokes equations.' *AIAA Paper 87-1107, Proc. AIAA 8th Computational Fluid Dynamics Conference*, pp. 55–69.
- Volpe, G., Siclari, M. J., and Jameson, A. (1987). 'A new Euler method for fighter type configurations.' *AIAA Paper 87-1160, Proc. AIAA 8th Computational Fluid Dynamics Conference.*
- Warming, R. F., and Beam, R. M. (1978). 'On the construction and application of implicit factored schemes for computational fluid dynamics.' *SIAM-AMS Proc.*, **11**, 85–129.

PROBLEMS

Problem 18.1

Obtain equation (18.1.15) and deduce the stability conditions by applying the method described in Chapter 8, Section 8.6.3 of Volume 1.

Show that conditions (18.1.6) are necessary and sufficient for the Von Neumann stability.

Hint: Since (18.1.15) is a scalar equation, G is equal to its eigenvalue λ .

Write (18.1.15) as a polynomial $P(\lambda)$.

Define the associated polynomial $\bar{P}(\lambda)$:

$$\bar{P}(\lambda) = \xi\lambda^2 - [1 + 2\xi - I\sigma(\theta - 1)\sin\phi]\lambda + (1 + \xi - I\sigma\theta\sin\phi)$$

Obtain

$$P_1(\lambda) = (1 + 2\xi + \sigma^2\theta^2\sin^2\phi)\lambda + I\sigma(1 + 2\xi)\sin\phi - (1 + 2\xi) - \sigma^2\theta(\theta - 1)\sin^2\phi$$

The solution to $P_1(\lambda) = 0$ should satisfy $|\lambda| \leq 1$.

Problem 18.2

Obtain equation (18.1.20) for the equivalent differential equation of scheme (18.1.10) up to the terms in u_{xxxx} included.

Problem 18.3

Derive the expression (18.1.21) for the numerical group velocity of the Beam and Warming schemes (18.1.10), with $\xi = 0$.

Problem 18.4

Obtain the amplification factor (18.1.26) for the linearized form of equation (18.1.24).

Problem 18.5

Apply the method of Problem 18.1 to equation (18.1.24) containing the explicit fourth-derivative dissipation terms. Show that one obtains the condition (18.1.29) after having defined the stability condition from the solution of $P_1(\lambda) = 0$.

Hint: The solution of $P_1(\lambda) = 0$ can be written as

$$\lambda = 1 - \frac{X(\varepsilon_E, \phi) + \theta\sigma^2\sin^2\phi + I\sigma\sin\phi[1 + 2\xi - X(\varepsilon_E, \phi)\theta]}{1 + 2\xi + \theta^2\sigma^2\sin^2\phi}$$

where

$$X(\varepsilon_E, \phi) = 4\varepsilon_E(1 - \cos\phi)^2$$

Problem 18.6

Apply the method of Problem 18.1 to scheme (18.1.31) containing the explicit and the implicit dissipation terms. Show that one obtains the condition (18.1.35) after having defined the stability condition from the solution of $P_1(\lambda) = 0$.

Hint: The solution of $P_1(\lambda) = 0$ can be written as

$$\lambda = 1 - \frac{(1 + Y)X + \theta\sigma^2\sin^2\phi + I\sigma\theta\sin\phi[1 + 2\xi + Y - \theta X]}{(1 + Y)(1 + 2\xi + Y) + \theta^2\sigma^2\sin^2\phi}$$

where

$$X = X(\varepsilon_E, \phi) = 4\varepsilon_E(1 - \cos\phi)^2$$

$$Y = Y(\varepsilon_I, \phi) = 2\varepsilon_I(1 - \cos\phi)$$

Problem 18.7

Solve Burgers equation for the cases shown in Figure 18.1.1 with the Euler implicit scheme and reproduce the results shown in this figure. Experiment with different CFL numbers.

Problem 18.8

Repeat Problem 18.7 with the backward difference scheme $\theta = 1, \xi = \frac{1}{2}$.

Problem 18.9

Repeat Problem 18.7 with the trapezoidal scheme $\theta = \frac{1}{2}, \xi = 0$. Comment and explain the increased convergence difficulties.

Problem 18.10

Reproduce the results shown in Figure 18.1.5 by solving Burgers equation with the Beam and Warming scheme and explicit artificial viscosity of fourth order.

Problem 18.11

Repeat Problem 18.10 with the MacCormack–Baldwin artificial dissipation.

Problem 18.12

Solve the shock tube problem of Figure 18.1.8 with Beam and Warming's scheme (18.1.24).

Problem 18.13

Work out explicitly the discrete form of the two tridiagonal systems (18.2.7).

Problem 18.14

Write the explicit form of the diagonalized implicit schemes (18.2.11) and compare with (18.2.13). Comment on the difference in computational work between these two possibilities.

Problem 18.15

Apply the diagonal form (18.2.11) and (18.2.13) to the shock tube problem of Figure 18.1.8 and compare with the results of the non-diagonal algorithm.

Apply different dissipation models and compare their performance.

Problem 18.16

Consider a two-stage Runge–Kutta method, written as

$$\begin{aligned} U^{(0)} &= U^n \\ U^{(1)} &= U^n - \alpha_1 \Delta t R(U^n) \equiv U^n + \Delta U^{(1)} \\ U^{n+1} &= U^n - \Delta t R(U^{(1)}) \end{aligned}$$

where, in a two-dimensional case, R is a centrally discretized form of $(\partial_x f + \partial_y g)$, for instance, following equation (18.1.1) in a Cartesian mesh.

If $R(U^{(1)})$ is approximated by a Taylor expansion, with

$$R(U^{(1)}) = R(U^n) + \Delta t \left(\frac{\partial R}{\partial U} \right) \Delta U^{(1)}$$

show that for $\alpha_1 = \frac{1}{2}$ one obtains the Lax–Wendroff scheme in the linear case.

In the non-linear case, compare the present formulation with the distributive formulas applied to a Cartesian mesh, and show that they lead to the same non-linear variant of Lax–Wendroff.

Hint: Calculate $(\partial R / \partial U) \Delta U^{(1)}$:

$$\begin{aligned} \frac{\partial R}{\partial U} \Delta U^{(1)} &= (\partial_x A + \partial_y B) \Delta U^{(1)} \\ &= -\alpha_1 \Delta t (\partial_x A + \partial_y B) (\partial_x f + \partial_y g)^n \\ &= -\alpha_1 \Delta t (\partial_x A + \partial_y B) R^{(n)} \end{aligned}$$

Obtain the discretized form of

$$U^{n+1} = U^n - \Delta t [1 - \alpha_1 \Delta t (\partial_x A + \partial_y B)] R^{(n)}$$

Problem 18.17

Solve the nozzle problem of Figure 18.1.6 with the Jameson scheme and fourth-order Runge–Kutta time integration. Compare the convergence rates with and without residual averaging.

Chapter 19

The Treatment of Boundary Conditions

In the preceding chapters, no particular reference was made to the associated boundary conditions, although this is an essential aspect of the practical application of a scheme into a working code.

The reader who has attempted to apply any of the methods described in the previous sections to a flow in a finite domain, for instance a stationary, one-dimensional nozzle flow, is immediately faced with the problem of how to discretize the equations at the boundary points.

Since we deal with hyperbolic propagation-dominated systems, the following essential questions have to be answered:

- (1) How many conditions of physical origin are to be imposed at a given boundary?
- (2) How are the remaining variables to be defined at the boundaries?
- (3) How are these conditions to be formulated and discretized in order to be compatible with the order of accuracy and the stability conditions of the internal scheme?

We will first present an analysis of these questions, and of their answers, for one-dimensional Euler flows.

The outcome of the one-dimensional analysis is actually of direct application to multi-dimensional flows. Indeed, as seen in Section 16.5, the number and type of conditions at a boundary of a multi-dimensional domain are defined by the eigenvalue spectrum of the Jacobians associated with the normal to the boundary. This defines locally quasi-one-dimensional propagation properties. Therefore, we will give a detailed discussion of the one-dimensional boundary treatments for the Euler equations in Section 19.1, while the multi-dimensional aspects will be dealt with in Section 19.2.

Section 19.3 gives a brief mention of far-field boundary conditions, while Section 19.4 discusses the question of the Kutta condition with Euler calculations.

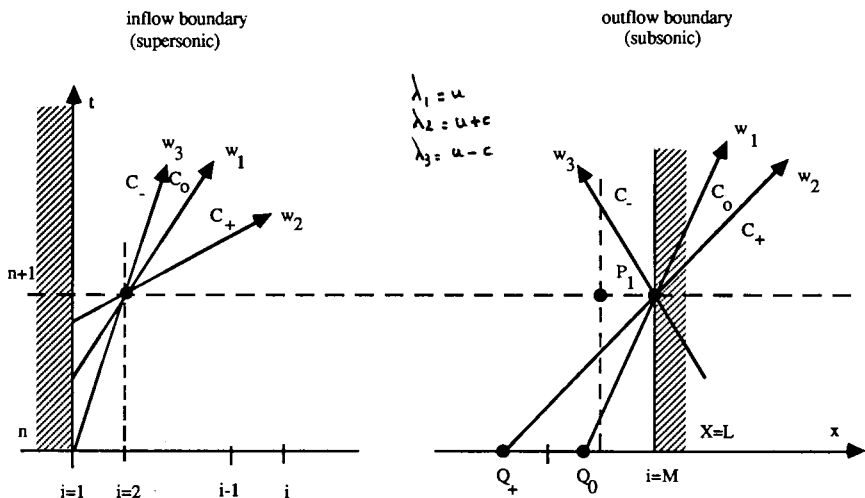


Figure 19.1.1 Boundary conditions for a supersonic inlet and subsonic outlet in a one-dimensional flow

19.1 ONE-DIMENSIONAL BOUNDARY TREATMENT FOR EULER EQUATIONS

If a one-dimensional flow problem has to be solved in a range $0 \leq x \leq L$, where $x = 0$ is the inflow boundary and $x = L$ the outflow boundary, the application of any scheme requires the knowledge of the flow variables at the points $x = 0$ and $x = L$. We will consider that the space interval $(0, L)$ is divided into $(M - 1)$ cells of length Δx , ranging from $i = 1$ at $x = 0$ to $i = M$ at $x = L$ (Figure 19.1.1).

For instance, writing the explicit Lax-Wendroff scheme at the point next to the inflow boundary, $i = 2$, leads to

$$U_2^{n+1} - U_2^n = -\frac{\tau}{2}(f_3 - f_1)^n + \frac{\tau^2}{2}[A_{3/2}(f_3 - f_2) - A_{1/2}(f_2 - f_1)]^n \quad (19.1.1)$$

where the right-hand side is taken at time level n . The values of the dependent variable vector U_1 at point $x = 0$ have to be determined in some way, since one cannot write equation (19.1.1) at $i = 1$ as this would require values of the flow variables at $i = -1$, which lies outside the computational domain.

If an explicit scheme is applied, the influence of the boundary values propagate numerically one space step at a time, that is a change in U_1 at time n will influence U_2 at time $(n + 1)$, U_3 at time $(n + 2)$ and so on.

On the other hand, an implicit scheme couples all the points at the same time level and a change in U_1 at time $n\Delta t$ influences all the U_i at the next time step, through the solution of the implicit (tridiagonal) system, if the boundary conditions are treated in an implicit way. This can best be seen on the following example of a Euler backward integration of the Beam and Warming scheme

($\theta = 1, \xi = 0$):

$$(1 + \tau \bar{\delta} A_i^n) \Delta U_i = -\tau \bar{\delta} f_i^n \quad (19.1.2)$$

Explicitly the system to solve at each time step is

$$\tau A_{i+1}^n \Delta U_{i+1} + 2\Delta U_i - \tau A_{i-1}^n \Delta U_{i-1} = -\tau (f_{i+1}^n - f_{i-1}^n) \quad (19.1.3)$$

At point $i = M - 1$, the equation becomes

$$\tau A_M^n \Delta U_M + 2\Delta U_{M-1} - \tau A_{M-2}^n \Delta U_{M-2} = -\tau (f_M^n - f_{M-2}^n) \quad (19.1.4)$$

and the way the information on ΔU_M is introduced will influence the solution algorithm and all the ΔU_i . Therefore, the influence of the implementation of the boundary conditions on the behaviour of the scheme may be considered as stronger with implicit methods as compared to explicit schemes.

If all the variables were known at a boundary from the knowledge of the physical input, there would be no difficulty in solving equation (19.1.1). However, this is generally not the case with hyperbolic equations.

The number of physical variables that can be imposed freely at a boundary is dependent on the propagation properties of the system and in particular on the information propagated from the boundary *towards the inside* of the flow region. See Section 16.4.4 for a discussion of these properties.

Since each characteristic direction can be considered as transporting a given information, expressed as a combination of conservative or primitive flow variables, the quantities transported from the inside of the domain towards the boundary will influence and modify the situation along this boundary.

Hence, only variables transported from the boundaries towards the interior can be freely imposed at the boundaries as *physical boundary conditions*. The remaining variables will depend on the computed flow situations and are therefore part of the solution. However, from a numerical point of view, in order to solve for U_2^{n+1} in equation (19.1.1), that is to compute the solution at the following time step, information about all the components of U_1^n is required in addition to the allowed physical conditions. This additional information, called *numerical boundary conditions*, has to be consistent with the physical properties of the flow, as well as compatible with the discretized equations.

The number of physical conditions has been defined in Section 16.4.4 as a function of the flow situation at the boundary (see Table 16.1). Since the total number of dependent variables is three in a one-dimensional flow (N in general), the number N_n of numerical boundary conditions to be added to the discretized system of equations is equal to

$$N_n = N - N_p \quad (19.1.5)$$

where N_p is the number of physical conditions.

19.1.1 Characteristic boundary conditions

The propagation properties in a one-dimensional flow are expressed in a straightforward way by the characteristic variables, or equivalently by the

Table 19.1. Physical and numerical boundary conditions for one-dimensional flows

	Subsonic	Supersonic
Inlet	Physical conditions: w_1, w_2	Physical conditions: w_1, w_2, w_3
	Numerical conditions: w_3	Numerical conditions: none
Outlet	Physical conditions: w_3	Physical conditions: none
	Numerical conditions: w_1, w_2	Numerical conditions: w_1, w_2, w_3

Riemann invariants. The form of the missing information is therefore defined by the variables associated with the outgoing characteristics (Figures 16.4.7 and 19.1.1).

Table 16.1 can now be completed with the requirements on the numerical boundary conditions, and this is presented in Table 19.1, referring to the notations of Section 16.4 for the characteristic variables W with components w_1, w_2, w_3 .

Hence, the number as well as the form of the missing information is theoretically known. For instance, at a subsonic outlet, one should impose the characteristic variable w_3 as the physical boundary condition and add, as numerical conditions, the characteristic equations for w_1 and w_2 discretized in a suitable way.

This forms the basis of the *characteristic boundary method*, which adds the Riemann invariants or the compatibility equations for the outgoing characteristics to the imposed physical boundary conditions, in order to obtain the missing equations for points $i = 1$ and $i = M$; see also Moretti (1981) for a general discussion and earlier references.

For instance, using the Riemann invariants one can apply the following relations at point P_1 of Figure 19.1.1, referring to equations (16.4.33):

$$\left(\frac{p}{\rho^\gamma}\right)_{P_1} = \left(\frac{p}{\rho^\gamma}\right)_{Q_0} \equiv w_1 \quad (19.1.6)$$

$$\left(u + \frac{2c}{\gamma - 1}\right)_{P_1} = \left(u + \frac{2c}{\gamma - 1}\right)_{Q_+} \equiv w_2 \quad (19.1.7)$$

$$\left(u - \frac{2c}{\gamma - 1}\right)_{P_1} \equiv w_3^{(P)} \quad (19.1.8)$$

where the variables at points Q_+ and Q_0 are known, as can be seen from Figure 19.1.1. The quantity $w_3^{(P)}$ is the imposed physical boundary condition. The system of these three equations determines all the quantities in point P_1 and define the vector U_i^{n+1} at $i = M$.

19.1.2 Compatibility relations

An alternative to the characteristic method is to apply the compatibility relations in differential form, discretizing them in an appropriate manner.

For a quasi-one-dimensional nozzle flow of area S , this would lead to the following equations (see equations (16.4.17)) at the subsonic outlet point P_1 of Figure 19.1.1, assuming $u > 0$:

$$\left(\frac{\partial \rho}{\partial t} - \frac{1}{c^2} \frac{\partial p}{\partial t}\right) + u \left(\frac{\partial \rho}{\partial x} - \frac{1}{c^2} \frac{\partial p}{\partial x}\right) = 0 \quad (19.1.9)$$

$$\left(\frac{\partial u}{\partial t} + \frac{1}{\rho c} \frac{\partial p}{\partial t}\right) + (u + c) \left(\frac{\partial u}{\partial x} + \frac{1}{\rho c} \frac{\partial p}{\partial x}\right) = -\frac{uc}{S} \frac{dS}{dx} \quad (19.1.10)$$

$$B(u, \rho, p) = 0 \quad (19.1.11)$$

where $B(u, \rho, p) = 0$ is the imposed physical boundary condition.

These equations have to be discretized at point P_1 , $i = M$, by using only interior information, that is one has to apply one-sided differencing only. An example of this approach can be found in Steger *et al.* (1980).

This is fully compatible with the mathematical analysis of boundary conditions and of the well-posedness of an initial boundary value problem, as analysed by Kreiss (1968, 1970). Indeed, the scalar hyperbolic equation $u_t + au_x = 0$ is well posed in the sense of Kreiss, that is the boundary conditions are not over- or underspecified and the solution depends continuously on the initial and boundary data if a boundary condition is imposed at $x = 0$ when $a > 0$ and at $x = L$ when $a < 0$.

In addition, the same condition corresponds also to the stability requirements of the upwind differencing. Indeed, as seen in Chapter 10 in Volume 1, the upwind scheme applied at $i = M$:

$$u_M^{n+1} = u_M^n - \sigma(u_M^n - u_{M-1}^n) \quad (19.1.12)$$

is stable for $a > 0$ and $\sigma < 1$ but unstable for $a < 0$, as is easily seen from the Von Neumann amplification factor $G = 1 - \sigma + \sigma e^{-i\phi}$.

Since the numerical conditions (19.1.9) and (19.1.10) correspond precisely to the characteristics with positive speeds of propagation, they will be stable under an upwind differencing. On the other hand, the physical boundary condition replaces the negative characteristic which would have been unstable under a backward discretization.

This consistency and harmony between the physical, mathematical and numerical properties is, of course, to be expected but is nevertheless worth mentioning.

The above considerations do not resolve, by far, all the problems connected with the implementation of the boundary conditions. If the characteristic boundary method is the most rigorous one from a physical point of view, various other ways of expressing the information corresponding to the outgoing characteristics can be defined. These are known as *extrapolation* techniques and will be discussed in the following sections. Other forms for the physical boundary conditions can also be defined, such as the *non-reflecting* boundary conditions, which are a particular formulation of the characteristic equations (Engquist and Majda, 1977, 1979; Hedstrom, 1979).

In addition, the Euler equations are generally solved in conservative form, and the physical boundary conditions on the characteristics have to be expressed as a function of the conservative variables. On the other hand, the physical boundary conditions are derived in many cases from experimental set-ups and are given in terms of measurable quantities such as the primitive variables ρ , u , p . For instance, the flow conditions in a nozzle are dominated for fixed inlet conditions by the downstream value of the pressure.

Various combinations of primitive or conservative variables have therefore to be selected as physical boundary conditions, raising several questions:

- (1) Which combinations of primitive (or conservative) variables may be applied as physical boundary conditions, in order to reconstruct the information contained in the incoming and outgoing characteristics? If this is not possible, the selected combination leads to an ill-posed problem. This will be investigated in Section 19.1.3.
- (2) What is the interrelation between physical boundary conditions at inlet and at outlet? Is any combination of non-characteristic variables equally valid in defining a well-posed problem with a unique solution? Wornom and Hafez (1984) have pointed out that certain combinations are to be excluded and this will also be discussed in Section 19.1.3.
- (3) What is the influence of the boundary treatment on the stability and accuracy of the basic scheme, also called the *interior scheme*? This is a crucial topic, since stable interior schemes can be strongly affected by unadapted boundary treatments, leading to possible instability of the complete scheme or to the reduction of unconditional to conditional stability. The theoretical analysis of the influence of boundary schemes on stability and accuracy is a difficult task and some results are available for simple problems which will be mentioned in Section 19.1.4.

Most of the research work in the field of the analysis of boundary schemes for initial boundary value problems is of a mathematical and theoretical nature. We refer the interested reader to the important contributions of Kreiss (1968, 1970, 1974); Osher (1969a, 1969b); Gustafsson *et al.* (1972); Gustafsson and Kreiss (1979); Trefethen (1983, 1984, 1985); and to the more complete references listed in these publications and in the review of Higdon (1986).

The non-mathematical-oriented reader will find much benefit in consulting the publications by Yee (1981), Yee *et al.* (1982), Beam *et al.* (1981) and Warming *et al.* (1983), which summarize the state of the art oriented towards the applied numerical scientists and focusing on the applications to the system of Euler equations.

19.1.3 Characteristic boundary conditions as a function of conservative and primitive variables

The problem will be well posed if the full information on the ingoing and outgoing characteristics can be recovered from the imposed combinations of

conservative or primitive variables. Since the transformation matrices between the characteristic W , primitive V and conservative variables U are known, it is not difficult to investigate the conditions under which an imposed combination of variables leads to a well-posed problem.

The following transformation matrices between the variables W, V and U have been defined in Section 16.4, for arbitrary variations Δ :

$$\Delta W = L^{-1} \Delta V \tag{19.1.13}$$

$$\Delta W = L^{-1} M^{-1} \Delta U \equiv P^{-1} \cdot \Delta U \tag{19.1.14}$$

The matrices L^{-1} and P^{-1} are given in their one-dimensional form by equations (16.4.9) and (16.4.11). The three set of variables are

$$\Delta W = \begin{pmatrix} \Delta \rho - \frac{1}{c^2} \Delta p \\ \Delta u + \frac{1}{\rho c} \Delta p \\ \Delta u - \frac{1}{\rho c} \Delta p \end{pmatrix} \equiv \begin{pmatrix} \Delta w_1 \\ \Delta w_2 \\ \Delta w_3 \end{pmatrix} \quad U = \begin{pmatrix} \rho \\ \rho u \\ \rho E \end{pmatrix} \quad V = \begin{pmatrix} \rho \\ u \\ p \end{pmatrix} \tag{19.1.15}$$

The well-posedness analysis has to be performed on the linearized equations whereby the coefficients of the matrices L^{-1} and P^{-1} are considered as constants, equal to their value on the boundaries. Consequently, the variations Δ are small perturbations around the local boundary values, which will be indicated by a subscript 0.

The analysis procedure can be systematized as follows (Yee, 1981). If the transformation matrix, say between W and V , is reordered such that the imposed set of physical boundary conditions is separated from the remaining variables, the information along the characteristics corresponding to the numerical boundary condition must allow these remaining variables to be defined. Referring to Figure 19.1.1 and the subsonic outlet point P_1 , one physical boundary condition is allowed, say pressure p . The transformation relation (19.1.13) is written with the 'physical' characteristic w_3 on top (see Table 19.1):

$$\Delta W \equiv \begin{pmatrix} \Delta w_3 \\ \Delta w_1 \\ \Delta w_2 \end{pmatrix} = \begin{pmatrix} -1 & 0 & 1 \\ \frac{1}{\rho c} & 1 & 0 \\ \frac{1}{\rho c} & 0 & 1 \end{pmatrix}_0 \cdot \begin{pmatrix} \Delta p \\ \Delta \rho \\ \Delta u \end{pmatrix} \tag{19.1.16}$$

The numerical conditions, obtained from (19.1.16),

$$\Delta w_1 = \frac{-\Delta p}{c_0^2} + \Delta \rho \tag{19.1.17}$$

$$\Delta w_2 = \frac{\Delta p}{\rho_0 c_0} + \Delta u \quad (19.1.18)$$

can clearly be solved for the remaining variables ρ and u at the boundary, since p is known.

Formally writing ΔW^P for the characteristics corresponding to the physical boundary conditions and ΔW^N for the remaining characteristics defining the numerical information from the interior towards the boundaries, equation (19.1.16) is formalized as follows:

$$\Delta W = \begin{vmatrix} \Delta W^P \\ \Delta W^N \end{vmatrix} = \begin{vmatrix} (L^{-1})_I^P & (L^{-1})_{II}^P \\ (L^{-1})_I^N & (L^{-1})_{II}^N \end{vmatrix} \begin{vmatrix} \Delta V^I \\ \Delta V^{II} \end{vmatrix} \quad (19.1.19)$$

The group of variables V^I represents the *imposed* physical conditions while the group V^{II} represents the *free* variables to be defined by the numerical or internal information. The transformation matrix L^{-1} is subdivided into the appropriate submatrices. In the case of equation (19.1.16) one has $W^P = w_3$:

$$W^N = \begin{vmatrix} w_1 \\ w_2 \end{vmatrix} \quad V^I = p \quad V^{II} = \begin{vmatrix} \rho \\ u \end{vmatrix} \quad (19.1.20)$$

and

$$(L^{-1})_I^P = \frac{-1}{\rho c} \quad (L^{-1})_{II}^P = (0, 1) \quad (19.1.21)$$

$$(L^{-1})_I^N = \begin{vmatrix} -1 \\ c^2 \\ 1 \\ \rho c \end{vmatrix} \quad (L^{-1})_{II}^N = \begin{vmatrix} 1 & 0 \\ 0 & 1 \end{vmatrix} \quad (19.1.22)$$

The condition for well-posedness is that V^{II} can be recovered from the information carried by the characteristics W^N which intersect the boundary from the interior of the flow domain. Writing

$$\Delta W^N = (L^{-1})_I^N \Delta V^I + (L^{-1})_{II}^N \Delta V^{II} \quad (19.1.23)$$

the free variables V^{II} are defined by

$$\Delta V^{II} = \frac{1}{(L^{-1})_{II}^N} [\Delta W^N - (L^{-1})_I^N \Delta V^I] \quad (19.1.24)$$

Hence, the condition for well-posedness is that the matrix $(L^{-1})_{II}^N$ is non-singular, that is the condition of non-zero determinant

$$\det |(L^{-1})_{II}^N| \neq 0 \quad (19.1.25)$$

has to be satisfied. This can be applied for the various combinations of primitive variables at inlet and at outlet.

At a subsonic outlet, equation (19.1.16) shows that any of three variables ρ , u , p can be chosen as a physical boundary condition, since none of the submatrices defining W^N is zero.

Subsonic inlet

At a subsonic inlet, W^P is formed by w_1 and w_2 , while $W^N = w_3$ and one has

$$\Delta \begin{vmatrix} W^P \\ W^N \end{vmatrix} = \begin{vmatrix} 1 & 0 & \frac{-1}{c^2} \\ 0 & 1 & \frac{1}{\rho c} \\ 0 & 1 & \frac{-1}{\rho c} \end{vmatrix}_0 \cdot \Delta \begin{vmatrix} \rho \\ u \\ p \end{vmatrix} \quad (19.1.26)$$

Since one of the elements of the submatrix defining W^N (0 1 $-1/\rho c$) is zero, namely the element corresponding to the density ρ , the choice (u, p) as a physical boundary condition is not well posed. Indeed, since

$$\Delta W^N = \Delta u - \frac{1}{(\rho c)_0} \Delta p \quad (19.1.27)$$

one cannot define $\Delta \rho$ at the boundary from the information on ΔW^N . For any other combination involving ρ as a physical condition, equation (19.1.27) will allow the determination of the remaining free variable.

The same considerations can be applied to the conservative variables U and the matrix P^{-1} instead of L^{-1} . Examining matrix P^{-1} (equation (16.4.11)), it is seen that there are no zero elements and hence any possible combination of variables as physical boundary conditions will be well-posed.

This analysis can also be extended to other combination of variables, say X , by setting up the transformation matrix $\Delta W = K \cdot \Delta X$ and investigating the submatrices of K (see Problems 19.1 and 19.2).

At supersonic boundaries, either all or none of the variables have to be imposed and the problem is always well posed.

The above-described procedure defines the allowable combinations of variables at a given boundary without relation to the selection of variables at the other boundary. This question applies only to flow situations that are subsonic at both boundaries and is actually not a trivial question, since it has been observed (Wornom and Hafez, 1984) that certain combinations can give rise to non-unique steady-state solutions.

Wornom and Hafez show that the steady-state subsonic nozzle flow with equal inlet and outlet areas leads to non-unique solutions if the same variable is specified at outlet and at inlet.

This is easily shown from the stationary conservation laws, the subscripts 0 and 1 referring to the two end-points $x = 0$ and $x = L$:

$$(\rho u S)_0 = (\rho u S)_1 \quad (19.1.28)$$

$$H = \left(\frac{\gamma}{\gamma - 1} \frac{p}{\rho} + \frac{u^2}{2} \right)_0 = \left(\frac{\gamma}{\gamma - 1} \frac{p}{\rho} + \frac{u^2}{2} \right)_1 \quad (19.1.29)$$

$$\left(\frac{p}{\rho^\gamma}\right)_0 = \left(\frac{p}{\rho^\gamma}\right)_1 \quad (19.1.30)$$

If ρ and p are imposed at inlet and p at outlet, that is ρ_0 , p_0 and p_1 are fixed, the other variables have to be defined from

$$\rho_1^\gamma = \rho_0^\gamma \frac{p_1}{p_0} \quad (19.1.31)$$

$$u_1^2 \left(\frac{\rho_1 S_1}{\rho_0 S_0} - 1 \right) = \frac{2\gamma}{\gamma - 1} \left(\frac{p_1}{\rho_1} - \frac{p_0}{\rho_0} \right) \quad (19.1.32)$$

If the imposed boundary conditions are such that $p_1 = p_0$, corresponding to a subsonic inviscid flow without shocks, then $\rho_1 = \rho_0$ and the right-hand side of equation (19.1.32) vanishes. Hence, the coefficient of u_1^2 has also to be zero in order for a flow to exist. This leaves u_1 undetermined and so the problem is not well posed. Hence, the computed distribution of flow variables will depend on the initial conditions. Therefore, when the flow conditions are identical at the two boundaries, one should not apply the same variable twice as the boundary condition.

Summarizing, all combinations of conservative and primitive variables can be selected as physical boundary conditions, with the exception of the pair (u, p) at a subsonic inlet, if one has to determine the missing information from the characteristic variables. In this case, the imposed conditions should contain the density; for instance, (ρ, p) or (ρ, u) are well-posed boundary conditions.

Note, however, that this restriction does not apply with other boundary treatments where the characteristic variables are explicitly determined at the boundaries.

In the particular case of identical subsonic inflow and outflow situations, the outlet boundary condition should contain the third variable, that is u_1 has to be associated with (p_0, ρ_0) or p_1 has to be coupled to (u_0, ρ_0) . This restriction is, however, not necessary when the inlet and outlet flow conditions are different.

19.1.4 Extrapolation methods

Next to the direct application of the characteristic and compatibility relations, many other methods can be applied in order to implement numerical boundary conditions.

Various forms are listed below as a sample of the most popular methods, although many other approaches can be defined. They are based on extrapolations of the internal variables towards the boundary.

The listed formulas are at most of first order, which is generally sufficient for second-order schemes, but quadratic extrapolation formulas can be used as well.

The following methods can be applied to any set of variables—conservative, primitive or characteristic—at an inlet or an outlet boundary. In order to stress this fact, we will use the variable X to represent either U, V, W or any other

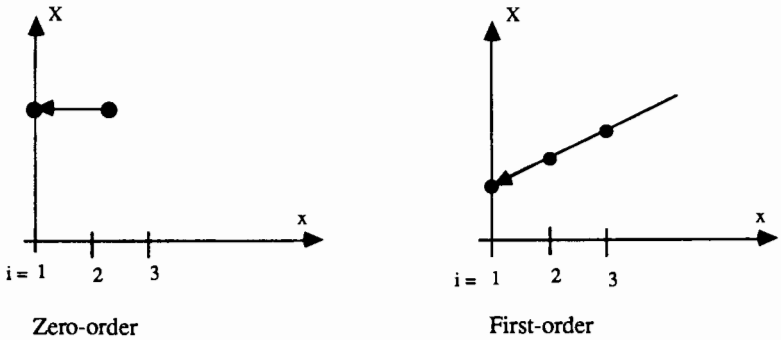


Figure 19.1.2 Illustration of various forms of variable extrapolation. Space extrapolation of variable X at fixed time

combination, and write the conditions for an outlet boundary $i = M$. The transposition to inlet conditions is straightforward, replacing $i = M$ by $i = 1$, $i = (M - 1)$ by $i = 2$ and so on (Figures 19.1.2 to 19.1.4).

A. Space extrapolation

Zero-order extrapolation

$$X_M^{n+1} = X_{M-1}^{n+1} \quad (19.1.33)$$

or

$$\Delta X_M = \Delta X_{M-1} \quad (19.1.34)$$

where

$$\Delta X = X^{n+1} - X^n \equiv \Delta X^n \quad (19.1.35)$$

First-order extrapolation

$$X_M^{n+1} = 2X_{M-1}^{n+1} - X_{M-2}^{n+1} \quad (19.1.36)$$

or

$$\Delta X_M^n = 2\Delta X_{M-1}^n - \Delta X_{M-2}^n \quad (19.1.37)$$

B. Space-time extrapolation

Zero order

$$X_M^{n+1} = X_{M-1}^n \quad (19.1.38)$$

or

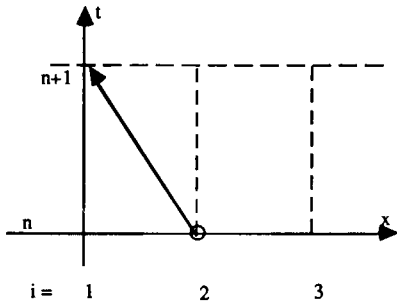
$$\Delta X_M^n = \Delta X_{M-1}^{n-1} \quad (19.1.39)$$

First order space/zero order in time

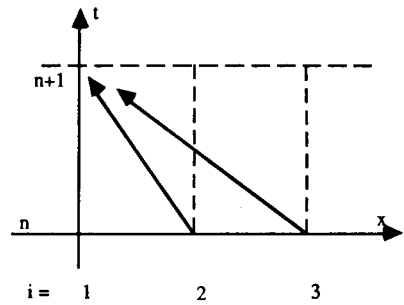
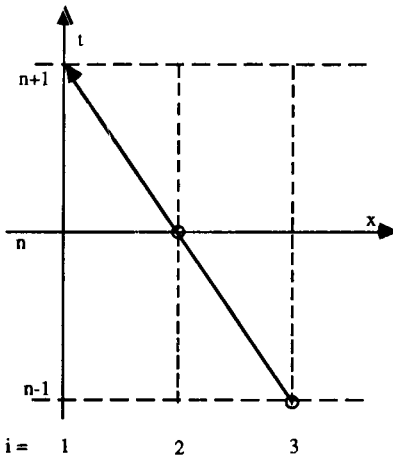
$$X_M^{n+1} = 2X_{M-1}^n - X_{M-2}^n \quad (19.1.40)$$

or

$$\Delta X_M^n = 2\Delta X_{M-1}^{n-1} - \Delta X_{M-2}^{n-1} \quad (19.1.41)$$



Zero order

First order in space / zero
order in time

First order in space / first order in time

Figure 19.1.3 Illustration of various forms of variable extrapolation. Space-time extrapolation

First order in space and time

$$X_M^{n+1} = 2X_{M-1}^n - X_{M-2}^{n-1} \quad (19.1.42)$$

or

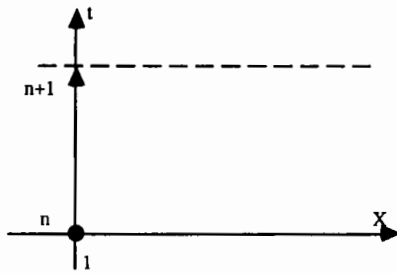
$$\Delta X_M^n = 2\Delta X_{M-1}^{n-1} - \Delta X_{M-2}^{n-2} \quad (19.1.43)$$

*C. Time extrapolation**Zero order*

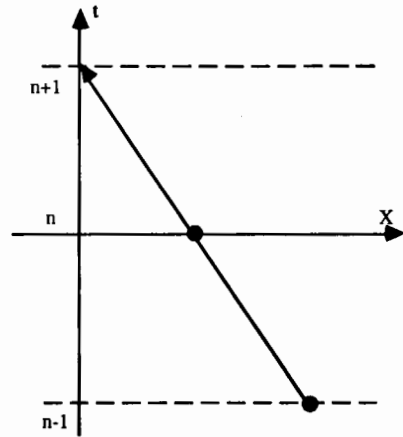
$$X_M^{n+1} = X_M^n \quad (19.1.44)$$

or

$$\Delta X_M^n = 0 \quad (19.1.45)$$



Zero order



First order

Figure 19.1.4 Illustration of various forms of variable extrapolation. Time extrapolation of variable X at fixed position

First order

$$X_M^{n+1} = 2X_M^n - X_M^{n-1} \quad (19.1.46)$$

or

$$\Delta X_M^n = \Delta X_M^{n-1} \quad (19.1.47)$$

Note that Figure 19.1.3 is a representation in the space-time plane $x-t$, while Figures 19.1.2 and 19.1.4 are representations of the variable X as a function of space or time.

The space-extrapolation techniques can be considered either as an explicit or as an implicit treatment of the numerical boundary conditions and are adapted to explicit and implicit schemes. On the other hand, the space-time extrapolations are explicit in nature, while the pure time extrapolations are well adapted to implicit (tridiagonal) schemes in Δ form.

The extrapolation techniques are discussed in some detail by Griffin and Anderson (1977) and by Gottlieb and Turkel (1978) for applications to the two-step Lax-Wendroff type of schemes, such as the Richtmyer or MacCormack schemes. They show, for instance, that the space-extrapolation methods do not destabilize these schemes nor reduce the stability limits.

With regard to accuracy, an important theorem by Gustafsson (1975) proves that, for linear equations, the boundary scheme can be one order lower than the interior scheme without reducing the global order of accuracy of the complete scheme. Hence, the zero-order space-accurate boundary schemes will reduce the overall accuracy of second-order schemes, while this will not be the case for the first-order boundary scheme.

With regard to implicit methods, the available results can be summarized, following Yee *et al.* (1982), as follows:

- (1) All A -stable interior schemes remain unconditionally stable with the implicit space extrapolation.
- (2) Coupled to space-time extrapolations, the implicit schemes will tend to lose their unconditional stability. An interesting example is given in the above-mentioned reference of the implicit Euler scheme ($\theta = 1$, $\xi = 0$), which is unconditionally stable for an odd number of mesh points but becomes conditionally stable for an even number of mesh points.
- (3) Generally, when coupled to other implicit boundary schemes, the interior implicit A -stable schemes remain unconditionally stable, while they reduce to conditional stability when coupled with explicit boundary schemes.

These results are based on linearized theory, but have been generally confirmed by numerical tests on non-linear equations such as Burgers equation and the Euler equations. We note also here that the unconditional stability referred to is to be interpreted as allowing very large CFL values to be applied for steady-state computations. We refer the reader to the cited references for more precise mathematical definitions of the stability criteria.

Another approach

Another family of numerical boundary conditions consists in discretizing the equations at the boundary points in a one-sided manner and adding this equation to the interior scheme. For instance, considering equation (19.1.1) for the Lax-Wendroff scheme, one could add a first-order appropriate upwind equation for U_1 (see the next chapter for more details on the upwind formulation with mixed sign eigenvalues) and provide in this way the missing information.

19.1.5 Practical implementation methods for numerical boundary conditions

Since the various forms for the numerical boundary conditions can be applied to any of the variables, a large number of non-equivalent formulations can be defined. For instance, a space-extrapolation method can be applied to the conservative variables, as, for instance, Lerat *et al.* (1984), or to the characteristic variables, following Yee *et al.* (1982), or to the primitive variables, or to any other combination of variables. In addition, various forms of extrapolation can be used for any of the above choice of variables. Due to the non-linearity of the flow equations, these choices are not equivalent and lead to different boundary treatments.

As another alternative, one can discretize directly the compatibility equations associated with the outgoing characteristics, or add to the internal scheme a one-sided discretization of the conservation equations or of the non-conservative form of the equations, coupled at the boundary with the physical conditions.

We will describe in this section a few of the methods that can be applied, since it is not possible to cover all the possibilities. We encourage the reader to experiment with as many methods as possible, since the numerical treatment of the boundary conditions is an essential aspect of a numerical simulation.

Characteristic extrapolation method

The transformation between the different set of variables follows the framework described in Section 19.1.2, and we will illustrate it on the example of a space extrapolation on the characteristic variables with a scheme based on the conservative variables and boundary conditions imposed on the primitive variables. This is the method adapted by Yee *et al.* (1982) and is an alternative to the one-sided discretization of the compatibility equations corresponding to the outgoing characteristics.

Referring to equation (19.1.24), the numerical characteristic variables ΔW^N are defined by an extrapolation, say equation (19.1.37), where Δ represents a time increment:

$$\Delta W^N|_M = 2\Delta W^N|_{M-1} - \Delta W^N|_{M-2} \tag{19.1.48}$$

The values at $i = (M - 1)$ and $i = (M - 2)$ are obtained from the primitive variables by an explicit evaluation following equation (19.1.23):

$$\Delta V_i^N = (L_i^{-1})_i^N \cdot \Delta V_i^I + (L_i^{-1})_{ii}^N \cdot \Delta V_i^{II} \quad \text{for } i = M - 1, M - 2 \tag{19.1.49}$$

where the matrix elements are evaluated at time level n . Equation (19.1.24) then gives

$$\Delta V_M^{II} = \frac{1}{(L_M^{-1})_{ii}^N} \Delta W_M^N \tag{19.1.50}$$

where $\Delta V_M^I = 0$ has been introduced since this indicates that the variables V_M^I are fixed by the physical boundary conditions. In a time-dependent problem ΔV_M^I will not be zero and determined by the imposed time variation.

Finally, the free variables V_M^{II} are transformed to the conservative variables by application of the matrix M , evaluated at time level n :

$$\Delta U_M = M_M \begin{vmatrix} \Delta V^I \\ \Delta V_M^{II} \end{vmatrix} = M_M \begin{vmatrix} 0 \\ \Delta V_M^{II} \end{vmatrix} \tag{19.1.51}$$

Subsonic outflow boundary, outflow pressure imposed

Referring to Figure 19.1.1 and equations (19.1.16) to (19.1.22), which define the different submatrices, we have for ΔW^N at points $i = M - 1$ and $M - 2$, following equation (19.1.49),

$$\Delta W_i^N \equiv \Delta \begin{vmatrix} w_1 \\ w_2 \end{vmatrix}_i = \begin{vmatrix} -1 \\ c^2 \\ 1 \\ \rho c \end{vmatrix}_i \Delta p_i + \begin{vmatrix} 1 & 0 \\ 0 & 1 \end{vmatrix}_i \Delta \begin{vmatrix} \rho \\ u \end{vmatrix}_i \tag{19.1.52}$$

and

$$\Delta W_M^N = 2 \begin{vmatrix} \frac{-\Delta p}{c^2} + \Delta \rho \\ \frac{\Delta p}{\rho c} + \Delta u \end{vmatrix}_{M-1} - \begin{vmatrix} \frac{-\Delta p}{c^2} + \Delta \rho \\ \frac{\Delta p}{\rho c} + \Delta u \end{vmatrix}_{M-2} = \begin{vmatrix} \Delta w_1 \\ \Delta w_2 \end{vmatrix}_M \quad (19.1.53)$$

The primitive free variables ΔV_M^{II} are obtained from equation (19.1.50) with

$$\frac{1}{(L_M^{-1})_{\text{II}}^M} = \begin{vmatrix} 1 & 0 \\ 0 & 1 \end{vmatrix} \quad (19.1.54)$$

$$\Delta V_M^{\text{II}} = \begin{vmatrix} \Delta \rho \\ \Delta u \end{vmatrix}_M = \begin{vmatrix} 1 & 0 \\ 0 & 1 \end{vmatrix} \begin{vmatrix} \Delta w_1 \\ \Delta w_2 \end{vmatrix}_M \quad (19.1.55)$$

and the corresponding conservative variables are obtained from equation (19.1.51):

$$\Delta U_M = M \begin{vmatrix} \Delta \rho \\ \Delta u \\ 0 \end{vmatrix}_M = \begin{vmatrix} 1 & 0 & 0 \\ u & \rho & 0 \\ \frac{u^2}{2} & \rho u & \frac{1}{\gamma-1} \end{vmatrix}_M \begin{vmatrix} \Delta w_1 \\ \Delta w_2 \\ 0 \end{vmatrix}_M = \begin{vmatrix} \Delta \rho \\ \Delta(\rho u) \\ \Delta(\rho E) \end{vmatrix}_M \quad (19.1.56)$$

where the coefficients of the matrix M are evaluated at time level n . One finally obtains the equation, for instance for $\Delta \rho$,

$$\Delta \rho_M + \left(\frac{2\Delta p}{c^2} \right)_{M-1} - 2 \cdot \Delta \rho_{M-1} - \left(\frac{\Delta p}{c^2} \right)_{M-2} + \Delta \rho_{M-2} = 0 \quad (19.1.57)$$

which has to be added to the interior scheme equations written up to the point $M-1$.

Equation (19.1.56) can be considered as an explicit or an implicit boundary scheme. For an implicit interior scheme with a tridiagonal matrix structure such as equations (19.1.3) and (19.1.4), the above equation (19.1.57) and the two others for $\Delta(\rho u)_M$ and $\Delta(\rho E)_M$ provide the additional equations needed for ΔU_M .

An alternative consists in the elimination of ΔU_M in equation (19.1.4) by introducing equation (19.1.56) without adding additional equations. One should take care to maintain the block tridiagonal structure of the systems. Indeed, this structure might be lost for some combinations when equations of the form (19.1.57) are added as additional equations.

Example 19.1.1 MacCormack scheme with time extrapolation of characteristic variables

Consider the original explicit MacCormack scheme under the form (17.2.31)

with the source term Q :

$$\begin{aligned}\overline{\Delta U}_i &= -\tau(f_{i+1}^n - f_i^n) + \Delta t Q_i^n \\ \overline{\overline{\Delta U}}_i &= \tau(\overline{f}_i - \overline{f}_{i-1}) + \Delta t \overline{Q}_i \\ \Delta U_i^n &= \frac{1}{2}(\overline{\Delta U}_i + \overline{\overline{\Delta U}}_i)\end{aligned}\quad (\text{E19.1.1})$$

Boundary conditions are required for each step separately which have to be compatible with the conditions on the global scheme.

The first equation of (E19.1.1) defines the predictor boundary values at the inlet $\overline{\Delta U}_1$ and the second equation can be used to obtain a corrector boundary value at the outlet $\overline{\overline{\Delta U}}_M$, since the forward predictor step defines ΔU_1 from the variables in point $i = 2$ and similarly for the backward corrector at outlet.

In order to obtain global boundary values a predictor boundary correction at the outlet $\overline{\overline{\Delta U}}_M$ and a corrector boundary correction at the inlet $\overline{\overline{\Delta U}}_1$ are required. Characteristic information at the boundaries together with the physically imposed boundary conditions are applied to calculate $\overline{\overline{\Delta U}}_1$ and $\overline{\overline{\Delta U}}_M$.

(a) Inlet boundary correction $\overline{\overline{\Delta U}}_1$

(i) Subsonic inlet

At a subsonic inlet, we select density and pressure as the physical boundary conditions and the velocity u is to be defined numerically. With

$$\begin{aligned}\rho &= \rho^* && \text{physical boundary condition} \\ p &= p^* && \text{physical boundary condition} \\ u &= u^{\text{num}} && \text{numerical boundary condition}\end{aligned}$$

the characteristic variables at the inlet at the corrector step are defined as follows:

$$\overline{\overline{\Delta w}}_1 = \overline{\overline{\Delta \rho}} - \frac{1}{c^2} \overline{\overline{\Delta p}} \quad (\text{E19.1.2a})$$

$$\overline{\overline{\Delta w}}_2 = \Delta u^{\text{num}} + \frac{1}{\rho c} \overline{\overline{\Delta p}} \quad (\text{E19.1.2b})$$

$$\overline{\overline{\Delta w}}_3 = \Delta w_3^{\text{num}} = \Delta u^{\text{num}} - \frac{1}{\rho c} \overline{\overline{\Delta p}} \quad (\text{E19.1.2c})$$

The boundary corrections $\overline{\overline{\Delta V}}$ for the corresponding primitive variables V will be consistent if the updating step

$$V^{n+1} = V^n + \frac{1}{2}(\overline{\overline{\Delta V}} + \overline{\overline{\Delta V}}) \quad (\text{E19.1.3})$$

maintains the constancy of the imposed variables ρ^* and p^* ; that is at a subsonic inlet, the corrector boundary values are related to the imposed variables and

to the calculated predictors at inlet by

$$\overline{\overline{\Delta\rho}} = 2(\rho^* - \rho^n) - \overline{\Delta\rho} \quad (\text{E19.1.4a})$$

$$\overline{\overline{\Delta p}} = 2(p^* - p^n) - \overline{\Delta p} \quad (\text{E19.1.4b})$$

The velocity Δu_1^{num} is calculated from (E19.1.2c) by the time extrapolation

$$\Delta w_3^{\text{num}} = \overline{\Delta w_3} \quad \text{or} \quad \Delta w_3^{\text{num}} = 0 \quad (\text{E19.1.5})$$

leading to

$$\overline{\overline{\Delta u}} = \Delta u^{\text{num}} = \frac{-1}{\rho c} \overline{\overline{\Delta p}} + \Delta w_3^{\text{num}} \quad (\text{E19.1.6})$$

These corrections are easily transformed into conservative corrections $\overline{\overline{\Delta U_1}}$.

Note that generally the initial solution will satisfy the physical boundary conditions and in this case the first terms in equations (E19.1.4) will be zero, that is $\rho^n = \rho^*$ and $p^n = p^*$ leading to $\overline{\overline{\Delta\rho}} = -\overline{\Delta\rho}$ and $\overline{\overline{\Delta p}} = -\overline{\Delta p}$.

(ii) *Supersonic inlet*

All three variables are imposed and the boundary corrections can be written directly in terms of conservative variables U :

$$\overline{\overline{\Delta U_1}} = 2(U_1^* - U_1^n) - \overline{\Delta U_1} \quad (\text{E19.1.7})$$

where U_1^* is obtained by transforming the physical imposed primitive variables to conservative variables.

(b) *Outlet boundary correction $\overline{\overline{\Delta U_M}}$*

(i) *Subsonic outlet*

At a subsonic exit, where the pressure is imposed the characteristic predictor values are defined by

$$\overline{\Delta w_1} = \Delta \rho^{\text{num}} - \frac{1}{c^2} \overline{\Delta p} \quad (\text{E19.1.8a})$$

$$\overline{\Delta w_2} = \Delta u^{\text{num}} + \frac{1}{\rho c} \overline{\Delta p} \quad (\text{E19.1.8b})$$

$$\overline{\Delta w_3} = \Delta u^{\text{num}} - \frac{1}{\rho c} \overline{\Delta p} \quad (\text{E19.1.8c})$$

with

$$\overline{\Delta p} = p^* - p^n \quad (\text{E19.1.9})$$

The variables $\Delta \rho^{\text{num}}$ and Δu^{num} are calculated from (E19.1.8a) and (E19.1.8b) respectively using a zero-order or first-order extrapolation in time for the corrections $\overline{\Delta w_1}$ and $\overline{\Delta w_2}$; that is

$$\overline{\Delta w_k^n} = 0 \quad k = 1, 2 \quad \text{zero-order extrapolation} \quad (\text{E19.1.10})$$

$$\overline{\Delta w_k^n} = \Delta w_k^{n-1} \quad k = 1, 2 \quad \text{first-order extrapolation} \quad (\text{E19.1.11})$$

The primitive corrections are then finally given by

$$\overline{\Delta \rho} = \Delta \rho^{\text{num}} = \overline{\Delta w_1} + \frac{1}{c^2} \overline{\Delta p} \quad (\text{E19.1.12})$$

$$\overline{\Delta u} = \Delta u^{\text{num}} = \overline{\Delta w_2} - \frac{1}{\rho c} \overline{\Delta p} \quad (\text{E19.1.13})$$

which are easily transformed to conservative corrections $\overline{\Delta U_M}$.

(ii) *Supersonic outlet*

Three numerical boundary conditions have to be imposed. One can directly work with conservative corrections using the following possibilities: a first-order extrapolation in time

$$\overline{\Delta U_N^n} = \Delta U_N^{n-1} \quad (\text{E19.1.14})$$

or a zero-order extrapolation, which gives excellent results,

$$\overline{\Delta U_N^n} = 0 \quad (\text{E19.1.15})$$

Compatibility relations with time-differenced physical boundary conditions

This approach, introduced by Chakravarthy (1983), is based on a systematization of the characteristic method, as illustrated by equations (19.1.9) to (19.1.11), whereby the physical boundary conditions are discretized in a time differential form.

The idea behind this formulation relies on the fact that the compatibility relations are obtained by multiplying the conservative Euler equations by the left eigenvectors of the Jacobian matrix A , as seen in Chapter 16.

At a boundary only the characteristics with negative (outgoing) eigenvalues may be considered, since they provide information from inside the domain, while the characteristics with positive eigenvalues have to be replaced by the physical boundary conditions. Hence at a boundary the matrix P^{-1} , grouping the left eigenvectors as lines, will have the lines associated with the incoming characteristics zeroed out, in order to maintain only valid information. The remaining equations can be derived from the physical boundary conditions by differentiation in order to define a system of three by three equations at a boundary, which is to be added to the system applied at the internal points.

With the notation of equation (19.1.19), the characteristic compatibility equations (16.4.19) can be written as

$$\frac{\partial}{\partial t} \begin{vmatrix} W^P \\ W^N \end{vmatrix} + \Lambda \frac{\partial}{\partial x} \begin{vmatrix} W^P \\ W^N \end{vmatrix} = L^{-1} \tilde{Q} = P^{-1} Q \quad (\text{19.1.58})$$

or with (16.3.39), as a function of the conservative variables, as

$$\frac{\partial}{\partial t} \left| \frac{W^P}{W^N} \right| + \left| \frac{(P^{-1})^P}{(P^{-1})^N} \right| A \frac{\partial}{\partial x} \left| \frac{U^I}{U^{II}} \right| = P^{-1} Q \quad (19.1.59)$$

where A is the Jacobian of the conservative variables. Note that the factor $A \partial U / \partial x$ can be replaced by the conservative flux derivative $\partial f / \partial x$.

Following the procedure described by equations (19.1.9) to (19.1.11), the variables W^P , which correspond to incoming characteristics, have to be replaced by the physical boundary conditions $B(U) = 0$, where U stands for the conservative variables, for instance.

A fully combined treatment is obtained by taking the time derivative of the boundary conditions

$$\frac{\partial B}{\partial t} = 0 = \frac{\partial B}{\partial U} U_t, \quad (19.1.60)$$

where $\partial B / \partial U$ is the Jacobian matrix of the B functions with respect to U . Introducing this equation for the physical boundary terms, the full system at the boundaries then becomes

$$\frac{\partial}{\partial t} \left| \frac{B}{W^N} \right| + \Lambda \frac{\partial}{\partial x} \left| \frac{0}{W^N} \right| = \left| \frac{0}{(P^{-1})^N} \right| Q \quad (19.1.61)$$

or with $\Delta W = P^{-1} \Delta U$,

$$\left| \frac{\partial B}{\partial U} \right| \frac{\partial U}{\partial t} + \left| \frac{0}{(P^{-1})^N} \right| A \frac{\partial U}{\partial x} = \left| \frac{0}{(P^{-1})^N} \right| Q \quad (19.1.62)$$

Explicitly, the equations (19.1.62) are discretized after isolating $\partial U / \partial t$ in the following way. Defining the two matrices P_1, P_2 ,

$$P_1 = \left| \frac{\frac{\partial B}{\partial U}}{(P^{-1})^N} \right| \quad (19.1.63)$$

$$P_2 = \left| \frac{0}{(P^{-1})^N} \right| \quad (19.1.64)$$

the equations (19.1.62) are discretized after multiplication by P_1^{-1} , which is non-singular by construction as a consequence of the well-posedness of the selected boundary treatment:

$$\frac{\partial U}{\partial t} + (P_1^{-1} P_2 A) \frac{\partial U}{\partial x} = (P_1^{-1} P_2) Q \quad (19.1.65)$$

or

$$\frac{\partial U}{\partial t} + P_1^{-1} P_2 \frac{\partial f}{\partial x} = (P_1^{-1} P_2) Q \quad (19.1.66)$$

The system (19.1.66) can be discretized in relation to the considered scheme, that is explicitly or implicitly. In both cases, the flux term $\partial f/\partial x$ will have to be differenced in a one-sided way, forward at an inlet boundary and backward at an outlet section.

When an implicit scheme is selected, these equations can be discretized as follows, with $P^* \equiv P_1^{-1}P_2$, in the line of the Beam and Warming schemes:

$$(1 + \tau P^* \delta^- A^n)_M \Delta U_M^n = P_1^{-1} (P_2 Q)_M^n - \tau P^* \delta^- f_M^n \quad (19.1.67)$$

for an outflow boundary and a similar equation at the inflow boundary with a forward differencing operator δ^+ instead of δ^- .

The examples shown in Figure 18.1.6 to 18.1.8 have been obtained with this treatment of the boundary conditions and a first-order upwind discretization of (19.1.67). Note that equation (19.1.67) can also be applied with a second-order backward difference, leading to a second-order accurate boundary scheme.

It is to be noted that the boundary equations (19.1.65) and (19.1.66) are not in conservation form and, furthermore, the upwind discretization at the boundaries is not consistent with the interior scheme from the point of view of global conservation. For instance, if the interior scheme is based on a central differencing of the fluxes $\bar{\delta} f_i$ and if at the boundary one would apply a first-order upwind formula $\delta^- f_i = f_i - f_{i-1}$, this would leave a conservation error of $(f_{M-1} + f_M)/2 + (f_M - f_{M-1}) = (3f_M - f_{M-1})/2$. For strict conservation the sum $\sum_{i=1}^{M-1} \bar{\delta} f_i + (\delta^- f_M)$ should depend only on f_1 and f_M and not on the fluxes at interior points.

For the implicit schemes of Lerat (Section 17.4) with $\alpha = 0$, the explicit step is the physical one, and will require a correct boundary treatment of an explicit nature. The implicit step, being of a mathematical nature, can allow a simplified treatment, such as $\Delta U = 0$ at the boundaries.

Example 19.1.2 Subsonic outlet boundary, imposed exit pressure

The method just described is applied to a subsonic exit section, with imposed pressure, directly in the conservative variables. The matrix P^{-1} (equation (16.4.11)) is split as follows, keeping the usual order of the equations, that is writing first $(P^{-1})^N$:

$$P^{-1} = \begin{array}{c} (P^{-1})^N \\ (P^{-1})^P \end{array} \equiv \left| \begin{array}{ccc} 1 - \frac{\gamma-1}{2} \frac{u^2}{c^2} & (\gamma-1) \frac{u}{c^2} & -\frac{\gamma-1}{c^2} \\ \left(\frac{\gamma-1}{2} u^2 - uc \right) \frac{1}{\rho c} & [c - (\gamma-1)u] \frac{1}{\rho c} & \frac{\gamma-1}{\rho c} \\ \hline -\left(\frac{\gamma-1}{2} u^2 + uc \right) \frac{1}{\rho c} & (c + (\gamma-1)u) \frac{1}{\rho c} & -\frac{\gamma-1}{\rho c} \end{array} \right| \quad (E19.1.16)$$

The condition $B(U) = 0$ is given by

$$B(U) = p - p_1 = 0 \quad (\text{E19.1.17})$$

where p_1 is a constant. The Jacobian $\partial B / \partial U$ is actually formed by the last line of the matrix M^{-1} :

$$\frac{\partial B}{\partial U} = \left| \begin{array}{ccc} \frac{\gamma-1}{2} u^2 & -(\gamma-1)u & \gamma-1 \end{array} \right| \quad (\text{E19.1.18})$$

The matrices P_1 and P_2 are defined here as

$$P_1 = \left| \begin{array}{c} (P^{-1})^N \\ \frac{\partial B}{\partial U} \end{array} \right| = \left| \begin{array}{ccc} 1 - \frac{\gamma-1}{2} \frac{u^2}{c^2} & (\gamma-1) \frac{u}{c^2} & -\frac{\gamma-1}{c^2} \\ \left(\frac{\gamma-1}{2} u^2 - uc \right) \frac{1}{\rho c} & [c - (\gamma-1)u] \frac{1}{\rho c} & \frac{\gamma-1}{\rho c} \\ \frac{\gamma-1}{2} u^2 & -(\gamma-1)u & \gamma-1 \end{array} \right| \quad (\text{E19.1.19})$$

$$P_2 = \left| \begin{array}{c} (P^{-1})^N \\ 0 \end{array} \right| = \left| \begin{array}{ccc} 1 - \frac{\gamma-1}{2} \frac{u^2}{c^2} & (\gamma-1) \frac{u}{c^2} & -\frac{\gamma-1}{c^2} \\ \left(\frac{\gamma-1}{2} u^2 - uc \right) \frac{1}{\rho c} & [c - (\gamma-1)u] \frac{1}{\rho c} & \frac{\gamma-1}{\rho c} \\ 0 & 0 & 0 \end{array} \right| \quad (\text{E19.1.20})$$

The matrix $P^* = P_1^{-1} P_2$ is derived by direct algebraic manipulations:

$$P^* = \left| \begin{array}{ccc} 1 - \frac{\gamma-1}{2} \frac{u^2}{c^2} & (\gamma-1) \frac{u}{c^2} & \frac{1-\gamma}{c^2} \\ \frac{\gamma-1}{2c} u^2 \left(1 - \frac{u}{c} \right) & 1 + \frac{\gamma-1}{c} u \left(\frac{u}{c} - 1 \right) & \frac{\gamma-1}{c} \left(1 - \frac{u}{c} \right) \\ -\frac{u^2}{2} \left[1 + (\gamma-1) \frac{u}{c} \left(\frac{u}{2c} - 1 \right) \right] & u \left[1 + (\gamma-1) \frac{u}{c} \left(\frac{u}{2c} - 1 \right) \right] & -(\gamma-1) \frac{u}{c} \left(\frac{u}{2c} - 1 \right) \end{array} \right| \quad (\text{E19.1.21})$$

Example 19.1.3 Subsonic inlet—pressure and density fixed

There is only one numerical boundary condition corresponding to the third characteristic. In this case, $(P^{-1})^N$ and $(P^{-1})^P$ are reversed in comparison to the previous example and we have

$$B(U) = \left| \begin{array}{c} \rho - \rho^* \\ p - p^* \end{array} \right| = 0 \quad (\text{E19.1.22})$$

where ρ^* and p^* are the imposed values.

The Jacobian $\partial B/\partial U$ is formed by the second and last rows of M^{-1} :

$$\frac{\partial B}{\partial U} = \begin{vmatrix} 1 & 0 & 0 \\ \frac{\gamma-1}{2}u^2 & -(\gamma-1)u & (\gamma-1) \end{vmatrix} \quad (\text{E19.1.23})$$

The matrices P_1 and P_2 become

$$P_1 = \begin{vmatrix} 1 & 0 & 0 \\ \frac{\gamma-1}{2}u^2 & -(\gamma-1)u & \gamma-1 \\ -\left(\frac{\gamma-1}{2}u^2 + uc\right)\frac{1}{\rho c} & [c + (\gamma-1)u]\frac{1}{\rho c} & -\frac{\gamma-1}{\rho c} \end{vmatrix} \quad (\text{E19.1.24})$$

$$P_2 = \begin{vmatrix} 0 & 0 & 0 \\ 0 & 0 & 0 \\ -\left(\frac{\gamma-1}{2}u^2 + uc\right)\frac{1}{\rho c} & [(c + (\gamma-1)u)]\frac{1}{\rho c} & -\frac{\gamma-1}{\rho c} \end{vmatrix} \quad (\text{E19.1.25})$$

The matrix $P^* = P_1^{-1}P_2$ is derived by direct algebraic manipulations:

$$P^* = \begin{vmatrix} 0 & 0 & 0 \\ -u\left(1 + \frac{\gamma-1}{2c}u\right) & 1 + (\gamma-1)\frac{u}{c} & -\frac{\gamma-1}{c} \\ -u^2\left(1 + \frac{\gamma-1}{2c}u\right) & \left[1 + (\gamma-1)\frac{u}{c}\right] & -\frac{\gamma-1}{c}u \end{vmatrix} \quad (\text{E19.1.26})$$

Example 19.1.4 Application to MacCormack and Beam and Warming schemes

Equation (19.1.66) is written with $P^* = P_1^{-1}P_2$:

$$\frac{\partial U}{\partial t} + P^* \frac{\partial f}{\partial x} = P^* Q \quad (\text{E19.1.27})$$

This equation, valid at the boundaries, will be discretized in a one-sided way. A first-order explicit scheme seems to be a good choice, since it has to be combined with the explicit MacCormack scheme.

For an inlet boundary $i = 1$ one would write

$$\Delta U_1^n = -\tau P_1^* \delta^+ f_1^n + \Delta t P_1^* Q_1^n \quad (\text{E19.1.28})$$

and for an outlet boundary $i = M$,

$$\Delta U_M^n = -\tau P_M^* \delta^- f_M^n + \Delta t P_M^* Q_M^n \quad (\text{E19.1.29})$$

For the Beam and Warming scheme, equation (E19.1.27) is discretized in an implicit way with one-sided differences.

For an inlet boundary $i = 1$ we have, with an implicit treatment of the source term where $C = \partial Q / \partial U$ is here the Jacobian of the source term.

$$(1 + \tau P_1^* \delta^+ A_1^n - \Delta t P_1^* C_1^n) \Delta U_1^n = -\tau P_1^* \delta^+ f_1^n + \Delta t P_1^* Q_1^n \quad (\text{E19.1.30})$$

For an outlet boundary $i = M$,

$$(1 + \tau P_M^* \delta^- A_M^n - \Delta t P_M^* C_M^n) \Delta U_M^n = -\tau P_M^* \delta^- f_M^n + \Delta t P_M^* Q_M^n \quad (\text{E19.1.31})$$

Equations (E19.1.30) and (E19.1.31) represent the extra boundary equations completing the blocktridiagonal system of Beam and Warming. More explicitly they can be written as follows:

$$Y \Delta U_1^n + Z \Delta U_2^n = \text{RHS}_1 \quad \text{inlet boundary} \quad (\text{E19.1.32})$$

with

$$\begin{aligned} Y &= 1 - \tau P_1^* A_1^n - \Delta t P_1^* C_1^n \\ Z &= \tau P_1^* A_2^n \\ \text{RHS}_1 &= -\tau P_1^* (f_2^n - f_1^n) + \Delta t P_1^* Q_1^n \end{aligned} \quad (\text{E19.1.33})$$

At the outlet boundary

$$X \Delta U_{M-1}^n + Y \Delta U_M^n = \text{RHS}_M \quad \text{outlet boundary} \quad (\text{E19.1.34})$$

with

$$\begin{aligned} Y &= 1 + \tau P_M^* A_M^n - \Delta t P_M^* C_M^n \\ X &= -\tau P_M^* A_{M-1}^n \\ \text{RHS}_M &= -\tau P_M^* (f_M^n - f_{M-1}^n) + \Delta t P_M^* Q_M^n \end{aligned} \quad (\text{E19.1.35})$$

In general, since the physical boundary conditions are imposed as time derivatives $\partial_t B = 0$ and linearized as equation (19.1.60), the non-linearity of the boundary conditions will lead to small errors on the exact condition $B(U) = 0$. Hence, it is recommended to update the imposed variables, for instance pressure in Example 19.1.1, after each time step in order to satisfy exactly the imposed values. An alternative to the updating, which is actually more consistent with an implicit approach, is to replace equation (19.1.60) by a Newton iteration

$$B(U^{n+1}) = B(U^n) + \frac{\partial B}{\partial U} (U^{n+1} - U^n) \quad (\text{19.1.68})$$

which is a discretized form of equation (19.1.60). Under the condition that the solution at time step $n + 1$ satisfies exactly the boundary condition $B(U^{n+1}) = 0$, equation (19.1.68) can be written with the boundary residual in the right-hand side as

$$\left(\frac{\partial B}{\partial U} \right)^n \Delta U^n = -B(U^n) \quad (\text{19.1.69})$$

This can easily be introduced in equations (19.1.61) to (19.1.67) by adding to the right-hand side the matrix $\begin{vmatrix} -B \\ 0 \end{vmatrix}$, leading to the following equation, instead of (19.1.62):

$$\begin{vmatrix} \frac{\partial B}{\partial U} \\ (P^{-1})^N \end{vmatrix} \frac{\partial U}{\partial t} + \begin{vmatrix} 0 \\ (P^{-1})^N \end{vmatrix} A \frac{\partial U}{\partial x} = \begin{vmatrix} -B \\ (P^{-1})^N Q \end{vmatrix} \tag{19.1.70}$$

and equation (19.1.66) becomes

$$\frac{\partial U}{\partial t} + P_1^{-1} P_2 \frac{\partial f}{\partial x} = P_1^{-1} \begin{vmatrix} -B \\ (P^{-1})^N Q \end{vmatrix} \tag{19.1.71}$$

In the discretized form of equation (19.1.67), this modification leads to the boundary scheme

$$(1 + \tau P^* \delta^- A^n)_M \Delta U_M^n = -\tau P^* \delta^- f_M^n + P_1^{-1} \begin{vmatrix} -B^n \\ (P^{-1})^N Q \end{vmatrix} \tag{19.1.72}$$

The first group of equations are in fact $B(U) = 0$ at time level n .

A comparison between this last method and the implicit characteristic extrapolation method is shown in Figures 19.1.5 and 19.1.6. They correspond to the same case and the same conditions as Figure 18.1.7, in particular the same physical boundary conditions, identical CFL numbers of 40 and the same artificial dissipation coefficients. The convergence rates of the three cases are practically identical, reaching a residual reduction of eight orders of magnitude in 100 time steps.

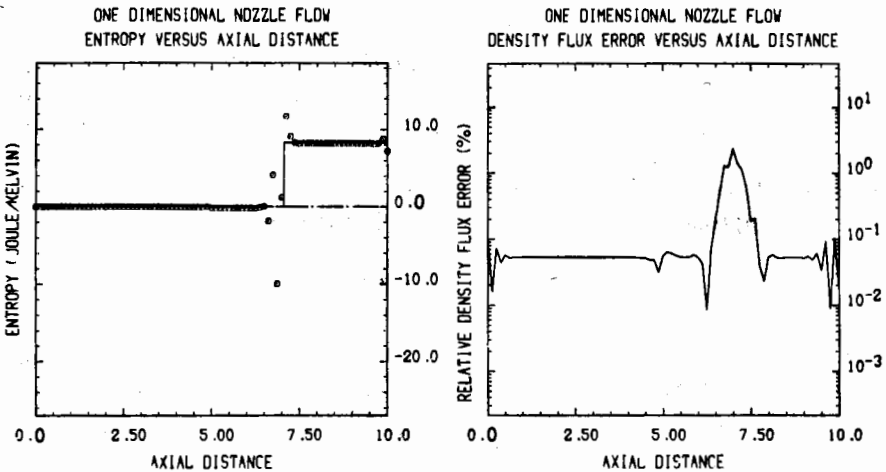


Figure 19.1.5 Mass flux error and entropy distribution obtained with the Beam and Warming scheme and first-order characteristic extrapolation as boundary treatment

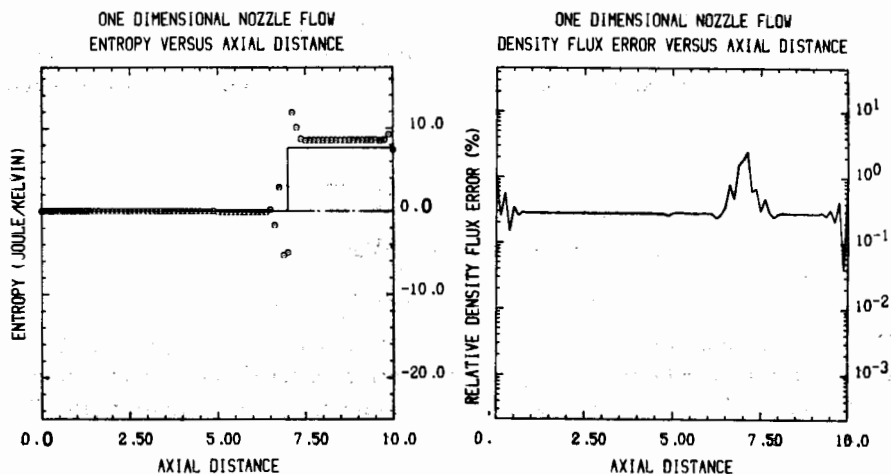


Figure 19.1.6 Mass flux error and entropy distribution obtained with the Beam and Warming scheme and zero-order characteristic extrapolation as boundary treatment

Figure 18.1.7 is obtained with the implicit characteristic treatment, while Figure 19.1.5 and 19.1.6 show the error evolution and entropy plots for the first-order extrapolation on the characteristic variables and the zero-order extrapolation respectively.

The results of Mach and density distributions can not be distinguished from those shown in Figure 18.1.7, but the error curves show an increase in the error level of the density flux which remains limited for the first-order extrapolation but reaches one order of magnitude for the zero-order extrapolation. This is to be expected since Gustafsson's theorem predicts that the coupling of a second-order accurate interior scheme with a zero-order boundary treatment reduces the overall order of accuracy of the complete scheme. This can also be seen on the entropy variation which shows an increased error in the region downstream of the shock.

19.1.6 Non-reflecting boundary conditions

This approach is an alternative for the expression of *physical* boundary conditions.

When imposing a constant pressure at a subsonic exit section under the form $p^{n+1} = p^*$ or $\Delta p = 0$, where $\Delta p = p^{n+1} - p^n = p^* - p^n$ as considered in Examples 19.1.1 and 19.1.2, one actually allows perturbation waves to be reflected at the boundaries. Indeed, since the amplitude of the local perturbation wave carried by the incoming characteristic is $\Delta w_3 = \Delta u - \Delta p / \rho c$, imposing $\Delta p = 0$ amounts to the generation of an incoming wave of intensity $\Delta w_3 = \Delta u$ reflected from the exit boundary.

The non-reflecting boundary condition (Engquist and Majda, 1977; Hedstrom, 1979) expresses the physical boundary conditions as the requirement that the local perturbations propagated along incoming characteristics be made to vanish: that is

$$\frac{\partial w_k}{\partial t} = 0 \quad \text{for all } k \text{ such that } \lambda_k \text{ enters the domain} \quad (19.1.73)$$

In discretized form this condition is expressed as

$$\Delta w_k = 0 \quad \text{for all } k \text{ such that } \lambda_k \text{ enters the domain} \quad (19.1.74)$$

This condition is automatically satisfied with the characteristic approach (19.1.6) to (19.1.8), but it can be applied with other treatments of the numerical boundary conditions (see Problems 19.6 and 19.7). For a subsonic outlet, equation (19.1.74) becomes

$$\Delta w_3 = \Delta u - \frac{\Delta p}{\rho^n c^n} = 0 \quad (19.1.75)$$

For a subsonic inlet, the non-reflecting boundary conditions would be

see (16.4.10) p. 162

$$\begin{aligned} \Delta w_1 &= \Delta \rho - \frac{\Delta p}{c^{2n}} = 0 \\ \Delta w_2 &= \Delta u + \frac{\Delta p}{\rho^n c^n} = 0 \end{aligned} \quad (19.1.76)$$

It is to be noted that this reasoning remains valid as long as shocks do not cross the boundary, since the characteristic variables are not constant across a shock. Hence the above conditions will generate a reflection when a shock passes through a boundary. However, if the shock is of strength ϵ , the Riemann variables change by an amount $O(\epsilon^2)$ through the shock and produce a reflection of this order of magnitude (Hedstrom, 1979).

In the presence of source terms, the characteristic equations are defined by equation (16.4.19) or

$$\frac{\partial w_k}{\partial t} + \lambda_k \frac{\partial w_k}{\partial x} = l^{(k)} Q \quad (19.1.77)$$

where $l^{(k)}$ is the left eigenvector of the Jacobian associated with λ_k . At a fixed position of the inlet or outlet boundaries, equation (19.1.73) is generalized as

$$\frac{\partial w_k}{\partial t} = l^{(k)} Q \quad \text{for all } k \text{ such that } \lambda_k \text{ enters the domain} \quad (19.1.78)$$

For a nozzle of cross-section $S(x)$, equation (19.1.75) for a subsonic exit becomes

see (16.4.23)

$$\Delta w_3 = \Delta u - \frac{\Delta p}{\rho^n c^n} = \frac{1}{S} \frac{dS}{dx} u^n c^n \quad (19.1.79)$$

Computations show, in particular with unsteady flows but also for stationary conditions, that this procedure provides an improved accuracy at the boundaries and we refer to the listed references for specific examples; see also Thompson (1987) for additional examples.

In steady-state computations and an imposed pressure at a subsonic exit, the non-reflecting condition (19.1.75) does not ensure that $p = p^*$, and a strict application of this equation might lead to a steady state depending on the initial data. An *ad hoc* cure to this situation has been proposed by Rudy and Strickwerda (1980). It consists in replacing equation (19.1.73) for the incoming characteristic by the condition $\alpha > 0$:

$$\frac{\partial u}{\partial t} - \frac{1}{\rho c} \frac{\partial p}{\partial t} - \frac{\alpha}{\rho c} (p - p^*) = 0 \quad \text{at } i = M \quad (19.1.80)$$

For any finite value of α the steady-state solution will satisfy the condition $p = p^*$.

The parameter α has to be optimized and some guidelines are provided by Rudy and Strickwerda (1980). For the two-dimensional test cases analysed by these authors with the MacCormack scheme, the convergence rate to steady state was strongly dependent on the parameter α . The optimum value of α decreases with increasing Mach number, from roughly 0.1 to 0.2 at Mach number 0.8 to a value close to 1 for Mach numbers of 0.4. However, these values are strongly problem dependent. In any case, the convergence rate was considerably better compared to the case where the condition $p = p^*$ at exit was used.

Equation (19.1.80) can be discretized in an implicit way, leading to

$$\Delta p_M = (\rho^n c^n \Delta u + \alpha \Delta t \Delta p^*)_M \frac{1}{1 + \alpha \Delta t} \quad (19.1.81)$$

where $\Delta p = p^{n+1} - p^n$ and $\Delta p^* = p^* - p^n$, or in an explicit way

$$\Delta p_M = (\rho^n c^n \Delta u + \alpha \Delta t \Delta p^*)_M \quad (19.1.82)$$

Better results are obtained with the implicit form (19.1.81).

An interesting combination for the expression of boundary conditions, in particular for unsteady problems, is to combine the compatibility equations for the outgoing waves with the non-reflective condition for the incoming characteristics. This corresponds to an application of the procedure developed in Section 19.1.5 with the replacement of the equation $\partial B / \partial t = 0$ by equation (19.1.78). This replacement maintains equation (19.1.65) with $P_1 = P^{-1}$, the complete diagonalization matrix of the Jacobian (E19.1.16). A straightforward interpretation of the equation obtained in this way can be given in terms of flux splitting concepts and will be discussed in Section 20.2.4.

Note that, for stationary problems, equation (19.1.80) might be used in this approach, instead of (19.1.78).

19.2 MULTI-DIMENSIONAL BOUNDARY TREATMENT

Multi-dimensional flows contain a variety of boundaries, which can be grouped into:

- (1) Free surfaces, either far-field boundaries in external flows or inlet and outlet sections of internal flow systems (Figures 19.2.1 and 19.2.2).

These are the boundaries through which the flow enters or leaves the computational domain. In external flow problems, free boundaries are generally located far enough from the body such that free-stream conditions can be considered although, as will be seen next, higher accuracy is obtained when some far-field corrections, taking into account the finite distance between the body and the outer boundaries of the computational domain, are introduced.

In internal flow systems, ducts or cascades, these boundaries refer to the inlet and outlet surfaces. For cascades, one has in addition periodic surfaces, resulting from the periodicity of the cascade geometry. These surfaces are not to be considered as external boundaries, since the periodicity condition of equality of all physical flow quantities at corresponding points E, F results in treating these points as internal points, without other boundary treatment.

- (2) Solid body surfaces, either bodies immersed in a flow or bounding walls in ducts and cascades.

19.2.1 Physical and numerical boundary conditions

In all cases, the number of physical boundary conditions to be imposed at the boundary surfaces is determined by the characteristic properties.

Referring to the presentation in Section 16.5, the number of physical conditions to be imposed at a boundary with the normal vector \vec{n} pointing towards the flow domain is defined by the signs of the eigenvalues of the matrix

$$K = \vec{A} \cdot \vec{1}_n = A\hat{n}_x + B\hat{n}_y \quad (19.2.1)$$

where $\vec{1}_n$ is the unit vector normal to the surface, with components (\hat{n}_x, \hat{n}_y) in a two-dimensional Cartesian coordinate system.

Remember that A and B are the Jacobians of the conservative x and y components of the flux vector, with respect to the conservative variables. The matrix

$$\tilde{K} = \vec{\tilde{A}} \cdot \vec{1}_n = \tilde{A}\hat{n}_x + \tilde{B}\hat{n}_y \quad (19.2.2)$$

formed by the Jacobians of the flux components with respect to the primitive variables has the same eigenvalues.

The eigenvalues of the matrix K are $\vec{v} \cdot \vec{1}_n$, $\vec{v} \cdot \vec{1}_n$, $\vec{v} \cdot \vec{1}_n + c$, $\vec{v} \cdot \vec{1}_n - c$ in a two-dimensional flow.

The first two eigenvalues are equal to the normal component of the velocity vector, v_n . The two remaining eigenvalues are associated with the acoustic waves

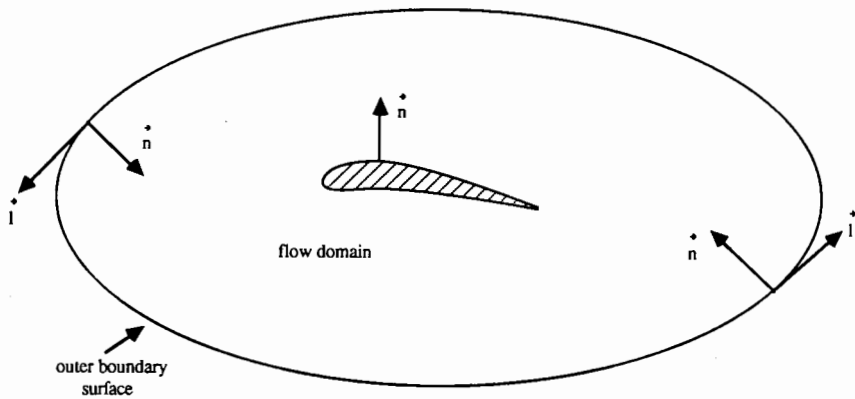
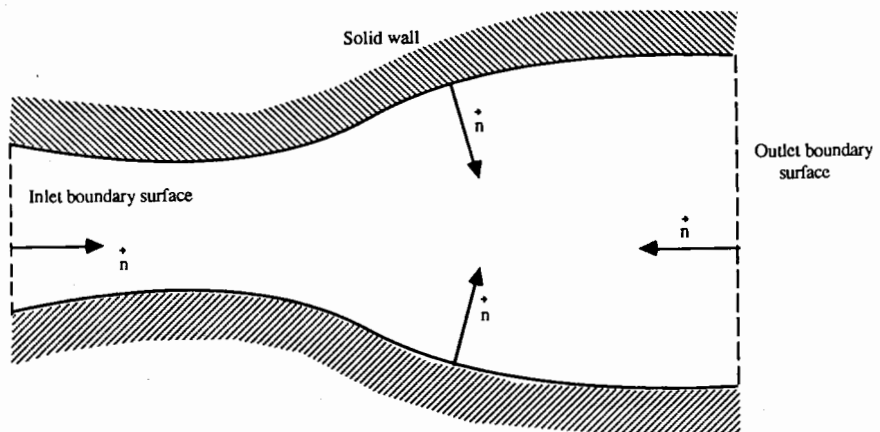
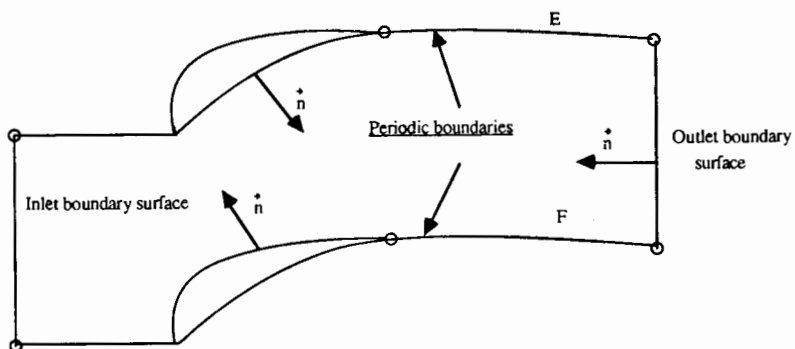


Figure 19.2.1 External flow boundary configuration



(a) Duct flow



(b) Cascade flow

Figure 19.2.2 Internal flow boundary configuration

and are equal to $v_n \pm c$. Hence the sign of these eigenvalues will be determined by the velocity components normal to the boundary surfaces.

Note that in a three-dimensional flow, the eigenvalue v_n appears three times.

The associated wave propagation speeds in the direction $\bar{1}_n$ are $\lambda \cdot \bar{1}_n$ where λ represents any of the above eigenvalues, according to equation (16.3.11). Hence, when λ is positive, the information carried by the associated characteristics propagates *from the boundary towards* the interior of the flow domain and a physical boundary condition has to be imposed.

On the other hand, when the eigenvalue λ is negative, information is propagated from the flow domain towards the boundary, influencing thereby the boundary surface conditions. These effects have therefore to be expressed numerically, through numerical boundary conditions.

If the *inlet flow* is subsonic in the direction *normal* to the entry surface, three eigenvalues are positive (four in a three-dimensional situation) and one is negative. Therefore, three (or four) quantities will have to be fixed by the physical flow conditions at the inlet of the flow domain, while the remaining one will be determined by the interior conditions, through a numerical boundary condition (Figure 19.2.3).

Two thermodynamic variables will generally be determined by the upstream stagnation conditions. Most currently, stagnation pressure and temperature can be imposed, or, equivalently, entropy and stagnation enthalpy. The third (and fourth) physical variable(s) will be defined by one (or two) velocity component(s). The remaining velocity component will result from the numerical boundary treatment.

An equivalent option often applied in internal flows, such as channels or cascade computations, is to specify inlet Mach number or velocity magnitude, and have the inlet flow angle defined by the computed flow, or, inversely, fix the incident flow angle, determining inlet Mach number from the computed flow.

In addition, when the flow is choked, that is when the sonic velocity is reached in a minimum area section which is lower than, or equal to, the critical section the mass flow rate cannot be imposed, but has to be calculated from the flow properties through a numerical procedure.

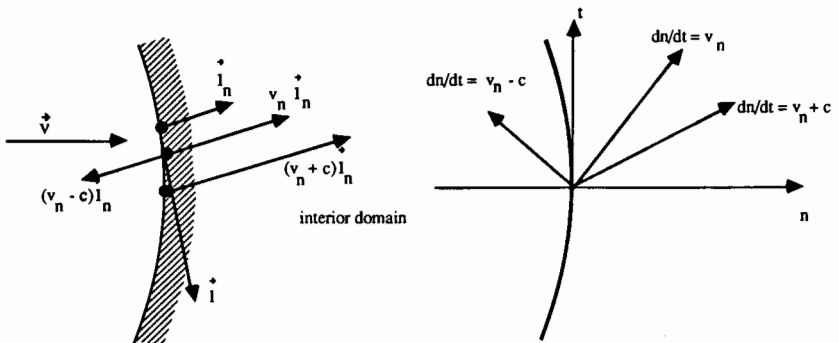


Figure 19.2.3 Subsonic inlet boundary in two-dimensional flows

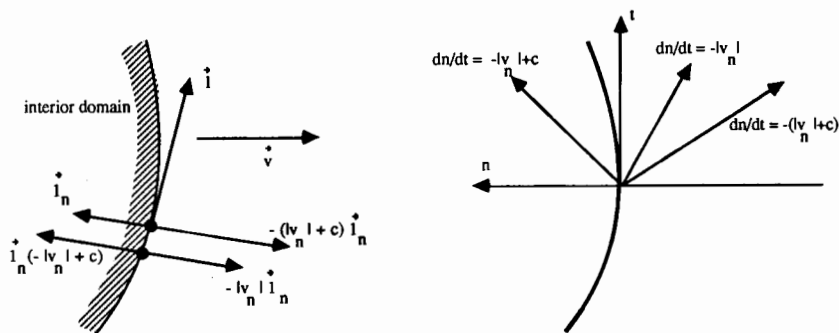


Figure 19.2.4 Subsonic outlet boundary in two-dimensional flows

At an *outlet boundary*, with subsonic normal velocity, three (four) eigenvalues are negative, since the normals are defined as pointing towards the interior flow domain. Three (four) numerical boundary conditions have therefore to be set, while the fourth (fifth) condition, associated with the positive eigenvalue $(-|v_n| + c)$, propagates information from the boundary towards the flow region. It is consequently associated with a physical boundary condition (Figure 19.2.4).

The most appropriate physical condition, particularly for internal flows and corresponding to most experimental situations, consists in fixing the downstream static pressure. This can also be applied for external flow problems. However, in this latter case, free-stream velocity is generally imposed.

If the flow is supersonic normal to the inlet surface, all boundary conditions are physical.

With the same circumstances at the outlet, all eigenvalues are of negative sign and no physical conditions have to be given. All the boundary variables are defined by the interior flow, for instance via extrapolation formulas.

At a *solid wall boundary*, the normal velocity is zero, since no mass or other convective flux can penetrate the solid body. Hence, only one eigenvalue is positive and only one physical condition can be imposed, namely $v_n = 0$. The other variables at the wall, in particular velocity and pressure, have to be determined by extrapolation from the interior to the boundary (Figure 19.2.5).

An important effect of the numerical boundary procedure is to ensure that unwanted perturbations, generated in the computational domain, for instance the transients in a steady-state flow, leave the domain without being reflected at the boundaries. This implies that the propagation of these perturbations is compatible with the characteristic propagation properties of the Euler equations, as expressed by the compatibility relations or the equations for the characteristic variables.

When this is not the case, the accuracy of the computation can be greatly affected by the reflection occurring at the boundaries. It is therefore recommended to apply, as in the one-dimensional case, characteristic or compatibility relations as boundary procedures.

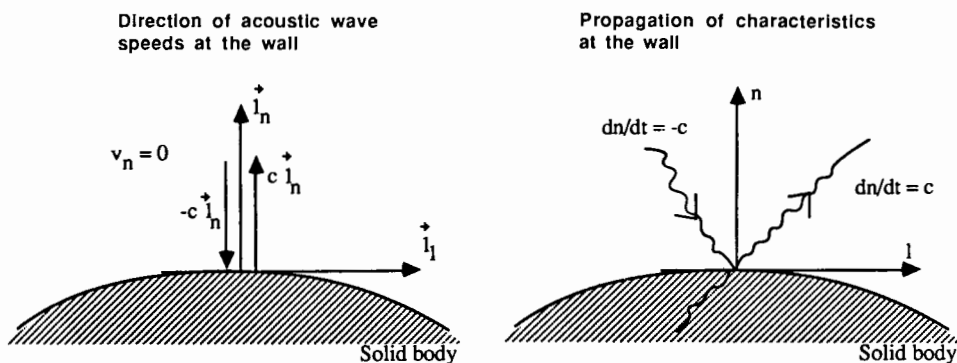


Figure 19.2.5 Solid wall boundary in two-dimensional flows

19.2.2 Multi-dimensional compatibility relations

The compatibility or characteristic relations can be written, for an arbitrary propagation direction, under the various formulations presented in Section 16.5.

They differ from their one-dimensional counterpart by the presence of contributions to the convective transport of characteristic quantities, arising from variations of velocity and pressure in the surface normal to the considered propagation direction. This is best seen in equation (16.5.46), which is the compatibility relation associated with the acoustic waves of celerity $v_n \pm c$.

This equation is reproduced here for the direction \vec{n} normal to the surface as

$$d_b^\pm R_n^\pm = \mp c \vec{l} \cdot (\vec{l} \cdot \vec{\nabla}) \vec{v} \quad (19.2.3)$$

where

$$d_b^\pm = \frac{\partial}{\partial t} + (\vec{v} \pm c \vec{l}_n) \cdot \vec{\nabla} \quad (19.2.4)$$

and with \vec{l} representing unit directions in the surface, that is normal to \vec{n} , namely

$$\vec{l} \cdot \vec{n} = 0 \quad (19.2.5)$$

The Riemann variables R_n^\pm associated with the direction n are defined by

$$R_n^\pm = \vec{v} \cdot \vec{l}_n \pm \frac{2c}{\gamma - 1} \quad (19.2.6)$$

as in the one-dimensional case.

It is seen here that these variables are generally not invariants, in the sense of being transported along an associated bicharacteristic, as a consequence of the presence of the right-hand side in equation (19.2.3).

The other characteristic relations are contained in the equations (16.5.51) to

(16.5.52) and are reproduced here for a two-dimensional flow and the direction \vec{n} :

$$\delta W = \begin{vmatrix} \delta w_1 \\ \delta w_2 \\ \delta w_3 \\ \delta w_4 \end{vmatrix} = \begin{vmatrix} \delta\rho - \frac{\delta p}{c^2} \\ \hat{n}_y \delta u - \hat{n}_x \delta v \\ \vec{l}_n \cdot \delta \vec{v} + \frac{\delta p}{\rho c} \\ -\vec{l}_n \cdot \delta \vec{v} + \frac{\delta p}{\rho c} \end{vmatrix} \quad (19.2.7)$$

The characteristic system becomes

$$\begin{aligned} \left(\frac{\partial}{\partial t} + \vec{v} \cdot \vec{\nabla} \right) w_1 &= 0 \\ \left(\frac{\partial}{\partial t} + \vec{v} \cdot \vec{\nabla} \right) w_2 &= \frac{c}{2} (\hat{n}_x \partial_y - \hat{n}_y \partial_x) (w_3 + w_4) = -\frac{1}{\rho} (\vec{l} \cdot \vec{\nabla}) p \\ \left[\frac{\partial}{\partial t} + (\vec{v} + c \vec{l}_n) \cdot \vec{\nabla} \right] w_3 &= c (\hat{n}_x \partial_y - \hat{n}_y \partial_x) w_2 = -c \vec{l} \cdot (\vec{l} \cdot \vec{\nabla}) \vec{v} \\ \left[\frac{\partial}{\partial t} + (\vec{v} - c \vec{l}_n) \cdot \vec{\nabla} \right] w_4 &= c (\hat{n}_x \partial_y - \hat{n}_y \partial_x) w_2 = -c \vec{l} \cdot (\vec{l} \cdot \vec{\nabla}) \vec{v} \end{aligned} \quad (19.2.8)$$

The first equation of (19.2.8) describes the constancy of entropy along a streamline, while the second characteristic equation has no equivalent in one-dimensional flows and represents the propagation of vorticity waves. The last two characteristic equations are identical to equation (19.2.3).

We recall here that these equations are to be considered as a shorthand form for the combination of primitive variable variations defined by (19.2.7) since, as pointed out in Chapter 16, the variables w cannot always be determined. However, if the flow is close to uniform, as in a far-field region of an immersed body, then the characteristic variables can be linearized around the uniform flow variables and W can always be defined, as seen in Chapter 16, Section 16.5.

If the *pressure and the velocity are uniform in the boundary surface*, that is

$$\vec{l} \cdot \vec{\nabla} p = 0 \quad \text{and} \quad (\vec{l} \cdot \vec{\nabla}) \vec{v} = 0 \quad (19.2.9)$$

then the right-hand sides of all the equations (19.2.8) vanish and one recovers locally a one-dimensional situation.

19.2.3 Far-field treatment for steady-state flows

A simple treatment of the inlet and outlet boundaries for stationary flows can be defined when (19.2.9) is valid (Thomas and Salas, 1986), where the

compatibility relations associated with the acoustic waves reduce to

$$R_n^+ = v_n + \frac{2c}{\gamma - 1} = \text{constant along the path } \bar{v} + c\bar{1}_n \quad (19.2.10)$$

$$R_n^- = v_n - \frac{2c}{\gamma - 1} = \text{constant along the path } \bar{v} - c\bar{1}_n \quad (19.2.11)$$

Subsonic inlet boundary

The first relation corresponds to the positive, incoming, characteristic and is associated with the physical boundary condition. Hence, the values at the boundary, indicated by a subscript B, are obtained from

$$R_{nB}^+ = v_{nB} + \frac{2c_B}{\gamma - 1} = V_{n\infty} + \frac{2c_\infty}{\gamma - 1} \quad (19.2.12)$$

where \bar{V}_∞ is the free-stream velocity and c_∞ the free stream speed of sound.

The second relation (19.2.11) is associated with a numerical boundary condition and has to be estimated from inside the domain by an appropriate extrapolation from the mesh points close to the boundary surface. Hence,

$$R_{ni}^- = v_{nB} - \frac{2c_B}{\gamma - 1} = v_{ni} - \frac{2c_i}{\gamma - 1} \quad (19.2.13)$$

where the subscript i refers to a value at an internal mesh point along the direction $\bar{v} - c\bar{1}_n$ or alternatively along the normal direction, since the boundary variations along the tangent to the surface have been assumed to vanish.

The boundary values of the normal velocity and sound speed are obtained by adding and subtracting equations (19.2.12) and (19.2.13), leading to

$$v_{nB} = \frac{R_{nB}^+ + R_{ni}^-}{2} \quad (19.2.14)$$

$$c_B = (R_{nB}^+ - R_{ni}^-) \frac{\gamma - 1}{4} \quad (19.2.15)$$

The second characteristic relation can be simplified if the local coordinate system is oriented such that the x direction is along the normal. In this case, the variable w_2 reduces to the tangential velocity v_t and the compatibility relation becomes

$$\begin{aligned} v_t &= \text{constant along the directions } \bar{v} \text{ or } \bar{n} \\ s &= \text{constant along the direction } \bar{v} \text{ or } \bar{n} \end{aligned} \quad (19.2.16)$$

both variables being associated to the physical free-stream values; that is

$$v_{tB} = v_{t\infty} \quad (19.2.17)$$

$$s_B = s_\infty \quad (19.2.18)$$

The above treatment does not indicate that the stagnation enthalpy is constant and equal to its imposed value, since H is not associated with a characteristic variable. This is an extremely important aspect for steady calculations and should be enforced. This can be achieved in several ways, for instance by defining the speed of sound along the boundary by

$$c_B^2 = \left(\frac{H_\infty - \bar{v}_B^2}{2} \right) (\gamma - 1) \quad (19.2.19)$$

instead of equation (19.2.15).

Alternatively, one could replace equation (19.2.12) or (19.2.18) by the condition

$$H_B = H_\infty \quad (19.2.20)$$

Subsonic outlet boundary

The same relations apply at the outlet, with the difference that the quantities R_{nB}^- , v_{nB} and s_B are determined from the internal values. Remember that we define the direction of the normal towards the inside of the computational domain, that is $v_n > 0$ at the inlet and $v_n < 0$ at the outlet.

The fourth relation for R_{nB}^+ is defined by the physical condition of fixed pressure:

$$R_{nB}^+ = -|v_{nB}| + \frac{2c_B}{\gamma - 1} = R_{n\infty}^+ = -|v_{n\infty}| + \frac{P_\infty}{\rho_\infty c_\infty} \quad (19.2.21)$$

If the flow is not uniform in the boundary surfaces the complete form (19.2.3) of the characteristic equations have to be used.

An equivalent formulation to the one just described can be defined by a direct extension of the treatment of Section 19.1.3 where the variables R_n^\pm are replaced by the characteristic variables Δw_3 and Δw_4 , while v_t and s are replaced by Δw_2 and Δw_1 respectively.

Also, the treatment of Chakravarthy, combining the time-differenced physical boundary conditions with the characteristic equations associated with the negative eigenvalues into one system of equations at the boundaries, can be extended in a straightforward way to two and three dimensions (Chakravarthy, 1983; Rai and Chaussee, 1983).

It is to be observed that other directions than the normal to the boundary surface may be selected in applying the characteristic relations. One interesting choice results from an analysis of Bayliss and Turkel (1982) which has been shown by Roe (1986) to correspond to a direction making an angle θ with the incident velocity directions, supposed to be aligned with the x axis, such that $\tan \theta = \beta^2 y / (x - \beta R M_\infty)$ with $\beta^2 = 1 - M_\infty^2$ and $R^2 = y^2 + x^2 / \beta^2$.

19.2.4 Solid wall boundary

At a solid wall one characteristic enters the flow domain and a single physical boundary condition is to be imposed. This condition is expressed by the

vanishing of the normal velocity

$$v_n = 0 \quad (19.2.22)$$

As a consequence, all convective flux components through the solid wall will vanish in the computation of the flux terms and the normal component of the flux vector reduces to the following expression in a two-dimensional flow:

$$\vec{F} \cdot \vec{1}_n = \begin{vmatrix} 0 \\ p\hat{n}_x \\ p\hat{n}_y \\ 0 \end{vmatrix} \quad (19.2.23)$$

Hence, only the pressure contribution remains at the walls.

The variables other than the normal velocity, in particular the tangential velocity, the pressure and another thermodynamic variables, for instance total enthalpy or entropy, have to be obtained from the interior flow. Here again these variables can be extrapolated directly from their values at points adjacent to the wall surface, or the conservation equations can be solved for mesh points on the boundary from a one-sided discretization.

A third alternative consists in applying the characteristic relations discretized in a one-sided way from the wall towards the inside of the flow field. It is essential to observe here that the simplified form of the compatibility relations, namely equations (19.2.10), (19.2.11) and (19.2.16), are not valid here, since the assumption of uniform velocity and pressure in the boundary surface is certainly not satisfied at a solid wall boundary. Hence the full form (19.2.7) and (19.2.8) has to be applied at the walls.

These relations are applied in differential form in the combined treatment of Chakravarthy, where the equation for w_3 , associated with a positive characteristic, is replaced by the time-differenced form of the physical boundary condition (19.2.22) (Chakravarthy, 1983; Rai and Chaussee, 1983).

Determination of the wall pressure

The numerical determination of the wall pressure is an essential element in any computation with solid boundaries and various methods can be applied in order to obtain the wall pressures.

Extrapolation from adjacent points This is the simplest approach, whereby an extrapolation, generally linear or quadratic, is applied from neighbouring points to the wall along a mesh point line.

When mesh points are located on the wall, as in Figure 19.2.6, one can also solve the Euler equations with one-sided discretizations to find all the variables in addition to the vanishing normal velocity.

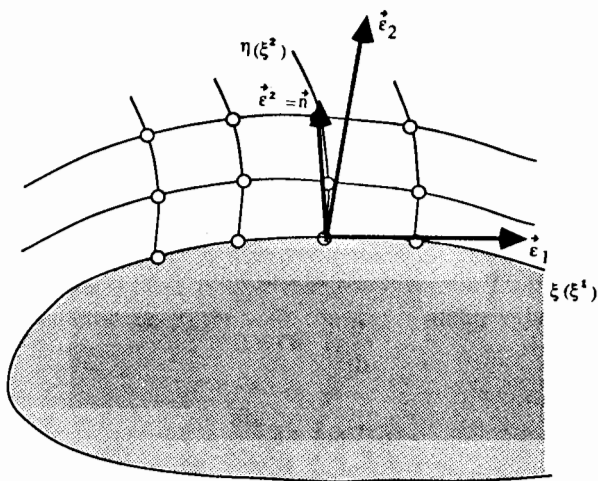


Figure 19.2.6 Streamwise curvilinear coordinates at solid boundary

Compatibility relations at the wall The wall pressure can be obtained from a one-sided discretization of the compatibility relations (19.2.8), considered as a system where the equation for w_3 is replaced by the physical boundary condition.

These equations couple streamwise and normal derivatives of the pressure, for instance the equation for w_4 becomes at the solid wall

$$-\frac{1}{\rho c} \frac{\partial p}{\partial t} - \frac{1}{R_w} v_l^2 - \frac{v_l}{\rho c} \frac{\partial p}{\partial l} + \frac{1}{\rho} \frac{\partial p}{\partial n} = c \bar{\nabla} \cdot \bar{v} \quad (19.2.24)$$

where R_w is the wall radius of curvature and ∂l is the elementary arc length along the wall. If the continuity equation is subtracted from equation (19.2.24), after having replaced the density variations by the isentropic pressure variations, that is under the form

$$\frac{1}{\rho c} \frac{\partial p}{\partial t} + c \bar{\nabla} \cdot \bar{v} + \frac{\bar{v}}{\rho c} \cdot \bar{\nabla} p = 0 \quad (19.2.25)$$

one is left with the following equation, which is nothing else than the normal projection of the momentum equation at the wall:

$$\frac{1}{R_w} v_l^2 = \frac{1}{\rho} \frac{\partial p}{\partial n} \quad (19.2.26)$$

Hence a third way, recommended initially by Rizzi (1978), consists in discretizing directly the normal momentum equation at the wall.

Normal momentum equation Equation (19.2.26) is discretized in a one-sided way along the normal to the solid wall boundary.

In practical computations, however, one has seldom a mesh system formed by normals to the wall, that is mesh points aligned along the wall normals. Consequently, equation (19.2.26) is difficult to discretize as it stands and a more appropriate form is based on the projection of the momentum equation in arbitrary curvilinear coordinates, (ξ, η) in two dimensions, with the coordinate line $\eta = \text{constant}$ being the wall surface (Figure 19.2.6).

Projecting the momentum equation along the normal to the wall corresponds to taking the second contravariant component, if one defines $\xi = \xi^1$ and $\eta = \xi^2$. From the vanishing normal velocity at the wall,

$$\frac{d}{dt}(\vec{v} \cdot \vec{n}) = 0 \tag{19.2.27a}$$

one has

$$-\vec{n} \cdot \vec{\nabla} p + \rho \vec{v} \cdot \frac{d\vec{n}}{dt} = 0 \tag{19.2.27b}$$

For stationary walls, the second term reduces to the streamwise derivative

$$-\vec{n} \cdot \vec{\nabla} p + \rho \vec{v} \cdot (\vec{v} \cdot \vec{\nabla}) \vec{n} = 0 \tag{19.2.28}$$

With \vec{n} equal to the unit vector $\vec{1}_n$ along the normal, this equation leads directly to equation (19.2.26).

Taking $\vec{n} = \vec{e}^{-2} = \vec{\nabla} \eta$ leads to

$$\begin{aligned} \vec{e}^{-2} \cdot \vec{\nabla} p &= \frac{\partial p}{\partial n} \sqrt{\eta_x^2 + \eta_y^2} \\ &= g^{2a} \partial_a p = (\xi_x \eta_x + \xi_y \eta_y) \frac{\partial p}{\partial \xi} + (\eta_x^2 + \eta_y^2) \frac{\partial p}{\partial \eta} \\ &= \rho \vec{v} \cdot (\vec{v} \cdot \vec{\nabla}) \vec{n} = -\rho \vec{n} \cdot (\vec{v} \cdot \vec{\nabla}) \vec{v} \\ &= -\rho \vec{U} \vec{n} \cdot \frac{\partial \vec{v}}{\partial \xi} = -\rho \vec{U} \left(\eta_x \frac{\partial u}{\partial \xi} + \eta_y \frac{\partial v}{\partial \xi} \right) \end{aligned} \tag{19.2.29}$$

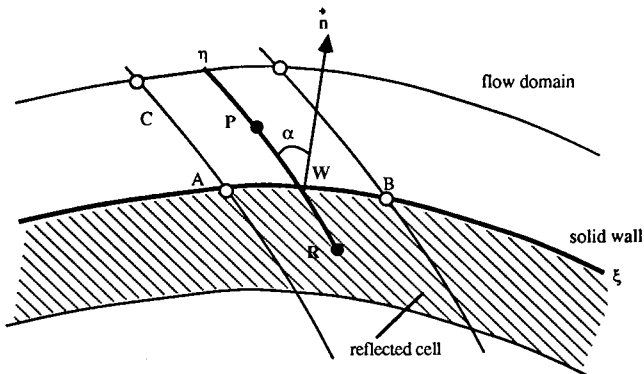


Figure 19.2.7 Reflected boundary cell at a solid boundary

The contravariant ξ component \tilde{U} of the velocity vector is defined by

$$\tilde{U} = \xi_x u + \xi_y v \quad (19.2.30)$$

where the subscripts on ξ and η indicate partial derivatives. This formula can be applied to estimate $\partial p / \partial n$ by calculating the metric coefficients from the mesh point coordinates. Note that alternative expressions can also be obtained from these equations (see Problem 19.20).

A current implementation technique is based on the definition of reflected cells as shown in Figure 19.2.7, where the flow variables are defined as to ensure vanishing normal velocities at the wall; that is one defines the conditions at the reflected point R by

$$\begin{aligned} \rho_R &= \rho_P \\ v_{IR} &= v_{IP} \\ v_{nR} &= -v_{nP} \\ p_R &= p_P - \left(\frac{\partial p}{\partial \eta} \right)_w \Delta \eta_{RP} \end{aligned} \quad (19.2.31)$$

The derivative in the direction of the curvilinear coordinate η is related to the normal pressure gradient by relations (19.2.29). The derivative $\partial p / \partial \eta$ is estimated at the wall and the wall values of all the variables are obtained from the arithmetic average between P and R. Hence,

$$p_w = \frac{p_P + p_R}{2} = p_P - \frac{1}{2} \left(\frac{\partial p}{\partial \eta} \right)_w \Delta \eta_{RP} \quad (19.2.32a)$$

If the radius of curvature is known, $\partial p / \partial n$ is given by equation (19.2.26) and $\partial p / \partial \eta$ is estimated directly from

$$\frac{\partial p}{\partial n} = \frac{\partial p}{\partial \eta} \left(\frac{\partial \eta}{\partial n} \right) + \frac{\partial p}{\partial \xi} \left(\frac{\partial \xi}{\partial n} \right) = \frac{\partial p}{\partial \eta} \frac{1}{\cos \alpha} + \frac{\partial p}{\partial \xi} \tan \alpha \quad (19.2.32b)$$

where the angle α is obtained from $\cos \alpha = (\text{area of cell}) / (AB \cdot AC)$ and $\partial p / \partial \xi$ can be approximated with a central finite difference of p along the solid wall.

A further improvement is obtained by the replacement of the second reflection condition on the tangential velocity at the wall by the condition of vanishing wall vorticity if the flow conditions are irrotational. In this case, the discretization of the following equation leads to an alternative to the third equation (19.2.31)

$$\frac{\partial v_t}{\partial n} + \frac{v_t}{R_w} = 0 \quad (19.2.33)$$

The normal derivative of the tangential velocity is estimated from the chain rule as in equation (19.2.32b). If the η direction is normal to ξ , equation (19.2.33) can be approximated as follows:

$$\frac{v_{IP} - v_{IR}}{\Delta \eta_{RP}} + \frac{v_{IP} + v_{IR}}{2R_w} = 0 \quad (19.2.34)$$

from which the tangential velocity in the reflected cell v_{IR} can be estimated, leading to

$$v_{IR} = v_{IP} \frac{1 + \Delta\eta_{RP}/R_w}{1 - \Delta\eta_{RP}/R_w} \quad (19.2.35)$$

19.2.5 Non-reflective boundary conditions

As in one dimension, non-reflective boundary conditions can be imposed as physical boundary conditions in order to prevent the outgoing waves from producing unwanted reflections at the boundaries.

Referring to the characteristic equations (19.2.7) and (19.2.8), written in the condensed form

$$\frac{\partial w_k}{\partial t} + (\vec{a}_k \cdot \vec{\nabla}) w_k = b_k \quad k = 1, \dots, 4 \quad (19.2.36)$$

where b_k represents the right-hand side of equations (19.2.8) and $\vec{a}_k = \lambda_k \vec{1}_n$.

For all characteristics corresponding to incoming waves in the direction normal to the boundary, that is with positive eigenvalues λ , the non-reflective boundary condition becomes

$$\frac{\partial w_k}{\partial t} = b_k \quad \text{for all } \lambda_k > 0 \quad (19.2.37)$$

For instance, at a subsonic outlet section where $\lambda_4 > 0$, this condition is written as

$$\vec{1}_n \cdot \frac{\partial \vec{v}}{\partial t} - \frac{1}{\rho c} \frac{\partial p}{\partial t} = c \frac{\partial v_t}{\partial l} \quad (19.2.38)$$

where the right-hand side represents the tangential variations of the velocity components in the boundary surface. When these variations are zero, either for uniform conditions in the exit surface or for normal exit velocities, then condition (19.2.38) is identical locally to the one-dimensional form.

The adaptation of Rudy and Strickwerda (1980) can be applied in the following form, instead of (19.2.38) for an imposed exit pressure p^* :

$$\frac{\partial v_n}{\partial t} - \frac{1}{\rho c} \frac{\partial p}{\partial t} - \frac{\alpha}{\rho c} (p - p^*) = c \frac{\partial v_t}{\partial l} \quad (19.2.39)$$

where $\alpha > 0$ has to be calibrated empirically.

19.3 THE FAR-FIELD BOUNDARY CORRECTIONS

In external as well as internal flow problems the inlet and outlet boundaries are assumed to be located far enough from the main flow region so that the influence of the flow disturbances does not affect the free-stream values.

Since these disturbances generally require long distances to damp out, the boundaries will have to be situated, in practice, at an appreciable distance from the source of the disturbances, for instance an airfoil in an external flow problem. In this latter case, a distance of the order of or larger than 50 chords between the airfoil and the far-field boundary is not uncommon.

These large distances have to be filled either with a very large number of mesh points in the far-field region, where on the other hand the flow variations are often unimportant, or with very large mesh cells having reduced accuracy. Both situations are undesirable and could be overcome if an approximate behaviour of the far-field flow would be known and matched to the interior flow field by an adaptation of the boundary conditions. As a consequence, the external boundaries could be taken closer to the disturbed flow region with a reduction in the total number of mesh points, reducing the total computational cost while improving the accuracy.

An approximate description of the far field can easily be obtained by introducing a perturbation field to the uniform flow and expressing it as an asymptotic series in a perturbation parameter. In the inviscid far field, the perturbation satisfies the small disturbance potential equation

$$(1 - M_\infty^2)\phi'_{x'x'} + \phi'_{y'y'} = 0 \quad (19.3.1)$$

where x' and y' are directions along and normal to the free-stream velocity and M_∞ the associated Mach number. The potential ϕ' is the isentropic disturbance field defining the perturbation velocities as

$$\vec{v}' = \vec{\nabla}\phi' \quad (19.3.2)$$

A solution can be obtained as a series expansion in function of x' and y' , or of corresponding polar coordinates. For external flow problems, a solution can be found of the form (see, for instance, Thomas and Salas, 1986)

$$\begin{aligned} u' &= \sum_{k=1}^{\infty} \frac{1}{r^k} [b'_k \cos(k\theta) + c'_k \sin(k\theta)] \\ v' &= \sum_{k=1}^{\infty} \frac{1}{r^k} [b'_k \sin(k\theta) + c'_k \cos(k\theta)] \end{aligned} \quad (19.3.3)$$

where r is the radius measured from the quarter chord of the airfoil and θ the polar angle. The coefficients can be obtained numerically by matching this expansion to the numerical solution along a boundary at a certain distance from the airfoil, such as the surface S_1 on Figure 19.3.1.

In the case of an isolated airfoil, however, theoretical far-field expansions can

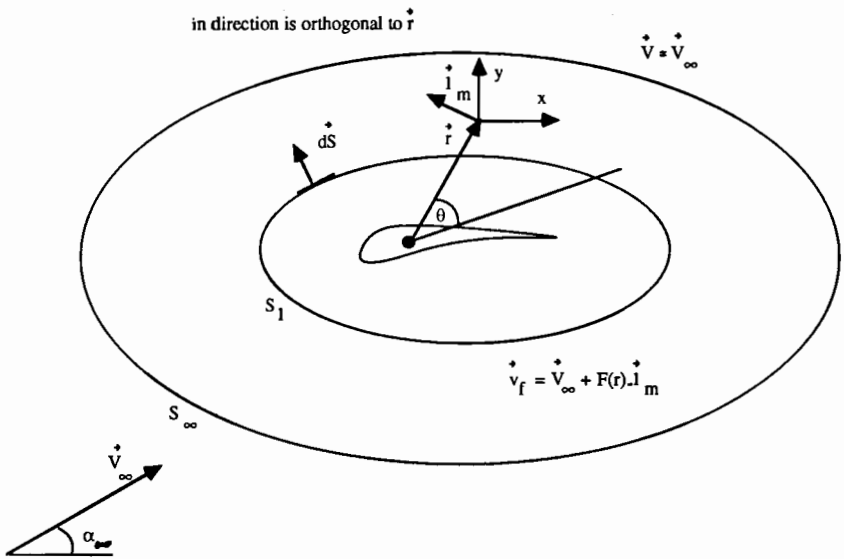


Figure 19.3.1 Far-field boundaries for flow along airfoil

be derived for thin airfoils, where the b' coefficients are related to the thickness distribution and the c' coefficients to the circulation.

To the lowest order one obtains the corrections u_f and v_f to the far-field velocities, expressed as fractions of the free-stream velocity \vec{V}_∞ , under an incidence angle of α_∞ :

$$\begin{aligned} \frac{u_f}{|\vec{V}_\infty|} &= \cos \alpha_\infty + F \sin \theta \\ \frac{v_f}{|\vec{V}_\infty|} &= \sin \alpha_\infty - F \cos \theta \end{aligned} \tag{19.3.4}$$

where F is defined as a function of the circulation Γ by

$$F = \frac{\Gamma}{|\vec{V}_\infty|} \frac{\beta}{2\pi r} \frac{1}{1 - M_\infty^2 \sin^2(\theta - \alpha_\infty)} \tag{19.3.5}$$

with

$$\beta = \sqrt{1 - M_\infty^2} \tag{19.3.6}$$

The circulation Γ is obtained from the lift coefficient

$$C_L = \frac{2\Gamma}{|\vec{V}_\infty|c} \tag{19.3.7}$$

for an airfoil with chord c , where the lift coefficient is calculated from a momentum flux balance over an arbitrary closed contour S around the airfoil.

The axial and normal forces L_x and L_y , expressed as coefficients, normalized by the free-stream dynamic pressure and the chord c , are calculated from the

following momentum balance (see, for instance, Yu *et al.*, 1983, for an overview of drag and lift calculations):

$$C_x = \frac{2L_x}{\rho_\infty(U_\infty^2 + V_\infty^2)c} = \frac{-2}{\rho_\infty(U_\infty^2 + V_\infty^2)c} \oint_S [\rho u(\vec{v} \cdot d\vec{S}) + p \vec{1}_x \cdot d\vec{S}] \quad (19.3.8)$$

$$C_y = \frac{2L_y}{\rho_\infty(U_\infty^2 + V_\infty^2)c} = \frac{-2}{\rho_\infty(U_\infty^2 + V_\infty^2)c} \oint_S [\rho v(\vec{v} \cdot d\vec{S}) + p \vec{1}_y \cdot d\vec{S}] \quad (19.3.9)$$

The corrected far-field velocities are to be introduced in the boundary conditions, replacing the velocities with the subscript B in the relations of Section 19.2.2.

The application of this correction leads to an improvement in the accuracy and allows the far-field boundary to be placed at distances of the order of five chords without penalty on the accuracy. An example, from Pulliam and Steger (1985), shows the variation of lift coefficient with the outer distance of the boundaries for an NACA 0012 airfoil at subsonic incidence conditions.

Figure 19.3.2 compares the variation of the lift coefficient with and without the far-field corrections, (19.3.4) to (19.3.6), demonstrating the spectacular improvement.

A more general formulation, valid for external and internal flows, has been developed by Gustafsson (1982), Ferm and Gustafsson (1982), Gustafsson and Ferm (1986), Verhoff (1985), Hirsch and Verhoff (1989). In this approach the Euler equations are linearized in the far field and analytical solutions are obtained for the perturbations from the uniform conditions at infinity, as a Fourier series expansion in the direction along the boundary, allowing also far field perturbations for the entropy waves. The coefficients of the expansion are written in the form of exponentials in the incoming direction, normal to the boundary. The linearized form of the compatibility equations (19.2.8) can be written as follows

$$\frac{\partial w'_1}{\partial \tau} + M_\infty \frac{\partial w'_1}{\partial x} = 0 \quad (19.3.10a)$$

$$\frac{\partial w'_2}{\partial \tau} + M_\infty \frac{\partial w'_2}{\partial x} + \frac{1}{2} \frac{\partial (w'_3 + w'_4)}{\partial y} = 0 \quad (19.3.10b)$$

$$\frac{\partial w'_3}{\partial \tau} + (M_\infty + 1) \frac{\partial w'_3}{\partial x} + \frac{\partial w'_2}{\partial y} = 0 \quad (19.3.10c)$$

$$\frac{\partial w'_4}{\partial \tau} + (M_\infty - 1) \frac{\partial w'_4}{\partial x} + \frac{\partial w'_2}{\partial y} = 0 \quad (19.3.10d)$$

where the dash indicates perturbations from the free stream values.

Considering the internal nozzle flow of Figure 19.3.3, an expansion of the form

$$w'_2 = \sum_{m=1}^{\infty} h_m(x) \sin \frac{m\pi y}{b} \quad (19.3.11a)$$

$$w'_3 = \sum_{m=1}^{\infty} f_m(x) \cos \frac{m\pi y}{b} \tag{19.3.11b}$$

$$w'_4 = \sum_{m=1}^{\infty} g_m(x) \cos \frac{m\pi y}{b} \tag{19.3.11c}$$

is considered.

Since the first characteristic variable, which is proportional to the entropy, is purely convected and decoupled from the other equations, we can solve separately for the entropy perturbation and remove the corresponding equation from the system (19.3.10).

The choice of the Fourier terms results from the flow tangency boundary condition at the solid walls $y = \pm b/2$. Introducing these solutions in the stationary form of equations (19.3.10) leads to the following system, for an arbitrary Fourier mode m , writing M instead of M_{∞} , the free stream Mach number and removing the subscript m on the amplitudes f, g and h .

$$\begin{aligned} (M + 1) \frac{\partial f}{\partial x} + \frac{m\pi}{b} h &= 0 \\ (M - 1) \frac{\partial g}{\partial x} + \frac{m\pi}{b} h &= 0 \\ M \frac{\partial h}{\partial x} - \frac{m\pi}{2b} (f + g) &= 0 \end{aligned} \tag{19.3.12}$$

For each Fourier mode, solutions of the form

$$\begin{vmatrix} f \\ g \\ h \end{vmatrix} = \begin{vmatrix} f \\ g \\ h \end{vmatrix}_0 e^{-\mu x} \tag{19.3.13}$$

can be applied in the inflow region, with x measured from the boundary on. The coefficients μ are eigenvalues of the system (19.3.12) and the amplitudes are proportional to the eigenvectors of this system. The general solution is of the form

$$\begin{vmatrix} f \\ g \\ h \end{vmatrix} = C_1 \begin{vmatrix} 1 \\ -1 \\ 0 \end{vmatrix} + C_2 \begin{vmatrix} \frac{\beta}{M + 1} \\ -\beta \\ \frac{1 - M}{1} \end{vmatrix} e^{-(m\pi/b\beta)x} + C_3 \begin{vmatrix} -\beta \\ M + 1 \\ \frac{\beta}{1 - M} \\ 1 \end{vmatrix} e^{(m\pi/b\beta)x} \tag{19.3.14}$$

From the properties of the characteristic variables it is known that w'_2 and w'_3 are characteristics propagating from left to right (for positive u), while w'_4 is propagating right to left for a subsonic flow, since they correspond respectively to wave speeds u , $u + c$ and $u - c$. Hence, in order to determine the far field disturbances we express the amplitudes of the incoming characteristic perturbations as zero at infinity, **leading to a correction on the physical boundary conditions for finite distances**, and the amplitudes of the outgoing characteristics are defined by the numerical solution at the boundary.

Hence, for the variables associated with the outgoing waves, a relation is obtained for the coefficients C by developing the numerically obtained internal solution at the boundary AA ($x = 0$), for instance, as a Fourier series in y .

Figure 19.3.4 shows an example, from Verhoff (1985), of a two dimensional nozzle flow comparing the computed solutions on the boundaries and in the constant area regions, with and without the far-field matching procedure.

The figures compare the Mach number distributions for the nozzle mesh shown in Figure 19.3.4 (a), when boundary conditions are applied at the sections AA and BB (solid line) or at the limits of the computational domain (dashed line).

Figure 19.3.4 (b) is obtained with characteristic-type boundary conditions, while Figure 19.3.4 (c) applies the perturbation expansion. As can be seen, the error introduced by applying these boundary conditions in sections AA and BB is very small, demonstrating the effectiveness of adapted far field corrections.

Another example is shown in the following figures for the transonic flow through a similar nozzle, demonstrating the validity of this boundary treatment for non-isentropic flows. Figure 19.3.5 shows the isoMach number distributions in the central part of the long channel, with the presence of a curved shock, resulting in a non uniform entropy downstream of the shock, comparing the results obtained for the extended and restricted domains, the latter with uncorrected (b) and corrected (c) boundary treatment.

The Mach number distributions on the lower and upper walls are shown on Figure 19.3.6, for the three cases of Figure 19.3.5. There is a shift in the shock position by one mesh cell, which is not very significant even on this relatively coarse mesh. The improvement due to the boundary corrections is clearly seen. Another measure of the corrections concerns the inlet angles; the corrected inlet angle for the short channel is 2.6 degrees, to be compared with the value of 2.7 degrees calculated along the same section of the long channel, while in the uncorrected case the inlet angle is fixed at zero degrees. Another display of the effects of the boundary treatment is shown on Figure 19.3.7 where the Mach number profiles are compared at inlet and outlet of the short channel. The differences between the dashed lines and the plus-symbols indicate the amplitude of the corrections on the short channel, while the solid line is the reference value from the long channel. The small difference between the latter and the corrected values of the short channel computation (+ symbols) is probably due to the fact that the boundaries of the long channel have not been taken far enough. This confirms again the efficiency of this boundary treatment.

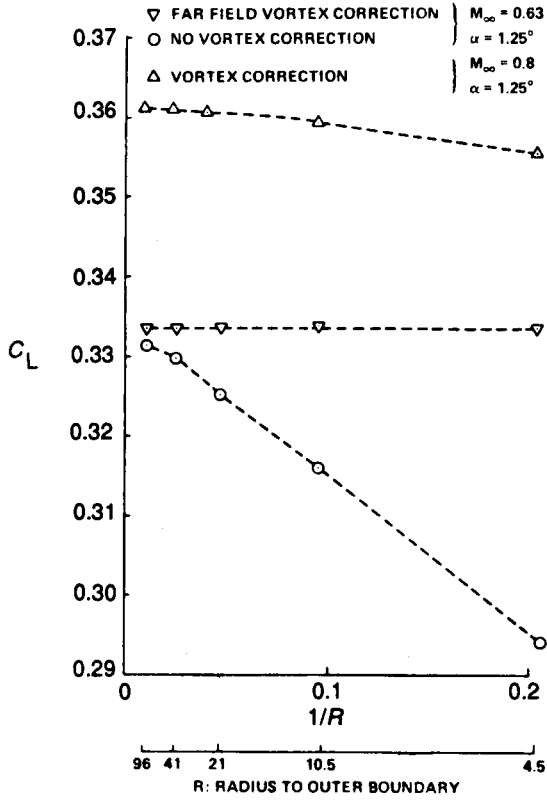


Figure 19.3.2 Effect on lift of varying outer boundary distances with and without vortex correction. (From Pulliam and Steger, 1985)

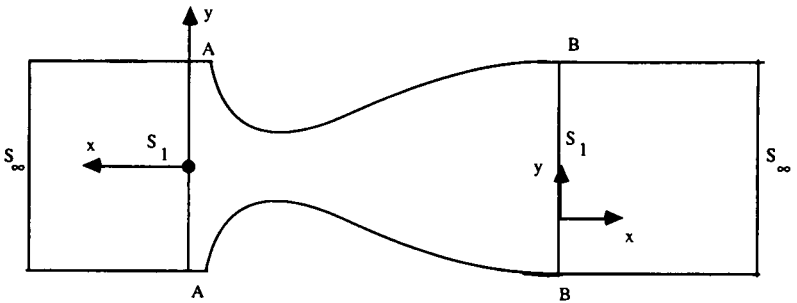
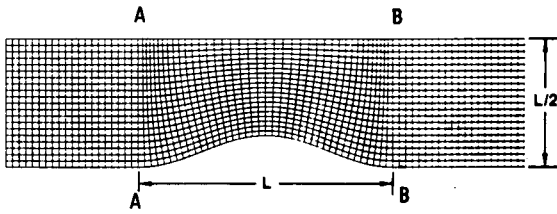
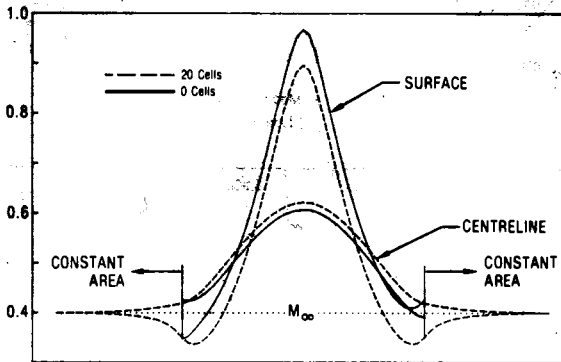


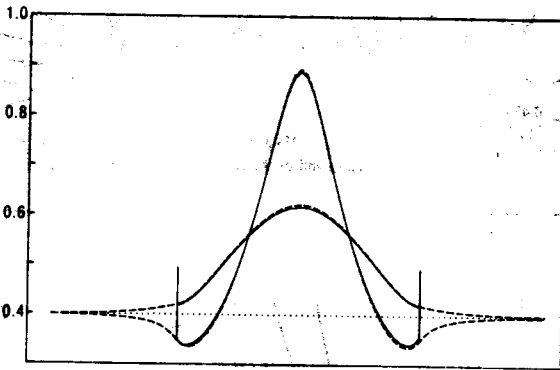
Figure 19.3.3 Far-field regions for nozzle flow. The regions left of AA and right of BB are considered as far field



(a) Nozzle geometry and grid



(b) Mach numbers distribution obtained with characteristic - type boundary conditions. Solid line : boundaries in AA, BB



(c) Mach number distribution obtained with perturbation boundary conditions. Solid line : boundaries in AA, BB

Figure 19.3.4 Comparison of characteristic and perturbation boundary conditions. (Courtesy A. Verhoff, McDonnell Aircraft Co., USA)

Therefore we suggest applying and deriving perturbative far field corrections whenever possible. It always reduces considerably the extension of the computational domain, while maintaining the required accuracy.

Applications of the Fourier series development of the flow disturbances along

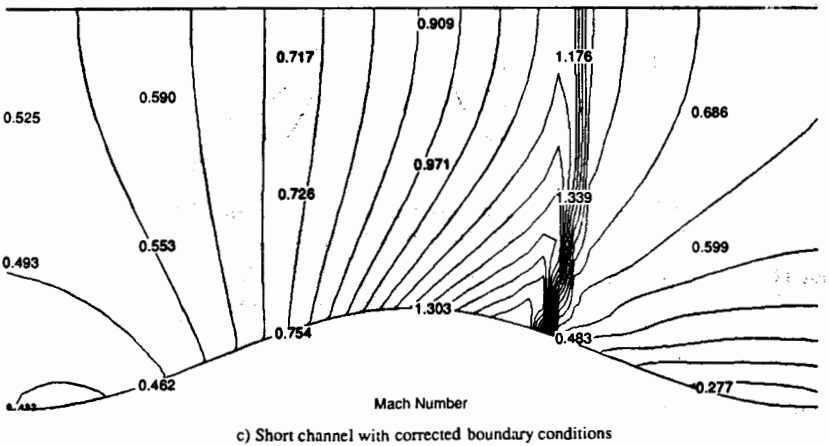
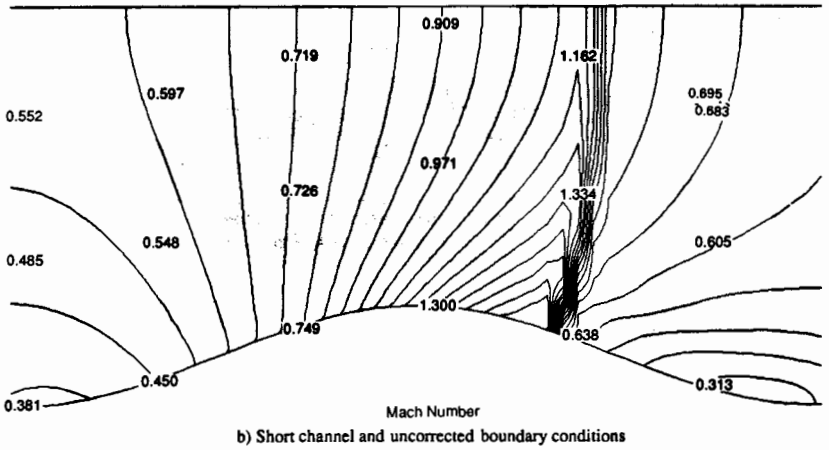
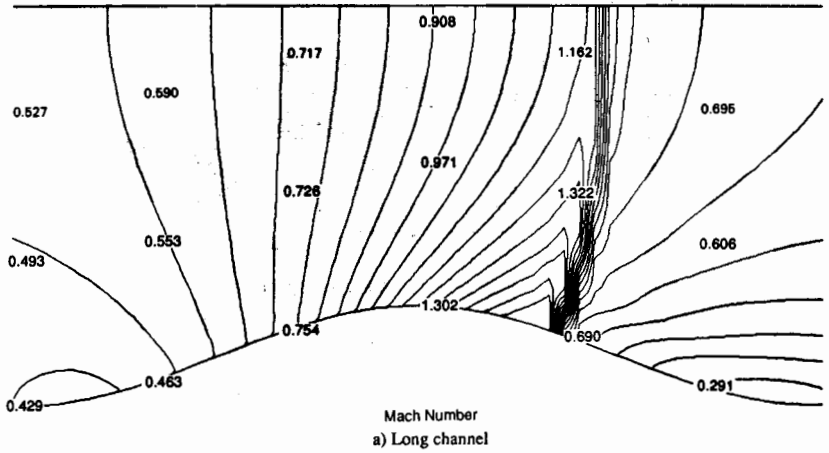


Figure 19.3.5 Comparison of iso-Mach lines in the central part of the sinusoidal channel at transonic conditions

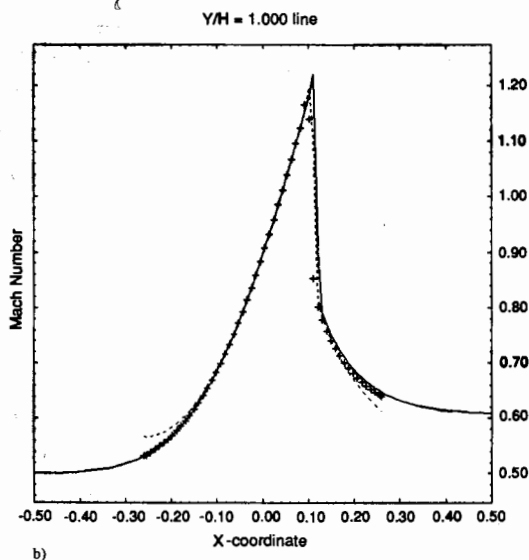
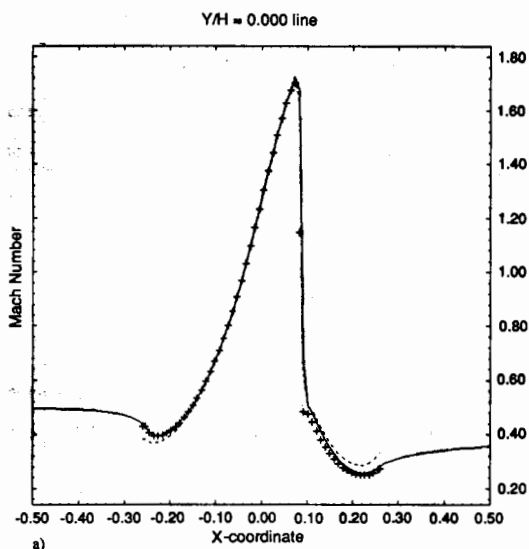


Figure 19.3.6 Comparison of Mach number distributions in the central part of the sinusoidal channel at transonic conditions on lower (a) and upper (b) walls
 Solid line: long channel
 Dashed line: short channel and uncorrected boundary conditions
 ++ symbols: short channel with corrected boundary conditions

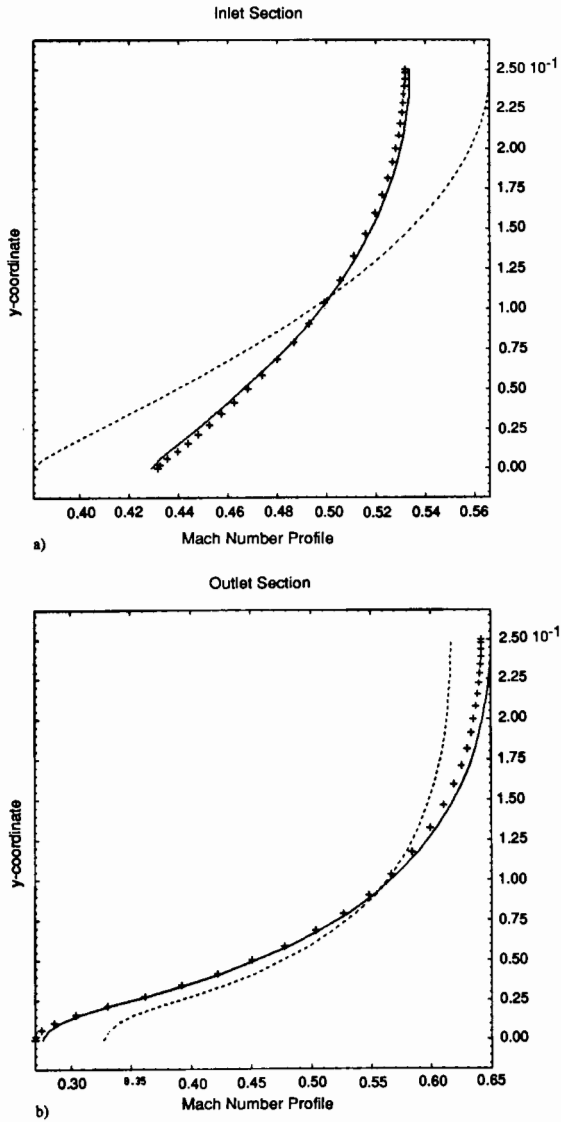


Figure 19.3.7 Comparison of Mach number distributions along the inlet (a) and exit (b) stations of the short sinusoidal channel at transonic conditions
 Solid line: long channel
 Dashed line: short channel and uncorrected boundary conditions
 ++ symbols: short channel with corrected boundary conditions

the boundaries have also been applied by Giles (1988), (1989) within the context of non-reflective boundary conditions.

It is of interest to notice the differences between the non-reflective boundary conditions and the far field corrections obtained by the above approach. Although the basic idea remains the same, namely to avoid incoming disturbances, the former approach expresses this condition at the finite distance location of the computational boundary, while the latter approach expresses this condition at infinity. From this requirement, an exact linearized solution is obtained in the far field. Hence the far field corrections give rise to incoming disturbances at finite distances which tend to zero at infinity. This is the correct physical assumption while the non-reflective conditions are approximations when expressed at finite distances.

However, linearized exact solutions cannot always be easily obtained and in these cases the application of non-reflective conditions at finite distances is the next best approximation.

19.4 THE KUTTA CONDITION

It is well known that inviscid flows over lifting bodies, such as airfoils, have an infinity of solutions depending on a free parameter, namely the circulation around the airfoil.

The Kutta condition states that the closest approximation to the physical, viscous reality is obtained for the value of the circulation which locates the downstream stagnation point at the sharp trailing edge of the airfoil.

This condition, which can be implemented in a variety of ways, is essential in potential flows in order to compute lifting airfoils. As seen in Chapter 13, a jump in potential equal to the circulation has to be introduced along a cut in the computational domain, simulating a singularity-vortex sheet. The intensity of the potential discontinuity is determined, for instance, by imposing equal pressures or velocities at the trailing edge points on the pressure and suction surfaces.

At a Workshop on inviscid transonic flow computations (Rizzi and Viviani, 1981), it appeared that computations based on the Euler equations, and which did not implement any form of Kutta condition, still produced accurate results, with the correct value of the circulation.

This has been confirmed since then by many computations on two-dimensional as well as three-dimensional airfoils and wings; see, for instance, Rizzi (1982, 1985).

It seems, therefore, that it is not necessary to impose a Kutta condition on calculations with time-dependent Euler flow models in order to obtain the correct lift on airfoils with sharp trailing edges. This remarkable result implies

the existence of some mechanism in the pseudo-time evolution of the computed Euler solutions, which reproduces and simulates the essential physical phenomena leading to the generation of circulation and lift.

It is well known (see, for instance, Prandtl, 1952, pp. 50–52, 69–70; Batchelor, 1970) that this mechanism is of a transient nature and is induced by the presence of an eddy at the trailing edge, generating a surface of discontinuity in the inviscid flow. In a viscous flow this surface of discontinuity will diffuse into a thin shear layer and form the wake of the airfoil.

Indeed, at the initial instants the flow behaves in an irrotational manner with a stagnation point *S* on the suction surface inducing a turning of the flow around the sharp trailing edge (Figure 19.4.1(a)).

Around the trailing edge, very strong velocity gradients exist since the inviscid, incompressible velocity tends to infinity at *P* and the compressible flow will expand up to zero vacuum pressure. By some mechanism, an eddy is formed at *P*, preventing the infinite velocities or the vacuum conditions, and a surface of discontinuity appears, also called a vortex sheet, along which the two flows from the pressure and suction sides merge with a discontinuity in the tangential velocity (Figure 19.4.1(b)).

Note that the generation of this surface of discontinuity is not in contradiction with Kelvin's theorems on the impossibility of vorticity creation in inviscid flows, since there are no streamlines that join points on the two sides of the surface of discontinuity. Therefore this surface is a possible weak solution of the Euler equations, in the same way as shocks.

The counterclockwise velocity induced by the eddy on the suction surface moves the stagnation point *S* towards the trailing edge *P*. As long as the stagnation point remains on the upper airfoil side, the discontinuity surface rolls up and feeds the eddy intensity, increasing the induced velocity which tends to move *S* towards *P*. After some short time, the stagnation point has indeed reached the trailing edge and the eddy is transported by convection downstream of the airfoil (Figure 19.4.1(c)).

Finally, a circulation appears around the airfoil, equal and opposite to the circulation around the downstream convected eddy (Figure 19.4.1(d)) such that the total circulation around any contour enclosing the airfoil and the rolling-up eddy is zero according to Kelvin's theorem.

This sequence of events can not be simulated with potential flows, since this isentropic, irrotational flow model does not allow for vortex sheets with a discontinuity in tangential velocities.

With the Euler flow model, on the other hand, vortex sheets can be captured by the computations and this transient sequence of events can be simulated numerically and inviscidly as soon as some mechanism exists that would trigger the generation of the trailing edge eddy of Figure 19.4.1(b).

Prandtl (1952) does not specify by which mechanism a trailing edge eddy can be produced, but it is clear from his remarks (pp. 51 and 58) that viscosity plays

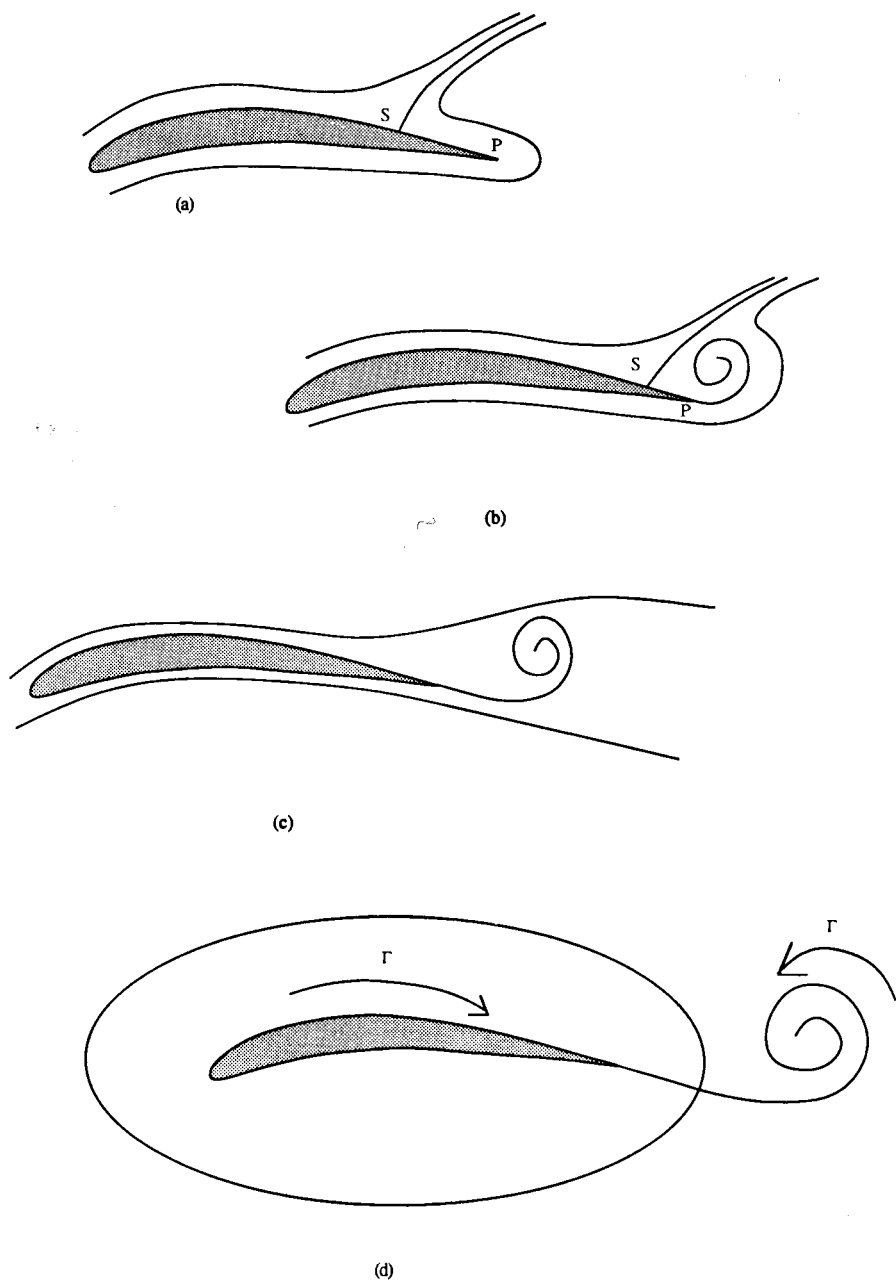
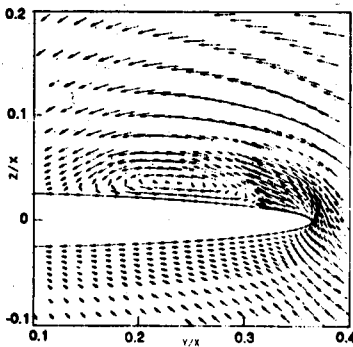


Figure 19.4.1 Mechanism behind the generation of lift on an airfoil

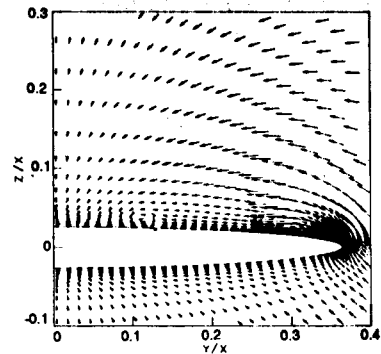
an essential, if not dominating, role in the vorticity generation at the trailing edge that feeds the eddy. Once this eddy is created the sequence of events described above proceeds in an inviscid way.

It is clear, therefore, that in the Euler computations that do not require the imposition of the Kutta condition, some mechanism has to exist that generates vorticity around the trailing edge in order to initiate the production of circulation. Remember, also, that in a real flow the physical circulation around airfoils is equal to the total amount of vorticity generated in the wall regions by viscosity (and eventually by non-uniform shocks). This vorticity feeds the downstream convected eddy.

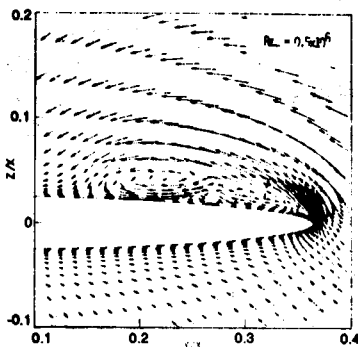
One possible mechanism can therefore be connected to the numerical dissipation present in every scheme, either from additional artificial viscosity or from the internal dissipation of the scheme needed for stability, both of which are proportional to the gradients of the flow variables and in particular of the



(a) Crossflow velocity vectors:
coarse grid Euler



(b) Crossflow velocity vectors: fine
grid Euler



(c) Crossflow velocity vectors:
conical Navier - Stokes

Figure 19.4.2 Effects of numerical dissipation on the vorticity generation in Euler flow solutions.
(From Newsome, 1985)

velocity. This provides a mechanism for the numerical generation of vorticity (and entropy) at the scale of the mesh. With the very strong velocity gradients at the sharp edge, even very small amounts of viscosity or dissipative effects will generate local entropy layers and hence induce vorticity.

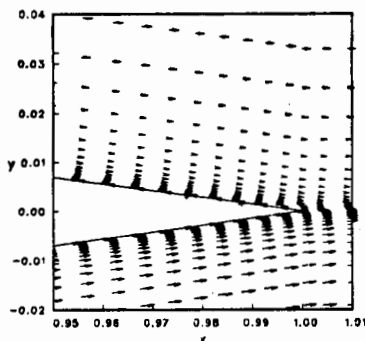
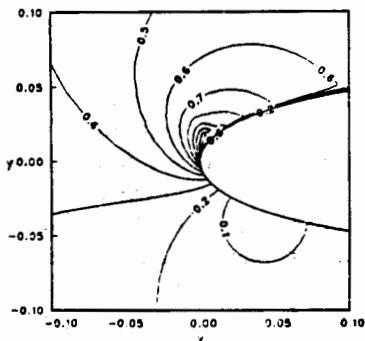
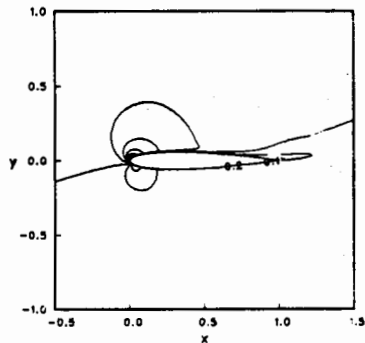
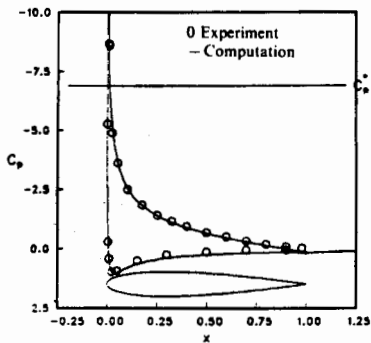
This is confirmed by various computations on coarse and fine grids (Barton and Pulliam, 1984; Newsome, 1985), which clearly show the numerical generation of vorticity or entropy layers by numerical dissipative effects. In this second reference (Newsome, 1985) an interesting test is run for a conical delta wing at supersonic Mach numbers and 10° incidence. This flow shows experimentally a large leading edge separation vortex and a smaller secondary viscous vortex, both of which are obtained with a Navier–Stokes computation (Figure 19.4.2c). The large separation vortex is also obtained with the Euler flow model on a coarse grid, although the smaller vortex (of viscous origin) does not appear. The coarse grid calculations are run without the imposition of a Kutta condition.

When the Euler flow is computed on a fine grid and the dissipation gradually switched off, the leading edge separation disappears from the computed solution, which is, however, a valid, converged solution of the Euler equations. When the Kutta condition is explicitly introduced in the fine grid calculations, the large local leading edge separation zone is recovered (Figure 19.4.2a, b).

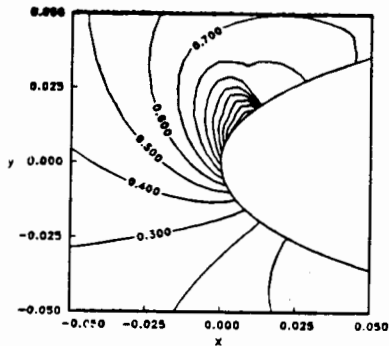
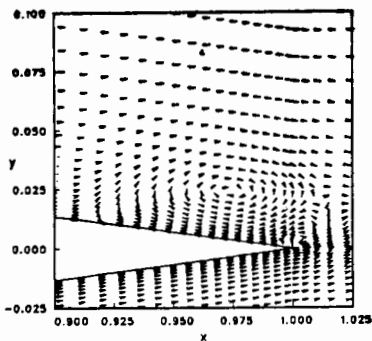
These interesting computations seem to confirm that numerical dissipation plays an essential role in the local generation of vorticity, and in addition also shows that some caution has to be exercised when interpreting numerical Euler solutions with large separated regions. Results can be obtained that are valid numerical solutions to the inviscid flow models, but that can not be considered as acceptable approximations to the limit of viscous flows for very high Reynolds numbers.

This is also shown by Barton and Pulliam (1984) for the flow along airfoils at subsonic free-stream velocities and high angles of attack. Figure 19.4.3 shows a computation of the flow along a NACA 0012 airfoil at an incident Mach number of 0.301 and 15° incidence, comparing a Navier–Stokes with a Euler computation on a fine mesh. The viscous, this shear layer computation gives a steady flow, fully confirmed by experimental data (Figure 19.4.3(a)), while the Euler solution is an unsteady flow with large separated vortex regions. This unsteady Euler flow is induced by the generation of vorticity due to a small normal recompression shock in the leading edge region, resulting from the strong leading edge expansion caused by the high incidence (Figure 19.4.3(b)). Although not a good approximation of the corresponding Navier–Stokes flow, it is nevertheless to be considered as a correct solution of the inviscid Euler equations.

The viscous solution exhibits also a strong leading edge acceleration which remains, however, fully subsonic, so that the generated vorticity, due only to the boundary layer vorticity, is not sufficient to induce the unsteady flow pattern generally produced by large amounts of concentrated vorticity, exemplified by the Von Karman vortex street periodic flow structure.



(a) Thin shear layer Navier-Stokes calculation



(b) Euler solution

Figure 19.4.3 Comparison between Euler and Navier-Stokes solutions for flow over a NACA 0012 airfoil at 15° incidence and 0.3 Mach number. (From Barton and Pulliam, 1984)

This suggests another mechanism that could contribute to the initial creation of an eddy at sharp edges as put forward by Rizzi (1982). In this mechanism, the large acceleration at the sharp edge leads to local supersonic flows with the subsequent creation of expansion fans, shocks and contact discontinuities, much like in the shock tube problem. The transient appearance of the shock wave creates vorticity and induces the vortex sheet surface to roll up into the eddy. Once the stagnation point is at the sharp edge, the local supersonic expansion disappears.

Note that the whole procedure described here is strongly dependent on the presence of a sharp edge. If the trailing or leading edges are rounded, then the above mechanisms do not operate and a Kutta condition is necessary to obtain lift on the smooth body. However, the position of the stagnation point at which the Kutta condition is to be imposed can only be determined by viscous considerations.

19.5 SUMMARY

Various methods can be adopted for the implementation of boundary conditions and any of these methods can be discretized in a variety of ways, applying various extrapolation formulas or different discretizations of the differential form of the characteristic relations.

A particular choice or combination of boundary conditions can have a considerable influence on the accuracy and even on the stability properties of the computational scheme; see, for instance, Trefethen (1983) and Foreman (1986) for examples and discussions of boundary condition influences.

It is strongly recommended to test, with any scheme, many options and combinations of implementations, by monitoring carefully the behaviour of variables at the boundaries, displaying local errors and following the conservation of variables such as total enthalpy for stationary flow problems or entropy. For instance, in test problems where exact or reference solutions are available, one should plot the detailed error evolution at the boundaries. This reveals the detailed boundary behaviour of the solution and allows the wave reflections and influence on accuracy, stability and convergence rate of the boundary treatment to be controlled.

References

- Barton, J. T., and Pulliam, T. H. (1984). 'Airfoil computation at high angles of attack, inviscid and viscous phenomena.' *AIAA Paper 84-0524*, AIAA 22nd Aerospace Sciences Meeting.
- Batchelor, G. K. (1970). *An Introduction to Fluid Dynamics*, Cambridge: Cambridge University Press.
- Bayliss, A., and Turkel E. (1982). 'Far field boundary conditions for compressible flows.' *Journal Computational Physics*, **48**, 182-99.
- Beam, R. M., Warming, R. F., and Yee, H. C. (1981). 'Stability analysis for numerical boundary conditions and implicit difference approximations of hyperbolic equations.'

- In *Numerical Boundary Condition Procedures*, NASA CP 2201, pp. 257–82, NASA AMES Research Center.
- Chakravarthy, S. R. (1983). 'Euler equations—implicit schemes and boundary conditions.' *AIAA Journal* **21**, 699–706.
- Engquist, B., and Majda, A. (1977). 'Absorbing boundary conditions for the numerical simulation of waves.' *Mathematics of Computation*, **31**, 629–51.
- Engquist, B., and Majda, A. (1979). 'Radiation boundary conditions for acoustic and elastic wave calculations.' *Comm. Pure and Applied Mathematics*, **32**, 312–58.
- Ferm, L., Gustafsson, B. (1982). 'A downstream boundary procedure for the Euler equations.' *Computers and Fluids*, **10**, 261–276.
- Foreman, M. G. G. (1986). 'An accuracy analysis of boundary conditions for the forced shallow water equations.' *Journal Computational Physics*, **64**, 334–67.
- Giles, M. B. (1988). 'Non-reflecting boundary conditions for the Euler equations.' *Technical Report TR-88-1, MIT Computational Fluid Dynamics Laboratory, Massachusetts Institute of Technology, USA.*
- Giles, M. B. (1989). 'Non-reflecting boundary conditions for Euler equation calculations.' *AIAA Paper-89-1942, Proc. AIAA 9th Computational Fluid Dynamics Conference*, 143–152.
- Gottlieb, D., and Turkel, E. (1978). 'Boundary conditions for multistep finite difference methods for time-dependent equations.' *Journal Computational Physics*, **26**, 181–96.
- Griffin, M. D., and Anderson, J. D. (1977). 'On the application of boundary conditions to time dependent computations for quasi one dimensional fluid flows.' *Computers and Fluids*, **5**, 127–37.
- Gustafsson, B. (1975). 'The convergence rate for difference approximations to mixed initial boundary value problems.' *Mathematics of Computation*, **29**, 396–406.
- Gustafsson, B. (1982). 'The choice of numerical boundary conditions for hyperbolic systems.' *Journal of Computational Physics*, **48**, 270–283.
- Gustafsson, B., Ferm, L. (1986). 'Far field boundary conditions for steady state solutions to hyperbolic systems.' In *Nonlinear Hyperbolic Problems*. (Eds. C. Carasso, P. Raviart, D. Serre), *Lecture Notes in Mathematics*, Vol. **1270**, Springer Verlag, Berlin.
- Gustafsson, B., and Kreiss, H. O. (1979). 'Boundary conditions for time dependent problems with an artificial boundary.' *Journal Computational Physics*, **30**, 333–51.
- Gustafsson, B., Kreiss, H. O., and Sundström, A. (1972). 'Stability theory of difference approximations for mixed initial boundary value problems, II.' *Mathematics of Computation*, **26**, 649–86.
- Hedstrom, G. W. (1979). 'Non reflecting boundary conditions for non linear hyperbolic systems.' *Journal Computational Physics*, **30**, 222–37.
- Higdon, R. L. (1986). 'Initial boundary value problems for linear hyperbolic systems.' *SIAM Review*, **28**, 177–217.
- Hirsch, Ch., Verhoff, A. (1989). 'Far field numerical boundary conditions for internal and cascade flow computations.' *AIAA Paper-89-1943, Proc. AIAA 9th Computational Fluid Dynamics Conference*, pp. 154–168.
- Kreiss, H. O. (1968). 'Stability theory for difference approximations of mixed initial boundary value problems, I.' *Mathematics of Computation*, **22**, 703–14.
- Kreiss, H. O. (1970). 'Initial boundary value problem for hyperbolic systems.' *Comm. Pure and Applied Mathematics*, **23**, 273–98.
- Kreiss, H. O. (1974). 'Boundary conditions for hyperbolic differential equations.' *Proc. Dundee Conference on Numerical Solution of Differential Equations, Lecture Notes in Mathematics*, **363**, Berlin: Springer Verlag.
- Lerat, A., Sides, J., and Daru, V. (1984). 'Efficient computation of steady and unsteady transonic flows by an implicit solver.' In W. G. Habashi, (ed.), *Advances in Computational Transonics*, Pineridge Press.
- Moretti, G. (1981). 'A physical approach to the numerical treatment of boundaries in gas dynamics.' In *Numerical Boundary Condition Procedures*, NASA CP 2201, pp. 73–96, NASA AMES Research Center.

- Osher, S. (1969a). 'Systems of difference equations with general homogeneous boundary conditions.' *Trans. Am. Math. Soc.*, **137**, 177–201.
- Osher, S. (1969a). 'Stability of difference approximations of dissipative type for mixed initial-boundary value problems I.' *Mathematics of Computation*, **23**, 335–40.
- Newsome, R. W. (1985). 'A comparison of Euler and Navier–Stokes solutions for supersonic flow over a conical delta wing.' *AIAA Paper 856-0111*, AIAA 23rd Aerospace Sciences Meeting.
- Prandtl L. (1952). *Essentials of Fluid Dynamics*, London: Blackie and Sons Ltd.
- Pulliam, T. H., and Steger, J. L. (1985). 'Recent improvements in efficiency, accuracy and convergence for implicit approximate factorization algorithms.' *AIAA Paper-85-0360*, AIAA 23rd Aerospace Sciences Meeting.
- Rai, M. M., and Chaussee, D. S. (1983). 'New implicit boundary procedures: theory and applications.' *AIAA Paper 83-0123*, AIAA 21st Aerospace Sciences Meeting.
- Rizzi, A. W. (1978). 'Numerical implementation of solid-body boundary conditions for the Euler equations.' *ZAMM*, **58**, 301–4.
- Rizzi, A. (1982). 'Damped Euler equation method to compute transonic flow around wing–body combinations.' *AIAA Journal*, **20**, 1321–8.
- Rizzi, A. (1985). 'Test cases for inviscid flow field methods.' *AGARD Report AR-211*.
- Rizzi, A., and Viviand, H. (eds) (1981). Proc. GAMM Workshop on Numerical Methods for the Computation of Inviscid Transonic Flows with Shock Waves. *Notes on Numerical Fluid Dynamics*, Vol. 3, Braunschweig/Wiesbaden: Vieweg.
- Roe, P. L. (1986). 'Remote boundary conditions for unsteady multidimensional aerodynamic computations.' *ICASE Report 86-75*, NASA Langley Research Center.
- Rudy, D. H., and Strickwerda, J. C. (1980). 'A non-reflecting outflow boundary condition for subsonic Navier–Stokes calculations.' *Journal Computational Physics*, **36**, 55–70.
- Steger, J. L., Pulliam, T. H., and Chima, R. V. (1980). 'An implicit finite difference code for inviscid and viscous cascade flows.' *AIAA Paper 80-1427*, AIAA 13th Fluid and Plasma Dynamics Conference, July 1980.
- Thomas, J. L., and Salas, M. D. (1986). 'Far field boundary conditions for transonic lifting solutions to the Euler equations.' *AIAA Journal*, **24**, 1074–80.
- Thompson, K. W. (1987). 'Time dependent boundary conditions for hyperbolic systems.' *Journal Computational Physics*, **68**, 1–24.
- Trefethen, L. N. (1983). 'Group velocity interpretation of the stability theory of Gustafsson, Kreiss and Sundström.' *Journal Computational Physics*, **49**, 199–217.
- Trefethen, L. N. (1984). 'Instability of difference models for hyperbolic initial boundary value problems.' *Comm. Pure and Applied Mathematics*, **37**, 329–67.
- Trefethen, L. N. (1985). 'Stability of finite difference models containing two boundaries or interfaces.' *Mathematics of Computation*, **45**, 279–300.
- Verhoff, A. (1985). 'Modeling of computational and solid surface boundary conditions for fluid dynamics calculations.' *AIAA Paper 85-1496*, Proc. AIAA 7th Computational Fluid Dynamics Conference.
- Warming, R. F., Beam, R. M., and Yee, H. C. (1983). 'Lecture notes on the stability of difference approximations for initial boundary value problems.' *NASA Report TM-84318*.
- Wornom, S. F., and Hafez, M. M. (1984). 'A rule for selecting analytical boundary conditions for the conservative quasi-one-dimensional nozzle flow equations.' *AIAA Paper 84-0431*, AIAA 22nd Aerospace Sciences Meeting.
- Yee, H. C. (1981). 'Numerical approximations of boundary conditions with applications to inviscid gas dynamics.' *NASA Report TM-81265*.
- Yee, H. C., Beam, R. M., and Warming, R. F. (1982). 'Boundary approximation for implicit schemes for one-dimensional inviscid equations of gas dynamics.' *AIAA Journal*, **20**, 1203–11.
- Yu, N. J., Chen, H. C., Samant, A. A., and Rubbert, P. E. (1983). 'Inviscid drag calculations for transonic flows.' *AIAA Paper 83-1928*, Proc. AIAA 6th Computational Fluid Dynamics Conference, pp. 283–92.

PROBLEMS

Problem 19.1

Investigate the well-posedness of the system of variables (s, c, u) with regard to the acceptable combinations of boundary variables for a subsonic inlet and outlet section, following the method of Section 19.1.3. Refer also to Problem 16.19.

Problem 19.2

Repeat Problem 19.1 for the variables (ρ, u, s) and $(\rho, \rho u, p)$. Refer to Problems 16.20 and 16.21.

Problem 19.3

Apply the boundary treatment by characteristic extrapolation of Section 19.1.5 to a subsonic inlet section in a one-dimensional flow, considering that ρ and u are given as physical boundary conditions. Determine the boundary relations for p and for the conservative variables.

Problem 19.4

Work out the boundary procedure for MacCormack's scheme applying first-order space extrapolation on the conservative variables.

Consider the four possibilities for sub/supersonic inlet/outlet sections with ρ and u fixed at a subsonic inlet and p fixed at a subsonic outlet.

Apply the relation $\rho E = p/(\gamma - 1) + \rho u^2/2$ to obtain p at the inlet and ρE at the outlet.

Work out this procedure for the variables U and for the variations ΔU .

Hint: In the second case write at the inlet $\Delta p/(\gamma - 1) = \Delta(\rho E) - u\Delta(\rho u) - u^2\Delta\rho/2$ where $\Delta(\rho E)$ is extrapolated. At the outlet $\Delta\rho$ and $\Delta(\rho u)$ are extrapolated and Δp is known and generally equal to zero.

Problem 19.5

Reproduce the boundary treatment of Example 19.1.3, based on compatibility relations and time-differenced physical boundary conditions, for imposed values of u and p at the subsonic inlet.

Find the matrices P_1 , P_2 and P^* .

Problem 19.6

Redefine the boundary procedure based on characteristic extrapolation with MacCormack's scheme, as developed in Example 19.1.1, with the non-reflecting conditions for the physical boundary values.

Problem 19.7

Repeat Problem 19.6 with a first-order extrapolation of the conservative variables as numerical boundary conditions.

Problem 19.8

Solve the one-dimensional stationary nozzle flow with the MacCormack scheme and first-order extrapolated boundary conditions on the conservative variables.

Consider the different cases of Problem 16.26 for the diverging nozzle and of Problem 16.27 for the converging–diverging nozzle.

Plot the errors in mass flux and the entropy and compare the results with the exact solution.

Compare with the zero-order extrapolated boundary conditions.

Problem 19.9

Solve the one-dimensional stationary nozzle flow with the MacCormack scheme and characteristic first-order extrapolated boundary conditions, following Example 19.1.1.

Consider the different cases of Problem 16.26 for the diverging nozzle and of Problem 16.27 for the converging–diverging nozzle.

Plot the errors in mass flux and the entropy and compare the results with the exact solution.

Compare with the zero-order extrapolated boundary conditions.

Problem 19.10

Repeat the previous problem by introducing the non-reflecting boundary conditions.

Compare also with the form (19.1.81) for the non-reflecting condition at exit.

Problem 19.11

Develop Chakravarthy's boundary treatment for a subsonic inlet, with enthalpy h and entropy s as physical imposed variables. Work out all the matrices and equations and write them out explicitly.

Problem 19.12

Solve the one-dimensional stationary nozzle flow with the MacCormack scheme and the boundary treatment of Example 19.1.4, with p , ρ and u as boundary variables.

Consider the different cases of Problem 16.26 for the diverging nozzle and of Problem 16.27 for the converging–diverging nozzle.

Plot the errors in mass flux and the entropy and compare the results with the exact solution.

Compare with the zero-order extrapolated boundary conditions.

Problem 19.13

Solve the one-dimensional stationary nozzle flow with the Beam and Warming scheme and various boundary extrapolation formulas on the conservative variables, with p , u and ρ as boundary variables.

Consider the different cases of Problem 16.26 for the diverging nozzle and of Problem 16.27 for the converging–diverging nozzle.

Plot the errors in mass flux and the entropy and compare the results with the exact solution.

Compare with the zero-order extrapolated boundary conditions.

Problem 19.14

Solve the one-dimensional stationary nozzle flow with the Beam and Warming scheme $\theta = 1$, $\xi = 0$ and the characteristic boundary treatment, with p , u and ρ as boundary variables. Test different discretizations, comparing first- and second-order one-sided difference formulas.

Consider the different cases of Problem 16.26 for the diverging nozzle and of Problem 16.27 for the converging-diverging nozzle.

Plot the errors in mass flux and the entropy and compare the results with the exact solution.

Compare with the zero-order extrapolated boundary conditions.

Problem 19.15

Solve the one-dimensional stationary nozzle flow with the Beam and Warming scheme $\theta = 1$, $\xi = 0$ and the boundary treatment of Example 19.1.4.

Consider the different cases obtained in Problems 16.26 and 16.27.

Plot the errors in mass flux and the entropy and compare the results with the exact solution.

Problem 19.16

Solve the shock tube problem for the first case of Problem 16.25 with MacCormack's scheme, applying the compatibility relations for the numerical conditions and the non-reflective relations for the physical boundary conditions. Perform the calculations for a sufficient number of time steps until the waves reach the exit boundary.

Observe the effects of the non-reflective condition by a comparison with a one-sided discretization of the compatibility relation for the incoming characteristic.

Problem 19.17

Define the matrix transformations for a two-dimensional flow between the characteristic variables and various appropriate combinations of primitive variables ρ, u, v, p , following the methodology of Section 19.1.3, for

- (a) a subsonic inlet,
- (b) a subsonic outlet,
- (c) a solid wall boundary.

Determine which combinations lead to an ill-posed boundary formulation.

Problem 19.18

Define the two-dimensional matrix transformations between the characteristic variables and various appropriate combinations of the variables s, u, v, H , following the methodology of Section 19.1.3, for

- (a) a subsonic inlet,
- (b) a subsonic outlet
- (c) a solid wall boundary.

Determine which combinations lead to an ill-posed boundary formulation.

Problem 19.19

Work out the boundary formulation of Section 19.1.5 for a two-dimensional flow, for

- (a) a subsonic inlet with s, H, u fixed,
- (b) a subsonic outlet with p fixed,
- (c) a solid wall boundary with vanishing normal velocity.

Write out the different matrices and the final boundary system of equations.

Problem 19.20

Show from equations (19.2.28) and (19.2.29) that the normal pressure gradient can be written as

$$\frac{\partial p}{\partial n} = \rho \tilde{U} \bar{v} \cdot \frac{\partial \bar{\mathbf{1}}_n}{\partial \xi} = \rho \tilde{U} \left(u \frac{\partial \eta_x}{\partial \xi} + v \frac{\partial \eta_y}{\partial \xi} \right)$$

or as

$$\frac{\partial p}{\partial n} = - \frac{\rho \tilde{U}}{\sqrt{\eta_x^2 + \eta_y^2}} \bar{n} \cdot \frac{\partial \bar{v}}{\partial \xi} = - \frac{\rho \tilde{U}}{\sqrt{\eta_x^2 + \eta_y^2}} \left(\eta_x \frac{\partial u}{\partial \xi} + \eta_y \frac{\partial v}{\partial \xi} \right)$$

Problem 19.21

Consider the two-dimensional oblique shock reflection on a flat plate and discretize on a rectangular mesh defined as a cell-centred finite volume mesh, whereby no mesh points are located on the plate; refer to Figure 19.2.7.

Apply the Jameson scheme to this problem with determination of the pressure from the reflected cell method of equations (19.2.31) and (19.2.32).

Compare the convergence rates with and without residual smoothing.

Problem 19.22

Solve the reflected shock problem on a flat plate with the Beam and Warming scheme from a discretization with a cell vertex finite volume or, equivalently, a finite difference discretization, whereby the mesh points are on the flat plate.

Obtain the wall variables from the resolution of the difference equations at the wall by applying the interior central discretization scheme after introduction of reflected wall cells.

Compare with a discretization based on the compatibility relations at the wall for the determination of the wall variables.

Problem 19.23

Repeat Problem 19.22 by replacing the time integration by a fourth-order Runge-Kutta method, following Jameson's approach but keeping the same space discretization.

Compare the details of the boundary treatment with the procedure of Problem 19.21.

Problem 19.24

Work out in detail the discretized form for the wall pressure in the case of a curved wall as in Figure 19.2.7, following the relations (19.2.31) and (19.2.32) for a reflected wall cell.

Problem 19.25

Work out equation (19.2.34) when the η direction is not perpendicular to the wall surface, following the development of equation (19.2.32).

Chapter 20

Upwind Schemes for the Euler Equations

The schemes discussed in Chapters 17 and 18 are based on central space discretizations and have a symmetry with respect to a change in sign of the Jacobian eigenvalues which does not distinguish upstream from downstream influences. Hence the physical propagation of perturbations along characteristics, typical of hyperbolic equations, is not considered in the definition of the numerical model.

The family of upwind schemes, whose origin may be taken back to Courant, Isaacson and Reeves (1952), is directed towards an introduction of the physical properties of the flow equations into the discretized formulation and has led to the family of techniques known as upwinding, covering a variety of approaches, such as flux vector splitting, flux difference splitting and various 'flux controlling' methods.

Other schemes based on characteristic formulations, such as the λ scheme of Moretti (1979), also rely on the physical propagation information contained in the equations. They are, however, non-conservative and require some shock fitting in the presence of discontinuities.

As seen earlier, all second-order central schemes generate oscillations in the vicinity of discontinuities, which have to be damped by the addition of artificial dissipation terms. Constructing schemes which take into account the essential physical properties of the equations aim at preventing the creation of unwanted oscillations.

In smooth regions of the flow, where the flow variables can be considered as continuous, the central schemes based on Taylor series expansions can be applied with any order of accuracy. This will be the case even for supersonic flows, the apparent contradiction between the physical one-way propagation of waves and the symmetrical central differenced schemes which are direction independent, being resolved by considering the analytic continuation properties of smooth functions. The validity of Taylor series expansions expresses, indeed, a most remarkable property of continuous functions, namely that it suffices to know the value of a continuous function in a *single* point, together with a sufficiently high number of derivatives in that same point, to be able to reconstruct the function in an increasingly large domain around that point. In

the limit, the complete *local* knowledge of a function, that is the knowledge of its value and all its derivatives in a single point, is equivalent to the knowledge of the function everywhere. However, as soon as discontinuities appear this information is destroyed and more physical input is required in order to resolve the non-linear behaviour.

The introduction of physical properties in the discretization process of the Euler equations can be done at different levels.

The first level introduces only information on the sign of the eigenvalues, whereby the flux terms are split and discretized directionally according to the sign of the associated propagation speeds. This leads to the *flux vector splitting* methods and will be described in Sections 20.2 to 20.4.

A higher level of introduction of physical properties into the definition of the scheme can, however, be defined, following the very remarkable scheme of Godunov (1959). In Godunov's method, the conservative variables are considered as piecewise constant over the mesh cells at each time step and the time evolution is determined by the exact solution of the Riemann (shock tube) problem at the inter-cell boundaries. Hence, properties derived from the exact *local solution* of the Euler equations are introduced in the discretization. This approach has been extended to higher orders, as well as to variants, whereby the local Riemann problem is only approximately solved through approximate Riemann solvers. They are referred to sometimes as *flux difference splitting* methods and we will refer to the family of methods which call on exact or approximate local properties of basic solutions to the Euler equations as *Godunov-type* methods.

Section 20.1 introduces the principles of the upwind schemes, while the basic concepts and properties of flux vector splitting are discussed in Section 20.2. The first-order discretization techniques applied to one-dimensional flux vector splitting are presented in Section 20.3 and extended to multi-dimensions in Section 20.4. Section 20.5 presents the basic first-order Godunov scheme and the approximate Riemann solvers of Roe and Osher.

The schemes presented in this chapter are restricted to first-order accuracy, while higher-order upwind schemes will be discussed in Chapter 21.

20.1 THE BASIC PRINCIPLES OF UPWIND SCHEMES

The original scheme of Courant *et al.* (1952) was based on the characteristic form of the equations $u_t + au_x = 0$ and a discretization depending on the sign of the eigenvalue a .

With a first-order forward difference in time, namely the explicit Euler method, it has been noted that the central difference of u_x leads to an unstable scheme. However, with a one-sided differencing the following scheme can be considered for $a > 0$:

$$u_i^{n+1} = u_i^n - \sigma(u_i^n - u_{i-1}^n) \quad (20.1.1)$$

Its amplification function is

$$G = 1 - 2\sigma \sin^2 \frac{\phi}{2} - I\sigma \sin \phi \quad (20.1.2)$$

which is represented by a circle in the complex G plane, with centre at $(1 - \sigma)$ on the real axis and radius σ , as seen in Chapter 8 in Volume 1. Hence scheme (20.1.1) will be stable for values of the Courant number σ between zero and one:

$$0 \leq \sigma \leq 1 \quad (20.1.3)$$

but unstable for negative characteristic speeds. The truncation error ε_T is

$$\varepsilon_T = \frac{a \Delta x}{2} (1 - \sigma) u_{xx} \quad (20.1.4)$$

showing that the scheme is only first-order accurate in space and time and that the equivalent equation has a dissipative term with a numerical viscosity coefficient equal to $a \Delta x (1 - \sigma)/2$.

It is to be observed that this viscosity term vanishes for $a = 0$, that is when the characteristic eigenvalues pass through zero, as will be the case in stagnation regions and at sonic transitions. Comparing with the numerical viscosity introduced by the Lax–Friedrichs scheme, which is also first-order accurate, it is seen from equation (17.1.8) that in this latter scheme the numerical dissipation never vanishes and is higher than (20.1.4) by a factor equal to $(\sigma + 1)/\sigma$.

Hence, the upwind scheme may be expected to lead to a better representation of discontinuities. This is clearly seen on Figure 20.1.1, displaying the solutions to Burgers equation for a moving discontinuity at $\sigma = 0.5$ after 80 time steps. This property of vanishing dissipation at sonic transitions is needed in order to be able to resolve sharp discontinuities, but can also lead to non-physical shocks.

Notice the odd–even oscillations of the Lax–Friedrichs scheme.

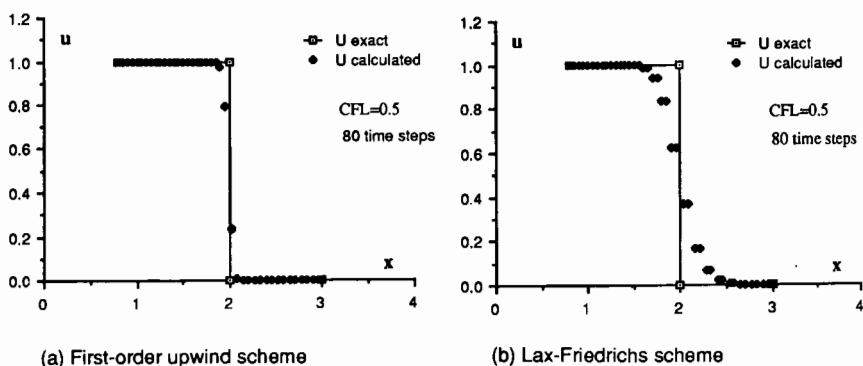


Figure 20.1.1 Solution to Burgers equation for a moving discontinuity

For negative propagation speeds, $a < 0$, the following one-sided scheme is stable:

$$u_i^{n+1} - u_i^n = -\sigma(u_{i+1}^n - u_i^n) \quad (20.1.5)$$

The amplification matrix is

$$G = 1 + 2\sigma \sin^2 \frac{\phi}{2} - I\sigma \sin \phi \quad (20.1.6)$$

and is lower than one in modulus for

$$-1 \leq \sigma \leq 0 \quad (20.1.7)$$

This shows that an upwind scheme cannot be simultaneously stable for both positive and negative eigenvalues. Steger and Warming (1981) give arguments to support this property for any non-symmetrical upwind sided scheme.

Schemes (20.1.1) and (20.1.5) are called *upwind schemes*. They apply a discretization that depends on the propagation direction of the wave or on the sign of the convection velocity a .

This also affects the boundary conditions. Scheme (20.1.1), valid for $a > 0$, will be solved by prescribing a physical boundary condition at the left side, for $i = 1$, and no numerical condition is required at the downstream end of the domain. The reverse applies to the scheme (20.1.5) which will be solved by sweeping the mesh from the downstream end, where a physical boundary condition will be applied, and no condition is necessary at $i = 1$. This is of course in full agreement with physical propagation phenomena.

A visual representation is given in Figure 20.1.2. The points involved in the discretization are always on the side of the intersection of the characteristic with the x axis; P_+ for $a > 0$ and P_- for $a < 0$.

The solution in point i at $t = (n+1)\Delta t$ will only be influenced by the information at $t = n\Delta t$ which can be transported by the characteristic. The CFL condition expresses that all of the information physically influencing point P , which is contained in the physical domain of dependence (P_-, P, P_+), should be allowed to influence numerically the solution in P . This has already been discussed in Chapter 8 in Volume 1.

When u represents a Riemann variable, we obtain the first-order λ scheme of Moretti (1979), which is then equivalent to the Courant *et al.* scheme.

The Euler equations have generally mixed sign eigenvalues and both schemes (20.1.1) and (20.1.5) can be combined in the following way. Defining positive and negative projections of the eigenvalues

$$a^+ = \max(a, 0) = \frac{1}{2}(a + |a|) \quad (20.1.8)$$

$$a^- = \min(a, 0) = \frac{1}{2}(a - |a|) \quad (20.1.9)$$

we obtain the general form for the *first-order accurate upwind scheme written for the linearized scalar form of the Euler equations*:

$$u_i^{n+1} - u_i^n = -\tau [a^+(u_i^n - u_{i-1}^n) + a^-(u_{i+1}^n - u_i^n)] \quad (20.1.10)$$

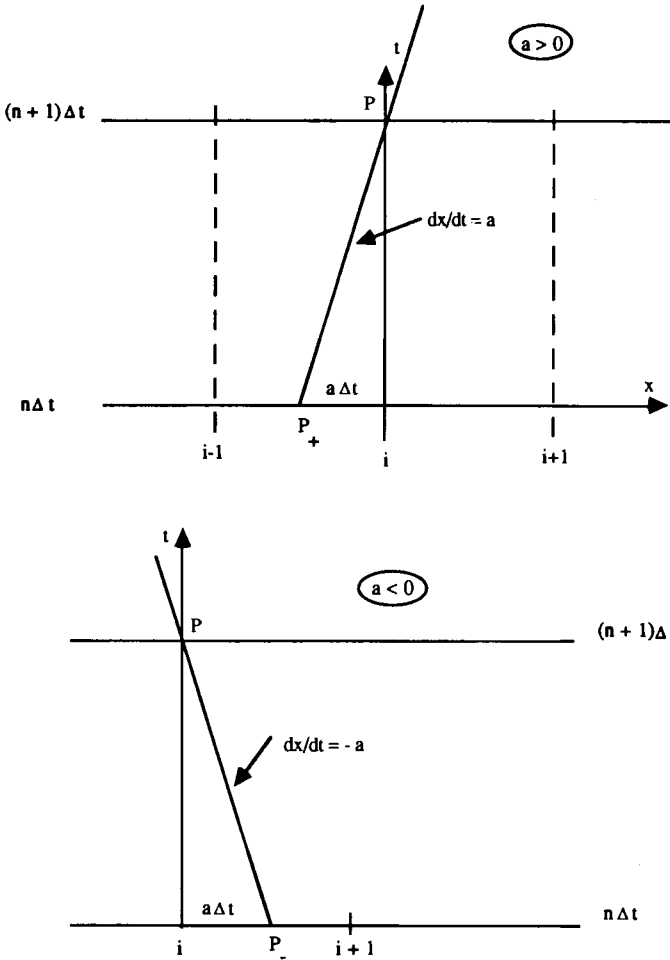


Figure 20.1.2 Characteristic properties and upwind discretization

The stability limit is now

$$|\sigma| = \tau|a| \leq 1 \tag{20.1.11}$$

Observe that a^+ is always positive (or zero), a^- is always negative (or zero) and that a problem of undeterminacy exists when $a = 0$, which has to be treated carefully.

Equation (20.1.1) can be interpreted as an integration of $du/dt = 0$ along the characteristic $dx/dt = a$ by finding $u(P_+)$ through a linear interpolation between i and $i - 1$ at level n , and writing $u_{P_+}^{n+1} = u_{P_+}^n = u_i^n - \sigma(u_i^n - u_{i-1}^n)$.

It is interesting to observe at this point that the Lax-Wendroff scheme can also be interpreted in the same way by performing a quadratic symmetric

interpolation between the three points $i - 1, i, i + 1$ in order to estimate $u(P_+)$. Indeed, with the second-order interpolation formula

$$u(x) = u_i + \frac{u_{i+1} - u_{i-1}}{2\Delta x}(x - x_i) + \frac{u_{i+1} - 2u_i + u_{i-1}}{2\Delta x^2}(x - x_i)^2 \quad (20.1.12)$$

the Lax-Wendroff scheme is obtained from this relation at $x - x_i = -a\Delta t$

$$u_p^{n+1} = u_{p+}^n = u_i^n - \frac{\sigma}{2}(u_{i+1}^n - u_{i-1}^n) + \frac{\sigma^2}{2}(u_{i+1}^n - 2u_i^n + u_{i-1}^n) \quad (20.1.13)$$

This shows one way of defining second-order upwind schemes, for instance by a quadratic interpolation between $i, i - 1$ and $i - 2$. A general presentation of this approach can be found in Yang (1986).

It is interesting to compare again this first-order scheme with the Lax-Friedrichs method. Equation (20.1.10) can be recast into a form which brings up the stabilization process of the unstable central scheme introduced by the upwinding process. Equation (20.1.10) is written as

$$u_i^{n+1} - u_i^n = -\frac{\sigma}{2}(u_{i+1}^n - u_{i-1}^n) + \frac{\tau}{2}|a|(u_{i+1}^n - 2u_i^n + u_{i-1}^n) \quad (20.1.14)$$

showing the presence of a numerical viscosity of the form $\Delta x^2|\sigma|u_{xx}/2$ added to an otherwise centrally discretized scheme. Hence, two options can be taken in order to take properly into account the propagation properties of an hyperbolic equation. Either one applies an upwind, directionally biased space discretization, or one uses central discretization without paying attention to the direction of propagation, but introduces an adapted artificial viscosity term. As described in Chapter 15, this technique has been largely applied for steady transonic potential flow computations. As an additional comparison, the Lax-Wendroff scheme has the same form as (20.1.14) but with $\sigma^2/2$ as the coefficient of the centrally discretized u_{xx} term. Rewriting equation (20.1.10) in still another form, namely

$$u_i^{n+1} = \tau a^+ u_{i-1}^n + (1 - \tau|a|)u_i^n + (-\tau a^-)u_{i+1}^n \quad (20.1.15)$$

it is seen that all weight coefficients of the right-hand side contributions to the solution at level $n + 1$ are positive when the CFL condition (20.1.11) is satisfied. This is illustrated in Figure 20.1.3.

This property is necessary and sufficient for a scheme to be *monotone* as defined by Godunov (1959). This will be discussed more in detail in Chapter 21. Let us, however, mention here that a monotone scheme has the property of not allowing the creation of new extrema and does not allow unphysical discontinuities. However, they cannot have an order of accuracy higher than one.

When applied to *linear* systems of equations, the scalar form of the first-order upwind scheme can be applied to each of the decoupled characteristic equations separately. With the diagonal matrix of the eigenvalues Λ , defined by equation (16.4.16), the schemes (20.1.14) written for the three characteristics can be

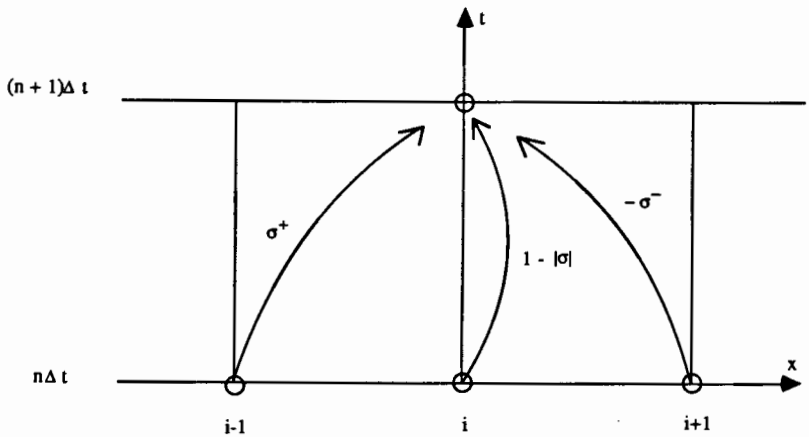


Figure 20.13 Weight coefficients in the distributive interpretation of the first-order upwind scheme

grouped as

$$W_i^{n+1} - W_i^n = -\frac{\tau}{2}\Lambda(W_{i+1}^n - W_{i-1}^n) + \frac{\tau}{2}|\Lambda|(W_{i+1}^n - 2W_i^n + W_{i-1}^n) \quad (20.1.16)$$

where W is the vector of the characteristic variables (16.4.18) and $|\Lambda|$ is the diagonal matrix of the absolute value of the eigenvalues. Reverting back to the conservative variables through the transformation (16.3.39) and defining the absolute value of the Jacobian by

$$|A| = P|\Lambda|P^{-1} \quad (20.1.17)$$

leads to the conservative form of the first-order upwind scheme

$$U_i^{n+1} - U_i^n = -\frac{\tau}{2}(f_{i+1}^n - f_{i-1}^n) + \frac{\tau}{2}|A|(U_{i+1}^n - 2U_i^n + U_{i-1}^n) \quad (20.1.18)$$

Note that scheme (20.1.18) has the numerical flux

$$f_{i+1/2}^* = \frac{f_{i+1} + f_i}{2} - |A| \frac{U_{i+1} - U_i}{2} \quad (20.1.19)$$

The stability condition is

$$\frac{\Delta t}{\Delta x} |\lambda_{\max}| \leq 1 \quad (20.1.20)$$

This scheme is uniquely defined by equation (20.1.18) when the system is linear. When applied to non-linear systems, it is not clear at which point the Jacobian matrix A has to be evaluated. In addition, one requires the schemes to be in conservative form. The flux splitting method of the following section is one way of combining upwind discretization with conservation.

20.2 ONE-DIMENSIONAL FLUX VECTOR SPLITTING

Since the Euler equations form a coupled system in the conservative variables and since the correct capture of discontinuities requires a conservative formulation, a more general definition of upwind schemes is necessary in order to define a splitting of the fluxes according to the signs of the eigenvalues. This can be achieved in the following way, introduced by Steger and Warming (1981).

20.2.1 Steger and Warming flux vector splitting

If the homogeneous Euler equations are put in characteristic form, equation (16.4.19),

$$\frac{\partial W}{\partial t} + \Lambda \frac{\partial W}{\partial x} = 0 \quad (20.2.1)$$

the upwind scheme (20.1.10) can be applied to each of the three characteristic variables separately, with the definitions

$$\lambda_k^+ = \frac{\lambda_k + |\lambda_k|}{2} \quad (20.2.2a)$$

$$\lambda_k^- = \frac{\lambda_k - |\lambda_k|}{2} \quad (20.2.2b)$$

for each of the eigenvalues of Λ :

$$\Lambda = \begin{vmatrix} \lambda_1 & \cdot & \cdot \\ \cdot & \lambda_2 & \cdot \\ \cdot & \cdot & \lambda_3 \end{vmatrix} = \begin{vmatrix} u & & \\ & u+c & \\ & & u-c \end{vmatrix} \quad (20.2.3)$$

This defines two diagonal matrices Λ^\pm :

$$\Lambda^\pm = \begin{vmatrix} \lambda_1^\pm & & \\ & \lambda_2^\pm & \\ & & \lambda_3^\pm \end{vmatrix} = \begin{vmatrix} \frac{u \pm |u|}{2} & & \\ & \frac{(u+c) \pm |u+c|}{2} & \\ & & \frac{(u-c) \pm |u-c|}{2} \end{vmatrix} \quad (20.2.4)$$

where Λ^+ has only positive eigenvalues, Λ^- only negative eigenvalues, and such that

$$\Lambda = \Lambda^+ + \Lambda^- \quad |\Lambda| = \Lambda^+ - \Lambda^- \quad (20.2.5)$$

or

$$\lambda_k = \lambda_k^+ + \lambda_k^- \quad |\lambda_k| = \lambda_k^+ - \lambda_k^- \quad (20.2.6)$$

The quasi-linear coupled equations are obtained from the characteristic form by the transformation matrix P , with the Jacobian A satisfying

$$A = P \Lambda P^{-1} \quad (20.2.7)$$

Hence an upwind formulation can be obtained with the Jacobians

$$A^+ = P \Lambda^+ P^{-1} \quad A^- = P \Lambda^- P^{-1} \quad (20.2.8)$$

with

$$A = A^+ + A^- \quad (20.2.9a)$$

$$|A| = A^+ - A^- \quad (20.2.9b)$$

The fluxes associated with these split Jacobians are obtained from the remarkable property of homogeneity of the flux vector $f(U)$. As noted earlier (Section 16.2), $f(U)$ is an homogeneous function of degree one of U . Hence, one has

$$f = A \cdot U \quad (20.2.10)$$

and the following flux splitting can be defined:

$$f^+ = A^+ \cdot U \quad f^- = A^- \cdot U \quad (20.2.11)$$

with

$$f = f^+ + f^- \quad (20.2.12)$$

This *flux vector* splitting, based on (20.2.2), has been introduced by Steger and Warming (1981). The split fluxes f^+ and f^- are also homogeneous functions of degree one in U .

It is important to notice that the splitting (20.2.2) is not unique, even under the restriction (20.2.5). For instance, the following splitting has been applied by Steger (1978):

$$\begin{aligned} \lambda_1^+ &= \frac{u + |u|}{2} & \lambda_1^- &= \frac{u - |u|}{2} \\ \lambda_2^+ &= \lambda_1^+ + c & \lambda_2^- &= \lambda_1^- \\ \lambda_3^+ &= \lambda_1^+ & \lambda_3^- &= \lambda_1^- - c \end{aligned} \quad (20.2.13)$$

which verifies equation (20.2.5), $\lambda_k^+ + \lambda_k^- = \lambda_k$.

Subsonic flow

For a subsonic flow, the third eigenvalue $\lambda_3 = u - c$ is negative and the two others are positive. Hence

$$\Lambda^+ = \begin{vmatrix} u & & \\ & u + c & \\ & & 0 \end{vmatrix} \quad \Lambda^- = \begin{vmatrix} 0 & & \\ & 0 & \\ & & u - c \end{vmatrix} \quad (20.2.14)$$

The Jacobians A^+ and A^- are obtained from (20.2.8) with the matrices P and

P^{-1} given by equations (16.4.11) and (16.4.12). Starting with A^- , which has more zero elements, one obtains (see Problem 20.1)

$$f^- = \frac{\rho(u-c)}{2\gamma} \begin{vmatrix} 1 \\ (u-c) \\ \frac{(u-c)^2}{2} + \left(\frac{3-\gamma}{\gamma-1}\right)\frac{c^2}{2} \end{vmatrix} \quad (20.2.15)$$

and f^+ is obtained from $f^+ = f - f^-$, where the energy has been expressed as a function of the sonic velocity by

$$\varepsilon = \rho E = \frac{\rho c^2}{\gamma(\gamma-1)} + \frac{\rho u^2}{2} \quad (20.2.16)$$

$$f^+ = \frac{\rho}{2\gamma} \begin{vmatrix} (2\gamma-1)u+c \\ 2(\gamma-1)u^2 + (u+c)^2 \\ (\gamma-1)u^3 + \frac{(u+c)^3}{2} + \frac{3-\gamma}{2(\gamma-1)}(u+c)c^2 \end{vmatrix} \quad (20.2.17)$$

A general calculation for an arbitrary splitting:

$$\bar{\Lambda} = \begin{vmatrix} \bar{\lambda}_1 & & \\ & \bar{\lambda}_2 & \\ & & \bar{\lambda}_3 \end{vmatrix} \quad (20.2.18)$$

performed by Steger and Warming, gives the corresponding flux as (see also Problem 20.2)

$$\bar{f} = P\bar{\Lambda}P^{-1}U = \frac{\rho}{2\gamma} \begin{vmatrix} 2(\gamma-1)\bar{\lambda}_1 + \bar{\lambda}_2 + \bar{\lambda}_3 \\ 2(\gamma-1)\bar{\lambda}_1 u + \bar{\lambda}_2(u+c) + \bar{\lambda}_3(u-c) \\ (\gamma-1)\bar{\lambda}_1 u^2 + \frac{\bar{\lambda}_2}{2}(u+c)^2 + \frac{\bar{\lambda}_3}{2}(u-c)^2 + \frac{3-\gamma}{2(\gamma-1)}(\bar{\lambda}_2 + \bar{\lambda}_3)c^2 \end{vmatrix} \quad (20.2.19)$$

Before presenting some schemes based on the flux vector splitting, it is important to notice a certain number of properties of the split fluxes.

20.2.2 Properties of split flux vectors

A first important remark to be made here is that the whole concept of flux splitting as defined by equations (20.2.9) to (20.2.11) is totally dependent on the fact that the fluxes are homogeneous functions of degree one in U . One cannot therefore directly apply this approach to a general scalar flux function $f(u)$, since the only homogeneous scalar flux function of degree one is the linear case $f = au$. For instance, the flux of Burgers equation $f = u^2/2$ is homogeneous of

degree two and has the Jacobian $a(u) = df/du = u$, leading to the relation $f = au/2$ instead of the scalar version of equation (20.2.10). Upwind methods that are not dependent on the homogeneity property of the fluxes will be discussed in Section 20.5 in relation to Godunov-type methods.

The splittings (20.2.9) and (20.2.11) give

$$\begin{aligned} A &= A^+ + A^- \\ f &= AU = f^+ + f^- = A^+U + A^-U \end{aligned} \quad (20.2.20)$$

and

$$\frac{\partial f}{\partial U} = A = \frac{\partial f^+}{\partial U} + \frac{\partial f^-}{\partial U} = A^+ + A^- \quad (20.2.21)$$

but one has *not* generally the equality of the split Jacobians, that is

$$\frac{\partial f^+}{\partial U} \neq A^+ \quad \text{and} \quad \frac{\partial f^-}{\partial U} \neq A^- \quad (20.2.22)$$

This can be verified by a direct calculation for the Steger–Warming flux splitting (see Problem 20.4).

More importantly, these matrices have not the same set of eigenvalues. By construction, the eigenvalues of A^+ and A^- are the positive and negative eigenvalues of A , that is λ_k^+ and λ_k^- , but this is not true for $\partial f^+/\partial U$ and $\partial f^-/\partial U$.

However, Steger and Warming (1981) report that $f_u^+ \equiv \partial f^+/\partial U$ has only positive eigenvalues and $f_u^- \equiv \partial f^-/\partial U$ has only negative eigenvalues. Lerat (1983) has given an analytical proof of this property for the one-dimensional Euler equations for a perfect gas, under the condition that the specific heat ratio γ satisfies the condition $1 < \gamma < \frac{5}{3}$ (see also Problem 20.5).

The non-equality of f_u^+ and A^+ on the one hand and of f_u^- and A^- on the other hand has very important consequences with regard to the definition of upwind schemes based on the concept of flux vector splitting. Indeed, we can write the conservation equations in split form as

$$\frac{\partial U}{\partial t} + \frac{\partial f^+}{\partial x} + \frac{\partial f^-}{\partial x} = 0 \quad (20.2.23)$$

which becomes, in quasi-linear form,

$$\frac{\partial U}{\partial t} + f_u^+ \frac{\partial U}{\partial x} + f_u^- \frac{\partial U}{\partial x} = 0 \quad (20.2.24)$$

Alternatively, we can first write the quasi-linear form and split the Jacobians afterwards, that is

$$\frac{\partial U}{\partial t} + A \frac{\partial U}{\partial x} = \frac{\partial U}{\partial t} + A^+ \frac{\partial U}{\partial x} + A^- \frac{\partial U}{\partial x} = 0 \quad (20.2.25)$$

These two formulations are not identical, as a consequence of equations (20.2.22), showing that the two operations of splitting the fluxes and introducing the

quasi-linearization do not commute. Only (20.2.25) corresponds to the direct generalization of the uncoupled equations (20.1.10) and therefore keeps the same physical characteristics which are separated according to their sign. Equation (20.2.24) does not represent a decomposition of the physical characteristics, but is the only linearization consistent with the conservative form (20.2.23).

Connection with the eigenvectors of the Jacobian matrix A

The split fluxes can be related to the eigenvectors of the Jacobian matrix A , in particular to the right eigenvectors, that constitute the columns of the matrix P (see Section 16.4). This leads to a simple way of computing the Jacobian A^\pm and the associated fluxes f^\pm (Lerat, 1983).

The set of left (or right) eigenvectors $l^{(j)}$ (or $r^{(j)}$) associated with the eigenvalue λ_j of A are linearly independent by definition of the hyperbolic character of the Euler equations. Hence, any function of the conservative variables can be expressed as linear combinations of the left (or the right) eigenvectors considered as basic vectors spanning the U space. In particular, we have

$$U = \sum_{j=1}^3 \alpha_j(U) r^{(j)}(U) \quad (20.2.26)$$

where α_j are the coefficients of the expansion and can be considered as the projection of U in the base $r^{(j)}$.

Since the $r^{(j)}$ vectors are defined up to a normalization constant (see equation (16.4.8)), we can always normalize each $r^{(j)}$ such that $\alpha_j = 1$. The appropriate normalization factors can be derived by inspection of equation (16.4.12) which defines the matrix P and which is repeated here for convenience. The matrix P

$$P = \begin{vmatrix} 1 & \frac{\rho}{2c} & -\frac{\rho}{2c} \\ u & \frac{\rho(u+c)}{2c} & -\frac{\rho(u-c)}{2c} \\ \frac{u^2}{2} & \frac{\rho(H+uc)}{2c} & -\frac{\rho(H-uc)}{2c} \end{vmatrix} \quad (20.2.27)$$

contains the right eigenvectors $r^{(j)}$ as columns with the normalization defined by $\alpha = \beta = \delta = 1$ in equation (16.4.8).

If $\alpha_j = 1$, equation (20.2.26) shows that the sum of the elements along the same line of P must be equal to the elements of U . This leads to the following renormalized eigenvectors $r^{(j)}$ (see Problem 16.24):

$$r^{(1)} = \rho \frac{\gamma-1}{\gamma} \begin{vmatrix} 1 \\ u \\ \frac{u^2}{2} \end{vmatrix} \quad r^{(2)} = \frac{\rho}{2\gamma} \begin{vmatrix} 1 \\ u+c \\ H+uc \end{vmatrix} \quad r^{(3)} = \frac{\rho}{2\gamma} \begin{vmatrix} 1 \\ u-c \\ H-uc \end{vmatrix} \quad (20.2.28)$$

where the perfect gas relations

$$p = (\gamma - 1)\rho e$$

$$E = e + \frac{u^2}{2} = H - \frac{p}{\rho} \quad (20.2.29)$$

have been introduced. Equation (20.2.26) now becomes

$$U = \sum_{j=1}^3 r^{(j)} \quad (20.2.30)$$

The flux vector f can also be projected in the space $r^{(j)}$, applying the homogeneity property of the fluxes in the Euler equations,

$$f = AU = \sum_{j=1}^3 Ar^{(j)} \quad (20.2.31)$$

Since $r^{(j)}$ is an eigenvector of A associated with the eigenvalue λ_j ,

$$f = \sum_{j=1}^3 \lambda_j r^{(j)} \quad (20.2.32)$$

showing that the projections of the flux vector on the basis $r^{(j)}$ are precisely the corresponding eigenvalues. This can be verified by a direct calculation (see Problem 20.7).

The split fluxes can now be defined with equations (20.2.11) and (20.2.2) to (20.2.9) as follows:

$$f = \sum_{j=1}^3 (\lambda_j^+ + \lambda_j^-) r^{(j)} = f^+ + f^- \quad (20.2.33)$$

with

$$f^+ = \sum_{j=1}^3 \lambda_j^+ r^{(j)} \quad f^- = \sum_{j=1}^3 \lambda_j^- r^{(j)} \quad (20.2.34)$$

This applies also to the arbitrary splitting of equation (20.2.18), where the flux \bar{f} , associated with a set of partial eigenvalues $\bar{\lambda}_j$, becomes

$$\bar{f} = \sum_{j=1}^3 \bar{\lambda}_j r^{(j)} \quad (20.2.35)$$

which should be identical to equation (20.2.19).

20.2.3 Van Leer's flux splitting

The Jacobian of the split fluxes f_u^+ and f_u^- as defined above are not continuously differentiable, since they have a discontinuous slope at sonic velocities. This can best be seen from the mass flux components, expressed as a function of the variables $\rho, c, M = u/c$, introducing the Mach number M . Since $f_1 = \rho u = \rho c M$ is linear in M , a plot of $f/\rho c$ as a function of Mach number illustrates the properties we wish to put forward. Since $f^+ = f$ for supersonic flows $u > c$, and

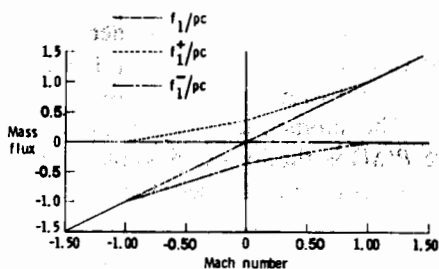
considering negative as well as positive velocities, we have (see also Problem 20.7)

$$f_1^+ = \begin{cases} 0 & \text{for } M \leq -1 \\ \frac{\rho c}{2\gamma}(M+1) & \text{for } -1 \leq M \leq 0 \\ \frac{\rho c}{2\gamma}[(2\gamma-1)M+1] & \text{for } 0 \leq M \leq 1 \\ f_1 & \text{for } M > 1 \end{cases} \quad (20.2.36)$$

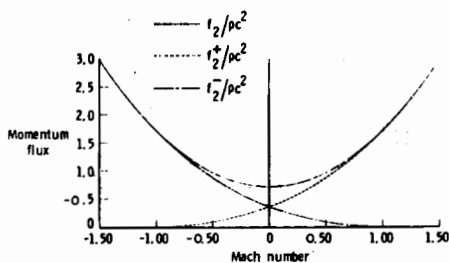
Similarly,

$$f_1^- = \begin{cases} f_1 & \text{for } M \leq -1 \\ \frac{\rho c}{2\gamma}[(2\gamma-1)M-1] & \text{for } -1 \leq M \leq 0 \\ \frac{\rho c}{2\gamma}(M-1) & \text{for } 0 \leq M \leq 1 \\ 0 & \text{for } M > 1 \end{cases} \quad (20.2.37)$$

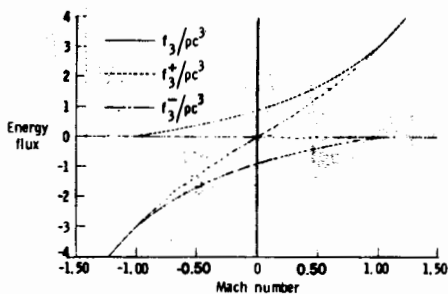
The variations of f_1^\pm are shown in Figure 20.2.1(a). The discontinuity in the



(a) Mass flux



(b) Momentum flux



(c) Energy flux

Figure 20.2.1 Mach number dependence of the Steger–Warming split fluxes. (From Anderson *et al.*, 1986a)

slope of f_1^\pm when the eigenvalues go to zero (at sonic and stagnation points) is clearly seen. Figures 20.2.1(b) and 20.2.1(c) show similarly the momentum fluxes f_2^\pm divided by ρc^2 and the energy fluxes divided by ρc^3 , both as a function of Mach number.

This will cause certain difficulties since a discontinuity in slope at the sonic transition might occur on the computed solution (Steger and Warming, 1981). This is illustrated later in Figure 20.3.7, which shows the results of a shock tube flow computation with a first-order upwind scheme based on the Steger-Warming flux splitting. The 'glitch' at the sonic transition is clearly seen.

Van Leer (1982) has introduced a flux splitting different from (20.2.15), (20.2.17) by imposing a certain number of conditions on f^+ and f^- satisfying (20.2.12). In particular, f^\pm and the associated Jacobians f_u^\pm are requested to be continuous functions of Mach number and expressed as polynomials of the lowest possible order. In addition, the eigenvalues of f_u^+ must be positive or zero and those of f_u^- negative or zero, with one eigenvalue equal to zero in the subsonic range $|M| < 1$. This last condition is fulfilled by the Jacobians A^+ and A^- but generally not by f_u^+ and f_u^- .

Since for $M \geq 1$, $f^+ = f$ and for $M \leq -1$, $f^- = f$, the symmetry properties of each flux component f_j^\pm must be the same as those of the total flux, that is

$$f_j^+(M) = \pm f_j^-(-M) \quad \text{if } f_j(M) = \pm f_j(-M) \quad (20.2.38)$$

The above conditions require the flux components to be proportional to $(M \pm 1)^n$, with $n \geq 2$ for vanishing slopes at $M = \mp 1$. The lowest possible order is $n=2$. The simplest expression for the mass flux component is then $f_1^\pm(M) = \rho c(M \pm 1)^2/4$. The momentum flux component can be defined as $f_2^\pm = f_1^\pm \cdot P(M)$, where $P(M)$ is the lowest possible polynomial in M , namely first order. The energy flux component is selected under the condition that one of the eigenvalues of the split flux Jacobians f_u^\pm should vanish in the range $0 < M < 1$. Hence f_3^\pm is taken to be proportional to $f_2^{\pm 2}/f_1^\pm$. This leads to the following form (Van Leer, 1982):

$$f_{\text{VL}}^+ = \frac{\rho}{4c} (u+c)^2 \begin{vmatrix} 1 \\ \frac{(\gamma-1)u+2c}{\gamma} \\ \frac{[(\gamma-1)u+2c]^2}{2(\gamma^2-1)} \end{vmatrix}$$

$$= \frac{\rho c}{4} (M+1)^2 \begin{vmatrix} 1 \\ \frac{2c}{\gamma} \left(1 + \frac{\gamma-1}{2} M\right) \\ \frac{2c^2}{\gamma^2-1} \left(1 + \frac{\gamma-1}{2} M\right)^2 \end{vmatrix} \quad (20.2.39)$$

The negative part of the flux is given by

$$f_{\text{VL}}^- = f - f_{\text{VL}}^+ = -\frac{\rho c}{4}(M-1)^2 \left[\begin{array}{c} 1 \\ \frac{2c}{\gamma} \left(-1 + \frac{\gamma-1}{2} M \right) \\ \frac{2c^2}{\gamma^2-1} \left(1 - \frac{\gamma-1}{2} M \right)^2 \end{array} \right]$$

$$= -\frac{\rho}{4c}(u-c)^2 \left[\begin{array}{c} 1 \\ \frac{(\gamma-1)u-2c}{\gamma} \\ \frac{[2c-(\gamma-1)u]^2}{2(\gamma^2-1)} \end{array} \right] \quad (20.2.40)$$

One has clearly $f_{j,\text{VL}}^+(M) = -f_{j,\text{VL}}^-(-M)$ for the first ($j=1$) and third ($j=3$) components, which are uneven in M ($f_1 = \rho u = \rho c M$ and $f_3 = \rho u H = \rho c^3 M [1/(\gamma-1) + M^2/2]$) and $f_{2,\text{VL}}^+(M) = f_{2,\text{VL}}^-(-M)$ for the momentum flux component $f_2 = \rho u^2 + p = \rho c^2 (1 + \gamma M^2)/\gamma$, which is an even function of M . The continuity of the slopes $\partial f^+/\partial M$ at $M=1$ is readily checked, while at $M=-1$ it is guaranteed by the presence of the factor $(M+1)^2$, which has a vanishing derivative at $M=-1$ (see also Problem 20.9).

The Van Leer split flux components are represented in Figure 20.2.2 as a function of M , and the continuity of slopes at sonic and stagnation points is clearly seen.

A direct but lengthy calculation, identifying the obtained splitting with the general form (20.2.19), leads to the following eigenvalue decomposition:

$$\lambda_{1,\text{VL}}^+ = \frac{c}{4}(M+1)^2 \left[1 - \frac{(M-1)^2}{\gamma+1} \right] \quad (20.2.41a)$$

$$\lambda_{2,\text{VL}}^+ = \frac{c}{4}(M+1)^2 \left[3 - M + \frac{\gamma-1}{\gamma+1}(M-1)^2 \right] \quad (20.2.41b)$$

$$\lambda_{3,\text{VL}}^+ = \frac{c}{2(\gamma+1)}(M+1)^2(M-1) \left(1 + \frac{\gamma-1}{2} M \right) \quad (20.2.41c)$$

Note that $\lambda_{3,\text{VL}}^+$ is negative in the range $0 < M < 1$, although the eigenvalues of the Jacobian of the corresponding split flux are positive or zero.

The negative parts are obtained from

$$\begin{aligned} \lambda_{1,\text{VL}}^- &= -\lambda_{1,\text{VL}}^+(-M) \\ \lambda_{2,\text{VL}}^- &= -\lambda_{2,\text{VL}}^+(-M) \\ \lambda_{3,\text{VL}}^- &= -\lambda_{3,\text{VL}}^+(-M) \end{aligned} \quad (20.2.42)$$

A direct calculation shows that the relations (20.2.6) are satisfied.

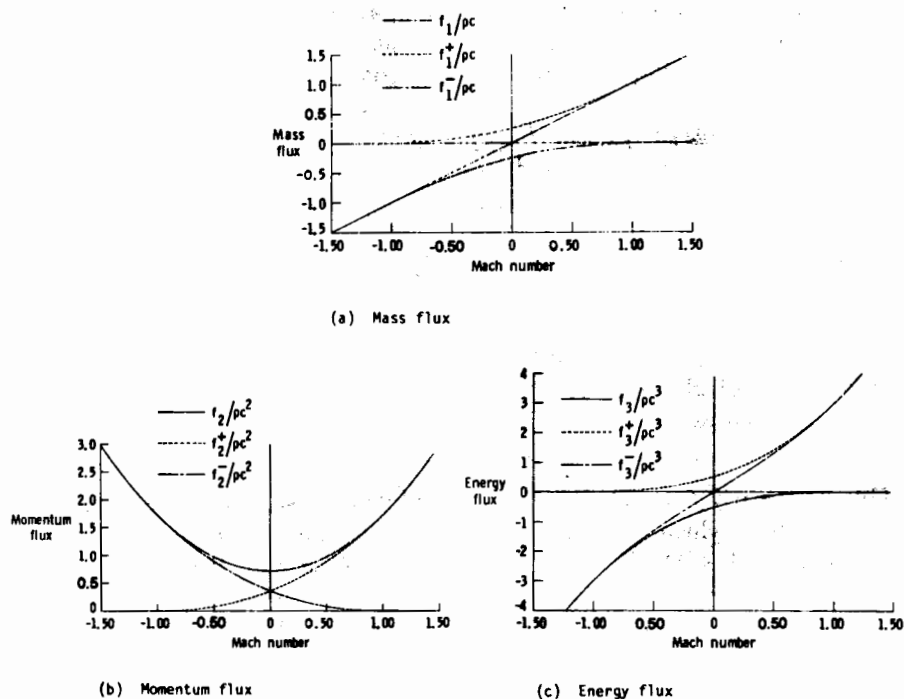


Figure 20.2.2 Mach number dependence of the Van Leer split fluxes. (From Anderson *et al.*, 1986a)

This eigenvalue splitting is obviously strongly distinct from the Steger-Warming choice. The vanishing of one of the eigenvalues of $f_{u,VL}^\pm$ for $|M| \leq 1$ forces a steady shock transition over two mesh cells (Van Leer, 1982).

A variant of the splitting (20.2.39), (20.2.40) has been applied by Hänel *et al.* (1987), with the aim of ensuring the constancy of the stagnation enthalpy H for stationary flows. Referring to Figure 20.3.1, the steady-state solution of a first-order upwind discretization is obtained from the balance of fluxes $f_{i-1}^+ + f_i^- = f_i^+ + f_{i+1}^-$ and when applied to the energy component the above splittings do not lead to the constancy of H over the cell $i(i-1/2, i+1/2)$ (see Problem 20.14). This is a weakness of the flux splitting approach, which is not shared by the central schemes which solve $f_{i-1} = f_{i+1}$, leading to $H_{i-1} = H_{i+1}$ when mass conservation is satisfied. The error is, however, of the order of the truncation error.

Since the energy flux $f_3 = \rho u H = \rho c M H$, a valid splitting of the third component is

$$f_3^\pm = f_1^\pm H \quad (20.2.43)$$

The third component of (20.2.39) can be written as $f_3^\pm = f_1^\pm [H - (M \mp 1)^2 c^2 / (\gamma + 1)]$, indicating that the choice (20.2.43) satisfies the conditions of slope

continuity at sonic and stagnation points. However, there is no longer any vanishing eigenvalue of the split flux Jacobians in the range $|M| \leq 1$; refer also to Problem 20.10.

The energy flux in the Van Leer splitting can be generalized to the form

$$f_3^\pm = f_1^\pm [H - c^2 P(M \pm 1)] \quad (20.2.44)$$

where $P(M \pm 1)$ is a polynomial in $M \pm 1$. If it is requested that the slopes $\partial f^+ / \partial M$ are continuous at $M = 1$, then P should be a polynomial in $(M - 1)$, for f^+ of second degree or higher. The lowest degree is two, leading to the original choice of (20.2.39). Other properties could be put forward (see, for instance, Problem 20.15), and use can be made of this degree of freedom for extending the flux splittings to non-perfect gases (Vinokur and Liu, 1988; Liou *et al.*, 1988).

20.2.4 Non-reflective boundary conditions and split fluxes

The non-equality of A^\pm and f_\pm^\pm has also an impact on the treatment of boundary conditions by methods connected to the characteristic approach. The compatibility relations for the outgoing characteristics are written as follows, referring to Section 19.1,

$$\frac{\partial W^N}{\partial t} + \Lambda \frac{\partial W^N}{\partial x} = P^{-1} Q \quad (20.2.45)$$

where the superscript N stands for numerical boundary condition and where W^N represents the number of outgoing characteristics.

At a subsonic inlet, W^N stands for the third characteristic w_3 and (20.2.45) represents one equation, while at a subsonic exit W^N stands for the characteristics w_1 and w_2 so that (20.2.45) represents two equations. To fix our ideas, let us suppose that the outgoing characteristics correspond to positive eigenvalues. The above equation can then be written as

$$\frac{\partial W^N}{\partial t} + \Lambda^+ \frac{\partial W^N}{\partial x} = P^{-1} Q \quad (20.2.46)$$

The non-reflecting condition (19.1.78) for the incoming characteristics is then associated with the negative eigenvalues and corresponds to the condition $\partial W^P / \partial t = P^{-1} Q$. Hence, when combined with the above compatibility equation as described at the end of Section 19.1.5, the three equations obtained in this way can be written as

$$\frac{\partial W}{\partial t} + \Lambda^+ \frac{\partial W}{\partial x} = P^{-1} Q \quad (20.2.47)$$

Reverting back to conservative variables, one obtains, in the presence of a source term Q , where A^+ is defined from the Steger-Warming flux splitting

(20.2.2), the non-conservative formulation

$$\frac{\partial U}{\partial t} + A^+ \frac{\partial U}{\partial x} = Q \quad (20.2.48)$$

These boundary conditions have to be discretized in an upwind way, for instance at an exit boundary point $i = M$,

$$U_M^{n+1} - U_M^n = -\tau A_M^+(U_M - U_{M-1}) + \Delta t \cdot Q_M \quad (20.2.49)$$

On the other hand, the alternative conservative formulation of the numerical conditions

$$\frac{\partial U}{\partial t} + \frac{\partial f^+}{\partial x} = Q \quad (20.2.50)$$

discretized as

$$U_M^{n+1} - U_M^n = -\tau(f_M^+ - f_{M-1}^+) + \Delta t \cdot Q \quad (20.2.51)$$

has not the same physical significance, since the eigenvalues of f_u^+ are not equal to the eigenvalues Λ^+ of A^+ . Hence along the path of the f_u^+ eigenvalues, the Riemann invariants are not constant as is the case when applying equation (20.2.48). Therefore, this formulation is not physically consistent and *should not be applied* with the split flux vectors f^+ and f^- .

When the incorrect boundary treatment (20.2.51) is applied, for instance to the one-dimensional shock tube problem, reflected waves are produced at the exit boundary. This will not be the case with the formulation (20.2.49). Therefore, equation (20.2.48) represents a consistent formulation for the compatibility relations in combination with the non-reflective condition.

20.3 ONE-DIMENSIONAL UPWIND DISCRETIZATIONS BASED ON FLUX VECTOR SPLITTING

The definition of fluxes with Jacobian eigenvalues always having a positive or negative sign, like f^+ and f^- , allows a general definition of upwind schemes in conservation form, although these eigenvalues are not equal to those of A .

Writing the system of Euler equations in the form of equation (20.2.23)

$$\frac{\partial U}{\partial t} + \frac{\partial f^+}{\partial x} + \frac{\partial f^-}{\partial x} = 0 \quad (20.3.1)$$

the basic idea of the upwind scheme will be realized if f_x^+ is discretized with a backward difference and f_x^- with a forward difference.

20.3.1 First-order explicit upwind schemes

The following explicit first-order scheme is the obvious conservative generalization of the upwind scheme (20.1.10) (Steger and Warming, 1981):

$$\begin{aligned} U_i^{n+1} - U_i^n &= -\tau(f_i^+ - f_{i-1}^+)^n - \tau(f_{i+1}^- - f_i^-)^n \\ &= -\tau[f_i^+ + f_{i+1}^- - (f_{i-1}^+ + f_i^-)]^n \end{aligned} \quad (20.3.2)$$

This scheme is first-order accurate in space and time. It can also be written, after isolating the central difference terms, like in (20.1.18) by introducing the absolute value flux

$$|f| = f^+ - f^- = |A|U \quad (20.3.3)$$

where

$$|A| = P|\Lambda|P^{-1} \quad (20.3.4)$$

$$U_i^{n+1} - U_i^n = -\frac{\tau}{2}(f_{i+1} - f_{i-1})^n + \frac{\tau}{2}(|f|_{i+1} - 2|f|_i + |f|_{i-1})^n \quad (20.3.5)$$

showing an artificial viscosity term proportional to the second derivative of the absolute flux value $|f|$.

Comparing with the Lax-Wendroff scheme, we can transform equation (20.3.2) in a form that explicits the absolute value Jacobian $|A|$. Up to second-order accuracy, one can write, after a Taylor expansion valid for smooth variations,

$$|f|_{i+1} - |f|_i = |A|_{i+1/2}(U_{i+1} - U_i) + O(\Delta x)(U_{i+1} - U_i) \quad (20.3.6)$$

Hence, equation (20.3.2) becomes, to the same first-order accuracy,

$$\begin{aligned} U_i^{n+1} - U_i^n &= -\frac{\tau}{2}(f_{i+1} - f_{i-1})^n + \frac{\tau}{2}[|A|_{i+1/2}(U_{i+1} - U_i) \\ &\quad - |A|_{i-1/2}(U_i - U_{i-1})]^n + O(\Delta U^2) \end{aligned} \quad (20.3.7)$$

while the Lax-Wendroff scheme, which is second-order accurate, can be written

$$U_i^{n+1} - U_i^n = -\frac{\tau}{2}(f_{i+1} - f_{i-1})^n + \frac{\tau^2}{2}[A_{i+1/2}^2(U_{i+1} - U_i) - A_{i-1/2}^2(U_i - U_{i-1})]^n \quad (20.3.8)$$

The differences between the two schemes can be viewed as the replacement of the first-order coefficients $\tau|A|/2$ by a second-order coefficients $\tau^2 A^2/2$ in the pseudo-viscosity terms, which stabilize the unstable central difference scheme (see also Problem 20.10).

Equations (20.3.2) and (20.3.7) are equivalent formulations of the first-order conservative upwind scheme for smooth variations of U . In terms of a numerical flux f^* , one can write the conservative upwind scheme (20.3.2) as

$$U_i^{n+1} - U_i^n = -\tau \delta f_{i+1/2}^* \quad (20.3.9)$$

with

$$f_{i+1/2}^* = f_i^+ + f_{i+1}^- \quad (20.3.10a)$$

or, up to second-order accuracy,

$$f_{i+1/2}^* = \frac{1}{2}(f_i + f_{i+1}) - \frac{1}{2}|A_{i+1/2}|(U_{i+1} - U_i) + O(\Delta U^2) \quad (20.3.10b)$$

↑
|A_{i+1/2}|

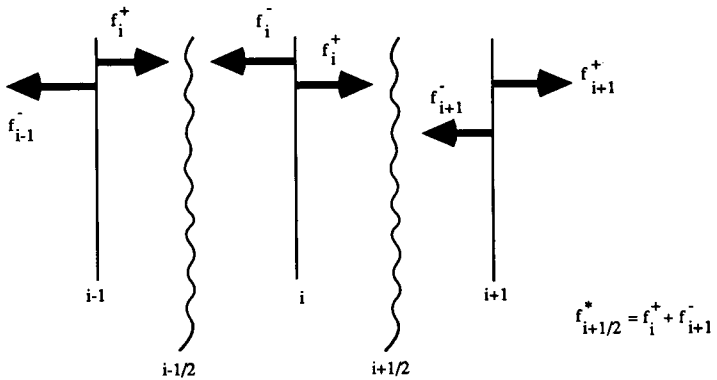


Figure 20.3.1 Interpretation of numerical fluxes associated with the first-order upwind scheme

This has an interesting physical interpretation, as seen from Figure 20.3.1. The flux contribution to the time variation of the solution at point i is described by the balance between the fluxes $f_{i+1/2}^*$ and $f_{i-1/2}^*$. If the fluxes f^+ and f^- are attached to the characteristics of positive and negative signs, it is seen that $f_{i+1/2}^*$ is the sum of the fluxes entering the cell $(i, i + 1)$, namely f_i^+ and f_{i+1}^- , and similarly for $f_{i-1/2}^*$, which is formed by the fluxes entering the cell $(i, i - 1)$.

20.3.2 Stability conditions for first-order flux vector splitting schemes

The stability conditions of scheme (20.3.2) have to be considered carefully. In the strict linear case, $f = au$, the stability condition reduces to the CFL condition of equation (20.1.11), $|\sigma| \leq 1$. However, in the non-linear case of equation (20.3.2), the Jacobians of f^\pm are not equal to A^\pm , as seen in the previous section, and, even more significant, their eigenvalues are different. Hence, if a local linearization is performed, around a given state U^n , equation (20.3.2) becomes

$$U_i^{n+1} - U_i^n = -\tau f_u^{+n}(U_i - U_{i-1})^n - \tau f_u^{-n}(U_{i+1} - U_i)^n \quad (20.3.11)$$

where f_u^{+n} and f_u^{-n} are the linearized values taken by the Jacobians of f^+ and f^- for $U = U^n$. The amplification matrix G becomes, from a Von Neumann analysis,

$$G - 1 = -2\tau(f_u^+ - f_u^-) \sin^2 \frac{\phi}{2} - I\tau(f_u^+ + f_u^-) \sin \phi \quad (20.3.12)$$

Introducing the matrix

$$|f_u| = f_u^+ - f_u^- \quad (20.3.13)$$

which is different from $|A|$ because of equation (20.2.22), one has

$$G = 1 - 2\tau|f_u| \sin^2 \frac{\phi}{2} - I\tau A \sin \phi \quad (20.3.14)$$

The stability condition is given by the requirement of the spectral radius of G being lower or equal to one.

A difficulty arises here since $|f_u|$ and A have, generally, not the same set of eigenvalues. However, an estimation of the eigenvalues of the matrix G can be obtained by first transforming G with the similarity transformation matrix P which diagonalizes A . Since G and

$$\bar{G} = P^{-1}GP \quad (20.3.15)$$

have the same eigenvalues, one can as well analyse the eigenvalues of

$$\bar{G} = 1 - 2\tau|E| \sin^2 \frac{\phi}{2} - I\tau\Lambda \sin \phi \quad (20.3.16)$$

where $|E|$ is the transformed matrix of $|f_u|$ and Λ the diagonal matrix of the eigenvalues of A :

$$|E| = P^{-1}|f_u|P = P^{-1}f_u^+P - P^{-1}f_u^-P \quad (20.3.17)$$

A numerical estimation of the eigenvalues of \bar{G} shows that they reach their maximum value for the high-frequency limit $\phi = \pi$. Hence, the maximum eigenvalue of \bar{G} , or its spectral radius $\rho(\bar{G})$, is given by

$$\rho(\bar{G}) = 1 - 2\tau\rho(|E|) \quad (20.3.18)$$

where $\rho(|E|)$ is the spectral radius of $|E|$. The stability condition of the flux split scheme (20.3.2) is therefore given by $\rho(\bar{G}) \leq 1$, that is by

$$\tau|e|_{\max} \leq 1 \quad (20.3.19)$$

where $|e|_{\max}$ is the maximum eigenvalue of $|E|$, instead of the linear CFL condition, written for $u > 0$:

$$\text{CFL} = \tau|u + c|_{\max} = \tau|\lambda|_{\max} \leq 1 \quad (20.3.20)$$

where $|\lambda|_{\max}$ represents the maximum eigenvalue of the Jacobian A . Hence, the stability limits of the scheme (20.3.2) are defined by the eigenvalues of $|f_u|$ and not by the Jacobian eigenvalues of $|A|$.

An explicit calculation performed by Lerat (1983) for a shock tube problem with an initial pressure ratio of 2.8 and equal temperatures on both sides of the diaphragm shows that the condition (20.3.19) corresponds to a CFL number limit $\tau|u + c|_{\max}$ below one; in particular, for this case the stability limit (20.3.19) corresponds to $\text{CFL} \leq 0.858$ instead of one according to equation (20.3.20).

Figure 20.3.2 presents computed results for this shock tube problem at $\text{CFL} = 0.9$ and 0.85 . The instability of the computed solutions at $\text{CFL} = 0.90$ clearly demonstrates the validity of the stability limit (20.3.19).

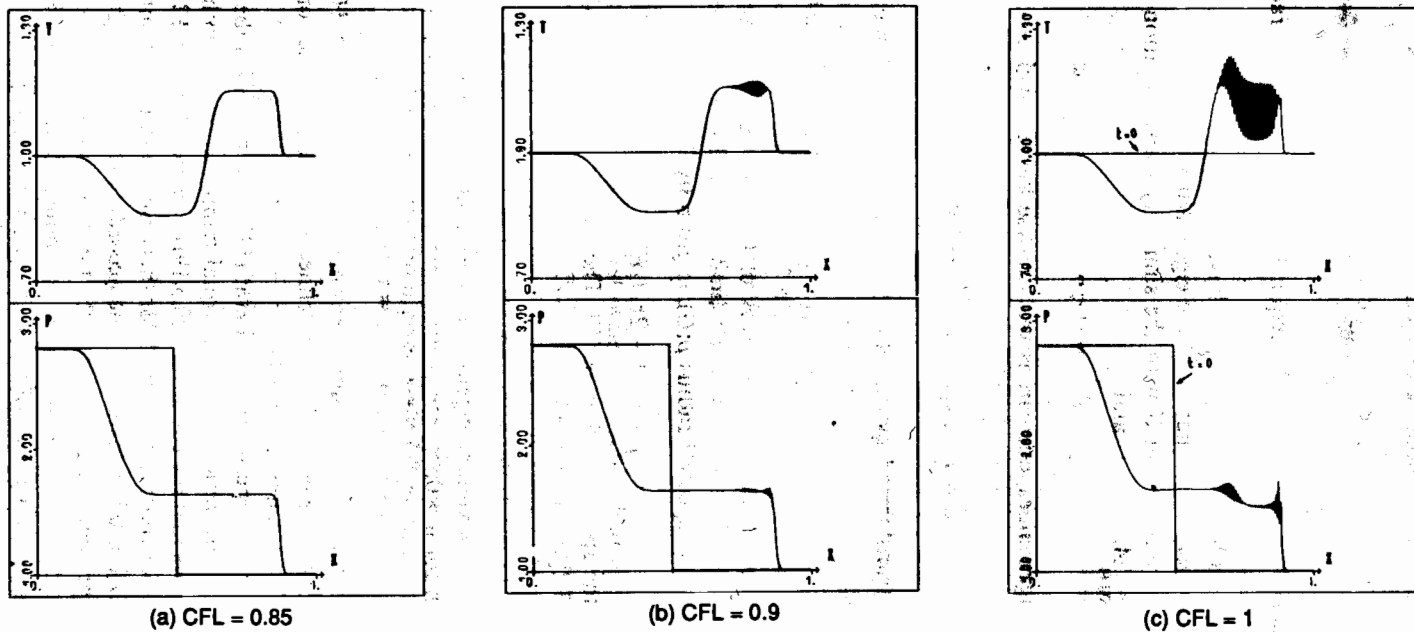
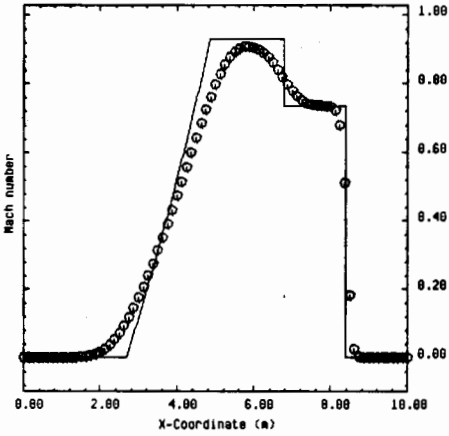


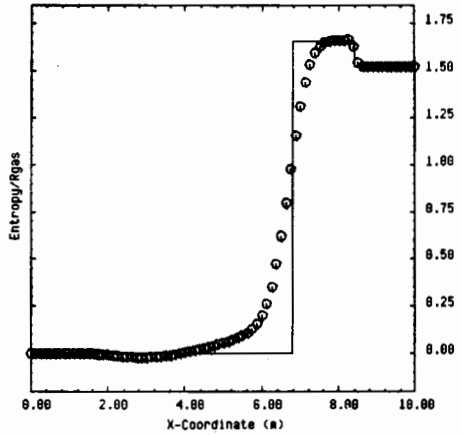
Figure 20.3.2 Shock tube problem with first-order Steger-Warming flux splitting. (From Lerat, 1983)

35 time steps

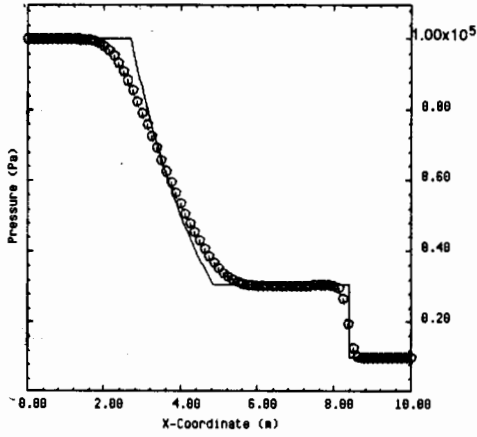
Shock Tube Flow
Solution at t = 6.2 msec.



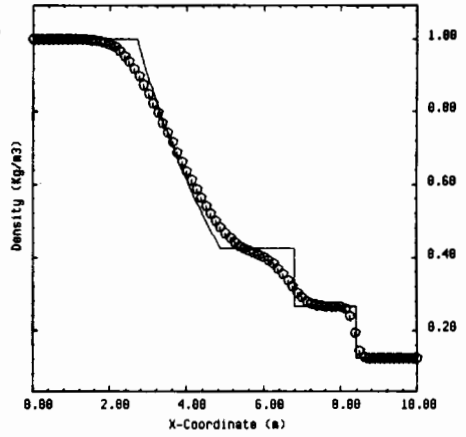
Shock Tube Flow
Solution at t = 6.2 msec.



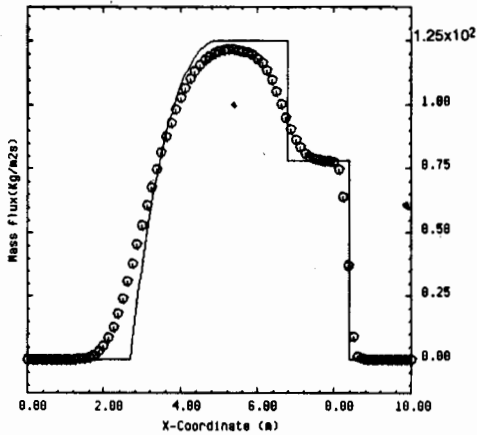
Shock Tube Flow
Solution at t = 6.2 msec.



Shock Tube Flow
Solution at t = 6.2 msec.



Shock Tube Flow
Solution at t = 6.2 msec.



Shock Tube Flow
Solution at t = 6.2 msec.

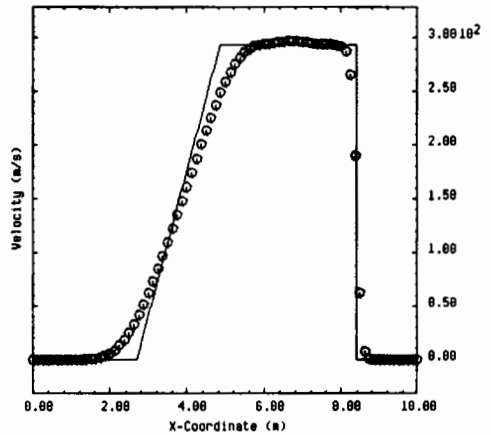


Figure 20.3.3 Computation of the shock tube problem with a first-order scheme and the flux vector splitting of Steger and Warming

pressure ratio $P_L/P_R = 10$

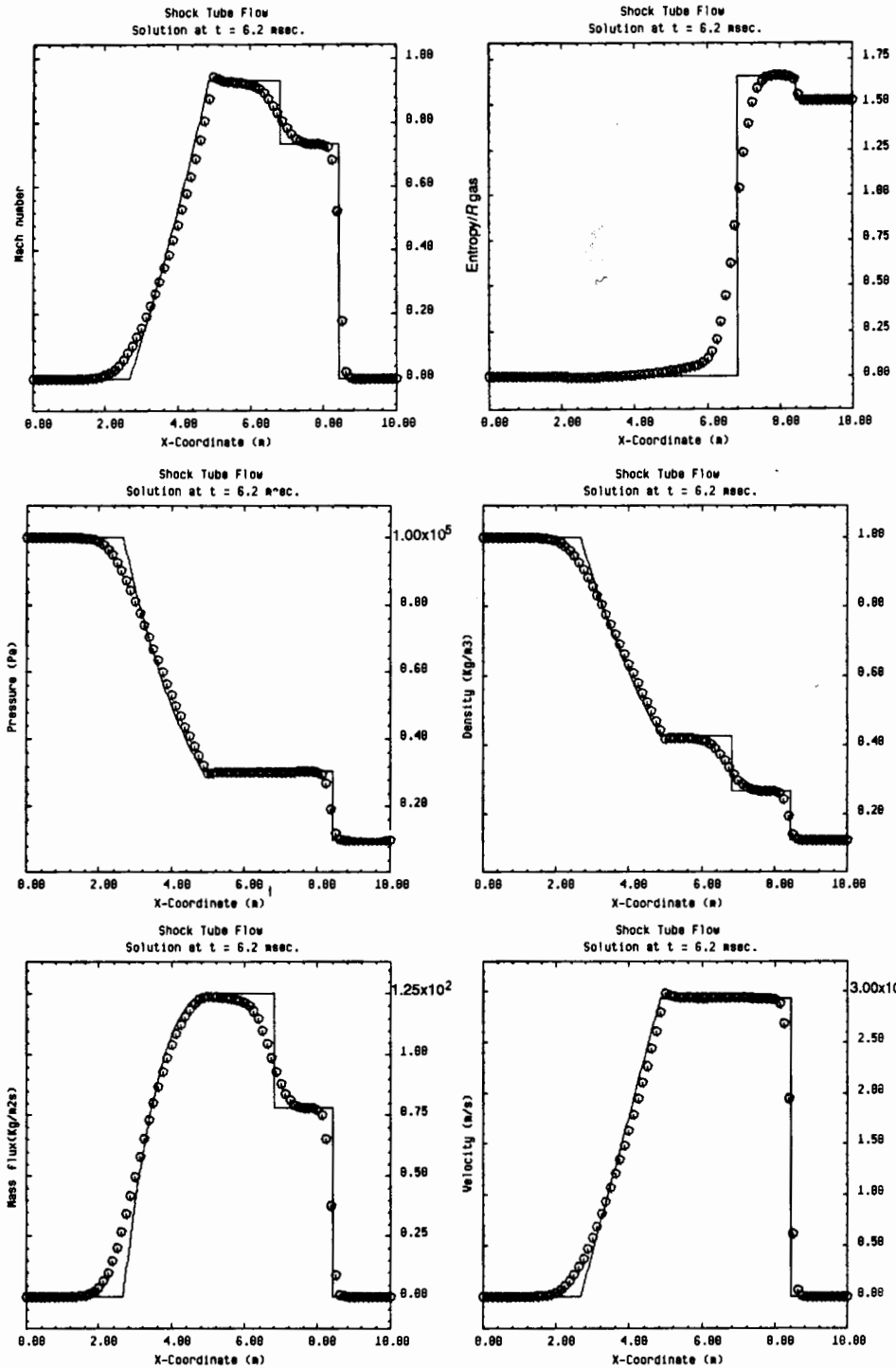
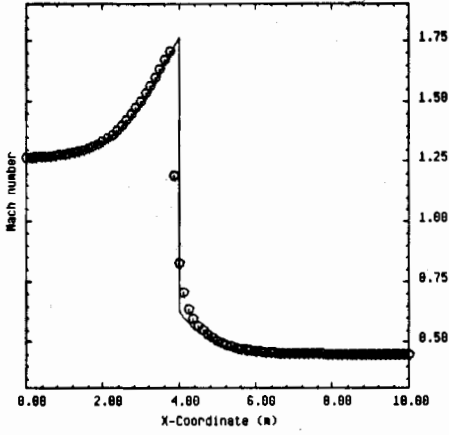
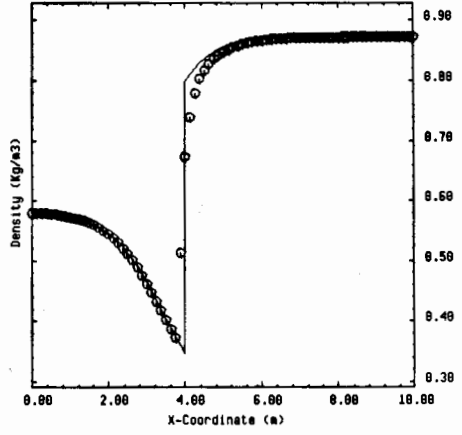


Figure 20.34 Computation of the shock tube problem with a first-order scheme and the flux vector splitting of Van Leer

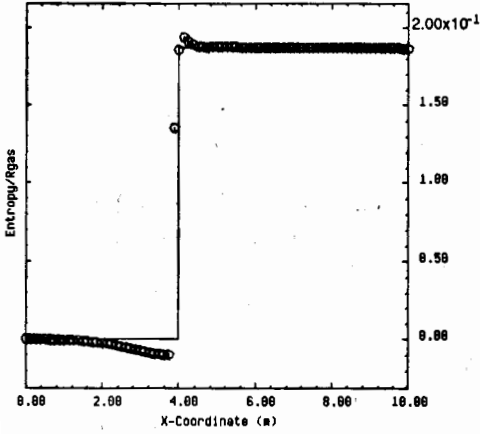
Divergent Nozzle Flow
Steady State



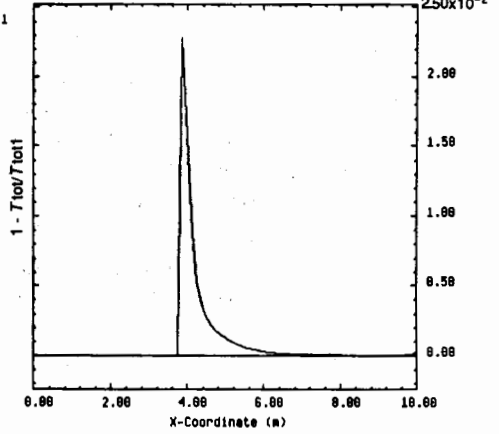
Divergent Nozzle Flow
Steady State



Divergent Nozzle Flow
Steady-State



Divergent Nozzle Flow
Steady State



Divergent Nozzle Flow
Steady State

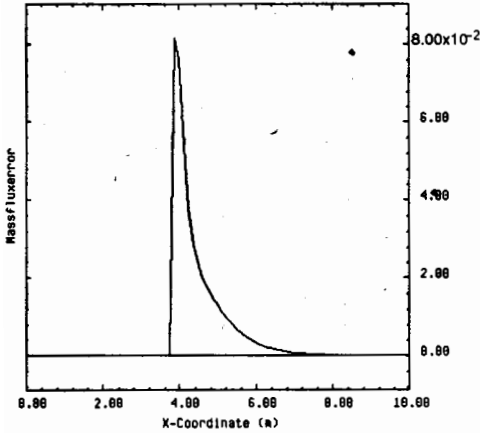


Figure 20.3.5 Computation of the shock transition in a divergent nozzle with a first-order flux vector splitting scheme of Steger and Warming

For the Van Leer splitting, a practical stability condition is given by Van Leer (1982), for $u > 0$:

$$\tau(u+c)_{\max} \leq \frac{2\gamma + M(3-\gamma)}{\gamma + 3} \quad \text{for } M < 1 \quad (20.3.21)$$

Figures 20.3.3 and 20.3.4 show a comparison, on the shock tube problem with a pressure ratio of 10 after 35 time steps, between the Steger and Warming flux vector splitting and the flux splitting defined by Van Leer, both at CFL = 0.95 with the first-order upwind scheme (20.3.2). Van Leer's fluxes give a marked improvement of the expansion region, although in both cases the contact discontinuity is poorly represented.

This is a general property of flux splitting schemes, since sharp transitions require a vanishing dissipation when crossing discontinuities. Since this does not happen at contact discontinuities, they will tend to diffuse continuously with time. To circumvent this difficulty non-linear devices will have to be introduced (see Chapter 21). Note also that Roe's and Osher's approximate Riemann solvers, to be presented in Section 20.5, detect stationary contact discontinuities and hence better preserve their sharpness.

With regard to shocks, the Van Leer splitting has, by construction, a vanishing eigenvalue of the split flux Jacobians in the range $0 < M < 1$ and leads to sharp stationary shock transitions, over two cells. Since the Steger–Warming splitting does not have this property, shocks will be more smeared out. These properties are clearly illustrated in Figures 20.3.5 and 20.3.6, comparing the two methods on a shock transition in a divergent nozzle. Observe that in both cases there is no mass flux, nor total temperature error upstream of the shock. This results from the adaptation of the upwind procedure with the supersonic flow in this region, preventing errors to propagate upstream.

Figure 20.3.7 shows the results of a computation with the Steger–Warming flux splitting for a shock tube problem with an initial pressure discontinuity of 100, corresponding to the test case of Figure 16.6.9. The expansion fan reaches supersonic velocities and a sonic transition occurs at the initial position of the diaphragm $x = 5$.

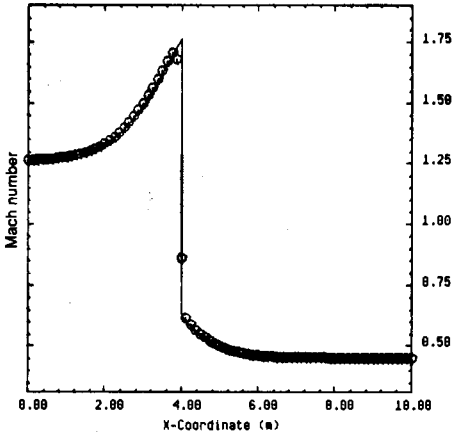
Observe the small discontinuity at the sonic point transition as a consequence of the slope discontinuity of the components f^+ and f^- . This can be corrected by a modification proposed by Buning and Steger (1982), whereby the eigenvalues are redefined as

$$\lambda^\pm = \frac{\lambda \pm \sqrt{\lambda^2 + \varepsilon^2}}{2} \quad (20.3.22)$$

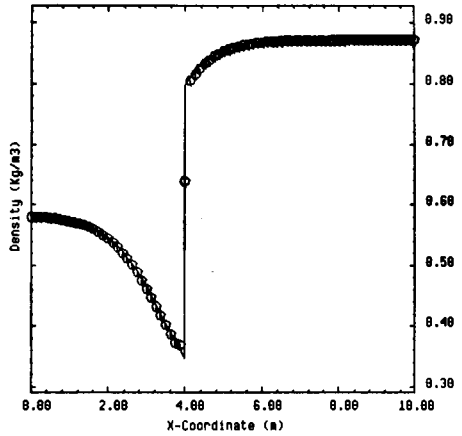
where ε is a small number. This leads to a smooth transition through the sonic points, as can be seen from Figure 20.3.8, at the expense of introducing some small error.

First-order schemes are not sufficiently accurate for practical purposes and the passage to second-order schemes is essential. This will be discussed in the following Chapter 21.

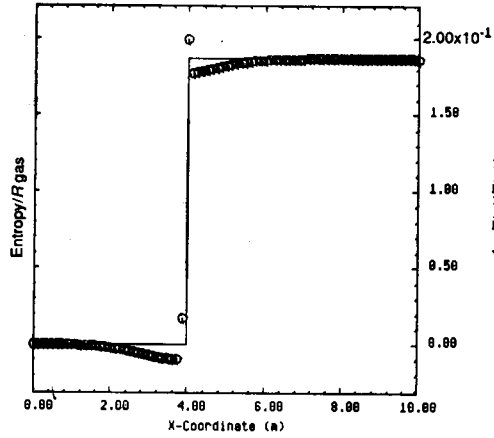
Divergent Nozzle Flow
Steady State



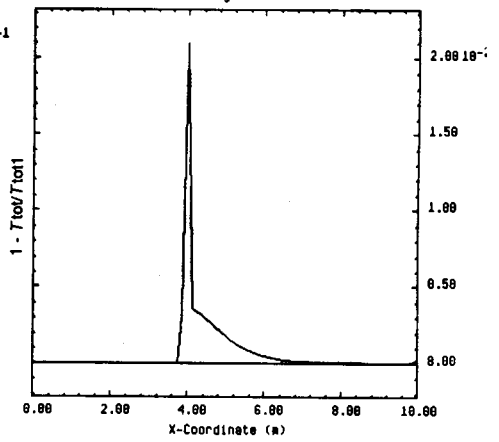
Divergent Nozzle Flow
Steady State



Divergent Nozzle Flow
Steady State



Divergent Nozzle Flow
Steady State



Divergent Nozzle Flow
Steady State

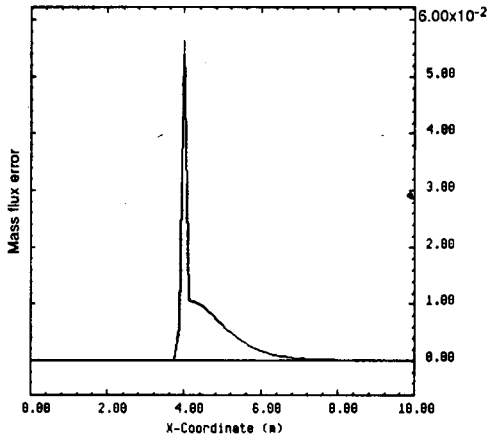


Figure 20.3.6 Computation of the shock transition in a divergent nozzle with a first-order flux vector splitting scheme of Van Leer

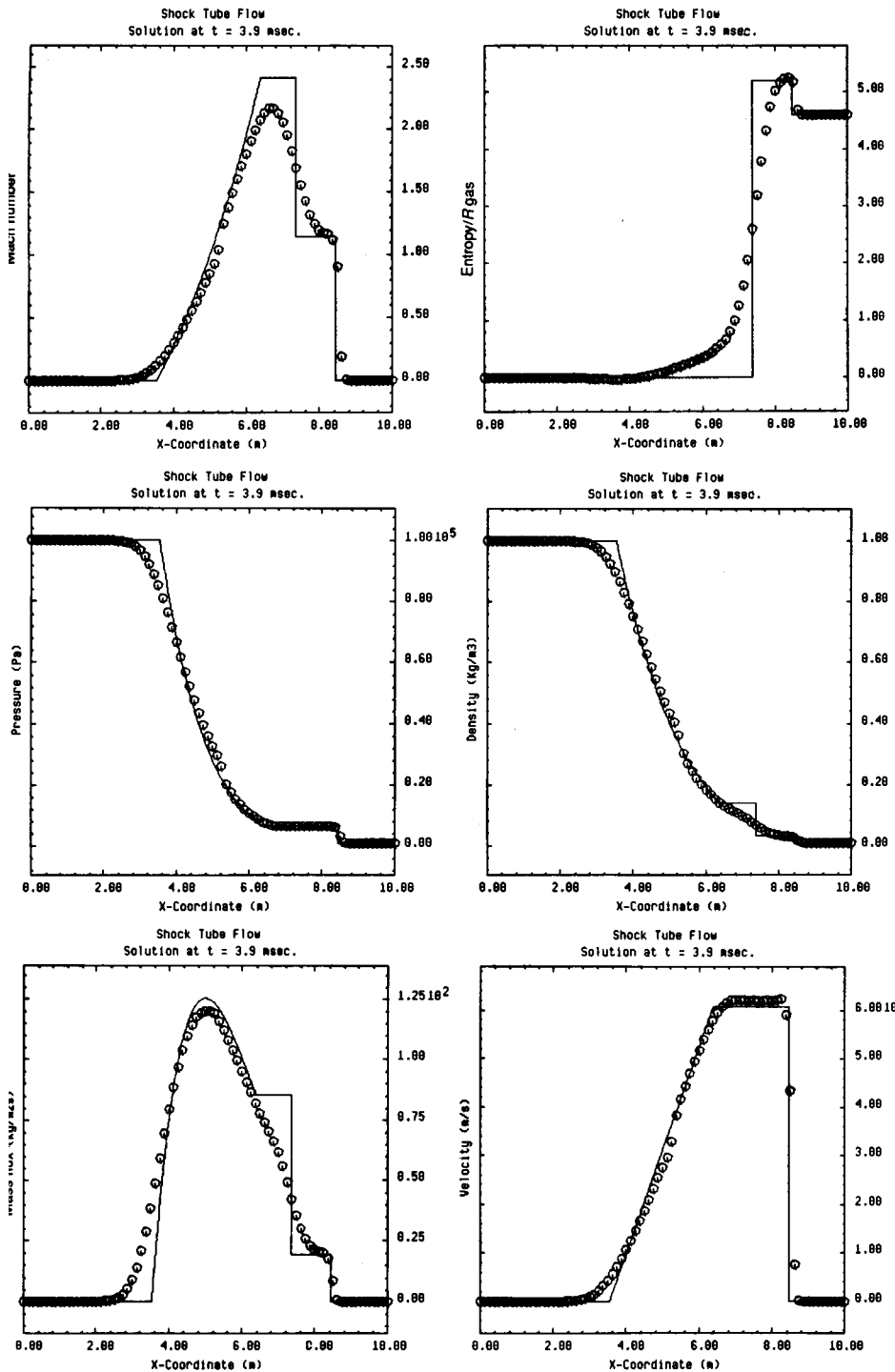


Figure 20.3.7 Computation of the shock tube problem of Figure 16.6.9 with a first-order scheme and the flux vector splitting of Steger and Warming, with $\varepsilon = 0$

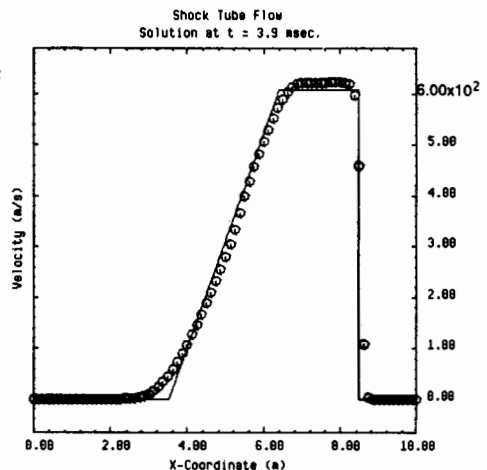
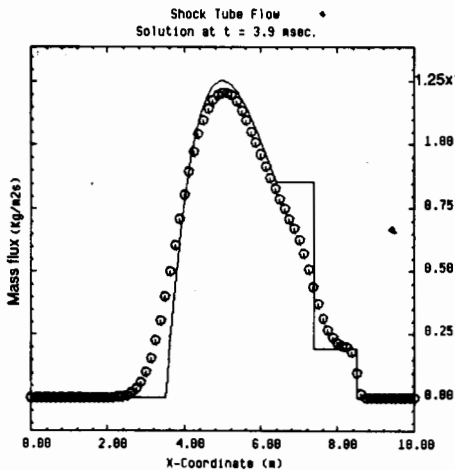
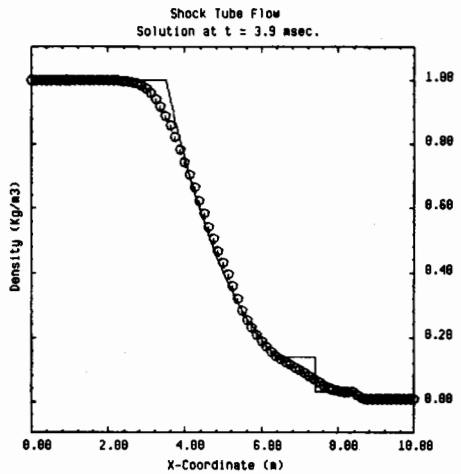
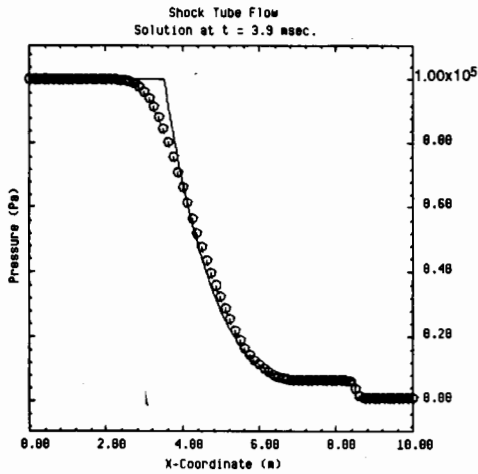
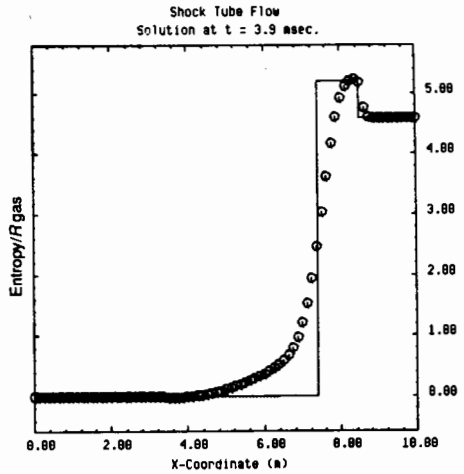
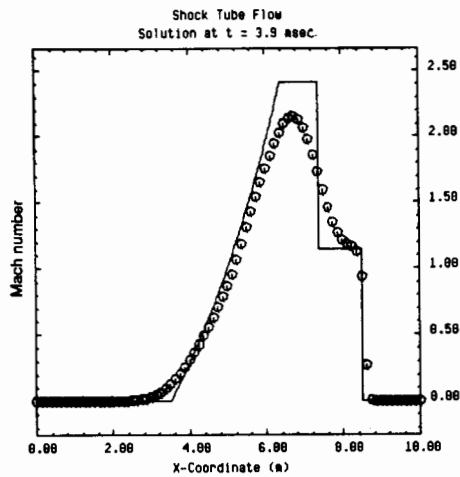


Figure 20.3.8 Computation of the shock tube problem of Figure 16.6.9 with a first-order scheme and the flux vector splitting of Steger and Warming, with $\epsilon \neq 0$

20.3.3 Non-conservative first-order upwind schemes

Several non-conservative schemes can be derived from the split form of the Euler equations, based on the splitting of the Jacobian following equations (20.2.8) and (20.2.9).

Considering the quasi-linear equation (20.2.25), a first-order accurate upwind discretization can be defined as

$$U_i^{n+1} - U_i^n = -\tau A_{i-1/2}^+(U_i - U_{i-1})^n - \tau A_{i+1/2}^-(U_{i+1} - U_i)^n \quad (20.3.23)$$

This method has been applied by Chakravarthy *et al.* (1980) under the name of split coefficient matrix method and is a direct generalization of the Courant, Isaacson and Reeves characteristic upwind scheme. A less accurate variant of this scheme consists in taking A^+ and A^- at a mesh point, leading to

$$U_i^{n+1} - U_i^n = -\tau A_i^+(U_i - U_{i-1})^n - \tau A_i^-(U_{i+1} - U_i)^n \quad (20.3.24)$$

Since these schemes are not in conservative form, they will require some form of shock fitting in order to obtain the correct shock intensities. Otherwise the discontinuities are not correctly captured.

Another family of non-conservative upwind schemes has been extensively developed by Moretti under the name of λ schemes (Moretti, 1979, 1986; see also Dadone and Napolitano, 1983; Moretti and Zannetti, 1984; Favini and Zannetti, 1986).

These schemes are based on the compatibility relations, using the Riemann variables as unknowns and discretizing the equations in an upwind way according to the sign of the associated characteristic speeds. Since the characteristic relations explicitly express the conservation of entropy along a streamline, the inclusion of shock fitting is an essential part of the formulation.

20.4 MULTI-DIMENSIONAL FLUX VECTOR SPLITTING

The flux splitting upwind methods can readily be extended to multi-dimensional flows by applying the one-dimensional splitting to each flux component separately according to the sign of the associated eigenvalues.

Considering a two-dimensional flow in a Cartesian coordinate system

$$\frac{\partial U}{\partial t} + \frac{\partial f}{\partial x} + \frac{\partial g}{\partial y} = 0 \quad (20.4.1)$$

the Jacobians A and B of the flux components f and g can be diagonalized by the matrices P_1 and P_2 derived from the general matrix P of Example 16.5.1 which diagonalizes the combination

$$K = \vec{A} \cdot \vec{\kappa} \quad (20.4.2)$$

by setting respectively $\vec{\kappa} = \vec{1}_x$ and $\vec{\kappa} = \vec{1}_y$.

The two-dimensional Jacobian A has the eigenvalues $u, u, u + c, u - c$, and the

transformation by the matrix P_1 leads to the diagonal matrix Λ_1 :

$$P_1^{-1}AP_1 = \begin{vmatrix} u & & & \\ \cdot & u & & \\ \cdot & \cdot & u+c & \\ \cdot & \cdot & \cdot & u-c \end{vmatrix} = \Lambda_1 \quad (20.4.3)$$

where P_1 is defined by setting $\kappa_x = 1$ and $\kappa_y = 0$ in equation (E16.5.3). Similarly, the matrix B is diagonalized to

$$P_2^{-1}BP_2 = \begin{vmatrix} v & & & \\ \cdot & v & & \\ \cdot & \cdot & v+c & \\ \cdot & \cdot & \cdot & v-c \end{vmatrix} = \Lambda_2 \quad (20.4.4)$$

where P_2 is defined by setting $\kappa_x = 0$ and $\kappa_y = 1$ in equation (E16.5.3).

Separating the positive from the negative eigenvalues in Λ leads to the definition of the split Jacobians A^\pm and B^\pm as well as to the split fluxes f^\pm and g^\pm , following the steps of Section 20.2.

For a supersonic flow in the x direction,

$$\begin{aligned} f^+ &= f \\ f^- &= 0 \end{aligned} \quad (20.4.5)$$

and for a subsonic flow, one would have

$$\Lambda_1^+ = \begin{vmatrix} u & \cdot & \cdot & \cdot \\ \cdot & u & \cdot & \cdot \\ \cdot & \cdot & u+c & \cdot \\ \cdot & \cdot & \cdot & 0 \end{vmatrix} \quad (20.4.6)$$

and

$$\Lambda_1^- = \begin{vmatrix} 0 & \cdot & \cdot & \cdot \\ \cdot & 0 & \cdot & \cdot \\ \cdot & \cdot & 0 & \cdot \\ \cdot & \cdot & \cdot & u-c \end{vmatrix} \quad (20.4.7)$$

with

$$\begin{aligned} A^+ &= P_1 \Lambda_1^+ P_1^{-1} \\ A^- &= P_1 \Lambda_1^- P_1^{-1} \end{aligned} \quad (20.4.8)$$

and similar definitions for B .

The split fluxes are defined by

$$\begin{aligned} f^\pm &= A^\pm \cdot U \\ g^\pm &= B^\pm \cdot U \end{aligned} \quad (20.4.9)$$

20.4.1 Steger and Warming flux splitting

Following equations (20.2.18) and (20.2.19), a flux splitting of the Steger-Warming type can be defined for a general eigenvalue matrix

$$\bar{\Lambda}_1 = \begin{vmatrix} \bar{\lambda}_1 & & & \\ \cdot & \bar{\lambda}_1 & & \\ \cdot & \cdot & \bar{\lambda}_2 & \\ \cdot & \cdot & \cdot & \bar{\lambda}_3 \end{vmatrix} \quad (20.4.10)$$

leading to a split flux

$$\bar{f} = \frac{\rho}{2\gamma} \begin{vmatrix} \alpha \\ \alpha u + c(\bar{\lambda}_2 - \bar{\lambda}_3) \\ \alpha v \\ \alpha \frac{u^2 + v^2}{2} + uc(\bar{\lambda}_2 - \bar{\lambda}_3) + c^2 \frac{\bar{\lambda}_2 + \bar{\lambda}_3}{\gamma - 1} \end{vmatrix} \quad (20.4.11)$$

where

$$\alpha = 2(\gamma - 1)\bar{\lambda}_1 + \bar{\lambda}_2 + \bar{\lambda}_3 \quad (20.4.12)$$

For the same splitting, the flux component \bar{g} would be given by

$$\bar{g} = \frac{\rho}{2\gamma} \begin{vmatrix} \alpha \\ \alpha u \\ \alpha v + c(\bar{\lambda}_2 - \bar{\lambda}_3) \\ \alpha \frac{u^2 + v^2}{2} + vc(\bar{\lambda}_2 - \bar{\lambda}_3) + c^2 \frac{\bar{\lambda}_2 + \bar{\lambda}_3}{\gamma - 1} \end{vmatrix} \quad (20.4.13)$$

The corresponding three-dimensional expressions can be found in the original reference (Steger and Warming, 1981).

20.4.2 Van Leer flux splitting

The Van Leer splitting is extended to two dimensions by the following expression:

$$f_{\text{VL}}^{\pm} = f_{1,\text{VL}}^{\pm} \begin{vmatrix} 1 \\ \frac{(\gamma - 1)u \pm 2c}{\gamma} \\ v \\ \frac{v^2}{2} + \frac{[(\gamma - 1)u \pm 2c]^2}{2(\gamma^2 - 1)} \end{vmatrix} \quad (20.4.14)$$

where the split mass flux component $f_{1,\text{VL}}^{\pm}$ is defined as in the one-dimensional

case by

$$f_{1,vL}^{\pm} = \pm \frac{\rho}{4c} (u \pm c)^2 \quad (20.4.15)$$

Similarly, the split flux component associated to the y direction is given by

$$g_{vL}^{\pm} = g_{1,vL}^{\pm} \left| \begin{array}{c} 1 \\ u \\ \frac{(\gamma - 1)v \pm 2c}{\gamma} \\ \frac{u^2}{2} + \frac{[(\gamma - 1)v \pm 2c]^2}{2(\gamma^2 - 1)} \end{array} \right| \quad (20.4.16)$$

with

$$g_{1,vL}^{\pm} = \pm \frac{\rho}{4c} (v \pm c)^2 \quad (20.4.17)$$

The three-dimensional split fluxes are to be found in the original reference (Van Leer, 1982) or in Anderson *et al.* (1986b).

20.4.3 Arbitrary meshes

In practical computations one deals mostly with arbitrary meshes, considered either in a finite volume approach or in a curvilinear coordinate system ξ, η .

In both cases, the upwind characterization is based on the signs of the eigenvalues of the matrix

$$K^{(n)} = \bar{A} \cdot \bar{1}_n = A \hat{n}_x + B \hat{n}_y \quad (20.4.18)$$

where the unit vector along the considered cell face is introduced.

The fluxes will be decomposed by their components

$$F^{(n)} = \bar{F} \cdot \bar{1}_n = f \hat{n}_x + g \hat{n}_y \quad (20.4.19)$$

and separated into positive and negative parts according to the sign of the eigenvalues of $K^{(n)}$ as described above, considering the normal direction as a local coordinate direction.

For a general eigenvalue splitting (20.2.2), the normal flux projection (20.4.19) is decomposed by a Steger-Warming flux splitting as

$$F_{\pm}^{(n)} = \frac{\rho}{2\gamma} \left| \begin{array}{c} \alpha \\ \alpha u + c(\lambda_2^{\pm} - \lambda_3^{\pm}) \hat{n}_x \\ \alpha v + c(\lambda_2^{\pm} - \lambda_3^{\pm}) \hat{n}_y \\ \alpha \frac{u^2 + v^2}{2} + cv_n(\lambda_2^{\pm} - \lambda_3^{\pm}) + c^2 \frac{\lambda_2^{\pm} + \lambda_3^{\pm}}{\gamma - 1} \end{array} \right| \quad (20.4.20)$$

where the eigenvalues of the matrix K are defined as

$$\begin{aligned}\lambda_1 &= \vec{v} \cdot \vec{I}_n \equiv v_n \\ \lambda_2 &= \vec{v} \cdot \vec{I}_n + c \\ \lambda_3 &= \vec{v} \cdot \vec{I}_n - c\end{aligned}\quad (20.4.21)$$

and the \pm sign indicates the positive or negative parts respectively.

The parameter α is defined as in (20.4.12) by

$$\alpha = 2(\gamma - 1)\lambda_1^\pm + \lambda_2^\pm + \lambda_3^\pm \quad (20.4.22)$$

In the curvilinear coordinate system ξ, η , selecting the normal components amounts to work with the contravariant components of the dependent variable and flux vectors.

In three dimensions, a similar form is readily obtained, defining the velocity squared as $q^2 = u^2 + v^2 + w^2$:

$$F_\pm^{(n)} = \frac{\rho}{2\gamma} \begin{vmatrix} \alpha \\ \alpha u + c(\lambda_2^\pm - \lambda_3^\pm)\hat{n}_x \\ \alpha v + c(\lambda_2^\pm - \lambda_3^\pm)\hat{n}_y \\ \alpha w + c(\lambda_2^\pm - \lambda_3^\pm)\hat{n}_z \\ \alpha \frac{q^2}{2} + cv_n(\lambda_2^\pm - \lambda_3^\pm) + c^2 \frac{\lambda_2^\pm + \lambda_3^\pm}{\gamma - 1} \end{vmatrix} \quad (20.4.23)$$

For the Van Leer splitting a general form for curvilinear coordinates, whereby the splitting is defined according to the Mach number components in a coordinate direction, has been given in Thomas *et al.* (1985). For finite volume schemes, this is best expressed under the form of the splitting of the normal projection of the flux, according to the normal Mach number $M_n = v_n/c$. The following expression can be applied

$$F_{\pm, \text{VL}}^{(n)} = f_\pm^m \begin{vmatrix} 1 \\ u + \frac{\hat{n}_x(-v_n \pm 2c)}{\gamma} \\ v + \frac{\hat{n}_y(-v_n \pm 2c)}{\gamma} \\ w + \frac{\hat{n}_z(-v_n \pm 2c)}{\gamma} \\ \frac{q^2 - v_n^2}{2} + \frac{[(\gamma - 1)v_n \pm 2c]^2}{2(\gamma^2 - 1)} \end{vmatrix} \quad (20.4.24)$$

where f_\pm^m is the split mass flux component defined by

$$f_\pm^m = \pm \frac{\rho c (M_n \pm 1)^2}{4} \quad (20.4.25)$$

In multi-dimensional flows, the flux splitting approach is based on a locally one-dimensional eigenvalue decomposition, implying the assumption of propagation of information in the directions normal to the cell faces. This leads to a mesh dependence of the multi-dimensional flux splitting, see Section 20.7.

20.5 THE GODUNOV-TYPE SCHEMES

As mentioned in the introduction to this chapter, we can go a step further in the interaction between discretization method and physical properties by introducing information from the local exact solutions to the Euler equations. This most original idea has been introduced by Godunov (1959).

In Godunov's method, the solution is considered as piecewise constant over each mesh cell at a fixed time and the evolution of the flow to the next time step results from the wave interactions originating at the boundaries between adjacent cells. The cell interfaces separate two different fluid states U_L at the left side and U_R at the right side, and the resulting local interaction can be exactly resolved since the initial conditions at time $t = n \Delta t$ correspond to the Riemann or shock tube problem.

As seen in Section 16.6.3, this problem has an exact solution generally composed of a shock wave, a contact discontinuity and an expansion fan separating regions of uniform flow conditions. The solutions to the Riemann problem at each cell interface produces a perturbation of the piecewise constant fluid state, resulting from the propagating waves over the time interval Δt . Each wave carries information in an upwind manner and hence the resulting state will only depend on the local physical properties. In order to define completely the interaction between adjacent cells, the time interval over which the waves are allowed to propagate should be limited by the condition that the adjacent Riemann problems do not interfere. This leads to a form of CFL condition.

The new piecewise constant approximation at time $t = (n + 1)\Delta t$ is then obtained by averaging, over each cell, the fluid states resulting from the perturbation waves. This produces an explicit conservative scheme, which is, however, of first-order accuracy as will be shown next. Actually Godunov's scheme was the first successful conservative upwind scheme. A detailed description of the method and applications to numerous flow problems, as it has been experienced by Godunov and his coworkers over a time span of nearly twenty years, is given in Godunov *et al.* (1979).

As a consequence of the averaging procedure, much of the details of the Riemann solutions are lost. Since the exact solution of the Riemann problem requires the resolution of a non-linear algebraic equation which can be quite time consuming, approximate Riemann solutions could be considered, reducing the computational work at each interface. The most interesting approximate Riemann solvers have been developed by Roe (1981a) and Osher (Osher, 1981; Osher and Solomon, 1982). They will be summarized in the following sections.

20.5.1 The basic Godunov scheme

Three steps are involved in Godunov's method in order to define the solution at time $t = (n + 1)\Delta t$ from the known solution at $t = n\Delta t$:

Step 1 Define a piecewise constant approximation of the solution at $t = n\Delta t$. This is illustrated in Figure 20.5.1(a). Since the piecewise constant approximation is an average of the solution over the cell of size Δx , the spatial error is of the order Δx and hence the resulting scheme will be first-order accurate in space.

Note that this approximation corresponds to a finite volume representation whereby the discrete values represent averages of the state variables over the cells. This is to be compared with the alternate representation whereby the discrete variables are considered as nodal values of smoothly varying functions.

Exact relations for the averaged cell values can be obtained from the integral conservation laws. Integrating the conservation equation $\partial U/\partial t + \partial f/\partial x = 0$

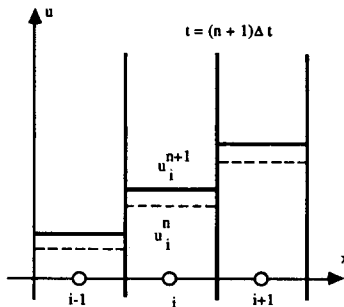
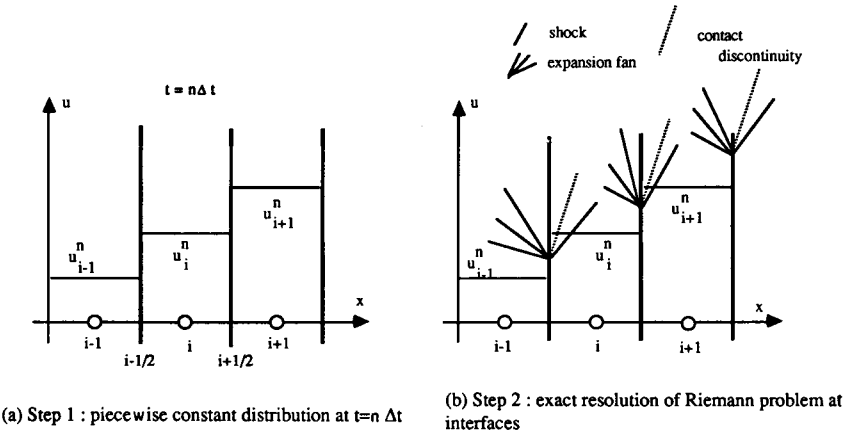


Figure 20.5.1 The three basic steps of Godunov's method

over x in the domain (a, b) gives the general relation

$$\frac{d}{dt} \int_a^b U(x, t) dx = f(a, t) - f(b, t) \quad (20.5.1)$$

and if further integrated in time, from $t = n \Delta t$ to $t = (n + 1) \Delta t$, we obtain the exact relation

$$\int_a^b U^{n+1}(x) dx - \int_a^b U^n(x) dx = -\Delta t [\hat{f}(U(b)) - \hat{f}(U(a))] \quad (20.5.2)$$

where \hat{f} is the time average of the physical flux between $n \Delta t$ and $(n + 1) \Delta t$.

Defining the average state variable over the cell $(i - \frac{1}{2}, i + \frac{1}{2})$ as

$$\bar{U}_i = \frac{1}{\Delta x} \int_{i-1/2}^{i+1/2} U(x, t) dx \quad (20.5.3)$$

the integral conservation relation (20.5.3) becomes

$$\bar{U}_i^{n+1} - \bar{U}_i^n = -\frac{\Delta t}{\Delta x} [\hat{f}(U_{i+1/2}) - \hat{f}(U_{i-1/2})] \quad (20.5.4)$$

This is again an exact relation in conservation form. It expresses the variation, over the time interval Δt , of the cell-averaged state variables as resulting from the balance of the time-averaged fluxes at the boundaries of the cell. Observe that the conservation equation (20.5.4) is of the same form as the general expression of a numerical scheme in conservation form (20.3.9). Hence the numerical flux of a scheme is to be considered as an approximation to the time average of the physical flux at the cell interfaces and the mesh point variables U_i^n as a representation of the cell averages.

Step 2 Obtain the solution for the local Riemann problem at the cell interfaces.

This is the physical step of the whole procedure. The discontinuities at the interfaces are resolved in a superposition of waves satisfying locally the conservation equations. This is illustrated in Figure 20.5.1(b), where the basic components of the one-dimensional Riemann problem solution are shown.

The original Godunov method is based on the exact solution of the Riemann problems. However, approximate solutions can be applied as an alternative and two of them will be described in the following subsection.

If we denote by $U^{(R)}(x/t, U_L, U_R)$ the exact solution of the Riemann problem with initial conditions

$$\begin{aligned} U &= U_L & x < 0 \\ U &= U_R & x > 0 \end{aligned} \quad (20.5.5)$$

we know from Section 16.6.3 that the exact solution is a unique function of initial conditions and of the ratio x/t . Hence in each interval $(i, i + 1)$, the local

exact solution is given by

$$U^{(R)}(x, t) = U^{(R)}\left(\frac{x - (i + 1/2)\Delta x}{t - n\Delta t}, U_i^n, U_{i+1}^n\right) \quad i\Delta x < x < (i + 1)\Delta x \quad (20.5.6)$$

Step 3 Average the state variables after a time interval Δt .

The state variables obtained after step 2 are averaged over each cell defining a new piecewise constant approximation resulting from the wave propagation during the time interval Δt (Figure 20.5.1(c)). In order to be consistent, the time interval Δt should be limited such that the waves issued at an interface do not interact with the waves created at the adjacent interfaces. Otherwise the situation inside a cell would be influenced by interacting Riemann problems. This leads to the CFL condition $|a_{\max}|\Delta t < \Delta x/2$, where a_{\max} is the maximum wave speed in the cell eigenvalue of the local Jacobian matrix.

The piecewise constant approximation at time level $n + 1$ is therefore defined by

$$\overline{U}_i^{n+1} = \frac{1}{\Delta x} \int_{i-1/2}^{i+1/2} U^{(R)}(x, (n + 1)\Delta t) dx \quad (20.5.7)$$

Since the integration covers two half-cells influenced by different Riemann problems, the solution at $n + 1$ can be split into two contributions:

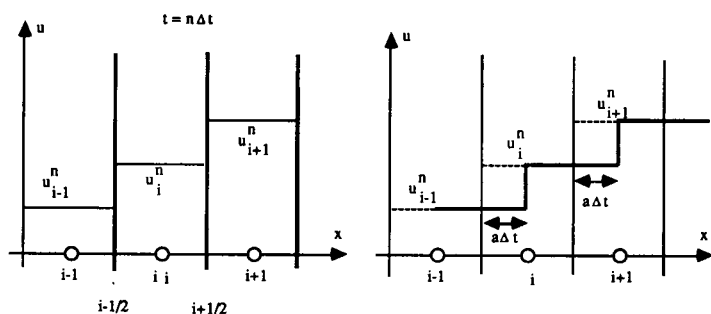
$$\overline{U}_i^{n+1} = \frac{1}{\Delta x} \int_0^{\Delta x/2} U^{(R)}\left(\frac{\xi}{\Delta t}, U_{i-1}^n, U_i^n\right) d\xi + \frac{1}{\Delta x} \int_{-\Delta x/2}^0 U^{(R)}\left(\frac{\xi}{\Delta t}, U_i^n, U_{i+1}^n\right) d\xi \quad (20.5.8)$$

where $\xi = 0$ corresponds to the cell interfaces, origins of the Riemann problems.

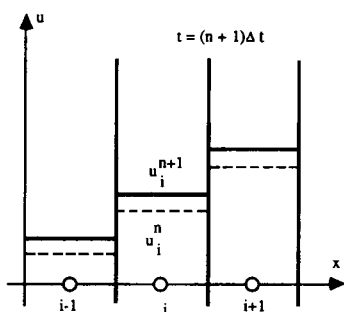
The first and third steps are actually of a numerical nature and can be considered as a ‘projection stage’, independent of the second, physical, step, the ‘evolution stage’, following the terminology of Van Leer (1977a, 1977b). Therefore, they can be modified without influencing the physical input, for instance by replacing the piecewise constant approximation by a piecewise linear variation inside each cell, leading to the definition of second-order space-accurate schemes (Van Leer, 1979). This will be discussed in more detail in Section 21.2.

In the following we will remove the overbars from the discrete state variables but it has to be kept in mind that they represent average states.

The basic steps of the Godunov approach can best be made clear when applied first to the simple linear scalar convection equation $u_t + au_x = 0$, with $a > 0$. The first step is shown in Figure 20.5.2(a) and is independent of the equation to be solved. The second, physical, step is obtained from the exact solution of the equation at the interface. For the linear convection equation, the discontinuity at the interface is translated over the distance $a\Delta t$ without modification, resulting in the situation shown in Figure 20.5.2(b) for $a > 0$. The new approximation at time level $n + 1$ results from the averaging of this new

(a) Step 1 : piecewise constant distribution at $t = n \Delta t$

(b) Step 2 : exact convection of discontinuity at interfaces

(c) Step 3 : averaging of new state after time interval Δt Figure 20.5.2 Godunov's method for the linear wave equation with $a > 0$

state. Since the exact linear solution is

$$u^{(n)}(x, t) = u^n[x - a(t - n \Delta t)] \quad (20.5.9)$$

the new average value in cell i is obtained as

$$\begin{aligned} u_i^{n+1} &= \frac{1}{\Delta x} \int_{i-1/2}^{i+1/2} u^n(x - a \Delta t) dx = \frac{1}{\Delta x} [a \Delta t u_{i-1}^n + (\Delta x - a \Delta t) u_i^n] \\ &= u_i^n - a \frac{\Delta t}{\Delta x} (u_i^n - u_{i-1}^n) \end{aligned} \quad (20.5.10)$$

We recognize here the first-order upwind scheme and the condition that the discontinuity at $(i - \frac{1}{2})$ does not leave cell i is the CFL condition

$$a \frac{\Delta t}{\Delta x} < 1 \quad (20.5.11)$$

When a is negative, the discontinuities propagate to the left and the above

procedure leads to (see Problem 20.18)

$$u_i^{n+1} = u_i^n - a \frac{\Delta t}{\Delta x} (u_{i+1}^n - u_i^n) \tag{20.5.12}$$

Hence, for an arbitrary sign we obtain the general upwind scheme (20.1.10).
but written for the cell averages $u_i^{n+1} \approx \bar{u}_i^{n+1}$ instead of the gridpoint values $u_i^{n+1} \approx u(x_i, (n+1)\Delta t)$

Godunov's numerical flux

The discrete form of Godunov's scheme is obtained from equation (20.5.8) by application of the conservation formula (20.5.2), since $U^{(R)}$ is an exact solution of the conservation equations and therefore satisfies equation (20.5.2). The first of the integrals in the right-hand side of equation (20.5.8) is calculated as follows:

$$\frac{1}{\Delta x} \int_0^{\Delta x/2} U^{(R)}\left(\frac{\xi}{\Delta t}, U_{i-1}^n, U_i^n\right) d\xi = \frac{1}{2} U_i^n - \frac{\Delta t}{\Delta x} [f(U_i) - f(U^{(R)}(0, U_{i-1}^n, U_i^n))] \tag{20.5.13}$$

The first term results from the fact that the solution at time $t = n\Delta t$ is the piecewise constant state U_i^n .

The flux terms are both constant in time, since the flux at $\xi = \Delta x/2$ is equal to $f(U_i^n)$ as long as the waves generated at $(i - \frac{1}{2})$ do not reach point i . This will be the case if the time step Δt is chosen to satisfy the condition

$$\Delta t |a_{\max}| < \frac{\Delta x}{2} \tag{20.5.14}$$

as a consequence of the following property of the Riemann solution, as seen in Section 16.6.3:

$$U^{(R)}\left(\frac{x}{t}, U_L, U_R\right) = \begin{cases} U_L & \text{for } x/t < a_{\min} \\ U_R & \text{for } x/t > a_{\max} \end{cases} \tag{20.5.15}$$

where a_{\min} and a_{\max} are the smallest and largest wave speeds. Note that generally one would have $a_{\min} = a_L$ and $a_{\max} = a_R$.

The second flux term is associated with the Riemann solution at the interface $\xi = 0$ and is therefore independent of time since the Riemann solution depends only on the ratio ξ/t . Hence the time-averaged fluxes of equation (20.5.13) are equal to the corresponding flux values. Similarly the second integral in equation (20.5.8) is obtained as

$$\frac{1}{\Delta x} \int_{-\Delta x/2}^0 U^{(R)}\left(\frac{\xi}{\Delta t}, U_i^n, U_{i+1}^n\right) d\xi = \frac{1}{2} U_i^n + \frac{\Delta t}{\Delta x} [f(U_i) - f(U^{(R)}(0, U_i^n, U_{i+1}^n))] \tag{20.5.16}$$

and Godunov's scheme can be written as

$$U_i^{n+1} = U_i^n - \frac{\Delta t}{\Delta x} [f(U^{(R)}(0, U_i^n, U_{i+1}^n)) - f(U^{(R)}(0, U_{i-1}^n, U_i^n))] \tag{20.5.17}$$

or, introducing the following notation for the Riemann solutions at the interfaces,

$$U_{i+1/2}^{(R)} = U^{(R)}(0, U_i^n, U_{i+1}^n) \quad (20.5.18a)$$

$$U_i^{n+1} = U_i^n - \frac{\Delta t}{\Delta x} [f(U_{i+1/2}^{(R)}) - f(U_{i-1/2}^{(R)})] \quad (20.5.18b)$$

The scheme is clearly in conservation form with the numerical flux

$$f_{i+1/2}^{*(G)} = f(U_{i+1/2}^{(R)}) \quad (20.5.19)$$

equal to the value taken by the physical flux for the Riemann solution at the interface.

Since the derivation takes place on a cell by cell basis, the Godunov scheme is easily extended to arbitrary meshes (see Problem 20.19). A generalization to time-varying and adaptive grids is developed in Harten and Hyman (1983).

The CFL condition (20.5.14) is established here under the requirement of non-interacting Riemann problems in order to obtain the simplest numerical flux and does not result from a stability limit on an amplification factor of the numerical scheme. Therefore the Godunov scheme could be extended to larger values of the CFL number if interactions between neighbouring Riemann problems are taken into account. Attempts in that direction have been developed by Leveque (1983, 1984, 1985) with an approximate treatment of the wave interactions, demonstrating the feasibility of Godunov schemes with larger time steps. However, when applied to the Euler equations the wave interactions can become quite complicated.

Godunov's scheme contains all the physics of the Euler equations, including proper representations of shocks and contact discontinuities. In addition, Godunov (1959) showed that the scheme does not accept expansion shocks, that is it satisfies an entropy condition (to be introduced in the following chapter), and that it is monotone.

Godunov's scheme for a scalar conservation law

More insight into the structure and properties of the Godunov scheme for non-linear conservation laws can be obtained in the case of a single conservation law, with arbitrary flux function $f(u)$.

The initial value problem for a scalar conservation equation

$$\begin{aligned} \frac{\partial u}{\partial t} + \frac{\partial f}{\partial x} &= 0 \\ u(x, 0) &= u_0(x) \end{aligned} \quad (20.5.20)$$

has generally discontinuous solutions, satisfying the Rankine-Hugoniot relations for a discontinuity propagating at speed C (see equation (16.1.19)) which becomes here

$$f(u_R) - f(u_L) = C(u_R - u_L) \quad (20.5.21a)$$

or

$$f(u_R) - Cu_R = f(u_L) - Cu_L \quad (20.5.21b)$$

where u_R and u_L are the states right and left of the discontinuity. The function $f(u) - Cu$ is therefore continuous.

The Riemann problem for the scalar equation (20.5.20) is defined by the initial conditions

$$u(x, 0) = \begin{cases} u_L & \text{for } x < 0 \\ u_R & \text{for } x \geq 0 \end{cases} \quad (20.5.22)$$

The solution of equation (20.5.20) with these initial conditions exists for arbitrary values of u_L and u_R and is a unique function of x/t for $t > 0$. It can be shown (Lax, 1971) that its values lie between u_L and u_R .

Denoting the Riemann solution by $u^{(R)}(x, t) = u^{(R)}(x/t, u_L, u_R)$, a remarkable closed-form formula for this solution has been found by Osher (1984), valid for arbitrary flux functions $f(u)$. We refer the reader to this reference for a proof.

Defining $\zeta = x/t$, Osher's formulas are as follows:

If $u_L < u_R$:

$$f(u^{(R)}(\zeta)) - \zeta u^{(R)}(\zeta) = \min_{u \in [u_L, u_R]} [f(u) - \zeta u] \quad (20.5.23a)$$

and

$$u^{(R)}(\zeta) = -\frac{d}{d\zeta} \left\{ \min_{u \in [u_L, u_R]} [f(u) - \zeta u] \right\} \quad (20.5.23b)$$

If $u_L > u_R$:

$$f(u^{(R)}(\zeta)) - \zeta u^{(R)}(\zeta) = \max_{u \in [u_L, u_R]} [f(u) - \zeta u] \quad (20.5.24a)$$

and

$$u^{(R)}(\zeta) = -\frac{d}{d\zeta} \left\{ \max_{u \in [u_L, u_R]} [f(u) - \zeta u] \right\} \quad (20.5.24b)$$

From these expressions a simple formula can be derived for the numerical flux (20.5.19) of Godunov's scheme, which is defined by the flux values at $\zeta = 0$. Hence, from equations (20.5.23a) and (20.5.24a),

$$f_{i+1/2}^{*(G)} = \begin{cases} \min_{u_i \leq u \leq u_{i+1}} f(u) & \text{if } u_i < u_{i+1} \\ \max_{u_i \geq u \geq u_{i+1}} f(u) & \text{if } u_i > u_{i+1} \end{cases} \quad (20.5.25)$$

When the flux is a convex function of u , that is $d^2 f/du^2 > 0$, as it is the case for the Euler equations or Burger's equation, the above relation states that when f is monotone between u_i and u_{i+1} the appropriate end point value has to be taken. When a critical sonic point $u = u^*$ exists in this interval, defined

by the vanishing first derivative $f'(u^*) = 0$, then either this point or an end value is selected.

Example 20.5.1 Godunov's scheme for Burgers equation

Consider the flux function $f = u^2/2$ of Burgers equation. For arbitrary values of u_i and u_{i+1} the exact solution of the Riemann problem with initial conditions

$$u = \begin{cases} u_i & \text{for } \xi < 0 \\ u_{i+1} & \text{for } \xi > 0 \end{cases} \quad (\text{E20.5.1})$$

has been derived in Section 16.6.2.

If $u_i > u_{i+1}$ the solution is a shock propagating at speed $C_{i+1/2} = (u_i + u_{i+1})/2$ and

$$u^{(R)}\left(\frac{\xi}{t}, u_i, u_{i+1}\right) = \begin{cases} u_i & \text{for } \xi/t < C_{i+1/2} \\ u_{i+1} & \text{for } \xi/t > C_{i+1/2} \end{cases} \quad (\text{E20.5.2})$$

If $u_i < u_{i+1}$ the solution is an expansion fan and the Riemann solution is

$$u^{(R)}\left(\frac{\xi}{t}, u_i, u_{i+1}\right) = \begin{cases} u_i & \text{for } \xi/t < u_i \\ \frac{\xi}{t} & \text{for } u_i < \xi/t < u_{i+1} \\ u_{i+1} & \text{for } \xi/t > u_{i+1} \end{cases} \quad (\text{E20.5.3})$$

It is seen from equation (20.5.25) ^{and the figures p 452} that for the quadratic flux function $f = u^2/2$ the numerical flux for Godunov's scheme is

$$f_{i+1/2}^{*(G)} = \begin{cases} \frac{1}{2}u_{i+1}^2 & \text{if } u_i \text{ and } u_{i+1} \text{ are both negative} \\ \frac{1}{2}u_i^2 & \text{if } u_i \text{ and } u_{i+1} \text{ are both positive} \end{cases} \quad (\text{E20.5.4})$$

When u_i and u_{i+1} have opposite signs, one has

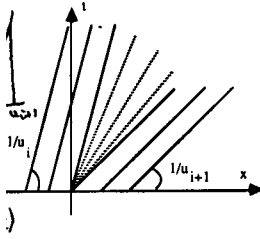
$$f_{i+1/2}^{*(G)} = \begin{cases} 0 & \text{if } u_i < 0 < u_{i+1} \quad (\text{expansion fan}) \\ \frac{1}{2}u_i^2 & \text{if } u_i > 0 > u_{i+1} \quad \text{and } C_{i+1/2} > 0 \\ \frac{1}{2}u_{i+1}^2 & \text{if } u_i > 0 > u_{i+1} \quad \text{and } C_{i+1/2} < 0 \end{cases} \quad (\text{E20.5.5})$$

The various cases are illustrated in Figure 20.5.3 where the characteristics with slopes $1/u_i$ and $1/u_{i+1}$ are shown. When they meet a shock is created, while an expansion fan appears when the characteristics diverge. The wave speed $a(u) = df/du = u$ vanishes at the 'sonic' value $u^* = 0$ and, in analogy with the Euler equations, positive values of u are considered as 'supersonic' and negative values as 'subsonic'. The flux function is minimum at the critical sonic value $u = u^*$ and separating the supersonic and subsonic values through the definitions

$$\begin{aligned} u^+ &= \max(u, u^* = 0) \\ u^- &= \min(u, u^* = 0) \end{aligned} \quad (\text{E20.5.6})$$

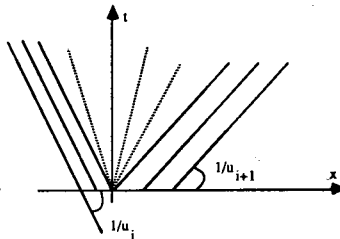
① $u_i < u_{i+1}$: Expansion

expansion fan



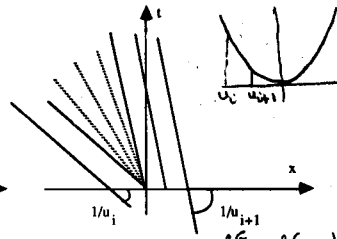
$0 < u_i < u_{i+1}$

'Supersonic' expansion



$u_i < 0 < u_{i+1}$

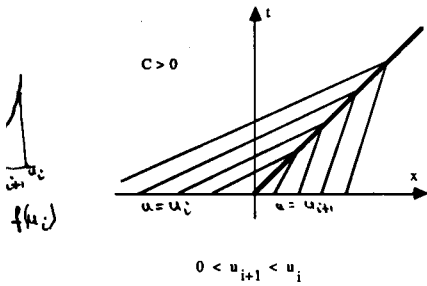
'Transonic' expansion



$u_i < u_{i+1} < 0$

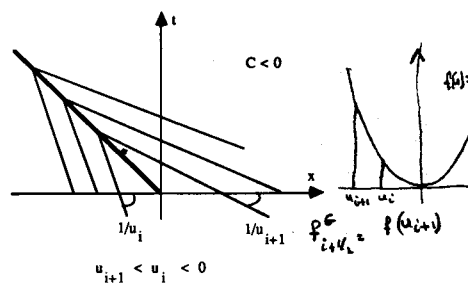
'Subsonic' expansion

② $u_i > u_{i+1}$: Shock



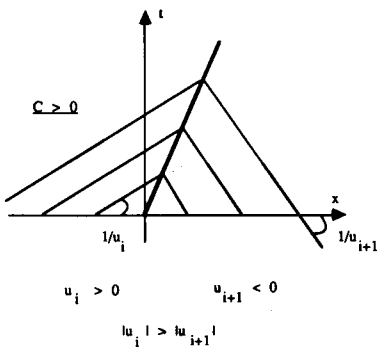
$0 < u_{i+1} < u_i$

'Supersonic' Shock



$u_{i+1} < u_i < 0$

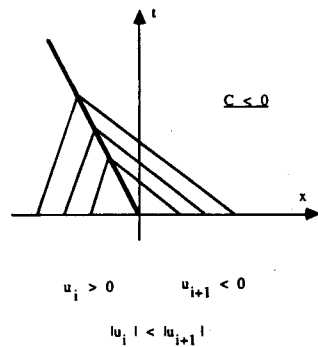
'Subsonic' Shock



$u_i > 0 \quad u_{i+1} < 0$

$|u_i| > |u_{i+1}|$

'Transonic' Shock



$u_i > 0 \quad u_{i+1} < 0$

$|u_i| < |u_{i+1}|$

Figure 20.5.3 Representation of different Riemann solutions for Burgers equation

with the properties

$$\begin{aligned} u^+ + u^- &= u \\ u^+ - u^- &= |u| \end{aligned} \quad (\text{E20.5.7})$$

the numerical flux of Godunov's scheme can be written as (Van Leer, 1984)

$$f_{i+1/2}^{*(G)} = \max \left[\frac{1}{2}(u_{i+1}^-)^2, \frac{1}{2}(u_i^+)^2 \right] \quad (\text{E20.5.8})$$

For the Euler equations we have to solve exactly the Riemann problem following the procedure of Section 16.6.3. This requires the solution of a non-linear equation at each cell interface and is quite time consuming. Since the exact solution is averaged over the cell, we can also consider approximate Riemann solutions which would require less computational work. A variety of possibilities can be defined and the most interesting *approximate Riemann solvers* derived by Osher and Roe will be discussed next.

20.5.2 Osher's approximate Riemann solver

This approximate Riemann solution originated from the upwind method developed by Engquist and Osher (1980, 1981) for scalar conservation laws.

The generalization of the linear upwind scheme (20.1.1) for the scalar conservation law (20.5.20) is straightforward when the Jacobian function $a(u) = df/du$ is of constant sign, say $a(u) > 0$:

$$u_i^{n+1} = u_i^n - \tau(f_i^n - f_{i-1}^n) \quad \text{if } a(u) > 0 \quad (20.5.26)$$

Similarly, a forward difference scheme can be written if the propagation speed $a(u) < 0$.

For a convex flux function, for which the second derivative has a constant sign, for instance $f''(u) > 0$, a unique critical or 'sonic' value u^* is obtained from

$$a(u^*) = 0 \quad (20.5.27)$$

The difficulty in defining an upwind scheme appears when $a(u)$ changes sign, that is at sonic and shock points. It is not at all obvious how to handle this transition from upstream to downstream differencing without creating local non-linear instabilities or non-physical expansion shocks while maintaining a sharp transition for physical acceptable shocks.

Examples of these difficulties have been discussed in the framework of the stationary potential equation in Chapter 15. The switching process of Murman and Cole can be written here as follows. Defining the switching function $\mu(u)$:

$$\mu = \begin{cases} 1 & \text{if } u \geq u^* \text{ or } a(u) \geq 0 \\ 0 & \text{if } u < u^* \text{ or } a(u) < 0 \end{cases} \quad (20.5.28)$$

and the positive and negative flux parts:

$$\begin{aligned} f^+(u) &= \mu(u)f(u) \\ f^-(u) &= [1 - \mu(u)]f(u) \end{aligned} \quad (20.5.29)$$

with

$$f = f^+ + f^- \quad (20.5.30)$$

the scheme

$$u_i^{n+1} - u_i^n = -\tau[f^+(u_i) - f^+(u_{i-1})] - \tau[f^-(u_{i+1}) - f^-(u_i)] \quad (20.5.31)$$

is completely defined when the numerical value of the switching is chosen. When the switch function μ is evaluated at the cell interface, the numerical flux of this Murman–Cole scheme can be written as

$$f_{i+1/2}^{*(MC)} = \mu_{i+1/2} f_i + (1 - \mu_{i+1/2}) f_{i+1} \quad (20.5.32)$$

Other choices can be considered (see also Problem 20.24).

With the definition (20.5.27), this numerical flux can also be written as

$$f_{i+1/2}^{*(MC)} = \frac{1}{2}(f_{i+1} + f_i) - \frac{1}{2}\text{sgn}(a_{i+1/2})(f_{i+1} - f_i) \quad (20.5.33)$$

and if $a_{i+1/2}$ is calculated via

$$a_{i+1/2} = \frac{f_{i+1} - f_i}{u_{i+1} - u_i} \quad (20.5.34)$$

it is seen from the Rankine–Hugoniot relations (20.5.21) that $a_{i+1/2}$ is equal to the shock speed $C_{i+1/2}$ where the cells i and $(i+1)$ are connected through a shock discontinuity. Hence, in all cases one has

$$f_{i+1/2}^{*(MC)} = \begin{cases} f_{i+1} & \text{if } C_{i+1/2} \leq 0 \\ f_i & \text{if } C_{i+1/2} > 0 \end{cases} \quad (20.5.35)$$

Therefore, when compared with the exact Riemann solution at the interface $(i + \frac{1}{2})$, the Murman–Cole scheme (20.5.32) considers only shock transitions, without distinguishing between compressions $u_i > u_{i+1}$ and expansions $u_i < u_{i+1}$.

In particular, for Burgers equation treated in Example 20.5.1, $C_{i+1/2} = (u_i + u_{i+1})/2$ and equation (20.5.35) is to be compared with (E20.5.5) which distinguishes the expansion from the shock transition. Consequently, this scheme will allow expansion shocks (see Chapter 15 and Problem 20.23).

Engquist and Osher's scheme for a scalar conservation law

Engquist and Osher's approach provides a method to perform this transition or 'switch', leading to a monotone conservative scheme which excludes expansion shocks and resolves discontinuities with at most two interior points. In addition Engquist and Osher prove that the resulting scheme is stable under a CFL condition $\Delta t |a_{\max}| < \Delta x$.

The essential component of the scheme is tied to the way the positive and negative parts of the flux function are defined. They are given in the Engquist and Osher scheme, for convex flux functions, by

$$\begin{aligned} f^+(u) &= f[\max(u, u^*)] \\ f^-(u) &= f[\min(u, u^*)] \end{aligned} \quad (20.5.36)$$

with
$$f = f^+ + f^- \quad (20.5.37)$$

and discretized with equation (20.5.31). The associated numerical flux is

$$f_{i+1/2}^{*(EO)} = f[\max(u_i, u^*)] + f[\min(u_{i+1}, u^*)] \quad (20.5.38)$$

This is extended as follows for arbitrary non-convex fluxes:

$$\begin{aligned} f^+(u) &= \int_0^u \mu(\xi) f'(\xi) d\xi \\ f^-(u) &= \int_0^u [1 - \mu(\xi)] f'(\xi) d\xi \end{aligned} \quad (20.5.39)$$

where the switching function $\mu(u)$ is, with $f'(u) = a(u)$,

$$\mu(u) = \begin{cases} 1 & \text{if } a(u) \geq 0 \\ 0 & \text{if } a(u) < 0 \end{cases} \quad (20.5.40)$$

An alternative expression for the definitions (20.5.39) is

$$\begin{aligned} f^+(u) &= \int_0^u \max[f'(\xi), 0] d\xi \equiv \int_0^u a^+(\xi) d\xi \\ f^-(u) &= \int_0^u \min[f'(\xi), 0] d\xi \equiv \int_0^u a^-(\xi) d\xi \end{aligned} \quad (20.5.41)$$

and equation (20.5.37) holds if the flux function is normalized to $f(0) = 0$.

The first-order upwind scheme (20.5.31) becomes

$$u_i^{n+1} - u_i^n = -\frac{\Delta t}{\Delta x} \left\{ \int_{u_{i-1}}^{u_i} \max[f'(u), 0] du + \int_{u_i}^{u_{i+1}} \min[f'(u), 0] du \right\} \quad (20.5.42a)$$

or

$$u_i^{n+1} - u_i^n = -\frac{\Delta t}{\Delta x} \left\{ \int_{u_{i-1}}^{u_i} \mu(u) f'(u) du + \int_{u_i}^{u_{i+1}} [1 - \mu(u)] f'(u) du \right\} \quad (20.5.42b)$$

The generalized numerical flux for arbitrary scalar flux functions is

$$\begin{aligned} f_{i+1/2}^{*(EO)} &= f_i^+ + f_{i+1}^- \\ &= \int_0^{u_i} \mu(u) f'(u) du + \int_0^{u_{i+1}} [1 - \mu(u)] f'(u) du \end{aligned} \quad (20.5.43)$$

and can also be written alternatively as (see Problem 20.25)

$$\begin{aligned} f_{i+1/2}^{*(EO)} &= f_i + \int_{u_i}^{u_{i+1}} [1 - \mu(u)] f'(u) du \equiv f_i + \int_{u_i}^{u_{i+1}} a^-(u) du \\ &= f_{i+1} - \int_{u_i}^{u_{i+1}} \mu(u) f'(u) du \equiv f_{i+1} - \int_{u_i}^{u_{i+1}} a^+(u) du \\ &= \frac{1}{2}(f_i + f_{i+1}) - \frac{1}{2} \int_{u_i}^{u_{i+1}} |a(u)| du \end{aligned} \quad (20.5.44)$$

A unique property of the Engquist–Osher numerical flux is its differentiability with respect to its arguments u_i and u_{i+1} as a consequence of the presence of the integrals in the above equation. This property is not shared by the Godunov numerical flux, nor by the Murman–Cole numerical flux, at the sonic transition over a stationary shock, that is at the points where $u_{i+1} < u^* < u_i$ with $f(u_i) = f(u_{i+1})$.

Example 20.5.2 Engquist–Osher’s scheme for Burgers equation

For $f = u^2/2$ equation (20.5.44) becomes

$$f_{i+1/2}^{*(EO)} = \frac{1}{4}(u_i^2 + u_{i+1}^2) - \frac{1}{2} \int_{u_i}^{u_{i+1}} |u| du \tag{E20.5.9}$$

Applying this expression to the various situations of Example 20.5.1, it is seen that

$$f_{i+1/2}^{*(EO)} = \begin{cases} \frac{1}{2}u_{i+1}^2 & \text{if } u_i \text{ and } u_{i+1} \text{ are both negative} \\ \frac{1}{2}u_i^2 & \text{if } u_i \text{ and } u_{i+1} \text{ are both positive} \end{cases} \tag{E20.5.10}$$

When u_i and u_{i+1} have opposite signs, one has

$$f_{i+1/2}^{*(EO)} = \begin{cases} 0 & \text{if } u_i < 0 < u_{i+1} \text{ (expansion fan)} \\ \frac{1}{2}(u_i^2 + u_{i+1}^2) & \text{if } u_i > 0 > u_{i+1} \text{ (transonic shock)} \end{cases} \tag{E20.5.11}$$

Compared to the Godunov scheme, this scheme differs only by the representation of the shock transition. As shown by Van Leer (1984), the Engquist–Osher scheme replaces the shock in the exact Riemann solution by an ‘overtuned’ centred compression wave. This is a consequence of the smooth transitions involved in the phase space integral defining the numerical flux. Consequently, discontinuous transitions are excluded in the approximate Riemann solution. This will appear even more clearly in the extension of this scheme to systems of conservation laws. However, after averaging to obtain the new piecewise approximation at time $(n + 1)\Delta t$, shocks are represented as sharp transitions over no more than two cells. The above relations can be summarized by the formula

$$f_{i+1/2}^{*(EO)} = \frac{1}{2}[(u_{i+1}^-)^2 + (u_i^+)^2] \tag{E20.5.12}$$

Osher’s scheme for systems of conservation laws

The extension to systems of hyperbolic equations has been developed on the basis of the generalization of the third form (20.5.44) for the numerical flux of the scalar case (Osher, 1981; Osher and Solomon, 1982).

The integral in the last expression of equation (20.5.44) is replaced by an integral in the phase space of the variable U (having n components, with $n = 3$ for the one-dimensional Euler equations), and the function $|a(u)|$ is replaced by the absolute value of the Jacobian matrix $|A(U)|$, defined according to equation

(20.2.9b). Hence the numerical flux of Osher's scheme for a system of conservation laws becomes

$$f_{i+1/2}^{*(O)} = \frac{1}{2}(f_i + f_{i+1}) - \frac{1}{2} \int_{U_i}^{U_{i+1}} |A(U)| dU \quad (20.5.45)$$

The integration path in phase space from U_i to U_{i+1} is split over all simple wave solutions defined in Section 16.4.5.

Each of the n simple wave solutions,

$$\frac{dU^{(j)}}{dw} = r^{(j)} \quad j = 1, \dots, n \quad (20.5.46)$$

associated with the eigenvalue $\lambda_{(j)}(w)$ and the right eigenvector $r^{(j)}(w)$, defines a wave path in phase space. As seen in Section 16.4.5, $(n - 1)$ Riemann invariants can be defined along each of these wave paths. Hence if a certain order is selected, there is a unique decomposition of the integration path from U_i to U_{i+1} into simple wave paths. The order selected by Osher for theoretical reasons, which allow certain properties to be proved, is the order of decreasing eigenvalues. Starting from point i , one follows the right eigenvector associated with the eigenvalue $\lambda = u + c$ and then the path associated with $\lambda = u$, and point $(i + 1)$ is attained along the path connected to the eigenvalue $(u - c)$. This is illustrated in Figure 20.5.4. Note that in practice the reverse order can also be selected (Hemker and Spekreijse, 1986), and corresponds actually to a more physical interpretation, since the waves are taken in increasing order of propagation speed.

The unique position, in the U space, of the intermediate points $(i + \frac{1}{3})$ and $(i + \frac{2}{3})$ between i and $(i + 1)$ is obtained from the constancy of the two Riemann invariants along each of the three simple wave paths. This provides six relations for the six unknowns $U_{i+1/3}$ and $U_{i+2/3}$. Considering the invariants s (entropy)

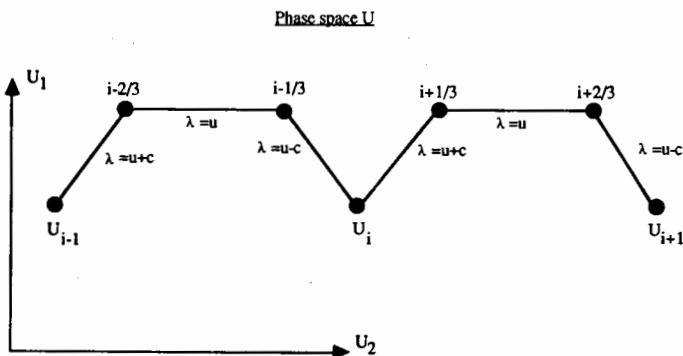


Figure 20.5.4 Integration paths in phase space for Osher's scheme and the one-dimensional Euler equations

and $u - 2c/(\gamma - 1)$ along the path $(U_i, U_{i+1/3})$, we can write

$$s_{i+1/3} = s_i$$

$$u_{i+1/3} - \frac{2c_{i+1/3}}{\gamma - 1} = u_i - \frac{2c_i}{\gamma - 1} \tag{20.5.47}$$

Along the wave path associated with $\lambda = u$, the quantities u and p remain invariant and hence

$$u_{i+1/3} = u_{i+2/3}$$

$$p_{i+1/3} = p_{i+2/3} \tag{20.5.48}$$

while along the third path, s and $u + 2c/(\gamma - 1)$ are constant. Hence,

$$s_{i+2/3} = s_{i+1}$$

$$u_{i+2/3} + \frac{2c_{i+2/3}}{\gamma - 1} = u_{i+1} + \frac{2c_{i+1}}{\gamma - 1} \tag{20.5.49}$$

The solutions to this system are easily found and are left as an exercise to the reader, so that the integration path is completely determined.

Since the integration paths follows only the simple wave solutions of the Euler equations, the approximate Riemann solution involved in this decomposition depends only on characteristics and hence does not contain discontinuous transitions. This generalizes Van Leer's (1984) analysis on the basis of Burgers equation.

Along each subpath $\Gamma(j)$, the integration of $|A|$ in equation (20.5.45) takes on a simple expression, since

$$\int_{\Gamma(j)} |A| dU = \int_{\Gamma(j)} |A| r^{(j)} dw = \int_{\Gamma(j)} |\lambda_{(j)}| r^{(j)} dw \tag{20.5.50}$$

the numerical flux (20.5.45) can be written as

$$f_{i+1/2}^{*(0)} = \frac{1}{2}(f_i + f_{i+1}) - \frac{1}{2} \sum_j \int_{\Gamma(j)} |\lambda_{(j)}| r^{(j)} dw \tag{20.5.51}$$

Alternative expressions generalizing the formulas (20.5.44) are

$$f_{i+1/2}^{*(0)} = f_i + \sum_j \int_{\Gamma(j)} \lambda_{(j)}^- r^{(j)} dw \tag{20.5.52a}$$

$$f_{i+1/2}^{*(0)} = f_{i+1} - \sum_j \int_{\Gamma(j)} \lambda_{(j)}^+ r^{(j)} dw \tag{20.5.52b}$$

where λ^\pm are the positive, respectively negative, eigenvalues. These expressions clearly show the upwind nature of the scheme: the flux at the interface $(i + \frac{1}{2})$ is obtained by correcting the flux of the adjacent cell, i or $(i + 1)$, by the contributions from all the simple waves that connect the boundary to the interior of the considered cell (Figure 20.5.5).

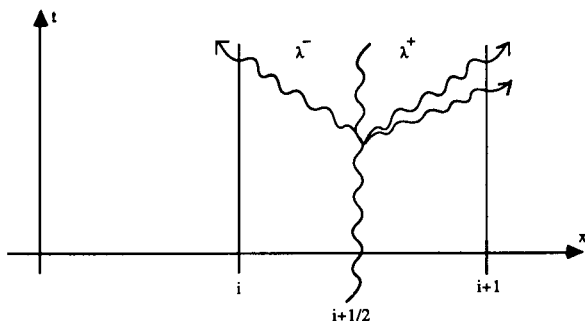


Figure 20.5.5 Illustration of the upwind character of Osher's numerical flux

For practical calculations the integrals are evaluated in terms of the flux values at the end-points of the wave paths or at the sonic points. Indeed, we have to distinguish (following Lax, 1957) between genuinely non-linear waves for which the eigenvalues $\lambda_{(j)}$ are not constant along the simple wave associated with the j th right eigenvector, that is for which

$$\frac{d\lambda_{(j)}}{dw} = \frac{d\lambda_{(j)}}{dU} \cdot r^{(j)} \neq 0 \quad (20.5.53)$$

and the linearly degenerate waves that satisfy

$$\frac{d\lambda_{(j)}}{dw} = \frac{d\lambda_{(j)}}{dU} \cdot r^{(j)} = 0 \quad (20.5.54)$$

The second case applies to the contact waves associated with the eigenvalue $\lambda = u$, while the eigenvalues $\lambda = u \pm c$ correspond to genuinely non-linear acoustic waves.

Along the paths associated with $\lambda = u$, the eigenvalue remains constant and hence

$$\int_{r^{(j)}} |A| dU = \text{sgn}(u) [f(U_{i+2/3}) - f(U_{i+1/3})] \quad (20.5.55)$$

In the genuinely non-linear case, the non-zero gradient of λ can always be normalized to 1 by an appropriate normalization of the right eigenvectors. Hence equation (20.5.53) can be set to

$$\frac{d\lambda_{(j)}}{dw} = \frac{d\lambda_{(j)}}{dU} \cdot r^{(j)} = 1 \quad (20.5.56)$$

equating the U gradient of λ to its associated left eigenvector.

With this choice, λ is a monotone function of the wave path parameter w (refer to Figure 16.4.8), and a unique sonic point U^* exists defined by $\lambda(U^*) = 0$ at which λ changes sign. The integral of $|A|$ will therefore depend on the existence

of eventual sonic points along the wave path. For instance, from i to $(i + \frac{1}{3})$, one has

$$\int_{U_i}^{U_{i+1/3}} A^+ dU = \begin{cases} f(U_{i+1/3}) - f(U_i) & \text{if } \lambda(U_i) > 0 \text{ and } \lambda(U_{i+1/3}) > 0 \\ f(U_{i+1/3}^*) - f(U_i) & \text{if } \lambda(U_i) > 0 \text{ and } \lambda(U_{i+1/3}) < 0 \\ f(U_{i+1/3}) - f(U_{i+1/3}^*) & \text{if } \lambda(U_i) < 0 \text{ and } \lambda(U_{i+1/3}) > 0 \\ 0 & \text{if } \lambda(U_i) < 0 \text{ and } \lambda(U_{i+1/3}) < 0 \end{cases} \quad (20.5.57)$$

The integrals for A^- are similarly constructed and we refer the reader to the mentioned references for details of demonstration of the scheme properties. The scheme is shown to converge to the physically correct weak solutions, excluding expansion shocks and resulting in sharp, monotone shock profiles, with at most two interior cells.

Extensions to multi-dimensional flows can be developed along the same lines by considering local one-dimensional Riemann problems in the direction normal to the cell boundaries. Practical applications of the method can be found in Chakravarthy and Osher (1983a, 1983b), Osher and Chakravarthy (1983) and Hemker and Spekreijse (1986).

20.5.3 Roe's approximate Riemann solver

The approximate Riemann solver developed by Roe (1980, 1981; see also Roe, 1985, 1986d) is based on a characteristic decomposition of the flux differences while ensuring the conservation properties of the scheme.

Referring to the first-order linear numerical flux (20.1.19), the schemes presented in this chapter can be regarded as defining different representations of the $|A|$ term for non-linear systems of conservation equations. This can also be seen by comparing with equations (20.3.10) and (20.5.45).

In the light of Godunov-type methods this reflects different ways of resolving the Riemann problem at the cell interfaces and Roe's approach is an ingenious way of extending the linear wave decomposition, which is the exact linear solution to Riemann's problem, to non-linear equations. Therefore, before presenting this approach, we will reinterpret the linear first-order upwind schemes as a sum of simple wave contributions, generalizing the scalar scheme (20.1.10) to systems of equations.

Reinterpretation of upwind schemes for linear systems

The first-order upwind scheme for a linear system can be written as

$$U_i^{n+1} - U_i^n = -\tau A^+ \delta^- U_i - \tau A^- \delta^+ U_i \quad (20.5.58)$$

or

$$U_i^{n+1} - U_i^n = -\tau \delta^- f_i^+ - \tau \delta^+ f_i^-$$

and the associated numerical flux takes different forms, δ representing here the

central difference operator

$$\begin{aligned} f_{i+1/2}^* &= f_i^+ + f_{i+1}^- = \frac{1}{2}(f_i + f_{i+1}) - \frac{1}{2}|A|(U_{i+1} - U_i) \\ &= f_i + \delta f_{i+1/2}^- \\ &= f_{i+1} - \delta f_{i+1/2}^+ \end{aligned} \quad (20.5.59)$$

The variations δU can be expressed as a sum of simple wave contributions as seen in Section 16.3, referring in particular to equation (16.3.40).

Considering the transformation from conservative to characteristic variables (16.3.39), $\delta U = P\delta W$, written as

$$\delta U = \sum_j \partial w_j r^{(j)} \equiv \sum_j \delta U^{(j)} \quad (20.5.60)$$

this relation expresses the variations δU of the conservative variables as a sum of simple waves $r^{(j)}$ with amplitudes ∂w_j . Each fraction $\delta U^{(j)}$ represents the contribution from the j th wave to the total variation δU . For the one-dimensional Euler equations (see Section 16.4), the right eigenvectors are the columns of the matrix P (equation (16.4.12)) and the ∂W variables are given by equation (16.4.18). Hence,

$$\delta U = \partial w_1 \begin{vmatrix} 1 \\ u \\ u^2/2 \end{vmatrix} + \frac{\rho}{2c} \partial w_2 \begin{vmatrix} 1 \\ u+c \\ H+uc \end{vmatrix} + \frac{\rho}{2c} \partial w_3 \begin{vmatrix} 1 \\ u-c \\ H-uc \end{vmatrix} \quad (20.5.61)$$

where each term represents one of the $\delta U^{(j)}$, with $f_{\text{form}}(6.4.9)-(c.4.18)$:

$$\begin{aligned} \partial w_1 &= \delta \rho - \frac{\delta p}{c^2} \\ \partial w_2 &= \delta u + \frac{\delta p}{\rho c} \\ \partial w_3 &= \delta u - \frac{\delta p}{\rho c} \end{aligned} \quad (20.5.62)$$

In these notations ∂w represents the particular combinations in the above equation, where δ is, for instance, the central difference operator acting on the variables defined at $(i + \frac{1}{2})$. We choose to maintain this notation in order to express the link with the characteristic variables and to point out that the ∂w quantities are combinations of differences. In the linearized case, the δU appearing in the first form of equation (20.5.59) is expressed by the sum on the $\delta U^{(j)}$, with, for instance,

$$\delta U_{i+1/2}^{(2)} = U_{i+1}^{(2)} - U_i^{(2)} = \left[\frac{(u_{i+1} - u_i) + (p_{i+1} - p_i)}{\rho c} \right] r_{i+1/2}^{(2)} \left[\frac{(u_{i+1} - u_i) + \frac{p_{i+1} - p_i}{\rho c}}{c} \right] r_{i+1/2}^{(2)}$$

In a linear system, with constant values of the variables, this decomposition is unambiguously defined, while the difficulty with the non-linear equations is to

determine the proper way for the evaluation of the coefficients in front of the δ terms. We consider for the time being that the equations are linearized and that all the coefficients are constants. In this case, we can write the flux variations as

$$\delta f = A\delta U = A \sum_j \partial w_j r^{(j)} = \sum_j \lambda_{(j)} \partial w_j r^{(j)} \quad (20.5.63)$$

with $\lambda_{(1)} = u$, $\lambda_{(2)} = u + c$ and $\lambda_{(3)} = u - c$. The positive and negative contributions can be simply sorted out by

$$\delta f^+ = A^+ \delta U = \sum_j \lambda_{(j)}^+ \partial w_j r^{(j)} \quad (20.5.64)$$

$$\delta f^- = A^- \delta U = \sum_j \lambda_{(j)}^- \partial w_j r^{(j)}$$

where λ^+ are the positive, respectively negative, eigenvalues. The numerical flux of the scheme can be obtained by estimating the $|A|$ term in equation (20.5.59) as

$$\delta |f| = |A| \delta U = \sum_j |\lambda_{(j)}| \partial w_j r^{(j)} \quad (20.5.65)$$

The different forms of the first-order upwind numerical flux become, with an evaluation of the wave components at point $(i + \frac{1}{2})$ and δ the central first difference,

$$\begin{aligned} f_{i+1/2}^* &= \frac{1}{2}(f_i + f_{i+1}) - \frac{1}{2} \sum_j |\lambda_{(j)}| \partial w_j r^{(j)} \\ &= f_i + \sum_j \lambda_{(j)}^- \partial w_j r^{(j)} \\ &= f_{i+1} - \sum_j \lambda_{(j)}^+ \partial w_j r^{(j)} \end{aligned} \quad (20.5.66)$$

The parallelism with equations (20.5.51), (20.5.52) is obvious, as is the upwind nature of the scheme (see Figure 20.5.5).

Roe's generalization of the above relations to nonlinear equations is based on a linearization which maintains the above forms while ensuring the conservative property of the resulting scheme.

Roe's scheme for the one-dimensional Euler equations

The conservative property of the wave decomposition requires that the sum (20.5.63), where the variables $\lambda, r, \partial w$ are functions of U_i and U_{i+1} , still reduces to a flux difference as in the linear case. This is certainly not a trivial problem. A simple idea which comes up for equation (20.5.63) would be to define the

Jacobian matrix A at the mid-points $(i + \frac{1}{2})$, for instance

$$f_{i+1} - f_i = A \left(\frac{U_i + U_{i+1}}{2} \right) (U_{i+1} - U_i) \equiv A_{i+1/2} (U_{i+1} - U_i) \quad (20.5.67)$$

However, if the eigenvalues and right eigenvectors of this Jacobian matrix are taken as the basis for the simple wave decomposition, the sum of all the contributions would not produce an expression of an exact difference of flux terms. This would be the case for a quadratic function such as Burgers equation for which one has

$$f_{i+1} - f_i = \frac{u_{i+1}^2 - u_i^2}{2} = \frac{1}{2}(u_i + u_{i+1})(u_{i+1} - u_i) \quad (20.5.68)$$

but since $A(U_i, U_{i+1})$ is not a quadratic function of the U variables, this choice is not a valid candidate. Hence a matrix $\bar{A}(U_i, U_{i+1})$ is sought with the following properties:

(1) For any pair U_i, U_{i+1} one should have *exactly*

$$f_{i+1} - f_i = \bar{A}(U_i, U_{i+1})(U_{i+1} - U_i) \quad (20.5.69)$$

(2) For $U_i = U_{i+1} = U$ the matrix $\bar{A}(U, U) = A(U) \equiv \partial f / \partial U$.

(3) \bar{A} has real eigenvalues with linearly independent eigenvectors.

Once such a matrix is defined the above wave decompositions can be written without any change. The eigenvalues of this matrix can be considered as the wave speeds of the approximate Riemann problem and the right eigenvectors as the associated waves.

Independently of the particular form of the \bar{A} matrix, its definition indicates the nature of the Riemann problem approximation it provides. Its eigenvalues C satisfy the relations

$$f_{i+1} - f_i = C(U_{i+1} - U_i) \quad (20.5.70)$$

which are identical to the Rankine–Hugoniot relations for a discontinuity of speed C between the states U_i and U_{i+1} . The projection on the corresponding eigenvector is the intensity of the jump over this discontinuity. Hence the approximate Riemann solver contained in the definition (20.5.69) recognizes only, and exactly, discontinuities. This is to be compared with Osher's approximation which recognizes only continuous transitions.

A consequence of this fact is that the method will not be able to identify properly an expansion fan containing a sonic point and in particular a stationary expansion for which $f_i = f_{i+1}$ and $U_i \neq U_{i+1}$ will appear as an expansion shock.

Construction of the Roe matrix

Roe (1981b) observes that the column vectors U and f can be expressed as

quadratic functions of the variable Z defined by

$$Z = \sqrt{\rho} \begin{vmatrix} 1 \\ u \\ H \end{vmatrix} \quad (20.5.71)$$

This is easily verified and one obtains for a perfect gas, using the relations

$$\rho E = \rho H - p = \frac{p}{\gamma - 1} + \frac{\rho u^2}{2} \quad (20.5.72)$$

$$U = \begin{vmatrix} z_1^2 \\ z_1 z_2 \\ \frac{z_1 z_3}{\gamma} + \frac{(\gamma - 1) z_2^2}{2\gamma} \end{vmatrix} \quad (20.5.73)$$

and

$$f = \begin{vmatrix} z_1 z_2 \\ \frac{(\gamma - 1) z_1 z_3}{\gamma} + \frac{(\gamma - 1) z_2^2}{2\gamma} \\ z_2 z_3 \end{vmatrix} \quad (20.5.74)$$

Hence one can apply the following identity for quadratic functions, valid for arbitrary variations $\delta a_{i+1/2} = a_{i+1} - a_i$, where the overbar indicates an arithmetic average $\bar{a} = (a_{i+1} + a_i)/2 \equiv a_{i+1/2}$:

$$\delta(ab)_{i+1/2} = \bar{a} \delta b_{i+1/2} + \bar{b} \delta a_{i+1/2} \quad (20.5.75)$$

When applied to U as given by equation (20.5.73), we have identically

$$U_{i+1} - U_i \equiv \bar{B}(Z_{i+1} - Z_i) \quad (20.5.76)$$

with

$$\bar{B} = \begin{vmatrix} 2\bar{z}_1 & 0 & 0 \\ \bar{z}_2 & \bar{z}_1 & 0 \\ \frac{\bar{z}_3}{\gamma} & \frac{\gamma - 1}{\gamma} \bar{z}_2 & \frac{\bar{z}_1}{\gamma} \end{vmatrix} \quad (20.5.77)$$

An analogous elementary calculation gives for the flux difference the identity

$$f_{i+1} - f_i \equiv \bar{C}(Z_{i+1} - Z_i) \quad (20.5.78)$$

with

$$\bar{C} = \begin{vmatrix} \bar{z}_2 & \bar{z}_1 & 0 \\ \frac{\gamma - 1}{\gamma} \bar{z}_3 & \frac{\gamma + 1}{\gamma} \bar{z}_2 & \frac{\gamma - 1}{\gamma} \bar{z}_1 \\ 0 & \bar{z}_3 & \bar{z}_2 \end{vmatrix} \quad (20.5.79)$$

Observe that the vectors U and f are homogeneous functions of degree two in Z , while the matrices \bar{B} and \bar{C} are homogeneous of degree one in Z . Remember

also that the flux f is homogeneous of order one in U . However, the above properties are not dependent on the homogeneous relations between f and U .

Combining equations (20.5.77) and (20.5.79) produces the desired linearization represented by equation (20.5.69):

$$\bar{A} = \bar{C}\bar{B}^{-1} \quad (20.5.80)$$

A straightforward calculation (see Problem 20.27) shows a very remarkable result: the matrix \bar{A} is *identical to the local Jacobian* given by equation (E16.2.3), when expressed as a function of the variables u and H , if these variables are replaced by an average weighted by the square root of the densities.

These particular averages are defined by setting $R_{i+1/2} = \sqrt{\rho_{i+1}/\rho_i}$:

$$\begin{aligned} \bar{\rho}_{i+1/2} &= \sqrt{\rho_{i+1}\rho_i} \equiv R_{i+1/2}\rho_i \\ \bar{u}_{i+1/2} &= \frac{\bar{z}_2}{\bar{z}_1} = \frac{(u\sqrt{\rho})_{i+1} + (u\sqrt{\rho})_i}{\sqrt{\rho_{i+1}} + \sqrt{\rho_i}} \equiv \frac{R_{i+1/2}u_{i+1} + u_i}{R_{i+1/2} + 1} \\ \bar{H}_{i+1/2} &= \frac{\bar{z}_3}{\bar{z}_1} = \frac{(H\sqrt{\rho})_{i+1} + (H\sqrt{\rho})_i}{\sqrt{\rho_{i+1}} + \sqrt{\rho_i}} \equiv \frac{R_{i+1/2}H_{i+1} + H_i}{R_{i+1/2} + 1} \end{aligned} \quad (20.5.81)$$

The eigenvectors and eigenvalues of the linearized matrix \bar{A} can now be obtained without further calculations. It suffices to replace the local variables in all the wave decomposition terms, developed in Section 20.5.3 for the linear case, by the above averages. Roe and Pike (1984) have shown that these averages are the unique choice satisfying the definition (20.5.69). It is also easily seen that this result remains unchanged for multi-dimensional flows.

Roe's scheme is therefore completely defined and can be summarized as follows:

- (1) For each cell $(i, i+1)$, calculate the above averaged values as well as the associated averaged speed of sound by

$$\bar{c}^2 = (\gamma - 1) \left(\bar{H} - \frac{\bar{u}^2}{2} \right) \quad (20.5.82)$$

Note that the formulas containing the variable R are computationally more efficient, since only one square root has to be evaluated per cell.

- (2) Calculate the eigenvalues and eigenvectors of the linearized matrix $\bar{A}(U_i, U_{i+1})$. They are obtained by

$$\bar{\lambda}_{(1)} = \bar{u} \quad \bar{\lambda}_{(2)} = \bar{u} + \bar{c} \quad \bar{\lambda}_{(3)} = \bar{u} - \bar{c} \quad (20.5.83) \quad \bar{\lambda}_{(3)} = \bar{u} - \bar{c}$$

with the eigenvectors

$$\bar{r}^{(1)} = \begin{vmatrix} 1 \\ \bar{u} \\ \bar{u}^2 \\ 2 \end{vmatrix} \quad \bar{r}^{(2)} = \begin{vmatrix} 1 \\ \bar{u} + \bar{c} \\ \bar{H} + \bar{u}\bar{c} \end{vmatrix} \frac{\bar{\rho}}{2\bar{c}} \quad \bar{r}^{(3)} = \begin{vmatrix} 1 \\ \bar{u} - \bar{c} \\ \bar{H} - \bar{u}\bar{c} \end{vmatrix} \frac{\bar{\rho}}{2\bar{c}} \quad (20.5.84)$$

All these variables are considered at $(i + \frac{1}{2})$.

- (3) Calculate the wave amplitudes, all quantities evaluated at $(i + \frac{1}{2})$:

$$\begin{aligned}\partial w_1 &= \delta p - \frac{\delta p}{c^2} \\ \partial w_2 &= \delta u + \frac{\delta p}{\rho c} \\ \partial w_3 &= \delta u - \frac{\delta p}{\rho c}\end{aligned}\tag{20.5.85}$$

$$\begin{aligned}\delta u_{i+1/2} &= u_{i+1} - u_i \\ \delta p_{i+1/2} &= p_{i+1} - p_i \\ \delta \rho_{i+1/2} &= \rho_{i+1} - \rho_i\end{aligned}\tag{20.5.86}$$

- (4) Evaluate the numerical flux of Roe's scheme by any of the following formula:

$$\begin{aligned}f_{i+1/2}^{*(R)} &= \frac{1}{2}(f_i + f_{i+1}) - \frac{1}{2} \sum_j |\bar{\lambda}_{(j)}^-| \partial w_j \bar{r}^{(j)} \\ &= f_i + \sum_j \bar{\lambda}_{(j)}^- \partial w_j \bar{r}^{(j)} \\ &= f_{i+1} - \sum_j \bar{\lambda}_{(j)}^+ \partial w_j \bar{r}^{(j)}\end{aligned}\tag{20.5.87}$$

where the \pm sign on the eigenvalues represents positive and negative values respectively.

For scalar non-linear equations the matrix \bar{A} reduces to a scalar function and the averaged propagation speed is defined, from equation (20.5.69), by

$$\bar{a}_{i+1/2} = \begin{cases} \frac{f_{i+1} - f_i}{u_{i+1} - u_i} & \text{if } u_{i+1} \neq u_i \\ a(u_i) & \text{if } u_{i+1} = u_i \end{cases}\tag{20.5.88}$$

It is seen that (20.5.88) is the Rankine-Hugoniot relation: hence the averaged propagation speed considered in Roe's scheme is equal to the speed of the discontinuities.

The numerical flux for the first-order scheme becomes

$$\begin{aligned}f_{i+1/2}^* &= \frac{1}{2}(f_i + f_{i+1}) - \frac{1}{2} |\bar{a}_{i+1/2}| (u_{i+1} - u_i) \\ &= f_i \quad \text{if } \bar{a}_{i+1/2} > 0 \\ &= f_{i+1} \quad \text{if } \bar{a}_{i+1/2} < 0\end{aligned}\tag{20.5.89a}$$

and is actually identical to the Murman and Cole scheme (20.5.33) for the scalar case. Roe's scheme can also be written as

$$f_{i+1/2}^{*(R)} = \frac{1}{2}(f_i + f_{i+1}) - \frac{1}{2} \text{sgn}(\bar{a}_{i+1/2}) (f_{i+1} - f_i)\tag{20.5.89b}$$

Example 20.5.3 Roe's scheme for Burgers equation

For Burgers equation the averaging defined by equation (20.5.69) is straightforward since the flux function is quadratic. Hence

$$\bar{a}_{i+1/2} = \frac{u_{i+1} + u_i}{2} \quad (\text{E20.5.13})$$

and

$$f_{i+1} - f_i = \bar{a}_{i+1/2}(u_{i+1} - u_i) \quad (\text{E20.5.14})$$

Observe that $\bar{a}_{i+1/2}$ is the propagation speed of the discontinuity (u_{i+1}, u_i) .

The numerical flux is defined by

$$f_{i+1/2}^{*(R)} = \begin{cases} \frac{1}{2}u_{i+1}^2 & \text{if } \bar{a}_{i+1/2} \leq 0 \\ \frac{1}{2}u_i^2 & \text{if } \bar{a}_{i+1/2} > 0 \end{cases} \quad (\text{E20.5.15})$$

and is identical to the Murman–Cole flux (20.5.35).

Summarizing the above results, it is seen that equations (20.5.87) and (20.5.89) are formally identical to their linear counterpart on a local basis; that is within each cell $(i, i+1)$, Roe's scheme solves the piecewise linear problem

$$\frac{\partial U}{\partial t} + \bar{A} \frac{\partial U}{\partial x} = 0 \quad \text{with } \bar{A} = \bar{A}(U_i, U_{i+1}) \quad (\text{E20.5.90a})$$

and the numerical flux

$$f_{i+1/2}^{*(R)} = \frac{1}{2}(f_i + f_{i+1}) - \frac{1}{2}|\bar{A}_{i+1/2}|(U_{i+1} - U_i) \quad (\text{E20.5.90b})$$

where the second term is expanded in eigenvectors of \bar{A} , representing propagating discontinuities satisfying the Rankine–Hugoniot relations.

Removing the expansion shock

The numerical flux of Roe's method differs from the exact Godunov flux for Burgers equation in the case of an expansion with a sonic transition. For an initial stationary expansion shock located in mesh point j ,

$$u_i = \begin{cases} -1 & \text{for } i < j \\ +1 & \text{for } i > j \end{cases} \quad (\text{E20.5.91})$$

equation (E20.5.15) shows that the balance of numerical fluxes is zero, since $f_{i+1/2}^{*(R)} = f_{i-1/2}^{*(R)} = u_i^2/2$ for $i \leq j$ and $f_{i+1/2}^{*(R)} = f_{i-1/2}^{*(R)} = u_{i+1}^2/2$ for $i > j$. Hence the initial expansion shock remains a stationary solution at all times. This is confirmed in Figure 20.5.6 where the solution to Burgers equation for an initial stationary expansion shock is shown. It can be compared to the result of the Lax–Friedrichs scheme which follows the correct solution, represented by a continuous expansion.

The reason behind this undesirable situation it to be found in the fact that

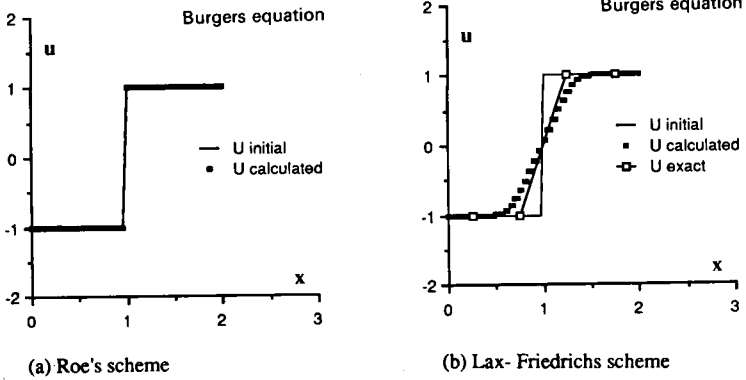


Figure 20.5.6 Solution to Burgers equation for an initial stationary expansion shock

the approximate Riemann solver of Roe's scheme does not see the sonic point. In Osher's scheme the detection of the sonic point is essential and therefore the above expansion shock will not remain a solution. Indeed, in this case $f_{i+1/2}^{*(EO)} = 0$ and $f_{i-1/2}^{*(EO)} = u_i^2/2$ for $i = j$ while $f_{i-1/2}^{*(EO)} = 0$ and $f_{i+1/2}^{*(EO)} = u_{i+1}^2/2$ for $i = j + 1$, and we obtain

$$\begin{aligned}
 u_i^{n+1} &= u_i^n + \frac{\tau u_i^{n2}}{2} & \text{for } i = j \\
 u_{i+1}^{n+1} &= u_{i+1}^n - \frac{\tau u_{i+1}^{n2}}{2} & \text{for } i = j + 1
 \end{aligned}
 \tag{20.5.92}$$

showing that the expansion shock resolves in an expansion fan. The difference between Roe's and Osher's approximate Riemann solvers is illustrated in Figure 20.5.7 for the case of a sonic point within the interval (u_L, u_R) . The former connects the two states by a direct, discontinuous jump, while the latter includes the sonic point as an intermediate step. This effect is also seen on the shock tube computation of Figure 20.5.9.

Hence, in order to cure the problem, an additional flux contribution can be introduced in Roe's scheme when an expansion through a sonic point is detected, and added to the upstream point while being subtracted from the downstream point in order to ensure conservation (Roe and Pike, 1984).

For Burgers equation, the additional flux can be set equal to $u_j u_{j+1}/2$ and added to point $i = j$, while subtracted from point $i = j + 1$. Note that this flux is negative.

An alternative technique to avoid the expansion shock is advocated by Harten and Hyman (1983). It consists in introducing a local expansion fan in the approximate Riemann solution when an expansion is detected through a sonic point. This can be realized by modifying the modulus of the eigenvalue $|\lambda|$ in

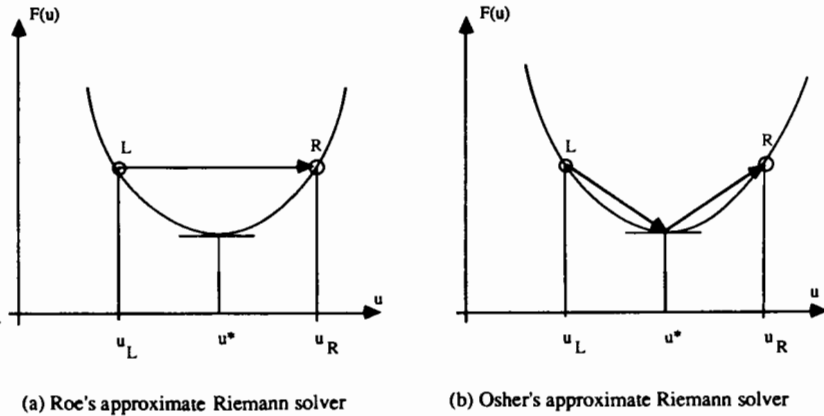


Figure 20.5.7 Transition from state L to state R according to (a) Roe's approximate Riemann solver and (b) Osher's approximate Riemann solver

equation (20.5.87) for the corresponding wave as follows:

$$|\bar{\lambda}|_{\text{mod}} = \begin{cases} |\bar{\lambda}|_{i+1/2} & \text{if } |\bar{\lambda}|_{i+1/2} \geq \varepsilon \\ \varepsilon & \text{if } |\bar{\lambda}|_{i+1/2} < \varepsilon \end{cases} \quad (20.5.93)$$

The quantity ε is derived on the basis of

$$\varepsilon = \max [0, (\bar{\lambda}_{i+1/2} - \lambda_i), (\lambda_{i+1} - \bar{\lambda}_{i+1/2})] \quad (20.5.94)$$

The zero in the maximum function automatically eliminates this correction for compression shocks.

A fully equivalent choice (Harten and Hyman, 1983) is given by

$$|\bar{\lambda}|_{\text{mod}} = \begin{cases} |\bar{\lambda}|_{i+1/2} & \text{if } |\bar{\lambda}|_{i+1/2} \geq \varepsilon \\ \frac{1}{2} \left(\frac{\bar{\lambda}_{i+1/2}^2}{\varepsilon} + \varepsilon \right) & \text{if } |\bar{\lambda}|_{i+1/2} < \varepsilon \end{cases} \quad (20.5.95)$$

with the advantage of a continuously differentiable correction.

Figure 20.5.8 shows results obtained for the stationary nozzle flow with Roe's scheme and Figure 20.5.9 displays similar results for the shock tube problem with a sonic transition in the expansion fan. A small expansion shock appears as discussed above. The shock is sharply captured, as is to be expected, but the contact discontinuity is strongly smeared.

20.5.4 Other Godunov-type methods

Other approximate Riemann solvers could be defined and we refer the reader to Harten *et al.* (1983), where general conditions for the definition of approximate Riemann solvers are given and several alternatives are analysed, although little practical use has been made of them.

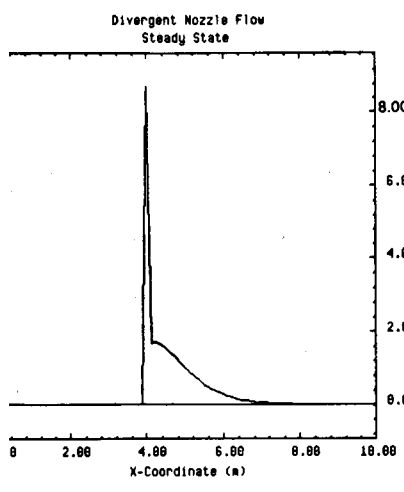
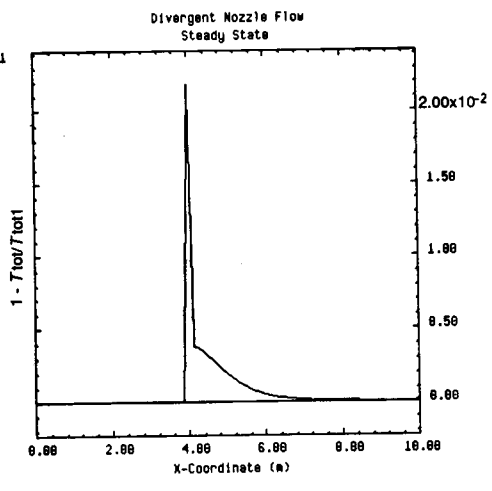
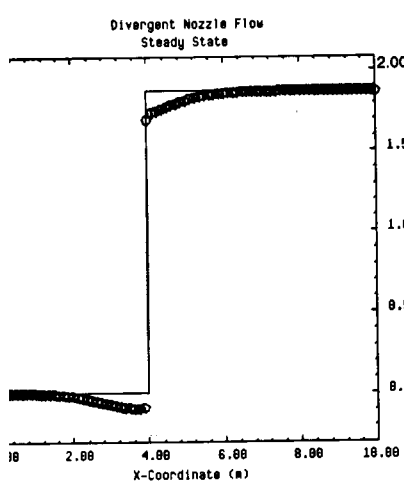
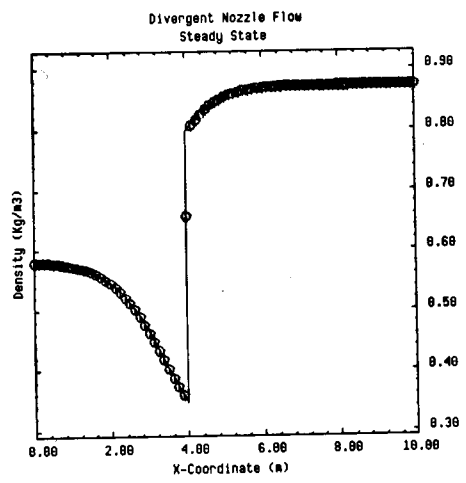
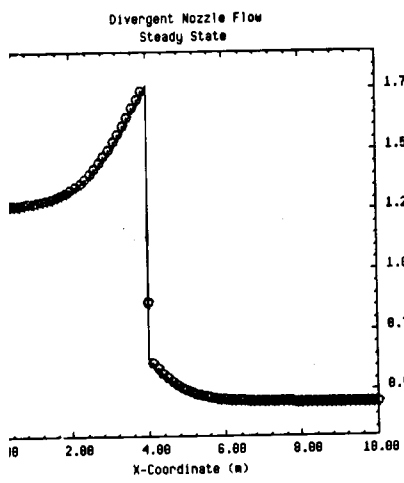


Figure 20.58 Computation of a stationary nozzle flow with a first-order scheme and Roe's Riemann solver

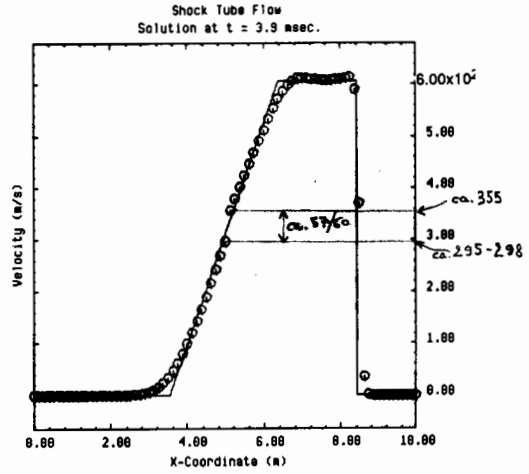
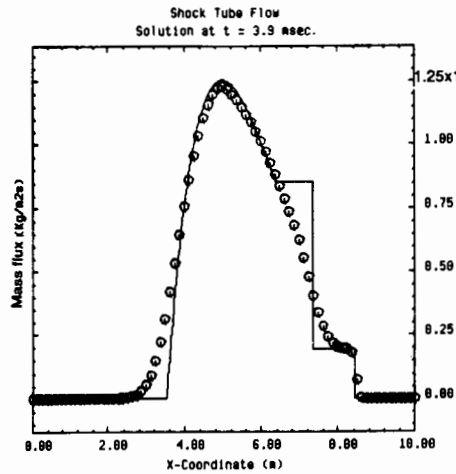
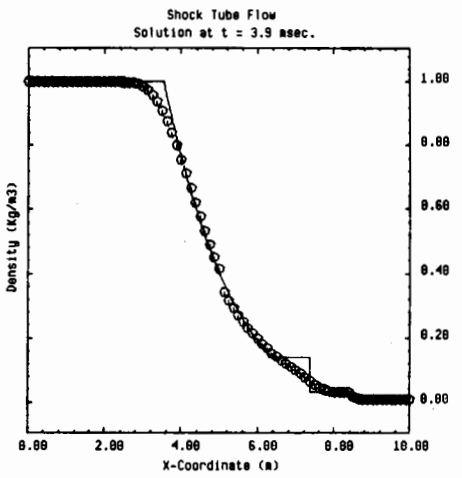
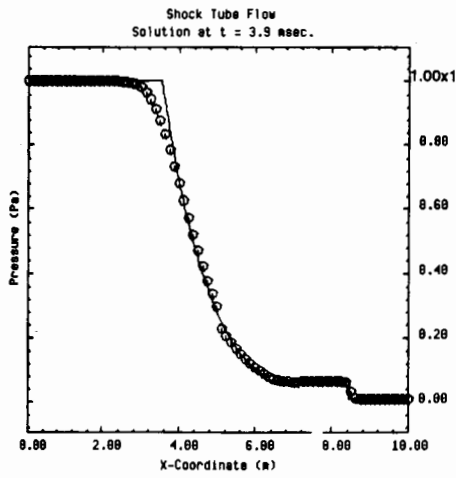
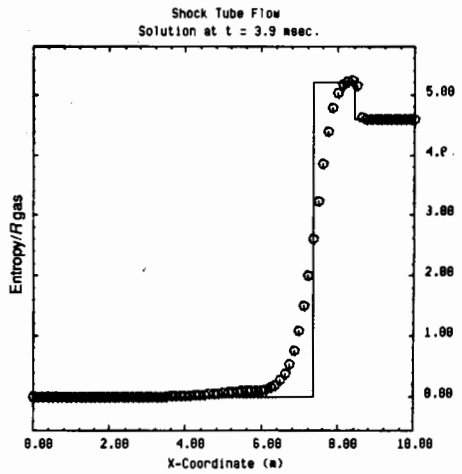
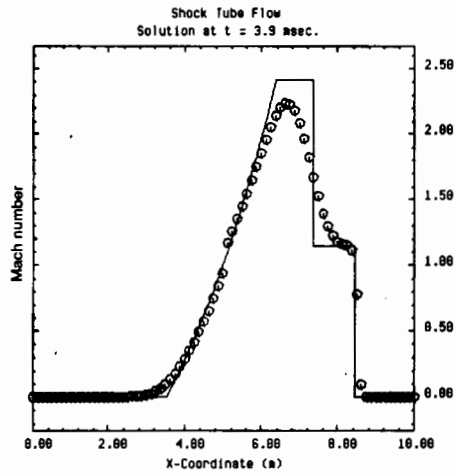


Figure 20.5.9 Computation of the shock tube problem with a first-order scheme and Roe's Riemann solver
 strong shock
 pressure ratio = 100
 with or without the Harten-Hyman correction?
 this is not clear! I believe without (from arrow)

Variants of Roe's flux difference splitting have been applied by Lombard *et al.* (1983) and Dick (1988), the latter in solving the stationary Euler equations with relaxation methods for the primitive variables.

Glimm's random choice method

A most original approach, based like Godunov's method on the solution of local Riemann problems, is the random choice method proposed by Glimm (1965) and further analysed and applied by Chorin (1976, 1977); see also Chorin and Marsden (1982).

As in Godunov's method, the solution is represented as piecewise constant at a given time step and advanced in time by solving Riemann problems at the cell interfaces. However, instead of averaging the wave distribution at time $(n+1)\Delta t$ as in Godunov's method, Glimm's method takes as the new approximation inside each cell the value of the exact solution at a randomly chosen point inside the cell. Convergence of this process has been proven by Glimm and it is shown that it resolves discontinuities with unlimited sharpness without under- or overshoots. In addition, Harten and Lax (1981) showed that these essential properties are maintained if the exact Riemann solution is replaced by appropriate approximate Riemann solutions.

Additional applications of Glimm's method can be found in Colella (1982) and Sod (1985).

20.5.5 Summary

The various options for first-order conservative upwind schemes can be expressed in a unified way through the numerical flux formulation. Referring to equation (20.5.4) we write all the first-order explicit upwind schemes as

$$U_i^{n+1} - U_i^n = -\frac{\Delta t}{\Delta x}(f_{i+1/2}^* - f_{i-1/2}^*) \quad (20.5.96a)$$

where

$$f_{i+1/2}^* = f^*(U_i, U_{i+1}) \quad (20.5.96b)$$

with the following options:

Flux vector splitting: $f_{i+1/2}^{*(FS)} = f^-(U_{i+1}) + f^+(U_i)$

Godunov scheme: $f_{i+1/2}^{*(G)} = f(U_{i+1/2}^{(R)}(0, U_i, U_{i+1}))$

Osher scheme: $f_{i+1/2}^{*(O)} = \frac{1}{2}(f_i + f_{i+1}) - \frac{1}{2} \sum_j \int_{\Gamma(j)} |\lambda_{(j)}| r^{(j)} dw$

Roe scheme: $f_{i+1/2}^{*(R)} = \frac{1}{2}(f_i + f_{i+1}) - \frac{1}{2} \sum_j |\bar{\lambda}_{(j)}| \partial w_j \bar{r}^{(j)}$

With the addition of the expansion fan corrections to Roe's scheme, all these

first-order schemes satisfy the properties of monotonicity and of convergence to the physical acceptable weak solutions of the Euler equations.

The difficult problem of extending the upwind schemes to second-order accuracy, while maintaining these properties and avoiding the production of oscillations around discontinuities, is the subject of the following chapter.

20.6 FIRST-ORDER IMPLICIT UPWIND SCHEMES

The numerical fluxes summarized in equation (20.5.96) represent approximations to the physical fluxes at the cell interfaces, in the line of equation (20.5.4). Hence the numerical flux balance over a cell represents a discretization of the spatial terms of the Euler equations and can be combined with appropriate time-integration schemes, such as implicit schemes, in the line of the approach developed in Chapter 18.

For any first-order upwind flux (20.5.96), a semi-discretized system of ordinary differential equations in time can be defined as

$$\frac{du_i}{dt} = -\frac{1}{\Delta x}(f_{i+1/2}^* - f_{i-1/2}^*) \equiv -\frac{1}{\Delta x}\delta f_i^* \quad (20.6.1)$$

Implicit upwind schemes can now be developed by applying the time-linearization procedure and linear multi-step time-integration methods, as introduced in Chapter 18 for the central discretized schemes.

Equation (18.1.5) applied to equation (20.6.1), that is after an upwind space discretization selecting $\xi = 0$, leads to

$$\Delta U_i = -\tau[\theta\delta f_i^{*n} + (1-\theta)\delta f_i^{*n+1}] \quad (20.6.2)$$

The linearization of the flux term at time level $n+1$ is defined in general terms for a first-order upwind scheme as follows, taking into account that the numerical flux only depends on two consecutive mesh point values:

$$f_{i+1/2}^* = f^*(U_i, U_{i+1}) \quad (20.6.3)$$

$$f_{i\pm 1/2}^{*n+1} = f_{i\pm 1/2}^{*n} + \frac{\partial f^{*n}}{\partial U_i}\Delta U_i + \frac{\partial f^{*n}}{\partial U_{i\pm 1}}\Delta U_{i\pm 1} + O(\Delta U^2) \quad (20.6.4)$$

Following Section 9.4 in Volume 1, the derivatives of the numerical flux with respect to the first or second variable are represented respectively by g_1 and g_2 , defined by

$$\frac{\partial f^*}{\partial U_i} \equiv g_{1,i} \quad \frac{\partial f^*}{\partial U_{i+1}} \equiv g_{2,i+1} \quad (20.6.5)$$

With the above linearization the general form of an implicit first-order upwind scheme can be written as

$$\Delta U_i + \tau(1-\theta)[(g_{1,i} - g_{2,i})\Delta U_i + g_{2,i+1}\Delta U_{i+1} - g_{1,i-1}\Delta U_{i-1}]^n = -\tau\delta f_i^{*n} \quad (20.6.6)$$

For a flux vector splitting scheme, one has, with the notations of Section 20.3,

$$g_1 = f_u^+ \quad g_2 = f_u^- \quad (20.6.7)$$

and a first-order implicit flux vector splitting scheme can be defined by

$$[1 + \tau\theta(\delta^- f_{ui}^+ + \delta^+ f_{ui}^-)]\Delta U_i^n = -\tau(\delta^- f_i^+ + \delta^+ f_i^-)^n \quad (20.6.8)$$

where f_u^\pm are the Jacobians of the split fluxes, generally not equal to A^\pm , the split Jacobians.

The solution of the implicit scheme requires the inversion of block tridiagonal systems, since g_1 and g_2 are 3×3 matrices. An important property can be observed from equation (20.6.6), as a consequence of the upwind wave decomposition, namely that the tridiagonal system is always diagonal dominant. Indeed, writing equation (20.6.6) for a linear system as

$$\alpha \Delta U_i + \beta \Delta U_{i+1} + \gamma \Delta U_{i-1} = -\delta f_i^{*n} \quad (20.6.9)$$

with

$$\beta = (1 - \theta)g_2$$

$$\alpha = \frac{1}{\tau} - \beta - \gamma \quad (20.6.10)$$

$$\gamma = -(1 - \theta)g_1$$

For the flux splitting scheme (20.6.7), β and γ are both negative and α is positive, satisfying the diagonal dominance condition

$$\alpha > |\beta| + |\gamma| \quad (20.6.11)$$

This property remains valid for all the Riemann solvers of Section 20.5, as can be seen from equations (20.5.52) for the Osher scheme or equation (20.5.87) for Roe's scheme. By selecting the appropriate formula for the numerical fluxes it is readily seen that g_1 contains only contributions from positive eigenvalues (see, for instance, equation (20.5.52b) for Osher's scheme) while g_2 has only negative contributions (equation (20.5.52a)).

An important consequence of the diagonal dominance property is the guarantee it provides that iterative relaxation schemes, applied to the implicit operators, will converge. This is not so essential for one-dimensional problems, where the system is only tridiagonal, but it becomes of larger interest for multi-dimensional cases where the implicit operators are block pentadiagonal in two-dimensional first-order upwind schemes and block heptadiagonal in similar three-dimensional problems (Dadone and Napolitano, 1983; Chakravarthy, 1984).

It will be seen in Chapter 21 that this property can remain valid for higher-order upwind schemes if non-linear flux limiters are introduced in order to avoid the appearance of numerical oscillations in the computed solutions.

20.7 MULTI-DIMENSIONAL FIRST-ORDER UPWIND SCHEMES

The extension of the first-order upwind schemes to multi-dimensional problems can be done formally in a simple way, treating each flux component in an upwind manner in its own direction on a local one-dimensional basis.

On a Cartesian mesh and in two dimensions, the flow equations are written as

$$\frac{\partial U}{\partial t} + \frac{\partial f}{\partial x} + \frac{\partial g}{\partial y} = 0 \tag{20.7.1}$$

where f and g are the x and y projections of the flux vector.

For a selected scheme, numerical fluxes can be defined separately for the two components and attributed to the faces of the cell centred on point (i, j) (Figure 20.7.1). Considering a flux vector splitting, one would write

$$U_{ij}^{n+1} - U_{ij}^n = -\frac{\Delta t}{\Delta x} (f_{i+1/2,j}^* - f_{i-1/2,j}^*) - \frac{\Delta t}{\Delta y} (g_{i,j+1/2}^* - g_{i,j-1/2}^*) \tag{20.7.2}$$

with

$$\begin{aligned} f_{i+1/2,j}^* &= f_{i+1,j}^- + f_{ij}^+ \\ g_{i,j+1/2}^* &= g_{i,j+1}^- + g_{ij}^+ \end{aligned} \tag{20.7.3}$$

where the splitting criteria are based on the eigenvalues of A for f and on the eigenvalues of B for the g component.

For Godunov-type methods the numerical fluxes are obtained from the solution (exact or approximate) of the Riemann problem in the directions normal to the cell interfaces. For each cell two Riemann problems have to be solved, one in the x direction based on the Jacobian A of the flux component f and one in the y direction associated with the flux component g and Jacobian B . Hence the variations δU between adjacent cells are split into different contributions according to the considered direction. Taking Roe's approximate

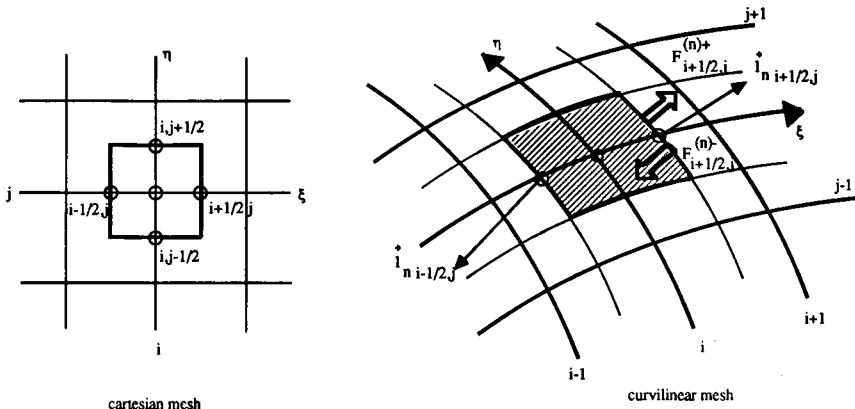


Figure 20.7.1 Two-dimensional cells in arbitrary and Cartesian coordinates

Riemann solver we can write the numerical fluxes in the following condensed way:

$$f_{i+1/2,j}^{*(R)} = \frac{1}{2}(f_{ij} + f_{i+1,j}) - \frac{1}{2}|\bar{A}|_{i+1/2,j}(U_{i+1,j} - U_{ij}) \quad (20.7.4)$$

where the second term is decomposed into simple waves, eigenvectors of the matrix \bar{A} with eigenvalues $\bar{\lambda}^A = \bar{u}, \bar{u}, \bar{u} + \bar{c}, \bar{u} - \bar{c}$, and ∂w variations in the x direction:

$$|\bar{A}|_{i+1/2,j}(U_{i+1,j} - U_{ij}) = \sum_k |\bar{\lambda}_{(k)}^A| \partial w_k \bar{r}^{(k)A} \quad (20.7.5)$$

while the numerical flux in the y direction is

$$g_{i,j+1/2}^{*(R)} = \frac{1}{2}(g_{ij} + g_{i,j+1}) - \frac{1}{2}|\bar{B}|_{i,j+1/2}(U_{i,j+1} - U_{ij}) \quad (20.7.6)$$

where the second term is decomposed into simple waves, eigenvectors of the matrix \bar{B} with eigenvalues $\bar{\lambda}^B = \bar{v}, \bar{v}, \bar{v} + \bar{c}, \bar{v} - \bar{c}$, and ∂w variations in the y direction:

$$|\bar{B}|_{i,j+1/2}(U_{i,j+1} - U_{ij}) = \sum_k |\bar{\lambda}_{(k)}^B| \partial w_k \bar{r}^{(k)B} \quad (20.7.7)$$

Hence two distinct set of waves are considered in the discretization in order to simulate the same physical behaviour.

This decomposition into one-dimensional wave patterns introduces a dependence on the mesh orientation and creates a strong numerical diffusion transverse to the direction of the wave speed vector. This can best be seen on the linear scalar convection equation

$$\frac{\partial u}{\partial t} + a \frac{\partial u}{\partial x} + b \frac{\partial u}{\partial y} = 0 \quad (20.7.8)$$

expressing that the quantity u is constant in the direction of the convection velocity.

For $a > 0$ and $b > 0$, the first-order upwind scheme (20.7.3) reduces to

$$u_{ij}^{n+1} - u_{ij}^n = -\frac{a \Delta t}{\Delta x} (u_{ij} - u_{i-1,j}) - \frac{b \Delta t}{\Delta y} (u_{ij} - u_{i,j-1}) \quad (20.7.9)$$

Defining $\sigma_x = a \Delta t / \Delta x$ and $\sigma_y = b \Delta t / \Delta y$, the computational molecule is shown in Figure 20.7.2. The consequence of the one-dimensional decomposition appears in the dependence of the scheme on the points Q and S, while point R does not contribute. This is to compared to the exact solution $u_p = u_T$ while scheme (20.7.9) has a stationary solution

$$u_p = \frac{\sigma_x u_Q + \sigma_y u_S}{\sigma_x + \sigma_y} \quad (20.7.10)$$

The error introduced is highest for a convection at 45° to the mesh, where the exact solution is $u_p = u_R$. Figure 20.7.3 compares the computational molecule corresponding to the exact solution with scheme (20.7.9), whose stationary

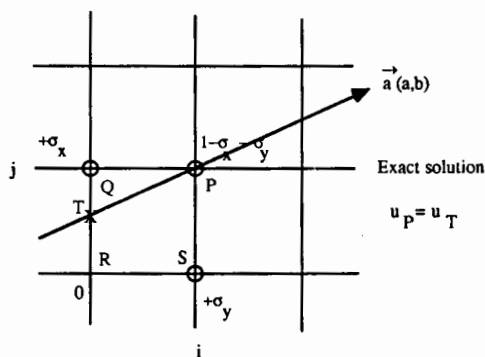


Figure 20.7.2 Computational molecule for two-dimensional first-order upwind scheme

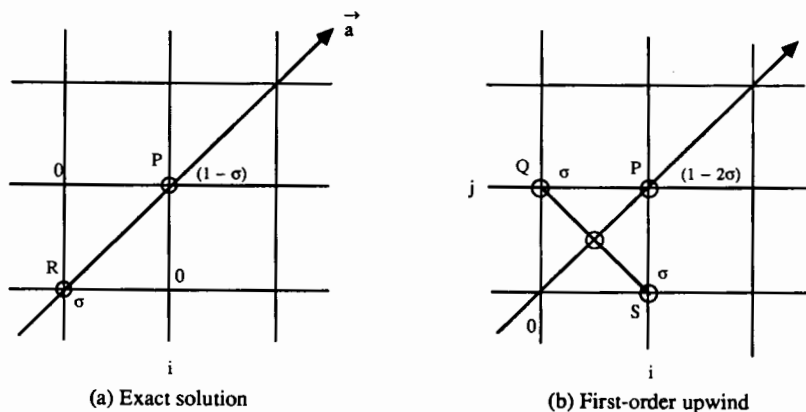


Figure 20.7.3 First-order upwind scheme and exact solution for a convection velocity at 45° to the mesh

solution is in this case $u_p = (u_Q + u_S)/2$. If the initial state is formed by a propagating discontinuity separating two constant states, this numerical solution generates considerable cross-diffusion. Hence this upwind scheme has poor directional properties since it is dependent on the mesh orientation.

It should also be mentioned that the necessary and sufficient condition for Von Neumann stability of scheme (20.7.9) is $|\sigma_x| + |\sigma_y| \leq 1$ (see Problem 20.3). (20.32)

The weakness of the above scheme finds its origin in the independence of the x and y discretizations, defined respectively by the A and B matrices, while the two-dimensionality of the physical flow interconnects the variations in both directions. For instance, if the flow is assumed to have a local linear variation in the direction transverse to the propagation speed, then the exact solution

would satisfy the relation, for a and b positive, $u_{ij} - u_{i-1,j} = u_T - u_Q = -(u_Q - u_R)b/a = -(u_{i-1,j} - u_{i-1,j-1})b/a$.

This gives a guideline towards the definition of schemes with reduced cross-diffusion.

Fractional step methods

Fractional step methods (Yanenko, 1979; see also Chapter 11 in Volume 1) form another general framework for the generation of two-dimensional algorithms, with some interaction between the two directions, although the approach is based on one-dimensional decompositions. A fractional step formulation of equation (20.7.1) would be

$$\frac{\partial \bar{U}}{\partial t} + \frac{\partial f}{\partial x} = 0 \quad (20.7.11a)$$

followed by the discretization of

$$\frac{\partial \bar{U}}{\partial t} + \frac{\partial g}{\partial y} = 0 \quad (20.7.11b)$$

With upwind numerical fluxes, an explicit fractional step discretization of first-order accuracy would replace scheme (20.7.2) by

$$\bar{U}_{ij} - U_{ij}^n = -\frac{\Delta t}{\Delta x} (f_{i+1/2,j}^* - f_{i-1/2,j}^*) \quad (20.7.12a)$$

followed by

$$U_{ij}^{n+1} - \bar{U}_{ij} = -\frac{\Delta t}{\Delta y} (\bar{g}_{i,j+1/2}^+ - \bar{g}_{i,j-1/2}^+) \quad (20.7.12b)$$

Applied to the linear convection equation (20.7.8) the fractional step convection algorithm becomes

$$\begin{aligned} \bar{u}_{ij} - u_{ij}^n &= -\sigma_x(u_{ij} - u_{i-1,j}) \\ u_{ij}^{n+1} - \bar{u}_{ij} &= -\sigma_y(\bar{u}_{ij} - \bar{u}_{i,j-1}) \end{aligned} \quad (20.7.13a)$$

or

$$\begin{aligned} u_{ij}^{n+1} - u_{ij}^n &= -\sigma_x(u_{ij} - u_{i-1,j}) - \sigma_y(u_{ij} - u_{i,j-1}) \\ &\quad + \sigma_x \sigma_y (u_{ij} - u_{i-1,j} - u_{i,j-1} + u_{i-1,j-1}) \end{aligned} \quad (20.7.13b)$$

Compared to scheme (20.7.9), an additional contribution appears corresponding to the discretization of a mixed xy derivative, representing some form of two-dimensional interaction. The associated computational molecule is illustrated in Figure 20.7.4.

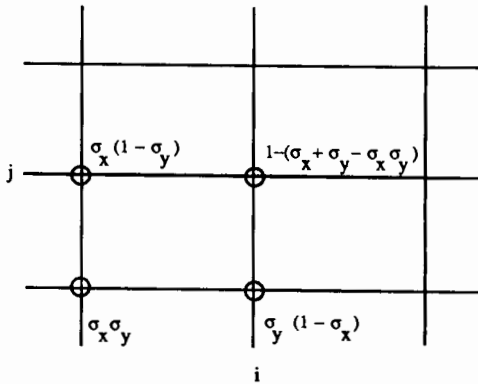


Figure 20.7.4 Computational molecule for a two-dimensional first-order upwind scheme obtained from the fractional step method

Other convection algorithms with two-dimensional properties have been suggested by Raithby (1976) and Rice and Schnipke (1985), drawing the first-order schemes closer to a streamline tracking procedure.

In Raithby's scheme the variable at a cell interface $(i + \frac{1}{2}, j)$ is interpolated to the centerline i between the points (i, j) and $(i, j - 1)$, according to the ratio $\alpha \equiv \sigma_y / 2\sigma_x$ (Figure 20.7.5).

If $\alpha < 1$ the convection velocity from Q intersects the segment PS and the value of u at point T is linearly interpolated between P and S. If $\alpha > 1$ (Figure 20.7.5(b)), the value at T is approximated by point S. This combines to

$$u_{i+1/2,j} = \begin{cases} (1 - \alpha)u_{ij} + \alpha u_{i,j-1} & \text{if } \alpha < 1 \\ u_{i,j-1} & \text{if } \alpha > 1 \end{cases} \quad (20.7.14)$$

or

$$u_{i+1/2,j} = (1 - \beta)u_{ij} + \beta u_{i,j-1} \quad \text{with } \beta = \min(1, \alpha) \quad (20.7.15)$$

In a similar fashion, the values at $(i, j + \frac{1}{2})$ are determined by

$$u_{i+1/2,j} = (1 - \bar{\beta})u_{ij} + \bar{\beta}u_{i-1,j} \quad (20.7.16)$$

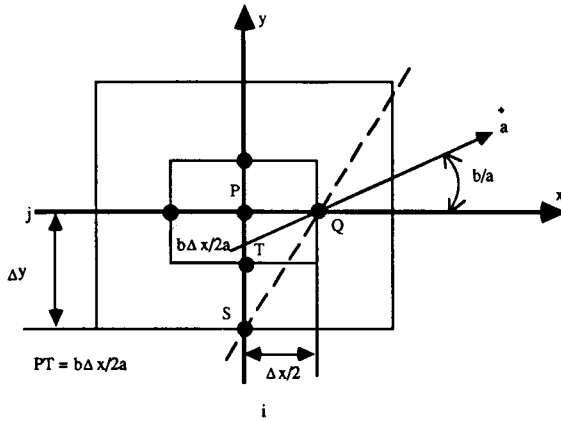
with

$$\bar{\beta} = \min(1, \bar{\alpha}) \quad \bar{\alpha} = \frac{\sigma_x}{2\sigma_y} \quad (20.7.17)$$

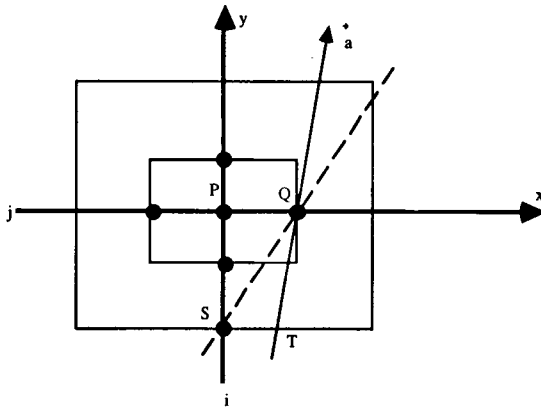
The resulting scheme, obtained from the flux balance of the contour around P, becomes

$$\begin{aligned}
 u_{ij}^{n+1} &= u_{ij}^n - \sigma_x(u_{i+1/2,j} - u_{i-1/2,j}) - \sigma_y(u_{i,j+1/2} - u_{i,j-1/2}) \\
 &= u_{ij}^n - \sigma_x[\beta u_{i,j-1} + (1-\beta)u_{ij} - \bar{\beta}u_{i-1,j-1} - (1-\bar{\beta})u_{i-1,j}] \\
 &\quad - \sigma_y[\bar{\beta}u_{i-1,j} + (1-\bar{\beta})u_{ij} - \beta u_{i-1,j-1} - (1-\beta)u_{i,j-1}] \quad (20.7.18)
 \end{aligned}$$

The schemes corresponding to non-positive values of a and b are derived in a similar way.



(a) $\sigma_y < \sigma_x$



(b) $\sigma_y > 2\sigma_x$

Figure 20.7.5 First-order upwind scheme in two dimensions, following Raithby (1976)

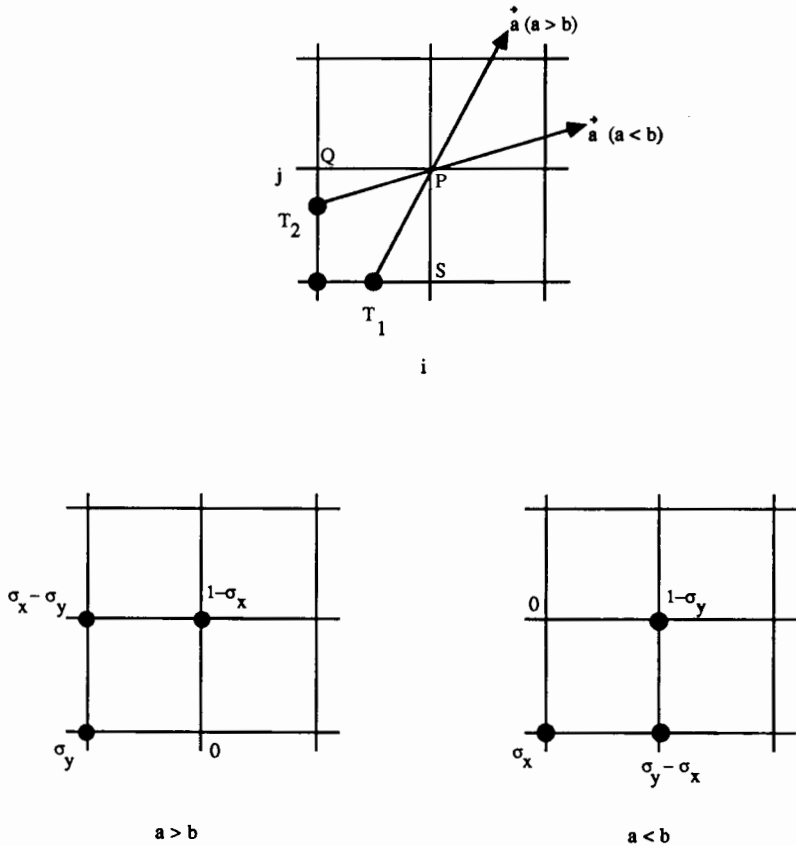


Figure 20.7.6 First-order upwind scheme in two dimensions, following Rice and Schnipke (1985)

This scheme reproduces the exact solution for a convection velocity at 45° to a Cartesian mesh.

In Rice and Schnipke's (1985) method (Figure 20.7.6) the values of the convected quantities at P are approximated by the upstream values at T_1 or T_2 according to the direction of the convection speed. For $a > 0$ and $b > 0$ with $a < b$,

$$u_{ij}^{n+1} = u_{ij}^n - \sigma_x(u_{i,j-1} - u_{i-1,j-1}) - \sigma_y(u_{ij} - u_{i,j-1}) \quad (20.7.19)$$

and for $a > b$,

$$u_{ij}^{n+1} = u_{ij}^n - \sigma_x(u_{ij} - u_{i-1,j}) - \sigma_y(u_{i-1,j} - u_{i-1,j-1}) \quad (20.7.20)$$

An exact solution is again recovered for a convection at 45° to the mesh. An extension to systems of hyperbolic equations the conservative form can be defined after a wave decomposition, applying the convection algorithms to each wave separately.

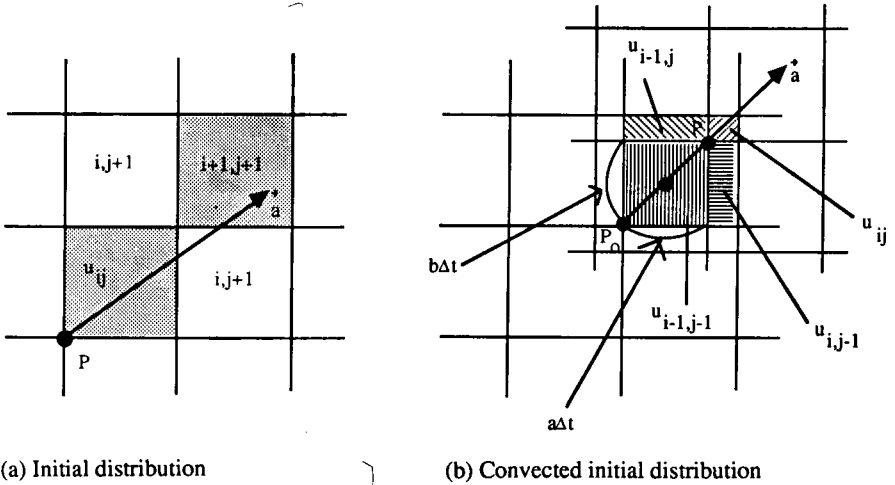


Figure 20.7.7 Two-dimensional Godunov method for a scalar convection equation: (a) initial piecewise distribution and (b) convected distribution over time step Δt

Godunov-type approach for two-dimensional convection

In the line of the Godunov-type approach an algorithm can be derived from the convection over a time interval Δt of an initial, piecewise constant distribution of the state variable over each cell (Figure 20.7.7), followed by an averaging of the newly obtained distribution. Point P undergoes a displacement of components $a \Delta t, b \Delta t$ and cell (i, j) receives contributions from the convected cells as shown in Figure 20.7.7(b). A straightforward averaging of this new distribution leads to

$$u_{ij}^{n+1} = \frac{1}{\Delta x \Delta y} \{ ab \Delta t^2 u_{i-1,j-1} + (\Delta y - b \Delta t) a \Delta t u_{i-1,j} + (\Delta x - a \Delta t) b \Delta t u_{i,j-1} + (\Delta x - a \Delta t)(\Delta y - b \Delta t) u_{ij} \} \tag{20.7.21}$$

This scheme is identical to the fractional step scheme (20.7.13). It can also be written in a conservative form as follows:

$$u_{ij}^{n+1} = u_{ij}^n - \sigma_x(u_{i+1/2,j}^* - u_{i-1/2,j}^*) - \sigma_y(u_{i,j+1/2}^* - u_{i,j-1/2}^*) \tag{20.7.22}$$

with

$$u_{i+1/2,j}^* = u_{ij}^n - \frac{1}{2} \sigma_y(u_{ij}^n - u_{i,j-1}^n) \tag{20.7.23a}$$

$$u_{i,j+1/2}^* = u_{ij}^n - \frac{1}{2} \sigma_x(u_{ij}^n - u_{i-1,j}^n) \tag{20.7.23b}$$

Equation (20.7.23a) can be considered as an approximation for the flux value at the interface $(i + \frac{1}{2}, j)$, resulting from a propagation over a time interval $\Delta t/2$ in the y direction. Similar interpretations are obtained for the other cell faces.

Additional considerations concerning multi-dimensional convection schemes can be found in Van Leer (1983) and Colella (1984).

Attempts to define two-dimensional upwind schemes which do not reduce to products of one-dimensional upwind operators can be found in Roe and Baines (1982, 1984). Further developments, based on a wave decomposition essentially determined by the flow properties and free from mesh dependence effects, are considered by Roe (1986a, 1986b), Deconinck *et al.* (1986), Hirsch *et al.* (1987), (1989), Powell and Van Leer (1989).

References

- Anderson, W. K., Thomas, J. L., and Van Leer, B. (1986a). 'Comparison of finite volume flux vector splittings for the Euler equations.' *AIAA Journal*, **24**, 1453–60.
- Anderson, W. K., Thomas, J. L., and Whitfield, D. L. (1986b). 'Multigrid acceleration of the flux split Euler equations.' *AIAA Paper 86-0274*, AIAA 24th Aerospace Sciences Meeting.
- Buning, P. G., and Steger, J. L. (1982). 'Solution of the two-dimensional Euler equations with generalized coordinate transformations using flux vector splitting.' *AIAA Paper 82-0971*, AIAA/ASME 3rd Joint Thermophysics Conference.
- Chakravarthy, S. R. (1984). 'Relaxation methods for unfactored implicit upwind schemes.' *AIAA Paper 84-0165*, AIAA 22nd Aerospace Sciences Meeting.
- Chakravarthy, S. R., and Osher, S. (1983a). 'Numerical experiments with the Osher upwind scheme for the Euler equations.' *AIAA Journal*, **21**, 1241–68.
- Chakravarthy, S. R., and Osher, S. (1983b). 'High resolution applications of the Osher upwind scheme for the Euler equations.' *AIAA Paper 86-1943*, *Proc. AIAA 6th Computational Fluid Dynamics Conference*, pp. 363–73.
- Chakravarthy, S. R., Anderson, D. A., and Salas, M. D. (1980). 'The split coefficient matrix method for hyperbolic systems of gas dynamic equations.' *AIAA Paper 80-0268*, AIAA 19th Aerospace Sciences Meeting.
- Chorin, A. J. (1976). 'Random choice solution of hyperbolic systems.' *Journal Computational Physics*, **22**, 517–33.
- Chorin, A. J. (1977). 'Random choice methods with application to reacting gas flows.' *Journal Computational Physics*, **25**, 253–71.
- Chorin, A. J., and Marsden, J. E. (1982). *A Mathematical Introduction to Fluid Mechanics*, New York: Springer Verlag.
- Colella, P. (1982). 'Glimm's method for gas dynamics.' *SIAM Journal for Sci. Stat. Comp.*, **3**, 76. Colella
- Colella, P. (1984). 'Multidimensional upwind methods for hyperbolic conservation laws.' *Report LBL-17023*, Lawrence Berkeley Laboratory, University of California, Berkeley, California.
- Courant, R., Isaacson, E., and Reeves, M. (1952). 'On the solution of nonlinear hyperbolic differential equations by finite differences.' *Comm. Pure and Applied Mathematics*, **5**, 243–55.
- Dadone, A., and Napolitano, M. (1983). 'An implicit lambda scheme.' *AIAA Journal*, **21**, 1391–9.
- Deconinck, H., Hirsch, C., and Peuteman, J. (1986). 'Characteristic decomposition methods for the multidimensional Euler equations.' *Proc. Tenth International Conference on Numerical Methods in Fluid Dynamics, Lecture Notes in Physics*, Vol. 264, pp. 216–21. Springer Verlag, Berlin.
- Dick, E. (1988). 'A flux difference splitting method for steady Euler equations.' *Journal Computational Physics*, **76**, 19–32.

- Engquist, B., and Osher, S. (1980). 'Stable and entropy satisfying approximations for transonic flow calculations.' *Mathematics of Computation*, **34**, 45–75.
- Engquist, B., and Osher, S. (1981). 'One-sided difference approximations for nonlinear conservation laws.' *Mathematics of Computation*, **36**, 321–52.
- Favini, B., and Zannetti, L. (1986). 'On conservative properties and non-conservative forms of Euler solvers.' *Proc. Tenth International Conference on Numerical Methods in Fluid Dynamics, Lecture Notes in Physics*, Vol. 264, pp. 270–5. Springer Verlag, Berlin.
- Glimm, J. (1965). 'Solutions in the large for nonlinear hyperbolic systems of equations.' *Comm. Pure and Applied Mathematics*, **18**, 697–715.
- Godnov, S. K. (1959). 'A difference scheme for numerical computation of discontinuous solution of hydrodynamic equations.' *Math. Sbornik*, **47**, 271–306 (in Russian). Translated US Joint Publ. Res. Service, *JPRS 7226* (1969).
- Godunov, S., Zabrodine, A., Ivanov, M., Kraiko, A., and Prokopov, G. (1979). *Resolution Numerique des Problems Multidimensionnels de la Dynamique des Gaz*. Moscow, USSR: Editions MIR.
- Hänel, D., Schwane, R., and Seider, G. (1987). 'On the accuracy of upwind schemes for the solution of the Navier–Stokes equations.' *AIAA Paper 87-1105, Proc. AIAA 8th Computational Fluid Dynamics Conference*, pp. 42–6.
- Harten, A., and Hyman, J. M. (1983). 'Self adjusting grid methods for one-dimensional hyperbolic conservation laws.' *Journal Computational Physics*, **50**, 235–69.
- Harten, A., and Lax, P. D. (1981). 'A random choice finite difference scheme for hyperbolic conservation laws.' *SIAM Journal Numerical Analysis*, **18**, 289–315.
- Harten, A., Lax, P. D., and Van Leer, B. (1983). 'On upstream differencing and Godunov-type schemes for hyperbolic conservation laws.' *SIAM Review*, **25**, 35–61.
- Hemker, P. W., and Spekrijse, S. P. (1986). 'Multiple grid and Osher's scheme for the efficient solution of the steady Euler equations.' *Applied Numerical Mathematics*, **2**, 475–93.
- Hirsch, Ch., Lacor, C., and Deconinck, H. (1987). 'Convètion algorithms based on a diagonalization procedure for the multidimensional Euler equations.' *AIAA Paper 87-1163, Proc. AIAA 8th Computational Fluid Dynamics Conference*, pp. 667–76.
- Hirsch, Ch., Lacor, C. (1989). 'Upwind algorithms based on a Diagonalization of the multidimensional Euler equations.' *AIAA-Paper 89-1958, AIAA 9th Computational Fluid Dynamics Conference*.
- Lax, P. D. (1957). 'Hyperbolic systems of conservation laws II.' *Comm. Pure and Applied Mathematics*, **11**, 537–66.
- Lax, P. D. (1971). 'Shock waves and entropy. In E. H. Zarantonello (ed.), *Contributions to Nonlinear Functional Analysis*, pp. 603–34, New York: Academic Press.
- Lerat, A. (1983). 'Proprietes d'homogeneite et decomposition des flux en dynamique des gaz.' *Journal de Mecanique Theorique et Appliquee*, **2**, 185–213.
- Leveque, R. J. (1983). 'Some preliminary results using a large time step generalization of Godunov's method.' In F. Angrand et al. (eds), *Numerical Methods for the Euler Equations of Fluid Dynamics*, Philadelphia: SIAM Publications.
- Leveque, R. J. (1984). 'Convergence of a large time step generalization of Godunov's method for conservation laws.' *Comm. Pure and Applied Mathematics*, **37**, 463–77.
- Leveque, R. J. (1985). 'A large time step generalization of Godunov's method for systems of conservation laws.' *SIAM Journal Numerical Analysis*, **22**, 1051–73.
- Liou, M. S., Van Leer, B., and Shuen, J. S. (1988). 'Splitting of inviscid fluxes for real gases.' *NASA Report TM 100856, ICOMP-88-7*, NASA Lewis Research Center.
- Lombard, C. K., Bardina, J., Venkatapathy, E., and Olinger, J. (1983). 'Multidimensional formulation of CSCM—an upwind flux difference, eigenvector split method for the compressible Navier–Stokes equations.' *AIAA Paper 83-1895, Proc. AIAA 6th Computational Fluid Dynamics Conference*, pp. 649–64.
- Moretti, G. (1979). 'The λ -scheme.' *Computers and Fluids*, **7**, 191–205.

- Moretti, G. (1987). 'A technique for integrating two-dimensional Euler equations.' *Computer and Fluids*, **15**, 59–75.
- Moretti, G., and Zannetti, L. (1984). 'A new and improved computational technique for two-dimensional, unsteady, compressible flows.' *AIAA Journal*, **22**, 758–65.
- Napolitano, M., and Dadone, A. (1985). 'Implicit lambda methods for three-dimensional compressible flows.' *AIAA Journal*, **23**, 1343–7.
- Osher, S. (1981). 'Numerical solution of singular perturbation problems and hyperbolic systems of conservation laws.' In O. Axelsson *et al.* (eds), *Mathematical Studies*, No. 47, Amsterdam: North Holland.
- Osher, S. (1984). 'Riemann solvers, the entropy condition and difference approximations.' *SIAM Journal Numerical Analysis*, **21**, 217–35.
- Osher, S., and Chakravarthy, S. R. (1983). 'Upwind schemes and boundary conditions with applications to Euler equations in general coordinates.' *Journal Computational Physics*, **50**, 447–81.
- Osher, S., and Solomon, F. (1982). 'Upwind difference schemes for hyperbolic systems of conservation laws.' *Mathematics of Computation*, **38**, 339–74.
- Powell, K. G., Van Leer, B. (1989). 'A genuinely multidimensional upwind cell-vertex scheme for the Euler equations.' AIAA Paper 89-0095, AIAA 27th Aerospace Sciences Meeting.
- Raithby, G. D. (1976). 'Skew upstream differencing schemes for problems involving fluid flows.' *Computer Methods in Applied Mechanics and Engineering*, **9**, 153–64.
- Rice, J. G., and Schnipke, R. J. (1985). 'A monotone streamline upwind finite element method for convection dominated flows.' *Computer Methods in Applied Mechanics and Engineering*, **48**, 313–27.
- Roe, P. L. (1981a). 'The use of the Riemann problem in finite difference schemes.' *Lecture Notes in Physics*, Vol. 141, pp. 354–9, Berlin: Springer Verlag.
- Roe, P. L. (1981b). 'Approximate Riemann solvers, parameter vectors and difference schemes.' *Journal Computational Physics*, **43**, 357–72.
- Roe, P. L. (1985). 'Upwind schemes using various formulations of the Euler equations.' In F. Angrand *et al.* (eds), *Numerical Methods for the Euler Equations of Fluid Dynamics*, Philadelphia: SIAM Publications.
- Roe, P. L. (1986a). 'Characteristic based schemes for the Euler equations.' *Annual Review of Fluid Mechanics*, **18**, 337–65.
- Roe, P. L. (1986b). 'Discrete models for the numerical analysis of time-dependent multidimensional gas dynamics.' *Journal Computational Physics*, **63**, 458–76.
- Roe, P. L., and Baines, M. J. (1982). 'Algorithms for advection and shock problems.' *Proc. 4th GAMM Conference on Numerical Methods in Fluid Mechanics*, Braunschweig, Vieweg.
- Roe, P. L., and Baines, M. J. (1984). 'Asymptotic behaviour of some non-linear schemes for linear advection.' *Proc. 5th GAMM Conference on Numerical Methods in Fluid Mechanics*, Braunschweig, Vieweg.
- Roe, P. L., and Pike, J. (1984). 'Efficient construction and utilisation of approximate Riemann solutions.' In R. Glowinski and J. L. Lions (eds), *Computing Methods in Applied Sciences and Engineering*, Amsterdam: North Holland.
- Sod, G. A. (1985). 'A random choice method with application to reaction-diffusion systems in combustion.' *Comp. and Maths. Appl.*, **II**.
- Steger, J. L. (1978). 'Coefficient matrices for implicit finite difference solution of the inviscid fluid conservation law equations.' *Computer Methods in Applied Mechanics and Engineering*, **13**, 175–88.
- Steger, J. L., and Warming, R. F. (1981). 'Flux vector splitting of the inviscid gas-dynamic equations with applications to finite difference methods.' *Journal Computational Physics*, **40**, 263–93.
- Thomas, J. L., Van Leer, B., and Walters, R. W. (1985). 'Implicit flux-split schemes for

- the Euler equations.' *AIAA Paper 85-1680*, AIAA 18th Fluid Dynamics, Plasma Dynamics and Lasers Conference.
- Van Leer, B. (1977a). 'Towards the ultimate conservative difference scheme. III: Upstream-centered finite difference schemes for ideal compressible flow.' *Journal of Computational Physics*, **23**, 263–275.
- Van Leer, B. (1977b). 'Towards the ultimate conservative difference scheme. IV: A new approach to numerical convection.' *Journal of Computational Physics*, **23**, pp. 276–299.
- Van Leer, B. (1979). 'Towards the ultimate conservative difference scheme. V: A second order sequel to Godunov's method.' *Journal of Computational Physics*, **32**, 101–136.
- Van Leer, B. (1982). 'Flux vector splitting for the Euler equations.' *Proc. 8th International Conference on Numerical Methods in Fluid Dynamics*, Berlin: Springer Verlag.
- Van Leer, B. (1983). 'Multidimensional explicit difference schemes for hyperbolic conservation laws.' *ICASE Report 172254*, NASA Langley Research Center.
- Van Leer, B. (1984). 'On the relation between the upwind differencing schemes of Godunov, Engquist–Osher and Roe.' *SIAM Journal Sci. Stat. Computing*, **5**, 1–20.
- Whitfield, D. L., and Janus, J. M. (1984). 'Three dimensional unsteady Euler equations solution using flux vector splitting.' *AIAA Paper 84-1552*, AIAA 17th Fluid Dynamics, Plasma Dynamics and Lasers Conference.
- Yanenko, N. N. (1979). *The Method of Fractional Steps*, New York: Springer Verlag.
- Yang, J. Y. (1986). 'Higher order flux difference splitting schemes for the Euler equations using upstream interpolations.' *Proc. 6th GAMM Conference on Numerical Methods in Fluid Mechanics, Notes on Numerical Fluid Mechanics*, Vol. 13, pp. 391–98, Braunschweig/Wiesbaden, Vieweg.

PROBLEMS

Problem 20.1

Obtain the conservative Steger and Warming split fluxes f^+ and f^- for a subsonic flow, with the splitting (20.2.14). Verify the homogeneity property of f^+ and f^- and derive the Jacobians A^+ and A^- as a function of the conservative variables.

Problem 20.2

Obtain the general transformed flux \bar{f} given by equation (20.2.19) for the eigenvalue splitting (20.2.18).

Problem 20.3

Derive the split fluxes for the decomposition (20.2.13) and compare with the expressions (20.2.15) and (20.2.17).

Problem 20.4

Show by an explicit calculation that the Jacobians of the split fluxes $\partial f^+ / \partial U$ and $\partial f^- / \partial U$ are not equal to A^+ and A^- respectively.

Show also that the orthogonality property $A^+(A^-U) = 0$ is always satisfied.

Problem 20.5

Find the eigenvalue equation of the matrices f_u^+ and f_u^- for the splitting of Steger and Warming (20.2.15), (20.2.17). Show that there is no zero eigenvalue in the range $|M| < 1$.

Hint: Consider the set of variables (ρ, c, M) .

Calculate the Jacobian of the split fluxes as a function of these variables $J \equiv \partial f^+ / \partial(\rho, c, M)$. Show that the independent term in the third-order polynomial in λ , obtained from $\det(J - \lambda) = 0$, is equal to $\det(J)$.

Problem 20.6

Show that the isentropic system of the Euler equations for the variables $U(\rho, \rho u)$ with the isentropic condition $p/\rho^\gamma = \text{constant}$ does not have a homogeneous flux of order one in U .

Hint: Show that the corresponding flux does not satisfy condition (20.2.10).

Problem 20.7

Verify by an explicit calculation that the flux f can be written as equation (20.2.32) for the normalization (20.2.28).

Prove also equations (20.2.36) and (20.2.37) by applying the relations (20.2.34).

Write out the corresponding decompositions for the two other flux components of the Steger–Warming splitting.

Hint: Obtain, for $0 \leq M \leq 1$,

$$f_2^+ = \frac{\rho c^2}{2\gamma} [2(\gamma - 1)M^2 + (M + 1)^2] \quad f_2^- = \frac{\rho c^2}{2\gamma} (M - 1)^2$$

and apply the symmetry relation $f_2^+(M) = f_2^-(-M)$ for the domain $-1 \leq M \leq 0$.

Similarly, the third component is given in the region $0 \leq M \leq 1$ by the relations

$$f_3^+ = \frac{\rho c^2}{4\gamma} \left[2(\gamma - 1)M^3 + (M + 1)^3 + \frac{3 - \gamma}{\gamma - 1} (M + 1) \right]$$

$$f_3^- = \frac{\rho c^2}{4\gamma} (M - 1) \left[(M - 1)^2 + \frac{3 - \gamma}{\gamma - 1} \right]$$

and apply the symmetry relation $f_3^+(M) = -f_3^-(-M)$ for the domain $-1 \leq M \leq 0$.

Problem 20.8

Obtain the eigenvalues (20.2.41) associated with the Van Leer flux splitting and show that they satisfy equations (20.2.6).

Problem 20.9

Show that the Van Leer split fluxes (20.2.39) have the same slopes in function of M , at $M = \pm 1$, as the corresponding unsplit flux components.

Show that these properties remain valid for the alternative definition of the split energy flux (20.2.43).

Show also that this property is not satisfied by the Steger–Warming flux splitting.

Problem 20.10

Calculate the eigenvalues λ of the Jacobian of Van Leer's split flux f_{VL}^+ defined by equation (20.2.39). Show that one of the eigenvalues is zero and that the non-zero eigenvalues are positive for $1 < \gamma < 3$ in the range $0 < M < 1$.

Show also that there is no zero eigenvalue for the alternative choice (20.2.43).

Hint: Consider the set of variables (ρ, c, M) .

Calculate the Jacobian of the split fluxes as a function of these variables $J \equiv \partial f^+ / \partial (\rho, c, M)$. Show that the first eigenvalue is zero by observing that the

independent term in the third-order polynomial in λ , obtained from $\det(J - \lambda) = 0$, is equal to $\det(J)$, which is zero for the Van Leer splitting (20.2.39).

The two remaining eigenvalues are solutions of the quadratic equation in λ :

$$\lambda^2 - \lambda \frac{3c}{2}(1 + M) \left\{ 1 - \frac{\gamma - 1}{12(\gamma + 1)}(M - 1) \left[M^2 - 3 \frac{\gamma + 2}{\gamma} \right] \right\} + \frac{c^2}{4}(1 + M)^3 \left\{ 1 - \frac{M - 1}{8\gamma(\gamma + 1)} [4\gamma(\gamma - 1)(M - 1) + (\gamma + 1)(3 - \gamma)] \right\} = 0$$

Problem 20.11

Consider the general form of a first-order explicit scheme for the linear convection equation, where the centrally discretized convection term has been stabilized by a term of the form $(\Delta x^2/2\Delta t)(\alpha u_x)_x$.

Show that the obtained scheme is

$$u_i^{n+1} - \hat{u}_i^n = -\frac{\tau}{2}(f_{i+1} - f_{i-1})^n + \frac{1}{2}[\alpha_{i+1/2}(u_{i+1} - u_i) - \alpha_{i-1/2}(u_i - u_{i-1})]^n$$

Analyse the linear stability of this scheme, applying the procedure of Section 8.6.2, Chapter 8 in Volume 1, and show that the artificial viscosity coefficient α has to satisfy the condition $\sigma^2 \leq \alpha \leq 1$.

Observe that the upper limit corresponds to the Lax–Friedrichs scheme and the lower limit to the Lax–Wendroff scheme, while the first-order upwind scheme is associated with the choice $\alpha = |\sigma|$.

Problem 20.12

Derive the two-dimensional Steger–Warming split flux components associated with the contravariant components of the flux vector in a curvilinear coordinate system ξ, η .

Show that the Cartesian form remains valid if the Cartesian velocity components are replaced by the contravariant velocity components.

Problem 20.13

Derive the Van Leer flux splitting for the isenthalpic one-dimensional Euler equations, written for the variables ρ and ρu with $H = \text{constant}$, by applying the definition conditions of Section 20.2.3.

Hint: Define the Mach number with respect to the critical velocity c^* , for which the lowest eigenvalue vanishes. Obtain $c^{*2} = 2(\gamma - 1)H/(\gamma + 1)$ and, with $M = u/c^*$, the following positive parts of the mass and momentum fluxes $f_{\text{mass}}^+ = \rho c^*(M + 1)^2/4$ and $f_{\text{mom}}^+ = f_{\text{mass}}^+(\gamma + 1)c^*/\gamma$.

Problem 20.14

Show that the balance of fluxes over cell $i(i - \frac{1}{2}, i + \frac{1}{2})$, defined by $f_{i-1}^+ + f_i^- = f_i^+ + f_{i+1}^-$, does not ensure the constancy of stagnation enthalpy, neither with the Steger–Warming nor the Van Leer splittings, for stationary flow conditions.

Assume mass conservation over the cell and apply the above discretization to the split energy fluxes, considering subsonic flow conditions. Calculate the error with respect to the condition $H_{i-1} = H_{i+1}$ by performing a Taylor expansion of the remaining terms.

Problem 20.15

Derive the eigenvalue decomposition for the modified Van Leer splitting (20.2.39) with the third component replaced by (20.2.44) and compare with the splitting given by equations (20.2.41).

Define a splitting such that $\lambda_3^+ = 0$ for subsonic flows $M < 1$ and show that it corresponds to the choice $P(M-1) = (M-1)[1/(\gamma-1) + (M-1)]/\gamma$ and to $f_3^+ = f_1^+ [H - c^2(M-1)/\gamma(\gamma-1) - c^2(M-1)^2/\gamma]$. Show that this flux component has a slope discontinuity at $M = 1$.

Hint: Obtain

$$\lambda_{1,\text{VL}}^+ = \frac{c}{4}(M+1)^2[M(2-M) + \gamma P(M-1)]$$

$$\lambda_{2,\text{VL}}^+ = \frac{c}{4}(M+1)^2[3 - M + (\gamma-1)(M-1)^2 - \gamma(\gamma-1)P(M-1)]$$

$$\lambda_{3,\text{VL}}^+ = \frac{c}{4}(M+1)^2\{(M-1)[2 - M + \gamma(M-1)] - \gamma(\gamma-1)P(M-1)\}$$

Problem 20.16

Apply the first-order upwind scheme with the Steger and Warming flux splitting to the stationary nozzle problem of Problem 16.26 selecting a transonic case with and without a shock.

Compare the results after the eigenvalue modification of equation (20.3.22) and observe the effects of increasing the parameter ε .

Repeat with the Van Leer splitting (20.2.39), (20.2.40) and compare with the alternative variant (20.2.43).

Problem 20.17

Apply the first-order upwind scheme with the flux splitting of Steger and Warming to the shock tube problem of Problem 16.25, case 1. Repeat the same computations for higher shock intensities applying the initial conditions of case 2.

Compare the results after the eigenvalue modification of equation (20.3.22) and observe the effects of increasing the parameter ε .

Repeat with the Van Leer splitting (20.2.39), (20.2.40) and compare with the alternative variant (20.2.43).

Problem 20.18

Apply the flux vector splitting scheme (20.3.10) to the Burgers equation following the analysis of Example 20.5.1.

Write $f^\pm = a^\pm u/2$ with $a = u$ and show that the scheme is identical to the Engquist–Osher scheme applied to the same equation.

Problem 20.19

Apply the Godunov method to the linear convection equation with $a < 0$.

Draw the corresponding figure to Figure 20.5.2 and show that the upwind scheme (20.5.12) is obtained.

Problem 20.20

Derive the general expression of the Godunov scheme on an arbitrary mesh, where the points x_i are randomly distributed. Consider the cell interfaces located at points $x_{i+1/2} = (x_i + x_{i+1})/2$.

Show that the relations (20.5.8) and (20.5.16) remain valid with the substitution of Δx by $(\Delta x_{i-1} + \Delta x_i)/2$ where $\Delta x_i = x_{i+1} - x_i$.

Show that the first-order upwind scheme (20.5.10) remains valid with the same replacement.

Problem 20.21

Consider an arbitrary mesh point distribution in the domain (a, b) with $\Delta x_i = x_{i+1/2} - x_{i-1/2} = (x_{i+1} - x_{i-1})/2$ and such that the flux is periodic, that is $f(a) = f(b)$. Apply the general form of the conservation law (20.5.4) for the cell-averaged state variables and show the following discrete form of the conservative condition on an arbitrary mesh:

$$\sum_i \Delta \bar{U}_i \Delta x_i \equiv \sum_i \frac{(\overline{U_i^{n+1}} - \overline{U_i^n})(x_{i+1} - x_{i-1})}{2} = 0$$

Consider the first-order upwind scheme on an arbitrary mesh under the form

$$u_i^{n+1} = u_i^n - a \Delta t \frac{u_i^n - u_{i-1}^n}{x_i - x_{i-1}}$$

and show that this generalization of the upwind scheme on an arbitrary mesh is not conservative, since it does not satisfy the above relation.

Compare also with the result of the previous problem.

Problem 20.22

By applying the integral conservation law (20.5.2) on the interval $[i\Delta x, (i+1)\Delta x]$ to the Riemann solution (20.5.6), show the following property, valid for all times $n\Delta t < t < (n+1)\Delta t$, with Δt restricted by the condition $\Delta t |a_{\max}| < \Delta x/2$:

$$\frac{1}{\Delta x} \int_{- \Delta x/2}^{\Delta x/2} U^{(R)} \left(\frac{\xi}{t}, U_i^n, U_{i+1}^n \right) d\xi = \frac{1}{2} (U_i^n + U_{i+1}^n) - \frac{\Delta t}{\Delta x} [f(U_{i+1}^n) - f(U_i^n)]$$

Problem 20.23

Consider the Godunov method for Burgers equation following Example 20.5.1.

Derive the numerical flux for all the configurations of Figure 20.5.3 and show that the expression (E20.5.8) is valid in all cases.

Problem 20.24

Solve Burgers equation with Godunov's method for the initial conditions of a stationary shock, $u = 1$ for $x < 0$ and $u = -1$ for $x > 0$.

Repeat for an initial expansion shock, $u = -1$ for $x < 0$ and $u = 1$ for $x > 0$, and note that the numerical solution correctly produces an expansion fan between the values -1 and $+1$.

Solve the same problems with Murman and Cole's first-order upwind method (20.5.32) and observe that the expansion shock remains as a valid solution of this scheme.

Problem 20.25

Show on the example of Burgers equation that the Murman–Cole scheme with the numerical flux

$$f_{i+1/2}^{*(MC)} = \mu_i f_i + (1 - \mu_{i+1}) f_{i+1}$$

instead of (20.5.32), is identical to the Engquist and Osher scheme.

Analyse all the cases of Figure 20.5.3.

Problem 20.26

Obtain the relations (20.5.44) for the Engquist–Osher numerical flux and derive the relations of Example 20.5.2 for Burgers equation by analysing all the cases.

Solve the Burgers equation for the initial data of Problem 20.24 and distinguish between moving and stationary shocks.

Problem 20.27

Work out the equations (20.5.47) to (20.5.49) defining the intermediate states in the Osher scheme.

Develop completely the algorithm by applying the relations (20.5.57) and their analogue for the negative part of the Jacobian.

Problem 20.28

Apply the first-order upwind Osher scheme to the stationary nozzle of Problem 16.26 selecting a transonic case with and without a shock.

Adapt the boundary conditions to the wave decomposition of the scheme.

Problem 20.29

Obtain the matrices \bar{B} and \bar{C} of equations (20.5.77) and (20.5.79) and by a direct application of equation (20.5.80) the Roe matrix \bar{A} .

Show that the matrix \bar{A} is identical to the local Jacobian given by equation (E16.2.3), when expressed as a function of the variables u and H , if these variables are replaced by the weighted averages (20.5.81).

Problem 20.30

Apply the first-order Roe scheme to the shock tube problem of Problem 16.25, case 1.

Repeat the same computations for higher shock intensities applying the initial conditions of case 2.

Problem 20.31

Develop the Roe-averaged matrix for the stationary two-dimensional supersonic flow treated in Example 16.4.2. Show the validity of the averaging of the variables defined in the one-dimensional case.

Problem 20.32

Perform a Von Neumann stability analysis of the two-dimensional first-order upwind scheme (20.7.9).

Write the scheme by extracting central difference terms, in the line of equation (20.1.14), and apply the results of Section 8.6.2 in Volume 1.

Show that the necessary and sufficient condition for Von Neumann stability of scheme (20.7.9) is $|\sigma_x| + |\sigma_y| \leq 1$.

Problem 20.33

Apply a flux splitting decomposition on the Lax–Wendroff scheme (17.2.5).

Show that the numerical flux (17.2.8) can be written as

$$f_{i+1/2}^{*LW} = f_i^+ + f_{i+1}^- + \frac{1}{2}(1 - \tau A_{i+1/2}^+) \delta f_{i+1/2}^+ - \frac{1}{2}(1 + \tau A_{i+1/2}^-) \delta f_{i+1/2}^-$$

where A can be defined as a Roe Matrix

Hint: Introduce $f = f^+ + f^-$ and $A = A^+ + A^-$ and take into account that $A^+ \cdot A^- = A^- \cdot A^+ = 0$.

Chapter 21

Second-order Upwind and High-resolution Schemes

The straightforward replacement of the first-order upwind space differences by appropriate second-order accurate formulas leads to deficiencies similar to those encountered with central schemes, namely the generation of oscillations around discontinuities.

This is somehow disappointing since one of the motivations behind upwind schemes is the hope that the introduction of physical propagation properties in the discretization will prevent the generation of oscillations in the numerical solutions. This is only partly fulfilled in the sense that for non-linear equations, such as the Euler equations, oscillation-free results can be obtained for weak stationary discontinuities. However, this is not a general property, since it can be shown theoretically that linear second-order upwind schemes always generate oscillations (Engquist and Osher, 1981).

A deeper analysis is therefore necessary to achieve the goals of oscillation-free, second-order schemes able to represent accurately shock as well as contact discontinuities. A systematic analysis of the conditions required by a scheme to satisfy these properties has been developed, initiated by Godunov (1959) who introduced the important concept of monotonicity. For non-linear equations the concept of bounded total variation of the solution is more general and has been introduced by Harten (1983) as a criterion to ensure that unwanted oscillations are not generated by a numerical scheme.

The converged solution should also be physically acceptable and the formalization of this requirement under the form of an entropy condition has been developed by Lax (1973) through the concept of entropy function.

General families of schemes satisfying these conditions can be defined (Harten, 1983, 1984; Osher, 1984), but it is shown that these schemes can only be first-order accurate. The only way to overcome this limitation, while satisfying the required conditions, is to introduce non-linear components. Non-linear discretizations imply that the schemes will be non-linear even when applied to linear equations. This important concept was introduced initially by Van Leer (1973, 1974) and Boris and Book (1973, 1976) under the form of 'limiters', which control the gradients of the computed solution such as to prevent the appearance of over- or undershoots.

We will review these concepts and their consequences in this chapter after a

presentation of a general framework for the generation of second-order upwind schemes.

Various approaches can be followed in this direction and a general framework has been set by Van Leer (1977b, 1979) in a series of papers leading to a second-order Godunov method satisfying all of the above-mentioned conditions and where many of the ideas at the basis of modern high-resolution schemes have been developed. This will form the content of Section 21.1, where the upwind fluxes with second-order accuracy in space are derived first. The adaptations necessary to generate an explicit scheme with second-order accuracy in time are presented separately.

Section 21.2 introduces the concept of high-resolution schemes and the requirements for preventing unwanted oscillations with higher-order schemes. This covers the concepts of entropy condition and monotonicity expressed through the total variation diminishing (TVD) conditions.

Section 21.3 introduces the non-linear limiters for upwind TVD schemes with second-order accuracy in space, basically for semi-discretized formulations while Section 21.4 discusses the time-integration methods and their implications for the TVD properties. Examples for one- and multi-dimensional Euler equations are presented in Section 21.5.

21.1 GENERAL FORMULATION OF HIGHER-ORDER UPWIND SCHEMES

Second-order spatial accuracy can be achieved by introducing more upwind points in the schemes. The procedure to be followed here is based on an extension of the Godunov approach, as described in Section 20.5.1, following Van Leer (1977b, 1979). It has been noted that the projection stage, whereby the solution is projected in each cell ($i - \frac{1}{2}, i + \frac{1}{2}$) on piecewise constant states, is the cause of the first-order space accuracy of the Godunov schemes. This stage is completely decoupled from the physical stage where the Riemann problems are solved at the interfaces of the cells.

Hence, it is sufficient to modify the first projection stage without modifying the Riemann solver, in order to generate higher spatial approximations. The state variables at the interfaces are thereby obtained from an extrapolation between the neighbouring cell averages. This method for the generation of second-order upwind schemes via *variable extrapolation* is often referred to in the literature as the MUSCL approach, this acronym standing for Monotone Upstream-centred Schemes for Conservation Laws, after the name of the first code applying this method as developed by Van Leer (1979).

Time-integration methods based on a separate time and space discretization following the approach of Chapter 18, such as linear multi-step methods (implicit schemes) or multi-stage Runge-Kutta techniques, can then directly be applied to the modified numerical flux.

For explicit schemes the time discretization should also be raised to second or higher order, giving rise to combined space-time discretizations in the linear

in van Leer's spelling

of the Lax–Wendroff approach. This will require an additional step between the projection stage and the physical stage.

21.1.1 Higher-order projection stages—variable extrapolation or MUSCL approach

Representing the numerical approximation of the solution as a piecewise constant is equivalent to a first-order spatial discretization. Hence a linear approximation of the solution on each cell is a second-order space discretization, while a quadratic representation on each cell leads to a third-order spatial discretization. This is easily understood since a linear solution is exactly resolved in the first case and a quadratic solution is exactly represented in the second case. The generated truncation errors are respectively of the order Δx^2 and Δx^3 .

In the representation of the conservation laws based on equation (20.5.4), the discrete state variables are representative of the *average* state within the cells and the piecewise linear or quadratic distributions have to average out to these values. Let us consider the general local representation, valid within cell i , at a given instant, Figure 21.1.1:

$$U(x) = U_i + \frac{1}{\Delta x}(x - x_i)\delta_i U + \frac{3\kappa}{2\Delta x^2} \left[(x - x_i)^2 - \frac{\Delta x^2}{12} \right] \delta_i^2 U \quad x_{i-1/2} < x < x_{i+1/2} \quad (21.1.1)$$

where U_i is the average value, defined by

$$U_i = \frac{1}{\Delta x} \int_{x_{i-1/2}}^{x_{i+1/2}} U(x) dx \quad (21.1.2)$$

and $\delta_i U, \delta_i^2 U$ are estimations of the first and second derivatives within cell i . The form of the Δx^2 term in this representation results from the definition (21.1.2). i.e. $\frac{\delta_i U}{\Delta x} \approx U'$

For $3\kappa = 1$, equation (21.1.1) is a correct Taylor development up to third order and this parabolic representation then generates a third-order accurate space discretization. For other values of the parameter κ the above representation is considered as linear with various truncation terms. Observe that the nodal value within the cell, $U(x_i)$, is equal to the average value U_i only for $\kappa = 0$, since

$$U(x_i) = U_i - \frac{\kappa}{8} \delta_i^2 U \quad (21.1.3)$$

Hence, this approach differs from a finite element representation which is based on nodal values (Figure 21.1.1).

In order to define completely the representation, the derivatives $\delta_i U$ and $\delta_i^2 U$ have to be estimated. If we require these gradients to depend only on quantities

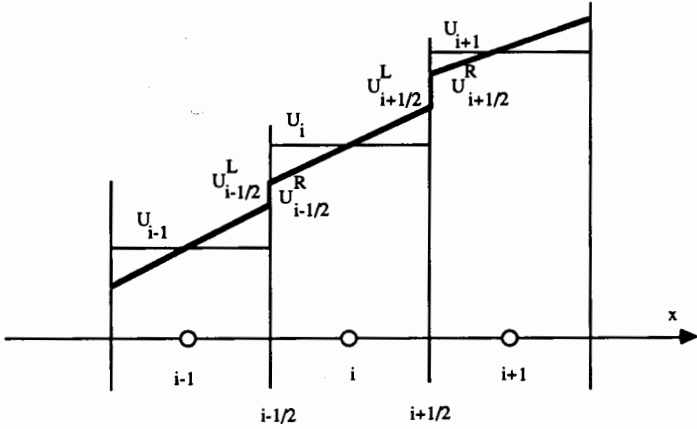


Figure 21.1.1 Piecewise linear representation within cells

of adjacent cells, the only choice is to use central differences of *averaged* values; that is

$$\delta_i U = \frac{U_{i+1} - U_{i-1}}{2} \quad (21.1.4a)$$

$$\delta_i^2 U = U_{i+1} - 2U_i + U_{i-1} \quad (21.1.4b)$$

Actually, the resolution of the Riemann problem or the numerical flux estimation requires only the values at the cell boundaries. Setting $x = x_i \pm \Delta x/2$ within cell i gives the interface values

$$\begin{aligned} U_{i+1/2}^L &= U_i + \frac{1}{2} \delta_i U + \frac{\kappa}{4} \delta_i^2 U \\ &= U_i + \frac{1}{4} (1 - \kappa) (U_i - U_{i-1}) + \frac{1}{4} (1 + \kappa) (U_{i+1} - U_i) \end{aligned} \quad (21.1.5a)$$

$$\begin{aligned} U_{i-1/2}^R &= U_i - \frac{1}{2} \delta_i U + \frac{\kappa}{4} \delta_i^2 U \\ &= U_i - \frac{1}{4} (1 + \kappa) (U_i - U_{i-1}) - \frac{1}{4} (1 - \kappa) (U_{i+1} - U_i) \end{aligned} \quad (21.1.5b)$$

where the superscripts L and R refer to the left and right sides at the considered boundary.

The first term on the right-hand side corresponds to the first-order schemes discussed in the previous chapter, and it is the additional dependence on adjacent points that gives the schemes a higher-order accuracy in space. Both options can be combined via the introduction of a parameter ε , such that $\varepsilon = 0$ for a first-order scheme and $\varepsilon = 1$ for a higher-order scheme, defining

$$U_{i+1/2}^L = U_i + \frac{\varepsilon}{4} [(1 - \kappa)(U_i - U_{i-1}) + (1 + \kappa)(U_{i+1} - U_i)] \quad (21.1.6)$$

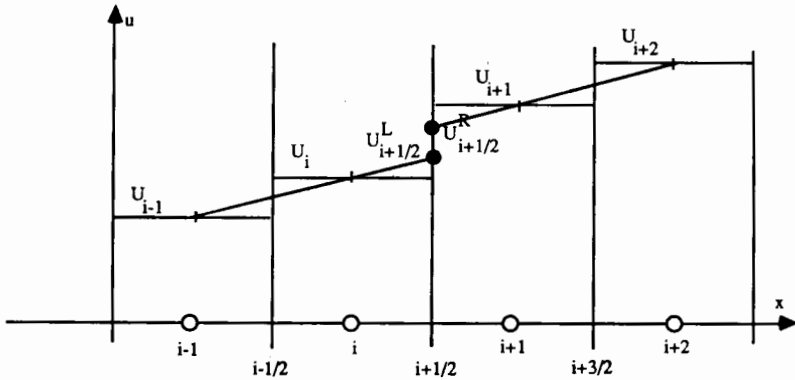


Figure 21.1.2 Linear one-sided extrapolation of interface values for $\kappa = -1$

and similarly for the extrapolated values at the right of $(i + \frac{1}{2})$ within cell $(i + 1)$:

$$U_{i+1/2}^R = U_{i+1} - \frac{\epsilon}{4} [(1 + \kappa)(U_{i+1} - U_i) + (1 - \kappa)(U_{i+2} - U_{i+1})] \quad (21.1.7)$$

The interface values can be considered as resulting from a combination of backward and forward extrapolations. In particular $\kappa = -1$ corresponds to a linear one-sided extrapolation at the interface between the averaged values at the two upstream cells i and $(i - 1)$ (Figure 21.1.2):

$$U_{i+1/2}^L = U_i + \frac{\epsilon}{2}(U_i - U_{i-1}) \quad \kappa = -1 \quad (21.1.8)$$

$$U_{i+1/2}^R = U_{i+1} - \frac{\epsilon}{2}(U_{i+2} - U_{i+1}) \quad \kappa = -1 \quad (21.1.9)$$

leading to a second-order fully one-sided scheme, as will be seen next.

For $\kappa = 0$ the interface value is approximated by a linear interpolation between one upstream and one downstream cell:

$$U_{i+1/2}^L = U_i + \frac{\epsilon}{4}(U_{i+1} - U_{i-1}) \quad \kappa = 0 \quad (21.1.10)$$

$$U_{i+1/2}^R = U_{i+1} - \frac{\epsilon}{4}(U_{i+2} - U_i) \quad \kappa = 0 \quad (21.1.11)$$

Observe that with $\kappa = 1$ the interface values are the arithmetic mean of the adjacent cell values and the upwind character is totally lost. This corresponds to a central scheme since there is no discontinuity at the cell interfaces.

Indeed, the discontinuity at the interface is defined by

$$\begin{aligned} U_{i+1/2}^R - U_{i+1/2}^L &= -\frac{1}{4}(1 - \kappa)(U_{i+2} - 3U_{i+1} + 3U_i - U_{i-1}) \\ &= -\frac{1}{4}(1 - \kappa)\frac{\partial^3 U}{\partial x^3} \Delta x^3 + O(\Delta x^4) \end{aligned} \quad (21.1.12)$$

where the difference formula (4.2.56) in Volume 1 has been applied at $(i + \frac{1}{2})$. This difference is seen to be of third order except for $\kappa = 1$, where it is at least of fourth order. The value $\kappa = \frac{1}{2}$ corresponds to the QUICK scheme of Leonard (1979). Note also that for any value of κ , the following relation holds within each cell i :

$$U_{i+1/2}^L - U_{i-1/2}^R = \frac{1}{2}(U_{i+1} - U_{i-1}) \quad (21.1.13)$$

but

$$U_{i+1/2}^L + U_{i-1/2}^R = 2U_i + \frac{\kappa}{4}(U_{i+1} - 2U_i + U_{i-1}) \quad (21.1.14)$$

21.1.2 Numerical flux for higher-order upwind schemes

Once the discontinuities at the cell interfaces have been defined, the second step of the Godunov approach can be applied, namely the resolution of the Riemann problem or, more generally, the definition of the numerical fluxes representing the selected approximation to the physical fluxes at the cell interfaces.

Any of the upwind numerical fluxes summarized in equation (20.5.96) can be applied with the above interfaces values. If the first-order scheme is defined by the numerical flux

$$f_{i+1/2}^* = f^*(U_i, U_{i+1}) \quad (21.1.15a)$$

the second-order *space*-accurate numerical flux is obtained from

$$f_{i+1/2}^{*(2)} = f^*(U_{i+1/2}^L, U_{i+1/2}^R) \quad (21.1.15b)$$

and the semi-discretized upwind scheme of second-order accuracy in space is

$$\frac{dU_i}{dt} = -\frac{1}{\Delta x}(f_{i+1/2}^{*(2)} - f_{i-1/2}^{*(2)}) \quad (21.1.15c)$$

This generalizes the first-order schemes to which the above equation reduces when the variable $\varepsilon = 0$. For example, a higher-order flux splitting method is obtained from

$$f_{i+1/2}^{*(2)} = f^+(U_{i+1/2}^L) + f^-(U_{i+1/2}^R) \quad (21.1.16)$$

Another example is the first-order Roe scheme, whose numerical flux is given by equation (20.5.89):

$$f_{i+1/2}^{*(R)} = \frac{1}{2}(f_i + f_{i+1}) - \frac{1}{2}|A|_{i+1/2}(U_{i+1} - U_i) \quad (21.1.17a)$$

with A defined as the Roe matrix, such that

$$A_{i+1/2}(U_{i+1} - U_i) = f_{i+1} - f_i \quad (21.1.17b)$$

Its extension to second-order spatial accuracy is written as follows:

$$f_{i+1/2}^{*(2)} = \frac{1}{2}[f(U_{i+1/2}^L) + f(U_{i+1/2}^R) - |A|_{i+1/2}^{(2)}(U_{i+1/2}^R - U_{i+1/2}^L)] \quad (21.1.18a)$$

with

$$A_{i+1/2}^{(2)}(U_{i+1/2}^R - U_{i+1/2}^L) = f(U_{i+1/2}^R) - f(U_{i+1/2}^L) \quad (21.1.18b)$$

All the second-order upwind schemes necessarily involve at least five mesh points.

The higher-order space discretization of the physical flux balance is thereby, in principle, completely defined. The mention 'in principle' points to the additional modifications to be introduced in order to avoid oscillations around discontinuities. This will be achieved via the introduction of non-linear limiters, to be discussed in the following sections.

21.1.3 Second-order space- and time-accurate upwind schemes based on variable extrapolation

For schemes based on separate time and space discretizations, such as linear multi-step methods leading to implicit schemes or Runge–Kutta methods, the higher-order extension of the space discretization is hereby completed. However, this is not the case for explicit schemes based on combined space–time discretizations, in the line of the Lax–Wendroff approach.

A simple explicit Euler time integration applied to equation (21.1.15c) would lead to the scheme of first-order accuracy in time:

$$U_i^{n+1} = U_i^n - \tau(f_{i+1/2}^{*(2)} - f_{i-1/2}^{*(2)}) \quad (21.1.19)$$

This scheme is, however, linearly *unconditionally unstable*, although the instability may be considered as weak (see Problem 21.1).

Since the instability arises from the first-order time differencing whose second-order truncation error, $-\Delta t u_{tt}/2 = -a^2 \Delta t u_{xx}/2$, is not compensated by a similar term from the second-order space difference (the first term of the truncation error is proportional to a third-order derivative), second-order time differencing has to be considered.

This can be obtained if the physical step of the Riemann solution is introduced *after a propagation, over a time step $\Delta t/2$, of the waves produced at the interfaces*.

In order to make the procedure clear, let us consider the linear convection equation and a local linear representation of the solution, with $\kappa = 0$ (Figure 21.1.3). At $t = n\Delta t$ the solution is represented within cell i by

$$u^n(x) = u_i^n + \frac{(x - x_i)(u_{i+1}^n - u_{i-1}^n)}{2\Delta x} \quad x_{i-1/2} < x < x_{i+1/2} \quad (21.1.20)$$

The exact solution of the Riemann problem is a pure convection:

$$u^{(R)}(x, t) = u^n(x - at) \quad (21.1.21)$$

and the approximation at time level $n + 1$ is defined by the cell averages of the exact solution after a time interval Δt :

$$u_i^{n+1} = \frac{1}{\Delta x} \int_{i+1/2}^{i-1/2} u^n(x - a\Delta t) dx \quad (21.1.22a)$$

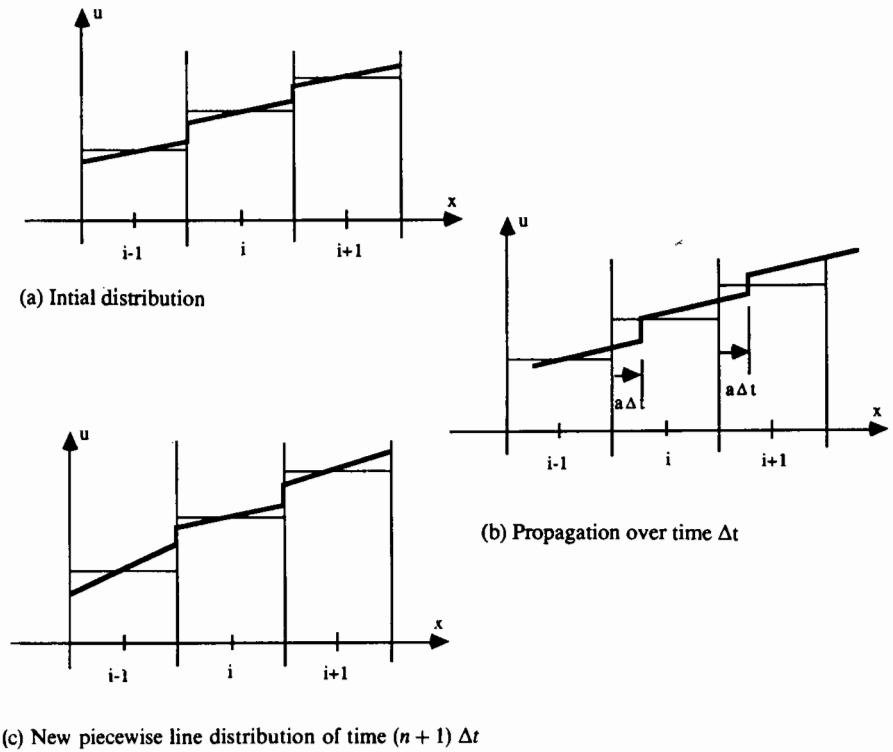


Figure 21.1.3 Second-order Godunov-type scheme for the linear convection equation

which becomes after exact integration

$$u_i^{n+1} = \frac{\sigma}{2} [u_{i-1/2}^L + u^n(x_{i-1/2} - a\Delta t)] + \frac{1}{2}(1 - \sigma) [u_{i-1/2}^R + u^n(x_{i+1/2} - a\Delta t)] \quad (21.1.22b)$$

With equations (21.1.10) and (21.1.11) the scheme becomes

$$u_i^{n+1} - u_i^n = -\sigma(u_i - u_{i-1})^n - \frac{\sigma}{4}(1 - \sigma)(u_{i+1} - u_i - u_{i-1} + u_{i-2})^n \quad (21.1.23)$$

where one recognizes the scheme presented by Fromm (1968).

Introducing the cell boundary values through equations (21.1.5) and selecting the symmetric choice $\kappa = 0$ for the gradient of the linear distribution of the state variable, Fromm's scheme is rewritten as

$$u_i^{n+1} - u_i^n = -\sigma \left[\left(u_{i+1/2}^L - \frac{\sigma}{2} \delta_i u^n \right) - \left(u_{i-1/2}^L - \frac{\sigma}{2} \delta_{i-1} u^n \right) \right] \quad (21.1.24)$$

The terms in brackets can be considered as resulting from a propagation of the

intercell values over a time step $\Delta t/2$, before the wave decomposition at the cell interfaces, since the contribution $-\sigma \delta u/2$ is obtained from the application of the first-order scheme over $\Delta t/2$. With

$$\overline{\Delta u}_i = -\frac{\sigma}{2} \delta_i u^n \quad (21.1.25a)$$

equation (21.1.24) is written as

$$u_i^{n+1} - u_i^n = -\sigma [(u_{i+1/2}^L + \overline{\Delta u}_i) - (u_{i-1/2}^L + \overline{\Delta u}_{i-1})] \quad (21.1.25b)$$

An extension of Fromm's scheme to general upwind discretizations has been applied along these lines by Van Leer (1979) and Van Albada *et al.* (1982).

A general formulation of second-order space- and time-accurate upwind schemes can be obtained as follows, based on equation (11.5.7) (Chapter 11 in Volume 1).

The first step defines intermediate values after a propagation over a time interval $\Delta t/2$:

$$\bar{U}_i = U_i^n - \frac{\Delta t}{2\Delta x} (f_{i+1/2}^* - f_{i-1/2}^*) \quad (21.1.26a)$$

where f^* is any of the *first-order numerical fluxes* (20.5.96). $f_{i\pm 1/2}^*$

The second step defines the interface variables as second-order extrapolations to the intermediate values \bar{U} :

$$U_{i+1/2}^{L*} = \bar{U}_i + \frac{1}{4} [(1 - \kappa)(U_i - U_{i-1}) + (1 + \kappa)(U_{i+1} - U_i)] \quad (21.1.26b)$$

$$U_{i+1/2}^{R*} = \bar{U}_{i+1} - \frac{1}{4} [(1 + \kappa)(U_{i+1} - U_i) + (1 - \kappa)(U_{i+2} - U_{i+1})]$$

The forward and backward gradients of U will be modified subsequently to ensure monotonicity. \leftarrow
 $U_{i\pm 1/2}$

The last step defines the second-order numerical flux as

$$f_{i+1/2}^{*(2)} = f^*(U_{i+1/2}^{L*}, U_{i+1/2}^{R*}) \quad (21.1.26c)$$

and the final scheme is

$$U_i^{n+1} - U_i^n = -\tau (f_{i+1/2}^{*(2)} - f_{i-1/2}^{*(2)}) \quad (21.1.26d)$$

If the first step (21.1.26a) is suppressed, the resulting flux is second-order accurate in space and (21.1.26d) is first order in time and hence unstable.

It is important to observe here that the propagation step (21.1.26a) and the approximation on the interface values (21.1.26b) do not have to be conservative. They could be performed on the characteristic variables for instance. The conservative property of the scheme is ensured by the third step which defines the numerical flux.

Applied to the linear convection equation and a first-order numerical flux, the above scheme is stable for $0 < \sigma < (1 - \kappa)$. It becomes identical to the second-order upwind scheme of Warming and Beam (1976) for $\kappa = -1$ (see

Problem 21.5) and represents a non-linear generalization of the unique second-order upwind scheme (9.3.12) (Chapter 9 in Volume 1) on the support $(i, i-1, i-2)$.

21.1.4 Linearized analysis of second-order upwind schemes

The linearized form of the second-order upwind scheme is obtained for $f = au$, with $a > 0$, $\sigma = a \Delta t / \Delta x$ and all the right-hand side terms taken at level n , for $\kappa = -1$ (Warming and Beam, 1976):

$$u_i^{n+1} - u_i^n = -\frac{\sigma}{2}(3u_i - 4u_{i-1} + u_{i-2})^n + \frac{\sigma^2}{2}(u_i - 2u_{i-1} + u_{i-2})^n \quad (21.1.27)$$

This scheme appears as a Lax-Wendroff-type scheme (17.2.4) where the space derivatives are discretized with upwind formulas. The scheme can also be written as a correction to the first-order upwind scheme

$$u_i^{n+1} - u_i^n = -\sigma(u_i - u_{i-1})^n - \frac{\sigma}{2}(1 - \sigma)(u_i - 2u_{i-1} + u_{i-2})^n \quad (21.1.28a)$$

or as a correction to the Lax-Wendroff scheme

$$\begin{aligned} u_i^{n+1} - u_i^n &= -\frac{\sigma}{2}(u_{i+1} - u_{i-1})^n + \frac{\sigma^2}{2}(u_{i+1} - 2u_i + u_{i-1})^n \\ &\quad + \frac{\sigma}{2}(1 - \sigma)(u_{i+1} - 3u_i + 3u_{i-1} - u_{i-2})^n \end{aligned} \quad (21.1.28b)$$

where the last term appears as a discretization of a dispersion term of the form $\sigma(1 - \sigma)\Delta x^3 u_{xxx} / 2$.

The amplification factor is given by

$$G - 1 = -2\sigma[1 - (1 - \sigma)\cos\phi] \sin^2 \frac{\phi}{2} - I\sigma \sin\phi \left[1 + 2(1 - \sigma)\sin^2 \frac{\phi}{2} \right] \quad (21.1.29)$$

and the modulus of G is given by

$$|G|^2 = 1 - \sigma(1 - \sigma)^2(2 - \sigma)(1 - \cos\phi)^2 \quad (21.1.30)$$

showing that the stability limit is $0 \leq \sigma \leq 2$ (see Figure 21.1.4).

It can be seen also that the phase error is a leading phase error for $\sigma < 1$ and is lagging for $\sigma > 1$, while the central second-order schemes all give lagging phase errors. This is illustrated in Figure 21.1.5, displaying the convection of a square wave at $\sigma = 0.5$ and at $\sigma = 1.5$.

Observe that the second-order upwind schemes do generate oscillations at discontinuous transitions. Hence, additional investigations are required to prevent these undesirable features.

In order to obtain a better time accuracy in the representation of wave motion, Fromm (1968) combined the above scheme and the Lax-Wendroff scheme,

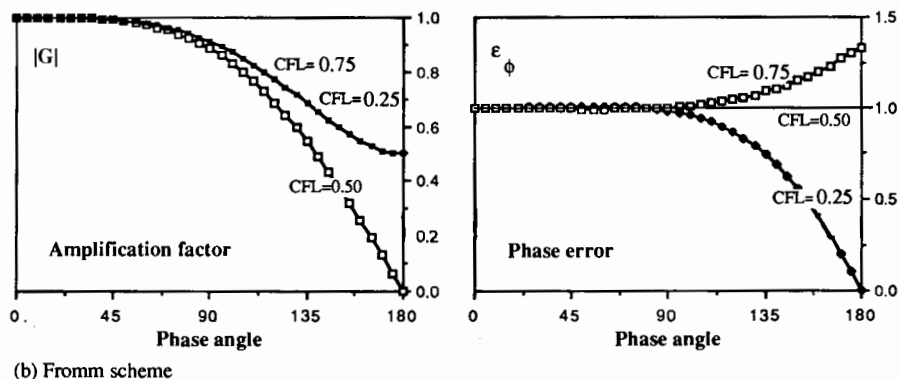
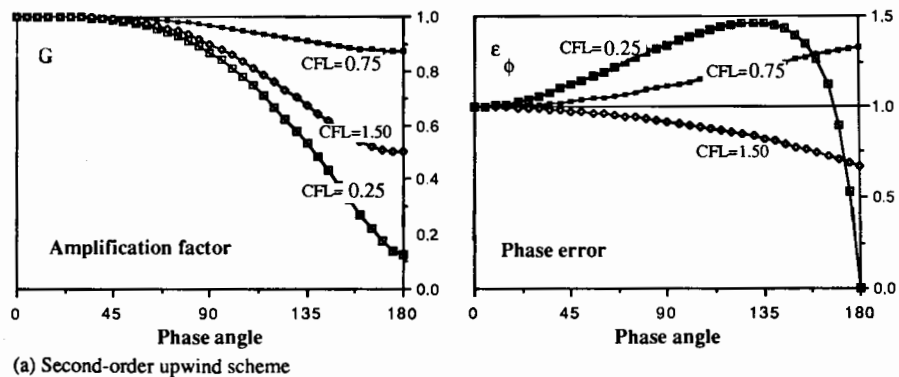
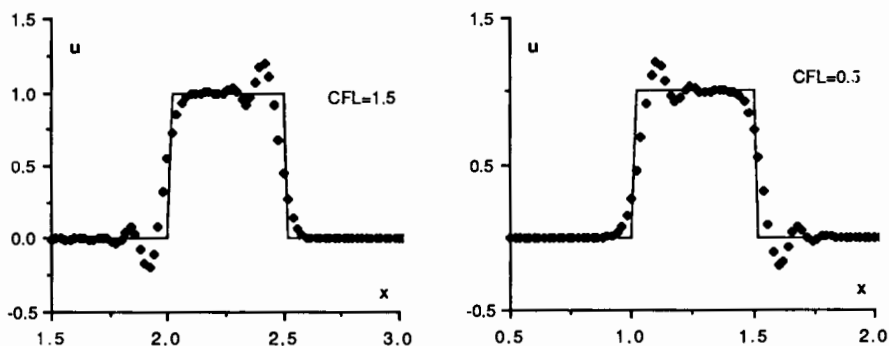


Figure 21.1.4 Amplitude and phase errors for the second-order upwind scheme of Warming and Beam and for Fromm's scheme



taking the arithmetic mean of both, with the aim of reducing the phase errors. This leads to Fromm's scheme

$$u_i^{n+1} - u_i^n = -\frac{\sigma}{4}(u_{i+1} + 3u_i - 5u_{i-1} + u_{i-2})^n + \frac{\sigma^2}{4}(u_{i+1} - u_i - u_{i-1} + u_{i-2})^n \quad (21.1.31)$$

It can also be written as a correction to the first-order upwind scheme

$$u_i^{n+1} - u_i^n = -\sigma(u_i - u_{i-1})^n - \frac{\sigma}{4}(1 - \sigma)(u_{i+1} - u_i - u_{i-1} + u_{i-2})^n \quad (21.1.32a)$$

or as a correction to the Lax-Wendroff scheme

$$u_i^{n+1} - u_i^n = -\frac{\sigma}{2}(u_{i+1} - u_{i-1})^n + \frac{\sigma^2}{2}(u_{i+1} - 2u_i + u_{i-1})^n + \frac{\sigma}{4}(1 - \sigma)(u_{i+1} - 3u_i + 3u_{i-1} - u_{i-2})^n \quad (21.1.32b)$$

where, compared to scheme (21.1.28b), the artificial dispersion represented by the last term has been reduced by half.

The amplification function is

$$G = 1 - 2\sigma \left[\sigma + (1 - \sigma) \sin^2 \frac{\phi}{2} \right] \sin^2 \frac{\phi}{2} - I\sigma \sin \phi \left[1 + (1 - \sigma) \sin^2 \frac{\phi}{2} \right] \quad (21.1.33)$$

and is also second-order accurate.

Fromm's scheme is stable for $0 \leq \sigma \leq 1$ and has indeed an improved phase behaviour (see Figure 21.1.4).

Note that the spatial discretization in scheme (21.1.32) is not fully one-sided, as (21.1.28), since it contains a contribution from point $(i + 1)$ for $\sigma > 0$. compare (21.1.28) and (21.1.32)

The extension to two dimensions is straightforward, following the derivations of Section 20.7. More details are given in Section 21.1.7 for finite difference formulations. A finite volume formulation of explicit second-order upwind schemes can be found in Borrel and Montagne (1985).

Another higher-order Godunov method has been developed by Woodward and Colella (1984a, 1984b) under the name of Piecewise Parabolic Method, while a second-order solution of the Riemann problem has been proposed by Ben-Artzi and Falcovitz (1984).

21.1.5 Numerical flux for higher-order upwind schemes— flux extrapolation

In the approach of the previous section the state variables are extrapolated to the cell interfaces. The fluxes at the cell boundaries are then calculated from these values. In this section the alternative option is taken whereby the fluxes in the cells are directly extrapolated to the boundaries, defining an interface

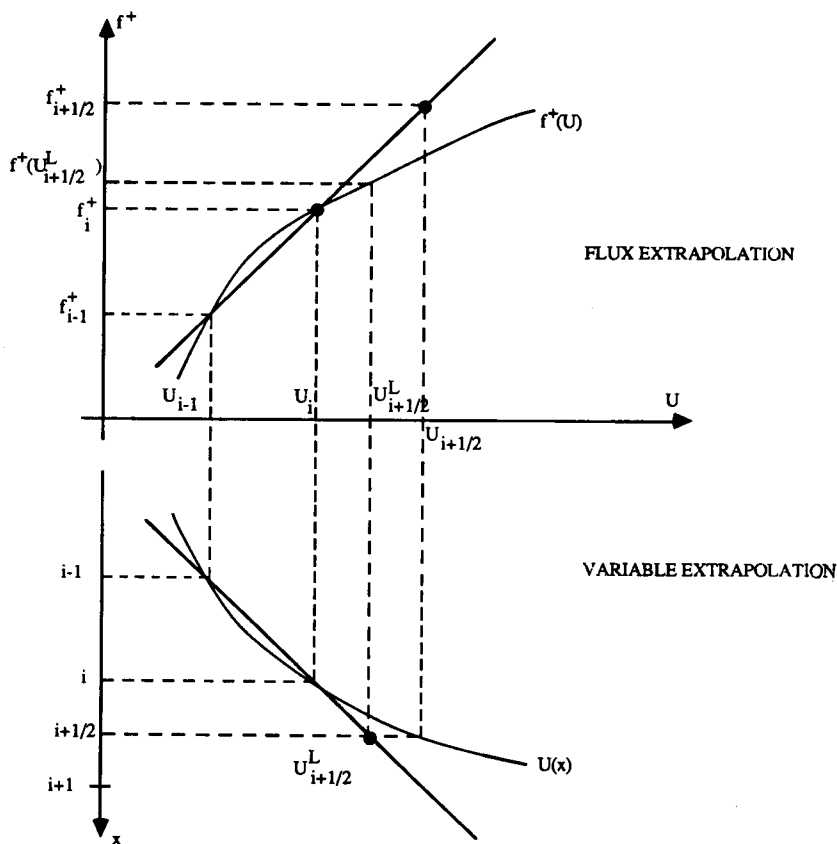


Figure 21.1.6 Comparison between flux extrapolation and variable extrapolation (MUSCL) methods for second-order upwind schemes

flux equal to the numerical flux of the scheme. Since the fluxes are non-linear functions of the basic dependent variables, this is not identical to an extrapolation of the variables to the cell faces followed by an evaluation of the fluxes (see Figure 21.1.6).

The extrapolation formulas for the fluxes are the same as the formulas applied to the variables. A general backward extrapolation of the positive flux is defined as

$$f_{i+1/2}^{+b} = f_i^+ + \frac{\epsilon}{4} [(1 - \kappa)(f_i^+ - f_{i-1}^+) + (1 + \kappa)(f_{i+1}^+ - f_i^+)] \quad (21.1.34a)$$

A forward extrapolation is applied to the negative part of the flux:

$$f_{i+1/2}^{-f} = f_{i+1}^- - \frac{\epsilon}{4} [(1 + \kappa)(f_{i+1}^- - f_i^-) + (1 - \kappa)(f_{i+2}^- - f_{i+1}^-)] \quad (21.1.34b)$$

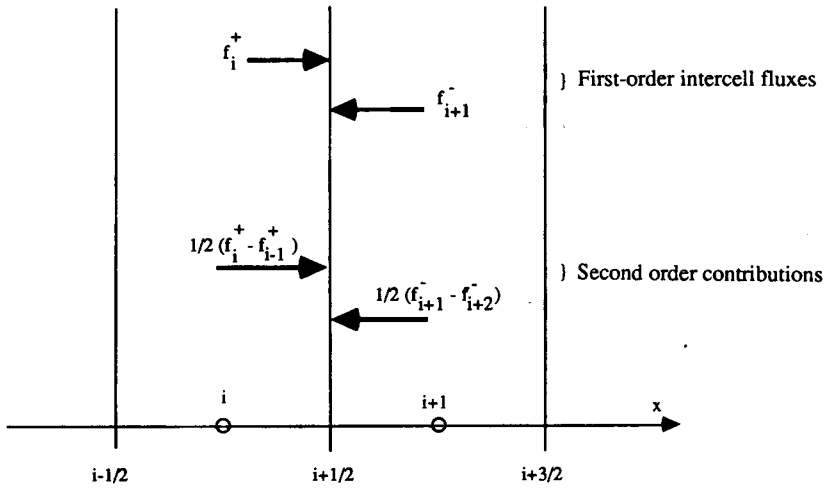


Figure 21.1.7 Second-order contributions to first-order upwind fluxes

The parameter κ defines the weight of the flux difference contributions and the second-order numerical flux is obtained from

$$f_{i+1/2}^{*(2)} = f_{i+1/2}^{+b} + f_{i+1/2}^{-f} \tag{21.1.34c}$$

For $\kappa = 1$ one obtains the symmetrical formula

$$f_{i+1/2}^{+b} + f_{i+1/2}^{-f} = \frac{f_i + f_{i+1}}{2}$$

leading to second-order space-centred schemes.

For $\kappa = -1$ one obtains the fully upwind scheme, in semi-discretized form (see Figure 21.1.7):

$$\frac{dU}{dt} = -\frac{1}{2\Delta x}(3f_i^+ - 4f_{i-1}^+ + f_{i-2}^+) - \frac{1}{2\Delta x}(-3f_i^- + 4f_{i+1}^- - f_{i+2}^-) \tag{21.1.35a}$$

which can also be written as

$$\frac{dU_i}{dt} = -\frac{1}{\Delta x} \delta^- [(1 + \frac{1}{2}\delta^-)f_i^+ + (1 - \frac{1}{2}\delta^+)f_{i+1}^-] \tag{21.1.35b}$$

The differences of positive and negative flux components can be defined in a general manner as differences between the first-order numerical flux and the physical flux:

$$f_{i+1/2}^* - f_i = \delta^+ f_i^- = \delta f_{i+1/2}^- \tag{21.1.36a}$$

$$f_{i-1/2}^* - f_i = -\delta^- f_i^+ = -\delta f_{i-1/2}^+ \tag{21.1.36b}$$

and represent the contributions to the flux differences arising from the negative, respectively positive, waves. This is also valid for all the Godunov-type methods, as can be seen from equations (20.5.52) and (20.5.87).

The numerical flux (21.1.34) can be generalized to any of the first-order Godunov-type schemes presented in Section 20.5, after introduction of the relations (21.1.36) defining the positive and negative flux differences. Equation (21.1.34) takes the following form, where f^* is the *first-order numerical flux*:

$$f_{i+1/2}^{*(2)} = f_{i+1/2}^* + \frac{1}{2} \left[\frac{1-\kappa}{2} (f_i - f_{i-1/2}^*) + \frac{1+\kappa}{2} (f_{i+1} - f_{i+1/2}^*) \right] \\ + \frac{1}{2} \left[\frac{1+\kappa}{2} (f_i - f_{i+1/2}^*) + \frac{1-\kappa}{2} (f_{i+1} - f_{i+3/2}^*) \right] \quad (21.1.37)$$

The numerical fluxes (21.1.37) are of second-order accuracy for all values of the parameter κ , as can be seen by rewriting the above equation as a correction to the central scheme:

$$f_{i+1/2}^{*(2)} = \frac{1}{2} (f_i + f_{i+1}) - \frac{1-\kappa}{4} (f_{i+3/2}^* - 2f_{i+1/2}^* + f_{i-1/2}^*) \quad (21.1.38)$$

Hence these schemes contain a second-order correction $-[(1-\kappa)/4]\Delta x^2 \partial^2 f^* / \partial x^2$ to the central scheme.

An explicit scheme, with second-order accuracy in time, is obtained by adding a first integration step over $\Delta t/2$ with the associated first order scheme:

$$\bar{U}_i = U_i^n - \frac{\Delta t}{2\Delta x} (f_{i+1/2}^* - f_{i-1/2}^*) \quad (21.1.39a)$$

followed by the definition of the second-order flux:

$$\overline{f_{i+1/2}^{*(2)}} = \overline{f_{i+1/2}^*} + \frac{1}{2} \left[\frac{1-\kappa}{2} (f_i - f_{i-1/2}^*) + \frac{1+\kappa}{2} (f_{i+1} - f_{i+1/2}^*) \right] \\ + \frac{1}{2} \left[\frac{1+\kappa}{2} (f_i - f_{i+1/2}^*) + \frac{1-\kappa}{2} (f_{i+1} - f_{i+3/2}^*) \right] \quad (21.1.39b)$$

with

$$\overline{f_{i+1/2}^*} = f^*(\bar{U}_i, \bar{U}_{i+1}) \quad (21.1.39c)$$

Finally, the solution at time level $n+1$ is obtained from

$$U_i^{n+1} - U_i^n = -\tau (\overline{f_{i+1/2}^{*(2)}} - \overline{f_{i-1/2}^{*(2)}}) \quad (21.1.39d)$$

A comparison between (21.1.15b) and (21.1.37) has been presented by Anderson *et al.* (1986a), in conjunction with an implicit time-integration and a flux vector splitting scheme, showing that the MUSCL approach has smoother properties with better defined shocks. Figure 21.1.8 shows a comparison of a

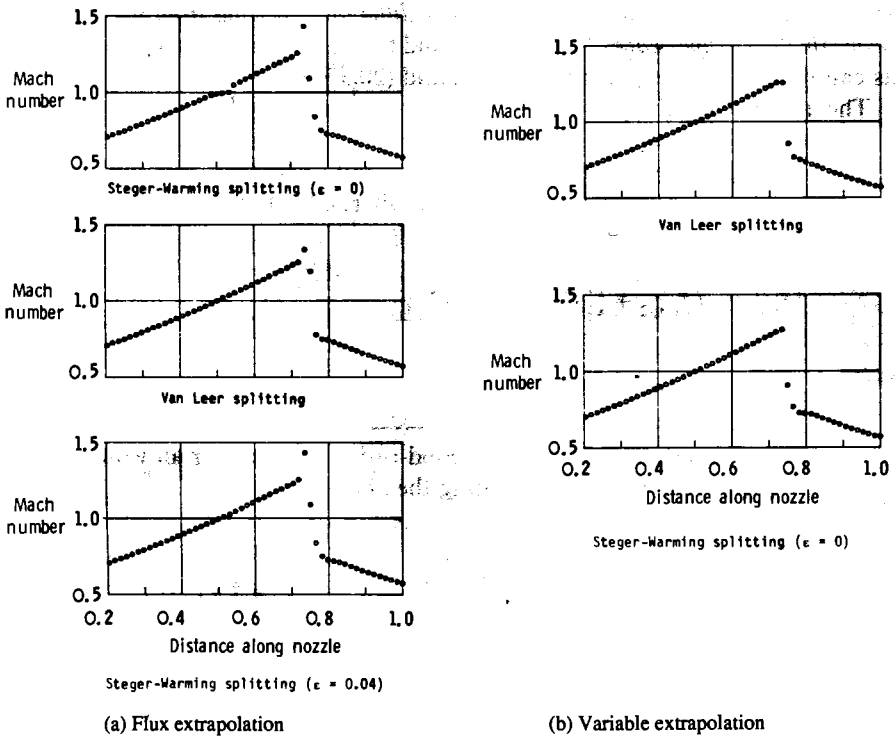


Figure 21.1.8 One-dimensional transonic nozzle flow calculated with second-order flux splitting schemes: (a) flux extrapolation and (b) variable extrapolation. (From Anderson *et al.*, 1986a)

stationary convergent-divergent transonic nozzle flow calculated with the extrapolated fluxes (Figure 21.1.8(a)), for both the Steger-Warming and Van Leer flux splittings. The same computation performed with the extrapolated variables is shown in Figure 21.1.8(b). Figure 21.1.8(a) reveals overshoots at the shock in both cases, as well as a small discontinuity at the sonic transition with the Steger-Warming flux splitting, as already noticed earlier.

The modification (20.3.22) removes the sonic point discontinuity, which does not appear with the Van Leer splitting in this case.

Comparing with Figure 21.1.8(b), it can be seen that the MUSCL approach also removes the sonic point discontinuity of the Steger-Warming splitting, and leads to a sharper shock definition without any overshoot.

The reason behind the better behaviour of the extrapolated variable approach can be connected to the fact that the fluxes are evaluated at the local cell values, while in the flux extrapolation approach, the splitting depends on the flow variables at various mesh points. Consequently better differentiability properties are also achieved in the former option; see also Mulder and Van Leer (1983). However, this does not ensure that numerical oscillations will not appear with higher-order upwind schemes, since they are present in the linear case, as seen from Figure 21.1.5. What is shown here is that the variable extrapolation method

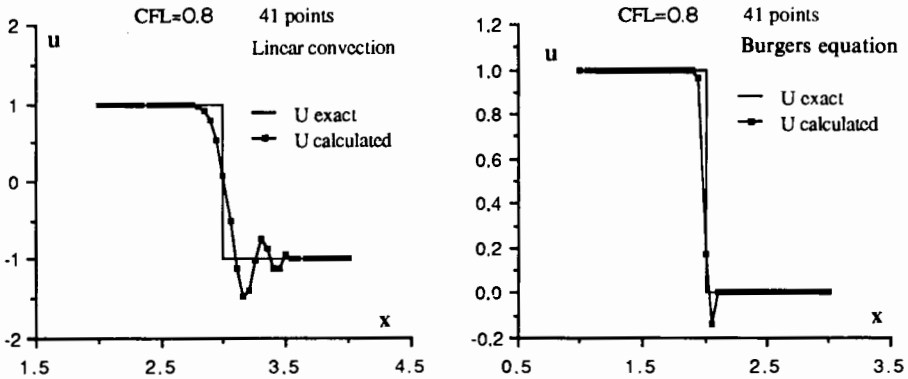


Figure 21.1.9 Comparison of a moving shock computation based on linear and Burgers equation with a second-order upwind scheme

makes better use of the inherent dissipation due to the specific non-linearities of the flow equations, as already discussed in Chapter 9 in Volume 1 in relation to Burgers equation.

Figure 21.1.9 shows a computation of the linear convection and Burgers equation for a moving shock, with scheme (21.1.39) and $\kappa = -1$. The linear oscillations are strongly reduced by the non-linearity of Burgers equation, but do not disappear completely.

This is confirmed by a computation of the same shock tube problem as displayed in Figure 20.3.3, but with the second-order upwind scheme (21.1.39), with $\kappa = -1$ and a Van Leer flux splitting. Figure 21.1.10 shows the behaviour of the different variables where overshoots at the contact and shock transitions can be noticed.

Flux splitting is therefore not sufficient to prevent the appearance of oscillations at shocks and other abrupt flow transitions with second-order schemes. In order to avoid this and achieve monotone and sharp shock transitions, it will be necessary to introduce non-linear corrections known as *limiters*.

Another, linearly equivalent, algorithm for second-order upwind schemes in space and time is obtained by performing an approximate Taylor expansion of the updating step (21.1.39c). For a flux splitting scheme we have

$$\begin{aligned} f^+(\bar{U}_i) &\simeq f_i^+ - \frac{\tau}{2} A_i^+ \cdot \delta^-(f_i^+ + f_{i+1}^-) + O(\tau^2) \\ &\simeq f_i^+ - \frac{\tau}{2} A_{i-1/2}^+ \cdot \delta f_{i-1/2}^+ + O(\tau^2) \end{aligned} \quad (21.1.40a)$$

$$\begin{aligned} f^-(\bar{U}_i) &\simeq f_i^- - \frac{\tau}{2} A_i^- \cdot \delta^-(f_i^+ + f_{i+1}^-) + O(\tau^2) \\ &\simeq f_i^- - \frac{\tau}{2} A_{i+1/2}^- \cdot \delta f_{i+1/2}^- + O(\tau^2) \end{aligned} \quad (21.1.40b)$$

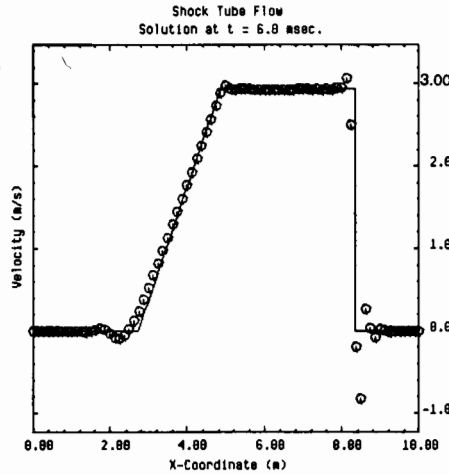
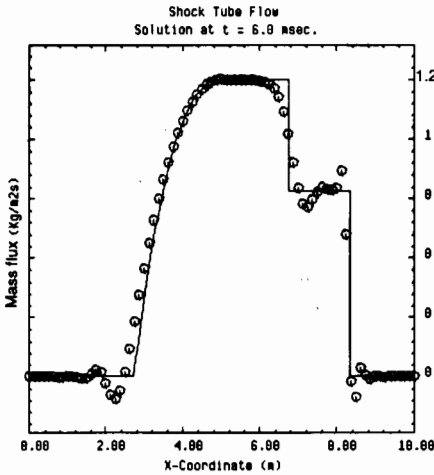
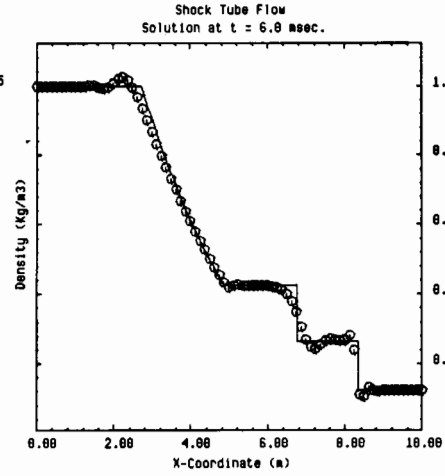
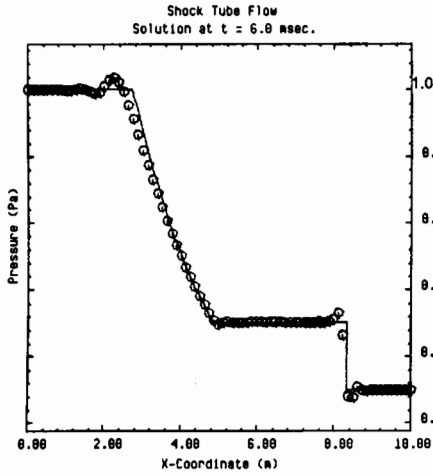
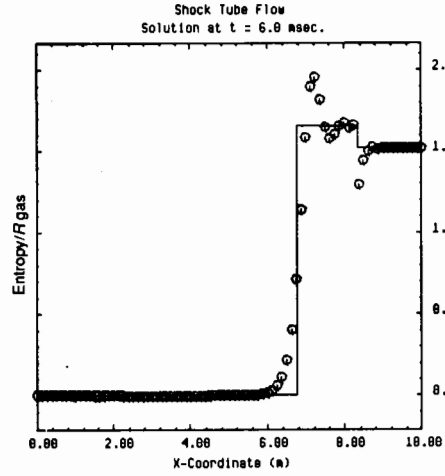
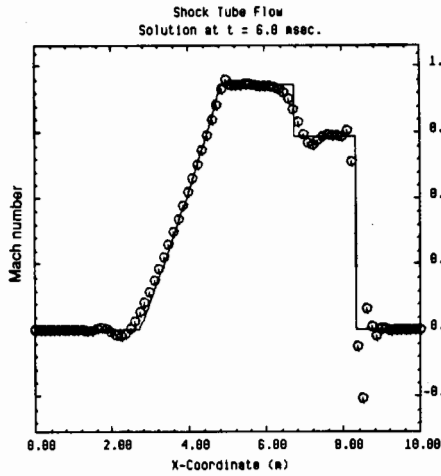


Figure 21.1.10 Shock tube problem calculated with a second-order Van Leer flux splitting scheme

where the orthogonality property of the Jacobian matrices $A^+ \cdot A^- = A^- \cdot A^+ = 0$ has been applied. A second-order space- and time-accurate numerical flux is hereby defined as

$$\overline{f_{i+1/2}^{*(2)}} = f_i^+ + f_{i+1}^- + \frac{1}{2}(1 - \tau A_{i-1/2}^+) \delta f_{i-1/2}^+ - \frac{1}{2}(1 + \tau A_{i+3/2}^-) \delta f_{i+3/2}^- \quad (21.1.41)$$

and generalized to any first-order upwind scheme as follows:

$$\overline{f_{i+1/2}^{*(2)}} = f_{i+1/2}^* + \frac{1}{2}(1 - \tau A_{i-1/2}^+) (f_i - f_{i-1/2}^*) - \frac{1}{2}(1 + \tau A_{i+3/2}^-) (f_{i+3/2}^* - f_{i+1}) \quad (21.1.42)$$

where the Jacobians are appropriately defined.

The scheme (21.1.41) can also be derived from a Lax–Wendroff approach coupled to a flux splitting and one-sided differencing (see Problem 21.15).

A third alternative for the definition of upwind schemes with second-order accuracy in time and space has been applied by Steger and Warming (1981). The predictor step defines an intermediate state solution of the first-order scheme after a propagation over a full time step Δt , instead of the half time step considered above:

$$\bar{U}_i = U_i^n - \tau (f_{i+1/2}^* - f_{i-1/2}^*)^n \quad (21.1.43a)$$

With

$$\overline{f_{i+1/2}^*} = f^*(\bar{U}_i, \bar{U}_{i+1}) \quad (21.1.43b)$$

the solution at time level $n + 1$ results from the corrector step

$$U_i^{n+1} = U_i^n - \tau (\overline{f_{i+1/2}^{*(2)}} - \overline{f_{i-1/2}^{*(2)}}) \quad (21.1.43c)$$

with the following numerical flux, obtained from $\overline{f_{i+1/2}^{*(2)}}$ by an updating of half of the first-order numerical flux in order to ensure second-order accuracy in time; refer to equation (11.2.10) (Chapter 11 in Volume 1). Considering a fully upwind scheme, with $\kappa = -1$,

$$\overline{f_{i+1/2}^{*(2)}} = \frac{1}{2}(f_{i+1/2}^* + \overline{f_{i+1/2}^*}) + \frac{1}{2} \delta^- f_i^+ - \frac{1}{2} \delta^+ f_{i+1}^- \quad (21.1.44a)$$

or

$$\overline{f_{i+1/2}^{*(2)}} = \frac{1}{2}(f_{i+1/2}^* + \overline{f_{i+1/2}^*}) + \frac{1}{2}(f_i - f_{i-1/2}^*) - \frac{1}{2}(f_{i+3/2}^* - f_{i+1}) \quad (21.1.44b)$$

This can obviously be translated into the variable extrapolation method by applying the definition (21.1.44) to the U variables and extending to other values of κ .

Another approach to second-order upwind schemes has been developed by Roe, (Roe and Baines, 1982; Roe, 1985) as a generalization of the interpretation of the Lax–Wendroff scheme as a distribution formula of first-order flux variations. The basic concept is described in Section 17.2 and we refer the reader to Roe's original work for more details.

Example 21.1.1 Roe second-order scheme for a scalar conservation equation

The first-order Roe scheme for a scalar conservation law is defined by

equation (20.5.89):

$$f_{i+1/2}^{*(R)} = \frac{1}{2}(f_i + f_{i+1}) - \frac{1}{2}|a|_{i+1/2}(u_{i+1} - u_i) \quad (\text{E21.1.1})$$

with

$$a_{i+1/2} = \frac{f_{i+1} - f_i}{u_{i+1} - u_i} \quad (\text{E21.1.2})$$

With

$$f_i - f_{i-1/2}^{*(R)} = \frac{1}{2}(a + |a|)_{i-1/2}(u_i - u_{i-1}) \equiv a_{i-1/2}^+(u_i - u_{i-1}) \quad (\text{E21.1.3})$$

$$f_{i+1} - f_{i+3/2}^{*(R)} = -\frac{1}{2}(a - |a|)_{i+3/2}(u_{i+2} - u_{i+1}) \equiv -a_{i+3/2}^-(u_{i+2} - u_{i+1}) \quad (\text{E21.1.4})$$

the second-order numerical flux becomes with $\kappa = -1$

$$\begin{aligned} f_{i+1/2}^{*(2)} &= f_{i+1/2}^{*(R)} + \frac{1}{2}a_{i-1/2}^+(u_i - u_{i-1}) - \frac{1}{2}a_{i+3/2}^-(u_{i+2} - u_{i+1}) \\ &= \frac{1}{2}(f_i + f_{i+1}) - \frac{1}{2}|a|_{i+1/2}(u_{i+1} - u_i) + \frac{1}{2}a_{i-1/2}^+(u_i - u_{i-1}) \\ &\quad - \frac{1}{2}a_{i+3/2}^-(u_{i+2} - u_{i+1}) \end{aligned} \quad (\text{E21.1.5})$$

Second-order accuracy in time is obtained from equation (21.1.39) as

$$\overline{f_{i+1/2}^{*(2)}} = \overline{f_{i+1/2}^{*(R)}} + \frac{1}{2}a_{i-1/2}^+(u_i - u_{i-1}) - \frac{1}{2}a_{i+3/2}^-(u_{i+2} - u_{i+1}) \quad (\text{E21.1.6})$$

An alternative to the second-order accuracy in time is provided by equation (21.1.41), which becomes here

$$\begin{aligned} \overline{f_{i+1/2}^{*(2)}} &= f_{i+1/2}^{*(R)} + \frac{1}{2}(1 - \tau a_{i-1/2}^+)a_{i-1/2}^+(u_i - u_{i-1}) \\ &\quad - \frac{1}{2}(1 + \tau a_{i+3/2}^-)a_{i+3/2}^-(u_{i+2} - u_{i+1}) \end{aligned} \quad (\text{E21.1.7})$$

21.1.6 Implicit second-order upwind schemes

Implicit second-order upwind schemes can be derived by application of the linear multi-step methods, discussed in Chapter 18, to the general numerical fluxes (21.1.15) or (21.1.34).

Considering the form (21.1.35) for the sake of simplicity, a second-order space-accurate implicit scheme with time-linearized implicit operators is

$$[(1 + \xi) + \tau\theta(\delta^b f_{U_i}^+ + \delta^f f_{U_i}^-)]^n \Delta U_i = -\tau(\delta^b f_i^+ + \delta^f f_i^-)^n + \xi \Delta U^{n-1} \quad (\text{21.1.45})$$

where the second-order, three-point, one-sided difference operators

$$\delta^b f_i^+ \equiv \frac{1}{2}(3f_i^+ - 4f_{i-1}^+ + f_{i-2}^+) = (1 + \frac{1}{2}\delta^-)\delta^- f_i^+ \quad (\text{21.1.46a})$$

$$\delta^f f_i^- \equiv \frac{1}{2}(-3f_i^- + 4f_{i+1}^- - f_{i+2}^-) = (1 - \frac{1}{2}\delta^+)\delta^- f_{i+1}^- \quad (\text{21.1.46b})$$

are introduced. The subscript U indicates a partial derivative and the quantities f_U^+ and f_U^- are the Jacobians of the split fluxes. They reduce to the split Jacobians A^+ and A^- in the linear case.

In this second-order scheme, the left-hand side implicit operator reduces to

the resolution of a block pentadiagonal system. Although efficient algorithms can be applied to the solution of pentadiagonal systems similar to the Thomas algorithm for tridiagonal systems (see, for instance, Marchuk, 1975), it still requires roughly twice as many operations to solve. This can also be seen if an approximate factorization of the implicit operator is performed into two block tridiagonal factors, leading for instance to the scheme, with $\xi = 0$.

$$(1 + \tau\theta\delta^b f_{\bar{u}_i}^+)(1 + \tau\theta\delta^f f_{\bar{u}_i}^-)\Delta U_i = -\tau(\delta^b f_i^+ + \delta^f f_i^-)^n \quad (21.1.47)$$

which is solved in two steps:

$$(1 + \tau\theta\delta^b f_{\bar{u}_i}^+)\overline{\Delta U}_i = -\tau(\delta^b f_i^+ + \delta^f f_i^-)^n \quad (21.1.48a)$$

followed by

$$(1 + \tau\theta\delta^f f_{\bar{u}_i}^-)\Delta U_i = \overline{\Delta U}_i \quad (21.1.48b)$$

Other factorizations are obviously possible, but since the implicit operator does not condition the space accuracy of the scheme which, as seen in Chapter 18, is uniquely determined by the explicit right-hand side residual, one could also keep the first-order Jacobian differences of equation (20.6.8), with a second-order left-hand side.

Hence, a second-order space-accurate implicit scheme could be applied as

$$[(1 + \xi) + \tau\theta(\delta^- f_{\bar{u}_i}^+ + \delta^+ f_{\bar{u}_i}^-)]^n \Delta U_i = -\tau(\delta^b f_i^+ + \delta^f f_i^-)^n + \xi \Delta U_i^{n-1} \quad (21.1.49)$$

where the left-hand side implicit operator now reduces to a block tridiagonal system.

Steger and Warming (1981) and Buning and Steger (1982) actually apply a further factorization of the implicit operator into two bidiagonal factors of the form

$$\left(1 + \tau \frac{\theta}{1 + \xi} \delta^- f_{\bar{u}_i}^+\right) \left(1 + \tau \frac{\theta}{1 + \xi} \delta^+ f_{\bar{u}_i}^-\right) \Delta U_i = -\frac{\tau(\delta^b f_i^+ + \delta^f f_i^-)^n - \xi \Delta U_i^{n-1}}{1 + \xi} \quad (21.1.50)$$

This can now be solved by two successive sweeps through the mesh, each sweep corresponding to one of the two following steps:

$$\left(1 + \tau \frac{\theta}{1 + \xi} \delta^- f_{\bar{u}_i}^+\right) \overline{\Delta U}_i = -\frac{\tau(\delta^b f_i^+ + \delta^f f_i^-)^n - \xi \Delta U_i^{n-1}}{1 + \xi} \quad (21.1.51a)$$

$$\left(1 + \tau \frac{\theta}{1 + \xi} \delta^+ f_{\bar{u}_i}^-\right) \Delta U_i = \overline{\Delta U}_i \quad (21.1.51b)$$

Writing out the implicit operators explicitly leads to

$$(1 + \xi + \tau\theta f_{\bar{u}_i}^+)\overline{\Delta U}_i - \tau\theta f_{\bar{u}_{i-1}}^+ \overline{\Delta U}_{i-1} = -\tau(\delta^b f_i^+ + \delta^f f_i^-)^n + \xi \Delta U_i^{n-1} \quad (21.1.52a)$$

$$\left(1 - \tau \frac{\theta}{1 + \xi} f_{\bar{u}_i}^-\right) \Delta U_i + \tau \frac{\theta}{1 + \xi} f_{\bar{u}_{i+1}}^- \Delta U_{i+1} = \overline{\Delta U}_i \quad (21.1.52b)$$

The first step is lower bidiagonal and is solved by a sweep through the mesh from left to right, that is from $i = 1$ to $i = M$, while the second step is an upper bidiagonal matrix which is solved by sweeping backwards from $i = M$ to $i = 1$.

Other bidiagonal factorizations have been analysed by Lombard *et al.* (1983) and the reader is referred to these references and to Casier *et al.* (1983) for a discussion of bidiagonal schemes applied to the Euler equations.

The non-factored schemes, with $\xi = 0$ in order to restrict to two-level schemes, are generalized to any upwind scheme by

$$[1 + \tau\theta(\delta^- f_{ui}^+ + \delta^+ f_{ui}^-)]\Delta U_i = -\tau\delta f_{i+1/2}^{*(2)} \quad (21.1.53)$$

In this equation the various options for the upwind definition of the numerical fluxes, as discussed above, can be introduced, although the MUSCL approach should be recommended. The implicit operators are the Jacobians of the positive and negative parts of the corresponding first-order numerical fluxes.

The interested reader is referred to Mulder and Van Leer (1983) for an application with Roe's approximate Riemann solver and to Rai and Chakravarthy (1984) for an approach based on Osher's scheme. However, other options are open whereby the left-hand side is derived from flux splittings or approximate Riemann solvers different from those selected for the right-hand side; see, for instance, Liou and Van Leer (1988).

21.1.7 Implicit second-order upwind schemes in two dimensions

Referring to Section 20.7, two-dimensional implicit upwind schemes are best defined by a straightforward extension of equation (21.1.53), with $\Delta x = \Delta y$:

$$[1 + \tau\theta(\delta_x^- f_{u,ij}^+ + \delta_x^+ f_{u,ij}^- + \delta_y^- g_{u,ij}^+ + \delta_y^+ g_{u,ij}^-)]\Delta U_{ij}^n = -\tau(\delta_x f_{i+1/2,j}^{*(2)} + \delta_y g_{i,j+1/2}^{*(2)}) \quad (21.1.54)$$

see, for instance, Deese (1983, 1985) and Whitfield and Janus (1984).

Considering Figure 21.1.11, the fluxes at the mid-point cell faces can be written as in the one-dimensional case, by an extrapolation of the split fluxes on the upwind side of the considered cell face.

Alternatively, the split fluxes can be calculated at the cell faces after an upwind extrapolation of the variables.

We consider here the fully one-sided case $\kappa = -1$ and leave the extension to arbitrary κ values as an exercise to the reader. For instance, in the first case one would define ($\varepsilon = 1$ for a second-order scheme)

$$f_{i+1/2,j}^{+b} = f_{ij}^+ + \frac{\varepsilon}{2}(f_{ij}^+ - f_{i-1,j}^+) \quad (21.1.55a)$$

and

$$f_{i+1/2,j}^{-f} = f_{i+1,j}^- - \frac{\varepsilon}{2}(f_{i+2,j}^- - f_{i+1,j}^-) \quad (21.1.55b)$$

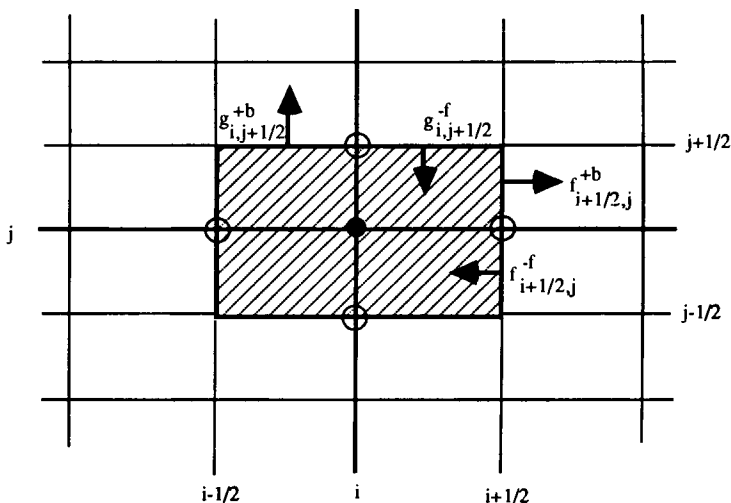


Figure 21.1.11 Upwind discretizations in two dimensions

with

$$f_{i+1/2,j}^{*(2)} = f_{i+1/2,j}^{+b} + f_{i+1/2,j}^{-f} \quad (21.1.55c)$$

The other flux components are defined similarly by

$$g_{i,j+1/2}^{+b} = g_{ij}^{+} + \frac{\varepsilon}{2}(g_{ij}^{+} - g_{i,j-1}^{+}) \quad (21.1.56a)$$

and

$$g_{i,j+1/2}^{-f} = g_{i,j+1}^{-} - \frac{\varepsilon}{2}(g_{i,j+2}^{-} - g_{i,j+1}^{-}) \quad (21.1.56b)$$

with

$$g_{i,j+1/2}^{*(2)} = g_{i,j+1/2}^{+b} + g_{i,j+1/2}^{-f} \quad (21.1.56c)$$

In the variable-extrapolation method, the relations (21.1.55) and (21.1.56) are applied to the variables $U_{i\pm 1/2,j}$ and $U_{i,j\pm 1/2}$, defining, for instance, left and right fully one-sided components:

$$U_{i+1/2,j}^L = U_{ij} + \frac{\varepsilon}{2}(U_{ij} - U_{i-1,j}) \quad (21.1.57a)$$

and

$$U_{i+1/2,j}^R = U_{i+1,j} - \frac{\varepsilon}{2}(U_{i+2,j} - U_{i+1,j}) \quad (21.1.57b)$$

The other flux components are defined similarly by

$$U_{i,j+1/2}^L = U_{ij} + \frac{\varepsilon}{2}(U_{ij} - U_{i,j-1}) \quad (21.1.58a)$$

and

$$U_{i,j+1/2}^R = U_{i,j+1} - \frac{\epsilon}{2}(U_{i,j+2} - U_{i,j+1}) \quad (21.1.58b)$$

The cell face fluxes are obtained in this case by the extension of equation (21.1.15):

$$f_{i+1/2,j}^{*(2)} = f^+(U_{i+1/2,j}^L) + f^-(U_{i+1/2,j}^R) \quad (21.1.59a)$$

$$g_{i,j+1/2}^{*(2)} = g^+(U_{i,j+1/2}^L) + g^-(U_{i,j+1/2}^R) \quad (21.1.59b)$$

The left-hand side implicit operator of the two-dimensional scheme (21.1.54) is a block pentadiagonal matrix. In order to reduce the computational cost an ADI factorization as discussed in Section 11.2 in Volume 1 can be applied (Steger and Warming, 1981; Anderson *et al.*, 1986a).

However, it can be observed that the schemes of the form (21.1.54) have an implicit operator which is diagonally dominant as a consequence of the flux splitting, as seen in Section 20.7.

As a consequence one might apply a variety of iterative relaxation methods for the solution of the algebraic system (Chakravarthy, 1984; Napolitano and Dadone, 1985) without resorting to a factorization which limits the extension to higher Courant numbers as a result of the factorization error proportional to Δt^2 (or Δt^3 in three-dimensional problems).

Various iterative methods such as Jacobi, point and line Gauss-Seidel eventually in Zebra formulations, have been tested by Thomas *et al.* (1985) for two- and three-dimensional flow calculations with the upwind flux splitting methods. In addition, as soon as the implicit operators are considered as an algebraic system, to be solved by iterative techniques such as presented in Chapter 12 in Volume 1, convergence accelerations via multi-grid methods have to be considered; see, for instance, Mulder (1985), Anderson *et al.* (1986b) and Hemker and Spekrijse (1986) for a representative analysis and presentation of results.

21.1.8 Summary

The following expressions for a second-order space-accurate upwind numerical flux can be applied, considering a first-order upwind numerical flux f^* .

1a. Based on variable extrapolation—MUSCL approach

$$U_{i+1/2}^L = U_i + \frac{1}{4}[(1 - \kappa)(U_i - U_{i-1}) + (1 + \kappa)(U_{i+1} - U_i)] \quad (21.1.60a)$$

$$U_{i+1/2}^R = U_{i+1} - \frac{1}{4}[(1 + \kappa)(U_{i+1} - U_i) + (1 - \kappa)(U_{i+2} - U_{i+1})] \quad (21.1.60b)$$

$$f_{i+1/2}^{*(2)} = f^*(U_{i+1/2}^L, U_{i+1/2}^R) \quad (21.1.60c)$$

1b. Based on flux extrapolation

$$f_{i+1/2}^{+b} = f_i^+ + \frac{1}{4}[(1 - \kappa)(f_i - f_{i-1/2}^*) + (1 + \kappa)(f_{i+1} - f_{i+1/2}^*)] \quad (21.1.61a)$$

$$f_{i+1/2}^{-f} = f_{i+1}^- - \frac{1}{4}[(1 + \kappa)(f_{i+1/2}^* - f_i) + (1 - \kappa)(f_{i+3/2}^* - f_{i+1})] \quad (21.1.61b)$$

$$f_{i+1/2}^{*(2)} = f_{i+1/2}^{+b} + f_{i+1/2}^{-f} \quad (21.1.61c)$$

Second-order upwind schemes in space and time are obtained after introduction of an additional predictor step, for instance over a half time step $\Delta t/2$:

$$\bar{U}_i = U_i^n - \frac{\Delta t}{2\Delta x}(f_{i+1/2}^* - f_{i-1/2}^*) \quad (21.1.62)$$

2a. Based on variable extrapolation—MUSCL approach

$$U_{i+1/2}^{L*} = \bar{U}_i + \frac{1}{4}[(1 - \kappa)(U_i - U_{i-1}) + (1 + \kappa)(U_{i+1} - U_i)] \quad (21.1.63a)$$

$$U_{i+1/2}^{R*} = \bar{U}_{i+1} - \frac{1}{4}[(1 + \kappa)(U_{i+1} - U_i) + (1 - \kappa)(U_{i+2} - U_{i+1})] \quad (21.1.63b)$$

$$\bar{f}_{i+1/2}^{*(2)} = f^*(U_{i+1/2}^{L*}, U_{i+1/2}^{R*}) \quad (21.1.63c)$$

2b. Based on flux extrapolation

Defining

$$\bar{f}_{i+1/2}^* = f^*(\bar{U}_i, \bar{U}_{i+1}) \quad (21.1.64)$$

the numerical flux is obtained as

$$\begin{aligned} f_{i+1/2}^{*(2)} = \bar{f}_{i+1/2}^* + \frac{1}{2} \left[\frac{1 - \kappa}{2}(f_i - f_{i-1/2}^*) + \frac{1 + \kappa}{2}(f_{i+1} - f_{i+1/2}^*) \right] \\ + \frac{1}{2} \left[\frac{1 + \kappa}{2}(f_i - f_{i+1/2}^*) + \frac{1 - \kappa}{2}(f_{i+1} - f_{i+3/2}^*) \right] \end{aligned} \quad (21.1.65)$$

A third formulation is defined for $\kappa = -1$:

$$f_{i+1/2}^{*(2)} = f_{i+1/2}^* + \frac{1}{2}(1 - \tau A_{i-1/2}^+)(f_i - f_{i-1/2}^*) - \frac{1}{2}(1 + \tau A_{i+3/2}^-)(f_{i+3/2}^* - f_{i+1}) \quad (21.1.66)$$

All these options are linearly identical.

21.2 THE DEFINITION OF HIGH-RESOLUTION SCHEMES

The observations made in the previous sections that an upwind algorithm by itself is not sufficient to avoid the appearance of oscillations around discontinuities with second-order schemes made it clear that a more fundamental approach is required in order to understand the mechanism of the generation of over- and undershoots in the numerical solutions.

The physical solutions to the Euler and Navier–Stokes equations, however, do not seem to allow the appearance of new extrema in the evolution of the flow variables. This can be proven at least for one-dimensional flows. Therefore the numerical generation of oscillations is due to the numerical treatment of the second-order approximation, since the first-order schemes are free of these undesirable over- and undershoots.

Considering the approach to second-order accuracy developed in Section 21.1 in the line of Godunov's method, it was noted that the passage from first- to second-order accuracy in space was fully contained in the representation of the state variables as piecewise linear within each cell, instead of piecewise constant. Next to the cell average, the additional variable is the slope of the linear variation, and therefore oscillations will be created when the slope in a cell becomes larger than the difference of adjacent mean values. As seen from Figure 21.2.1, if the slope in cell i is too large, the solution to the linear convection equation at time step $n + 1$, obtained after a translation $a \Delta t$ of the distribution at time $n \Delta t$, will lead to a cell-averaged value $u_i^{n+1} < u_{i-1}^{n+1}$, while at level n one had $u_i^n > u_{i-1}^n$ and hence an undershoot in the solution at time $n + 1$ will appear.

Hence, in order to define a scheme without overshoots around discontinuities, one should avoid excessive large gradients. Therefore the previous schemes will be controlled at each time step and within each cell, in such a way as to keep the gradients within the proper bounds.

It should be remembered at this point that the approach towards high-resolution upwind schemes consists in *preventing* the generation of oscillations by acting on their production mechanism, as opposed to central schemes where oscillations are allowed to appear and are subsequently damped by artificial dissipation terms that act as a low bypass filter.

In a landmark paper, Godunov (1959) showed that all monotone linear schemes can be at most of first-order accuracy. Hence, any linear procedure by

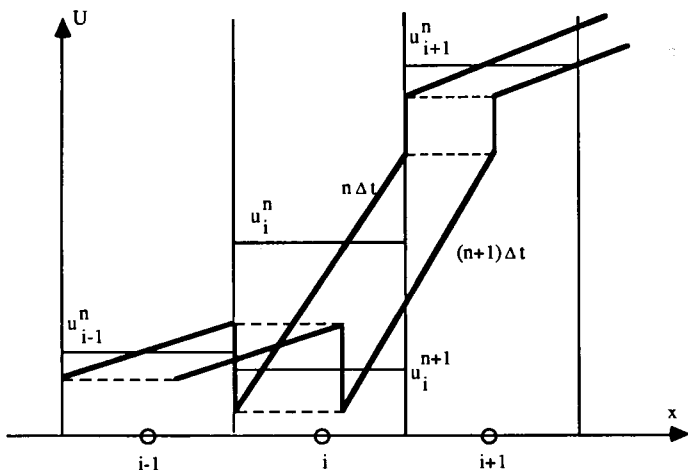


Figure 21.2.1 Generation of oscillations in numerical solutions

which the gradients would be limited in second-order schemes will not fulfil the requested goal, and the only way around this difficulty is to introduce *non-linear* correction factors, called *limiters*. They have been introduced initially by Van Leer (1973) and independently by Boris and Book (1973).

Since the role of these limiters is to force the numerics to follow closely the variation bounded properties of the Euler solutions, it is essential to first define and express mathematically the 'non-oscillatory' properties of the Euler solutions. These properties will be expressed by

- (1) The entropy condition,
- (2) Monotonicity,
- (3) Total variation diminishing (TVD) schemes.

The first condition is not connected to the non-oscillatory behaviour, but to the fact that certain first-order upwind schemes, such as Roe's scheme, admit expansion shock solutions, as seen in Section 20.5. These solutions are not acceptable physically, since they are associated with a decrease in entropy which is not allowed by the second principle of thermodynamics. They have therefore to be rejected and the mathematical formulation of this condition, known as the entropy condition, has to be introduced in the formalization of the properties to be satisfied by a numerical scheme.

The formal theory of approximate solutions to non-linear conservation laws has been developed essentially for scalar equations or for linear systems in one dimension, for which most of the properties to be discussed in this section have been proven. Very little has, up to now, been proven for multi-dimensional problems or for non-linear systems.

Basic contributions to these theoretical developments can be found in Godunov (1959), Lax (1973), Van Leer's series of papers (1973 to 1979) concerning second-order Godunov schemes and monotonicity, Harten *et al.* (1976), Majda and Osher (1979), Crandall and Majda (1980), Harten and Lax (1981), Harten (1983, 1984) who introduced the concept of total variation diminishing (TVD) schemes, Osher (1984), Osher and Chakravarthy (1984) and several others to be found as references in these papers.

21.2.1 The generalized entropy condition for inviscid equations

The system of inviscid equations (Euler equations, potential flow models) admits non-differentiable, that is discontinuous, solutions, which from a mathematical point of view cannot satisfy the differential equations, but are valid solutions of the integral form of the conservation laws or, more generally, solutions of the so-called weak form of the equations. These solutions are to be considered in the distributional sense, with the discontinuity jump satisfying the Rankine-Hugoniot relations.

However, several discontinuous solutions can exist, not all of them having a physical meaning. A criterion has therefore to be defined allowing the correct solution to be selected.

Based on physical arguments, namely the second principle of thermodynamics (which states that in any physical realizable adiabatic evolution the entropy can only increase during the transformation of the system), only compression shocks are retained and expansion shocks, which correspond to a negative entropy variation, are excluded, since they cannot occur in real flows. Since inviscid flow models do not have any built-in dissipative mechanism, such as viscosity effects, an additional condition has to be added to the system of equations in order to select the correct discontinuity or shock and reject the non-physical ones. This condition is therefore called the *entropy condition*.

An excellent, mathematically rigorous and far-reaching analysis of the entropy condition for inviscid flows has been developed by Lax (1973). His analysis is based on the properties of the one-dimensional hyperbolic conservation law

$$\frac{\partial u}{\partial t} + \frac{\partial f}{\partial x} = 0 \quad (21.2.1)$$

but its extension to multi-dimensional forms is straightforward. We will summarize in the following the main results of Lax's analysis.

In analogy with the properties of physical compression shocks, the condition to be satisfied by the discontinuous solutions of the hyperbolic conservation law is that the wave speed $a(u) = df/du$ is such that

$$a_R = a(U_R) < C < a(u_L) = a_L \quad (21.2.2)$$

where C is the speed of propagation of the discontinuity (which satisfies the Rankin–Hugoniot relations) and u_R and u_L are values of u on the right and left sides of the discontinuity. This form of the *entropy condition* indicates that the characteristics on either side of the discontinuity surface Σ will ultimately intersect the discontinuity.

This is illustrated in Figure 21.2.2 and shows that for such solutions every

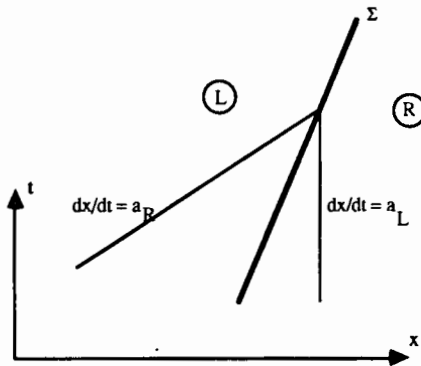


Figure 21.2.2 Intersection of a compression shock discontinuity surface with left and right characteristics

point on Σ can be connected by a backward-going characteristic to a point on the initial data line at $t = 0$.

A discontinuity satisfying the Rankine–Hugoniot relations and the entropy condition is therefore a compression shock.

For convex flux functions $f(u)$, that is such that

$$\frac{da(u)}{du} = f_{uu} > 0 \quad (21.2.3)$$

it is shown that the entropy condition leads to a unique generalized solution for any given set of initial data. Actually, the convexity condition can be relaxed by a *generalized entropy condition* for any flux function f if it is realized that $a(u)$ is the tangent to the flux function $f(u)$.

If $u_R < u_L$, one should have

$$f(\alpha u_R + (1 - \alpha)u_L) \leq \alpha f(u_R) + (1 - \alpha)f(u_L) \quad (21.2.4a)$$

and if $u_L < u_R$,

$$f(\alpha u_R + (1 - \alpha)u_L) \geq \alpha f(u_R) + (1 - \alpha)f(u_L) \quad (21.2.4b)$$

These conditions are to be interpreted geometrically as requiring that for $u_R < u_L$ the curve $f(u)$ lies below the chord (Figure 21.2.3) and for $u_R > u_L$ the curve $f(u)$ lies above the chord.

Note that the fluxes f occurring in the Euler equations have the convexity property. The slope of the chord RL in Figure 21.2.3 represents the speed of propagation of the discontinuity joining the states u_R and u_L , since in accordance with the Rankine–Hugoniot relation (16.1.19) applied to the scalar equation (21.2.1), one has

$$C = \frac{f(u_R) - f(u_L)}{u_R - u_L} \quad (21.2.5)$$

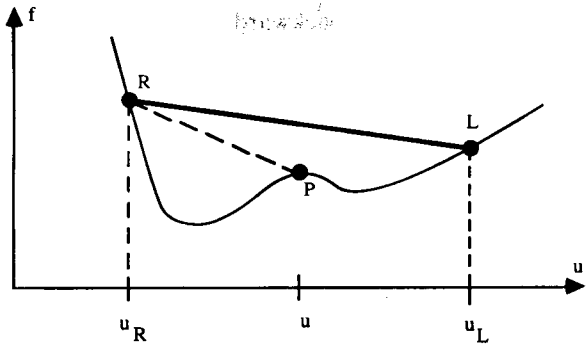
The graphical representation of the entropy condition leads to the formulation of the *Oleinik condition*, also called *condition E*, namely that the slope RP is lower than the slope of RL for any u between u_L and u_R when $u_R < u_L$. Hence one should have

$$\frac{f(u) - f(u_R)}{u - u_R} \leq \frac{f(u_L) - f(u_R)}{u_L - u_R} \leq \frac{f(u_L) - f(u)}{u_L - u} \quad \text{for } u_R \leq u \leq u_L \quad (21.2.6)$$

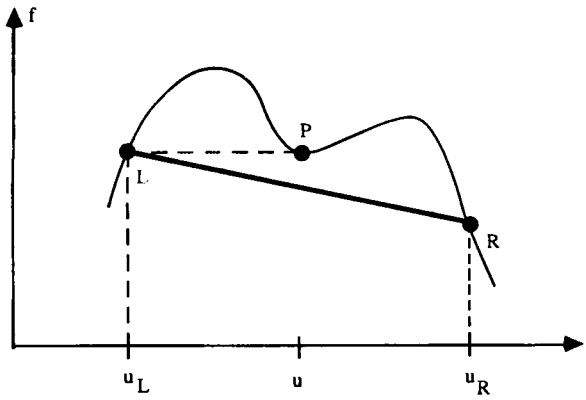
More importantly for practical applications, every initial value problem has a generalized unique solution, satisfying the entropy condition, that can be considered as the limit, for vanishing coefficients ν , of the parabolic equation

$$u_t + f_x = \nu u_{xx} \quad (21.2.7)$$

If u is the velocity of the fluid, the right-hand side is typical of the viscosity term in the one-dimensional Navier–Stokes equation. This extremely important result gives indications for the practical implementation of the entropy condition in numerical computations of inviscid flows. If *appropriate artificial viscosity*



(a) Condition on flux function for $u_R < u_L$



(b) Condition on flux function for $u_R > u_L$

Figure 21.2.3 Graphical representation of entropy conditions for a general, non-convex flux function

terms are added to the discretized equations, non-physical discontinuities will never appear.

The generalization to systems of conservation law is as follows. The hyperbolic system (21.2.1) of n equations written in one-dimensional space

$$U_t + Au_x = 0 \tag{21.2.8}$$

where $A = \partial F / \partial U$ is the Jacobian matrix of the flux vector, has n real and distinct eigenvalues λ_k , labelled in increasing order. The problem is genuinely non-linear if

$$\bar{r}_k \cdot \bar{\nabla} \lambda_k \neq 0 \tag{21.2.9}$$

where \bar{r}_k is the right eigenvector of A corresponding to the eigenvalue λ_k , and linearly degenerate otherwise.

The entropy condition is expressed by the requirement that for *some index* k , $1 \leq k \leq n$,

$$\lambda_k(U_R) < C < \lambda_k(U_L) \quad (21.2.10a)$$

while for the other characteristics

$$\lambda_{k+1}(U_R) > C > \lambda_{k+1}(U_L) \quad (21.2.10b)$$

This means that k characteristics reach the discontinuity from the left. Such a discontinuity is called a k shock by Lax, while if the k th characteristic is degenerate, then the speed of propagation of the discontinuity is

$$C = \lambda_k(u_L) = \lambda_k(u_R) \quad (21.2.11)$$

and one has a *contact discontinuity*.

The concept of the entropy condition can be further conceptualized by the introduction of an 'entropy' function $S(u)$, which satisfies a conservation law. If S and G are functions of U , the conservation law for the quantity S

$$\frac{\partial S}{\partial t} + \frac{\partial G}{\partial x} = 0 \quad (21.2.12)$$

is satisfied if, taking into account (21.2.8),

$$A \frac{\partial S}{\partial U} = \frac{\partial G}{\partial U} \quad (21.2.13)$$

This represents a system of n partial differential equations for S and G . For $n \geq 2$ the system is overdetermined and has generally no solutions. However for the Euler equations non-trivial solutions do indeed exist.

Since the solutions satisfying the entropy equations can be considered as the limits for ν going to zero of continuous solutions of the system of equations with an artificial viscosity

$$U_t + AU_x = \nu U_{xx} \quad (21.2.14)$$

it can be shown that, for *convex entropy functions* $S(U)$, that is satisfying the condition

$$\frac{\partial^2 S}{\partial u_i \partial u_j} > 0 \quad (21.2.15)$$

the following inequality should hold:

$$\frac{\partial S(U)}{\partial t} + \frac{\partial G(U)}{\partial x} \leq 0 \quad (21.2.16)$$

for any solution U of (21.2.14) in the limit $\nu \rightarrow 0$.

Actually, these conditions lead also to another formulation of the entropy condition: across a shock discontinuity, the following jump inequality is valid:

$$C[S_L - S_R] - [G_L - G_R] \leq 0 \quad (21.2.17)$$

The formulations (21.2.16) or (21.2.17) are fully equivalent to the previous expressions of the entropy condition, namely equations (21.2.10) or (21.2.2) for a single scalar equation.

The importance of the concept of entropy function lies in the fact that equation (21.2.16) has to be satisfied also at the discrete level by the numerical scheme; that is the solutions to any conservative scheme

$$U_i^{n+1} - U_i^n = -\tau(f_{i+1/2}^* - f_{i-1/2}^*) \quad (21.2.18a)$$

should satisfy an entropy inequality of the form

$$S_i^{n+1} - S_i^n \leq -\tau(G_{i+1/2}^* - G_{i-1/2}^*) \quad (21.2.18b)$$

where G^* is the numerical entropy flux. The entropy function S_i is a function of U_i and $G_{i+1/2}^* = G^*(U_{i-k+1}, \dots, U_{i+k})$.

A current choice, used in theoretical proofs of convergence applied to a single scalar conservation law, is

$$\begin{aligned} S(u) &= |u - z| \\ G(u) &= [f(u) - f(z)] \cdot \text{sgn}(u - z) \end{aligned} \quad (21.2.19)$$

where z is an arbitrary number and $\text{sgn}(x)$ is the sign function equal to 1 for $x > 0$ and to -1 for $x < 0$. It has been shown by Kruskov (1970) that two solutions u and v which satisfy the entropy condition

$$\frac{\partial |u - z|}{\partial t} + \frac{\partial [f(u) - f(z)] \cdot \text{sgn}(u - z)}{\partial x} \leq 0 \quad (21.2.20)$$

have the following bound in the L^1 norm:

$$\|u(x, t) - v(x, t)\|_{L^1} \leq \|u(x, t_0) - v(x, t_0)\|_{L^1} \quad (21.2.21)$$

for all $t > t_0$, and inversely. This condition ensures the existence and uniqueness of the solutions to the scalar conservation law $u_t + f_x = 0$ (Kruskov, 1970; Diperna, 1983).

At the discrete level, the property (21.2.21) becomes

$$\|u^m - v^m\|_{L^1} \leq \|u^n - v^n\|_{L^1} \quad \text{for all } m \geq n \geq 0 \quad (21.2.22a)$$

where

$$\|u^n - v^n\|_{L^1} = \sum_i |u_i^n - v_i^n| = \sum_i (u_i^n - v_i^n) \cdot \text{sgn}(u_i^n - v_i^n) \quad (21.2.22b)$$

Example 21.2.1 Entropy function for linear wave equation

If the linear wave equation $u_t + au_x = 0$ is multiplied by u , leading to

$$\frac{\partial u^2}{\partial t} + a \frac{\partial u^2}{\partial x} = 0 \quad (E21.2.1)$$

a possible convex entropy function is $S = u^2$ and the associated flux is $G = au^2$.

Observe that equations (21.2.13) and (21.2.15) are satisfied. The scheme

$$u_i^{n+1} = u_i^n - \sigma(u_{i+1/2}^n - u_{i-1/2}^n) \quad (\text{E21.2.2})$$

applied to equation (E21.2.1) leads to the following entropy condition, to be satisfied by all solutions:

$$(u_i^{n+1})^2 - (u_i^n)^2 + \sigma(u_{i+1/2}^n - u_{i-1/2}^n)(u_{i+1/2}^n + u_{i-1/2}^n) \leq 0 \quad (\text{E21.2.3})$$

21.2.2 Monotonicity condition

A scheme is considered as monotone if it does not lead to an oscillatory behaviour of the numerical solution, as illustrated in Figure 21.2.4. The 'smooth' behaviour of a numerical solution can result from different conditions, the strongest being monotonicity, while a weaker condition will be connected to the total variation.

The condition of monotonicity is best expressed by writing the general form of a numerical scheme applied to the scalar conservation equation $u_t + f_x = 0$ under the form

$$u_i^{n+1} = H(u_{i-k}^n, u_{i-k+1}^n, \dots, u_{i+k}^n) \quad (21.2.23)$$

The scheme (21.2.23) is said to be monotone if H is a monotone increasing function of each of its arguments, that is

$$\frac{\partial H}{\partial u_j}(u_{i-k}, u_{i-k+1}, \dots, u_{i+k}) \geq 0 \quad \text{for all } i-k \leq j \leq i+k \quad (21.2.24)$$

Observe that the function H is completely defined by the numerical flux of the scheme, with

$$u_i^{n+1} = H(u_{i-k}^n, u_{i-k+1}^n, \dots, u_{i+k}^n) \equiv u_i^n - \tau(f_{i+1/2}^* - f_{i-1/2}^*) \quad (21.2.25a)$$

$$f_{i+1/2}^* = f^*(u_{i-k+1}^n, u_{i-k+2}^n, \dots, u_{i+k}^n) \quad (21.2.25b)$$

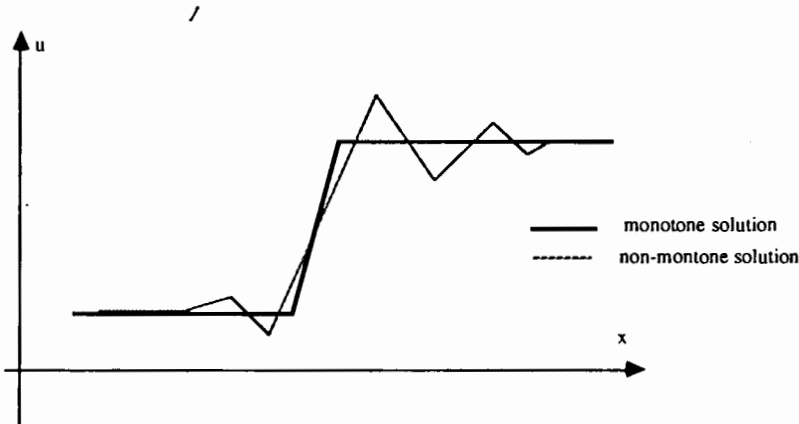


Figure 21.2.4 Monotone and non-monotone behaviour of a numerical solution

Hence the numerical flux of a monotone scheme is non-decreasing in its first argument and non-increasing in its last argument:

$$\frac{\partial f_{i+1/2}^*}{\partial u_{i-k+1}} \geq 0 \quad \frac{\partial f_{i+1/2}^*}{\partial u_{i+k}} \leq 0 \quad (21.2.26)$$

For any linear scheme written in the form

$$u_i^{n+1} = \sum_k b_k u_{i+k}^n \quad (21.2.27)$$

the condition of monotonicity requires all the coefficients b_k to be non-negative.

Example 21.2.2

Consider the linear form of the first-order upwind scheme applied to the scalar convection equation $u_t + au_x = 0$, with $a > 0$:

$$u_i^{n+1} = \sigma u_{i-1}^n + (1 - \sigma)u_i^n \quad (E21.2.4)$$

This scheme is monotone for $0 < \sigma \leq 1$, that is within its stability region.

On the other hand, the second-order Lax–Wendroff scheme, written as

$$u_i^{n+1} = \frac{\sigma}{2}(1 + \sigma)u_{i-1}^n + (1 - \sigma^2)u_i^n + \frac{\sigma}{2}(\sigma - 1)u_{i+1}^n \quad (E21.2.5)$$

is clearly not monotone since $|\sigma| \leq 1$ for stability and the third coefficient is negative.

The second-order upwind scheme (21.1.27), written as

$$u_i^{n+1} = \frac{\sigma}{2}(\sigma - 1)u_{i-2}^n + \sigma(2 - \sigma)u_{i-1}^n + \left(1 - \frac{\sigma}{2}\right)(\sigma - 1)u_i^n \quad (E21.2.6)$$

is also non-monotone since the first coefficient is negative for $0 < \sigma < 1$, while the third coefficient is negative for $1 < \sigma < 2$.

Similar considerations apply to two- and three-dimensional schemes. For instance, the two-dimensional upwind scheme (20.6.9) is monotone for $0 < \sigma_x + \sigma_y \leq 1$, corresponding to its stability domain.

Properties of monotone schemes

It is shown by Harten *et al.* (1976) that the converged solutions to a monotone scheme always correspond to physically acceptable states. In other words, monotone schemes do not produce non-physical solutions, such as expansion shocks, and therefore satisfy the entropy condition as defined in Section 21.2.1.

Another formulation of the relation between monotonicity and the entropy condition is presented by B. Keyfitz in an Appendix to Harten *et al.* (1976),

where it is shown that the condition (21.2.22) is necessary and sufficient for monotonicity.

This property can be explained by the close relation between monotonicity and the presence of viscosity terms in the equivalent differential equation of monotone schemes. Indeed, a straightforward computation of the Taylor series expansion of the functional H around u_i , taking into account the consistency relation

$$H(u, u, \dots, u) = u \quad (21.2.28)$$

and denoting by H_j the partial derivative of H with respect to its j th argument with the convention $H_j \equiv 0$ for $j > k$ or $j < -k$, leads to the following equivalent differential equation (Harten *et al.*, 1976), $\tau = \Delta t / \Delta x$:

$$u_t + f_x = \Delta t [\beta(u) u_x]_x \quad (21.2.29a)$$

$$\beta(u) = \frac{1}{2\tau^2} \left[\sum_{j=-k}^{j=+k} j^2 H_j(u, u, \dots, u) - \tau^2 a(u) \right] \quad (21.2.29b)$$

From the monotonicity condition $H_j \geq 0$, the properties

$$\sum_{j=-k}^{j=+k} H_j(u, u, \dots, u) = 1 \quad (21.2.30a)$$

$$\sum_{j=-k}^{j=+k} j H_j'(u, u, \dots, u) = -\tau a(u) \quad (21.2.30b)$$

and the Schwarz's inequality, we obtain

$$\begin{aligned} \tau^2 a^2(u) &= (\sum j H_j)^2 = (\sum j \sqrt{H_j} \sqrt{H_j})^2 \\ &\leq \sum j^2 H_j \cdot \sum H_j = \sum j^2 H_j \end{aligned} \quad (21.2.31)$$

showing that $\beta(u)$ is always positive. As equation (21.2.29) is of the form (21.2.7) its solutions satisfy the entropy condition. Consequently, conservative monotone schemes for the non-linear equation (21.2.1) are only of first-order accuracy.

This represents a severe limitation, since first-order accuracy is insufficient for practical purposes, the corresponding schemes being too diffusive. Hence, conditions less severe than monotonicity have to be defined, allowing the definition of schemes, with an accuracy higher than one generating entropy-satisfying solutions without overshoots at shocks and contact discontinuities. Schemes of this type are called *high-resolution schemes*.

A weaker condition than monotonicity is provided by the concept of total variation of a numerical solution introduced by Harten (1983, 1984). The condition of total variation boundedness is more general than monotonicity and is sufficient to guarantee the convergence of the numerical solution of a conservative scheme to the weak solutions of the scalar conservation law (21.2.1). However, unlike monotonicity, this condition does not ensure the satisfaction of the entropy condition.

21.2.3 Total variation diminishing (TVD) schemes

The concept of bounded total variation finds its origin in an important property of a scalar conservation law $u_t + f_x = 0$: the total variation of any physically admissible solution

$$\text{TV} = \int \left| \frac{\partial u}{\partial x} \right| dx$$

does not increase in time (Lax, 1973).

The *total variation in x* (TV) of a discrete solution to a scalar conservation law is defined by

$$\text{TV}(u) \equiv \sum_i |u_{i+1} - u_i| \quad (21.2.32)$$

A numerical solution is said to be of *bounded total variation* or *total variation stable* if the total variation is uniformly bounded in t and Δx .

A numerical *scheme* is said to be *total variation diminishing* if

$$\text{TV}(u^{n+1}) \leq \text{TV}(u^n) \quad (21.2.33)$$

If the following monotonicity properties are maintained as a function of t :

- (1) No new local extrema in x can be created;
- (2) The value of a local minimum is non-decreasing, the value of a local maximum is non-increasing;

then the scheme is said to be *monotonicity preserving*. This condition states that a scheme is monotonicity preserving if u^{n+1} remains monotone when u^n is monotone. In other words, monotone profiles are preserved during the time evolution of the discrete solutions and overshoots will not be created.

The following hierarchy exists between these properties:

- (1) All monotone schemes are TVD.
- (2) All TVD schemes are monotonicity preserving.

Note that the first property immediately results from the condition (21.2.22), which is necessary and sufficient for monotonicity, when the choice $v_i = u_{i+1}$ is made.

For linear schemes of the form (21.2.27), monotonicity preservation leads to the same conditions as monotonicity. Therefore any linear TVD scheme is a monotone scheme and hence only *first-order accurate*.

However, this restriction does not apply to *non-linear* schemes, which can be made TVD while having second-order accuracy. This possibility explains the importance of the TVD concept in the generation of high-resolution schemes.

Let us consider a three-point conservative scheme for the scalar conservation law (21.2.1), written in numerical flux form. In order to derive TVD conditions it is necessary to rewrite the scheme under an increment from, that is as a combination of mesh point differences $\delta u_{i+1/2} \equiv u_{i+1} - u_i$.

The semi-discretized equation

$$\frac{du_i}{dt} = -\frac{1}{\Delta x} (f_{i+1/2}^* - f_{i-1/2}^*) \quad (21.2.34a)$$

$$f_{i+1/2}^* = f^*(u_i, u_{i+1}) \quad (21.2.34b)$$

is written as

$$\frac{du_i}{dt} \equiv -\frac{1}{\Delta x} (C_{i+1/2}^- \delta u_{i+1/2} + C_{i-1/2}^+ \delta u_{i-1/2}) \quad (21.2.35)$$

Comparing with equation (21.2.34), setting $u_i = u_{i-1}$ and applying the consistency condition $f^*(u, u) = f(u)$ gives

$$C_{i+1/2}^- \delta u_{i+1/2} = f_{i+1/2}^* - f_i \equiv a_{i+1/2}^- (u_{i+1} - u_i) \quad (21.2.36a)$$

and similarly

$$C_{i-1/2}^+ \delta u_{i-1/2} = f_i - f_{i-1/2}^* \equiv a_{i-1/2}^+ (u_i - u_{i-1}) \quad (21.2.36b)$$

C^+ and C^- contain the contributions from the waves with positive, respectively negative, wave speeds with the above definitions of a^\pm .

Note also the relation

$$C_{i+1/2}^+ + C_{i+1/2}^- = \frac{f_{i+1} - f_i}{u_{i+1} - u_i} = \frac{\delta f_{i+1/2}}{\delta u_{i+1/2}} \equiv a_{i+1/2} \quad (21.2.37)$$

which is to be considered as a condition for the scheme (21.2.35) to be conservative.

The considered schemes can also be written as a central scheme plus a dissipation term following equation (17.3.23), that is

$$f_{i+1/2}^* = \frac{1}{2}(f_i + f_{i+1}) - \frac{1}{2}\bar{D}_{i+1/2} \delta u_{i+1/2} \quad (21.2.38)$$

where \bar{D} can be considered as the numerical viscosity coefficient of the scheme. The function \bar{D} defines uniquely the three-point scheme and can be related to the C^\pm coefficients. Equation (21.2.36) leads to

$$C_{i+1/2}^- = \frac{1}{2}(a_{i+1/2} - \bar{D}_{i+1/2}) \quad (21.2.39a)$$

$$C_{i+1/2}^+ = \frac{1}{2}(a_{i+1/2} + \bar{D}_{i+1/2}) \quad (21.2.39b)$$

where $a_{i+1/2}$ is defined by equation (21.2.37).

Inversely, the numerical viscosity coefficient \bar{D} is obtained from the C^\pm coefficients via

$$\bar{D}_{i+1/2} = C_{i+1/2}^+ - C_{i+1/2}^- \quad (21.2.40)$$

Conditions for three-point TVD schemes

Conditions for schemes to be TVD have been derived by Harten (1983, 1984) for three-point explicit and implicit schemes and generalized by Jameson and Lax (1984) to multi-point schemes.

The semi-discretized scheme (21.2.35) is TVD if and only if

$$C_{i+1/2}^+ \geq 0 \quad C_{i+1/2}^- \leq 0 \quad (21.2.41)$$

This is easily shown, following the arguments of Jameson and Lax (1984). Subtracting equations (21.2.35) at $(i+1)$ and at i and defining the sign function $s_{i+1/2} = \text{sgn}(\delta u_{i+1/2})$ gives

$$\begin{aligned} \frac{d\text{TV}(u)}{dt} &= \sum_i s_{i+1/2} \frac{d(u_{i+1} - u_i)}{dt} \\ &= \frac{1}{\Delta x} \sum_i s_{i+1/2} [(C^- - C^+)_{i+1/2} \delta u_{i+1/2} - C_{i+3/2}^- \delta u_{i+3/2} + C_{i-1/2}^+ \delta u_{i-1/2}] \\ &= \frac{1}{\Delta x} \sum_i [s_{i+1/2} (C_{i+1/2}^- - C_{i+1/2}^+) - C_{i+1/2}^- s_{i-1/2} + C_{i+1/2}^+ s_{i+3/2}] \delta u_{i+1/2} \end{aligned} \quad (21.2.42)$$

The TVD condition requires the right-hand side to be non-positive. This will be the case if the term in brackets is of opposite sign to $\delta u_{i+1/2}$ for all δu . In particular, for

$$\delta u_{i+1/2} = 1 \quad \delta u_{i+3/2} = \delta u_{i-1/2} = 0$$

leading to the conditions (21.2.41). Observe that these conditions only depend on the *space discretization of the flux gradient*.

If equation (21.2.35) is integrated with an explicit Euler method, the resulting scheme

$$u_i^{n+1} = u_i^n - \frac{\Delta t}{\Delta x} (C_{i+1/2}^- \delta u_{i+1/2} + C_{i-1/2}^+ \delta u_{i-1/2})^n \quad (21.2.43)$$

is TVD under the conditions (21.2.41) and the additional CFL-like condition (Harten, 1983):

$$\tau(C_{i+1/2}^+ - C_{i+1/2}^-) \leq 1 \quad (21.2.44)$$

Indeed, the total variation at time level $n+1$ is obtained as

$$\begin{aligned} \text{TV}(u^{n+1}) &= \sum_i |u_i^{n+1} - u_i^n| \\ &= \sum_i |[1 - \tau(C^+ - C^-)_{i+1/2}] \delta u_{i+1/2} \\ &\quad - \tau C_{i+3/2}^- \delta u_{i+3/2} + \tau C_{i-1/2}^+ \delta u_{i-1/2}| \\ &\leq \sum_i \{ [1 - \tau(C^+ - C^-)_{i+1/2}] |\delta u_{i+1/2}| \\ &\quad - \tau C_{i+3/2}^- |\delta u_{i+3/2}| + \tau C_{i-1/2}^+ |\delta u_{i-1/2}| \} \end{aligned} \quad (21.2.45)$$

where the relations (21.2.41) have been used to obtain the last line. Rearranging the second and third sums it is seen that the first term has to be negative, since

in this case

$$\begin{aligned} \text{TV}(u^{n+1}) &\leq \sum_i \{ [1 - \tau(C^+ - C^-)_{i+1/2}] |\delta u_{i+1/2}| \\ &\quad - \tau C_{i+1/2}^- |\delta u_{i+1/2}| + \tau C_{i+1/2}^+ |\delta u_{i+1/2}| \} \\ &= \sum_i |\delta u_{i+1/2}| = \text{TV}(u^n) \end{aligned} \quad (21.2.46)$$

The TVD conditions can also be expressed as a function of the numerical dissipation coefficient \bar{D} (Tadmor, 1984a). The explicit scheme (21.2.43) is TVD if the numerical dissipation satisfies the following conditions:

$$\tau |a|_{i+1/2} \leq \tau \bar{D}_{i+1/2} \leq 1 \quad (21.2.47)$$

The lower boundary on \bar{D} results from the conditions (21.2.41) on the semi-discretized formulation (21.2.35) and indicates that the dissipation coefficients of a TVD scheme has to be equal or greater than the dissipation of Roe's first-order upwind scheme for which $\bar{D} = |a|$. The upper bound on \bar{D} is the CFL-like condition (21.2.43) for the explicit scheme and corresponds to the dissipation of the Lax–Friedrichs scheme.

It is interesting to observe at this point that the first-order explicit scheme applied to the scalar convection equation, with the numerical flux (21.2.38), is Von Neumann stable in the larger domain $\tau^2 a^2 = \sigma^2 \leq \tau \bar{D} \leq 1$ (see Problem 20.11).

Example 21.2.3 First-order upwind scheme for a scalar conservation law

The simplest generalization of the linear first-order upwind scheme is given by Murman and Cole's version (20.5.33), which is identical to Roe's scheme in this case, as seen from equation (20.5.89). With the definition (20.5.34), one has

$$C_{i+1/2}^+ + C_{i+1/2}^- = a_{i+1/2} \quad (E21.2.7)$$

and

$$C_{i+1/2}^- = \frac{a_{i+1/2} - |a|_{i+1/2}}{2} \equiv a_{i+1/2}^- \quad (E21.2.8a)$$

$$C_{i+1/2}^+ = \frac{a_{i+1/2} + |a|_{i+1/2}}{2} \equiv a_{i+1/2}^+ \quad (E21.2.8b)$$

It is seen from equations (21.2.41) that all the first-order upwind schemes presented in Chapter 20 are TVD.

The third condition (21.2.44) for the explicit first-order upwind schemes is satisfied for the CFL condition

$$\tau(a^+ - a^-)_{i+1/2} = \tau |a|_{i+1/2} \leq 1 \quad (E21.2.9)$$

The numerical viscosity function \bar{D} is given here, in agreement with equation (20.5.89), by

$$\bar{D}_{i+1/2} = |a|_{i+1/2} \quad (E21.2.10)$$

The following property is of essential importance: any *three-point TVD scheme is of first-order accuracy*.

This can be seen from a truncation error analysis of the scheme (21.2.43), following the approach of Section 9.4 (chapter 9 in Volume 1). From equation (17.3.25), the lowest-order truncation term is

$$\frac{\Delta x}{2} [(\bar{D} - \tau a^2)u_x]_x \quad (21.2.48)$$

and the TVD conditions (21.2.47) result in the inequalities

$$\bar{D} - \tau a^2 \geq |a|(1 - \tau|a|) \geq 0 \quad (21.2.49)$$

Hence the considered three-point TVD schemes are only first-order accurate.

Therefore schemes of the form (21.2.35) or (21.2.43) can only be made TVD if *more than three points are involved in the definition of the numerical fluxes*. In addition, as stated above, a linear TVD scheme is always of first-order accuracy, independently of the number of points involved. Hence the procedure to follow in order to transform a three-point scheme into a higher-order TVD scheme is to *introduce more points in a non-linear way*. This will be developed in Section 21.3.

Conditions for linear multi-point TVD schemes

If a multi-point TVD scheme is constructed by non-linear adaptations of three-point schemes, then the general form (21.2.35) will remain valid, with, however, a general dependence of the C^\pm coefficients on more than two points. For instance, a five-point scheme of the form (21.2.35) will be defined by relations

$$\begin{aligned} C_{i+1/2}^- &= C^-(u_{i+2}, u_{i+1}, u_i, u_{i-1}) \\ C_{i-1/2}^+ &= C^+(u_{i+1}, u_i, u_{i-1}, u_{i-2}) \end{aligned} \quad (21.2.50)$$

The conditions (21.2.41) and (21.2.44) remain valid for this five-point scheme to be TVD.

However, for linear multi-point schemes, generalized TVD conditions have been derived by Jameson and Lax (1984). In semi-discretized form, the following $2J + 1$ point scheme

$$\frac{du_i}{dt} = -\frac{1}{\Delta x} \sum_{k=1}^J (C_{i+k-1/2}^{-(k)} \delta u_{i+k-1/2} + C_{i-k+1/2}^{+(k)} \delta u_{i-k+1/2}) \quad (21.2.51)$$

is TVD if and only if

$$C_{i+1/2}^{-(1)} \leq C_{i+1/2}^{-(2)} \leq \dots \leq C_{i+1/2}^{-(k)} \leq 0 \quad (21.2.52a)$$

$$C_{i+1/2}^{+(1)} \geq C_{i+1/2}^{+(2)} \geq \dots \geq C_{i+1/2}^{+(k)} \geq 0 \quad (21.2.52b)$$

generalizing equation (21.2.41).

The explicit scheme

$$u_i^{n+1} = u_i^n - \tau \sum_{k=1}^J (C_{i+k-1/2}^{-(k)} \delta u_{i+k-1/2} + C_{i-k+1/2}^{+(k)} \delta u_{i-k+1/2})^n \quad (21.2.53)$$

is TVD under the same conditions and the additional CFL-like condition

$$\tau(C_{i+1/2}^{+(1)} - C_{i+1/2}^{-(1)}) \leq 1 \quad (21.2.54)$$

which is identical to the condition (21.2.44).

The general implicit scheme

$$\begin{aligned} & u_i^{n+1} - \tau \sum_{k=1}^J (B_{i+k-1/2}^{-(k)} \delta u_{i+k-1/2} + B_{i-k+1/2}^{+(k)} \delta u_{i-k+1/2})^{n+1} \\ &= u_i^n - \tau \sum_{k=1}^J (C_{i+k-1/2}^{-(k)} \delta u_{i+k-1/2} + C_{i-k+1/2}^{+(k)} \delta u_{i-k+1/2})^n \end{aligned} \quad (21.2.55)$$

is TVD if and only if the implicit coefficients B satisfy the conditions

$$B_{i+1/2}^{+(1)} \leq B_{i+1/2}^{+(2)} \leq \dots \leq B_{i+1/2}^{+(k)} \leq 0 \quad (21.2.56a)$$

$$B_{i+1/2}^{-(1)} \geq B_{i+1/2}^{-(2)} \geq \dots \geq B_{i+1/2}^{-(k)} \geq 0 \quad (21.2.56b)$$

and the explicit coefficients satisfy the conditions (21.2.52) and (21.2.54).

Example 21.2.4 Second-order upwind schemes

Consider the linearized second-order upwind schemes (21.1.35), with $f^\pm = a^\pm u$, written here as a multi-point scheme:

$$\frac{du_i}{dt} = -\frac{a^+}{2\Delta x} [3(u_i - u_{i-1}) - (u_{i-1} - u_{i-2})] - \frac{a^-}{2\Delta x} [3(u_{i+1} - u_i) - (u_{i+2} - u_{i+1})] \quad (E21.2.11)$$

Hence the coefficients of the expansion (21.2.51) are

$$\begin{aligned} C_{i+3/2}^{-(1)} &= \frac{3}{2}a^- & C_{i+3/2}^{-(2)} &= \frac{-1}{2}a^- \\ C_{i-1/2}^{+(1)} &= \frac{3}{2}a^+ & C_{i-3/2}^{+(2)} &= \frac{-1}{2}a^+ \end{aligned} \quad (E21.2.12)$$

It is seen from equations (21.2.52) that if the coefficients $C^{\pm(1)}$ satisfy the TVD conditions, the coefficients $C^{\pm(2)}$ have the wrong sign. Therefore, the second-order schemes of Section 21.1 are not TVD and oscillations will appear around discontinuities.

Another way of treating the above scheme is to write it in the form (21.2.35), that is

$$\frac{du_i}{dt} = -\frac{a^+}{2\Delta x} \left(3 - \frac{u_{i-1} - u_{i-2}}{u_i - u_{i-1}} \right) (u_i - u_{i-1}) - \frac{a^-}{2\Delta x} \left(3 - \frac{u_{i+2} - u_{i+1}}{u_{i+1} - u_i} \right) (u_{i+1} - u_i) \quad (E21.2.13)$$

defining the coefficients

$$C_{i-1/2}^+ = \frac{a^+}{2} \left(3 - \frac{u_{i-1} - u_{i-2}}{u_i - u_{i-1}} \right) \quad (\text{E21.2.14a})$$

$$C_{i+1/2}^- = \frac{a^-}{2} \left(3 - \frac{u_{i+2} - u_{i+1}}{u_{i+1} - u_i} \right) \quad (\text{E21.2.14b})$$

The ratios appearing in the right-hand side can become large enough such as to dominate the first term. Hence, if the ratios

$$\frac{u_i - u_{i-1}}{u_{i+1} - u_i} \geq 3 \quad \text{and} \quad \frac{u_{i+2} - u_{i+1}}{u_{i+1} - u_i} \geq 3 \quad (\text{E21.2.15})$$

the schemes are not TVD.

The way to render the second-order upwind schemes TVD will consist in restricting these gradients, in a non-linear way, to values below 3.

This analysis of the TVD properties of second-order upwind schemes can be extended to the general flux (21.1.61). Writing the semi-discretized scheme associated with this numerical flux, with the choice $\kappa = -1$, produces the form

$$\begin{aligned} \frac{du_i}{dt} = & -\frac{1}{2\Delta x} \left(3 - \frac{f_{i-1} - f_{i-3/2}^*}{f_i - f_{i-1/2}^*} \right) (f_i - f_{i-1/2}^*) \\ & -\frac{1}{2\Delta x} \left(3 - \frac{f_{i+3/2}^* - f_{i+1}}{f_{i+1/2}^* - f_i} \right) (f_{i+1/2}^* - f_i) \end{aligned} \quad (\text{E21.2.16})$$

Relating this scheme to the form (21.2.35), the definitions (21.2.36) are extended to second-order upwind schemes as follows:

$$C_{i-1/2}^+ \delta u_{i-1/2} = \frac{1}{2} \left(3 - \frac{f_{i-1} - f_{i-3/2}^*}{f_i - f_{i-1/2}^*} \right) (f_i - f_{i-1/2}^*) \quad (\text{E21.2.17a})$$

$$C_{i+1/2}^- \delta u_{i+1/2} = \frac{1}{2} \left(3 - \frac{f_{i+3/2}^* - f_{i+1}}{f_{i+1/2}^* - f_i} \right) (f_{i+1/2}^* - f_i) \quad (\text{E21.2.17b})$$

The second factors represent the three-point increments of equation (21.2.36). Here, again, the flux ratios in the first factors can exceed the value of 3 and the schemes are generally not TVD.

Example 21.2.5 Lax–Wendroff scheme for the linear convection equation

Let us write the linear Lax–Wendroff scheme applied to the scalar convection equation $u_t + au_x = 0$ as

$$u_i^{n+1} = u_i^n - \sigma(u_i^n - u_{i-1}^n) + \frac{\sigma}{2}(1 - \sigma)(u_i^n - u_{i-1}^n) - \frac{\sigma}{2}(1 - \sigma)(u_{i+1}^n - u_i^n) \quad (\text{E21.2.18})$$

The Lax–Wendroff scheme is hereby written in incremental form as a

second-order correction to the first-order upwind scheme. The C^\pm coefficients become, in the case of $a > 0$,

$$\begin{aligned} C_{i-1/2}^+ &= \frac{a(1+\sigma)}{2} \\ C_{i-1/2}^- &= \frac{a(1-\sigma)}{2} \end{aligned} \quad (\text{E21.2.19})$$

Under the CFL condition, the C^- coefficient is positive and hence the TVD condition (21.2.41) is not satisfied. If $a < 0$ then the C^+ coefficient is negative and the first of the TVD conditions will not be fulfilled.

TVD schemes and the entropy condition

It has already been stated that the TVD condition does not ensure the satisfaction of the entropy condition. An example is given by Roe's scheme, which has been shown to admit stationary expansion shock solutions.

A detailed analysis of the additional constraints to be imposed on a TVD scheme in order to satisfy an entropy condition can be found in Osher (1984) and Osher and Chakravarthy (1984). In particular, Osher (1984) introduced the concept of E-schemes which generate TVD and entropy-satisfying solutions.

A consistent scheme is called an E-scheme if its numerical flux function satisfies

$$[f_{i+1/2}^* - f(u)] \cdot \text{sgn}(u_{i+1} - u_i) \leq 0 \quad \text{for all } u \text{ between } u_i \text{ and } u_{i+1} \quad (21.2.57)$$

Note that this definition is not restricted to three-point schemes.

From the definitions (21.2.36), it is seen that the TVD conditions (21.2.41) are always fulfilled and hence an E-scheme is TVD. In addition, if the scheme has a three-point support, equation (21.2.26) shows that three-point monotone schemes are E-schemes.

The usefulness of E-schemes is, however, restricted by the fact that *E-schemes are at most first-order accurate*, as shown by Osher (1984). When applied to Roe's scheme (20.5.89), whose numerical flux is

$$f_{i+1/2}^{*(R)} = \frac{1}{2}(f_i + f_{i+1}) - \frac{1}{2}|a|_{i+1/2} \delta u_{i+1/2} \quad (21.2.58)$$

where $a_{i+1/2}$ is defined by equation (21.2.37), the E-scheme condition becomes

$$\frac{f_i + f_{i+1} - 2f(u)}{\delta u_{i+1/2}} \leq |a|_{i+1/2} \quad \text{for all } u \text{ between } u_i \text{ and } u_{i+1} \quad (21.2.59)$$

As can be seen from Figure 21.2.5 for a convex flux function, this condition is always satisfied, unless the interval $(i, i+1)$ contains the sonic point u^* , defined by $f(u^*) = 0$. In this case $|a|$ can vanish and the condition is not fulfilled, allowing the appearance of expansion shocks. Hence, if $u_i < u^* < u_{i+1}$, that is for an expansion through the sonic point, $|a|$ should be redefined in such a way that

$$\begin{aligned} \max [f_i + f_{i+1} - 2f(u)] &= f_i + f_{i+1} - 2 \min [f(u)] \\ &= f_i + f_{i+1} - 2f(u^*) \leq |a| \delta u_{i+1/2} \end{aligned} \quad (21.2.60a)$$

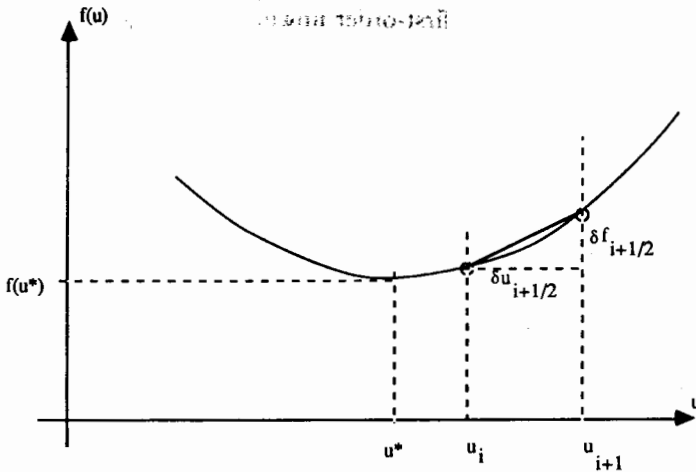


Figure 21.2.5 Scalar, convex flux function with sonic point

or

$$f_{i+1/2}^{*(R)} < f(u^*) \quad \text{for } u_i < u^* < u_{i+1} \quad (21.2.60b)$$

This is achieved with the modifications (20.5.93) to (20.5.95).

In order to obtain a guideline for making second-order TVD schemes satisfy the entropy condition, Osher and Chakravarthy (1984) define a weaker condition than the E-scheme condition (21.2.57).

The inequality

$$\int_{u_i}^{u_{i+1}} S_{uu}(u) [f_{i+1/2}^* - f(u)] du \leq 0 \quad (21.2.61)$$

where $S(u)$ is a convex entropy function with $S_{uu}(u) \geq 0$ is sufficient for ensuring the entropy condition of the scheme. This condition can be satisfied for all convex entropy functions S if the scheme is an E-scheme, but then it is only first-order accurate. Hence a weaker condition can be required, namely that it is only to be satisfied for a single entropy function, for instance $S(u) = u^2/2$. The interested reader is referred to Osher and Chakravarthy (1984) for an example of an application to second-order upwind TVD schemes.

21.3 SECOND-ORDER TVD SEMI-DISCRETIZED SCHEMES WITH LIMITERS

The methodology for the definition of second-order, high-resolution TVD schemes is now clear and can be set as follows:

- (1) Select a first-order monotone numerical flux.
- (2) Extend the numerical flux to second-order accuracy.

- (3) Restrict the amplitude of the gradients appearing in the additional terms, via *non-linear limiters*, such as to ensure the TVD conditions.
- (4) Select a time-integration scheme and adapt, if necessary, the choice of the limiters to the additional TVD conditions.
- (5) Check, if possible, the entropy condition for the ‘limited’ higher-order scheme.

The first two steps have been defined previously and the third step will be developed in this section.

We will first discuss the TVD properties for the semi-discretized formulation with numerical fluxes of second-order accuracy in *space*. This forms the TVD basis when time-integration schemes are applied independently of the space discretization as described in Chapter 18. For second (or higher)-order schemes based on combined space–time discretizations, the influence of the Δt^2 terms will have to be treated separately.

21.3.1 Definition of limiters for the linear convection equation

We consider first the linear convection equation $u_t + au_x = 0$ and the second-order upwind scheme as presented in Example 21.2.4. In order to make the scheme TVD we restrict the variations δu appearing in the *second-order terms* via a non-linear limiting function Ψ . Rewriting equation (E21.2.11) as a first-order scheme plus correction terms

$$\begin{aligned} \frac{du_i}{dt} = & -\frac{a^+}{\Delta x} [(u_i - u_{i-1}) + \frac{1}{2}(u_i - u_{i-1}) - \frac{1}{2}(u_{i-1} - u_{i-2})] \\ & -\frac{a^-}{\Delta x} [(u_{i+1} - u_i) + \frac{1}{2}(u_{i+1} - u_i) - \frac{1}{2}(u_{i+2} - u_{i+1})] \end{aligned} \quad (21.3.1)$$

the variations in the second and third terms within the square brackets will be limited as follows:

$$\begin{aligned} \frac{du_i}{dt} = & -\frac{a^+}{\Delta x} [(u_i - u_{i-1}) + \frac{1}{2}\Psi_{i-1/2}^+(u_i - u_{i-1}) - \frac{1}{2}\Psi_{i-3/2}^+(u_{i-1} - u_{i-2})] \\ & -\frac{a^-}{\Delta x} [(u_{i+1} - u_i) + \frac{1}{2}\Psi_{i+1/2}^-(u_{i+1} - u_i) - \frac{1}{2}\Psi_{i+3/2}^-(u_{i+2} - u_{i+1})] \end{aligned} \quad (21.3.2)$$

Since equation (E21.2.15) shows that the TVD conditions are to be expressed as a function of ratios of consecutive variations, the limiters Ψ should also be defined as a function of these ratios. Defining

$$r_{i+1/2}^+ = \frac{u_{i+2} - u_{i+1}}{u_{i+1} - u_i} \quad r_{i+1/2}^- = \frac{u_i - u_{i-1}}{u_{i+1} - u_i} \quad (21.3.3)$$

as the ratios of $\delta u_{i+1/2} = u_{i+1} - u_i$ with the forward and backward gradients, $\delta u_{i+3/2} = u_{i+2} - u_{i+1}$ and $\delta u_{i-1/2} = u_i - u_{i-1}$, the limiting functions can be

considered to depend on two of these ratios, depending on the associated upwind direction. Hence, the general form will be taken as

$$\Psi_{i-1/2}^+ = \Psi(r_{i-1/2}^+, r_{i+1/2}^+) \quad (21.3.4a)$$

for the terms associated to positive waves and

$$\Psi_{i+1/2}^- = \Psi(r_{i+1/2}^-, r_{i+3/2}^-) \quad (21.3.4b)$$

for the negative wave contributions.

The TVD conditions (21.2.41) are obtained by writing equation (21.3.2) in the incremental form (21.2.35):

$$\begin{aligned} \frac{du_i}{dt} = & -\frac{a^+}{\Delta x} \left[1 + \frac{1}{2}\Psi_{i-1/2}^+ - \frac{1}{2} \frac{\Psi_{i-3/2}^+}{r_{i-3/2}^+} \right] (u_i - u_{i-1}) \\ & -\frac{a^-}{\Delta x} \left[1 + \frac{1}{2}\Psi_{i+1/2}^- - \frac{1}{2} \frac{\Psi_{i+3/2}^-}{r_{i+3/2}^-} \right] (u_{i+1} - u_i) \end{aligned} \quad (21.3.5)$$

leading to the TVD conditions

$$1 + \frac{1}{2}\Psi_{i-1/2}^+ - \frac{1}{2} \frac{\Psi_{i-3/2}^-}{r_{i-3/2}^+} \geq 0 \quad (21.3.6a)$$

$$1 + \frac{1}{2}\Psi_{i+1/2}^- - \frac{1}{2} \frac{\Psi_{i+3/2}^-}{r_{i+3/2}^-} \geq 0 \quad (21.3.6b)$$

In order to restrict the generality of the limiting functions Ψ , it will be assumed that they depend only on a *single upwind* gradient. Furthermore, in order to restrict the support of the scheme, the closest occurring gradients are selected. Hence, we define the following dependence:

$$\Psi_{i-1/2}^+ = \Psi(r_{i-1/2}^+) \quad \Psi_{i-3/2}^+ = \Psi(r_{i-3/2}^+) \quad (21.3.7a)$$

while limiters associated with negative waves are expressed as

$$\Psi_{i+1/2}^- = \Psi(r_{i+1/2}^-) \quad \Psi_{i+3/2}^- = \Psi(r_{i+3/2}^-) \quad (21.3.7b)$$

A discussion of several options for a more general dependence of the limiting functions (21.3.4) can be found in Roe (1984), in the framework of the Lax-Wendroff schemes.

The TVD conditions (21.3.6) become

$$\frac{\Psi(r_{i-3/2}^+)}{r_{i-3/2}^+} - \Psi(r_{i-1/2}^+) \leq 2 \quad (21.3.8a)$$

$$\frac{\Psi(r_{i+3/2}^-)}{r_{i+3/2}^-} - \Psi(r_{i+1/2}^-) \leq 2 \quad (21.3.8b)$$

These two conditions are similar and of the form

$$\frac{\Psi(r)}{r} - \Psi(s) \leq 2 \quad (21.3.9)$$

for all values of r and s .

A detailed analysis of the properties of the Ψ limiters has been given by Sweby (1984) and also, from a different standpoint, by Roe (1985).

The above functional relations can be satisfied by a large variety of Ψ functions. However, a certain number of constraints can be identified or imposed. First of all, we restrict Ψ to be a positive function, that is

$$\Psi(r) \geq 0 \quad \text{for } r \geq 0 \quad (21.3.10)$$

In addition, when $r < 0$, that is when an extremum is encountered in the variation of the solution u , it seems logical to set $\Psi = 0$ corresponding to a zero slope in the interval considered (see Figure 21.3.1). This avoids non-monotone behaviours with changes of slope directions, at the expense of a certain loss of accuracy. When $\Psi = 0$ the scheme reduces to first-order accuracy. Hence, we set

$$\Psi(r) = 0 \quad \text{for } r \leq 0 \quad (21.3.11a)$$

With these assumptions, we have the sufficient condition

$$0 \leq \Psi(r) \leq 2r \quad (21.3.11b)$$

Additional conditions are obtained by imposing the same Ψ limiters to the explicit second-order Warming and Beam scheme (21.1.28a) derived from equation (21.3.2) by an appropriate time integration. The 'limited' version of the Warming and Beam scheme, for $a > 0$, is written in the form

$$u_i^{n+1} = u_i^n - \sigma(u_i - u_{i-1})^n - \frac{\sigma}{2}(1 - \sigma)\delta^- [\Psi(r_{i-1/2}^+) (u_i - u_{i-1})^n] \quad (21.3.12)$$

With reference to equation (21.2.43) and the condition (21.2.44), we have

$$0 \leq \tau C_{i-1/2}^+ = \sigma \left\{ 1 + \frac{1}{2}(1 - \sigma) \left[\Psi(r_{i-1/2}^+) - \frac{\Psi(r_{i-3/2}^+)}{r_{i-3/2}^+} \right] \right\} \leq 1 \quad (21.3.13a)$$

$$C_{i+1/2}^- = 0 \quad (21.3.13b)$$

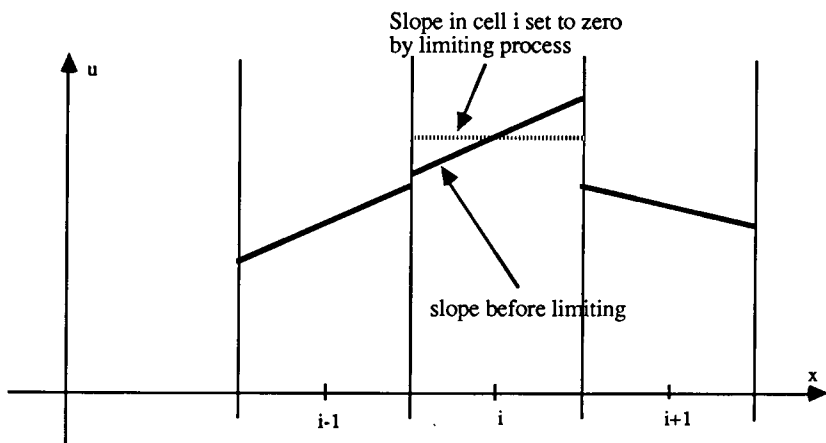


Figure 21.3.1 Slope limiting at an extremum for $\Psi(r_{i-1/2}^+)$

This leads to the following condition, for arbitrary values r and s :

$$\frac{\Psi(r)}{r} - \Psi(s) \leq \frac{2}{1-\sigma} \tag{21.3.14a}$$

and to

$$\Psi(s) - \frac{\Psi(r)}{r} \leq \frac{2}{\sigma} \tag{21.3.14b}$$

These equations can be satisfied in the range $0 \leq \sigma \leq 1$ if, in addition to the conditions (21.3.11), we impose

$$\Psi(r) \leq 2 \tag{21.3.15}$$

Therefore, the second-order upwind scheme will be TVD if the limiting function Ψ lies within the shaded area of Figure 21.3.2, which summarizes the above relations as

$$0 \leq \Psi(r) \leq \min(2r, 2) \tag{21.3.16}$$

Weaker conditions are considered by Roe (1985), namely

$$\frac{\Psi(r)}{r} \leq \frac{2}{1-\sigma} \tag{21.3.17a}$$

and

$$\Psi(r) \leq \frac{2}{\sigma} \tag{21.3.17b}$$

It is interesting to observe that the 'unlimited', non-TVD second-order upwind scheme of Warming and Beam corresponds to $\Psi = 1$. On the other hand,

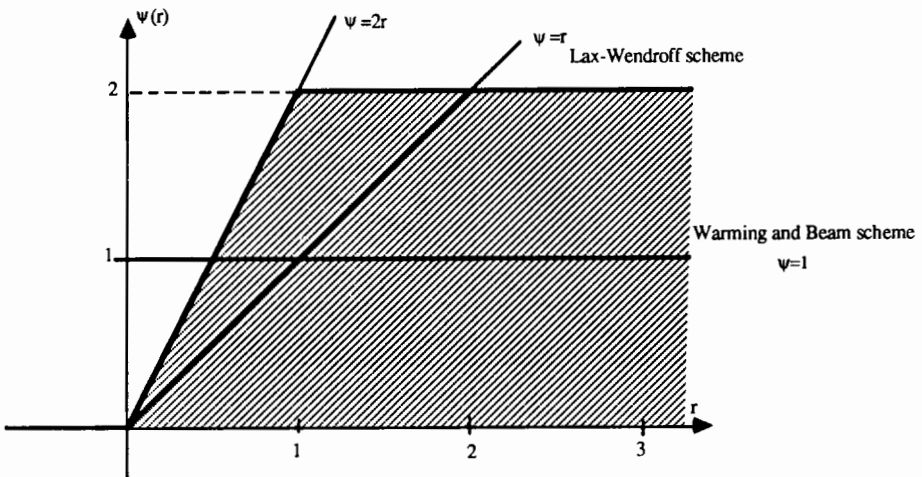


Figure 21.3.2 TVD region for the limiter function $\Psi(r)$ associated with second-order upwind schemes

equation (21.3.12) reduces to the Lax–Wendroff scheme for $\Psi(r) = r$, as can be observed by comparison with equation (E21.2.18). These two cases are plotted in Figure 21.3.2 and it is seen that they both fall outside the TVD region, as expected. Note also that both schemes satisfy the condition $\Psi(1) = 1$, which is a necessary requirement for second-order accuracy.

Indeed, in the smooth parts of the flow, that is almost everywhere, the values of r are close to one and if $\Psi \simeq 1$ the ‘limited’ schemes will maintain their second-order accuracy in the major parts of the flow, with the exception of the points or regions with sharp extrema in the variation of u . This can be seen from a Taylor expansion of r , for instance

$$r_{i+1/2}^- \simeq \frac{\Delta x u'_i - \Delta x^2 u''_i/2 + \dots}{\Delta x u'_i + \Delta x^2 u''_i/2 + \dots} \simeq 1 - \Delta x \frac{u''_i}{u'_i} + \dots \quad (21.3.18)$$

Hence r will deviate significantly from unity in regions where u is close to an extremum or has sharp gradients.

The above developments can also be reformulated in order to define a ‘limited’ form of the Lax–Wendroff scheme, by

$$u_i^{n+1} = u_i^n - \sigma(u_i^n - u_{i-1}^n) - \frac{\sigma}{2}(1 - \sigma)\delta^- [\Psi(r_{i+1/2}^-)(u_{i+1}^n - u_i^n)] \quad (21.3.19)$$

leading to the same conditions (21.3.17) on the Ψ functions (see Problem 21.23).

Actually, the analysis of TVD Lax–Wendroff schemes was at the basis of the present generalization of the concept of limiters (Davis, 1984; Roe, 1984; Sweby, 1984). It may seem surprising that this led to the same constraints on the limiter function Ψ , but demonstrates, on the other hand, the generality of the hereby defined limiters. In addition, as observed by Sweby (1984), the fact that the second-order (in time) explicit upwind scheme of Warming and Beam and the second-order explicit Lax–Wendroff schemes can both be made TVD by the same set of limiters allows the definition of a subset of the TVD region of Figure 21.3.2, where the ‘limited’ explicit schemes remain globally second-order accurate in time and space.

It has been noticed in Section 9.3 in Volume 1 that any linear second-order explicit scheme on the support $(i-2, i-1, i, i+1)$ can be obtained as a linear combination of the Warming and Beam and the Lax–Wendroff schemes. Consequently, any second-order ‘limited’ scheme could be based on a limiter function Ψ , which lies between the lines $\Psi = r$ and $\Psi = 1$, and remains within the shaded TVD area. This domain for second-order explicit TVD schemes is shown in Figure 21.3.3. As reported by Sweby (1984), the regions outside the lines $\Psi = r$ and $\Psi = 1$ lead to schemes that are overcompressive, that is turning sine waves into square wave forms.

Observe that all the limiters in this region contain the point $r = 1$, $\Psi = 1$ requested for second-order accuracy.

Various limiter functions have been defined in the literature. Van Leer (1974)

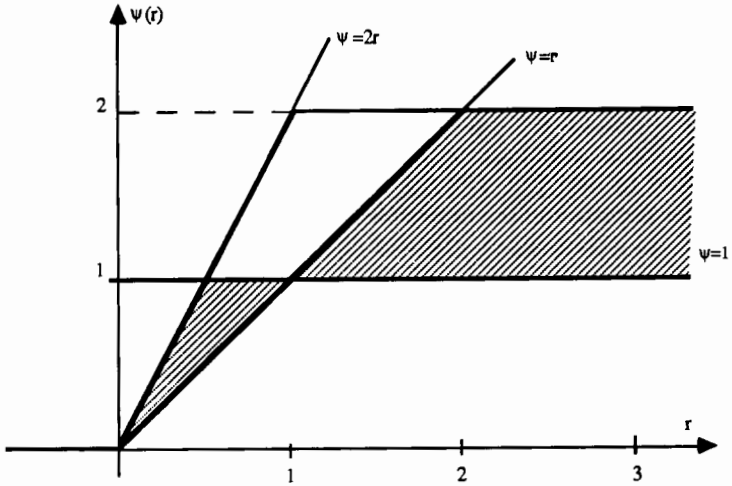


Figure 21.3.3 Limiter region for second-order TVD schemes

applied initially the formula

$$\Psi(r) = \frac{r + |r|}{1 + r} \quad (21.3.20)$$

shown in Figure 21.3.4(a). A similar limiter, with a smoother behaviour, has been applied by Van Albada *et al.* (1982):

$$\Psi(r) = \frac{r^2 + r}{1 + r^2} \quad (21.3.21)$$

It has the property of tending to 1 for large values of r .

The lowest boundary of the considered TVD domain is an often-applied limiter, although its resolution at contact discontinuities is not too good. It is shown in Figure 21.3.4(b) and can be represented by

$$\Psi(r) = \begin{cases} \min(r, 1) & \text{if } r > 0 \\ 0 & \text{if } r \leq 0 \end{cases} \quad (21.3.22)$$

and is a particular case of the *minmod* function, defined as the function that selects the number with the smallest modulus from a series of numbers when they all have the same sign, and zero otherwise. For two arguments:

$$\text{minmod}(x, y) = \begin{cases} x & \text{if } |x| < |y| \text{ and } xy > 0 \\ y & \text{if } |x| > |y| \text{ and } xy > 0 \\ 0 & \text{if } xy < 0 \end{cases} \quad (21.3.23a)$$

or in compact form:

$$\text{minmod}(x, y) = \text{sgn}(x) \cdot \max [0, \min (|x|, \text{sgn}(x) \cdot y)] \quad (21.3.23b)$$

Equation (21.3.22) can therefore be written as $\Psi(r) = \text{minmod}(1, r)$.

The upper limit of the second-order TVD domain has been considered by Roe (1985) under the nickname of 'Superbee' and shown to have excellent resolution properties for contact discontinuities. It is shown in Figure 21.3.4(c) and defined by

$$\Psi(r) = \max [0, \min (2r, 1), \min (r, 2)] \quad (21.3.24)$$

This limiter actually amplifies certain contributions, when $\Psi > 1$, while remaining within the TVD bounds. This explains the property of this 'Superbee' limiter in counteracting the excessive spreading of contact discontinuities

The limits of the TVD region are members of a family of limiters, based on a single parameter β in the range $1 < \beta < 2$ (Sweby, 1984):

$$\Psi(r) = \max [0, \min (\beta r, 1), \min (r, \beta)] \quad 1 \leq \beta \leq 2 \quad (21.3.25)$$

These β limiters are shown in Figure 21.3.4(d).

All of these limiters share the symmetry property

$$\frac{\Psi(r)}{r} = \Psi\left(\frac{1}{r}\right) \quad (21.3.26)$$

indicating that forward and backward gradients are treated in the same way. Alternatively, this property ensures that the limited gradients remain associated with a linear variation of the u variable within each cell. This will be shown in the following subsection.

Finally, let us mention for completeness the limiter used by Chakravarthy and Osher (1983):

$$\Psi(r) = \max [0, \min (r, \beta)] \quad 1 \leq \beta \leq 2 \quad (21.3.27)$$

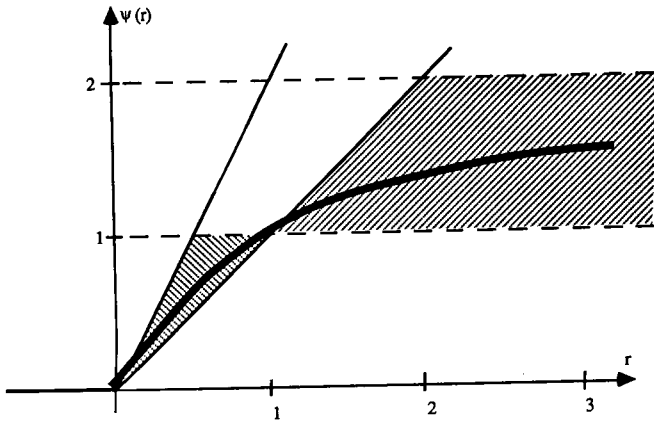
shown in Figure 21.3.4(e). Note that this limiter does not satisfy the symmetry condition (21.3.26).

It is important to observe at this point that all TVD schemes are strictly non-linear due to the dependence on the δu ratios, even when applied to the linear convection equation.

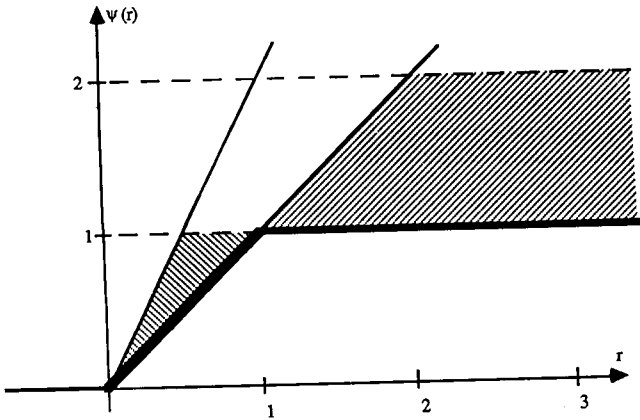
More insight into the action of the limiters is obtained by considering the specific contribution of the second-order terms of scheme (21.3.2) to the new solution at point i at time level $n + 1$.

The second term $(u_i - u_{i-1})$ is modified by a non-linear correction $\Psi(u_i - u_{i-1})$. With the 'minmod' limiter, we actually set the following restrictions:

- (1) If the gradient $(u_{i+1} - u_i)/\Delta x < (u_i - u_{i-1})/\Delta x$, that is if $r < 1$, $\Psi(r) = r$ and the contribution $(u_i^n - u_{i-1}^n)$ to u_i^{n+1} is replaced by the smaller quantity $(u_{i+1}^n - u_i^n)$.
- (2) If $r > 1$, the contribution $(u_i - u_{i-1})$ remains unchanged.



(a)



(b)

Figure 21.3.4 Limiters for second-order TVD schemes

- (a) Van Leer's limiter $\psi = (r + |r|)/(1 + r)$
- (b) Minmod limiter $\psi(r) = \text{minmod}(r, 1)$
- (c) Roe's 'Superbee' limiter $\psi = \max[0, \min(2r, 1), \min(r, 2)]$
- (d) General β -limiters $\psi = \max[0, \min(\beta r, 1), \min(r, \beta)]$
- (e) Chakravarthy and Osher limiter $\psi(r) = \max[0, \min(r, \beta)]$

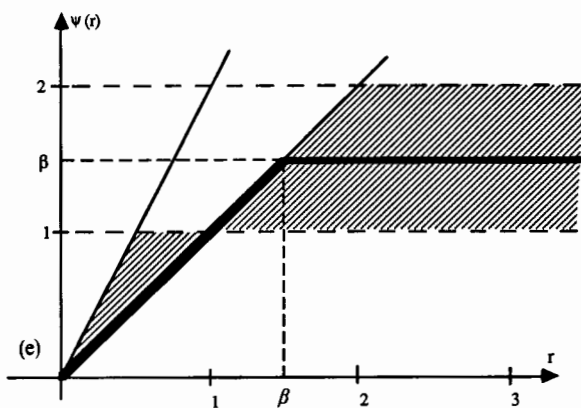
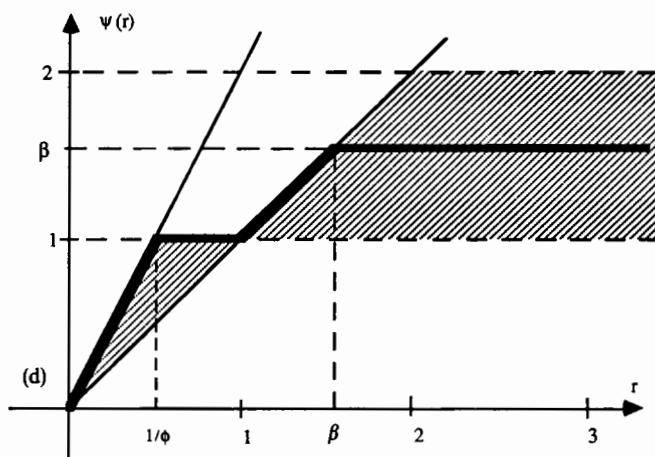
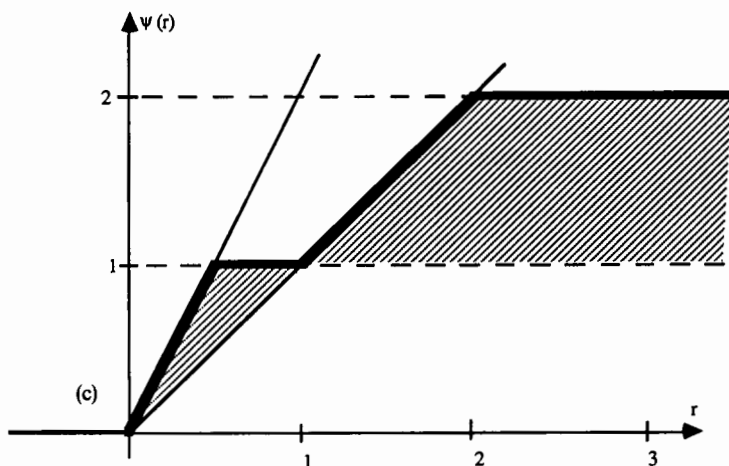


Figure 21.3.4 (Continued)

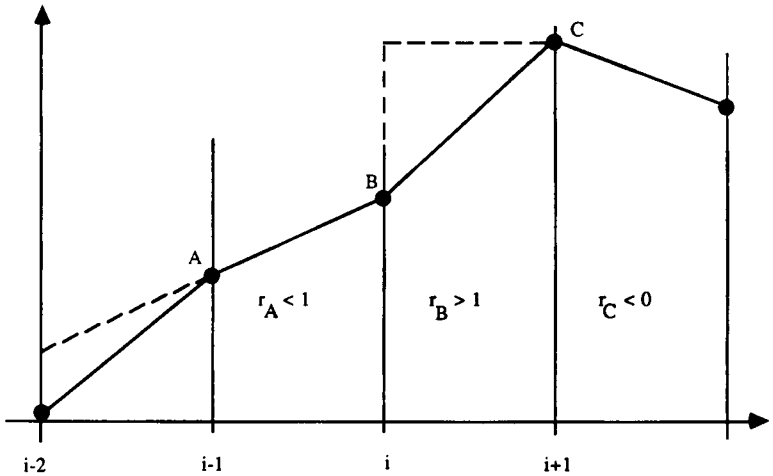


Figure 21.3.5 Typical behaviour of oscillatory solution and effect of minmod limiter

- (3) If the slopes of consecutive intervals change sign, the updated point i receives no contribution from the upstream interval.

Referring to Figure 21.3.5, point A is associated with a ratio $r < 1$ and the contribution to $u(A)$ at time level $n + 1$ is restricted to the smaller, downstream variation $u(B) - u(A)$. At point B, $r > 1$ and the second-order contribution to $u(B)$ at level $n + 1$ remains unchanged. At point C, $r < 0$ and the contribution to $u(C)$ from the upstream interval is set to zero.

With the 'Superbee' limiter, on the other hand, some contributions are enhanced instead of reduced, while remaining within the TVD region. If $r < \frac{1}{2}$, $\Psi = 2r$ and the contribution $(u_i^n - u_{i-1}^n)$ to u_i^{n+1} is replaced by the smaller quantity $2(u_{i+1}^n - u_i^n)$, while for $\frac{1}{2} < r < 1$, the larger quantity is kept. For $1 < r < 2$, $\Psi = r$ and again the larger quantity is transferred as a contribution to the updated solution. Finally, for $r > 2$ the smaller quantity $2(u_i - u_{i-1})$ is transferred. Figure 21.3.6 reflects the effects of the Superbee limiter, where the dashed lines are the corrected slopes as they contribute to the downstream nodes.

The specific effect of the limiters on smooth flows can be seen from a comparison of Figure 21.3.7, which displays the results of the convection of a low-frequency sinusoidal wave. The linear convection equation is solved with the second-order limited upwind scheme (21.3.12), applying the minmod and the Superbee limiters. Figure 21.3.7(a) is obtained with the first-order upwind scheme and the excessive dissipation inherent to all first-order schemes is apparent, when compared to the exact solution. Figure 21.3.7(b) shows the improvement obtained with the standard second-order upwind scheme (21.1.27), at the expense of oscillations appearing at the slope discontinuities, typical of all second-order schemes. The introduction of the limiters in the second-order

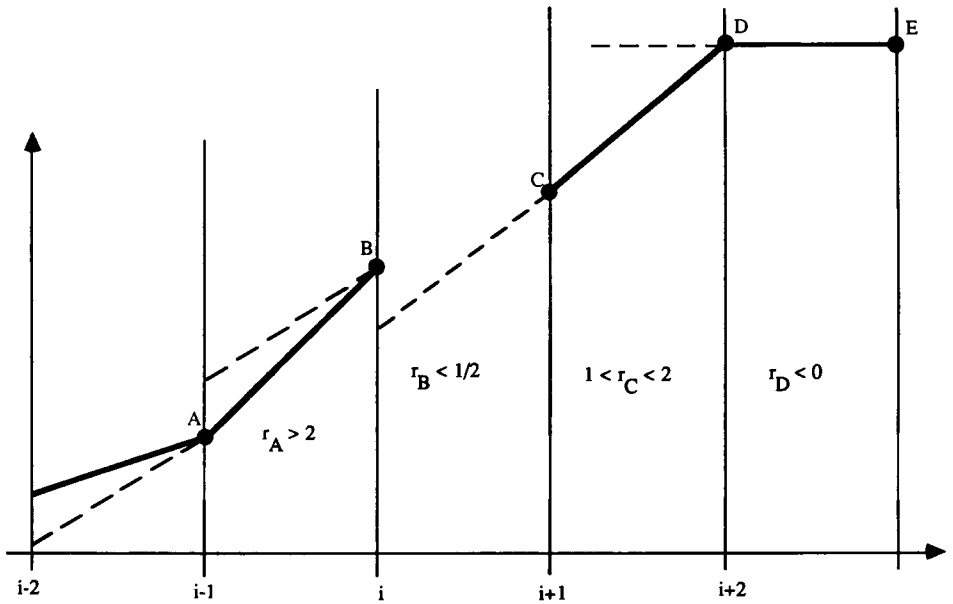


Figure 21.3.6 Typical behaviour of oscillatory solution and effect of Superbee limiter

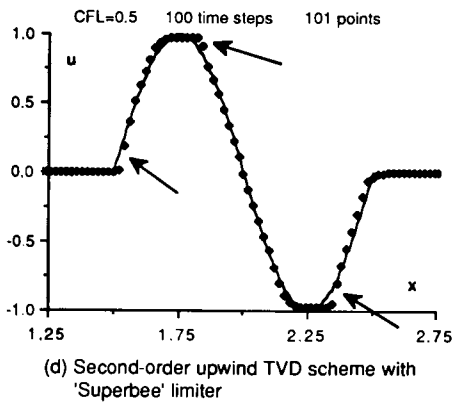
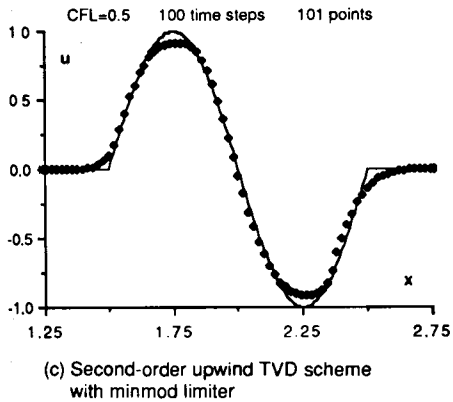
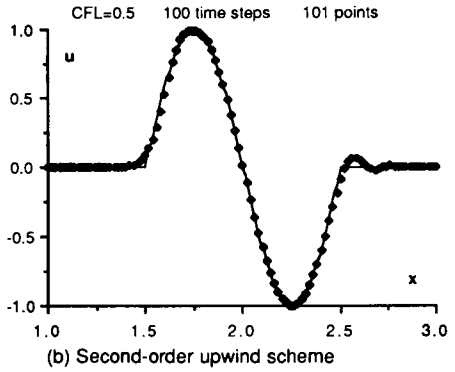
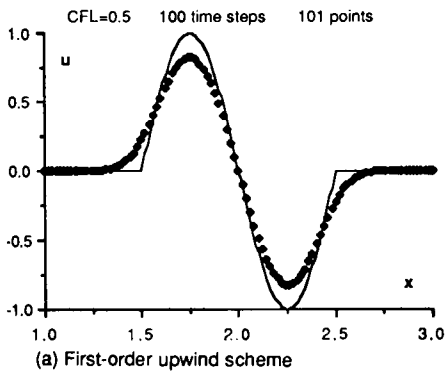
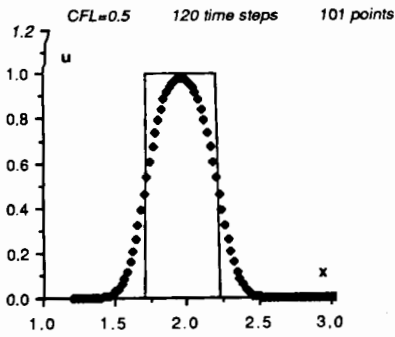
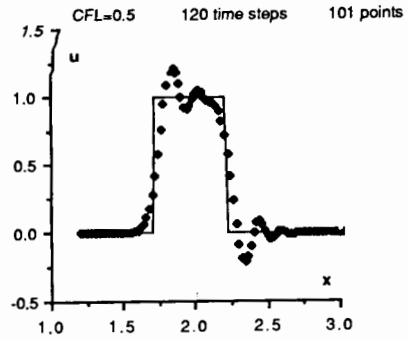


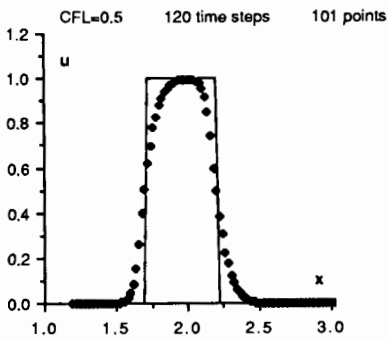
Figure 21.3.7 Effects of limiters on the linear convection of a sinusoidal wave



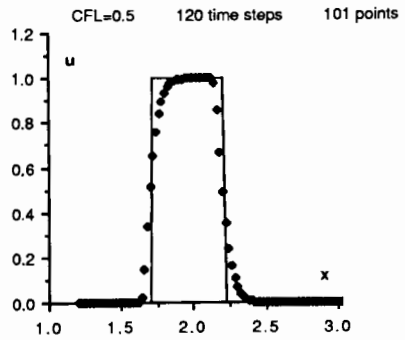
(a) First-order upwind scheme



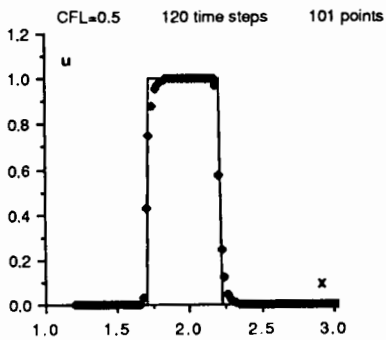
(b) Second-order upwind scheme



(c) Second-order TVD upwind scheme with minmod limiter



(d) Second-order TVD upwind scheme with Van Leer limiter



(e) Second-order TVD upwind scheme with 'Superbee' limiter

Figure 21.38 Effects of limiters on the linear convection of a square wave after 120 time steps

upwind scheme removes completely the oscillations, producing monotone profiles. However, the minmod limiter reduces locally the accuracy of the solution around the extrema, as seen in Figure 21.3.7(c), bringing it close to first order as a consequence of equation (21.3.11a). Finally, Figure 21.3.7(d) shows the behaviour of the Superbee limiter where its overcompressive property is clearly seen. The maxima are flattened and the gradients are made steeper. This is well adapted for sharp discontinuities but not too adequate for smooth profiles.

An overruling of condition (21.3.11a) has been suggested by Hartwich *et al.* (1988) by setting $\Psi(r) = \max[\beta, \min(r, 1)]$ with $\beta = -1$ as a generalization of the minmod limiter, to which it reduces when $\beta = 0$.

Attempts to maintain uniform second-order accuracy of non-oscillatory schemes have been developed by Harten and Osher (1987) by enlarging the TVD concept to a broader class of schemes, designated as essentially non-oscillatory (ENO), at the cost, however, of an increased complexity of the schemes.

The effects of the limiters on shock/contact discontinuities can be seen from the convection of a square wave. Figures 21.3.8 and 21.3.9 compare the linear

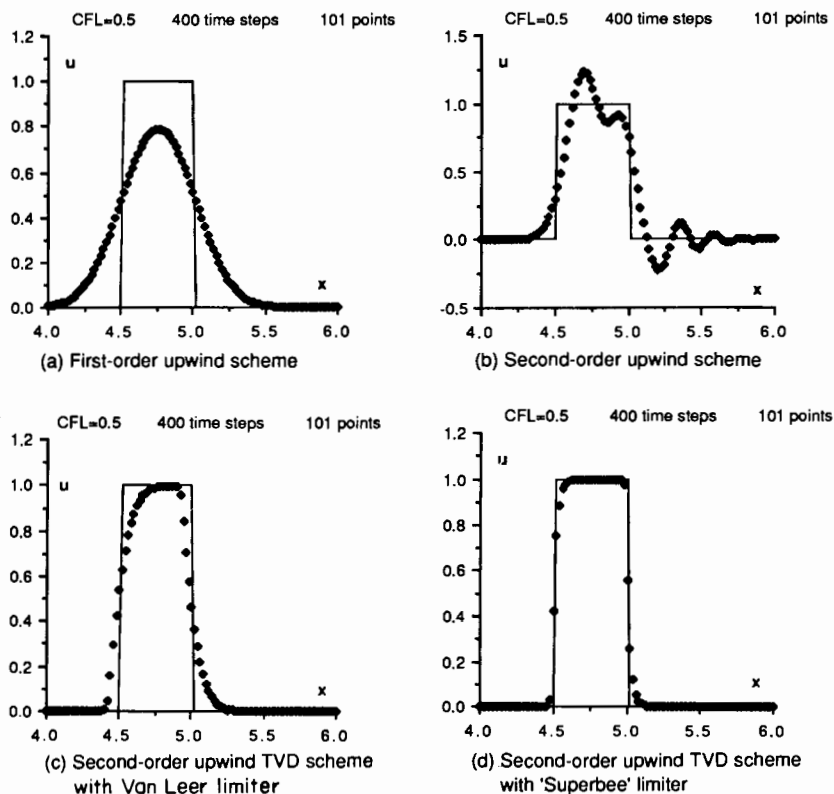


Figure 21.3.9 Effects of limiters on the linear convection of a square wave after 400 time steps

convection of a square wave after 120 and 400 time steps at a Courant number of 0.5. Figures 21.3.8(a) and 21.3.9(a) are obtained with the first-order upwind scheme, showing its excessive diffusion; Figures 21.3.8(b) and 21.3.9(b) are obtained with the second-order upwind scheme, showing the strong oscillations around the discontinuities. Figures 21.3.8(c), (d), (e) are computed with the minmod, Van Leer and Superbee limiters respectively and generate monotone profiles. The minmod limiter, however, is still too diffusive, while the Superbee limiter produces excellent results, with extremely sharp discontinuities. The Van Leer limiter has properties between the previous two. Superbee maintains the sharpness of the profile indefinitely, as can be seen by comparing with a similar calculation after 400 time steps, shown in Figure 21.3.9(c). The points in the transition region are practically unchanged from time step 120 to time step 400, while it is seen that the Van Leer limiter still continues to generate a small, but continuous, diffusion of the transition profiles.

21.3.2 General definition of flux limiters

The limiters defined in the previous section can now easily be generalized to non-linear scalar conservation equations by an appropriate redefinition of the slope ratios (21.3.3).

Considering the second-order upwind numerical flux (21.1.35) associated with a first-order monotone numerical flux f^* , the TVD form of the corresponding semi-discretized scheme is written as

$$\frac{du_i}{dt} = -\frac{1}{\Delta x} \delta^- [f_{i+1/2}^* + \frac{1}{2} \Psi_{i-1/2}^+ (f_i - f_{i-1/2}^*) + \frac{1}{2} \Psi_{i+3/2}^- (f_{i+1} - f_{i+3/2}^*)] \quad (21.3.28)$$

The limiter functions Ψ^\pm are defined as functions of the flux difference ratios

$$r_{i+1/2}^+ = \frac{f_{i+2} - f_{i+3/2}^*}{f_{i+1} - f_{i+1/2}^*} \quad r_{i+1/2}^- = \frac{f_{i-1} - f_{i-1/2}^*}{f_i - f_{i+1/2}^*} \quad (21.3.29)$$

Note that for a flux splitting scheme, the above definitions reduce to

$$r_{i+1/2}^+ = \frac{f_{i+2}^+ - f_{i+1}^+}{f_{i+1}^+ - f_i^+} \quad r_{i+1/2}^- = \frac{f_i^- - f_{i-1}^-}{f_{i+1}^- - f_i^-} \quad (21.3.30)$$

and are indeed a straightforward generalization of the definitions (21.3.3).

With the assumptions (21.3.7), equation (21.3.28) becomes

$$\begin{aligned} \frac{du_i}{dt} = & -\frac{1}{\Delta x} \left[1 + \frac{1}{2} \Psi(r_{i-1/2}^+) - \frac{1}{2} \frac{\Psi(r_{i-3/2}^+)}{r_{i-3/2}^+} \right] (f_i - f_{i-1/2}^*) \\ & - \frac{1}{\Delta x} \left[1 + \frac{1}{2} \Psi(r_{i+1/2}^-) - \frac{1}{2} \frac{\Psi(r_{i+3/2}^-)}{r_{i+3/2}^-} \right] (f_{i+1/2}^* - f_i) \end{aligned} \quad (21.3.31a)$$

or with the definitions (21.2.36)

$$\begin{aligned} \frac{du_i}{dt} = & -\frac{1}{\Delta x} \left[1 + \frac{1}{2} \Psi(r_{i-1/2}^+) - \frac{1}{2} \frac{\Psi(r_{i-3/2}^+)}{r_{i-3/2}^+} \right] a_{i-1/2}^+ (u_i - u_{i-1}) \\ & - \frac{1}{\Delta x} \left[1 + \frac{1}{2} \Psi(r_{i+1/2}^-) - \frac{1}{2} \frac{\Psi(r_{i+3/2}^-)}{r_{i+3/2}^-} \right] a_{i+1/2}^- (u_{i+1} - u_i) \end{aligned} \quad (21.3.31b)$$

Comparing with the incremental form (21.2.35) and the TVD properties of the first-order reference scheme, the TVD conditions (21.3.6) for the second-order scheme are obtained. Hence, the previously defined limiters are fully valid with, however, the adapted definitions (21.3.29) for the ratios of flux differences.

Example 21.3.1 Second-order semi-discretized TVD Roe scheme

The first-order Roe scheme for a scalar conservation law is defined by the numerical flux

$$f_{i+1/2}^{*(R)} = \frac{1}{2}(f_i + f_{i+1}) - \frac{1}{2}|a|_{i+1/2}(u_{i+1} - u_i) \quad (E21.3.1)$$

or, equivalently,

$$f_{i+1/2}^{*(R)} = \frac{1}{2}(f_i + f_{i+1}) - \frac{1}{2} \operatorname{sgn}(a_{i+1/2}) \cdot (f_{i+1} - f_i) \quad (E21.3.2)$$

With

$$f_i - f_{i-1/2}^{*(R)} = \frac{1}{2}(a + |a|)_{i-1/2}(u_i - u_{i-1}) \equiv a_{i-1/2}^+(u_i - u_{i-1}) \quad (E21.3.3)$$

$$f_i - f_{i+1/2}^{*(R)} = -\frac{1}{2}(a - |a|)_{i+1/2}(u_{i+1} - u_i) \equiv -a_{i+1/2}^-(u_{i+1} - u_i) \quad (E21.3.4)$$

the second-order TVD numerical flux in equation (21.3.28) becomes

$$f_{i+1/2}^{*(2)} = f_{i+1/2}^{*(R)} + \frac{1}{2} \Psi_{i-1/2}^+ a_{i-1/2}^+ (u_i - u_{i-1}) - \frac{1}{2} \Psi_{i+3/2}^- a_{i+3/2}^- (u_{i+2} - u_{i+1}) \quad (E21.3.5)$$

The limiter is defined as

$$\Psi_{i-1/2}^+ = \Psi(r_{i-1/2}^+) = \Psi \left[\frac{a_{i+1/2}^+(u_{i+1} - u_i)}{a_{i-1/2}^+(u_i - u_{i-1})} \right] \quad (E21.3.6)$$

$$\Psi_{i+3/2}^- = \Psi(r_{i+3/2}^-) = \Psi \left[\frac{a_{i+1/2}^-(u_{i+1} - u_i)}{a_{i+3/2}^-(u_{i+2} - u_{i+1})} \right] \quad (E21.3.7)$$

An alternative formulation is given by the following expression, assuming the limiter has the symmetry property $\Psi(r) = r\Psi(1/r)$:

$$f_{i+1/2}^{*(2)} = f_{i+1/2}^{*(R)} + \frac{1}{2} \Phi^+ a_{i+1/2}^+ (u_{i+1} - u_i) - \frac{1}{2} \Phi^- a_{i+1/2}^- (u_{i+1} - u_i) \quad (E21.3.8)$$

where Φ^\pm are the limiters for the inverse variables

$$\Phi^+ = \Psi \left[\frac{a_{i-1/2}^+(u_i - u_{i-1})}{a_{i+1/2}^+(u_{i+1} - u_i)} \right] \quad (E21.3.9)$$

$$\Phi^- = \Psi \left[\frac{a_{i+3/2}^-(u_{i+2} - u_{i+1})}{a_{i+1/2}^-(u_{i+1} - u_i)} \right] \quad (E21.3.10)$$

Observe that the unlimited form of scheme (E21.3.8), obtained with $\Phi^\pm = 1$, is the second-order central scheme of numerical flux equal to $(f_i + f_{i+1})/2$, which is already known to generate instabilities.

21.3.3 Limiters for variable extrapolation—MUSCL—method

With the variable extrapolation—MUSCL—method, described in Section 21.1.1, the piecewise constant approximation of the first-order Godunov-type schemes is replaced by a piecewise linear (or eventually quadratic) approximation. As noticed earlier, in particular with Figure 21.2.1, the slopes of the linear variations have to be limited in order to avoid overshoots in the numerical solution. A careful analysis of Figure 21.2.1 shows that the overshoots would be avoided if the interface values were to remain between the adjacent average cell values; that is, referring to the definitions of Section 21.1, if

$$u_{i-1/2}^R \geq u_{i-1} \quad (21.3.32a)$$

$$u_{i+1/2}^L \leq u_{i+1} \quad (21.3.32b)$$

with $u_{i-1} < u_{i+1}$ remembering that u_i and u_{i-1} are cell-averaged quantities.

In order to ensure these monotonicity conditions, limiters are introduced in the definitions (21.1.6) and (21.1.7) of the extrapolated interface values. Setting $\varepsilon = 1$ for second-order spatial accuracy, the slopes are restricted as follows, the 'tilde' indicating monotonicity-satisfying quantities:

$$\tilde{u}_{i+1/2}^L = u_i + \frac{1}{4}[(1 - \kappa)\Phi_{i-1/2}^+(u_i - u_{i-1}) + (1 + \kappa)\Phi_{i+1/2}^-(u_{i+1} - u_i)] \quad (21.3.33)$$

with

$$\Phi_{i-1/2}^+ = \Phi(r_{i-1/2}^+) \quad \Phi_{i+1/2}^- = \Phi(r_{i+1/2}^-) \quad (21.3.34)$$

The slope limiters Φ^\pm are defined as in (21.3.7), and writing r^L for $r_{i-1/2}^+$ as defined by equation (21.3.3), we have

$$\tilde{u}_{i+1/2}^L = u_i + \frac{1}{4} \left[(1 - \kappa)\Phi(r^L) + (1 + \kappa)r^L\Phi\left(\frac{1}{r^L}\right) \right] (u_i - u_{i-1}) \quad (21.3.35)$$

with

$$r^L = \frac{u_{i+1} - u_i}{u_i - u_{i-1}} \quad (21.3.36)$$

The left interface value can be written as

$$\tilde{u}_{i+1/2}^L = u_i + \frac{1}{2}\Psi^L(u_i - u_{i-1}) \quad (21.3.37)$$

with

$$\Psi^L = \frac{1}{2} \left[(1 - \kappa)\Phi(r^L) + (1 + \kappa)r^L\Phi\left(\frac{1}{r^L}\right) \right] \quad (21.3.38)$$

For $\kappa = -1$ the limiter Ψ is equal to $\phi(r)$: $\Psi = \Phi(r)$.

Similarly, the right interface value is 'limited' as follows:

$$\tilde{u}_{i+1/2}^R = u_{i+1} - \frac{1}{4}[(1 - \kappa)\Phi_{i+3/2}^-(u_{i+2} - u_{i+1}) + (1 + \kappa)\Phi_{i+1/2}^+(u_{i+1} - u_i)] \quad (21.3.39)$$

with

$$\Phi_{i+1/2}^+ = \Phi(r_{i+1/2}^+) \quad \Phi_{i+3/2}^- = \Phi(r_{i+3/2}^-) \quad (21.3.40)$$

Defining

$$r^R = \frac{u_{i+1} - u_i}{u_{i+2} - u_{i+1}} \quad (21.3.41)$$

equation (21.3.39) can be written as

$$\tilde{u}_{i+1/2}^R = u_{i+1} - \frac{1}{2}\Psi^R(u_{i+2} - u_{i+1}) \quad (21.3.42a)$$

with

$$\Psi^R = \frac{1}{2} \left[(1 - \kappa)\Phi(r^R) + (1 + \kappa)r^R\Phi\left(\frac{1}{r^R}\right) \right] \quad (21.3.42b)$$

to be compared to equation (21.1.9).

An alternative form is as follows:

$$\tilde{u}_{i+1/2}^R = u_{i+1} - \frac{1}{2}\hat{\Psi}^R(u_{i+1} - u_i) \quad (21.3.43a)$$

with

$$\hat{\Psi}^R = \frac{1}{2} \left[\frac{(1 - \kappa)\Phi(r^R)}{r^R} + (1 + \kappa)\Phi\left(\frac{1}{r^R}\right) \right] \quad (21.3.43b)$$

With the above definitions, the second-order upwind schemes defined in Section 21.1.5 are made TVD by defining the numerical flux of the semi-discretized schemes as

$$f_{i+1/2}^{*(2)} = f^*(\tilde{u}_{i+1/2}^L, \tilde{u}_{i+1/2}^R) \quad (21.3.44)$$

For example, a higher-order flux splitting method defined by

$$f_{i+1/2}^{*(FS)} = f^+(\tilde{u}_{i+1/2}^L) + f^-(\tilde{u}_{i+1/2}^R) \quad (21.3.45)$$

is TVD under the conditions (21.3.17). Indeed, in the linear case the numerical flux (21.3.45) reduces to

$$f_{i+1/2}^{*(FS)} = a^+ \tilde{u}_{i+1/2}^L + a^- \tilde{u}_{i+1/2}^R \quad (21.3.46)$$

and leads to the semi-discretized scheme

$$\frac{du_i}{dt} = -\frac{a^+}{\Delta x}(\tilde{u}_{i+1/2}^L - \tilde{u}_{i-1/2}^L) - \frac{a^-}{\Delta x}(\tilde{u}_{i+1/2}^R - \tilde{u}_{i-1/2}^R) \quad (21.3.47)$$

which is identical in form to equation (21.3.2). Hence, the generalized limiters Ψ have to satisfy the conditions (21.3.17).

Consequently, any of the limiters of Section 21.3.1 can be selected for Ψ . In addition, the fully upwind scheme $\kappa = -1$ is completely identical to scheme (21.3.2) and therefore the slope limiters Φ are also identical to the Ψ limiters.

On the other hand, the relations (21.3.38) and (21.3.43) show that $\Psi = \Phi$ for all values of κ if Φ satisfies the symmetry property (21.3.26), that is if

$$\Phi(r) = r\Phi\left(\frac{1}{r}\right) \quad (21.3.48)$$

Since this property is satisfied by all the limiters considered previously, with the exception of (21.3.27), the TVD formulation of the second-order upwind schemes obtained with the variable extrapolation—MUSCL—method is completely defined when one of these limiters is chosen.

Special consideration is to be given to the choice (21.3.27) for the slope limiter $\Phi(r)$, leading to

$$\Psi(r) = \frac{1}{2}[(1 - \kappa) \min\text{mod}(r, \beta) + (1 + \kappa) \min\text{mod}(1, \beta r)] \quad \beta \geq 1 \quad (21.3.49)$$

The conditions $\Psi(r) < \min(2, 2r)$ imply restrictions on the parameter β :

$$1 \leq \beta \leq \frac{3 + \kappa}{1 + \kappa} \quad \text{if } r < 1 \quad \text{and} \quad \beta r < 1 \quad (21.3.50a)$$

For larger values of r ,

$$1 \leq \beta \leq \frac{3 - \kappa}{1 - \kappa} \quad \text{if } r \geq \beta \quad (21.3.50b)$$

In the intermediate range $1/\beta < r < \beta$, $\Psi(r)$ is independent of β and always lies in the TVD region of Figure 21.3.4.

Alternative variant

Instead of the general form of equation (21.3.33) for u^L we can also select from the start $\Phi^+ = \Phi^-$ and define monotone variable extrapolations by the relation (21.3.37) with Ψ defined by

$$\tilde{\Psi}_{i-1/2} = \frac{1}{2}[(1 - \kappa) + (1 + \kappa)r^L]\Phi(r^L) \quad (21.3.51)$$

instead of (21.3.38).

The same approach for the right interface variable u^R leads to the expression (21.3.42) with, however, Ψ defined by

$$\tilde{\Psi}_{i+3/2} = \frac{1}{2}[(1 - \kappa) + (1 + \kappa)r^R]\Phi(r^R) \quad (21.3.52)$$

instead of (21.3.43). This introduction of the limiters in the MUSCL approach actually consists of the replacement of the factor ε in equations (21.1.6) and (21.1.7) by the limiter function $\Phi(r)$. The non-limited case is associated with $\Phi = 1$.

It is interesting to observe that the limited variables will have a linear distribution over each cell, that is

$$\hat{u}_{i+1/2}^L - u_i = u_i - \hat{u}_{i-1/2}^R \quad (21.3.53)$$

if the symmetry property (21.3.48) is satisfied by the $\tilde{\Psi}$ or $\hat{\Psi}$ limiters. It is easily

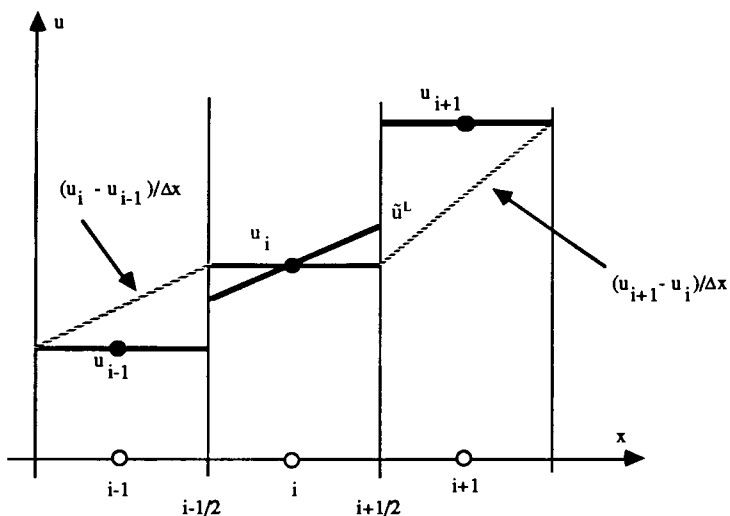
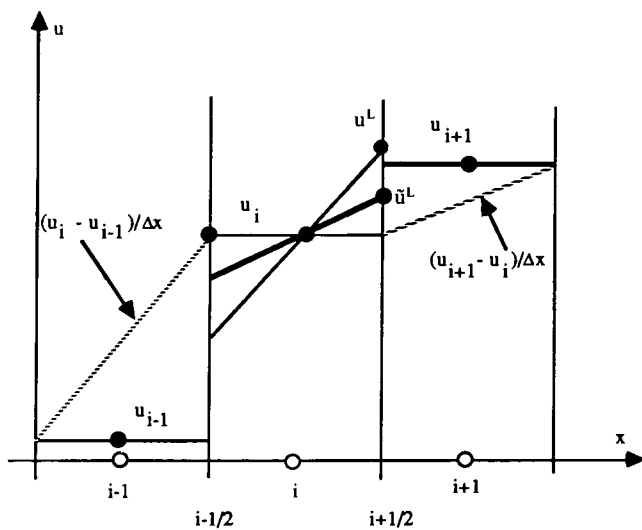
(a) Gradient ratio $r > 1$ (b) Gradient ratio $r < 1$

Figure 21.3.10 Effect of minmod limiter on variable extrapolation

seen that this is the case if the Φ limiters satisfy this symmetry condition. Therefore, and although not essential, it may be useful to include this condition, which treats forward and backward gradients in the same way.

It should also be mentioned at this point that somewhat more restrictive conditions for generalized, semi-discretized MUSCL schemes to be TVD have been derived by Osher (1985) for general first-order E-schemes. Osher (1985) obtains the following sufficient conditions:

$$0 \leq \Psi(r) \leq 1 \quad \text{and} \quad 0 \leq \frac{\Psi(r)}{r} \leq 1 \quad (21.3.54a)$$

or

$$0 \leq \Psi(r) \leq \min(1, r) \quad (21.3.54b)$$

to be compared with condition (21.3.17). This corresponds to the lower limit of the TVD region of Figure 21.3.3, that is to the minmod limiter (21.3.22).

The practical effects of the limiters on the extrapolated variables at the cell interfaces are illustrated in Figure 21.3.10. With the definition (21.3.36) for the ratio of consecutive gradients, Figure 21.3.10(a) corresponds to a ratio $r > 1$. With the minmod limiter $\Psi(r) = \min\text{mod}(r, 1)$, equation (21.3.37) will select a slope $(u_i - u_{i-1})$. For $r < 1$ the selected slope is $(u_{i+1} - u_i)$, leading to the interface value \tilde{u}^L instead of the unlimited value u^L , which would be obtained for $\kappa = -1$, as shown in Figure 21.3.10(b).

21.4 TIME-INTEGRATION METHODS FOR TVD SCHEMES

The second-order space-accurate TVD numerical fluxes of the previous sections have now to be associated with a time-integration method.

As already noticed in relation to the central schemes in Chapters 17 and 18, two families of time-integration methods can be defined: the separate time and space discretizations, based on linear multi-step (implicit) methods or Runge-Kutta time-integration schemes, or the combined space-time methods in the line of the Lax-Wendroff technique. The former approach generates numerical fluxes which are independent of the time step and are more appropriate for steady-state calculations, while the latter can be considered as better adapted for time-dependent flows, without excluding, however, the application of any of these schemes to the other family of problems.

With the first approach, the numerical fluxes of the semi-discretized formulation can be applied without additional considerations, the resulting time-dependent scheme remaining TVD with, however, the additional CFL-like condition (21.2.54) for explicit as well as implicit schemes.

With the combined space-time approach, the second-order time-integration method generates additional space-discretized terms, which can affect the monotonicity preservation of the semi-discretized TVD numerical fluxes. Hence, the numerical flux of the time-dependent scheme will have to be analysed and redefined in an appropriate way in order to ensure the TVD conditions.

The simplest explicit time integration is the first-order Euler method, which is unconditionally unstable for second-order space-accurate flux discretizations. However, and very remarkably indeed, making the scheme TVD via the non-linear limiters has the unexpected consequence of generating a conditionally stable, first order in time and second order in space upwind scheme.

21.4.1 Explicit TVD schemes of first-order accuracy in time

Let us consider the general form of the semi-discretized scheme (21.3.31). If a first-order Euler method is selected as time integration, then the following scheme is obtained:

$$u_i^{n+1} = u_i^n - \tau \left[1 + \frac{1}{2} \Psi(r_{i-1/2}^+) - \frac{1}{2} \frac{\Psi(r_{i-3/2}^+)}{r_{i-3/2}^+} \right] (f_i - f_{i-1/2}^*)^n - \tau \left[1 + \frac{1}{2} \Psi(r_{i+1/2}^-) - \frac{1}{2} \frac{\Psi(r_{i+3/2}^-)}{r_{i+3/2}^-} \right] (f_{i+1/2}^* - f_i)^n \quad (21.4.1)$$

As already stated, the non-limited form of this scheme with $\Psi = 1$ is linearly, unconditionally unstable. It is therefore remarkable to observe that the *non-linear* TVD version of the same scheme is *conditionally stable* under the TVD condition (21.2.44), since the boundedness of the total variation of the solution ensures the stability of the scheme. We now define local, positive and negative CFL numbers through

$$\sigma_{i+1/2}^+ = \tau \frac{f_{i+1} - f_{i+1/2}^*}{u_{i+1} - u_i} = \tau \frac{f_{i+1}^+ - f_i^+}{u_{i+1} - u_i} \quad (21.4.2a)$$

$$\sigma_{i+1/2}^- = \tau \frac{f_{i+1/2}^* - f_i}{u_{i+1} - u_i} = \tau \frac{f_{i+1}^- - f_i^-}{u_{i+1} - u_i} \quad (21.4.2b)$$

with the properties

$$\sigma_{i+1/2}^+ + \sigma_{i+1/2}^- = \sigma_{i+1/2} = \tau \frac{f_{i+1} - f_i}{u_{i+1} - u_i} = \tau a_{i+1/2} \quad (21.4.3)$$

$$\sigma_{i+1/2}^+ - \sigma_{i+1/2}^- = |\sigma|_{i+1/2} = \tau \left| \frac{f_{i+1} - f_i}{u_{i+1} - u_i} \right| = \tau |a|_{i+1/2} \quad (21.4.4)$$

Equation (21.4.1) defines the C^\pm coefficients as

$$\tau C_{i-1/2}^+ = \sigma_{i-1/2}^+ \left[1 + \frac{1}{2} \Psi(r_{i-1/2}^+) - \frac{1}{2} \frac{\Psi(r_{i-3/2}^+)}{r_{i-3/2}^+} \right] \quad (21.4.5a)$$

$$\tau C_{i+1/2}^- = \sigma_{i+1/2}^- \left[1 + \frac{1}{2} \Psi(r_{i+1/2}^-) - \frac{1}{2} \frac{\Psi(r_{i+3/2}^-)}{r_{i+3/2}^-} \right] \quad (21.4.5b)$$

and the TVD condition (21.2.44) becomes

$$\tau(C_{i+1/2}^+ - C_{i+1/2}^-) \leq \tau |a|_{i+1/2} \left(\frac{1 + \alpha}{2} \right) \leq 1 \quad (21.4.6)$$

where the limiter Ψ is selected under the constraint

$$\left| \Psi(s) - \frac{\Psi(r)}{r} \right| \leq \alpha \quad (21.4.7)$$

where $0 < \alpha \leq 2$ for second-order accuracy. Hence, the first order in time and second order in space upwind TVD scheme (21.4.1) is stable under the CFL condition,

$$|\sigma| \leq \frac{2}{2 + \alpha} \quad (21.4.8)$$

With the minmod limiter $\Psi(r) = \text{minmod}(r, 1)$ the scheme is stable for $|\sigma| < \frac{2}{3}$, while the Superbee limiter, for instance, would lead to a restriction $|\sigma| < \frac{1}{2}$. These conditions are generally far too restrictive for stationary problems.

In these cases implicit schemes are a most interesting option, even more so because the TVD condition ensures that the implicit operators are diagonal dominant.

21.4.2 Implicit TVD schemes

A general implicit linear multi-step scheme applied to the second-order TVD semi-discretized equations can be written as, taking $\xi = 0$ to avoid three time levels,

$$\Delta u_i^n + \tau \theta (f_{i+1/2}^{*(2)n+1} - f_{i-1/2}^{*(2)n+1}) = -\tau(1 - \theta)(f_{i+1/2}^{*(2)n} - f_{i-1/2}^{*(2)n}) \quad (21.4.9)$$

The left-hand side implicit operators are linearized in time, as

$$f^{*(2)n+1} = f^{*(2)n} + f_u^{*(2)n}(u^{n+1} - u^n) \quad (21.4.10)$$

where the subscript u indicates a derivative. The Jacobians of the second-order numerical fluxes are generally computationally expensive, leading also to implicit operators with a five-point support and hence to pentadiagonal matrices. Therefore, as seen in Section 21.1.7, the left-hand side is often replaced by a first-order upwind operator, leading to a scheme of the form

$$[1 + \tau \theta (\delta^- f_{ui}^+ + \delta^+ f_{ui}^-)]^n \Delta u_i = -\tau (f_{i+1/2}^{*(1)n} - f_{i-1/2}^{*(1)n}) \quad (21.4.11)$$

Since the first-order fluxes are monotone, the TVD conditions (21.2.56) will be satisfied and the TVD property on the right-hand side will ensure that the solutions remain TVD under the additional condition (21.2.54). The latter generate a CFL-like restriction for the scheme to be TVD without affecting the linear unconditional stability condition for $\theta \geq \frac{1}{2}$.

However, full advantage of the TVD properties can be taken if the incremental

form (21.2.35) is introduced in the implicit part and time-linearized, leading to

$$[1 + \tau\theta(C_{i+1/2}^- \delta^+ + C_{i-1/2}^+ \delta^-)]^n \Delta u_i^n = -\tau(f_{i+1/2}^{*(2)} - f_{i-1/2}^{*(2)})^n \quad (21.4.12)$$

where the right-hand side can be defined as in equation (21.3.31).

Observe that the implicit part is now globally second-order accurate in space, with the exception of points where the gradient ratios r differ strongly from $r = 1$.

Working out the implicit operator gives, dropping the mesh point indication on the C^\pm coefficients,

$$[1 + \theta\tau(C^+ - C^-)]\Delta u_i + \theta\tau C^- \Delta u_{i+1} - \theta\tau C^+ \Delta u_{i+1} = -\tau(f_{i+1/2}^{*(2)} - f_{i-1/2}^{*(2)})^n \quad (21.4.13)$$

Hence, the TVD conditions (21.2.41) ensures that the left-hand side matrix is diagonal dominant by lines and by columns. The CFL-like condition (21.2.54) becomes here (see also Problem 21.17)

$$\tau(1 - \theta)(C_{i+1/2}^+ - C_{i+1/2}^-) \leq 1 \quad (21.4.14)$$

Note that the implicit part is not in conservation form. This does not affect the steady-state solution which is determined by the vanishing right-hand side residuals, which are conservative. However, the transient solutions lose the conservation property.

The diagonal dominance of the implicit TVD operators becomes particularly interesting for multi-dimensional problems (Chakravarthy, 1984).

Additional investigations and variants of TVD implicit schemes can be found in Yee and Harten (1985) and Yee (1986a), while the application of Runge-Kutta methods to TVD upwind schemes has been attempted by Turkel and Van Leer (1984).

The definition of explicit TVD schemes with second-order accuracy in time requires more attention. Several methods have been developed, the earliest being the flux corrected transport (FCT) method of Boris and Book (1973, 1976), which has been generalized by Salezack (1979). This method, although less firmly grounded from a theoretical point of view, is the first to have introduced the concept of non-linear flux limiting. Its essential idea is to add to a first-order monotone solution a limited amount of the difference between the second-order and first-order fluxes. This difference, which corrects the excessive dissipation of the first-order schemes, is called an *antidiffusive* flux contribution and is restricted, in a non-linear way, to the amount necessary to remove the first-order diffusion without creating unwanted overshoots or oscillations, typical of the second-order schemes. This approach can be adapted in a straightforward way to the generation of second-order explicit TVD schemes, either through flux extrapolation or through the variable extrapolation—MUSCL—method.

Another approach has been followed by Roe (1985) and Sweby (1984), based on a TVD formulation of the Lax-Wendroff scheme, written as a first-order upwind scheme plus centrally discretized 'antidiffusive' terms. The latter are then limited following the TVD criteria.

Zalesak

Finally the method developed by Harten (1983, 1984) introduces a *modified flux* to a first-order upwind flux, leading to second-order accuracy followed by TVD limiting.

21.4.3 Explicit second-order TVD schemes

If a second-order accurate time integration is selected, such as scheme (21.1.39), then it can be seen from equation (21.1.39b) that the second-order time integration only affects the way the first-order numerical flux is treated. The predictor step (21.1.39a) based on the first order scheme produces a monotone intermediate solution and the second order space terms in (21.1.39b) will be 'limited' in the same way as in (21.3.28). Hence the following scheme can be considered as the TVD variant of scheme (21.1.39), taking $k = -1$:

$$\bar{u}_i = u_i^n - \frac{\tau}{2} \delta^- f_{i+1/2}^* \quad (21.4.15a)$$

$$\overline{f_{i+1/2}^*} = f^*(\bar{u}_i, \bar{u}_{i+1}) \quad (21.4.15b)$$

$$u_i^{n+1} = u_i^n - \tau \delta^- \left[\overline{f_{i+1/2}^*} + \frac{1}{2} \Psi_{i-1/2}^+ (f_i^n - f_{i-1/2}^*) + \frac{1}{2} \Psi_{i+3/2}^- (f_{i+1}^n - f_{i+3/2}^*) \right] \quad (21.4.15c)$$

The solution \bar{u} is a stable monotone solution and hence the contributions form the numerical flux $\overline{f^*}$ are also monotone, as easily shown following, for instance, Problem 21.28. However, this flux generates additional space terms which might influence the TVD conditions on the limiters of equation (21.4.15c).

In order to analyse this dependence, we consider the application of the scheme (21.4.15) to the linear convection equation with second-order upwind discretization.

Considering $a > 0$, equation (21.4.15c) becomes,

$$u_i^{n+1} = u_i^n - \sigma \left[1 + \frac{1}{2} (\Psi_{i-1/2}^+ - \sigma) - \frac{1}{2} \frac{\Psi_{i-3/2}^+ - \sigma}{r_{i-3/2}^+} \right] (u_i^n - u_{i-1}^n) \quad (21.4.16)$$

The TVD conditions are

$$0 \leq \sigma \left[2 + \Psi(s) - \sigma - \frac{\Psi(r) - \sigma}{r} \right] \leq 2 \quad (21.4.17)$$

with $s = r_{i-1/2}^+$ and $r = r_{i-3/2}^+$ and reduce to the sufficient conditions for $\Psi > 0$:

$$0 \leq \Psi(r) \leq (2 - \sigma)r + \sigma \quad (21.4.18a)$$

$$0 \leq \Psi(r) \leq \frac{2}{\sigma} \quad (21.4.18b)$$

As can be seen from Figure 21.4.1, all the previously defined limiters satisfy these conditions which reduce, in the range $0 < \sigma \leq 1$, to $\Psi(r) \leq \min(2, 2r)$. The

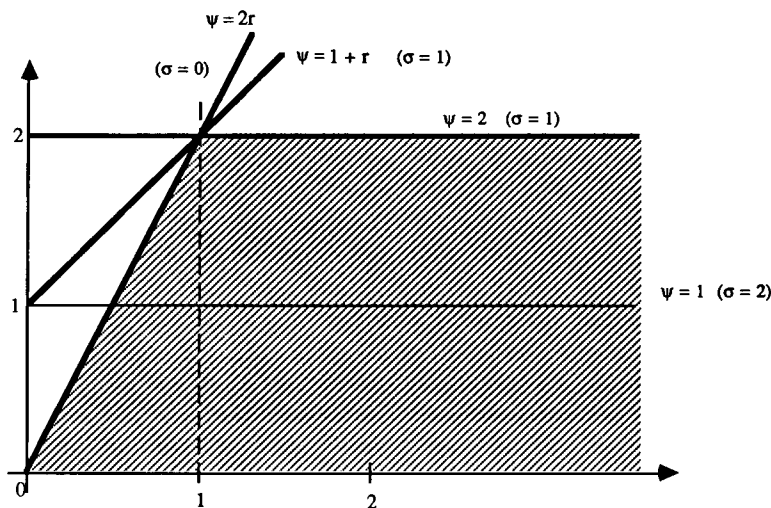


Figure 21.4.1 TVD region for second-order explicit upwind scheme following conditions (21.4.18)

scheme is hereby completely defined and can also be worked out following the developments of Section 21.3.2.

Note that the limited terms in equation (21.4.15c) represent the difference (prior to limiting) between the second- and the first-order numerical fluxes, that is the difference $f^{*(2)} - f^*$. This is the antidiffusive flux considered in the FCT method of Boris and Book.

Explicit second-order schemes with variable extrapolation—MUSCL—approach

Based on the linear equivalence, the second-order TVD explicit MUSCL approach is obtained by combining the second-order schemes (21.1.26) with the relations of Section 21.3.3. Hence an explicit second-order scheme based on variable extrapolation is defined by the following steps:

$$u_i = u_i^n - \frac{\Delta t}{2\Delta x} (f_{i+1/2}^{*(2)} - f_{i-1/2}^{*(2)}) \quad (21.4.19a)$$

$$\tilde{u}_{i+1/2}^L = \bar{u}_i + \frac{1}{2} \hat{\Psi}^L(u_i - u_{i-1}) \quad (21.4.19b)$$

$$\tilde{u}_{i+1/2}^R = \bar{u}_{i+1} - \frac{1}{2} \hat{\Psi}^R(u_{i+1} - u_i) \quad (21.4.19c)$$

The second-order numerical flux is then defined by

$$f_{i+1/2}^{\overline{*(2)}} = f^*(\tilde{u}_{i+1/2}^L, \tilde{u}_{i+1/2}^R) \quad (21.4.20a)$$

$$u_i^{n+1} - u_i^n = -\tau (f_{i+1/2}^{\overline{*(2)}} - f_{i-1/2}^{\overline{*(2)}}) \quad (21.4.20b)$$

Here again the Ψ limiters obey the restrictions developed above.

TVD formulation of the Lax–Wendroff scheme

A third approach to second-order explicit TVD schemes is based on Roe's adaptation of the Lax–Wendroff scheme to upwind discretizations (Roe, 1985), further generalized by Sweby (1984) to any first-order approximate Riemann solver. This approach was initiated by the application of TVD concepts to the Lax–Wendroff scheme (Davis, 1984; Roe, 1984). However, it can also be considered as a direct application of TVD limiters to the second-order (in space and time) numerical flux (21.1.42). Although equation (21.1.42) is a second-order upwind scheme, the limiting procedure leads to a very remarkable and unexpected unification of upwind and central explicit second-order TVD schemes. Namely, *one step explicit and TVD second-order upwind schemes can be made identical to the TVD centrally discretized Lax–Wendroff schemes* if the limiters satisfy the symmetry property (21.3.26).

This is easily seen on the corresponding linearized equations (21.3.12) and (21.3.19) (see also Problem 21.23), but can be shown for a general upwind scheme. The Lax–Wendroff numerical flux (17.2.8) can be transformed into an equivalent flux splitted form by decomposing the fluxes and the Jacobians into their positive and negative parts (see also Problem 20.33). Defining the Jacobians as Roe matrices leads to the numerical flux

$$f_{i+1/2}^{*\text{LW}} = f_i^+ + f_{i+1}^- + \frac{1}{2}(1 - \tau A_{i+1/2}^+) \delta f_{i+1/2}^+ - \frac{1}{2}(1 + \tau A_{i+1/2}^-) \delta f_{i+1/2}^- \quad (21.4.21)$$

Observe that an equivalent formulation is obtained by replacing A^+ and A^- by the full Jacobian A , since $A^+ f^- = A^- f^+ = 0$.

Compared with the upwind numerical flux (21.1.42), rewritten here for convenience,

$$\overline{f_{i+1/2}^{*(2)}} = f_i^+ + f_{i+1}^- + \frac{1}{2}(1 - \tau A_{i-1/2}^+) \delta f_{i-1/2}^+ - \frac{1}{2}(1 + \tau A_{i+3/2}^-) \delta f_{i+3/2}^- \quad (21.4.22)$$

they differ by the mesh point locations where the flux components are evaluated. In the Lax–Wendroff scheme, both positive and negative waves are evaluated at the same point, giving rise to the central discretization. In the upwind scheme the evaluation points are selected in the direction 'downwind' to the wave speed.

In the scalar case, with the definitions (21.4.2) to (21.4.4), these two schemes can be written as

$$f_{i+1/2}^{*\text{LW}} = f_i^+ + f_{i+1}^- + \frac{1}{2}(1 - \sigma_{i+1/2}^+) \delta f_{i+1/2}^+ - \frac{1}{2}(1 + \sigma_{i+1/2}^-) \delta f_{i+1/2}^- \quad (21.4.23)$$

$$\overline{f_{i+1/2}^{*(2)}} = f_i^+ + f_{i+1}^- + \frac{1}{2}(1 - \sigma_{i-1/2}^+) \delta f_{i-1/2}^+ - \frac{1}{2}(1 + \sigma_{i+3/2}^-) \delta f_{i+3/2}^- \quad (21.4.24)$$

This scheme is made TVD following the treatment of Section 21.3.2, equation (21.3.28), by

$$f_{i+1/2}^{\overline{*(2)}} = f_i^+ + f_{i+1}^- + \frac{1}{2} \Psi_{i-1/2}^+ (1 - \sigma_{i-1/2}^+) \delta f_{i-1/2}^+ - \frac{1}{2} \Psi_{i+3/2}^- (1 + \sigma_{i+3/2}^-) \delta f_{i+3/2}^- \quad (21.4.25)$$

where the limiters are considered as functions of the following ratios:

$$r_{i+1/2}^+ = \frac{(1 - \sigma_{i+3/2}^+) \delta f_{i+3/2}^+}{(1 - \sigma_{i+1/2}^+) \delta f_{i+1/2}^+} = \frac{(1 - \sigma_{i+3/2}^+) a_{i+3/2}^+ (u_{i+2} - u_{i+1})}{(1 - \sigma_{i+1/2}^+) a_{i+1/2}^+ (u_{i+1} - u_i)} \quad (21.4.26a)$$

$$r_{i+1/2}^- = \frac{(1 + \sigma_{i-1/2}^-) \delta f_{i-1/2}^-}{(1 + \sigma_{i+1/2}^-) \delta f_{i+1/2}^-} = \frac{(1 + \sigma_{i-1/2}^-) a_{i-1/2}^- (u_i - u_{i-1})}{(1 + \sigma_{i+1/2}^-) a_{i+1/2}^- (u_{i+1} - u_i)} \quad (21.4.26b)$$

These definitions are a logical extension of equation (21.3.30).

Introducing the flux differences at $(i + \frac{1}{2})$, equation (21.4.25) takes the form

$$\begin{aligned} f_{i+1/2}^{*(2)} = & f_i^+ + f_{i+1}^- + \frac{1}{2} \left[\frac{\Psi(r_{i-1/2}^+)}{r_{i-1/2}^+} \right] (1 - \sigma_{i+1/2}^+) \delta f_{i+1/2}^+ \\ & - \frac{1}{2} \left[\frac{\Psi(r_{i+3/2}^-)}{r_{i+3/2}^-} \right] (1 + \sigma_{i+1/2}^-) \delta f_{i+1/2}^- \end{aligned} \quad (21.4.27)$$

With the symmetry property (21.3.26), $\Psi(r)/r = \Psi(1/r)$, this upwind scheme becomes *identical to the limited TVD Lax-Wendroff scheme*:

$$\begin{aligned} f_{i+1/2}^{*LW}|_{TVD} = & f_i^+ + f_{i+1}^- + \frac{1}{2} \Psi \left(\frac{1}{r_{i-1/2}^+} \right) (1 - \sigma_{i+1/2}^+) \delta f_{i+1/2}^+ \\ & - \frac{1}{2} \Psi \left(\frac{1}{r_{i+3/2}^-} \right) (1 + \sigma_{i+1/2}^-) \delta f_{i+1/2}^- \end{aligned} \quad (21.4.28)$$

The TVD scheme (21.4.28) reduces to equation (21.3.19) for the scalar convection equation with $a > 0$.

Equation (21.4.28) can also be written as the Lax-Wendroff numerical flux plus TVD terms; this amounts to the replacement of Ψ by $(\Psi - 1)$. Hence, any two-step variant of the Lax-Wendroff scheme can be applied instead and made TVD.

From the derivations of Section 21.3.1 it is readily seen that all the symmetric limiters for second-order schemes can be applied here. Consequently, the numerical flux (21.4.25), or (21.4.28) to which it is identical, is a second-order space- and time-accurate TVD flux, under the CFL-like condition (21.4.8).

The presence of the functional dependence on $r_{i+3/2}$ is required by the necessity of obtaining a five-point scheme in order to satisfy the TVD and second-order accuracy conditions.

Harten's modified flux method

If the first-order upwind scheme has a truncation error of the form (21.2.29), its solutions are second-order approximations of this equivalent differential equation. Hence if the truncation error is subtracted from the original flux as an antidiffusive flux, the solutions of the resulting equation will be second-order approximations of the original equation. These contributions have to be limited in order to obtain a TVD scheme. Hence, writing equation (21.2.29) under the

form

$$u_t + f_x = g_x \quad (21.4.29a)$$

with

$$g(x) = \Delta t \beta(u) u_x \quad (21.4.29b)$$

the application of the original first-order scheme to the conservation law with the modified flux function ($f + g$)

$$u_t + (f + g)_x = 0 \quad (21.4.30)$$

is a second-order approximation to $u_t + f_x = 0$.

For the first-order upwind scheme in the form of equation (E21.3.1)

$$f_{i+1/2}^* = \frac{1}{2}(f_i + f_{i+1}) - \frac{1}{2}|a|_{i+1/2}(u_{i+1} - u_i) \quad (21.4.31a)$$

the truncation error is given by

$$g(x) = \frac{\Delta x}{2}|a|(1 - \tau|a|)u_x + O(\Delta x^2) = \frac{\Delta x}{2\tau}|\sigma|(1 - |\sigma|)u_x + O(\Delta x^2) \quad (21.4.31b)$$

and the following numerical flux is second-order accurate in space and time (Harten, 1983):

$$f_{i+1/2}^{*(2)} = \frac{1}{2}(f_i + f_{i+1}) + \frac{1}{2}(g_i + g_{i+1}) - \frac{1}{2}|a + b|_{i+1/2}(u_{i+1} - u_i) \quad (21.4.32)$$

where g is discretized as

$$g_{i+1/2} = |a|_{i+1/2}(1 - |\sigma|_{i+1/2})\frac{u_{i+1} - u_i}{2} \equiv \frac{g_i + g_{i+1}}{2} \quad (21.4.33)$$

$$b_{i+1/2} = \frac{g_{i+1} - g_i}{u_{i+1} - u_i} \quad (21.4.34)$$

The scheme is TVD under the condition (21.2.47), which becomes here

$$\tau|a + b|_{i+1/2} \leq 1 \quad (21.4.35)$$

In order to satisfy this condition, the g values have to be 'limited'. For instance, by a minmod limiter (Harten, 1983),

$$g_i = \text{minmod}(g_{i-1/2}, g_{i+1/2}) \quad (21.4.36)$$

The reader is referred to the original references for additional details and proofs.

21.4.4 TVD schemes and artificial dissipation

The TVD approach can also be considered as a rational way to introduce artificial dissipation in central schemes. This is best seen when the TVD form of the Lax–Wendroff numerical flux (21.4.28) is compared with the general expression (17.3.4) for central second-order schemes plus artificial dissipation.

Equation (21.4.28) can be written as a central, or as a Lax–Wendroff, scheme plus dissipation terms. Indeed, writing Ψ^+ and Ψ^- for the limiters associated

with the positive and negative waves respectively, equation (21.4.28) becomes

$$f_{i+1/2}^{*\text{LW}}|_{\text{TVD}} = \frac{1}{2}(f_i + f_{i+1}) - \frac{1}{2}|a|_{i+1/2}(u_{i+1} - u_i) + \frac{1}{2}[\Psi^+(1 - \sigma^+)a^+ - \Psi^-(1 + \sigma^-)a^-]_{i+1/2}(u_{i+1} - u_i) \quad (21.4.37)$$

Since the limiter Ψ^+ acts only on the positive flux components, we can always assume that

$$\Psi^+ \cdot a^- = 0 \quad \text{or} \quad \Psi^+ \cdot f^- = 0 \quad (21.4.38a)$$

and similarly

$$\Psi^- \cdot a^+ = 0 \quad \text{or} \quad \Psi^- \cdot f^+ = 0 \quad (21.4.38b)$$

This allow us to write the above TVD numerical flux as

$$f_{i+1/2}^{*\text{LW}}|_{\text{TVD}} = \frac{1}{2}(f_i + f_{i+1}) - \frac{1}{2}|a|_{i+1/2}(u_{i+1} - u_i) + \frac{1}{2}(\Psi^+ + \Psi^-)[(1 - \sigma^+)a^+ - (1 + \sigma^-)a^-]_{i+1/2}(u_{i+1} - u_i) \quad (21.4.39a)$$

or

$$f_{i+1/2}^{*\text{LW}}|_{\text{TVD}} = \frac{1}{2}(f_i + f_{i+1}) - \frac{1}{2}|a|_{i+1/2}(u_{i+1} - u_i) + \frac{1}{2}(\Psi^+ + \Psi^-)[|a|(1 - |\sigma|)]_{i+1/2}(u_{i+1} - u_i) \quad (21.4.39b)$$

Considered as a correction to the Lax-Wendroff flux, we have

$$f_{i+1/2}^{*\text{LW}}|_{\text{TVD}} = \frac{1}{2}(f_i + f_{i+1}) - \frac{1}{2}\tau a_{i+1/2}^2(u_{i+1} - u_i) + \frac{1}{2}(\Psi^+ + \Psi^- - 1)[|a|(1 - |\sigma|)]_{i+1/2}(u_{i+1} - u_i) \quad (21.4.40)$$

The last term is the artificial dissipation term to be compared with the general expression (17.3.4), leading to

$$D_{i+1/2} = \frac{1}{2}(1 - \Psi^+ - \Psi^-)[|a|(1 - |\sigma|)]_{i+1/2} \quad (21.4.41)$$

where Ψ^\pm are defined as in equation (21.4.28).

For the linear convection equation with $a > 0$, Ψ^- does not contribute, and in the vicinity of $r \approx 1$, $(\Psi^+ - 1) \approx (r - 1) = O(\Delta x)$, as seen from equation (21.3.18). Hence the artificial dissipation is globally of second order, although at extrema it becomes of first order, reducing the scheme to first-order accuracy, as has already been noticed.

Note that this form of TVD artificial dissipation can be applied with any of the two-step predictor-corrector variants of the Lax-Wendroff scheme. For instance, a TVD MacCormack scheme can be defined as follows, for a scalar equation:

$$\bar{u}_i = u_i^n - \tau(f_{i+1} - f_i)^n \quad (21.4.42a)$$

$$\bar{u}_i = u_i^n - \tau(\bar{f}_i - \bar{f}_{i-1}) \quad (21.4.42b)$$

$$u_i^{n+1} = \frac{1}{2}(\bar{u}_i + \bar{u}_i) + \tau[D_{i+1/2}(u_{i+1} - u_i) - D_{i-1/2}(u_i - u_{i-1})] \quad (21.4.42c)$$

Figure 21.4.2 shows results obtained with the TVD MacCormack scheme on the same test case as Figures 21.3.8 and 21.3.9 for the linear convection equation.

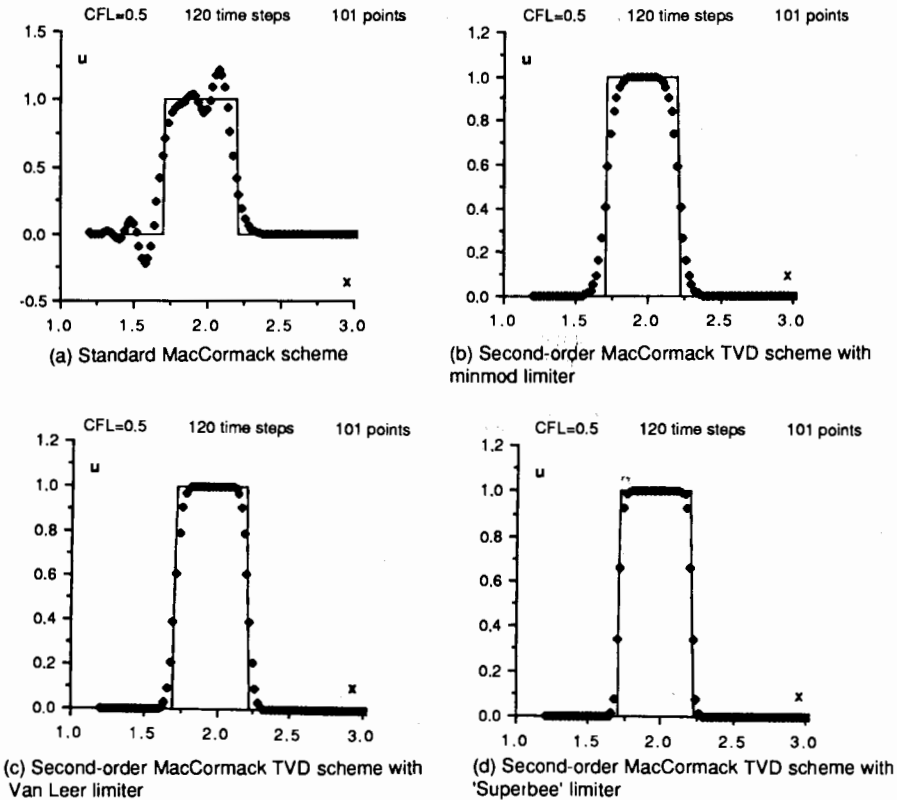


Figure 21.4.2 Effects of limiters on the linear convection of a square wave after 120 time steps

Here again the Superbee limiter leads to very sharp, non-diffusive transition profiles, as seen by comparing with the results after 400 time steps on Figure 21.4.3, while the other limiters shown, the minmod and the Van Leer limiters, still have some diffusive components. Note in particular the symmetrical shape of the profiles, compared to the similar profiles obtained with the upwind method which show traces of the upwind discretizations.

The TVD dissipation of the Lax–Wendroff scheme depends on the time step and is therefore less suitable for steady-state calculations. In order to derive TVD-based artificial dissipation terms in the line of the approach presented in Chapter 18, the above equations are written as follows:

$$f_{i+1/2}^{*LW}|_{TVD} = \frac{1}{2}(f_i + f_{i+1}) - \frac{1}{2}\tau a_{i+1/2}^2(\Psi^+ + \Psi^-)(u_{i+1} - u_i) + \frac{1}{2}(\Psi^+ + \Psi^- - 1)|a|_{i+1/2}(u_{i+1} - u_i) \quad (21.4.43)$$

If the second term, proportional to the time step, is dropped, an artificial dissipation which is suitable for separate space and time discretizations can be defined. This has been investigated by Yee (1985, 1986a, 1987a), applying the following scheme:

$$f_{i+1/2}^{*(2)}|_{TVD} = \frac{1}{2}(f_i + f_{i+1}) - \frac{1}{2}(1 - \Psi^+ - \Psi^-)|a|_{i+1/2}(u_{i+1} - u_i) \quad (21.4.44)$$

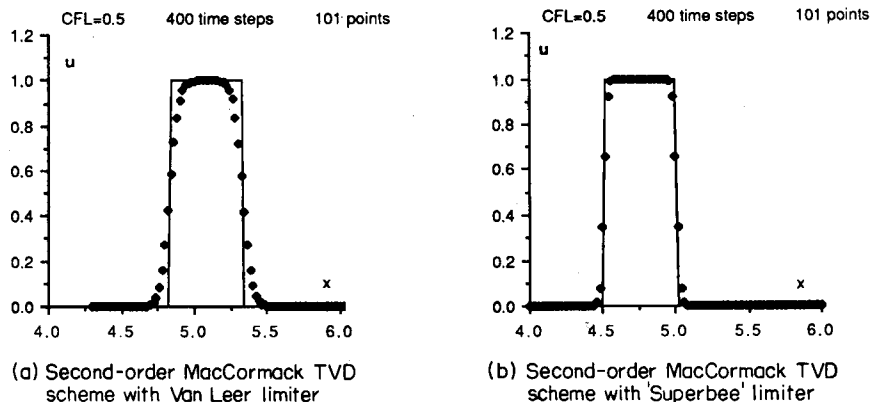


Figure 21.4.3 Effects of limiters on the linear convection of a square wave after 400 time steps

This numerical flux is of second-order accuracy in space in smooth flow regions.

Since the dependence on the Courant number σ , that is on the time step Δt , is removed, the gradient ratios have to be redefined. The following definitions appear as natural to the central formulation

$$r_{i+1/2}^+ = \frac{|a|_{i+3/2} \delta u_{i+3/2}}{|a|_{i+1/2} \delta u_{i+1/2}} \quad (21.4.45a)$$

$$r_{i+1/2}^- = \frac{|a|_{i-1/2} \delta u_{i-1/2}}{|a|_{i+1/2} \delta u_{i+1/2}} \quad (21.4.45b)$$

with

$$\Psi^+ \equiv \Psi\left(\frac{1}{r_{i-1/2}^+}\right) = \Psi(r_{i+1/2}^-) \quad (21.4.46a)$$

$$\Psi^- \equiv \Psi\left(\frac{1}{r_{i+3/2}^-}\right) = \Psi(r_{i+1/2}^+) \quad (21.4.46b)$$

Since these two limiters appear together we can set

$$Q_{i+1/2} = \Psi^+ + \Psi^- \equiv Q(r_{i+1/2}^-, r_{i+1/2}^+) \quad (21.4.47)$$

where the dependence on $\delta u_{i+3/2}$ is essential for the definition of a five-point scheme. In this case, setting Ψ^+ to zero when acting on negative waves, and similarly for Ψ^- , is no longer justified. Hence Q is considered as a new limiter to be defined by the appropriate TVD conditions.

Considering an explicit scheme in incremental form (21.2.35), we have

$$C_{i-1/2}^+ = \frac{1}{2} |a|_{i-1/2} \left[\operatorname{sgn}(a_{i-1/2}) + 1 - Q_{i-1/2} + \frac{\operatorname{sgn}(a_{i+1/2}) - 1 + Q_{i+1/2}}{r_{i+1/2}^-} \right] \quad (21.4.48a)$$

$$C_{i+1/2}^- = 0 \quad (21.4.48b)$$

For positive values of a , $a > 0$, the TVD conditions become

$$0 \leq \sigma_{i-1/2} \left(1 - \frac{1}{2} Q_{i-1/2} + \frac{1}{2} \frac{Q_{i+1/2}}{r_{i+1/2}^-} \right) \leq 1 \quad (21.4.49)$$

With the assumptions $Q \geq 0$ and $Q/r \geq 0$, the following sufficient conditions:

$$Q \leq 2 \quad (21.4.50a)$$

$$\frac{Q}{r^-} < \frac{2(1-\sigma)}{\sigma} \quad (21.4.50b)$$

are obtained. If $a < 0$, one obtains similarly

$$Q \leq 2 \quad (21.4.51a)$$

$$\frac{Q}{r^+} < \frac{2(1-|\sigma|)}{|\sigma|} \quad (21.4.51b)$$

With an implicit scheme of the form (21.4.12) the second condition becomes

$$0 < \frac{Q}{r^\pm} < \frac{2}{|\sigma|(1-\theta)} - 2 \quad (21.4.52)$$

implying the condition on the implicit parameter θ for a TVD artificial dissipation

$$|\sigma|(1-\theta) < 1 \quad (21.4.53)$$

For a backward Euler scheme $\theta = 1$, the scheme is unconditionally TVD.

Remember that this restriction on the Courant number σ is not a stability condition in the Von Neumann sense, since the implicit scheme (21.4.12) is unconditionally stable for $\theta \geq \frac{1}{2}$, but it will not remain TVD if $|\sigma|(1-\theta) \geq 1$.

For $\theta = \frac{1}{2}$ the implicit scheme is second-order accurate in time and the limits on $|\sigma|$ arising from equation (21.4.52) are $|\sigma| < 2$.

All of the previously defined limiters can be applied if Q is taken as $Q = \Psi(r^+) + \Psi(r^-)$, within the above restrictions. However, in order to maintain second-order accuracy in smooth flow regions, the quantity $(1-Q)$ should be proportional at least to the first power of Δx ; that is for $r^+ \simeq r^- \simeq 1$ one should have $Q \simeq 1 + O(\Delta x)$. For instance, selecting the minmod limiter (21.3.22) for Ψ would lead to

$$Q(r^-, r^+) = \minmod(1, r^-) + \minmod(1, r^+) - 1 \quad (21.4.54)$$

valid for $|\sigma|(1-\theta) < \frac{2}{3}$.

More general Q functions can be applied following Roe (1984), for instance,

$$Q(r^-, r^+) = \minmod(1, r^-, r^+) \quad (21.4.55a)$$

$$Q(r^-, r^+) = \minmod[2, 2r^-, 2r^+, (r^- + r^+)/2] \quad (21.4.55b)$$

The first limiter never exceeds 1 and will be valid for $|\sigma|(1-\theta) < \frac{2}{3}$, while the second is bounded by 2 and is valid for $|\sigma|(1-\theta) < \frac{1}{2}$.

21.4.5 TVD limiters and the entropy condition

Although the TVD conditions do not ensure the satisfaction of the entropy condition, it can be expected that if the reference first-order scheme is an E

scheme, the addition of 'limited' antidiffusive second-order terms would not destroy the diffusion at sonic expansions, which prevents entropy violating expansion shocks.

This property has been conjectured by Sweby (1984), where an argument is given in support of this behaviour. Indeed, considering the TVD scheme (21.4.28), the C^\pm coefficients of the incremental form (21.2.35) are a measure of the diffusion contribution of the associated waves. As long as these coefficients are not reduced (in absolute value), it may be considered that the overall diffusion is not reduced. At sonic expansions, where entropy violating discontinuities are observed with certain schemes, we have for convex f , $f'(u_{i-1/2}) < 0 < f'(u_{i+3/2})$, implying $a_{i-1/2}^- < 0$ and $a_{i+3/2}^- = 0$. Hence the C^\pm terms for the TVD Lax-Wendroff scheme (21.4.28) are increased, in absolute value, with respect to the first-order values (see Problem 21.33).

This is not a general proof but numerical experiences also seem to substantiate that second-order TVD schemes, based on a first-order entropy satisfying E-scheme, do not generate expansion shocks with the most current limiters. A more rigorous analysis, referred to in Section 21.2.3, is nevertheless to be applied for more general validations of the entropy condition.

A representative example is provided by Figure 21.4.4, which displays the results of Burgers equation for an initial square wave, after 50 and 100 time steps

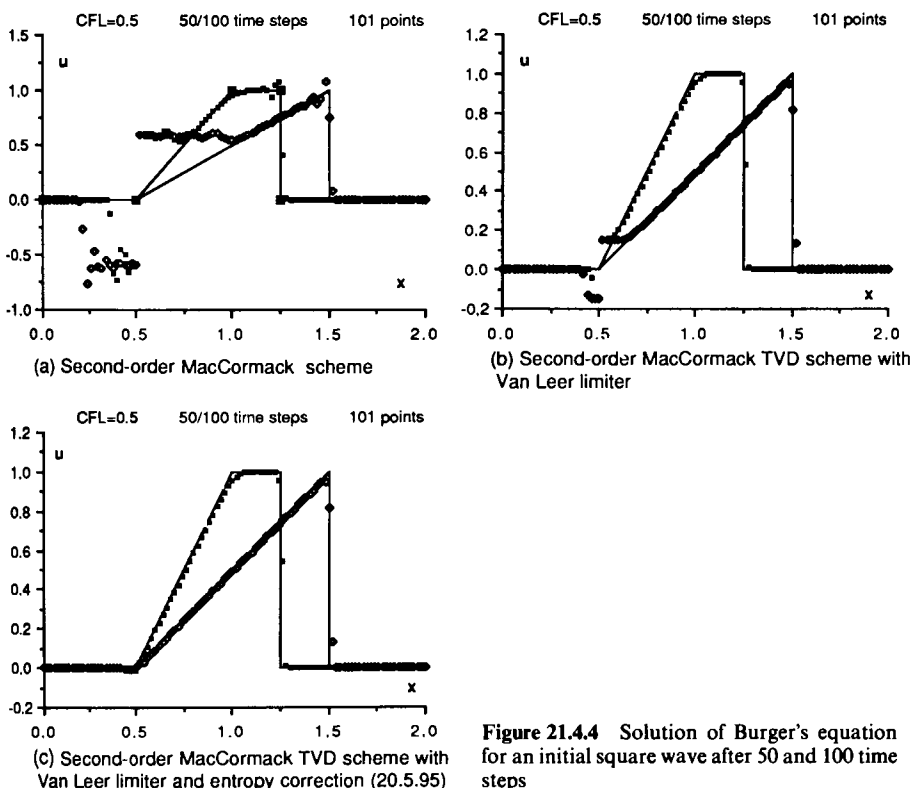


Figure 21.4.4 Solution of Burger's equation for an initial square wave after 50 and 100 time steps

steps, obtained with a MacCormack scheme that is known not to satisfy the entropy condition. Figure 21.4.4(a) shows the typical oscillations and an expansion shock at the foot of the expansion wave at the sonic point $u=0$. Applying the TVD MacCormack scheme with the Van Leer limiter removes all the oscillations, as seen from Figure 21.4.4(b), but does not suppress the expansion shock. This is realized on Figure 21.4.4(c) where the modification (20.5.95) is introduced, replacing $|a|$ in equation (21.4.41) by $\varepsilon^2/(a^2 + 2\varepsilon)$ when $|a| < \varepsilon$.

21.5 EXTENSION TO NON-LINEAR SYSTEMS AND TO MULTI-DIMENSIONS

The extension of the TVD and limiter concepts to nonlinear systems can be performed in a nonambiguous way, if the definitions (21.2.36) remain valid. This can be achieved by a limiting process on the variables in each of the coordinate directions separately, within the variable extrapolation method. Alternatively, the Roe linearization (20.5.69) and the decomposition (20.5.87) can be applied to each wave separately, the characteristic variations δw_j playing the role of the variations δu in the scalar case. Hence, the amplitudes δw_j are limited in the same way as the δu of the associated schemes, with the gradient ratios r defined accordingly as ratios of δw variations. The summation over all the waves is then performed after limiting. We refer the reader to the cited literature for more details.

Similarly, multidimensional problems are treated by local one-dimensional decomposition of the limiting process in directions normal to the cell faces of the finite volumes.

The following figures illustrate the performance of the TVD schemes and their adapted dissipative action in capturing accurately shocks and other discontinuities, without oscillations.

Figure 21.5.1 displays results of a computation of the shock tube problem shown previously, obtained with the second order TVD version of Roe's scheme, applying the variable extrapolation (MUSCL) approach and a minmod limiter on the characteristic variables. It is seen that the shock is sharply captured, the contact discontinuity is better resolved and no oscillations are produced. This result is particularly striking when compared to Figure 21.1.10 obtained without limiter with second order flux splitting. The application of the superbee limiter under the same conditions, shown on Figure 21.5.2, provides a marked improvement at the foot of the expansion fan and of the contact discontinuity which is sharply captured. This compares very favourably with the results obtained by the MacCormack scheme with added artificial dissipation, as shown in Chapter 17.

The same scheme applied to the diverging nozzle flow with shock is shown in Figure 21.5.3, with a minmod limiter. Here again excellent resolution is obtained, the shock being captured over two cells as expected, although a slight error on the entropy can still be noticed.

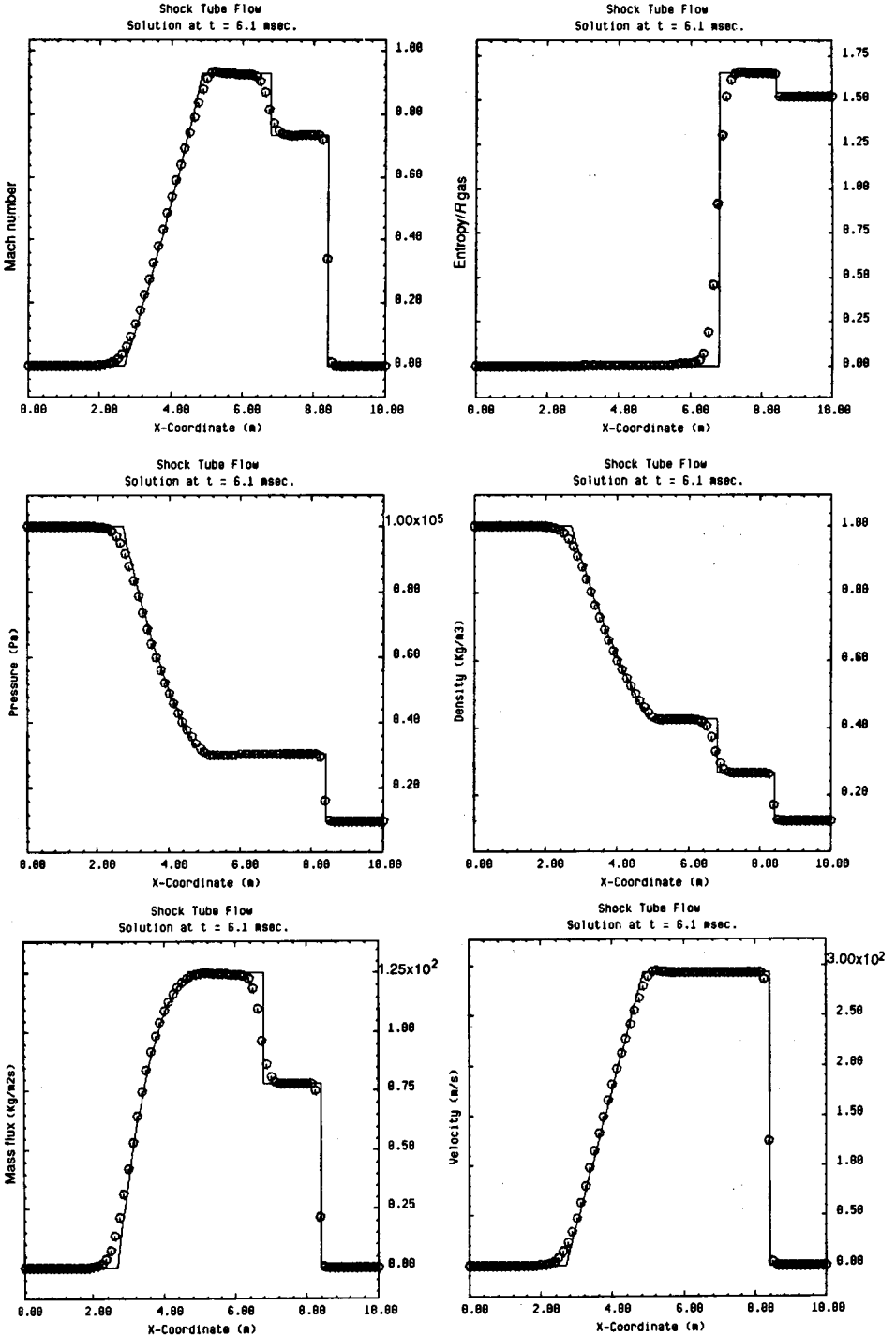


Figure 21.5.1 Computation of the shock tube problem with second order Roe TVD scheme and variable extrapolation (MUSCL) with minmod limiter.

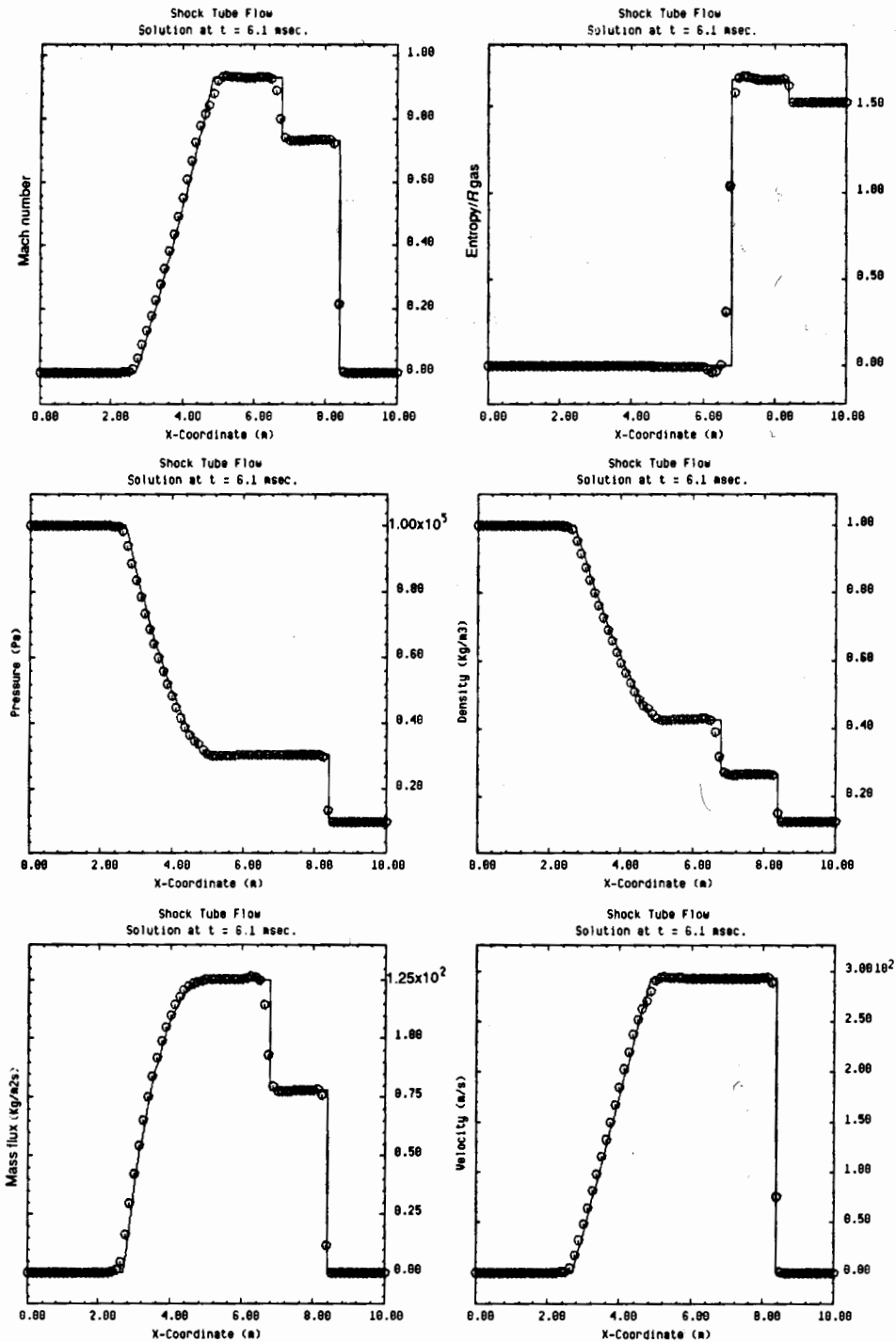


Figure 21.5.2 Computation of the shock tube problem with second order Roe TVD scheme and variable extrapolation (MUSCL) with superbee limiter.

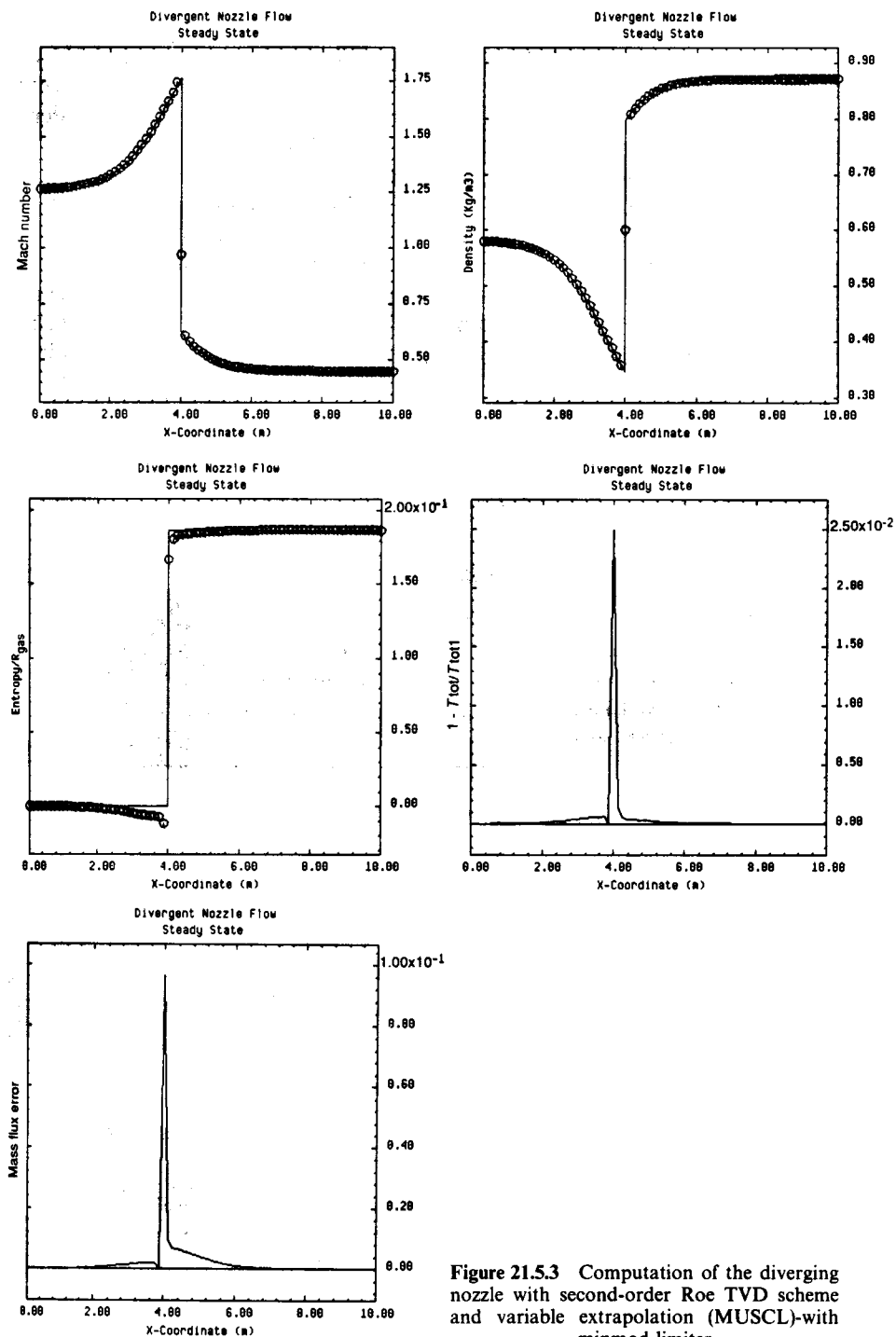


Figure 21.53 Computation of the diverging nozzle with second-order Roe TVD scheme and variable extrapolation (MUSCL)-with minmod limiter

Example 21.5.1 Shock impinging on an airfoil at 30° incidence

The following example covers the unsteady two-dimensional flow generated by a curved shock impinging on a NACA 0018 airfoil at an angle of attack $\alpha = 30^\circ$ and is typical of the level of high resolution attainable with second-order TVD schemes, without the need for adjustable parameters in artificial dissipation formulas. Figure 21.5.4 shows the schematics of the experiment and the results of a computation performed by Yee (1986b, 1987b) are shown in Figure 21.5.5. The computations are performed with the symmetric TVD scheme (21.4.44) and with a version of Harten's explicit upwind scheme (21.4.32) on a C-mesh of 299×79 points. The results are displayed at the times corresponding to the Schlieren pictures. The middle column indicates the density contours obtained with the upwind TVD scheme, while the third column is obtained from the symmetric TVD scheme. The incident and reflected shocks, the Mach stem and the slip lines are captured within three mesh points as well as the trailing edge vortices. The shock resolution of the central TVD scheme is slightly more diffusive than the upwind scheme. This can be seen by comparing the sharpness of the reflected shock on the pressure surface in the vicinity of the trailing edge.

Example 21.5.2 Three-dimensional flow in a butterfly valve

The very complex flow around a butterfly valve under incidence has been computed by Lacor and Hirsch (1988). The computations are performed with a flux vector splitting, in this case a Steger–Warming splitting, with variable extrapolation (MUSCL) and Van Albada limiter. An implicit scheme is applied.

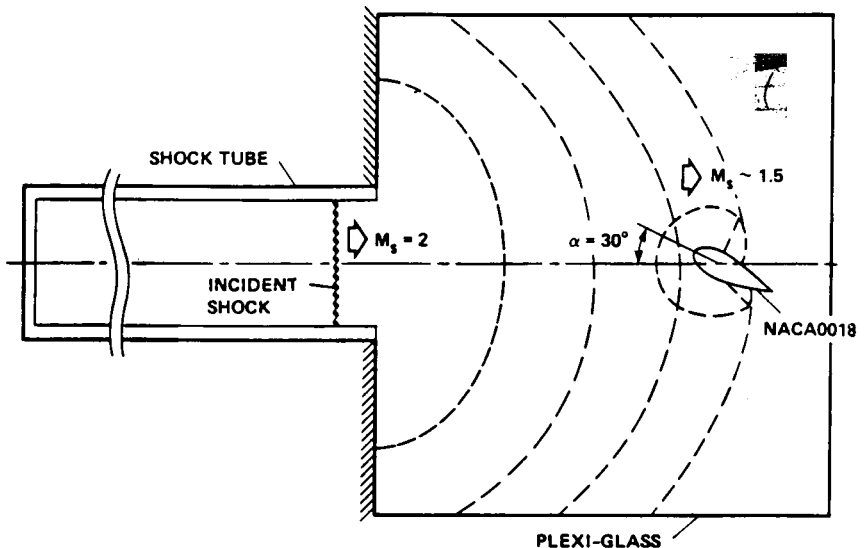


Figure 21.5.4 Schematics of the experimental set-up for the incident shock on a NACA 0018 under 30° incidence. (From Yee, 1987b)

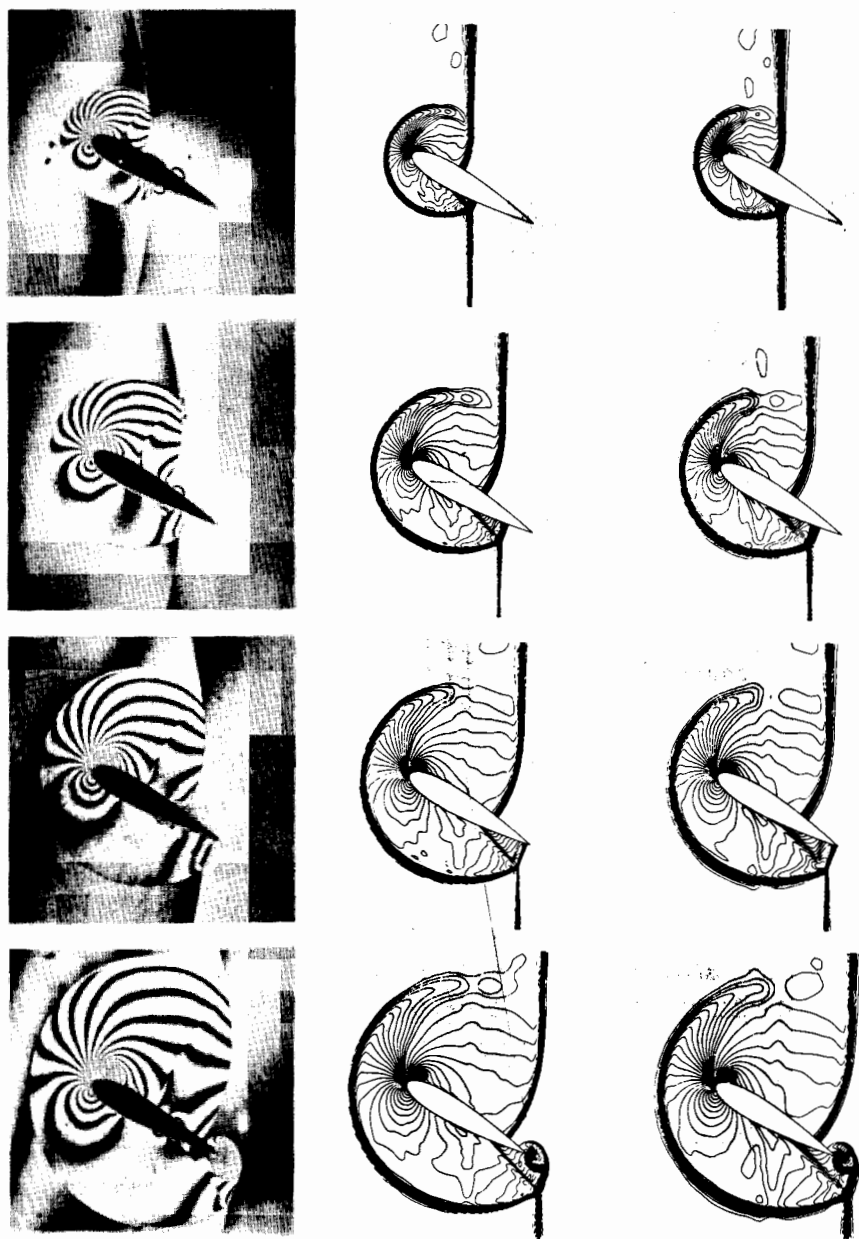


Figure 21.5.5 Density isolines obtained by the upwind TVD scheme and a central TVD scheme, compared to Schlieren pictures at the same instants of the shock-airfoil interaction. (From Yee, 1987b)

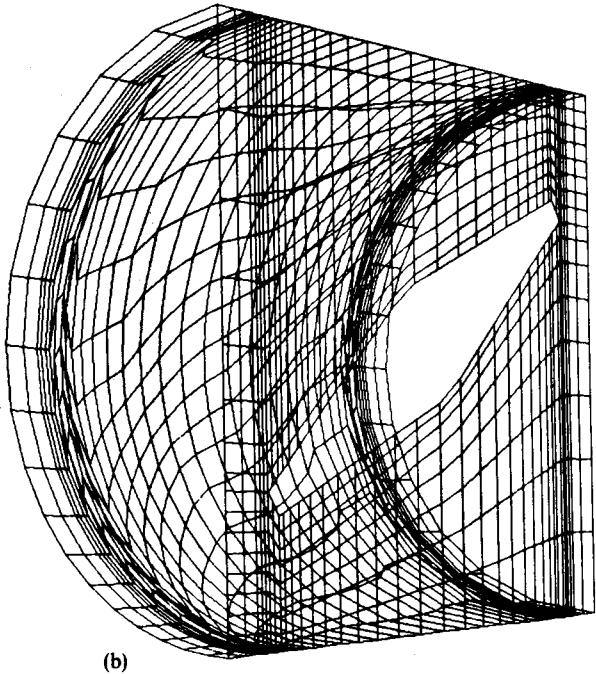
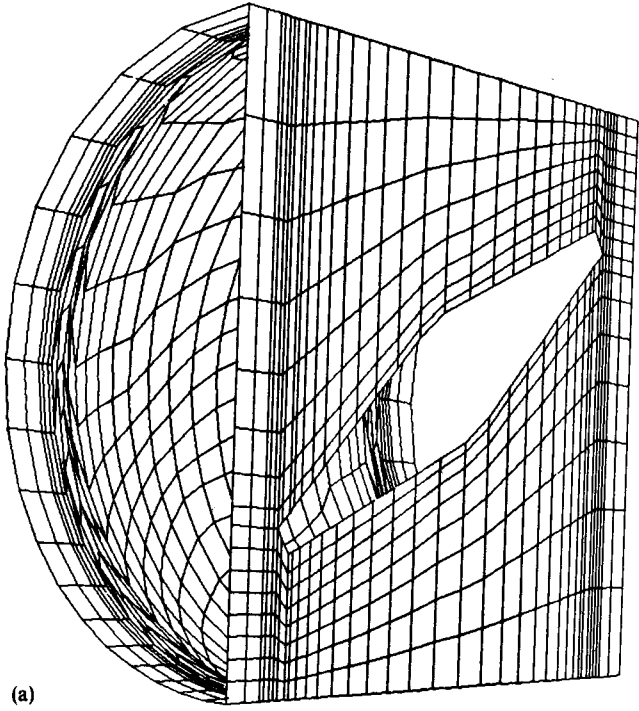


Figure 21.5.6 Part of the mesh and the geometry of a butterfly valve at 30° incidence

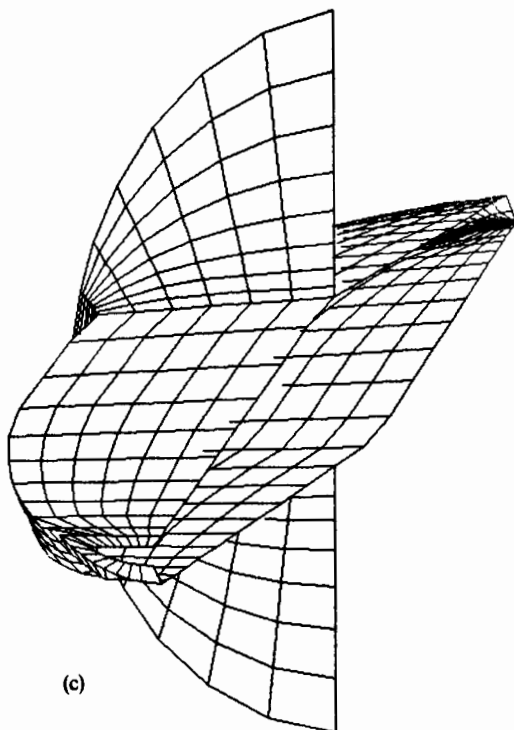


Figure 21.5.6 (Continued)

defined by the three-dimensional extension of equation (21.1.54). The implicit system is solved by relaxation, applying a non-linear double symmetric Gauss-Seidel method. Four consecutive sweeps into different directions are performed at each iteration.

Boundary conditions at the inlet are specified by stagnation temperature and pressure and the inlet flow angles. The normal velocity is extrapolated from the interior to the boundary. At the exit, static pressure is fixed and the remaining primitive variables are extrapolated. On solid walls the pressure is obtained from the normal pressure gradient and zero normal velocity. All the boundary conditions are treated implicitly.

The geometry of the valve with parts of the mesh are shown in Figure 21.5.6 for the valve opening angle of 30° on the horizontal direction. For symmetry reasons, the computations are performed on half of the duct. The operating point corresponds to a non-dimensionalized pressure drop of 0.25 and is close to choking. Note that in this inviscid computation, the operating point in the diagram pressure drop versus mass flow results from the computation and, as can be seen from the experimental data of Figure 21.5.7, is well predicted. This deserves some explanation as to the origin of the total pressure losses in an inviscid calculation. As can be seen from the calculated Mach number, static and total pressure distributions in the symmetry plane

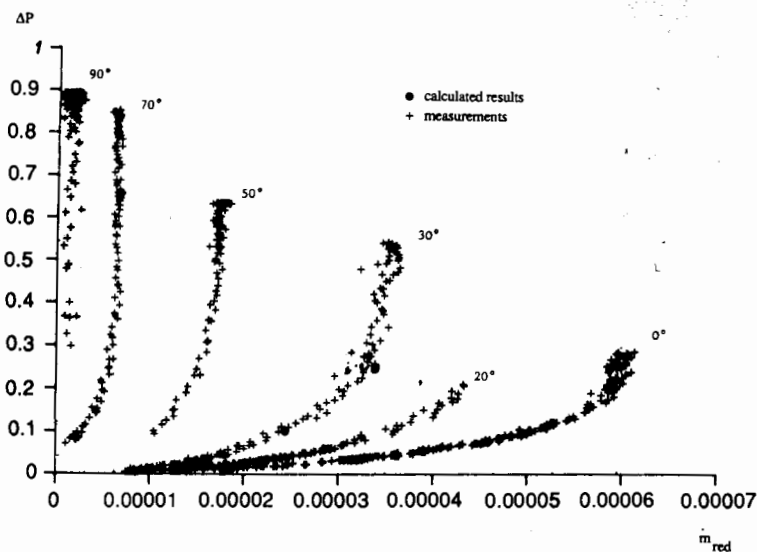


Figure 21.5.7 Comparison of calculated operating points (black circle) with experimental performance map at different opening angles of the butterfly valve at various incidence

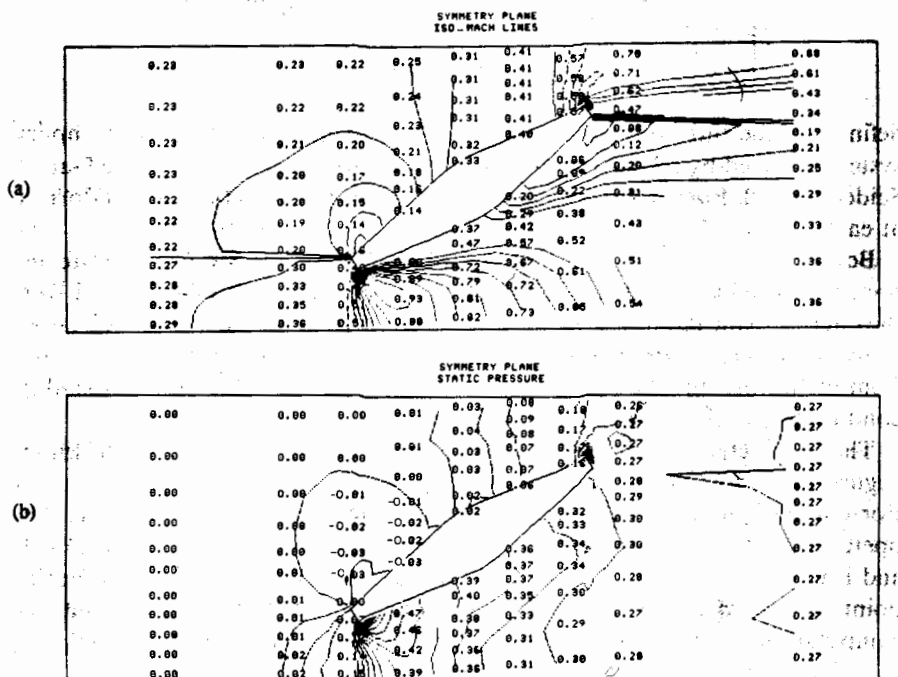


Figure 21.5.8 (a) Calculated Mach number, (b) static pressure, (c) total pressure and (d) velocities in the symmetry plane of the butterfly valve at 30° incidence and $\Delta p = 0.25$

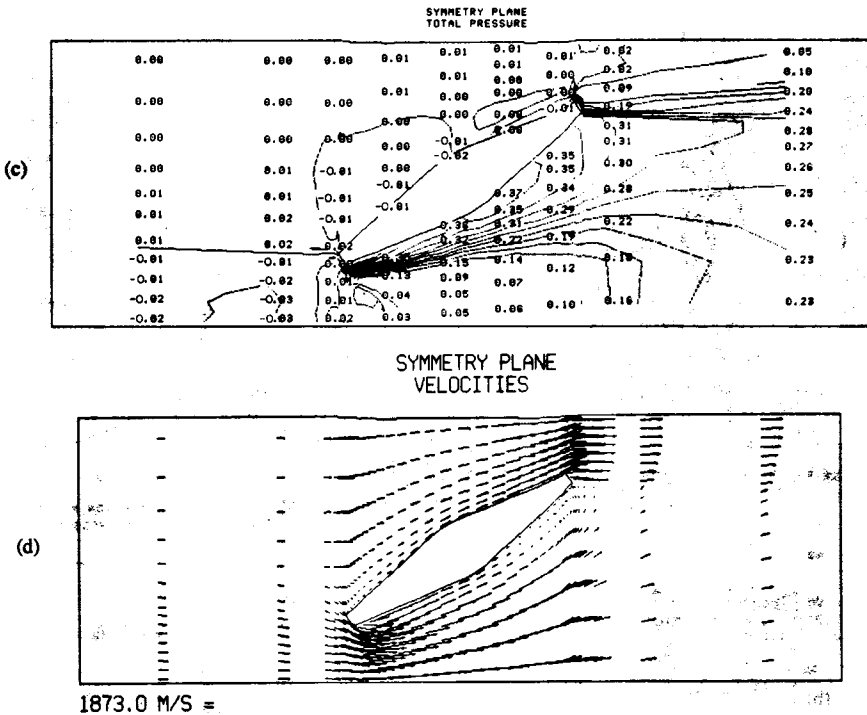


Figure 21.5.8 (Continued)

shown in Figure 21.5.8, vortex sheets at the leading and trailing edges of the valve are captured. The sheet is widened to a finite thickness by numerical diffusion. It has been shown by Powell *et al.* (1987) that any discretization of a vortex sheet, with at least one internal mesh point, necessarily results in a total pressure drop over the sheet, with an intensity imposed by the conservation laws and practically independent of the numerical diffusion. In addition, comparisons with Navier–Stokes calculations show that the genuine viscous contributions to the total pressure variation are generally small. This is fully confirmed by the present calculations and by comparison with the experimental data. Finally, Figure 21.5.9 shows Mach number, stagnation pressure and crossflow velocities in selected cross-sections, illustrating the complexity of the flow.

An interesting experimental investigation of the compressible flow conditions in butterfly valves has been performed by Morris and Dutton (1988). It is shown in Figure 21.5.10 which displays the Schlieren photographs of the flow at two pressure ratios with the corresponding static pressure distributions. The valve is inclined at 45° and has a flat plate configuration. Although the conditions are not identical to the geometry considered in the computations, the similarity between the theoretical and experimental results is striking. The captured vortex sheets and the static pressure distributions are indeed very similar. In particular

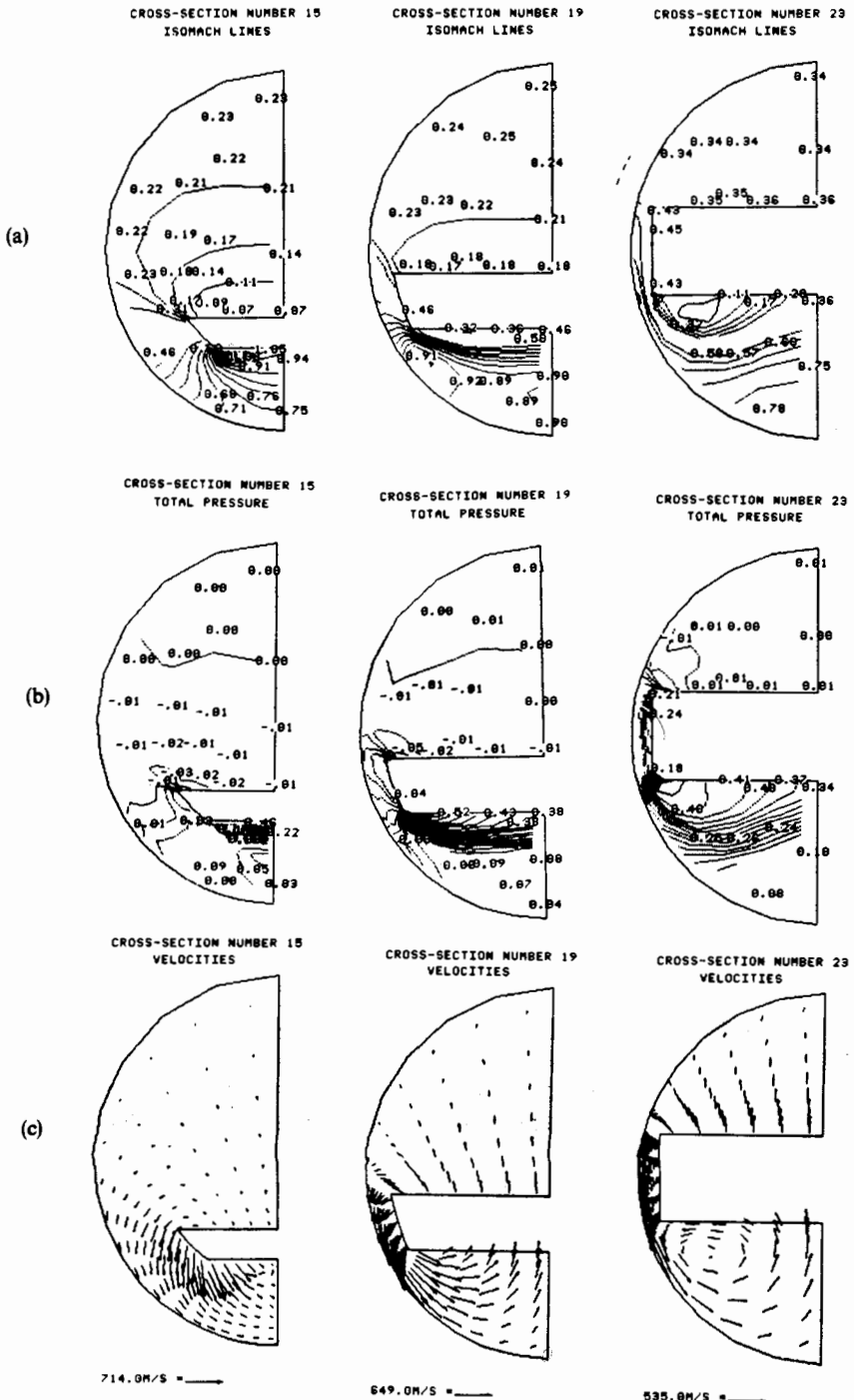
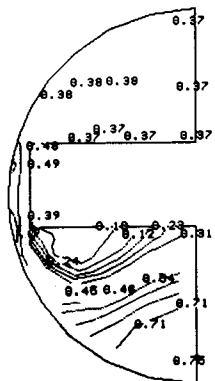
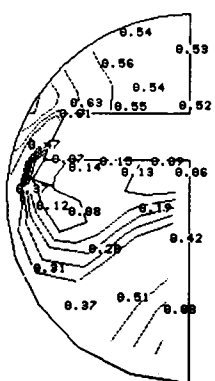
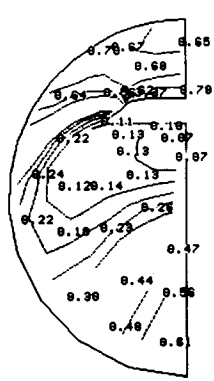
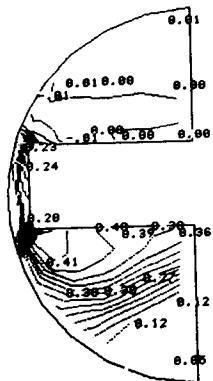
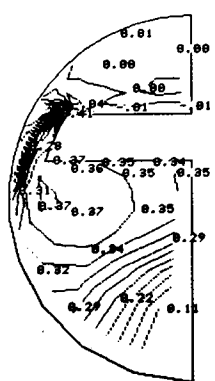
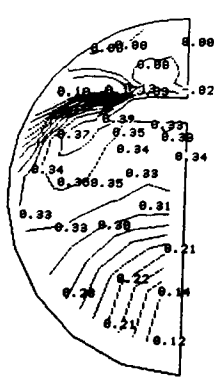
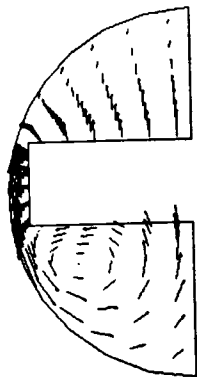
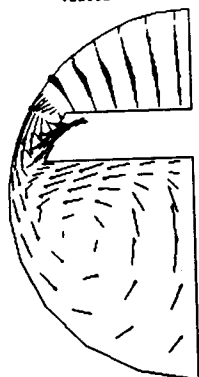
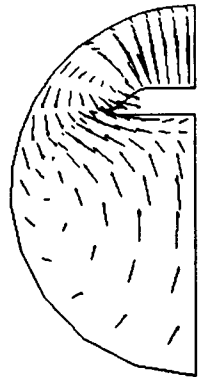


Figure 21.59 (a) Calculated Mach number, (b) total pressure and (c) velocities in several cross-sections of the butterfly valve at 30° incidence and $\Delta p = 0.25$

CROSS-SECTION NUMBER 24
ISOMACH LINESCROSS-SECTION NUMBER 28
ISOMACH LINESCROSS-SECTION NUMBER 32
ISOMACH LINESCROSS-SECTION NUMBER 24
TOTAL PRESSURECROSS-SECTION NUMBER 28
TOTAL PRESSURECROSS-SECTION NUMBER 32
TOTAL PRESSURECROSS-SECTION NUMBER 24
VELOCITIESCROSS-SECTION NUMBER 28
VELOCITIESCROSS-SECTION NUMBER 32
VELOCITIES

467.0M/S =

395.0M/S =

326.0M/S =

Figure 21.5.9 (Continued)

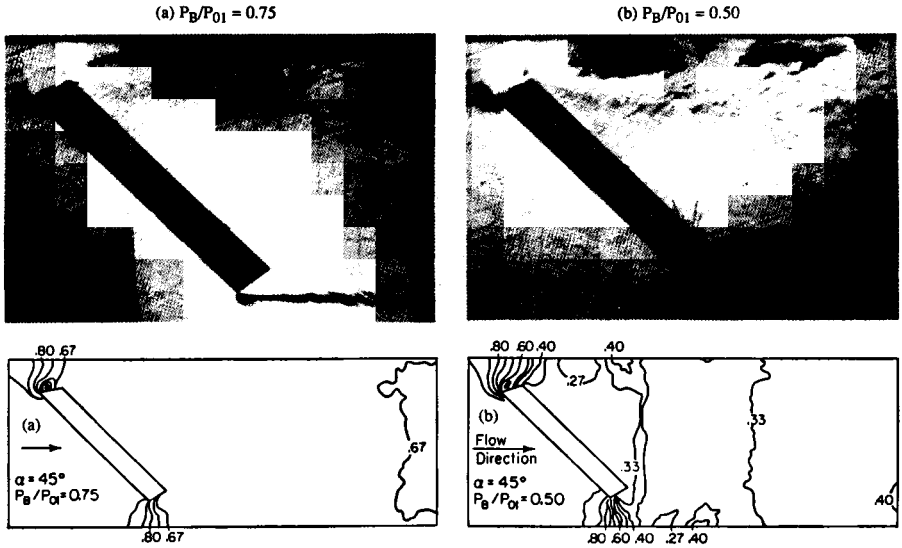


Figure 21.5.10

the fact that one of the vortex sheets is more diffused than the other is also well reproduced by the computation.

Conclusions

The concept of total variation has led to a rigorous formulation of higher-order monotonicity-preserving schemes. TVD schemes are globally second-order accurate, but reduce to first-order accuracy at local extrema of the solution. The TVD approach can also be used to generate artificial dissipation terms for central schemes, avoiding thereby the adaptation of 'empirical' constants attached to all of the artificial dissipation formulas discussed earlier in Section 17.3.

It can be proven that high-resolution schemes obtained via non-linear limiters converge to a unique weak solution if the entropy condition is satisfied.

These proofs are, however, restricted to one-dimensional non-linear scalar equations and to linear systems of hyperbolic equations. The extensions to one-dimensional non-linear systems is done in formal analogy to the scalar case.

The situation is even less firmly based for multi-dimensional problems since there is no clear extension of the TVD definitions to these cases. The straightforward extension of the one-dimensional definitions to multi-dimensions implies that a conservative TVD scheme for scalar conservation laws in two dimensions is at most first-order accurate (Goodman and Leveque, 1985). Hence, the extension of TVD schemes to multi-dimensions is performed on an *ad hoc* basis by local one-dimensional decompositions. Experiences with various schemes indicate, however, that oscillation-free results can be obtained in this way.

21.6 CONCLUSIONS TO PART VI

The methodology for obtaining numerical solutions of the full system of Euler equations has now come to a mature state. A large variety of efficient methods are available but objective recommendations seem hardly possible since none of the approaches has come out with undisputed advantages over the others. Hence, the final selection will most probably be a combination of subjective judgement, experience and personal non-rational choice.

The key elements in the choice of a method are:

- (1) The mesh: structured or unstructured, fixed or adaptative
- (2) The space discretization: central or upwind
- (3) The time integration: explicit or implicit

in addition to the large number of variants within these groups.

One of the most important problems in a high-level numerical simulation is related to the mesh generation and the mesh configuration.

A choice has to be made between structured and unstructured meshes. The former has the clear benefit of simplicity and straightforward treatment of the mesh, but in complex configurations it leads to severe constraints on the mesh generation. The unstructured, finite element-type meshes benefit from an extremely large flexibility at the expense of a heavier bookkeeping of the nodes and their connectivity. An intermediate option is the use of a multi-domain approach with appropriate interfaces.

In addition, with increasing numbers of mesh points, one attempts to optimize the ratio of accuracy to number of mesh points by concentrating mesh points in the regions of severe gradients, such as stagnation points and discontinuities. Since the location of these regions is not known *a priori*, a dynamic treatment can be developed, namely adaptive meshes, whereby the points are redistributed during the iteration process as a function of certain gradient detection parameters. This can be done by local refinements and (or) by moving existing mesh points of the initial mesh. This is an important concept and we refer the reader to the available literature.

Several finite element methods for Euler equations have been developed, either based on Lax–Wendroff-type methods, coupled with flux limiting on the main variables (Lohner *et al.*, 1987; Peraire *et al.*, 1987), or based on upwind considerations (Angrand *et al.*, 1983; Hughes and Mallet, 1986; Stoufflet *et al.*, 1987; Thareja *et al.*, 1988, and cited references). Most of these developments are combined with adaptive grids where the finite element flexibility comes at its full advantage.

Note also that finite volume methods are easily adapted to unstructured meshes and we refer to Figure 18.3.1, computed on an unstructured mesh, for a typical example.

From the point of view of the space discretization, the first choice is between central or upwind discretizations. The central schemes are the easiest to programme and lead to simple codes when applied with finite volume methods.

They require, however, the introduction of artificial dissipation terms, containing adjustable and problem-dependent parameters, which have generally to be calibrated for optimum performance. This might be considered as the main weakness of the central schemes, although a large body of experience with some of the most currently applied formulations is available. But clearly any new application will require a new calibration.

The other branch of the alternative lies in the upwind discretizations and we have presented the general framework for the generation of schemes with high resolution with second-, or higher, order space accuracy. These schemes are somewhat more time consuming to programme and the flux evaluations require more arithmetic operations compared to central schemes. However the introduction of the TVD limiters ensures the required mechanism for preventing unwanted oscillations and instabilities, without adjustable parameters. This is a strong advantage in complex flows, particularly in the presence of strong gradients and discontinuities and has to be considered as the main advantage of the upwind schemes. Although the multi-dimensional extension of the TVD concepts is theoretically not firmly established at this time, most *ad hoc* extensions perform excellently. The price for this extended and problem-independent formulation is a larger arithmetic operation count per mesh point, per iteration.

However one of the most spectacular outcomes of the analysis and development of TVD schemes is the bridge that can be established between the upwind and central discretizations, as discussed in Section 21.4.4. This allows central schemes to be formulated with an adapted dissipation satisfying TVD requirements and provides a most interesting compromise, since the basic flux evaluations can be performed with the simplicity of the central schemes.

With regard to the time integration, we have also seen that a variety of methods can be selected independently of the choice made for the space discretization. They can be grouped into two categories, explicit or implicit methods. The former are again simple to programme and imply a minimal cost per time step, but the CFL condition limits severely the maximum allowable time step. Implicit methods, on the other hand, allow, at least linearly, unlimited time steps at an increased computational cost per iteration and more laborious programming.

Some general guidelines can nevertheless be formulated. If the flow to be simulated is unsteady, a time-accurate solution is required and obviously one will look out for applying an explicit method. However, it is essential to determine the time scale of the physical unsteady phenomena under investigation and to compare it with the time step arising from the CFL condition. If the ratio of these two time scales is very high, a large number of numerical time steps will be needed to cover the physical time interval. In this case, implicit methods with time-accurate inversion of the implicit operators should be recommended.

For steady-state computations, the time history is not significant and explicit methods require the support of performant acceleration techniques, such as

multi-grid, to be cost effective. Although multi-grid with Lax–Wendroff-type methods have been successfully applied, most of the effective Euler codes do rely in some way on implicit methods. It is to be noted at this point that the explicit, multi-stage, Runge–Kutta methods, discussed in Chapter 18, which already allow a CFL number higher than one (close to three for a four-stage method), are enhanced by the so-called residual averaging, which is actually an implicit step.

A most promising approach is therefore to apply, with central as well as with upwind schemes, implicit operators that allow extremely high Courant numbers, in order to approach a Newton method. This can be achieved by calling on flux splitting concepts in order to generate diagonal-dominant implicit operators which can be solved by relaxation techniques coupled to multi-grid acceleration. Many variants can be selected at this point and the choice of the most cost-effective iteration scheme depends on the computer architecture. Many relaxation procedures can be tuned for easy vectorization, such as Zebra relaxation, but it can be expected that upcoming parallel machines will require adapted methods to take full benefit of their specific structure.

The combined evolution of computer hardware, in particular the availability of supercomputers, and algorithmic improvements allow today steady two-dimensional Euler solutions to be obtained in seconds of computer time. It is interesting to remember, for proper comparison, that in the 1970s numerical solutions of the two-dimensional Euler equations were attached to hours of computer time. Three-dimensional computations on simple geometries are on the level of minutes of CPU, with the best efficient codes. Introduction of Euler codes in the industrial design process is consequently of direct application.

With its established basis, Euler codes can now be applied to complex configurations such as the computation of the flow over a complete aircraft, the introduction of real gas effects, such as air in non-equilibrium, the flow in a complete turbomachinery stage, and so on.

References

- Anderson, W. K., Thomas, J. L., and Van Leer, B. (1986a). 'Comparison of finite volume flux vector splittings for the Euler equations.' *AIAA Journal*, **24**, 1453–60.
- Anderson, W. K., Thomas, J. L., and Whitfield, D. L. (1986b). 'Multigrid acceleration of the flux split Euler equations.' *AIAA Paper 86-0274*, AIAA 24th Aerospace Sciences Meeting.
- Angrand, F., Dervieux, A., Boulard, V., Periaux, J., and Vijayasundaram, G. (1983). 'Transonic Euler simulations by means of finite element explicit schemes.' *AIAA Paper 83-1924, Proc. AIAA 6th Computational Fluid Dynamics Conference*, pp. 267–73.
- Ben-Artzi, M., and Falcovitz, J. (1984). 'A second order Godunov-type scheme for compressible fluid dynamics.' *Journal Computational Physics*, **55**, 1–32.
- Boris, J. P., and Book, D. L. (1973). 'Flux corrected transport: I. SHASTA, a fluid transport algorithm that works.' *Journal Computational Physics*, **11**, 38–69.
- Boris, J. P., and Book, D. L. (1976). 'Solution of the continuity equation by the method of flux corrected transport.' *Journal Computational Physics*, **16**, 85–129.
- Borrel, M., and Montagne, J. L. (1985). 'Numerical study of a non-centered scheme with

- application to aerodynamics.' *AIAA Paper 85-1497, Proc. AIAA 7th Computational Fluid Dynamics Conference*, pp. 88-97.
- Buning, P. G., and Steger, J. L. (1982). 'Solution of the two-dimensional Euler equations with generalized coordinate transformations using flux vector splitting.' *AIAA Paper 82-0971, AIAA/ASME 3rd Joint Thermophysics Conference*.
- Casier, F., Deconinck, H., and Hirsch, Ch. (1983). 'A class of central bidiagonal schemes with implicit boundary conditions for the solution of Euler's equations.' *AIAA Paper 83-0126, AIAA 21st Aerospace Sciences Meeting*; see also *AIAA Journal*, **22**, 1556-63.
- Chakravarthy, S. R. (1984). 'Relaxation methods for unfactored implicit upwind schemes.' *AIAA Paper 84-0165, AIAA 22nd Aerospace Sciences Meeting*.
- Chakravarthy, S. R., and Osher, S. (1983). 'High resolution applications of the Osher upwind scheme for the Euler equations.' *AIAA Paper 83-1943, Proc. AIAA 6th Computational Fluid Dynamics Conference*, pp. 363-73.
- Crandall, M. G., and Majda, A. (1980). 'Monotone difference approximations for scalar conservation laws.' *Mathematics of Computation*, **34**, 1-34.
- Davis, S. F. (1984). 'TVD finite difference schemes and artificial viscosity.' *ICASE Report 84-20, NASA CR-172373, NASA Langley Research Center*.
- Deese, J. E. (1983). 'Numerical experiments with the split flux vector form of the Euler equations.' *AIAA Paper 83-0122, AIAA 21st Aerospace Sciences Meeting*.
- Deese, J. E. (1985). 'Split flux vector solutions of the Euler equations for three dimensional configurations.' *AIAA Paper 85-0434, AIAA 23rd Aerospace Sciences Meeting*.
- Diperna, R. J. (1983). 'Convergence of approximate solutions to conservation laws.' *Arch. Rat. Mechanics and Analysis*, **82**, 27-70.
- Engquist, B., and Osher, S. (1981). 'One-sided difference approximations for nonlinear conservation laws.' *Mathematics of Computation*, **36**, 321-52.
- Fromm, J. E. (1968). 'A method for reducing dispersion in convective difference schemes.' *Journal Computational Physics*, **3**, 176-89.
- Godunov, S. K. (1959). 'A difference scheme for numerical computation of discontinuous solution of hydrodynamic equations.' *Math. Sbornik*, **47**, 271-306 (in Russian). Translated US Joint Publ. Res. Service, *JPRS 7226* (1969).
- Goodman, J. B., and Leveque, R. J. (1985). 'On the accuracy of stable schemes for 2D scalar conservation laws.' *Mathematics of Computation*, **45**, 156-71.
- Harten, A. (1983). 'High resolution schemes for hyperbolic conservation laws.' *Journal Computational Physics*, **49**, 357-93.
- Harten, A. (1984). 'On a class of high resolution total variation stable finite difference schemes.' *SIAM Journal Numerical Analysis*, **21**, 1-23.
- Harten, A., and Lax, P. D. (1981). 'A random choice finite difference scheme for hyperbolic conservation laws.' *SIAM Journal Numerical Analysis*, **18**, 289-315.
- Harten, A., and Osher, S. (1987). 'Uniformly high-order accurate nonoscillatory schemes I.' *SIAM Journal Numerical Analysis*, **24**, 279-309.
- Harten, A., Hyman, J. M., and Lax, P. D. (1976). 'On finite difference approximations and entropy conditions for shocks.' *Comm. Pure and Applied Mathematics*, **29**, 297-322.
- Hartwich, P.-M., Hsua, C. H., and Liu, C. H. (1988). 'Total variation diminishing (TVD) schemes of uniform accuracy.' *NASA TM 100552, NASA Langley Research Center*.
- Hemker, P. W., and Spekrijse, S. P. (1986). 'Multiple grid and Osher's scheme for the efficient solution of the steady Euler equations.' *Applied Numerical Mathematics*, **2**, 475-93.
- Hughes, T. J. R., and Mallet, M. (1986). 'A new finite element formulation for computational fluid dynamics: III. The generalized streamline operator for multi-dimensional advective-diffusive systems.' *Computer methods of Applied Mechanics and Engineering*, **58**, 305-28.
- Jameson, A., and Lax, P. D. (1984). 'Conditions for the construction of multi-point total variation diminishing difference schemes.' Department of Mechanical and Aerospace Engineering, University of Princeton, *MAE Report 1650*.

- Kruskov, S. N. (1970). 'First order quasi-linear equations in several independent variables.' *Math. USSR Sbornik*, **10**, 217-43.
- Lacor, C., and Hirsch, C. (1988). 'Numerical simulation of the three-dimensional flow around a butterfly valve.' *Proc., International Symposium on Fluid Dynamics in Non-Rotating Turbomachinery Components*, ASME Winter Annual Meeting, FED-Vol. 69, pp. 1-12, Chicago, USA.
- Lax, P. D. (1973). *Hyperbolic Systems of Conservation Laws and the Mathematical Theory of Shock Waves*, Philadelphia: SIAM Publications.
- Leonard, B. P. (1979). 'A stable and accurate convective modelling procedure based on quadratic upstream interpolation.' *Computer Methods of Applied Mechanics and Engineering*, **19**, 59-98.
- Liou, M. S., and Van Leer, B. (1988). 'Choice of implicit and explicit operators for the upwind differencing method.' *AIAA Paper 88-0624*, AIAA 26th Aerospace Sciences Meeting.
- Lohner, R., Morgan, K., Peraire, J., and Vahdati, M. (1987). 'Finite element flux-corrected transport for the Euler and Navier-Stokes equations.' *Int. Journal Numerical Methods Fluids*, **7**, 1093-109.
- Lombard, C. K., Bardina, J., Venkatapathy, E., and Olinger, J. (1983). 'Multidimensional formulation of CSCM—an upwind flux difference eigenvector split method for the compressible Navier-Stokes equations.' *AIAA Paper 83-1895*, *Proc. AIAA 6th Computational Fluid Dynamics Conference*, pp. 649-64.
- Majda, A., and Osher, S. (1979). 'Numerical viscosity and entropy condition.' *Comm. Pure and Applied Mathematics*, **32**, 797-838.
- Marchuk, G. I. (1975). *Methods of Numerical Mathematics*, Berlin: Springer Verlag.
- Morris, M. J., Dutton, J. C. (1988). 'Compressible flowfield characteristics of butterfly valves.' *ASME Paper 88-WA/FE-12*, *ASME 1988 Winter Annual Meeting, Chicago, USA*.
- Mulder, W. A. (1985). 'Multigrid relaxation for the Euler equations.' *Journal Computational Physics*, **60**, 235-52.
- Mulder, W. A., and Van Leer, B. (1983). 'Implicit upwind methods for the Euler equations.' *AIAA Paper 83-1930*, *Proc. AIAA 6th Computational Fluid Dynamics Conference*, pp. 303-10.
- Napolitano, M., and Dadone, A. (1985). 'Implicit lambda methods for three-dimensional compressible flows.' *AIAA Journal*, **23**, 1343-7.
- Oleinik, O. A. (1957). 'Discontinuous solutions of nonlinear differential equations.' *Uspekhi Mat. Nauk*, **12**, 3-73 (in Russian). English translation in *Am. Math. Soc. Trans., Series 2*, **26**, 95-172.
- Osher, S. (1984). 'Riemann solvers, the entropy condition and difference approximations.' *SIAM Journal Numerical Analysis*, **21**, 217-35.
- Osher, S. (1985). 'Convergence of generalized MUSCL schemes.' *SIAM Journal Numerical Analysis*, **22**, 947-61.
- Osher, S., and Chakravarthy, S. R. (1984). 'High resolution schemes and the entropy condition.' *SIAM Journal Numerical Analysis*, **21**, 955-84.
- Peraire, J., Vahdati, M., Morgan, K., and Zienkiewicz, O. C. (1987). 'Adaptive remeshing for compressible flow computations.' *Journal Computational Physics*, **72**, 449-66.
- Powell, K. G., Murman, E. M., Perez, E. S., and Baron, J. R. (1987). 'Total pressure loss in vortical solutions of the conical Euler equations.' *AIAA Journal*, **25**, 360-8.
- Rai, M. M., and Chakravarthy, S. (1984). 'An implicit form for the Osher upwind scheme.' *AIAA Paper-84-0088*, AIAA 22nd Aerospace Sciences Meeting.
- Roe, P. L. (1984). 'Generalized formulation of TVD Lax-Wendroff schemes.' *ICASE Report 84-53*, NASA CR-172478, NASA Langley Research Center.
- Roe, P. L. (1985). 'Some contributions to the modelling of discontinuous flows.' *Proc. 1983 AMS-SIAM Summer Seminar on Large Scale Computing in Fluid Mechanics, Lectures in Applied Mathematics*, Vol. 22, pp. 163-93. SIAM, Philadelphia.

- Roe, P. L., and Baines, M. J. (1982). 'Algorithms for advection and shock problems.' *Proc. 4th GAMM Conference on Numerical Methods in Fluid Mechanics*, Braunschweig, Vieweg.
- Z Salezka, S. T. (1979). 'Fully multidimensional flux-corrected transport.' *Journal of Computational Physics*, **31**, 355-62.
- Steger, J. L., and Warming, R. F. (1981). 'Flux vector splitting of the inviscid gas-dynamic equations with applications to finite difference methods.' *Journal Computational Physics*, **40**, 263-93.
- Stoufflet, B., Periaux, J., Fezoui, F., and Dervieux, A. (1987). 'Numerical simulation of 3D hypersonic Euler flows around space vehicles using adapted finite elements.' *AIAA Paper 87-0560*, AIAA 25th Aerospace Sciences Meeting.
- Sweby, P. K. (1984). 'High resolution schemes using flux limiters for hyperbolic conservation laws.' *SIAM Journal Numerical Analysis*, **21**, 995-1011.
- Tadmor, E. (1984). 'The large time behavior of the scalar, genuinely nonlinear Lax-Friedrichs scheme.' *Mathematics of Computation*, **43**, 353-68.
- Thareja, R. R., Steward, J. R., Hassan, O., Morgan, K., and Peraire, J. (1988). 'A point implicit unstructured grid solver for the Euler and Navier-Stokes equations.' *AIAA Paper 88-0036*, AIAA 21st Aerospace Sciences Meeting.
- Thomas, J. L., Van Leer, B., and Walters, R. W. (1985). 'Implicit flux-split schemes for the Euler equations.' *AIAA Paper 85-1680*, AIAA 18th Fluid Dynamics, Plasma Dynamics and Lasers Conference.
- Turkel, E., and Van Leer, B. (1984). 'Flux vector splitting and Runge-Kutta methods for the Euler equations.' *ICASE Report 84-27*, NASA CR 172415, NASA Langley Research Center.
- Van Albada, G. D., Van Leer, B., and Roberts, W. W. (1982). 'A comparative study of computational methods in cosmic gas dynamics.' *Astron. Astrophysics*, **108**, 76-84.
- Van Leer, B. (1973). 'Towards the ultimate conservative difference scheme. I. The quest of monotonicity.' *Lecture Notes in Physics*, Vol. 18, pp. 163-68. Springer Verlag, Berlin.
- Van Leer, B. (1974). 'Towards the ultimate conservative difference scheme. II. Monotonicity and conservation combined in a second order scheme.' *Journal Computational Physics*, **14**, 361-70.
- Van Leer, B. (1977a). 'Towards the ultimate conservative difference scheme. III. Upstream-centered finite difference schemes for ideal compressible flow.' *Journal Computational Physics*, **23**, 263-75.
- Van Leer, B. (1977b). 'Towards the ultimate conservative difference scheme. IV. A new approach to numerical convection.' *Journal Computational Physics*, **23**, 276-99.
- Van Leer, B. (1979). 'Towards the ultimate conservative difference scheme. V. A second order sequel to Godunov's method.' *Journal Computational Physics*, **32**, 101-36.
- Warming, R. F., and Beam, R. W. (1976). 'Upwind second order difference schemes and applications in aerodynamic flows.' *AIAA Journal*, **24**, 1241-9.
- Woodward, P. R., and Colella, P. (1984a). 'The numerical simulation of two-dimensional fluid flow with strong shocks.' *Journal Computational Physics*, **54**, 115-73.
- Woodward, P. R., and Colella, P. (1984b). 'The piecewise parabolic method (PPM) for gas dynamical calculations.' *Journal Computational Physics*, **54**, 174-201.
- Yee, H. C. (1985). 'On symmetric and upwind TVD schemes.' *Proc. 6th GAMM Conference on Numerical Methods in Fluid Mechanics*, pp. 399-407, Braunschweig: Vieweg.
- Yee, H. C. (1986a). 'Linearized form of implicit TVD schemes for multidimensional Euler and Navier-Stokes equations.' *Computers and Mathematics with Applications*, **12A**, 413-32.
- Yee, H. C. (1986b). 'Numerical experiments with a symmetric high resolution shock-capturing scheme.' *NASA TM 88325*, NASA AMES Research Center.
- Yee, H. C. (1987a). 'Construction of explicit and implicit symmetric TVD schemes and their applications.' *Journal Computational Physics*, **68**, 151-79.

- Yee, H. C. (1987b). 'Upwind and symmetric shock-capturing schemes.' *NASA TM 89464*, NASA AMES Research Center.
- Yee, H. C., and Harten, A. (1985). 'Implicit TVD schemes for hyperbolic conservation laws in curvilinear coordinates.' *AIAA Paper 85-1513, Proc. AIAA 7th Computational Fluid Dynamics Conference*, pp. 228-41.

PROBLEMS

Problem 21.1

Show that the straightforward second-order generalization of the first-order upwind scheme, obtained by taking second-order one-sided differences in space with a first-order difference in time, is unconditionally unstable. Consider the scheme

$$u_i^{n+1} - u_i^n = -\frac{\tau}{2}(3f_i^+ - 4f_{i-1}^+ + f_{i-2}^+) - \frac{\tau}{2}(-3f_i^- + 4f_{i+1}^- - f_{i+2}^-)$$

Perform a Von Neumann analysis on the linearized equation obtained with $f = au$ and $a > 0$, and show that the instability arises from the low-frequency errors.

Obtain the truncation error by a Taylor expansion and show that the instability arises from the first-order time differencing which generates a second-derivative term in the truncation error of the form αu_{xx} , with $\alpha < 0$.

Hint: Consider a linear case with $a > 0$, and analyse the scheme

$$u_i^{n+1} - u_i^n = -\frac{\sigma}{2}(3u_i - 4u_{i-1} + u_{i-2})$$

Obtain

$$G = 1 - \sigma(1 - \cos \phi)^2 - I\sigma \sin \phi(2 - \cos \phi)$$

Consider the modulus of G in the low-frequency limit by performing a Taylor expansion around $\phi = 0$ and show that $|G| > 1$.

Consider the case $\phi = \pi$ in the expression of the amplification factor and note that the high frequencies are damped.

Problem 21.2

Obtain the amplification factor for the second-order upwind scheme (21.1.27). Calculate the diffusion and dispersion errors as a function of the Courant number σ and the phase angle ϕ . Show that the phase error is a leading error, that is $\epsilon_\phi > 1$, for $\sigma < 1$ and a lagging error for $1 < \sigma \leq 2$.

Obtain the stability condition $0 \leq \sigma \leq 2$.

Problem 21.3

Analyse the stability and error properties of Fromm's scheme (21.1.31). Obtain the stability condition and the results of Figure 21.1.6.

Problem 21.4

Obtain the counterpart of the second-order one-sided scheme (21.1.27) for flux functions with negative eigenvalues.

Take the Lax-Wendroff formulation as a starting point with forward first and second differences and obtain the scheme

$$u_i^{n+1} - u_i^n = -\frac{\sigma}{2}(-3u_i + 4u_{i+1} - u_{i+2}) + \frac{\sigma^2}{2}(u_i - 2u_{i+1} + u_{i+2})$$

Problem 21.5

Consider the second-order upwind scheme (21.1.26) applied to the linear scalar convection equation with $a > 0$ and consider the first-order upwind numerical flux.

Show that the following scheme is obtained:

$$u_i^{n+1} - u_i^n = -\frac{\sigma}{2}(u_{i+1} - u_{i-1})^n + \frac{\sigma^2}{2}(u_{i+1} - 2u_i + u_{i-1})^n \\ + \frac{\sigma}{4}(1 - \kappa - 2\sigma)(u_{i+1} - 3u_i + 3u_{i-1} - u_{i-2}^n)$$

Show that these schemes are second order in space and time for all values of κ and that the resulting scheme reduces to the second-order upwind Warming and Beam scheme for $\kappa = -1$.

Perform a Von Neumann analysis and obtain the stability conditions as a function of κ as $0 < \sigma < 1 - \kappa$.

Hint: Write the amplification factor and analyse the high-frequency behaviour.

Problem 21.6

Consider the second-order upwind scheme (21.1.26) applied to the linear scalar convection equation with $a > 0$, whereby the first step (21.1.26a) is replaced by the step (21.1.25a)

$$\bar{u}_i = u_i^n - \frac{\sigma}{2} \delta_i u^n$$

with

$$\delta_i u = \frac{1}{4}(1 - \kappa)(u_i - u_{i-1}) + \frac{1}{4}(1 + \kappa)(u_{i+1} - u_i)$$

Show that the resulting schemes reduce to Fromm's scheme for $\kappa = 0$, to the second-order upwind Warming and Beam scheme for $\kappa = -1$ and to the Lax-Wendroff scheme for $\kappa = 1$, if the basic first-order numerical flux is the first-order upwind scheme.

Problem 21.7

Apply the second-order upwind scheme (21.1.43) with the Steger and Warming flux splitting to the stationary nozzle of Problem 16.26 selecting a transonic case with and without a shock.

Problem 21.8

Repeat Problem 21.7 with the alternative non-linear variant (21.1.65).

Problem 21.9

Apply the second-order upwind scheme (21.1.65) with the flux splitting of Steger and Warming and $\kappa = -1$ to the shock tube problem of Problem 16.25, case 1. Repeat the same computations for higher shock intensities applying the initial conditions of case 2.

Observe the evolution of the results with increasing shock intensities.

Compare the results after the eigenvalue modification of equation (20.3.22) and observe the effects of increasing the parameter ε .

Problem 21.10

Repeat Problem 21.9 with the alternative non-linear variant (21.1.43).

Problem 21.11

Repeat Problem 21.7 with the variable extrapolation (MUSCL) approach (21.1.63).

Problem 21.12

Repeat Problems 21.7 to 21.11 with the Van Leer flux splitting.

Problem 21.13

Repeat Problem 21.7 with Roe's scheme (20.5.90).

Problem 21.14

Obtain equations (21.1.37) and (21.1.38).

Problem 21.15

Apply the Lax-Wendroff technique in order to obtain an explicit second-order scheme in space and time, by using upwind approximations for the discretization of $\partial f / \partial x$.

Hint: Referring to equation (17.2.4), apply the second-order upwind discretization (21.1.35) to $\partial f / \partial x$ and flux splitted upwind differences for the term $\partial_x(A \partial f_x)$. The resulting scheme is

$$U_i^{n+1} - U_i^n = -\tau \delta^- [(f_i^+ + f_{i+1}^-) + \frac{1}{2} \delta^- f_i^+ - \frac{1}{2} \delta^+ f_{i+1}^-]^n \\ + \frac{\tau^2}{2} [\delta^+ (A_i^- \delta^+ f_i^-) + \delta^- (A_i^+ \delta^- f_i^+)]^n$$

Show that this scheme is linearly equivalent to the second-order schemes (21.1.39) and (21.1.43) for $\kappa = -1$, making use of the property $A^+ A^- U = A^- A^+ U = 0$ and expanding the flux terms in these two-step schemes.

Problem 21.16

Consider three-point scalar conservative schemes written in incremental form (21.2.35).

Show that the derivative of the numerical fluxes with respect to the first and second arguments are given by

$$\frac{\partial f^*(u_i, u_{i+1})}{\partial u_i} = a_i - C_{i+1/2}^- \\ \frac{\partial f^*(u_i, u_{i+1})}{\partial u_{i+1}} = a_{i+1} - C_{i+1/2}^+$$

Show that for all first-order upwind schemes the derivative with respect to the first argument is positive, while the derivative of the numerical flux with respect to the second argument is negative. Explain why these schemes can be considered as TVD.

Problem 21.17

Obtain the TVD conditions for the implicit *three-point* schemes

$$u_i^{n+1} = u_i^n - \tau \theta (f_{i+1/2}^* - f_{i-1/2}^*)^{n+1} - \tau (1 - \theta) (f_{i+1/2}^* - f_{i-1/2}^*)^n$$

Write this scheme in incremental form

$$u_i^{n+1} = u_i^n - \tau\theta(C_{i+1/2}^- \delta u_{i+1/2} + C_{i-1/2}^+ \delta u_{i-1/2})^{n+1} \\ - \tau(1-\theta)(C_{i+1/2}^- \delta u_{i+1/2} + C_{i-1/2}^+ \delta u_{i-1/2})^n$$

and show that the scheme is TVD under the conditions (21.2.41) and the additional condition

$$\tau|a|_{i+1/2} \leq \tau D_{i+1/2} \leq \frac{1}{1-\theta}$$

where D is defined by equation (21.2.38). Note that these conditions imply that $0 \leq \theta \leq 1$.

Problem 21.18

Show by applying the definition (20.5.25) for the numerical flux of Godunov's scheme applied to a scalar flux function $f(u)$ that the numerical flux of an E-scheme is such that

$$f_{i+1/2}^* \leq f_{i+1/2}^{*(G)} \quad \text{if } u_{i+1} < u_i \\ f_{i+1/2}^* \geq f_{i+1/2}^{*(G)} \quad \text{if } u_{i+1} > u_i$$

Problem 21.19

Show that the Engquist–Osher scheme for a scalar conservation law, defined by equation (20.5.37), is an E-scheme. Show also that condition (21.2.44) reduces to

$$\tau \max[f'(u)] \leq 1$$

Problem 21.20

Prove equation (21.2.59) and show that the definitions (20.5.93) to (20.5.95) satisfy equation (21.2.60), in order to remove expansion shocks with Roe's scheme applied to a convex scalar conservation law.

Problem 21.21

Show that the Lax–Friedrich scheme for a scalar conservation law is a TVD scheme under the conditions (21.2.41) and (21.2.44).

Show also that the Lax–Friedrichs scheme is an E-scheme and hence satisfies an entropy condition.

Problem 21.22

Write the limited form of the second-order upwind scheme for the linear convection equation for $a < 0$, following the developments of equation (21.3.12).

Obtain the TVD conditions and show that they lead to the conditions (21.3.14) and hence to (21.3.16).

Problem 21.23

Obtain the limited form (21.3.19) of the Lax–Wendroff scheme

$$u_i^{n+1} = u_i^n - \sigma(u_i - u_{i-1})^n - \frac{\sigma}{2}(1-\sigma)\delta^- [\Psi(r_{i+1/2}^-)(u_{i+1} - u_i)^n]$$

and derive the TVD conditions. Show that equations (21.3.14) and (21.3.15) are recovered, leading to the TVD conditions of Figure 21.3.2.

Show also that the upwind TVD scheme (21.3.12) reduces identically to the limited Lax–Wendroff scheme if the limiter Ψ is chosen to satisfy the symmetry condition (21.3.26). This is a very remarkable property of second-order TVD schemes.

Hint: Write the scheme under the form (21.2.43), selecting $C^- \equiv 0$.

Repeat the calculations by selecting $C^+ \equiv 0$ and show that the same relations are again obtained.

Problem 21.24

Show that equation (21.3.28) reduces to the form (21.3.2) for the linear convection equation. Obtain equation (21.3.31).

Problem 21.25

Show that equations (21.3.32) imply the following restriction on the slopes of the linear variation, for $\kappa = 0$ and with reference to Figure 21.1.1 and equation (21.1.4):

$$\delta_i u \leq 2\delta^+ u_i \quad \text{and} \quad \delta_i u \leq 2\delta^- u_i$$

Show that these conditions applied to the ‘limited’ extrapolations (21.3.35) and (21.3.39) are satisfied if the limiters Ψ obey the relation $\Psi(r) \leq 2r$ and $\Psi \leq 2$.

Show also that the choice of the minmod limiter $\Psi(r) = \text{minmod}(r, 1)$ corresponds to limited slopes such that

$$[\delta_i u]_{\text{lim}} = \min(\delta^+ u_i, \delta^- u_i)$$

Problem 21.26

Show that the limiter (21.3.49) corresponds to limited interface values defined by

$$\bar{u}_{i+1/2} = u_i + \frac{1}{4}[(1 - \kappa) \text{minmod}(\delta^+ u_i, \beta \delta^- u_i) + (1 + \kappa) \text{minmod}(\delta^- u_i, \beta \delta^+ u_i)]$$

with $1 < \beta < (3 - \kappa)/(1 - \kappa)$.

Compare the cases $\beta = 1$ and $\beta = 2$ and plot the limiter (21.3.53) for $\kappa = 0$ and $\kappa = -1$.

Problem 21.27

Consider the second-order TVD Roe numerical flux given by equation (E21.3.7).

Write the scheme in the incremental form (21.2.35) and define the C^\pm coefficients.

Show that the TVD conditions (21.2.41) are indeed satisfied.

Problem 21.28

Show that the scheme restricted to the first part of the second-order space- and time-accurate upwind scheme (21.1.39), namely

$$\bar{u}_i = u_i^n - \frac{\tau}{2}(f_{i+1/2}^* - f_{i-1/2}^*)^n$$

with

$$\overline{f_{i+1/2}^*} = f^*(\bar{u}_i, \bar{u}_{i+1})$$

and

$$u_i^{n+1} = u_i^n - \tau(\overline{f_{i+1/2}^*} - \overline{f_{i-1/2}^*})$$

is only first-order accurate, monotone and hence TVD.

Extend the linearized form of this scheme to the general form, where γ is a free

parameter:

$$u_i^{n+1} - u_i^n = -\sigma(u_i - u_{i-1})^n + \sigma\gamma(u_i - 2u_{i-1} + u_{i-2})^n$$

and obtain the Von Neumann stability conditions for $\sigma > 0$, $2\gamma \leq 1$ and $\sigma(1 - 2\gamma) \leq 1$ and the TVD conditions $0 \leq \gamma \leq 1$ and $\sigma(1 - \gamma) \leq 1$.

Observe why the second-order Warming and Beam upwind scheme is not TVD.

Hint: Apply the two-step scheme to the linear convection equation, with $a > 0$, and a first-order upwind scheme as predictor step and obtain

$$u_i^{n+1} - u_i^n = -\sigma(u_i - u_{i-1})^n + \frac{\sigma^2}{2}(u_i - 2u_{i-1} + u_{i-2})^n$$

Show that the monotonicity condition (21.2.24) and the TVD condition (21.2.52b) are satisfied. Show also that this scheme is first order and stable under the CFL condition $0 < \sigma \leq 1$.

Problem 21.29

Obtain equation (21.4.16) and prove the TVD conditions (21.4.18).

Following the developments of Section 21.3.2, work out explicitly the scheme (21.4.15c).

Problem 21.30

Show that the limited Lax–Wendroff scheme with the numerical flux (21.4.28) is TVD under the CFL-like condition (21.4.8).

Hint: Obtain the C coefficients of the incremental form (21.2.43) and apply the TVD conditions.

Problem 21.31

Show that the sum of the terms $(f + g)$ in the numerical flux (21.4.32) of Harten's modified flux approach is equal to the Lax–Wendroff terms, prior to limiting.

Work the scheme out for a linear convection equation and compare with the limited Lax–Wendroff scheme (21.3.19), selecting the minmod limiter $\Psi(r) = \text{minmod}(1, r)$.

Problem 21.32

Obtain the expressions (21.4.48) for the numerical flux (21.4.43).

Problem 21.33

Prove the relations (21.4.51) and show that $Q/r^\pm < 1$ for the CFL-like condition $|\sigma| < \frac{2}{3}$ while $Q/r < 2$ for $|\sigma| < \frac{1}{2}$.

Problem 21.34

Write explicitly the C^\pm coefficients of the incremental form (21.2.43) for the TVD Lax–Wendroff scheme (21.4.28) and show that these coefficients are increased, in absolute value, with respect to the first-order values in the situation of a sonic expansion as described in Section 21.4.4.

PART VII: THE NUMERICAL SOLUTION OF THE NAVIER–STOKES EQUATIONS

Solving the full system of Navier–Stokes equations is the ultimate goal of a numerical flow simulation. It is accepted, indeed, that all the properties of a continuous flow system can be described by the Navier–Stokes equations.

For laminar flows, the only requested input to the flow equations are the dependence relations of the viscosity and heat conductivity coefficients, with pressure and temperature. Within the framework of continuum mechanics, these relations can only be obtained from *empirical* information. The accuracy of the final computation will be a function of the accuracy of these empirical data. However, for accepted viscosity and heat conduction coefficients, once the constitutive relations defining the nature of the fluid are defined, all possible flow configurations can be simulated numerically.

The situation is more uncertain for turbulent flows, since, at the level of the Reynolds-averaged Navier–Stokes equations, the uncertainty connected with the semi-empirical turbulence models will require a control of the accuracy of the computed flow properties by comparison with experimental data, in particular for the validation of sensitive variables such as wall shear stresses and heat transfer coefficients. However, the need for empirical turbulence information is not required at the level of the direct numerical simulation of turbulence.

At this level, direct solution of the Navier–Stokes equations in the Reynolds number range where turbulent instabilities occur allow the computation of the stochastic, turbulent fluctuating quantities, out of which Reynolds-averaged mean flow variables can be extracted.

The computational resources requested for practical computations at this highest level of flow simulation are several orders of magnitude above the level of computer power expected in the near future. As a consequence, only very simplified flow systems are computed today at this level of approximation. However, the data base generated in this way can be used to test and/or validate various assumptions at the basis of turbulence models. The interested reader might consult the Proceedings of a Workshop held in 1987 (Moin *et al.*, 1987)

or the summary report of Hunt (1988), describing the outcome of such an attempt.

Although direct simulation of turbulence will become increasingly important in the future, we will not discuss this field of computational fluid dynamics. The interested reader may refer to the following contributions, representative of the present state of the art (Rogallo and Moin, 1984; Kim *et al.*, 1987; Moin and Moser, 1988). Instead we will limit ourselves to the laminar or Reynolds-averaged Navier–Stokes equations.

This last part on Navier–Stokes equations is conceived as a concise presentation. Since most of the flow situations encountered in practice have high Reynolds numbers, they are dominated by convective effects. Hence, many of the various schemes developed for the Euler equations can be applied with the addition of the shear stress and heat conduction terms, which are always *centrally discretized* since they correspond to diffusive effects.

With the exception of the turbulence models, there is therefore not much to add to the description of the discretization techniques described in Chapters 17 to 21 and we will illustrate the numerical solution of the Navier–Stokes equations through typical examples.

The vanishing of the density–time derivative in the continuity equation for incompressible flows, on the other hand, creates some difficulties when the above-mentioned schemes have to be applied. This will require some special treatment.

Chapter 22 presents some essential properties of the system of coupled compressible Navier–Stokes equations, as well as an introduction to the Reynolds-averaged equations and the associated turbulence models.

Chapter 23 covers a discussion of the discretization techniques for the compressible Navier–Stokes equations in a time-dependent formulation based on the schemes developed for the Euler equations. The incompressible Navier–Stokes equations are treated separately and the pseudo-compressibility method for stationary flows as well as the pressure correction methods are introduced.

In particular, the pressure-correction methods can be applied to the stationary as well as the non-stationary Navier–Stokes equations. In the former case, they can also be applied within the framework of the parabolized Navier–Stokes approximation through a single downstream marching procedure, when experience confirms that the computed states are effectively stationary.

Chapter 22

The Properties of the System of Navier–Stokes Equations

The full system of compressible Navier–Stokes equations, for a Newtonian fluid, has been derived in Chapter 1 and discussed in Section 2.1 (Volume 1).

The differential conservative form of the equations, in terms of the fluxes, will have strong similarities with the Euler equations. Actually, this similarity will go very far, since compressibility is associated with high velocities and therefore with high Reynolds numbers. As a consequence, all of the schemes discussed in Part VI on the Euler equations can be applied to the discretization of the compressible Navier–Stokes equations.

22.1 MATHEMATICAL FORMULATION OF THE NAVIER–STOKES EQUATIONS

The Navier–Stokes equations can be cast, like the Euler system, in various forms after addition of the viscous and heat conduction terms. The reference form, connected to the integral conservation laws, is the conservative formulation.

22.1.1 Conservative form of the Navier–Stokes equations

Referring to Section 2.1 of Chapter 2 and to Chapter 16, the equations can be written as follows:

$$\frac{\partial}{\partial t} \begin{vmatrix} \rho \\ \rho \vec{v} \\ \rho E \end{vmatrix} + \vec{\nabla} \cdot \begin{vmatrix} \rho \vec{v} \\ \rho \vec{v} \otimes \vec{v} + p\vec{I} - \vec{\tau} \\ \rho \vec{v} H - \vec{\tau} \cdot \vec{v} - k\vec{\nabla} T \end{vmatrix} = \begin{vmatrix} 0 \\ \rho \vec{f}_e \\ \rho \vec{f}_e \cdot \vec{v} + q_H \end{vmatrix} \quad (22.1.1)$$

or

$$\frac{\partial U}{\partial t} + \vec{\nabla} \cdot \vec{F}_T = Q \quad (22.1.2)$$

The vector U of conservative variables is defined by equation (16.1.6) and the right-hand side is represented by the source vector Q . The flux vector \vec{F}_T contains

two components, the inviscid flux \bar{F} defined by equation (16.1.7) and a viscous contribution \bar{F}_v with Cartesian components (f_v, g_v, h_v) .

With the introduction of the total stress tensor $\bar{\sigma}$, \bar{I} being the unit tensor:

$$\bar{\sigma} = -\rho\bar{I} + \bar{\tau} \quad (22.1.3)$$

we can write the flux vector \bar{F}_T as

$$\bar{F}_T = \bar{F} - \bar{F}_v = \begin{vmatrix} \rho\bar{v} \\ \rho\bar{v} \otimes \bar{v} + p\bar{I} \\ \rho\bar{v}H \end{vmatrix} + \begin{vmatrix} 0 \\ -\bar{\tau} \\ -\bar{\tau} \cdot \bar{v} - k\bar{\nabla}T \end{vmatrix} = \bar{v}U - \begin{vmatrix} 0 \\ \bar{\sigma} \\ \bar{\sigma} \cdot \bar{v} + k\bar{\nabla}T \end{vmatrix} \quad (22.1.4)$$

and the Navier-Stokes equations as

$$\frac{\partial U}{\partial t} + \bar{\nabla} \cdot (\bar{F} - \bar{F}_v) = Q \quad (22.1.5)$$

We assume a perfect gas constitutive relation defined, for instance, by equation (16.2.16) and a Newtonian fluid defined by the two viscosity coefficients λ and μ , following equation (1.3.3) of Volume 1:

$$\tau_{ij} = \mu(\partial_i v_j + \partial_j v_i) + \lambda(\bar{\nabla} \cdot \bar{v})\delta_{ij} \quad (22.1.6)$$

Although this is the most general form for a Newtonian viscous fluid, we will consider the range of fluid behaviour within local thermodynamic equilibrium, for which the Stokes relation $3\lambda + 2\mu = 0$ is valid. Hence, the shear stresses become

$$\tau_{ij} = \mu(\partial_i v_j + \partial_j v_i) - \frac{2}{3}\mu(\bar{\nabla} \cdot \bar{v})\delta_{ij} \quad (22.1.7)$$

The temperature T is related to the conservative variable ρE by

$$T = \frac{1}{c_v} \left(E - \frac{\bar{v}^2}{2} \right) = \frac{e}{c_v} \quad (22.1.8)$$

where c_v is the specific heat under constant volume.

Note that the heat conduction flux $\bar{q}_c = -k\bar{\nabla}T$ is sometimes expressed as a function of the internal energy gradient as

$$\bar{q}_c = -\frac{\mu\gamma}{Pr} \bar{\nabla}e \quad (22.1.9a)$$

or

$$\bar{q}_c = -\frac{\mu}{Pr} \bar{\nabla}h \quad (22.1.9b)$$

where the Prandtl number Pr is introduced.

The components of \bar{F}_v are, in Cartesian coordinates,

$$f_v = \begin{vmatrix} 0 \\ \tau_{xx} \\ \tau_{xy} \\ \tau_{xz} \\ \tau_{xx}u + \tau_{xy}v + \tau_{xz}w + k \frac{\partial T}{\partial x} \end{vmatrix} = \begin{vmatrix} 0 \\ 2\mu \frac{\partial u}{\partial x} - \frac{2}{3}\mu(\bar{\nabla} \cdot \bar{v}) \\ \mu \left(\frac{\partial u}{\partial y} + \frac{\partial v}{\partial x} \right) \\ \mu \left(\frac{\partial u}{\partial z} + \frac{\partial w}{\partial x} \right) \\ 2\mu \frac{\partial u}{\partial x} u + \mu \left(\frac{\partial v}{\partial x} + \frac{\partial u}{\partial y} \right) v + \mu \left(\frac{\partial w}{\partial x} + \frac{\partial u}{\partial z} \right) w - \frac{2}{3}\mu(\bar{\nabla} \cdot \bar{v})v + k \frac{\partial T}{\partial x} \end{vmatrix} \quad (22.1.10)$$

$$g_v = \begin{vmatrix} 0 \\ \tau_{yx} \\ \tau_{yy} \\ \tau_{yz} \\ \tau_{yx}u + \tau_{yy}v + \tau_{yz}w + k \frac{\partial T}{\partial y} \end{vmatrix} = \begin{vmatrix} 0 \\ \mu \left(\frac{\partial u}{\partial y} + \frac{\partial v}{\partial x} \right) \\ 2\mu \frac{\partial v}{\partial y} - \frac{2}{3}\mu(\bar{\nabla} \cdot \bar{v}) \\ \mu \left(\frac{\partial v}{\partial z} + \frac{\partial w}{\partial y} \right) \\ \mu \left(\frac{\partial v}{\partial x} + \frac{\partial u}{\partial y} \right) u + 2\mu \frac{\partial v}{\partial y} v + \mu \left(\frac{\partial w}{\partial y} + \frac{\partial v}{\partial z} \right) w - \frac{2}{3}\mu(\bar{\nabla} \cdot \bar{v})v + k \frac{\partial T}{\partial y} \end{vmatrix} \quad (22.1.11)$$

$$h_v = \begin{vmatrix} 0 \\ \tau_{zx} \\ \tau_{zy} \\ \tau_{zz} \\ \tau_{zx}u + \tau_{zy}v + \tau_{zz}w + k \frac{\partial T}{\partial z} \end{vmatrix} = \begin{vmatrix} 0 \\ \mu \left(\frac{\partial w}{\partial x} + \frac{\partial u}{\partial z} \right) \\ \mu \left(\frac{\partial v}{\partial z} + \frac{\partial w}{\partial y} \right) \\ 2\mu \frac{\partial w}{\partial z} - \frac{2}{3}\mu(\bar{\nabla} \cdot \bar{v}) \\ \mu \left(\frac{\partial w}{\partial x} + \frac{\partial u}{\partial z} \right) u + \mu \left(\frac{\partial v}{\partial z} + \frac{\partial w}{\partial y} \right) v + 2\mu \frac{\partial w}{\partial z} w - \frac{2}{3}\mu(\bar{\nabla} \cdot \bar{v})w + k \frac{\partial T}{\partial z} \end{vmatrix} \quad (22.1.12)$$

22.1.2 Integral form of the Navier–Stokes equations

The integral form of the Navier–Stokes equations is the basis for all finite volume formulations. For an arbitrary control volume S , enclosing the volume Ω ,

equation (22.1.5) becomes

$$\frac{\partial}{\partial t} \int_{\Omega} U \, d\Omega + \oint_S \bar{F} \cdot d\bar{S} - \oint_S \bar{F}_v \cdot d\bar{S} = \int_{\Omega} Q \, d\Omega \tag{22.1.13}$$

Comparing to the Euler equations (16.1.1) to (16.1.3), the above equation leads to the same form with the addition of the shear and heat conduction terms expressed as boundary fluxes. The continuity equation is unchanged from the inviscid form

$$\frac{\partial}{\partial t} \int_{\Omega} \rho \, d\Omega + \oint_S \rho \bar{v} \cdot d\bar{S} = 0 \tag{22.1.14}$$

while the momentum equations have an additional shear stress term

$$\frac{\partial}{\partial t} \int_{\Omega} \rho \bar{v} \, d\Omega + \oint_S (\rho \bar{v} \otimes \bar{v} + p) d\bar{S} = \oint_S \bar{\tau} \cdot d\bar{S} + \int_{\Omega} \rho \bar{f}_e \, d\Omega \tag{22.1.15}$$

The energy conservation equation differs from the inviscid form by the presence of heat conduction and the work of the shear stresses:

$$\frac{\partial}{\partial t} \int_{\Omega} \rho E \, d\Omega + \oint_S \rho H \bar{v} \cdot d\bar{S} = \oint_S (\bar{\tau} \cdot \bar{v}) \cdot d\bar{S} + \oint_S k \frac{\partial T}{\partial n} dS + \int_{\Omega} (\rho \bar{f}_e \cdot \bar{v} + q_H) \, d\Omega \tag{22.1.16}$$

where $\partial T / \partial n$ is the temperature gradient in the direction normal to the boundary S .

22.1.3 Shock waves and contact layers

Due to viscosity effects and heat conduction, the inviscid discontinuities, such as shocks and contact discontinuities, are transformed into sharp but continuous

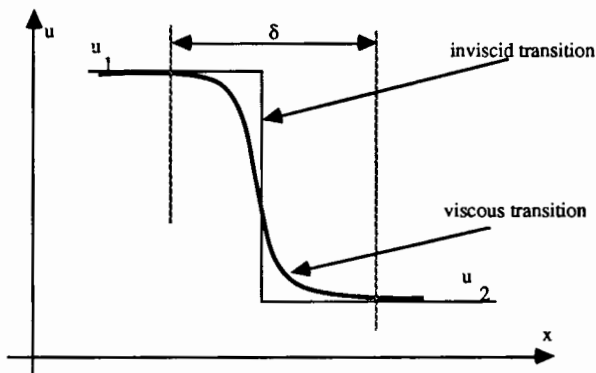


Figure 22.1.1 Viscosity and heat conduction effects on an inviscid discontinuity

variations (Figure 22.1.1). Therefore, the Navier–Stokes equations do not have solutions (in the weak sense) with discontinuous variations.

The distance δ over which the sharp shock transition takes place is of the order of $\nu^*/[u] \simeq \nu/[a^*(M - 1)]$ (Liepmann and Roshko, 1957), where ν^* is the viscosity at sonic conditions, $[u]$ the finite jump in velocity over the corresponding inviscid discontinuity, a^* the critical speed of sound and M the supersonic Mach number upstream of the shock. Hence, an internal structure over a thickness δ arises, conditioned by a balance between viscous and thermal effects, which can be resolved by a viscous computation.

However, this thickness δ is very small; for instance with a viscosity for air of $22 \times 10^{-6} \text{ m}^2/\text{s}$ and an upstream Mach number of $M_1 = 1.5$ we would have

$$\delta \simeq \frac{22 \times 10^{-6}}{300 \times 0.5} = 10^{-7} \text{ m} = 10^{-4} \text{ mm} \quad (22.1.17)$$

This distance is too small, in practice, to be resolved by a computational mesh and therefore, unless an exceptionally fine mesh is set up, the internal structure will not be computed. As a consequence, shocks will appear and be treated in the same way as in inviscid flows, that is they will be dominated by the numerical rather than by the physical dissipation.

22.1.4 Mathematical properties and boundary conditions

Compared to the Euler equations, the presence of viscosity and heat conduction transforms the conservation laws of momentum and energy into second-order partial differential equations. Hence, in the unknowns \bar{v} and e , these equations are parabolic in time and space and elliptic in space in the steady-state conditions. They are said to be parabolic–elliptic.

The continuity equation, on the other hand, is hyperbolic in space and time since it remains a first-order differential equation, considered as an equation for the density ρ .

The coupled system of the Navier–Stokes equations is therefore a hybrid system, being parabolic–hyperbolic in time and space but becoming of mixed elliptic–hyperbolic nature in space for the stationary formulation.

As discussed in Chapter 3 in Volume 1, elliptic operators of second order require one boundary condition on the whole boundary of the domain.

Therefore the Navier–Stokes equations require a greater number of boundary conditions than the Euler equations. More precisely, it is known, from the analysis of Gustafsson and Sundström (1978) (see also Dutt, 1988) that at an inflow boundary five boundary conditions have to be imposed, while four boundary conditions are required at an outflow boundary for three-dimensional viscous flows. The Euler equations, on the other hand, require five inflow conditions if the inlet velocity is supersonic but only four at subsonic inlet velocities. Also, as seen in Chapter 16, no conditions are to be imposed at a supersonic exit boundary and only one at a subsonic exit boundary for inviscid flows.

It is clear that the viscous boundary conditions have to be compatible with the inviscid conditions in the limit of vanishing viscosities. Otherwise, a non-physical boundary layer behaviour can appear with solutions behaving like $\exp(-x/\nu)$ when $\nu \rightarrow 0$, as shown by Gustafsson and Sundström (1978). Consequently, the additional viscous conditions should contain at most first-order streamwise derivatives and be defined in such a way that they can be assimilated to some form of extrapolated numerical boundary condition for vanishing viscosity.

Hence, the momentum and energy equations will require the velocity and temperature, or derivatives of these quantities, or a combination of function values and derivatives, to be fixed at the boundaries.

No-slip boundary condition at solid walls

Physical experience has to be used in order to determine the nature of the conditions to impose along solid wall boundaries. Within the framework of continuum mechanics, all known experiments indicate that the relative velocity between the fluid and the solid wall is zero. This is called the *no-slip* condition and is expressed by

$$\vec{v} = \vec{v}_w \quad \text{at solid walls} \quad (22.1.18)$$

where \vec{v}_w is the displacement velocity of the wall in the considered reference system.

For the temperature, either the wall temperature is fixed

$$T = T_w \quad \text{at solid walls} \quad (22.1.19)$$

or the heat flux is determined by the physical conditions, that is

$$-k \frac{\partial T}{\partial n} = q_w \quad (22.1.20)$$

where q_w is the wall heat flux. For an adiabatic wall $q_w = 0$.

The second thermodynamic variable at the solid wall can be obtained either by extrapolation from the inside or by applying the normal pressure equation. At a solid boundary with a no-slip condition, the momentum equation projected on the normal direction reduces to

$$\frac{\partial p}{\partial n} = (\vec{V} \cdot \vec{\tau})_n \quad (22.1.21)$$

where n refers to the normal direction and can be discretized appropriately as discussed in Chapter 19. For thin shear layers at high Reynolds numbers, this might be replaced by the boundary layer approximation

$$\frac{\partial p}{\partial n} = 0 \quad (22.1.22)$$

which can be used as an acceptable alternative for the pressure boundary condition.

In- and outflow boundaries

Along inlet boundaries, through which the flow enters the domain, the velocity and thermodynamic fields have to be given.

Along outlet boundaries, this is not generally possible, since the flow is strongly dependent on its evolution in the computed domain. Therefore, conditions on the normal derivative of \vec{v} and T are more appropriate, for instance, if the geometrical conditions allow for it:

$$\frac{\partial \vec{v}}{\partial n} = 0 \quad (22.1.23)$$

$$k \frac{\partial T}{\partial n} = 0 \quad (22.1.24)$$

Other forms of extrapolation from the inside towards the boundary can also be imposed; for instance, by expressing that tangential shear stress components vanish in far-field regions (Dutt, 1988).

One has to be aware that the problem of the appropriate boundary conditions and the nature of their numerical formulation is a most essential topic in the simulation of Navier–Stokes flows. Since there is no absolute and universal rule for the selection of boundary conditions, in particular along outlet flow boundaries, it is strongly recommended that the influence of the selected conditions on the computed flow properties be carefully controlled numerically.

22.2 REYNOLDS-AVERAGED NAVIER–STOKES EQUATIONS

The Reynolds-averaged Navier–Stokes equations are derived by averaging the viscous conservation laws over a time interval T , following the definitions of Section 2.2 in Volume 1. The time interval T is chosen large enough with respect to the time scale of the turbulent fluctuations, but has to remain small with respect to the time scales of other time-dependent effects. When this is possible, the time-dependent Reynolds-averaged continuity equation remains unchanged for the average densities and velocities, if density-weighted averaged velocities are defined, as shown in Section 2.2.

For any quantity A , the fluctuation A' is defined by

$$A = \bar{A} + A' \quad (22.2.1)$$

where

$$\bar{A}(\vec{x}, t) = \frac{1}{T} \int_{-T/2}^{T/2} A(\vec{x}, t + \tau) d\tau \quad (22.2.2)$$

is the mean turbulent-averaged value. The corresponding density-weighted

average is defined through

$$\tilde{A} = \frac{\overline{\rho A}}{\bar{\rho}} \quad (22.2.3)$$

with

$$A = \tilde{A} + A'' \quad (22.2.4)$$

and

$$\overline{\rho A''} = 0 \quad (22.2.5)$$

The averaged continuity equation becomes

$$\frac{\partial}{\partial t} \bar{\rho} + \bar{\nabla} \cdot (\bar{\rho} \bar{\mathbf{v}}) = 0 \quad (22.2.6)$$

The averaged momentum equations lead to the introduction of the Reynolds stress tensor, to be added to the averaged viscous stresses, as seen from equation (2.2.7), which is repeated here. Hence, all variables are considered as averaged quantities (density and pressure as time averages and velocities as density-weighted averages):

$$\frac{\partial}{\partial t} (\bar{\rho} \bar{\mathbf{v}}) + \bar{\nabla} \cdot (\bar{\rho} \bar{\mathbf{v}} \otimes \bar{\mathbf{v}} + \bar{\rho} \bar{\mathbf{I}} - \bar{\boldsymbol{\tau}}^v - \bar{\boldsymbol{\tau}}^R) = 0 \quad (22.2.7)$$

where the *Reynolds stresses* $\bar{\boldsymbol{\tau}}^R$ are defined by

$$\bar{\boldsymbol{\tau}}^R = -\overline{\rho \mathbf{v}'' \otimes \mathbf{v}''} \quad (22.2.8a)$$

In Cartesian coordinates,

$$\tau_{ij}^R = -\overline{\rho v_i'' v_j''} \quad (22.2.8b)$$

where \mathbf{v}'' designates the turbulent fluctuating velocity vector.

It is to be observed that all the effects of the turbulence on the averaged momentum conservation are contained in the Reynolds stress term.

22.2.1 Turbulent-averaged energy equation

The derivation of the turbulent-averaged energy conservation equation is more complicated since a distinction has to be made between the averaged total energy \tilde{E} and the total energy of the averaged flow \hat{E} . These two quantities differ by the kinetic energy of the turbulent fluctuations.

If we define the *mean turbulent total energy* by the straightforward relation, the overbar indicating the time average,

$$\bar{\rho} \tilde{E} = \overline{\rho E} = \overline{\rho \left(e + \frac{\mathbf{v}^2}{2} \right)} \quad (22.2.9)$$

we obtain

$$\tilde{E} = \tilde{e} + \tilde{k} + k \equiv \hat{E} + k \quad (22.2.10)$$

where \tilde{k} is the kinetic energy of the mean flow per unit mass,

$$\bar{\rho}\tilde{k} = \bar{\rho} \frac{\bar{v}^2}{2} \quad (22.2.11)$$

and k is the turbulent kinetic energy; thus

$$\bar{\rho}k = \rho \frac{\overline{v''^2}}{2} \equiv \overline{\rho k''} \quad (22.2.12)$$

is defined as the average of the kinetic energy k'' of the turbulent fluctuations. Similarly, the averaged total enthalpy is defined by

$$\tilde{H} = \tilde{E} + \frac{\bar{p}}{\bar{\rho}} = \tilde{h} + \tilde{k} + k \equiv \hat{H} + k \quad (22.2.13)$$

where \hat{H} is the stagnation enthalpy of the averaged flow.

The fluctuating components are given by

$$H'' = h'' + \bar{v}'' \cdot \bar{v}'' + k'' - k \quad (22.2.14)$$

and a similar relation for the fluctuating total energy E'' is

$$E'' = e'' + \bar{v}'' \cdot \bar{v}'' + k'' - k \quad (22.2.15)$$

A conservative form of the turbulent energy equation is obtained by averaging the energy conservation equation, in the absence of external sources, leading to

$$\frac{\partial}{\partial t} (\bar{\rho}\tilde{E}) + \bar{\nabla} \cdot (\bar{\rho}\tilde{H}\bar{v}) = \bar{\nabla} \cdot (-\bar{F}_D + \bar{v} \cdot \bar{\tau} - \overline{\rho H'' v''}) \quad (22.2.16)$$

where the heat diffusive flux $\bar{F}_D = -(\mu c_p / Pr) \nabla \bar{T}$.

It is seen that the influence of the turbulent fluctuations on the energy balance of the time-averaged flow is expressed by a *turbulent heat flux vector*, equal to $(-\overline{\rho H'' v''})$.

This last equation can be written in another form by an explicit calculation of the turbulent heat flux term, using equation (22.2.14). Introducing also the equation for the turbulent kinetic energy, a simplified form for the conservation of the total energy of the averaged flow can be obtained (see, for instance, Cebeci and Smith, 1974):

$$\frac{\partial}{\partial t} (\bar{\rho}\hat{E}) + \bar{\nabla} \cdot (\bar{\rho}\hat{H}\bar{v}) = \bar{\nabla} \cdot (-\bar{F}_D + \bar{v} \cdot \bar{\tau}^T - \overline{\rho h'' v''}) \quad (22.2.17)$$

where the total shear stress tensor $\bar{\tau}^T$ is defined by

$$\bar{\tau}^T = \bar{\tau}^v + \bar{\tau}^R \quad (22.2.18)$$

as the sum of the averaged viscous stresses $\bar{\tau}^v$ and the Reynolds stresses $\bar{\tau}^R$.

Similarly, a total, turbulent heat flux term F_D^T can be defined as

$$\bar{F}_D^T = -\frac{\mu c_p}{P_r} \bar{\nabla} T + \overline{\rho h'' v''} \quad (22.2.19)$$

22.3 TURBULENCE MODELS

Although the set of Reynolds-averaged Navier–Stokes equations (22.2.6), (22.2.7) and (22.2.18) is formally equivalent to the laminar form (22.1.1) it cannot be used without additional information. Indeed, the averaged procedure has produced the Reynolds stress term $\bar{\tau}^R$ and the turbulent heat diffusion \bar{F}_D^T . Since these quantities are unknown, in particular their relation to the mean flow variables, the application of the Reynolds-averaged equations to the computation of turbulent flows requires the introduction of some modellization of these unknown relations, based on theoretical considerations coupled to unavoidable empirical information. This information is considered to be contained in the *turbulence models*, to be added to the averaged Navier–Stokes equations.

Many different models, ranging from simple *algebraic* to *second-order closure* models, have been developed.

In the second-order closure models, transport equations for the second-order correlations $\overline{\rho v_i'' \cdot v_j''}$ and $\overline{v_i'' \cdot h''}$ are deduced from the Navier–Stokes equations and the third-order correlations appearing in the equations are modelled as a function of the second-order correlations. These models are quite general but require the solution of a system of transport equations for each of the second-order correlations. The computational effort involved is large and it seems from the available experience, with the important exception of atmospheric flows (Zeman, 1981), that this complexity can be avoided for simple flow configurations and that simpler models such as the first-order models, to be discussed next, can provide an acceptable approximation of the influence of turbulent transport and diffusion on the mean flow quantities.

We will summarize in the following some of the most important models used in practical calculations over the last years and recent reviews of turbulence models can be found in Frost and Moulden (1977), Rodi (1980, 1982), Kline *et al.* (1982), Launder *et al.* (1984), Patel *et al.* (1985) and Lakshminarayana (1986).

An important assumption with regard to the influence of compressibility on the turbulence models is based on Morkovin's hypothesis (Morkovin, 1964). According to this hypothesis, the effects of density fluctuations on the turbulence structure will remain small for Mach numbers below 5 for boundary layers and wakes and below 1.5 for jets (Bradshaw, 1977).

This implies that the turbulence models, based on density-averaged quantities will remain valid with the empirical data taken from incompressible flow experiments, within these limits on Mach number. However, this might not be true any more in high-temperature flows, such as the flows in combustion chambers, and for these cases, more complex data and models are necessary.

In the first-order closure models the Reynolds stresses are expressed through an eddy viscosity, following Boussinesq's (1877) original assumption:

$$\tau_{ij}^R \equiv -\overline{\rho v_i'' v_j''} = \mu_T [\partial_i \tilde{v}_j + \partial_j \tilde{v}_i - \frac{2}{3}(\overline{\mathbf{V}} \cdot \overline{\mathbf{v}}) \delta_{ij}] - \frac{2}{3} \bar{\rho} k \delta_{ij} \quad (22.3.1)$$

where μ_T is a *turbulent eddy viscosity* coefficient. The last term has to be introduced to ensure consistency for $i = j$, since τ_{ii}^R is equal to twice the turbulent kinetic energy $\bar{\rho} k$.

Similarly, the turbulent heat flux vector (22.2.19) will be modelled by

$$\overline{\mathbf{F}}_D^T = -k_T \overline{\mathbf{V}} \overline{T} \quad (22.3.2)$$

or

$$\overline{\mathbf{F}}_D^T = -\gamma \frac{\mu_T}{Pr_T} \overline{\mathbf{V}} \overline{\tilde{e}} \quad (22.3.3)$$

defining a turbulent thermal conductivity coefficient k_T or the corresponding diffusivity coefficient κ_T through a turbulent Prandtl number:

$$Pr_T = \mu_T \frac{c_p}{k_T} = \frac{\nu_T}{\kappa_T} = \frac{\mu_T}{\bar{\rho} \kappa_T} \quad (22.3.4)$$

where the kinematic turbulent viscosity ν_T has been introduced.

Introducing these expressions into the turbulent-averaged Navier–Stokes equations leads to a system than is formally identical to the Navier–Stokes equations (22.1.1) where the molecular viscosity ν is multiplied by $(1 + \nu_T/\nu)$ and the thermal conductivity coefficient k is replaced by $(k + k_T)$. In addition the turbulent kinetic energy contribution to the normal stresses, the last term in equation (22.3.1), will generally be included in the mean pressure \bar{p} .

The system of Reynolds-averaged Navier–Stokes equation becomes in this representation

$$\frac{\partial}{\partial t} \begin{vmatrix} \bar{\rho} \\ \bar{\rho} \overline{\mathbf{v}} \\ \bar{\rho} \overline{E} \end{vmatrix} + \overline{\mathbf{V}} \cdot \begin{vmatrix} \bar{\rho} \overline{\mathbf{v}} \\ \rho(\overline{\mathbf{v}} \otimes \overline{\mathbf{v}}) + \overline{\mathbf{P}} \overline{\mathbf{I}} - \overline{\boldsymbol{\tau}}^T \\ \bar{\rho} \overline{\mathbf{v}} \overline{H} - \overline{\boldsymbol{\tau}}^T \cdot \overline{\mathbf{v}} - (k + k_T) \overline{\mathbf{V}} \overline{T} \end{vmatrix} = \begin{vmatrix} 0 \\ \bar{\rho} \overline{\mathbf{f}}_e \\ W_t + q_H \end{vmatrix} \quad (22.3.5a)$$

with

$$\overline{\boldsymbol{\tau}}_{ij}^T = (\mu + \mu_T) [\partial_i \tilde{v}_j + \partial_j \tilde{v}_i - \frac{2}{3}(\overline{\mathbf{V}} \cdot \overline{\mathbf{v}}) \delta_{ij}] \quad (22.3.5b)$$

$$\overline{\mathbf{P}} = \bar{p} + \frac{2}{3} \bar{\rho} k \quad (22.3.5c)$$

This is the easiest approach to the turbulent-averaged Navier–Stokes equations and the various models in this group are distinguished from one another by the way these two coefficients are estimated.

The first-order models can be classified according to the number of additional transport equations for the turbulent quantities they require. The algebraic models, also called the zero equation models, do not require any differential equation for the turbulence quantities and are therefore the simplest and easiest

models to use. Methods using one or two additional differential equations are therefore called one-equation and two-equation models.

22.3.1 Algebraic models

The most currently applied algebraic turbulence models are based on the original two-layer model developed by Cebeci and Smith (1974) for boundary layer applications. A modified formulation, adapted to Navier–Stokes computations, has been developed by Baldwin and Lomax (1978).

Cebeci–Smith model

The turbulent boundary layer is considered to be formed by two regions, an inner and an outer region, with different expressions for the eddy viscosity coefficient. For the inner region the algebraic models provide semi-empirical expressions for ν_T through the mixing length l defined by

$$\nu_T^{(i)} = l^2 |\bar{\nabla}_x \bar{v}| \quad (22.3.6)$$

In a two-dimensional boundary layer along a surface aligned with the x axis and with normal direction y , the vorticity in equation (22.3.6) reduces to the shear $\partial u/\partial y$.

Representative models for the mixing length are given by the classical representation of Prandtl $l = Ky$, corrected by Van Driest (1956):

$$l = Ky(1 - e^{-(y+/A)}) \quad (22.3.7)$$

where $K = 0.41$ is the Von Karman constant; the parameter A has been calibrated with boundary layer data to be $A = 26$. The variable y_+ is defined by

$$y_+ = \frac{y}{\nu} \sqrt{\frac{\tau_0}{\rho}} \quad (22.3.8)$$

where τ_0 is the wall shear stress and y denotes the distance to the wall.

Correction terms on the coefficient A for non-zero pressure gradients can be found in Cebeci and Bradshaw (1984). In the outer layer, the eddy viscosity is defined by

$$\nu_T^{(o)} = 0.00168 \bar{v}_e \delta^* F \quad (22.3.9)$$

where \bar{v}_e is the external velocity at the boundary layer edge and δ^* is the boundary layer displacement thickness

$$\delta^* = \int_0^\infty \left(1 - \frac{\bar{v}}{\bar{v}_e}\right) dy \quad (22.3.10)$$

The function F represents the influence of the intermittency at the edge of the

boundary layer and is given by the empirical formula

$$F = \frac{1}{1 + 5.5(y/\delta)^6} \quad (22.3.11)$$

where δ is the boundary layer thickness. An additional intermittency factor which takes into account the laminar-turbulent transition region can be found in Cebeci and Bradshaw (1984).

The switching from the inner to the outer value of the eddy viscosity occurs at the position y_c where the inner value becomes equal to the outer value; that is (Figure 22.3.1)

$$\begin{aligned} v_T &= v_T^{(i)} & \text{if } y < y_c \\ v_T &= v_T^{(o)} & \text{if } y > y_c \end{aligned} \quad (22.3.12)$$

This model has mainly been developed for boundary layer flows and requires some modifications for free shear layers such as wakes. In this case the outer value can be used for the whole wake region.

One of the drawbacks of the Cebeci and Smith model is the need for the calculation of the velocity at the edge of the boundary layer. In order to avoid

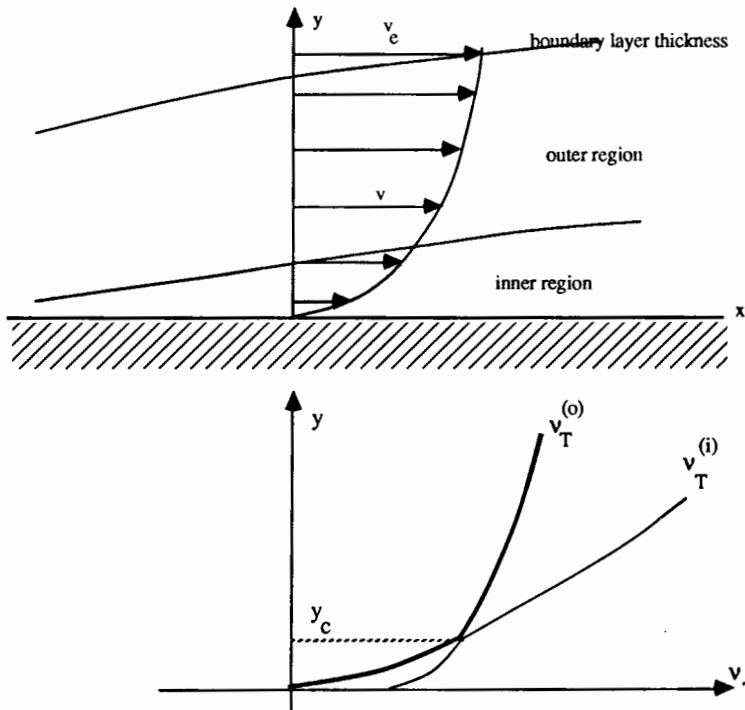


Figure 22.3.1 Two-layer edge viscosity model

this calculation, Baldwin and Lomax (1978) modified the estimation of the outer part of the eddy viscosity.

Baldwin–Lomax model

The outer eddy viscosity coefficient is defined by

$$\nu_T^{(o)} = 0.0168\beta F y_{\max} \Gamma_{\max} \quad (22.3.13)$$

The intermittency function F is expressed by

$$F = \frac{1}{1 + 5.5(\alpha y/y_{\max})^6} \quad (22.3.14)$$

The function Γ is defined by

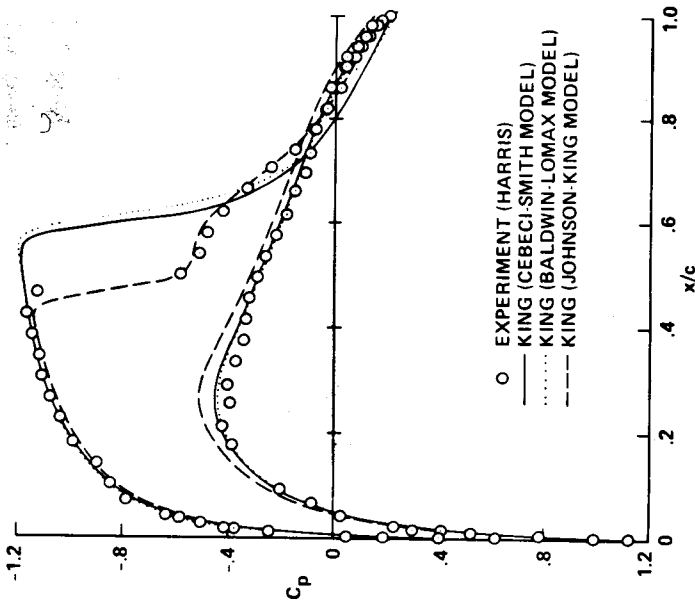
$$\Gamma = y(1 - e^{-y^{1/4}})|\bar{\nabla}x\bar{v}| \quad (22.3.15)$$

and y_{\max} is the value where Γ attains its maximum value Γ_{\max} . The constants α and β are generally taken equal to $\alpha = 0.3$ and $\beta = 1.6$, although other values have been applied (York and Knight, 1985). A discussion of the range and limitations of this model can be found in Visbal and Knight (1983).

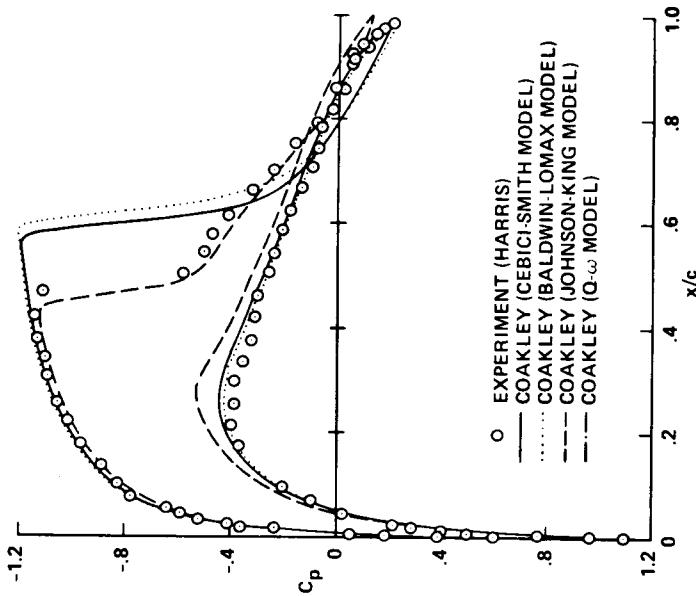
The algebraic models have been extensively used for thin, attached shear layers at moderate Mach numbers (Cebeci and Smith, 1974; Kline *et al.*, 1982), with very acceptable results. However, as soon as separation of the boundary layer is approached, the algebraic models give rise to poor predictions. Attempts to relate some of the empirical constants appearing in both the Cebeci–Smith and Baldwin–Lomax models with the wake factor of Coles' law of the wall enable an improved dependence with pressure gradients (Granville, 1987; Stock and Haase, 1987).

These limitations are related to the theoretical limits of the mixing length hypothesis, which implies that the eddy viscosity is zero if the mean velocity gradient vanishes. This can lead to inconsistencies, in particular in the vicinity of separation or reattachment points. In addition, the algebraic models are not able to take into account the transport and diffusion of turbulence and therefore history effects can not be simulated. These deficiencies will mainly appear in complex flow configurations, such as recirculating or separated flows.

An interesting model which appears to give a significant improvement over the above-mentioned models has been presented by Johnson and King (1985). It is essentially based on the observation that the effects of strong adverse pressure gradients, as occurring in shock–boundary layer interactions, for instance, can be modelled by the evolution of the maximum values of the Reynolds stress. The eddy viscosity is therefore related to the maximum Reynolds stress for which an ordinary differential equation is derived in order to follow its development in the streamwise direction. Compared to the other models, the Johnson–King approach leads to better predictions of shock-induced separation on airfoil surfaces, as can be seen from Figures 22.3.2 and 22.3.3, obtained by King (1987) and Coackley (1987) and reported by Holst

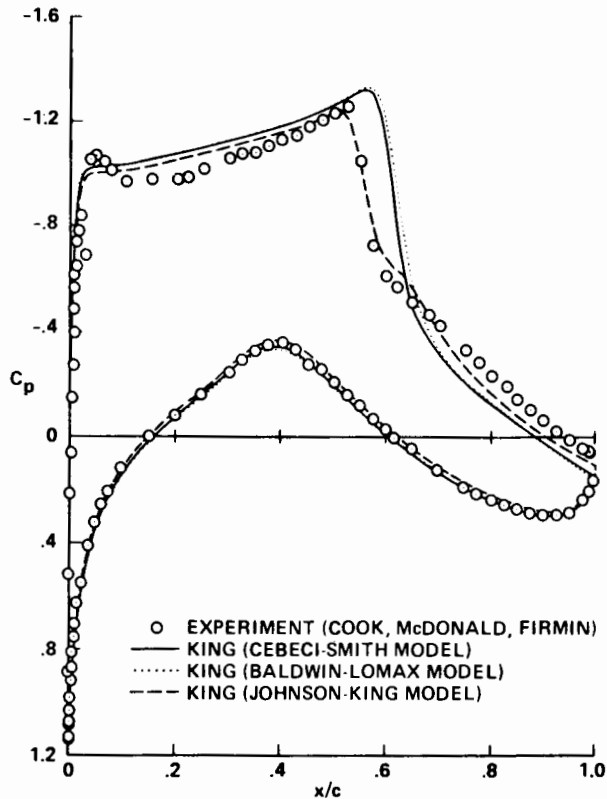


(a) Turbulence model variations due to King (1987)

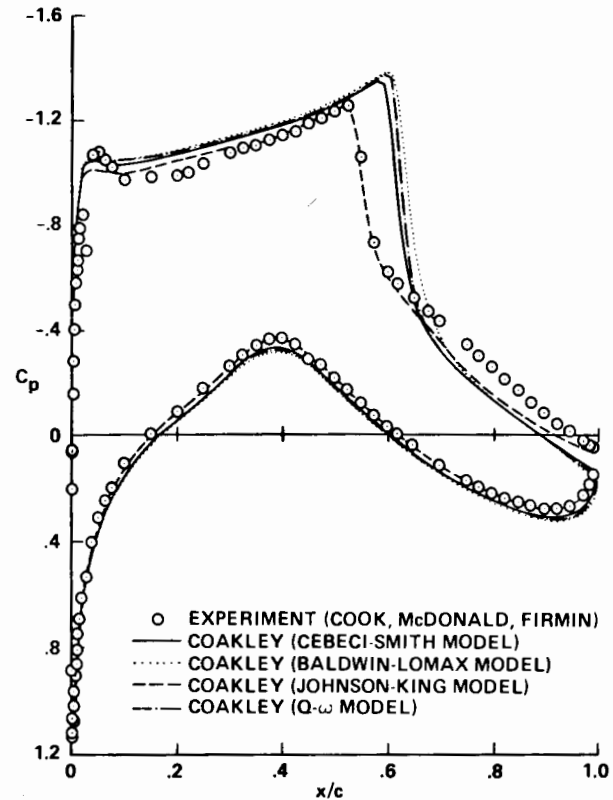


(b) Turbulence model variations due to Coakley (1987)

Figure 22.3.2 Navier-Stokes computations with different turbulence models on a NACA 0012 airfoil at incident Mach number of 0.799 and 2.26° incidence at Reynolds number of 9.0×10^6 . (From Holst, 1987)



(a) Turbulence model variations due to King (1987)



(b) Turbulence model variations due to Coakley (1987)

Figure 22.3.3 Navier-Stokes computations with different turbulence models on an RAE 2822 airfoil at incident Mach number of 0.725 and 2.92° incidence at Reynolds number of 6.5×10^6 . (From Holst, 1987)

(1987). Figures 22.3.2 and 22.3.3 compare the results of a two-dimensional Navier–Stokes computation performed with different turbulence models for transonic conditions on NACA 0012 and RAE 2822 airfoils. In both cases, which correspond to a shock-induced separation, the Johnson–King model gives excellent agreement with the available experimental data. Both calculations have been performed with different schemes and give very consistent results, indicating that the turbulence dependence is free of numerical effects. In addition Coackley's calculations include also a two-equation model which does not perform better than the algebraic models of Cebeci–Smith and Baldwin–Lomax. It seems, therefore, that the monitoring of the maximum Reynolds stress is a good indicator for the memory effects in turbulent separation. Other comparisons reported by Holt (1987) show that the above models do predict similar behaviour in non-separated regions.

22.3.2 One- and two-equation models— k - ϵ models

More sophisticated methods have been developed based on transport equations for some basic turbulence properties such as the turbulent kinetic energy and the turbulent dissipation.

One-equation models have been developed for the kinetic energy k but the results were not considered as sufficiently accurate, and the best results have been obtained by the two-equation models, the so-called k - ϵ models, which are based on transport equations for the kinetic energy of the turbulence k and for the turbulent dissipation ϵ .

The various models rely on the Prandtl–Kolmogorov expression

$$\nu_T = C_\nu k^{1/2} L \quad (22.3.16)$$

where $k^{1/2}$ and L act as representative velocity and length scales of the turbulence. Also, from dimensional arguments, the dissipation ϵ can be written as

$$\epsilon = C_\epsilon \frac{k^{3/2}}{L} \quad (22.3.17)$$

and equation (22.3.16) as

$$\nu_T = C_\mu \frac{k^2}{\epsilon} = \frac{\mu_T}{\bar{\rho}} \quad (22.3.18)$$

The structure of these equations have the general form of a transport equation. The various terms of the turbulent kinetic energy equation (22.2.23) can be modelled, leading to the following form (see, for instance, Launder and Spalding, 1972):

$$\frac{\partial}{\partial t}(\bar{\rho}k) + \bar{\nabla} \cdot (\bar{\rho}k \bar{v}) = \bar{\nabla} \cdot (\mu_k \bar{\nabla} k) + (\bar{\tau}^R \cdot \bar{\nabla}) \cdot \bar{v} - \bar{\rho}\epsilon + Q_k \quad (22.3.19)$$

The first term on the right-hand side is a diffusion term, while the second term,

denoted by P , is the production of turbulent energy by the work of the main flow against the Reynolds stresses $\bar{\tau}^R$. The third term is the dissipation contribution.

An equation of a similar nature is assumed for the dissipation ε :

$$\frac{\partial}{\partial t}(\bar{\rho}\varepsilon) + \bar{\nabla} \cdot (\bar{\rho}\varepsilon\bar{v}) = \bar{\nabla} \cdot (\mu_\varepsilon \bar{\nabla}\varepsilon) + C_{\varepsilon 1} P \frac{\varepsilon}{k} - C_{\varepsilon 2} \bar{\rho} \frac{\varepsilon^2}{k} + Q_\varepsilon \quad (22.3.20)$$

where P is the production term of the k equation (22.3.19). The terms Q_k and Q_ε are additional terms introduced by various authors in order to obtain better agreement in specific flow situations. In the standard k - ε model, both contributions are zero, $Q_k = Q_\varepsilon = 0$.

The eddy diffusivities μ_k and μ_ε associated with the kinetic energy and dissipation equations respectively are defined by

$$\mu_k = \mu + \frac{\mu_T}{\sigma_k} \quad \text{and} \quad \mu_\varepsilon = \mu + \frac{\mu_T}{\sigma_\varepsilon} \quad (22.3.21)$$

The five constants σ_k , σ_ε , C_μ , $C_{\varepsilon 1}$ and $C_{\varepsilon 2}$ have to be defined empirically. Typical values, which are valid for a wide range of applications, are

$$\begin{array}{lll} C_\mu = 0.09 & C_{\varepsilon 1} = 1.45 - 1.55 & C_{\varepsilon 2} = 1.92 - 2.00 \\ f_2 = 1 & \sigma_k = 1 & \sigma_\varepsilon = 1.3 \end{array} \quad (22.3.22)$$

Equations (22.3.19) and (22.3.20) can be solved with $k = \varepsilon = 0$ as boundary conditions along solid smooth walls, although other conditions are applicable, such as $\partial\varepsilon/\partial n = 0$. Another approach, which has perhaps more physical support, consists in fixing the values of k and ε at a point outside the viscous sublayer and relating these values to the logarithmic law of the wall, known to be valid for turbulent flows along smooth solid walls.

This approach, based on wall functions in order to define the boundary conditions, has been introduced by Chieng and Launder (1980). A more detailed discussion can be found in Viegas and Rubesin (1983) and Patel *et al* (1985) where comparisons are made and compressibility effects discussed.

With regard to the turbulent heat diffusivity, the simplest assumption consists in assuming a constant value of the turbulent Prandtl number. A typical value used for air flows is

$$Pr_T = 0.9 \quad (22.3.23)$$

The values of these constants can vary from one investigator to the other or can be made dependent on various parameters such as a turbulent Reynolds number $R_T = k^2/\varepsilon$, as for instance in the Jones and Launder (1972) or Wilcox and Rubesin (1980) models.

In Jones and Launder (1972), the basic model is extended to cover also low Reynolds number flows including relaminarization. This requires taking into account the increasing influence of the molecular viscosity at low Reynolds numbers.

Other modifications can be found in the literature (Chien, 1982; Wilcox and Rubesin, 1980; Coackley, 1983), which can all be considered as variants of the Jones–Launder model. A general review of corrections to the k – ε models for low Reynolds numbers can be found in Patel *et al.* (1985), while adaptations of the basic model for axisymmetric flows as well as for the influence of buoyancy are discussed by Rodi (1980).

An interesting and systematic study of the sensitivity of the various coefficients of equation (22.3.20) has been performed by Raiszadeh and Dwyer (1983). This analysis shows, at least for the incompressible round jet treated by the authors, that the most sensitive parameters are the coefficients $C_{\varepsilon 1}$ and $C_{\varepsilon 2}$. This confirms similar observations made by Rodi (1980).

The two-equation models have been applied to a large variety of flow situations and are able to predict, with the same set of constants, complex flows such as separated and three-dimensional flows, and present an acceptable compromise between economy of calculations and accuracy of the results.

Reported experiments with various models, as well as a discussion of some of the difficulties encountered, can be found in Kline *et al.* (1982), Marvin (1982), Coackley (1983), Sugavanam (1983), Viegas and Rubesin (1983), Visbal and Knight (1983), Laksminarayana (1986), Holt (1987) and Rubesin (1989).

22.3.3 Algebraic Reynolds stress models

These models can be considered as intermediate between the first-order models, such as the k – ε models, and the second-order methods which solve transport equations for all the components of the Reynolds stress tensor.

In the algebraic Reynolds stress models, algebraic relations are applied between the components $-\overline{\rho v_j'' v_j''}$, the turbulent kinetic energy k and the dissipation ε , with coefficients as a function of the mean velocity gradients. This leads, for instance, to expressions for the C_μ coefficient of equation (22.3.18) as a function of the ratio P/ε , tending to $C_\mu = 0.09$ for $P/\varepsilon > 1.5$ (Launder, 1982).

More generally, these methods also provide a framework for the introduction of curvature, rotation and other additional effects on the turbulence structure, within the k – ε models, and appear to give improved results for complex turbulent flows.

According to a review by Laksminarayana (1986), the algebraic Reynolds stress models, coupled to the k – ε equations, provide a most useful and generally valid formulation of turbulence modelling methods within the framework of the k – ε models. The area of turbulence modelling for Reynolds-averaged Navier–Stokes equations will undoubtedly be the central problem of this level of approximation in the near future and a great deal of effort is still required to reach a satisfactory situation.

A particularly important and difficult problem is connected to the prediction of laminar–turbulent transition. Very few reliable criteria have been developed in the past, although a poor prediction of transition can have dramatic effects on calculated results, particularly with shock-induced separations.

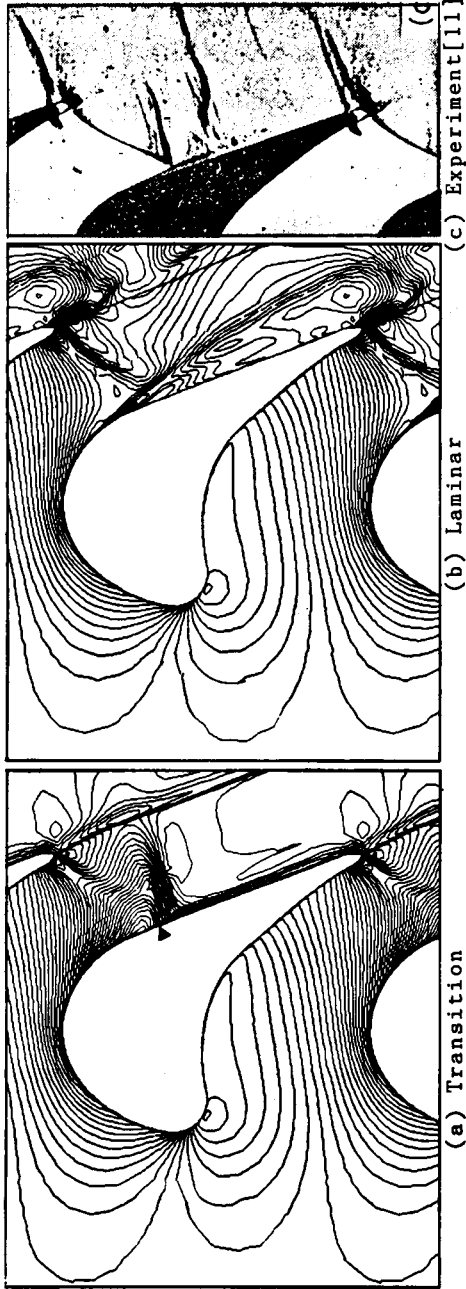


Figure 22.3.4 Computed density contours and Schlieren picture for a high-turning transonic cascade at an exit Mach number of 0.91, an inlet angle of 60° and $Re = 8.6 \times 10^5$. (From Nakahashi *et al.*, 1987)

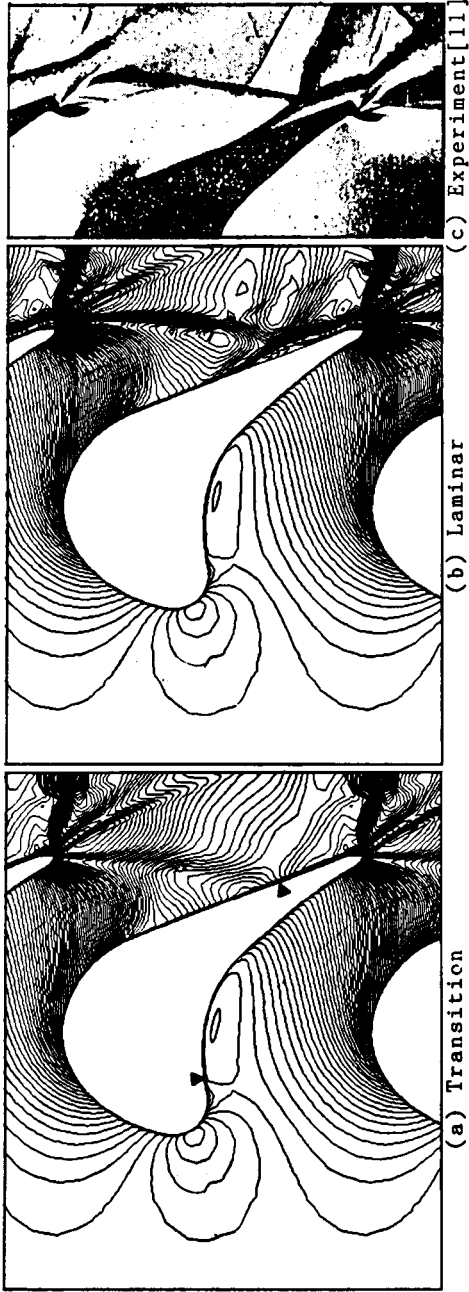


Figure 22.3.5 Computed density contours and Schlieren picture for a high-turning transonic cascade at an exit Mach number of 1.43, an inlet angle of 40° and $Re = 8.6 \times 10^5$. (From Nakahashi *et al.*, 1987)

A spectacular example is provided by the calculations of Nakahashi *et al.* (1987) of the two-dimensional flow in a turbine cascade, with a Baldwin–Lomax turbulence model and a simple transition criteria based on the maximum eddy viscosity becoming higher than an imposed value. Figure 22.3.4(a) shows the computed density lines with transition prediction at the point indicated by a triangle on the suction surface. The transition is predicted at the point of impingement of the shock, inducing a small turbulent separation. Figure 22.3.4(b) corresponds to an assumed laminar flow and shows a massive separation due to the shock–boundary layer interaction, the computed flow on the suction side becoming unsteady. Comparing this to the Schlieren picture in figure 22.3.4(c) it is seen that the turbulent calculations provide excellent agreement. However, for the same cascade at a higher exit Mach number of 1.43 and 20° negative incidence with respect to the design value of 60°, the turbulent calculations do not indicate separation, while the experiments are in good agreement with the laminar data, as seen from Figure 22.3.5. In this case, the inaccurate transition prediction led to the strongly inaccurate flow field of Figure 22.3.5(a).

Hence it can be considered that whatever the numerical qualities of a Navier–Stokes code, its results will be strongly dependent on the transition prediction model. This extremely important topic still requires considerable research.

22.4 SOME EXACT ONE-DIMENSIONAL SOLUTIONS

In the one-dimensional case, several exact solutions can be obtained for the linear convection–diffusion equation:

$$\frac{\partial u}{\partial t} + a \frac{\partial u}{\partial x} = \nu \frac{\partial^2 u}{\partial x^2} \quad (22.4.1)$$

and for Burgers ‘viscous’ equation:

$$\frac{\partial u}{\partial t} + u \frac{\partial u}{\partial x} = \nu \frac{\partial^2 u}{\partial x^2} \quad (22.4.2)$$

The solutions of concern in the present context relate to the influence of viscosity on ‘inviscid’ states such as a travelling or stationary discontinuity and, on the other hand, for boundary-layer-type situations. In the former case we will consider solutions for an initial discontinuity located at $t = 0$ and, in the latter, we will consider a boundary value problem with fixed values at $x = 0$ and $x = L$.

22.4.1 Solutions to the linear convection–diffusion equation

Initial discontinuity

We consider an initial discontinuity at $x = 0$, defined by

$$\begin{aligned} u &= u_1 & x > 0, & t = 0 \\ u &= u_2 & x < 0, & t = 0 \end{aligned} \quad (22.4.3)$$

and the boundary conditions at infinity:

$$\begin{aligned} u &= u_1 & x &\rightarrow \infty \\ u &= u_2 & x &\rightarrow -\infty \end{aligned} \quad (22.4.4)$$

In the inviscid case, the solution is a propagating discontinuity, while the effects of viscosity will tend to diffuse the initial discontinuity. An exact solution can be obtained for all times t , expressed in terms of the error function $\text{erfc}(x)$:

$$u(x, t) = A - B \text{erfc}\left(\frac{x - at}{2\sqrt{vt}}\right) \quad (22.4.5)$$

with

$$A = \frac{u_2 + u_1}{2} \quad B = \frac{u_2 - u_1}{2} \quad (22.4.6)$$

The error function can be approximated for numerical applications by the following expansion, with an accuracy better than 5×10^{-4} :

$$aa(x) = 1 + 0.278393x + 0.230389x^2 + 0.000972x^3 + 0.078108x^4 \quad (22.4.7)$$

$$\text{erfc}(x) = 1 - \frac{1}{aa(x)}$$

The solution is illustrated in Figure 22.4.1.

Stationary boundary-layer-type solution

The steady-state solution to the boundary value problem

$$\begin{aligned} a \frac{\partial u}{\partial x} &= v \frac{\partial^2 u}{\partial x^2} & 0 \leq x \leq L \\ u(0) &= u_0 & x = 0 \\ u(L) &= u_L & x = L \end{aligned} \quad (22.4.8)$$

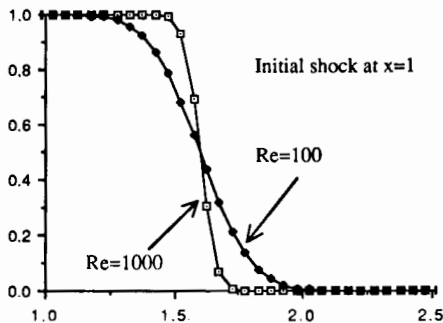


Figure 22.4.1 Solution to the linear convection-diffusion equation for an initial discontinuity at different times

has been already referred to in Chapter 10 in Volume 1 and the solution is given in equation (10.5.13). With a Reynolds number Re defines by $Re = aL/\nu$, the solution is

$$\frac{u - u_0}{u_0 - u_L} = \frac{e^{Re(x/L)} - 1}{e^{Re} - 1} \quad (22.4.9)$$

22.4.2 Solutions to Burgers equation

A large variety of solutions to Burgers equation are available and can be found in Whitham (1974) and in Benton and Platzman (1972). This last reference contains an extensive, if not exhaustive, compilation of available exact solutions to the 'viscous' Burgers equation.

Initial discontinuity

We will consider only the initial discontinuity and the initial value problem (22.4.3), (22.4.4). An asymptotic solution, valid for large times, is given for an initial shock, that is for $u_2 > u_1$, by

$$u = u_1 + \frac{u_2 - u_1}{1 + \exp[B(x - At)/\nu]} \quad (22.4.10a)$$

which can also be written as

$$u = A - B \tanh\left[\frac{B(x - At)}{2\nu}\right] \quad (22.4.10b)$$

The diffusing shock propagates with the 'inviscid' velocity equal to A . Hence, the transformation $x - At = X$ is a stationary shock structure at $X = 0$.

For practical calculations, this solution might be considered as accurate for

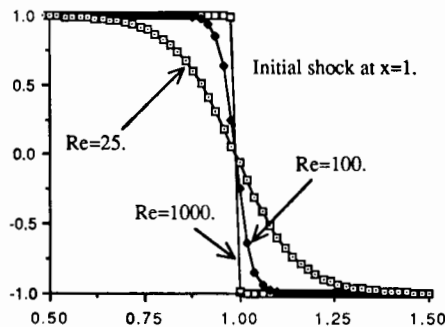


Figure 22.4.2 Solution to Burgers equation for an initial discontinuity at different Reynolds numbers.

a number of time steps n , such that

$$n\Delta t > \frac{8\nu}{B^2} \quad (22.4.11a)$$

or

$$n > \frac{8N}{\text{CFL} \times \text{Re}} \frac{U}{B} \quad (22.4.11b)$$

where CFL and Re are the Courant and Reynolds numbers of the computation, which is performed on a domain of finite length L with N mesh points. U is the maximum velocity used in the definition of the Reynolds number.

The solution is shown in Figure 22.4.2.

22.4.3 Other simple test cases

Two-dimensional viscous flows can be tested for the uniform flow along a flat plate, developing a laminar boundary layer, whose behaviour is given by the well-established Blasius solution.

An intermediate, simpler case is the laminar flow between two parallel plates, or within a circular straight duct, whose solution is the parabolic Poiseuille profile. The geometry is two dimensional, but the solution depends only on a single space variable.

Another variant of the flow between two plates is provided by the Couette problem, for which the upper plate is moving at a constant velocity relative to the bottom one. Details on these flows can be found in nearly any textbook on basic fluid mechanics.

References

- Baldwin, B., and Lomax, H. (1978). 'Thin layer approximation and algebraic model for separated turbulent flow.' *AIAA Paper 78-0257*, AIAA 16th Aerospace Sciences Meeting.
- Benton, E. R., and Platzman, G. W. (1972). 'Solutions to the one-dimensional Burgers equation.' *Quart. Appl. Math.*, **30**, 195–212.
- Boussinesq, J. (1877). *Theorie de l'Écoulement Tourbillonnant*, Vol. 23, pp. 46–50, Paris: Comptes-Rendus de l'Académie des Sciences.
- Bradshaw, P. (1977). 'Compressible turbulent shear layers.' *Annual Review of Fluid Mechanics*, **9**, 33–54.
- Cebeci, T., and Bradshaw, P. (1984). *Physical and Computational Aspects of Convective Heat Transfer*, New York: Springer Verlag.
- Cebeci, T., and Smith, A. M. O. (1974). *Analysis of Turbulent Boundary Layers*, New York: Academic Press.
- Chien, J. Y. (1982). 'Predictions of channel boundary layer flows with a low Reynolds number turbulence model.' *AIAA Journal*, **20**, 33–8.
- Chiang, C. C., and Launder, B. E. (1980). 'On the calculation of turbulent heat transport downstream from an abrupt pipe expansion.' *Numerical Heat Transfer*, **3**, 189–207.
- Coackley, T. J. (1983). 'Turbulence modeling methods for the compressible Navier–Stokes equations.' *AIAA Paper 83-1693*, AIAA 16th Fluid and Plasma Dynamics Conference.

- Coackley, T. J. (1987). 'Numerical simulation of viscous transonic flows.' *AIAA Paper 87-0416*, AIAA 25th Aerospace Sciences Meeting.
- Dutt, P. (1988). 'Stable boundary conditions and difference schemes for Navier-Stokes equations.' *SIAM Journal Numerical Analysis*, **25**, 245-67.
- Frost, W., and Moulden, T. H. (eds) (1977). *Handbook of Turbulence*, Vol. 1, New York: Plenum Press.
- Granville, P. S. (1987). 'Baldwin-Lomax factors for turbulent boundary layers in pressure gradients.' *AIAA Journal*, **25**, 1624-7.
- Gustafsson, B., and Sundström A. (1978). 'Incompletely parabolic problems in fluid dynamics.' *SIAM Journal Applied Mathematics*, **35**, 343-57
- Holst, T. L. (1987). 'Viscous transonic airfoil workshop compendium of results.' *AIAA Paper 87-1460*, AIAA 19th Fluid Dynamics, Plasma Dynamics and Lasers Conference.
- Hunt, J. C. R. (1988). 'Studying turbulence using direct numerical simulation: 1987 Center for Turbulence Research NASA Ames/Stanford Summer Programme.' *Journal of Fluid Mechanics*, **190**, 375-92.
- Johnson, D. A. and King, L. S. (1985). 'A mathematically simple turbulence closure model for attached and separated turbulent boundary layers.' *AIAA Journal*, **23**, 1684-92.
- Jones, W. P., Launder, B. E. (1972). 'The prediction of laminarization with a two-equation model of turbulence'. *International Developments in Heat Transfer*, **15**, 303-314.
- Kim, J., Moin, P., and Moser R. D. (1987). 'Turbulence statistics in fully developed channel flow at low Reynolds number.' *Journal of Fluid Mechanics*, **177**, 133-66.
- King, L. S. (1987). 'A comparison of turbulence closure models for transonic flows about airfoils.' *AIAA Paper 87-0418*, AIAA 25th Aerospace Sciences Meeting.
- Kline, S. J., Cantwell, B. J., and Lilley, G. M. (1982). *Proceedings of the 1980-81 AFOSR-HTTM-Stanford Conference on Complex Turbulent Flows*, Vols I, II, III, Thermosciences Division, University of Stanford, Stanford, California.
- Lakshminarayana, B. (1986). 'Turbulence modelling for complex shear flows.' *AIAA Journal*, **24**, 1900-17.
- Launder, B. E. (1982). 'A generalized algebraic stress transport hypothesis.' *AIAA Journal*, **20**, 436.
- Launder, B. E., and Spalding, B. (1972). *Mathematical Models of Turbulence*, New York: Academic Press.
- Launder, B. E. Reynolds, W. C., and Rodi, W. (1984). *Turbulence Models and Their Applications*, Paris, France: Editions Eyrolles.
- Liepmann, H. W., and Roshko, A. (1957). *Elements of Gas Dynamics*, New York: John Wiley and Sons.
- Marvin, J. G. (1982). Turbulence modelling for computational aerodynamics.' *AIAA Paper 82-0164*, AIAA 20th Aerospace Sciences Meeting.
- Moin, P., and Moser R. D. (1988). 'Characteristic eddy decomposition of turbulence in a channel.' *Journal of Fluid Mechanics*.
- Moin, P., Reynolds, W. C., and Kim, J. (1987). 'Studying turbulence using numerical simulation databases.' *Report CTR-S87, Proc. 1987 Summer Program, Center for Turbulence Research, NASA Ames Research Center*.
- Morkovin, M. V. (1964). 'Effects of compressibility on turbulent flow.' In A. Favre (ed.), *The Mechanics of Turbulence*, New York: Gordon and Breach.
- Nakahashi, K., Nozaki, O., Kikuchi, K., and Tamura, A. (1987). 'Navier-Stokes computations of two- and three-dimensional cascade flow fields.' *AIAA Paper 87-1315*, AIAA 19th Fluid Dynamics, Plasma Dynamics and Lasers Conference.
- Patel, V. C., Rodi, W., and Scheurer, G. (1985). 'Turbulence models for near-wall and low-Reynolds number flows: a review.' *AIAA Journal*, **23**, 1308-19.
- Raiszadeh, F., and Dwyer, H. A. (1983). 'A study with sensitivity analysis of the $k-\epsilon$ turbulence model applied to jet flows.' *AIAA Paper 83-0285*, AIAA 21st Aerospace Sciences Meeting.

- Rodi, W. (1980). *Turbulence Models and Their Application in Hydraulics*, Delft, Netherlands: International Association for Hydraulic Research (IAHR).
- Rodi, W. (1982). 'Examples of turbulence models for incompressible flows.' *AIAA Journal*, **20**, 72-9.
- Rogallo, R. S., and Moin, P. (1984). 'Numerical simulation of turbulent flows.' *Annual Review of Fluid Mechanics*, **16**, 99-137.
- Rubeshin, M. W. (1989). 'Turbulence modelling for aerodynamic flows' *AIAA Paper 89-0606*, AIAA 27th Aerospace Sciences Meeting.
- Stock, H. W., and Haase, W. (1987). 'The determination of turbulent length scales in algebraic turbulence models for attached and slightly separated flows using Navier-Stokes methods.' *AIAA Paper 87-1302*, AIAA 19th Fluid Dynamics, Plasma Dynamics and Lasers Conference.
- Sugavanam, A. (1983). 'Near-wake computations with Reynolds stress models.' *AIAA Paper 83-1696*, AIAA 16th Fluid and Plasma Dynamics Conference.
- Van Driest, E. R. (1956). 'On turbulent flow near a wall.' *Journal of Aeronautical Sciences*, **23**, 1007-11.
- Viegas, J. R., and Rubeshin, M. W. (1983). 'Wall-function boundary conditions in the solution of the Navier-Stokes equations for complex compressible flows.' *AIAA Paper 83-1694*, AIAA 16th Fluid and Plasma Dynamics Conference.
- Visbal, M., and Knight, D. (1983). 'Evaluation of the Baldwin-Lomax turbulence model for two-dimensional shock wave boundary layer interactions.' *AIAA Paper 83-1697*, AIAA 16th Fluid and Plasma Dynamics Conference.
- Whitham, G. B. (1974). *Linear and Nonlinear Waves*, New York: John Wiley and Sons.
- Willcox, D. C. and Rubeshin, N. W. (1980). 'Progress in turbulence modeling for complex flow fields including effects of compressibility.' *NASA TP 1517*.
- York, B., and Knight, D. (1985). 'Calculation of two-dimensional turbulent boundary layers using the Baldwin-Lomax model.' *AIAA Journal*, **23**, 1849-50.
- Zeman, O. (1981). 'Progress in the modeling of planetary boundary layers.' *Annual Review of Fluid Mechanics*, **13**, 253-72.

Chapter 23

Discretization Methods for the Navier–Stokes Equations

The numerical resolution of the Navier–Stokes equations at high Reynolds numbers relies largely on the methods developed for inviscid flows. Most of the schemes applied to the Euler equations can be used for the Navier–Stokes equations by discretizing centrally the viscous and heat conduction terms.

We will briefly review this extension for the schemes discussed in the previous chapters and point out specific problems.

One of the essential differences with inviscid flow computations is to be found in the mesh to be defined for viscous problems. If the viscous shear layers are to be resolved with sufficient accuracy, it is necessary to define a large number of points in these regions, generally between ten and twenty in the direction normal to the solid boundaries. In the streamwise direction, however, the mesh point density will generally be determined by the inviscid pressure gradient and be therefore similar to a ‘Euler’ mesh. At high Reynolds numbers and attached boundary layers, this leads to cells with a very large aspect ratio, particularly in the immediate vicinity of the solid walls. Indeed, the first point in the boundary layer is generally taken at a distance of the order of the viscous sublayer thickness, that is $y_+ \simeq 1-10$, while the streamwise distance of the points will be of at least the order of the boundary layer thickness, that is $\delta_+ \simeq 1000$. Consequently, aspect ratios larger than 100 are not uncommon for the first cells in a ‘Navier–Stokes’ mesh (Figure 23.1.1), with the obvious consequences on the accuracy of the computation. Adequate discretization formulas have therefore to be applied if the same accuracy on the viscous terms were required in all directions.

Note that the thin shear layer approximation, discussed in Chapter 2 in Volume 1, neglects all the streamwise derivatives in the boundary layer regions, since they are generally much smaller than the normal gradients and also are evaluated with less accuracy, due to the large aspect ratio of the mesh cells.

Another important problem is connected to the presence of dissipation terms in the discretized Euler equations, which could interfere with the physical dissipation represented by the molecular and turbulent viscosity.

As mentioned in Chapter 22, the mesh resolution is never fine enough to resolve the diffusive effects of viscosity and heat conduction in regions of severe gradients such as shocks. Therefore artificial dissipation, on the scale of the

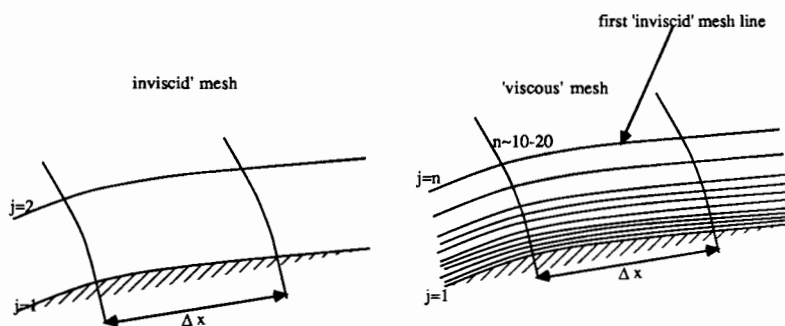


Figure 23.1.1 Typical differences between an 'inviscid' and a 'viscous' mesh in solid wall regions

mesh, has to be introduced even with Navier–Stokes calculations, at least at high Reynolds numbers. This is provided by the dissipation introduced in the inviscid equations, which is applied also for the viscous computations. Hence a particular attention is required to control the numerical dissipation in order not to influence, or even dominate, the physical effects and alter thereby the viscous flow solution. More details on this point will be given in relation to the particular schemes to be discussed in the following sections.

The central discretization of the diffusion terms is fairly straightforward in finite difference formulations and some indications for the application to general meshes within the framework of finite volume or finite element methods are presented in Section 23.1.

Section 23.2 is devoted to a presentation of the extension of the Euler schemes to the computation of compressible Navier–Stokes flows, via the time-dependent formulation.

Section 23.3 presents some current approaches to the resolution of the incompressible Navier–Stokes equations. The absence of the time derivative of the density creates difficulties with the current Euler-type schemes, which become generally extremely slow in convergence at very low Mach numbers, although most of them can be applied to reasonable low levels, of the order of $M \approx 0.05$ – 0.1 .

23.1 DISCRETIZATION OF VISCOUS AND HEAT CONDUCTION TERMS

Independently of the choice of the basic Euler scheme, central or upwind, the *viscous and thermal diffusion terms are always centrally discretized*. This is fairly straightforward on Cartesian meshes, but can be algebraically more complicated on arbitrary mesh systems. With finite difference schemes, the general transformation formulas to curvilinear coordinates can be applied.

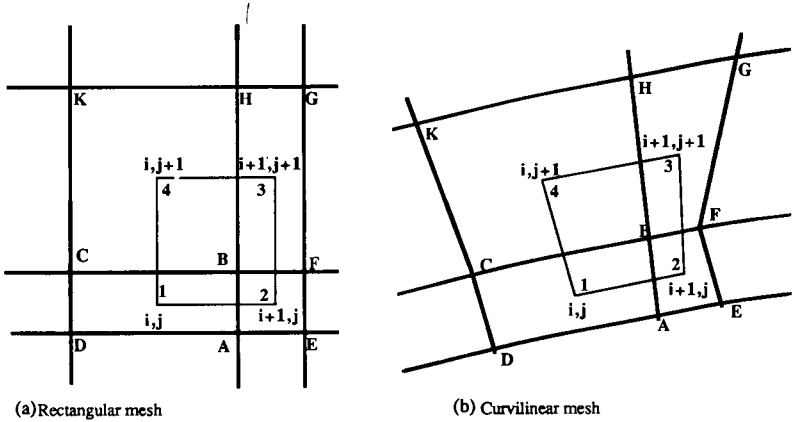


Figure 23.1.2 Finite volume mesh discretization, rectangular and curvilinear

An alternative and general procedure is obtained from finite volume methods and the application of the derivative approximations to be found in Chapter 6 in Volume 1.

Referring to equation (22.1.15), the viscous terms in the momentum balance at point (i, j) , written for the control volume ABCD of Figure 23.1.2, contribute terms of the form $\Sigma(\bar{\tau} \cdot \Delta \bar{S})$, where the summation extends over the four sides. For side AB, the contribution is

$$\bar{\tau}_{AB} \cdot \Delta \bar{S}_{AB} = (\tau_{xx} \Delta S_x + \tau_{xy} \Delta S_y)_{AB} \tag{23.1.1}$$

with

$$\begin{aligned} \Delta S_{x,AB} &= \Delta y_{AB} = y_B - y_A \\ \Delta S_{y,AB} &= -\Delta x_{AB} = -(x_B - x_A) \end{aligned} \tag{23.1.2}$$

Since the shear stresses are proportional to velocity derivatives, all velocity gradients could be evaluated directly at the interfaces; for instance for the x derivatives by the formula

$$\left. \frac{\partial u}{\partial x} \right|_{AB} \simeq \frac{u_{i+1,j} - u_{ij}}{x_{i+1,j} - x_{ij}} \tag{23.1.3}$$

The y derivatives can be estimated from formulas similar to those applied for the potential function derivatives in Chapter 14; for instance

$$\left. \frac{\partial u}{\partial y} \right|_{AB} \simeq \frac{1}{2} \frac{u_{i+1,j+1} - u_{i+1,j-1}}{y_{i+1,j+1} - y_{i+1,j-1}} + \frac{1}{2} \frac{u_{i,j+1} - u_{i,j-1}}{y_{i,j+1} - y_{i,j-1}} \tag{23.1.4}$$

When combined with similar contributions on the other cell faces, central discretized expressions appear with second-order accuracy on uniform meshes (see Problem 23.1).

Another option would be to evaluate the shear stresses at points A and B:

$$\bar{\tau}_{AB} = \frac{1}{2} (\bar{\tau}_A + \bar{\tau}_B) \tag{23.1.5}$$

where $\bar{\tau}_b$ is the average shear stress over the volume 1234.

The velocity derivatives at point B can be estimated from formulas such as (6.2.29) (Chapter 6 in Volume 1) when the flow variables are defined in the cell centres 1, 2, 3, 4:

$$\left(\frac{\partial u}{\partial x}\right)_B = \frac{(u_2 - u_4)(y_3 - y_1) - (u_3 - u_1)(y_2 - y_4)}{(x_2 - x_4)(y_3 - y_1) - (x_3 - x_1)(y_2 - y_4)} \quad (23.1.6a)$$

with a similar relation for the y derivative:

$$\left(\frac{\partial u}{\partial y}\right)_B = \frac{(x_2 - x_4)(u_3 - u_1) - (x_3 - x_1)(u_2 - u_4)}{(x_2 - x_4)(y_3 - y_1) - (x_3 - x_1)(y_2 - y_4)} \quad (23.1.6b)$$

These formulas are independent of the location of point B, leading to a loss in accuracy for strongly varying mesh cells, when point B is not close to the centre of cell 1234. In this case better accuracy is obtained from a finite element representation within the cell, considered as a bilinear element. Referring to Chapter 5 in Volume 1 for more details, the derivatives can be obtained from

$$u_B = \sum_{I=1}^4 u_I N_I(x, y) \quad (23.1.7)$$

and

$$\left.\frac{\partial u}{\partial x}\right|_B = \sum_{I=1}^4 u_I \frac{\partial N_I(x, y)}{\partial x} \quad (23.1.8)$$

with a similar relation for the y derivatives. The interpolation functions $N_I(x, y)$ and their gradients are obtained via isoparametric transformations.

The same formulas can be applied for the heat flux terms in the energy equation.

23.2 TIME-DEPENDENT METHODS FOR COMPRESSIBLE NAVIER-STOKES EQUATIONS

The time-dependent approach for the numerical resolution of the compressible Navier-Stokes equations relies fully on the methods developed for the Euler equations. Most of these methods can be directly applied with the addition of the shear and heat conduction terms, discretized following the guidelines of Section 23.1.

We will consider successively the central and the upwind schemes and maintain the distinction between combined and separate space-time discretizations. The first option corresponds to the Lax-Wendroff family (Chapter 17) and the second to the central schemes with various time integrations, such as the implicit multi-step time integration of the Beam and Warming schemes or the explicit Runge-Kutta multi-stage method as developed by Jameson (Chapter 18).

The basic properties of the schemes in the presence of viscous terms will be analysed essentially on the one-dimensional scalar equation, written as

$$\frac{\partial u}{\partial t} + \frac{\partial f}{\partial x} = \frac{\partial \tau}{\partial x} \quad (23.2.1a)$$

or

$$\frac{\partial u}{\partial t} + \frac{\partial f_T}{\partial x} = 0 \quad (23.2.1b)$$

where the shear stress $\tau = \nu \partial u / \partial x$, f representing the inviscid flux. The conservative form is made apparent by defining a total flux $f_T = f - f_\nu$ with $f_\nu = \tau$:

$$f_T = f - \nu \frac{\partial u}{\partial x} \quad (23.2.1c)$$

In the linear case $f = au$ and equation (23.2.1a) reduces to the standard form of the convection–diffusion equation:

$$\frac{\partial u}{\partial t} + a \frac{\partial u}{\partial x} = \nu \frac{\partial^2 u}{\partial x^2} \quad (23.2.2)$$

23.2.1 First-order explicit central schemes

The straightforward central discretization of second-order space accuracy in finite difference form (Figure 23.2.1) leads to the semi-discretized system of ordinary differential equations in time:

$$\frac{du_i}{dt} = -\frac{f_{i+1} - f_{i-1}}{2\Delta x} + \frac{\tau_{i+1/2} - \tau_{i-1/2}}{\Delta x} \quad (23.2.3)$$

where the shear stress term at the intercell boundaries is defined by

$$\tau_{i+1/2} = \frac{\nu_{i+1/2}(u_{i+1} - u_i)}{\Delta x} \quad (23.2.4)$$

The explicit scheme obtained from a first-order accurate, forward time difference

$$u_i^{n+1} - u_i^n = -\frac{\Delta t}{2\Delta x} (f_{i+1}^n - f_{i-1}^n) + \frac{\Delta t}{\Delta x} (\tau_{i+1/2}^n - \tau_{i-1/2}^n) \quad (23.2.5)$$

reduces in the linear case to the scheme, with $\sigma = a\Delta t/\Delta x$ as the Courant number:

$$u_i^{n+1} - u_i^n = -\frac{\sigma}{2}(u_{i+1}^n - u_{i-1}^n) + \frac{\nu\Delta t}{\Delta x^2}(u_{i+1}^n - 2u_i^n + u_{i-1}^n) \quad (23.2.6)$$

already investigated in Chapter 10 in Volume 1.

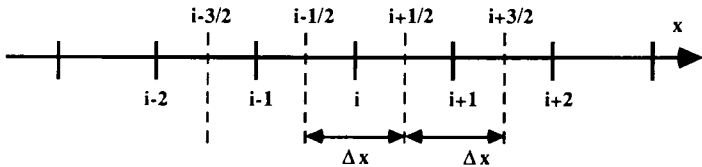


Figure 23.2.1 One-dimensional space discretization

The stability conditions can be written as

$$\sigma^2 \leq 2\beta \leq 1 \quad (23.2.7a)$$

with $\beta = \nu\Delta t/\Delta x^2$, or, introducing the mesh Reynolds number $R = a\Delta x/\nu$,

$$\sigma \leq \frac{R}{2} \leq \frac{1}{\sigma} \quad (23.2.7b)$$

This scheme is, however, not recommended, since an oscillatory behaviour of the numerical solution appears for mesh Reynolds numbers above 2, implying the necessity for very fine meshes in the viscous regions.

Note at this point that the Lax–Friedrichs scheme for the convection diffusion equation (23.2.2) is unconditionally unstable (see Problem 23.5).

Therefore, explicit central schemes for the viscous equations should be at least of second-order accuracy. This leads us to the Lax–Wendroff schemes, since the leapfrog-type schemes, based on central time differences, are not well adapted to diffusive equations (see Problems 23.6 and 23.7).

23.2.2 One-step Lax–Wendroff schemes

Application of the one-step Lax–Wendroff approach to the viscous flow equations leads to a scheme with a complicated structure and requiring more than three-point support in order to achieve second-order accuracy in space and time.

Applying the developments of Section 17.2.1, we have

$$u^{n+1} = u^n - \Delta t \frac{\partial f_{\mathcal{T}}}{\partial x} + \frac{\Delta t^2}{2} \frac{\partial}{\partial x} \left(A_{\mathcal{T}} \frac{\partial f_{\mathcal{T}}}{\partial x} \right) + O(\Delta t^3) \quad (23.2.8)$$

where $A_{\mathcal{T}}$ is the Jacobian of the total flux

$$A_{\mathcal{T}} = \frac{\partial f_{\mathcal{T}}}{\partial u} \quad (23.2.9)$$

The Jacobian can be calculated directly as follows for the scalar equation:

$$A_{\mathcal{T}} \Delta u = \left[\frac{\partial f}{\partial u} - \frac{\partial}{\partial u} \left(v \frac{\partial u}{\partial x} \right) \right] \Delta u = \left(a - v \frac{\partial}{\partial x} \right) \Delta u \quad (23.2.10)$$

where a is the inviscid Jacobian. The Δt^2 term of equation (23.2.8) then becomes

$$\frac{\partial}{\partial x} \left(A_{\mathcal{T}} \frac{\partial f_{\mathcal{T}}}{\partial x} \right) = \frac{\partial}{\partial x} \left(a \frac{\partial f}{\partial x} \right) - \frac{\partial}{\partial x} \left(a \frac{\partial \tau}{\partial x} \right) - \frac{\partial}{\partial x} \left(v \frac{\partial^2 f}{\partial x^2} \right) + \frac{\partial}{\partial x} \left(v \frac{\partial^2 \tau}{\partial x^2} \right) \quad (23.2.11)$$

All the terms have to be discretized centrally.

Since this leads to complicated formulas, the two-step versions of the Lax–Wendroff schemes, such as the MacCormack scheme, should be preferred since they avoid the explicit computation of the Jacobians.

23.2.3 Two-step Lax–Wendroff schemes

The most popular of the two-step Lax–Wendroff schemes is undoubtedly the MacCormack method. The MacCormack schemes (17.2.29) or (17.2.30) remain unchanged, with the replacement of the inviscid flux f by the total flux f_T . For instance, the forward–backward version (17.2.29) becomes

$$\bar{u}_i = u_i^n - \frac{\Delta t}{\Delta x} (f_{T,i+1}^n - f_{T,i}^n) \quad (23.2.12a)$$

$$u_i^{n+1} = \frac{1}{2}(u_i^n + \bar{u}_i) - \frac{\Delta t}{2\Delta x} (\bar{f}_{T,i} - \bar{f}_{T,i-1}) \quad (23.2.12b)$$

In order to maintain overall second-order accuracy, the shear stress terms have to be discretized as follows. In the predictor, the total flux is obtained from

$$f_{T,i} = f_i - \tau_{i-1/2} = f_i - \frac{v_{i-1/2}(u_i - u_{i-1})}{\Delta x} \quad (23.2.13)$$

while in the corrector, the viscous terms are taken at $(i + 1/2)$:

$$\bar{f}_{T,i} = \bar{f}_i - \bar{\tau}_{i+1/2} = \bar{f}_i - \frac{\bar{v}_{i+1/2}(\bar{u}_{i+1} - \bar{u}_i)}{\Delta x} \quad (23.2.14)$$

Hence, compared to the inviscid version, the MacCormack scheme (23.2.12) becomes

$$\bar{u}_i = u_i^n - \frac{\Delta t}{\Delta x} (f_{i+1}^n - f_i^n) + \frac{\Delta t}{\Delta x^2} [v_{i+1/2}(u_{i+1} - u_i) - v_{i-1/2}(u_i - u_{i-1})] \quad (23.2.15a)$$

$$u_i^{n+1} = \frac{1}{2}(u_i^n + \bar{u}_i) - \frac{\Delta t}{2\Delta x} (\bar{f}_i - \bar{f}_{i-1}) + \frac{\Delta t}{2\Delta x^2} (\bar{v}_{i+1/2}(\bar{u}_{i+1} - \bar{u}_i) - \bar{v}_{i-1/2}(\bar{u}_i - \bar{u}_{i-1})) \quad (23.2.15b)$$

Its numerical flux can be written as

$$f_{T,i+1/2}^* = \frac{1}{2}(f_{i+1}^n + \bar{f}_i) - \frac{1}{2}(\tau_{i+1/2}^n + \bar{\tau}_{i+1/2}) \quad (23.2.16)$$

The overall scheme has a five-point support and reduces in the linear case to the one-step Lax–Wendroff scheme (23.2.8) to (23.2.10) (see Problem 23.8).

The backward–forward version, corresponding to equation (17.2.30), is defined similarly by a permutation of the definitions (23.2.13) and (23.2.14); that is equation (23.2.14) is applied at the predictor level and (23.2.13) is used for the corrector. The resulting numerical flux remains unchanged from the form (23.2.16).

As for the inviscid case, it is recommended that one alternates between the two versions in order to avoid a systematic accumulation of errors.

The Von Neumann stability of the scheme cannot be obtained analytically and a sufficient condition can be defined from the analysis of the following

section. In particular, the stability condition

$$\sigma + 2\beta \leq 1 \quad \text{or} \quad \Delta t \leq \frac{\Delta x^2}{|a|\Delta x + 2\nu} \quad (23.2.17)$$

can be applied as a practical guideline. This condition has been suggested by Tannehill *et al.* (1975) on empirical grounds and is confirmed by the more general analysis of the next section.

For the system of one-dimensional Navier–Stokes equations, a is the maximum eigenvalue $u + c$ (for u positive), and ν is to be taken as the maximum of the viscosity coefficient and the thermal diffusivity $k/(\rho c_v)$, that is $\nu \rightarrow \max [v, k/(\rho c_v)]$.

The extension to multi-dimensions follows the methodology discussed in Chapter 17, section 17.2, and does not cause particular difficulties.

Practical Example Two-dimensional flow in a turbine cascade

The flow in the turbine rotor of the US space shuttle main engine fuel pump has been calculated by Chima (1985) with a Lax–Wendroff-type method and a multi-grid acceleration. Details of the method are also described in Chima and Johnson (1985).

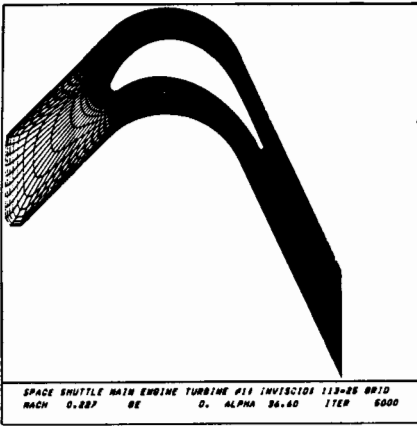
The algebraic turbulence model of Baldwin and Lomax is applied on a C-mesh, shown in Figure 23.2.2(a), of 113×41 points. At inflow, stagnation pressures and temperatures are imposed, together with the inlet flow angle. At exit, the static pressure is specified and at the solid surface, no-slip and fixed temperature conditions are selected.

The flow is fully subsonic with an incident Mach number of 0.225, an inlet flow angle of 36.6° and a Reynolds number of 4.17×10^6 .

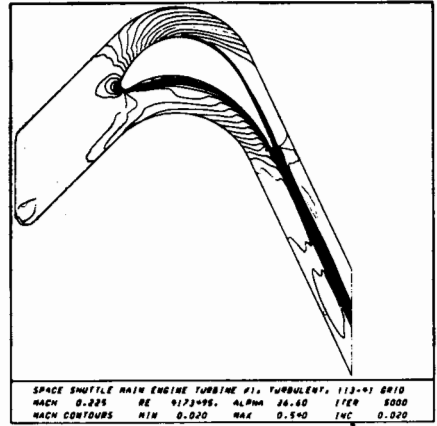
Figure 23.2.2 shows: (b) the computed Mach number lines, (c) the total pressure contours and (d) the computed velocity field. A small separation bubble is seen on the pressure side of the blade, which does not affect significantly the blade pressure distribution, but could have a significant influence on the heat transfer.

MacCormack's method is one of the most efficient versions of the two-step Lax–Wendroff schemes from the point of view of operation count, but requires a very large number of time steps to converge to a stationary solution. This approach is well adapted for time-dependent problems, but in order to be competitive with other methods for steady flows, it should be inserted in a multi-grid acceleration framework. Additional variants and investigations on multi-grid Lax–Wendroff-type schemes can be found in Davis *et al.* (1984) and Chima *et al.* (1987), where comparisons with other central, multi-grid schemes are presented. Generally, the multi-grid convergence rate is reduced in the presence of viscous terms, when compared to the similar inviscid calculation.

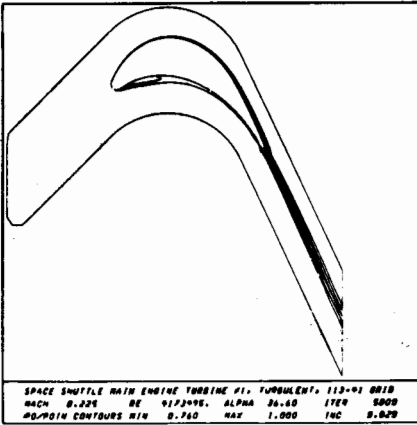
As mentioned above, there is still a need for the addition of artificial dissipation at high Reynolds numbers, as confirmed by the results of Figure 23.2.3. The viscous Burgers equation is solved with the MacCormack method, without any artificial dissipation terms or limiters, for an expansion fan at different Reynolds numbers. As seen from Figure 21.4.4, in the inviscid case the scheme generates



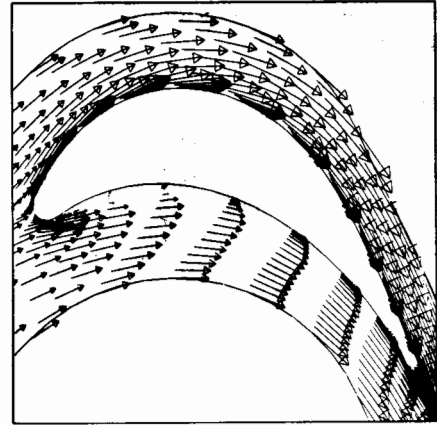
(a) Computational grid for space shuttle main engine fuel pump turbine rotor. C-mesh of 113x41 points



(b) Viscous Mach number contours for space shuttle main engine fuel pump turbine rotor. Iso-Mach lines



(c) Viscous total pressure contours for space shuttle main engine fuel pump turbine rotor



(d) Viscous velocity vectors for space shuttle main engine fuel pump turbine rotor. Velocity field

Figure 23.2.2 Navier–Stokes computation of a turbine rotor flow with a MacCormack multi-grid method by Chima (1985). (Courtesy R. Chima, NASA Lewis Research Center, USA)

an unphysical expansion shock and overshoots. At a Reynolds number of 100, the physical viscosity produces sufficient dissipation to reproduce the correct smooth solution. At $Re = 1000$ some overshoot appears at the foot of the expansion, while at $Re = 10000$ there is not enough dissipation on the scale of the mesh to avoid the expansion shock. Hence, this case requires the same treatment as inviscid calculations.

The most general formulation of the viscous two-step variants of the Lax–Wendroff schemes is obtained by extending the S_4^β schemes of Lerat and Peyret, presented in Section 17.2.3, to the viscous flow equations.

MacCormack scheme-viscous Burgers equation

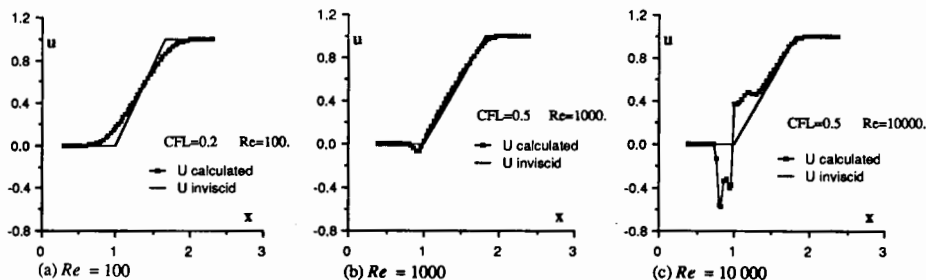


Figure 23.2.3 Application of MacCormack's scheme, without artificial dissipation, to the viscous Burgers equation. The continuous line is the inviscid expansion fan solution

In a one-dimensional framework, referring to equation (23.2.1), the schemes (17.2.39) are generalized as follows:

$$\begin{aligned} \bar{u}_i = & u_i^n + \beta(u_{i+1}^n - u_i^n) - \alpha \frac{\Delta t}{\Delta x} (f_{i+1}^n - f_i^n) \\ & + \alpha \frac{\Delta t}{\Delta x} [\gamma(\tau_{i+3/2}^n - \tau_{i+1/2}^n) + (1-\gamma)(\tau_{i+1/2}^n - \tau_{i-1/2}^n)] \end{aligned} \quad (23.2.18a)$$

$$\begin{aligned} u_i^{n+1} = & u_i^n - \frac{\Delta t}{2\alpha\Delta x} [(\alpha + \beta - 1)(f_i^n - f_{i-1}^n) + (\alpha - \beta)(f_{i+1}^n - f_i^n) + \bar{f}_i - \bar{f}_{i-1}] \\ & + \frac{\Delta t}{2\alpha\Delta x} [\beta(\bar{\tau}_{i-1/2} - \bar{\tau}_{i-3/2}) + (1-\beta)(\bar{\tau}_{i+1/2} - \bar{\tau}_{i-1/2}) \\ & + (2\alpha - 1)(\tau_{i+1/2}^n - \tau_{i-1/2}^n)] \end{aligned} \quad (23.2.18b)$$

These schemes depend on the three parameters α, β, γ and are second order in space and time. Their numerical flux can be written as

$$\begin{aligned} f_{i+1/2}^* = & \frac{1}{2\alpha} [(\alpha - \beta)f_{i+1}^n + (\alpha + \beta - 1)f_i^n + \bar{f}_i \\ & - (2\alpha - 1)\tau_{i+1/2}^n - \beta\bar{\tau}_{i-1/2} - (1-\beta)\bar{\tau}_{i+1/2}] \end{aligned} \quad (23.2.19)$$

The choice $\alpha = 1, \beta = \gamma = 0$ is the forward-backward MacCormack scheme (23.2.15), (23.2.16), while $\alpha = 1, \beta = \gamma = 1$ is the backward-forward version. Remember also that $\alpha = \beta = 1/2$ is the two-step Richtmeyer scheme.

The scheme (23.2.18) has a seven-point support for general values of β and γ unless $\beta = \gamma = 0$ or $\beta = \gamma = 1$. In order to avoid seven-point schemes, which are not very convenient close to solid boundaries, five-point extensions can be defined if the time accuracy is restricted to first order in the viscous case, following the original scheme of Thommen (1966). The latter is a viscous extension of the Richtmeyer scheme $\alpha = \beta = 1/2$.

Hence an alternative generalization of Lerat and Peyret's S_α^β schemes is defined

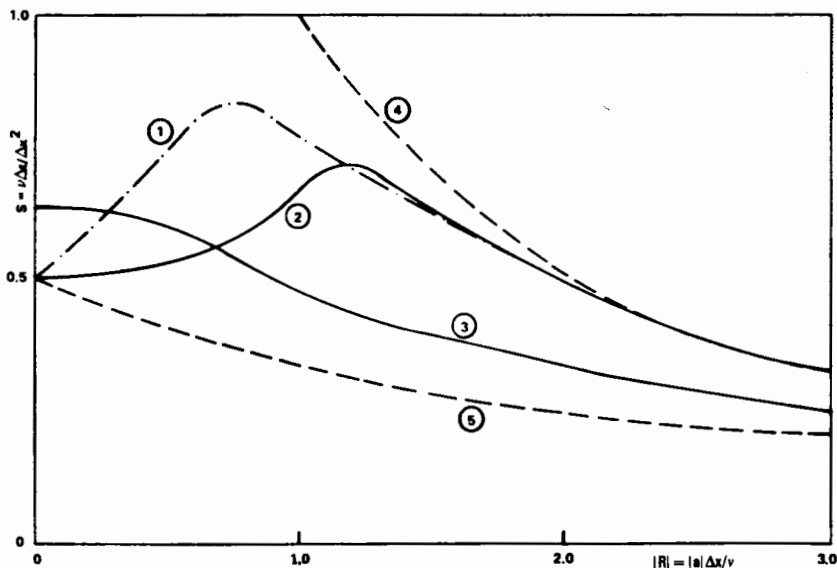
by modifying the corrector step of equation (23.2.18):

$$\begin{aligned} \bar{u}_i = & u_i^n + \beta(u_{i+1}^n - u_i^n) - \alpha \frac{\Delta t}{\Delta x} (f_{i+1}^n - f_i^n) \\ & + \alpha \frac{\Delta t}{\Delta x} [\gamma(\tau_{i+3/2}^n - \tau_{i+1/2}^n) + (1-\gamma)(\tau_{i+1/2}^n - \tau_{i-1/2}^n)] \end{aligned} \quad (23.2.20a)$$

$$\begin{aligned} u_i^{n+1} = & u_i^n - \frac{\Delta t}{2\alpha \Delta x} [(\alpha + \beta - 1)(f_i^n - f_{i-1}^n) + (\alpha - \beta)(f_{i+1}^n - f_i^n) + \bar{f}_i - \bar{f}_{i-1}] \\ & + \frac{\Delta t}{\Delta x} (\tau_{i+1/2}^n - \tau_{i-1/2}^n) \end{aligned} \quad (23.2.20b)$$

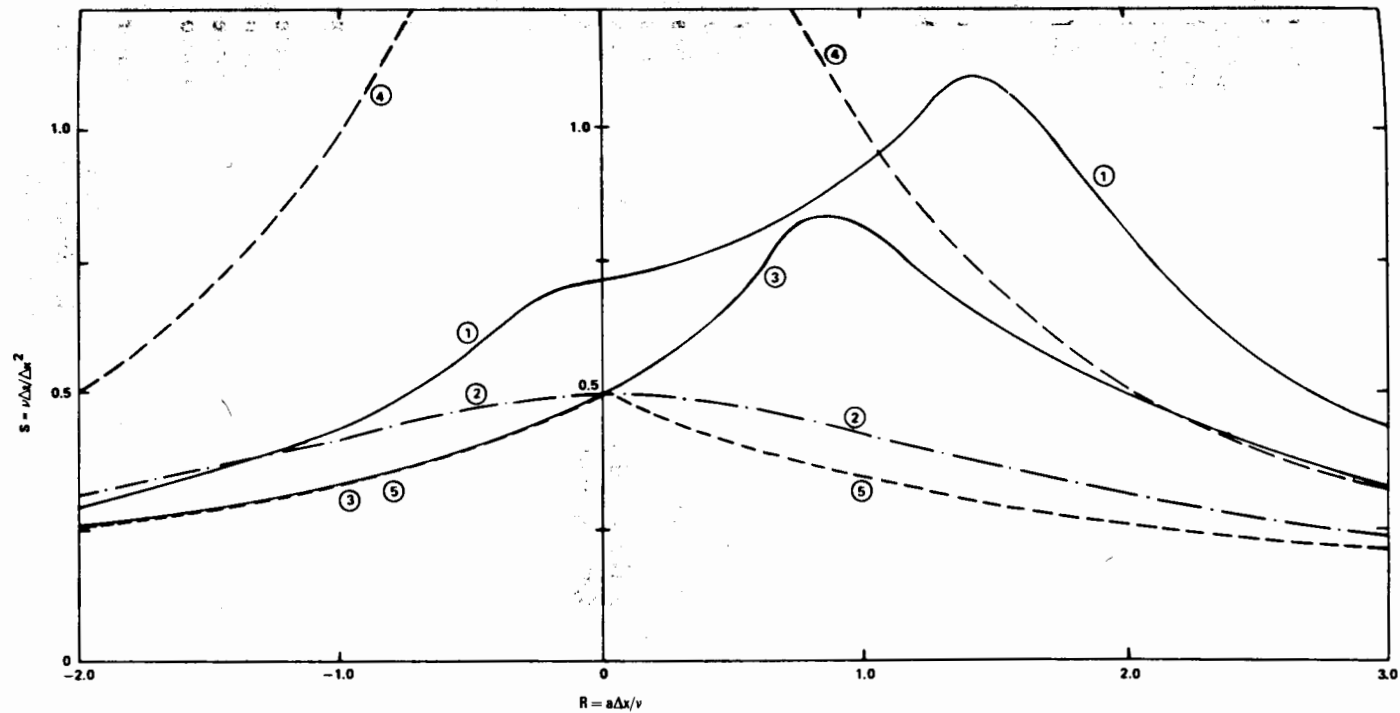
Observe that the second step does not require new evaluations of the viscous terms. The above scheme is first order in time and second order in space, reducing to second order at steady state, and has a numerical flux defined by

$$f_{i+1/2}^* = \frac{1}{2\alpha} [(\alpha - \beta)f_{i+1}^n + (\alpha + \beta - 1)f_i^n + \bar{f}_i - 2\alpha\tau_{i+1/2}^n] \quad (23.2.21)$$



- ① The variant $\alpha = \beta = \gamma = 1/2$ (Richtmyer type)
- ② The MacCormack scheme $\alpha = 1, \beta = \gamma = 0$ or 1
- ③ An 'optimal' scheme $\alpha = 1 + \sqrt{5}/2, \beta = \gamma = 1/2$ (Lerat-Peyret)
- ④ The CFL condition $\sigma = 1$
- ⑤ The condition (23.2.17)

Figure 23.2.4 Stability limits for the second-order schemes (23.2.18). (From Peyret and Taylor, 1983)



- ① The variant $\alpha = 1, \beta = 1/2, \gamma = 0$ of scheme (23.2.19)
- ② Thommen's scheme $\alpha = \beta = \gamma = 1/2$
- ③ The schemes (23.2.20) with arbitrary α, β and $\gamma = 0$
- ④ The CFL condition $\sigma = 1$
- ⑤ The condition (23.2.17)

Figure 23.2.5 Stability limits for the second-order schemes (23.2.18) and (23.2.20). (From Peyret and Taylor, 1983)

Thommen's (1966) original scheme corresponds to $\alpha = \beta = \gamma = 1/2$ and allows an exact linear stability analysis, leading to

$$\frac{\Delta t}{\Delta x^2} (a^2 \Delta t + 2\nu) \leq 1 \quad (23.2.22)$$

For the other schemes, analytical stability conditions cannot be obtained and a numerical investigation is presented by Peyret and Taylor (1983) in a diagram $\nu \Delta t / \Delta x^2$, $R = a \Delta x / \nu$, which is reproduced here as Figure 23.2.4. It corresponds to the second-order schemes (23.2.18) and contains a comparison between the stability limits for: (1) the variant $\alpha = \beta = \gamma = \frac{1}{2}$; (2) the MacCormack scheme; (3) an 'optimal' scheme $\alpha = 1 + \sqrt{5}/2$, $\beta = \gamma = \frac{1}{2}$; (4) the CFL condition $\sigma = 1$ and (5) the condition (23.2.17). The schemes are stable in the region below the corresponding curve.

The important conclusion is that the condition (23.2.17) can be applied as a valid sufficient condition of stability for all second-order variants of the viscous Lax–Wendroff schemes.

Figure 23.2.5 contains additional results for the schemes (23.2.20), which are only first order in time. It contains a comparison between the stability limits for: (1) the variant $\alpha = 1$, $\beta = \frac{1}{2}$, $\gamma = 0$ of scheme (23.2.18); (2) Thommen's scheme; (3) the schemes (23.2.20) with arbitrary α , β and $\gamma = 0$; (4) the CFL condition $\sigma = 1$ and (5) the condition (23.2.17). Here again condition (23.2.17) is generally valid as a sufficient condition for linear Von Neumann stability.

It should be added at this point that the implicit Lax–Wendroff-type schemes of Lerat, discussed in Section 17.4, have been extended to the Navier–Stokes equations by Hollanders *et al.* (1985) and that implicit versions of MacCormack's scheme, with flux splitted implicit operators, have been investigated by Kordulla and MacCormack (1985) showing interesting convergence properties.

23.2.4 Central schemes with separate space and time discretization

The central schemes with separate space and time discretizations are all based on the same central discretization of the flux gradients, which reduce in one-dimensional flows to equation (23.2.3). As discussed in Chapter 18, artificial dissipation terms have to be added to the right-hand side.

The addition of the viscous and heat conduction terms does not modify the general approach described in Chapter 18, but the artificial dissipation has to be reduced in the viscous layers if loss of accuracy is to be avoided, for instance by multiplication with a factor which goes linearly, or quadratically, to zero with Mach number.

Most of the central methods apply the Jameson combination of non-linear second- and fourth-order damping terms and a discussion of the effects of these terms on accuracy and convergence rates of Navier–Stokes solutions, for two- and three-dimensional flows, can be found in Pulliam (1986), Swanson and Turkel (1987) and Caughey and Turkel (1988).

With *Kunge–Kutta time-integration* methods, the extension of the approach discussed in Section 18.3 is straightforward (Martinelli *et al.*, 1986; Dawes, 1986; Martinelli and Jameson, 1988). The main difference lies in the removal of the enthalpy damping terms, since these are not valid for stationary Navier–Stokes flows where the stagnation enthalpy is not constant over the flow field.

When *multi-step implicit time-integration* methods are applied, following the original approach of Briley and McDonald (1975) and Beam and Warming (1978), additional contributions from the viscous terms have to be considered in the implicit operators.

Reproducing the development of Section 18.1 for the viscous equation (23.2.1), considered here as a system, equation (18.1.5) becomes, with $\xi = 0$,

$$\left(1 + \Delta t \theta \frac{\partial}{\partial x} A_T^n\right) \Delta U^n = -\Delta t \left(\frac{\partial f}{\partial x} - \frac{\partial f_v}{\partial x} \right)^n + \left(\theta - \frac{1}{2} \right) O(\Delta t^2) \quad (23.2.23)$$

We have written the dependent variable as U instead of u in accordance with our convention for systems of equations. A_T is the Jacobian of the total flux $f_T = f - f_v$:

$$A_T = \frac{df_T}{dU} = A - \frac{df_v}{dU} \quad (23.2.24)$$

where A is the inviscid Jacobian and reduces to equation (23.2.10) for scalar equations.

Compared to the inviscid case, the calculation of the Jacobian matrix is somewhat more complicated, due to the presence of the viscous terms which are also a function of velocity derivatives. Considering $f_v = f_v(U, U_x)$, where U_x is the x derivative of U , the viscous part of the Jacobian is calculated from

$$\frac{df_v}{dU} \Delta U = \frac{\partial f_v}{\partial U} \Delta U + \frac{\partial f_v}{\partial U_x} \Delta U_x = \frac{\partial f_v}{\partial U} \Delta U + \frac{\partial f_v}{\partial U_x} (\Delta U)_x \equiv A_1 \Delta U + A_2 (\Delta U)_x \quad (23.2.25)$$

Following Beam and Warming (1978), the viscous Jacobians are combined in equation (23.2.23) as follows:

$$\begin{aligned} \frac{\partial}{\partial x} A_T \Delta U &= \frac{\partial}{\partial x} [A \Delta U - A_1 \Delta U - A_2 (\Delta U)_x] \\ &= \frac{\partial}{\partial x} \left[(A - A_1 + A_{2x}) \Delta U - \frac{\partial}{\partial x} (A_2 \Delta U) \right] \end{aligned} \quad (23.2.26)$$

where $A_{2x} \equiv \partial A_2 / \partial x$.

For the one-dimensional Euler equations we obtain the following expressions, assuming constant values of viscosity and thermal conductivity coefficients with time, although these coefficients may depend on other variables such as

temperature (see Problem 23.10):

$$A_2 = \frac{1}{\rho} \begin{vmatrix} 0 & 0 & 0 \\ -\frac{4\mu u}{3} & \frac{4\mu}{3} & 0 \\ -\frac{4\mu u^2}{3} - \frac{k}{c_v}(E - u^2) & \left(\frac{4\mu}{3} - \frac{k}{c_v}\right)u & \frac{k}{c_v} \end{vmatrix} \quad (23.2.27)$$

and

$$A_{2x} - A_1 = \frac{1}{\rho} \begin{vmatrix} 0 & 0 & 0 \\ -\frac{4\mu_x u}{3} & \frac{4\mu_x}{3} & 0 \\ -\frac{4\mu_x u^2}{3} - \left(\frac{k}{c_v}\right)_x (E - u^2) & \left(\frac{4\mu}{3} - \frac{k}{c_v}\right)_x u & \left(\frac{k}{c_v}\right)_x \end{vmatrix} \quad (23.2.28)$$

Note that this last combination is a homogeneous function of the gradients of viscosity and thermal conductivity. Hence this matrix vanishes for constant values of these coefficients.

With central discretizations, the implicit scheme (23.2.23) becomes

$$\left\{ 1 + \frac{\Delta t}{\Delta x} \theta \left[\bar{\delta}(A_i^n + A_{2x,i}^n - A_{1,i}^n) - \frac{1}{\Delta x} \delta^2 A_{2,i}^n \right] \right\} \Delta U_i^n = -\frac{\Delta t}{\Delta x} [\bar{\delta} f_i^n - \delta f_{v,t+1/2}^n] \quad (23.2.29)$$

and the viscous terms maintain the block tridiagonal structure of the implicit operator.

The treatment of the artificial dissipation terms follows the developments of Chapter 18 and has to be included in the implicit operator.

The generalization to multi-dimensions is formally straightforward. Denoting by B_T and C_T the Jacobians of the total fluxes in the y and z directions, the implicit scheme can be written for a three-dimensional problem, in condensed form, as

$$\left[1 + \Delta t \theta \left(\frac{1}{\Delta x} \bar{\delta}_x A_T^n + \frac{1}{\Delta y} \bar{\delta}_y B_T^n + \frac{1}{\Delta z} \bar{\delta}_z C_T^n \right) \right] \Delta U_{ijk}^n = -\Delta t R_{ijk}^n \quad (23.2.30)$$

where the residual R is equal to the right-hand side of equation (23.2.29) plus similar terms in the y and z directions (or a finite volume generalization in an arbitrary mesh system). The implicit operator is block heptadiagonal (block pentadiagonal in two-dimensions) and can be reduced by the standard factorization approach of Beam and Warming, as described in Section 18.2 and in Section 11.4 in Volume 1, leading to

$$\left(1 + \theta \frac{\Delta t}{\Delta x} \bar{\delta}_x A_T^n \right) \left(1 + \theta \frac{\Delta t}{\Delta y} \bar{\delta}_y B_T^n \right) \left(1 + \theta \frac{\Delta t}{\Delta z} \bar{\delta}_z C_T^n \right) \Delta U_{ijk}^n = -\Delta t R_{ijk}^n \quad (23.2.31)$$

each factor being resolved separately.

The implicit formulation of the multi-dimensional Navier–Stokes equations requires, however, some additional care, since the viscous fluxes depend on all the space derivatives of the flow variables. For instance, the x flux component f_v is a function of not only U and U_x but also of U_y and U_z . Hence, the development (23.2.25) of the Jacobians becomes

$$\begin{aligned} \frac{df_v}{dU} \Delta U &= \frac{\partial f_v}{\partial U} \Delta U + \frac{\partial f_v}{\partial U_x} \Delta U_x + \frac{\partial f_v}{\partial U_y} \Delta U_y + \frac{\partial f_v}{\partial U_z} \Delta U_z \\ &\equiv A_1 \Delta U + A_2 (\Delta U)_x + A_3 (\Delta U)_y + A_4 (\Delta U)_z \end{aligned} \quad (23.2.32)$$

The terms $\partial[A_3(\Delta U)_y]/\partial x$ and $\partial[A_4(\Delta U)_z]/\partial x$ in the implicit operator contain mixed derivatives and lead to difficulties with the approximate factorization. Therefore the mixed derivative terms are generally treated explicitly. Also the cost of the block tridiagonal inversions of each factor can be reduced by applying the diagonalized variant of Section 18.2.1. A further simplification can be obtained by neglecting completely the viscous terms in the implicit operator. Although this might affect the convergence rate, it leads to a significant reduction in the computational effort.

Additional considerations concerning the practical application of this approach are described in Pulliam (1984) and Pulliam and Steger (1985).

It is known that the errors due to the factorization reduce the unconditional stability of the implicit scheme (23.2.30). This is easily understood by considering that the leading error in (23.2.31) is proportional to

$$\Delta t^3 \bar{\delta}_x A_T \cdot \bar{\delta}_y B_T \cdot \bar{\delta}_z C_T \Delta U \quad (\Delta t^2 \bar{\delta}_x A_T \cdot \bar{\delta}_y B_T \Delta U \text{ in two dimensions}) \quad (23.2.33)$$

which becomes increasingly large when Δt is increased. Since for steady-state problems, one aims at applying the largest possible time step (high CFL numbers) in order to reach the converged state in the least possible number of iterations, alternative options are currently considered.

Besides factorization, a variety of solution techniques can be applied to the inversion of the implicit operators of equation (23.2.30). In particular, by applying flux splitting decompositions to the inviscid Jacobian matrices, diagonal dominance can be achieved, allowing the application of relaxation techniques, as described in Section 21.1.7. Alternatively, LU decompositions are also considered, also based on flux splitting considerations. Some examples of these attempts can be found in Obayashi and Kuwahara (1984), MacCormack (1985), Jameson and Yoon (1987) and Rieger and Jameson (1988).

Example 23.2.1 Secondary flow in turbine cascades

The central finite volume discretization is applied by Subramanian and Bozzola (1987) with Jameson-type artificial viscosity and a four-stage Runge–Kutta time-integration method.

Boundary conditions are fixed on solid surfaces by the zero normal flux condition at the solid boundary cell faces, where the pressure is obtained from

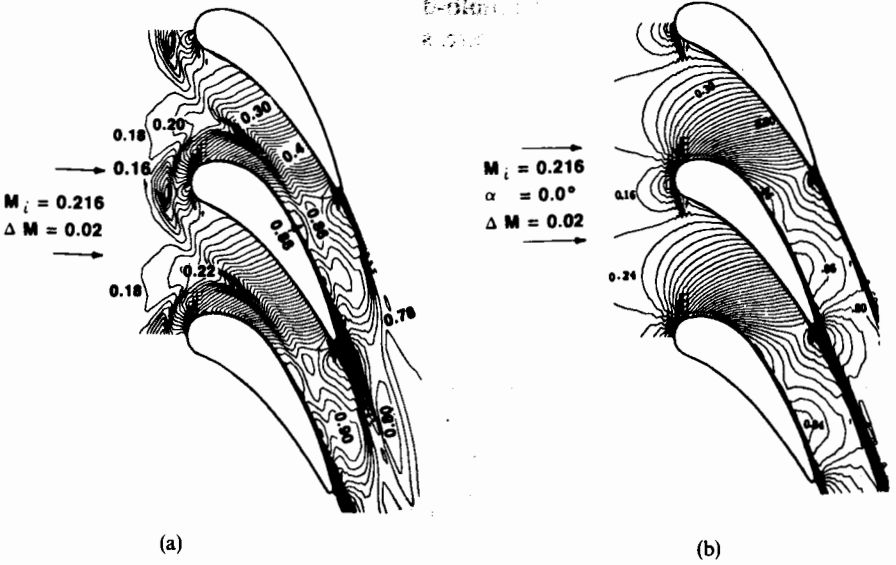


Figure 23.2.6 Iso-Mach lines (a) at 1.2 per cent span and (b) at mid-span for an annular untwisted turbine cascade. (From Subramanian and Bozzola, 1987)

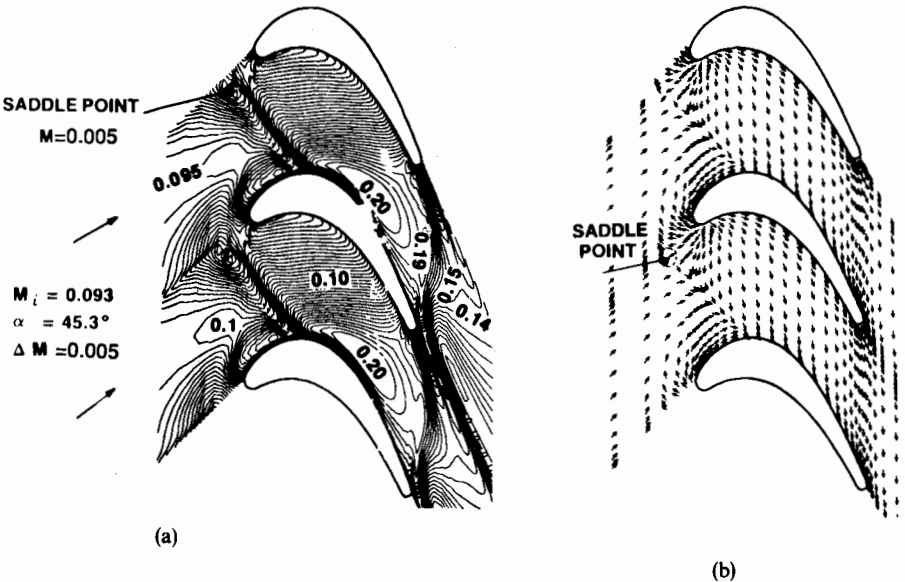


Figure 23.2.7 (a) Iso-Mach lines and (b) velocity directions at 1.2 per cent span for the Langston linear turbine cascade. (From Subramanian and Bozzola, 1987)

the normal pressure gradient. On inflow boundaries, total pressure and temperature are fixed together with the inlet flow angle and the remaining information is obtained from the extrapolated left-running Riemann invariant. At outflow boundaries the static pressure is fixed, the other variables being extrapolated.

The turbulence input is obtained from the Baldwin–Lomax model.

Figure 23.2.6 relates to the flow in a three-dimensional, annular, untwisted turbine cascade, tested at NASA. An H-mesh of $31 \times 71 \times 21$ points is used. The incident Mach number is 0.216 under 0° inlet angle.

Figure 23.2.6(a) and (b) displays the calculated Mach number isolines at 1.2 per cent of the hub end wall and at mid-span, showing the secondary flow pattern and the horseshoe vortex around the leading edge. An interaction between the secondary flow and the blade suction surface boundary layer can be noticed. This effect is much more pronounced for the linear cascade of Figure 23.2.7, tested by Langston *et al.* (1977), at a Reynolds number of 5.9×10^5 and 44.7° inlet angle at low inlet Mach number. The iso-Mach lines at a section at 1.2 per cent of the end wall are shown in Figure 23.2.7(a) and the corresponding velocity directions can be seen in Figure 23.2.7(b). The horseshoe vortex interacts strongly with the suction surface boundary layer and a significant corner stall appears, in agreement with experimental data. In addition the secondary flow deviates the wake towards the adjacent blade, indicating a severe roll-up action of the secondary flow.

Example 23.2.2 Hypersonic flow over HERMES space shuttle

The Navier–Stokes fluxes are centrally discretized by a finite volume method, with artificial viscosity terms and an implicit time integration, derived from a Newton iteration for the steady-state solutions. The implicit operator is decomposed via an LU factorization (Rieger and Jameson, 1988). The following figures show representative results obtained for a configuration of the European HERMES space shuttle. Figure 23.2.8 shows the surface and several cross-sectional meshes, with a total of $97 \times 129 \times 65$ mesh points.

The subsonic far-field boundary conditions are derived from local one-dimensional characteristic relations and treated explicitly. Free-stream values are imposed at a supersonic inflow far field, while first-order extrapolation of the conservative variables is applied at supersonic outflow boundaries. At solid surfaces, vanishing normal pressure is applied with adiabatic conditions.

Results are shown for an incident Mach number of 8.0 and 30° incidence, a Reynolds number of 10^6 per unit length and laminar viscosity.

Figure 23.2.9 shows the Mach number distribution in the symmetry plane with a detailed view of the nose region. The front bow shock and the canopy shock are clearly resolved. The Mach number distribution in cross-section $x = 12.7$ m is shown in Figure 23.2.10, with a close-up view of the vehicle surface region, and is compared to an inviscid calculation in Figure 23.2.11. These two solutions are very close in the outer part of the shock layer, but strong differences

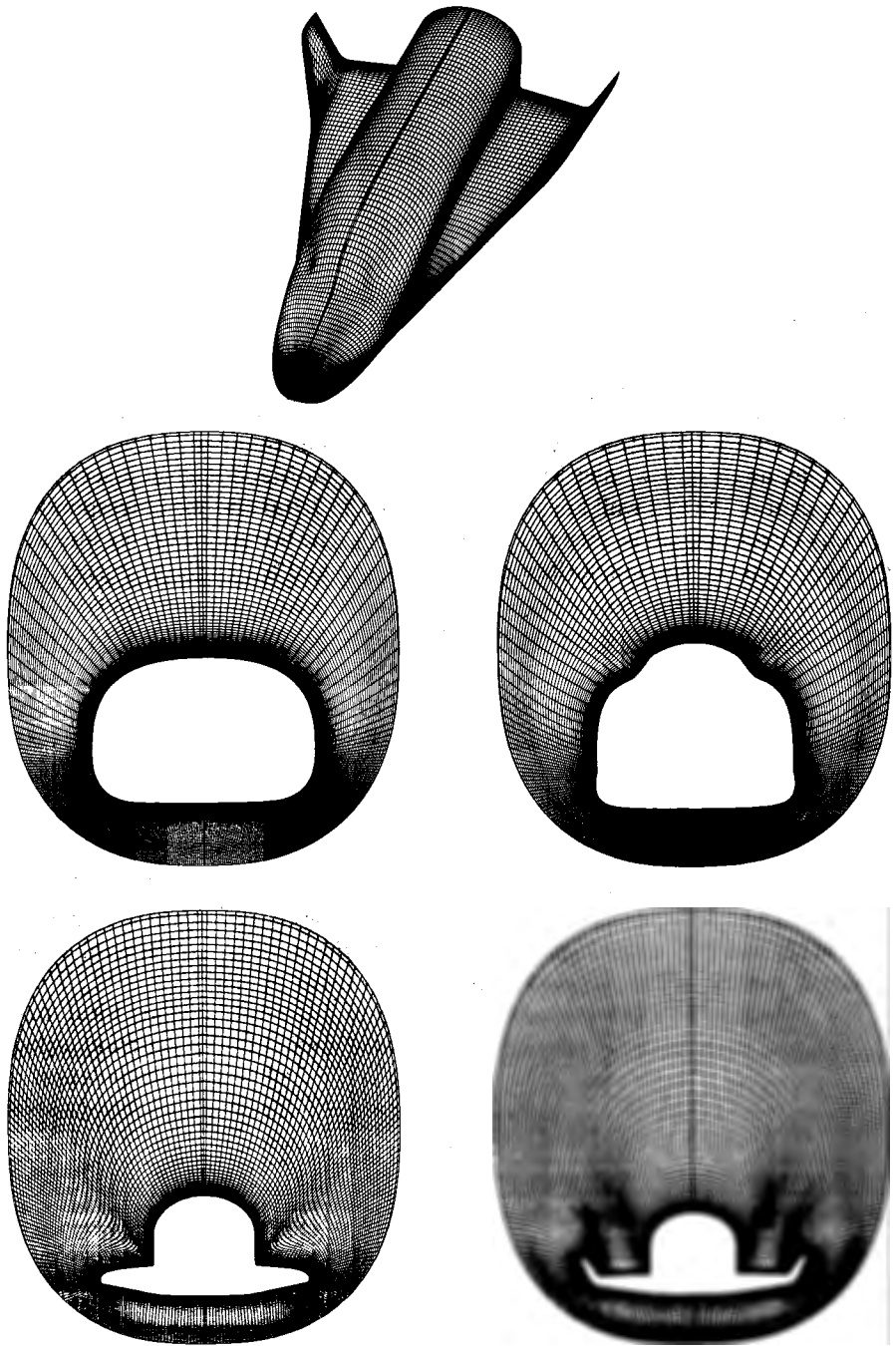


Figure 23.2.8 Mesh distribution on the surface and at various cross-sections of the HERMES space shuttle. (From Rieger and Jameson, 1988. Courtesy H. Rieger, Dornier GmbH)



Figure 23.2.9 Mach number distribution in the symmetry plane of the HERMES space shuttle with detailed view of the nose region. (From Rieger and Jameson, 1988. Courtesy H. Rieger, Dornier GmbH)

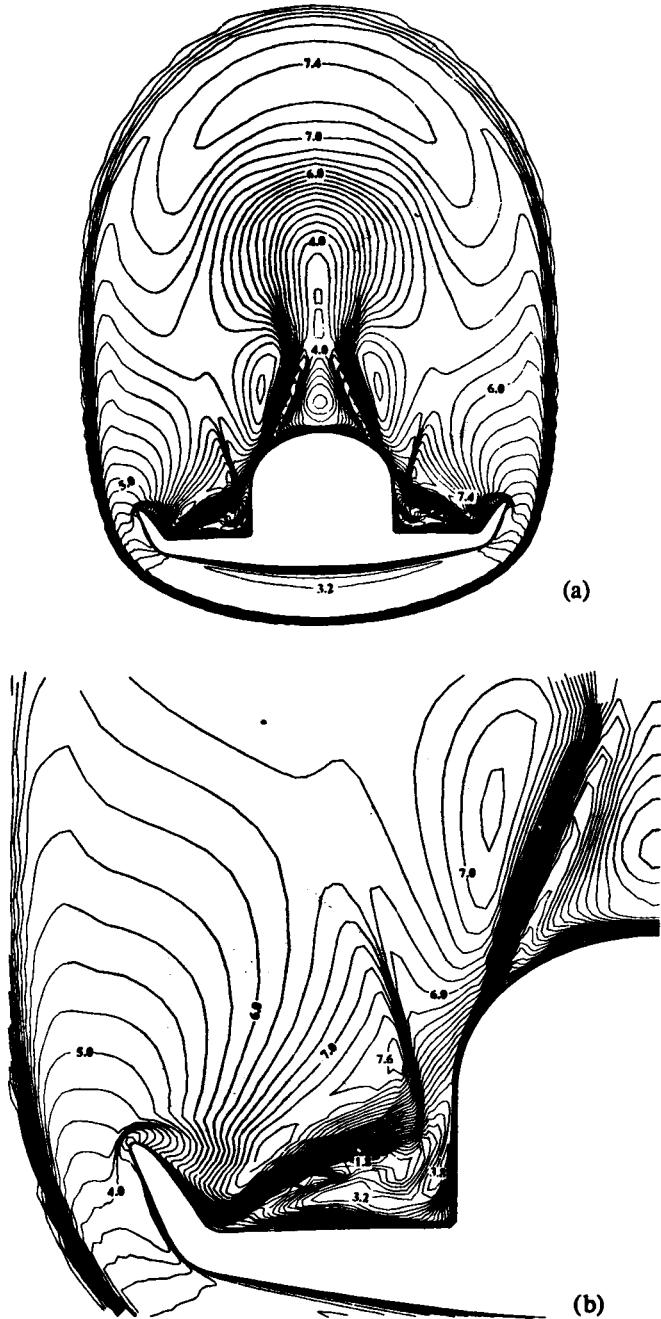


Figure 23.2.10 Mach number distribution (a) in cross-section $x = 12.7$ of the HERMES space shuttle, from viscous calculation, with (b) detailed view of Mach number in surface region and (c) velocity field in surface region. (From Rieger and Jameson, 1988. Courtesy H. Rieger, Dornier GmbH)

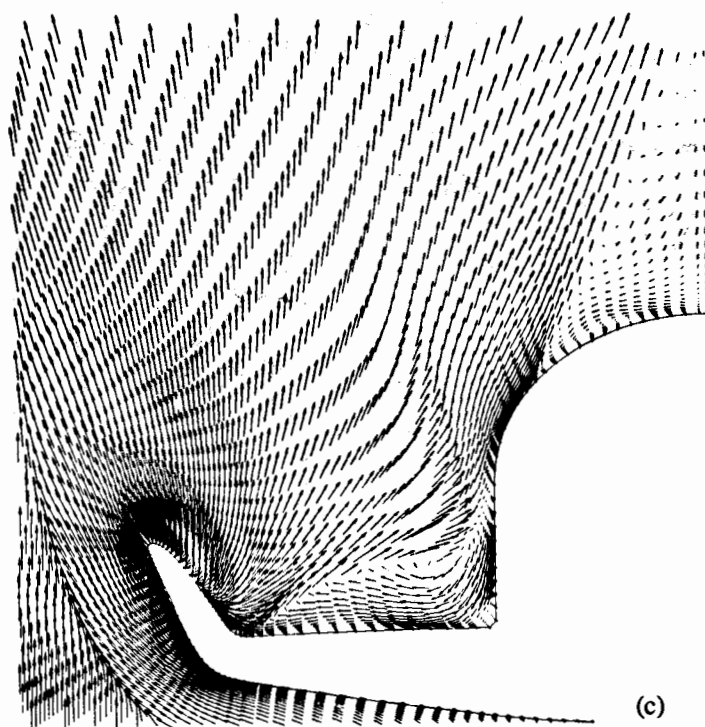


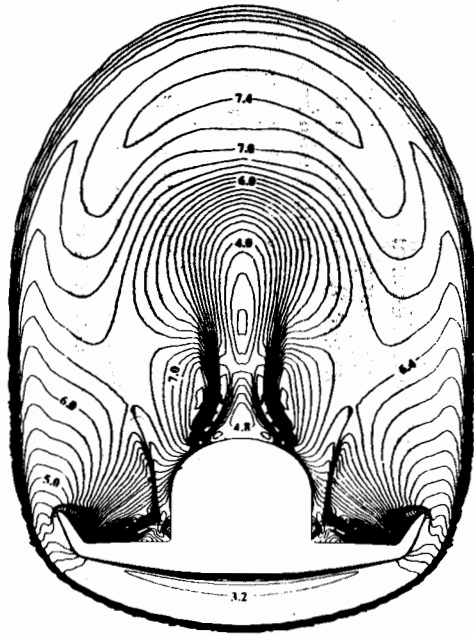
Figure 23.2.10 (Continued)

are observed in the vicinity of the walls. The inviscid calculation shows a crossflow shock above the wing and the cargo bay, which is strongly smoothed in the viscous case. This shock is first aligned along the diagonal to the vertical fuselage wall and then undergoes a 90° change of direction. In addition a shock wave appears at the winglet leading edge. A closer look at the inviscid solution shows some unphysical behaviour (Figure 23.2.11(b)), with peak Mach numbers of 15. In the viscous case, Figure 23.2.10(b) and (c) show peak Mach numbers of the order of the free-stream value.

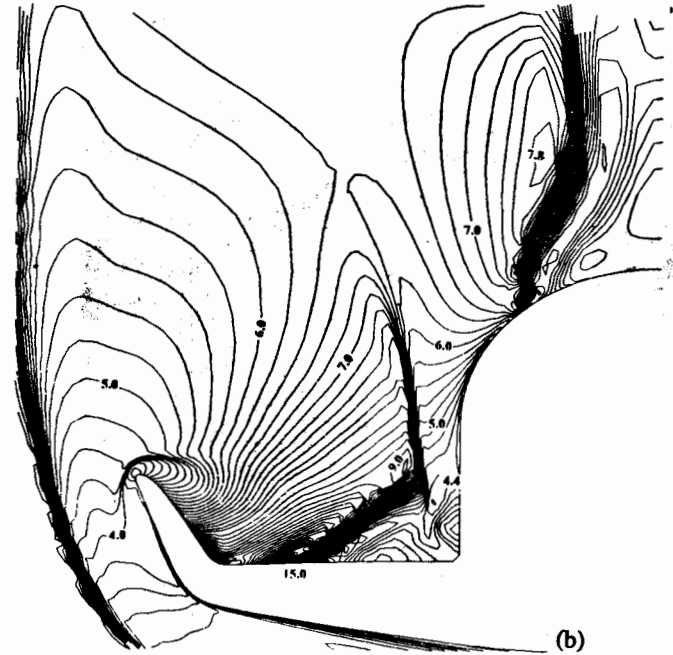
Example 23.2.3 Flow around a pitching NACA 0015 airfoil

The flow around a rapidly pitching airfoil has been calculated by Visbal and Shang (1987) with the implicit approximate factorization scheme of Beam and Warming and a three-point backward time integration. The grid is fixed to the oscillating airfoil.

Free-stream boundary conditions are fixed in the far field and all variables are extrapolated on the outflow boundary. On the airfoil surface no-slip

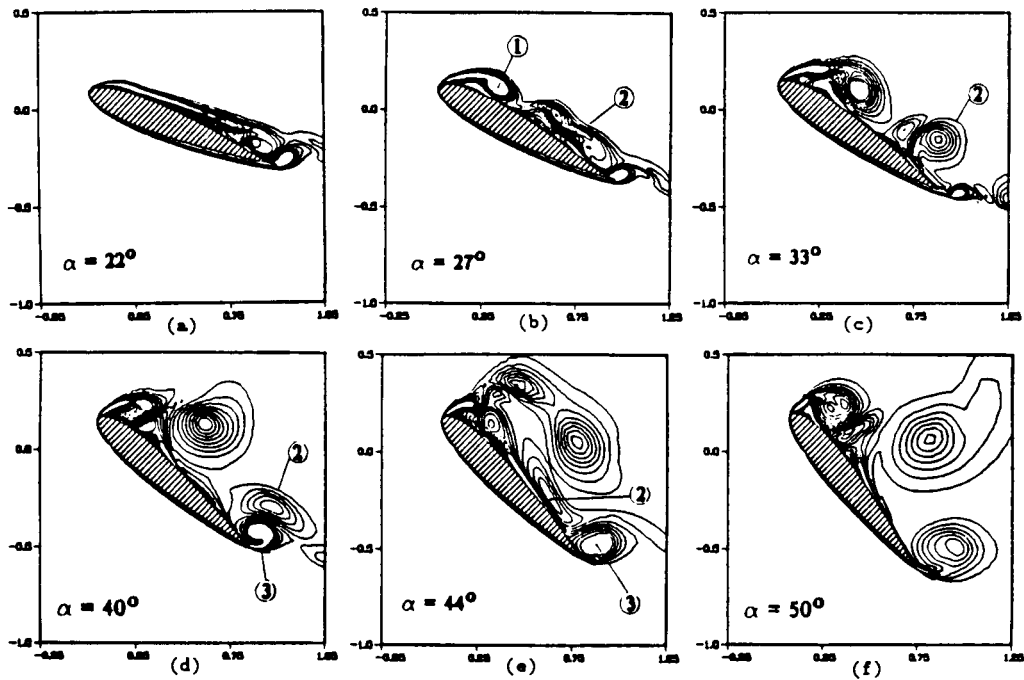


(a)



(b)

Figure 23.2.11 Mach number distribution (a) in cross-section $x = 12.7$ of the HERMES space shuttle, from inviscid calculation, with (b) detailed view of Mach number in surface region. (From Rieger and Jameson, 1988. Courtesy H. Rieger, Dornier GmbH)



Evolution of Vorticity Field

- ① Leading Edge Vortex
- ② Shear Layer Vortex
- ③ Trailing Edge Vortex

Figure 23.2.12 Evolution of vorticity field with time-varying incidence angle on a pitching NACA 0015 airfoil. (From Visbal and Shang, 1987)

isothermal conditions are imposed together with the normal pressure gradient, taken equal to the local inertia force resulting from the airfoil instantaneous acceleration.

The computation is performed for an incident Mach number of 0.2 and Reynolds number of 10^4 . Although the flow is unsteady, the ratio of the time constant of the oscillation (reduced frequency of 0.2) and the Courant number allowed a CFL number for the calculation close to 100, while maintaining a resolution of 200 time steps per cycle.

Figure 23.2.12 shows the vorticity field at different instantaneous incidence angles computed for an O-mesh of 203×101 points and a laminar flow assumption. The extremely complex vortical structure can be analysed as well as the interaction between the different vortices. A more detailed analysis of the flow can be found in the mentioned reference.

23.2.5 Upwind schemes

The upwind schemes discussed in Chapters 20 and 21 can be applied in a straightforward way to the computation of viscous flows by addition of the centrally discretized viscous terms.

The first-order upwind method, although rarely applied in practice due to its limited first-order accuracy, provides a reference with regard to stability conditions. Indeed, considering a one-dimensional system, a flux splitting on the convection terms leads to the scheme

$$U_i^{n+1} - U_i^n = -\frac{\Delta t}{\Delta x}(f_{i+1}^- - f_i^-) - \frac{\Delta t}{\Delta x}(f_i^+ - f_{i-1}^+) + \frac{\Delta t}{\Delta x}(\tau_{i+1/2}^n - \tau_{i-1/2}^n) \quad (23.2.34)$$

corresponding to a numerical flux

$$f_{T,i+1/2}^* = f_{i+1}^- + f_i^+ - \tau_{i+1/2}^n \quad (23.2.35)$$

When applied to the linear convection–diffusion equation (23.2.2), with $a > 0$, we have

$$u_i^{n+1} - u_i^n = -\sigma(u_i - u_{i-1})^n + \frac{v\Delta t}{\Delta x^2}(u_{i+1}^n - 2u_i^n + u_{i-1}^n) \quad (23.2.36)$$

Applying the methods of Section 8.6 in Volume 1, an exact Von Neumann stability condition is derived and is given by equation (23.2.17) (see Problem 23.12). As seen from Figures 23.2.4 and 23.2.5, this condition provides a sufficient criterion for all the Lax–Wendroff-type schemes.

In practical computations, the second-order methods of Chapter 21 are applied, either with explicit time integrations or with an implicit formulation in the line of Section 21.1.7, solved either by ADI factorizations or relaxation techniques, as referred to also in the previous section, coupled preferably to a multi-grid method to accelerate convergence for steady-state problems.

Referring to Section 21.1, a second-order space-accurate inviscid upwind numerical flux is defined by equation (21.1.37), for instance with fully backward extrapolation ($\kappa = -1$)

$$f_{i+1/2}^{*(2)} = f_{i+1/2}^* + \frac{1}{2}(f_i - f_{i-1/2}^*) + \frac{1}{2}(f_{i+1} - f_{i+3/2}^*) \quad (23.2.37)$$

As illustrated in Figure 21.1.7, the second and third terms represent the second-order corrections to the first-order numerical flux f^* . Hence it is sufficient to add the viscous terms to this flux, since they are discretized with second-order accuracy. The second-order space-accurate upwind flux for the viscous equations is therefore obtained by replacing the inviscid flux f^* by the total flux f_{τ}^* , defined by equation (23.2.35), leading to

$$f_{\tau,i+1/2}^{*(2)} = f_{\tau,i+1/2}^* + \frac{1}{2}(f_i - f_{i-1/2}^*) + \frac{1}{2}(f_{i+1} - f_{i+3/2}^*) \quad (23.2.38)$$

The contributions of the viscous terms to the implicit operators can be taken into account, as discussed in the previous section. The interested reader will find more details in Chakravarthy *et al.* (1985) in applications to various upwind schemes.

For explicit schemes with second-order accuracy in space and time, a two-step procedure can be defined, following, for instance, equation (21.1.39). The second-order accuracy in time is obtained by introducing predictor values in the first term of equation (21.1.37) obtained after an integration of the first-order scheme over $\Delta t/2$. This corresponds to the second-order time-integration scheme (11.5.7) in Volume 1. The similar procedure leads here to the following scheme, corresponding to $\kappa = -1$:

$$\bar{U}_i = U_i^n - \frac{\Delta t}{2\Delta x} (f_{\tau,i+1/2}^* - f_{\tau,i-1/2}^*) \quad (23.2.39a)$$

followed by

$$\overline{f_{\tau,i+1/2}^{*(2)}} = \overline{f_{\tau,i+1/2}^*} + \frac{1}{2}(f_i - f_{i-1/2}^*) + \frac{1}{2}(f_{i+1} - f_{i+3/2}^*) \quad (23.2.39b)$$

and

$$U_i^{n+1} - U_i^n = -\frac{\Delta t}{\Delta x} (\overline{f_{\tau,i+1/2}^{*(2)}} - \overline{f_{\tau,i-1/2}^{*(2)}}) \quad (23.2.39c)$$

Note that the first-order viscous numerical flux is evaluated with the predictor variables. The remaining corrections in (23.2.39b) are necessary to obtain second-order accuracy in space for the convection terms, and do not require viscous contributions, since the viscous terms are already second-order accurate at each step.

An important problem is related to the accuracy of the upwind schemes in the viscous-dominated regions. It has been pointed out in the previous chapters that the upwind schemes have a 'built-in' dissipation which is made apparent when writing its numerical flux as a central term plus additional contributions, following equation (21.1.38) for a second-order space-accurate upwind scheme.

The behaviour of these additional contributions, equal to the central discretization of $-(1-\kappa)\Delta x^2 \partial^2 f^*/\partial x^2$, where f^* is the numerical flux of the first-order upwind scheme, depends on the dissipation of the first-order scheme. The latter can be written in the form of equation (21.2.38), making the dissipation term apparent.

When applied to a viscous computation, the dissipation \bar{D} , proportional to Δx , might compete with the viscous contributions and lead to a loss of accuracy. This has been investigated by Van Leer *et al.* (1987). From formulas (20.5.96), it is seen that Roe and Osher's approximate Riemann solvers have dissipation contributions proportional to the eigenvalues of the discrete approximation A to the flux Jacobian. Roe and Osher's approximations to A have vanishing eigenvalues at shocks and contact discontinuities. This explains the sharp shock resolution of these schemes and their better resolution of contact discontinuities. This last property is of particular concern in boundary layer regions, since a boundary layer can be considered as an inviscid shear layer submitted to a viscous diffusion. The flux vector splitting schemes of first order have a numerical flux which can be written as equation (20.3.10b). Although the Van Leer splitting ensures that one eigenvalue on the Jacobian of the split fluxes vanishes over a shock transition, it does not vanish at a contact discontinuity, and neither does the Steger-Warming flux splitting. Hence it is to be expected that the flux vector splitting schemes will produce excessive dissipation in the boundary layer regions, in comparison with Roe or Osher's schemes. This is confirmed by the following figures, from Van Leer *et al.* (1987), showing the near-wall temperature profile in the flow around a circular cone at zero degree of incidence.

With conical bodies, the flow can be greatly simplified, since the flow will maintain the *conical symmetry*, that is all flow properties remain invariant on rays passing through the apex. All derivatives in the 'conical direction' vanish and the flow can be described by a two-dimensional model. Referring to Figure 23.2.13, the conical variables are defined by $X = x$, $Y = y/x$ and $Z = z/x$, and the conical flow depends only on Y and Z . This is strictly true for the inviscid part, since the viscous terms depend also on the distance $r = (x^2 + y^2 + z^2)^{1/2}$ to the apex, which appears in a Reynolds number factor on the viscous and heat conduction terms (actually a term $1/Re$). For a circular cone, the flow reduces to one dimension since it depends only on the angle θ between the streamline and the cone.

The calculations correspond to an incident Mach number of 7.95, $Re = 0.42 \times 10^6$ on a 10° cone with adiabatic boundary conditions. Hence the wall temperature has to be calculated and is a very sensitive quantity. The results display T/T_∞ as a function of θ , the value at the wall being close to 11.73. Figure 23.2.14 shows results obtained with the first-order Van Leer flux vector splitting and 18, 37 and 74 points in the boundary layer, compared to the results obtained with Roe's scheme. With Roe's fluxes the solution is practically independent of the number of points in the boundary layer, while the Van Leer fluxes do not generate the correct wall temperature even with 74 points in the

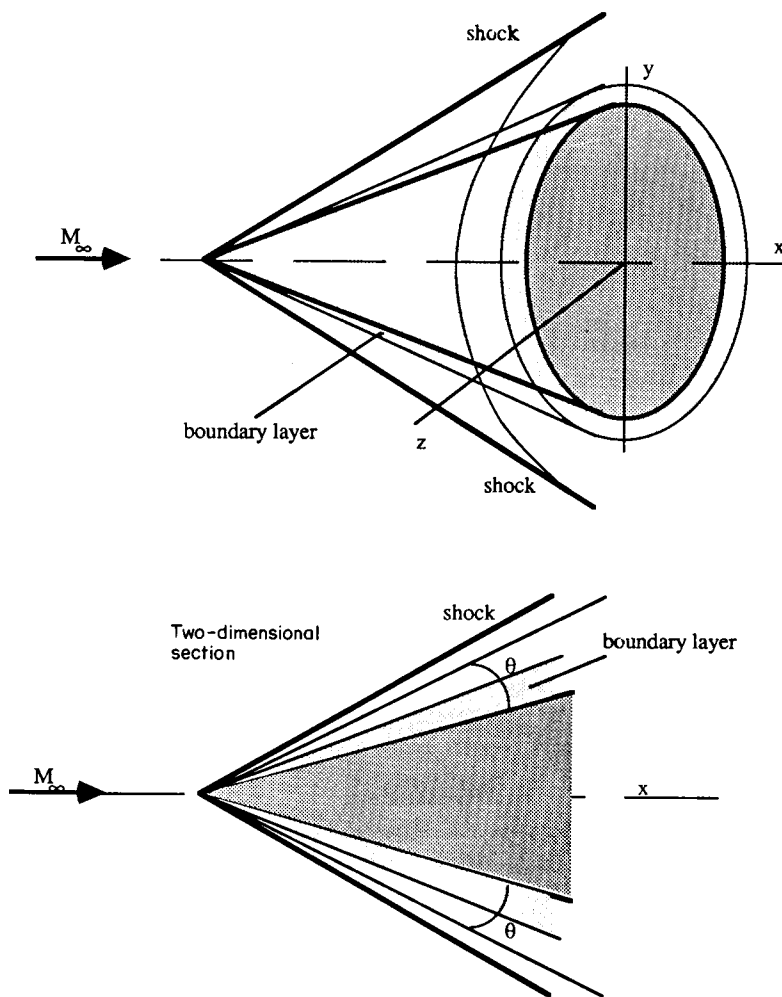
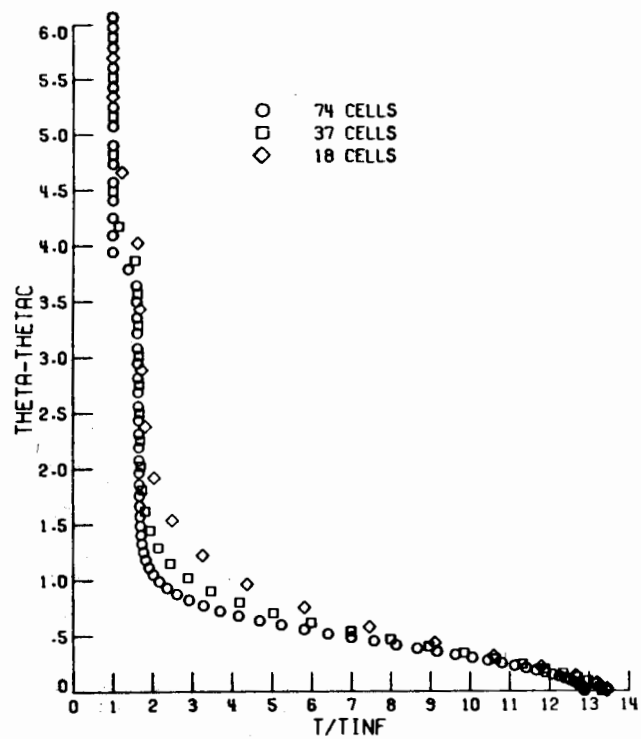


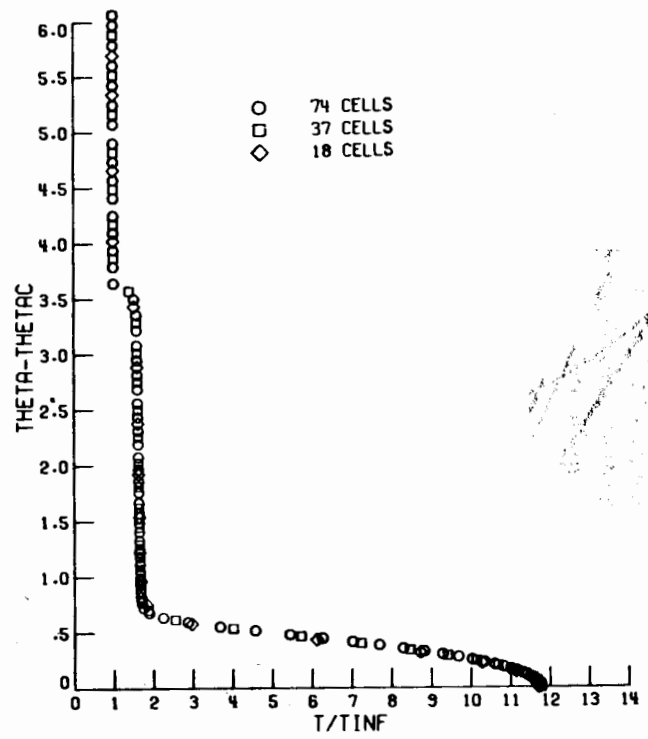
Figure 23.2.13 Geometry of conical flow configuration

viscous layer. Note also that the shock is better resolved with Roe's scheme. Figure 23.2.15 shows similar results obtained with the second-order flux vector upwind and MacCormack schemes. The results are clearly improved on the finest mesh, but on the coarse mesh are not even close to the first-order Roe scheme, which gives unchanged results with second-order accuracy. On the other hand, MacCormack's scheme gives excellent results in the boundary layer, although the shock resolution is not as good as expected from a central scheme. The good behaviour of the Lax-Wendroff-type schemes can be understood from the numerical flux (17.2.22), showing a dissipation term that is quadratic in the Jacobian eigenvalues, as seen from equation (17.2.24). Hence it tends to zero quadratically for vanishing eigenvalues.



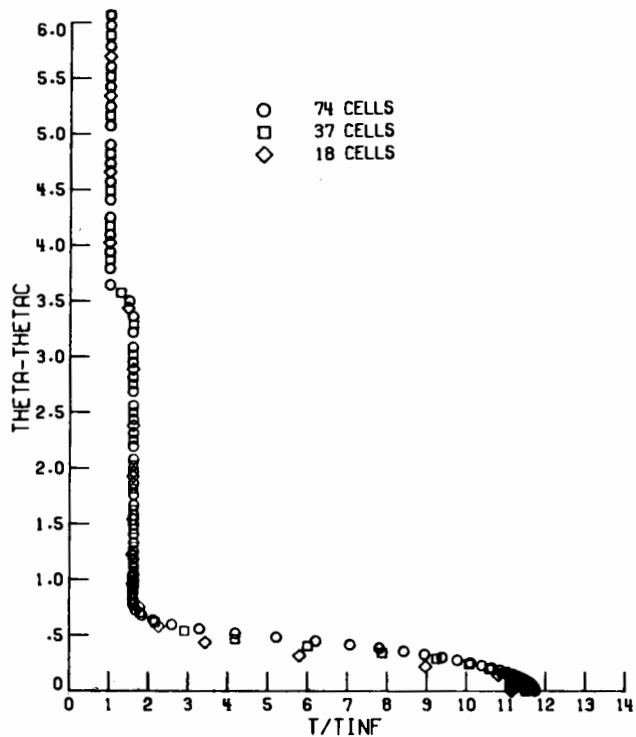
MACH 7.95 10-DEGREE CONE ADIABATIC WALL
SPATIAL CONVERGENCE STUDY

(a)

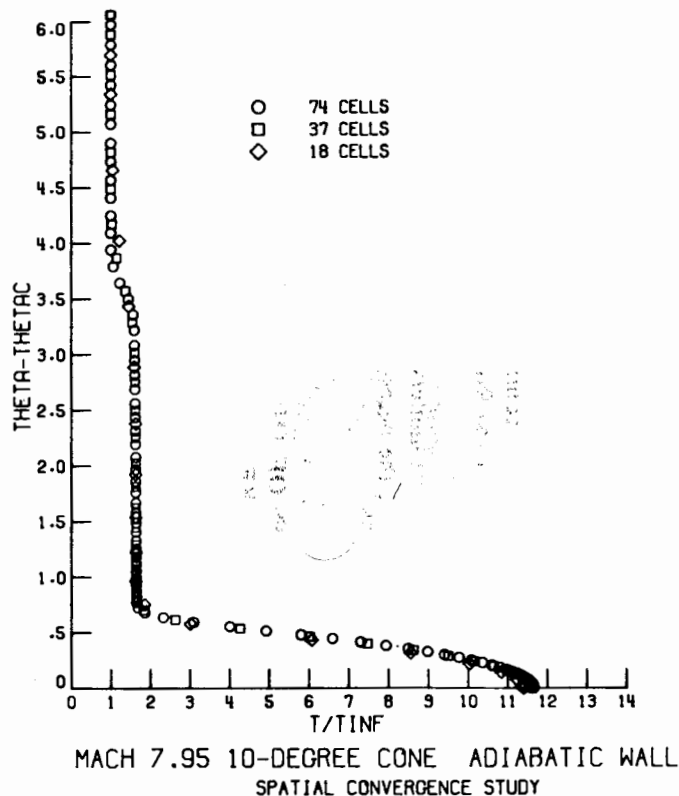


(b)

Figure 23.2.14 Comparison of first-order accurate solutions for the wall temperature in conical hypersonic flow, obtained with (a) Van Leer flux splitting, (b) Roe approximate Riemann solver, and 18, 37 and 74 mesh points in the boundary layer. (From Van Leer *et al.*, 1987)



(a)



(b)

Figure 23.2.15 Comparison of second-order accurate solutions for the wall temperature in conical hypersonic flow, obtained with (a) Van Leer flux splitting, (b) MacCormack scheme, and 18, 37 and 74 mesh points in the boundary layer. (From Van Leer *et al.*, 1987)

This property is actually at the basis of the unsatisfactory behaviour of these schemes at shock discontinuities, where the dissipation terms vanish too rapidly, while this same property is an asset in viscous regions. On the other hand, the limited flux vector upwind schemes have an adequate level of vanishing dissipation at shocks but too much at contact discontinuities.

It appears, therefore, that the behaviour of the upwind schemes in the viscous regions depends on the way they resolve the contact–shear layer discontinuities. This explains the excellent behaviour of the Roe and Osher schemes, as well as the MacCormack scheme.

Additional results on the effects of the limiters in the viscous regions can be found in Hänel *et al.* (1987), showing the necessity to reduce the influence of the limiters in the viscous regions.

23.3 DISCRETIZATION OF THE INCOMPRESSIBLE NAVIER–STOKES EQUATIONS

The discretization of the incompressible Navier–Stokes equations requires particular consideration since the time derivative of the density no longer appears. Hence the time-dependent methods suitable for the compressible equations cannot be applied without adaptation.

Several methods have been developed in order to treat this particular situation. For stationary flows, a structure similar to the compressible equations can be recovered by adding an artificial compressibility term under the form of the time derivative of the pressure added to the continuity equation. When steady state is reached, this term vanishes. This is the pseudo-compressibility method introduced by Chorin (1967) (see also Yanenko, 1971).

For time-dependent problems, the current approach consists in solving the time-dependent momentum equations in connection with a Poisson equation for the pressure obtained by taking the divergence of the momentum equations and expressing the condition of the divergence-free velocity field. This method can obviously also be applied to stationary problems and is referred to as the pressure correction method.

Alternative methods, based on variables other than the primitive, rely on a streamfunction–vorticity formulation. This approach is limited to two-dimensional flows and will therefore not be treated here. The interested reader can refer to Roache (1972), Cebeci *et al.* (1981) and Peyret and Taylor (1983) for a discussion of this approach and further references.

23.3.1 Incompressible Navier–Stokes equations

The mass conservation equation reduces to

$$\bar{\nabla} \cdot \bar{v} = 0 \quad (23.3.1)$$

which appears as a constraint to the general time-dependent equation of motion, written here in conservative form after division by the constant density and in

presence of external forces:

$$\frac{\partial \vec{v}}{\partial t} + \vec{\nabla} \cdot (\vec{v} \otimes \vec{v} + P\vec{I} - \vec{\tau}) = \vec{f}_e \quad (23.3.2)$$

where $P = p/\rho$ and τ is defined here as the shear stress (22.1.6) divided by the density, that is

$$\tau_{ij} = \nu(\partial_i v_j + \partial_j v_i) \quad (23.3.3)$$

The non-conservative form is written as

$$\frac{\partial \vec{v}}{\partial t} + (\vec{v} \cdot \vec{\nabla})\vec{v} = -\vec{\nabla}P + \vec{\nabla} \cdot \vec{\tau} + \vec{f}_e \quad (23.3.4)$$

which reduces to the following form for flows with constant viscosity:

$$\frac{\partial \vec{v}}{\partial t} + (\vec{v} \cdot \vec{\nabla})\vec{v} = -\vec{\nabla}P + \nu \Delta \vec{v} + \vec{f}_e \quad (23.3.5)$$

The equation for the temperature field can be obtained through application of equation (1.5.15) in Volume 1, where the divergence-free condition for the velocity field is introduced. It can be written as

$$\rho \frac{de}{dt} = \varepsilon_v + \vec{\nabla} \cdot (k\vec{\nabla}T) + q_H \quad (23.3.6)$$

where ε_v is the dissipation term, defined by

$$\varepsilon_v = \rho(\vec{\tau} \cdot \vec{\nabla}) \cdot \vec{v}$$

notice that in (1.5.13) Vol. 1
 $\varepsilon_v = (\vec{\tau} \cdot \vec{\nabla}) \cdot \vec{v}$ without the factor ρ

For constant thermal coefficients, this equation becomes

$$\frac{\partial T}{\partial t} + \vec{\nabla} \cdot (\vec{v}T) = E_v + \frac{k}{\rho c_v} \Delta T + \frac{q_H}{\rho c_v} \quad (23.3.8)$$

where the velocity can equally be put outside the divergence operator.

An equation for the pressure can be obtained by taking the divergence of the momentum equation and introducing the divergence-free velocity condition, leading to the following relation for constant viscosity:

$$\frac{1}{\rho} \Delta p = -\vec{\nabla} \cdot (\vec{v} \cdot \vec{\nabla})\vec{v} + \vec{\nabla} \cdot \vec{f}_e \quad (23.3.9)$$

which is a Poisson equation for the pressure for a given velocity field. Note that the right-hand side contains only products of first-order velocity derivatives, because of the incompressibility condition. Indeed, in tensor notations, the velocity term in the right-hand side is equal to $(\partial_j v_i) \cdot (\partial_i v_j)$.

For flows with constant viscosity, the temperature is decoupled and the basic variables will be pressure and velocity. The temperature distribution can then be found from the solution of equation (23.3.8) for the known velocity field.

23.3.2 Pseudo-compressibility method

The pseudo-compressibility method, which applies to the computation of stationary incompressible flows, consists in replacing the continuity equation (23.3.1) by the following, time-dependent, equation:

$$\frac{1}{\beta^2} \frac{\partial P}{\partial t} + \bar{\nabla} \cdot \bar{v} = 0 \quad (23.3.10)$$

The parameter β has the dimensions of a velocity and represents a pseudo-speed of sound of the transformed system.

The incompressible flow equations take on thereby an hyperbolic character, with pseudo-pressure waves propagating with finite speed. Note that the incompressible limit corresponds to an infinite speed of sound, that is to zero Mach numbers. The pseudo-wave speeds depend on the parameter β , which will play an important role in determining the convergence rate and stability of the method. It will have to be adjusted for optimum convergence to steady state.

The transient behaviour has hereby lost its physical meaning, which is only recovered at steady state, where the divergence-free condition is satisfied.

This method was introduced initially by Chorin (1967) and frequently applied since; see, for instance, Temam (1977), Steger and Kutler (1977), Peyret and Taylor (1983), Chang and Kwak (1984), Choi and Merkle (1985), Rizzi and Eriksson (1985), Kwak *et al.* (1986), Soh (1987) and the mentioned references.

The hyperbolic properties can best be obtained from a one-dimensional analysis of the inviscid part of the equations, following the method of Chapter 3 in Volume 1.

The pseudo-incompressible system becomes, in one dimension,

$$\frac{1}{\beta^2} \frac{\partial P}{\partial t} + \frac{\partial u}{\partial x} = 0 \quad (23.3.11a)$$

$$\frac{\partial u}{\partial t} + \frac{\partial u^2}{\partial x} + \frac{\partial P}{\partial x} = 0 \quad (23.3.11b)$$

Observe that we consider here the conservative form of the momentum equation, since the non-conservative form (23.3.5) is not equivalent to the conservative form (23.3.2) as a consequence of the pseudo-compressibility term in the continuity equation. The equivalence is, of course, restored at steady state and this indicates that the conservative equations should be discretized. Writing the equations in matrix form for the vector $U = (P, u)^T$,

$$\frac{\partial}{\partial t} \begin{vmatrix} P \\ u \end{vmatrix} + \begin{vmatrix} 0 & \beta^2 \\ 1 & 2u \end{vmatrix} \frac{\partial}{\partial x} \begin{vmatrix} P \\ u \end{vmatrix} = 0 \quad (23.3.12a)$$

or in condensed notation

$$\frac{\partial U}{\partial t} + A \frac{\partial U}{\partial x} = 0 \quad (23.3.12b)$$

The eigenvalues λ of A are readily obtained as (see Problem 23.13).

$$\lambda_{\pm} = u \pm \sqrt{u^2 + \beta^2} \quad (23.3.13)$$

showing that they are real and of opposite sign. Consequently, the flow remains subsonic with respect to the pseudo-sonic speed $c = (u^2 + \beta^2)^{1/2}$. Note that this pseudo-sonic speed depends on the flow velocity.

The parameter β has to be chosen large enough, since the flow perturbations are propagated with the pseudo-pressure wave speeds. A useful guideline is indicated by Chang and Kwak (1984), based on the ratio of time scales for propagation of pressure and diffusion of viscosity effects. The pressure waves require a time of the order

$$\Delta t_p \simeq \frac{L}{|u - c|} \quad (23.3.14)$$

to propagate over a distance L , L being the length of the computational domain. On the other hand, it is known that the viscous effects diffuse, during a time span t , over a distance δ proportional to \sqrt{vt} , say $\delta = 2\sqrt{vt}$. Hence the time for viscous effects to diffuse over a distance δ can be written as

$$\Delta t_v \simeq \frac{Re\delta^2}{4u_{ref}L} \quad (23.3.15)$$

where u_{ref} is a reference velocity and the Reynolds number $Re = u_{ref}L/\nu$. It is required for good convergence properties that the viscous regions do not follow too closely the unphysical, transient pseudo-pressure wave variations. Hence, the condition

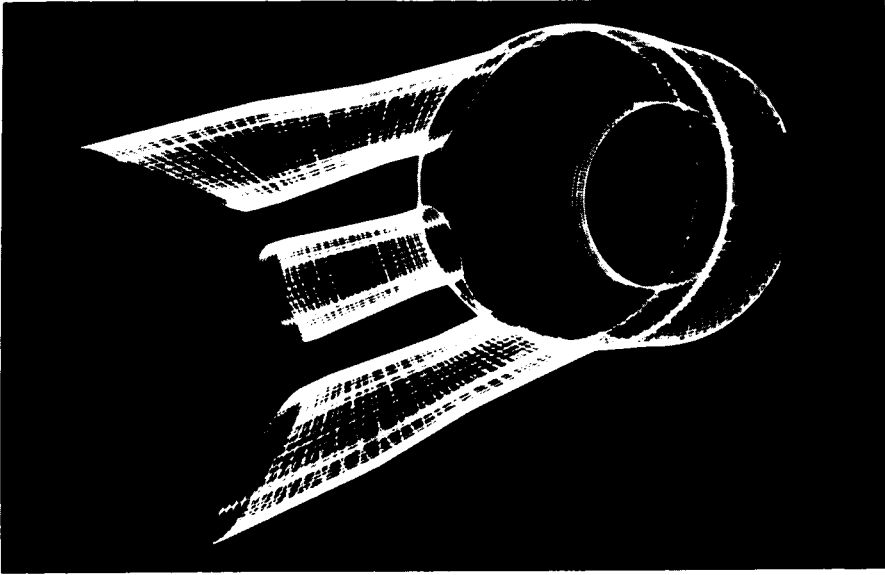
$$\Delta t_p \ll \Delta t_v \quad (23.3.16)$$

leads to

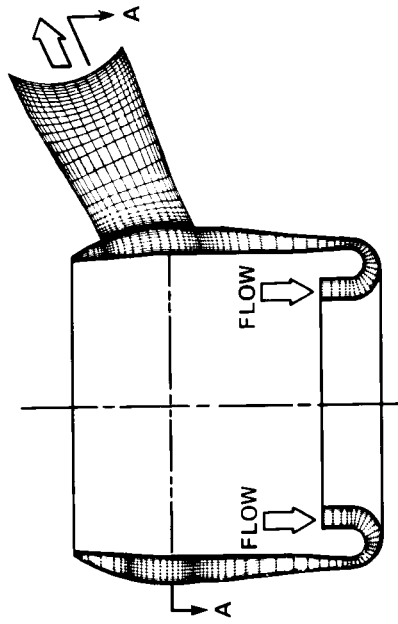
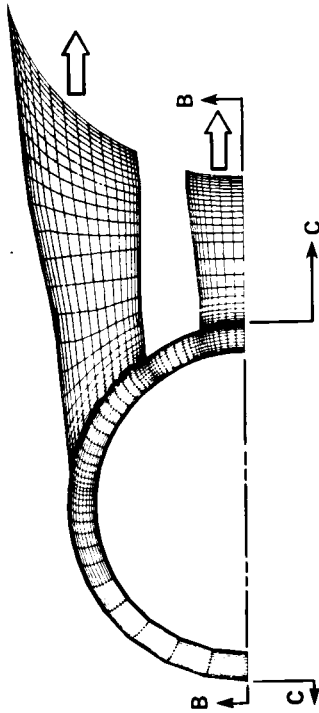
$$\frac{\beta^2}{u_{ref}^2} \gg \left(1 + \frac{L}{\delta} \frac{4}{Re}\right)^2 - 1 \quad (23.3.17)$$

For a duct flow, L might be taken as the length of the duct and δ as the half-width. For a ratio of $L/\delta = 20$ and $Re = 100$, the lower limit on the right-hand side of equation (23.3.17) is 2.24 and is equal to 0.166 for $Re = 1000$. Numerical experiments performed by Chang and Kwak (1984) confirm the extreme sensitivity of the method to the value of β . For the calculation of the return duct, shown in Figure 23.3.2(c), which corresponds to a ratio $L/\delta = 20$ and $Re = 1000$, a value of $\beta^2/u_{ref}^2 = 0.3$ did not allow convergent results to be obtained. Optimal convergence was obtained for $\beta^2/u_{ref}^2 = 5$ to 10, while divergence appeared at values around 100. Similar results were obtained at other values of the Reynolds number and are also confirmed by the calculations of Soh (1987).

For external flow problems, the choice of β is less restrictive and if δ is considered as the boundary layer thickness, $4L/\delta \simeq Re$ and the right-hand side

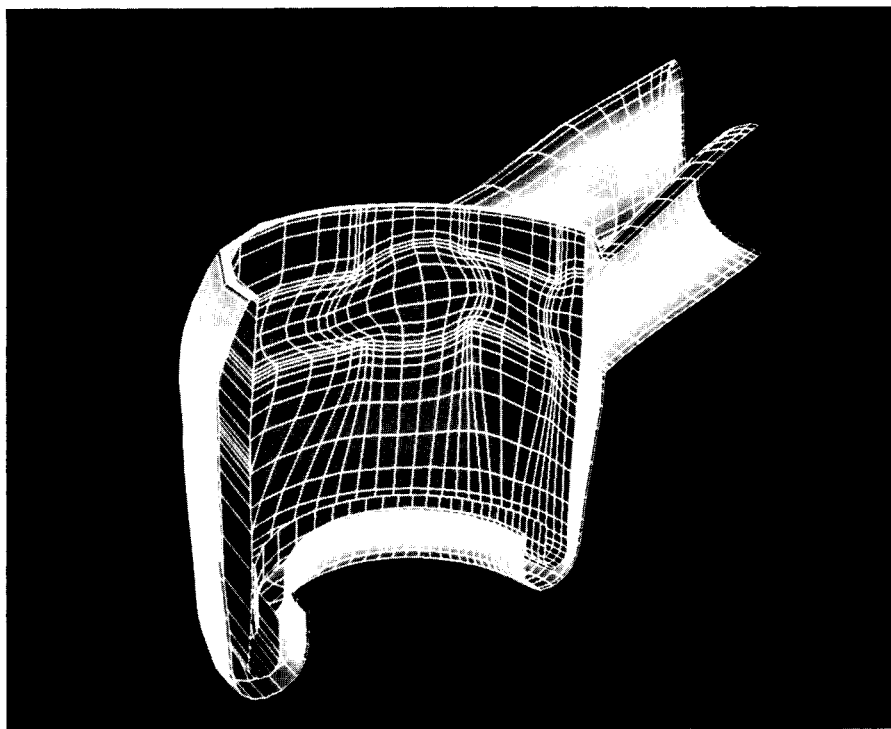


(b) Surface view, showing the turnaround duct and the transfer tubes



(a) Cross - sectional view

Figure 23.3.1 Three-dimensional grid of the hot gas manifold of the NASA Space Shuttle main engine. (From Chang *et al.*, 1985a. Courtesy, D. Kwak, NASA Ames Research Center, USA)



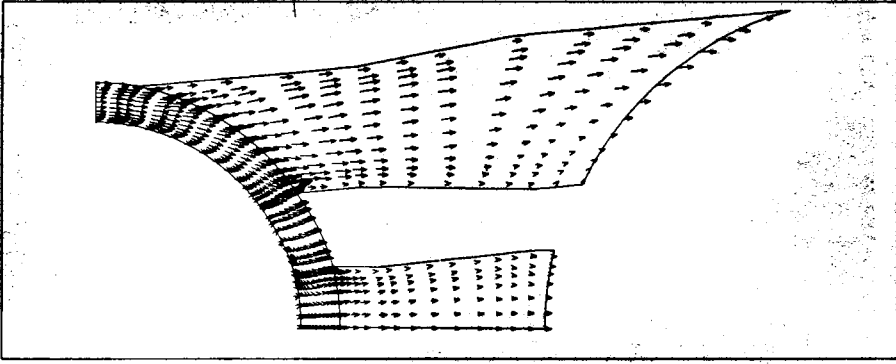
(c) Surface view

Figure 23.3.1 (Continued)

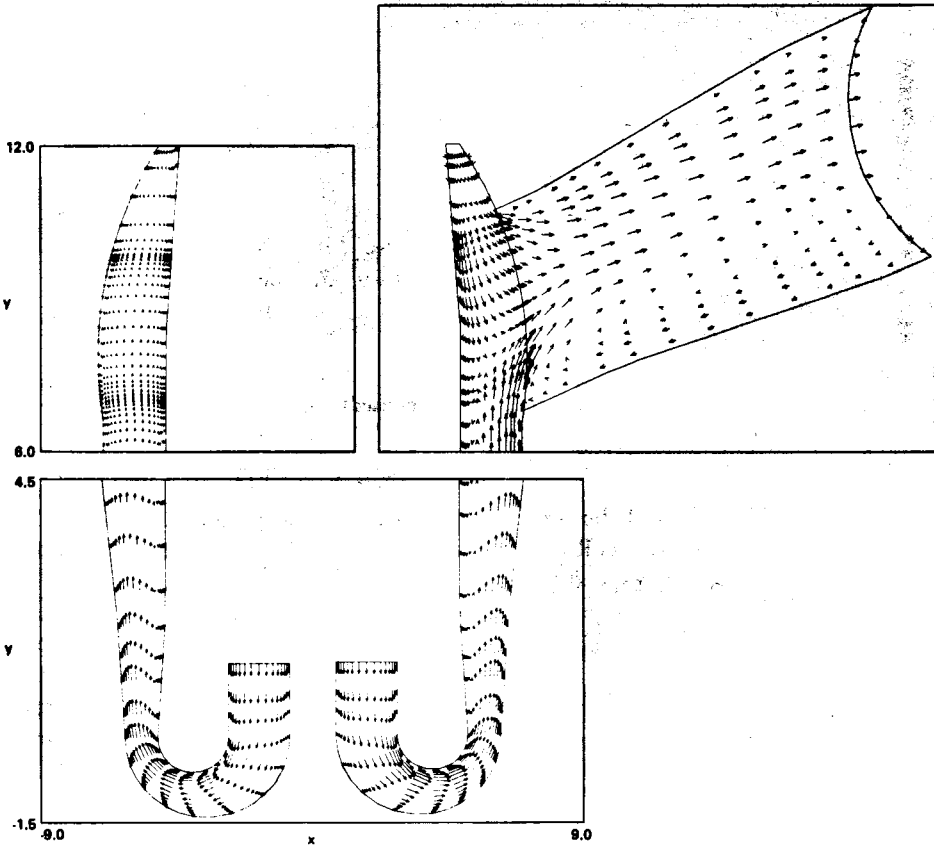
of equation (23.3.17) is of the order of 1. This ratio is also confirmed by Choi and Merkle (1985) as well as Rizzi and Eriksson (1985), based on considerations of uniform pseudo-wave speed propagation.

The upper limit on β is connected to the numerical solution technique. Since the transient has no physical significance, the time integration would best be implicit and the obvious choice is a multi-step method, although Runge–Kutta schemes have also been applied (Rizzi and Eriksson, 1985). Coupled to a central discretization of the convection and diffusion fluxes, the implicit schemes are of the family of the Beam and Warming schemes, discussed in Chapter 18. When applied on a cell-centred finite volume mesh, where pressure and velocity are stored in the cell centres, artificial dissipation terms have to be added to damp the odd–even oscillations, typical of central schemes. This can be done as in Chapter 18, but care has to be taken that the artificial dissipation terms remain of a lower order of magnitude compared to the viscous dissipation. Other space discretizations will be discussed in Section 23.3.4.

The limitation of the error connected to the approximate factorization puts an upper limit on β of the order of the inverse of the time step (Kwak *et al.*, 1986).



(a) Velocity field in horizontal cross-section



(b) Velocity field in vertical cross-sections of transfer tube and turnaround duct

Figure 23.3.2 Computed velocity field at Reynolds number of 1000. (From Chang *et al.*, 1985a. Courtesy D. Kwak, NASA Ames Research Center, USA)

An interesting analysis and extension of the pseudo-compressibility method has been developed by Turkel (1986), where additional artificial time-dependent terms are also added to the momentum equations.

Example 23.3.1 Three-dimensional incompressible flow in a complex duct system

The flow in the turnaround duct and the three transfer tubes of the hot gas manifold (HGM) of the NASA Space Shuttle main engine have been computed by Chang *et al.* (1985a). The numerical method is an implicit Beam and Warming scheme for the pseudo-compressible equations with linear implicit and explicit artificial dissipation.

The geometry of this internal flow system is fully three dimensional, as can be seen from Figure 23.3.1, showing a cross-sectional and surface view of the HGM with the mesh distribution of the boundaries of the flow region.

The results of a laminar computation at a Reynolds number of 1000 are shown in Figure 23.3.2 where the computed flow field is presented in the horizontal (a) and vertical (b) cross-sections. The flow is highly non-uniform and a large separation region appears downstream of the entrance to the transfer tubes. Also a large separation bubble can be seen after the 180° turning of the flow. Figures 23.3.3 and 23.3.4 show the flow in the cross-sections of the transfer tubes, namely near the entrance, at mid-section and near the exit plane. Strong-swirling flows are observed in the entrance sections, which dissipate towards the exit sections.

This is a most complex internal flow and these calculations, which provide information unobtainable from experiments, led to a new design of the system with improved flow conditions. A calculation for turbulent flow conditions has been performed by the same authors on the redesigned geometry (Chang, *et al.*, 1985b).

The pseudo-compressibility method allows discretization of the stationary incompressible equations by applying the schemes developed for compressible flows. Although most of the applications apply central differencing, upwind TVD concepts can be applied (Hartwich and Hsu, 1986, 1987). The main difficulty is connected with the great dependence of the convergence of the method on the parameter β , which has to be optimized empirically. In addition the method applies only to steady-state problems. Since many flow situations are unsteady, in particular all flows with large separation regions appear to be unsteady, methods have to be developed for the computation of three-dimensional unsteady, incompressible flows.

Most of these methods are based on the resolution of the Poisson equation for the pressure in order to satisfy the divergence-free condition for the velocity. They are generally known as pressure correction methods.

23.3.3 Pressure correction methods

The methods falling in this class can be applied to the stationary as well as to the time-dependent incompressible flow equations. They consist of a basic

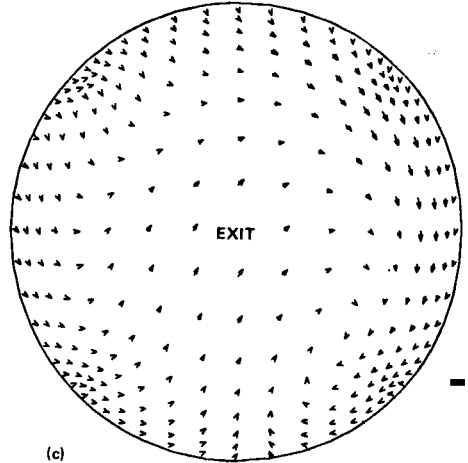
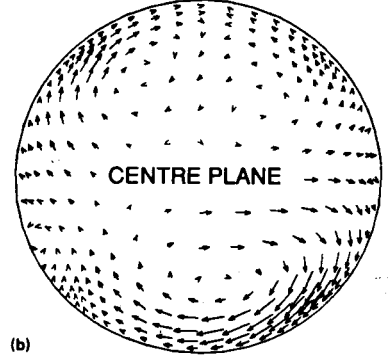
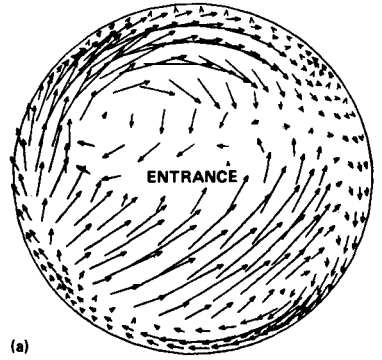
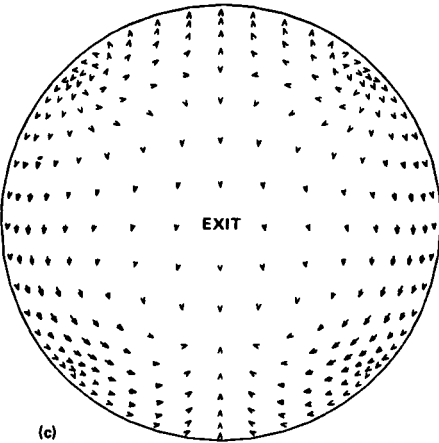
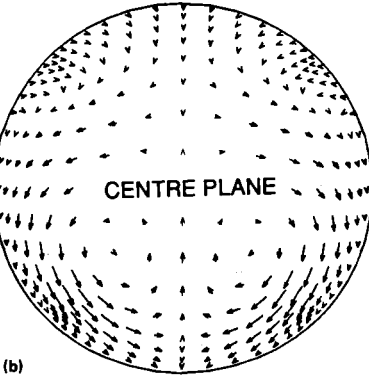
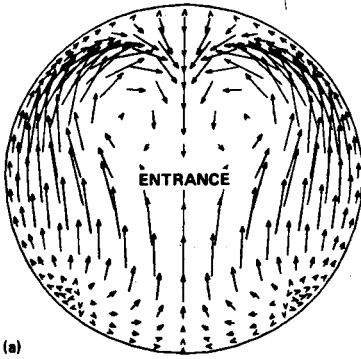


Figure 23.3.3 Velocity field in three cross-sections of the centre duct, $Re = 1000$. (From Chang *et al.*, 1985a. Courtesy D. Kwak, NASA Ames Research Center, USA)

Figure 23.3.4 Velocity field in three cross-sections of the outer duct, $Re = 1000$. (From Chang *et al.*, 1985a. Courtesy D. Kwak, NASA Ames Research Center, USA)

iterative procedure between the velocity and the pressure fields. For an initial approximation of the pressure, the momentum equation can be solved to determine the velocity field. The obtained velocity field does not satisfy the divergence-free continuity equation and has therefore to be corrected. Since this correction has an impact on the pressure field, a related pressure correction is defined, obtained by showing that the corrected velocity satisfies the continuity equation. This leads to a Poisson equation for the pressure correction.

The method was originally applied by Harlow and Welch (1965) in the MAC (Marker-And-Cell) method for the computation of free surface incompressible flows. It is connected to a fractional step method, also called projection method, developed independently by Chorin (1968) and Temam (1969); see also Temam (1977).

The method can be summarized as follows, after selection of a time-integration scheme for the momentum equations, considering the pressure gradient as known. For reasons of simplicity and in order to point out the essential properties of the pressure correction approach, we will select an explicit method of first-order accuracy in time, although it is not recommended in practice. Even for time-dependent problems, the time step restriction imposed by the stability conditions for the parabolic, convection-diffusion, momentum equations is generally much smaller than the physical time constant of the flow. Hence, the time steps allowed by the requirements of physical accuracy are large enough to allow the larger numerical time steps of implicit schemes.

Hence, we consider for the time being the explicit discretization

$$\frac{\bar{v}^* - \bar{v}^n}{\Delta t} = -\bar{\nabla} \cdot (\bar{v} \otimes \bar{v})^n - \bar{\nabla} P^* + \nu \Delta \bar{v}^n \quad (23.3.18)$$

where P^* is the assumed pressure field and \bar{v}^* the intermediate velocity field, obtained from the solution of (23.3.18) and which does not satisfy the continuity equation. Hence the final values are defined by adding corrections to the intermediate values

$$\bar{v}^{n+1} = \bar{v}^* + \bar{v}' \quad P^{n+1} = P^* + P' \quad (23.3.19)$$

where the final values with superscript $n+1$ have to be solutions of the scheme

$$\frac{\bar{v}^{n+1} - \bar{v}^n}{\Delta t} = -\bar{\nabla} \cdot (\bar{v} \otimes \bar{v})^n - \bar{\nabla} P^{n+1} + \nu \Delta \bar{v}^n \quad (23.3.20a)$$

$$\bar{\nabla} \cdot \bar{v}^{n+1} = 0 \quad (23.3.20b)$$

Introducing (23.3.19) in the above equation and subtracting (23.3.18) leads to the following relation between the pressure and velocity corrections:

$$\bar{v}' = -\Delta t \bar{\nabla} P' \quad (23.3.21)$$

Note that expressing the velocity correction as a gradient of a scalar function conserves the vorticity of the intermediate velocity field; that is the correction field is a potential flow.

Taking the divergence of (23.3.20a) gives the Poisson equation for the pressure

$$\Delta P' = \frac{1}{\Delta t} \bar{\nabla} \cdot \bar{v}^* \quad (23.3.22)$$

which is equivalent to

$$\Delta P^{n+1} = \frac{D^n}{\Delta t} + \nu \Delta D^n - D^{n2} - (\bar{v}^n \cdot \bar{\nabla}) D^n - \bar{\nabla} \cdot (\bar{v}^n \cdot \bar{\nabla}) \bar{v}^n \quad (23.3.23)$$

where

$$D^n \equiv \bar{\nabla} \cdot \bar{v}^n \quad (23.3.24)$$

Equation (23.3.9) contains only the last term of the right-hand side of equation (23.3.23), since this equation was obtained by assuming divergence-free velocity. In the numerical process, the velocity at level n might not satisfy exactly the divergence-free condition. In this case, the above equation is more accurate and gives better convergence properties. This situation is more likely to occur in stationary computations where n represents an iteration count. With time-dependent calculations, it is recommended that mass conservation at each time step be satisfied accurately, in particular by discretizing the integral form of the mass conservation law on a finite volume mesh.

The Poisson equation for the pressure is solved with Neumann boundary conditions on the normal pressure gradient, obtained by taking the normal component of equations (23.3.20a) or (23.3.21). The details of the implementation depend on the selected space discretization and on the mesh.

An additional condition is essential for the numerical accuracy of the resolution of the pressure equation, namely that the compatibility condition, obtained from Green's theorem applied to the Poisson equation, should be identically satisfied by the space discretization. Applied to equation (23.3.22), for instance, we should have identically, for the integral of the normal pressure gradient on the boundary Γ of the computational domain Ω ,

$$\oint_{\Gamma} \frac{\partial P'}{\partial n} d\Gamma = \int_{\Omega} \frac{\bar{\nabla} \cdot \bar{v}'}{\Delta t} d\Omega = \frac{1}{\Delta t} \oint_{\Gamma} \bar{v}' \cdot d\bar{S} \quad (23.3.25)$$

A similar relation is to be satisfied for P^{n+1} if equation (23.3.23) is solved instead.

It might be of interest to observe at this point that a simple way to satisfy numerically the compatibility relation (23.3.25) is to write the pressure equation in conservation form, as

$$\bar{\nabla} \cdot \left(\bar{\nabla} P' - \frac{1}{\Delta t} \bar{v}^* \right) = 0 \quad (23.3.26)$$

and apply the various discretization methods discussed in Chapter 14.

The fractional step, or projection method, is based on a slightly different definition of the intermediate step (23.3.18), whereby the pressure term is

removed, leading to

$$\frac{\bar{v}^* - \bar{v}^n}{\Delta t} = -\bar{\nabla} \cdot (\bar{v} \times \bar{v})^n + \nu \Delta \bar{v}^n \quad (23.3.27)$$

Equations (23.3.20) remain unchanged and by subtracting we obtain

$$\frac{\bar{v}^{n+1} - \bar{v}^*}{\Delta t} = -\bar{\nabla} P^{n+1} \quad (23.3.28)$$

Taking the divergence leads to the pressure equation

$$\Delta P^{n+1} = \frac{1}{\Delta t} \bar{\nabla} \cdot \bar{v}^* \quad (23.3.29)$$

instead of (23.3.22).

Most of the applications are based on implicit time discretizations of the momentum equations, applying the multi-step methods discussed in Chapter 18, followed by an ADI approximate factorization. Applying the same linearization procedures, which are strongly simplified here due to the incompressibility and the linearity of the viscous terms in isothermal flows, equation (23.3.18) could be replaced by a backward Euler method, which is first order in time and unconditionally stable:

$$\frac{\bar{v}^* - \bar{v}^n}{\Delta t} = -\bar{\nabla} \cdot (\bar{v}^n \otimes \bar{v}^*) - \bar{\nabla} P^* + \nu \Delta \bar{v}^* \quad (23.3.30a)$$

followed by

$$\frac{\bar{v}^{n+1} - \bar{v}^n}{\Delta t} = -\bar{\nabla} \cdot (\bar{v}^n \otimes \bar{v}^{n+1}) - \bar{\nabla} P^{n+1} + \nu \Delta \bar{v}^{n+1} \quad (23.3.30b)$$

Subtracting for the corrections (23.3.19) leads to the correction equation

$$\frac{\bar{v}'}{\Delta t} = -\bar{\nabla} \cdot (\bar{v}^n \otimes \bar{v}') - \bar{\nabla} P' + \nu \Delta \bar{v}' \quad (23.3.31)$$

Since this equation defines the corrections, it can be simplified by dropping the viscous and convection terms, leading to equation (23.3.21).

Here again the fractional step method consists in removing the pressure term from equation (23.3.30a).

The numerical resolution of the Poisson equation for the pressure is a crucial step of the whole approach, since the overall efficiency of the code will depend on its performance. Hence all possible convergence optimization and acceleration techniques should be applied. In particular preconditioning and multi-grid techniques are strongly recommended for this step of the computation, and eventually for other steps.

In connection with stationary formulations, the pressure correction methods have been developed by Patankar and Spalding (1972) and Patankar (1980) and largely applied in practice; see, for instance, Raithby and Schneider (1979), Ghia

et al. (1981), Cebeci *et al.* (1981), Peyret and Taylor (1983), Van Doormaal and Raithby (1984), Freitas *et al.* (1985), Chan *et al.* (1987) and cited references.

Finally, it should be mentioned that the pressure correction methods can also be applied to the parabolized Navier–Stokes equations. Referring to Section 2.4 in Volume 1, when the mainstream direction is the x coordinate the stationary equations can be solved by an explicit marching procedure in the x direction and an implicit ADI or other relaxation technique in the cross-planes. The parabolic properties of the approximation ensures that a single sweep of the mesh in the x direction is sufficient; see, for, instance Ghia and Sokhey (1977) and Pouagare and Lakshminarayana (1986), where the latter solves directly for the primitive variables, without a Poisson equation for the pressure. Other approaches to the parabolized Navier–Stokes equations have been developed by S. Rubin and coworkers; see, for instance, Rubin and Reddy (1983a, 1983b) Reddy and Rubin (1988) and cited references.

For the full Navier–Stokes equations, the pressure equation is solved by additional iterative steps over the x direction; the approach is sometimes referred to as fully elliptic.

23.3.4 Selection of the space discretization

The choice of a space discretization is, as for compressible flows, between centred or upwind methods, at least for the convection terms, since the diffusive contributions are always centrally discretized.

Central schemes

The central discretization for the convection terms suffers from the well-known odd–even decoupling and requires the addition of some higher-order artificial dissipation terms to create the required damping of high-frequency errors. Examples of artificial dissipation terms have been discussed in Chapter 18 and can be applied as well to incompressible flows. In particular the linear fourth-order dissipation should be appropriate.

However, the absence of the time derivative of the density in the continuity equation creates an additional uncoupling in the centrally discretized equations, when applied with classical cell-centred finite volume, or finite difference, meshes. This is best illustrated on a one-dimensional example (Bernard and Thompson, 1984).

A simplified, one-dimensional analogue of the pressure correction method can be written as follows, neglecting the viscous and non-linear convection terms, for the momentum equation:

$$\frac{\partial u}{\partial t} = - \frac{\partial P}{\partial x} \quad (23.3.32a)$$

and for the continuity equation:

$$\frac{\partial u}{\partial x} = 0 \quad (23.3.32b)$$

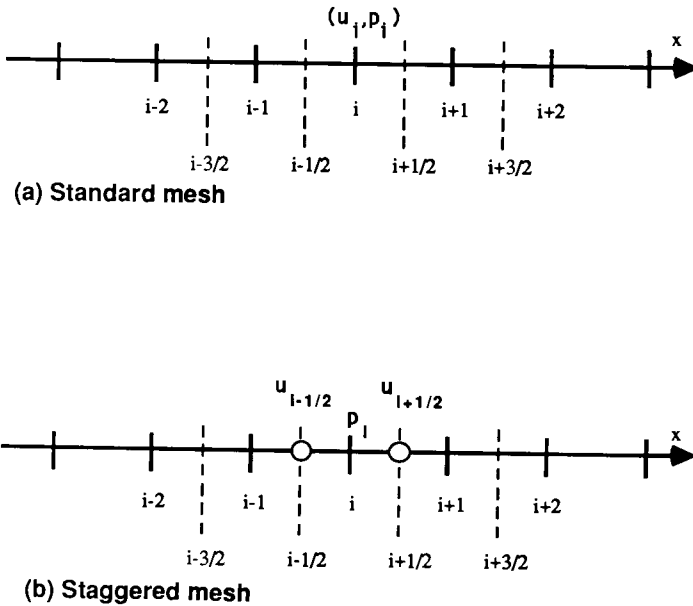


Figure 23.3.5 One-dimensional finite difference meshes

With an explicit time-integration and central space discretization on the standard mesh of Figure 23.3.5, equations (23.3.20) and (23.3.23) reduce to

$$u_i^{n+1} = u_i^n - \frac{\Delta t}{2\Delta x} (P_{i+1}^{n+1} - P_{i-1}^{n+1}) \quad (23.3.33a)$$

Taking the x derivative of this equation and showing that the velocity at level $n+1$ satisfies the continuity equation gives the Poisson equation for the pressure in a one-dimensional form, $\partial^2 P / \partial x^2 = \Delta t (\partial u / \partial x)^n$:

$$P_{i+1}^{n+1} - 2P_i^{n+1} + P_{i-1}^{n+1} = \frac{\Delta x}{2\Delta t} (u_{i+1}^n - u_{i-1}^n) \quad (23.3.33b)$$

As can be seen, the pressure at point i is not influenced by the velocity u_i^n and in return u_i^{n+1} is not affected by P_i^{n+1} . Hence velocity and pressure are decoupled on even and odd points (see also Chapter 4 in Volume 1 for an illustration of analogue cases).

This decoupling is not present with compressible flows due to the density-velocity coupling in the continuity equation. It will generate additional high-frequency oscillations, requesting the introduction of artificial dissipation terms.

A cure to this undesirable situation has been introduced by Harlow and Welch (1965), under the form of a *staggered mesh*, where the velocity and pressure are not defined in the same mesh points. As seen in Figure 23.3.5(b), the velocity

is defined at the half mesh points or at the cell faces in a finite volume interpretation. The central discretization (23.3.33) now becomes

$$u_{i+1/2}^{n+1} = u_{i+1/2}^n - \frac{\Delta t}{\Delta x} (P_{i+1}^{n+1} - P_i^{n+1}) \quad (23.3.34a)$$

$$P_{i+1}^{n+1} - 2P_i^{n+1} + P_{i-1}^{n+1} = \frac{\Delta x}{\Delta t} (u_{i+1/2}^n - u_{i-1/2}^n) \quad (23.3.34b)$$

and points i (pressure) and $(i + \frac{1}{2})$ (velocity) are coupled in both equations.

Staggered meshes are currently applied with central discretizations and the most popular two-dimensional arrangement is shown in Figure 23.3.6, where the u and v velocity components are located on different cell faces.

The equations are discretized in *conservation form*, the control volumes depending on the considered equation. Mass conservation is discretized on the volume centred on point (i, j) , while x -momentum conservation is expressed for the volume centred on the location of u , that is $(i + \frac{1}{2}, j)$. Similarly, y -momentum conservation is expressed for the volume centred on the location of v , that is $(i, j + \frac{1}{2})$. This is left as an exercise for the reader (see Problem 23.18).

The Poisson equation for the pressure is obtained from the divergence of the

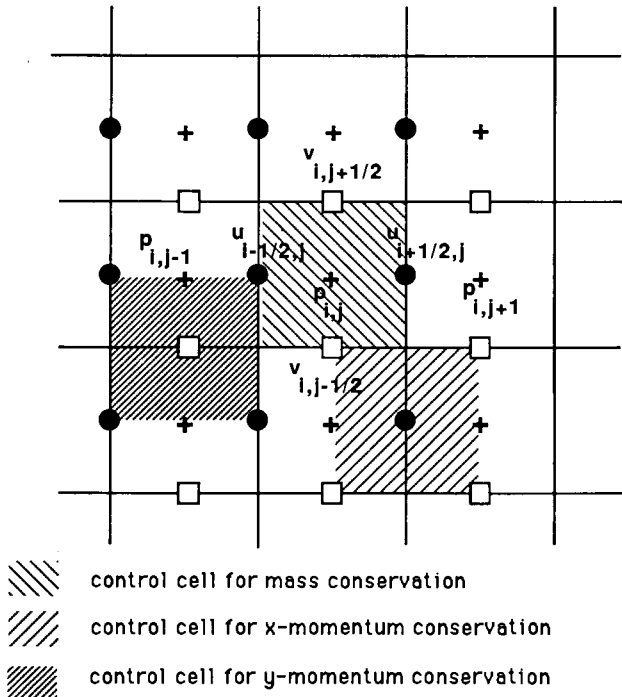


Figure 23.3.6 Staggered, two-dimensional finite difference mesh for centrally discretized pressure correction methods

discretized momentum equation. *Hence, this step should be performed by exactly the same discrete operations as applied to express mass conservation.* This is required for global consistency and conservation. It is fairly straightforward on a Cartesian mesh, but becomes essential on arbitrary meshes. Actually, this requirement will be automatically fulfilled if the pressure equation is considered under the divergence form (23.3.26) and discretized exactly like the condition of zero divergence for the velocity.

As with current cell-centred finite volumes, the boundaries of the computational domain are located on cell faces.

Upwind schemes

The alternative to the central discretization is to apply upwind differences on the convection terms as a function of the sign of the velocity components. This approach is also widely applied in practice, and particular attention has been given to the multi-dimensional aspects of the upwind extrapolation (see Section 20.7). An interesting approach has also been presented by Dick (1988) for the solution of the steady incompressible Navier–Stokes equations, applying a flux vector splitting to the convective terms.

It is clear, however, that first-order upwind discretizations produce excessive numerical dissipation and should not be applied. Second-order upwind difference formulas, following the developments of Chapter 21, should be applied instead and for flow situations with severe gradients, non-linear limiters can be introduced in order to avoid non-monotone behaviour of the computed solutions.

Many contributions have been developed in this direction, particularly for stationary incompressible flow models, independently of the progress in the field of high-speed compressible flows, described in Chapter 21.

The main conclusion of these investigations towards the definition of accurate space discretizations for complex recirculating flows is the confirmation of the superiority of the second-order upwind schemes over their first-order counterpart (Han *et al.*, 1981; Shyy, 1985; Shyy and Correa, 1985; Syed *et al.*, 1985; Castro and Jones, 1987). Applications of non-linear limiters to this family of steady incompressible flows have also been reformulated recently by Gaskell and Lau (1987) and Leonard (1987).

The reader is referred to the cited literature and to some recent applications, for instance Tamura *et al.* (1988), Rosenfeld *et al.* (1988) and Freitas and Street (1988).

Finite element discretizations

Many computations of incompressible Navier–Stokes flows have been developed with finite element discretizations, and an extensive literature exists on the subject to which we refer the reader for detailed information. Several books are available: Chung (1978), Girault and Raviart (1981), Taylor and Hughes

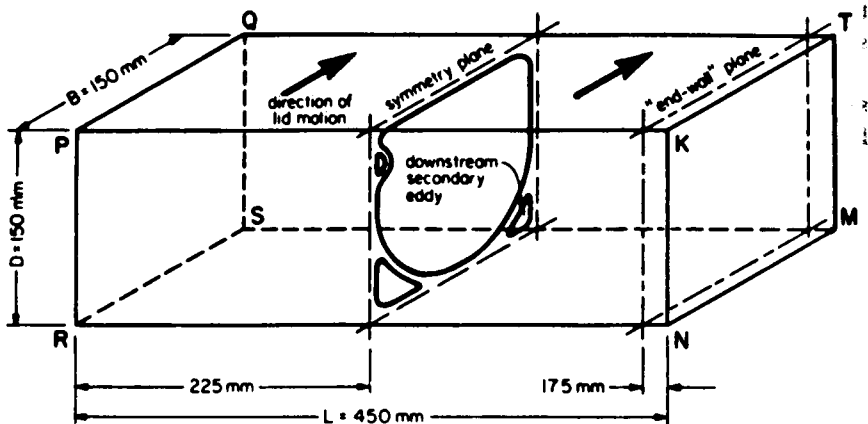
(1981), Thomasset (1981), Baker (1983), Glowinski (1983) and Pironneau (1988). Additional references and basic contributions can be found in Bristeau *et al.* (1980), Hughes *et al.* (1979), Brooks and Hughes (1982) and Gresho *et al.* (1984).

Example 23.3.2 Three-dimensional recirculation flow

The shear-driven cavity flow for a constant density incompressible fluid has been investigated in great detail by Freitas *et al.* (1985) and Freitas and Street (1988) for a three-dimensional cavity at a Reynolds number of 3200. This flow, triggered by an upper wall moving at constant speed, has an extremely complex physical structure. It is highly unsteady, although the boundary conditions are stationary, and possesses significant secondary motion in the spanwise direction and a complex three-dimensional pattern. The geometrical configuration is shown in Figure 23.3.7.

At the start of the upper wall motion, a primary recirculating flow exists due to the shear motion, generating a pressure-driven secondary flow in planes parallel to the end walls. The secondary flow establishes a spanwise cellular pattern. Finally Taylor-Görtler (TG) vortices develop from the interaction between the primary flow and the viscous end wall regions, modifying the primary and secondary flow configurations.

The calculations have been performed on a $32 \times 32 \times 45$ mesh for the half-cavity with a pressure correction method and an upwind discretization of



BOUNDARY DEFINITIONS

END-WALL : PQSR	SIDE-WALL UPSTREAM : PKNR
: KTMN	DOWNSTREAM : QTMS
LID : PQTK	LOWER HORIZ. : SMNR

Geometric and general flow definitions

Figure 23.3.7 Geometric and general flow definitions. (From Freitas and Street, 1988)

the convection terms, a time-accurate mode covering the first 25 minutes after onset of the flow.

The primary recirculating flow at several spanwise locations is represented in Figure 23.3.8 through particle track diagrams and velocity field.

The most spectacular features of this calculation are the capturing of the Taylor–Görtler instability, which is shown in Figure 23.3.9 for a time span of 180s starting at $t = 20$ minutes. It is seen that the pairs of TG vortices, which are not symmetric, vary strongly in size and in space–time locations.

The spectral density distribution of this unsteady flow pattern shows a $-5/3$ power dependence with frequency, typical of three-dimensional turbulent flows in equilibrium, in the region of the flow not directly influenced by the TG vortices. On the other hand, it has a -3 power dependence with frequency in the TG dominated regions, which is typical of two-dimensional turbulence and

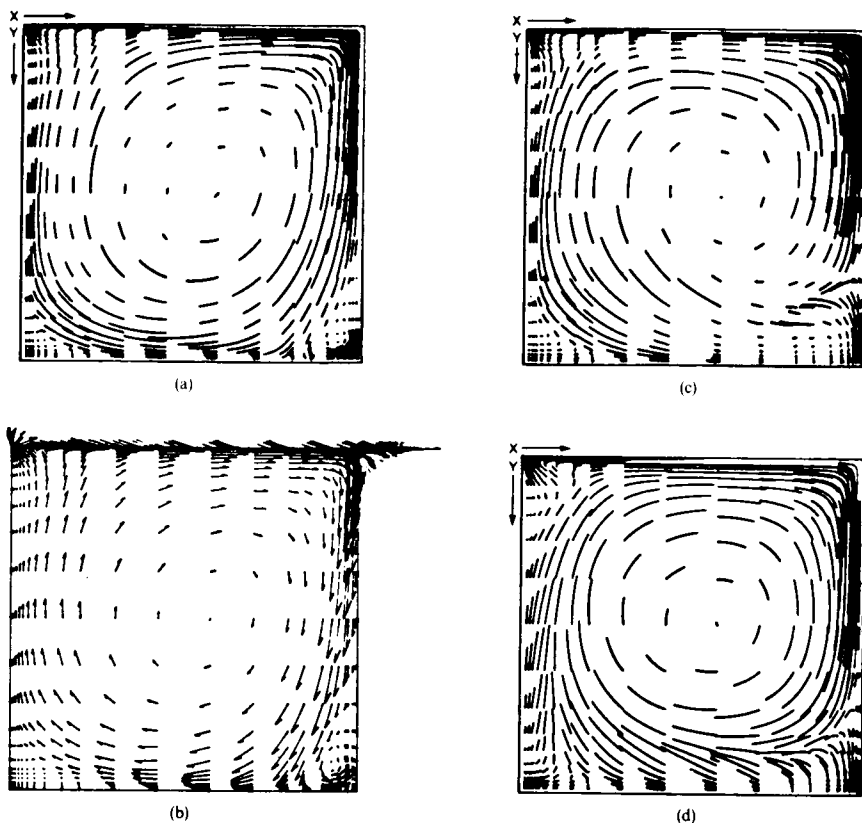


Figure 23.3.8 Four seconds particle track and vector fields at selected spanwise locations. Velocity field at time = 20 min. (a) Particle track field on a plane 40 mm from end wall. (b) Vector field on a plane 40 mm from end wall. (c) Particle track field on a plane 10 mm from end wall. (d) Particle track field on symmetry plane. (From Freitas and Street, 1988)

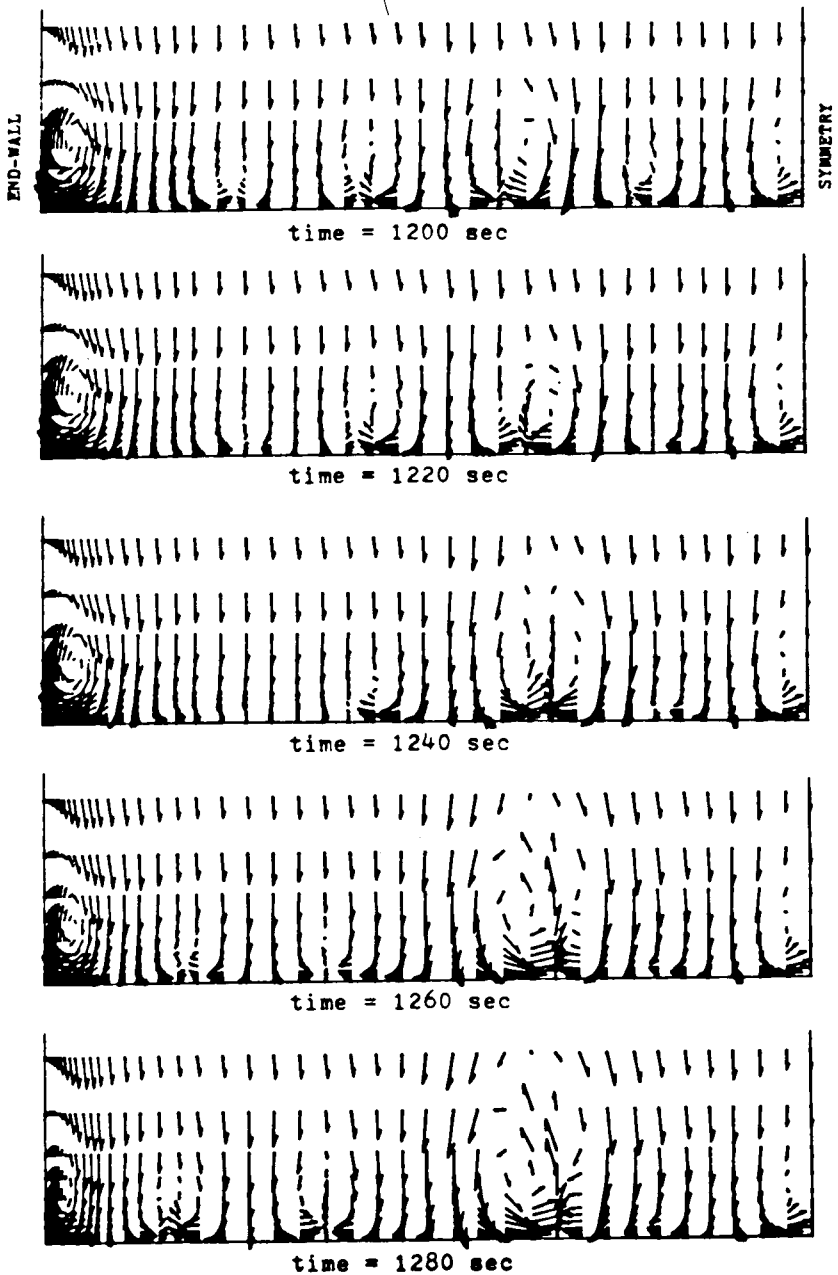
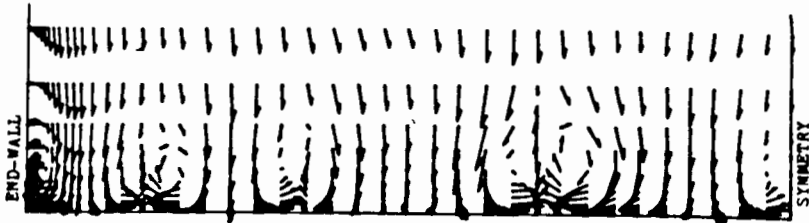
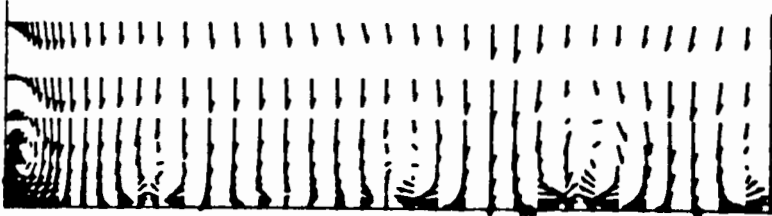


Figure 23.3.9 Temporal variation of TG vortices on a plane 35 mm from downstream wall, after $t = 20$ minutes. (From Freitas and Street, 1988)



time = 1300 sec



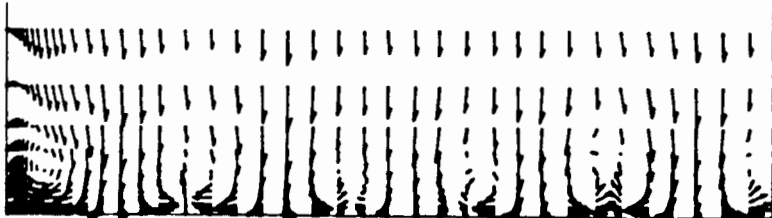
time = 1320 sec



time = 1340 sec



time = 1360 sec



time = 1380 sec

Figure 23.3.9 (Continued)

organized, non-equilibrium, states. This remarkable simulation is at the onset of direct turbulence modelling since this highly unsteady flow possesses limited regions of turbulence.

23.4 CONCLUSIONS TO PART VII

The applications of numerical simulations of the full Reynolds-averaged Navier-Stokes equations are developing rapidly for basic and industrial applications. The methods for high-speed compressible viscous flows do rely mostly on the schemes developed for the Euler equations with the addition of centrally discretized diffusion terms. This last step does not pose any problem and the basis for this field of application can now be considered as well established.

For incompressible flows, on the other hand, particular resolution techniques are developed, a distinction being made between stationary and unsteady formulations.

The considerable development of computer hardware enables Navier-Stokes solutions to be obtained in short computer times on available supercomputers, at least for two-dimensional and simple three-dimensional configurations. This consideration has led us to the subjective decision not to discuss in detail the approximate Navier-Stokes models, such as the thin shear layer or parabolized Navier-Stokes models, although, as shown by several examples in Chapter 2 in Volume 1, many situations are found where they present a valid approximation.

Many difficulties still remain for the numerical simulation of Reynolds-averaged Navier-Stokes flows, most of them being more of a physical nature than of numerical origin.

The first problem we wish to mention at this point is connected with the experimental observation that most of the external viscous flows with large separated regions become unsteady. The classical example is the periodic vortex street created in the wake of a cylinder under uniform and constant incident flow conditions, as a consequence of the fact that all free shear layers are basically unstable. With more complex configurations and varying incidence angles it is not known *a priori* from which value the flow will become locally unsteady. Hence, reliable Navier-Stokes codes should be able to detect the onset of unsteadiness of the physical flows and eventually simulate the larger scale (as opposed to turbulence scale) unsteadiness.

This problem appears also, but perhaps to a lesser extent, with internal flow configurations, where the geometrical confinement can restrict the extent of viscous separated regions and limit their unsteadiness, although it might not be able to suppress it locally.

This brings us to another major problem, namely the turbulence modelling within the Reynolds-averaged Navier-Stokes approximation. This is most likely to be a major concern for the validation of Navier-Stokes codes and requires considerable research effort for the understanding and modellization of

turbulence phenomena, including the predictions of transition. Recent validations have shown that the accurate prediction of the shape and extent of the three-dimensional separated region on a wing could not be improved by mesh refinement, up to 1.1×10^6 mesh points, unless the turbulence model were to be adapted to take into account non-equilibrium effects. The predictions were then strongly improved without the necessity to call for such dense meshes (Kaynak and Flores, 1987).

Hence, with the numerical procedures reaching a mature and well-established status, with experience accumulating on the relative effects of numerics and physics, the application of numerical simulations of viscous flows is reaching the goal set up at the origin: to predict accurately complex flow situations occurring in nature and in technology, including multi-phase, multi-component, chemical reacting systems.

With the available reliability and knowledge of the numerics we are now able to apply widely the numerical simulation tools towards the final objective of understanding, and eventually controlling, the physical phenomena at the basis of natural and industrial flow processes.

References

- Baker, A. J. (1983). *Finite Element Computational Fluid Mechanics*, New York: Hemisphere Publishing Co., McGraw-Hill Co.
- Beam, R. M., and Warming, R. F. (1978). 'An implicit factored scheme for the compressible Navier-Stokes equations.' *AIAA Journal*, **16**, 393-402.
- Bernard, R. S., and Thompson, J. F. (1984). 'Mass conservation on regular grids for incompressible flow.' *AIAA Paper 84-1669*, AIAA 17th Fluid Dynamics, Plasmadynamics and Lasers Conference.
- Briley, W. R., and McDonald, H. (1975). 'Solution of the three-dimensional Navier-Stokes equations by an implicit technique.' *Proc. Fourth International Conference on Numerical Methods in Fluid Dynamics, Lectures Notes in Physics*, Vol. 35, Berlin: Springer.
- Bristeau, M. D., Glowinski, R., Mantel, B., Periaux, J., Perrier, P., and Pironneau, O. (1980). 'A finite element approximation of Navier-Stokes equations for viscous incompressible fluids. Iterative methods of solution. In *Approximation Methods for Navier-Stokes Problems, Lecture Notes in Mathematics*, Vol. 771, pp. 78-123, New York: Springer Verlag.
- Brooks, A. N., and Hughes, T. J. R. (1982). 'Streamline upwind/Petrov-Galerkin formulations for convection dominated flows with particular emphasis on the incompressible Navier-Stokes equations.' *Computer Methods in Applied Mechanics and Engineering*, **32**, 199-259.
- Castro, I. P., and Jones, J. M. (1987). 'Studies in numerical computations of recirculating flows.' *Int. Journal Numerical Methods Fluids*, **7**, 793-823.
- Caughy, D. A., and Turkel, E. (1988). 'Effects of numerical dissipation on finite volume solutions of compressible flow problems.' *AIAA Paper 88-0621*, AIAA 26th Aerospace Sciences Meeting.
- Cebeci, T., Hirsh, R. S., Keller, H. B., and Williams, P. G. (1981). 'Studies of numerical methods for the plane Navier-Stokes equations.' *Computer Methods in Applied Mechanics and Engineering*, **27**, 13-44.
- Chakravarthy, S. R., Szema, K.-Y., Goldberg, U. C., Gorski, J. J., and Osher, S. (1985).

- 'Application of a new class of high accuracy TVD schemes to the Navier–Stokes equations.' *AIAA Paper 85-0165*, AIAA 23rd Aerospace Science Meeting.
- Chan, D. C., Sindir, M. M., Gosman, A. D. (1987). 'Numerical flow simulation of passages with strong curvature and rotation using a three-dimensional Navier–Stokes solver.' *AIAA Paper 87-1354*, AIAA 19th Fluid Dynamics, Plasmadynamics and Lasers Conference.
- Chang, J. L., and Kwak, D. (1984). 'On the method of pseudo compressibility for numerically solving incompressible flows.' *AIAA Paper 84-0252*, AIAA 22nd Aerospace Sciences Meeting.
- Chang, J. L., Kwak, D., Dao, S. C., and Rosen, R. (1985a). 'A three-dimensional incompressible flow simulation method and its application to the space Shuttle main engine—Part I—Laminar flow.' *AIAA Paper 85-0175*, AIAA 23rd Aerospace Sciences Meeting.
- Chang, J. L., Kwak, D., Dao, S. C., and Rosen, R. (1985b). 'A three-dimensional incompressible flow simulation method and its application to the Space Shuttle main engine—Part II—Turbulent flow.' *AIAA Paper 85-1670*, AIAA 18th Fluid Dynamics, Plasmadynamics and Lasers Conference.
- Chima, R. V. (1985). 'Analysis of inviscid and viscous flows in cascades with an explicit multiple grid algorithm.' *AIAA Journal*, **23**, 1556–63.
- Chima, R. V., and Johnson, G. M. (1985). 'Efficient solution of the Euler and Navier–Stokes equations with a vectorized multiple-grid algorithm.' *AIAA Journal*, **23**, 23–32.
- Chima, R. V., Turkel, E., and Schaffer, S. (1987). 'Comparison of three multigrid methods for the Euler and Navier–Stokes equations.' *Report NASA TM 88878*, NASA Lewis Research Center.
- Choi, D., and Merkle C. L. (1985). 'Application of time iterative schemes to incompressible flow.' *AIAA Journal*, **23**, 1518–24.
- Chorin, A. J. (1967). 'A numerical method for solving incompressible viscous flow problems.' *Journal Computational Physics*, **2**, 12–26.
- Chorin, A. J. (1968). 'Numerical solution of the Navier–Stokes equations.' *Mathematics of Computation*, **23**, 341–54.
- Chung, T. J. (1978). *Finite Element Analysis in Fluid Dynamics*, New York: McGraw Hill.
- Davis, R. L., Ni, R. H., and Bowley, W. W. (1984). 'Prediction of compressible laminar viscous flows using a time-marching control volume and multiple-grid technique.' *AIAA Journal*, **22**, 1573–81.
- Dawes, W. N. (1986). 'A pre-processed implicit algorithm for 3D viscous compressible flows.' In D. Rues and W. Kordulla (eds), *Proc. 6th GAMM Conference on Numerical Methods in Fluid Dynamics, Notes on Numerical Fluid Mechanics*, Vol. 13, pp. 70–77, Braunschweig: Vieweg.
- Dick, E. (1988) 'A flux vector splitting method for steady Navier–Stokes equations.' *Int. Journal Numerical Methods Fluids*, **8**, 317–26.
- Freitas, C. J., and Street, R. L. (1988). 'Non-linear transient phenomena in a complex recirculating flow: a numerical investigation.' *Int. Journal. Numerical Methods Fluids*, **8**, 769–802.
- Freitas, C. J., Street, R. L., Findikakis, A. N., and Koseff J. R. (1985). 'Numerical simulation of three-dimensional flow in a cavity.' *Int. Journal Numerical Methods Fluids*, **5**, 561–75.
- Gaskell, P. H., and Lau, A. K. C. (1987). 'Curvature compensated convective transport: SMART, a new boundedness preserving transport algorithm.' *Int. Journal Numerical Methods Fluids*, **8**, 617–41.
- Ghia, U., and Sokhey, J. S. (1977). 'Laminar incompressible viscous flow in curved ducts of rectangular cross sections.' *Trans. ASME, Journal of Fluids Engineering*, **99**, 640–8.
- Ghia, U., Ghia, K., Rubin, S., and Khosla, P. K. (1981). 'Study of incompressible flow separation using primitive variables.' *Computer and Fluids*, **9**, 123–42.

- Girault, V., and Raviart, P. A. (1981). *Finite Element Approximation of the Navier–Stokes Equations, Lecture Notes in Mathematics*, Vol. 749, New York: Springer Verlag.
- Glowinski, R. (1983). *Numerical Methods for Non-Linear Variational Problems*. 2nd edn, New York: Springer Verlag.
- Gresho, P. M., Chan, S. T., Lee, R. L., and Upson, C. D. (1984). 'A modified finite element method for solving the time-dependent incompressible Navier–Stokes equations. Part 1: Theory; Part II: Applications.' *Int. Journal Numerical Methods Fluids*, **4**, 557–98; 619–40.
- Han, T., Humphrey, J. A. C., and Launder, B. E. (1981). 'A comparison of hybrid and quadratic-upstream differencing in high Reynolds number elliptic flows.' *Computer Methods in Applied Mechanics and Engineering*, **29**, 81–95.
- Hänel, D., Schwane, R., and Seider, G. (1987). 'On the accuracy of upwind schemes for the solution of the Navier–Stokes equations.' *AIAA Paper 87-1105, Proc. AIAA 8th Computational Fluid Dynamics Conference*, pp. 42–6.
- Harlow, F. H., and Welch, J. E. (1965). 'Numerical calculation of time-dependent viscous incompressible flow of fluid with free surface.' *Physics of Fluids*, **8**, 2182–9.
- Hartwich, P. M., and Hsu, C. H. (1986). 'An implicit flux difference splitting scheme for three-dimensional incompressible Navier–Stokes solutions to leading edge vortex flows.' *AIAA Paper 86-1839*, AIAA 18th Fluid Dynamics, Plasma Dynamics and Lasers Conference.
- Hartwich, P. M., and Hsu, C. H. (1987). 'High resolution upwind schemes for the three-dimensional incompressible Navier–Stokes equations.' *AIAA Paper 87-0547*, AIAA 23rd Aerospace Sciences Meeting.
- Hollanders, H., Lerat, A., and Peyret, R. (1985). 'Three-dimensional calculation of transonic viscous flows by an implicit method.' *AIAA Journal*, **23**, 1670–8.
- Hughes, T. J. R., Liu, W. K., and Brooks, A. N. (1979). 'Finite element analysis of incompressible viscous flows by the penalty function formulation.' *Journal Computational Physics*, **30**, 1–60.
- Jameson, A., and Yoon, S. (1987). 'Lower-upper implicit schemes with multiple grids for the Euler equations.' *AIAA Journal*, **25**, 929–35.
- Kaynak, U., and Flores, J. (1987). 'Advances in the computation of transonic flows over finite wings.' *AIAA Paper 87-1195*, AIAA 19th Fluid Dynamics, Plasma Dynamics and Lasers Conference.
- Kordulla, W., and MacCormack, R. W. (1985). 'A new predictor–corrector scheme for the simulation of three-dimensional compressible flow with separation.' *AIAA Paper 85-1502-CP*, AIAA 7th Computational Fluid Dynamics Conference.
- Kwak, D., Chang, J. L., Shanks, S. P., and Chakravarthy, S. (1986). 'A three-dimensional incompressible Navier–Stokes flow solver using primitive variables.' *AIAA Journal*, **24**, 390–6.
- Langston, L. S., Nice, M. L., and Hooper, R. M. (1977). 'Three-dimensional flow within a turbine cascade passage.' *ASME Journal of Engineering for Power*, **99**, 21–8.
- Leonard, B. P. (1987). 'SHARP simulation of discontinuities in highly convective steady flows.' *NASA Report TM-100240, ICOMP-87-9*, NASA Lewis Research Center.
- Leonard, B. P. (1988). 'Universal limiter for transient interpolation modeling of the advective transport equations: The ULTIMATE conservative difference scheme.' *NASA Report TM-100916, ICOMP-88-11*, NASA LEWIS Research Center.
- MacCormack, R. W. (1985). 'Current status of numerical solutions of the Navier–Stokes equations.' *AIAA Paper 85-0032*, AIAA 23rd Aerospace Sciences Meeting.
- Martinelli, L., and Jameson, A. (1988). 'Validation of a multigrid method for the Reynolds averaged equations.' *AIAA Paper 88-0414*, AIAA 26th Aerospace Sciences Meeting.
- Martinelli, L., Jameson, A., and Grasso, F. (1986). 'A multigrid method for the Navier–Stokes equations.' *AIAA Paper 86-0208*, AIAA 24th Aerospace Sciences Meeting.
- Obayashi, S., and Kuwahara, K. (1984). 'LU factorization of an implicit scheme for the

- compressible Navier–Stokes equations.' *AIAA Paper 84-1670*, AIAA 16th Fluid Dynamics, Plasma Dynamics and Lasers Conference.
- Patankar, S. V. (1980). *Numerical Heat Transfer and Fluid Flow*, New York: Hemisphere Publishing Co./McGraw-Hill Co.
- Patankar, S. V., and Spalding, D. B. (1972). 'A calculation procedure for heat, mass and momentum transfer in three-dimensional parabolic flows.' *Int. Journal Heat Mass Transfer*, **15**, 1787–806.
- Peyret, R., and Taylor, T. D. (1983). *Computational Methods for Fluid Flow*, New York: Springer Verlag.
- Pironneau, O. (1988). *Finite Element Methods for Fluids*, Chichester, J. Wiley & Sons.
- Pouagare, M., and Laksminarayana, B. (1986). 'A space marching method for viscous incompressible internal flows.' *Journal Computational Physics*, **64**, 389–415.
- Pulliam, T. H. (1984). 'Euler and Thin layer Navier-Stokes codes: ARC2D, ARC3D.' *Proc. Computational Fluid Dynamics User's Workshop*. The University of Tennessee Space Institute, Tullahoma, Tennessee.
- Pulliam, T. H. (1986). 'Artificial dissipation models for the Euler equations.' *AIAA Journal*, **24**, 1931–40.
- Pulliam, T. H., and Steger, J. L. (1985). 'Recent improvements in efficiency, accuracy and convergence for implicit approximate factorization algorithms.' *AIAA Paper 85-0360*, AIAA 23rd Aerospace Sciences Meeting.
- Raithby, G. D., and Schneider, G. E. (1979). 'Numerical solution of problems in incompressible fluid flow: treatment of the velocity–pressure coupling.' *Numerical Heat Transfer*, **2**, 417–40.
- Reddy, D. R., and Rubin, S. G. (1988). 'Consistent boundary conditions for reduced Navier–Stokes (RNS) scheme applied to three-dimensional internal viscous flows.' *AIAA Paper 88-0714*, AIAA 26th Aerospace Sciences Meeting.
- Rieger, H., and Jameson, A. (1988). 'Solution of the three-dimensional compressible Euler and Navier–Stokes equations by an implicit LU scheme.' *AIAA paper 88-0619*, AIAA 26th Aerospace Sciences Meeting.
- Rizzi, A., and Eriksson, L. E. (1985). 'Computation of inviscid incompressible flow with rotation.' *Journal Fluid Mechanics*, **153**, 275–312.
- Roache, P. J. (1972). *Computational Fluid Dynamics*, Albuquerque, New Mexico: Hermosa Publications.
- Rosenfeld, M., Kwak, D., and Vinokur, M. (1988). 'A solution method for the unsteady and incompressible Navier–Stokes equations in generalized coordinate systems.' *AIAA Paper 88-0718*, AIAA 26th Aerospace Sciences Meeting.
- Rubin, S. G., and Reddy, D. R. (1983a). 'Analysis of global pressure relaxation for flows with strong pressure interaction and separation.' *Computers and Fluids*, **11**, 281–306.
- Rubin, S. G., and Reddy, D. R. (1983b). 'Global solution procedures for incompressible laminar flow with strong pressure interaction and separation.' In T. Cebeci (ed.), *Numerical and Physical Aspects of Aerodynamic Flows*, Vol. II, pp. 79–96, New York: Springer Verlag.
- Shyy, W. (1985). 'A study of finite difference approximations to steady state convection dominated flow problems.' *Journal Computational Physics*, **57**, 415–38.
- Shyy, W., and Correa, S. M. (1985). 'A systematic comparison of several numerical schemes for complex flow calculations.' *AIAA Paper 85-0440*, AIAA 23rd Aerospace Sciences Meeting.
- Soh, W. Y. (1987). 'Time marching solution of incompressible Navier–Stokes equations for internal flow.' *Journal Computational Physics*, **70**, 232–52.
- Steger, J. L., and Kutler, P. (1977). 'Implicit finite difference procedures for the computation of vortex wakes.' *AIAA Journal*, **15**, 581–90.
- Subramanian, S. V., and Bozzola, R. (1987). 'Numerical simulation of three-dimensional flow fields in turbomachinery blade rows using the compressible Navier–Stokes

- equations.' *AIAA Paper 87-1314*, AIAA 19th Fluid Dynamics, Plasma Dynamics and Lasers Conference.
- Swanson, R. C., and Turkel, E. (1987). 'Artificial dissipation and central difference schemes for the Euler and Navier–Stokes equations.' *AIAA Paper 87-1107, Proc. AIAA 8th Computational Fluid Dynamics Conference*, pp. 55–69.
- Tannehill, J. C., Holst, T. L., and Rakich, J. V. (1975). 'Numerical computation of two-dimensional viscous blunt body flows with an impinging shock.' *AIAA Paper 75-0154*, AIAA 13th Aerospace Sciences Meeting.
- Taylor, C., and Hughes, T. G. (1981). *Finite Element Programming of the Navier–Stokes Equations*, Swansea, UK: Pineridge Press.
- Temam, R. (1969). 'Sur l'approximation de la solution des equations de Navier–Stokes par la méthode des pas fractionnaires', (I): *Arch. Rational Mech. Anal.*, **32**, 135–153; (II): *Arch. Rational Mech. Anal.*, **33**, 377–385.
- Temam, R. (1977). *Navier–Stokes Equations*, Amsterdam: North Holland Publishing Co.
- Thomasset, F. (1981). *Implementation of Finite Element Methods for Navier–Stokes Equations*, Springer Series in Computational Physics, New York: Springer Verlag.
- Thommen, H. U. (1966). 'Numerical integration of the Navier–Stokes equations.' *Z. Angew. Math. Phys.*, **17**, 369–84.
- Turkel, E. (1986). 'Preconditioned methods for solving the incompressible and low speed compressible equations.' *NASA CR-178086 Report, ICASE Report 86-14*, NASA Langley Research Center.
- Van Doormaal, J. P., and Raithby G. D. (1984). 'Enhancements of the SIMPLE method for predicting incompressible fluid flows.' *Numerical Heat Transfer*, **7**, 147–63.
- Van Leer, B., Thomas, J. L., Roe, P. L., and Newsome, R. W. (1987). 'A comparison of numerical flux formulas for the Euler and Navier–Stokes equations.' *AIAA Paper 87-1104, Proc. AIAA 8th Computational Fluid Dynamics Conference*, pp. 36–41.
- Visbal, M. R., and Shang, J. S. (1987). 'Numerical investigation of the flow structure around a rapidly pitching airfoil.' *AIAA Paper 87-1424*, AIAA 19th Fluid dynamics, Plasma Dynamics and Lasers Conference.
- Yanenko, N. N. (1971). *The Method of Fractional Steps*, New York: Springer Verlag.

PROBLEMS

Problem 23.1

Apply formulas of the form (23.1.3) and (23.1.4) to define the discretization of the shear stress terms in the momentum equation with a finite volume approach for the rectangular and curvilinear meshes of Figure 23.1.2. Consider cell ABCD and derive also the expressions for a Cartesian mesh.

Problem 23.2

Apply formulas of the form (23.1.6) to define the discretization of the shear stress terms in the momentum equation with a finite volume approach for the rectangular and curvilinear meshes of Figure 23.1.2. Consider cell ABCD and derive also the expressions for a Cartesian mesh. Compare with the results of Problem 23.1.

Problem 23.3

Apply formulas of the form (23.1.6), with (23.1.5) to define the discretization of the shear stress terms in the momentum equation with a finite volume approach for the rectangular and curvilinear meshes of Figure 23.1.2. Consider cell ABCD in a cell-vertex method, with variables defined in ABCD. Compare with the results of Problem 23.1.

Problem 23.4

Apply the finite element representation (23.1.7), (23.1.8) to define the discretization of the shear stress terms in the momentum equation with a finite volume approach for the rectangular and curvilinear meshes of Figure 23.1.2. Consider cell ABCD and derive also the expressions for a Cartesian mesh. Compare with the results of Problems 23.1 and 23.3.

Problem 23.5

Apply the Lax–Friedrichs scheme to the convection–diffusion equation (23.2.2):

$$u_i^{n+1} = \frac{1}{2}(u_{i+1}^n + u_{i-1}^n) - \frac{\sigma}{2}(u_{i+1}^n - u_{i-1}^n) + \frac{v\Delta t}{\Delta x^2}(u_{i+1}^n - 2u_i^n + u_{i-1}^n)$$

Show that this scheme is unconditionally unstable.

Develop the equivalent differential equation of this scheme and prove that the instability originates from the combination of a first-order accuracy on the convection term and on the time integration, combined with second-order accuracy of the viscous diffusion term.

Problem 23.6

Consider the leapfrog scheme applied to the convection–diffusion equation (23.2.2):

$$u_i^{n+1} - u_i^{n-1} = -\sigma(u_{i+1}^n - u_{i-1}^n) + \frac{2v\Delta t}{\Delta x^2}(u_{i+1}^n - 2u_i^n + u_{i-1}^n)$$

Show that this scheme is unconditionally unstable, by applying a Von Neumann analysis, following the methods of Section 8.6 in Volume 1. Confirm this analysis by the application of the matrix method (Chapter 10), looking at the spectrum of the space-discretized terms.

Hint: Observe that the spectrum of the space-discretization operators has eigenvalues with negative real parts, while the time integration allows only for imaginary eigenvalues.

Problem 23.7

Consider the leapfrog scheme of Problem 23.6 applied to the convection–diffusion equation (23.2.2) and stabilized by the Dufort–Frankel method:

$$u_i^{n+1} - u_i^{n-1} = -\sigma(u_{i+1}^n - u_{i-1}^n) + \frac{2v\Delta t}{\Delta x^2}(u_{i+1}^n - u_i^{n+1} - u_i^{n-1} + u_{i-1}^n)$$

Show by applying the method of Section 8.6.3 in Volume 1 that the scheme is stable under the CFL condition $|\sigma| \leq 1$. Observe that this condition is independent of viscosity.

Show also by developing the equivalent differential equation that the scheme is not consistent unless $\Delta t/\Delta x$ tends to zero when $\Delta t \rightarrow 0$ and $\Delta x \rightarrow 0$.

Problem 23.8

Work out MacCormack's scheme (23.2.15) for the linear convection–diffusion equation, expressing all the corrector terms as a function of the variable u at time step n . Show that it is identical to the one-step Lax–Wendroff scheme (23.2.8) to (23.3.10) when appropriate

central difference formulas are selected for the second- and third-order derivatives. Refer to Chapter 4 in Volume 1 for a summary of finite difference formulas.

Hint: Obtain the following scheme, with $\sigma = a\Delta t/\Delta x$ and $\beta = \Delta t/\Delta x^2$:

$$u_i^{n+1} - u_i^n = -\frac{\sigma}{2}(u_{i+1}^n - u_{i-1}^n) + \left(\frac{\beta + \sigma^2}{2}\right)(u_{i+1}^n - 2u_i^n + u_{i-1}^n) \\ - \frac{\sigma\beta}{2}(u_{i+2}^n - 2u_{i+1}^n + 2u_{i-1}^n - u_{i-2}^n) + \frac{\beta^2}{2}(u_{i+2}^n - 4u_{i+1}^n + 6u_i^n - 4u_{i-1}^n + u_{i-2}^n)$$

Observe that the last three terms are the linear discretization of equation (23.2.11), applying the formulas (4.2.44) and (4.2.58) of Chapter 4 in Volume 1 at half-integer mesh points.

Problem 23.9

Develop in detail Thommen's scheme (23.2.20) with $\alpha = \beta = \gamma = \frac{1}{2}$ and obtain the stability condition (23.2.22). Compare with the corresponding version of scheme (23.2.18).

Problem 23.10

Obtain the viscous Jacobian matrices (23.2.27), (23.2.28).

Hint: Express the velocity and temperature derivatives in the one-dimensional form of the viscous flux (22.1.10) as a function of the conservative variables.

$$\text{Obtain } f_v = (0; 4\mu u_x/3; 4\mu u u_x/3 + kT_x)^T.$$

Problem 23.11

Develop the Beam and Warming implicit scheme (23.2.29) for the one-dimensional scalar equation (23.2.1).

By linearizing to equation (23.2.2), perform a Von Neumann stability analysis and show that the scheme is unconditionally stable for $\theta > \frac{1}{2}$.

Investigate the effects on the stability from neglecting the viscous terms in the implicit operator, applying the method of Section 8.6 in Volume 1.

Problem 23.12

Show by applying the method of Section 8.6.3 in Volume 1 that the scheme (23.2.36) is stable under the condition (23.2.17).

Problem 23.13

Consider the one-dimensional pseudo-compressible system (23.3.12).

Derive the eigenvalues of the matrix A and obtain the characteristic variables as well as the compatibility relations.

Hint: The characteristic variables are

$$\partial w = \partial u + \frac{\partial P}{u + c} \quad \text{with } c^2 = u^2 + \beta^2$$

Problem 23.14

Consider the two-dimensional pseudo-compressible form of the incompressible flow equations obtained by neglecting the viscous terms, generalizing equation (23.3.12) for the variables $U = (P, u, v)^T$. Obtain the eigenvalues of this hyperbolic system for waves propagating in the direction κ defined by the unit vector $\bar{1}_\kappa$.

Hint: The system can be written as follows:

$$\frac{\partial U}{\partial t} + A \frac{\partial U}{\partial x} + B \frac{\partial U}{\partial y} = 0$$

with

$$A = \begin{vmatrix} 0 & \beta^2 & 0 \\ 1 & 2u & 0 \\ 0 & v & u \end{vmatrix} \quad B = \begin{vmatrix} 0 & 0 & \beta^2 \\ 0 & v & u \\ 1 & 0 & 2v \end{vmatrix}$$

and the eigenvalues of the matrix $A\kappa_x + B\kappa_y$, where κ_x and κ_y are the Cartesian components of the unit vector in the κ -direction, are $\bar{v} \cdot \bar{1}_\kappa$ ($\equiv v_\kappa$), $v_\kappa \pm \sqrt{v_\kappa^2 + \beta^2}$.

Problem 23.15

Derive equation (23.3.23).

Problem 23.16

Work out the implicit scheme (23.3.30) in the two-dimensional case as a system of two equations in the velocity components u, v , and obtain the pressure correction equation.

Compare with the formulation obtained from Problem 23.14 by removing the equation for the pressure and adding the viscous terms. Linearize the Jacobian matrices and observe that the result is not identical to equations (23.3.30). Explain these differences and their origin.

Problem 23.17

Develop the implicit scheme (23.3.30) for the two-dimensional case as a system of two equations in the velocity components u, v , considering a fractional step method whereby the pressure term is removed from equation (23.3.30). Derive the Poisson equation for the pressure.

Problem 23.18

Work out in detail the upwind schemes (23.2.37) and (23.2.39) applied to the linear convection equation.

Compare with the MacCormack scheme.

Problem 23.19

Discretize the incompressible momentum and continuity equations on the staggered mesh of Figure 23.3.6, selecting the indicated finite volumes. The values at alternate points are obtained by averaging the surrounding mesh point values.

Define various linearizations for the convection terms.

Problem 23.20

Apply the schemes referred to in Problem 23.18 to the linear convection–diffusion equation for an initial shock discontinuity and compare with the exact solution.

Investigate the influence of the Reynolds number.

Problem 23.21

Repeat Problem 23.20 for Burgers equation.

Index

- Acoustic waves 194, 292, 376, 378, 459
ADI factorization, method 61, 88–92,
265, 296, 327, 336, 515, 648, 665
Airfoil 10, 15, 18, 26, 31, 57, 65, 66, 74,
92, 105, 108, 110–117, 269, 270,
280, 292, 385–387, 395–401, 574,
613, 645
Aliasing effect 308
Amplification factor, matrix 51, 83, 87,
88, 228, 230, 232, 236, 243, 251,
252, 261, 265, 288, 291, 292, 294,
312, 316–321, 336, 337, 410, 411,
428, 429, 502, 504
Approximate factorization 61, 88–92, 639,
659, 665
Approximate Riemann solver 127, 409,
434, 443, 453–469, 514, 562
Artificial compressibility, density 61,
67–70, 84–87, 89, 117
Artificial dissipation (viscosity) 58, 61,
62–67, 71, 81, 85, 86, 105, 117,
127, 240, 270, 273–283, 290, 315–
326, 368, 398, 413, 521, 523, 527,
529, 574, 624, 631, 636, 659, 666
of Jameson 279–280, 327, 328, 636,
639
of MacCormack–Baldwin 279, 281
of TVD schemes 564–570, 574
of Von Neumann–Richtmyer 274–278
Artificial mass flux (flux upwinding) °
70–76, 117
A-stability 310, 357
Backward differencing (*see* Upwind
differencing)
Beam–Warming scheme 126, 129, 279,
286, 287, 289, 307–334, 345, 364,
366–369, 627, 637, 659
Bicharacteristics 152, 177, 186, 188–192,
195, 376
Boundary conditions 14–18, 19, 26,
36–38, 66, 81, 90, 115, 126, 157,
171–173, 191–192, 211, 225, 240,
246, 270, 284, 295, 308, 309, 411,
601–603, 639
Dirichlet 17, 36, 81
for Euler equations 344–401
far-field 15, 372, 377–379, 385–395
implicit 290, 357, 359
Neumann 17, 18, 19, 36, 43, 90, 664
non-reflecting 191, 348, 369–371, 384,
425–426
numerical 173, 191, 195, 240, 346,
347–353, 360, 362, 370, 372–375,
378, 411, 425
periodic 18, 83
physical 171–173, 191, 346–353,
358, 360–363, 367, 369, 372–375,
378–381, 384, 389, 411
reflecting 36
solid wall 14, 36, 37, 372, 375,
379–384, 602
Boundary layer 15, 117, 399, 602,
608–613, 650, 657
Box scheme 246
Burgers' equation 196–204, 225, 226,
249, 250, 313, 319, 321, 357, 410,
417, 450–453, 456, 458, 463, 467,
509, 570, 620–621, 631
Cascade flow 17, 18, 31, 42, 47, 115, 372,
374, 618, 631, 639

- Central difference, discretization 27, 30, 62, 64–66, 68, 76, 125, 126, 226, 232, 234, 235, 243, 246, 251, 254, 280, 281, 283, 408, 409, 413, 424, 427, 493, 496, 497, 507, 518, 529, 552, 625, 659, 666–669
schemes with independent time integration 129, 305–339, 494, 499, 537, 556, 566, 636–648
- Centrifugal force 134
- CFL condition (*see* Courant–Friedrichs–Lewy)
- Channel (duct) flow 17, 157, 158, 257, 330–333, 372, 374, 389, 657, 661
- Characteristic 10, 11, 132, 197, 201–208, 254, 346, 357–380, 384, 408, 409–416, 419, 451, 458, 460, 520–523
boundary conditions 346–379, 387, 425–426
formulation of Euler equations (*see* Euler equations)
speed, velocity 151, 152, 162, 163, 239, 410, 438
surface 10, 11, 14, 151, 152, 186, 191, 194
variables 157–195, 238, 329, 346, 353, 357–362, 369, 370, 379, 395, 415, 461–462, 501
- Circulation 15, 18, 115, 386, 395, 396
- Clebsch representation 116
- Compatibility relations (equations) 150–195, 347–349, 353, 357, 362–369, 375–381, 387, 425, 426, 438
- Conditioning operator (*see* Preconditioning)
- Conjugate gradient method 77, 99
- Conservation form, law, scheme 4–6, 18, 19, 27, 39, 61, 66, 99, 105, 112, 113, 132, 199, 224, 225, 227, 235, 249, 273, 283, 292, 327, 349, 352, 357, 364, 380, 414, 426, 427, 443–445, 448–449, 453–457, 460–462, 481, 495, 501, 511, 519–528, 531, 654, 656, 657, 668
of Euler equations (*see* Euler equations)
of Navier–Stokes (*see* Navier–Stokes)
of potential equation (*see* Potential equation)
- Conservative variables 132, 138–149, 154, 156, 180–184, 274, 349, 350, 353, 357–363, 414, 415, 419, 425, 461, 597
- Consistency condition 225, 285, 529
- Contact discontinuity 71, 127, 132, 135–137, 168–171, 204–206, 225, 250, 275, 322, 401, 434, 443, 449, 469, 493, 523, 527, 543, 549, 600, 650
- Continuity equation (*see* Mass conservation)
- Contravariant components 13, 31, 35, 37, 75, 382, 383, 442
- Convection equation 125, 196, 224, 226, 227, 234, 272, 328, 446, 476–483, 499, 501, 509, 518, 526, 531, 534, 537–550, 560, 565
- Convection–diffusion equation 69, 618–620, 629, 648
- Coriolis force 133
- Corrected viscosity scheme 233–234
- Courant (CFL) number 226–228, 238, 243, 246, 284, 286, 289–292, 295, 296, 313, 315, 316, 319, 322, 368, 410, 411, 515, 550, 557, 567, 568, 621, 628, 636
- Courant–Friedrichs–Lewy (CFL) condition 228, 236, 246, 260, 261, 264, 283, 287, 292, 308, 335, 428, 429, 443, 446–449, 454, 530, 531, 533, 535, 556–559, 563
- Covariant components 13
- Critical condition 211
mass flow 211
section 211–213
- Crococ’s equation 114
- Curvilinear coordinates, mesh 5, 31–36, 67, 74, 76, 89, 92, 135, 307, 327, 382, 441, 442, 625
- Cylindrical coordinates 6
- Diagonal dominance 29, 285, 288, 289, 290, 329, 474, 516, 559, 639
- Diffusion error, properties (*see* Dissipation error, properties)
- Direct method 77, 85, 87
- Dirichlet boundary condition (*see* Boundary conditions)
- Dispersion error, properties 196, 228–229, 236, 237, 285, 292, 313, 318, 502, 504
- Dissipation (viscous) 601, 659
error, properties 196, 225, 228–229, 237, 250, 283, 285, 287, 288, 292, 313, 318
numerical (*see* Numerical dissipation) in the sense of Kreiss 229, 237, 285, 287, 288, 291, 313

- Dissipative mechanism, scheme, term 196, 204, 227, 246, 272–283, 288, 289–291, 294, 308, 318, 334, 335, 339, 398, 399, 529, 624, 650
- Domain of dependence 11, 51, 57, 61, 77–81, 169, 262, 411
- Domain of influence 11, 169
- Duct flow (*see* Channel flow)
- Elliptic equation, method 9, 26, 51, 57
- Energy (conservation) equation 4, 5, 132, 146, 274, 280, 335, 336, 600, 604–606
- Enthalpy 133
damping 335, 637
stagnation (total) enthalpy 4, 133, 335, 374, 379, 380, 424, 605, 637
- Entropy 19, 76, 114, 115, 117, 137, 164, 165, 168, 173, 194, 206, 211, 243, 258, 270, 271, 322, 369, 377, 380, 388, 389, 399, 438, 457
condition 63, 135, 138, 171, 196, 204, 449, 493, 494, 519–527, 535–537, 570
function 523–525, 536
inequality 138, 523, 524
- Equation of state 134
- Equivalent differential equation 237, 250, 269, 285, 527, 563
- Euler equations 69, 71, 76, 105, 110, 115, 117, 125–585, 596, 601, 625–627
characteristic formulation 150–157, 415, 416
conservative form 132–138, 199, 224, 225, 227, 235, 249, 273, 283, 292, 327, 349, 352, 357, 364, 380, 414, 418, 419
mathematical formulation 132–213
non-conservative, quasi-linear, form 138–149, 150, 186, 357, 408, 418
simple wave solutions 173–176
- Euler explicit method 308, 310, 499, 530, 557
- Euler implicit method 310, 313, 318, 322
- Expansion fan 170, 202–208, 243, 326, 401, 443, 451, 463, 468–472, 631
- Expansion shock 57, 63, 71, 72, 137, 171, 196, 204, 243, 246, 273, 275, 308, 449, 453, 454, 460, 463, 467–469, 519, 520, 526, 535, 570, 632
- Explicit method, scheme 224, 225, 226, 232, 246, 265, 283, 287, 308, 345, 346, 494, 499, 541, 557, 560
- Extrapolation method (for boundary conditions) 348, 353–362, 368, 378, 380, 602
- Finite difference formula, method 26, 27–31, 34, 36, 41, 43, 58, 61, 307, 327, 625
- Finite difference operators 28, 35, 61, 92, 232, 286, 504
- Finite element method 18, 19, 26, 33, 42–47, 49, 61, 68, 69, 83, 85, 92, 104, 495, 583, 627, 669–670
- Finite volume method 18, 19, 26, 38–42, 234, 256, 263, 307, 327, 334, 441, 442, 444, 504, 626, 638, 664
- Flux
antidiffusive 559, 561, 563, 570
corrected transport 559, 561
difference splitting 127, 408, 409
extrapolation 504–517
homogeneity property 139–141, 416–420, 465
limiters 474, 550–552
mass 37, 68, 76, 243, 275, 281, 322, 420, 434, 600, 601, 603–604
modified 563–564
numerical (*see* Numerical)
upwinding (*see* Artificial flux)
vector splitting 127, 371, 408, 409, 415–443, 507–511, 553, 577, 639
viscous 274, 598, 637, 649
- Fourier analysis, mode 50, 83, 228, 336, 337, 387, 393
- Fractional-step method 265, 478, 482, 664, 665
- Fromm's scheme 500, 501, 504
- Galerkin method 42–47
- Gauss–Seidel line, point iteration (*see* Relaxation method)
- Gaussian quadrature 45
- Godunov method (scheme) 127, 409, 443–453, 456, 472, 494, 504, 518
numerical flux 448–453, 456, 467
- Godunov-type method (schemes) 127, 409, 418, 443–472, 475, 482, 507, 552
- Group velocity 150, 315
- Heat conduction equation, flux 26, 598, 625–627, 636
- High frequency errors 85, 104, 237, 243, 273, 285, 291, 294, 308, 313, 315, 336, 337, 666

Homogeneous, flux 139

High resolution schemes 493–582

Hybrid equations 157

Hyperbolic equation (problem) 9, 10, 12, 57, 79, 80, 127, 132, 143, 157, 225, 232, 310, 334, 335, 344, 346, 348, 408, 413, 419, 456, 481, 520, 522, 656

Ill-posed problem 349

Implicit difference formulas 311

dissipation 319–325

operator 86, 88, 311

Implicit scheme 88, 224, 246, 265, 308, 311, 337, 345, 346, 356, 357, 364, 494, 556, 638, 659

of Beam and Warming (*see* Beam–Warming scheme)

of Lerat (*see* Lerat)

upwind schemes 473–474, 512–517, 558–559

Incompressible flow 396, 606

potential equation 42, 50

Navier–Stokes equation 596, 654, 675

Interior scheme 344, 349, 356, 359, 364

Irrotational condition (flow) 4, 9, 257, 383, 396

Isentropic condition, flow, law 4, 17, 19,

165, 173, 190, 211, 213, 270, 381

potential model 6, 57, 76, 104–112, 114, 115, 385

shock 76, 105, 116

Isoparametric transformation (mapping) 33

Iterative method on density 47–51

Jacobian matrix 49, 50, 51, 57, 77, 83, 84, 363

diagonalization of 153, 160, 178–184

of flux (vector) 138–149, 177, 197, 224, 235, 237, 238, 255, 258, 266, 288, 322, 372, 414–429, 438–439, 453, 446, 456, 463, 474, 475, 511–514, 522, 558, 562, 629, 637, 639

eigenvalues 150–161, 177–180, 228, 231, 243, 288, 290, 344, 408, 415–429, 438–443, 457, 462, 463, 650

left eigenvectors 150, 153–155, 158–161, 175, 177–180, 193, 194, 362, 370, 419

right eigenvectors 154, 156, 175, 179, 238, 419–420, 457–463, 522–523

Jameson's multistage method 126, 307, 334–339

Kutta–Joukowski condition 18, 115, 116, 344, 395–401

Laminar flow 595, 621

Laplace equation 28, 42, 45, 47, 50, 51, 83, 85

Lax–Friedrichs scheme 125, 226–235, 238, 258, 272, 281, 413, 467, 629

Lax–Wendroff (family of) scheme 125, 126, 224–296, 307, 308, 345, 356, 357, 412, 413, 427, 495, 499, 502, 511, 526, 534, 538, 541, 556, 559, 562–566, 570, 627, 629–636, 648, 651

Leap frog scheme 238, 258, 308, 310, 629

Least squares approach 47

Left eigenvectors (*see* Jacobian matrix)

Lerat implicit schemes of Lax–Wendroff type 283–296

Lerat and Peyret schemes 126, 226, 246–250, 258, 267–271, 632, 633

Limiters 127, 474, 493, 499, 509, 519, 536–582, 631

Linearization 47, 49, 309, 473, 512

Line relaxation (*see* Relaxation)

Local time step 284, 335

MacCormack method, scheme 126, 226, 239–246, 249, 255, 258, 261–272, 275, 326, 335, 356, 359–362, 366, 371, 565, 570, 629–636, 651

Mach angle 12

cone, conoid 12, 152, 184–186, 191

line 163

Mapping 31, 33

Mass conservation (equation) 4, 19, 20, 38, 132, 146, 274, 381, 424, 654, 656, 664, 666, 668–669

flux (*see* Flux)

Mesh Reynolds (Péclet) number 629

Method of lines 273

Metric coefficients, tensor 33, 34–36, 38, 41, 89, 92, 327, 383

Momentum equation 132, 146, 189, 274, 381, 382, 387, 602, 604, 654, 656, 663, 665, 668

Monotone scheme, monotonicity 71, 413, 449, 473, 501, 518–519, 525–528, 535, 536, 549, 552, 558–560

Multigrid method 61, 77, 80, 98–104, 105, 253, 255, 257, 284, 334, 337, 339, 515, 631, 648, 665

Multistage method (*see* Runge–Kutta multistage method)

- Multistep method 307–312, 473, 494, 499, 512, 556, 637, 659
 Murman–Cole method, scheme 58–61, 62, 65, 71, 77, 453–454, 456, 466, 467, 531
 MUSCL approach (*see* Variable extrapolation)
 Navier–Stokes equations 125, 271, 274, 307, 309, 329, 399, 518, 521, 595–675
 conservation form 597–599
 mathematical formulation 597–621
 Reynolds averaged 595, 596, 603–607
 Neumann boundary condition (*see* Boundary conditions)
 Newton method 23, 49, 207, 367
 Nine-point formula for Laplace equation
 Nonconservative form (scheme) 6, 26, 61, 138–149, 150, 186, 357, 408, 438, 655
 of Euler equations (*see* Euler equations)
 of potential equation (*see* Potential flows)
 Nonlinearity, non-linear form, properties 26, 47, 196, 224, 237, 240, 249, 250, 269, 275, 280, 281, 284, 292, 293, 308, 357, 367, 414, 443, 449, 453, 459–462, 493, 494, 502, 505, 509, 519, 527, 528, 532, 534, 543, 550, 557, 559, 570
 Nonlinear limiters (*see* Limiters)
 Non-reflecting boundary conditions (*see* Boundary conditions)
 Non-uniqueness of potential flow 104–112
 Normal mode analysis 272
 Nozzle flow 115, 211–213, 241–243, 246, 275, 295, 321, 348, 349, 352, 370, 389, 434, 469, 508
 Numerical boundary conditions (*see* Boundary conditions)
 domain of dependence 262, 264
 dissipation, viscosity (*see also* Artificial dissipation, viscosity) 226, 227, 269, 273, 410, 413, 476, 531
 flux 225, 229, 235, 237, 240–241, 250, 268, 273, 274, 275, 279, 281, 283, 293, 311, 414, 427, 445, 448–462, 466–467, 472–476, 494, 496, 498–499, 501, 505–507, 512, 514, 516–517, 525–526, 532–537, 550–553, 556, 560–567, 630, 648–650
 phase speed 229
 One-dimensional flow 157–176
 Oscillations 41, 127, 224, 232, 237, 243, 246, 249, 250, 270, 272, 273, 275, 280, 281, 308, 313, 315, 319, 326, 408, 422, 473, 474, 493, 494, 499, 502, 508, 517, 518, 546, 549, 550, 559, 659, 667
 nonlinear 71, 250, 309
 Odd–even decoupling 41, 232, 273, 308, 411, 666–667
 Operator splitting 265
 Osher's approximate Riemann solver 127, 409, 434, 453–460, 468, 474, 514, 650
 Over-relaxation (*see* Relaxation method)
 Parabolic equation 9, 310, 521
 Parabolized Navier–Stokes equations (PNS) 666
 Perfect gas 5, 7, 134, 139, 141, 147, 418, 420, 464, 598
 Periodic boundary conditions (*see* Boundary conditions)
 Phase error (*see* Dispersion error)
 Physical boundary conditions (*see* Boundary conditions)
 Poisson equation for pressure 654–655, 661–664, 668
 Positive definiteness 23, 51, 57, 77
 Potential flows 1–124, 280, 327, 395, 396, 453, 519, 626, 663
 boundary conditions 14–18, 19, 26, 36–38, 66
 conservative form 4–6, 18, 26, 27, 61, 66, 76, 105, 108
 discontinuities, shocks 14, 17, 18, 19, 26, 57, 63, 72, 76, 105, 108, 110, 112, 114–117
 integral or weak formulation 18–23
 isentropic 6, 57, 76, 104–112, 114–117
 iteration schemes 77–104
 mathematical formulation 4–25
 non-conservative form 6, 9, 26, 29, 61, 62–66, 76, 108
 non-isentropic 104, 112–117
 relaxation method 77–88
 small disturbance (perturbation) form 7, 58, 63, 65, 71, 83, 88, 114, 385
 transonic 57–117, 280, 335, 413
 unsteady 9
 Prandtl number 598, 607, 614
 Prandtl–Glauert small disturbance equation 8
 Preconditioning 51, 77, 78, 82, 99

- Predictor-corrector 224, 238–241, 247–249, 261, 263, 266, 268, 360–362, 630
- Pressure correction method 654, 661–670
- Primitive variables 132, 145–149, 154, 156, 176–180, 186, 195, 349, 350, 353, 357–362, 372
- Pseudo-compressibility 654, 656–661
- Pseudo-path line 184–186, 189, 195
- Rankine–Hugoniot relations 19, 76, 105, 112, 114, 116, 135–137, 199, 212, 271, 449, 454, 463, 466, 467, 519–521
- Real fluids 141, 520
- Region of dependence (*see* Domain of dependence)
- Relaxation method 474, 648
 - equivalent differential equation 78, 79, 80
 - for potential equation (*see* Potential flows)
 - successive line 61, 77–81, 85, 88, 89
 - zebra 99, 516
- Residual 78, 90, 241, 294, 334–337, 513
- Reynolds number 125, 399, 596, 597, 602, 615, 621, 624–625, 631–632, 657
- Reynolds stress 604–607, 610, 613–618
- Richtmyer scheme 238, 258–261, 356, 633
- Riemann invariants 176, 346, 347, 426, 457
 - problem, solution 127, 170, 204–211, 243–245, 275, 281, 322, 401, 409, 422, 426, 429–432, 443–454, 460, 463, 472, 474, 475, 494, 496, 504, 509
 - variables 162–165, 173, 190, 207, 370, 376, 411
- Right eigenvectors (*see* Jacobian matrix)
- Roe's approximate Riemann solver 127, 409, 434, 460–469, 474, 475, 498, 504, 650
- Roe linearization 238, 463
- Rotated difference scheme 64, 79
- Rotational flow 257
- Runge–Kutta multistage method 126, 307, 308, 334–337, 494, 556, 559, 627, 637, 639, 659
- Second order upwind scheme 493–582
- Secondary flows 332–334, 639
- Semi-discretized form 309, 473, 494, 498, 506, 529–534, 536–558, 628
- Separate space–time integration (*see* Central schemes)
- Shear layer 194, 396, 609, 610, 624
- Shear stress 598, 605, 626, 628
- Shock–boundary layer interaction 76, 618
- Shock fitting 408, 438
- Shock transition wave 14, 17, 18, 19, 26, 57, 63, 72, 76, 105, 108, 110, 112, 114–117, 127, 132, 135–137, 168–171, 176, 199–201, 204–213, 225, 240, 243, 249, 250, 257, 270–272, 275, 280, 281, 290, 308, 313, 315, 322–326, 369, 370, 389, 398, 401, 424, 434, 438, 443, 450–454, 456, 469, 493, 507–509, 527, 549, 574, 600, 615, 650–654
- Shock tube problem (*see* Riemann problem)
- Simple wave (solutions) 173–176, 238, 457–463, 476
- Slip lines 137, 574
- Small disturbance approximation (*see* Potential flows)
- Sonic condition, point, velocity 8, 11, 14, 17, 22, 58, 63, 69, 71, 72, 76, 145, 243, 273, 275, 290, 315, 374, 378, 379, 420–425, 434, 451–453, 456, 459–460, 463–469, 508, 509, 535, 570, 601
- Source term 158, 241, 242, 322, 360, 367, 370, 597
- Space-centred discretization (*see* Central difference)
- Spacelike variable, direction 14, 22, 50, 185
- Spectral radius 228, 294, 296, 329, 429
- Speed of sound (*see* Sonic velocity)
- Stability analysis, condition, properties 92, 225, 228, 230, 231, 233, 236, 260–262, 265, 285, 287, 288, 307, 310, 313, 316–321, 335, 348, 349, 356, 476, 502, 526, 531, 557, 568, 629–631, 636
 - conditional 84, 85, 88, 126, 246, 357, 557
 - unconditional 86, 87, 88, 283, 284, 289, 290, 294, 308, 328, 357, 639
 - for upwind schemes 410–412, 414, 428–434
- Stagnation enthalpy (*see* Enthalpy)
 - pressure (loss) 115, 116, 257, 332, 333, 374, 577
 - temperature 243, 374, 434, 577
- Staggered mesh 667–669

- Steady state (stationary) form, solution
 157, 165–168, 201, 229, 233, 241,
 246, 263, 272, 280, 284, 291, 293,
 296, 311, 316, 319, 322, 329, 335,
 357, 371, 377–379, 424, 476, 556,
 559, 631, 634, 648, 654, 656
 potential flow 5, 7, 9, 20, 49
- Steger–Warming flux splitting 127,
 415–418, 422, 424, 425, 434,
 440–442, 508, 577, 650
- Stiffness matrix 43, 45
- Streamline coordinates 64
- Subsonic flow 9, 11, 13, 14, 17, 18, 22,
 26, 29, 42, 49, 50, 57, 58, 63, 65, 68,
 72, 77, 79, 92, 117, 168–169, 172,
 173, 186, 192, 211–213, 295, 351,
 352, 353, 358, 360, 361, 364, 365,
 370, 375, 378, 379, 384, 387, 416,
 422, 425, 439, 451, 601, 657
- Successive over-relaxation, SOR (*see*
 Over-relaxation)
- Supercritical airfoil 112
- Supersonic flow, region, velocities 9,
 11–14, 17, 18, 22, 29, 42, 50,
 57–117, 156, 165, 168–169, 172,
 173, 186, 192, 211–213, 239, 246,
 257, 295, 339, 352, 361, 362, 375,
 401, 408, 420, 434, 439, 451, 601
- Switch factor, switching function 65–72,
 453–455
- Taylor expansion, series 235, 248–249,
 283, 285, 292, 313, 408, 427, 509,
 527, 541
- Thin-shear layer 602, 624–625
- Thomas algorithm 81, 308, 513
- Three-dimensional flow, problem 9, 36,
 39, 42, 49, 58, 61, 77, 92, 104, 117,
 177, 188, 192–194, 225, 257, 264,
 309, 328, 339, 372, 379, 395,
 441–442, 474, 515, 526, 574, 601,
 636, 638, 661, 670
- Time-dependent (equation) approach 284,
 358
- Time like variable, direction 9, 12, 13, 14,
 22, 50, 75, 80
- Total enthalpy (*see* Enthalpy)
- Total pressure (*see* Stagnation temperature)
- Total temperature (*see* Stagnation tempera-
 ture)
- Total variation diminishing (TVD)
 schemes 127, 281, 494, 519, 527–582
- Transonic flow 14, 17, 26, 42, 57–117,
 243, 257, 269, 280, 335, 389
- Trapezoidal method, scheme 287, 289,
 310, 313, 318
- Tridiagonal system 77, 81, 88, 89, 90,
 294, 295, 308, 311, 327–329, 336,
 359, 474, 513
- Truncation error 27, 227, 234, 239, 241,
 246, 249, 250, 269, 272, 273, 274,
 281, 285, 290, 293, 313, 329, 424,
 495, 499, 532
- Turbomachinery flow 272
- Turbulence models 595, 596, 606–618,
 674
 algebraic model 608–613, 631
 algebraic Reynolds stress model
 615–618
 one- and two-equation (k - ϵ) model
 613–615
- Turbulent flow 595, 603–618
 eddy viscosity 607–614, 618
- Two step method, scheme 234, 253, 296,
 327, 649
 Lax–Wendroff schemes 238–250,
 258–272
 Lerat implicit schemes 289, 290
- Unicity 23
- Unsteady flow, phenomena 9, 204, 272,
 284, 285, 292–294, 296, 371
- Upwind differencing, discretization
 62–69, 75, 80, 263, 348, 357, 364
 schemes 126, 127, 280, 281, 408–582,
 648–654, 669
- Van Leer flux splitting 127, 420–425,
 434, 440–442, 508, 509, 650
- Variable extrapolation 494–505, 507,
 508, 514–517, 552–556, 559, 561,
 577
- Variational principle (formulation) 19,
 42
- Viscid–inviscid interaction 15, 76
- Viscosity 125, 273, 274, 283, 398, 399,
 521, 595, 598–602, 607, 618, 619,
 655
- Von Neumann analysis, method 77,
 80, 228, 230, 231, 236, 251,
 252, 260, 265, 285, 287, 312,
 316–321, 428, 476, 531, 568,
 630, 636, 648
- Vortex sheet 137, 396
- Vorticity (equation) 37, 110, 114,
 194, 332, 377, 383, 396–401,
 608, 654

Wake 396, 609

Wave equation 196, 225

number, vector 177, 188, 195, 196
(phase) speed 150, 151, 176, 177,

374, 476, 520, 529, 562

propagation, reflections 191, 280

surface (*see* Characteristic surface)

Wave-like solutions 150

Weak formulation 18–23, 42, 43

Weak instability 328

Weak solution 396, 460, 473, 601

Weighted residual method 43

NUMERICAL COMPUTATION of INTERNAL and EXTERNAL FLOWS

Volume 2:

Computational Methods for Inviscid and Viscous Flows

C. Hirsch, *Vrije Universiteit Brussel, Brussels, Belgium*

This second volume deals with the applications of computational methods to the problems of fluid dynamics. It complements the first volume to provide an excellent reference source in this vital and fast growing area. The author includes material on the numerical computation of potential flows and on the most up-to-date methods for Euler and Navier-Stokes equations. The coverage is comprehensive and includes detailed discussion of numerical techniques and algorithms, including implementation topics such as boundary conditions. Problems are given at the end of each chapter and there are comprehensive reference lists.

Of increasing interest, the subject has powerful implications in such crucial fields as aeronautics and industrial fluid dynamics. Striking a balance between theory and application, the combined volumes will be useful for an increasing number of courses, as well as to practitioners and researchers in computational fluid dynamics.

Contents

Preface

Nomenclature

PART V: THE NUMERICAL COMPUTATION OF POTENTIAL FLOWS

Chapter 13 The Mathematical Formulations of the Potential Flow Model

Chapter 14 The Discretization of the Subsonic Potential Equation

Chapter 15 The Computation of Stationary Transonic Potential Flows

PART VI: THE NUMERICAL SOLUTION OF THE SYSTEM OF EULER EQUATIONS

Chapter 16 The Mathematical Formulation of the System of Euler Equations

Chapter 17 The Lax-Wendroff Family of Space-centred Schemes

Chapter 18 The Central Schemes with Independent Time Integration

Chapter 19 The Treatment of Boundary Conditions

Chapter 20 Upwind Schemes for the Euler Equations

Chapter 21 Second-order Upwind and High-resolution Schemes

PART VII: THE NUMERICAL SOLUTION OF THE NAVIER-STOKES EQUATIONS

Chapter 22 The Properties of the System of Navier-Stokes Equations

Chapter 23 Discretization Methods for the Navier-Stokes Equations

Index

ISBN 0-471-92452-0



BIBLIOTHÈQUES UNIVERSITÉ DE MONTRÉAL



3 1225 02026 8351

JOHN WILEY & SONS

Chichester · New York · Brisbane · Toronto ·

A Wiley · Interscience Publication